NEURAL PROSTHESES FOR LOCOMOTION

EDITED BY: Daniel P. Ferris, Mikhail Lebedev, Yury Ivanenko, Kyuhwa Lee, Yoshio Sakurai and Irina N. Beloozerova
PUBLISHED IN: Frontiers in Neuroscience, Frontiers in Human Neuroscience and Frontiers in Neurology

frontiers Research Topics

frontiers

ISSN 1664-8714
ISBN 978-2-88971-939-6
DOI 10.3389/978-2-88971-939-6

About Frontiers

Frontiers is more than just an open-access publisher of scholarly articles: it is a pioneering approach to the world of academia, radically improving the way scholarly research is managed. The grand vision of Frontiers is a world where all people have an equal opportunity to seek, share and generate knowledge. Frontiers provides immediate and permanent online open access to all its publications, but this alone is not enough to realize our grand goals.

Frontiers Journal Series

The Frontiers Journal Series is a multi-tier and interdisciplinary set of open-access, online journals, promising a paradigm shift from the current review, selection and dissemination processes in academic publishing. All Frontiers journals are driven by researchers for researchers; therefore, they constitute a service to the scholarly community. At the same time, the Frontiers Journal Series operates on a revolutionary invention, the tiered publishing system, initially addressing specific communities of scholars, and gradually climbing up to broader public understanding, thus serving the interests of the lay society, too.

Dedication to Quality

Each Frontiers article is a landmark of the highest quality, thanks to genuinely collaborative interactions between authors and review editors, who include some of the world's best academicians. Research must be certified by peers before entering a stream of knowledge that may eventually reach the public - and shape society; therefore, Frontiers only applies the most rigorous and unbiased reviews.
Frontiers revolutionizes research publishing by freely delivering the most outstanding research, evaluated with no bias from both the academic and social point of view. By applying the most advanced information technologies, Frontiers is catapulting scholarly publishing into a new generation.

What are Frontiers Research Topics?

Frontiers Research Topics are very popular trademarks of the Frontiers Journals Series: they are collections of at least ten articles, all centered on a particular subject. With their unique mix of varied contributions from Original Research to Review Articles, Frontiers Research Topics unify the most influential researchers, the latest key findings and historical advances in a hot research area! Find out more on how to host your own Frontiers Research Topic or contribute to one as an author by contacting the Frontiers Editorial Office: frontiersin.org/about/contact

NEURAL PROSTHESES FOR LOCOMOTION

Topic Editors:
Daniel P. Ferris, University of Florida, United States
Mikhail Lebedev, Skolkovo Institute of Science and Technology, Russia
Yury Ivanenko, Santa Lucia Foundation (IRCCS), Italy
Kyuhwa Lee, Wyss Center for Bio and Neuroengineering, Switzerland
Yoshio Sakurai, Doshisha University, Japan
Irina N. Beloozerova, Georgia Institute of Technology, United States

Citation: Ferris, D. P., Lebedev, M., Ivanenko, Y., Lee, K., Sakurai, Y., Beloozerova, I. N., eds. (2021). Neural Prostheses for Locomotion. Lausanne: Frontiers Media SA. doi: 10.3389/978-2-88971-939-6

Table of Contents

frontiers in Neuroscience

EDITORIAL
published: 04 November 2021
doi: 10.3389/fnins.2021.788021

Editorial: Neural Prostheses for Locomotion

Yury Ivanenko[1,2*], *Daniel P. Ferris*[3], *Kyuhwa Lee*[4], *Yoshio Sakurai*[5], *Irina N. Beloozerova*[6] *and Mikhail Lebedev*[2,7]

[1] Laboratory of Neuromotor Physiology, IRCCS Fondazione Santa Lucia, Rome, Italy, [2] V. Zelman Center for Neurobiology and Brain Restoration, Skolkovo Institute of Science and Technology, Moscow, Russia, [3] J. Crayton Pruitt Family Department of Biomedical Engineering, University of Florida, Gainesville, FL, United States, [4] Wyss Center for Bio and Neuroengineering, Genève, Switzerland, [5] Graduate School of Brain Science, Doshisha University, Kyoto, Japan, [6] School of Biological Sciences, Georgia Institute of Technology, Atlanta, GA, United States, [7] Center for Bioelectric Interfaces, National Research University Higher School of Economics, Moscow, Russia

Keywords: locomotion, exoskeletons, neuromodulation, brain computer interface, EEG, EMG, locomotor-related disorders, neurorehabilitation

Editorial on the Research Topic

Neural Prostheses for Locomotion

During the last decade, we have seen a rapid development of neural prostheses, the systems that connect the brain to external assistive and rehabilitation devices. While this work was dominated by the research on neural prostheses that enable sensorimotor functions of the arm and hand, there has also been a growing interest in neural prostheses that restore locomotion, the ability to move in space. Brain-controlled wheelchairs and exoskeletons represent examples of such neural prostheses.

The collection of articles in this Research Topic present and discuss available evidence, conceptual frameworks, neuroprosthetic designs and practical questions concerning application of neural prostheses to gait assistance and rehabilitation. The Research Topic covers a range of issues such as control schemes, robotic aspects, effectiveness, characteristics of motor performance, neural underpinnings, ethics, significance for neurological disorders, motor learning, and recovery of locomotor function. The contributions are summarized below in 7 thematic categories: (i) reviews and perspectives, (ii) animal studies, (iii) balance control, (iv) prostheses for locomotion, (v) myoelectric control, (vi) electroencephalography (EEG)-based systems for lower limb prosthesis control, and (vii) combined effects of spinal cord neuromodulation and exoskeleton gait training in paralyzed individuals.

REVIEWS AND PERSPECTIVES

Two review articles included in the Research Topic assess the current state of assistive devices for locomotion and their perspectives for development. The review by Tariq et al. discusses a number of key features of the EEG-based activity mode recognition and the potentials of EEG-based brain computer interfaces for enabling locomotion and improving its rehabilitation. The authors consider incorporation of neural technologies in various devices for locomotion, such as wearable lower-limb exoskeletons, orthoses, prostheses, wheelchairs, and assistive-robot devices. The performance of these devices could be improved by BCIs that recognize user intent and provide a communication channel. The EEG communication signals employed by these BCIs are sensorimotor rhythms, event-related potentials and visual evoked potentials. The authors develop a framework for such neural technologies and suggest using this framework for the development of the next generation of intent-based multifunctional controllers for individuals suffering from neuromotor disorders, trauma to nervous system, or limb amputation.

OPEN ACCESS

Edited and reviewed by:
Michela Chiappalone,
Italian Institute of Technology (IIT), Italy

***Correspondence:**
Yury Ivanenko
y.ivanenko@hsantalucia.it

Specialty section:
This article was submitted to Neuroprosthetics, a section of the journal Frontiers in Neuroscience

Received: *01 October 2021*
Accepted: *14 October 2021*
Published: *04 November 2021*

Citation:
Ivanenko Y, Ferris DP, Lee K, Sakurai Y, Beloozerova IN and Lebedev M (2021) Editorial: Neural Prostheses for Locomotion. Front. Neurosci. 15:788021. doi: 10.3389/fnins.2021.788021

In an opinion article, Bissolotti et al. discuss the limiting factors and evaluate some ethical questions regarding the domestic use of robotic exoskeletons for gait assistance in people affected by spinal cord injury (SCI). While the literature supports the effectiveness of different types of exoskeletons used in a clinical setting to treat such conditions as spasticity, balance impairment and abnormal blood pressure, multiple issues arise when such gait training systems are adapted for the home environments. These issues include high cost of the device and related inequality in the access to health care services, level of competence reached after training to use the device, risk of cardiovascular and metabolic diseases, high risk of osteoporosis of the paretic limbs, skin lesions, deep venous thrombosis and pelvic floor impairment. The article discusses the countermeasures to counteract the negative effects that could increase therapeutic efficacy and decrease inequality in the access to health care services and devices.

ANIMAL STUDIES

Several articles report testing neural technologies in animal models of locomotion. In a rabbit amputation model, Millevolte et al. tested and demonstrated the potential for the housing and engagement of a sieve electrode within the medullary canal of long bones as part of an osseointegrated neural prosthesis. Mottaghi et al. investigated cortico-basal ganglia beta oscillations in a rat model of unilateral Parkinson's Disease (PD) and analyzed the effects of deep brain stimulation. They concluded that this model accurately represents many of the motor and electrophysiological symptoms of PD, which makes it a useful tool for pre-clinical testing of new treatments. Park et al. developed a prototype of a powered transtibial prosthesis for the use in a feline model of prosthetic gait. In this prosthesis, the linear actuator operates the prosthetic ankle joint with the control signals that emulate myoelectric activity of muscles; there is a close match between the locomotor patterns produced by the prosthesis and by cats during level walking.

BALANCE CONTROL

Three articles address the issue of improving balance control. Buettner et al. describe a virtual balancing apparatus that can modify gravity (e.g., for patients who are unable to balance their full body weight), damping, inertia. The apparatus can be also used to examine the effects of support surface perturbations. It may be well-suited to simulate conditions which could otherwise only be realized in space experiments and to examine the potential benefit for patients of virtual balance training. Sozzi et al. report the effects and the time-course of stabilization produced by a haptic cue provided by a walking cane. They argue that this type of haptic information has many of the features of the direct fingertip contact. They also suggest that the processing time of haptic input from a walking aid should be taken into consideration when designing prostheses for locomotion. Furthermore, Sozzi et al. assess balance improvement in subjects with low vision by adding the haptic input from a cane or fingertip. The authors discuss the ways visual and haptic information could be integrated in in the devices for balance training.

PROSTHESES FOR LOCOMOTION

Three articles analyze available evidence for using robotic devices for the benefit of patients with gait impairments. Malcolm et al. use a biomimetic approach to design prostheses with bi-articular actuation components. In their study, the effect of a bi-articular and spring configuration were tested that mimicked the m. gastrocnemius action; this design was compared to the mono-articular configuration and configuration without a spring. The authors discuss the specific effects of different exoskeleton configurations on metabolic cost and muscle activation that could be useful for providing customized assistance for specific gait impairments. Jayaraman et al. describe the impact of using powered knee-ankle prostheses in two transfemoral amputees. The participants gained the ability to walk with gait kinematics similar to normal gait patterns observed in a healthy limb. These results indicate that powered prosthetic components have a considerable potential to provide safe and efficient gait for individuals with above-the-knee amputation. Finally, van Dijsseldonk et al. report a framework for measuring the effects of training with the Rewalk exoskeleton on the ability to perform basic and advanced skills in people with complete spinal cord injury.

MYOELECTRIC CONTROL

Myoelectric control of neuroprostheses for walking is a prominent theme in this Research Topic. This is a biologically inspired approach, where electromyography (EMG) feedback from lower-limb muscles assists walking in an exoskeleton or contributes to hybrid rehabilitation systems that combine functional electrical stimulation (FES) and a robotic exoskeleton.

Grazi et al. report a novel assistive control strategy for a robotic hip exoskeleton that relies on the use of the gastrocnemius medialis EMG signal instead of a hip flexor muscle, to control the hip flexion torque and improve the reliability of the control system. Since the presence of moderate to severe spasticity can significantly impair gait kinematics and prevent such individuals from walking in an exoskeleton, Ekelem and Goldfarb applied peroneal stimulation (timed with the exoskeleton swing phase) to acutely suppress extensor spasticity in SCI subjects through the recruitment of the flexion withdrawal reflex. While the common peroneal stimulation had only acute effects (it did not have a significant effect on modified Ashworth scores), it suppressed extensor tone, significantly aided flexion in the hip and ankle joints and enabled improved exoskeletal walking for persons with severe spasticity.

Zhang et al. propose a novel cooperative control strategy, which could realize arbitrary distribution of torque generated by functional electrical stimulation and exoskeleton. Two muscle groups (quadriceps and hamstrings) were stimulated to generate active torque for knee joint in synchrony with torque

compensation from the exoskeleton. Experimental evaluation of the hybrid FES-exoskeleton system was conducted in five healthy subjects and four paraplegic patients. The system enabled cooperative control of torque distribution, trajectory tracking, and phase synchronization. Furthermore, Alibeji et al. describe a hybrid neuroprosthesis for walking that combines FES with a powered lower limb exoskeleton. This system has an electrical actuator at the hip and knee joints. The control framework mimics muscle synergy, where FES of the hamstrings and quadriceps muscle group of each leg restores walking in patients with paraplegia. The system was tested in an able-bodied subject and a patient with an incomplete SCI. Another article on myoelectric control (Karunakaran et al.) reports the orthotic and therapeutic effects due to continuous use of a foot drop stimulator (using FES to stimulate the peroneal nerve) in children with foot drop and hemiplegia secondary to brain injury. The authors report that this treatment improves spatial gait asymmetry and increases dorsiflexion and toe displacement during swing. These are a potentially long-lasting effects.

Several articles evaluate the efficiency of the Hybrid Assistive Limb (HAL) exoskeleton, a unique device that performs real-time collection of bioelectric signals from the patient to support and enhance voluntary gait. HAL exoskeletons are equipped with surface EMG electrodes that percutaneously detect minimal bioelectric signals generated by the patient's muscles (hip and knee flexors and extensors). Additionally, floor reaction force signals could be detected caused by patient's intended weight shifts. Sczesny-Kaiser et al. assess the effects and safety of body-weight supported treadmill training with the use of the HAL exoskeleton in patients with limb-girdle muscular dystrophy. All patients involved in this study benefitted from the training. Sczesny-Kaiser et al. report a crossover clinical trial comparing conventional physiotherapy and HAL supported treadmill therapy in chronic stroke patients with hemiparesis. The authors demonstrate the efficiency of individualized therapy based on this approach. Puentes et al. report the effects of HAL therapy in myelopathy (caused by ossification of the posterior longitudinal ligament) patients by performing the principal component analysis of the kinematic data. In this study, HAL therapy improved walking and gait coordination in patients by reshaping their gait pattern. Furthermore, Puentes et al. report an improvement in the intersegmental coordination (assessed by planar covariation of elevation angles) for the paretic and non-paretic side after early HAL intervention in hemiparetic stroke patients. Tan et al. show that muscle synergy analysis can be used as a tool to quantify the change and improvements in neuromuscular coordination of lateral symmetry during gait training in stroke patients with the help of the HAL exoskeleton. Finally, Shimizu et al. describe a case of voluntary ambulation triggered by upper limb activity using the HAL exoskeleton in patients with complete paraplegia after spinal cord injury. The HAL electrodes for the hip and knee flexion-extension were placed on the anterior and posterior sides of the upper limbs contralaterally corresponding to each of the lower limbs. The results suggest that an upper-limb-triggered HAL ambulation is a feasible option for rehabilitation of patients with complete quadri/paraplegia caused by chronic SCI.

ELECTROENCEPHALOGRAPHY (EEG)-BASED SYSTEMS FOR CONTROLLING LOWER LIMB PROSTHESES

A group of articles report and analyze the usage of EEG signals for the control of prostheses for locomotion. Murphy et al. assess the benefits of using an EEG-based BCI for lower-limb prostheses. The feasibility of such systems is supported by the implementation of a reliable knee-locking switch based on a EEG rhythm-feedback training for swing phase during walking and for sitting down in a transfemoral amputee. Ortiz et al. describe a new tool based on the Stockwell transform for the analysis of the EEG signals during gait cycle. Extraction of instantaneous EEG characteristics with this method was successfully tested in healthy individuals and patients with lower limb disabilities. Mejia Tobar et al. examine the classification of ankle flexion and extension movements from cortical current sources estimated by a hierarchical variational Bayesian method they use EEG and fMRI recordings. The presented method is also applicable to real-time BCIs and has the potential to identify neural patterns to control exoskeletons, prostheses and functional electrical stimulators. Wei et al. investigate the feasibility of gait phase recognition based on EEG combined with EMG using the corticomuscular interaction analysis and the time–frequency cross mutual information method. They report good recognition for three different walking speeds and discuss a theoretical basis for gait recognition based on EEG and EMG recordings during patient rehabilitation with lower limb exoskeletons.

COMBINED EFFECTS OF SPINAL CORD NEUROMODULATION AND EXOSKELETON WALK TRAINING IN PARALYZED INDIVIDUALS

Finally, a promising approach is based on neuromodulation of the spinal circuitry during walking in the exoskeleton. This method is particularly beneficial for gait rehabilitation after SCI. This approach makes use of the activation of central pattern generation circuits that largely depend on the presence of a sustained excitatory drive (as it can be elicited by non-invasive transcutaneous electrical spinal cord stimulation either without or with specific pharmacological neuromodulation) combined with the over-ground step training in an exoskeleton. In particular, Gad et al. in a case study report that spinal cord stimulation combined with pharmacological treatment enhanced the level of effort and improved the coordination patterns of the lower limb muscles, resulting in a continuous stepping motion in the exoskeleton along with the improvements in autonomic functions including cardiovascular and thermoregulation. In a large cohort of SCI patients, Shapkova et al. show that percutaneous electrical stimulation of the lumbar enlargement and exoskeleton-induced walking work together well to assist walking in SCI patients. Particularly, anti-spastic stimulation at high frequency enabled individuals with severe spasticity

to be able to use the exoskeleton for walking. Overall, this study showed that the 2-week intensive synergistic effect of exoskeleton-assisted walking and the simultaneous spinal cord stimulation improve gait and neurological signs in chronic SCI, including complete paralysis.

Taken together, this Research Topic demonstrates the growth of interest to using neural prostheses for the restoration of locomotion in patients with neurological disorders that impair gait.

AUTHOR CONTRIBUTIONS

All authors listed have made a substantial, direct and intellectual contribution to the work, and approved it for publication.

FUNDING

This work was supported by the Russian Science foundation Grant 21-75-30024, USA National Science Foundation (NSF) Grant # 1912557, and the Italian Ministry of Health (Ricerca Corrente, IRCCS Fondazione Santa Lucia).

ACKNOWLEDGMENTS

We would like to thank all authors and reviewers for their contributions to this Research Topic. The editors also thank Frontiers team for professional help with this Research Topic.

Conflict of Interest: The authors declare that the research was conducted in the absence of any commercial or financial relationships that could be construed as a potential conflict of interest.

Publisher's Note: All claims expressed in this article are solely those of the authors and do not necessarily represent those of their affiliated organizations, or those of the publisher, the editors and the reviewers. Any product that may be evaluated in this article, or claim that may be made by its manufacturer, is not guaranteed or endorsed by the publisher.

frontiers in Neuroscience

CASE REPORT
published: 08 June 2017
doi: 10.3389/fnins.2017.00333

Weight Bearing Over-ground Stepping in an Exoskeleton with Non-invasive Spinal Cord Neuromodulation after Motor Complete Paraplegia

Parag Gad[1], *Yury Gerasimenko*[1,2], *Sharon Zdunowski*[1], *Amanda Turner*[1], *Dimitry Sayenko*[1], *Daniel C. Lu*[3,4] *and V. Reggie Edgerton*[1,3,4,5,6]*

[1] Department of Integrative Biology and Physiology, University of California, Los Angeles, Los Angeles, CA, United States, [2] Pavlov Institute of Physiology, St. Petersburg, Russia, [3] Department of Neurosurgery, University of California, Los Angeles, Los Angeles, CA, United States, [4] Brain Research Institute, University of California, Los Angeles, Los Angeles, CA, United States, [5] Department of Neurobiology, University of California, Los Angeles, Los Angeles, CA, United States, [6] Institut Guttmann, Hospital de Neurorehabilitació, Institut Universitari adscrit a la Universitat Autònoma de Barcelona, Barcelona, Spain

OPEN ACCESS

Edited by:
Mikhail Lebedev,
Duke University, United States

Reviewed by:
Wiktor Sieklicki,
Gdańsk University of Technology, Poland
Giuseppe Carbone,
University of Cassino, Italy
Yury Ivanenko,
Fondazione Santa Lucia (IRCCS), Italy

***Correspondence:**
V. Reggie Edgerton
vre@ucla.edu

Specialty section:
This article was submitted to Neuroprosthetics, a section of the journal Frontiers in Neuroscience

Received: *20 March 2017*
Accepted: *29 May 2017*
Published: *08 June 2017*

Citation:
Gad P, Gerasimenko Y, Zdunowski S, Turner A, Sayenko D, Lu DC and Edgerton VR (2017) Weight Bearing Over-ground Stepping in an Exoskeleton with Non-invasive Spinal Cord Neuromodulation after Motor Complete Paraplegia. Front. Neurosci. 11:333. doi: 10.3389/fnins.2017.00333

We asked whether coordinated voluntary movement of the lower limbs could be regained in an individual having been completely paralyzed (>4 year) and completely absent of vision (>15 year) using two novel strategies—transcutaneous electrical spinal cord stimulation at selected sites over the spine as well as pharmacological neuromodulation by buspirone. We also asked whether these neuromodulatory strategies could facilitate stepping assisted by an exoskeleton (EKSO, EKSO Bionics, CA) that is designed so that the subject can voluntarily complement the work being performed by the exoskeleton. We found that spinal cord stimulation and drug enhanced the level of effort that the subject could generate while stepping in the exoskeleton. In addition, stimulation improved the coordination patterns of the lower limb muscles resulting in a more continuous, smooth stepping motion in the exoskeleton along with changes in autonomic functions including cardiovascular and thermoregulation. Based on these data from this case study it appears that there is considerable potential for positive synergistic effects after complete paralysis by combining the over-ground step training in an exoskeleton, combined with transcutaneous electrical spinal cord stimulation either without or with pharmacological modulation.

Keywords: spinal cord injury, exoskeleton, spinal cord stimulation, non-invasive neuromodulation, neural prostheses for locomotion, locomotion rehabilitation

INTRODUCTION

The mammalian spinal cord is capable of generating locomotor output independent of any input from the brain using locomotor related neuronal circuitries. After complete mid-thoracic transection of the spinal cord, paralyzed cats can stand, and step when appropriate proprioceptive input is provided to the lumbosacral networks that contain the pattern generator circuitry (Rossignol et al., 2007; Rossignol and Frigon, 2011). The animals can learn to fully support their

hindquarters, and to step at a range of speeds and loads (de Leon et al., 1999a,b). Adult paralyzed rats can relearn to step with a combination of neuromodulatory strategies including locomotor training, pharmacological intervention, and epidural stimulation (Courtine et al., 2009; Musienko et al., 2012; Gad et al., 2013, 2015). Paralyzed rats can step forward, sideways, backwards as well as climb stairs voluntarily (Shah et al., 2012). Recently we have suggested a novel neuromodulation strategy of motor control using non-invasive transcutaneous spinal cord stimulation combined with administering a monoaminergic agent. We have demonstrated that transcutaneous spinal cord stimulation at lumbosacral segments can induce coordinated stepping like movements in paralyzed individuals when their lower limbs are suspended in a gravity neutral device (Gorodnichev et al., 2012; Gerasimenko Y. et al., 2015). Also this strategy has enabled voluntary control of stepping-like motions in 5/5 individuals with chronic complete motor paralysis (Gerasimenko Y. P. et al., 2015).

Here, we use this non-invasive stimulation technology, painless cutaneous enabling motor control (pcEmc) to determine the feasibility of re-establishing functional brain spinal cord connectivity that enables a subject with complete motor paralysis to move upon volitional intent and perform work that can assist a robotic exoskeletal device in generating over-ground stepping.

The use of robotic-like devices to improve locomotion in patients with paralysis has been tested with mixed results (Ferris et al., 2005; Esquenazi et al., 2012; Strausser et al., 2012; McDaid et al., 2013). In experimental studies in animals, we developed an assist-as-needed (AAN) robotic treadmill device with arms to move the legs in a step-like trajectory so that the mice could be trained with an allowable variation in window diameter and temporal pattern controlled with a graded force field (Cai et al., 2006). Several Exoskeleton devices have been developed to allow human subjects to step over-ground with varying efforts from the subject including some that are approved by FDA such as the ReWalk, Indego, EKSO Bionics and others that are still experimental (Esquenazi et al., 2012; del-Ama et al., 2012). Some of the experimental units include a brain computer interface (Lebedev and Nicolelis, 2011; Onose et al., 2016) or muscle stimulators (del-Ama et al., 2014), however, each of these units bypass the automaticity that is intrinsic to the spinal networks and do not allow voluntary effort from the subjects and the inter-step variability to allow the spinal networks to relearn stepping (Ziegler et al., 2010).

EKSO Bionics is a battery powered wearable bionic suit with motors at the hips and knees which enables individuals with lower extremity motor impairment to stand and voluntarily step over-ground with weight-bearing and alternating gait. The EKSO GT robotic exoskeleton is a class I medical device (United States FDA) which provides functional rehabilitation in the form of over-ground weight bearing stepping in subjects with spinal cord injuries (complete and incomplete) and stroke. The device works in two modes namely the "max assist" and "variable assist." In max assist, the pilot (patient) has to initiate a step by unweighting one leg which triggers the motors on the EKSO to move the entire limb in a step like trajectory. In this mode, 100% assistance is offered during the entire step cycle. However, the variable assist mode actively allows the subject to voluntarily assist, even when the subject exerts minimal voluntary influence on the robot.

Thus, the objective of the study was to test the combinatorial effects of non-invasive electrical spinal cord stimulation, pharmacological neuromodulation with a robotic device that allows one to voluntarily assist the robot during over-ground stepping. We hypothesized that tonic pcEmc can modulate the paralyzed spinal networks so that the subject can voluntarily engage these networks to assist stepping, as observed in spinal mice, when training in the EKSO. The present results demonstrate that locomotor spinal networks can be neuromodulated with pcEmc to physiological states, similar to that observed in paralyzed mice with epidural stimulation that enables sensory input to serve as a source of neural control to generate stepping. Based on our previous observation with epidural stimulation we also hypothesized that the plasticity occurring in the spinal cord would re-enable improved voluntary control of lower limbs other than during stepping, as well as cardio-vascular function.

METHODS

Clinical Status

The subject was an adult between the age of 35 and 40 years at the time of the study. The subject was diagnosed with a detached retina at the age between 20 and 25 years leading to complete blindness. In 2010 the subject fell from a 2nd story balcony hitting a concrete floor causing a spinal cord injury at T9 and L1 vertebral levels. The subject was initially (immediately after the injury), 24 months post injury and immediately before the study was initiated, was diagnosed as American Spinal Injury Association Impairment Scale (AIS) A (no sensation or movement below the level of injury) motor complete injury and had no motor function of trunk or leg muscles and used a suprapubic catheter to enable bladder emptying. Despite being diagnosed as AIS A, the spinal locomotor circuitry in the lumbosacral spinal cord was active and responsive to stimulation (**Figure 1A**) that was varied based on the site of stimulation with the generation of late responses (latency $>$ 100 ms) and increased muscle activity while voluntarily attempting dorsiflexion or plantarflexion (**Figures 1B,C**). The subject had been training (inconsistently) with the EKSO Bionics suit for over 24 months and had completed ∼180,000 steps prior to the experiment. The subject used crutches while stepping in the EKSO during the entire period of the study. The subject signed an informed consent form which was approved by the Institutional Review Board (IRB) at the University of California, Los Angeles (UCLA).

Experimental Procedures

Training: Walking in the EKSO Bionics

The study was divided into four phases, baseline, stim only, drug only, and drug+stim (1 week each). EMG and EKSO robot data were collected at the end of each phase of the study. Further, self-scored data from the subject were collected everyday (see below for details).

To establish and define a functional baseline the subject walked in the EKSO for a period of 4 weeks without pcEmc

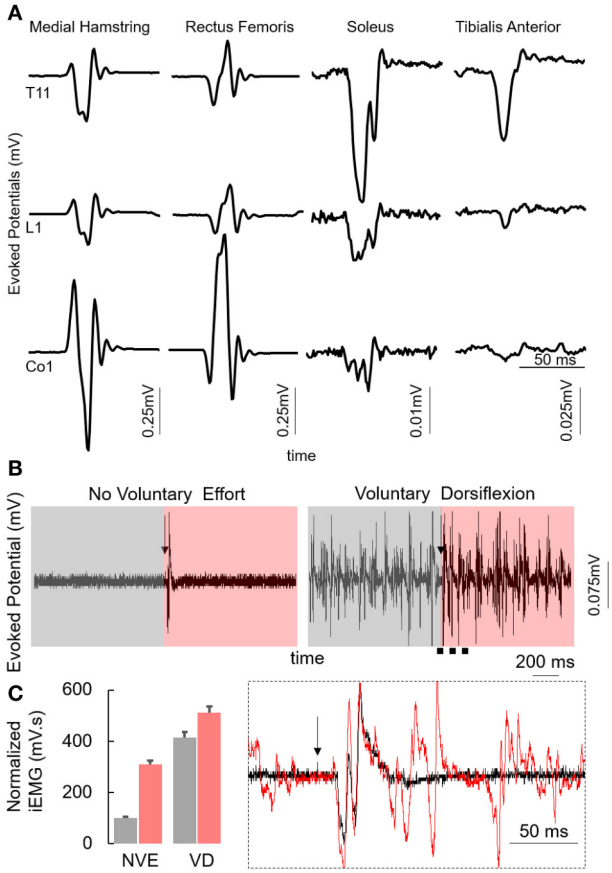

FIGURE 1 | (A) Average motor evoked potentials ($n = 5$) at 200 mA while stimulating the T11, L1, and Co1 vertebral levels with the subject in supine position from the multiple lower limb muscles. **(B)** Average motor evoked potentials ($n = 3$) from the MG muscles with the subject in supine position at T11 (110 mA) vertebral level during control conditions (No Voluntary Effort, NVE) or with the subjects voluntarily attempting to maximally dorsiflex (Voluntary Dorsiflexion, VD). Box inset: zoomed in view during NVE and voluntary dorsiflexion 1 s before the stim pulse (gray) and 1 s after the stim pulse (red). Note the black arrow marks the stimulation pulse. **(C)** Normalized mean+SD integrated EMG for the duration highlighted in **(B)**. Inset represents the zoomed in view of the region marked by black dotted line. Each of these data were collected at PreStim time point.

in variable assist mode for 1 h/day, 5 days/week. Each 1-h session was divided into blocks of 15 min with 5 min break in between. At the end of the 4-week period, EKSO training with neuromodulation was initiated. Neuromodulation consisted of 1 week of pcEmc only followed by 1 week of pharmacological enabling motor control (fEmc) followed by 1 week of pcEmc and fEmc. Each day of training consisted of 5–10 min warm up block, followed by three 20 min blocks with or without pcEmc based on the phase of the study. Blood pressure and heart rate readings were recorded at the end of each block.

Neuromodulation Parameters

Non-invasive spinal cord stimulation at T11 and/or Co1 was administered using a specific stimulation waveform that minimizes discomfort, even when used at energies required to transcutaneously reach the spinal cord (Gerasimenko Y. P. et al., 2015). pcEmc was delivered using a 2.5 cm diameter electrode (Lead Lok, Sandpoint, United States) placed midline on the skin between spinous processes T11–T12 (simply T11) or over Co1 as a cathode and two 5.0 × 10.2 cm^2 rectangular plates made of conductive plastic (Ambu, Ballerup, Germany) placed symmetrically on the skin over the iliac crests as anodes. pcEmc was delivered at Thorasic T11 – 30 Hz and/or Coccyx bone segment (Co1) – 5 Hz, the intensities of stimulation were determined based on optimum efficacy and feedback from the subject. fEmc was administered with 10 mg tablets twice a day (prescribed by the MD on the study).

Testing

Baseline (pre-train) data were collected after 4 weeks of training. An external pressure sensor (FSR 1 sq. inch) was attached to the right heel at the same site as the internal pressure sensor on the EKSO. This FSR pressure sensor was connected to the EMG system (Delsys System) allowing us to synchronize the data generated by the EKSO and the EMG system. At the end of each phase, ability to step in the EKSO was tested both with and without pcEmc. Data were synchronized, band pass filtered and analyzed using custom scripts written in Matlab (Mathworks). 30 consecutive steps when the subject was stepping was chosen to perform the data analysis including calculating mean assistance data from the EKSO, mean integrated EMG from proximal, and distal muscles. Similarly, ability to flex specific joints was tested at the end of each phase with and without pcEmc.

EKSO Bionics

The EKSO device can work in two modes namely the "max assist" and "variable assist." In max assist, the pilot (patient) has to initiate a step by unweighting one leg which triggers the motors on the EKSO to move the entire limb in a step like trajectory. In this mode, 100% assistance is offered during the entire step cycle. However, in the variable assist mode actively allows the subject to voluntarily assist, even when the subject voluntarily exerts minimal influence on the robot.

During training, the EKSO device was operated in variable assist mode enabling the subject to generate voluntary effort to move forward and maintain a predetermined trajectory. During the course of each step, if the subject's voluntary effort was not sufficient to maintain the trajectory, the onboard computer provided the required assistance to complete the step as planned. The EKSO device contained multiple position sensors (hip, knee, torso) that prevented the subject from falling and recorded 74 parameters (sampled at 500 Hz) including the assistance provided and current drawn by the motors which are directly related to the subjects' efforts to enable weight bearing stepping.

Kinematics and EMG Recordings

Bipolar surface electrodes were placed bilaterally on the soleus, medial gastrocnemius (MG), tibialis anterior (TA), medial hamstring (HM), and vastus lateralis (VL) muscles as described previously (Gerasimenko Y. P. et al., 2015). Electromyography (EMG) signals were amplified differentially (bandwidth of 10

Hz to 10 kHz) and acquired at 10 KHz using a 16-channel hard-wired A/D board and customized LabVIEW software (National Instruments, Austin, TX) acquisition program. To minimize artifacts from the stimulation, the EMG signals were passed through a band-pass filter using a six-order band-pass Butterworth filter (30–1,000 Hz). The filtered EMG signals were analyzed off-line to compute the amplitude, duration, and timing of individual bursts. Angular displacements at hip and knee joints in both legs were recorded with goniometers.

Self-Scoring by Subject

The subject self-scored on various parameters including (1) muscle tone during stepping, (2) sensation during stepping, (3) sensation in legs every morning, (4) body perspiration during stepping, (5) hand to leg coordination: This scores the perception of the subject's ability to move the upper and lower extremity as a synchronous in a smooth and synchronous manner rather than indiscreet interrupted components.

RESULTS

Active vs. Passive Stepping

Stepping passively (in variable assist mode) or in max assist in the EKSO resulted in minimal activation of lower extremity muscles and autonomic function (perspiration etc) over the course of the entire period of testing each day as well as weeks of training. Active voluntary effort during stepping resulted in increased EMG activity especially in proximal muscles, heart rate and blood pressure along with decrease in assistance provided by the EKSO. The decreased assistance was accompanied by increased EMG activity in proximal and distal muscles (**Figure 2**). Further, in the presence of stimulation, active stepping resulted in less assistance and higher levels of EMG activity (**Figure 3A**). The changing mean assistance, motor current and activation patterns of muscles varied with the site of stimulation (**Figures 3B,C**). However, the most effective pattern of stimulation (least mean assistance and maximum EMG activity) was observed during a combination of T11 and Co1 stimulation (**Figures 3D,E**). fEmc alone, on the other hand, required a higher level of assistance by the EKSO compared to pcEmc and voluntary effort. A combination of pcEmc and fEmc resulted in lowest levels of robotic assistance (**Figure 3C**). The mean step cycle duration in the presence of stim only reduced from 2.13 s (baseline) to 2.03 s (stim only). However, in the presence of drug the mean step cycle increased to 2.07 s and decreased to 2.00 s with stim+drug. The profile for assistance provided during the course of an average step cycle resulted in a unique pattern of activation of the EKSO compared to when the subject exerted a voluntary effort. These patterns of assistance were consistent with the mean assistance provided. In summary, the absence of pcEmc required higher levels of assistance by the EKSO compared to presence of pcEmc.

Voluntary Control While in Supine

At the end of each test session, we tested the subject's ability to voluntarily flex his knee with and without pcEmc while lying in a supine position. Without pcEmc, the subject was not capable of flexing his knee but bursting activity was sometimes observed in distal (TA, soleus, and MG) but not in the proximal muscles (VL, RF, and ST). However, in the presence of pcEmc at T11 (30 Hz) and Co1 (5 Hz), the subject was capable of flexing his knee on command (**Figure 4**) with an alternating bursting pattern corresponding to flexion and extension of proximal muscles with little activity in distal muscles. In the presence of fEmc only, however, the subject was not capable of successfully flexing his knee but generated robust bursting pattern in proximal muscle with little activity in the distal muscles. Further, a combination of pcEmc and fEmc resulted in robust bursting pattern with little change in knee angle.

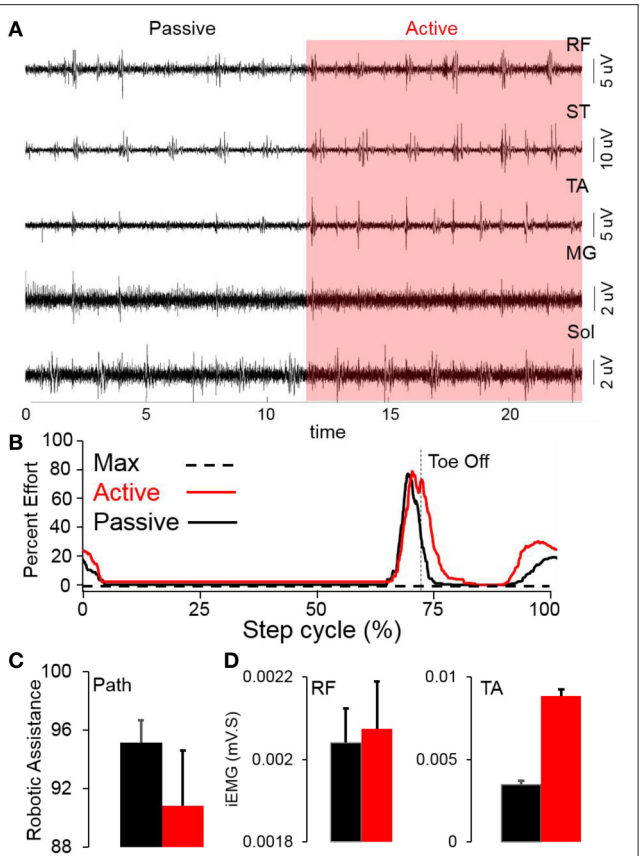

FIGURE 2 | (A) Raw EMG from multiple leg muscles while stepping in the EKSO without (passive) and with (red highlight) voluntary effort (active) **(B)** Average percent effort ($n = 30$ steps) during either active or passive stepping during a normalized step cycle. **(C)** Mean+SD ($n = 30$ steps) robotic work during stepping in the EKSO (%). **(D)** Mean+SD ($n = 30$ steps) integrated EMG in rectus femoris (RF) and tibialis anterior (TA) while stepping in the EKSO in active (red) or passive (black) modes.

The changes in stepping patterns were accompanied by changes in cardiovascular function (recorded via BP and HR during every training session). The average systolic BP and HR during a single session increased with each phase and was maximum during the combination of pcEmc and fEmc (**Figure 5A**). Along with changes in EMG patterns and robotic assistance, the subject self-reported changes in muscle tone, sensation, perspiration both during stepping as well as during the rest of the day and hand to leg coordination during

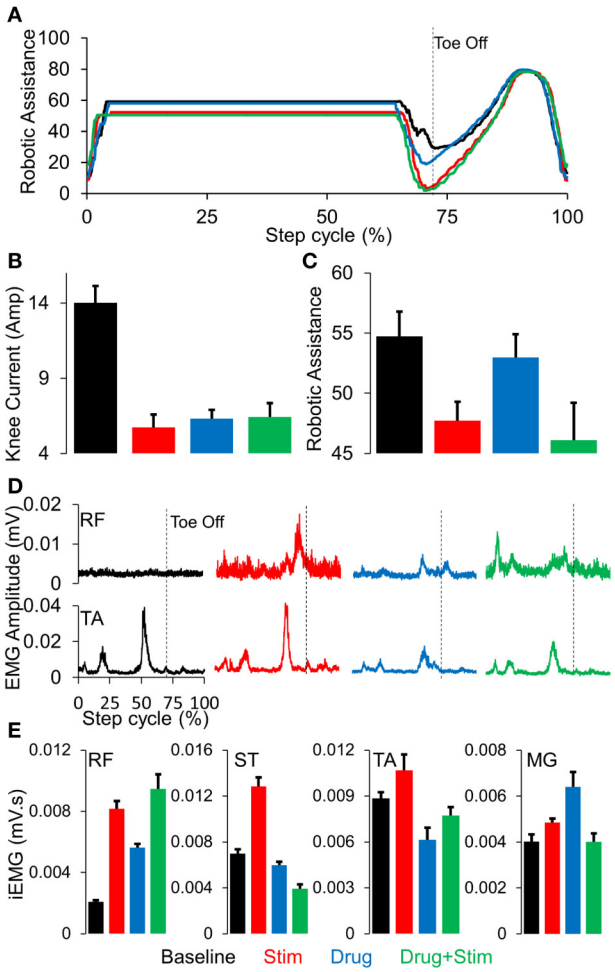

FIGURE 3 | (A) Average robotic assistance ($n = 30$ steps) during a complete normalized step cycle during baseline (black), stim (red), drug (blue), and stim+drug (green) phases while stepping in active mode. **(B)** mean+SD ($n = 30$ steps) knee current in the conditions mentioned above. **(C)** mean+SD ($n = 30$ steps) robotic assistance in the conditions mentioned above. **(D)** Average ($n = 30$ steps) linear envelope for the RF and TA muscles while stepping in the EKSO, **(E)** Mean+SD ($n = 30$ steps) integrated EMG while stepping in the EKSO in active mode for the conditions mentioned above. RF, Rectus Femoris; ST, Semitendinosus; TA, Tibialis Anterior; MG, Medial Gastrocnemius.

stepping. Each of the above variables were higher during either pcEmc or pcEmc+fEmc phases as compared to fEmc only and lowest during baseline (**Figure 5B**). Further, the trends in the self-reported scores followed the same patterns as the robotic assistance demonstrating the integrated nature of the subject's efforts and the assistance offered by the robot.

DISCUSSION

Using completely non-invasive interventions, we have demonstrated the ability to neuromodulate the lumbosacral spinal cord to enable function of locomotor networks of a human subject that has been completely paralyzed for more than 4 years. This is consistent with our previous findings with five subjects (Gerasimenko Y. P. et al., 2015). The interventions tested included a combination of non-invasive spinal cord stimulation, pharmacological activation via a monoaminergic agonist (Buspirone), and over-ground weight bearing stepping in an exoskeleton. It has been shown that activation of the lumbar enlargement via transcutaneous electrical stimulation facilitates passive locomotion and robust patterns of EMG activity in lower extremity muscles in SCI patients (Minassian et al., 2007; Hofstoetter et al., 2013, 2015). Recently we have shown that transcutaneous spinal cord neuromodulation (pcEmc) can be used to both initiate oscillatory movement and enable voluntary oscillatory movements in motor complete subjects. These oscillatory movements were further amplified with a combination of pcEmc and fEmc over the course of 18 weeks (Gerasimenko Y. P. et al., 2015).

Stepping in the EKSO Bionics device provides a unique opportunity for subjects with spinal cord injuries to experience over-ground weight bearing stepping (Strausser et al., 2012). However, a unique and perhaps essential advantage of the EKSO Bionics device is the ability to voluntarily engage the lower limbs while stepping, by engaging both supraspinal and spinal networks in a synergistic manner. The EKSO Bionics is capable of functioning in two modes, the maximum assistance mode in which the subject is expected to initiate a step cycle (by shifting his weight to the contralateral side) with the EKSO completing the step cycle with the parameters provided, i.e. step cycle, toe height, swing time etc. while maintaining the decided trajectory. In contrast, while stepping with the variable assistance mode, once the subject initiates a step, the EKSO only provides assistance during the swing phase based on the amount of effort the pilot applies. However, if and when various joints of the active limb falls out of the window of error that is allowed, assistance is provided to ensure the trajectory is maintained and the swing phase is completed as planned. This "assist as needed" paradigm allows the subject to engage the lumbosacral spinal networks to control one limb at a time to complete a swing phase while the contralateral limb goes through a passive stance phase. In addition, pcEmc can modulate the excitability of the spinal neural networks to a state of higher state of excitability that enables re-connectivity of cortical networks to spinal networks projecting to the appropriate motor pools with a relatively high level agonist-antagonistic coordination that supports the generation of standing and stepping.

We have reported similar changes in modulating the physiological state of the lumbosacral spinal cord in four out of the first four subjects diagnosed as AIS A, tested with epidural implants over the L1-S1 spinal levels within weeks of implantation (Harkema et al., 2011; Angeli et al., 2014). The results show continuous recovery in voluntary motor control as a result of daily motor training, but only in the presence of epidural stimulation. In a study of 564 human cadavers with SCI, Kakulas (1999) reported that many of the cadavers had axons within the spinal cord white matter remaining across lesion site even though they were clinically assessed as

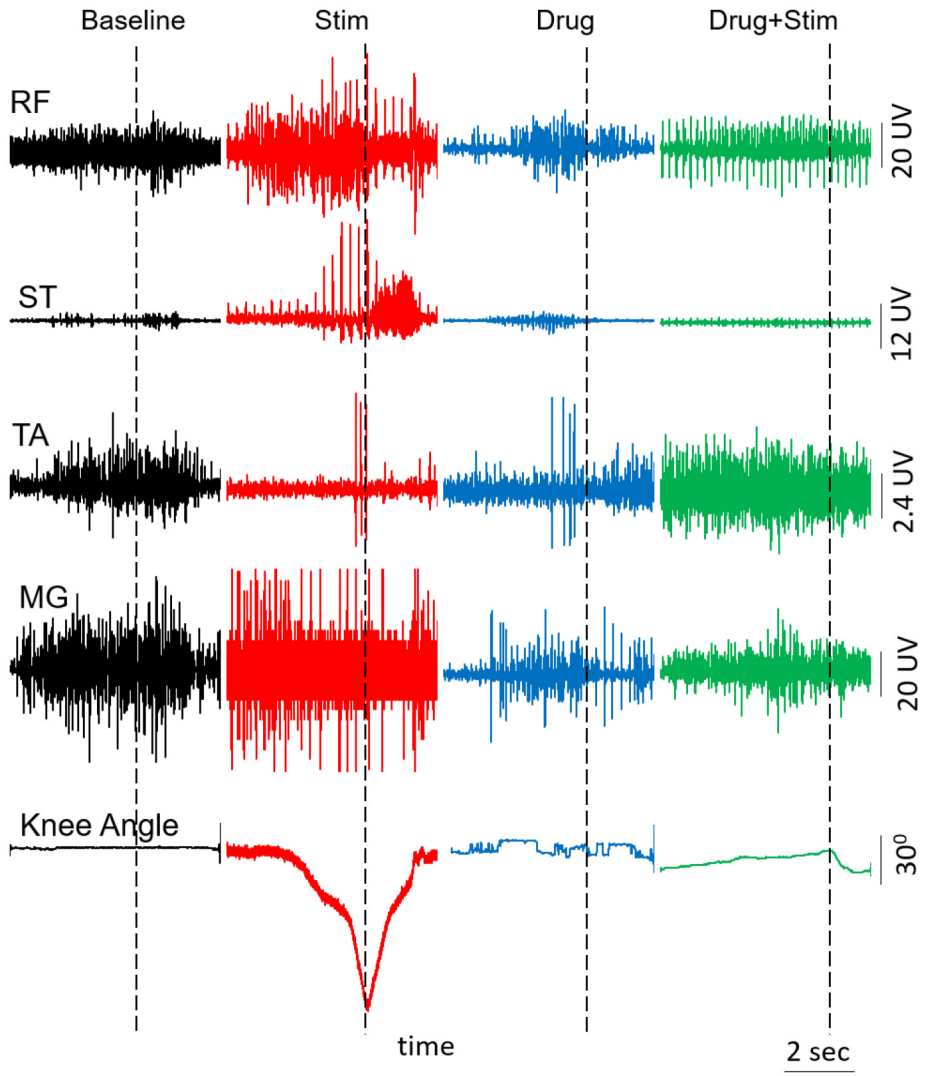

FIGURE 4 | EMG activity and knee angle excursion when attempting voluntary knee flexion when the subject is in a supine position with and without Stim and/or drug. RF, Rectus Femoris; ST, Semitendinosus; TA, Tibialis Anterior; MG, Medial Gastrocnemius.

motor complete. The changes in both locomotor and autonomic systems that we observed in this study provides further evidence that spinal networks of individuals clinically diagnosed at AIS A can be physiologically neuromodulated to a higher and more functional state even with non-invasive neuromodulatory procedures.

Three important aspects of over-ground training in the exoskeleton vs. locomotor training with a body weight support come to light. Firstly, while stepping in an exoskeleton, only one person is needed to spot the subject to avoid falls as compared to 3–4 trainers while stepping on a treadmill. Secondly, while walking in the EKSO Bionics device, the subjects are capable of using their upper bodies, trunk muscles, arms to further enhance their locomotor abilities. Thirdly, over-ground stepping in the EKSO challenges the system to a higher degree compared to stepping with a body-weight support system since the patient has to actively balance the upper body and generate coordinated movements between the arms, trunk and lower limbs. Obviously, the unique feature of the EKSO is that it generates overground stepping kinematics that can be influenced by the subject's effort. The overhead support allowing overground mobility has no means for assisting the limb kinematics. The overhead support devices on a treadmill either imposes uniform kinematics which is markedly non-physiological or relies on multiple skilled therapists. It should be noted that multiple robotic suits are being developed for overground stepping (experimental and FDA approved) with unique sets of built in features (Lebedev and Nicolelis, 2011; del-Ama et al., 2012; Esquenazi et al., 2012; McDaid et al., 2013). Comparing the various features of the different robotic exoskeletons is an important question but that is beyond the scope of the current report.

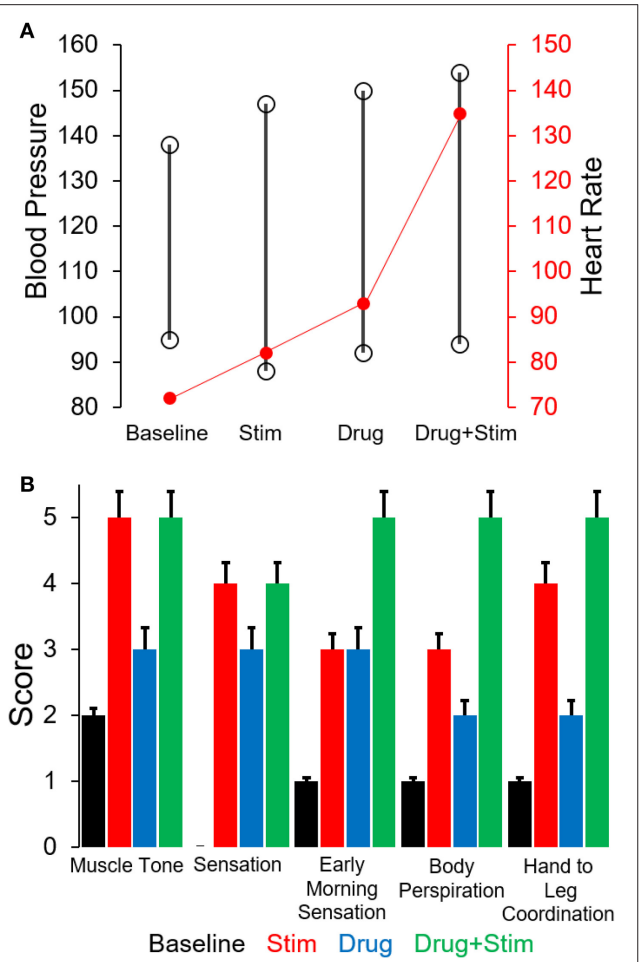

FIGURE 5 | (A) Average cardiovascular function (Blood pressure and Heart rate) during the different phases of training. **(B)** Average score (self-scored by subject, 0 = low, 5 = high) on various parameters during the course of various phases of training.

The present data also demonstrates that the interneuronal spinal networks that normally generates a largely random-stochastic bursting pattern of excitation of the motoneurons can be neuromodulated using a non-invasive mode of stimulation as can occur with epidural stimulation after complete paralysis (Angeli et al., 2014). Convergence of somatosensory and descending motor inputs in combination with spinal cord stimulation and pharmacological activation of interneurons, and perhaps to some degree motoneurons, results in the re-emergence of not only some level of "automated" locomotor movements but also those that can be under more voluntary control (Gerasimenko Y. P. et al., 2015). Once the functionally non-responsive neural networks become electrically responsive, it appears that they can be transformed to a physiological state which is sufficient for them to be re-engaged and even be controlled with the presentation of proprioceptive and cutaneous ensembles of sensory input normally linked to a motor task. It is this new dynamic physiological state which enables it to learn with training.

A more general point to be derived from the present data, when combined with other similar observations (Rejc et al., 2015), questions the validity of several dogmatic concepts, namely, (1) there is limited plasticity after more than a year after a spinal-complete lesion, thus, precluding significant levels of functional recover and (2) with a clinically complete spinal lesion there are no viable cellular components intrinsic to the lesion that can provide a means for supraspinal-spinal re-connectivity. These results in conjunction with our recent report of five subjects with motor complete spinal injuries greater than a year post lesion regaining voluntary influence of lower limb movements within one treatment session with pcEmc raise new and critical questions about the biology of the lesion of a "complete" spinal injury (Gerasimenko Y. P. et al., 2015). The question becomes, to what extent can spared but perhaps functionally incompetent descending axons within the lesion site be transformed to electrically competent networks below the injury using non-invasive painless spinal cord stimulation. If this transformation can be achieved, it appears that descending supraspinal input, proprioception and neuromodulatory inputs projecting to interneuronal networks projecting to different motor pools can generate the appropriate EMG and behavioral response. With long term training, there appears to be an emergence of improved synaptic connections among the spinal interneurons projecting to motoneurons resulting in more "normal stochastic and coordinated bursting patterns" from agonist and antagonistic motor pools compared with dormant networks before training that seems to have formed aberrant functional connections in response to an extensive "denervation" phenomenon within and among spinal networks distal to the lesion.

AUTHOR CONTRIBUTIONS

PG: Conducted the study, performed data analysis and wrote and edited the manuscript. YG: Conducted the study, wrote and edited the manuscript. SZ: Conducted the study and performed data analysis. AT: Coordinated the study and edited the manuscript. DS: Performed data analysis. DL: Provided medical guidance and edited the manuscript. VE: Conceived the study. Performed data analysis. Wrote and edited the manuscript.

ACKNOWLEDGMENTS

This research was funded by the Christopher & Dana Reeve Foundation, Broccoli Foundation, and the Walkabout Foundation. The research was conducted in the UCLA Clinical and Translational Research Center (CTRC) supported by National Center for Advancing Translational Science (NCATS) UCLA CTSI Grant Number UL1TR000124.

REFERENCES

Angeli, C. A., Edgerton, V. R., Gerasimenko, Y. P., and Harkema, S. J. (2014). Altering spinal cord excitability enables voluntary movements after chronic complete paralysis in humans. *Brain* 137(Pt 5), 1394–1409. doi: 10.1093/brain/awu038

Cai, L. L., Fong, A. J., Otoshi, C. K., Liang, Y., Burdick, J. W., Roy, R. R., et al. (2006). Implications of assist-as-needed robotic step training after a complete spinal cord injury on intrinsic strategies of motor learning. *J. Neurosci.* 26, 10564–10568. doi: 10.1523/JNEUROSCI.2266-06.2006

Courtine, G., Gerasimenko, Y., van den Brand, R., Yew, A., Musienko, P., Zhong, H., et al. (2009). Transformation of nonfunctional spinal circuits into functional states after the loss of brain input. *Nat. Neurosci.* 12, 1333–1342. doi: 10.1038/nn.2401

del-Ama, A. J., Gil-Agudo, A., Pons, J. L., and Moreno, J. C. (2014). Hybrid FES-robot cooperative control of ambulatory gait rehabilitation exoskeleton. *J. Neuroeng. Rehabil.* 11:27. doi: 10.1186/1743-0003-11-27

del-Ama, A. J., Koutsou, A. D., Moreno, J. C., de-los-Reyes, A., Gil-Agudo, A., and Pons, J. L. (2012). Review of hybrid exoskeletons to restore gait following spinal cord injury. *J. Rehabil. Res. Dev.* 49, 497–514. doi: 10.1682/JRRD.2011.03.0043

de Leon, R. D., London, N. J., Roy, R. R., and Edgerton, V. R. (1999a). Failure analysis of stepping in adult spinal cats. *Prog. Brain Res.* 123, 341–348. doi: 10.1016/S0079-6123(08)62869-1

de Leon, R. D., Tamaki, H., Hodgson, J. A., Roy, R. R., and Edgerton, V. R. (1999b). Hindlimb locomotor and postural training modulates glycinergic inhibition in the spinal cord of the adult spinal cat. *J. Neurophysiol.* 82, 359–369.

Esquenazi, A., Talaty, M., Packel, A., and Saulino, M. (2012). The ReWalk powered exoskeleton to restore ambulatory function to individuals with thoracic-level motor-complete spinal cord injury. *Am. J. Phys. Med. Rehabil.* 91, 911–921. doi: 10.1097/PHM.0b013e318269d9a3

Ferris, D. P., Sawicki, G. S., and Domingo, A. (2005). Powered lower limb orthoses for gait rehabilitation. *Top. Spinal Cord Inj. Rehabil.* 11, 34–49. doi: 10.1310/6GL4-UM7X-519H-9JYD

Gad, P., Choe, J., Nandra, M. S., Zhong, H., Roy, R. R., Tai, Y. C., et al. (2013). Development of a multi-electrode array for spinal cord epidural stimulation to facilitate stepping and standing after a complete spinal cord injury in adult rats. *J. Neuroeng. Rehabil.* 10:2. doi: 10.1186/1743-0003-10-2

Gad, P., Roy, R. R., Choe, J., Creagmile, J., Zhong, H., Gerasimenko, Y., et al. (2015). Electrophysiological biomarkers of neuromodulatory strategies to recover motor function after spinal cord injury. *J. Neurophysiol.* 113, 3386–3396. doi: 10.1152/jn.00918.2014

Gerasimenko, Y., Gorodnichev, R., Moshonkina, T., Sayenko, D., Gad, P., and Reggie Edgerton, V. (2015). Transcutaneous electrical spinal-cord stimulation in humans. *Ann. Phys. Rehabil. Med.* 58, 225–231. doi: 10.1016/j.rehab.2015.05.003

Gerasimenko, Y. P., Lu, D. C., Modaber, M., Zdunowski, S., Gad, P., Sayenko, D. G., et al. (2015). Noninvasive reactivation of motor descending control after paralysis. *J. Neurotrauma* 32, 1968–1980. doi: 10.1089/neu.2015.4008

Gorodnichev, R. M., Pivovarova, E. A., Pukhov, A., Moiseev, S. A., Savokhin, A. A., Moshonkina, T. R., et al. (2012). [Transcutaneous electrical stimulation of the spinal cord: non-invasive tool for activation of locomotor circuitry in human]. *Fiziol. Cheloveka* 38, 46–56.

Harkema, S., Gerasimenko, Y., Hodes, J., Burdick, J., Angeli, C., Chen, Y., et al. (2011). Effect of epidural stimulation of the lumbosacral spinal cord on voluntary movement, standing, and assisted stepping after motor complete paraplegia: a case study. *Lancet* 377, 1938–1947. doi: 10.1016/S0140-6736(11)60547-3

Hofstoetter, U. S., Hofer, C., Kern, H., Danner, S. M., Mayr, W., Dimitrijevic, M. R., et al. (2013). Effects of transcutaneous spinal cord stimulation on voluntary locomotor activity in an incomplete spinal cord injured individual. *Biomed. Tech. (Berl).* doi: 10.1515/bmt-2013-4014. [Epub ahead of print].

Hofstoetter, U. S., Krenn, M., Danner, S. M., Hofer, C., Kern, H., McKay, W. B., et al. (2015). Augmentation of voluntary locomotor activity by transcutaneous spinal cord stimulation in motor-incomplete spinal cord-injured individuals. *Artif. Organs* 39, E176–E186. doi: 10.1111/aor.12615

Kakulas, B. A. (1999). The applied neuropathology of human spinal cord injury. *Spinal Cord* 37, 79–88. doi: 10.1038/sj.sc.3100807

Lebedev, M. A., and Nicolelis, M. A. (2011). Toward a whole-body neuroprosthetic. *Prog. Brain Res.* 194, 47–60. doi: 10.1016/B978-0-444-53815-4.00018-2

McDaid, A., Kora, K., Xie, S., Lutz, J., and Battley, M. (2013). "Human-inspired Robotic Exoskeleton (HuREx) for Lower Limb Rehabilitation," in *2013 IEEE International Conference on Mechatronics and Automation* (Kagawa: ICMA), 19–24.

Minassian, K., Persy, I., Rattay, F., Pinter, M. M., Kern, H., and Dimitrijevic, M. R. (2007). Human lumbar cord circuitries can be activated by extrinsic tonic input to generate locomotor-like activity. *Hum. Mov. Sci.* 26, 275–295. doi: 10.1016/j.humov.2007.01.005

Musienko, P., Heutschi, J., Friedli, L., R., van den Brand, and Courtine, G. (2012). Multi-system neurorehabilitative strategies to restore motor functions following severe spinal cord injury. *Exp. Neurol.* 235, 100–109. doi: 10.1016/j.expneurol.2011.08.025

Onose, G., Cardei, V., Craciunoiu, S. T., Avramescu, V., Opris, I., Lebedev, M. A., et al. (2016). Mechatronic wearable exoskeletons for bionic bipedal standing and walking: a new synthetic approach. *Front. Neurosci.* 10:343. doi: 10.3389/fnins.2016.00343

Rejc, E., Angeli, C., and Harkema, S. (2015). Effects of lumbosacral spinal cord epidural stimulation for standing after chronic complete paralysis in humans. *PLoS ONE* 10:e0133998. doi: 10.1371/journal.pone.0133998

Rossignol, S., and Frigon, A. (2011). Recovery of locomotion after spinal cord injury: some facts and mechanisms. *Annu. Rev. Neurosci.* 34, 413–440. doi: 10.1146/annurev-neuro-061010-113746

Rossignol, S., Schwab, M., Schwartz, M., and Fehlings, M. G. (2007). Spinal cord injury: time to move? *J. Neurosci.* 27, 11782–11792. doi: 10.1523/JNEUROSCI.3444-07.2007

Shah, P. K., Gerasimenko, Y., Shyu, A., Lavrov, I., Zhong, H., Roy, R. R., et al. (2012). Variability in step training enhances locomotor recovery after a spinal cord injury. *Eur. J. Neurosci.* 36, 2054–2062. doi: 10.1111/j.1460-9568.2012.08106.x

Strausser, K. A., Swift, T. A., Zoss, A. B., Kazerooni, H., and Bennett, B. C. (2012). "Mobile exoskeleton for spinal cord injury: development and testing," in *Proceedings of the Asme Dynamic Systems and Control Conference and Bath/Asme Symposium on Fluid Power and Motion Control (Dscc 2011),* vol 2 (Arlington, VA), 419–425.

Ziegler, M. D., Zhong, H., Roy, R. R., and Edgerton, V. R. (2010). Why variability facilitates spinal learning. *J. Neurosci.* 30, 10720–10726. doi: 10.1523/JNEUROSCI.1938-10.2010

Conflict of Interest Statement: VE, YG, DL, and PG, researchers on the study team hold shareholder interest in NeuroRecovery Technologies and hold certain inventorship rights on intellectual property licensed by The Regents of the University of California to NeuroRecovery Technologies and its subsidiaries.

The other authors declare that the research was conducted in the absence of any commercial or financial relationships that could be construed as a potential conflict of interest.

frontiers in Neuroscience

ORIGINAL RESEARCH
published: 08 August 2017
doi: 10.3389/fnins.2017.00449

Treadmill Training with HAL Exoskeleton—A Novel Approach for Symptomatic Therapy in Patients with Limb-Girdle Muscular Dystrophy—Preliminary Study

Matthias Sczesny-Kaiser[1], Rebecca Kowalewski[1], Thomas A. Schildhauer[2], Mirko Aach[3], Oliver Jansen[2], Dennis Grasmücke[3], Anne-Katrin Güttsches[1], Matthias Vorgerd[1] and Martin Tegenthoff[1]*

[1] Department of Neurology, BG-University Hospital Bergmannsheil Bochum, Ruhr University Bochum, Bochum, Germany, [2] Department of General and Trauma Surgery, BG-University Hospital Bergmannsheil Bochum, Ruhr University Bochum, Bochum, Germany, [3] Department of Spinal Cord Injury, BG-University Hospital Bergmannsheil Bochum, Ruhr University Bochum, Bochum, Germany

OPEN ACCESS

Edited by:
Daniel P. Ferris, University of Florida, United States

Reviewed by:
Sabato Santaniello, University of Connecticut, United States
Juri Taborri, Sapienza Università di Roma, Italy

***Correspondence:**
Matthias Sczesny-Kaiser
matthias.sczesny-kaiser@rub.de

Specialty section:
This article was submitted to Neuroprosthetics, a section of the journal Frontiers in Neuroscience

Received: *07 March 2017*
Accepted: *24 July 2017*
Published: *08 August 2017*

Citation:
Sczesny-Kaiser M, Kowalewski R, Schildhauer TA, Aach M, Jansen O, Grasmücke D, Güttsches AK, Vorgerd M and Tegenthoff M (2017) Treadmill Training with HAL Exoskeleton—A Novel Approach for Symptomatic Therapy in Patients with Limb-Girdle Muscular Dystrophy—Preliminary Study. Front. Neurosci. 11:449. doi: 10.3389/fnins.2017.00449

Purpose: Exoskeletons have been developed for rehabilitation of patients with walking impairment due to neurological disorders. Recent studies have shown that the voluntary-driven exoskeleton HAL® (hybrid assistive limb) can improve walking functions in spinal cord injury and stroke. The aim of this study was to assess safety and effects on walking function of HAL® supported treadmill therapy in patients with limb-girdle muscular dystrophy (LGMD).

Materials and Methods: Three LGMD patients received 8 weeks of treadmill training with HAL® 3 times a week. Outcome parameters were 10-meter walk test (10 MWT), 6-minute walk test, and timed-up-and-go test (TUG). Parameters were assessed pre and post training and 6 weeks later (follow-up).

Results: All patients completed the therapy without adverse reactions and reported about improvement in endurance. Improvements in outcome parameters after 8 weeks could be demonstrated. Persisting effects were observed after 6 weeks for the 10 MWT and TUG test (follow-up).

Conclusions: HAL® treadmill training in LGMD patients can be performed safely and enables an intensive highly repetitive locomotor training. All patients benefitted from this innovative method. Upcoming controlled studies with larger cohorts should prove its effects in different types of LGMD and other myopathies.

Keywords: muscular dystrophy, exoskeleton, locomotor training, walking, rehabilitation

INTRODUCTION

Limb girdle muscular dystrophies (LGMD) are rare neuromuscular diseases with an estimated prevalence ranging from 0.43 per 100,000 for subtype 2I (LGMD 2I) and 0.94 per 100,000 for subtype 2A (LGMD 2A; Fanin et al., 2005; Narayanaswami et al., 2014; Thompson and Straub, 2016). They are a pathophysiologically diverse group of degenerative myopathies with the

common feature of floppy para- or quadriparesis with proximal pronouncement and muscular atrophy. Basically, LGMDs and divided into two groups due to different modes of inheritance. The LGMD1 group has an autosomal dominant inheritance, whereas LGMD2 are autosomal recessive. Involvement of cardiac and respiratory muscles, joint contractures and extramuscular anomalies occur irregularly depending on the subtype, the underlying genetic defect and affected structural protein (Thompson and Straub, 2016). For example, cardiac involvement is observed often in LGMD 2B whereas has not yet been reported for LGMD 2A, suggesting different pathophysiological mechanisms in both diseases. Different genetic mutations have been identified as the cause of fiber degeneration and strength loss. Intensive genetic and proteomic research over the last 10 years helped to understand the disease and clinical manifestations. Another nomenclature of LGMDs can be done depending on the specific protein function that is defective. So, different pathways and subcellular structures can be involved, e.g., dystrophin-glycoprotein complex, sarcomere, glycosylation, signal transduction, nuclear function, and trafficking. These pathological mechanisms may lead to loss of sarcomere integrity, error in glycosylation of alpha-dystroglycan, defects in muscle repair and dissociation of the sarcomere. For example, LGMD 2A is the most frequent LGMD worldwide. Underlying mutations are located in the Calpain-3-gene that encodes a muscle-specific nonlysosomal protease that is supposed to be mainly involved in disassembly of the sarcomere and muscle cytoskeleton to allow for proper protein turnover during muscle remodeling (Taveau et al., 2003; Kramerova et al., 2007a,b). The clinically manifestations can vary and the phenotypic spectrum is broad; cardiac involvement has not been reported yet and stands in great contrast with other types of LGMD (Kramerova et al., 2007a). In contrast, LGMD 2I is caused by a mutation in the fukutin-related protein gene (*FKRP*) at chromosome 19. It leads to secondary laminin alpha2 deficiency and an abnormal glycosylation of alpha-dystroglycan (Brockington et al., 2001a,b). The clinical spectrum of this subtype ranges from severe and Duchenne-like phenotypes to mild dystrophies with mild elevated creatine kinase (CK) levels (Mercuri et al., 2003). However, genetic and protein defects for all subtypes are still not yet known. Today, LGMD1 A–H and LGMD2 A–W are described (Nigro and Savarese, 2014) today. Clinically, muscle weakness is usually slowly progressive over years. Resultant reduced endurance and cardiovascular fitness, fatigue, exercise intolerance and a more sedentary lifestyle are common symptoms of patients with LGMD. Sooner or later but depending on subtype, most patients need physical assistance for walking and activities of daily living.

Inspite of growing and innovative pharmaceutical investigations for degenerative and even hereditary neurological disorders, disease-specific therapy for LGMD is not yet available (Thompson and Straub, 2016). A few study groups still try to find therapies that start at genetic level. Initial laboratory approaches have been undertaken for precise genetic therapy in LGMD 2B and 2D (Turan et al., 2016). Other study groups have tried to diminish secondary effects of muscle degeneration like inflammation with immune suppressive therapies or to prevent cardiac involvement (Chen et al., 2016; Heydemann, 2016). None of these approaches are established and safe medical therapies, today. Nonetheless, patients suffering from LGMD cannot profit from these new investigations. Therefore, exercise therapies play an important role in patients with LGMD (Siciliano et al., 2015).

Even many studies have been conducted in this area, little is known about the best and most effective physiotherapy for each different myopathy. Standard rehabilitation therapy programs could not be established yet. Most studies struggle with the problem of small case numbers, unclear subtype of LGMD, unclear genetic mutation and heterogeneous causes of myopathy that has been included to the study. One should be very careful in extrapolating training effects from one disease to another, since the molecular defects are so different, which warrants many more investigations of individual muscle diseases.

Generally, two different types for physical therapy can be divided: (a) strength training and (b) aerobic exercise training (Siciliano et al., 2015). **Strength training programs** aiming at certain target muscles report transient increase in muscle strength, but without knowing the optimal resistance needed (Lindeman et al., 1995; Sveen et al., 2013). Strength exercise should be supervised because of possible long-lasting myalgia and increase of (CK) indicating therapy-induced muscular injury (da Luz et al., 2011). Studies examining various exercise protocols are limited because of small sample sizes and wide clinical heterogeneity, again. Several studies showed that walking rehabilitation programs with **aerobic endurance training** can improve muscle strength and self-assessed muscle function (Ansved, 2003; Vissing et al., 2014). For example, Vissing et al. investigated 6 patients with LGMD 2L, so called anoctamin 5 myopathy (Vissing et al., 2014). They performed systematically aerobic training with a bicycle ergometer for 10 weeks. The authors could show improvement of oxidative capacity and muscle strength without further increase of CK or muscle soreness. Further studies from the same scientific group have demonstrated similar positive results for aerobic training in Becker's dystrophy (Sveen et al., 2008), LGMD 2I (Sveen et al., 2007), and facioscapulohumeral muscular dystrophy (Olsen et al., 2005). However, aerobic training seems to play a useful and safe effect in some subtypes of LGMD.

Today, treadmill training (TT) is a very useful tool to enhance locomotor function in diseases presenting with walking disturbance, e.g., stroke and spinal cord injury (SCI; Protas et al., 2001; Srivastava et al., 2016). It requires partially preserved stability of the trunk and residual active muscle innervation of the lower extremities. Combined with a body weight support (BWSTT), it is a regularly used and safe tool to applicate an aerobic endurance training. BWSTT can be assessed also in patients with impaired cardiac and pulmonary function. Its advantage is a very high repetition frequency of gait cycle that can lead to more intensive learning and training effect (Daly and Ruff, 2007). BWSTT can especially improve the stance phase of gait, i.e., the symmetrical weight shift (Visintin and Barbeau, 1994), symmetrical activation of the quadriceps muscles during limb loading (Trueblood, 2001) and faster walking (Visintin et al., 1998; Daly and Ruff, 2004, 2007). Because BWSTT has some lacks of results in some gait training studies considering brain plasticity and for the swing phase of gait, it is

reasonable to combine BWSTT with other interventions. Daly et al. combined BWSTT with functional electrical stimulation (FES) in stroke survivors. They showed that the combination offered the capability of practice of the greatest number of gait components for which two motor learning principles associated with CNS plasticity could be satisfied: practice of close-to-normal movement and repetition of that practice (Daly and Ruff, 2007). Some studies using BWSTT/TT in myopathies can be found in literature. In particular, Taivassalo used TT in patients with metabolic and non-metabolic myopathies performing a short-term aerobic training at low intensity. Both groups benefited (Taivassalo et al., 1998, 1999). Controlled studies aiming on the effect of BWSTT/TT compared to other training methods on different types of myopathy are not available so far. Clear recommendations on BWSTT/TT application and other types of training methods in myopathies do not exist today.

In the last decades, BWSTT has been combined with neurorobotic devices also (Blaya and Herr, 2004; Pohl et al., 2007; Michmizos et al., 2015). All of these devices provide repetitive, accurate and reproducible practice and represent task-specific training. A new generation of robotics are exoskeletons. They are wearable mobile machines with a frame and actuators on hip and knee joints. One commercially available exoskeleton is the hybrid assistive limb® (HAL®; Kawamoto et al., 2013, 2014). It detects electromyographic signals via surface electrodes from the ventral and dorsal thigh (Cyberdyne Inc., Japan). In contrast to other robotic devices that provide automatic passive motion, HAL® enables gait training with voluntarily driven by muscle activity. Today, it used as a training tool only, not as an aid for domestic field. In studies, it used in combination with BWSTT throughout. Studies on patients with SCI and stroke have demonstrated beneficial effects on walking function and on neuronal plasticity (Kubota et al., 2013; Aach et al., 2014; Cruciger et al., 2014; Sczesny-Kaiser et al., 2015). Aach et al. showed in a pilot study and in a larger study including 55 patients with chronic SCI that BWSTT with HAL® led to functional improvement assessed by walking tests like 10-meter walk test and 6-minutes walk test. The authors used an intensive training program with 5 sessions per week over 12 weeks. An improvement of ∼50% could be expected (Aach et al., 2014; Grasmücke et al., 2017). Even a cortical reorganization indicating neuronal plasticity could be observed. Using electrophysiological methods, unused leg representations in the postcentral gyrus were activated even after years post ictus (Sczesny-Kaiser et al., 2015). Similar results have been reported for chronic stroke patients (Yoshimoto et al., 2016). Walking speed increased about 56%. A comparison with other rehabilitation programs like Bobath has not been performed so far. Past experience with HAL® training in patients with chronic gait impairment demonstrated that this exoskeleton and training program can induce additional functional improvements. Because patients with chronic myopathy rely on physiotherapy only, HAL® might be a new training tool for exercise training. Looking for HAL® training in myopathies, only one case has been reported using HAL® in a patient with ocularpharyngodistal myopathy (Hasegawa et al., 2015). Authors stated that no adverse events occurred and that patient's walking parameters were stable. Further application of HAL®-training in myopathies or muscular dystrophies does not exist. Because HAL® exoskeleton is a promising and novel rehabilitation tool utilizing patients' active and voluntarily driven muscular activity, we evaluated the effect on walking functions in three LGMD patients before and after an 8-week period of HAL®-supported treadmill training. By means of the results of this small study, upcoming studies with larger groups should be planned. We want to establish a novel and innovative therapy program for patients with myopathies.

MATERIALS AND METHODS

Subjects

Three outpatients of our neuromuscular center with LGMD were enrolled. Clinical details are shown in **Tables 1A,B**. Inclusion criteria were a clinically, histopathologically, or genetically determined LGMD with para- or quadriparesis and proximal pronouncement and muscular atrophy, and sufficient stability of the trunk. The patients were required to present preserved motor function of hip and knee extensor and flexor muscle groups in order to be able to trigger the exoskeleton (medical research council scale for muscle strength = MRC ≥ 1/5). Exclusion criteria were plegia (MRC 0/5), instability of the trunk, severe limitations of range of motion regarding hip and knee joints (i.e., leading to functional contractures), body weight >100 kg, non-consolidated fractures and severe heart insufficiency. All patients provided written informed consent (ethic approval no. 4733-13, Medical faculty, Ruhr University Bochum). The study was performed in accordance with the Declaration of Helsinki. The clinical assessment and muscle strength score were evaluated before the protocol by a skilled operator.

The Exoskeletal Training

All patients underwent an 8-week training period of body-weight supported treadmill training (BWSTT) with HAL® exoskeleton. Each patient was scheduled 3 times a week resulting in 24 sessions. The actual time of walking with HAL® was max. 30 min. The exoskeleton was voluntarily triggered by EMG-signals from the extensor and flexor muscles of hip and knee detected via surface EMG electrodes. Voluntary motion was magnified and adjusted the muscle activity in accordance with the patient's intention. During therapy, the velocity of the treadmill (Woodway USA, WI, USA) was set individually between comfortable and maximum speed tolerated by the patient. Initially, the bodyweight support was individually pre-set at up to 50% of patient's body weight and individually reduced in subsequent training sessions (see **Figure 1**).

HAL®-Supported Treadmill Parameters

Some treadmill-bounded parameters were assessed. The distance on treadmill in meters for each session, the velocity on treadmill and the time on treadmill were recorded and documented by the therapist.

Primary Outcome Measurements

To assess the training effect, all tests were performed *without* HAL® exoskeleton. We used the 10-meter walk test (10 MWT)

TABLE 1 | A and B: Clinical data of LGMD patients.

A			
No.	**Age range**	**Diagnosis**	**Genetics**
1	40-45	LGMD 2A	Compound heterozygous *CAPN3*-mutations in exon 3 c.390G>C (p.Trp130Cys) and in exon 4: c.550delA
2	55-60	LGMD 2I	Homozygous *FKRP*-mutation in exon 4: c.826C>A (p.Leu276Ile)
3	60-65	LGMD (of unknown subtype)	No mutations detected in next generation sequencing panel including *CAPN3*-, *DYSF*-, *FKRP*-genes

B				
No.	**Age range at disease onset**	**Proximal muscle strength of lower extremities (MRC)**	**Extraskeletal muscular involvement**	**Physical assistance**
1	10–15	1–2/5	None	Electric wheelchair
2	45–50	2–3/5	Cardiac, mild lowered left ventricular function	Wheeled walker
3	45–50	2–3/5	None	Walking stick

M, man; F, female; LGMD, limb-girdle muscular dystrophy; MRC, medical research council.

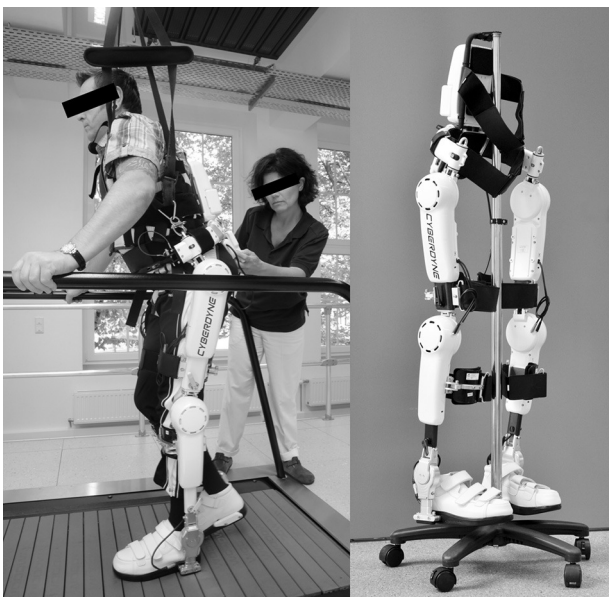

FIGURE 1 | Training setting. The patient is performing body-weight supported treadmill training with the HAL® exoskeleton. The physiotherapist supervises the session. Left picture: Copyright V. Daum, Bergmannsheil Bochum; with informed and written consent obtained from both, the patient and the therapist; right picture: Copyright and courtesy of Cyberdyne Care Robotics GmbH, Bochum, Germany. Appropriate permissions have been obtained from the copyright holders for the publication of both images.

at each daily training session (Bohannon et al., 1996). Data from the first and the last day have been taken for baseline and end of the training data. We took it daily in order to give a feedback to the patient, to motivate her/him. The 10 MWT measured the time needed to walk a 10 m distance. The timed-up-and-go test (TUG) describes the time and assistance required for standing up from the wheelchair, walk 3 m, turn around, walk back and sit down (Podsiadlo and Richardson, 1991). The 6-minute walk test (6 MWT) evaluates the distance covered when walking for 6 min (Balke, 1963). TUG test and 6 MWT were done at the beginning and at the end of the 8-week training period. If possible, all three tests were assessed 6 weeks after the end of the training period again (follow-up assessment, see **Figure 2**).

Secondary Outcome Measurements

To assess motor and balance functions, the motor-related section of the Functional Independence Measure (FIM) (Keith et al., 1987) and the Berg Balance Scale (BBS) (Berg et al., 1992) were documented at baseline and after the 8-week training period (Ottenbacher et al., 1996; Ravaud et al., 1999; Bérard et al., 2005). Both scales were tested by a physical therapist with long-time experience in neurological disorders and myopathies.

Self-Reported Changes in Condition and Symptoms, Adverse Events

Before and after each training session, patients were asked if they had any negative symptoms and adverse events. Furthermore, after the whole training session, patients completed a modified questionnaire grading changes in physical endurance, leg muscle strength, and physical activity (Sveen et al., 2007).

RESULTS

Exoskeletal Training

All three patients completed 24 sessions each. Patients #2 and #3 performed follow-up assessment after 6 weeks. Patient #1 was lost to follow-up. Adverse reactions did not occur. Assessed data can be divided into two categories: (a) HAL®-supported treadmill parameters and (b) primary outcome parameters *without* HAL®. Treadmill parameters were recorded online and demonstrate the velocity on treadmill, how long the patients could perform the exercise on the treadmill and the distance walked on treadmill. These parameters should improve, otherwise the training has to be considered not suitable for this patient. Improvement in treadmill bounded parameters are the basis of a successful training.

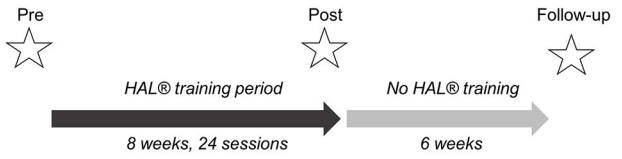

FIGURE 2 | Study design. Three measurements: pre-, post-, and follow-up assessments. Additionally, 10 MWT was performed before and after each training session. Follow-up assessments were done 6 weeks after completion of HAL® training period.

HAL®-Supported Treadmill Parameters

All patients showed increased distance covering on treadmill, increased training time with a maximum of 30 min and increased velocity on treadmill (see **Figures 3A–C**). A five-fold distance, four-fold increase of velocity and a maximum time on treadmill (30 min) have been reached in all patients.

Primary Outcome Parameters

Figures 4A–C show the results of all walking parameters 10 MWT, TUG test, and 6 MWT. At baseline 10 MWT showed similar impairment at a mild stage for all 3 patients. Six MWT and TUG test demonstrated different degree of impairment reflecting different subtypes of LGMD. But, assessed *without* HAL® exoskeleton, all patients showed clearly decreased time in 10 MWT, increased distance in 6 MWT and decreased time in TUG test after 24 training sessions. In the follow up assessments, 10 MWT and TUG test data revealed preserved training effects in both patients compared to baseline data. This effect could not be observed for 6 MWT data. Statistical analysis was not performed due to small data.

Secondary Outcome Measurements

Patient #2 showed increased BBS-score of 5 points after training period. BBS-scores of patients #1 and #3 varied only by 1 point. Considering the motor section of FIM, patient #3 increased by 6 points after HAL® therapy whereas patient #2 did not exhibit any change (see **Figures 5A,B**). Patient #1 could increase his performance by 3 points.

Self-Reported Improvements and Adverse Events

Patient #1 and #2 did not report any adverse events. Patient #3 felt general weakness for about 1–2 h after the training session without myalgia or stiff muscles. Furthermore, all three patients told about better physical endurance after 8 weeks of HAL® training (see **Table 2**).

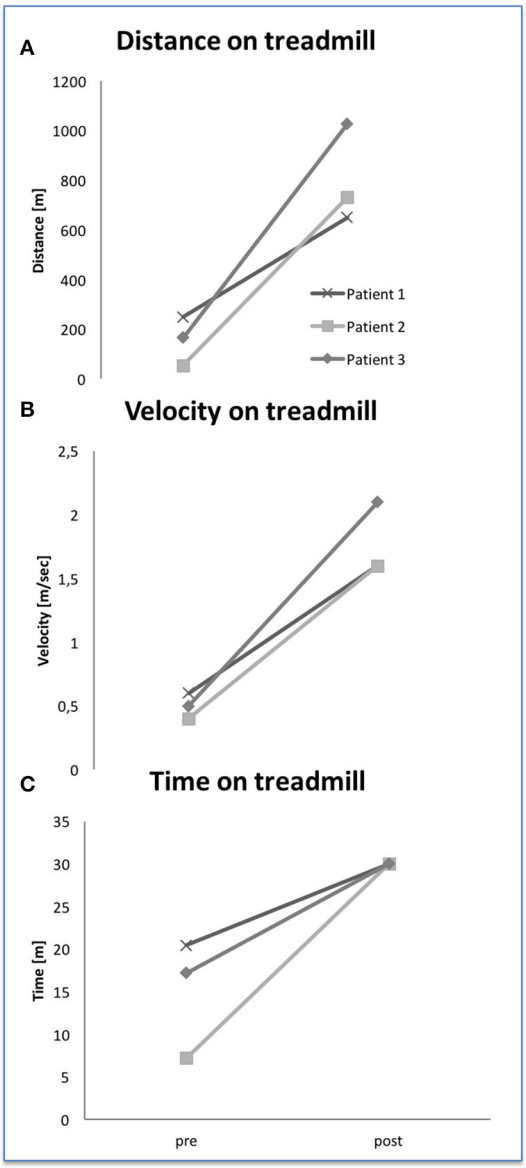

FIGURE 3 | Treadmill parameter with HAL® exoskeleton at baseline and after 24 training sessions **(A–C)**.

DISCUSSION

This study shows that HAL®-assisted BWSTT is a safe and effective method for aerobic exercise training in ambulatory patients with LGMD. All patients showed increased *treadmill-bounded* and HAL®-*dependent* walking parameter, i.e., walking distance, velocity on treadmill and time on treadmill. No patient reported about sustained worsening of symptoms. These results indicate a good acceptance of this new robotic training method and give the basic for an effective therapy. HAL® supports the patients efficiently to complete treadmill training sessions and to improve walking distances on treadmill. HAL®-training enables a highly repetitive and intensive locomotor training in LGMD-patients with mild to severe impaired walking functions. Like previously described, TT cannot cover all parts of gait phases; TT is more effective when combined with other training methods. In our study, we combined with a voluntarily driven exoskeleton. In this combination, more importantly, we found improved HAL®-*independent* walking parameters (10 MWT, 6 MWT, TUG) which were paralleled by self-reported improvements.

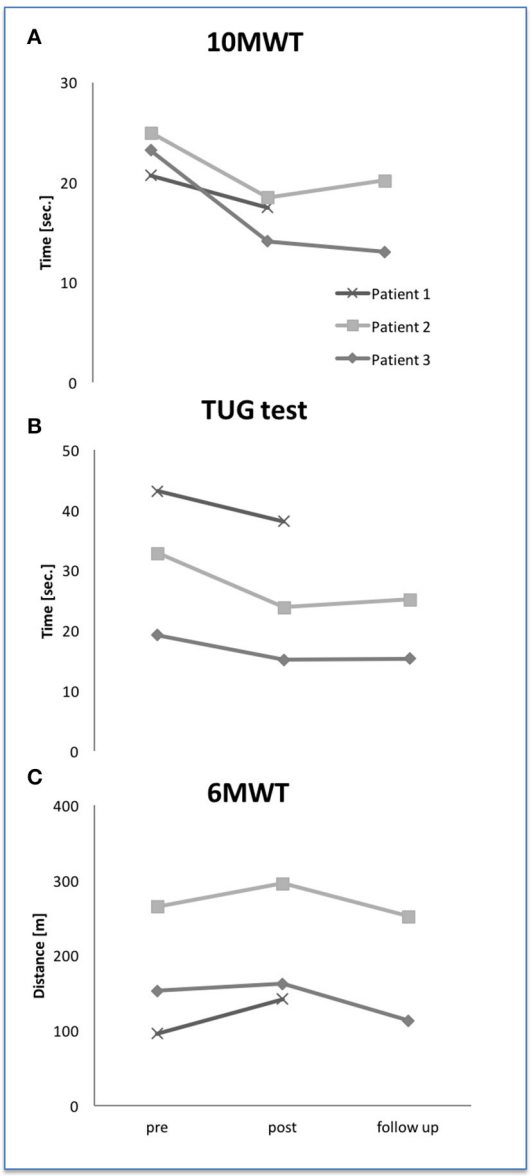

FIGURE 4 | Walking abilities at baseline, after 24 HAL® training sessions and follow up 6 weeks later. Ten MWT, 10-meter walk test **(A)**; TUG, timed-up-and-go **(B)**; 6 MWT, 6-minute walk test **(C)**.

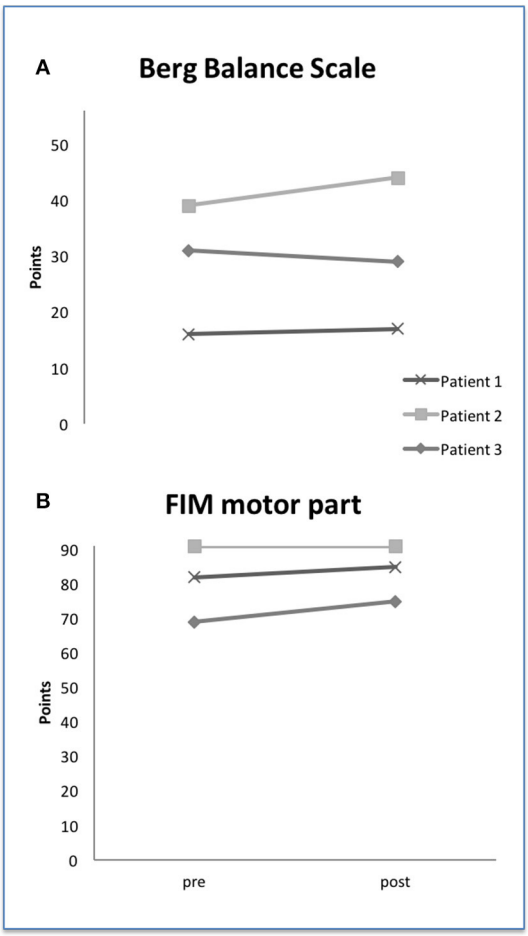

FIGURE 5 | Berg-Balance Scale **(A)** and FIM motor part **(B)** at baseline and after HAL® training. FIM, functional independence measure.

TABLE 2 | Self-reported training-induced changes of physical fatique, endurance, muscle strength and walking distance.

Patient	Physical fatique	Physical endurance	Leg muscle strength	Walking distance
#1	0	+	0	0
#2	+	+	+	+
#3	0	+	0	+

+, improvement; 0, no change; –, worsening.

Compared to other HAL® BWSTT studies, we found similar improvements with ∼30–50% for walking speed. The effects on TUG test were in two patients (#1, #3) smaller; patient #2 clearly improved in TUG test ∼30%. Again, we can see different effects on different types of myopathy. The effects on 6 MWT were smaller. These results indicate different effects of HAL®-supported BWSTT on different aspects of gait, too. Ten MWT mainly reflects walking speed and an efficient sequence of gait phases whereas TUG test aims on safety, balance and functional mobility. Six MWT includes cardiopulmonary fitness. Parameter of pulmonary and cardiac functions were not assessed in this study. One might speculate only about the possible reason for the lack of improvement in 6 MWT. A comparison with aerobic exercise studies on LGMD patients assessed by Sveen (Sveen et al., 2007) and Vissing (Vissing et al., 2014) is not available. Sveen and Vissing used parameters for cardiopulmonary fitness like V_{O2} and plasma lactate levels. These parameters were not collected in our study. Taivassalos' studies on metabolic and non-metabolic myopathies using TT assessed different parameters, too phosphorus magnetic resonance spectroscopy (Taivassalo et al., 1998, 1999). Thus, our study results cannot be compared with previous studies dealing in this field.

Remarkably, training effects measured with 10 MWT and TUG persisted for at least 6 weeks. The effect on 6 MWT could

not be detected at follow-up. The reason for this observation remains unclear. Maybe a short-time factor like motivation might play a role. Missing effects on cardiopulmonary functions might be another reason. Since cardiopulmonary parameters like V_{O2} were not revealed, this question remains unanswered.

In order to answer the question whether HAL® training effects are limited to walking function or can also lead to better motor and balance functions in daily living, FIM and BBS were assessed. The results of both parameters were inconsistent and have to be tested in a larger cohort. The observed score changes are small and do not exceed the required minimal detectable change. One might see a tendency for patient #2 in BBS. The patient also improved in TUG test that includes balance functions also. So, both values (BBS and TUG test) might be considered as a concordant result. Patient #2 reported about frequent falls that reduced after training period for a time. Whether this can be a systematic result, upcoming studies have to investigate this issue.

This is the first HAL® study specifically focused on patients with LGMD. Patients with this disease present with proximal paresis. Because HAL® robot suit supports proximal joints and muscle groups, these patients might benefit the most from this therapy. As mentioned above, two single case reports have been published including one distal and one proximal pronounced myopathy (Asai et al., 2014; Hasegawa et al., 2015). Like the patient with BMD and proximal pronounced paresis, all our LGMD patients improved in HAL®-independent walking parameters. In contrast to this, the OPDM patient's walking function did not improve whereas treadmill associated parameters increased. These two single cases underline that HAL® training is more effective in patients with proximal paresis. So, from our point of view, it is necessary to adapt HAL®-training and take into account the physical condition and pattern of paresis. Another critical point is the training frequency and training time. The whole training session lasted about 90 min, the net walking time 30 min. Coming up from our previous SCI study and to take possible myalgias into account, we reduced the frequency from 5 times a week to 3 times a week (Aach et al., 2014; Nilsson et al., 2014). The question which frequency might be optimal should be tested in upcoming systematic studies.

Considering that these patients suffer from chronic degenerative and dystrophic myopathy, these results are encouraging, offering the possibility to use a novel approach of symptomatic therapy. Even though our study does not allow conclusions on interference with natural course of LGMD or potential long-term effects as compared to conventional physiotherapy, the results are encouraging for upcoming controlled HAL®-studies in larger groups of patients with muscular dystrophy. The anatomical or pathophysiological origins of positive effects on walking functions remain unclear. Different effects on muscular and neuronal systems can be discussed but were not investigated in detail in this study.

Instead of our positive results, some limitations should be discussed. This study is based on only three LGMD patients without a control group. All patients were ambulatory patients of our neuromuscular center and are not representative of the disease with respect to age, gender, and clinical aspect, thus the findings cannot be generalized to the whole LGMD population. Specific measurements looking for increased endurance capacity (lactate, respiratory function, cardiovascular measurements) and serum CK levels were not collected. In future studies, these parameters should be implemented.

We can conclude that our study investigating HAL®-assisted body-weight supported treadmill training in patients with LGMD showed feasibility and safety. Moreover, for the first time, our data show that this voluntarily driven exoskeleton can improve walking functions. With respect to the limited data of three patients only, it encourages us to undertake further studies with larger cohorts and different types of LGMD.

AUTHOR CONTRIBUTIONS

MS, RK, OJ, DG had substantial contributions to the conception and design of the work, acquired data and analyzed the data, drafted the work, and finally approved the final version to be published. MA, AG, MV, TS, and MT participated in the coordination, the design and drafted the manuscript and made critical revisions of the manuscript.

ACKNOWLEDGMENTS

We thank Dr. Silke Lissek, Ph.D., for proof reading. We also thank Professor Yoshiyuki Sankai, CEO of Cyberdyne Inc., that produces the HAL® exoskeleton. He provided exclusively technical and advisory support.

REFERENCES

Aach, M., Cruciger, O., Sczesny-Kaiser, M., Höffken, O., Meindl, R. C., Tegenthoff, M., et al. (2014). Voluntary driven exoskeleton as a new tool for rehabilitation in chronic spinal cord injury: a pilot study. *Spine J.* 14, 2847–2853. doi: 10.1016/j.spinee.2014.03.042

Ansved, T. (2003). Muscular dystrophies: influence of physical conditioning on the disease evolution. *Curr. Opin. Clin. Nutr. Metab. Care* 6, 435–439. doi: 10.1097/01.mco.0000078987.18774.d9

Asai, T., Ojima, I., Minami, S., Takeshima, Y., and Matsuo, M. (2014). Gait training for becker's muscular dystrophy using robot suit hybrid assistive limb. *Phys. Med. Rehabil. Int.* 1, 1–4.

Balke, B. (1963). A simple field test for the assessment of physical fitness. Rep 63-6. *Rep. Civ. Aeromed. Res. Inst.* US 6, 1–8.

Bérard, C., Payan, C., Hodgkinson, I., Fermanian, J., and MFM Collaborative Study Group (2005). A motor function measure for neuromuscular diseases. Construction and validation study. *Neuromuscul. Disord* 15, 463–470. doi: 10.1016/j.nmd.2005.03.004

Berg, K. O., Maki, B. E., Williams, J. I., Holliday, P. J., and Wood-Dauphinee, S. L. (1992). Clinical and laboratory measures of postural balance in an elderly population. *Arch. Phys. Med. Rehabil.* 73, 1073–1080.

Blaya, J. A., and Herr, H. (2004). Adaptive control of a variable-impedance ankle-foot orthosis to assist drop-foot gait. *IEEE Trans. Neural Syst. Rehabil. Eng.* 12, 24–31. doi: 10.1109/TNSRE.2003.823266

Bohannon, R. W., Andrews, A. W., and Thomas, M. W. (1996). Walking speed: reference values and correlates for older adults. *J. Orthop. Sports Phys. Ther.* 24, 86–90. doi: 10.2519/jospt.1996.24.2.86

Brockington, M., Blake, D. J., Prandini, P., Brown, S. C., Torelli, S., Benson, M. A., et al. (2001a). Mutations in the fukutin-related protein gene (FKRP)

cause a form of congenital muscular dystrophy with secondary laminin alpha2 deficiency and abnormal glycosylation of alpha-dystroglycan. *Am. J. Hum. Genet.* 69, 1198–1209. doi: 10.1086/324412

Brockington, M., Yuva, Y., Prandini, P., Brown, S. C., Torelli, S., Benson, M. A., et al. (2001b). Mutations in the fukutin-related protein gene (FKRP) identify limb girdle muscular dystrophy 2I as a milder allelic variant of congenital muscular dystrophy MDC1C. *Hum. Mol. Genet.* 10, 2851–2859. doi: 10.1093/hmg/10.25.2851

Chen, L., Huang, J., Ji, Y., Zhang, X., Wang, P., Deng, K., et al. (2016). Tripartite motif 32 prevents pathological cardiac hypertrophy. *Clin. Sci.* 130, 813–828. doi: 10.1042/CS20150619

Cruciger, O., Tegenthoff, M., Schwenkreis, P., Schildhauer, T. A., and Aach, M. (2014). Locomotion training using voluntary driven exoskeleton (HAL) in acute incomplete SCI. *Neurology* 83, 474–474. doi: 10.1212/WNL.0000000000000645

da Luz, C. R., Nicastro, H., Zanchi, N. E., Chaves, D. F., and Lancha, A. H. (2011). Potential therapeutic effects of branched-chain amino acids supplementation on resistance exercise-based muscle damage in humans. *J. Int. Soc. Sports Nutr.* 8:23. doi: 10.1186/1550-2783-8-23

Daly, J. J., and Ruff, R. L. (2004). Feasibility of combining multi-channel functional neuromuscular stimulation with weight-supported treadmill training. *J. Neurol. Sci.* 225, 105–115. doi: 10.1016/j.jns.2004.07.006

Daly, J. J., and Ruff, R. L. (2007). Construction of efficacious gait and upper limb functional interventions based on brain plasticity evidence and model-based measures for stroke patients. *Sci. World J.* 7, 2031–2045. doi: 10.1100/tsw.2007.299

Fanin, M., Nascimbeni, A. C., Fulizio, L., and Angelini, C. (2005). The frequency of limb girdle muscular dystrophy 2A in northeastern Italy. *Neuromuscul. Disord.* 15, 218–224. doi: 10.1016/j.nmd.2004.11.003

Grasmücke, D., Zieriacks, A., Jansen, O., Fisahn, C., Sczesny-Kaiser, M., Wessling, M., et al. (2017). Against the odds: what to expect in rehabilitation of chronic spinal cord injury with a neurologically controlled Hybrid Assistive Limb exoskeleton. A subgroup analysis of 55 patients according to age and lesion level. *Neurosurg. Focus* 42:E15. doi: 10.3171/2017.2.FOCUS171

Hasegawa, M., Haga, N., Fujiwara, S., Yokota, K., Nakahara, Y., and Sankai, Y. (2015). Robotic rehabilitation for a patient with oculopharyngodistal myopathy. *Physiotherapy* 101, eS427–eS632. doi: 10.1016/j.physio.2015.03.3352

Heydemann, A. (2016). Severe murine limb-girdle muscular dystrophy type 2C pathology is diminished by FTY720 treatment. *Muscle Nerve* 1:1314362. doi: 10.1002/mus.25503

Kawamoto, H., Kamibayashi, K., Nakata, Y., Yamawaki, K., Ariyasu, R., Sankai, Y., et al. (2013). Pilot study of locomotion improvement using hybrid assistive limb in chronic stroke patients. *BMC Neurol.* 13:141. doi: 10.1186/1471-2377-13-141

Kawamoto, H., Kandone, H., Sakurai, T., Ariyasu, R., Ueno, Y., Eguchi, K., et al. (2014). Development of an assist controller with robot suit HAL for hemiplegic patients using motion data on the unaffected side. *Conf. Proc. IEEE Eng. Med. Biol. Soc.* 2014, 3077–3080. doi: 10.1109/EMBC.2014.6944273

Keith, R. A., Granger, C. V., Hamilton, B. B., and Sherwin, F. S. (1987). The functional independence measure: a new tool for rehabilitation. *Adv. Clin. Rehabil.* 1, 6–18.

Kramerova, I., Beckmann, J. S., and Spencer, M. J. (2007a). Molecular and cellular basis of calpainopathy (limb girdle muscular dystrophy type 2A). *Biochim. Biophys. Acta* 1772, 128–144. doi: 10.1016/j.bbadis.2006.07.002

Kramerova, I., Kudryashova, E., Venkatraman, G., and Spencer, M. J. (2007b). Calpain 3 participates in sarcomere remodeling by acting upstream of the ubiquitin-proteasome pathway. *Hum. Mol. Genet.* 16, 1006–1006. doi: 10.1093/hmg/ddm044

Kubota, S., Nakata, Y., Eguchi, K., Kawamoto, H., Kamibayashi, K., Sakane, M., et al. (2013). Feasibility of rehabilitation training with a newly developed wearable robot for patients with limited mobility. *Arch. Phys. Med. Rehabil.* 94, 1080–1087. doi: 10.1016/j.apmr.2012.12.020

Lindeman, E., Leffers, P., Spaans, F., Drukker, J., Reulen, J., Kerckhoffs, M., et al. (1995). Strength training in patients with myotonic dystrophy and hereditary motor and sensory neuropathy: a randomized clinical trial. *Arch. Phys. Med. Rehabil.* 76, 612–620. doi: 10.1016/S0003-9993(95)80629-6

Mercuri, E., Brockington, M., Straub, V., Quijano-Roy, S., Yuva, Y., Herrmann, R., et al. (2003). Phenotypic spectrum associated with mutations in the fukutin-related protein gene. *Ann. Neurol.* 53, 537–542. doi: 10.1002/ana.10559

Michmizos, K. P., Rossi, S., Castelli, E., Cappa, P., and Krebs, H. I. (2015). Robot-aided neurorehabilitation: a pediatric robot for ankle rehabilitation. *IEEE Trans. Neural Syst. Rehabil. Eng.* 23, 1056–1067. doi: 10.1109/TNSRE.2015.2410773

Narayanaswami, P., Weiss, M., Selcen, D., David, W., Raynor, E., Carter, G., et al. (2014). Evidence-based guideline summary: diagnosis and treatment of limb-girdle and distal dystrophies: report of the guideline development subcommittee of the American Academy of Neurology and the practice issues review panel of the American Association of Neuromuscular & Electrodiagnostic Medicine. *Neurology* 83, 1453–1463. doi: 10.1212/WNL.0000000000000892

Nigro, V., and Savarese, M. (2014). Genetic basis of limb-girdle muscular dystrophies: the 2014 update. *Acta Myol.* 33, 1–12.

Nilsson, A., Vreede, K. S., Häglund, V., Kawamoto, H., Sankai, Y., and Borg, J. (2014). Gait training early after stroke with a new exoskeleton–the hybrid assistive limb: a study of safety and feasibility. *J. Neuroeng. Rehabil.* 11:92. doi: 10.1186/1743-0003-11-92

Olsen, D. B., Ørngreen, M. C., and Vissing, J. (2005). Aerobic training improves exercise performance in facioscapulohumeral muscular dystrophy. *Neurology* 64, 1064–1066. doi: 10.1212/01.WNL.0000150584.45055.27

Ottenbacher, K. J., Hsu, Y., Granger, C. V., and Fiedler, R. C. (1996). The reliability of the functional independence measure: a quantitative review. *Arch. Phys. Med. Rehabil.* 77, 1226–1232. doi: 10.1016/S0003-9993(96)90184-7

Podsiadlo, D., and Richardson, S. (1991). The timed "Up & Go": a test of basic functional mobility for frail elderly persons. *J. Am. Geriatr. Soc.* 39, 142–148. doi: 10.1111/j.1532-5415.1991.tb01616.x

Pohl, M., Werner, C., Holzgraefe, M., Kroczek, G., Mehrholz, J., Wingendorf, I., et al. (2007). Repetitive locomotor training and physiotherapy improve walking and basic activities of daily living after stroke: a single-blind, randomized multicentre trial (DEutsche GAngtrainerStudie, DEGAS). *Clin. Rehabil.* 21, 17–27. doi: 10.1177/0269215506071281

Protas, E. J., Holmes, S. A., Qureshy, H., Johnson, A., Lee, D., and Sherwood, A. M. (2001). Supported treadmill ambulation training after spinal cord injury: a pilot study. *Arch. Phys. Med. Rehabil.* 82, 825–831. doi: 10.1053/apmr.2001.23198

Ravaud, J. F., Delcey, M., and Yelnik, A. (1999). Construct validity of the functional independence measure (FIM): questioning the unidimensionality of the scale and the "value" of FIM scores. *Scand. J. Rehabil. Med.* 31, 31–41. doi: 10.1080/003655099444704

Sczesny-Kaiser, M., Höffken, O., Aach, M., Cruciger, O., Grasmücke, D., Meindl, R., et al. (2015). HAL® exoskeleton training improves walking parameters and normalizes cortical excitability in primary somatosensory cortex in spinal cord injury patients. *J. Neuroeng. Rehabil.* 12:68. doi: 10.1186/s12984-015-0058-9

Siciliano, G., Simoncini, C., Giannotti, S., Zampa, V., Angelini, C., and Ricci, G. (2015). Muscle exercise in limb girdle muscular dystrophies: pitfall and advantages. *Acta Myol.* 34, 3–8.

Srivastava, A., Taly, A. B., Gupta, A., Kumar, S., and Murali, T. (2016). Bodyweight-supported treadmill training for retraining gait among chronic stroke survivors: a randomized controlled study. *Ann. Phys. Rehabil. Med.* 59, 235–241. doi: 10.1016/j.rehab.2016.01.014

Sveen, M.-L., Andersen, S. P., Ingelsrud, L. H., Blichter, S., Olsen, N. E., Jønck, S., et al. (2013). Resistance training in patients with limb-girdle and becker muscular dystrophies. *Muscle Nerve* 47, 163–169. doi: 10.1002/mus.23491

Sveen, M.-L., Jeppesen, T. D., Hauerslev, S., Køber, L., Krag, T. O., and Vissing, J. (2008). Endurance training improves fitness and strength in patients with Becker muscular dystrophy. *Brain* 131, 2824–2831. doi: 10.1093/brain/awn189

Sveen, M.-L., Jeppesen, T. D., Hauerslev, S., Krag, T. O., and Vissing, J. (2007). Endurance training: an effective and safe treatment for patients with LGMD2I. *Neurology* 68, 59–61. doi: 10.1212/01.wnl.0000250358.32199.24

Taivassalo, T., De Stefano, N., Argov, Z., Matthews, P. M., Chen, J., Genge, A., et al. (1998). Effects of aerobic training in patients with mitochondrial myopathies. *Neurology* 50, 1055–1060. doi: 10.1212/WNL.50.4.1055

Taivassalo, T., De Stefano, N., Chen, J., Karpati, G., Arnold, D. L., and Argov, Z. (1999). Short-term aerobic training response in chronic myopathies. *Muscle Nerve* 22, 1239–1243. doi: 10.1002/(SICI)1097-4598(199909)22:9<1239::AID-MUS11>3.0.CO;2-W

Taveau, M., Bourg, N., Sillon, G., Roudaut, C., Bartoli, M., and Richard, I. (2003). Calpain 3 is activated through autolysis within the active site and lyses sarcomeric and sarcolemmal components. *Mol. Cell. Biol.* 23, 9127–9135. doi: 10.1128/MCB.23.24.9127-9135.2003

Thompson, R., and Straub, V. (2016). Limb-girdle muscular dystrophies - international collaborations for translational research. *Nat. Rev. Neurol.* 12, 294–309. doi: 10.1038/nrneurol.2016.35

Trueblood, P. R. (2001). Partial body weight treadmill training in persons with chronic stroke. *Neurorehabilitation* 16, 141–153.

Turan, S., Farruggio, A. P., Srifa, W., Day, J. W., and Calos, M. P. (2016). Precise correction of disease mutations in induced pluripotent stem cells derived from patients with limb girdle muscular dystrophy. *Mol. Ther.* 24, 685–696. doi: 10.1038/mt.2016.40

Visintin, M., and Barbeau, H. (1994). The effects of parallel bars, body weight support and speed on the modulation of the locomotor pattern of spastic paretic gait. A preliminary communication. *Paraplegia* 32, 540–553. doi: 10.1038/sc.1994.86

Visintin, M., Barbeau, H., Korner-Bitensky, N., and Mayo, N. E. (1998). A new approach to retrain gait in stroke patients through body weight support and treadmill stimulation. *Stroke* 29, 1122–1128. doi: 10.1161/01.STR.29.6.1122

Vissing, C. R., Preisler, N., Husu, E., Prahm, K. P., and Vissing, J. (2014). Aerobic training in patients with anoctamin 5 myopathy and hyperckemia. *Muscle Nerve* 50, 119–123. doi: 10.1002/mus.24112

Yoshimoto, T., Shimizu, I., and Hiroi, Y. (2016). Sustained effects of once-a-week gait training with hybrid assistive limb for rehabilitation in chronic stroke: case study. *J. Phys. Ther. Sci.* 28, 2684–2687. doi: 10.1589/jpts.28.2684

Conflict of Interest Statement: MS, RK, MA, OJ, DG, AG, MV, and MT declare that the research was conducted in the absence of any commercial or financial relationships that could be construed as a potential conflict of interest. TS reports personal fees from Cyberdyne, Inc. outside the submitted work.

frontiers in Neuroscience

ORIGINAL RESEARCH
published: 26 September 2017
doi: 10.3389/fnins.2017.00531

Virtual Balancing for Studying and Training Postural Control

*Daniela Buettner, Daniela Dalin, Isabella K. Wiesmeier and Christoph Maurer**

Department of Neurology and Neurophysiology, University Hospital Freiburg, Medical Faculty, Freiburg, Germany

Postural control during free stance has been frequently interpreted in terms of balancing an inverted pendulum. This even holds, if subjects do not balance their own, but an external body weight. We introduce here a virtual balancing apparatus, which produces torque in the ankle joint as a function of ankle angle resembling the gravity and inertial effects of free standing. As a first aim of this study, we systematically modified gravity, damping, and inertia to examine its effect on postural control beyond the physical constraints given in the real world. As a second aim, we compared virtual balancing to free stance to test its suitability for balance training in patients who are not able to balance their full body weight due to certain medical conditions. In a feasibility study, we analyzed postural control during free stance and virtual balancing in 15 healthy subjects. Postural control was characterized by spontaneous sway measures and measures of perturbed stance. During free stance, perturbations were induced by pseudorandom anterior-posterior tilts of the body support surface. In the virtual balancing task, we systematically varied the anterior-posterior position of the foot plate where the balancing forces are zero following a similar pseudorandom stimulus profile. We found that subjects' behavior during virtual balancing resembles free stance on a tilting platform. This specifically holds for the profile of body excursions as a function of stimulus frequencies. Moreover, non-linearity between stimulus and response amplitude is similar in free and virtual balancing. The overall larger stimulus induced body excursions together with an altered phase behavior between stimulus and response could be in part explained by the limited use of vestibular and visual feedback in our experimental setting. Varying gravity or damping significantly affected postural behavior. Inertia as an isolated factor had a mild effect on the response functions. We conclude that virtual balancing may be well suited to simulate conditions which could otherwise only be realized in space experiments or during parabolic flights. Further studies are needed to examine patients' potential benefit of virtual balance training.

Keywords: virtual, postural control, balancing, inverted pendulum, model

OPEN ACCESS

Edited by:
Daniel P. Ferris,
University of Florida, United States

Reviewed by:
Andrew Sawers,
University of Illinois at Chicago, United States
Martin Lotze,
University of Greifswald, Germany

****Correspondence:***
Christoph Maurer
christoph.maurer@uniklinik-freiburg.de

Specialty section:
This article was submitted to Neuroprosthetics, a section of the journal Frontiers in Neuroscience

Received: *14 July 2017*
Accepted: *12 September 2017*
Published: *26 September 2017*

Citation:
Buettner D, Dalin D, Wiesmeier IK and Maurer C (2017) Virtual Balancing for Studying and Training Postural Control. Front. Neurosci. 11:531. doi: 10.3389/fnins.2017.00531

INTRODUCTION

Free stance is controlled by the central nervous system (CNS) using sensory signals derived from visual, vestibular and proprioceptive afferent information (Dichgans et al., 1976; Lestienne et al., 1976; Nashner and Berthoz, 1978; Freyler et al., 2014; Ritzmann et al., 2015). Stabilization of the center of mass of the human body resembles balancing an inverted pendulum (Ritzmann et al., 2015). Muscle forces are used to provide an appropriate torque (Dichgans et al., 1976), which counteracts gravitational and inertial forces.

The ability to stand freely is often characterized by analyzing spontaneous sway (Prieto et al., 1996; Qu et al., 2009). Spontaneous sway reflects the small fluctuations of body position during standing. These fluctuations show similar patterns in free stance as well as when balancing an external weight through a moveable platform (Fitzpatrick et al., 1992; Fitzpatrick and McCloskey, 1994; Loram and Lakie, 2002). The similarity covers many features of spontaneous sway, like, e.g., amplitude, velocity, and major frequency content. The diagnostic value of spontaneous sway for evaluating stance behavior has been repeatedly questioned. In contrast, studying postural reactions to external perturbations seem to provide a deeper inside into the mechanisms of stance (Peterka, 2002; Maurer and Peterka, 2005; Masani et al., 2006; Lockhart and Ting, 2007; Welch and Ting, 2009; Vette et al., 2010; Davidson et al., 2011; van der Kooij and Peterka, 2011; Nishihori et al., 2012; Engelhart et al., 2014; Pasma et al., 2014). However, whether postural reactions subsequent to external perturbations are similar between free standing and balancing an external weight, is unknown as yet.

The virtual balance paradigm introduced here allows for analyzing both, spontaneous fluctuations and motor reactions to external perturbations. Instead of a physical weight which is balanced through a foot plate, we simulated balancing a weight through a foot plate by measuring the platform to body position, i.e., the ankle joint angle, and calculating the appropriate torque signal, which is then fed back into the system as an ankle torque. We hypothesize that free standing postural reactions could be well mimicked by a virtual balance paradigm after optimizing control parameters.

An important feature of the virtual balance paradigm relates to the nearly free choice of gravitational load, body inertia, and joint damping. From literature, it is well known that postural control is load-dependent (Freyler et al., 2014; Ritzmann et al., 2015). Earlier studies dealing with over- and under-loading were performed with astronauts in space (Layne et al., 2001; Loomer, 2001; di Prampero and Narici, 2003), in free fall conditions (Nomura et al., 2001; Miyoshi et al., 2003), with partial weight-bearing (Ali and Sabbahi, 2000; Phadke et al., 2006; Hwang et al., 2011; Freyler et al., 2014), under hypergravity (Miyoshi et al., 2003), with extra weight (Dietz et al., 1989; Ali and Sabbahi, 2000), or using water buoyancy (Dietz et al., 1989; Nakazawa et al., 2004). It has been demonstrated that load variation is associated with changes in angle torque (Mergner and Rosemeier, 1998; Nakazawa et al., 2004), in the use of somatosensory signals (Paloski et al., 1993; Bloomberg et al., 1997; Layne et al., 2001), and changes in neuromuscular activity (Dietz et al., 1989; Avela et al., 1994; Ali and Sabbahi, 2000; Pöyhönen and Avela, 2002). However, despite the substantial amount of load-related articles, the underlying neuromuscular mechanisms and functional consequences for balance control are poorly understood.

The paradigm of modifying gravitational load and inertia seems to be particularly helpful in patients who are not capable of supporting their own body weight, e.g., due to trauma or muscle weakness. It is well known that neural mechanisms employed to perform balancing are different from those used to, e.g., apply ankle torque against an external resistance, including the different sensory perceptions (Fitzpatrick and McCloskey, 1994). Here, we aimed to examine the individual effects of gravity, damping and inertia on postural control that could otherwise only be realized in space experiments or during parabolic flights. Moreover, we aimed at comparing virtual balancing with free stance to investigate its similarity and suitability for balance training in patients who are not able to balance their full body weight and/ or are prone to falls. Finally, virtual balancing may allow for adapting gravitational load and inertia to patients' needs.

MATERIALS AND METHODS

In this feasibility study, subjects were tested by recording spontaneous sway, as well as motor reactions to external perturbations during free stance, and, in addition, using a virtual balance apparatus.

Subjects

We measured postural control of 15 young people (9 female, 6 male, 23.8 years ± 2.14 [mean age ± SD]). We excluded people suffering from any disease that may interact with postural control. For that, each subject was carefully examined for intact vestibular and proprioceptive function. Further exclusion criteria included any acute or chronic disease that may influence the general condition of health. Anthropometric data of subjects are given in **Table 1**.

Procedures during Free Standing

Spontaneous sway and perturbed stance were assessed on a custom-built motion platform (**Figure 1A**). Subjects were told to stand upright in a relaxed position. For safety reasons and

TABLE 1 | Anthropometric data of subjects.

Subject	Height (cm)	Weight (kg)	BMI (kg/m^2)
1	172	57	19.3
2	180	71	21.9
3	174	73	24.1
4	174	70	23.1
5	173	68	22.7
6	183	70	20.9
7	197	76	19.6
8	182	80	24.2
9	180	70	21.6
10	158	58	23.2
11	160	45	17.6
12	160	51	19.9
13	157	48	19.5
14	163	55	20.7
15	164	71	26.4
Mean value ± SD	171.8 ± 11.06	64.2 ± 9.77	21.7 ± 2.23

9 female, 6 male; SD, standard deviation; BMI, body mass index; cm, centimeter; kg, kilogram; m, meter.

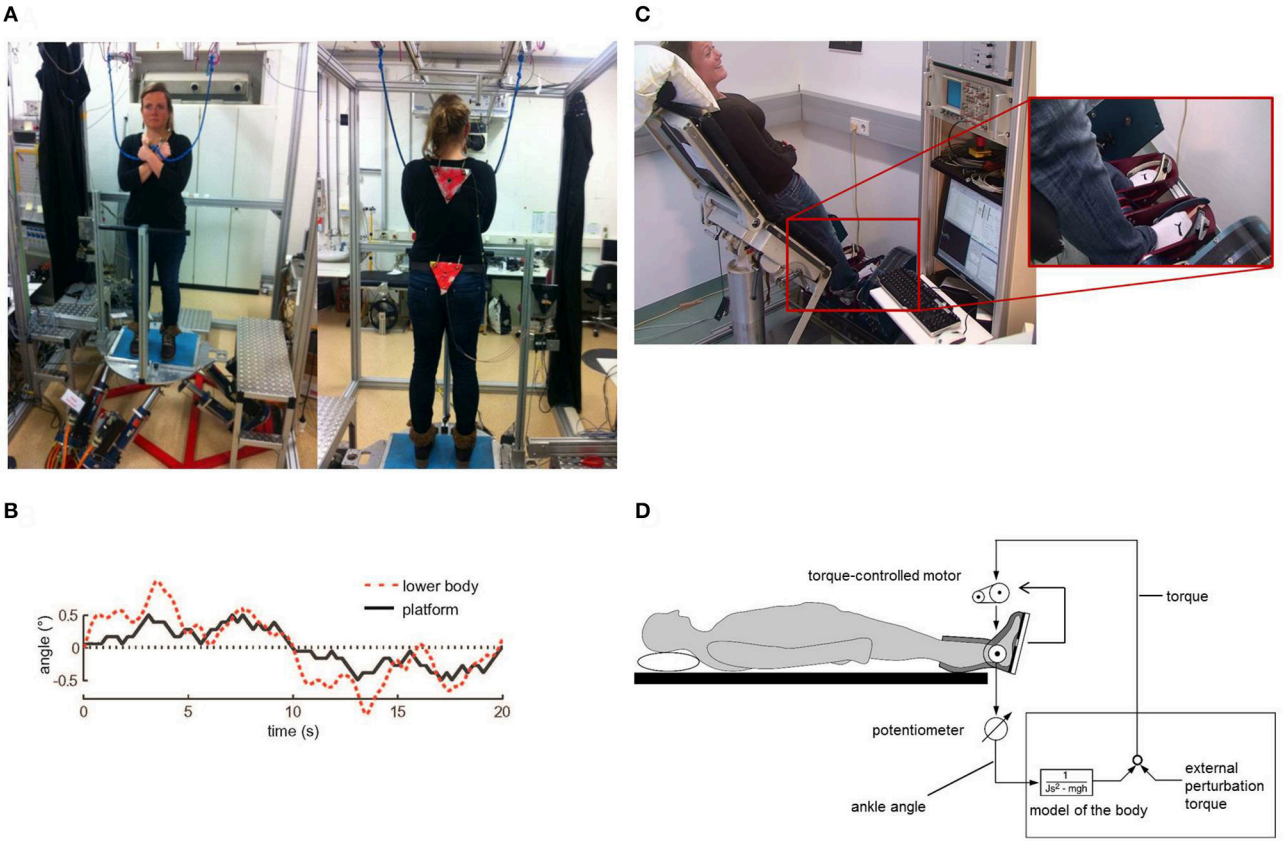

FIGURE 1 | Experimental setup. **(A)** Custom-built motion platform for measurements of spontaneous sway and perturbed stance. Angular excursions of the body and the platform were quantified with an optoelectronic camera system. **(B)** Example of a PRTS (pseudorandom ternary sequence) stimulus profile (black line) yielding to anterior-posterior rotational tilts of the platform with 1° peak-to-peak stimulus amplitude together with a healthy subject's postural reaction in terms of lower body excursion (red dotted line). **(C)** Custom-made platform for virtual balancing. Subjects were lying in an inclined position with their feet positioned on a tilting balance board. They moved their feet in the ankle joint in order to control the balance board. **(D)** Potentiometers and torque sensors measured position as well as torque of the balance board with respect to the body. Measured board tilts were transferred online into board torque commands using the real time simulation toolbox of Simulink/Matlab, running on a PC. The ankle angle-to-torque transformation followed the characteristics of an inverted pendulum body, including virtual gravity (mgh), inertia (J) and damping. Board torque commands were fed back to the board via a torque controlled electric motor. External perturbations, i.e., PRTS stimuli, were applied as shifts of the zero equilibrium point.

to prevent falls, the experimental setup included ropes that were fixed to the ceiling at a position which was about 30 cm in forward direction with respect to the foot position of the subjects. At the lower end of the ropes, there were two small wooden handles attached to the rope. The handles did not serve as a reference, because the subjects held them freely. Since they were attached via the loosely dangling ropes to the ceiling, they were meant to serve as a replacement for a body harness. If a subject felt unsafe, he/ she could have lowered the handles to put tension on the ropes. However, this event did not happen during the experiments. None of the subjects used the ropes to prevent falls. Subjects performed 2 trials of spontaneous sway and 8 trials of perturbed stance, each with eyes open and eyes closed. One trial lasted 1 min; between trials, a short break of about 10 s was taken.

We recorded center-of-pressure (COP) sway paths and 3-D angular positions of the body. The COP sway path was measured with the help of a force transducing platform (Kistler platform type 9286, Winterthur, Switzerland). 3-D angular excursions of the body (hip-to-ankle, shoulder-to-hip) were detected using an optoelectronic device with markers attached to shoulder and hip (Optotrak 3020, Waterloo, Canada). Each marker consisted of three light-emitting diodes fixed to a rigid triangle. Optotrak® and Kistler® output signals as well as the stimulus signals recorded with software programmed in LabView® (National Instruments, Austin, Texas, USA). COM height above the ankle joints was calculated according to tables from Winter (1995) using the measured heights of hip and shoulder markers. A detailed description of the experimental setup has been published previously (e.g., Wiesmeier et al., 2015).

External perturbations consisted of rotational platform tilts in the sagittal plane with the tilt axis passing through subject's ankle joints. Stimulus profiles followed a pseudorandom signal (PRTS, pseudorandom ternary sequence, see **Figure 1B**) using two different peak-to-peak amplitudes (0.5° and 1°). Postural reactions were evaluated at certain frequencies (0.05, 0.15, 0.3, 0.4, 0.55, 0.7, 0.9, 1.1, 1.35, 1.75, and 2.2 Hz), leading

to specific transfer functions between stimulus and postural reactions.

Procedures during Virtual Balancing

Virtual balancing was performed on a newly developed, custom-made platform. Subjects were lying in an inclined position with their feet positioned on a tilting board (**Figure 1C**). In this experimental setting, subjects did not move their own body. They solely moved their feet in the ankle joint in order to control the moveable balance board (**Figure 1D**). We measured position as well as torque of the balance board with respect to the body using potentiometers and torque sensors. The balance board was programed in such a way that its anterior-posterior torque was derived from its position. Similar to the gravitational effect in a free standing task, the virtual gravitational torque had a zero point at a board position orthogonal to the body vertical direction. Increasing board angles were accompanied by increasing torques away from the zero position, resembling unstable equilibrium. The inertial force was mimicked through an additional torque which was directed counter to the board acceleration. Damping was implemented by applying a counter-torque based on board velocity. Virtual gravity, inertia and damping were calculated with a compiled version of a Simulink/MATLAB® model (The MathWorks Inc., Natick, MA, USA) using the real-time simulation mode. Measured board tilts were transferred online into board torque commands, which were then fed back to the board via torque controlled electric motors. This condition resembled free standing on firm ground and produced spontaneous sway.

In the virtual external perturbation condition, we used a stimulus profile similar to free standing (PRTS, see above). This signal directly modified the zero-position of the equilibrium. The stimulus produced an additional torque. For example, if we aimed to simulate a one degree tilt of the platform during free standing, we added a torque with a size exactly resembling the gravitational torque of a one degree inclination from space vertical of a human body. Subjects tended to correct for this torque offset by moving the platform until a new equilibrium with minimal torque was found. This behavior is related to the free standing behavior on a tilting platform, where a platform tilt leads to a correction of the ankle angle until the body is close to vertical in space again, thereby minimizing gravitational torque.

Subjects were instructed to comfortably lean on the inclined backboard and fold their arms. We assured that no relevant body movements were elicited other than subjects' ankle joint movements controlling the balance board. Subjects were instructed to continuously balance the moveable platform and find the equilibrium point in a playful manner rather than to massively co-contract in order to block the platform in a certain position. Subjects were presented with 5 trials for practice. Subsequently, we systematically varied gravitational force of the virtual body (10, 20, and 40% of subjects' own body weight), inertial force (5, 10, and 20% of subjects' own body inertia), damping (5 and 10% of the gravitational force), and external perturbation (relating to 0, 0.25°, 0.5°, and 1° peak to peak body inclination, with respect to subjects' body metrics). The experimental protocol consisted of $3 \times 3 \times 2 \times 4 = 72$ trials in a randomized order. Each trial started with a 10 s period, where the torque with respect to the board position was ramping up to allow subjects for finding their equilibrium point. The duration and the stimulus profile of the subsequent measuring period closely resembled the trials during free standing.

Data Analyses

Data analysis was performed off-line with custom-made software programmed in MATLAB® (The MathWorks Inc., Natick, MA, USA). From upper body, lower body and center of pressure excursions in the free standing condition and board tilts in the virtual balancing condition, we calculated Root Mean Square (sway amplitude, RMS) and Mean velocity (sway velocity, MV) for characterizing spontaneous sway. Transfer functions from stimulus-response data were calculated by a discrete Fourier transform. Fourier coefficients of stimulus and response time series are used to determine GAIN and PHASE with respect to stimulus frequencies. GAIN (response sensitivity) shows the amplitude relationship between the external perturbation and the postural reaction (body angle during free standing, board angle during virtual balancing). PHASE is the relative delay between the stimulus and the reaction of the body.

Statistical analyses were performed using Microsoft Excel and statistic programs (JMP® and Statview by SAS Institute Inc., Cary, NC, USA). After testing normal distribution and homogeneity of variances with the Kolmogorov-Smirnov test, we used parametric methods for further analyses. Due to the expected dependency between the outcome measures within the balance tasks (real stance vs. virtual balancing), statistical significance was tested by an analysis of variance (ANOVA). The within-subjects factors for free spontaneous sway were visual condition, sway direction, and body segment (hip, shoulder). For perturbed stance, the within-subjects factors were visual condition, stimulus amplitude, stimulus frequency, and body segment (hip, shoulder). For the virtual balancing task, the within-subjects factors were gravity, damping, inertia, and stimulus amplitude. The level of statistical significance was set at $p = 0.05$.

The study was performed according to the ethical standards of the Declaration of Helsinki. It was approved by the ethics committee of the Medical Center of the University of Freiburg. All subjects gave their written informed consent prior to study participation.

RESULTS

Spontaneous Sway

Generally, the Root Mean Square (sway amplitude, RMS) of virtual balancing (3.15 cm) was significantly larger than the RMS of free stance (0.47 cm, eyes open). Moreover, the RMS during virtual balancing significantly depended on gravity (3.15 cm with a gravity effect of 40% vs. 2.80 cm with a gravity effect of 20% and 1.37 cm with 10%; $F = 23.04$, $p < 0.0001$, **Figure 2A**). In contrast, inertia and damping did not affect RMS. As with RMS, Mean Velocity (sway velocity, MV) of virtual balancing (5.39 cm/s) was significantly larger than the MV of free stance (0.43 cm/s; eyes open) and significantly depended on gravity (5.39 cm/s with a

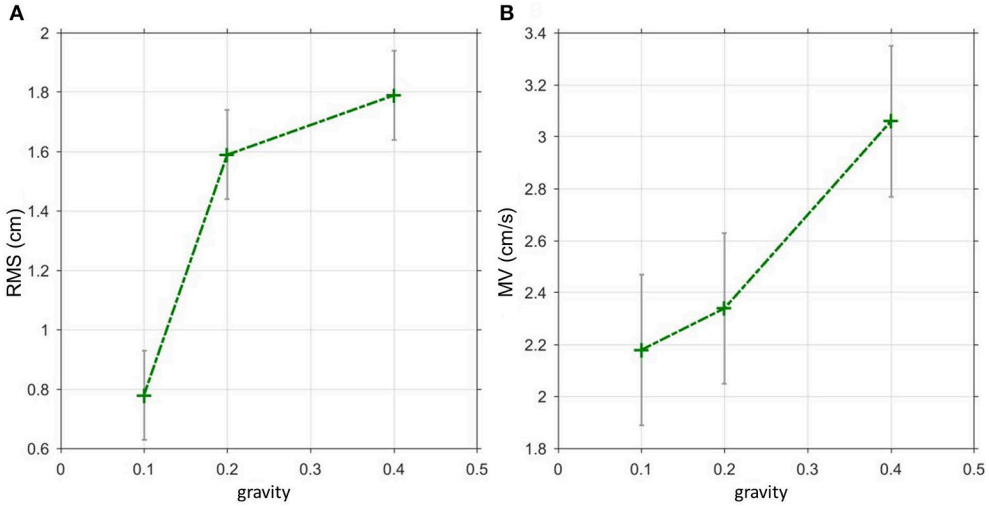

FIGURE 2 | Spontaneous sway during virtual balancing. **(A)** Root Mean Square (RMS) and **(B)** Mean Velocity (MV) as a function of the amount of virtual gravity.

gravity effect of 40% vs. 4.12 cm/s with a gravity effect of 20% and 3.84 cm/s with 10%; $F = 5.09$, $p = 0.0068$, **Figure 2B**). Inertia and Damping did not significantly affect MV.

Externally Perturbed Stance

The GAIN across all parameter settings and frequencies during virtual balancing (1.92, **Figure 3A**) was slightly larger than the GAIN of free stance (1.74, eyes open, **Figure 3B**). However, the difference between the two experimental sets was much smaller than that for spontaneous sway. The frequency influenced GAIN significantly during virtual balancing ($F = 19.2$, $p < 0.001$). Both virtual balancing and free stance showed the largest GAIN (>3.5) between a frequency of 0.15–0.55 Hz. With increasing frequency, GAIN values decreased. Interactions of stimulus amplitude and GAIN during virtual balancing (2.81 with 0.125 Nm and 1.92 with 0.5 Nm) and free stance (2 with 0.5° and 1.73 with 1°) were similar and indicated a non-linearity between stimulus amplitude and GAIN (**Figure 4A** virtual balancing, **Figure 4B** free stance). In the frequency-response curve the Phase showed a similar behavior during virtual balancing and free stance. Low frequencies induced low delay of phase while high frequencies induced a large delay of phase (**Figure 3C** virtual balancing, **Figure 3D** free stance). The coherence across all effects was slightly larger during virtual balancing (1.0) than during free stance (0.79).

Dependence of Motor Behavior from Gravity, Damping, Inertia, and Stimulus Amplitude

Stimulus amplitude, virtual gravity, and virtual damping significantly interacted with GAIN of the transfer function. Stimulus amplitudes were inversely correlated with GAIN ($F = 7.98$, $p = 0.0003$, **Figure 4A**). The largest stimulus (0.5 Nm) induced the least GAIN (1.92 vs. 2.26 with 0.25 Nm and 2.81 with 0.125 Nm). In contrast, the virtual gravitational force was directly correlated with GAIN ($F = 15.7$, $p < 0.0001$, **Figure 4C**). GAIN with a gravity of 40% (4.02) was larger than the GAIN with a gravity of 20% (3.16) and the GAIN with a gravity of 10% (2.81). A larger amount of damping [10%] diminished the GAIN (3.33; vs. 2.81 with smaller damping [5%]; $F = 7.64$, $p = 0.0057$, **Figure 4D**). Virtual inertia did not affect GAIN in a significant way ($F = 2.86$, $p = 0.058$).

All parameters, except from damping ($F = 1.85$; $p = 0.1733$), significantly interacted with PHASE of the transfer function. There was no linearity between PHASE and gravity (6.64° with gravity 0.4; 32.15° with gravity 0.2 and 13.87° with gravity 0.1; $F = 5.21$, $p = 0.0055$) and inertia (16.44° with 0.0003; −4.70° with 0.00015 and 13.87 with 0.000075; $F = 3.40$, $p = 0.0184$). In contrast the largest stimulus (0.5 Nm) induced the largest PHASE (69.56°) vs. 43.56° with 0.25 Nm and 13.87° with 0.125 Nm ($F = 23.4$; $p < 0.0001$, **Figure 4E**).

When adjusting stimulus amplitude, virtual gravity, virtual damping, and virtual inertia, to optimally resemble postural reactions of free standing, we isolated a parameter set of a large stimulus amplitude, low gravity and large damping values.

Individual Perception

Subjects valued each stimulus in terms of how much it resembles free standing. A scale 0 (close resemblance), 1 (indifferent), 2 (no resemblance) was given. Both stimulus amplitude and gravity significantly influenced the perception of resemblance to free standing (stimulus amplitude: $F = 56.0$, $p < 0.0001$, gravity: $F = 31.44$, $p < 0.0001$). The smaller a stimulus the higher the resemblance to free standing (0.13 with 0 Nm, 0.23 with 0.125 Nm, 0.44 with 0.25 Nm and 0.85 with 0.5 Nm). Interactions of gravity and resemblance to free standing during virtual balancing were proportional (0.13 with 0.1 cm/s, 0.3 with 0.2 cm/s and 0.54 with 0.4 cm/s;). Damping and inertia did not influence perception to a significant degree.

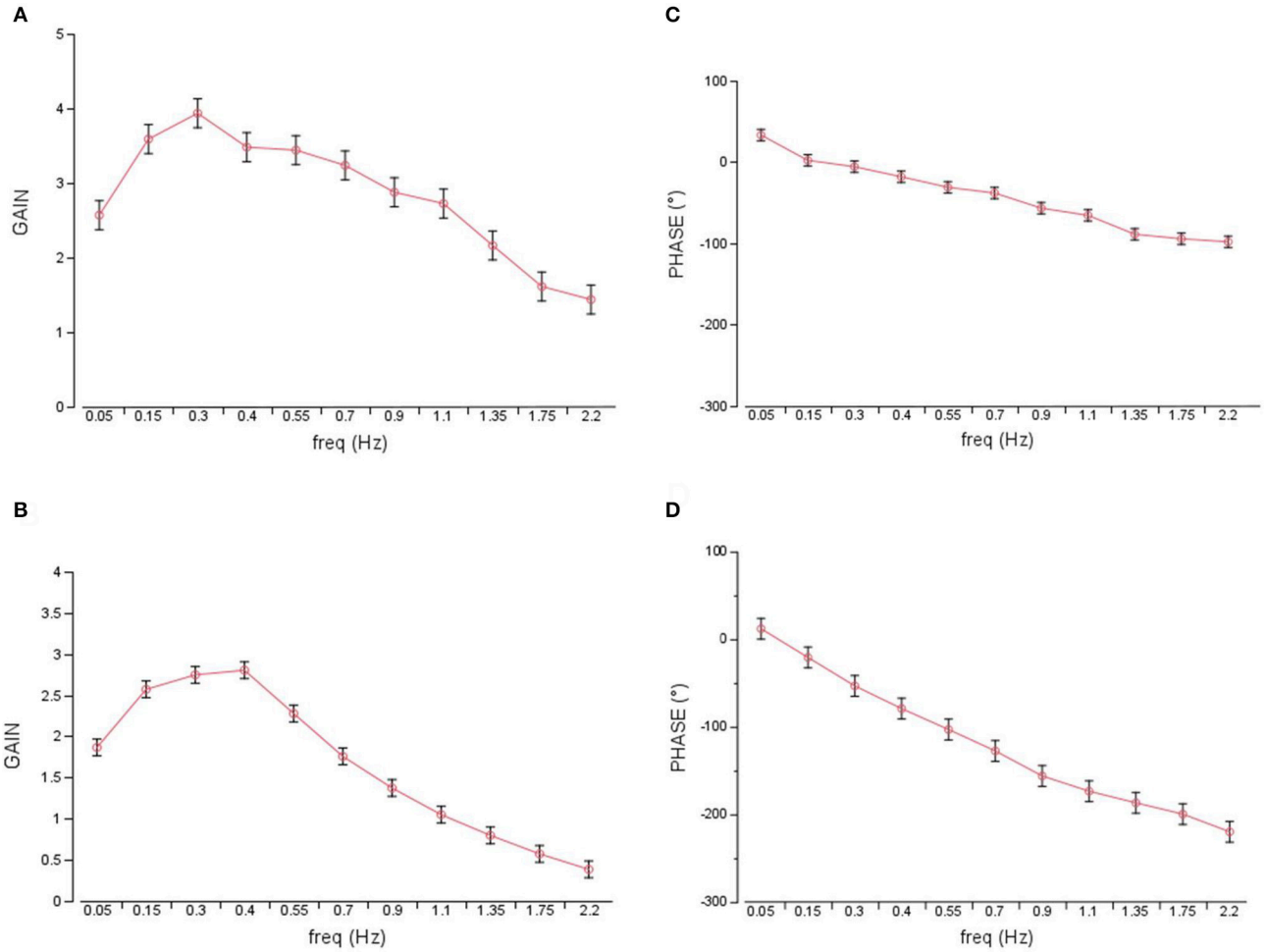

FIGURE 3 | GAIN and PHASE curves representing transfer functions of virtual balancing and free stance. GAIN during virtual balancing **(A)**, and during free stance **(B)** across all parameter settings, freq, frequency in Hz. Respective PHASE (in degree) during virtual balancing **(C)** and during free stance **(D)**.

DISCUSSION

We introduced here a virtual balancing paradigm, which calculates and delivers ankle torque in a real-time fashion. The applied torque directly depends on ankle angle position, velocity, and acceleration in a way that it resembles gravity and inertial effects of free standing. Balancing an external weight as a substitute for the own body has been evaluated before (Fitzpatrick and McCloskey, 1994; Loram and Lakie, 2002). Here, subjects did not balance themselves, or an external physical weight, but instead a virtual mass that was adapted to the biomechanical characteristics of the subjects in terms of body height and weight. By using the virtual balancing task, we were able to systematically and independently modify gravity, damping, and inertia, which are usually linked together in the real world. This enabled us to study their individual effects on postural control. Moreover, the modification of gravity, damping, and inertia may be used to train patients who are not able to stabilize their own body. First, we evaluated the effects of gravity, damping, and inertia on postural control. This will be presented in the following paragraphs. As a second aim, we compared virtual balancing to free stance to test its similarity and suitability for balance training in patients who are not able to balance their full body weight due to certain medical conditions. We will discuss that thereafter.

Spontaneous sway parameters clearly depended on virtual gravity. Sway amplitude (RMS) as well as sway velocity (MV) increased with increasing virtual gravity. These findings nicely reproduce results from Ritzmann et al. (2015), where overloading increased, and underloading decreased, postural sway amplitudes and frequencies. This was interpreted in part by a predominance of the ankle strategy as compared to hip strategy to organize postural control with increasing loads (Dietz et al., 1980). However, our experimental setup excluded any hip strategy. Any postural control effort was applied through the ankles. Another more simple explanation would relate to the positive correlation between ankle joint torques and gravity. As with any passive, spring-like stabilizing mechanism, increasing torque would lead

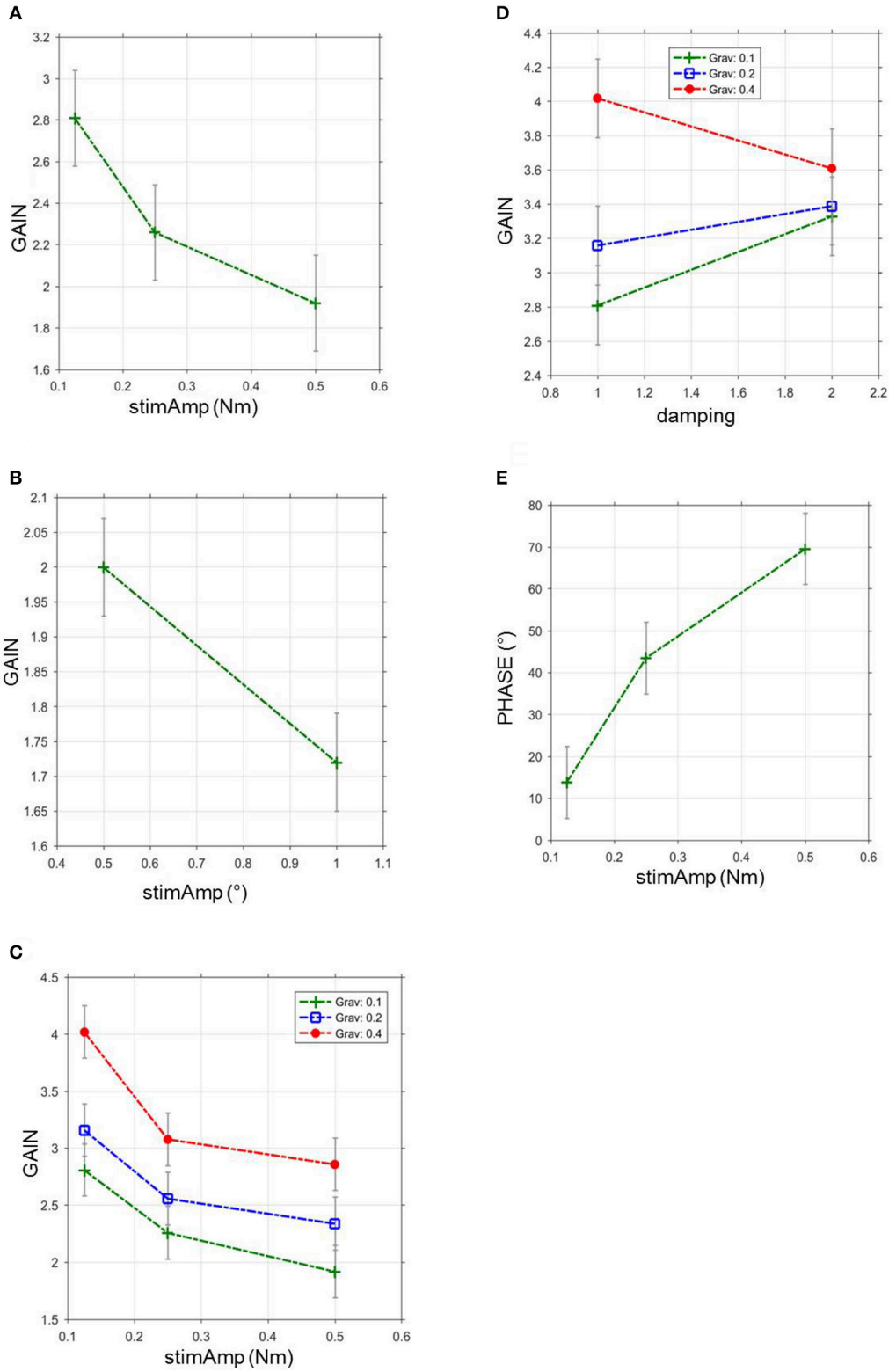

FIGURE 4 | GAIN and PHASE in relation to stimulus amplitude, gravitational force and damping during virtual balancing and free stance. **(A)** GAIN during virtual balancing as a function of stimulus amplitudes in Nm across all visual conditions and body segments, *stimAmp*, stimulus amplitude. **(B)** GAIN during free stance as a function of stimulus amplitudes in degrees across all visual conditions and body segments, *stimAmp*, stimulus amplitude. °, degree. **(C)** Influence of gravitational force and stimulus amplitude on GAIN during virtual balancing, *Grav*, gravitational force **(D)** Influence of gravitational force and damping on GAIN during virtual balancing. **(E)** Relation between stimulus amplitude and PHASE during virtual balancing.

to increasing body excursions. As a partial compensation, rapid strong reflex-induced postural reactions in distal muscles (Masani et al., 2013), and co-contraction (Bruhn et al., 2004; Hortobágyi et al., 2009; Nagai et al., 2011; Sayenko et al., 2012) may contribute to the frequency rise. Varying inertia and damping did not affect sway amplitude or velocity to a significant degree.

The relative size of postural reactions as a function of anterior-posterior platform tilts, exemplified by GAIN, positively correlated with the amount of gravity applied. This is again in line with the larger ankle torque leading to larger body excursions, as mentioned in the previous paragraph (Ritzmann et al., 2015). Damping worked as a velocity-related resistance against the movement of the foot plate. This behavior reduces excursions just like ankle rigidity would do. Consequently, increasing damping reduced GAIN. The effect of inertia on GAIN did not reach statistical significance. That may be, in part, due to the low values of the imposed inertia effect which was related to the technical feasibility. Because we technically had to feed back the second derivative (acceleration) of the platform position as a force signal, this signal contained a large degree of high frequency noise, which limited the stability of the whole platform system. Higher acceleration gains led to platform oscillations that were perceived by the subject and might have been able to bias the outcome. The stimulus size determined the GAIN in terms of a negative correlation. The larger the stimulus size the lower the relative postural reactions. This closely resembles the relationships in free standing on a moving platform (Peterka, 2002; Engelhart et al., 2014). The temporal relationship between stimulus and response as represented by PHASE, varied across stimulus conditions. However, the amount of the effects was small. Apart from the effect of stimulus amplitude, mean PHASE shifts varied between 4° and 32°. Stimulus amplitude positively correlated with PHASE with a range from 14° to 70°. This may be due to the change of postural strategy with larger stimuli, as, again, is also seen in free standing, and reported below.

In general, the virtual balance task presented here bear resemblance to free standing. Spontaneous sway measures such as sway amplitude (RMS) or sway velocity (MV) were larger in the virtual balance task. On a first look, the frequency distribution of postural reactions seemed to be similar. The similarity covers the GAIN dependency on stimulus frequency with a maximum GAIN around 0.3 Hz in both virtual balancing and free stance: With increasing frequency GAIN values decreased in both cases. Moreover, the non-linearity of postural responses as a function of stimulus size in terms of a GAIN reduction with larger stimulus sizes was similar. PHASE curves were similar in that low stimulus frequencies induced a small PHASE delay while high frequencies induced a large PHASE delay. Finally, the measure for reproducibility of the postural response, i.e., coherence, was similar.

In more detail, GAIN values of virtual balancing where larger than those of free stance and PHASE values of virtual balancing display a flattened profile as a function of frequency. Spontaneous sway and perturbed stance features of virtual balancing resemble abnormalities of vestibular loss patients (Maurer et al., 2006; Goodworth and Peterka, 2010). In fact, space cues (i.e., visual and vestibular feedback) are limited in the virtual balancing task due to the experimental setting. As the body is leaning against the backboard, the vestibular and visual systems sense zero movement, while the proprioceptive system detects the ankle angle representing the virtual body orientation. As such, vestibular and visual systems do not contribute to virtual balancing, which may impair an even closer resemblance to free standing. In future experiments, we will add visual contributions by displaying a virtual visual background according to the virtual body movements. Another limitation for the comparison between real stance and virtual balancing might have been that subjects' sway during real stance could have been affected by intermittent touch of the safety ropes which, in principle, have the potential to reduce sway as an additional space reference (Wing et al., 2011). Therefore, we aimed to avoid in our experimental setup that ropes ever touch the subject. The ropes, which served as a replacement for a body harness, were fixed to the ceiling at about 30 cm in forward direction with respect to the foot position of the subjects. We monitored the subjects during the experiments and touch did not occur.

When comparing our results during unperturbed and perturbed free stance to own earlier studies and to the literature (Prieto et al., 1996; Peterka, 2002; Maurer and Peterka, 2005; Maurer et al., 2006; Goodworth and Peterka, 2010; van der Kooij and Peterka, 2011; Engelhart et al., 2014; Wiesmeier et al., 2015) we did not find any major differences.

When adjusting the parameters of virtual balancing, i.e., stimulus amplitude, virtual gravity, virtual damping, and virtual inertia, to optimally resemble transfer functions of postural reactions of free standing, we found a large stimulus amplitude, low gravity and large damping values. However, our subjects felt maximal resemblance between virtual balancing and free standing at low stimulus amplitude, low gravity, and without any damping and inertia.

This discrepancy may, again, point to additional differences in the experimental settings of virtual vs. free balancing. During virtual balancing, subjects did not move their own body. Possible postural reactions were confined to the ankle joint. Even if the major postural reactions originate from the ankle joint in free standing, (Horak et al., 1989), the hip joint usually contributes to postural reactions, especially in the high frequency range. The virtual balancing task may, therefore, still elicit certain changes in the balancing strategy. Moreover, discrepancies between virtual balancing and free standing might be explained by the absence of space cues (see above).

Patients' benefit of virtual balancing may rely on the potentially increased mobility in a reduced gravity environment. Moreover, balancing could be trained without the threat to fall. Patient groups, who may benefit from such training, may include those who are not able to support their complete body weight like, e.g., hemiparetic/paraparetic patients or patients suffering from axial fractures. In this study we were able to show the feasibility of a virtual balancing paradigm. In a future version, the apparatus could be integrated into boots and may act as an exoskeleton around the ankle angle. The main purpose of such a training prosthesis is to rehearse balance, which is the major prerequisite for free walking. Further studies are needed to show

that practicing virtual balance affects free stance, and to evaluate which patients may benefit from such a training.

AUTHOR CONTRIBUTIONS

DB was responsible for data acquisition, analysis, and interpretation and contributed to writing the first draft. DD contributed to the conception of the work, to data analysis, and interpretation. IW contributed to data interpretation, drafted and edited the final manuscript for submission and revised the work critically. CM was responsible for the conception of the work, for data analysis and interpretation and wrote the first draft. All authors approved the final manuscript.

FUNDING

This work was supported by a European Union FP7 grant (EMBALANCE: Grant Agreement no 610454) and the Brainlinks-Braintools Cluster of Excellence funded by the German Research foundation (DFG, grant no ADV139).

REFERENCES

Ali, A. A., and Sabbahi, M. A. (2000). H-reflex changes under spinal loading and unloading conditions in normal subjects. *Clin. Neurophysiol.* 111, 664–670. doi: 10.1016/S1388-2457(99)00304-1

Avela, J., Santos, P. M., Kyröläinen, H., and Komi, P. V. (1994). Effects of different simulated gravity conditions on neuromuscular control in drop jump exercises. *Aviat. Space Environ. Med.* 65, 301–308.

Bloomberg, J. J., Peters, B. T., Smith, S. L., Huebner, W. P., and Reschke, M. F. (1997). Locomotor head-trunk coordination strategies following space flight. *J. Vestib. Res. Equilib. Orientat.* 7, 161–177. doi: 10.1016/S0957-4271(96)00169-3

Bruhn, S., Kullmann, N., and Gollhofer, A. (2004). The effects of a sensorimotor training and a strength training on postural stabilisation, maximum isometric contraction and jump performance. *Int. J. Sports Med.* 25, 56–60. doi: 10.1055/s-2003-45228

Davidson, B. S., Madigan, M. L., Southward, S. C., and Nussbaum, M. A. (2011). Neural control of posture during small magnitude perturbations: effects of aging and localized muscle fatigue. *IEEE Trans. Biomed. Eng.* 58, 1546–1554. doi: 10.1109/TBME.2010.2095500

di Prampero, P. E., and Narici, M. V. (2003). Muscles in microgravity: from fibres to human motion. *J. Biomech.* 36, 403–412. doi: 10.1016/S0021-9290(02)00418-9

Dichgans, J., Mauritz, K. H., Allum, J. H., and Brandt, T. (1976). Postural sway in normals and atactic patients: analysis of the stabilising and destabilizing effects of vision. *Agressol. Rev. Int. Physio-Biol. Pharmacol. Appl. Aux. Eff. Agres.* 17, 15–24.

Dietz, V., Mauritz, K. H., and Dichgans, J. (1980). Body oscillations in balancing due to segmental stretch reflex activity. *Exp. Brain Res.* 40, 89–95. doi: 10.1007/BF00236666

Dietz, V., Horstmann, G. A., Trippel, M., and Gollhofer, A. (1989). Human postural reflexes and gravity–an under water simulation. *Neurosci. Lett.* 106, 350–355. doi: 10.1016/0304-3940(89)90189-4

Engelhart, D., Pasma, J. H., Schouten, A. C., Meskers, C. G. M., Maier, A. B., Mergner, T., et al. (2014). Impaired standing balance in elderly: a new engineering method helps to unravel causes and effects. *J. Am. Med. Dir. Assoc.* 15, 227.e1–227.e6. doi: 10.1016/j.jamda.2013.09.009

Fitzpatrick, R., and McCloskey, D. I. (1994). Proprioceptive, visual and vestibular thresholds for the perception of sway during standing in humans. *J. Physiol.* 478(Pt 1), 173–186. doi: 10.1113/jphysiol.1994.sp020240

Fitzpatrick, R. C., Taylor, J. L., and McCloskey, D. I. (1992). Ankle stiffness of standing humans in response to imperceptible perturbation: reflex and task-dependent components. *J. Physiol.* 454, 533–547. doi: 10.1113/jphysiol.1992.sp019278

Freyler, K., Weltin, E., Gollhofer, A., and Ritzmann, R. (2014). Improved postural control in response to a 4-week balance training with partially unloaded bodyweight. *Gait Posture* 40, 291–296. doi: 10.1016/j.gaitpost.2014.04.186

Goodworth, A. D., and Peterka, R. J. (2010). Influence of bilateral vestibular loss on spinal stabilization in humans. *J. Neurophysiol.* 103, 1978–1987. doi: 10.1152/jn.01064.2009

Horak, F. B., Shupert, C. L., and Mirka, A. (1989). Components of postural dyscontrol in the elderly: a review. *Neurobiol. Aging* 10, 727–738. doi: 10.1016/0197-4580(89)90010-9

Hortobágyi, T., Solnik, S., Gruber, A., Rider, P., Steinweg, K., Helseth, J., et al. (2009). Interaction between age and gait velocity in the amplitude and timing of antagonist muscle coactivation. *Gait Posture* 29, 558–564. doi: 10.1016/j.gaitpost.2008.12.007

Hwang, S., Jeon, H. S., Kwon, O. Y., and Yi, C. H. (2011). The effects of body weight on the soleus H-reflex modulation during standing. *J. Electromyogr. Kinesiol.* 21, 445–449. doi: 10.1016/j.jelekin.2010.11.002

Layne, C. S., Mulavara, A. P., McDonald, P. V., Pruett, C. J., Kozlovskaya, I. B., and Bloomberg, J. J. (2001). Effect of long-duration spaceflight on postural control during self-generated perturbations. *J. Appl. Physiol. Bethesda Md 1985* 90, 997–1006.

Lestienne, F., Berthoz, A., Mascot, J. C., and Koitcheva, V. (1976). Effets posturaux induits par une scène visuelle en mouvement linéaire. *Agressologie* 17, 37–46.

Lockhart, D. B., and Ting, L. H. (2007). Optimal sensorimotor transformations for balance. *Nat. Neurosci.* 10, 1329–1336. doi: 10.1038/nn1986

Loomer, P. M. (2001). The impact of microgravity on bone metabolism *in vitro* and *in vivo*. *Crit. Rev. Oral Biol.* 12, 252–261. doi: 10.1177/10454411010120030401

Loram, I. D., and Lakie, M. (2002). Human balancing of an inverted pendulum: position control by small, ballistic-like, throw and catch movements. *J. Physiol.* 540, 1111–1124. doi: 10.1113/jphysiol.2001.013077

Masani, K., Vette, A. H., and Popovic, M. R. (2006). Controlling balance during quiet standing: proportional and derivative controller generates preceding motor command to body sway position observed in experiments. *Gait Posture* 23, 164–172. doi: 10.1016/j.gaitpost.2005.01.006

Masani, K., Sayenko, D. G., and Vette, A. H. (2013). What triggers the continuous muscle activity during upright standing? *Gait Posture* 37, 72–77. doi: 10.1016/j.gaitpost.2012.06.006

Maurer, C., and Peterka, R. J. (2005). A new interpretation of spontaneous sway measures based on a simple model of human postural control. *J. Neurophysiol.* 93, 189–200. doi: 10.1152/jn.00221.2004

Maurer, C., Mergner, T., and Peterka, R. J. (2006). Multisensory control of human upright stance. *Exp. Brain Res.* 171, 231–250. doi: 10.1007/s00221-005-0256-y

Mergner, T., and Rosemeier, T. (1998). Interaction of vestibular, somatosensory and visual signals for postural control and motion perception under terrestrial and microgravity conditions–a conceptual model. *Brain Res. Brain Res. Rev.* 28, 118–135. doi: 10.1016/S0165-0173(98)00032-0

Miyoshi, T., Nozaki, D., Sekiguchi, H., Kimura, T., Sato, T., Komeda, T., et al. (2003). Somatosensory graviception inhibits soleus H-reflex during erect posture in humans as revealed by parabolic flight experiment. *Exp. Brain Res.* 150, 109–113. doi: 10.1007/s00221-003-1414-8

Nagai, K., Yamada, M., Uemura, K., Yamada, Y., Ichihashi, N., and Tsuboyama, T. (2011). Differences in muscle coactivation during postural control between healthy older and young adults. *Arch. Gerontol. Geriatr.* 53, 338–343. doi: 10.1016/j.archger.2011.01.003

Nakazawa, K., Miyoshi, T., Sekiguchi, H., Nozaki, D., Akai, M., and Yano, H. (2004). Effects of loading and unloading of lower limb joints on the soleus H-reflex in standing humans. *Clin. Neurophysiol.* 115, 1296–1304. doi: 10.1016/j.clinph.2004.01.016

Nashner, L., and Berthoz, A. (1978). Visual contribution to rapid motor responses during postural control. *Brain Res.* 150, 403–407. doi: 10.1016/0006-8993(78)90291-3

Nishihori, T., Aoki, M., Jiang, Y., Nagasaki, S., Furuta, Y., and Ito, Y. (2012). Effects of aging on lateral stability in quiet stance. *Aging Clin. Exp. Res.* 24, 162–170. doi: 10.3275/7626

Nomura, T., Kawano, F., Ishihara, A., Sato, Y., Mitarai, G., Iwase, S., et al. (2001). Enhanced Hoffman-reflex in human soleus muscle during exposure to microgravity environment. *Neurosci. Lett.* 316, 55–57. doi: 10.1016/S0304-3940(01)02367-9

Paloski, W. H., Black, F. O., Reschke, M. F., Calkins, D. S., and Shupert, C. (1993). Vestibular ataxia following shuttle flights: effects of microgravity on otolith-mediated sensorimotor control of posture. *Am. J. Otol.* 14, 9–17.

Pasma, J. H., Engelhart, D., Schouten, A. C., van der Kooij, H., Maier, A. B., and Meskers, C. G. M. (2014). Impaired standing balance: the clinical need for closing the loop. *Neuroscience* 267, 157–165. doi: 10.1016/j.neuroscience.2014.02.030

Peterka, R. J. (2002). Sensorimotor integration in human postural control. *J. Neurophysiol.* 88, 1097–1118. doi: 10.1152/jn.00605.2001

Phadke, C. P., Wu, S. S., Thompson, F. J., and Behrman, A. L. (2006). Soleus H-reflex modulation in response to change in percentage of leg loading in standing after incomplete spinal cord injury. *Neurosci. Lett.* 403, 6–10. doi: 10.1016/j.neulet.2006.04.058

Pöyhönen, T., and Avela, J. (2002). Effect of head-out water immersion on neuromuscular function of the plantarflexor muscles. *Aviat. Space Environ. Med.* 73, 1215–1218.

Prieto, T. E., Myklebust, J. B., Hoffmann, R. G., Lovett, E. G., and Myklebust, B. M. (1996). Measures of postural steadiness: differences between healthy young and elderly adults. *IEEE Trans. Biomed. Eng.* 43, 956–966. doi: 10.1109/10.532130

Qu, X., Nussbaum, M. A., and Madigan, M. L. (2009). Model-based assessments of the effects of age and ankle fatigue on the control of upright posture in humans. *Gait Posture* 30, 518–522. doi: 10.1016/j.gaitpost.2009.07.127

Ritzmann, R., Freyler, K., Weltin, E., Krause, A., and Gollhofer, A. (2015). Load dependency of postural control–Kinematic and neuromuscular changes in response to over and under load Conditions. *PLoS ONE* 10:e0128400. doi: 10.1371/journal.pone.0128400

Sayenko, D. G., Masani, K., Vette, A. H., Alekhina, M. I., Popovic, M. R., and Nakazawa, K. (2012). Effects of balance training with visual feedback during mechanically unperturbed standing on postural corrective responses. *Gait Posture* 35, 339–344. doi: 10.1016/j.gaitpost.2011.10.005

van der Kooij, H., and Peterka, R. J. (2011). Non-linear stimulus-response behavior of the human stance control system is predicted by optimization of a system with sensory and motor noise. *J. Comput. Neurosci.* 30, 759–778. doi: 10.1007/s10827-010-0291-y

Vette, A. H., Masani, K., Nakazawa, K., and Popovic, M. R. (2010). Neural-mechanical feedback control scheme generates physiological ankle torque fluctuation during quiet stance. *IEEE Trans. Neural Syst. Rehabil. Eng. Publ. IEEE Eng. Med. Biol. Soc.* 18, 86–95. doi: 10.1109/TNSRE.2009.2037891

Welch, T. D., and Ting, L. H. (2009). A feedback model explains the differential scaling of human postural responses to perturbation acceleration and velocity. *J. Neurophysiol.* 101, 3294–3309. doi: 10.1152/jn.90775.2008

Wiesmeier, I. K., Dalin, D., and Maurer, C. (2015). Elderly use proprioception rather than visual and vestibular cues for postural motor control. *Front. Aging Neurosci.* 7:97. doi: 10.3389/fnagi.2015.00097

Wing, A. M., Johannsen, L., and Endo, S. (2011). Light touch for balance: influence of a time-varying external driving signal. *Philos. Trans. R. Soc. Lond. B Biol. Sci.* 366, 3133–3141. doi: 10.1098/rstb.2011.0169

Winter, D. (1995). Human balance and posture control during standing and walking. *Gait Posture* 3, 193–214. doi: 10.1016/0966-6362(96)82849-9

Conflict of Interest Statement: The authors declare that the research was conducted in the absence of any commercial or financial relationships that could be construed as a potential conflict of interest.

frontiers in Neuroscience

ORIGINAL RESEARCH
published: 21 November 2017
doi: 10.3389/fnins.2017.00649

Voluntary Ambulation by Upper Limb-Triggered HAL® in Patients with Complete Quadri/Paraplegia Due to Chronic Spinal Cord Injury

Yukiyo Shimizu[1], Hideki Kadone[2], Shigeki Kubota[3], Kenji Suzuki[4], Tetsuya Abe[5], Tomoyuki Ueno[1], Yuichiro Soma[1], Yoshiyuki Sankai[4], Yasushi Hada[1] and Masashi Yamazaki[5]*

[1] Department of Rehabilitation Medicine, University of Tsukuba Hospital, Tsukuba, Japan, [2] Center for Innovative Medicine and Engineering, University of Tsukuba Hospital, Tsukuba, Japan, [3] Division of Regenerative Medicine for Musculoskeletal System, Faculty of Medicine, University of Tsukuba, Tsukuba, Japan, [4] Center for Cybernics Research, University of Tsukuba, Tsukuba, Japan, [5] Department of Orthopaedic Surgery, Faculty of Medicine, University of Tsukuba, Tsukuba, Japan

Patients with complete paraplegia after spinal cord injury (SCI) are unable to stand or walk on their own. Standing exercise decreases the risk of decubitus ulcers, osteoporosis, and joint deformities in patients with SCI. Conventional gait training for complete paraplegia requires excessive upper limb usage for weight bearing and is difficult in cases of complete quadriplegia. The purpose of this study was to describe voluntary ambulation triggered by upper limb activity using the Hybrid Assistive Limb® (HAL) in patients with complete quadri/paraplegia after chronic SCI. Four patients (3 men, 1 woman) were enrolled in this study. The mean patient age ± standard deviation was 37.2 ± 17.8 (range, 20–67) years. Clinical evaluation before intervention revealed the following findings: case 1, neurological level C6, American Spinal Cord Injury Association impairment scale (AIS) grade B; case 2, T6, AIS A; case 3, T10 AIS A; and case 4, T11, AIS A. The HAL intervention consisted of 10 sessions. Each HAL session lasted 60–90 min. The HAL electrodes for hip and knee flexion-extension were placed on the anterior and posterior sides of the upper limbs contralaterally corresponding to each of the lower limbs. Surface electromyography (EMG) was used to evaluate muscle activity of the tensor fascia lata and quadriceps femoris (Quad) in synchronization with a Vicon motion capture system. The modified Ashworth scale (mAs) score was also evaluated before and after each session. All participants completed all 10 sessions. Cases 1, 2, and 3 demonstrated significant decreases in mAs score after the sessions compared to pre-session measurements. In all cases, EMG before the intervention showed no apparent activation in either Quad. However, gait phase dependent activity of the lower limb muscles was seen during voluntarily triggered ambulation driven by upper limb muscle activities. In cases 3 and 4, active contraction in both Quads was observed after intervention. These findings suggest that upper-limb-triggered HAL ambulation is a safe and feasible option for rehabilitation in patients with complete quadri/paraplegia caused by chronic SCI.

Keywords: chronic spinal cord injury, complete quadriplegia or paraplegia, gait analysis, rehabilitation, upper and lower limb coordination, hybrid Assistive Limb®

OPEN ACCESS

Edited by:
Yury Ivanenko, Fondazione Santa Lucia (IRCCS), Italy

Reviewed by:
Valentina La Scaleia, Università Tor Vergata Roma, Italy
Michael James MacLellan, Louisiana State University, United States

****Correspondence:***
Yukiyo Shimizu
shimiyukig@md.tsukuba.ac.jp

Specialty section:
This article was submitted to Neuroprosthetics, a section of the journal Frontiers in Neuroscience

Received: *31 August 2017*
Accepted: *08 November 2017*
Published: *21 November 2017*

Citation:
Shimizu Y, Kadone H, Kubota S, Suzuki K, Abe T, Ueno T, Soma Y, Sankai Y, Hada Y and Yamazaki M (2017) Voluntary Ambulation by Upper Limb-Triggered HAL® in Patients with Complete Quadri/Paraplegia Due to Chronic Spinal Cord Injury. Front. Neurosci. 11:649. doi: 10.3389/fnins.2017.00649

INTRODUCTION

Patients with complete paraplegia after spinal cord injury (SCI) are unable to stand or walk on their own. Standing exercise for patients with SCI decreases decubitus ulcers, osteoporosis, hip joint flexion, and adduction deformities and improves the performance of the cardiovascular and digestive systems (Karimi, 2011). Conventional gait training using orthoses for complete paraplegia requires locking of the knee joint in an extended position as well as excessive upper limb usage for weight bearing (Karimi, 2011), and it is difficult in cases of complete quadriplegia.

Robotic devices have recently been used in clinical settings for patients with chronic SCI. Exoskeleton robotic devices employed with a treadmill, such as the Lokomat (Hocoma, Switzerland) (Colombo et al., 2000) and LOPES (Veneman et al., 2007) and powered exoskeleton devices, such as the ReWalk (Robotics, Israel) (Miller et al., 2016), have angular sensors in the joints and pelvis as well as foot force pressure sensors. However, they have no sensors to detect the neuromuscular activation of the user.

In sensing a user's neuromuscular activation, our research has focused on another exoskeleton robot, the Hybrid Assistive Limb® (HAL, Cyberdyne Inc., Ibaraki, Japan). HAL is a wearable robot suit that assists the user in voluntary control of knee and hip joint motion by detecting signals from force/pressure sensors in the shoes or even very weak bioelectric signals on the skin surface. Power units on the bilateral hip and knee joints are comprised of angular sensors and actuators, and the control system consists of a cybernic voluntary control (CVC) mode, cybernic autonomous control (CAC) subsystem (Kawamoto and Sankai, 2005), and cybernic impedance control (CIC) mode. The HAL suit has a unique operating system, with a hybrid control system that includes the CVC, CAC, and CIC modes. The CAC mode can automatically move a user's leg using signals from the force-pressure sensors (Ikumi et al., 2017). The CVC mode can support the user's voluntary motion by providing assistive torque to each joint according to their voluntary muscle activity. The CIC mode can adjust to the user's motion while compensating for HAL's weight and joint viscosity.

Gait training with the HAL has been reported to improve gait ability in patients with chronic stroke (Kawamoto et al., 2013; Nilsson et al., 2014; Wall et al., 2015), chronic SCI (Aach et al., 2014; Sczesny-Kaiser et al., 2015; Wall et al., 2015; Ikumi et al., 2017; Shimizu et al., 2017b), and postoperative thoracic ossification of the posterior longitudinal ligament (Sakakima et al., 2013; Kubota et al., 2016, 2017; Fujii et al., 2017) in terms of gait speed, step length, and clinical functional evaluation.

We previously evaluated the application of HAL for single joints in a patient with complete C4 quadriplegia in order to restore elbow joint flexion using residual trapezius muscle activation. We found that the use of HAL that associated the residual muscle contraction to the elbow joint movement might activate the paralyzed muscle (Shimizu et al., 2017a).

We focused on remaining muscle activity in the upper limb in complete paraplegia. Previous studies have reported neural coupling of the upper and lower limbs in humans (Zehr and Duysens, 2004; Dietz, 2011; La Scaleia et al., 2014; Sylos-Labini et al., 2014). Arm-leg coordination was reported to be useful for gait assistive technology (Hassan et al., 2014; La Scaleia et al., 2014). Therefore, we concentrated on the structural analogy and symmetric motion of the shoulder and hip during gait. The lower extremities move synchronously and almost simultaneously with the contralateral upper extremities during natural locomotion. As we flex a shoulder, the contralateral hip flexes; and at the same time the other shoulder extends, with contralateral hip extension.

We hypothesized that triggering lower limb motion by upper limb muscle activity using HAL was feasible for the voluntary generation of gait composed of voluntarily driven hip and knee joint motions, in people with chronic SCI leading to complete paraplegia or quadriplegia with residual control over upper limb movement. In addition, we hypothesized that simulating the synergy of the upper and contralateral lower limbs in voluntary gait during HAL intervention may activate paralyzed lower limb muscles.

Here, we describe the feasibility and effects of upper limb-triggered HAL intervention for patients with complete paraplegia or quadriplegia caused by chronic SCI.

MATERIALS AND METHODS

Participants

Four patients (3 men, 1 woman) were enrolled in this study. The mean patient age ± standard deviation was 37.2 ± 17.8 (range, 20–67) years. Clinical evaluation before the intervention revealed the following findings: case 1, neurological level C6, American Spinal Cord Injury Association (ASIA) impairment scale (AIS) (Kirshblum et al., 2011) grade B; case 2, T6, AIS A; case 3, T10, AIS A; and case 4, T11, AIS A. International Standards for Neurological and Functional Classification of Spinal Cord Injury (ISNCSCI) lower extremity motor score (LEMS) was 0 in cases 1, 2, and 3, and 2 in case 4. Participants' clinical data are shown in **Table 1**.

This study was conducted in accordance with the Declaration of Helsinki, with approval from the Ethics Committee of the Tsukuba University Faculty of Medicine (approval no.: H26-22). All participants provided written informed consent for participation and publication, including the use of accompanying images.

HAL Intervention

Participants underwent 10 HAL sessions. The frequency of sessions ranged from 2 per week to 1–2 per month. Intervention for cases 1, 3, and 4 was performed on an outpatient basis, and no additional therapies were implemented during HAL intervention. In case 2, HAL intervention was performed as part of an inpatient stay at our hospital in addition to standard physical therapy. Before the intervention, active hip flexion and active knee extension were evaluated using a Trigno™ Lab Wireless electromyography (EMG) system (Delsys Inc., Boston, MA, USA).

Upper Limb-Triggered HAL (UT-HAL)

We designed the HAL intervention based on patients' residual muscle activity. The primary goal of HAL intervention was

TABLE 1 | Patient characteristics.

Case	1	2	3	4
Sex	Male	Male	Female	Male
Age	20	67	32	30
Reason for SCI	C3/4 fracture-dislocation	T5/6 Pyogenic Spondylitis	Spinal cord infarction	T12 burst fracture
Post injured period	3y 2 m	2y 3 m	6y 3 m	1y 9 m
AIS	C6 B	T6 A	T10 A	T11 A
Type of paralysis	Spastic	Spastic	Spastic	Flaccid
ISNCSCI UEMS	24	50	50	50
ISNCSCI LEMS	0	0	0	3
History of other gait training	None	None	Long leg brace	Long leg brace
Frequency	1 to 2/month	2/week	1 to 2/month	2/week

to achieve voluntary gait using voluntary activation of upper limb motion with the HAL system. On the basis of several previous studies on upper and lower limb coordination in human locomotion (Zehr and Duysens, 2004; Dietz, 2011; La Scaleia et al., 2014; Sylos-Labini et al., 2014), voluntary ambulation with HAL using upper limb activation involved motion intention from the anterior deltoid and posterior deltoid for contralateral hip flexion and extension, respectively, and motion intention from the biceps and triceps brachii for contralateral knee flexion and extension, respectively. We referred to the upper limb-triggered HAL session as the "UT-HAL" method (**Figure 1**).

The electric motors for the hip and knee joints are controlled in real-time to generate joint torque computed as a weighted difference of the activation of the flexor and extensor muscles. In equation, Thip=Gda*Ada-Gdp*Adp and Tknee=Gb*Ab-Gt*At are, respectively, the hip and knee joint torques generated by the motors, where Gda, Gdp, Gb, and Gt are the gain, and Ada, Adp, Ab, and At are the filtered activation of the anterior deltoid, posterior deltoid, biceps, and triceps muscles, respectively. Gda, Gdp, Gb, and Gt are adjusted for the user's comfort.

Knee Extension HAL

The secondary goal of HAL intervention was to regain active knee extension. In patients who were able to flex their hips, a second component was added to each HAL session. In addition to the first component, which involved voluntary gait using the patient's upper limb activation, the second component involved active knee extension using hip flexor activation, focusing on the hip flexor as the site of remaining muscle activation in patients who could not contract the knee extensors.

HAL Session

A typical HAL session lasted 60–90 min, including the time required to attach and detach the device (20 min). The gait session was ∼40 min, including a 10-min period of rest. The knee extension session lasted about 30 min including evaluation (10 min) of muscle activity during five repetitions of each of the following motions: active hip flexion; active knee extension; and active combined hip flexion and knee extension, such as in a kicking motion, before and after each HAL session.

A physiatrist was present in case of an emergency, a therapist and two assistants attached and detached the HAL, and an engineer implemented the gait analysis. For safety reasons, a walking device (All-in-One Walking Trainer, Ropox A/S, Naestved, Denmark) with a harness was used to prevent falls.

For participants without a history of ambulation training (cases 1 and 2), we initially used the CAC and CIC mode along with heavy assistance of three therapists, and as they became accustomed to ambulation training, upper limb-triggered methods were introduced.

Assessments

Assessments were performed before the intervention and during each HAL session. A surface EMG system was used to evaluate the muscle activity of the tensor fasciae lata (TFL) for hip flexion and the femoral quadriceps (Quad) for knee extension on both sides. We chose the TFL for the evaluation of hip flexion because the main hip flexor, the iliopsoas muscle, is located in the deep layer and thus is difficult to detect by surface EMG. We chose the vastus lateralis in the Quad because it is a simple knee extensor. The activity of each muscle was evaluated using EMG collected at 2,000 Hz and filtered with a 30- to 400-Hz band-pass filter using scripts on MATLAB 8.2 (Mathworks, Natick, MA, USA). Motion capture (Vicon MX with 16 T20S cameras, Vicon, Oxford, UK) was used to evaluate foot motion in synchronization with EMG. Following the Vicon plug-in gait marker set, auto-reflective markers were placed bilaterally on the feet, head of the second metatarsal bone of the toe, lateral malleolus of the ankle, and posterior peak of the calcaneus of the heel. The swing phase and stance phase within a gait cycle were extracted according to the movement trajectory of the markers. Heel strikes were detected as the lower peaks of the height of the heel markers, and toe lifts were detected as the lower peaks of the toe markers. The swing phase started with a toe lift and ended with the subsequent heel strike on the same side. The stance phase started with a heel strike and ended with the subsequent toe lift (Ivanenko et al., 2007).

We also evaluated the walking distance and bilateral modified Ashworth scale (mAs) score (range: 0–24; hip abduction, knee

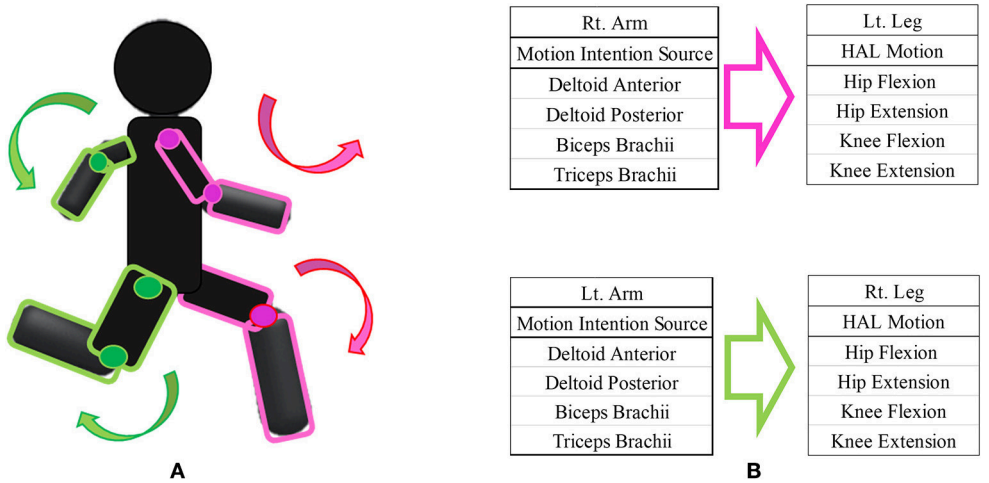

FIGURE 1 | Upper limb-triggered HAL (UT-HAL) method. **(A)** Schema of UT-HAL. **(B)** Picture of patient 1. Muscle activities from the anterior and posterior deltoid for contralateral hip flexion and extension and activities from the biceps and triceps brachii were used for contralateral knee flexion and extension. **(B-1)** Left leg flexion triggered by right arm flexion. **(B-2)** Right leg flexion triggered by left arm flexion.

extension, and ankle dorsiflexion; Bohannon and Smith, 1987) before and after each HAL session. The mAs scores before and after each HAL session were compared with the Wilcoxon signed-rank test. All analyses were performed using JMP® 10.0.2 (SAS Institute Inc., Cary, NC, USA); $P < 0.05$ were considered significant. Any adverse events associated with HAL intervention were also recorded.

RESULTS

All participants completed all 10 sessions. The only observed adverse event was redness caused by contact between the skin and harness in cases 1, 2, and 3 which was avoidable by using a cushion. **Figure 2** shows the walking distance in all cases; improvement was observed in cases 3 and 4 as the HAL intervention progressed. The decrease of the mAs score was statistically significant from before to after session; the each post-session mAs score decreased significantly compared to the pre-session mAs score in case 1 (from 9.9 ± 1.5 to 5.1 ± 2.2; $P = 0.004$), case 2 (from 15.3 ± 1.6 to 9.1 ± 2.5; $P = 0.029$), and case 3 (from 7.0 ± 1.2 to 6.2 ± 0.8; $P = 0.063$; **Figure 3**). In cases 1, 2, and 3, activation was observed in both Quads in the stance phase (**Figures 4–6**), which became more apparent as the sessions progressed. However, in all cases, surface EMG before the intervention showed no apparent activation in either Quad (refer to **Figures 6**, **7** for cases 3 and 4). In these graphs, we chose sessions that were representative of the progression of each subject throughout the UT-HAL sessions.

In cases 3 and 4, knee extension sessions were performed using the hip flexor as the trigger of knee extension. In both cases, active contraction in both Quads was observed after intervention. **Table 2** shows the neurological findings in all cases after intervention.

CASE DESCRIPTIONS

Case 1 (Figure 1B)

A 20-year-old male with complete quadriplegia and chronic cervical SCI due to cervical vertebral dislocation (C5/6) underwent HAL intervention with a total of 10 sessions, 1–2 per month, beginning 3 years and 2 months post-injury. He had the ability to perform daily activities independently with the help of a wheelchair, including transfer from/to the wheelchair and intermittent self-catheterization. Before intervention, manual muscle test (MMT) of the upper limb muscles was 5/5 for both deltoids, 5/5 for both biceps brachii, 2/2 for both triceps brachii, and 1/1 for both wrist flexor muscles. The muscle strength of his elbow extensors and wrist flexors had shown recovery; however, his lower limbs had remained in complete paraplegia. AIS was C6 B, ISNCSCI upper extremity motor score (UEMS) was 26/50, and LEMS was 0/50.

On evaluation before HAL intervention, there was no muscle activation in either TFL or Quad. As the patient had no history of ambulation training, in order to become accustomed to ambulation training, he started HAL sessions using CAC or CIC mode accompanied by heavy assistance from three therapists with an overhead harness. Activation in both Quads was observed in the stance phase from the first session. From the latter half of the fifth session, his upper limb was used as a trigger for lower limb movement, and activation became more apparent in the UT-HAL session than in previous sessions. **Figure 4A** shows surface EMG during the fifth session using CAC mode. There was some activation in both Quads, but no periodic activation in the right Quad. More periodic activation, from the end of swing phase to early stance phase, was observed during UT-HAL gait in the same fifth session (**Figure 4B**). More apparent activation was present in the sixth session, predominantly on the right side (**Figure 4C**).

Walking distance increased from 73.4 m (first session) to 200 m (tenth session; **Figure 2**). The mAs score decreased after

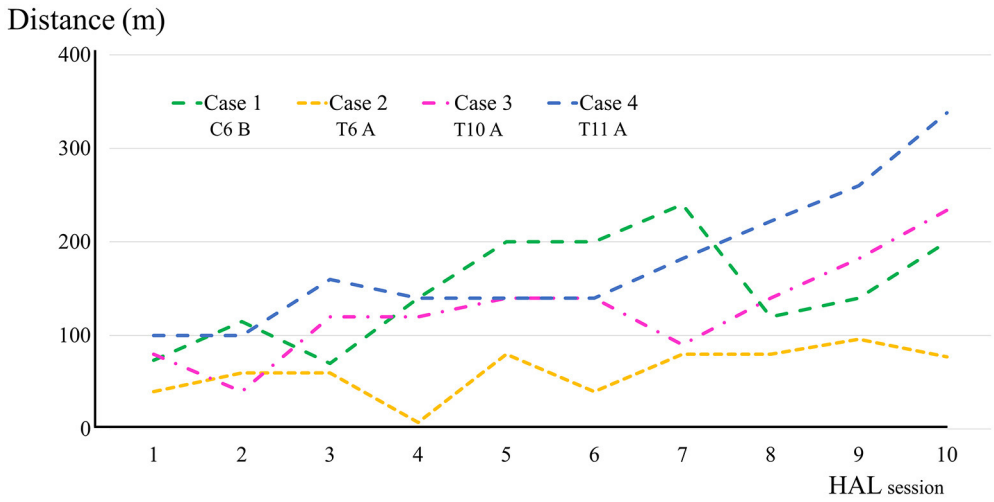

FIGURE 2 | Walking distance in each HAL session in cases 1–4.

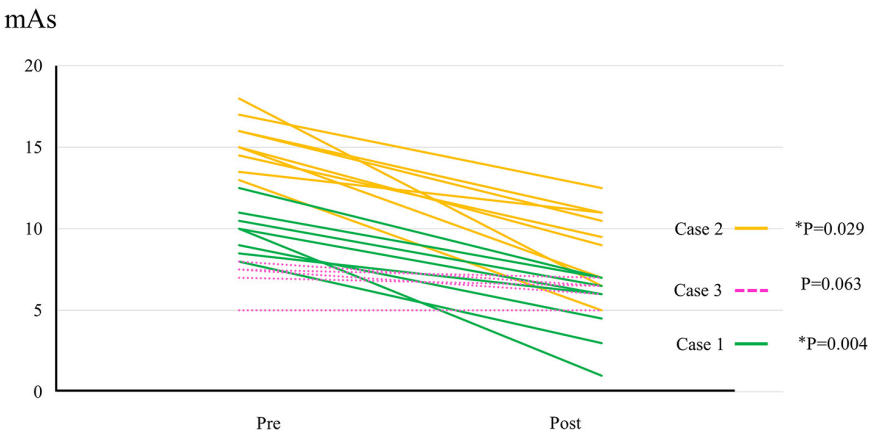

FIGURE 3 | The change of mAs score in cases 1–3. Data evaluated by the same examiner were available from 8 sessions in case 1, 9 sessions in case 2, and 5 sessions in case 3.

each HAL session compared to pre-session measurements; the mean scores before and after the sessions were 9.9 ± 1.5 and 5.1 ± 2.2, respectively ($P = 0.004$; **Figure 3**).

Case 2

A 67-year-old male with complete paraplegia and chronic SCI underwent HAL intervention 2 years and 3 months after the onset of complete paralysis caused by pyogenic spondylitis in the fifth and sixth thoracic vertebrae. He was admitted to our hospital to undergo HAL intervention. His main complaint was spasticity. The mAs scores on admission were as follows: total, 16; hip abduction, 3/2; knee extension, 3/2; and ankle dorsiflexion, 3/3; for the right and left sides, respectively. He underwent HAL sessions twice per week. He had the ability to perform daily activities with the help of a wheelchair and his wife, including transfer from/to the wheelchair. Before intervention, AIS was T6 A, ISNCSCI UEMS was 50/50, and LEMS was 0/50. There was no activation in either TFL or Quad.

As the patient had no history of ambulation training, he started HAL sessions using CAC or CIC mode and the heavy assistance of three therapists. Activation in both Quads was observed in the stance phase from the first session. UT-HAL sessions were started from the latter half of the third session, and more apparent activation was observed in the UT-HAL session than during CIC mode (**Figures 5A,B**).

Walking distance increased from 40 m (first session) to 77 m (tenth session; **Figure 2**). The mAs score after each HAL session decreased compared to pre-session measurements; the mean scores before and after each session were 15.3 ± 1.6 and 9.1 ± 2.5, respectively ($P = 0.029$; **Figure 3**).

Case 3

A 32-year-old female with complete paraplegia and chronic SCI due to spinal cord infarction underwent HAL intervention 6 years and 3 months after spinal cord infarction. She had the ability to perform daily activities with the help

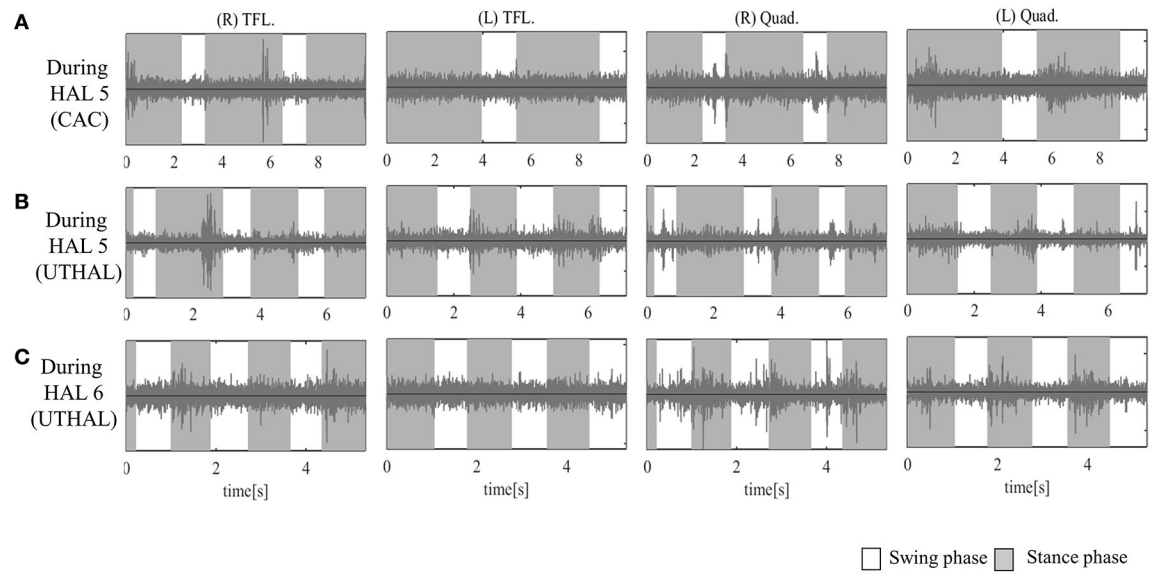

FIGURE 4 | Surface electromyography (EMG) of both TFLs and Quads in case 1. **(A)** During the fifth session using CAC mode, there was some activation in both Quads, and periodic activation only in the left. **(B)** During the fifth session in UT-HAL gait, there was more periodic activation, from the end of the swing phase to early stance phase, than in CAC mode. **(C)** During the sixth session in UT-HAL gait, there was more apparent activation, predominantly on the right side.

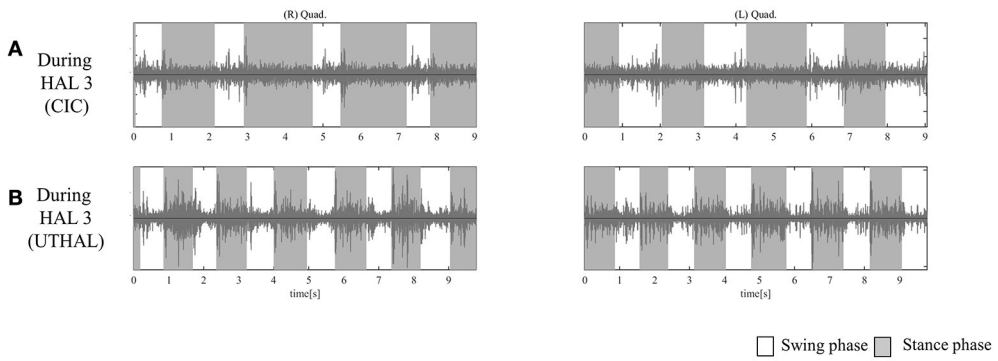

FIGURE 5 | EMG of both Quads in case 2. **(A)** During the third session using CIC mode, there was activation in both Quads in the stance phase. **(B)** During the same third session in UT-HAL gait, there was more apparent activation than during CIC mode.

of a wheelchair. She had a history of ambulation training using long leg braces. She underwent 1–2 HAL sessions per month.

Before intervention, AIS was T10 A, and ISNCSCI LEMS was 0/50. She was able to contract the right hip adductor slightly. She could not contract either TFL or Quad.

On evaluation before HAL intervention, there was no muscle activation in either TFL or Quad. From the first session, we used the upper limb as the trigger for limb motion. Some aperiodic activation in both TFLs and the right Quad was observed in the first session (**Figure 6C**).

On evaluation before the second session, she could contract the right TFL; therefore, we added a knee extension session using the right hip flexor as the trigger for right knee extension from the second session.

Figure 6A shows surface EMG in both TFLs and Quads before, during, and after the third knee HAL session. Before the HAL session, there was periodic activation in the right TFL and Quad. During the HAL session, activation was observed in both TFLs and Quads. After the session, there was rhythmic activation in the right TFL and Quad. Before the ninth session, periodic activation was observed in both TFLs and the right Quad; during the HAL session, activation was more apparent in both TFLs and Quads; and after the session, more obvious activation was observed in the right Quad. Some activation was also seen in the left Quad during hip flexion and knee extension (**Figure 6B**). **Figures 6C,D** shows surface EMG during the first and the tenth UT-HAL sessions, respectively. In the tenth session, more rhythmic activation was observed in both Quads during the stance phase, predominantly on the right side.

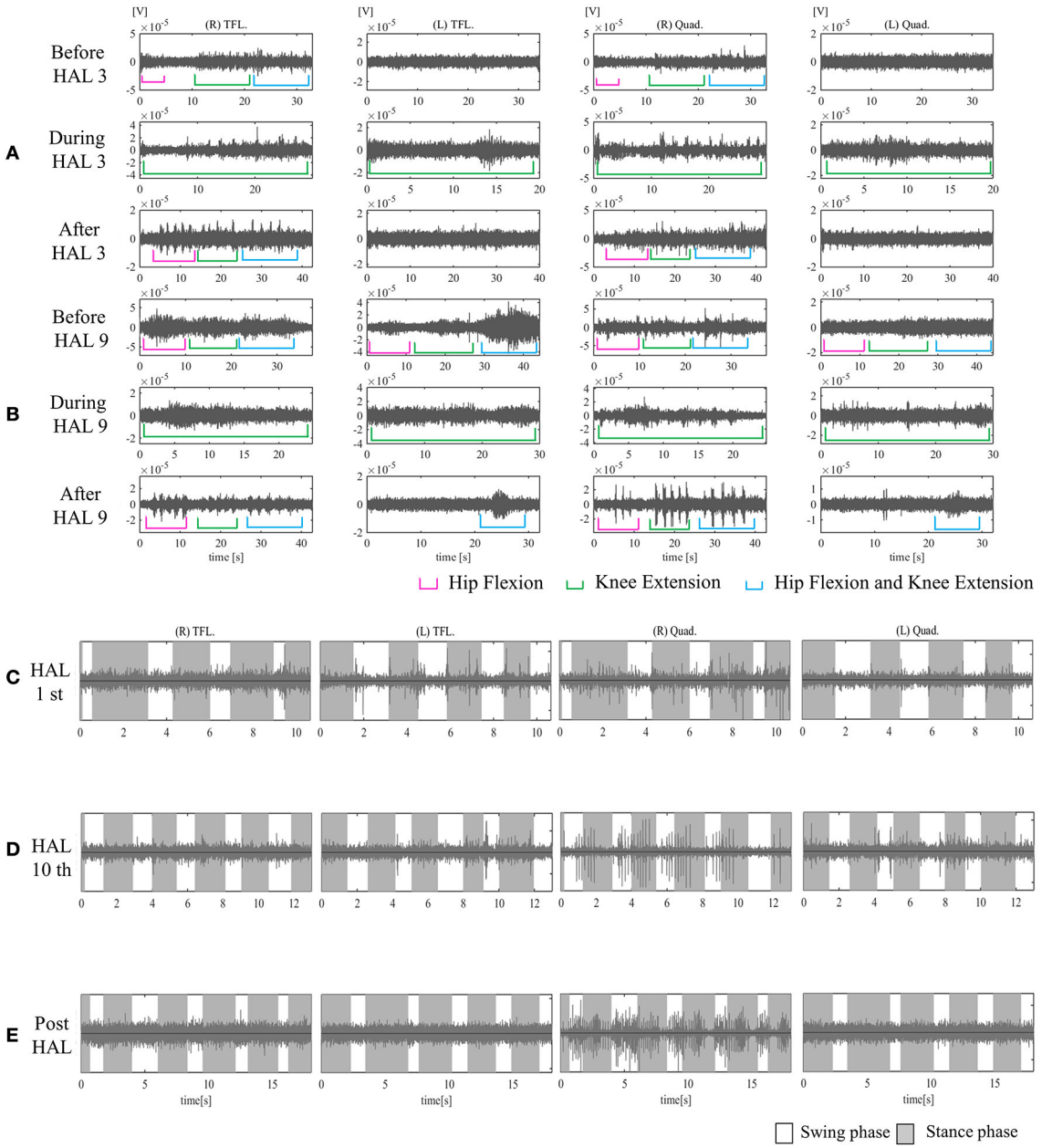

FIGURE 6 | EMG of both TFLs and Quads in case 3. **(A)** Before, during, and after the third knee HAL session. Before this session, there was periodic activation in the TFL and Quad only on the right side. During the HAL session, activation was observed in both TFLs and Quads. After the session, there was rhythmic activation in the right TFL and Quad. **(B)** Before, during, and after the ninth knee HAL session. Before the session, there was periodic activation in both TFLs and the right Quad; during the HAL session, activation was more apparent in both TFLs and Quads; and after the session, more obvious activation was observed in the right Quad, and some activation was seen in the left during hip flexion and extension. **(C)** During the first session in UT-HAL gait, there was some aperiodic activation in both TFLs and the right Quad. **(D)** During the tenth session in UT-HAL gait, there was more rhythmic activation in both Quads during the stance phase, predominantly on the right side. **(E)** During voluntary ambulation with a walker and overhead harness without HAL after the entire intervention, there was rhythmic activation in the right quad from the swing mid-phase to the early stance phase.

Figure 6E shows surface EMG during voluntary ambulation with a walker and overhead harness without HAL after the entire intervention. Rhythmic activation in the right quad was observed from the swing mid-phase to the early stance phase.

Walking distance increased from 80 m (first session) to 234 m (tenth session; **Figure 2**). After the intervention, the patient's hip flexor and knee extensor MMT score improved from 0/5 to 1/5 on both sides, and LEMS improved from 0 to 4 (**Table 2**).

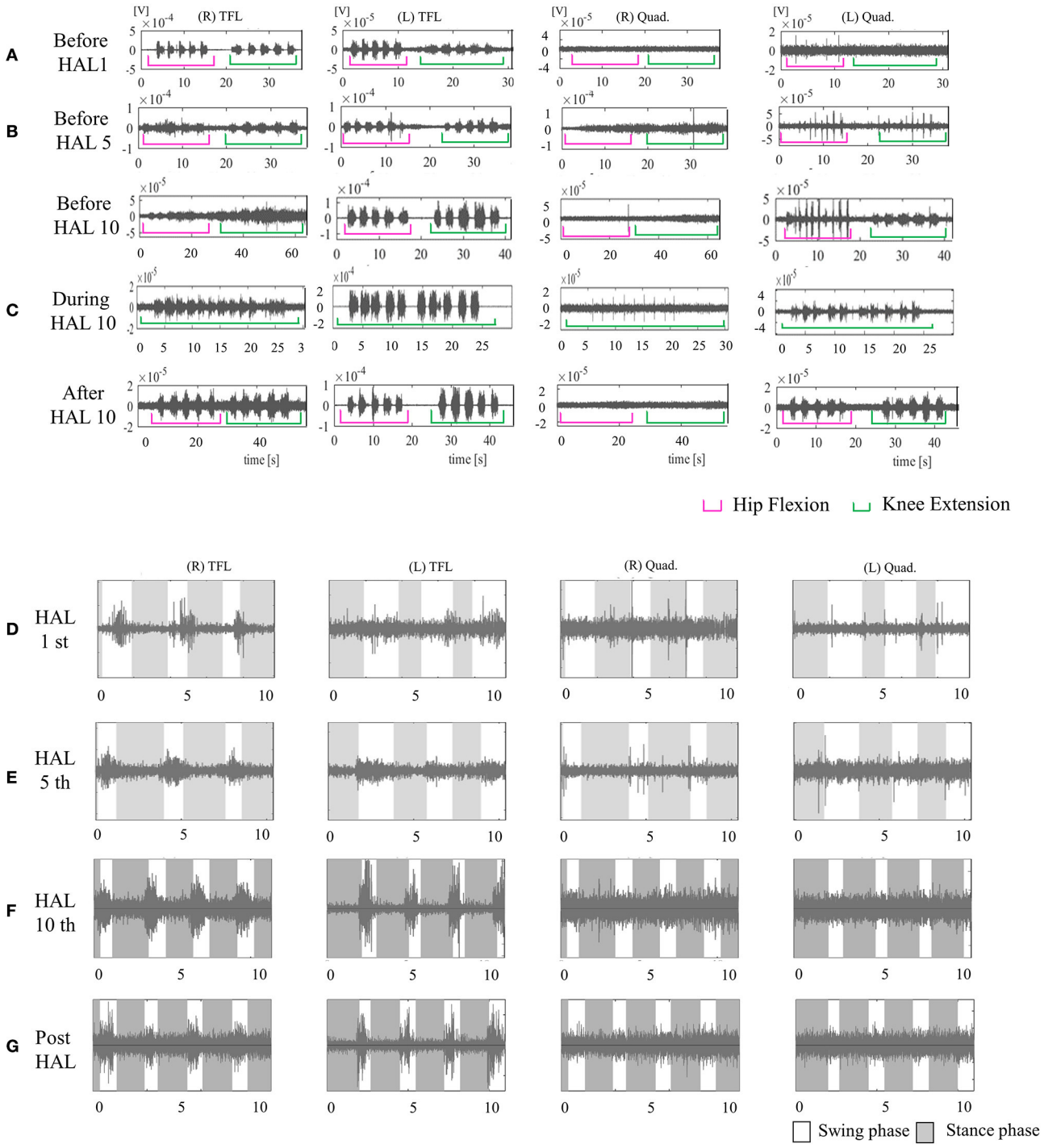

FIGURE 7 | EMG of both TFLs and Quads in case 4. **(A)** Before the first session, there was no voluntary contraction in either Quad. **(B)** Before the fifth session, there was voluntary contraction in the left Quad. **(C)** Before, during, and after the tenth knee HAL session. Before and during the session, there was periodic activation in the left Quad; during the session, the right Quad was also periodically activated. After the session, the left Quad was more periodically activated than before it. **(D)** During the first session in UT-HAL gait. **(E)** During the fifth session in UT-HAL gait. There was activation in both TFLs from the first to tenth sessions; there was no activation in either Quad in the first and fifth gait sessions. **(F)** During the tenth session in UT-HAL gait, there was slight periodic activation during swing phase. **(G)** During voluntary ambulation with a walker and overhead harness without HAL after the entire intervention, there was rhythmic activation in both TFLs, and no periodic activation in either Quad.

TABLE 2 | Neurological change after HAL intervention.

Case	1	2	3	4
AIS before HAL	C6 B	T6 A	T10 A	T11 A
AIS after HAL	C6 B	T6 A	T10 A	T11 C
LEMS before HAL	0	0	0	3
LEMS after HAL	0	0	4	7

The mAs score was reduced after each HAL session compared to pre-session measurements; the mean scores before and after each session were 7.0 ± 1.2 and 6.2 ± 0.8, respectively ($P = 0.063$; **Figure 3**).

Case 4

A 30-year-old male with complete paraplegia and chronic SCI due to twelfth vertebral burst fracture underwent the HAL intervention 1 year and 7 months post-injury. He had the ability to perform daily activities with the help of a wheelchair. He had a history of ambulation training with long leg braces or the assistance of two therapists. He underwent HAL sessions twice per week.

Before intervention, AIS was T11 A, and ISNCSCI LEMS was 3/50. MMT of the hip flexor was 1/5 on the right and 2/5 on the left. There was no voluntary contraction in either Quad (**Figure 7A**).

From the first session, we used both hip flexors as the trigger for knee extension in the knee extension HAL session, and the upper limb as the trigger of limb motion during the HAL ambulation session. Activation was observed in both TFLs during the gait session, predominantly in the swing phase, but not in either Quad (**Figure 7D**). On evaluation before the fifth session, voluntary contraction was observed in the left Quad (**Figure 7B**). Therefore, we placed electrodes at the recommended sites on both limbs in the latter five sessions and performed knee extension sessions triggered by both knee extensors and HAL ambulation sessions triggered by activation of both lower limbs. **Figure 7C** shows surface EMG in the tenth knee extension session. Before and during the session, there was periodic activation in the left Quad; during the session, the right Quad was also periodically activated. After the session, the left Quad was more periodically activated than before it. **Figures 7D–F** show EMG in the first, fifth, and tenth HAL ambulation sessions, respectively. There was activation in both TFLs from the first to tenth sessions, and no rhythmic activation in either Quad was observed in the first or fifth gait sessions. During the tenth gait session, there was slight periodic activation during the swing phase.

Figure 7G shows voluntary ambulation with a walker and overhead harness without HAL after the entire intervention. Rhythmic activation was observed in both TFLs, with no periodic activation in either Quad.

Walking distance increased from 100 to 338 m (**Figure 2**). The mAs score remained 0 before and after each session. After the intervention, the patient's hip flexor MMT score improved from 1/5 to 2/5 on the right, and from 2/5 to 3/5 on the left. Knee extensor MMT also improved from 0/5 to 1/5, and LEMS improved from 3 to 7 (**Table 2**).

DISCUSSION

In this study, we focused on residual upper limb muscle activity in complete quadri/paraplegia and coordination between the upper limbs and contralateral lower limbs in natural gait. In addition, we used voluntary contraction of the hip flexors as a trigger for knee extension. We observed neurological changes in two cases after the intervention.

For all cases, including patients with cervical SCI and high thoracic SCI who were considered ineligible to perform conventional walking training with orthoses, it was possible to perform movement of the paralyzed joints with voluntary control of the relevant muscle using HAL. Considering that the method was feasible in case 1, whose injury level was the highest of the among the patients presented in the study, this method is feasible for patients who has at least voluntary control the triceps muscle with MMT score greater than or equal to 1.

The operating system of HAL directly maps in real-time the detected neuromuscular activity to the assistive torque on the joints of the lower limbs, and therefore directly reflects the user's motion intention into the generated motion. By contrast, other exoskeleton robots such as the Lokomat (Colombo et al., 2000), LOPES (Veneman et al., 2007), and ReWalk (Miller et al., 2016) move paretic limbs automatically; therefore, the limbs are passively moved. We focused on exploiting the residual voluntary muscle activation of paraplegia patients. Using the HAL motion assist function in the context of upper-lower limb coordination during gait, voluntary ambulation was possible, and the improvement of muscle activities was observed.

The HAL has been reported to be a feasible tool for some types of neuromuscular disorders (Kawamoto et al., 2013; Kubota et al., 2013, 2017; Sakakima et al., 2013; Aach et al., 2014; Nilsson et al., 2014; Sczesny-Kaiser et al., 2015, 2017; Wall et al., 2015; Fujii et al., 2017; Ikumi et al., 2017; Shimizu et al., 2017b) and to improve ambulation in patients with chronic SCI (Aach et al., 2014; Sczesny-Kaiser et al., 2015; Wall et al., 2015; Ikumi et al., 2017; Kubota et al., 2017; Shimizu et al., 2017b). HAL is able to detect very weak neuromuscular activities, if any, using its surface electrodes and to provide motion assistance. In this sense, HAL is an effective tool for gait training in more severe cases of SCI. However, the conventional method using the CVC mode of HAL is not applicable in patients with complete paraplegia who have difficulty in detecting bioelectrical signals. The CAC mode uses a foot pressure sensor as a motion trigger, and pressure sensors are not effective for patients who cannot place their weight on both feet. Therefore, we chose upper limb motion as the voluntary trigger for lower limb movement during ambulation.

In utilizing upper extremity muscle activation, we focused on the structural analogy and symmetric motion between upper and contralateral lower limbs in natural gait. The upper and contralateral lower limbs move in synchrony and almost simultaneously during natural locomotion. Based

on this contralateral relationship of upper and lower limb movement during locomotion, we placed electrodes on the biceps and triceps brachii to drive contralateral knee flexion and extension, respectively, and on the anterior deltoid and posterior deltoid to drive contralateral hip flexion and extension, respectively.

A previous study reported that the paralyzed lower limb muscles of patients with SCI can be activated by passive leg movements, suggesting the residual function of the rhythmic pattern generator circuit after SCI (Kawashima et al., 2005). The rhythmic pattern generator is highly relevant to quadrupedal coordination during locomotion in humans (Dietz et al., 1995; Zehr and Duysens, 2004; Dietz, 2011). In fact, recent research has indicated that voluntary upper limb alternate movement generates locomotor-like movements (Sylos-Labini et al., 2014) and enhances muscle activation in the lower limbs (de Kam et al., 2013), and this property can be used in the control of legged exoskeletons (La Scaleia et al., 2014). From this perspective, we hypothesized that synergistic coordination of the upper and lower limbs during voluntary gait using HAL may activate lower limb muscles.

UT-HAL-assisted gait in SCI patients incorporates coordinated voluntary movement of the multiple joints of the upper and lower limbs. Since UT-HAL connects each of the upper limb muscles to the corresponding lower limb joint movements independently, the coordination of lower limb movement is realized solely by the coordinated voluntary activation of the upper limb muscles. Our hypothesis is that gait phase-dependent, voluntary, and coordinated activation of the upper limb muscles, in coherent combination with the voluntarily generated gait pattern of the lower limbs, may re-activate gait phase-dependent muscle activity in the lower limbs. This is difficult to implement by other assistive devices such as passive orthoses, other robots, or current functional electric stimulation systems (Karimi et al., 2014).

Our protocol included voluntary knee extension. Patients with paralysis of knee extensors use long leg braces in the knee-locked position for walking exercises; therefore, it is difficult for them to train with knee extensor movement during gait exercise. Gait with the HAL enabled users to extend their knee periodically in the stance phase according to the gait cycle without knee locking (Shimizu et al., 2017b).

In case 3, the patient was unable to contract the hip flexor before intervention. However upper limb-triggered HAL ambulation appeared to activate her paralyzed and disused hip flexors. Subsequently, we used improved muscle activation of the hip flexors as the trigger for knee extension.

We speculate that muscle activation acquired during voluntary ambulation using motion intention conferred by residual activity of the upper limb muscle and during voluntary knee extension using residual activity of the hip flexor may contribute to the improvement of paralyzed Quad muscle activation. Both sessions—knee extension with the hip flexor and locomotion with upper limb muscle activation—were effective in improving muscle activity in cases 3 and 4.

In addition, in case 3 (lower panels of **Figure 6**), the patient contracted the right TFL in the knee extension HAL session, while in the UT-HAL locomotion session the TFL activation was absent. In our opinion, it was easier to contract the TFL in the knee extension session than in the UT-HAL locomotion because during sitting, TFL contraction is accompanied by a simple single-joint motion of hip flexion, and it was easy for her to focus her attention on the motion. On the other hand, while walking, complex coordinated motion involving hip and knee flexion and extension is required, incorporating coordinated activation of multiple muscles. She could generate voluntary gait using UT-HAL and activate the right Quad in phase with the gait; however, she could not achieve the level of coordinated multiple muscle control during gait.

A similar discussion may apply to case 4 (lower panels of **Figure 7**). Quad activation was present during the knee extension HAL session, while in the UT-HAL locomotion session it was absent. The patient could contract both TFLs and left Quad independently. During walking, he could generate voluntary gait using UT-HAL and activate both TFLs in phase with the gait. However, he could not reach the level of including the newly activated left Quad in the coordinated activation of the muscles. We consider HAL intervention was effective for achieving voluntary contraction of single-joint muscles; however, a longer-term intervention might have been necessary in order for this patient to be able to perform coordinated muscle control including the newly activated muscles during gait.

Cases 1 and 2 had not experienced conventional walking training before the HAL intervention. They had complete paralysis in both lower extremities; however, during HAL ambulation, there was some activation in the TFLs and Quads. In addition, there was more apparent activation in UT-HAL sessions than in CAC sessions. We consider that ambulation with voluntary control have positively influenced periodic activation.

After intervention, the neurological levels in cases 1 and 2 were unchanged; however, in these cases, spastic paralysis evaluated by the mAs score after each session decreased from pre-session values. As spasticity was the main concern in case 2, this change represented meaningful clinical data. Regarding the reduction of spasticity, we previously reported a decrease of mAs after HAL gait training for a patient with C4 SCI (Ikumi et al., 2017). Spasticity negatively influences quality of life for many SCI patients by causing pain, joint contracture, and restricted activity of daily living (Adams and Hicks, 2005; van Cooten et al., 2015). Therefore, this method may be useful to reduce spasticity and related concerns.

One limitation of this protocol is that it is not suitable for patients who are unable to control upper limb muscles. In addition, it is challenging for patients with severe joint deformities or orthostatic hypotension. It is important for medical staff to evaluate skin problems or bruising in paralyzed areas because of their sensory deficiency. Moreover, although neurological improvement was observed in two cases in this study, we did not confirm the underlying mechanism behind this change. Future perspectives include neurological evaluation of this protocol using, for example, functional MRI of the spinal cord (Stroman et al., 2004) or spinal cord mapping of motor activity during gait (Ivanenko et al., 2008).

The ambulation protocol using HAL and voluntary upper limb muscle activation was feasible for complete paraplegic patients. Moreover, patients with injury to the cervical cord or upper thoracic cord, who have difficulty performing conventional gait training with orthoses, may experience decreased spasticity and activation of paralyzed muscles. It is applicable for patients with both spastic and flaccid-type paralysis and represents a novel option for such patients to perform voluntary controlled ambulation similar to natural gait by using their residual neuromuscular activities. Therefore, this HAL protocol may contribute to broadening gait rehabilitation for complete SCI patients.

CONCLUSIONS

This study reports the safety and feasibility of upper-limb-triggered HAL ambulation for patients with complete quadri/paraplegia caused by chronic SCI. Improvement of activation in both TFLs and Quads was observed for two cases, and decreased spasticity after each session was also observed for three cases with spastic-type paralysis. Therefore, voluntary upper limb muscle activation using HAL is a potential option for rehabilitation in complete quadri/paraplegic patients.

AUTHOR CONTRIBUTIONS

All authors participated in the design, execution, and analysis of these studies and have seen and approved the final version of the manuscript. YuSh and HK participated in the study design and drafted the manuscript. YuSh, HK, SK, and YuSo executed HAL interventions and performed the data analysis. YoS conceived the device and helped to draft the manuscript. KS, TU, TA, YH, and MY participated in the study design and helped to draft the manuscript. MY is the principal investigator of this study and participated in the design and coordination of the study. Furthermore, this manuscript has been revised by a professional editor whose first language is English.

FUNDING

This study was supported by Industrial Disease Clinical Research Grants of the Ministry of Health, Labor, and Welfare in Japan (14060101-01).

ACKNOWLEDGMENTS

We thank Mayuko Sakamaki and Yumiko Ito, Center for Innovative Medicine and Engineering (CIME), University of Tsukuba Hospital, for their excellent technical assistance.

REFERENCES

Aach, M., Cruciger, O., Sczesny-Kaiser, M., Hoffken, O., Meindl, R., Tegenthoff, M., et al. (2014). Voluntary driven exoskeleton as a new tool for rehabilitation in chronic spinal cord injury: a pilot study. *Spine J.* 14, 2847–2853. doi: 10.1016/j.spinee.2014.03.042

Adams, M. M., and Hicks, A. L. (2005). Spasticity after spinal cord injury. *Spinal Cord* 43, 577–586. doi: 10.1038/sj.sc.3101757

Bohannon, R. W., and Smith, M. B. (1987). Interrater reliability of a modified Ashworth scale of muscle spasticity. *Phys. Ther.* 67, 206–207. doi: 10.1093/ptj/67.2.206

Colombo, G., Joerg, M., Schreier, R., and Dietz, V. (2000). Treadmill training of paraplegic patients using a robotic orthosis. *J. Rehabil. Res. Dev.* 37, 693–700.

de Kam, D., Rijken, H., Manintveld, T., Nienhuis, B., Dietz, V., and Duysens, J. (2013). Arm movements can increase leg muscle activity during submaximal recumbent stepping in neurologically intact individuals. *J. Appl. Physiol.* 115, 34–42. doi: 10.1152/japplphysiol.00510.2012

Dietz, V. (2011). Quadrupedal coordination of bipedal gait: implications for movement disorders. *J. Neurol.* 258, 1406–1412. doi: 10.1007/s00415-011-6063-4

Dietz, V., Colombo, G., Jensen, L., and Baumgartner, L. (1995). Locomotor capacity of spinal cord in paraplegic patients. *Ann. Neurol.* 37, 574–582. doi: 10.1002/ana.410370506

Fujii, K., Abe, T., Kubota, S., Marushima, A., Kawamoto, H., Ueno, T., et al. (2017). The voluntary driven exoskeleton hybrid assistive limb (HAL) for postoperative training of thoracic ossification of the posterior longitudinal ligament: a case report. *J. Spinal Cord Med.* 40, 361–367. doi: 10.1080/10790268.2016.1142056

Hassan, M., Kadone, H., Suzuki, K., and Sankai, Y. (2014). Wearable gait measurement system with an instrumented cane for exoskeleton control. *Sensors* 14, 1705–1722. doi: 10.3390/s140101705

Ikumi, A., Kubota, S., Shimizu, Y., Kadone, H., Marushima, A., Ueno, T., et al. (2017). Decrease of spasticity after hybrid assistive limb(R) training for a patient with C4 quadriplegia due to chronic SCI. *J. Spinal Cord Med.* 40, 573–578. doi: 10.1080/10790268.2016.1225913

Ivanenko, Y. P., Cappellini, G., Dominici, N., Poppele, R. E., and Lacquaniti, F. (2007). Modular control of limb movements during human locomotion. *J. Neurosci.* 27, 11149–11161. doi: 10.1523/JNEUROSCI.2644-07.2007

Ivanenko, Y. P., Cappellini, G., Poppele, R. E., and Lacquaniti, F. (2008). Spatiotemporal organization of alpha-motoneuron activity in the human spinal cord during different gaits and gait transitions. *Eur. J. Neurosci.* 27, 3351–3368. doi: 10.1111/j.1460-9568.2008.06289.x

Karimi, M., Omar, A. H., and Fatoye, F. (2014). Spinal cord injury rehabilitation: which way forward? *Neurorehabilitation* 35, 325–340. doi: 10.3233/NRE-141124

Karimi, M. T. (2011). Evidence-based evaluation of physiological effects of standing and walking in individuals with spinal cord injury. *Iran. J. Med. Sci.* 36, 242–253.

Kawamoto, H., Kamibayashi, K., Nakata, Y., Yamawaki, K., Ariyasu, R., Sankai, Y., et al. (2013). Pilot study of locomotion improvement using hybrid assistive limb in chronic stroke patients. *BMC Neurol.* 13:141. doi: 10.1186/1471-2377-13-141

Kawamoto, H., and Sankai, Y. (2005). Power assist method based on phase sequence and muscle force condition for HAL. *Adv. Robot.* 19, 717–734. doi: 10.1163/1568553054455103

Kawashima, N., Nozaki, D., Abe, M. O., Akai, M., and Nakazawa, K. (2005). Alternate leg movement amplifies locomotor-like muscle activity in spinal cord injured persons. *J. Neurophysiol.* 93, 777–785. doi: 10.1152/jn.00817.2004

Kirshblum, S. C., Burns, S. P., Biering-Sorensen, F., Donovan, W., Graves, D. E., Jha, A., et al. (2011). International standards for neurological classification of spinal cord injury (revised 2011). *J. Spinal Cord Med.* 34, 535–546. doi: 10.1179/204577211X13207446293695

Kubota, S., Abe, T., Fujii, K., Marushima, A., Ueno, T., Haginoya, A., et al. (2016). Improvement of walking ability using hybrid assistive limb training in a patient with severe thoracic myelopathy caused by ossification of the posterior longitudinal ligament. A case report. *J. Spine* S7:003. doi: 10.4172/2165-7939.S7-003

Kubota, S., Abe, T., Kadone, H., Fujii, K., Shimizu, Y., Marushima, A., et al. (2017). Walking ability following hybrid assistive limb treatment for a patient with chronic myelopathy after surgery for cervical ossification

of the posterior longitudinal ligament. *J. Spinal Cord Med.* 20, 1–9. doi: 10.1080/10790268.2017.1313932

Kubota, S., Nakata, Y., Eguchi, K., Kawamoto, H., Kamibayashi, K., Sakane, M., et al. (2013). Feasibility of rehabilitation training with a newly developed wearable robot for patients with limited mobility. *Arch. Phys. Med. Rehabil.* 94, 1080–1087. doi: 10.1016/j.apmr.2012.12.020

La Scaleia, V., Sylos-Labini, F., Hoellinger, T., Wang, L., Cheron, G., Lacquaniti, F., et al. (2014). Control of leg movements driven by EMG activity of shoulder muscles. *Front. Hum. Neurosci.* 8:838. doi: 10.3389/fnhum.2014.00838

Miller, L. E., Zimmermann, A. K., and Herbert, W. G. (2016). Clinical effectiveness and safety of powered exoskeleton-assisted walking in patients with spinal cord injury: systematic review with meta-analysis. *Med. Devices* 9, 455–466. doi: 10.2147/MDER.S103102

Nilsson, A., Vreede, K. S., Haglund, V., Kawamoto, H., Sankai, Y., and Borg, J. (2014). Gait training early after stroke with a new exoskeleton–the hybrid assistive limb: a study of safety and feasibility. *J. Neuroeng. Rehabil.* 11:92. doi: 10.1186/1743-0003-11-92

Sakakima, H., Ijiri, K., Matsuda, F., Tominaga, H., Biwa, T., Yone, K., et al. (2013). A newly developed robot suit hybrid assistive limb facilitated walking rehabilitation after spinal surgery for thoracic ossification of the posterior longitudinal ligament: a case report. *Case Rep. Orthop.* 2013:621405. doi: 10.1155/2013/621405

Sczesny-Kaiser, M., Hoffken, O., Aach, M., Cruciger, O., Grasmucke, D., Meindl, R., et al. (2015). HAL(R) exoskeleton training improves walking parameters and normalizes cortical excitability in primary somatosensory cortex in spinal cord injury patients. *J. Neuroeng. Rehabil.* 12:68. doi: 10.1186/s12984-015-0058-9

Sczesny-Kaiser, M., Kowalewski, R., Schildhauer, T. A., Aach, M., Jansen, O., Grasmücke, D., et al. (2017). Treadmill training with HAL exoskeleton—a novel approach for symptomatic therapy in patients with limb-girdle muscular dystrophy—preliminary study. *Front. Neurosci.* 11:449. doi: 10.3389/fnins.2017.00449

Shimizu, Y., Kadone, H., Kubota, S., Ikumi, A., Abe, T., Marushima, A., et al. (2017a). Active elbow flexion is possible in C4 quadriplegia using hybrid assistive limb (HAL®) technology: a case study. *J. Spinal Cord Med.* 40, 456–462. doi: 10.1080/10790268.2017.1305036

Shimizu, Y., Nakai, K., Kadone, H., Yamauchi, S., Kubota, S., Ueno, T., et al. (2017b). The hybrid assistive limb(R) intervention for a postoperative patient with spinal dural arteriovenous fistula and chronic spinal cord injury: a case study. *J. Spinal Cord Med.* 29, 1–8. doi: 10.1080/10790268.2017.1329916

Stroman, P. W., Kornelsen, J., Bergman, A., Krause, V., Ethans, K., Malisza, K. L., et al. (2004). Noninvasive assessment of the injured human spinal cord by means of functional magnetic resonance imaging. *Spinal Cord* 42, 59–66. doi: 10.1038/sj.sc.3101559

Sylos-Labini, F., Ivanenko, Y. P., Maclellan, M. J., Cappellini, G., Poppele, R. E., and Lacquaniti, F. (2014). Locomotor-like leg movements evoked by rhythmic arm movements in humans. *PLoS ONE* 9:e90775. doi: 10.1371/journal.pone.0090775

van Cooten, I. P., Snoek, G. J., Nene, A. V., de Groot, S., and Post, M. W. (2015). Functional hindrance due to spasticity in individuals with spinal cord injury during inpatient rehabilitation and 1 year thereafter. *Spinal Cord* 53, 663–667. doi: 10.1038/sc.2015.41

Veneman, J. F., Kruidhof, R., Hekman, E. E., Ekkelenkamp, R., Van Asseldonk, E. H., and van der Kooij, H. (2007). Design and evaluation of the LOPES exoskeleton robot for interactive gait rehabilitation. *IEEE Trans. Neural Syst. Rehabil. Eng.* 15, 379–386. doi: 10.1109/TNSRE.2007.903919

Wall, A., Borg, J., and Palmcrantz, S. (2015). Clinical application of the hybrid assistive limb (HAL) for gait training-a systematic review. *Front. Syst. Neurosci.* 9:48. doi: 10.3389/fnsys.2015.00048

Zehr, E. P., and Duysens, J. (2004). Regulation of arm and leg movement during human locomotion. *Neuroscientist* 10, 347–361. doi: 10.1177/1073858404264680

Conflict of Interest Statement: YS is the C.E.O., shareholder, and director of CYBERDINE Inc., which produces the robot suit HAL. CYBERDINE was not involved in study design, data collection, analysis, writing or submission of this article.

The other authors declare that the research was conducted in the absence of any commercial or financial relationships that could be construed as a potential conflict of interest.

frontiers in Neuroscience

ORIGINAL RESEARCH
published: 28 November 2017
doi: 10.3389/fnins.2017.00660

Application of the Stockwell Transform to Electroencephalographic Signal Analysis during Gait Cycle

Mario Ortiz, Marisol Rodríguez-Ugarte, Eduardo Iáñez and José M. Azorín*

Brain-Machine Interface Systems Lab, Miguel Hernández University of Elche, Elche, Spain

The analysis of electroencephalographic signals in frequency is usually not performed by transforms that can extract the instantaneous characteristics of the signal. However, the non-steady state nature of these low voltage electrical signals makes them suitable for this kind of analysis. In this paper a novel tool based on Stockwell transform is tested, and compared with techniques such as Hilbert-Huang transform and Fast Fourier Transform, for several healthy individuals and patients that suffer from lower limb disability. Methods are compared with the Weighted Discriminator, a recently developed comparison index. The tool developed can improve the rehabilitation process associated with lower limb exoskeletons with the help of a Brain-Machine Interface.

Keywords: brain-machine interface, EEG analysis, fast fourier transform, gait intention, Hilbert-Huang transform, Stockwell transform

OPEN ACCESS

Edited by:
Mikhail Lebedev,
Duke University, United States

Reviewed by:
Rahul Goel,
University of Houston, United States
Guy Cheron,
Free University of Brussels, Belgium

****Correspondence:***
Mario Ortiz
mortiz@umh.es

Specialty section:
This article was submitted to Neuroprosthetics, a section of the journal Frontiers in Neuroscience

Received: *25 August 2017*
Accepted: *13 November 2017*
Published: *28 November 2017*

Citation:
Ortiz M, Rodríguez-Ugarte M, Iáñez E and Azorín JM (2017) Application of the Stockwell Transform to Electroencephalographic Signal Analysis during Gait Cycle. Front. Neurosci. 11:660. doi: 10.3389/fnins.2017.00660

1. INTRODUCTION

Reduced mobility is a serious handicap for people who have suffered a cerebrovascular accident, brain trauma or encephalitis. Orthesis and prosthesis devices have been developed in last years in order to assist people with severe motor limitations. Although EMG-based interfaces have been used in several applications for controlling these devices (Villarejo Mayor et al., 2017), the use of Brain-Machine Interfaces (BMIs) can be a more suitable option to control a speller or a wheel chair (Li et al., 2014) and especially exoskeletons, since they can improve the neuroplasticity in rehabilitation therapies (Cramer, 2008; Gharabaghi, 2016; Barrios et al., 2017).

The basis of a BMI is to extract the brain waves, normally by electroencephalography (EEG), process and translate them into commands to control a device. The electrical waves obtained are categorized by their frequency components and the location where they are acquired (Rao, 2013). Usually, the following frequency bands are considered: delta (0.1–4 Hz) which is associated with deep sleep (Amzica and Steriade, 1998), theta (4–7 Hz) which is associated with Rapid Eye Movement (REM) sleep and transition from sleep to waking (Cantero et al., 2003), alpha (8–15 Hz) which is associated with relaxed, but awake state with eyes closed (Da Silva, 2010) and beta (15–32 Hz) and gamma (>25 Hz) which are associated with movement and attentive focus (Rao, 2013). Depending on the author, the bands can slightly differ and overlap. Thus, it is hard to establish a precise limit for them. In literature, bands have received another designation; for instance, mu band (8–12 Hz) which is usually related to the event-related synchronization phenomenon (Pfurtscheller and Neuper, 1994). In Cheron et al. (2012), it was demonstrated that some EEG frequency bands (alpha, beta and gamma) are involved in the control of the walking pattern, and that it is possible to extract EEG signals event-related desynchronization/synchronization (ERD/ERS) (Severens et al., 2012; Wagner et al., 2012) from

the sensorimotor cortex controlling the contralateral foot placement. This confirmed the study of Gwin et al. (2011) which stated that electrocortical activity is coupled to gait cycle phase during treadmill walking. Cheron et al. (2012) also used the two most representative independent components of the sensorimotor cortex as input for a Dynamic Recurrent Neural Network (DRNN) learning identification toward the two principal components of the 3 elevation angles (foot, shank, and thigh) of one lower limb kinematics which can be easily interpreted by artificial actuators.

EEG signals are usually analyzed by Fourier transforms (FT). Due to the discrete nature of the data analyzed, signals are cut in several windows and processed (Fast Fourier Transform FFT or Short Time Fourier Transform STFT). Although the information extracted by each epoch can provide the evolution through time of the frequency components, other techniques could be more suitable for its time-frequency analysis due to the non-steady nature of EEG signals.

In literature, there are a few examples of these techniques, such as the wavelet transform (Subasi, 2005). However, it needs a good choice of the wavelet mother function which can make this process difficult. In our previous research (Ortiz et al., 2017), we introduced the application of a time-frequency analysis transform, the Hilbert Huang Transform (HHT) (Huang et al., 1998), in an offline scenario for lower limb detection of start and stop of gait cycle based on the ERD/ERS phenomenon. HHT combines a decomposition algorithm Empirical Mode Decomposition (EMD) and a mathematical transform Hilbert Transform (HT). This paper expands our previous research introducing a new transform, the Stockwell Transform (ST) (Stockwell et al., 1996), in order to compare its performance not only with HHT, but also with the FFT. Besides, the study is carried out in an offline and a pseudo-online scenario for better comparison of the techniques. In order to correctly measure the performance of the different proposals, the Weighted Discriminator index (WD) is used (Rodríguez-Ugarte et al., 2017).

The purpose of this work is to show how time-frequency techniques, such as the ST transform, improve the accuracy of the start and the stop detection of gait cycles through the EEG signal analysis, lowering the number of false detections. Sixteen different subjects (eight healthy and eight patients) participated in the research. Data was not only analyzed offline, but pseudo-online as this approach simulates the behavior of the BMI working with an external device in real time.

2. MATERIALS AND METHODS

This section provides information about the experimental setup, equipment used for EEG acquisition, motion capture system (MCS) and the data processing.

2.1. Experimental Setup

Data was collected on sixteen participants. Eight participants (labeled as H1-8) were healthy and did not have any known health issue. They were all right-handed, and were in the age range of 24–29 years (28.2 ± 3.0) at the time of the experiment. Additionally, there were eight patients (labeled as P1-8) of the National Hospital for Spinal Cord Injury in Toledo (Spain), and they were in the age range of 19–71 years (43.7 ± 18.4). This study was carried out in accordance with the recommendations of ethics committee of the Miguel Hernández University of Elche (Spain) with written informed consent from all subjects. All subjects gave written informed consent in accordance with the Declaration of Helsinki. The protocol was approved by the ethics committee of the Miguel Hernández University of Elche (Spain).

Healthy subjects performed ten different trials. However, certain patients due to limitations, tiredness and hardware detection problems completed less trials or some of the trials were not correctly accomplished. **Table 1** shows the number of trials considered for analysis by each subject.

Each trial consisted of 4 complete gait cycles, each one with two events: start and stop as can be seen in **Figure 1**. Each cycle followed the next pattern: relax, start intention of gait, gait, stop intention of gait and stop (out of the model analysis, although it can be considered as a relaxed state).

The purpose of the paper is to measure the performance of a BMI that detects the starts or stops of the gait cycle. Hence, two different models were considered, one for the detection of start and other for the detection of stop. The analysis was carried out considering each event (start or stop intention) as the active part of the model (state 1) and the previous state (relax or gait) as the non-active (state 0).

Data processing was not performed in real time. Two different approaches were considered in order to measure the performance of the methods and the classification model: offline and pseudo-online. Pseudo-online analysis simulated the behavior of the tool in real-time conditions. State labels (0 and 1) were defined based on the Inertial Measurement Units (IMU) activation. Active windows had a 4 s duration starting 2 s previously to the IMU activation. Non-active windows were considered before the active windows with a time gap of 0.5 s. In the case of the offline model, active windows had a duration of 4 s, covering the whole previous time of analysis for the pseudo-online model. Differences between the data windows are shown in **Figure 1** for both approaches. Nevertheless, data was sampled at 500 Hz and sent every 0.2 s in epochs of 1 s duration to the data processing tools. This allowed to treat the data in a similar way for all the methods tested.

2.2. Brain-Machine Interface

2.2.1. EEG Data Acquisition

EEG signals were recorded using a commercial device developed by Brain Products GmbH (Germany). 31 electrodes were used

TABLE 1 | Trials performed by subject.

Subject	H1–H8	P1	P2	P3	P4	P5	P6	P7	P8
Total number of trials	10	10	7	6	7	8	9	10	9
Trials used for pseudo-online model	1–6	1–6	1–4	1–4	1–4	1–5	1–6	1–6	1–6
Trials used for pseudo-online testing	7–10	7–10	5–7	5–6	5–7	6–8	7–9	7–10	7–9

with the help of an actiCAP for an easier placement. The system registered the EEG signals through the actiCHamp amplifier. They were wireless transmitted by a MOVE transmitter for offline and pseudo-online analyses at a sampling frequency rate of 500 Hz. Electrodes were positioned according to the International 10/10 system. **Figure 2A** shows healthy subject H4 walking during a trial. Although 31 electrodes were recorded, finally only nine electrodes were used. This is based on previous studies (Hortal et al., 2016b; Ortiz et al., 2017) and preliminary results of the methods tested on this paper for offline scenario. The electrodes chosen were those close to the electrode Cz (Fz, FC1, FC2, C3, Cz, C4, CP1, CP2, and Pz). The reference was positioned on the right ear lobe and the ground on AFz. **Figure 3** shows the electrode configuration used.

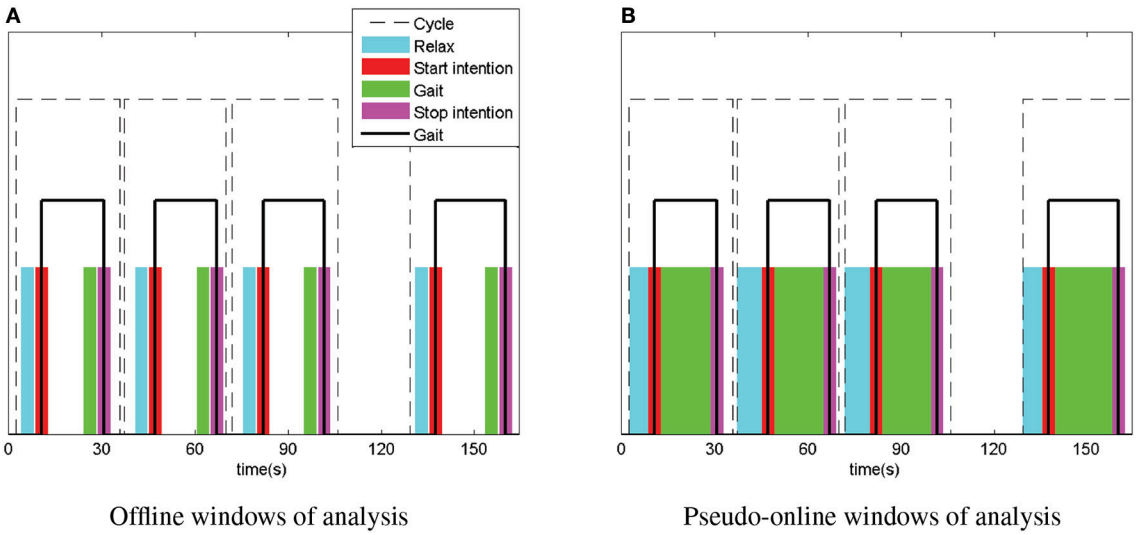

FIGURE 1 | Windows of analysis for offline and pseudo-online models. Time of simulation (broken line) for every trial contains 4 complete gait cycles (solid line). Intention windows (red and magenta) were considered as the active data of the model (state 1). Relax and gait windows (cyan and green) were considered as the non-active data of the model (state 0). The data represented in the figure correspond to the 10th trial of patient P1. **(A)** Offline windows of analysis. **(B)** Pseudo-online windows of analysis.

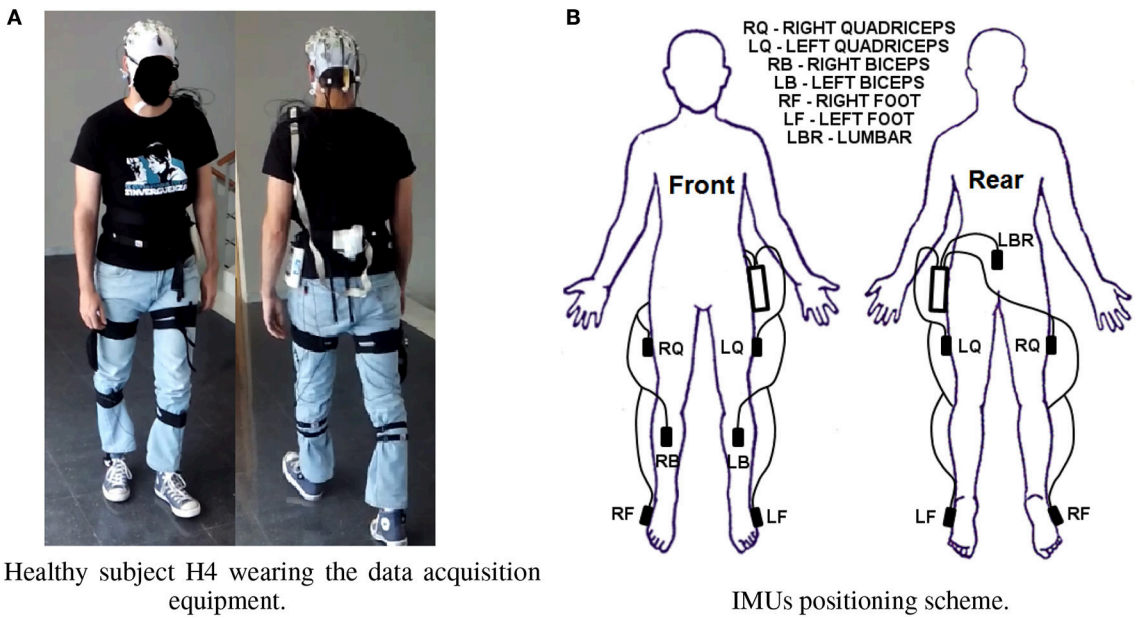

FIGURE 2 | Data acquisition equipment. **(A)** Shows subject H4 wearing the fixing bands for the IMUs, the actiCAP, and Move transmitter. **(B)** Shows a scheme for the positioning of the IMUs from front and rear view. **(A)** Healthy subject H4 wearing the data acquisition equipment. **(B)** IMUs positioning scheme.

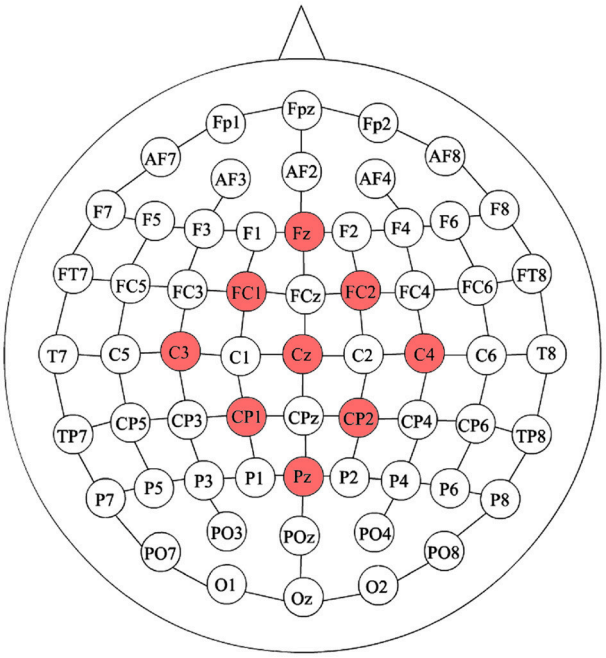

FIGURE 3 | Electrode configuration considered.

2.2.2. Motion Capture System

For the MCS a Tech MCS manufactured by Technaid S.L. (Spain) was used. The system consisted of seven wireless Inertial Measurement Units (IMUs) located on the following positions: three at each limb (foot, thigh and leg) and one on the lumbar position. **Figure 2** shows the exact position of the units. Each IMU had three different types of sensors: an accelerometer, a gyroscope and a magnetometer. Each IMU provided 19 parameters: 9 for rotation, 3 for acceleration, 3 for angular velocity, 3 for magnetic field and 1 for temperature. Rotation parameters were used to detect the initiation and stop of the movement. The data registered by each IMU were acquired through a HUB connected to the PC USB port at a sampling rate of 20 Hz. The MCS mission was to provide the feedback of gait state changes for accuracy calculation of the tests, i.e., the correct detection of the real initiation and stop of the gait.

2.2.3. Preprocessing

Reducing signal to noise ratio is important to improve the feature extraction, so pre-processing of data was needed for each epoch. Several filters were considered.

2.2.3.1. Hardware filter

As this depends on the equipment used for data acquisition, it was the same for all the measurements. The hardware used applied a low pass filter with a cut off frequency of 100 Hz and a notch filter at 50 Hz in order to mitigate the power line interference.

2.2.3.2. Spatial filter

The use of a spatial filter helps to minimize the contribution of the rest of the electrodes to each channel. This way the information of each sensor is better isolated (McFarland et al., 1997). In a previous study (Ortiz et al., 2017) a Laplacian (Lp) and a Common Average Reference (CAR) spatial filter were compared during offline analysis, obtaining Lp filter a better outcome in average than CAR for both event detection (7.8 % better comparison index for the FFT and 6.3 % better for the EMD). Therefore, Lp was the spatial filter used in this study. It aims to subtract the contribution of the rest of electrodes based on distance. Equation 1 shows how the filtered voltage is calculated for electrode *i*.

$$V_i^{Lp} = V_i - \sum_{i \neq j} g_{ij} \cdot V_j \tag{1}$$

Where V_i^{Lp} represents the voltage after filtering, V_j is the voltage without filtering, $j = 1:31$ and g_{ij}:

$$g_{ij} = \frac{\frac{1}{d_{ij}}}{\sum_{i \neq j} \frac{1}{d_{ij}}} \tag{2}$$

With d_{ij} representing the distance between the electrodes i and j based on the three dimensional Euclidean method.

2.2.3.3. Frequency filter

The application of the frequency filter depends on the algorithm or mathematical transform used for data analysis. In this research it was only used before the FFT processing. Based on our previous study (Ortiz et al., 2017) a 4th order Butterworth high-pass filter with a cut off frequency of 0.2 Hz was used to extract the DC component of the signal. HHT and ST methods are not affected by the low pass filter, so it would only increase the computing time without an improvement of the results.

2.2.4. Processing

Three different processing tools were tested to obtain the feature vector of the signal: FFT, HHT, and ST. The three methods were used to extract the data characteristics from the same frequency bands: 8–13, 13–32, and 32–50 Hz. They are related to alpha, beta (ERD/ERS phenomenon) and gamma (attentive focus) bands. Therefore, for all processing methods, each electrode provides three features. Following paragraphs describe the nature of these methods.

2.2.4.1. Fast fourier transform

Fourier transform (Bracewell and Bracewell, 1986) is one of the most extended tools in signal processing. The non-steady state nature of EEG signals is minimized thanks to the analysis of the signal in epochs. FFT provides information of the evolution in time (different epochs moving every 0.2 s) of the harmonic content. For each epoch and electrode, the harmonic content in each band was computed.

2.2.4.2. Hilbert huang transform

HHT was developed by Huang et al. (1998) as an improvement to Hilbert Transform (HT) application. It consists of a sifting process based on the envelopes of data. This process, called Empirical Mode Decomposition (EMD) separates a signal in

several Intrinsic Mode Functions (IMFs). The process can be described as follows:

1. Find the local extrema of $x(t)$.
2. Find the maximum envelope $e_+(t)$ of $x(t)$ by fitting a natural cubic spline through the local maxima. Then, repeat this step to find the minimum envelope, $e_-(t)$, by using the local minima.
3. Compute an approximation to the local average: $m(t) = (e_+(t) + e_-(t))/2$.
4. Find the proto-mode function: $p_i(t) = x(t) - m(t)$.
5. Check if $p_i(t)$ is an IMF:
   a. The number of extrema and the number of zero crossings may differ by no more than one.
   b. The local average is zero. The thresholds chosen to set this condition are critical to avoid over or undertraining. In this research the stopping criteria thresholds of Rilling et al. (2003) were followed.
   c. To avoid the extraction of accidental IMFs, the conditions must be accomplished in at least two to three consecutive iterations (three in our case).
6. If $p_i(t)$ is not an IMF, repeat the EMD sifting process by setting: $x(t) = p_i(t)$. If $p_i(t)$ is an IMF then set: $IMF_i(t) = p_i(t)$.

Every $IMF_i(t)$ is supposed to be monotonic if EMD is successfully applied. Therefore, $IMF_i(t)$ and its HT are orthogonal and instantaneous amplitude $a(t)$ and pulsation $\omega_i(t)$ can be computed through the analytical complex function $z_i(t)$ analysis (Huang et al., 1998) of every mode:

$$z_i(t) = IMF_i(t) + jHT(IMF_i(t)) = a_i(t)e^{j\phi_i(t)} \quad (3)$$

$$\omega_i(t) = \frac{d\phi_i(t)}{dt} \quad (4)$$

Once all the modes are extracted (see **Figure 4B** for an example), Hilbert Spectrum $H(\omega, t)$ (Huang et al., 1998) is calculated based on $a_i(t)$ and $\omega_i(t)$ for all the modes. $H(\omega, t)$ is computed as a function of energy (square amplitude) by frequency and time (right part of **Figure 4A**). As data volume of $H(\omega, t)$ can be too large, the Hilbert Marginal Spectrum $h(\omega)$ is computed as Equation (5). This is carried out for each epoch as:

$$h(\omega) = \int_{t_1}^{t_2} H(\omega, t)dt \quad (5)$$

Being $t_2 - t_1 = 1s$.

For each electrode and epoch the peak value of each frequency band is extracted as one feature of data. See **Figure 4A** for a clearer representation of $h(\omega)$ features. Notice that in **Figure 4A** $H(\omega, t)$ is represented in logarithmic square amplitude, instead of square amplitude, for a better visualization.

However, there are difficulties related to the algorithm nature of the EMD. The sifting process is sensitive to the thresholds defined in the algorithm (Rilling et al., 2003) and the sampling frequency (Rilling and Flandrin, 2006). Besides, it can be hard to extract components that present similar tones (Rilling et al., 2003; Rilling and Flandrin, 2008) which can affect to the quality of the $H(\omega, t)$ due to the lack of orthogonality of some of the modes.

2.2.4.3. Stockwell transform

Stockwell transform, also known as S-Transform (ST), was developed as a time-frequency decomposition tool (Stockwell et al., 1996). It overcomes some of the disadvantages of Short Time Fourier Transform (STFT) (better time-frequency resolution) based on a scalable localizing Gaussian window. It is defined as:

$$S(\tau, f) = \int_{-\infty}^{+\infty} x(t)\frac{|f|}{\sqrt{2\pi}}e^{-\frac{(\tau-t)^2 f^2}{2}}e^{-j2\pi ft} \quad (6)$$

One of the properties of ST is to define multiple frequency voices as one dimensional functions of time scale (τ) and frequency (f_i):

$$S(\tau, f_i) = A(\tau, f_i)e^{j\phi(\tau, f_i)} \quad (7)$$

Due to the orthogonal nature of voice functions, local frequency and amplitude can be computed which allows to obtain $H(\omega, t)$. Once it is created for each epoch, $h(\omega, t)$ is calculated in the same way that was explained for HHT in paragraph 2.2.4.2 and **Figure 4A**, obtaining the three features per electrode based on the $h(\omega)$ peaks per band. ST and HHT are similar in the way the features are extracted, but different in the way $H(\omega, t)$ is computed. The main advantage of ST is its analytical nature which makes it not dependable of any thresholds. However, although it improves the frequency resolution of FFT, it has still a worse frequency resolution the higher the frequency is. As the frequency bands related to the characteristics (8–50 Hz) are far from the Nyquist frequency (250 Hz), this is not a problem for our study.

2.2.5. Post-processing

Once the features were extracted per each electrode ($9 \times 3 = 27$ data vector per 1 s epoch). Two different tests were done: offline and pseudo-online.

First, it was necessary to create a model for the later test data identification. Each participant had this way four different models associated: one for type of event detection (start or stop) and one for approach (offline or pseudo-online). The model allowed to identify testing epochs as non-active (0 label for rest or gait) and active intention (1 label for start intention or stop intention).

2.2.5.1. Classifier

The classifier chosen was the Support Vector Machine (SVM) algorithm. The SVM is based on hyperplane separation by maximizing the margin between the nearest points of different classes (Steinwart and Christmann, 2008). SVM combined with non-linear kernels, such as the radial basis used for this research, results in a robust method (Hortal et al., 2016a; Sburlea et al., 2017). Other alternative classifiers such as Self-organizing maps (SOM) and Linear Discrimination Analysis (LDA) were also considered and tested for some of the healthy subjects at the first steps of the research. However, the higher time of processing required for the model creation in the case of the SOM classifier and the overall better results obtained by SVM were the reason to select it. In order to limit the volume of data presented, only SVM results are shown on this paper. The model creation and

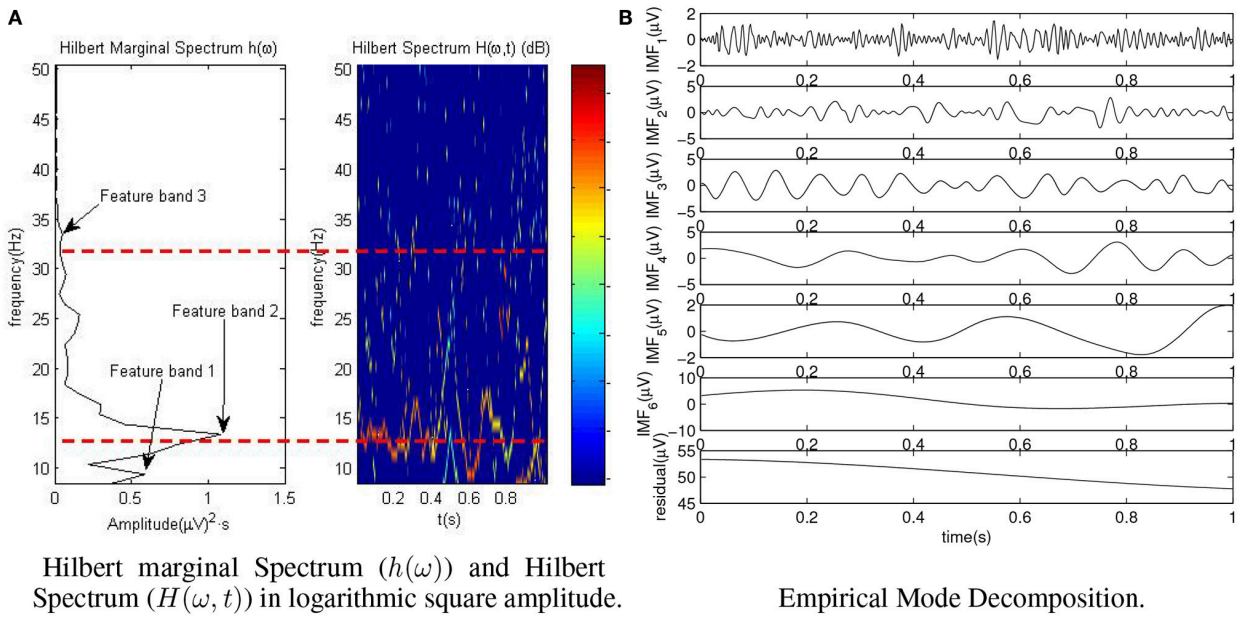

FIGURE 4 | Representation of Hilbert Spectrum ($H(\omega, t)$) and IMFs of an epoch for the healthy subject H4. Hilbert Spectrum is represented in logarithmic scale for better visualization. Marginal Spectrum $h(\omega)$ is shown as square amplitude per time. **(A)** Hilbert marginal Spectrum ($h(\omega)$) and Hilbert Spectrum ($H(\omega, t)$) in logarithmic square amplitude. **(B)** Empirical mode decomposition.

evaluation was carried out in a different way for offline and pseudo-online approaches.

In the case of offline analysis, subjects were evaluated by leave-one-out cross-validation. This means that for each participant, one trial was used for validation and the rest of the trials for modeling. For instance, in the case of a subject with ten trials registered, ten different models of nine trials were performed for start intention and another ten for stopping. The ten test trials were evaluated for each one of their models and finally the results were averaged.

For pseudo-online tests, the first trials were used to create the model and the last ones to test it as if they were processed in real time. Therefore, evaluation was carried out without leave-one-out cross-validation. In the case of healthy participants, the ratio was six tests for modeling and four for testing (6/4 ratio). As the number of trials for patients was inferior to ten in some cases, the ratio presented minor differences, e.g., P2 had a 4/3 ratio. **Table 1** shows the trials used for the model creation and testing by user. The indices associated with the test trials of each subject were also averaged.

For evaluation, each epoch, formed by a 27 features vector, was tested over the classifier and a label 0 or 1 was returned. This label was compared with the true nature of the epoch, based on the MCS data, and a result of a true (T) or false detection (F) was registered. The process is shown in **Figure 5**. This true and false vector was used afterwards for the index evaluation.

2.2.5.2. Evaluation indices

The most common way to evaluate the results is using the following indices: True Positive Rate (TPR), False Positive per Minute (FP/min) and Accuracy (Acc).

TPR indicates the percentage of true start or stop intention events detected. This was evaluated only for the active windows (red or magenta in **Figure 1**). The evaluation of a true event detection was a bit different for the two analysis. Offline, a number of $T > F$ was enough to consider a true event, while on pseudo-online, more than five consecutive T were needed to consider the whole event as true. A single trial TPR would be defined as:

$$TPR = \frac{Number\ of\ true\ event\ detections}{Number\ of\ true\ events} \tag{8}$$

Accuracy appoints how many start or stop intentions detected were really a true detection. This means that it has to be evaluated for active and non-active windows. In the case of non-active windows, a false detection was achieved when $F > T$ (offline) or more than five consecutive F were accounted (pseudo-online). In active windows, the calculation of a detection was the same as TPR. The Acc of a trial would be:

$$Acc = \frac{Number\ of\ true\ event\ detections}{Number\ of\ total\ event\ detections} \tag{9}$$

FP/min indicates the number of false detections per minute. It is an important index, because a high number would result in a disturbing operation of the mobility assistant device, in which the mechanism would be activated without the real subject desire. FP/min were computed for non-active windows when $F > T$ in the case of offline analysis. However, pseudo-online analysis is a bit different. As it tries to simulate the real-time behavior of the tool and several FP can occur during non-active windows, it was necessary to compute all the false activations and not only

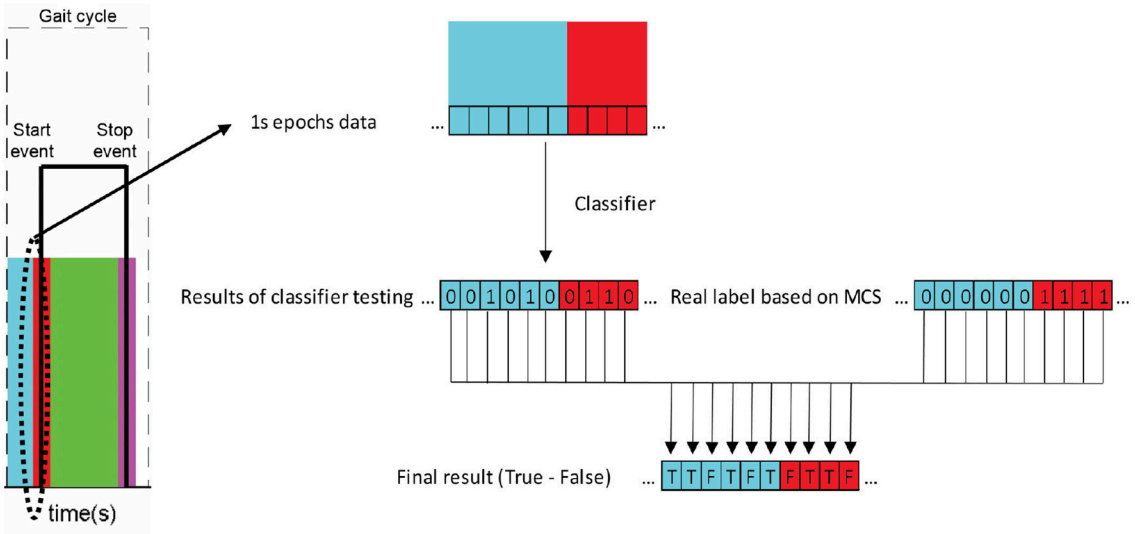

FIGURE 5 | Scheme of evaluation of data epochs tested on the classifier.

one by event. This way, a FP was computed each time more than five consecutives *F* were detected. The rest or gait windows (non-active) for the offline scenario have the same length than active windows: 4 s, i.e., 4/60 min, while for the pseudo-online scenario expand for the whole rest or gait time previous to the 0.5 gap between non-active and active windows per event. This can be seen in **Figure 1B** as cyan or green windows for the start and the stop models. FP/min can be expressed as:

$$FP/min = \frac{Number\ of\ false\ activations}{Rest\ or\ gait\ time\ windows\ in\ minutes} \quad (10)$$

It is important to remark that the three indices are necessary in order to correctly analyze the results. For instance, a trial test with 100% Acc and 0 FP/min could seem a perfect one, but it may only indicate that one of the four events of a trial was detected, being in this case the TPR only 25%. Although the previous indices provide a good information of the results, it can be difficult to compare them based on three independent indices. Consequently, in a previous research, a unified index called Weighted Discriminator (WD) was developed (Rodríguez-Ugarte et al., 2017). WD takes into account TPR, Acc and the False Positive Ratio (FPR) which provides the ratio of false positives per event:

$$WD = 0.4 \cdot TPR + 0.6 \cdot Acc - FPR \quad (11)$$

with TPR and FPR in p.u. and:

$$FPR = FP/min \cdot Duration\ of\ a\ single\ FP\ in\ mins \quad (12)$$

Being the duration for the offline analysis 4/60 min and 1/60 min for the pseudo-online one (equivalent to five consecutive detections represented by the gap of 0.2 s). WD can oscillate from a perfect performance value of 1 to the worst if value is −1. Therefore, WD acts as a comprehensive index to compare the performance of the different tests.

3. RESULTS

Results were obtained for the sixteen subjects and the offline and pseudo-online analysis. The comprehensive WD index was calculated from the determination of TPR, FP/min and Acc indices in order to evaluate the performance of the BMI in every case. WD index was statistically analyzed. A Shapiro-Wilks (S-W) test of normality was applied in order to detect outliers (Ghasemi and Zahediasl, 2012) and a factorial multivariate analysis of variance (MANOVA) was carried out to detect the significant differences between methods (ST/HHT/FFT), type of subject (healthy/patient) and type of event (start/stop) with the help of SPSS (Field, 2009).

3.1. Offline Analysis

As previously stated, offline analysis was carried out by leave-one-out cross-validation technique. WD acts as a measurement of the BMI performance. It was computed for each method, subject and model. This can be seen in **Tables 2–4**.

The S-W test indicated that P2 was an outlier for the HHT stop model ($p < 0.05$) and, as a consequence, it was not considered for the stop model.

In order to carry out a MANOVA test, it is needed to assess if the variances between groups are equal (assumption of sphericity). This test is known as Mauchly's test. In this case, assumption of sphericity was not violated ($p > 0.05$).

Then, it was performed the MANOVA analysis. The interaction between methods and type of event in the test of within-subjects presented significant differences [$F_{(2,\ 54)} = 10.80$, $p < 0.001$, $\eta^2 = 0.29$]. In order to see the cause of this, a pairwise comparison using Bonferroni confidence interval adjustment was

TABLE 2 | Offline results for the sixteen subjects.

Subject	Method	Start				Stop			
		TPR (%)	FP/min	Acc (%)	WD	TPR (%)	FP/min	Acc (%)	WD
H1	ST	87.50	3.75	77.83	**0.50**	75.00	1.13	92.17	**0.76**
	HHT	77.50	4.50	74.79	0.38	82.50	1.88	89.00	0.71
	FFT	65.00	3.75	71.50	0.38	80.00	2.63	85.17	0.61
H2	ST	87.50	2.63	88.00	**0.66**	85.00	1.50	91.50	**0.76**
	HHT	77.50	4.13	70.67	0.39	75.00	1.88	87.67	0.67
	FFT	70.00	3.00	79.33	0.51	80.00	2.25	84.83	0.64
H3	ST	82.50	2.63	84.83	**0.62**	82.50	0.75	95.50	**0.84**
	HHT	65.00	6.75	60.17	0.06	75.00	1.88	89.67	0.68
	FFT	70.00	5.25	75.21	0.29	77.50	2.63	82.00	0.58
H4	ST	95.00	1.50	93.33	**0.81**	87.50	0.38	98.00	**0.91**
	HHT	82.50	2.63	86.71	0.63	72.50	0.38	98.00	0.85
	FFT	80.00	1.13	93.00	0.78	85.00	2.25	88.17	0.68
H5	ST	88.00	2.10	87.14	**0.70**	82.00	1.50	92.14	**0.76**
	HHT	78.00	3.60	76.95	0.47	74.00	1.80	85.17	0.66
	FFT	72.00	2.10	85.14	0.62	84.00	3.60	83.06	0.53
H6	ST	90.00	2.70	84.79	0.64	66.00	0.90	93.33	**0.75**
	HHT	72.00	3.00	84.10	0.54	44.00	1.20	90.00	0.62
	FFT	82.00	1.80	89.31	**0.71**	58.00	2.70	78.50	0.48
H7	ST	86.00	3.90	81.25	**0.51**	82.00	0.60	96.00	**0.85**
	HHT	58.00	7.50	54.76	-0.06	50.00	3.60	67.48	0.30
	FFT	66.00	3.90	72.50	0.37	66.00	3.30	77.14	0.45
H8	ST	94.00	3.00	84.23	0.63	82.00	0.60	96.33	**0.86**
	HHT	64.00	4.20	68.52	0.32	38.00	0.30	86.67	0.65
	FFT	82.00	1.20	93.00	**0.79**	72.00	1.80	82.08	0.63
P1	ST	85.00	0.38	97.50	**0.89**	60.00	3.38	85.83	**0.47**
	HHT	77.50	1.50	84.00	0.69	47.50	1.88	70.50	0.46
	FFT	85.00	1.50	92.00	0.77	60.00	3.00	77.00	0.45
P2	ST	53.57	2.68	70.48	**0.41**	89.29	4.29	83.16	**0.50**
	HHT	96.43	9.64	64.49	-0.03	46.43*	7.50*	26.19*	-0.28*
	FFT	67.86	4.82	65.24	0.26	71.43	5.36	73.81	0.28
P3	ST	66.67	5.63	66.67	0.20	50.00	1.88	73.61	**0.49**
	HHT	54.17	6.25	47.50	-0.02	50.00	3.75	77.78	0.35
	FFT	58.33	4.38	69.44	**0.29**	50.00	5.63	56.94	0.07
P4	ST	92.86	2.68	86.90	**0.67**	57.14	2.68	68.57	0.42
	HHT	78.57	2.68	81.67	0.58	50.00	1.07	93.57	**0.67**
	FFT	78.57	2.68	84.52	0.60	57.14	3.75	71.19	0.34
P5	ST	90.63	2.34	89.64	**0.71**	71.88	1.41	90.63	**0.71**
	HHT	84.38	4.69	75.21	0.40	68.75	1.88	90.83	0.66
	FFT	84.38	3.75	80.68	0.51	68.75	2.34	85.42	0.59
P6	ST	84.00	3.00	83.93	0.59	72.00	2.40	87.52	**0.61**
	HHT	76.00	6.60	63.88	0.14	56.00	2.40	70.64	0.45
	FFT	86.00	3.00	84.57	**0.60**	68.00	2.10	83.81	0.60
P7	ST	72.00	5.10	69.72	0.28	64.00	3.00	79.00	**0.48**
	HHT	46.00	4.50	61.79	0.18	46.00	3.00	59.31	0.29
	FFT	68.00	4.50	70.42	**0.32**	58.00	2.70	77.64	0.47
P8	ST	80.00	2.00	89.42	0.69	91.11	1.67	94.44	0.79
	HHT	66.67	1.00	94.44	**0.75**	95.56	0.33	98.15	**0.94**
	FFT	86.67	3.00	82.01	0.59	93.33	1.00	94.44	0.86

*The data represent the average value of the trials (up to ten by subject) obtained by leave-one-out cross-validation technique for the different evaluation indices. Outliers identified by SPSS are marked by *. Best WD results by subject are marked in bold for the start and stop models.*

TABLE 3 | Offline results by method.

Method	Start				Stop			
	TPR (%)	FP/min	Acc (%)	WD	TPR (%)	FP/min	Acc (%)	WD
ST	83.45 ± 10.98	2.88 ± 1.27	83.48 ± 8.54	**0.60 ± 0.18**	73.88 ± 12.22	1.59 ± 0.93	88.97 ± 8.74	**0.70 ± 0.16**
HHT	72.14 ± 12.59	4.57 ± 2.30	71.85 ± 12.71	0.34 ± 0.27	61.65 ± 16.94	1.82 ± 1.08	83.63 ± 11.74	0.60 ± 0.19
FFT	75.11 ± 8.94	3.11 ± 1.31	80.49 ± 8.98	0.52 ± 0.19	70.51 ± 12.53	2.78 ± 1.05	80.49 ± 8.53	0.53 ± 0.18
Average	76.90 ± 11.75	3.52 ± 1.82	78.61 ± 11.20	0.49 ± 0.24	68.68 ± 14.69	2.06 ± 1.12	84.36 ± 10.19	**0.61 ± 0.19**

The data represent the average value ±, standard deviation by method for the subjects. P2 was not considered for the stop model as it was detected as outlier. Best results for start and stop models appear in bold.

TABLE 4 | WD Offline results by method and type of subject.

Method	Healthy		Patient	
	Start	Stop	Start	Stop
ST	**0.64 ± 0.10**	**0.81 ± 0.13**	**0.56 ± 0.24**	**0.57 ± 0.14**
HHT	0.34 ± 0.23	0.64 ± 0.16	0.33 ± 0.31	0.55 ± 0.23
FFT	0.56 ± 0.20	0.58 ± 0.09	0.49 ± 0.18	0.48 ± 0.24
Average	**0.51 ± 0.22**	**0.68 ± 0.14**	0.46 ± 0.26	0.53 ± 0.20

The data represent the average WD value ± standard deviation by method and type of subject: healthy or patient. P2 was not considered for the stop model as it was detected as outlier. Best results in bold.

performed. ST and FFT had no significant differences ($p > 0.05$), but HHT did ($p < 0.01$) for the start and stop models. On the other hand, the interaction, in the test of within-subjects, between methods and type of subject presented no significant differences ($p > 0.05$). The interaction between type of event and type of subjects in the test of between-subjects was also not significant ($p > 0.05$).

Regarding the WD value, ST obtained the best results for both start and stop models (bold text in **Table 3**). Although, there were no significant differences depending on the type of subject, WD results for healthy users were higher in average (bold text for average in **Table 4**). ST was also the method with the highest WD for both type of subjects as **Table 4** shows, but with a lower difference with the other methods for patients than for healthy subjects. HHT performance was irregular with the lowest WD results for the start model and the highest standard deviation in **Tables 3**, **4**.

3.2. Pseudo-Online Analysis

The actual application of the BMI is in a real-time situation where the patient is trying to activate the motion device with the BMI output. As the trials were acquired before the ST and HHT implementation by the authors, a pseudo-online approach was adopted to overcome this issue. In a pseudo-online scenario, it is simulated that epochs are processed as they are acquired. First trials were used for modeling, as stated in subsection 2.2.5.1, and the rest of them were reserved for testing (**Table 1**). It is important to notice that, FP/min was calculated in a different way as several false activations can be registered in real-time non-active windows. Therefore, this approach bring us a more realistic outcome of the BMI behavior, while offline tests gives information of the global performance when applying the different methods. A bad trial performance of a subject had a more relevant influence over the results, because not only an inferior number of trials is considered, but false detections can be multiple for each event.

Table 5 provides the TPR, FP/min, Acc, and WD results for the different methods and subjects whereas **Tables 6**, **7** show the average WD value for the three methods and type of subject. The results vary from the offline tests as there were differences in the way a detection was computed and the number of trials used for testing. This variation is more noticeable in the case of the number of FP/min, as a comparison between offline and pseudo-online tables shows. However, as the WD takes into account the FPR and the FP time length varies, WD still acts as a good index for the method comparison.

The S-W test of normality was passed for all the models ($p > 0.05$) and no outliers were detected. Hence, the sixteen subjects were considered for pseudo-online analysis.

Mauchly's test indicated that the assumption of sphericity was violated ($p < 0.05$). Therefore, it was needed to apply the corrector factor with the highest power, in this case Huynh-Feldt.

For the MANOVA analysis, the test of within-subjects effects presented no significant differences ($p > 0.05$) for the interaction between methods and type of event, and for the interaction between the methods and the type of subject, applying for both cases the corresponding corrector factor of Huynh-Feldt. The interaction between type of event and type of subject in the test of between-subjects effects presented significant differences [$F_{(1,\ 28)} = 6.34, p < 0.05, \eta^2 = 0.185$]. The pairwise comparison using Bonferroni confidence interval adjustment did not detect

TABLE 5 | Pseudo-online results for the sixteen subjects.

Subject	Method	Start				Stop			
		TPR (%)	FP/min	Acc (%)	WD	TPR (%)	FP/min	Acc (%)	WD
H1	ST	81.25	7.68	66.67	**0.56**	93.75	3.99	79.52	**0.79**
	HHT	68.75	6.43	58.75	0.52	68.75	3.36	75.18	0.67
	FFT	68.75	7.27	66.19	0.55	81.25	3.91	78.04	0.73
H2	ST	100.00	5.14	83.57	**0.82**	100.00	8.86	64.09	0.64
	HHT	56.25	4.10	55.36	0.49	68.75	0.65	93.75	**0.83**
	FFT	75.00	3.97	73.87	0.68	100.00	12.05	58.69	0.55
H3	ST	93.75	13.16	66.98	**0.56**	81.25	1.35	92.26	**0.86**
	HHT	68.75	10.27	59.38	0.46	43.75	0.00	75.00	0.63
	FFT	93.75	14.76	57.78	0.48	62.50	0.69	91.67	0.79
H4	ST	100.00	0.00	100.00	**1.00**	81.25	0.00	100.00	**0.93**
	HHT	62.50	7.44	40.21	0.37	25.00	0.00	75.00	0.55
	FFT	75.00	1.80	82.50	0.77	56.25	1.89	68.75	0.61
H5	ST	85.00	9.06	75.70	0.64	85.00	1.83	92.26	**0.86**
	HHT	75.00	4.34	86.31	**0.75**	55.00	3.64	66.67	0.56
	FFT	75.00	8.80	80.31	0.64	70.00	4.32	56.52	0.55
H6	ST	70.00	1.78	78.33	**0.72**	95.00	3.05	81.26	**0.82**
	HHT	65.00	4.66	73.61	0.62	35.00	3.03	52.50	0.40
	FFT	70.00	3.56	78.41	0.69	80.00	8.33	53.84	0.50
H7	ST	70.00	1.93	82.14	**0.74**	85.00	2.69	83.33	**0.80**
	HHT	30.00	7.74	27.68	0.16	40.00	3.60	56.25	0.44
	FFT	50.00	4.29	49.43	0.43	55.00	2.69	70.42	0.60
H8	ST	90.00	4.06	67.38	**0.70**	100.00	1.75	83.33	**0.87**
	HHT	50.00	3.45	50.00	0.44	55.00	2.73	57.50	0.52
	FFT	85.00	5.43	61.81	0.62	95.00	2.42	78.82	0.81
P1	ST	100.00	3.58	84.18	0.85	31.25	0.00	100.00	**0.73**
	HHT	100.00	2.13	89.58	**0.90**	37.50	0.00	75.00	0.60
	FFT	93.75	3.30	87.61	0.85	25.00	0.00	50.00	0.40
P2	ST	50.00	2.62	72.22	**0.59**	91.67	3.54	75.93	**0.76**
	HHT	100.00	21.42	60.58	0.41	100.00	40.14	36.25	-0.05
	FFT	33.33	3.33	35.71	0.29	58.33	2.42	77.78	0.66
P3	ST	62.50	0.00	100.00	0.85	87.50	13.33	30.30	0.31
	HHT	75.00	0.00	100.00	**0.90**	62.50	11.99	25.71	0.20
	FFT	50.00	0.00	100.00	0.80	75.00	13.28	38.87	**0.31**
P4	ST	83.33	0.00	100.00	**0.93**	91.67	18.04	37.87	0.29
	HHT	58.33	3.61	75.00	0.62	66.67	4.65	59.44	**0.55**
	FFT	41.67	0.00	100.00	0.77	66.67	8.51	42.73	0.38
P5	ST	83.33	4.72	75.56	**0.71**	50.00	1.65	74.29	0.62
	HHT	75.00	5.62	65.48	0.60	25.00	4.03	33.33	0.23
	FFT	50.00	1.23	91.67	0.73	58.33	1.46	69.05	**0.62**
P6	ST	73.33	2.85	79.17	**0.72**	86.67	3.04	79.74	**0.77**
	HHT	66.67	5.66	65.61	0.57	80.00	16.13	35.20	0.26
	FFT	40.00	5.00	57.62	0.42	73.33	11.20	38.33	0.34
P7	ST	65.00	6.82	61.16	**0.51**	85.00	11.78	50.87	**0.45**
	HHT	35.00	2.08	48.33	0.40	60.00	11.43	32.91	0.25
	FFT	35.00	3.95	42.50	0.33	45.00	3.23	59.72	0.48
P8	ST	80.00	7.41	73.61	0.64	100.00	0.85	96.67	**0.97**
	HHT	53.33	0.00	100.00	**0.81**	86.67	0.85	95.24	0.90
	FFT	86.67	6.22	76.67	0.70	73.33	2.54	89.26	0.79

Data represent the average value of the tested trials. No outliers were identified by SPSS. Best WD results appear in bold.

TABLE 6 | Pseudo-online results by method.

Method	Start				Stop			
	TPR (%)	FP/min	Acc (%)	WD	TPR (%)	FP/min	Acc (%)	WD
ST	80.47 ± 14.63	4.43 ± 3.67	79.17 ± 12.19	**0.72 ± 0.14**	84.06 ± 18.40	4.73 ± 5.34	76.36 ± 20.95	**0.72 ± 0.21**
HHT	64.97 ± 18.96	5.56 ± 5.04	65.99 ± 20.59	0.56 ± 0.20	56.85 ± 21.68	6.64 ± 10.11	59.06 ± 21.90	0.47 ± 0.25
FFT	63.93 ± 20.96	4.56 ± 3.64	71.38 ± 19.46	0.61 ± 0.17	67.19 ± 18.40	4.93 ± 4.28	63.91 ± 16.82	0.57 ± 0.16
Average	69.79 ± 19.54	4.85 ± 4.11	72.18 ± 18.26	**0.63 ± 0.18**	69.37 ± 22.24	5.44 ± 6.95	66.44 ± 20.92	0.59 ± 0.23

The data represent the average value ± standard deviation by method for the sixteen subjects. Best results for WD start and stop models appear in bold.

TABLE 7 | WD pseudo-online results by method and type of subject.

Method	Healthy		Patient	
	Start	Stop	Start	Stop
ST	**0.72 ± 0.14**	**0.82 ± 0.09**	**0.73 ± 0.14**	**0.61 ± 0.24**
HHT	0.48 ± 0.17	0.58 ± 0.14	0.65 ± 0.20	0.37 ± 0.30
FFT	0.61 ± 0.11	0.64 ± 0.12	0.61 ± 0.23	0.50 ± 0.17
Average	0.60 ± 0.17	**0.68 ± 0.15**	**0.66 ± 0.19**	0.49 ± 0.25

The data represent the average WD value ± standard deviation by method and type of subject: healthy or patient. Best results in bold.

differences for healthy subjects ($p > 0.05$), but it did for patients ($p < 0.05$). This indicated that patients performed significantly different depending on the start or stop event detection.

Regarding the WD value, ST obtained the best results for both start and stop models (bold text in **Table 6**), with lower FP/min and higher TPR and Acc. Looking at **Table 7**, WD results were similar in average for healthy subjects and patients, not showing the apparently superior performance that offline analysis attributed to healthy subjects. The same table also shows that ST presented the highest WD value for both healthy subjects and patients. HHT was again the method with the most irregular performance, as the lower WD value and higher standard deviation in **Tables 6**, **7** indicate. The HHT result was specially low in the case of the stop model of patients which was the reason of the previously detected difference in the pairwise comparison.

4. DISCUSSION

A new BMI based on ST has been compared to another signal analysis technique (HHT) and a traditional transform (FFT). The tests were done for sixteen different subjects: eight healthy and eight with lower limb disabilities. With the help of a recently developed comprehensive index (WD), the different processing methods were evaluated in an offline and a pseudo-online scenario.

From the point of view of the differences between start and stop event detection of gait, offline analysis seemed to perform better for the stop detection. However, the pseudo-online approach offered a similar performance in average, with the same WD value in the case of the ST method. In addition, statistical analysis showed no significant differences between the start and stop models. Therefore, as pseudo-online model is a more adequate way to represent the performance of the BMI in a real-time scenario, it can be concluded that both event detection models (start/stop) are similar.

Another conclusion is related to the individual performance of the sixteen participants. Results of **Tables 2**, **5** show that BMI performance was dependent on the subject, as the performance of each of them was substantially different. This means that the subjects need some time to get used to the BMI in order to improve their results. However, there were not significant differences between healthy subjects and patients in the MANOVA test. Therefore, it is not needed to personalize the BMI depending on the type of subject.

Regarding the different methods of analysis, indices showed that ST obtained the best results with better Acc and TPR, and even zero FP/min for certain subjects. All the models showed higher WD value in average for ST (bold text in the tables) which demonstrates the better performance of this transform. This is mainly due to the analytical nature of ST that makes it a more robust method than HHT. HHT had an irregular performance with the lowest WD value for the start offline model of both type of subjects and the stop pseudo-online model of patients (WD < 0.4), but with similar results to the other methods in the rest of the cases (WD > 0.55). HHT was also the method with the highest standard deviation for all the models. The cause of this irregular behavior is the EMD algorithm. EMD did not always achieve to extract the different components related to the bands of frequency considered in the paper. If the EMD of an epoch mixes several tones in a IMF, $H(\omega, t)$ is not computed correctly and the $h(\omega)$ does not provide the three features per electrode in a constant way, which affects the classifier and the event detection. FFT performed as the second best method, but as it is not based on instantaneous amplitude and frequency, provided a worse determination of the transition from a relax to a starting gait state, and from a gait to a stopping gait state than ST.

The comparison of this work with previous works is not trivial. First, there are not many studies about detection of intention of start and stop gait for lower limb that provide the three parameters: TPR, FP/min and Acc. In addition, the FP/min

can be computed differently depending on the approach. For instance, a different number of consecutive detections could be specified, or a statistical mode threshold could be used. And finally, WD is hardly used as a comparison index because it was recently developed.

In Jiang et al. (2015) an offline approach for single-trial detection of gait initiation from movement related cortical potentials was presented. The study, carried out for nine subjects, provided the following averaged results: TPR = 76.80 ± 8.97% and FP/min = 2.93 ± 1.09. No Acc was indicated in the paper, being TPR a bit lower and FP/min a bit higher than the offline ST results shown in **Table 3** for the start model (TPR = 83.45 ± 10.98% and FP/min = 2.88 ± 1.27). Looking at previous work of the authors based on FFT (Hortal et al., 2016b), **Table 2** of the reference shows averaged indices of TPR = 54.8 ± 9.3% and FP/min = 2.66 ± 2.24 for the offline start and stop gait intention of six subjects (no Acc provided). This example allows to compare the results in a similar scenario with more subjects under analysis. In our research, the same averaged indices (start and stop) show also an improvement: TPR = 78.82 ± 12.39% and FP/min = 2.25 ± 1.28.

It has been demonstrated that the BMI developed allows to detect the start and stop of gait intention through the use of EEG signals improving the accuracy obtained. Future research will aim the online implementation of the BMI with a motion assistant device. This approach could be useful in the context of the lower limb rehabilitation for patients that have suffered stroke.

AUTHOR CONTRIBUTIONS

MO is responsible for the design, implementation and data analysis. MR-U and EI developed the classifier module and MO adapted it. Data acquisition was designed and performed by EI. MO, MR-U, EI and JA contributed to the revision process. JA actively contributed as director of the work.

FUNDING

Research supported by the project Associate—Decoding and stimulation of motor and sensory brain activity to support long term potentiation through Hebbian and paired associative stimulation during rehabilitation of gait (DPI2014-58431-C4-2-R), funded by the Spanish Ministry of Economy and Competitiveness and by the European Union through the European Regional Development Fund (ERDF) "A way to build Europe". The acquisition wireless system of EEG signals with 32 channels from Brain Products has been partially financed by funds from the European Union (P.O. FEDER 2007/2013), with the management of Generalitat Valenciana (Spain).

REFERENCES

Amzica, F., and Steriade, M. (1998). Electrophysiological correlates of sleep delta waves. *Electroencephalogr. Clin. Neurophysiol.* 107, 69–83. doi: 10.1016/S0013-4694(98)00051-0

Barrios, L. J., Hornero, R., Pérez-Turiel, J., Pons, J. L., Vidal, J., and Azorín, J. M. (2017). State of the art in neurotechnologies for assistance and rehabilitation in spain: fundamental technologies. *Rev. Iberoamer. Autom. Inf. Indust.* 14, 346–354. doi: 10.1016/j.riai.2017.06.003

Bracewell, R. N., and Bracewell, R. N. (1986). *The Fourier Transform and Its Applications*. New York, NY: McGraw-Hill.

Cantero, J. L., Atienza, M., Stickgold, R., Kahana, M. J., Madsen, J. R., and Kocsis, B. (2003). Sleep-dependent θ oscillations in the human hippocampus and neocortex. *J. Neurosci.* 23, 10897–10903. Available online at: http://www.jneurosci.org/content/23/34/10897?ct=

Cheron, G., Duvinage, M., De Saedeleer, C., Castermans, T., Bengoetxea, A., Petieau, M., et al. (2012). From spinal central pattern generators to cortical network: integrated BCI for walking rehabilitation. *Neural Plast.* 2012:375148. doi: 10.1155/2012/375148

Cramer, S. C. (2008). Repairing the human brain after stroke. II. restorative therapies. *Ann. Neurol.* 63, 549–560. doi: 10.1002/ana.21412

Da Silva, F. L. (2010). "EEG: origin and measurement," in *EEG-fMRI: Physiological Basis, Technique, and Applications,* eds C. Mulert and L. Lemieux (Berlin; Heidelberg: Springer), 19–38. doi: 10.1007/978-3-540-87919-0_2

Field, A. (2009). *Discovering Statistics Using SPSS*. London, UK: Sage Publications.

Gharabaghi, A. (2016). What turns assistive into restorative brain-machine interfaces? *Front. Neurosci.* 10:456. doi: 10.3389/fnins.2016.00456

Ghasemi, A., and Zahediasl, S. (2012). Normality tests for statistical analysis: a guide for non-statisticians. *Int. J. Endocrinol. Metab.* 10:486. doi: 10.5812/ijem.3505

Gwin, J. T., Gramann, K., Makeig, S., and Ferris, D. P. (2011). Electrocortical activity is coupled to gait cycle phase during treadmill walking. *Neuroimage* 54, 1289–1296. doi: 10.1016/j.neuroimage.2010.08.066

Hortal, E., Planelles, D., Iáñez, E., Costa, A., Úbeda, A., and Azorín, J. M. (2016a). "Detection of gait initiation through a ERD-based brain-computer interface," in *Advances in Neurotechnology, Electronics and Informatics,* eds A. R. Londral and P. Encarnação (Cham: Springer), 141–150. doi: 10.1007/978-3-319-26242-0_10

Hortal, E., Úbeda, A., Iáñez, E., Azorín, J. M., and Fernández, E. (2016b). EEG-based detection of starting and stopping during gait cycle. *Int. J. Neural Syst.* 26:1650029. doi: 10.1142/S0129065716500295

Huang, N. E., Shen, Z., Long, S. R., Wu, M. C., Shih, H. H., Zheng, Q., et al. (1998). The empirical mode decomposition and the Hilbert spectrum for nonlinear and non-stationary time series analysis. *Proc. R. Soc. Lond. A Math. Phys. Eng. Sci.* 454, 903–995. doi: 10.1098/rspa.1998.0193

Jiang, N., Gizzi, L., Mrachacz-Kersting, N., Dremstrup, K., and Farina, D. (2015). A brain–computer interface for single-trial detection of gait initiation from movement related cortical potentials. *Clin. Neurophysiol.* 126, 154–159. doi: 10.1016/j.clinph.2014.05.003

Li, J., Ji, H., Cao, L., Zang, D., Gu, R., Xia, B., et al. (2014). Evaluation and application of a hybrid brain computer interface for real wheelchair parallel control with multi-degree of freedom. *Int. J. Neural Syst.* 24:1450014. doi: 10.1142/S0129065714500142

McFarland, D. J., McCane, L. M., David, S. V., and Wolpaw, J. R. (1997). Spatial filter selection for EEG-based communication. *Electroencephalogr. Clin. Neurophysiol.* 103, 386–394. doi: 10.1016/S0013-4694(97)00022-2

Ortiz, M., Iáñez, E., Rodriguez-Ugarte, M., and Azorín, J. (2017). "Empirical mode decomposition use in electroencephalography signal analysis for detection of starting and stopping intentions during gait cycle," in *26th IEEE International Symposium on Robot and Human Interactive Communications* (Lisbon: IEEE), 1–7.

Pfurtscheller, G., and Neuper, C. (1994). Event-related synchronization of mu rhythm in the EEG over the cortical hand area in man. *Neurosci. Lett.* 174, 93–96. doi: 10.1016/0304-3940(94)90127-9

Rao, R. P. (2013). *Brain-Computer Interfacing: An Introduction*. Cambridge, UK: Cambridge University Press.

Rilling, G., and Flandrin, P. (2006). "On the influence of sampling on the empirical mode decomposition," in *Acoustics, Speech and Signal Processing, 2006. ICASSP 2006 Proceedings. 2006 IEEE International Conference on*, Vol. 3 (Toulouse: IEEE), III.

Rilling, G., and Flandrin, P. (2008). One or two frequencies? The empirical mode decomposition answers. *IEEE Trans. Signal Process.* 56, 85–95. doi: 10.1109/TSP.2007.906771

Rilling, G., Flandrin, P., and Gonçalves, P. (2003). "On empirical mode decomposition and its algorithms," in *IEEE-EURASIP Workshop on Nonlinear Signal and Image Processing*, Vol. 3 (Grado: IEEER), 8–11.

Rodríguez-Ugarte, M., Iáñez, E., Ortíz, M., and Azorín, J. M. (2017). Personalized offline and pseudo-online BCI models to detect pedaling intent. *Front. Neuroinformatics* 11:45. doi: 10.3389/fninf.2017.00045

Sburlea, A. I., Montesano, L., and Minguez, J. (2017). Advantages of EEG phase patterns for the detection of gait intention in healthy and stroke subjects. *J. Neural Eng.* 14:036004. doi: 10.1088/1741-2552/aa5f2f

Severens, M., Nienhuis, B., Desain, P., and Duysens, J. (2012). "Feasibility of measuring event related desynchronization with electroencephalography during walking," in *Engineering in Medicine and Biology Society (EMBC), 2012 Annual International Conference of the IEEE* (San Diego, CA: IEEE), 2764–2767.

Steinwart, I., and Christmann, A. (2008). *Support Vector Machines*. New York, NY: Springer Science & Business Media.

Stockwell, R. G., Mansinha, L., and Lowe, R. (1996). Localization of the complex spectrum: the s transform. *IEEE Trans. Signal Process.* 44, 998–1001. doi: 10.1109/78.492555

Subasi, A. (2005). Automatic recognition of alertness level from EEG by using neural network and wavelet coefficients. *Expert Syst. Appl.* 28, 701–711. doi: 10.1016/j.eswa.2004.12.027

Villarejo Mayor, J. J., Costa, R. M., Frizera-Neto, A., and Bastos, T. F. (2017). Decoding of grasp and individuated finger movements based on low-density myoelectric signals. *Rev. Iberoam. Autom. Infor. Indust.* 14, 184–192. doi: 10.1016/j.riai.2017.02.001

Wagner, J., Solis-Escalante, T., Grieshofer, P., Neuper, C., Müller-Putz, G., and Scherer, R. (2012). Level of participation in robotic-assisted treadmill walking modulates midline sensorimotor EEG rhythms in able-bodied subjects. *Neuroimage* 63, 1203–1211. doi: 10.1016/j.neuroimage.2012.08.019

Conflict of Interest Statement: The authors declare that the research was conducted in the absence of any commercial or financial relationships that could be construed as a potential conflict of interest.

frontiers in Neuroscience

ORIGINAL RESEARCH
published: 12 December 2017
doi: 10.3389/fnins.2017.00699

A Framework for Measuring the Progress in Exoskeleton Skills in People with Complete Spinal Cord Injury

Rosanne B. van Dijsseldonk[1], Hennie Rijken[2], Ilse J. W. van Nes[2], Henk van de Meent[3] and Noel L. W. Keijsers[1,3]*

[1] Department of Research, Sint Maartenskliniek Research, Nijmegen, Netherlands, [2] Department of Rehabilitation, Sint Maartenskliniek, Nijmegen, Netherlands, [3] Department of Rehabilitation, Radboudumc, Nijmegen, Netherlands

For safe application of exoskeletons in people with spinal cord injury at home or in the community, it is required to have completed an exoskeleton training in which users learn to perform basic and advanced skills. So far, a framework to test exoskeleton skills is lacking. The aim of this study was to develop and test the hierarchy and reliability of a framework for measuring the progress in the ability to perform basic and advanced skills. Twelve participants with paraplegia were given twenty-four training sessions in 8 weeks with the Rewalk-exoskeleton. During the 2nd, 4th, and 6th training week the Intermediate-skills-test was performed consisting of 27 skills, measured in an hierarchical order of difficulty, until two skills were not achieved. When participants could walk independently, the Final-skills-test, consisting of 20 skills, was performed in the last training session. Each skill was performed at least two times with a maximum of three attempts. As a reliability measure the consistency was used, which was the number of skills performed the same in the first two attempts relative to the total number. Ten participants completed the training program. Their number of achieved intermediate skills was significantly different between the measurements $X_F^2(2) = 12.36$, $p = 0.001$. *Post-hoc* analysis revealed a significant increase in the median achieved intermediate skills from 4 [1–7] at the first to 10.5 [5–26] at the third Intermediate-skills-test. The rate of participants who achieved the intermediate skills decreased and the coefficient of reproducibility was 0.98. Eight participants met the criteria to perform the Final-skills-test. Their median number of successfully performed final skills was 16.5 [13–20] and 17 [14–19] skills in the first and second time. The overall consistency of >70% was achieved in the Intermediate-skills-test (73%) and the Final-skills-test (81%). Eight out of twelve participants experienced skin damage during the training, in four participants this resulted in missed training sessions. The framework proposed in this study measured the progress in performing basic and advanced exoskeleton skills during a training program. The hierarchical ordered skills-test could discriminate across participants' skill-level and the overall consistency was considered acceptable.

Keywords: spinal cord injury, exoskeleton, paraplegia, ambulation, skills

OPEN ACCESS

Edited by:
Mikhail Lebedev,
Duke University, United States

Reviewed by:
William Zev Rymer,
Rehabilitation Institute of Chicago, United States
Gelu Onose,
Carol Davila University of Medicine and Pharmacy, Romania

****Correspondence:***
Rosanne B. van Dijsseldonk
r.vandijsseldonk@maartenskliniek.nl

Specialty section:
This article was submitted to Neuroprosthetics, a section of the journal Frontiers in Neuroscience

Received: *29 August 2017*
Accepted: *28 November 2017*
Published: *12 December 2017*

Citation:
van Dijsseldonk RB, Rijken H, van Nes IJW, van de Meent H and Keijsers NLW (2017) A Framework for Measuring the Progress in Exoskeleton Skills in People with Complete Spinal Cord Injury. Front. Neurosci. 11:699. doi: 10.3389/fnins.2017.00699

INTRODUCTION

Worldwide the incidence of Spinal Cord Injury (SCI) is 180,000 cases per annum (Lee et al., 2014) of whom 50% have a complete lesion and become wheelchair-designated for their mobility (Wyndaele and Wyndaele, 2006). A lifetime of sitting has been associated with an increased risk of multiple secondary complications, such as pressure ulcers, spasticity, and worsening of bladder and bowel dysfunction (Jensen et al., 2013; Adriaansen et al., 2016). Exoskeletons (external active orthosis) make it possible for people with paraplegia to regain their standing and walking mobility by generating the basic motions for ambulation e.g., standing-up, sitting-down, standing, and walking. Similar to other standing and robotic gait training devices (Middleton et al., 1997; Dunn et al., 1998; Mirbagheri et al., 2015), exoskeletons have the potential to prevent secondary health complication (Miller et al., 2016). The main benefit of exoskeletons compared to other robotic gait training devices (such as Lokomat®) is that exoskeletons can be used at home and in the community outside of a clinical setting (Federici et al., 2015). However, several risks are identified with exoskeleton use such as falls, joint misalignment, skin damage, software malfunctions, electrical and fire hazard, and user errors (He et al., 2017). So far, the chance and extent of the risks are not well understood (He et al., 2017). Furthermore, manufacturers require an intensive training period before home and community use is allowed.

A prerequisite for safe and independent home and community exoskeleton use, is that users are able to perform basic and advanced exoskeleton skills. Previous research mainly focussed on the basic skills (sit-to-stand, stand-to-sit, and walking) and has shown that basic skills can be learned in a 25 sessions-training program with varying levels of assistance (Spungen et al., 2013; Kozlowski et al., 2015; Platz et al., 2016). The basic skills are highly relevant for use in a clinical setting, but for safe independent community use more advanced skills are required, including arresting gait on command, passing door thresholds, low curbs and ramps and controlling the input device (Spungen et al., 2013; Yang et al., 2015). The control of and interaction with the exoskeleton is diverse across the different exoskeletons available on the market. Moreover, some exoskeletons are more difficult or impossible to control dependent on the level and severity of the SCI of the user (Bryce et al., 2015). Several studies tested advanced skills in a limited number of motor complete SCI patients (Spungen et al., 2013; Hartigan et al., 2015; Kozlowski et al., 2015; Benson et al., 2016; Platz et al., 2016). However, the advanced skills were not tested in a systematic way and for example Spungen et al. concluded that the skills could have been introduced earlier in the training program (Spungen et al., 2013). So far, a systematic framework to structure, test and evaluate exoskeleton skills during a training program is lacking. Therefore, the aim of this study is to develop a framework to measure the progress in the ability to perform exoskeleton skills. The proposed framework consists of exoskeleton skills arranged into a hierarchy so that the difficulty increased with each tested skill. If the exoskeleton skills formed a true hierarchy and a skill was not achieved, it can be assumed that the participant would not achieve all higher skills and would achieve all lower skills. Therefore, arranging the skills into a hierarchy would reduce the time and effort of the exoskeleton-skills-test (Tyson and DeSouza, 2004). Furthermore, it is essential that the exoskeleton-skill-tests in the framework are reliable. Accordingly, the skills had to be performed consistent to reduce the change of misjudging the participants' skill-level.

Before an advanced exoskeleton skill-level can be achieved, an intensive training program with multiple training sessions per week over a longer period of time is required. The risk factors associated with such an intensive training program are still not well understood (He et al., 2017). However, it can be expected that such an intensive training program decreases the risk of falls, joint misalignment and user errors and increases the safety of exoskeleton home and community use. On the contrary, intensive exoskeleton use increases the risk of skin damage and bruises. Previous research concluded that in hospital training with an exoskeleton was safe (Zeilig et al., 2012; Esquenazi, 2013; Kolakowsky-Hayner et al., 2013; Kubota et al., 2013; Spungen et al., 2013). However, other studies disclosed mild to moderate skin damages in half of the participants (five out of ten) (Benson et al., 2016) (four out of seven) (Platz et al., 2016). Other reported complications were a fracture of the talus (Louie et al., 2015) and venous-lymphatic stasis in the lower limbs (Onose et al., 2016). Hence, assessing the occurrence of complications such as skin damage, muscle or joint pain, incontinence problems, device related errors, fractures, venous-lymphatic stasis, and falls during an exoskeleton training program is important for clinical recommendations.

In conclusion, the main objective of this study was to develop and test a framework for measuring the progress to perform basic and advanced exoskeleton skills in a group of individuals with motor complete SCI. The hierarchy and the reliability of the exoskeleton-skills-test in the framework was evaluated. As a secondary outcome, complications such as skin damage, muscle or joint pain, and incontinence problems resulting from the intensive exoskeleton training program were assessed.

MATERIALS AND METHODS

Participants

People with paraplegia who gained knowledge about the exoskeleton technology throughout the media and who were interested in testing the potential of an exoskeleton contacted the rehabilitation center of the Sint Maartenskliniek to participate in this study. Eligible persons were adult patients in the chronic phase (>6 months) with a motor complete SCI [American Spinal Injury Association Impairment Scale (AIS) A or B] between Thoracic 1 (Th1) and Lumbar 1 (L1). The exclusion criteria were physical factors that hamper proper functioning of the exoskeleton, such as severe spasticity (Modified Ashworth Scale > 3), taller than 1.90 m or smaller than 1.60 m, bodyweight above 100 kg, and restricted range of motion in the hip, knee, or ankle joint. Other exclusion criteria were inability to control crutches, unable to make a transfer from a chair to a wheelchair without the use of external support, and patients with conditions that could interfere with the motor learning process (e.g., stroke). Potential subjects with an increased risk of adverse events such as patients with osteoporosis, fractures of the lower extremities in the last 2 years, balance disorders, neurogenic

heterotopic ossification and pregnancy were also excluded. All participants gave written informed consent in accordance with the Declaration of Helsinki. The study was approved by the medical ethics committee of Arnhem-Nijmegen (2016-2418) and the internal review committee of the Sint Maartenskliniek.

Procedure

All exoskeleton training sessions and measurements were performed in the sports hall at the rehabilitation center. Prior to the start of the training a brief physical examination by a rehabilitation physician was performed, in which the in- and exclusion criteria of the study were checked. Participants were given twenty-four training sessions of 1.5-h over an 8 week period. Three physical therapists were trained by ReWalk™ Robotics to give the exoskeleton training. During each session at least two physical therapists were present to assure safety. The exoskeleton and the Lofstrand crutches were adjusted to the patients' body composition during the first training session. After each training the physical therapists notated the skills that were practiced. Participants kept a logbook during the entire study including any complications such as skin abrasions, muscle or joint pain, falls, and incontinence problems. The logbook was filled out at least three times a week. To assess the progress in achieved skills the participants' skill-level was tested every 2 weeks during a training session. In total the skill-level was assessed four times during the study, three times with the Intermediate-skills-test and one time with the Final-skills-test.

Intermediate- and Final-Skills-Test

The Intermediate-skills-test was performed in training week 2, 4, and 6. The Intermediate-skills-test consisted of 27 skills, which were measured separately of each other and were arranged into a hierarchy so that the difficulty increased with each skill. The intermediate skills were sorted into three categories; standing, walking, and advanced skills. Each subsequent category required more control of the user over the exoskeleton. Within each category the complexity of the skills also increased. In the standing skills the feet of the user remained roughly at the same place and participants learned to use their crutches, whereas there was displacement of the feet in the walking and advanced skills. In the walking skills, the increase of difficulty was related to the decrease in level of assistance and number of involuntary stops. In the advanced skills an additional task was performed while walking. The complexity of the task increased from walking turns with a decrease in number of involuntary stops to passing obstacles to passing obstacles that require raising or lowering of the center of mass (walk up and down a martial arts mat). An overview of the 27 skills of the Intermediate-skills-test is given in **Table 1**. Each intermediate skill was performed at least two times with a maximum of three attempts. An intermediate skill was considered achieved when the skill was performed independent without assistance of the exoskeleton trainer in at least two out of three attempts. The Intermediate-skills-test continued until two skills were not achieved. Participants were allowed to take rest between the various skills tested. A more detailed description of the Intermediate-skills-test is provided in Supplementary Table 1 (available online).

TABLE 1 | Assessed exoskeleton skills in the Intermediate-skills-test.

Category	Order	Intermediate skill
Standing skills	1	Weight shifting forward and backward and to the right and left
	2	Touching the wristband during standing
	3	Sit-to-stand
	4	Stand-to-sit
Walking skills	5	Walk 10 m with assistance (with max. 2 stops)
	6	Stop with the preferred leg
	7	Stop with the not preferred leg
	8	Walk 10 m without assistance (with max. 2 stops)
	9	Walk 10 m without assistance (without stops)
Advanced skills	10	Arrest gait at command
	11	Walk a 90° curve to the right (with max. 1 stop)
	12	Walk a 90° curve to the right (without stops)
	13	Walk a 90° curve to the left (with max. 1 stop)
	14	Walk a 90° curve to the left (without stops)
	15	Walk a 180° curve (radius 1.8 m) to the right (with max. 1 stop)
	16	Walk a 180° curve (radius 1.8 m) to the right (without stops)
	17	Walk a 180° curve (radius 1.8 m) to the left (with max. 1 stop)
	18	Walk a 180° curve (radius 1.8 m) to the left (without stops)
	19	Arrest gait nearby a vaulting box (height 1.1 m) and move a cone at chest height
	20	Pass a narrow passage (width 0.8 m) (with max. 1 stop)
	21	Arrest gait nearby a door (width 0.8 m), open the door away from you and enter (with max. 1 stop)
	22	Arrest gait nearby a door (width 0.8 m), open the door toward you and enter (with max. 1 stop)
	23	Arrest gait near a chair (height 0.5 m) and pivot turn to sit down
	24	Pass an upward and downward sloping doorstep (angle up 11.3°and down 16.7°, height 0.03 m) (with max. 1 stop)
	25	Walk up a martial arts mat (height 0.04 m) (with max. 1 stop)
	26	Walk down a martial arts mat (height 0.04 m) (with max. 1 stop)
	27	Walk a slalom around 4 badminton poles (distance between poles 3.0 m) (with max. 2 stops)

The Final-skills-test was performed during the last training week (week 8) in the final training session. A prerequisite for performing the Final-skills-test was that participants could control the remote control and walk without assistance of the exoskeleton trainer. The Final-skills-test consisted of a fixed set of 20 skills and was performed two times with a 5 min break in between. In contrast to the Intermediate-skills-test, the tested exoskeleton skills were measured in sequence during

the Final-skills-test, simulating daily life situations in which skills are rarely performed independent of each other. Moreover, performing skills in sequence made it more difficult to achieve a skill than performing skills independent from each other (e.g., arresting gait immediately after a sharp curve compared to arresting gait independent of the previous action). In the Final-skills-test the focus was on independent performance of skills and the number of stops was not taken into account. Furthermore, the basic intermediate skills (e.g., weight shifting, touching the wristband, sit-to-stand, and assisted walking) are required in performing most of the skills and were not tested separately. In order to assess the test in a sports hall with as little material as possible, the advanced intermediate skill of opening a door was not part of the Final-skills-test. To assure safety, the exoskeleton trainer walked behind the participant but did not intervene unless the participants lost their balance and could fall. The final skills were considered achieved when the participants performed the skills without assistance of the exoskeleton trainer. In **Figure 1** a schematic representation of the Final-skills-test is given.

Equipment

In this study, two wearable robotic exoskeletons that enable powered hip and knee motion from ReWalk™ Robotics were used; (1) the ReWalk™ Rehabilitation System and (2) the ReWalk™ Personal 6.0. The exoskeleton systems provided user-initiated mobility through the integration of a wearable brace support, a computer-based control system and motion sensors. The exoskeleton systems have the Class II FDA clearance for

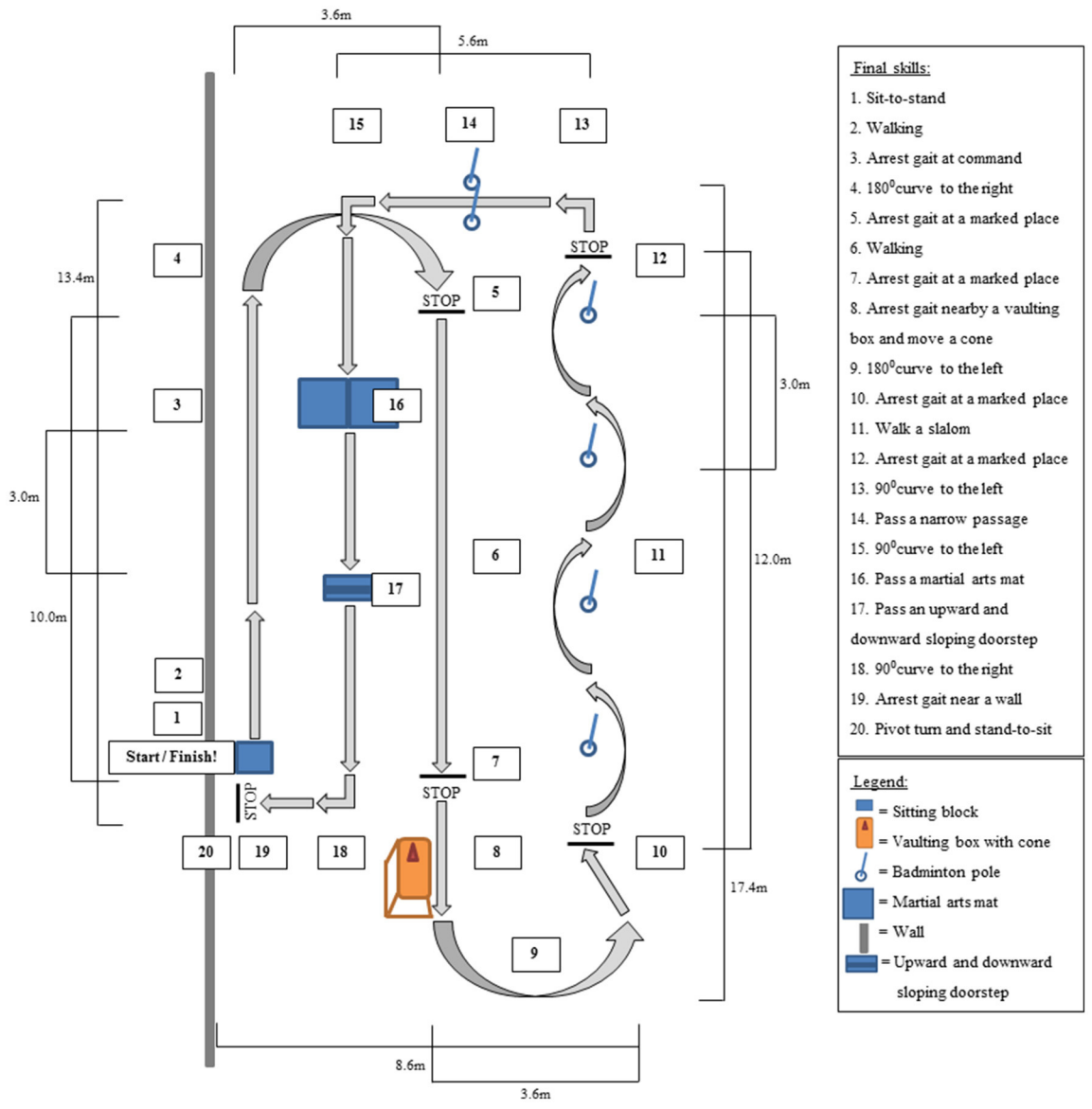

FIGURE 1 | Schematic representation of the top view of the Final-skills-test. Arrows represent the walking direction.

both use in a rehabilitation setting as well as personal use. All participants started training with the ReWalk™ Rehabilitation System. Only participants who met de criteria to perform the Final-skills-test used the ReWalk™ Personal 6.0 system as well.

Data and Statistical Analysis

To assess if the proposed framework measured the ability to perform basic and advanced exoskeleton skills throughout an exoskeleton program, the skill-tests in the framework should measure progression in the number of achieved skills and show distinct skill-levels between participants. The skills should be arranged into a hierarchical order of difficulty. Moreover, the skills tested in the framework should be performed consistent. In addition, the relation between the Intermediate- and Final-skills-test was determined.

Achieved Intermediate Skills

The number of achieved skills was analyzed using descriptive statistics (median and ranges). Differences in the number of achieved skills between the three Intermediate-skills-test was assessed with the non-parametric Friedman test ($\alpha = 0.05$). In case of a significant Friedman test, Wilcoxon *post-hoc* test with Bonferroni correction ($\alpha = 0.017$) was used to determine changes. The number of participants who showed the expected increase in number of achieved skills over the three intermediate measurements was determined. Each intermediate skill was also analyzed separately for the number of times a skill was achieved.

Hierarchy of the Skills

The hierarchy of the skills tested in the Intermediate-skills-test was analyzed according to two measurements (1) the rate of participants achieving each intermediate skill and (2) the coefficient of reproducibility (Tyson and DeSouza, 2004). Both tests are based on the theoretical expectation that the participants ability to achieve a skill would decrease as the difficulty of the task increased. For a more detailed description see Tyson and DeSouza (2004). The coefficient of reproducibility was calculated with the formula described by Tyson and DeSouza: Coefficient of reproducibility = 1 − scaling errors/(number of skills × number of observations; Tyson and DeSouza, 2004). In which scaling errors is the number of participants who did not achieve the skills in the predetermined order. Since participants progressed during the training each intermediate skills measurement was considered as a separate observation in the analysis. A coefficient of reproducibility of at least 0.9 was considered acceptable (Guttman, 1944; Tyson and DeSouza, 2004).

Achieved Final Skills

The number of achieved final skills was analyzed using descriptive statistics (median and ranges). Each final skill was also analyzed separately for the number of times a skill was achieved. The correlation between the number of achieved skills in each skills-test was assessed with Kendall's rank correlation coefficient (Kendall's Tau).

Consistency

The consistency in the number of exoskeleton skills which were performed the same in the first two attempts (successful-successful or failure-failure) relative to the total number of performed skills was used as a reliability measure of the Intermediate-skills-test and the Final-skills-test. An overall consistency of >70% was considered reliable. Each intermediate skill and final skill was also analyzed separately for the number of times a skill was tested, performed consistent and performed successful.

Complications

To assess the occurrence of complications during an exoskeleton training program both the physical therapists and participants filled out a logbook after each training session including any complications. The reported complications such as the number of skin damages, location of skin damages, incidence of reported muscle or joint pain, number of incontinence problems, device related errors, fractures, venous-lymphatic stasis and falls during the exoskeleton training program were analyzed using descriptive statistics.

RESULTS

Participants

Out of 12 participants 10 (83%) completed the training program. Reasons for not completing the training program were inability to learn the basic skills of the exoskeleton (stopped after seven training sessions and performed the first Intermediate-skills-test) and absence of perceived benefit (stopped after two training sessions and did not perform an Intermediate-skills-test). Eleven participants completed at least one Intermediate-skills-test, the data of these participants was used in the analysis of the hierarchy and consistency of the intermediate skills. Due to time constraints, one participant was not able to perform the skills a second time during the Final-skills-test. For this participant the set of final skills was repeated twice one week later. The data of the second Final-skills-test was only used for the consistency analysis whereas the first Final-skills-test was used for the analysis of the achieved skills after the training program. We do not expect that this had an impact on the outcome of the current study. An overview of the patient characteristics is given in **Table 2**.

TABLE 2 | Patient characteristics.

	Total (*N* = 12)
Gender (male/female)	7/5
Age (years), median [range]	42 [24–56]
Level of SCI, median [range]	Thoracic 9 [4–11]
Post-injury (months), median [range]	75 [24–276]
AIS* (A/B)	11/1

**AIS, American Spinal Injury Association Impairment Scale.*

Achieved Intermediate Skills

The Friedman test revealed a significant difference between the number of achieved intermediate skills between the measurements [$X_F^2(2) = 12.36$, $p = 0.001$]. *Post-hoc* analysis revealed that the achieved intermediate skills significantly increased from a median of 4 [1–7] at Intermediate-skills-test one to 10.5 [5–26] at Intermediate-skills-test three. There was no significant difference in the number of achieved skills between Intermediate-skills-test one and two and between two and three. **Figure 2** shows the achieved intermediate skills per participant. Five out of ten participants showed the expected increase in number of achieved skills over the three measurements.

Detailed *post-hoc* analysis revealed that five of the intermediate skills were achieved during all measurements (see completely green bars in **Figure 3**). Three out of five intermediate walking skills, and two advanced skills were achieved in approximately half of the tested times, these skills are highlighted with an "#"-sign in **Figure 3**.

Hierarchy of the Skills

In general, the rate of participants who achieved the intermediate skills decreased. In three skills, the "walk 10 m without stops," "180° curve tot the right without stops," and "open door toward"-skill, the number of participants who achieved the skills was smaller than skills later in the hierarchical order (**Figure 4**). The coefficient of reproducibility was 0.98 (number of scaling errors: 14, number of skills: 27 and number of observations: 31 (10 participants with three observations and one participant with one observations). The scaling errors occurred in nine different skills (Intermediate-skill 3, 4, 6, 7, 9, 10, 12, 16, and 22) and in eight out of eleven participants. Four scaling errors occurred in Intermediate-skills-test one, three in Intermediate-skills-test two, and seven in Intermediate-skills-test three.

Achieved Final Skills

Eight participants were able to walk without assistance between the 18th and 23th training session and therefore met the criteria to perform the Final-skills-test. The median number of successfully performed final skills in these participants was 16.5 [13–20] and 17 [14–19] skills in the first and second time. In the Final-skills-test, 15 skills were at least one time achieved by all eight subjects (see **Figure 5**). The martial arts mat was not achieved by half of the participants.

The number of achieved final skills in the first and the second time were significantly correlated ($r_\tau = 0.75$, $p < 0.05$) and not significantly different ($z = -0.71$, $p = 0.75$, effect size $= -0.18$). **Table 3** revealed the correlation between the various skills-tests. The number of achieved skill in none of the Intermediate-skills-tests were significantly correlated with the achieved skills in any other skill-tests.

Consistency

Eleven participants performed in total 235 intermediate skills, of which 171 (73%) were performed the same in the first two attempts (successful-successful or failure-failure).

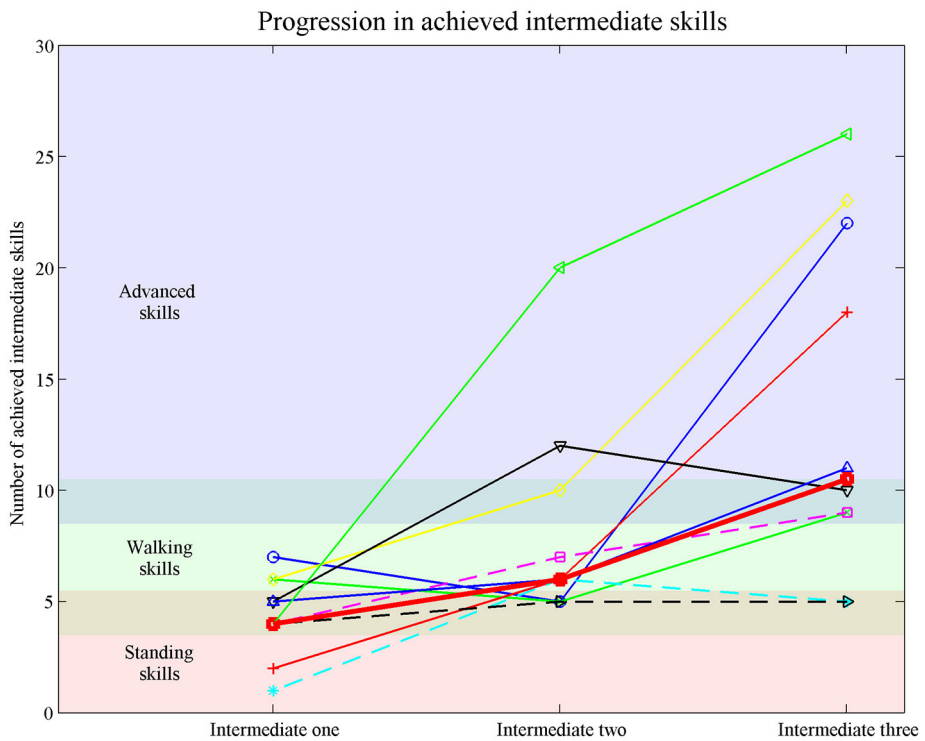

FIGURE 2 | Achieved intermediate skills measured with the Intermediate-skills-test one, two and three. Each line represents a participants. Thick red line represents the median achieved intermediate skills. Dotted lines represent participants who did not perform the Final-skills-test.

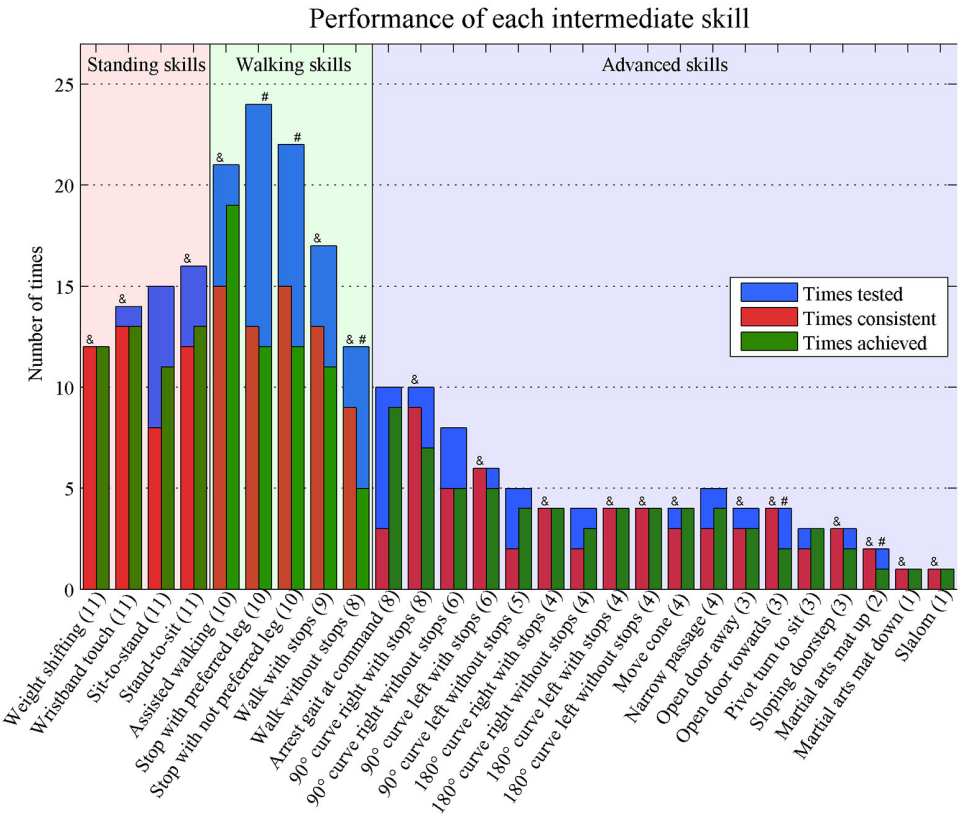

FIGURE 3 | Times performed consistent and achieved of each separate intermediate skill. Numbers in brackets represent the number of tested participants. Consistent = performed the same in the first two attempts (successful-successful or failure-failure). Achieved = at least two out of three successful attempts & = >70% performed consistent # = achieved in ∼50% of the times.

The number of participants who performed the skill, the number of times a skill was measured, the number of times a skill was performed consistent and the number of times a skill was achieved is shown for each intermediate skill in **Figure 3**. Eighteen skills were performed consistent in more than 70% of the times (highlighted with an "&"-sign in **Figure 3**). Of these skills, 10 skills were performed consistent during all Intermediate-skills-tests (see completely red bars in **Figure 3**).

Eight participant performed all twenty final skills twice resulting in a total of 160 final skills. They performed 130 (81%) final skills the same in both attempts. The median number of inconsistent performed skills per participant was 2.5 [0–9]. An overview of the consistent and inconsistent performances of each final skill is depicted in **Figure 5**. Most skills were performed consistently by seven (9 skills) or six (6 skills) participants. Two skills were performed consistently by all participants (highlighted with an "A"-sign in **Figure 5**), whereas three skills were performed inconsistent by three participants (180° curve to the right, slalom and martial arts mat) (highlighted with an "N"-sign in **Figure 5**).

Complications

Eight out of twelve participants experienced device related skin damage at the feet ($n = 3$), knee ($n = 5$), thigh ($n = 3$), pelvic ($n = 4$), and/or trunk ($n = 1$) area. In four participants the skin damage resulted in at least one missed training session, which was rescheduled at the end of the training period. In case of skin damage, extra padding was added to prevent reoccurrence of the complication. As a result, most skin damage occurred in the early phase of the training program. Seven participants reported muscle or joint pain during the training program around the hands/wrists ($n = 2$), arms ($n = 3$), shoulders ($n = 3$), neck ($n = 3$), trunk ($n = 1$), and/or back ($n = 3$). None of the complications evolved into serious adverse events. During the entire study the incidence of device related errors was three times in 218 training sessions. No incontinence problems, fractures, venous-lymphatic stasis or falls were mentioned by the participants or physical therapists in the study.

DISCUSSION

In the present study, a framework for measuring the ability to perform basic and advanced exoskeleton skills throughout an exoskeleton training program was developed and tested. Ten participants completed the training program and were tested during the 2nd, 4th, and 6th training week. They showed an increase in the achieved intermediate skills from four at the

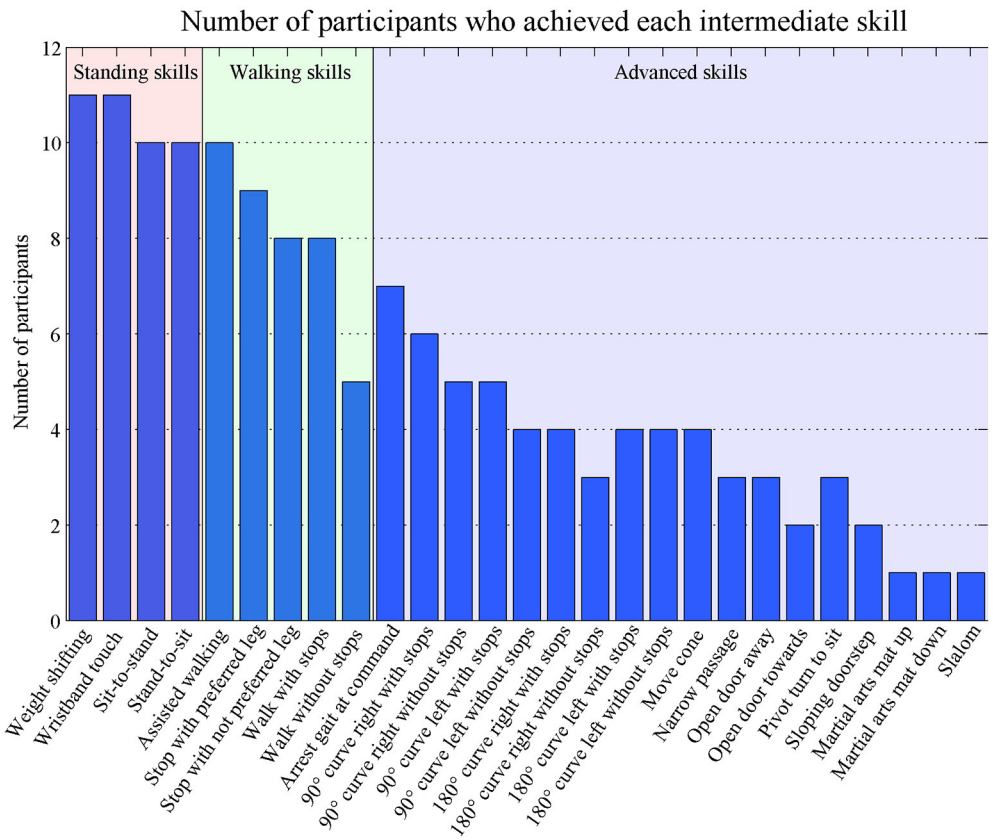

FIGURE 4 | Rates of achievement of each intermediate skill.

first to 10.5 at the third Intermediate-skills-test. The rate of participants who achieved the intermediate skills decreased and the coefficient of reproducibility was 0.98. In the last training week, eight participants successfully performed 16.5 and 17 skills in the Final-skills-test. An overall consistency of 73% in the Intermediate-skills-test and 81% in the Final-skills-test was achieved.

Similar to other assistive technologies, such as prostheses and to a lesser extent wheelchairs, exoskeleton community use is preceded with a training program. Although the type and extent of the risks of exoskeletons are yet to be understood (He et al., 2017), the risks associated with exoskeleton use seems higher than with prostheses or wheelchair. The advantage of a prostheses and a wheelchair is that it can be used independently for ambulation in an early phase. Therefore, clinical tests such as the timed up and go-test (Condie et al., 2006) or the mechanical efficiency (Leving et al., 2016) can be used to evaluate the progress in performance in using the assistive technologies. In contrast, most people are not able to perform basic ambulation skills at the start of an exoskeleton training program and multiple training sessions are needed before independent ambulation is possible. Assessing performance in using assistive technologies can also be done with standardized skills-tests. For wheeled mobility several skills-test, such as the wheelchair skills-test, are available (Fliess-Douer et al., 2010). Until now there were no standardized skills-test for exoskeleton performance. Several studies marked the training session in which a skill with an exoskeleton was performed with varying levels of trainer assistance (Spungen et al., 2013; Hartigan et al., 2015; Kozlowski et al., 2015; Benson et al., 2016; Platz et al., 2016). However, in these studies the performed exoskeleton skills were kept up in a logbook and the independent achievement of skills was not tested on a regular bases. The main objective of this study was to develop a framework for measuring the ability to perform basic and advanced exoskeleton skills throughout an exoskeleton training program.

A framework to assess the progress of exoskeleton skills should consist of tests measuring achieved skills in a hierarchical order of difficulty. As a consequence participants should progress during an intensive exoskeleton training program. Although the Friedman test revealed a significant difference in the number of achieved skills between the Intermediate-skills-tests, these results should be interpreted with care because several tied ranks were observed and a small number of participants were included. Nevertheless, the number of achieved intermediate skills significantly increased from 4 at the first to 10.5 at the third Intermediate-skills-test. Furthermore, nine and seven out of ten participants had an increase in the number of achieved skills between the first and second and the second and third Intermediate-skills-test, respectively. However, such an increase

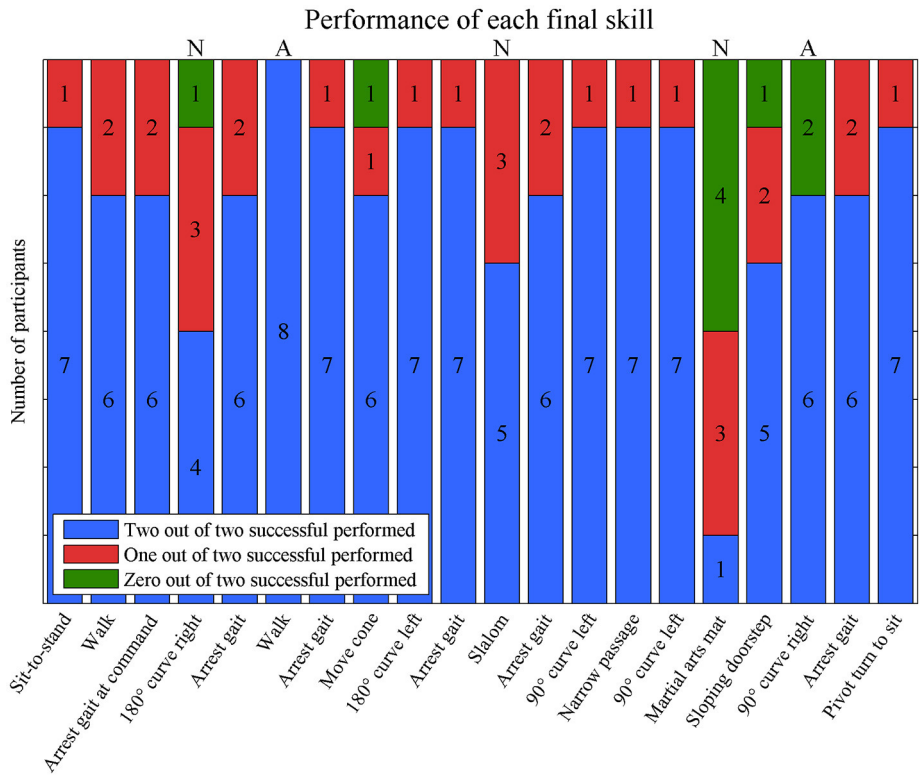

FIGURE 5 | The number of consistent performances of each final skill. Green bars represent inconsistent performances in which one out of two attempt was successful performed. Blue and red bars represent consistent performances. A = all performed consistent; N = <70% performed consistent.

TABLE 3 | Correlation (Kendall's tau) between all test moments.

	Intermediate-skills-test 1	Intermediate-skills-test 2	Intermediate-skills-test 3	Final-skills-test 1	Final-skills-test 2
Intermediate-skills-test 1		−0.15 (10)	0.29 (10)	0.08 (8)	0.21(8)
Intermediate-skills-test 2			0.37 (10)	0.00 (8)	−0.13(8)
Intermediate-skills-test 3				0.15 (8)	0.32(8)
Final-skills-test 1					0.75(8)*

Digits in brackets represent the number of participants.
**Correlation is significant at the 0.05 level.*

in number of achieved skills doesn't automatically indicate that the skills are in a correct order of difficulty. In the current study, two measures were used to assess the hierarchy. According to the coefficient of reproducibility (0.98) the intermediate skills were in the correct order of difficulty (Guttman, 1944; Tyson and DeSouza, 2004). The rate of the number of participants achieving each skill revealed three skills (walk 10 m without stops, 180° curve to the right without stops, and open door toward-skill) that were achieved by a larger number of participants in the subsequent skill. Detailed *post-hoc* analysis revealed that only an unachieved "walk 10 m without stops"-skill was followed by achieved skills in more than two observations (five observations). Covering a distance of 10 m without stops was the last basic skills before advanced skills were tested. The advanced skills consisted of an additional task during walking such as a sudden stop, curves or passing a doorstep, but a shorter distance of ∼3 m had to be covered. The length of the skill of walking a distance of 10 m increased the chance of errors and not achieving the skill. Two other studies (Spungen en Platz) also recorded the moment the 10 m walking skill was performed without assistance, four (Spungen et al., 2013) and one (Platz et al., 2016) out of seven participants were able to perform the skill independent within 24 training sessions. Indicating the difficulty of walking 10 m without assistance. In the current study each test session was scheduled in advance within a training session and an extra person was present during the skills-test. As a result, most participants were more stressed during the skills-test than during other training sessions. An increased stress level could evoke more spasticity (Fleuren et al., 2009) causing involuntary stops, which particularly influenced the achievement of the "10 m walking skill without stops"-skill. Because walking without stops is crucial in performing most advanced skills, we prefer to keep

the proposed order of the skills. However, for future research we would advise to change the order of the Intermediate-skills for the "walking curves" according to the preference of the patient.

In addition to assess the progression, the framework had to discriminate across participants. In all Intermediate-skills-tests, differences between participants were apparent. After 2 weeks of exoskeleton training participants were only able to perform basic skills, but varied between standing and walking skills. This was in line with the findings of Spungen et al. (2013). In the current study, all participants were able to perform all intermediate standing skills without assistance after 4 and 6 weeks of training, but differed in walking and advanced skills. In addition to differences across participants at the Intermediate-skills-tests, participants showed various learning curves. The low correlation between the three Intermediate-skills-tests (r_τ between -0.15 and 0.37) supports the various learning process across participants. In conclusion, the framework proposed in this study measured the progress in the ability to perform basic and advanced exoskeleton skills, had the skills in a hierarchical order of difficulty and could discriminate across participants.

A second important prerequisite of the framework is that the tested skills were reliable. An overall consistency of 73% in the Intermediate-skills-test and 81% in the Final-skills-test was achieved. Detailed analysis revealed several skills that had a consistency of <70% (see **Figures 3**, **5**). Remarkable was a lower consistency for the same skills in the Intermediate-skill-test compared to the Final-skill-test or vice versa. A consistency below 70% in the Intermediate-skill-test whereas a consistency above 70% in the Final-skill-test was met for the skills: sit-to-stand, stopping with the preferred or not preferred leg, arresting gait at command, passing a narrow passage, and pivot-turn to sit. The lower consistency of the intermediate skills were possibly due to the learning process. During the Intermediate-skills-test participants had to perform skills they practiced only once or twice without assistance. As a result, the skill was sometimes successfully performed by chance instead of competence and therefore participants were unable to perform the skill consistent. Therefore, we recommend that a skill should be performed at least two times when tested. The skills 180° curve to the right, slalom and martial arts mat had a low consistency in the Final-skills-test whereas a high consistency was obtained in the Intermediate-skills-test. These skills were performed by only a minority of the participants during the Intermediate-skills-tests indicating that most participants were only in the last training sessions at a level that they could practice these advanced skills. Nevertheless, the majority of the tested skills were performed consistent in the Intermediate- and Final-skills-test. Therefore, considering a skill achieved after two out of three successful attempts seems a good assumption to evaluate the skill-level.

In order to achieve exoskeleton skills, participants received multiple training sessions per week over an 8 week period. Such an intensive training program yields the potential of complications such as bruises and other skin damage. Most previous studies indicated that in hospital training with an exoskeleton was safe (Zeilig et al., 2012; Esquenazi, 2013; Kolakowsky-Hayner et al., 2013; Kubota et al., 2013; Spungen et al., 2013; Miller et al., 2016). Although other studies disclosed mild to moderate skin damages in half of the participants (five out of ten) (Benson et al., 2016) (four out of seven) (Platz et al., 2016), the intensity (session per week) and duration of the training period in this study was similar to most previous studies (Spungen et al., 2013; Benson et al., 2016; Miller et al., 2016; Platz et al., 2016). In the current study, eight out of twelve participants experienced skin damage during the training program. In four cases this skin damage resulted in at least one missed training. Whereas all skin damages reported in the study of Benson and none of the skin damages reported by Platz led to discontinuation of the training (Benson et al., 2016; Platz et al., 2016). Because of extra padding in the early phase of the training program, skin damage rarely occurred in the later phase. In addition, during the whole training program special care was taken to the correct joint alignment. Therefore, none of the patients had to reduce the training intensity in the later phase of the training program. Moreover, it suggests that special attention to joint alignment and padding during the training reduces the risk of skin damage.

In the current study, the Rewalk exoskeleton was used. In the current study, the ReWalk exoskeleton was used. Nowadays, there are multiple exoskeletons available on the market, which have their specific interaction with and control of the exoskeleton. As a consequence the hierarchical order of the skills in the framework might be slightly different between exoskeletons. The main difference between the current available exoskeletons for home and community is the control of initiation of gait, arresting of gait, and involuntary stops. For example, to initiate gait, the ReWalk and Ekso require a forward and lateral shift of the trunk, the Indego exoskeleton requires a forward trunk excursion, and the Rex exoskeleton does not require any trunk movement (Bryce et al., 2015). Despite the differences in interaction with and control of the exoskeleton, all skills proposed in the current study are relevant and applicable to the current available exoskeletons. Standing and walking skills are presumed to be achieved before users can perform additional advanced skills, which are mostly performed during walking. The first eight advanced skills, require less interaction with the environment. Within these skills a distinction was made in the fluency of the performance (with or without stops). Therefore, we expect that the hierarchical order of the first 18 intermediate skills can be applied to other exoskeletons. The hierarchical order of the last nine advanced skills might be slightly different across exoskeletons due to the difference in interaction with and control of the exoskeleton. However, achieving one of these skills indicates a highly advanced exoskeleton skill level.

The skills-tests proposed in this framework were based on independent performance of exoskeleton skills, but did not take the quality of the performance into consideration. For future research, the quality of how a skill is performed might be of interest in addition to if it is possible to perform a skill independent. Moreover, all exoskeleton skills in this study were assessed in a clinical setting and it remains unknown which skills are relevant and which skill-level is necessary for safe community use. Therefore, future research should focus on community use of an exoskeleton and its relation to the skill-level during the training period measured with the proposed framework.

CONCLUSION

The framework proposed in this study measured the progress in performing basic and advanced exoskeleton skills during a training program. The hierarchical ordered skills-test could discriminate across participants' skill-level. The overall consistency of the performed exoskeleton skills was considered acceptable.

DISCLOSURE

The exoskeleton training of the physiotherapists by ReWalk Robotics was given before the start of the study and ReWalk Robotics does not have any influence on the entire study.

AUTHOR CONTRIBUTIONS

All authors were involved in the design of the study. RvD, HR, and NK conceived and planned the experiments. RvD performed the data collection during the experiments. RvD and NK processed the experimental data, performed the analysis, drafted the manuscript and designed the figures. IvN, HvdM, and NK supervised the project. All authors discussed the results and contributed to the final manuscript.

SUPPLEMENTARY MATERIAL

The Supplementary Material for this article can be found online at: https://www.frontiersin.org/articles/10.3389/fnins.2017.00699/full#supplementary-material

REFERENCES

Adriaansen, J. J., Ruijs, L. E., van Koppenhagen, C. F., van Asbeck, F. W., Snoek, G. J., van Kuppevelt, D., et al. (2016). Secondary health conditions and quality of life in persons living with spinal cord injury for at least ten years. *J. Rehabil. Med.* 48, 853–860. doi: 10.2340/16501977-2166

Benson, I., Hart, K., Tussler, D., and van Middendorp, J. J. (2016). Lower-limb exoskeletons for individuals with chronic spinal cord injury: findings from a feasibility study. *Clin. Rehabil.* 30, 73–84. doi: 10.1177/0269215515575166

Bryce, T. N., Dijkers, M. P., and Kozlowski, A. J. (2015). Framework for assessment of the usability of lower-extremity robotic exoskeletal orthoses. *Am. J. Phys. Med. Rehabil.* 94, 1000–1014. doi: 10.1097/PHM.0000000000000321

Condie, E., Scott, H., and Treweek, S. (2006). Lower limb prosthetic outcome measures: a review of the literature 1995 to 2005. *J. Prosthet. Orthotics* 18, 13–45. doi: 10.1097/00008526-200601001-00004

Dunn, R. B., Walter, J. S., Lucero, Y., Weaver, F., Langbein, E., Fehr, L., et al. (1998). Follow-up assessment of standing mobility device users. *Assist. Technol.* 10, 84–93. doi: 10.1080/10400435.1998.10131966

Esquenazi, A. (2013). New bipedal locomotion option for individuals with thoracic level motor complete spinal cord injury. *J. Spinal Res. Fundation* 8, 26–28. Available online at: http://www.ryzur.com.cn/uploadfile/2016/0830/20160830115943895.pdf

Federici, S., Meloni, F., Bracalenti, M., and De Filippis, M. L. (2015). The effectiveness of powered, active lower limb exoskeletons in neurorehabilitation: a systematic review. *Neurorehabilitation* 37, 321–340. doi: 10.3233/NRE-151265

Fleuren, J. F., Voerman, G. E., Snoek, G. J., Nene, A. V., Rietman, J. S., and Hermens, H. J. (2009). Perception of lower limb spasticity in patients with spinal cord injury. *Spinal Cord* 47, 396–400. doi: 10.1038/sc.2008.153

Fliess-Douer, O., Vandelandewijck, Y. C., Lubel Manor, G., and Van Der Woude, L. H. (2010). A systematic review of wheelchair skills tests for manual wheelchair users with a spinal cord injury : towards a standardized outcome measure. *Clin. Rehabil.* 24, 867–886. doi: 10.1177/0269215510367981

Guttman, L. (1944). A basis for scaling qualitative data. *Am. Sociol. Rev.* 9, 139–150. doi: 10.2307/2086306

Hartigan, C., Kandilakis, C., Dalley, S., Clausen, M., Wilson, E., Morrison, S., et al. (2015). Mobility outcomes following five training sessions with a powered exoskeleton. *Top. Spinal Cord InJ. Rehabil.* 21, 93–99. doi: 10.1310/sci2102-93

He, Y., Eguren, D., Luu, T. P., and Contreras-Vidal, J. L. (2017). Risk management and regulations for lower limb medical exoskeletons : a review. *Med. Devices* 10, 89–107. doi: 10.2147/MDER.S107134

Jensen, M. P., Truitt, A. R., Schomer, K. G., Yorkston, K. M., Baylor, C., and Molton, I. R. (2013). Frequency and age effects of secondary health conditions in individuals with spinal cord injury: a scoping review. *Spinal Cord* 51, 882–892. doi: 10.1038/sc.2013.112

Kolakowsky-Hayner, S. A., Crew, J., Moran, S., and Shah, A. (2013). Safety and feasibility of using the EksoTM bionic exoskeleton to aid ambulation after spinal cord injury. *J. Spine* 4, 1–8. doi: 10.4172/2165-7939.S4-003

Kozlowski, A. J., Bryce, T. N., and Dijkers, M. P. (2015). Time and effort required by persons with spinal cord injury to learn to use a powered exoskeleton for assisted walking. *Top. Spinal Cord Inj. Rehabil.* 21, 110–121. doi: 10.1310/sci2102-110

Kubota, S., Nakata, Y., Eguchi, K., Kawamoto, H., Kamibayashi, K., Sakane, M., et al. (2013). Feasibility of rehabilitation training with a newly developed wearable robot for patients with limited mobility. *Arch. Phys. Med. Rehabil.* 94, 1080–1087. doi: 10.1016/j.apmr.2012.12.020

Lee, B. B., Cripps, R. A., Fitzharris, M., and Wing, P. C. (2014). The global map for traumatic spinal cord injury epidemiology: update 2011, global incidence rate. *Spinal Cord* 52, 110–116. doi: 10.1038/sc.2012.158

Leving, M. T., Vegter, R. J., de Groot, S., and van der Woude, L. H. (2016). Effects of variable practice on the motor learning outcomes in manual wheelchair propulsion. *J. Neuroeng. Rehabil.* 13, 1–15. doi: 10.1186/s12984-016-0209-7

Louie, D. R., Eng, J. J., Lam, T., and Spinal Cord Injury Research Team (SCIRE). (2015). Gait speed using powered robotic exoskeletons after spinal cord injury: a systematic review and correlational study. *J. Neuroeng, Rehabil.* 12, 1–10. doi: 10.1186/s12984-015-0074-9

Middleton, J. W., Yeo, J. D., Blanch, L., Vare, V., Peterson, K., and Brigden, K. (1997). Clinical evaluation of a new orthosis, the "Walkabout", for restoration of functional standing and short distance mobility in spinal paralysed individuals. *Spinal Cord* 35, 574–579. doi: 10.1038/sj.sc.3100459

Miller, L. E., Zimmermann, A. K., and Herbert, W. G. (2016). Clinical effectiveness and safety of powered exoskeleton-assisted walking in patients with spinal cord injury : systematic review with meta- analysis. *Med. Devices* 9, 455–466. doi: 10.2147/MDER.S103102

Mirbagheri, M. M., Kindig, M. W., and Niu, X. (2015). Effects of robotic-locomotor training on stretch reflex function and muscular properties in individuals with spinal cord injury. *Clin. Neurophysiol.* 126, 997–1006. doi: 10.1016/j.clinph.2014.09.010

Onose, G., Cârdei, V., Craciunoiu, S., Avramescu, V., Opris, I., Lebedev, M. A., et al. (2016). Mechatronic wearable exoskeletons for bionic bipedal standing and walking : a new synthetic approach. *Front. Neurosci.* 10:343. doi: 10.3389/fnins.2016.00343

Platz, T., Gillner, A., Borgwaldt, N., Kroll, S., and Roschka, S. (2016). Device-training for individuals with thoracic and lumbar spinal cord injury using a powered exoskeleton for technically assisted mobility : achievements and user satisfaction. *Biomed. Res. Int.* 2016, 1–10. doi: 10.1155/2016/8459018

Spungen, A. M., Asselin, P. K., Fineberg, D. B., Kornfeld, S. D., and Harel, N. Y. (2013). "Exoskeletal-assisted walking for persons with motor-complete paraplegia," in *Force Sustainment: Rehabilitation, Regeneration and Prosthetics for Re-Integration to Duty*, 6–1; 6–14. STO-MP-HFM-228. Available online at: http://www.ryzur.com.cn/uploadfile/2016/0830/20160830115519272.pdf

Tyson, S. F., and DeSouza, L. H. (2004). Development of the brunel balance assessment: a new measure of balance disability post stroke. *Clin. Rehabil.* 18, 801–810. doi: 10.1191/0269215504cr744oa

Wyndaele, M., and Wyndaele, J. J. (2006). Incidence, prevalence and epidemiology of spinal cord injury: what learns a worldwide literature survey? *Spinal Cord* 44, 523–529. doi: 10.1038/sj.sc.3101893

Yang, A., Asselin, P., Knezevic, S., Kornfeld, S., and Spungen, A. M. (2015). Assessment of in-hospital walking velocity and level of assistance in a powered exoskeleton in persons with spinal cord injury. *Top. Spinal Cord Inj. Rehabil.* 21, 100–109. doi: 10.1310/sci2102-100

Zeilig, G., Weingarden, H., Zwecker, M., Dudkiewicz, I., Bloch, A., and Esquenazi, A. (2012). Safety and tolerance of the ReWalkTM exoskeleton suit for ambulation by people with complete spinal cord injury: a pilot study. *J. Spinal Cord Med.* 35, 96–101. doi: 10.1179/2045772312Y.0000000003

Conflict of Interest Statement: The authors declare that the research was conducted in the absence of any commercial or financial relationships that could be construed as a potential conflict of interest.

frontiers in Neuroscience

ORIGINAL RESEARCH
published: 14 December 2017
doi: 10.3389/fnins.2017.00705

Haptic Cues for Balance: Use of a Cane Provides Immediate Body Stabilization

Stefania Sozzi[1], *Oscar Crisafulli*[2] *and Marco Schieppati*[3]*

[1] Centro Studi Attività Motorie, Istituti Clinici Scientifici Maugeri SPA SB, Institute of Pavia, IRCCS, Pavia, Italy, [2] Department of Neuroscience, Rehabilitation, Ophthalmology, Genetics and Maternal Child Health, University of Genoa, Genoa, Italy, [3] Department of Exercise and Sport Science, LUNEX International University of Health, Exercise and Sports, Differdange, Luxembourg

Haptic cues are important for balance. Knowledge of the temporal features of their effect may be crucial for the design of neural prostheses. Touching a stable surface with a fingertip reduces body sway in standing subjects eyes closed (EC), and removal of haptic cue reinstates a large sway pattern. Changes in sway occur rapidly on changing haptic conditions. Here, we describe the effects and time-course of stabilization produced by a haptic cue derived from a walking cane. We intended to confirm that cane use reduces body sway, to evaluate the effect of vision on stabilization by a cane, and to estimate the delay of the changes in body sway after addition and withdrawal of haptic input. Seventeen healthy young subjects stood in tandem position on a force platform, with eyes closed or open (EO). They gently lowered the cane onto and lifted it from a second force platform. Sixty trials per direction of haptic shift (Touch → NoTouch, T-NT; NoTouch → Touch, NT-T) and visual condition (EC-EO) were acquired. Traces of Center of foot Pressure (CoP) and the force exerted by cane were filtered, rectified, and averaged. The position in space of a reflective marker positioned on the cane tip was also acquired by an optoelectronic device. Cross-correlation (CC) analysis was performed between traces of cane tip and CoP displacement. Latencies of changes in CoP oscillation in the frontal plane EC following the T-NT and NT-T haptic shift were statistically estimated. The CoP oscillations were larger in EC than EO under both T and NT ($p < 0.001$) and larger during NT than T conditions ($p < 0.001$). Haptic-induced effect under EC (Romberg quotient NT/T ∼ 1.2) was less effective than that of vision under NT condition (EC/EO ∼ 1.5) ($p < 0.001$). With EO cane had little effect. Cane displacement lagged CoP displacement under both EC and EO. Latencies to changes in CoP oscillations were longer after addition (NT-T, about 1.6 s) than withdrawal (T-NT, about 0.9 s) of haptic input ($p < 0.001$). These latencies were similar to those occurring on fingertip touch, as previously shown. Overall, data speak in favor of substantial equivalence of the haptic information derived from both "direct" fingertip contact and "indirect" contact with the floor mediated by the cane. Cane, finger and visual inputs would be similarly integrated in the same neural centers for balance control. Haptic input from a walking aid and its processing time should be considered when designing prostheses for locomotion.

Keywords: sensorimotor integration, haptic sense, cane, standing balance, center of pressure, time to stabilization

OPEN ACCESS

Edited by:
Mikhail Lebedev,
Duke University, United States

Reviewed by:
Rahul Goel,
University of Houston, United States
Martina Mancini,
Oregon Health & Science University, United States

***Correspondence:**
Marco Schieppati
marco.schieppati@lunex-university.net

Specialty section:
This article was submitted to Neuroprosthetics, a section of the journal Frontiers in Neuroscience

Received: *31 August 2017*
Accepted: *01 December 2017*
Published: *14 December 2017*

Citation:
Sozzi S, Crisafulli O and Schieppati M (2017) Haptic Cues for Balance: Use of a Cane Provides Immediate Body Stabilization. Front. Neurosci. 11:705. doi: 10.3389/fnins.2017.00705

INTRODUCTION

Powered exoskeletons enable persons with various walking problems to ambulate over the ground. Several of these devices require the use of crutches to ambulate and maintain balance (Wang et al., 2015; see Asselin et al., 2016). Beyond their obvious mechanical effects (Bateni and Maki, 2005), crutches are a critical source of somatosensory inflow that provides information about body orientation with respect to the supporting surface through "extended physiological proprioception" (Simpson, 1974).

In this exploratory study, we asked whether the stabilizing effect on static balance of haptic information from a cane can be likened to that of haptic input from a light fingertip touch or to that of vision. It is well-known that haptic input reduces body sway during stance. Haptic input modifies spinal reflex excitability and the postural set even if it does not mechanically stabilize posture (Schieppati and Nardone, 1995; Jeka et al., 1996; Bove et al., 2006; Huang et al., 2009). The force exerted by the subjects onto a lightly touched stable frame need not be larger than 1 Newton (N) in order to induce the stabilizing effect (Kouzaki and Masani, 2008). The effect is similar to that obtained by opening the eyes with respect to standing eyes closed (Paulus et al., 1984; Sozzi et al., 2012; Honeine et al., 2015). Hence, addition of vision and haptic sense to the inherent proprioceptive inflow make the control of stance more effective (Jeka and Lackner, 1994, 1995; Sozzi et al., 2011, 2012; Honeine et al., 2015).

Haptic supplementation in elderly subjects or in patients with moderate to severe balance and gait impairment, as well as in blind subjects, is often dependent on their use of a cane (Jeka et al., 1996; Maeda et al., 1998; Hirahara et al., 2006; Albertsen et al., 2012; Guillebastre et al., 2012; Perreira et al., 2017; see Berglund, 2017, for an interesting point of view on the use of a cane). The cane would help these persons to compensate for their diminished cutaneous sensation from the feet (Peters et al., 2016) and to move independently while reducing their risk of falling, but it is normally used when standing as well, particularly in an unfamiliar environment or in presence of joint pain, or so. In people with neurological disorders of various nature, the cane is used to increase postural stability and to reduce the load on the weight–bearing lower extremities (Laufer, 2003; see Hamzat and Kobiri, 2008, for a complementary opinion).

The relevance of the supplementary haptic input for balance is further highlighted by the rapidity of the changes in sway as a consequence of adding or withdrawing the haptic or the visual information. Recently we estimated, in a population of young healthy subjects standing in tandem Romberg posture, the time-period necessary for the central nervous system to integrate the new sensory information and reweight its impact (or, in the case of withdrawal, to withstand the removal of the supplementary information and return to the proprioception-driven control; Sozzi et al., 2012; Honeine et al., 2015; see Honeine and Schieppati, 2014). In those experiments, the haptic information was a gentle touch (active or passive) of a firm surface exerted by the tip of the index finger or its removal by suddenly detaching surface and/or finger. The time necessary for the integration of haptic information, as assessed by the onset of the slightest detectable reduction in body sway, was >1 s, while that observed in the case of haptic withdrawal was significantly shorter. Next, a reweighting process led to a new dynamic steady-state in some 4–5 s in both cases. These time-intervals were not different from those measured by adding or withdrawing visual information (Sozzi et al., 2012).

With a cane, the haptic input is indirect, through a tool instead of by direct touch onto a stable frame with their own index finger. Sensory information would be produced by the cane touching the solid surface at some distance from the body, and by the subject being free to slide the cane on the ground. Conversely, in our previous investigations with finger touch, the solid surface touched by the fingertip was very close to the anterior surface of the trunk so that the vertical projection to the ground of this spot was at the border of the body's support surface defined by the feet position, and the wavering of the finger was very circumscribed (Sozzi et al., 2011, 2012; Honeine et al., 2015). The sensory input would also differ compared to that occurring on touching a frame with the finger because the perception of the contact would possibly rely on different sensory receptors. The contribution to the haptic input from upper limb muscle receptors (Rabin et al., 2008) would be perhaps more important for signaling the contact of the cane with the ground than the light-touch information from the skin of the fingertip.

Similar amounts of sway stabilization and similar latencies to stabilization for finger and cane touch would be in keeping with the hypothesis that an integration process is initiated by the haptic stimulus at the hand-cane interface, as if the fingers themselves touched a solid surface at the time-instant the cane touches the ground. A larger body sway and a longer latency to stabilization would speak instead of the need to include the computation of the actual location of the forearm and cane-tip touching-point into the reference frame for the control of body orientation in space. If the computation of the location of the touching point is necessary in order to reconstruct the image of the body-cane ensemble and calibrate the force of contact, stabilization might take more time with respect to when subject touches a solid surface with the fingertip directly.

We, therefore, assessed, in a population of normal young subjects standing in tandem feet position, the effect of cane use on body sway, and the time to stabilization or destabilization of balance, on adding or withdrawing the haptic input produced by the contact of the cane onto the ground. Our interest was three-fold: (a) to assess whether the use of the cane was indeed able to produce reduction of body sway, even if the cane was not fixed to the ground, and to measure the size of the effect; (b) to evaluate any effect of vision on the cane induced stabilization; (c) to estimate the latency at which the CNS incorporates the haptic information (or its withdrawal) connected with the cane stroke to the ground.

METHODS

Subjects

Seventeen (7 males and 10 females) healthy subjects participated in this study. Their mean values (±standard deviation, SD) for age, weight and height were 25.7 years ± 6.6, 61.4 kg

± 10.6 and 167 cm ± 8. All procedures were carried out in accordance with the Declaration of Helsinki and with the adequate understanding and written informed consent of each subject. The ethics committee of the "Istituti Clinici Scientifici Maugeri" had approved the experiment (# 757 CEC).

Task and Procedures

Subjects stood in tandem position on a force platform (Kistler 9286BA), with the great toe of the rear foot immediately behind the heel of the front foot, with eyes closed or with eyes open. With EO, subjects were simply asked to look in front of them, and not to stare at any specific target. The visual scene of the laboratory walls at 6 m distance contained both horizontal and vertical profiles and sharp contours. Subjects chose which foot was the rear foot (it was the right foot in 12 subjects). The tandem posture was utilized to enhance medio-lateral sway (Sozzi et al., 2011, 2012, 2013; Honeine et al., 2015). Subjects were asked to hold with their dominant hand (right hand for all subjects) a straight plastic cane of 1 m length and 100 g weight, instrumented with a reflective marker fixed on the tip of the cane.

After a verbal "go" signal given by the operator, subjects gently lowered the cane onto (or lifted it from) a second force platform equal to that mentioned above, which recorded the force applied by the cane. This force platform was placed in front of the subject and laterally spaced from the platform on which the subject stood (there was a distance of 55 cm from the center of the first to that of the second platform; **Figure 1A**). Successive "go" signals were given in a series, spaced by time intervals ranging each from 20 to 25 s, so that subjects periodically lowered the cane and withdrew it from the platform in sequence. A few practice trials were run to obtain touch forces on the platform smaller than 1 N. Subjects were asked not to move the cane in a reaction-time mode on hearing the verbal signal but to self-pace the movement necessary for lowering or lifting the cane from the ground when they felt so. Subjects underwent a series of at least 60 trials per direction of shift (Touch → NoTouch, T-NT; or vice versa NoTouch → Touch, NT-T) and per visual condition (EC or EO). Data were collected during 20 subsequent acquisition epochs of 240 s each (10 acquisition periods with EC and 10 with EO). Therefore, each epoch contained six haptic changes in which the cane was lowered onto the ground (NT-T) and six changes in which the cane was lifted (T-NT) from the ground. These epochs were then divided into trials, each of 30 s duration containing and centered on the change in haptic condition at $t = 15$ s. Then, equal-condition trials were aligned with the instant of the haptic shift and averaged. These big trial numbers were necessary in order to allow averaging of as many traces as possible in order to get consistent mean values for body oscillation and to reliably estimate the time following the shift in the sensory information, at which modifications occurred in body sway. Between each block of acquisition epochs, subjects were free to sit or move around for variable periods. The overall duration of the experimental session varied from 2 to 3 h, all conditions included.

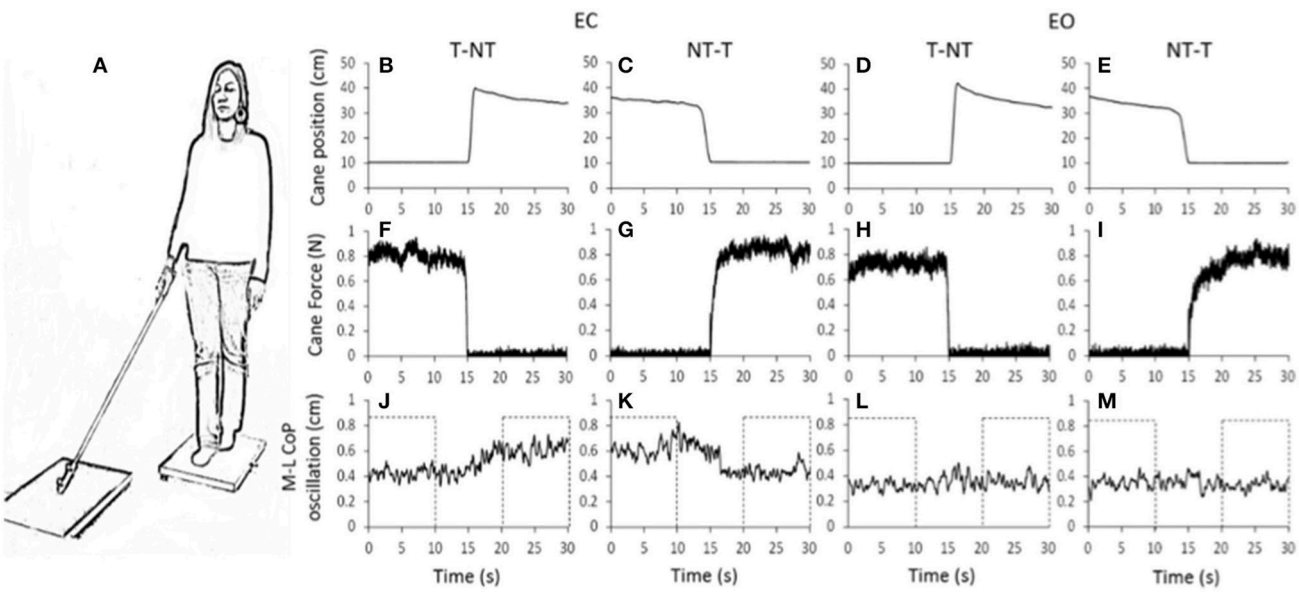

FIGURE 1 | (A) Subjects stood with feet in tandem position on a force platform, with EC or EO, the cane resting on a second platform. **(B–M)** shows the mean value of the recorded signals in one representative subject. **(B–E)** vertical position of the marker placed close to the cane tip. **(F–I)** force applied by the cane onto the ground. **(J–M)** medio-lateral CoP oscillations, larger during EC than EO. With EC, after a short delay from the instant at which the cane was lifted, the oscillation amplitude increased (**J**, $t = 15$ s). Conversely, after the NT-T shift **(K)** the oscillation diminished. With EO **(L,M)**, no differences were obvious in the oscillations after the changes in haptic condition. The dotted boxes in **(J–M)** show the time intervals in which the oscillations were considered stationary and not affected by the shift in haptic condition.

Center of Foot Pressure (CoP) and Cane Movement Recording

Force signals from the two platforms were acquired at 140 Hz (SMART-D system, BTS, Italy). The output of the platform onto which the subject stood was the instantaneous position of the Center of foot Pressure (CoP) along the sagittal (antero-posterior, A-P) and the frontal plane (medio-lateral, M-L) during the standing trials. To quantify the amplitude of the CoP oscillations on the frontal and sagittal plane, the traces were high-pass filtered with a 2nd order Butterworth filter (cut-off frequency 0.1 Hz), and then rectified with a software developed in Labview (National Instruments, USA).

The mean level of force exerted by the cane on the ground was computed from the vertical force recorded by the platform onto which the cane rested. The position in space of the marker fixed on the tip of the cane was also acquired at 140 Hz by means of an optoelectronic device composed of 12 cameras (Smart-D, BTS, Italy) and stored in a PC for off-line analysis.

For each subject and trial, a cross-correlation (CC) analysis was performed between the traces of the cane tip and of the CoP M-L displacement. The CC coefficient (R) at time lag = 0 s was calculated by means of a software developed in Labview. A positive coefficient indicated an in-phase displacement of cane and CoP in the M-L direction, a negative coefficient indicated anti-phase displacement. The time lag was the time interval at which the absolute value of R was maximum. A negative time lag indicates that cane movement lagged the CoP movement.

Mean Level of CoP Oscillation

For every trial recorded in each subject, the mean A-P and M-L oscillations of the CoP were computed under all haptic (NT and T) and visual (EC and EO) conditions at steady state. To this aim, each variable was averaged during the first and last 10 s periods of each trial containing a shift in sensory condition (see the dotted box in **Figure 1**). These periods did not contain the 10-s time interval centered on the sensory shift and were considered to be stationary and unaffected by the sensory shift (Sozzi et al., 2011, 2012; Honeine et al., 2015).

Mean Latency of Change in Body Sway Following the Sensory Shifts

The latencies of the changes in body sway following the haptic shift were measured only for the CoP oscillation in the frontal plane under EC condition. With EO, the effects of a shift in haptic information were small both in the frontal and sagittal plane. Further, even with EC, the presence or absence of haptic information influenced to a much larger extent the oscillation in the frontal than in the antero-posterior direction.

For each subject and condition of haptic shift (addition or withdrawal), we measured the latency following the sensory shift (cane put on the ground, NT-T) or cane off the ground (T-NT), at which M-L CoP oscillation diminished, or increased depending on the haptic-shift direction. Latency was estimated on the averaged traces of all the trials ($n = 60$) containing the sensory shift. Each successive mean value of the trace after the shift was compared to the mean value of the variable computed during the 15 s before the shift (reference value) by the one-sample Student's t-test with n = number of repetitions. The time after the shift, at which the t-value of the above comparisons bypassed the critical value corresponding to a 0.05 probability and remained above it for at least 100 ms, was taken as the time, at which the presence or absence of the haptic information began to affect the postural control mode (Sozzi et al., 2012; Schieppati et al., 2014).

Statistical Analyses

A 3-way repeated-measure ANOVA with direction of oscillation (M-L and A-P), presence or absence of haptic information (NT or T) and visual condition (EC and EO) was used to compare the mean levels of CoP oscillation calculated at steady state. The *post-hoc* analysis was made with Fisher's LSD test. The mean time-lags between cane and M-L CoP displacements were compared between visual conditions by paired Student's t-test. The mean latencies of the changes in M-L CoP oscillations with EC were compared between the two haptic-shift conditions by a paired Student's t-test. The software package used was Statistica (StatSoft, USA).

RESULTS

Effect of the Addition or Withdrawal of Haptic Information on Body Sway

Figure 1 shows the averaged traces of the recorded signals of one representative subject standing on the force platform (**Figure 1A**) during the T-NT and NT-T trials under EC (**Figures 1B,C,F,G,J,K**) and EO condition (**Figures 1D,E,H,I,L,M**). The first-row panels show the vertical position of the marker placed on the tip of the cane. When the cane was on the ground, the force recorded by the platform (middle row panels) was <1 N under both visual conditions. The difference between visual conditions in the force applied by the cane was not significant (paired t-test, $p = 0.10$). The bottom-row panels show that, under the EC condition, following the T-NT shift (at time $t = 15$ s in all panels), the values of the oscillations (**Figure 1J**) increased after a short delay from the instant of the sensory shift. Conversely, when the cane was lowered onto the ground (NT-T), the values of the M-L CoP oscillations (**Figure 1K**) diminished in amplitude. Under the EO condition, there were negligible differences in M-L CoP oscillations (**Figures 1L,M**) following the shift in haptic condition, for either NT-T or T-NT direction of shift. All subjects, particularly in the EC condition, referred that when the cane rested on the ground they felt more stable than during the period in which there was no cane reference.

Body Sway under Steady-State Condition

Figure 2 shows the mean values across subjects of the M-L and A-P oscillations of the CoP calculated at steady state under EC (**Figure 2A**) and EO (**Figure 2B**) conditions, with (T) or without (NT) the use of the cane. The CoP oscillations were greater along the M-L than the A-P direction [$F_{(1, 16)} = 44.64$, $p < 0.001$] during both the NT and the T condition (*post-hoc*, $p < 0.05$ for all comparisons).

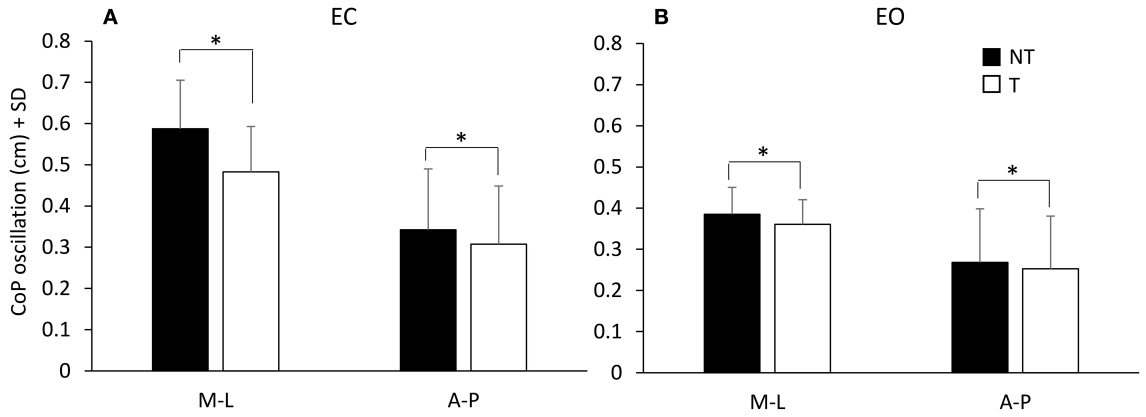

FIGURE 2 | Mean values of CoP oscillations at steady-state under EC **(A)** and EO **(B)** condition. Black bars refer to no-touch (NT) condition, white bars to touch (T) condition. The CoP oscillations were greater along the frontal (M-L) than the sagittal (A-P) plane and greater under EC than EO condition. CoP oscillations were greater during the NT condition than during T condition. *Indicates a significant difference ($p < 0.05$).

There was a difference between the two visual conditions [EC vs. EO; $F_{(1, 16)} = 76.73$, $p < 0.001$] since the oscillations were larger with EC than EO (NT and T collapsed). Oscillations were also larger during the NT period (black bars) than during the T period (white bars) [NT vs. T; $F_{(1, 16)} = 46.06$, $p < 0.001$]. There was an interaction between direction of oscillation (M-L and A-P) and visual condition [$F_{(1, 16)} = 13.23$, $p < 0.05$], an interaction between direction of oscillation and presence or absence of haptic information [$F_{(1, 16)} = 31.72$, $p < 0.001$], and an interaction between direction of oscillation, visual condition and presence or absence of haptic information [$F_{(1, 16)} = 18.13$, $p < 0.01$]. In fact, the presence of haptic information diminished the CoP oscillation more under EC than EO condition and more in M-L than A-P direction. The Romberg quotients NT/T (EC) and EC/EO (NT) for the M-L CoP oscillations were 1.22 ± 0.13 and 1.54 ± 0.33 SD, respectively, indicating that both haptic input and vision reduced body sway. The haptic effect was, however, smaller than that of vision (paired *t*-test on the Romberg quotients, $p < 0.001$). With EO, the Romberg quotient NT/T (1.07 ± 0.09 *SD*) indicated no major haptic-induced stabilization compared to the haptic effect with EC (paired *t*-test on the Romberg quotients, $p < 0.001$).

Cane-Tip Displacement Follows Body Oscillation

During the period in which the cane tip was resting on the ground, there was a good association between the movement of the cane and the CoP M-L oscillation (in the example reported in **Figure 3A**, $R = 0.837$, $p < 0.001$). When the CoP position moved to the right (positive values on the abscissa), also the cane moved to the right (positive values on the ordinate) and vice versa. The cane tip displacements were often smaller than those of the CoP. With EC, the CC coefficient calculated for the two traces was positive in the majority of subjects (15/17), ranging from −0.46 to 0.64 (all trials and subjects collapsed, mean $R = 0.43 \pm 0.34$ SD). With EO, the CC coefficient was positive in the majority of the subjects as well, ranging from −0.38 to 0.68 (mean $R = 0.47 \pm 0.32$ SD). Mean CC coefficients were slightly different between visual conditions (paired *t*-test, $p < 0.05$). The positive values of the CC coefficients indicate an overall in-phase movement of cane and CoP in the M-L direction. The mean time lag between cane and CoP displacement in the M-L direction (**Figure 3B**) was −37.7 ms ± 48.6 with EC and −27.7 ms ± 38.3 with EO (paired *t*-test, $p = 0.3$), indicating that the cane displacement lagged the CoP displacement regardless of the visual conditions.

The Delay from the Sensory Shift to the Change in Body Sway Is Longer with Addition than Removal of Haptic Input

The latencies of the changes in body sway on touching the ground with the cane or lifting it off ground were estimated for each subject on the mean M-L CoP oscillation trace under EC condition. The reason was that the changes in the levels of CoP oscillations, caused by the addition or removal of haptic information, were much greater in the M-L than A-P direction.

Figure 1 showed that, with a short delay following the shift in haptic condition (at $t = 15$ s), the oscillations increased when the cane was removed (T-NT condition) or decreased when the cane was put on the ground (NT-T condition). The latencies of the changes in oscillations calculated for each subject are reported in **Figure 4A** for the NT-T and for the T-NT condition. Latencies ranged from 0.76 to 2.98 s for the NT-T shift in haptic condition and from 0.45 to 1.7 for the T-NT shift, and were longer for the addition than for the withdrawal of haptic information. In **Figure 4B**, the mean latencies across subjects for the two sensory shifts are reported. Mean latencies were longer by about 0.7 s for the NT-T (1.64 s ± 0.6 SD) than for the T-NT condition (0.93 s ± 0.4 SD) (paired *t*-test, $p < 0.001$).

DISCUSSION

We investigated the changes occurring in the body sway of young healthy subjects standing in tandem position and performing the

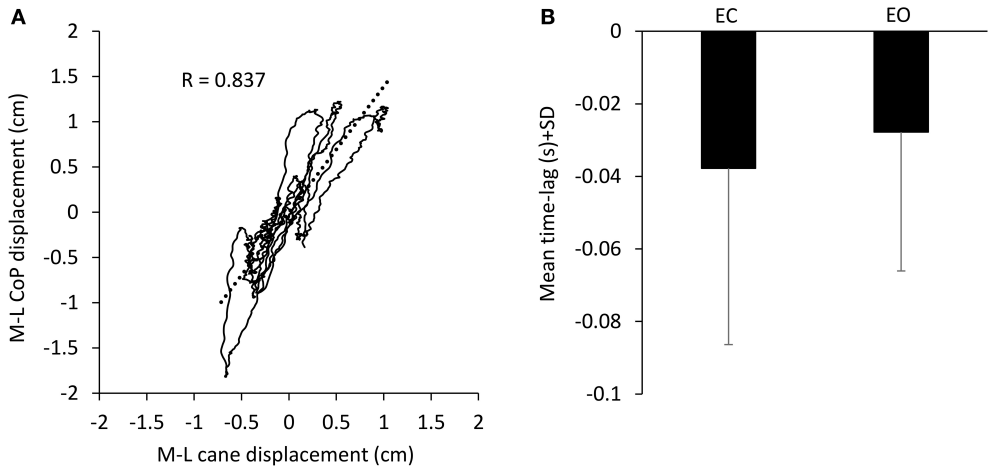

FIGURE 3 | Association between CoP and cane displacement. **(A)** The displacement of the CoP along the frontal plane (M-L) was plotted against the cane movement in the same plane recorded during one 10-s period in which the cane rested on the ground in one subject EC. When the CoP moved to the right (positive values in the ordinate) also the cane moved to the right (positive values in the abscissa). **(B)** Mean time-lag between CoP and cane movement across subjects. Negative values of time-lag indicate that the cane movements lagged the CoP movements.

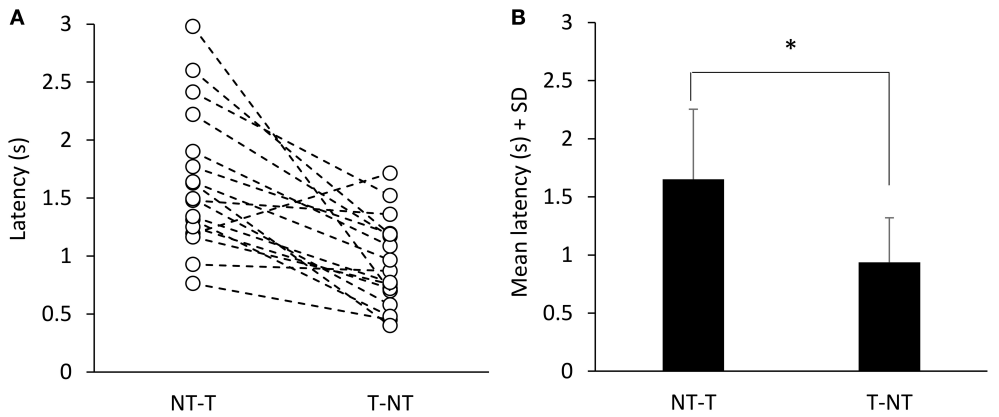

FIGURE 4 | Time intervals from haptic change to change in body oscillation when standing with EC. **(A)** Latencies of the changes in M-L CoP oscillations calculated for each subject. **(B)** Mean latencies across subjects. The latencies were longer for the NT-T shift than for the T-NT shift. *Indicates a significant difference ($p < 0.001$).

task of lowering a cane onto the ground or lifting it. We were specifically interested in estimating the latency at which body sway diminishes in response to the haptic input connected with the cane contact onto the ground (or at which sway increases on removing the cane).

In line with previous reports (Sozzi et al., 2011, 2012; Honeine et al., 2015), the CoP oscillations were smaller with EO than EC. With EC, oscillations were smaller with cane touch (T) compared to no touch (NT). With EO cane had little effect. All subjects felt more stable when the haptic input was available, and referred that standing in tandem was easier with than without the haptic input. The latencies to the initial changes in oscillation in response to the sensory shift, assessed on the EC data, were longer after addition (NT-T, about 1.6 s) than withdrawal (T-NT, about 0.9 s) of the haptic input.

It is well-known that standing humans sway less when vision is allowed (Straube et al., 1994; Sozzi et al., 2011; Sarabon et al., 2013). Haptic information from light finger touch produces body sway reduction as well (Jeka and Lackner, 1994; Jeka et al., 1996; Lackner et al., 1999; Bolton et al., 2011; Sozzi et al., 2012; Kanekar et al., 2013; Schieppati et al., 2014; Honeine et al., 2015). Hence, minor displacement of the visual field on the retina, or touch information from the fingertip, not granting mechanical stabilization (Lackner et al., 2001; Kouzaki and Masani, 2008), are sufficient for consistently reducing body sway. These effects are obvious when balance is critical, like standing with the feet in tandem position (Huang et al., 2009; Sozzi et al., 2011, 2012; Sarabon et al., 2013; Honeine et al., 2015). The visual and haptic information would be little exploited under quiet stance with feet parallel, but become relevant when balancing under unfavorable conditions (De Nunzio and Schieppati, 2007; Sozzi et al., 2011).

Visual or haptic input add to the proprioceptive information, to the cutaneous input from the foot soles, and to the vestibular input (Mergner et al., 2009; Billot et al., 2013; Bronstein, 2016). Thus, in spite of the visual and haptic inputs being just a fraction of the overall sensory inflow, they are not at all negligible for stabilization (Lackner et al., 1999).

Similar Stabilization by a Cane and Fingertip Touch

Here, we used a cane as a way for decreasing body sway during eyes-closed stance. This tool proved to be effective for stabilization, even when the cane exerted <1 N force on the ground, and even when the cane was not fixed to the ground, as in other investigations on this issue (Jeka et al., 1996; Maeda et al., 1998; Albertsen et al., 2010; Ustinova and Langenderfer, 2013; Oshita and Yano, 2016). Of note, the experiments were conducted under tandem stance, which is a challenging sway situation (Sozzi et al., 2013), in order to clearly detect differences between the condition with/without cane touch. Quiet stance with feet parallel would have required a much larger number of repetition to detect the onset of sway changes on adding/removing the haptic input, owing to the sensitivity of the analytical method.

In our study, the cane was free to move, as it would happen under natural circumstances, and its displacement on the force platform accompanied the oscillations of the center of foot pressure. Interestingly, it appeared that the cane was not used as a pivot to control body sway, exerting a force onto the ground in order to move the body; contrary, its translation normally followed the displacement of the center of foot pressure by some 40 ms (see **Figure 3**). This further suggests that the cane moves with the swaying body and that stabilization can be obtained through the haptic reference rather than using the cane as a mechanical support (Misiaszek et al., 2016). Whether such effect can transfer to different conditions, such as postural disturbances (Owings et al., 2000), or to reactive balance control (Schinkel-Ivy et al., 2016), or to walking (Rabin et al., 2015) is an important issue, worth specific investigation.

The Effect of Vision and the Interaction with Haptic Input

The reduction in the center of foot pressure oscillation with the cane resting on the ground under EC condition (diminution to 82%) was smaller than that obtained with vision (when standing without a cane, the diminution in sway amplitude on opening the eyes reached 67%). In a similar vein, the effect obtained with the cane was also somewhat smaller than that obtained by using the fingertip, as shown in a previous investigation (Sozzi et al., 2012; fingertip touch reduced sway to about 75%, no touch compared to touch, eyes closed). This value had been obtained in a different population of subjects matched for age and gender, but having comparable sway values eyes-closed under no-touch condition. Interestingly, roughly similar stabilizing effects of the haptic input have been also noted as a consequence of touching either a rough or a slippery surface (Jeka and Lackner, 1995).

When the cane was used while vision was allowed (eyes open all the time), the concurrent haptic information produced little extra reduction of the body sway compared to no-cane, as already observed (Albertsen et al., 2012), as if vision would largely overrule the haptic information provided by the cane (Krishnan and Aruin, 2011). The use of the cane did decrease body sway in the M-L plane with eyes open, but this decrease was limited as if an occlusion effect ensued. This would occur if haptic inflow and vision would share common mechanisms for stabilization. Besides, the steadying effect of vision was large, and the use of the cane (not exerting any mechanical action) may not easily further reduce the oscillations when subjects are standing in tandem. Not alternatively, oscillations would not diminish beyond a certain value, because a given body-sway stimulus is in any case required for activating proprioceptors and labyrinth and sending meaningful information to the brain (van Emmerick and van Wengen, 2000; Carpenter et al., 2010). But then again, in this case, a given body sway would also return a certain valuable input from the moving cane tip. The effect of haptic input from the cane would be a substitute for vision and become crucial during stance or walking in blind subjects or in sighted subjects with eyes closed, when absence of vision produces clear-cut effects on the spatial characteristics of gait requiring an increased computational brain effort (Oates et al., 2017; Oliveira et al., 2017). Of note, vision and touch reduce muscle activity and co-contraction of antagonist leg muscles, which is characteristic of the tandem stance (Sozzi et al., 2012, 2013), much as vision does during another challenging balance condition, such as counteracting continuous postural perturbations (Sozzi et al., 2016).

Sensori-Motor Integration Time

The congruence of haptic input from cane and visual input in enhancing body stability under steady-state condition had a counterpart in the substantial equivalence of the latency for the changes in body oscillation, on addition or on withdrawal of the corresponding sensory inputs. In the previous investigations mentioned above, though, the mean latency to stabilization onset on opening the eyes was about 1.2 s, hence just shorter than that following cane touch to the ground (they were instead equal on removing vision or touch; Sozzi et al., 2011, 2012; Honeine et al., 2015). However, the mean latencies to decrease and increase of sway (about 1.4 and 1 s, respectively), observed when the haptic input originated from light fingertip touch (Sozzi et al., 2012; Honeine et al., 2015) were similar to those measured in the present study. Overall, these data speak in favor of a substantial equivalence of the haptic information derived from a "direct" contact of fingertip with a stable surface and of the "indirect" contact with a stable surface mediated by the cane, and confirm a slightly longer latency for the integration of haptic compared to visual information.

The Effect of the Haptic Information from the Cane Is Not Affected by the Interaction with the Task Execution

The profile of the changes in body sway induced by the haptic information (or by its withdrawal) seemed not to be affected by the movement necessary to lift or lower the cane onto

the ground. This finding and conclusion were not anticipated, because movements of upper limb and hand for lowering or lifting the cane, though limited in extent and velocity, might have interfered with the exploitation of the haptic sensory input (Saradjian, 2015). Further, these movements might have produced anticipatory or corrective postural adjustments, possibly impeding appropriate reweighting of the new haptic sensory inputs because of other types of balance priorities (such as counteracting the task of gently lifting or lowering the cane). Or, the onset of the changes in oscillation might have been simply concealed by large CoP displacements connected to those tasks. The experiment was not designed for sorting out potentially interfering effects of anticipatory or corrective postural adjustments: however, these were rarely obvious in the individual CoP traces and disappeared on averaging multiple epochs. This points to small and asynchronous postural adjustments, and to the rather constant latency of the sway reducing (or increasing) effects of the changes in haptic input. Hence, we would suggest that the reweighting phenomenon must be robust, and possibly represents a priority for the postural control system, independent of the possible modulation of the haptic input itself, connected with the voluntary act of moving the cane, as occurs for other inputs along the thalamo-somatosensory cortex pathway (Bolton et al., 2012; Seki and Fetz, 2012; Song and Francis, 2015; Colino et al., 2017). In this light, these findings lend support to the conclusions of Saradjian et al. (2013) and Mouchnino et al. (2015) that the brain exerts dynamic control over the transmission of the afferent signals according to their current relevance during a critical balance condition.

Processing Time and Neural Circuits: Open Questions

Regardless of the modality and origin of the sensory information (at least for visual and haptic—finger or cane), the nervous system seems to react within roughly similar time intervals. It might be conjectured that the entry to the "posture stabilizing" centers is common to both visual and haptic inputs, and independent of any parallel pathway conveying inputs for different physiological functions. Admittedly, time intervals pertaining to different modalities may not be stated definitely in our test paradigm. The paradigm and analytical procedures are certainly accurate for detecting differences between addition and withdrawal of a sensory input, but may not detect subtle differences connected with the peripheral traveling and central processing of information from different sources.

The relatively long integration time may be an expression of the computation for shifting to a less energetically expensive pattern of stance control. The latency to change in the oscillation pattern is much longer than a reflex (∼50 ms), or a startle reaction (∼100 ms), or else a quick voluntary response (∼150 ms), and is even longer than the balance-correcting responses triggered by a perturbation of stance (∼200 ms) (Valls-Solé et al., 1999; Grüneberg et al., 2005; Sozzi et al., 2012; Honeine and Schieppati, 2014). Interestingly, the latencies to stabilization onset were somewhat longer but of the same order of magnitude as the time lag between motor command and body sway, estimated by means of cross-correlation analysis of leg muscle EMG activities and body sway size in subjects standing quietly without support (Masani et al., 2011). These authors found that the longer the time lag of the cross-correlation (up to half a second) the smaller the body sway, and concluded that a control strategy producing a longer preceding time for the motor command can stabilize the body more effectively. It is not unlikely that the values we found for latency to stabilization might have implied activation of the processes mentioned in Masani et al. (2011).

Processing of the haptic input for balance stabilization would be subserved by dedicated cortical networks, possibly at parietal cortex level (Kaulmann et al., 2017), while the more rapid shift toward a new state of increased sway on withdrawing the haptic input would be produced at subcortical level. Anticipated loss of balance (lifting the cane) would allow for the cortical pre-selection and optimization of brain stem postural activity (Jacobs and Horak, 2007; see Shadmehr, 2017). Removal of sensory inputs equally rapidly triggers a "default" reaction of the posture stabilizing centers to the sudden withdrawal of the critical haptic originating from finger and cane contact or vision, whereby body sway quickly shifts to a larger oscillation pattern (Sozzi et al., 2012; Honeine and Schieppati, 2014; Assländer and Peterka, 2016; Honeine et al., 2017). This is the consequence of the lack of critical information on the one hand and a condition for stronger proprioceptive and vestibular stimulation on the other.

Balance, Locomotion, and Neural Prostheses for Locomotion

We would, therefore, argue that haptic input as provided by using a cane is sufficient for improving balance, almost as a gentle fingertip touch of a stable structure or vision of the surrounding space. Hence, cane or crutches would provide an information which can be typically processed by the nervous system along with other, more "natural" (tactile, visual, vestibular) inputs. It is arguable that haptic input from such devices can be exploited not only during stance, but also during locomotion, all the more so when locomotion is aided by neural prostheses. Haptic inflow from cane would be crucial during gait initiation and cooperate with the anticipatory postural adjustments in helping weight distribution between both legs so as to produce the best stability conditions for optimal gait initiation (Caderby et al., 2017). In this line, Chastan et al. (2010) have mentioned the relevance of the somatosensory input for balance control during gait initiation. Further insight on the mechanisms of action of any haptic input finalized to reducing the oscillation of the center of pressure during the successive stance phases of walking would be welcome.

Walking velocity is clearly affected by postural instability in several clinical conditions, as in cerebellar and neuropathic diseases (Morton and Bastian, 2003; Nardone et al., 2009, 2014) or in patients with stroke (Hsiao et al., 2017), chronic obstructive pulmonary disease (Morlino et al., 2017) or Parkinson's disease (Giardini et al., submitted). Investigation on the timing of haptic-motor integration should be extended to a larger population of normal young subjects, to elderly persons and to visually impaired and neurological populations, such as

Parkinson's disease patients (Rabin et al., 2015). The findings of these investigations would prove useful in the design of new rehabilitation devices. Haptic control is needed for any locomotion exoskeleton, where step production consists of discrete shifts from one posture to another. Implementation of an appropriate time-lag between changes in haptic inflow and their effects on balance control would represent an important aspect of the design of the control system for exoskeletons (see Mergner, 2007; Peterka, 2009; O'Doherty et al., 2012). In a broader context, it is not unlikely that somatosensory prosthetics may help not only perception and action (O'Doherty et al., 2011; Tyler, 2015), but also contribute to creating an appropriate response in the domain of the control of the equilibrium. The findings of the present investigation might foster implementation of new technologies taking into account the "natural" time constraints of multi-modality sensory integration, and represent a step toward the building of biologically inspired balance- and locomotion devices.

AUTHOR CONTRIBUTIONS

SS: contributed with data collection, data analysis, and drafted the manuscript; OC: contributed with data collection and data analysis; MS: contributed with project creation, data analysis, and wrote and edited the manuscript.

FUNDING

This study was supported in part by the Ricerca Finalizzata grants (GR-2009-1471033 and RF-2011-02352379) from the Italian Ministry of Health.

REFERENCES

Albertsen, I. M., Temprado, J. J., and Berton, E. (2010). Effect of haptic supplementation on postural stabilization: a comparison of fixed and mobile support conditions. *Hum. Mov. Sci.* 29, 999–1010. doi: 10.1016/j.humov.2010.07.013

Albertsen, I. M., Temprado, J. J., and Berton, E. (2012). Effect of haptic supplementation provided by a fixed or mobile stick on postural stabilization in elderly people. *Gerontology* 58, 419–429. doi: 10.1159/000337495

Asselin, P. K., Avedissian, M., Knezevic, S., Kornfeld, S., and Spungen, A. M. (2016). Training persons with spinal cord injury to ambulate using a powered exoskeleton. *J. Vis. Exp.* doi: 10.3791/54071

Assländer, L., and Peterka, R. J. (2016). Sensory reweighting dynamics following removal and addition of visual and proprioceptive cues. *J. Neurophysiol.* 116, 272–285. doi: 10.1152/jn.01145.2015

Bateni, H., and Maki, B. E. (2005). Assistive devices for balance and mobility: benefits, demands, and adverse consequences. *Arch. Phys. Med. Rehabil.* 86, 134–145. doi: 10.1016/j.apmr.2004.04.023

Berglund, J. (2017). A balancing act: scientists seek to reduce the risk of falls in the elderly. *IEEE Pulse* 8, 21–24. doi: 10.1109/MPUL.2016.2647059

Billot, M., Handrigan, G. A., Simoneau, M., Corbeil, P., and Teasdale, N. (2013). Short term alteration of balance control after a reduction of plantar mechanoreceptor sensation through cooling. *Neurosci. Lett.* 535, 40–44. doi: 10.1016/j.neulet.2012.11.022

Bolton, D. A., Brown, K. E., McIlroy, W. E., and Staines, W. R. (2012). Transient inhibition of the dorsolateral prefrontal cortex disrupts somatosensory modulation during standing balance as measured by electroencephalography. *Neuroreport* 23, 369–372. doi: 10.1097/WNR.0b013e328352027c

Bolton, D. A., McIlroy, W. E., and Staines, W. R. (2011). The impact of light fingertip touch on haptic cortical processing during a standing balance task. *Exp. Brain Res.* 212, 279–291. doi: 10.1007/s00221-011-2728-6

Bove, M., Bonzano, L., Trompetto, C., Abbruzzese, G., and Schieppati, M. (2006). The postural disorientation induced by neck muscle vibration subsides on lightly touching a stationary surface or aiming at it. *Neuroscience* 143, 1095–1103. doi: 10.1016/j.neuroscience.2006.08.038

Bronstein, A. M. (2016). Multisensory integration in balance control. *Handb. Clin. Neurol.* 137, 57–66. doi: 10.1016/B978-0-444-63437-5.00004-2

Caderby, T., Yiou, E., Peyrot, N., de Viviés, X., Bonazzi, B., and Dalleau, G. (2017). Effects of changing body weight distribution on mediolateral stability control during gait initiation. *Front. Hum. Neurosci.* 11:127. doi: 10.3389/fnhum.2017.00127

Carpenter, M. G., Murnaghan, C. D., and Inglis, J. T. (2010). Shifting the balance: evidence of an exploratory role for postural sway. *Neuroscience* 171, 196–204. doi: 10.1016/j.neuroscience.2010.08.030

Chastan, N., Westby, G. W., du Montcel, S. T., Do, M. C., Chong, R. K., Agid, Y., et al. (2010). Influence of sensory inputs and motor demands on the control of the centre of mass velocity during gait initiation in humans. *Neurosci. Lett.* 469, 400–404. doi: 10.1016/j.neulet.2009.12.038

Colino, F. L., Lee, J. H., and Binsted, G. (2017). Availability of vision and tactile gating: vision enhances tactile sensitivity. *Exp. Brain Res.* 235, 341–348. doi: 10.1007/s00221-016-4785-3

De Nunzio, A. M., and Schieppati, M. (2007). Time to reconfigure balancing behaviour in man: changing visual condition while riding a continuously moving platform. *Exp. Brain Res.* 178, 18–36. doi: 10.1007/s00221-006-0708-z

Grüneberg, C., Duysens, J., Honegger, F., and Allum, J. H. (2005). Spatio-temporal separation of roll and pitch balance-correcting commands in humans. *J. Neurophysiol.* 94, 3143–3158. doi: 10.1152/jn.00538.2004

Guillebastre, B., Rougier, P. R., Sibille, B., Chrispin, A., Detante, O., and Pérennou, D. A. (2012). When might a cane be necessary for walking following a stroke? *Neurorehabil. Neural Repair* 26, 173–177. doi: 10.1177/1545968311412786

Hamzat, T. K., and Kobiri, A. (2008). Effects of walking with a cane on balance and social participation among community-dwelling post-stroke individuals. *Eur. J. Phys. Rehabil. Med.* 44, 121–126.

Hirahara, Y., Sakurai, Y., Shiidu, Y., Yanashima, K., and Magatani, K. (2006). Development of the navigation system for the visually impaired by using white cane. *Conf. Proc. IEEE Eng. Med. Biol. Soc.* 1, 4893–4896. doi: 10.1109/IEMBS.2006.260433

Honeine, J. L., Crisafulli, O., and Schieppati, M. (2017). Body sway adaptation to addition but not withdrawal of stabilizing visual information is delayed by a concurrent cognitive task. *J. Neurophysiol.* 117, 777–785. doi: 10.1152/jn.00725.2016

Honeine, J. L., Crisafulli, O., Sozzi, S., and Schieppati, M. (2015). Processing time of addition or withdrawal of single or combined balance-stabilizing haptic and visual information. *J. Neurophysiol.* 114, 3097–3110. doi: 10.1152/jn.00618.2015

Honeine, J. L., and Schieppati, M. (2014). Time-interval for integration of stabilizing haptic and visual information in subjects balancing under static and dynamic conditions. *Front. Syst. Neurosci.* 8:190. doi: 10.3389/fnsys.2014.00190

Hsiao, H., Gray, V. L., Creath, R. A., Binder-Macleod, S. A., and Rogers, M. W. (2017). Control of lateral weight transfer is associated with walking speed in individuals post-stroke. *J. Biomech.* 60, 72–78. doi: 10.1016/j.jbiomech.2017.06.021

Huang, C. Y., Cherng, R. J., Yang, Z. R., Chen, Y. T., and Hwang, I. S. (2009). Modulation of soleus H reflex due to stance pattern and haptic stabilization of posture. *J. Electromyogr. Kinesiol.* 19, 492–499. doi: 10.1016/j.jelekin.2007.07.014

Jacobs, J. V., and Horak, F. B. (2007). External postural perturbations induce multiple anticipatory postural adjustments when subjects cannot pre-select their stepping foot. *Exp. Brain Res.* 179, 29–42. doi: 10.1007/s00221-006-0763-5

Jeka, J. J., Easton, R. D., Bentzen, B. L., and Lackner, J. R. (1996). Haptic cues for orientation and postural control in sighted and blind individuals. *Percept. Psychophys.* 58, 409–423. doi: 10.3758/BF03206817

Jeka, J. J., and Lackner, J. R. (1994). Fingertip contact influences human postural control. *Exp. Brain Res.* 100, 495–502. doi: 10.1007/BF02738408

Jeka, J. J., and Lackner, J. R. (1995). The role of haptic cues from rough and slippery surfaces in human postural control. *Exp. Brain Res.* 103, 267–276. doi: 10.1007/BF00231713

Kanekar, N., Lee, Y. J., and Aruin, A. S. (2013). Effect of light finger touch in balance control of individuals with multiple sclerosis. *Gait Posture* 38, 643–647. doi: 10.1016/j.gaitpost.2013.02.017

Kaulmann, D., Hermsdörfer, J., and Johannsen, L. (2017). Disruption of right posterior parietal cortex by continuous Theta Burst Stimulation alters the control of body balance in quiet stance. *Eur. J. Neurosci.* 45, 671–678. doi: 10.1111/ejn.13522

Kouzaki, M., and Masani, K. (2008). Reduced postural sway during quiet standing by light touch is due to finger tactile feedback but not mechanical support. *Exp. Brain Res.* 188, 153–158. doi: 10.1007/s00221-008-1426-5

Krishnan, V., and Aruin, A. S. (2011). Postural control in response to a perturbation: role of vision and additional support. *Exp. Brain Res.* 212, 385–397. doi: 10.1007/s00221-011-2738-4

Lackner, J. R., DiZio, P., Jeka, J., Horak, F., Krebs, D., and Rabin, E. (1999). Precision contact of the fingertip reduces postural sway of individuals with bilateral vestibular loss. *Exp. Brain Res.* 126, 459–466. doi: 10.1007/s002210050753

Lackner, J. R., Rabin, E., and DiZio, P. (2001). Stabilization of posture by precision touch of the index finger with rigid and flexible filaments. *Exp. Brain Res.* 139, 454–464. doi: 10.1007/s002210100775

Laufer, Y. (2003). The effect of walking aids on balance and weight-bearing patterns of patients with hemiparesis in various stance positions. *Phys. Ther.* 83, 112–122. doi: 10.1093/ptj/83.2.112

Maeda, A., Nakamura, K., Otomo, A., Higuchi, S., and Motohashi, Y. (1998). Body support effect on standing balance in the visually impaired elderly. *Arch. Phys. Med. Rehabil.* 79, 994–997. doi: 10.1016/S0003-9993(98)90100-9

Masani, K., Vette, A. H., Abe, M. O., Nakazawa, K., and Popovic, M. R. (2011). Smaller sway size during quiet standing is associated with longer preceding time of motor command to body sway. *Gait Posture* 33, 14–17. doi: 10.1016/j.gaitpost.2010.08.012

Mergner, T. (2007). Modeling sensorimotor control of human upright stance. *Prog. Brain Res.* 165, 283–297. doi: 10.1016/S0079-6123(06)65018-8

Mergner, T., Schweigart, G., and Fennell, L. (2009). Vestibular humanoid postural control. *J. Physiol. Paris* 103, 178–194. doi: 10.1016/j.jphysparis.2009.08.002

Misiaszek, J. E., Forero, J., Hiob, E., and Urbanczyk, T. (2016). Automatic postural responses following rapid displacement of a light touch contact during standing. *Neuroscience* 316, 1–12. doi: 10.1016/j.neuroscience.2015.12.033

Morlino, P., Balbi, B., Guglielmetti, S., Giardini, M., Grasso, M., Giordano, C., et al. (2017). Gait abnormalities of COPD are not directly related to respiratory function. *Gait Posture* 58, 352–357. doi: 10.1016/j.gaitpost.2017.08.020

Morton, S. M., and Bastian, A. J. (2003). Relative contributions of balance and voluntary leg-coordination deficits to cerebellar gait ataxia. *J. Neurophysiol.* 89, 1844–1856. doi: 10.1152/jn.00787.2002

Mouchnino, L., Fontan, A., Tandonnet, C., Perrier, J., Saradjian, A. H., Blouin, J., et al. (2015). Facilitation of cutaneous inputs during the planning phase of gait initiation. *J. Neurophysiol.* 114, 301–308. doi: 10.1152/jn.00668.2014

Nardone, A., Godi, M., Grasso, M., Guglielmetti, S., and Schieppati, M. (2009). Stabilometry is a predictor of gait performance in chronic hemiparetic stroke patients. *Gait Posture* 30, 5–10. doi: 10.1016/j.gaitpost.2009.02.006

Nardone, A., Turcato, A. M., and Schieppati, M. (2014). Effects of balance and gait rehabilitation in cerebellar disease of vascular or degenerative origin. *Restor. Neurol. Neurosci.* 32, 233–245. doi: 10.3233/RNN-130315

Oates, A. R., Hauck, L., Moraes, R., and Sibley, K. M. (2017). The effects of haptic input on biomechanical and neurophysiological parameters of walking: a scoping review. *Gait Posture* 58, 232–239. doi: 10.1016/j.gaitpost.2017.08.004

O'Doherty, J. E., Lebedev, M. A., Ifft, P. J., Zhuang, K. Z., Shokur, S., Bleuler, H., et al. (2011). Active tactile exploration using a brain-machine-brain interface. *Nature* 479, 228–231. doi: 10.1038/nature10489

O'Doherty, J. E., Lebedev, M. A., Li, Z., and Nicolelis, M. A. (2012). Virtual active touch using randomly patterned intracortical microstimulation. *IEEE Trans. Neural Syst. Rehabil. Eng.* 20, 85–93. doi: 10.1109/TNSRE.2011.2166807

Oliveira, A. S., Schlink, B. R., Hairston, W. D., Konig, P., and Ferris, D. P. (2017). Restricted vision increases sensorimotor cortex involvement in human walking. *J. Neurophysiol.* 118, 1943–1951. doi: 10.1152/jn.00926.2016

Oshita, K., and Yano, S. (2016). Effect and immediate after-effect of lightly gripping the cane on postural sway. *J. Physiol. Anthropol.* 35:14. doi: 10.1186/s40101-016-0096-4

Owings, T. M., Pavol, M. J., Foley, K. T., and Grabiner, M. D. (2000). Measures of postural stability are not predictors of recovery from large postural disturbances in healthy older adults. *J. Am. Geriatr. Soc.* 48, 42–50. doi: 10.1111/j.1532-5415.2000.tb03027.x

Paulus, W. M., Straube, A., and Brandt, T. (1984). Visual stabilization of posture. Physiological stimulus characteristics and clinical aspects. *Brain* 107(Pt 4), 1143–1163. doi: 10.1093/brain/107.4.1143

Perreira, R. B., Collange Grecco, L. A. C., and Oliveira, C. S. (2017). Postural control in blind individuals: a systematic review. *Gait Posture* 57, 161–167. doi: 10.1016/j.gaitpost.2017.06.008

Peterka, R. J. (2009). Comparison of human and humanoid robot control of upright stance. *J. Physiol. Paris* 103, 149–158. doi: 10.1016/j.jphysparis.2009.08.001

Peters, R. M., McKeown, M. D., Carpenter, M. G., and Inglis, J. T. (2016). Losing touch: age-related changes in plantar skin sensitivity, lower limb cutaneous reflex strength, and postural stability in older adults. *J. Neurophysiol.* 116, 1848–1858. doi: 10.1152/jn.00339.2016

Rabin, E., Demin, A., Pirrotta, S., Chen, J., Patel, H., Bhambri, A., et al. (2015). Parkinsonian gait ameliorated with a moving handrail, not with a banister. *Arch. Phys. Med. Rehabil.* 96, 735–741. doi: 10.1016/j.apmr.2014.07.427

Rabin, E., DiZio, P., Ventura, J., and Lackner, J. R. (2008). Influences of arm proprioception and degrees of freedom on postural control with light touch feedback. *J. Neurophysiol.* 99, 595–604. doi: 10.1152/jn.00504.2007

Sarabon, N., Rosker, J., Loefler, S., and Kern, H. (2013). The effect of vision elimination during quiet stance tasks with different feet positions. *Gait Posture* 38, 708–711. doi: 10.1016/j.gaitpost.2013.03.005

Saradjian, A. H. (2015). Sensory modulation of movement, posture and locomotion. *Neurophysiol. Clin.* 45, 255–267. doi: 10.1016/j.neucli.2015.09.004

Saradjian, A. H., Tremblay, L., Perrier, J., Blouin, J., and Mouchnino, L. (2013). Cortical facilitation of proprioceptive inputs related to gravitational balance constraints during step preparation. *J. Neurophysiol.* 110, 397–407. doi: 10.1152/jn.00905.2012

Schieppati, M., and Nardone, A. (1995). Time course of 'set'-related changes in muscle responses to stance perturbation in humans. *J. Physiol.* 487(Pt 3), 787–796. doi: 10.1113/jphysiol.1995.sp020918

Schieppati, M., Schmid, M., and Sozzi, S. (2014). Rapid processing of haptic cues for postural control in blind subjects. *Clin. Neurophysiol.* 125, 1427–1439. doi: 10.1016/j.clinph.2013.11.011

Schinkel-Ivy, A., Singer, J. C., Inness, E. L., and Mansfield, A. (2016). Do quiet standing centre of pressure measures within specific frequencies differ based on ability to recover balance in individuals with stroke? *Clin. Neurophysiol.* 127, 2463–2471. doi: 10.1016/j.clinph.2016.02.021

Seki, K., and Fetz, E. E. (2012). Gating of sensory input at spinal and cortical levels during preparation and execution of voluntary movement. *J. Neurosci.* 32, 890–902. doi: 10.1523/JNEUROSCI.4958-11.2012

Shadmehr, R. (2017). Distinct neural circuits for control of movement vs. holding still. *J. Neurophysiol.* 117, 1431–1460. doi: 10.1152/jn.00840.2016

Simpson, D. C. (1974). "The choice of control system for the multimovement prosthesis: extended physiological proprioception (EPP)," in *The Control of Upper-Extremity Prostheses and Orthoses*, eds P. Herberts, R. Kadefors, R. Magnusson, and I. Petersen (Springfield, IL: Thomas C. Thomas), 146–150.

Song, W., and Francis, J. T. (2015). Gating of tactile information through gamma band during passive arm movement in awake primates. *Front. Neural Circuits* 9:64. doi: 10.3389/fncir.2015.00064

Sozzi, S., Do, M. C., Monti, A., and Schieppati, M. (2012). Sensorimotor integration during stance: processing time of active or passive addition or withdrawal of visual or haptic information. *Neuroscience* 212, 59–76. doi: 10.1016/j.neuroscience.2012.03.044

Sozzi, S., Honeine, J. L., Do, M. C., and Schieppati, M. (2013). Leg muscle activity during tandem stance and the control of body balance in the frontal plane. *Clin. Neurophysiol.* 124, 1175–1186. doi: 10.1016/j.clinph.2012.12.001

Sozzi, S., Monti, A., De Nunzio, A. M., Do, M. C., and Schieppati, M. (2011). Sensori-motor integration during stance: time adaptation of control mechanisms on adding or removing vision. *Hum. Mov. Sci.* 30, 172–189. doi: 10.1016/j.humov.2010.06.002

Sozzi, S., Nardone, A., and Schieppati, M. (2016). Calibration of the leg muscle responses elicited by predictable perturbations of stance and the effect of vision. *Front. Hum. Neurosci.* 10:419. doi: 10.3389/fnhum.2016.00419

Straube, A., Krafczyk, S., Paulus, W., and Brandt, T. (1994). Dependence of visual stabilization of postural sway on the cortical magnification factor of restricted visual fields. *Exp. Brain Res.* 99, 501–506. doi: 10.1007/BF00228986

Tyler, D. J. (2015). Neural interfaces for somatosensory feedback: bringing life to a prosthesis. *Curr. Opin. Neurol.* 28, 574–581. doi: 10.1097/WCO.0000000000000266

Ustinova, K. I., and Langenderfer, J. E. (2013). Postural stabilization by gripping a stick with different force levels. *Gait Posture* 38, 97–103. doi: 10.1016/j.gaitpost.2012.10.020

Valls-Solé, J., Rothwell, J. C., Goulart, F., Cossu, G., and Mu-oz, E. (1999). Patterned ballistic movements triggered by a startle in healthy humans. *J. Physiol.* 516(Pt 3), 931–938. doi: 10.1111/j.1469-7793.1999.0931u.x

van Emmerick, R. E. A., and van Wengen, E. E. H. (2000). On variability and stability in human movement. *J. Appl. Biomech.* 16, 394–406. doi: 10.1123/jab.16.4.394

Wang, S., Wang, L., Meijneke, C., van Asseldonk, E., Hoellinger, T., Cheron, G., et al. (2015). Design and control of the MINDWALKER exoskeleton. *IEEE Trans. Neural Syst. Rehabil. Eng.* 23, 277–286. doi: 10.1109/TNSRE.2014.2365697

Conflict of Interest Statement: The authors declare that the research was conducted in the absence of any commercial or financial relationships that could be construed as a potential conflict of interest.

frontiers in Neurology

PERSPECTIVE
published: 15 December 2017
doi: 10.3389/fneur.2017.00696

Electroencephalogram-Based Brain–Computer Interface and Lower-Limb Prosthesis Control: A Case Study

Douglas P. Murphy[1], Ou Bai[1,2], Ashraf S. Gorgey[1,3], John Fox[1], William T. Lovegreen[1], Brian W. Burkhardt[1], Roozbeh Atri[2], Juan S. Marquez[2], Qi Li[2] and Ding-Yu Fei[4]*

[1] Hunter Holmes McGuire VA Medical Center, Department of Veterans Affairs, Richmond, VA, United States, [2] Department of Electrical and Computer Engineering, Florida International University, Miami, FL, United States, [3] Department of Physical Medicine and Rehabilitation, Virginia Commonwealth University, Richmond, VA, United States, [4] Department of Biomedical Engineering, Virginia Commonwealth University, Richmond, VA, United States

Objective: The purpose of this study was to establish the feasibility of manipulating a prosthetic knee directly by using a brain–computer interface (BCI) system in a transfemoral amputee. Although the other forms of control could be more reliable and quick (e.g., electromyography control), the electroencephalography (EEG)-based BCI may provide amputees an alternative way to control a prosthesis directly from brain.

Methods: A transfemoral amputee subject was trained to activate a knee-unlocking switch through motor imagery of the movement of his lower extremity. Surface scalp electrodes transmitted brain wave data to a software program that was keyed to activate the switch when the event-related desynchronization in EEG reached a certain threshold. After achieving more than 90% reliability for switch activation by EEG rhythm-feedback training, the subject then progressed to activating the knee-unlocking switch on a prosthesis that turned on a motor and unlocked a prosthetic knee. The project took place in the prosthetic department of a Veterans Administration medical center. The subject walked back and forth in the parallel bars and unlocked the knee for swing phase and for sitting down. The success of knee unlocking through this system was measured. Additionally, the subject filled out a questionnaire on his experiences.

Results: The success of unlocking the prosthetic knee mechanism ranged from 50 to 100% in eight test segments.

Conclusion: The performance of the subject supports the feasibility for BCI control of a lower extremity prosthesis using surface scalp EEG electrodes. Investigating direct brain control in different types of patients is important to promote real-world BCI applications.

Keywords: prosthesis, brain–computer interfaces, lower limb, control, electroencephalography, rhythm modulation

OPEN ACCESS

Edited by:
Mikhail Lebedev, Duke University, United States

Reviewed by:
Janet S. Dufek, University of Nevada, Las Vegas, United States
Mario U. Manto, University of Mons, Belgium

****Correspondence:***
Ashraf S. Gorgey
ashraf.gorgey@va.gov

Specialty section:
This article was submitted to Neuroprosthetics, a section of the journal Frontiers in Neurology

Received: *05 September 2017*
Accepted: *05 December 2017*
Published: *15 December 2017*

Citation:
Murphy DP, Bai O, Gorgey AS, Fox J, Lovegreen WT, Burkhardt BW, Atri R, Marquez JS, Li Q and Fei D-Y (2017) Electroencephalogram-Based Brain–Computer Interface and Lower-Limb Prosthesis Control: A Case Study. Front. Neurol. 8:696. doi: 10.3389/fneur.2017.00696

INTRODUCTION

The National Limb Loss Information Center reported that there are approximately 1.7 million people living with limb loss in the United States (1). Most of new amputations occur due to complications from impairment of the vascular system, and amputations of this type account for 82% of limb loss discharges between 1988 and 1996 (2). Lower-limb amputations account for 97% of all dysvascular

limb loss discharges. A recent study of the prevalence of limb loss in the US estimated that one out of every 190 people has had an amputation, and this number may double by the year of 2050 (3).

Advanced Lower-Limb Prosthetic Technology

People who have received limb-amputation face staggering emotional and financial lifestyle changes. They require one or more prosthetic devices and services, which must be maintained for the rest of their lives (4). A transfemoral amputee (above the knee) must expend up to 60% more metabolic energy to walk than a person with two whole legs (5) and consume as much as three times the affected-side hip power and torque (6). Commercially available prostheses comprise spring structures that store and release elastic energy throughout each walking stance period (7). Because of their passive nature, such prostheses cannot generate more mechanical energy than that is stored during each walking step. In distinction, the human ankle performs positive net work and has a greater peak power over the stance period, especially at moderate to fast walking speeds (8, 9). Emerging powered prosthetic devices with an embedded microprocessor provide a net positive power to the user, allowing more user control with less energy expenditure (4). These devices include a powered transfemoral prosthesis developed by a Vanderbilt University team led by Sup et al. (10) and a spring ankle with regenerative kinetics (SPARKy) funded by the US Army (11). In addition to the above devices for research purposes, the C-Leg (by Otto Bock, Germany) adjusts the degree and speed of knee joint swing in millisecond intervals allowing for the user to move more effortlessly. The Proprio-foot (by Ossur, Iceland) provides adaptive dorsiflexion to reduce compensation needs from the amputees in stair ambulation (though not truly, actively powered) (12). Incorporating advanced technology developed by Dr. Herr at MIT (13), *iWalk Inc.* delivers a clinically available device, BiOM®, a leg system [shown in the figure, adapted from Aldridge et al. (14)] that replaces combined functions of the foot, ankle, and calf regions of the human body. By adding a reflexive torque response in powered plantar flexion, the BiOM emulates the sound side stance-phase kinetics to provide better symmetry and economy of motion for amputees (15).

Prior attempts at voluntary control of the elements of a prosthesis have focused on the use of electromyographic (EMG) signals from muscle groups that remain under voluntary control. Most of this work has centered around control systems for upper extremity prostheses. Targeted muscle reinnervation is a case in point (16). This method provides adequate control but creates the extra step of muscle activation to control prosthetic functions. The Brain–Computer Interface (BCI) takes out this step for a more direct control method. Furthermore, the EMG or mechanical sensor-based control (10, 17) is reactive to the kinematic movement on residual or healthy limbs. We are striving to provide a proactive means for control that allows users to make voluntary adjustments independently before changing terrains or gait types.

Invasive BCI systems employ either spike trains or local field potentials with the brain. At the cortical surface, electrocorticography is employed. In contrast, non-invasive BCI systems employ electroencephalography (EEG) on the scalp. Invasive BCIs feature a better signal quality because electrodes are placed much closer to the neurons than non-invasive BCIs. Most of the invasive BCIs have been explored for complicated and fast control of upper extremity prosthetics (18–20). A non-invasive BCI using EEG is portable, less expensive, and provides a good time-resolution in milliseconds. However, the signal quality of the EEG may be inferior to that of signals obtained through invasive means. Non-invasive BCI can further be categorized into stimulus-induced BCIs using steady-state visual-evoked potential or SSVEP (21), the P300 evoked potential (22, 23), or combined SSVEP and P300. When using these BCI signal methods, the users need to shift their eye gaze to a visual stimulator provided by a computer monitor or LED array placed in front of them. When using stimulus-induced BCIs, the users must tolerate the strong visual flashes from the stimulators. On the other hand, the non-stimulus BCIs employ a signal method of the event-related desynchronization (ERD) and event-related synchronization (24) in EEG associated with the motor imagery, i.e., kinetic imagination of users' limb movement without any physical movement. As this method does not require any overt motor action, it is ideal for patients with severe motor disability. For example, it can serve as a communication solution (e.g., a spelling device) for those "locked-in" persons who have totally lost motor control in conditions, such as amyotrophic lateral sclerosis patients in the late stage (25, 26).

One of the early pioneers of BCI was Dr. Jacques J. Vidal who helped establish the University of California Los Angeles Computer Science department. He coined the term "brain–computer interface" and initiated a project in that area. Since that time, studies have shown how subjects can alter images on computer screens, use a speller, reach out with robotic arms and other activities through the use of this system (27). A BCI system works through combining several systems. The initial task is to acquire a brain signal that is associated with a particular thought. This signal then is processed and amplified and funneled to drive a given device. The entire process can be compartmentalized into four phases: signal acquisition, feature extraction, feature translation, and device output. Signal acquisition can occur through surface scalp electrodes or through chips placed on or near the cortex intracranially. Prior studies have clearly demonstrated the capacity of a BCI system to control a switching mechanism. In part the results of these studies have motivated the one in this report (28).

Unmet Needs

The control parameters of a microprocessor-driven powered prosthesis are commonly optimized for level walking. The level walking-optimized control parameters do not apply to locomotion activities other than level walking. Consequently, walking on ice or mud, for example, is not addressed with optimal parameters. Currently, amputees have extreme difficulty in going upstairs/downstairs or up/down steep-slopes when using the prosthesis optimized for level walking. This sub-optimal status leads to an increased instability and an additional load to the amputee's intact limb (12). *How can prosthetic users efficiently adapt prosthetic parameters to altered situations and environments?* For instance, this problem exists when the user needs to go upstairs

or downstairs after optimization for level walking. Amputees are frequently confronted with environmental situations that challenge their ability to ambulate efficiently and safely. Difficulty or inability in surmount such situations can significantly curtail or obstruct the restoration of a normal life. Quality of life and well-being suffer (29–31). In addition, amputees may have a higher risk of falling if the prosthesis cannot adapt to altered situations, such as stair climbing or unpaved trails (32).

Efforts have been made in state-of-the-art powered prostheses to make them more adaptive; however, the current technologies are still not sufficient. A powered prosthesis can measure user-shifted weight using biomechatronic mechanisms to adapt to the user's weight changes; however, the microprocessor embedded in the prosthetic device has difficulty in sensing and adopting environmental changes. Because of this, the prosthesis power output is not able to adapt to the user's needs/volitions in dynamic situations and environments. For instance, when an able-bodied person walks across a street, that person may intend to run rather than walk to reduce the risk of being hit by a car that may suddenly appear. To support the amputee's effort to move faster, the powered prosthesis should provide increased reflex power like a biological leg. According to the biomechanical mechanism, the increased reflex power can be generated either by exerting a stronger ground reaction force or interposing a higher power gain (i.e., by parameter intervention). The former one requires that the user push harder on the residual limb to obtain an increased ground reaction force; this, however, may lead to potential damage due to the increased pressure between the socket and the residual limb (33, 34). Accordingly, the latter one is preferred as the user can receive increased power support while keeping the same level of ground reaction force. Because the prosthetic device has no ability to know the user's desire, amputees need a new mechanism to relay their volition to appropriately affect the prosthetic control parameters so that the prosthesis can subsequently provide adaptive support. Although the other forms of control could be more reliable and quick (e.g., EMG control), the EEG-based BCI may provide amputees an alternative way to control prosthesis directly from brain.

PURPOSE OF THIS STUDY

The prosthetic control parameters are commonly tuned to optimize level walking. User control of a prosthesis to manipulate prosthetic control parameters in real time is essential to allow for the prosthesis to adapt to altered situations and environments. Smooth, effortless user control of a prosthesis that mimics the performance of a natural biological limb can reduce the effort and the load from the user, who under the best circumstances will consume much more energy than able-bodied persons. This study proposes a volitional prosthesis control using BCIs (35, 36) to support comfortable and effortless user control of the prosthesis, in which users can control the prosthesis (parametric intervention) proactively by thought alone as shown in **Figure 1**. The automatic recognition of the user's volition with subsequent automatic adjustment of prosthetic control parameters will bring amputee gait closer to normal gait patterns, which can help the amputee increase motion functions (e.g., upslope/downslope) and reduce energy expenditure in altered situations and environments.

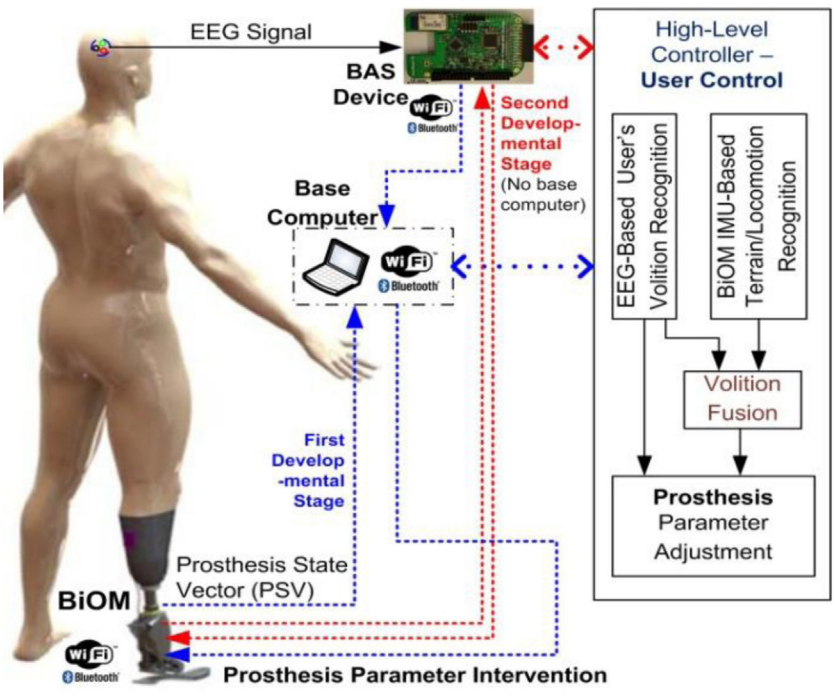

FIGURE 1 | Schematic diagram of user's direct control of prosthesis using brain–computer interface (BCI).

Meanwhile, recognition of the user's conscious intent with subsequent prosthetic control will provide the user an ownership sense of "I am the one in control of prosthetic adaptation." This sense of agency and control will improve the amputee's psychological and physical well-being (37, 38). Although this pilot study did not achieve this end point in its entirety, it does represent an important first step toward achieving the aforementioned goals. Therefore, the first step involves providing a mechanism for the prosthetic user to adjust his prosthesis with the speed and ease of thought in response to a simple environmental circumstance. Once a single switching system has successfully been achieved, then progression can occur to multiple switching systems and other more advanced control methods that would allow the prosthetic user to respond quickly and effectively to complex environmental situations.

BRAINBOARD SYSTEM TO SUPPORT BCI-BASED PROSTHETIC CONTROL

Developing a powerful BCI on a platform suitable for mobile use is a challenging task that would benefit from an open platform for enabling widespread, developmental efforts. To this end, an open-source hardware solution was implemented (https://github.com/gskelly), dubbed the BrainBoard, to allow researchers and developers to easily deploy wearable EEG-based BCI systems. It will allow for wireless data transmission to a device or host computer, along with some basic onboard processing for signal enhancement and noise rejection. The board is non-specific to any electrode arrangement and allows the use of up to eight signal electrodes. The BrainBoard was designed to function as a standalone board measuring 2.1″ × 2.5 ″. In addition to the hardware design, a basic software application programming interface was developed for the BrainBoard that allowed programmers to implement BCI algorithms both standard and novel. The high-level operating capability of the BrainBoard also makes it a possible host for existing BCI software.

The self-designed prototype of the light-weight, low-power consumption, battery-powered, and wireless-enabled BrainBoard for EEG/EMG recording using an ADS-1299 chip module (39) is illustrated in **Figure 2**. The ADS-1299 module is a low-cost, low-noise 24-bit analog front-end bio-potential measurement system recently distributed by Texas Instruments (Dallas, TX, USA). Using an ADS-1299 module greatly reduced the cost of the BrainBoard while maintaining high-quality amplification. A 32-bit MPU (AT32 Atmel AVR Microcontroller) was embedded in the BrainBoard for onboard real-time signal processing and data transmission. This self-developed BrainBoard provided high-precision EEG/EMG signal with less than 1.0 μV peak-to-peak noise. A low-power Bluetooth module RN42 (Roving Network, Los Gatos, CA, USA) was embedded to support wireless data transmission. The self-designed BrainBoard was designed to provide seamless recording and transmission of eight channels of 24-bit EEG/EMG signal with the sampling rate up to 1,000 Hz. The range of the wireless transmission can reach about 100 feet in an open space. Further, an IMU sensor was also embedded into the BrainBoard. A MPU-6050 (Gyro + Accelerometer) MEMS motion tracking chip device (InvenSense, San Jose, CA, USA) was employed. This chip provides a user-programmable gyro full-scale range from ±250, to ±2,000°/s and a user-programmable accelerometer full-scale range from ±2 to ±16 *g*, which meets the requirement for studying human locomotion.

FIGURE 2 | Open-source electroencephalography hardware platform.

CASE STUDY OF BCI-BASED KNEE UNLOCK

The current study is considered a proof of concept study aiming to examine our research hypothesis on one person as a feasibility pilot work. The study provides data to optimize both hardware and software to promote the goals of BCI use in lower extremity amputees. A 36-year-old male suffered a right transfemoral amputation as a sequel of the explosion of an improvised explosive device in an overseas conflict. This person is a full time transfemoral prosthetic wearer who ambulates without any additional aids such as a cane or crutches. IRB approval of the research design was obtained, and the subject agreed to the project and signed a consent form after receiving a full explanation of the study. The subject was then trained in the use of a BCI system to activate a switching mechanism. EEG electrodes were placed on his scalp. The design of this study included visits for training and one for the actual trial with the prosthesis. The first visit trained the subject in the use of the BCI system for control of a switch on a lower extremity prosthesis. Each training visit had two sessions. In the first session, EEG recordings were made when the subject engaged in motor imagery of his limb movement. These data were utilized to determine the necessary parameters for predicting the intention to move. In the second session, those parameters were used for real-time control of the switch on the lower extremity prosthesis. After the training visits the subject then used the BCI system to control a knee-locking mechanism on the prosthesis while he walked in the parallel bars.

ERD was obtained from a 32 channel EEG setup with dens sampling over motor areas on both hemispheres. This method was used in our previous BCI study (36). Six Electrodes (small metal disks) were placed on the subject's scalp over central motor areas on two hemispheres (C5, C3, C1, CZ, C2, and C4) and then secured with a plastic cap as shown in **Figure 3**.

A conductive gel was used to fill the space between the electrodes and the scalp to ensure good conductivity and minimize noise artifact. The EEG signals from the seven electrodes were referenced against the electrode on CZA (3 cm anterior to CZ). The EEG signals were amplified using a custom-made digital amplifier embedded with an ADS-1299 front-end system-on-chip bio-potential chip by Texas Instruments (Dallas, TX, USA). The EEG signals were then bandpassed (1–100 Hz) using a custom-made MATLAB tool box (BCI2VR). The ERD of the beta band (16–24 Hz) was calculated in real time against baseline activity when the subject was relaxed. The frequency band was determined by the ERD analysis of cued motor task managed in the first training session as shown in the **Figure 4**.

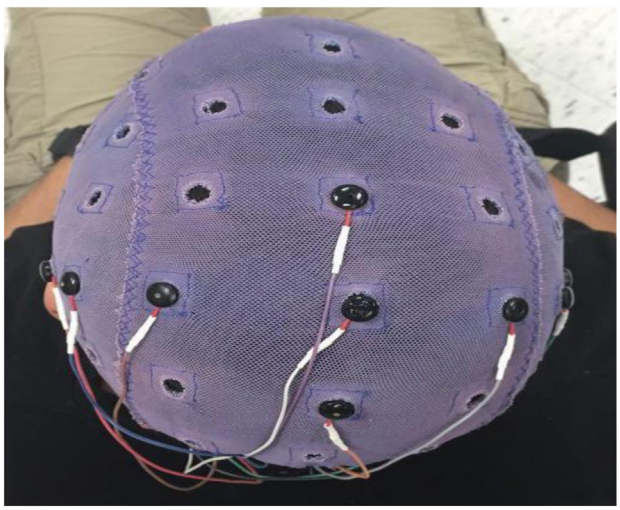

FIGURE 3 | The ECI conductive electro-gel by electro-cap.com was used in this current study.

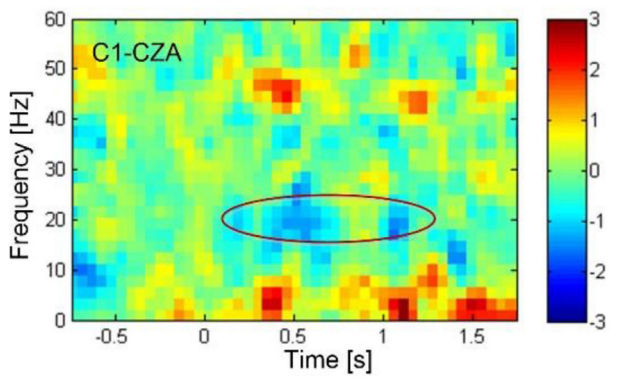

FIGURE 4 | The event-related desynchronization (ERD) plotted in blue color, showing the decrease in electroencephalography rhythmic amplitude as indicated in the circle, revealed in the beta band centered around 20 Hz starting 0.5 s after the sound cue was provided at 0 s. The ERD was associated with the actual toe extension. According to the time-spectral analysis of ERD, the beta band frequency from 16 to 24 Hz were determined for feedback training and subsequently for control of knee lock.

An off-line linear discrimination analysis model was made for online detection of the subject's intention to activate the switch by imaging his lower-limb movement. The algorithms as well as the BCI2VR tool box was provided in a previous study by one of the investigators (40).

Four training sessions occurred on four separate visits and were conducted before the trial. Each session lasted about 1.5 h (excluding the time for EEG setup). Custom-made software was developed to enable real time feedback from EEG. The frequency band was determined by ERD analysis. The training sessions started with wrist extension and toe extension movements on the healthy leg following a sound cue. After a reliable desynchronization in the beta band was observed, the subject was asked to imagine toe extension on the lost leg. At the beginning of the training, the ERD associated with the imagined toe extension was not reliable; the strategy was changed, and the subject was asked to move the hand, the intact leg and the residual limb. The subject was asked to imagine other types of motor activity such as walking forward. The goal was to generate a higher and more reliable ERD that could be found in the real-time feedback. In the first two training sessions, the subject was seated on a chair. The subject stood and walked during the third training session. The motor imagery task that generated the highest ERD was identified. In the fourth session, the sound cue was removed. The subject performed self-paced, imagined motor tasks, and the associated ERD was checked from the real-time feedback provided by the system.

During the training sessions, the subject was seated comfortably in an armchair with his hands and forearms supported. He was instructed to keep eye movements to a minimum including blinking, to minimize muscle action potential interference. The subject was asked to be as relaxed as possible to reduce or prevent other electrical or motion based noise. He was then asked to perform motor imagery of the amputated limb. Initially, he was asked to move the bar on a bar graph past a designated threshold point that appeared on a computer screen. When he could consistently achieve this activity more than 90% of the time, he was ready to activate the mechanism to unlock the prosthetic knee through BCI control.

A transfemoral prosthesis which is a well-fitting ischial containment socket, with gel seal-in suction liner for suspension, a modular single axis knee joint, with lock and extension assist (Otto Bock 3R33) and a solid ankle cushion heel foot, was modified with a rotary actuator that was controllable through a BCI system. The BCI program would unlock the knee, and an extension of the knee locked the prosthetic knee. The initiative to control the knee lock mechanism came from the test subject's thought after training in the use of the BCI hardware. The rotary actuator was manufactured in the prosthetics lab through utilization of components from a myoelectric wrist rotator (Otto Bock 10S17) and was powered by a 6-V lithium ion battery. This was connected to the BCI system and the manual locking system of the knee. Once the test subject was competent and reliable in locking and unlocking the knee, this person then performed short distance ambulation in the parallel bars with one of the investigators on either side for stabilization. The test subject rose from a seated position and locked the knee. The investigators tested the success of knee locking. The subject

then walked the length of the parallel bars, unlocking the knee for swing phase, turned around, returned to the wheelchair, unlocked the knee with the BCI mechanism and sat down. This procedure was repeated four times. The number of times the locking was successfully unlocked on the first effort was compared to the number of occasions in which the knee had to be unlocked. The custom-made program performed bandpass filtering and calculated ERD according to the baseline activity, which was collected when the subject was relaxing, in real time. The single-trial ERD calculated was feedback to the subject in real time without trial back-averaging. The knee lock was open only when the ERD was over a pre-set threshold. Since it was self-paced design, there was no inter-trial break. The BCI was turned off between testing segments to let the subject have a 5- to 15-min rest.

After a rest of at least 5–15 min the subject returned to the parallel bars. He came to a standing position. He walked the length of the parallel bars and back. The knee was locked for stance phase and unlocked for the swing phase. The subject took two more trips from one end to the other and back in the parallel bars. The success of unlocking the knee was again compared to occasions when unlocking was required.

After the trial the subject filled out a short survey, in which the subject indicated that the use of the BCI system was only mildly challenging to learn, and that once learned he developed complete confidence in his capacity to unlock the prosthetic knee through the system. The ultimate goal was to walk naturally. The subject was able to unlock the knee to sit in the five attempts. His success rates for the eight walking segments (each segment consisted of walking from one end of the parallel bars to the other and then a return to the starting point) were as follows: First segment, 100%; second segment, 77.8%; third segment, 100%; fourth segment, 100%; fifth segment, 50%; sixth segment, 83.3%; seventh segment, 71.4%; and eighth segment, 85.7%.

DISCUSSION

Human gait can be controlled either consciously or subconsciously. The EMG, including those by invasive procedures, can assist the prosthetic control without user's conscious involvement. Under this situation, the prosthetic control is achieved subconsciously. When walking on uneven terrain or transitioning from different gait modes, the human is usually consciously involved with the locomotion control, where human preserve the "sense of control." The proposed user's control of prosthesis using BCI would potentially provide the user this kind of conscious control. Further, the EMG-based approach is "reactive" that the alternation in control can only be implemented after the change of locomotion mode. For example, the prosthetic control can be adapted only after walking one-stair down. In contrast, the proposed approach would potentially shift the prosthetic control before moving downstairs. Further, EMG systems are brain to nerve to muscle to electrode to device. Surface EEG electrodes are brain to device. Because there are less interfaces, there is the potential for less error and a shorter response time and less effort required on the part of the user.

Investigating direct brain control in different types of patients is important to promote real-world BCI applications. This study demonstrates that, at least on a short-term basis, non-invasive scalp recorded EEG signals can be used successfully and reliably to manipulate a lock for a mechanical knee on a prosthesis. There is debate within the literature as to whether BCI control systems can move from implanted chips attached to the brain to scalp recorded systems due to the low signal to noise (S/N) ratios in the latter. In this study the S/N ratio was improved through use of a spatial filtering system with a Laplacian array (40).

Not only did the results indicate some level of mastery of the system but the subject developed confidence in his ability without any sense of added risk. The results did show less success in the later trials. Potentially, this could indicate some level of mental fatigue. Other factors such as distractibility could have played a role. Also, the electrode conductivity could have diminished if the gel had dried or the electrodes had shifted with a degradation in the contact with the skin. In prior studies, one investigator had reduced variance in ERD through use of a longer recording window and had reduced subject fatigue through limiting the time for body action imagery to 1 s (40). Similar tactics were used in this study to enhance reliability, although there was no relaxation window. Since the actual test was managed in a real-world scenario on the self-paced mode, the accurate recording of the delay in the attempt to the knee lock operation was not available. However, the subject reported that in most cases, he could unlock the knee within a very short time.

In order for a BCI system to integrate successfully into the daily use of a prosthesis, it must perform reliably on demand and must not activate spontaneously to reduce false positives (F/P). During the trials in this study there were no observed F/P. Unintentional and unexpected unlocking of the knee during stance phase would increase the risk of falls for the user. This phenomenon was not observed. More extensive testing and training would be required to confirm this sort of reliability. This testing could also include walking in more challenging environments such as stairs or uneven terrain.

Other BCI systems for prosthetic control have focused on upper extremity control systems (41, 42). Applying the BCI technology to lower extremity prostheses potentially offers a different set of advantages. These might include prosthetic manipulation or adjustment through a hands-free mechanism, the ability to adjust rapidly according to different environmental circumstances, and a more natural appearing control of the prosthesis. Current powered and intelligent lower extremity prostheses react to the motion and demands of the user. While these can dramatically improve prosthetic function, they still only offer a strictly passive method of control that is reactive and not proactive (43). The prosthesis has no way of predicting a change in terrain or the future demands of the user. Using BCI systems the user could communicate with a prosthesis using thought alone to actively manipulate the prosthesis. This more closely approximates the natural control of a limb.

Challenges that remain for the BCI management of a lower extremity prosthesis include increasing the reliability of

control and creating an adequate wireless system that is secure, dependable and wearer-friendly both for cosmesis and comfort. Furthermore, the current system only activates a switch to make a simple prosthetic adjustment. More complex systems would be desirable to increase prosthetic control options particularly for microprocessor ankle/foot systems and knees.

ETHICS STATEMENT

All aspects of the study design was conducted based on our IRB approved protocol, all participants were given and signed an approved consent form.

AUTHOR CONTRIBUTIONS

DM contributed to experimental design, data collection, and writing the article. OB contributed to experimental design, data collection, data analysis, and writing the article. AG contributed to data collection and writing the article. JF, WL, BB, RA, JM, QL, and DF were involved in experimental design and data collection.

ACKNOWLEDGMENTS

This work is partly supported by National Science Foundation (CNS-1552163).

REFERENCES

1. NLLI Center. *Amputation Statistics by Cause Limb Loss in the United States*. Manassas, VA: The Amputee Coalition (2008).
2. Adams PF, Hendershot GE, Marano MA. Current estimates from the National Health Interview Survey, 1996. *Vital Health Stat 10* (1999) 200:1–203.
3. Ziegler-Graham K, MacKenzie EJ, Ephraim PL, Travison TG, Brookmeyer R. Estimating the prevalence of limb loss in the United States: 2005 to 2050. *Arch Phys Med Rehabil* (2008) 89:422–9. doi:10.1016/j.apmr.2007.11.005
4. McGimpsey G, Bradford T. *Limb Prosthetics Services and Devices Critical Unmet Need: Market Analysis*. Worcester, MA: Bioengineering Institute Center for Neuroprosthetics, Worcester Polytechnic Institution (2010).
5. Waters RL, Perry J, Antonelli D, Hislop H. Energy cost of walking of amputees: the influence of level of amputation. *J Bone Joint Surg Am* (1976) 58:42–6. doi:10.2106/00004623-197658010-00007
6. Winter DA. *The Biomechanics and Motor Control of Human Gait: Normal, Elderly and Pathological*. Waterloo, ON: University of Waterloo Press (1991).
7. Seymour R. *Prosthetics and Orthotics: Lower Limb and Spinal*. Baltimore, MD: Lippincott Williams & Wilkins (2002).
8. Hof AL, Geelen BA, Van den Berg J. Calf muscle moment, work and efficiency in level walking; role of series elasticity. *J Biomech* (1983) 16:523–37. doi:10.1016/0021-9290(83)90067-2
9. Hansen AH, Childress DS, Miff SC, Gard SA, Mesplay KP. The human ankle during walking: implications for design of biomimetic ankle prostheses. *J Biomech* (2004) 37:1467–74. doi:10.1016/j.jbiomech.2004.01.017
10. Sup F, Bohara A, Goldfarb M. Design and control of a powered transfemoral prosthesis. *Int J Robot Res* (2008) 27:263–73. doi:10.1177/0278364907084588
11. Hitt JK, Bellman R, Holgate M, Suga TG, Hollander KW. The SPARKy (spring ankle with regenerative kinetics) project: design and analysis of a robotic transtibial prosthesis with regenerative kinetics. *6th International Conference on Multibody Systems, Nonlinear Dynamics, and Control*. Las Vegas, NV, USA: ASME (2007). p. 1587–96.
12. Alimusaj M, Fradet L, Braatz F, Gerner HJ, Wolf SI. Kinematics and kinetics with an adaptive ankle foot system during stair ambulation of transtibial amputees. *Gait Posture* (2009) 30:356–63. doi:10.1016/j.gaitpost.2009.06.009
13. Willyard C. Profile: Hugh Herr. *Nat Med* (2007) 13:1395. doi:10.1038/nm1207-1395
14. Aldridge JM, Sturdy JT, Wilken JM. Stair ascent kinematics and kinetics with a powered lower leg system following transtibial amputation. *Gait Posture* (2012) 36:291–5. doi:10.1016/j.gaitpost.2012.03.013
15. Geyer H, Herr H. A muscle-reflex model that encodes principles of legged mechanics produces human walking dynamics and muscle activities. *IEEE Trans Neural Syst Rehabil Eng* (2010) 18:263–73. doi:10.1109/TNSRE.2010.2047592
16. Kuiken TA, Li G, Lock BA, Lipschutz RD, Miller LA, Stubblefield KA, et al. Targeted muscle reinnervation for real-time myoelectric control of multifunction artificial arms. *JAMA* (2009) 301:619–28. doi:10.1001/jama.2009.116
17. Au S, Berniker M, Herr H. Powered ankle-foot prosthesis to assist level-ground and stair-descent gaits. *Neural Netw* (2008) 21:654–66. doi:10.1016/j.neunet.2008.03.006
18. Donoghue JP. Connecting cortex to machines: recent advances in brain interfaces. *Nat Neurosci* (2002) 5(Suppl):1085–8. doi:10.1038/nn947
19. Carmena JM, Lebedev MA, Crist RE, O'Doherty JE, Santucci DM, Dimitrov DF, et al. Learning to control a brain-machine interface for reaching and grasping by primates. *PLoS Biol* (2003) 1:E42. doi:10.1371/journal.pbio.0000042
20. Velliste M, Perel S, Spalding MC, Whitford AS, Schwartz AB. Cortical control of a prosthetic arm for self-feeding. *Nature* (2008) 453:1098–101. doi:10.1038/nature06996
21. Sutter EE, Tran D. The field topography of ERG components in man – I. The photopic luminance response. *Vision Res* (1992) 32:433–46. doi:10.1016/0042-6989(92)90235-B
22. Donchin E, Spencer KM, Wijesinghe R. The mental prosthesis: assessing the speed of a P300-based brain-computer interface. *IEEE Trans Rehabil Eng* (2000) 8:174–9. doi:10.1109/86.847808
23. Polich J. Updating P300: an integrative theory of P3a and P3b. *Clin Neurophysiol* (2007) 118:2128–48. doi:10.1016/j.clinph.2007.04.019
24. Wolpaw JR, McFarland DJ. Control of a two-dimensional movement signal by a noninvasive brain-computer interface in humans. *Proc Natl Acad Sci U S A* (2004) 101:17849–54. doi:10.1073/pnas.0403504101
25. Birbaumer N, Cohen LG. Brain-computer interfaces: communication and restoration of movement in paralysis. *J Physiol* (2007) 579:621–36. doi:10.1113/jphysiol.2006.125633
26. Daly JJ, Wolpaw JR. Brain-computer interfaces in neurological rehabilitation. *Lancet Neurol* (2008) 7:1032–43. doi:10.1016/S1474-4422(08)70223-0
27. Kuiken TA, Barlow AK, Hargrove LJ, Dumanian GA. Targeted muscle reinnervation for the upper and lower extremity. *Tech Orthop* (2017) 32:109–16. doi:10.1097/BTO.0000000000000194
28. Shih JJ, Krusienski DJ, Wolpaw JR. Brain-computer interfaces in medicine. *Mayo Clin Proc* (2012) 87:268–79. doi:10.1016/j.mayocp.2011.12.008
29. Varol HA, Sup F, Goldfarb M. Multiclass real-time intent recognition of a powered lower limb prosthesis. *IEEE Trans Biomed Eng* (2010) 57:542–51. doi:10.1109/TBME.2009.2034734
30. Huang H, Zhang F, Hargrove LJ, Dou Z, Rogers DR, Englehart KB. Continuous locomotion-mode identification for prosthetic legs based on neuromuscular-mechanical fusion. *IEEE Trans Biomed Eng* (2011) 58:2867–75. doi:10.1109/TBME.2011.2161671
31. Young AJ, Simon AM, Fey NP, Hargrove LJ. Intent recognition in a powered lower limb prosthesis using time history information. *Ann Biomed Eng* (2014) 42:631–41. doi:10.1007/s10439-013-0909-0
32. Vanicek N, Strike SC, McNaughton L, Polman R. Lower limb kinematic and kinetic differences between transtibial amputee fallers and non-fallers. *Prosthet Orthot Int* (2010) 34:399–410. doi:10.3109/03093646.2010.480964
33. Sanders JE, Goldstein BS, Leotta DF. Skin response to mechanical stress: adaptation rather than breakdown – a review of the literature. *J Rehabil Res Dev* (1995) 32:214–26.
34. Ali S, Abu Osman NA, Eshraghi A, Gholizadeh H, Abd Razak NA, Wan Abas WA. Interface pressure in transtibial socket during ascent and descent on stairs and its effect on patient satisfaction. *Clin Biomech (Bristol, Avon)* (2013) 28:994–9. doi:10.1016/j.clinbiomech.2013.09.004
35. Wolpaw JR, McFarland DJ, Neat GW, Forneris CA. An EEG-based brain-computer interface for cursor control. *Electroencephalogr Clin Neurophysiol* (1991) 78:252–9. doi:10.1016/0013-4694(91)90040-B
36. Bai O, Lin P, Vorbach S, Floeter MK, Hattori N, Hallett M. A high performance sensorimotor beta rhythm-based brain–computer interface

associated with human natural motor behavior. *J Neural Eng* (2008) 5:24. doi:10.1088/1741-2560/5/1/003
37. Reker GT, Peacock EJ, Wong PT. Meaning and purpose in life and well-being: a life-span perspective. *J Gerontol* (1987) 42:44–9. doi:10.1093/geronj/42.1.44
38. Ryan RM, Deci EL. Self-determination theory and the facilitation of intrinsic motivation, social development, and well-being. *Am Psychol* (2000) 55:68–78. doi:10.1037/0003-066X.55.1.68
39. Kelly G, Americo Nabuco Leva Ferreira de Freitas J, Bai O. BrainBoard: an open-source hardware/software platform for wearable EEG-based brain-computer interfaces. *The 6th International IEEE EMBS Conference on Neural Engineering*. San Diego, CA (2013).
40. Qian K, Nikolov P, Huang D, Fei D-Y, Chen X, Bai O. A motor imagery-based online interactive brain-controlled switch: paradigm development and preliminary test. *Neurophysiol Clin* (2010) 121:1304–13. doi:10.1016/j.clinph.2010.03.001
41. Ang KK, Guan C, Chua KSG, Ang BT, Kuah C, Wang C, et al. A clinical study of motor imagery-based brain-computer interface for upper limb robotic rehabilitation. *2009 Annual International Conference of the IEEE Engineering in Medicine and Biology Society*. Minneapolis, MN (2009). p. 5981–4.
42. Horki P, Solis-Escalante T, Neuper C, Müller-Putz G. Combined motor imagery and SSVEP based BCI control of a 2 DoF artificial upper limb. *Med Biol Eng Comput* (2011) 49:567–77. doi:10.1007/s11517-011-0750-2
43. Wong CK, Rheinstein J, Stern MA. Benefits for adults with transfemoral amputations and peripheral artery disease using microprocessor compared with nonmicroprocessor prosthetic knees. *Am J Phys Med Rehabil* (2015) 94:804–10. doi:10.1097/PHM.0000000000000265

Conflict of Interest Statement: The authors declare that the research was conducted in the absence of any commercial or financial relationships that could be construed as a potential conflict of interest.

frontiers in Neuroscience

ORIGINAL RESEARCH
published: 21 December 2017
doi: 10.3389/fnins.2017.00725

Cooperative Control for A Hybrid Rehabilitation System Combining Functional Electrical Stimulation and Robotic Exoskeleton

Dingguo Zhang[1], Yong Ren[1], Kai Gui[1], Jie Jia[2] and Wendong Xu[2]**

[1] State Key Laboratory of Mechanical Systems and Vibrations, Robotics Institute, Shanghai Jiao Tong University, Shanghai, China, [2] Huashan Hospital, School of Medicine, Fudan University, Shanghai, China

Functional electrical stimulation (FES) and robotic exoskeletons are two important technologies widely used for physical rehabilitation of paraplegic patients. We developed a hybrid rehabilitation system (FEXO Knee) that combined FES and an exoskeleton for swinging movement control of human knee joints. This study proposed a novel cooperative control strategy, which could realize arbitrary distribution of torque generated by FES and exoskeleton, and guarantee harmonic movements. The cooperative control adopted feedfoward control for FES and feedback control for exoskeleton. A parameter regulator was designed to update key parameters in real time to coordinate FES controller and exoskeleton controller. Two muscle groups (quadriceps and hamstrings) were stimulated to generate active torque for knee joint in synchronization with torque compensation from exoskeleton. The knee joint angle and the interactive torque between exoskeleton and shank were used as feedback signals for the control system. Central pattern generator (CPG) was adopted that acted as a phase predictor to deal with phase confliction of motor patterns, and realized synchronization between the two different bodies (shank and exoskeleton). Experimental evaluation of the hybrid FES-exoskeleton system was conducted on five healthy subjects and four paraplegic patients. Experimental results and statistical analysis showed good control performance of the cooperative control on torque distribution, trajectory tracking, and phase synchronization.

Keywords: knee exoskeleton, functional electrical stimulation, hybrid rehabilitation, cooperative control, central pattern generator

OPEN ACCESS

Edited by:
Daniel P. Ferris,
University of Florida, United States

Reviewed by:
Nitin Sharma,
University of Pittsburgh, United States
Kazutaka Takahashi,
University of Chicago, United States

****Correspondence:***
Dingguo Zhang
dgzhang@sjtu.edu.cn
Wendong Xu
wendongxu@fudan.edu.cn

Specialty section:
This article was submitted to Neuroprosthetics, a section of the journal Frontiers in Neuroscience

Received: *11 July 2017*
Accepted: *12 December 2017*
Published: *21 December 2017*

Citation:
Zhang D, Ren Y, Gui K, Jia J and Xu W (2017) Cooperative Control for A Hybrid Rehabilitation System Combining Functional Electrical Stimulation and Robotic Exoskeleton. Front. Neurosci. 11:725. doi: 10.3389/fnins.2017.00725

1. INTRODUCTION

Neurologic injuries such as stroke and spinal cord injury may cause paresis in patients and give rise to movement disability. Physical rehabilitation is highly necessary for paralyzed individuals to restore mobility of extremities. Functional electrical stimulation (FES) and robotic exoskeletons are two important technologies used widely in extremity rehabilitation.

Many FES systems have been developed by using either surface or implanted electrodes in the past decades (Popovic et al., 2001). As a neuro-rehabilitation approach that excites and activates muscles directly, FES can provide not only functional training but also therapeutic benefits to paralyzed patients. Although some advances in closed-loop control and multichannel selection

of muscles have achieved complex stimulation, it is still a complicated and tough problem of controlling FES to assist paralyzed individuals to move in a natural manner, mainly due to the nonlinearity and time variability of human musculoskeletal system (Zhang et al., 2007; Lynch and Popovic, 2008). The pathological muscle conditions and the poor controllability of FES result in insufficient joint torque to provide limbs movement and body support for patients (del Ama et al., 2012; Ha et al., 2012; Quintero et al., 2012). In addition, muscle fatigue is often induced under continuous electrical stimulation. In a word, these problems mentioned severely hinder the widespread usage of FES from becoming a popular treatment option.

Robotic exoskeleton is an alternative technology of extremity rehabilitation for paraplegic patients, and lower limb exoskeletons are designed to accomplish neuro-rehabilitation and replace the physical gait training effort of therapists (Dollar and Herr, 2008). The well-known representatives in the application of motor rehabilitation for lower limbs are Lokomat (Hocoma, Switzerland) (Colombo et al., 2000), LOPES (Veneman et al., 2007), POGO and PAM (Reinkensmeyer et al., 2006), ALEX (Banala et al., 2009), etc. The popular exoskeletons usually use electric actuators, hydraulic actuators, or pneumatic actuators (Fan and Yin, 2013; Vitiello et al., 2013). In comparison with FES, the therapeutic effect of robotic rehabilitation is limited, because it can merely provide assistive torque to limbs, the muscles are not stimulated actively, which are passively contracted or stretched. Therefore, it is an urgent demand to combine FES with exoskeletons, merging as hybrid rehabilitation systems that bring about not only functional but also physiological benefits to patients.

There is an increasing interest in developing hybrid rehabilitation systems, taking the advantages of FES and exoskeleton, and overcoming the limitations in separate application (To et al., 2008; del Ama et al., 2012). In general, there are two kinds of such hybrid rehabilitation systems, i.e., combination of FES and powerless (passive) orthoses, or combination of FES and powered (active) exoskeletons. The controlled-brake orthosis (CBO) developed by Goldfarb and Durfee (1996) used joint brakes to control the body movement generated by FES. An obvious deficiency of orthoses is the inability to generate active torque for joints. Compared with orthoses, powered exoskeletons using mechanical actuators can compensate insufficient torque generated by FES. Recently, some achievements in hybrid FES-exoskeleton systems have been made, such as WalkTrainer (Stauffer et al., 2009), Vanderbilt Exoskeleton (Ha et al., 2012), Kinesis (del Ama et al., 2014), iLeg (Chen et al., 2014) and so on. In WalkTrainer system, Stauffer et al. (2009) developed closed-loop control of FES that modulated muscle stimulation to minimize the interaction force between the wearer and the exoskeleton, or modulated the desired torques as a function of the gait cycle. That system did not take account for muscle fatigue compensation as the exoskeleton was not actively involved. In order to accomplish cooperative control of FES with the Vanderbilt Exoskeleton during walking, Ha et al. (2016) proposed a two-loop controller, where motor control loop and muscle control loop co-existed. In that manner, the motor control loop used joint angle feedback to control the output of the joint motor to track the desired joint trajectories, while the muscle control loop utilized joint torque profiles from previous steps to regulate the muscle stimulation for the subsequent step to minimize the motor torque contribution required for joint angle trajectory tracking. del Ama et al. (2014) proposed cooperative control to balance the effort between muscle stimulation and exoskeleton in hybrid system (Kinesis), which sought to minimize the interaction torque and realized hybrid ambulatory gait rehabilitation. The torque-time integral generated by FES was measured to estimate muscle fatigue and a learning method was used to modulate the stimulation strength so as to compensate the torque loss. Alibeji N. A. et al. (2015) and Alibeji et al. (2017) developed an adaptive control method inspired by muscle synergy to compensate for actuator redundancy and FES-induced muscle fatigue in a hybrid FES-exoskeleton system, which showed ability to coordinate FES of quadriceps and hamstrings muscles and electric motors at the hip joint and knee joint of the exoskeleton. Chen et al. (2014) designed an FES-assisted control strategy for a hybrid lower-limb rehabilitation system (iLeg), where active FES control was achieved via a combination of neural network based feedforward control and PD feedback control to realize torque control, and meanwhile impedance control was adopted for exoskeleton control. Tu et al. (2017) combined FES with exoskeleton to accomplish gait rehabilitation in a different way, where FES and exoskeleton made effect on different joints separately, i.e., exoskeleton was applied on hip and knee joints, and FES was applied on ankle joint. A sliding control algorithm called chattering mitigation robust variable control (CRVC) was used for cooperative control in that hybrid system.

This study aims to accomplish harmonic and elegant control between FES and exoskeleton and explore their combined function on single-joint movement. Different from previous works, the active roles of FES and exoskeleton can be set freely here, i.e., the contribution of FES and exoskeleton can be distributed arbitrarily under different circumstances with specified requirements. Meanwhile, the synchronization problem of different drivers (motor vs. muscle) is well solved. It is well known knee joints play very important roles in lower limb locomotion, and knee joint control is a benchmark in previous literature (Chang et al., 1997; Ferrarin et al., 2001; Hunt et al., 2004; Sharma et al., 2009; Alibeji N. et al., 2015). Therefore, a hybrid rehabilitation system called FEXO Knee is developed in this work, which combines FES with a knee exoskeleton. A novelty of the system is the interactive force can be measured, which can help realize the better cooperative control. Moreover, it is very interesting and challenging to synchronize the human leg (driven by biological muscles) and exoskeleton (driven by artificial motor) to accomplish one task together, which is particularly solved in this work. A new cooperative control scheme is proposed, which can achieve shank swing motion under the harmonized and synchronized action of FES and exoskeleton, and realize different contribution of FES and exoskeleton. In such a scheme, a biologically-inspired control method, central pattern generator (CPG), is adopted because CPG has some favorable properties in synchronization, entrainment, and robustness against disturbance in general

(Ijspeert, 2008). A combination of feedforward control and feedback control is used for FES and exoskeleton. A parameter regulator based on policy gradient method is designed to coordinate FES controller and exoskeleton controller adaptively. Five healthy subjects and four hemiplegic patients have participated in a series of experiments to test the cooperative control performance of FEXO Knee.

2. METHOD

2.1. FEXO Knee

The cooperative control of FES and exoskeleton is accomplished on our available prototype, FEXO Knee, which has two parts: a self-designed knee exoskeleton and a commercial FES device (RehaStim 2, Hasomed, Germany). The exoskeleton is composed of mechanical parts, electric motor, elastic actuator, sensors, and accessories. The function of exoskeleton is to generate assistive torque for rhythmic swing of human shank. It is designed for subjects with sitting posture, so it has a base bench that may be fixed on a table to hold the whole structure. The preliminary version (FEXO Knee I) has been reported in Ren and Zhang (2014). The new version (FEXO Knee II) is shown in **Figure 1**.

2.1.1. Mechanical Design and Actuation

The main mechanical frame of the knee exoskeleton is made of aluminum. The key part is the electric motor (i.e., an AC servo motor of Panasonic Corp., Japan), which has a maximum angular velocity of 5,000 rpm, 400 W rated power, and a nominal torque of 1.3 Nm. The planetary reducer combined with the motor has speed radio of 15:1, thus the output end of the reducer can generate a nominal torque of 19.5 Nm.

The output shaft of the reducer connects to an elastic component via a rigid coupler. The elastic component consists of six linear springs with a stiffness of 16.5 N/mm. The six springs with pre-contraction are placed between a three-spoke element and an output fixture (see **Figure 1**). The torque generated by the servo motor can be transmitted to the output fixture through a rotatory elastic module, which turns into a series elastic actuator (SEA) (Pratt and Williamson, 1995; Tsagarakis et al., 2009). For the whole elastic component, the stiffness is a variable and can be given by:

$$K_{SEA} = 6 \cdot K_A \cdot (R^2 + \frac{r_s^2}{3}) \cdot (2\cos\vartheta_s^2 - 1) \quad (1)$$

where K_{SEA} denotes the stiffness of the elastic component; K_A denotes the stiffness of a single linear spring; R denotes the spoke radius; r_s denotes the external radius of a single linear spring; ϑ_s is the net rotatory angle, which is the difference between motor output angle and actual exoskeleton rotation angle ($\vartheta_s = \vartheta_m - \vartheta_e^a$). According to the design size of the knee exoskeleton, we know $R = 0.027$ m, $r_s = 0.008$ m.

The mechanism that holds the human shank is fastened to the output fixture of the elastic component, and contains two adjustable shells. Two interactive force sensors are placed between the outer shell and the shank wrap. For safety purpose, the range of motion (ROM) of the joint is limited to $\pm 90^\circ$ for knee extension and flexion. The naturally drooping state of human shank is defined as the zero position.

2.1.2. Sensors

Two types of sensors are installed in the knee exoskeleton: an absolute encoder for measuring the joint angular position, and two interactive force sensors for measuring the mutual force between exoskeleton and shank. The encoder is fastened coaxially with the joint with resolution of 0.09°. The two interactive force sensors are respectively attached to the front and the rear of the shell, and please refer to component (6) in **Figure 1**. Each contains six distributed force sensing resistors (FSR 402, Interlink Electronics, USA) covered with a silicone board. The total interactive force is the summation of measured data from six calibrated FSR elements. The mutual torque (τ_{mut}) between exoskeleton and shank can be obtained through multiplying the interactive force by the force arm. According to the mechanical structure, the average force arm is 0.16 m for the knee exoskeleton. The mutual torque is defined as positive if it is acted on shank in extension direction and negative in flexion direction. For real-time control, FEXO Knee uses a data acquisition card (USB-6343, National Instrument, USA) to receive signals from these sensors, and the sampling frequency is 1 Hz. In fact, the interactive force sensors should be a highlight of this system, which can measure force variation generated by muscles (e.g., force decline due to muscle fatigue), and provide important information for cooperative control.

2.2. Control Scheme

In the FEXO Knee system, two different kinds of actuators (skeletal muscles and electric motor) should work together. The cooperative control is the kernel, which aims to achieve suitable synchronization and compliant interaction between the knee exoskeleton driven by electric motor and the human shank activated by FES. The control scheme of FEXO Knee is shown in **Figure 2**. The desired total torque (τ_k^d) for knee joint movement is supplied by summation of desired FES torque (τ_{FES}^d) and desired assistive torque from exoskeleton (τ_{exo}^{d2}). The torque distribution between them is regulated by two tunable gains (δ_{exo} and δ_{FES}). In fact, the exoskeleton should generate two parts of desired torque, compensating its own dynamics (τ_{exo}^{d1}), and contributing to knee joint movement (τ_{exo}^{d2}). In our system, the total torque output of exoskeleton is realized via SEA (τ_{SEA}^d), which is the summation of τ_{exo}^{d1} and τ_{exo}^{d2}. In practice, the actual output of SEA minus the actual torque for exoskeleton dynamics (τ_{exo}^{a1}) is the actual assistive torque for knee joint from exoskeleton (τ_{exo}^{a2}), which is measured by the interactive force sensors and indicated by τ_{mut}. Therefore, τ_{mut} is the same as τ_{exo}^{a2}.

The overall control architecture is mainly composed of four parts: (1) the reference trajectory generator based on the CPG model, (2) the feedfoward controller for modulating pulse width of FES, (3) the feedback controller of the knee exoskeleton used to compensate the insufficient part of torque generated by FES, and (4) the parameter regulator with online adaptive updating rules for key parameters.

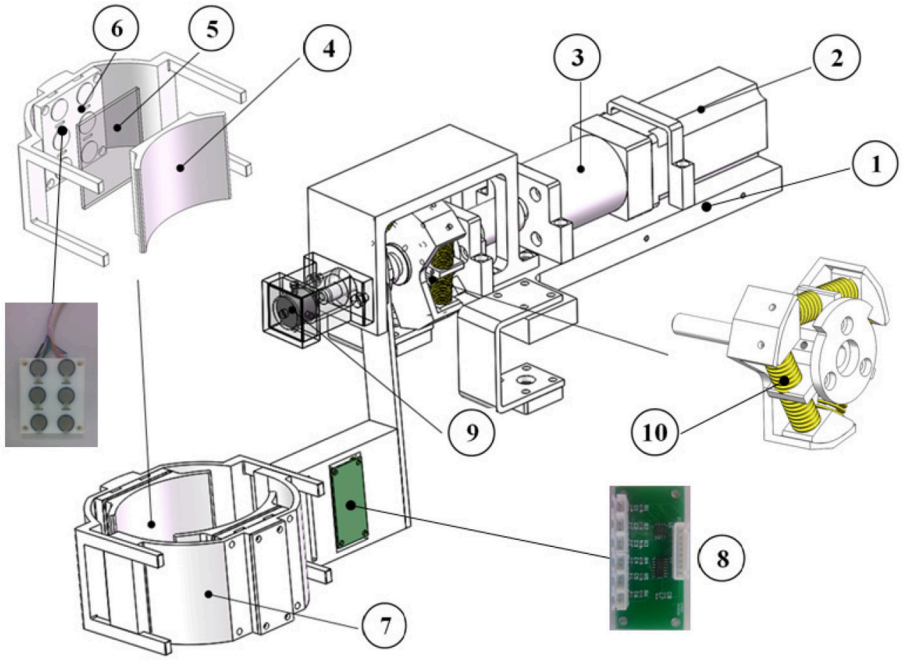

FIGURE 1 | Structure of exoskeleton in FEXO Knee: (1) base bench, (2) electric motor (AC servo motor), (3) reducer, (4) shank wrap, (5) silicone board, (6) interactive force sensors, (7) outer shell, (8) signal amplification circuit, (9) encoder, (10) linear springs.

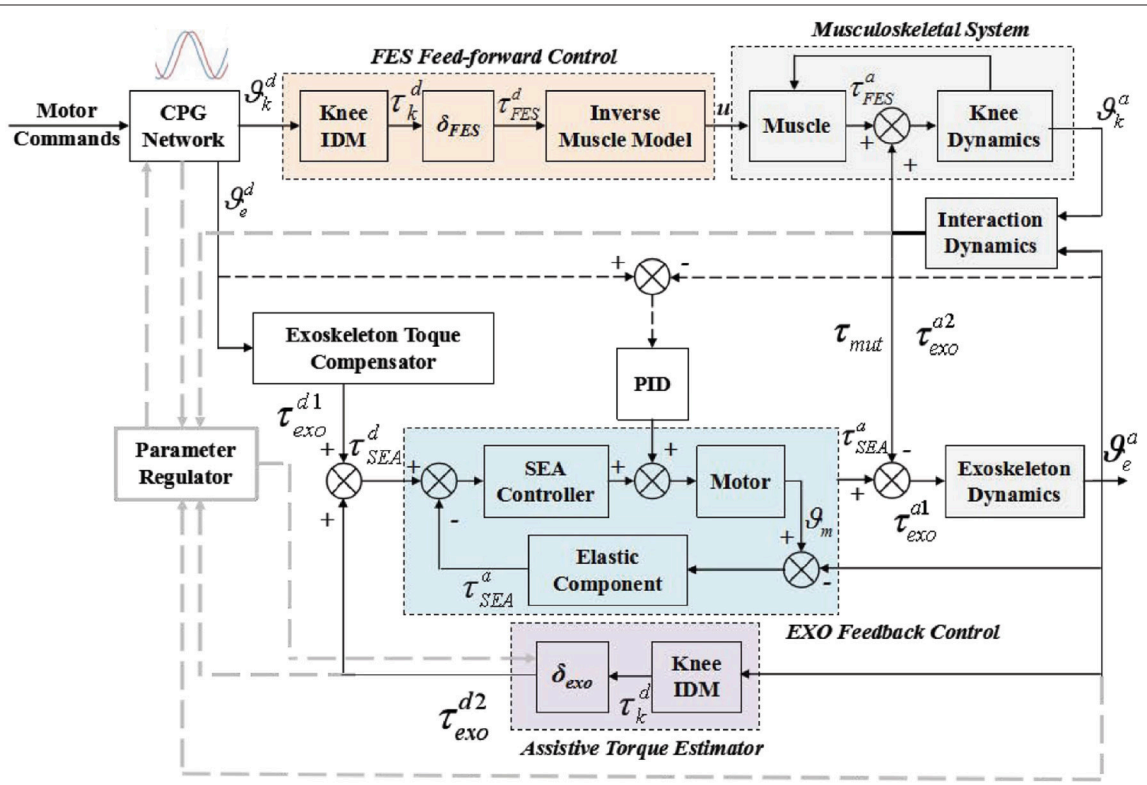

FIGURE 2 | Block diagram of cooperative control scheme for FES and exoskeleton in a hybrid rehabilitation system (FEXO Knee). The controlled plant includes knee musculoskeletal system and exoskeleton. The feedfoward control strategy is used for FES, and the feedback control strategy is for exoskeleton. CPG network and parameter regulator are in charge of synchronization of FES and exoskeleton.

2.2.1. CPG Network

According to previous research in neurophysiology, CPGs have been demonstrated to be a kind of neural control mechanism in central nervous system of animals, which can generate rhythmic locomotion independently. In addition, CPGs have some inherent advantages of entrainment, synchronization, robustness, which are desired features in the cooperative control of rhythmic movements. A variety of mathematical models have been developed to simulate the CPG function in a simplified form, which are widely used in robotic control, e.g., Matsuoka oscillators (Zhang and Hashimoto, 2012), Hopf oscillators (Righetti et al., 2006), and phase oscillators (Farzaneh and Akbarzadeh, 2012), etc. In this work, we use a phase oscillator, which was firstly adopted by Ijspeert et al. to control a salamander-like robot (Ijspeert et al., 2007). To make the model match our requirement, the original form of the phase oscillator is modified. Two mutually coupled nonlinear oscillators form the CPG network. The modified oscillator model is given by the following equations:

$$\dot{\phi}_i(t) = \omega_i(t) + \sum_j^2 \nu_{ij} \sin(\phi_j(t) - \frac{\omega_j}{\omega_i}\phi_i(t) - \Phi) \quad (2)$$

$$\ddot{\alpha}_i(t) = \mu_{\alpha i}[\frac{\mu_{\alpha i}}{4}(A_i - \alpha_i(t)) - \dot{\alpha}_i(t)] \quad (3)$$

$$\ddot{\omega}_i(t) = \mu_{\omega i}[\frac{\mu_{\omega i}}{4}(\Omega_i - \omega_i(t)) - \dot{\omega}_i(t)] \quad (4)$$

where ϕ_i, α_i, and ω_i are state variables, and denote the phase, amplitude and frequency of a nonlinear oscillator respectively; Φ is a variable that denotes the desired phase difference between two oscillators; A_i and Ω_i denote the desired amplitude and frequency of a oscillator respectively; $\mu_{\alpha i}$ and $\mu_{\omega i}$ are some positive parameters that represent the velocity of a oscillator transformed into a new locomotion state; ν_{ij} is a positive parameter that denotes the coupling weight between two oscillators. For all these parameters, the subscribe $i = 1, 2$.

In general, CPG has three basic output features (phase, amplitude, and frequency), which can be freely set based on requirement. This model uses nonlinear differential equations to realize CPG, which can generate smooth and stable trajectories even during transitional periods between different patterns. The output of a single nonlinear oscillator in CPG can be represented by:

$$\vartheta_i(t) = \alpha_i(t)\sin(\phi_i(t)) \quad (5)$$

where ϕ_i is a state variable and denotes the phase of the ith oscillator, ϑ_i denotes the output trajectory of the ith oscillator. Here, the two outputs ϑ_1 and ϑ_2 serve as the desired trajectories for knee joint (ϑ_k^d) and exoskeleton (ϑ_e^d).

Besides, the velocity and acceleration of the output trajectory can be conveniently obtained as follows:

$$\frac{d^k\vartheta_i}{dt^k}(t) = \alpha_i\omega_i^k \sin(\phi_i + \frac{\pi}{2}k). \quad (6)$$

Therefore, the desired angle, angular velocity and acceleration for knee joint ($\vartheta_k^d, \dot{\vartheta}_k^d, \ddot{\vartheta}_k^d$) and the exoskeleton ($\vartheta_e^d, \dot{\vartheta}_e^d, \ddot{\vartheta}_e^d$) can be generated by the two coupled oscillators.

The reference joint angle, angular velocity and acceleration generated by CPG can be used to estimate the desired torque. Besides, the phase difference between reference trajectories of FES and the exoskeleton (Φ) is one of the most important parameters in the control scheme, which can be online regulated to avoid possible confliction between human shank and knee exoskeleton. The desired motion commands (A_i, Ω_i, etc.) for different motor patterns are adjusted manually based on experimental protocol.

2.2.2. Feedfoward Control for FES

The feedfoward controller for FES contains three parts: (1) an inverse dynamics module, in which the inputs are the joint angle, angular velocity and acceleration provided by the CPG network, and the output is desired actuation torque of human knee joint; (2) a torque distribution gain δ_{FES}, which represents the percentage of torque that FES should provide; (3) an inverse muscle model, which is used to obtain the modulated stimulation pulse width as the output of FES.

An inverse dynamics model (IDM) of the knee joint movement (shank swing) is developed, which is used to calculate the desired torque in the feedfoward controller:

$$\tau_k^d(t) = I_s\ddot{\vartheta}(t) + B_s\dot{\vartheta}(t) + K_s\vartheta(t) + mgl_s\sin\vartheta(t) \quad (7)$$

where I_s[Nms^2/rad], m[kg] and l_s[m] are the segment (shank and foot) inertia, mass and equivalent length, respectively; B_s[Nms/rad] and K_s[Nm/rad] are the knee viscous damping and stiffness coefficients; $\vartheta(t)$[rad], $\dot{\vartheta}(t)$[rad/s] and $\ddot{\vartheta}(t)$[rad/s^2] denote the knee angle, angular velocity and acceleration, using the desired trajectory and its first and second derivatives (i.e., $\vartheta_k^d, \dot{\vartheta}_k^d, \ddot{\vartheta}_k^d$); $g = 9.81$ m/s^2 is the gravity constant; $\tau_k^d(t)$[Nm] denotes the total desired torque needed for knee joint.

The desired torque that should be generated by human muscles under electrical stimulation is a fraction of the estimated total torque obtained by IDM, i.e., $\tau_{FES}^d = \delta_{FES} \cdot \tau_k^d$, and the fraction is determined by the FES distribution gain δ_{FES}. An inverse muscle model based on Hill-type musculotendon actuator is used to acquire the pulse width of FES. The Hill-type model illustrates the activation and contraction dynamics of human muscles. A model-based control method is adopted, which used a piecewise linear recruitment function to describe the muscular activation dynamics, a Gaussian function to describe the torque-angle relation, and a linear function to approximate the torque-angular velocity relation (Ferrarin et al., 2001). The inverse muscle model can be given by:

$$a(t) = \tau_{FES}^d(t) \cdot \exp\left\{\left(\frac{\vartheta(t) + \pi/2 - \lambda_1}{\lambda_2}\right)^2\right\} \cdot (1 - \lambda_3\dot{\vartheta}(t))^{-1} \quad (8)$$

$$u(t) = \frac{a(t)(u_{sat} - u_{thres})}{u_{sf}} + u_{thres} \quad (9)$$

where $a(t)$[Nm] denotes the muscle activation; λ_1[rad], λ_2[rad] and λ_3[rad^{-1}s] are muscle and joint specific parameters used in the contraction dynamics; $u(t)$[μs] is the stimulation pulse width;

$u_{sat}[\mu s]$, $u_{thres}[\mu]$ and $u_{sf}[\mu]$ denote, respectively, the threshold, the saturation, and the scaling factor. These parameters are individual variables, which can be acquired through experimental indentification.

2.2.3. Feedback Control for Exoskeleton

The exoskeleton should provide two parts of torque: one is to support its own motion, and the other is for human knee joint motion. The exoskeleton torque compensator is designed firstly, in which the knee exoskeleton is considered independently without regard to the interaction with human leg. The desired driven torque (τ_{exo}^{d1}) for the exoskeleton dynamics itself is estimated through an impedance model given by:

$$\tau_{exo}^{d1} = I_e \ddot{\vartheta}_e^d + B_e \dot{\vartheta}_e^d + K_e \vartheta_e^d \tag{10}$$

where I_e, B_e, and K_e denote the inertia, viscous damping and stiffness of the exoskeleton, which are obtained by system identification in experiment. ϑ_e^d is the desired trajectories of exoskeleton provided by CPG. The human leg would not bear any burden from the exoskeleton if τ_{exo}^{d1} is completely generated by electric motor in this case.

The desired assistive torque (τ_{exo}^{d2}) that should be provided by the exoskeleton depends on a distribution gain δ_{exo}, which is a fraction of total torque of knee joint, i.e., $\tau_{exo}^{d2} = \delta_{exo} \cdot \tau_k^d$. We design δ_{exo} and δ_{FES} as a pair of distribution gains. In theory, $\delta_{exo} + \delta_{FES} = 1$. However, it has some difference in practice, because δ_{FES} is a fixed parameter, while δ_{exo} is a flexible parameter that is updated online by parameter regulator. The total torque of knee joint is also calculated according to the knee IDM Equation (7), but it should be acquired in a real-time approximation for feedback control, which needs the information of actual angular position, velocity and acceleration. In fact, the raw angle data measured by an encoder always contain noise signals, which would make the estimation very rough if we directly use the derivatives of the joint angle. In our control system, a state estimation method based on adaptive phase oscillators proposed by Ronsse et al. is used to acquire the angular position, velocity and acceleration (Ronsse et al., 2011, 2013). Thus, a relatively smooth estimation of total torque can be obtained. The product of the estimated total torque and the gain δ_{exo} is the desired assistive torque τ_{exo}^{d2} that the exoskeleton should provide. In ideal condition, τ_{exo}^{d2} should be equal to mutual torque τ_{mut}. In sum, the desired torque of SEA (τ_{SEA}^d) contains two parts, one is for masking the dynamics of the exoskeleton and the other is for providing necessary assistive torque.

The SEA controller realizes the torque control by a proportional-derivative (PD) method, and the control parameters k_{SEA}^p and k_{SEA}^d are tuned at 0.1 and 0.001 by trial and error. The mutual torque between human leg and the exoskeleton (τ_{mut}) is measured in real time, which represents the actual assistive torque for human leg or the resistant torque for the exoskeleton. Therefore, the actual output torque of SEA (τ_{SEA}^a) minus the mutual torque (τ_{mut}) is the actual exoskeleton torque (τ_{exo}^{a1}), which drives the exoskeleton itself.

Besides, a classical proportional-integral-derivative (PID) controller is implemented as a position controller to reduce the trajectory tracking error, and make the motion of exoskeleton smooth and accurate. The error signal is the difference between the reference trajectory and the actual angle of exoskeleton. The control parameters k_p, k_i, and k_d are tuned at 6.0, 0.12, and 0.01 by trial and error in the experiment. Even though the closed-loop PID is for angular position control, the absolute accuracy of trajectory tracking is not the most important issue in the control paradigm. Actually, the combination of SEA torque control and PID position control allows compliant interaction between the knee exoskeleton and the human leg, as well as appropriate trajectory tracking of knee joint.

2.2.4. Parameter Regulator

Parameter regulator is the key part in the cooperative control scheme, which aims to update two key parameters, Φ (cf. Equation 2) and δ_{exo}. Parameter regulator has three pairs of inputs (desired and actual angle, desired and actual angular velocity, desired and actual mutual torque), and two outputs (Φ and δ_{exo}). The two outputs are the online adaptive parameters. Please note angular velocity is not measured directly from sensors, and it is achieved by derivative operation of angle. Therefore, only two pairs of inputs are shown in the parameter regulator in **Figure 2**. Φ is for CPG, which can provide synchronization for FES and exoskeleton. δ_{exo} is for exoskeleton controller, which can make exoskeleton adaptively compensate the inadequate torque from FES (e.g., muscle fatigue).

Due to variations of different individuals in different situations, an online regulating strategy based on policy gradient methods is used to adjust these parameters (Kaelbling et al., 1996; Peters and Schaal, 2006). FEXO Knee mainly focuses on rhythmic locomotion, thus every period can be considered as a task trial. A fitness function is introduced to assess the motion performance:

$$J = \int_{t_0}^{t_f} (0.125e_\tau^2 + 1.2e_p^2 + 0.556e_v^2)dt \tag{11}$$

where t_0 and t_f represent the beginning and end of a trial; e_p, e_v and e_τ denote the position error of knee joint ($\vartheta_k^d - \vartheta_k^a$), the angular velocity error ($\dot{\vartheta}_k^d - \dot{\vartheta}_k^a$), and the assistive torque error ($\tau_{exo}^{d2} - \tau_{exo}^{a2}$), respectively. Actually, the mutual toque (τ_{mut}) is equal to τ_{exo}^{a2}. The updating rule of relevant parameters can be given by:

$$\delta_{exo,h+1} = \delta_{exo,h} - \gamma_\delta \nabla_{\delta_{exo}} J|_{\delta_{exo}=\delta_{exo,h}} \tag{12}$$

$$\Phi_{h+1} = \Phi_h - \gamma_\Phi \nabla_\Phi J|_{\Phi=\Phi_h} \tag{13}$$

where γ_δ and γ_Φ denote learning rates and $h \in \{0, 1, 2, \ldots\}$ is the updating number. The updating time window is three cycle periods (trial durations) for the two parameters, Φ and δ_{exo}, because of the partial derivatives in the discrete gradient descent method.

3. EXPERIMENTS AND RESULTS

Experiments were conducted on nine subjects for evaluating the performance of FEXO Knee with the cooperative control method proposed. The experiments were approved by the Ethics Committee of Shanghai Jiao Tong University, China. All subjects

were volunteers and signed the informed consent before the experiments.

3.1. Subjects

Five healthy subjects (H1∼H5) and four patients (P1∼P4) participated in the experiments. The basic information of the nine subjects is shown in **Table 1**. All the five healthy subjects had no history of neurological or muscular disease. All the four patients were hemiplegic. P1∼P3 had paralysis on right side, and P4 had paralysis on left side. The disease time of the four patients was all less than 10 months. The experiments on the hemiplegic patients were conducted in Shanghai Huashan People's Hospital.

Some parameters in IDM for each subject were estimated according to the anthropometric calculation method in Winter (2009). The mass of the segment (shank and foot) was estimated as 6.1% of the total body weight, the length as 28.5% of the total body height, the center of mass as 60.6% of the segment length, and the radius of gyration as 73.5% of the segment length. The inertia is calculated as the product between the segment mass and the square of the segment radius of gyration, i.e., $I = m(0.735l)^2$[Nms^2/rad]. Other parameters in IDM were estimated according to the empirical method in Ferrarin et al. (2001). This is a rough model of the actual knee dynamics, so the variations in stiffness K and the damping coefficient B during knee flexion and extension movement were not considered. The movement range of knee joint angle is $-35^\circ \sim +35^\circ$. The stiffness and damping coefficients were calculated by the equations: $K = \omega^2 I - mgl/2$[Nm/rad], $B = 2\eta\omega I$[Nms/rad] (Lin and Rymer, 1991). In experiments, η and ω of IDM were respectively tuned at 0.5 and 6 Hz for all subjects for simplicity, resulting an under-damped knee motion.

3.2. Experimental Setup and Protocol

Before the evaluation experiments, some parameters about the control system of FEXO Knee should be preset, which were grouped for CPG network, FES feedfoward controller, exoskeleton feedback controller, and parameter regulator.

The parameters of CPG network were determined by user requirement and literature (Ijspeert et al., 2007). The parameters for exoskeleton feedback controller were determined by simple system identification in experiments. The parameters for FES feedfoward controller were determined by experimental methods in the reference (Ferrarin et al., 2001), and some pilot tests on subjects. The parameters of regulator were determined by trial-and-error test and literature (Peters and Schaal, 2006). The general parameters for all the subjects are shown in **Table 2**. The subject-dependent parameters are shown in **Table 3**. Regarding parameter setting of FES, the pulse frequency was set at 50 Hz for all the subjects, the pulse amplitude I_a [mA] was a subject-dependent parameter, and the pulse width was the only controlled variable.

During experiment, the subject sat on a chair and wore FEXO Knee on the leg, two-channel FES surface electrodes were placed over the anterior and posterior thigh, targeting two muscle groups (quadriceps and hamstrings), as shown in **Figure 3**. The subject was told not to perform any voluntary movements during the experimental procedure.

The evaluation experiments were designed to assess the cooperative control performance of FEXO Knee under different FES levels. The purpose is to check if exoskeleton can provide the proper assistive torque for knee joint if FES makes different contribution. The experimental protocol is shown in **Figure 4**. In the experiments, each subject accomplished three sessions according to the FES level based on distribution gain (δ_{FES}). The distribution gain was arbitrarily chosen as $\delta_{FES} = 0.3, 0.5, 0.7$, meaning that the torque provided by FES accounted for 30, 50, and 70% of the total joint torque. In each session, the reference trajectories generated by the CPG module provided three kinds of motion patterns: Pattern 1–movement frequency 0.3 Hz and maximum angular amplitude $\pm 25^\circ$; Pattern 2–movement frequency 0.3 Hz and maximum angular amplitude $\pm 30^\circ$; Pattern 3–movement frequency 0.5 Hz and maximum angular amplitude

TABLE 1 | Information of subjects.

Subj.	Gender	Age	Height [cm]	Mass [kg]	Physical condition
H1	Male	24	168	61	Healthy
H2	Male	25	165	55	Healthy
H3	Male	24	170	65	Healthy
H4	Male	25	168	59	Healthy
H5	Male	25	170	73	Healthy
P1	Female	35	160	63	Brain Injury
P2	Male	61	160	70	Stroke
P3	Male	66	170	75	Stroke
P4	Male	64	156	58	Stroke

TABLE 2 | Common control parameters.

Parameter	Value	Parameter	Value	Parameter	Value
ν_{12}	2.0	$\mu_{\alpha 1,2}$	5.0	$\mu_{\omega 1,2}$	5.0
γ_δ	10^{-5}	γ_Φ	10^{-5}	μ_{sf} [μs]	15
λ_1[rad]	0.87	λ_2[rad]	1.13	λ_3[rad^{-1}s]	0.04
I_e[kgm^2]	0.04	B_e[Nms/rad]	2.0	K_e[Nm/rad]	3.50

TABLE 3 | Subject-specific stimulation parameters.

Subj.	μ_{sat}^{HAM} [μs]	μ_{sat}^{QUA} [μs]	μ_{thres}^{HAM} [μs]	μ_{thres}^{QUA} [μs]	I_a [mA]
H1	400	350	50	50	25
H2	400	370	50	50	30
H3	450	380	50	50	30
H4	380	370	50	50	25
H5	400	400	50	50	25
P1	260	260	100	100	30
P2	400	400	100	100	35
P3	420	420	100	100	40
P4	420	420	100	100	40

HAM, hamstrings; QUA, quadriceps.

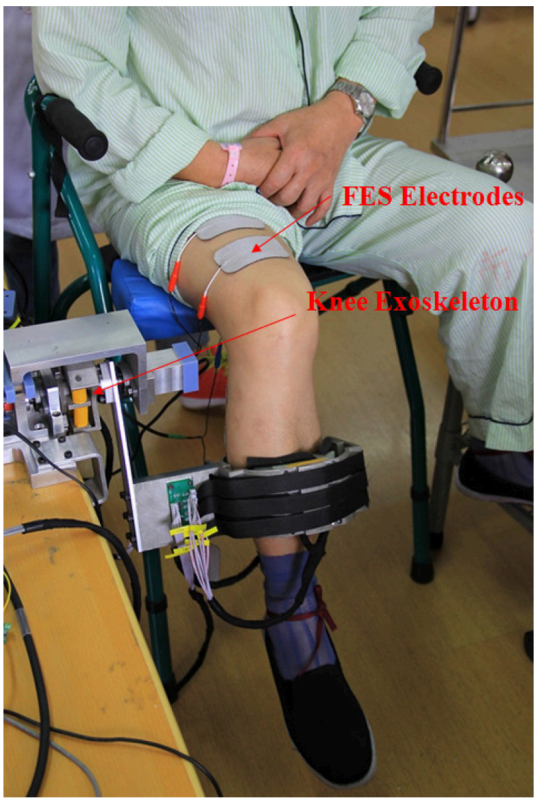

FIGURE 3 | Experimental setup of hybrid FES-exoskeleton rehabilitation system (FEXO Knee). A paralyzed patient (P3) wearing FEXO Knee was taking experiment, where outer shell of exoskeleton held the shank, and FES electrodes were attached to skin over targeted muscles (quadriceps and hamstrings).

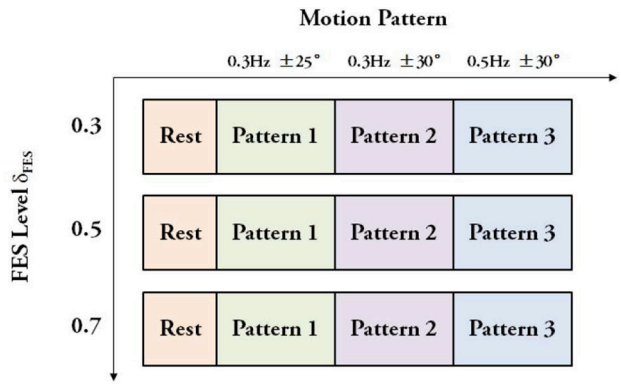

FIGURE 4 | Experimental protocol. Three sessions with different FES levels were conducted, and each session had three motion patterns.

±30°. There were breaks between the sessions for the subjects to rest. For healthy subjects, each motion pattern continued for 120 s. Considering the lower endurance of paralyzed patients, their experimental duration was a little shorter. The whole procedure of the experiments was carried out by the control software of FEXO Knee. During the steady state of evaluation experiments, no subjects reported confliction or disturbance between leg and exoskeleton using the FEXO Knee system.

3.3. Data Processing and Results

First of all, to obtain an intuitive view of the testing performance on FEXO Knee, arbitrarily the joint trajectories of the patient P2 during overall experimental procedure were presented in **Figure 5**. The good tracking performance between desired trajectory and actual knee joint angle is clearly observed. Especially, the trajectory is smooth and stable even during the transition periods between different motion patterns, which should be attributed to the merits of CPG.

To watch the performance including trajectories, torques, and controlled variables of FES in detail, the related real-time data of the healthy subject H3 under motion pattern 1 with the FES distribution gain at 0.3 were arbitrarily selected to show in **Figure 6**. We can see that the tracking performance is satisfactory, and the assistive effect of the knee exoskeleton (mutual torque) matches the desired values well. It demonstrates the efficiency of FEXO Knee, which can distribute the torque upon any requirements and keep FES-induced muscles and the exoskeleton work in a synchronized manner.

In our experimental paradigm, the interactive force sensors did not catch obvious muscle force decline due to muscle fatigue because of the simple swing motion without much effort and the short time for muscle stimulation. To imitate the muscle fatigue condition, we added an experiment to check the system performance in condition of muscle force decline. The real-time data on the healthy subject H2 are shown in **Figure 7**. When the muscle stimulation intensity was lowered in pre-setting program, the torque distribution gain (δ_{exo}) of the exoskeleton automatically increased. It means the exoskeleton adaptively compensated the torque needed, i.e., the measured mutual torque also increased accordingly. The self-adaption of the system is mainly due to the function of the parameter regulator. The error between desired assistive torque and actual mutual torque updated the exoskeleton gain (δ_{exo}) as shown in Equation (12). Please note that the updating time window for δ_{exo} is three cycle periods.

Five measures were proposed and analyzed, which could comprehensively evaluate the control performance of our system: (1) the absolute maximum amplitude of joint angle, (2) the duration of a single trial (i.e., a cycle period of knee joint movement), (3) the absolute maximum mutual torque between shank and exoskeleton, (4) the averaged error between reference trajectory of the exoskeleton and actual knee angle; (5) the averaged error between the desired assistive torque and measured mutual torque. The measures (1) and (4) indicates the position control performance. The measure (2) indicates the speed control performance. The measures (3) and (5) indicate the torque control performance. According to the experimental paradigm, there were totally nine conditions with different stimulation levels and motion patterns. The data during steady trials were extracted for evaluation and analysis, i.e., the trials 6∼35 were segmented for the healthy subjects and the trials 6∼25 for the patients. Each trial started from the zero position of knee joint.

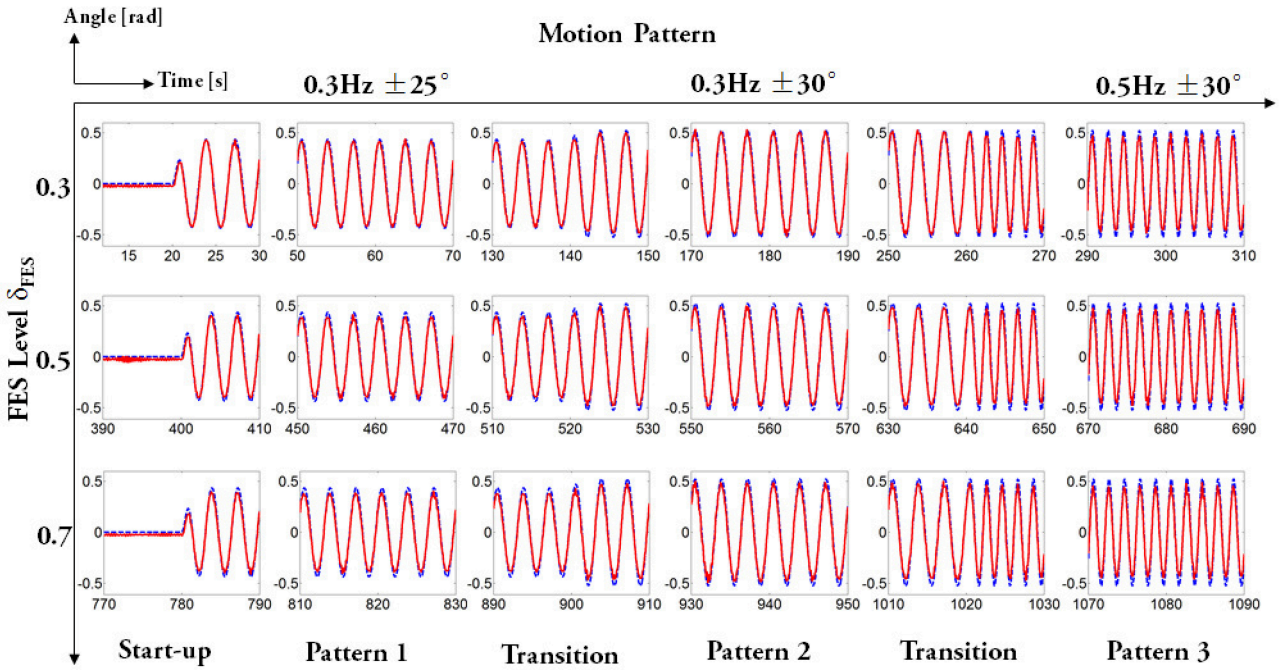

FIGURE 5 | Trajectory tracking of P2 during the overall experimental procedure. For each subfigure, the x axis is time and the y axis is joint angle. The whole evaluation experiment contained three sessions determined by FES levels, and for each session, subjects underwent a continuous procedure including three kinds of motion patterns. The dashed lines represent desired trajectories and solid lines represent actual joint angle.

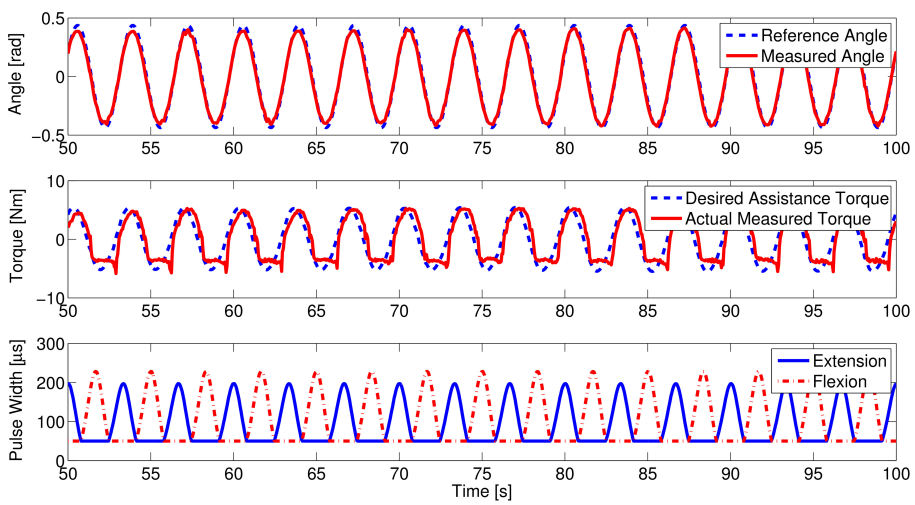

FIGURE 6 | Real-time data of the healthy subject H3. The upper figure shows the trajectory tracking curves, the middle figure shows the assistive performance of the knee exoskeleton, and the lower figure shows modulated pulse width of two FES channels targeting quadriceps for extension and hamstrings for flexion.

The data processing and statistical analysis were conducted in MATLAB (MathWorks, Natick, MA).

The experimental results regarding five measures (maximum angle, trial duration, angle error, torque error, and maximum mutual torque) are shown in the figures (**Figures 9**, **10**). The grand-averaged results of five healthy subjects and four patients are given separately. For every sub-figure, the lateral axis denotes the trial number (30 trials for healthy subjects, and 20 trials for hemiplegic subjects), and the solid lines represent the mean values across subjects and the shadow regions represent the standard errors of the mean values (±s.e.m) among subjects.

The statistical analysis was conducted to evaluate the general performance over the five healthy subjects and hemiplegic patients, respectively. The raw data were divided into trials, and each trial was equal to a complete cycle of knee extension and

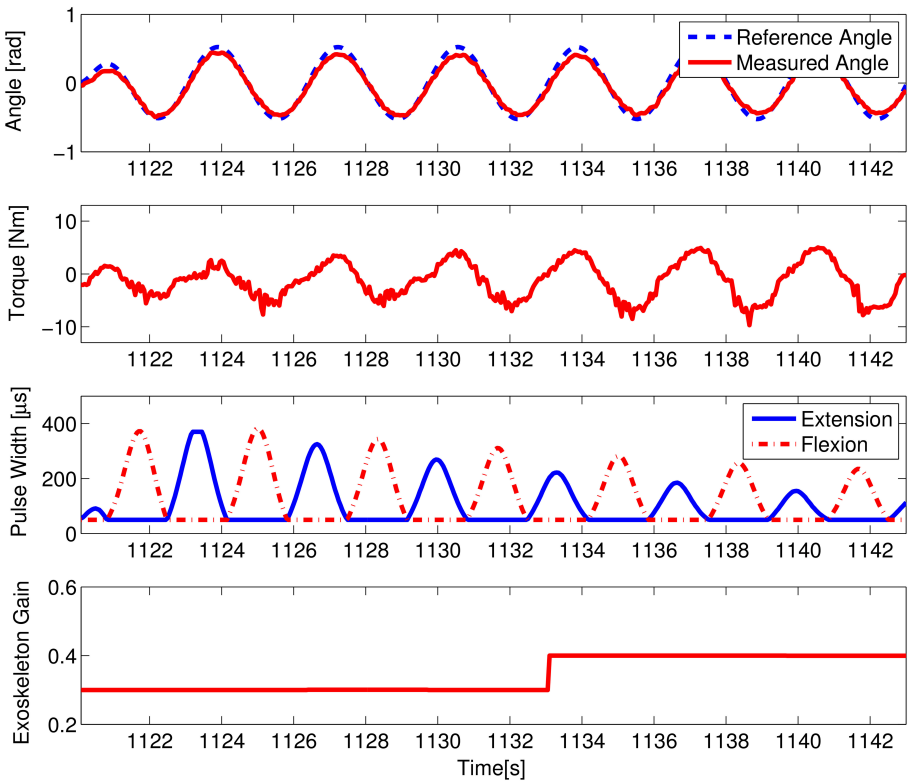

FIGURE 7 | System performance in case of muscle force decline on the healthy subject H2. The first figure shows the trajectory tracking curves, the second figure shows the measured maximum mutual torque, the third shows the modulated pulse width of the two FES channels, and the fourth shows the variations of the exoskeleton torque distribution gain.

flexion (30 trials for healthy subjects, and 20 trials for hemiplegic subjects).

Based on the experimental protocol as shown in **Figure 4**, there are two factors (motion pattern and FES level). A two-way ANOVA including two factors (motion pattern and FES level) was applied firstly, and the results showed no significant interaction between the two factors ($p = 0.96 > 0.1$ for healthy subjects and $p = 0.99 > 0.1$ for paralyzed patients). As we focused on the factor of FES level, a one-way ANOVA was used to evaluate the performance further. Maximum angle, trial duration, and maximum mutual torque are key measures, which can show the steady and adaptation performance of the system under different FES levels (δ_{FES}). In a single motion pattern, we checked the difference of the three measures among three FES levels.

Regarding statistical analysis on trial duration (see **Figure 8**), the FES level depending on torque distribution ratio is the unique factor. The ANOVA results do not show significant difference for the healthy subjects in different FES levels [motion pattern 1: $F_{(2,\,87)} = 0.05$, $p > 0.1$; motion pattern 2: $F_{(2,\,87)} = 0.22$, $p > 0.1$; motion pattern 3: $F_{(2,\,87)} = 0.04$, $p > 0.1$], as well as the patients [motion pattern 1: $F_{(2,\,57)} = 0.01$, $p > 0.1$; motion pattern 2: $F_{(2,\,57)} = 0.02$, $p > 0.1$; motion pattern 3: $F_{(2,\,57)} = 0.39$, $p > 0.1$]. It reveals that the variations of FES levels do not influence the trial duration of FEXO Knee in the same motion pattern. In other words, the swing frequency (motion speed) is steady, which is the desired merit for hybrid rehabilitation systems. Similarly, the ANOVA results show that variations of different FES levels do not have significant impact on actual maximum joint angle (see **Figure 9**). These results reflect that FEXO Knee can provide stable assistance for users. Even if FES is changing, the exoskeleton part can compensate the change in time, and achieve the desired motion features smoothly. However, in the same motion pattern, the maximum joint angle of paralyzed patients cannot keep a stale value in three FES levels, and there is a slight decrease as FES level increases (cf. **Figure 9**), which may be caused by the pathological conditions of muscles in the patients (weakness, atrophy, and rigid, etc.). When the FES level gets higher, the actual torque generated by patients' muscles is lower than expected, and the rigid knee joint prevents the exoskeleton from providing enough compensative torque, therefore, maximum joint angle cannot be fully reached. The actual torque generated by patients was smaller than healthy subjects, due to the weaker muscle activation of patients and the fact that the regulation of FES output depends on an open-loop control method. Nevertheless, even though some rough models (IDM, inverse muscular model, etc.) are used in the control scheme, the motion performance of FEXO Knee is satisfactory and no subjects have reported conflicted interaction between FES

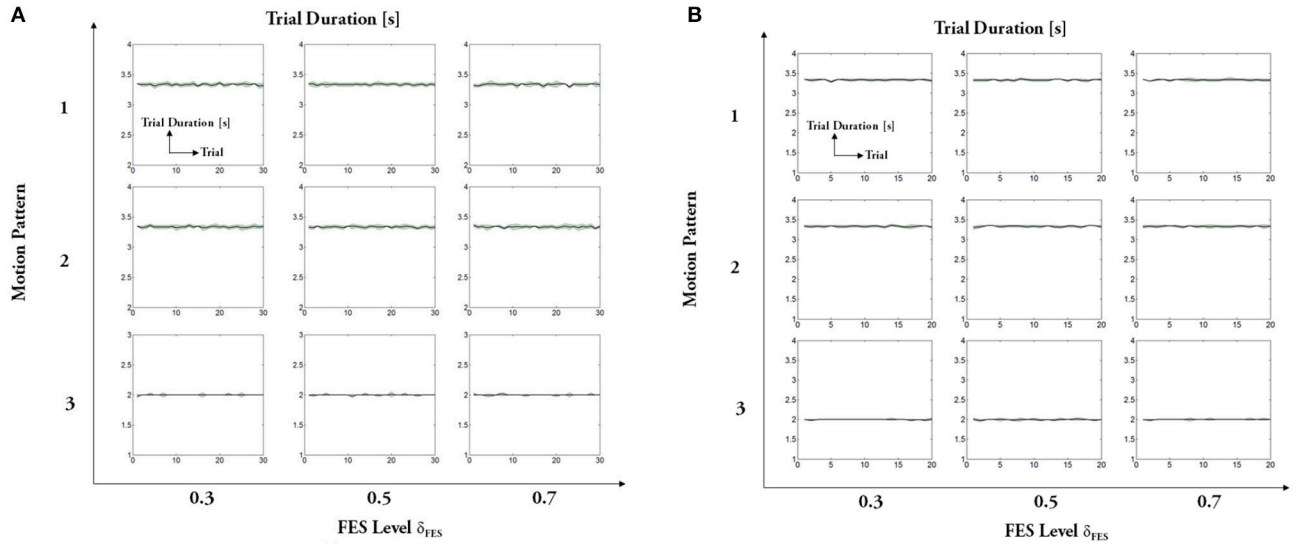

FIGURE 8 | Trial duration: **(A)** healthy subjects, **(B)** hemiplegic patients. For each subfigure, x-axis indicates the trial number and y-axis indicates the trial duration.

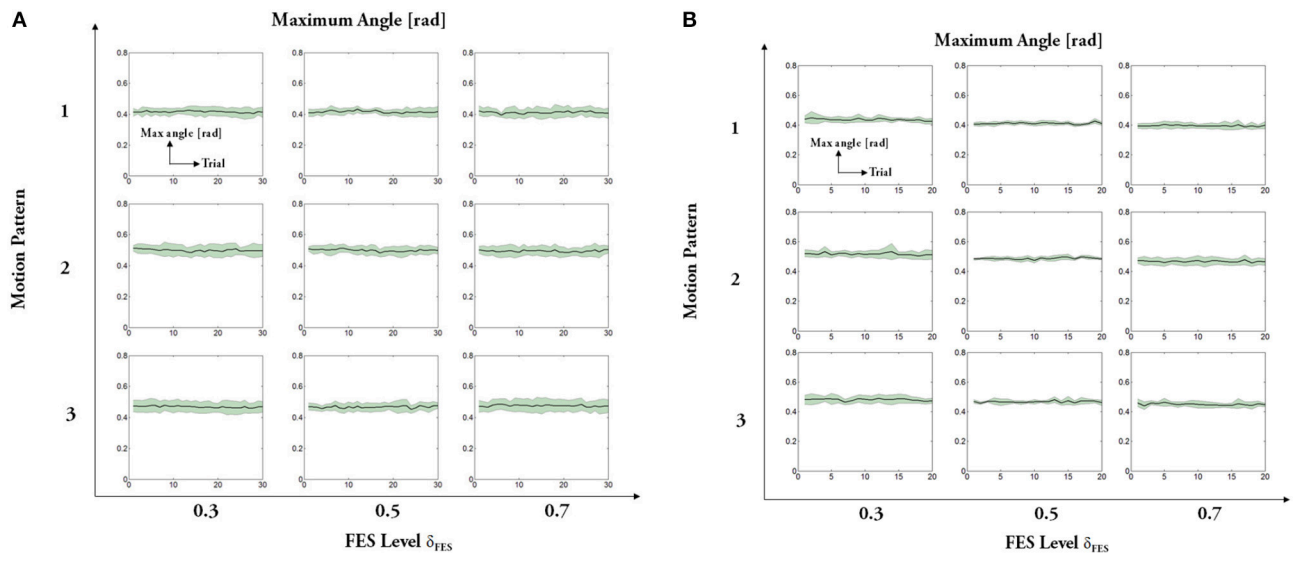

FIGURE 9 | Maximum amplitude of joint angle: **(A)** healthy subjects, **(B)** hemiplegic patients. For each subfigure, x-axis indicates the trial number and y-axis indicates the absolute maximum angle. Solid lines represent the mean values across all subjects and shadow regions represent the standard error of the mean (±s.e.m.), similarly hereinafter.

and the exoskeleton, which demonstrates the efficiency of the cooperative control strategy.

Regarding the absolute maximum mutual torque (see **Figure 10**), we can see that the assistive torque provided by the exoskeleton (measured mutual torque) declines as human muscles under FES generates larger force. The ANOVA results of the maximum mutual torque among different motion patterns are significant for healthy subjects [motion pattern 1: $F_{(2,\ 87)} = 31{,}696$, $p<0.01$; motion pattern 2: $F_{(2,\ 87)} = 30{,}417.54$, $p < 0.01$; motion pattern 3: $F_{(2,\ 87)} = 58{,}308.27$, $p < 0.01$], as well as the patients [motion pattern 1: $F_{(2,\ 87)} = 78{,}032.9$, $p < 0.01$; motion pattern 2: $F_{(2,\ 87)} = 131{,}176.09$, $p < 0.01$; motion pattern 3: $F_{(2,\ 87)} = 131{,}562.45$, $p < 0.01$]. The results reveal that the primary goal of FEXO Knee that aims to regulate the torque distribution between FES and the exoskeleton is accomplished to some extent.

Figures 11, **12** present results of other two measures: angle error (errors between the desired joint angle and the measured joint angle) and torque error (errors between the desired assistive torque and the measured mutual torque). The results reveal that the angle errors are kept in a relatively small range. From the results, we can also see that the averaged torque errors are limited

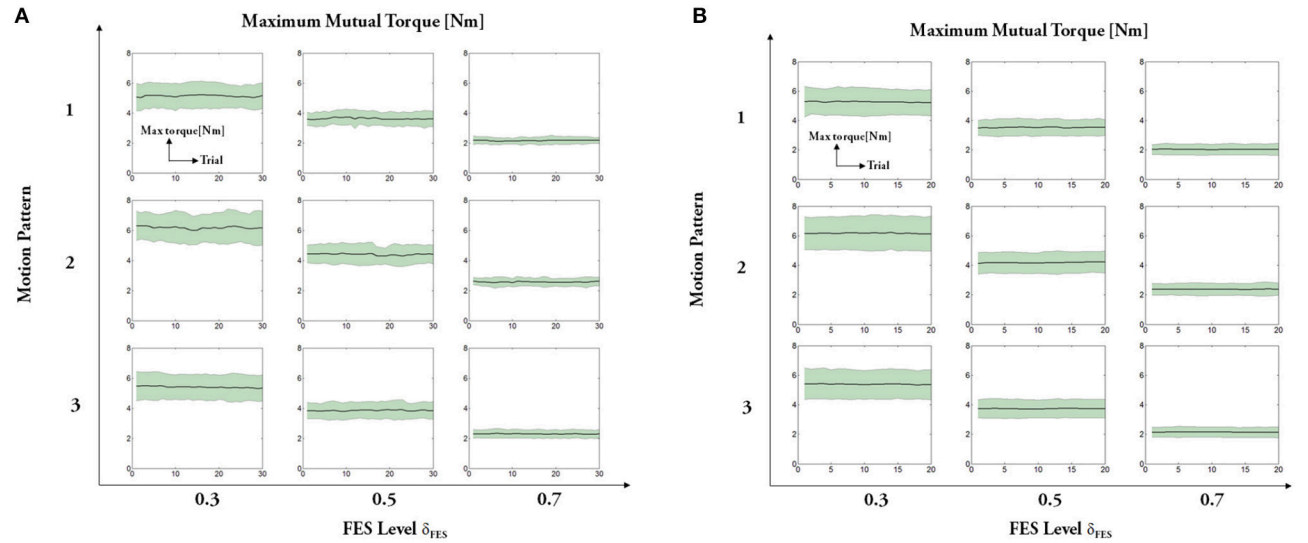

FIGURE 10 | Absolute maximum mutual torque: **(A)** healthy subjects, **(B)** hemiplegic patients. For each subfigure, x-axis indicates the trial number and y-axis indicates the measured maximum mutual torque between shank and exoskeleton.

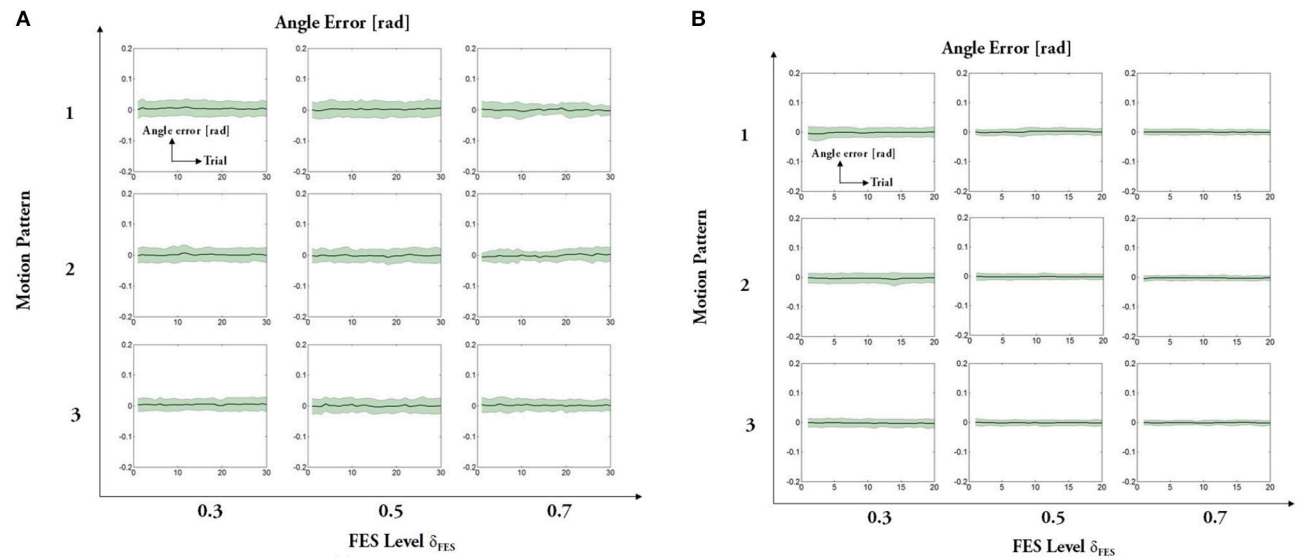

FIGURE 11 | Averaged error between the reference trajectory and the actual knee angle: **(A)** healthy subjects, **(B)** hemiplegic patients. For each subfigure, x-axis indicates the trial number and y-axis indicates the averaged angle error.

to ± 3 Nm, even if there are relatively large individual variations among the subjects. Given the fact the system does not seek the perfect torque tracking, the results are acceptable.

4. DISCUSSION

In this paper, a novel approach based on cooperative control was introduced for exploring hybrid FES-exoskeleton rehabilitation. A self-made hybrid rehabilitation device called FEXO Knee was developed as the experimental platform. The exoskeleton has a compliant mechanism driven by a rotatory elastic actuator, and this is a highlight of the system. Series elastic actuators (SEAs) possess some specific advantages compared with traditional rigid actuators, including tolerance to abrupt force shock, capacity of energy storage and release, and steady force control, etc. (Pratt and Williamson, 1995; Yu et al., 2015). Actually, the SEAs do not seek absolute accuracy of tracking position trajectory but compliant human-robot interaction, which is more important in human-machine system.

The muscle nonlinearity and the exoskeleton compliance would bring about phase confliction problems. Therefore, we

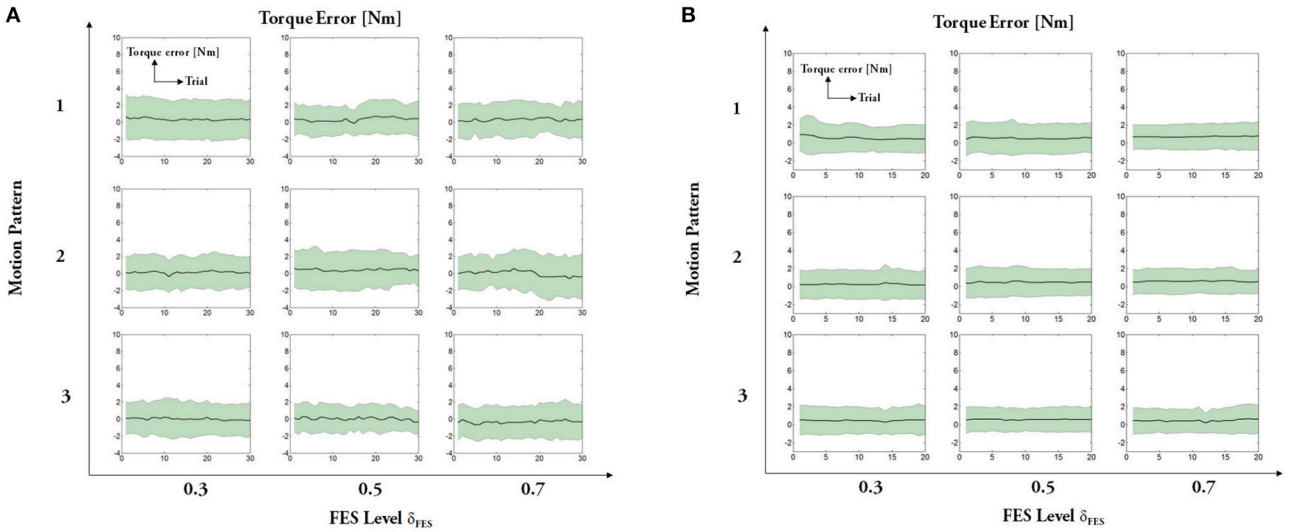

FIGURE 12 | Averaged error between the desired assistive torque and the measured mutual torque: **(A)** healthy subjects, **(B)** hemiplegic patients. For each subfigure, x-axis indicates the trial number and y-axis indicates the averaged torque error.

used a CPG network based on modified phase oscillators capable of online adjusting the phase difference to avoid possible out-of-phase trouble. CPGs possess some merits, which are especially favorable for the requirements of cooperative control in our hybrid system. Firstly, the CPG in this work has the capacity to generate stable oscillation, so as to keep robust under transient and slight disturbance. The state variables of the modified phase oscillator model can converge to the desired values while the convergent velocity is determined by some tunable values (cf. Equations 2–4). Secondly, the CPG has smooth transition capacity between different rhythmic oscillations after receiving commands from the higher level controller. As for the modified phase oscillators, the desired state values can be changed to form variable rhythmic patterns, and ensure the transition is continuous and smooth, which is essential to joint trajectory generation. Finally, the basic units (i.e., nonlinear oscillators) of the CPG has the capacity of establishing a network by coupling. The second term of Equation (2) reflects the coupling effect among phase oscillators. The coupling can be used to make different oscillators keep stable phase differences. Furthermore, the CPG as a network composed by these phase oscillators theoretically can generate any periodical trajectories. In the control scheme of FEXO Knee, the two nonlinear oscillators keep an adaptive phase difference with the help of a parameter regulator to avert possible conflictions between human leg and exoskeleton. Through the parameter regulator, sensory feedback is incorporated into CPG, thus a fully coupled dynamic system is accomplished in a big closed loop, and entrainment of CPG with plant output can make the whole system work in a synchronized way.

An advantage of the cooperative control is the arbitrary distribution of torque contribution between FES and exoskeleton. The tunable gains are set in feedfoward control of FES and feedback control of exoskeleton, respectively. Even though a lot of advanced control methods have been developed in controlling FES-actuated limbs to track reference trajectories accurately in previous research (Zhang et al., 2007), this work just adopted the feedfoward controller for FES to generate modulated pulse width based on an inverse muscular model. The control scheme of FEXO Knee does not aim to accomplish accurate position tracking merely by FES, but use a compliant actuator of exoskeleton to compensate the insufficient torque instead. The hybrid rehabilitation paradigm can overcome the deficiencies of FES and the exoskeleton, while achieving mutual promotion of these two technologies. Therefore, a simple but practical method is enough for FES controller.

Previous studies have introduced mechanical actuators to assist FES to achieve locomotion including swinging, walking and cycling, but the mutual interaction between skeletal muscles and mechanical actuators were rarely considered. Most hybrid rehabilitation systems intended to either reduce mechanical power consumption (Ha et al., 2012) or minimize the resistive torque caused by mechanical actuation (del Ama et al., 2014). It should be emphasized that the interactive force sensors are implemented in FEXO Knee. Based on the force sensors, the arbitrary torque distribution can be realized via the cooperative control. In our control strategy, the coordination between FES and the exoskeleton is ascribed to the torque distribution gain that denotes their actuating effort for limb locomotion, and the possible confliction is solved by adjusting the phase difference of their reference trajectories. It differs from the previous control methods in which muscular and mechanical actuation have separate control objectives. For example, Hunt et al. (2004) proposed an integrated control strategy containing two closed loops for hybrid FES cycling, which provided feedback control of leg power output (via automatic adjustment of stimulation intensity) and cycling cadence (via electric motor control), respectively. In fact, FEXO Knee aims to accomplish a general goal (desired angular position) while allotting the workload (assistive torque) between FES and exoskeleton in

arbitrary ratio, and this task is realized by the cooperative control.

Some evaluation experiments of FEXO Knee were conducted on both healthy subjects and hemiplegic patients. Different levels of FES were applied on the subjects, and the statistical analysis on the experimental data revealed that the cooperative control method could balance the effort of FES and the exoskeleton. Besides, the variations of stimulation strength did not influence the movement performance, i.e., the angular position and duration of each trial did not change, which verified the adaptability and robustness of the system. In clinical application, the cooperative control method used for dealing the torque distribution between FES and exoskeleton would be very helpful for patients.

The experimental results have shown the performance is satisfactory for both healthy subjects and paralyzed patients, and none reported significant confliction between leg and exoskeleton, which demonstrated the efficiency of the cooperative control strategy. FEXO Knee kept stable swing motion exhibited by the amplitude and period of joint motion, while the exoskeleton could adaptively compensate the insufficient part of necessary torque for shank swing, i.e., the mutual torque was changed accordingly (see **Figure 10**). The patients had pathological muscular conditions including weakness, atrophy, rigidness, and so on, so the actual torque generated by muscles of patients are lower than expected under FES. While the closed-loop control of exoskeleton could detect the torque error and position error, and thus automatically provided enough compensative torque to accomplish the desired motor pattern. In real FES clinical rehabilitation, paraplegic patients usually need to walk bearing their body weight for some time, so continuous and intensive electrical stimulation can cause significant muscle fatigue. In our experimental paradigm, the muscle fatigue phenomenon is not obvious because of the simple swing motion without much effort and short time for muscle stimulation. However, the proposed strategy is capable of dealing with muscle force decline like the situation of muscle fatigue. The parameter regulator can update the tunable gain (τ_{exo}) online, which works together with the closed-loop control mechanism of exoskeleton, is a trump card.

In future, some work should be conducted to improve the FEXO Knee system with cooperative control. The feedfoward controller for FES is based on a rough inverse model of human muscles under electrical stimulation, which still needs manual system identification. Some intelligent methods such as artificial neural networks may be used to accomplish automatic parameter identification facing individual variability, especially for paralyzed patients (Chang et al., 1997; Kurosawa et al., 2005). The FEXO Knee mainly focuses on rhythmic movements of knee joint, and we need extend its applications toward complex lower-limb movements such as walking. Therefore, a hybrid FES-exoskeleton system with multiple degrees of freedom is expected to be developed.

5. CONCLUSIONS

This paper presents a novel cooperative control scheme for better human-machine interaction and physical rehabilitation in a hybrid FES-exoskeleton system called FEXO Knee. Torque distribution between the two kinds of actuators (muscles under electrical stimulation and electrical motor with SEA) is regulated via tunable gains. A CPG network containing two modified phase oscillators generates reference motion of FES and the exoskeleton. Cooperative control adaptively adjusts the phase difference between the two oscillators to avoid unexpected conflictions between the two compliant mechanisms, allowing better interaction. The control method provides an effective solution for dealing with the coordination between FES and the exoskeleton in a hybrid system. The performance has been testified by some evaluation experiments on both healthy subjects and hemiplegic patients. We believe the FEXO Knee system for physical rehabilitation would be very promising for paraplegic patients to restore the extremity function.

AUTHOR CONTRIBUTIONS

DZ and WX conceived of the study and designed the experiments. YR, KG and DZ designed the system, conducted the experiment, and analyzed the data. JJ and WX performed the clinical test on the patients. DZ and YR drafted the manuscript.

FUNDING

This work was supported by the National Natural Science Foundation of China (No. 51475292), and the National High Technology Research and Development Program (863 Program) of China (2015AA020501).

ACKNOWLEDGMENTS

The authors would like to thank all the subjects in the evaluation experiments, and also thank the doctors and therapists for their active assistance in the clinical experiments on patients in Shanghai Huashan Hospital.

REFERENCES

Alibeji, N., Kirsch, N., Farrokhi, S., and Sharma, N. (2015). Further results on predictor-based control of neuromuscular electrical stimulation. *IEEE Trans. Neural Syst. Rehabil. Eng.* 23, 1095–1105. doi: 10.1109/TNSRE.2015.2418735

Alibeji, N., Kirsch, N., and Sharma, N. (2017). An adaptive low-dimensional control to compensate for actuator redundancy and fes-induced muscle fatigue in a hybrid neuroprosthesis. *Control Eng. Pract.* 59, 204–219. doi: 10.1016/j.conengprac.2016.07.015

Alibeji, N. A., Andrew, K. N., and Nitin, S. (2015). A muscle synergy-inspired adaptive control scheme for a hybrid walking neuroprosthesis. *Front. Bioeng. Biotechnol.* 3:203. doi: 10.3389/fbioe.2015.00203

Banala, S. K., Kim, S. H., Agrawal, S. K., and Scholz, J. P. (2009). Robot assisted gait training with active leg exoskeleton (ALEX). *IEEE Trans. Neural Syst. Rehabil. Eng.* 17, 2–8. doi: 10.1109/TNSRE.2008.2008280

Chang, G. C., Luh, J. J., Liao, G. D., Lai, J. S., Cheng, C. K., Kuo, B., et al. (1997). A neuro-control system for the knee joint position control with quadriceps stimulation. *IEEE Trans. Rehab. Eng.* 5, 2–11. doi: 10.1109/86.559344

Chen, Y. X., Hu, J., Peng, L., and Hou, Z. G. (2014). The FES-assisted control for a lower limb rehabilitation robot: simulation and experiment. *Rob. Biomimet.* 1:2. doi: 10.1186/s40638-014-0002-7

Colombo, G., Joerg, M., Schreier, R., and Dietz, V. (2000). Treadmill training of paraplegic patients using a robotic orthosis. *J. Rehabil. Res. Dev.* 37, 693–700.

del Ama, A. J., Gil-Agudo, A., Pons, J. L., and Moreno, J. C. (2014). Hybrid FES-robot cooperative control of ambulatory gait rehabilitation exoskeleton. *J. NeuroEng. Rehabil.* 11:27. doi: 10.1186/1743-0003-11-27

del Ama, A. J., Koutsou, A. D., Moreno, J. C., de-los Reyes, A., Gil-Agudo, and Pons, J. L. (2012). Review of hybrid exoskeletons to restore gait following spinal cord injury. *J. Rehabil. Res. Dev.* 49, 497–514. doi: 10.1682/JRRD.2011.03.0043

Dollar, A. M. and Herr, H. (2008). Lower extremity exoskeletons and active orthoses: challenges and state-of-the-art. *IEEE Trans. Rob.* 24, 144–158. doi: 10.1109/TRO.2008.915453

Fan, Y., and Yin, Y. (2013). Active and progressive exoskeleton rehabilitation using multisource information fusion from EMG and force-position EPP. *IEEE Trans. Biomed. Eng.* 60, 3314–3321. doi: 10.1109/TBME.2013.2267741

Farzaneh, Y., and Akbarzadeh, A. (2012). A bio-inspired approach for online trajectory generation of industrial robots. *Adapt. Behav.* 20, 191–208. doi: 10.1177/1059712312443842

Ferrarin, M., Palazzo, F., Riener, R., and Quintern, J. (2001). Model-based control of FES-induced single joint movements. *IEEE Trans. Neural Syst. Rehabil. Eng.* 9, 245–257. doi: 10.1109/7333.948452

Goldfarb, M., and Durfee, W. K. (1996). Design of a controlled-brake orthosis for FES-aided gait. *IEEE Trans. Rehabil. Eng.* 4, 13–24. doi: 10.1109/86.486053

Ha, K., Murray, S., and Goldfarb, M. (2016). An approach for the cooperative control of fes with a powered exoskeleton during level walking for persons with paraplegia. *IEEE Trans. Neural Syst. Rehabil. Eng.* 24:455. doi: 10.1109/TNSRE.2015.2421052

Ha, K. H., Quintero, H. A., Farris, R. J., and Goldfarb, M. (2012). "Enhancing stance phase propulsion during level walking by combining FES with a powered exoskeleton for persons with paraplegia," in *Proceedings Annual International Conference of the IEEE Engineering in Medicine and Biology Society (EMBC)* (San Diego, CA), 344–347.

Hunt, K. J., Stone, B., Negard, N. O., Schauer, T., Fraser, M. H., Cathcart, A. J., et al. (2004). Control strategies for integration of electric motor assist and functional electrical stimulation in paraplegic cycling: utility for exercise testing and mobile cycling. *IEEE Trans. Neural Syst. Rehabil. Eng.*12, 89–101. doi: 10.1109/TNSRE.2003.819955

Ijspeert, A. J. (2008). Central pattern generators for locomotion control in animals and robots: a review. *Neural Netw.* 21, 642–653. doi: 10.1016/j.neunet.2008.03.014

Ijspeert, A. J., Crespi, A., Ryczko, D., and Cabelguen, J.-M. (2007). From swimming to walking with a salamander robot driven by a spinal cord model. *Science* 315, 1416–1420. doi: 10.1126/science.1138353

Kaelbling, L. P., Littman, M. L., and Moore, A. W. (1996). Reinforcement learning: a survey. *J. Artif. Intell. Res.* 4, 237–285.

Kurosawa, K., Futami, R., Watanabe, T., and Hoshimiya, N. (2005). Joint angle control by FES using a feedback error learning controller. *IEEE Trans. Neural Syst. Rehabil. Eng.* 13, 359–371. doi: 10.1109/TNSRE.2005.847355

Lin, D. C., and Rymer, W. Z. (1991). A quantitative analysis of pendular motion of the lower leg in spastic human subjects. *IEEE Trans. Biomed. Eng.* 38, 906–918. doi: 10.1109/10.83611

Lynch, C. L., and Popovic, M. R. (2008). "Functional electrical stimulation: closed-loop control of induced muscle contractions," in *IEEE Control Systems Magazine,* Vol. 28, 40–50. doi: 10.1109/MCS.2007.914689

Peters, J., and Schaal, S. (2006). "Policy gradient methods for robotics," in *Proceedings IEEE/RSJ International Conference Robots and Systems (IROS)* (Beijing), 2219–2225.

Popovic, M. R., Keller, T., Pappas, I. P. I., Dietz, V., and Morari, M. (2001). Surface stimulation technology for grasping and walking neuroprostheses. *IEEE Eng. Med. Biol. Mag.* 20, 82–93. doi: 10.1109/51.897831

Pratt, G. A., and Williamson, M. M. (1995). "Series elastic actuator," in *Proceedings IEEE International Conference on Intelligent Robots and Systems (ICIRS)* (Pittsburgh, PA), 399–406.

Quintero, H. A., Farris, R. J., Ha, K. H., and Goldfarb, M. (2012). "Preliminary assessment of the efficacy of supplementing knee extension capability in a lower limb exoskeleton with FES," in *Proceedings Annual International Conference of the IEEE Engineering in Medicine and Biology Society (EMBC)* (San Diego, CA), 3360–3363.

Reinkensmeyer, D. J., Aoyagi, D., Emken, J. L., Galvez, J. A., Ichinose, W., Kerdanyan, G., et al. (2006). Tools for understanding and optimizing robotic gait training. *J. Rehabil. Res. Dev.* 43, 657–670. doi: 10.1682/JRRD.2005.04.0073

Ren, Y., and Zhang, D. G. (2014). "Fexo knee: a rehabilitation device for knee joint combining functional electrical stimulation with a compliant exoskeleton," in *Proceedings IEEE RAS and EMBS International Conference on Biomedical Robotics and Biomechatronics (BIOROB)* (São Paulo), 683–688.

Righetti, L., Buchli, J., and Ijspeert, A. J. (2006). Dynamic Hebbian learning in adaptive frequency oscillators. *Phys. D* 216, 269–281. doi: 10.1016/j.physd.2006.02.009

Ronsse, R., Rossi, S., Vitiello, N., Lenzi, T., Carrozza, M. C., and Ijspeert, A. J. (2013). Real-time estimate of velocity and acceleration of quasi-periodic signals using adaptive oscillators. *IEEE Trans. Rob.* 29, 783–791. doi: 10.1109/TRO.2013.2240173

Ronsse, R., Vitiello, N., Lenzi, T., Kieboom, J., Carrozza, M. C., and Ijspeert, A. J. (2011). Human-robot synchrony: flexible assistance using adaptive oscillators. *IEEE Trans Biomed Eng.* 58, 1001–1012. doi: 10.1109/TBME.2010.2089629

Sharma, N., Stegath, K., Gregory, C. M., and Dixon, W. E. (2009). Nonlinear neuromuscular electrical stimulation tracking control of a human limb. *IEEE Trans. Neural Syst. Rehabil. Eng.* 17, 576–584. doi: 10.1109/TNSRE.2009.2023294

Stauffer, Y., Allemand, Y., Bouri, M., Fourier, J., Clavel, R., Metrailler, P., et al. (2009). The WalkTrainer-a new generation of walking reeducation device combining orthoses and muscle stimulation. *IEEE Trans. Neural Syst. Rehabil. Eng.* 17, 38–45. doi: 10.1109/TNSRE.2008.2008288

To, C. S., Kobetic, R., Schnellenberger, J. R., Audu, M. L., and Triolo, R. J. (2008). Design of a variable constraint hip mechanism for a hybrid neuroprosthesis to restore gait after spinal cord injury. *IEEE/ASME Trans. Mechatron.* 13, 197–205. doi: 10.1109/TMECH.2008.918551

Tsagarakis, N. G., Laffranchi, M., and Vanderborght, B. (2009). "A compact soft actuator unit for small scale human friendly robots," in *Proceedings IEEE International Conference on Robotics and Automation (ICRA)* (Kobe), 4356–4362.

Tu, X., Li, J., Li, J., Su, C., Zhang, S., Li, H., et al. (2017). Model-based hybrid cooperative control of hip-knee exoskeleton and fes induced ankle muscles for gait rehabilitation. *Int. J. Pattern Recogn. Artif. Intell.* 31:1759019. doi: 10.1142/S0218001417590194

Veneman, J. F., Kruidhof, R., Hekman, E., Ekkelenkamp, R., Asseldonk, E. V., and van der Kooij, H. (2007). Design and evaluation of the LOPES exoskeleton robot for interactive gait rehabilitation. *IEEE Trans. Neural Syst. Rehabil. Eng.* 15, 379–386. doi: 10.1109/TNSRE.2007.903919

Vitiello, N., Lenzi, T., Roccella, S., Rossi, S. M. M. D., Cattin, E., Giovacchini, F., et al. (2013). NEUROExos: a powered elbow exoskeleton for physical rehabilitation. *IEEE Tran. Rob.* 29, 220–235. doi: 10.1109/TRO.2012.2211492

Winter, D. A. (2009). *Biomechanics and Motor Control of Human Movement, 4th Edn*. Hoboken, NJ: Wiley.

Yu, H., Huang, S., Chen, G., Pan, Y., and Guo, Z. (2015). Human robot interaction control of rehabilitation robots with series elastic actuators. *IEEE Trans. Rob.* 31, 1089–1100. doi: 10.1109/TRO.2015.2457314

Zhang, D. G., Guan, T. H., Widjaja, F., and Ang, W. T. (2007). "Functional electrical stimulation in rehabilitation engineering: a survey," in *Proceedings International Convention on Rehabilitation Engineering and Assistive Technology (i-Create)* (Singapore), 221–226.

Zhang, X., and Hashimoto, M. (2012). Synchronization-based trajectory generation method for a robotic suit using neural oscillators for hip joint support in walking. *Mechatronics* 22, 33–44. doi: 10.1016/j.mechatronics.2011.11.002

Conflict of Interest Statement: The authors declare that the research was conducted in the absence of any commercial or financial relationships that could be construed as a potential conflict of interest.

frontiers in Neuroscience

ORIGINAL RESEARCH
published: 08 January 2018
doi: 10.3389/fnins.2017.00733

Decoding of Ankle Flexion and Extension from Cortical Current Sources Estimated from Non-invasive Brain Activity Recording Methods

*Alejandra Mejia Tobar[1], Rikiya Hyoudou[1], Kahori Kita[2,3], Tatsuhiro Nakamura[3], Hiroyuki Kambara[1], Yousuke Ogata[1,3], Takashi Hanakawa[3], Yasuharu Koike[1,3] and Natsue Yoshimura[1,3]**

[1] Institute of Innovative Research, Tokyo Institute of Technology, Yokohama, Japan, [2] Center for Frontier Medical Engineering, Chiba University, Chiba, Japan, [3] Department of Advanced Neuroimaging, Integrative Brain Imaging Center, National Center of Neurology and Psychiatry, Tokyo, Japan

OPEN ACCESS

Edited by:
Yoshio Sakurai,
Doshisha University, Japan

Reviewed by:
Rolando Grave De Peralta Menendez,
Geneva Electrical Neuroimaging Group, Switzerland
Mikhail Lebedev,
Duke University, United States
Fumino Fujiyama,
Doshisha University, Japan

***Correspondence:**
Natsue Yoshimura
yoshimura@pi.titech.ac.jp

Specialty section:
This article was submitted to Neuroprosthetics, a section of the journal Frontiers in Neuroscience

Received: 30 August 2017
Accepted: 15 December 2017
Published: 08 January 2018

Citation:
Mejia Tobar A, Hyoudou R, Kita K, Nakamura T, Kambara H, Ogata Y, Hanakawa T, Koike Y and Yoshimura N (2018) Decoding of Ankle Flexion and Extension from Cortical Current Sources Estimated from Non-invasive Brain Activity Recording Methods. Front. Neurosci. 11:733. doi: 10.3389/fnins.2017.00733

The classification of ankle movements from non-invasive brain recordings can be applied to a brain-computer interface (BCI) to control exoskeletons, prosthesis, and functional electrical stimulators for the benefit of patients with walking impairments. In this research, ankle flexion and extension tasks at two force levels in both legs, were classified from cortical current sources estimated by a hierarchical variational Bayesian method, using electroencephalography (EEG) and functional magnetic resonance imaging (fMRI) recordings. The hierarchical prior for the current source estimation from EEG was obtained from activated brain areas and their intensities from an fMRI group (second-level) analysis. The fMRI group analysis was performed on regions of interest defined over the primary motor cortex, the supplementary motor area, and the somatosensory area, which are well-known to contribute to movement control. A sparse logistic regression method was applied for a nine-class classification (eight active tasks and a resting control task) obtaining a mean accuracy of 65.64% for time series of current sources, estimated from the EEG and the fMRI signals using a variational Bayesian method, and a mean accuracy of 22.19% for the classification of the pre-processed of EEG sensor signals, with a chance level of 11.11%. The higher classification accuracy of current sources, when compared to EEG classification accuracy, was attributed to the high number of sources and the different signal patterns obtained in the same vertex for different motor tasks. Since the inverse filter estimation for current sources can be done offline with the present method, the present method is applicable to real-time BCIs. Finally, due to the highly enhanced spatial distribution of current sources over the brain cortex, this method has the potential to identify activation patterns to design BCIs for the control of an affected limb in patients with stroke, or BCIs from motor imagery in patients with spinal cord injury.

Keywords: brain computer interface, walking, electroencephalography, functional magnetic resonance imaging

INTRODUCTION

Patients with walking impairments often use wheelchairs for transportation; however, this transportation means can cause pressure soars in the long-term if the patients do not perform pressure-relieving movements frequently (Stockton and Parker, 2002). Other devices such as exoskeletons and functional electrical stimulation (FES) systems allow patients to stand up and take steps however their control rely on the patient's unaffected motor abilities (pressing switches, trunk shifts, remaining muscle activity, etc.; Gancet et al., 2012; Contreras-Vidal et al., 2016). An alternative of control for these systems, which rely less heavily on the remaining motor abilities, is a brain-computer interface (BCI), in which brain signals are recorded and translated into control commands for assistive and communication devices (Wolpaw et al., 2002; Shih et al., 2012).

Breakthroughs in BCI have demonstrated the potential of this technology for motor rehabilitation, by controlling virtual environments and upper limb robots from implanted electrodes on the brain cortex (Wessberg et al., 2000; Serruya et al., 2002; Taylor et al., 2002; Carmena et al., 2003; Velliste et al., 2008; Hochberg et al., 2012). A study by Fitzsimmons et al. (2009) in non-human primates using implanted electrodes, demonstrated that it is possible to decode bipedal walking patterns (leg kinematics and EMG activities), from cortical ensembles in M1 and S1 during forward and backward walking tasks, showing the feasibility to use invasive BCIs for the restoration of gait in humans with intact locomotion centers in the brain. While invasive recordings can provide signals with high spatial resolution that allow for the decoding of more kinematic and physiological variables relevant to gait, the need for surgery limits the population that can access to this technology and, furthermore, there is always a risk of infection with implanted electrodes (Lesser et al., 2010). In this sense, non-invasive BCI techniques are preferred because they are safer and patients do not need to meet strict inclusion criteria to participate in this type of BCI studies. Among non-invasive techniques, electroencephalography (EEG) has a high temporal resolution and therefore is suitable for real time applications; nevertheless, movement artifacts and other sources of noise easily affect it. Despite its limitations, EEG is widely used in BCIs because of its portability.

Studies of BCIs based on binary classifications (i.e., detection of movement intention) using EEG have shown promising results for the development of assistive devices for gait restoration in patients with movement impairments (Waldert et al., 2008; King et al., 2013; Xu et al., 2014; Barsotti et al., 2015; Jiang et al., 2015; Severens et al., 2015; Yang et al., 2015; Pereira et al., 2017). Furthermore, long-term training with non-invasive BCIs has showed significant improvement in cortical plasticity in M1 and S1 areas in patients with paraplegia (Donati et al., 2016), demonstrating potential in the practical use of BCIs for the rehabilitation of walking impairments. However, in order to design a more natural non-invasive BCI for walking, it is necessary to classify more categories of motor tasks. Since the motor areas in the brain that represent right and left leg and foot are in close proximity (Meier et al., 2008), the multi-class classification of motor tasks in the lower limbs becomes a more challenging task for EEG signals.

To improve the spatial resolution and classification accuracies, various techniques to estimate cortical current sources from EEG, magnetoencephalography (MEG) and functional magnetic resonance imaging (fMRI) have been developed (Baillet et al., 2001). Among these techniques, we use a hierarchical Bayesian method that imposes fMRI as a hierarchical soft constraint on EEG for current source estimation (Sato et al., 2004; Yoshioka et al., 2008). This method was selected because it preserves the high temporal resolution of the EEG and the high spatial resolution of the fMRI, and it has been successfully implemented in previous offline BCI studies (Toda et al., 2011; Yoshimura et al., 2012, 2016; Kawase et al., 2017). In the context of this study, a current source can be defined as the average neuronal activation in each $3 \times 3 \times 3$ mm voxel in the brain cortex. The voxels from MRI provide information on the location and orientation of dipoles on the brain cortex, while from the fMRI data the region of interest (area prior) and the relative amplitudes of dipole currents (activity prior) are extracted. Area and activity priors are imposed as a soft constraint to estimate cortical current sources from the EEG data.

In our study, anatomically known areas in the brain contributing to motor planning and execution for ankle movements were obtained from the fMRI analysis. Each participant executed the same ankle movements as experimental tasks during both the fMRI and the EEG experiments, which were carried out separately on different days. Since from the fMRI information we can obtain good anatomical locations, with high resolution, for brain activations related to foot movements, we expect that the estimated current sources are a reasonable representation of the true current sources (group of neurons in each voxel) generated in the brain cortex. After current sources were estimated, we apply a multiclass classifier based on sparse logistic regression (SLR) (Yamashita et al., 2008), for the time series signals of the estimated current sources and EEG sensor signals, to classify ankle flexion and extension with two different force levels (i.e., nine tasks for both legs including a no-motion condition). This method was selected because it is suitable for brain activity data with high-dimensional features, and it has been reported to be more robust in the presence of irrelevant features when compared to other methods such as support vector machine and regularized logistic regression (Yamashita et al., 2008).

Our objective in this research is to estimate cortical current sources from EEG and fMRI recordings, and decode activation patterns in the brain for ankle flexion and extension movements at two force levels in both legs. These motor tasks were selected because of the major role these tasks play in the normal walking cycle, and because the classification of these tasks in healthy participants shows the feasibility to design control strategies for walking aids for patients with walking impairments. Based on the methods described here, classifiers can be created, for example, from motor imagery of ankle movements in patients with spinal cord injury, or from the healthy brain activation related to contralateral ankle or foot movement in patients affected by stroke.

MATERIALS AND METHODS

Participants

Eight healthy participants (5 males and 3 females) aged 22–50 years (Mean: 29.67 ± 8.81) participated in this study. Signed informed consents approved by the ethics committee of the National Center of Neurology and Psychiatry (NCNP) and Tokyo Institute of Technology were obtained from each participant prior to each experiment.

Experimental Design

Two types of experiments were conducted in different days: an fMRI and an EEG experiment. The experimental tasks consisted of isometric ankle flexion and extension at high (< ∼30% of maximum voluntary contraction level) and low force levels (about half of the high force) in each foot, yielding 8 active task conditions named "High Left Extension" (HLE), "High Left Flexion" (HLF), "High Right Extension" (HRE), "High Right Flexion" (HRF), "Low Left Extension" (LLE), "Low Left Flexion" (LLF), "Low Right Extension" (LRE), "Low Right Flexion" (LRF), and a resting control condition called "Still." Images showing the motor tasks throughout the experiments were created in Poser 2012 (Smith Micro Software, Inc., California, United States). In both fMRI and EEG experiments the same task pictures were shown, however in the EEG experiment, additional figures indicating the "blinking" and "set" intervals (fixed crosses before each task to reduce eye-movement artifacts in task periods), were included (**Figure 1**).

fMRI Experiment

The fMRI experiment was conducted to obtain the activated brain areas and the corresponding intensities to the experimental tasks. This information was used as prior for the cortical current sources estimation using the variational Bayesian multimodal encephalography (VBMEG) toolbox for Matlab (Sato et al., 2004).

A block design was used for the fMRI experiment. In total, the experiment consisted of 7 runs with 8 tasks blocks and one still (control) block per run, as detailed in **Figure 2A**. Each block consisted of one experimental task repeated 6 times during 2 s with 1 s rest (18 s per block). The experimental program was created using Presentation 16.3 (Neurobehavioral Systems, Inc., California, United States).

This experiment was conducted in the National Center of Neurology and Psychiatry (Tokyo, Japan) in a 3 Tesla Verio MRI Scanner (Siemens AG, Munich, Germany). Axial and sagittal scans were acquired for the T1-weighted structural images with a magnetization prepared rapid gradient-echo (MPRAGE). Both images were used during the preprocessing of fMRI; however, the sagittal image was also used to obtain a polygon model of the brain surface for each subject. In total, 48 slices were obtained for the axial images (repetition time = 2 s; echo time = 3.4 ms; flip angle = 8°, field of view = 192 × 192 mm; imaging matrix = 192 × 192; voxel size = 1 × 1 × 1 mm; inversion time = 0.99 ms), and 224 slices were acquired for the sagittal images (repetition time = 2 s; echo time = 3.41 ms; flip angle = 8°; field of view = 256 × 256 mm; imaging matrix = 256 × 256; voxel size = 1 × 1 × 1 mm; inversion time = 0.99 ms). T2*-weighted fMRI data was obtained with an echo planar imaging (EPI) with a generalized autocalibrating partial parallel acquisition (GRAPPA) method, recording 116 volumes per session (repetition time = 2 s; echo time = 13 ms; echo train length = 31 ms; flip angle = 90°; field of view = 192 × 192 mm; imaging matrix = 64 × 64; number of slices = 48; voxel size = 3 × 3 × 3 mm).

Electromyography (EMG) of ankle flexors and extensors was recorded during the fMRI experiment with the purpose of confirming task execution. EMG electrodes were attached prior to the fMRI experiment to the Tibialis Anterior (dorsiflexor), the Gastrocnemius (plantarflexor and knee flexor), the Soleus (plantarflexor), and the Extensor Hallucis Brevis (toes extensor) in both legs, and the participant was asked to practice the experimental tasks. EMG data in this experiment was collected with a BrainAmp ExG MR (Brain Products GmbH, Gilching, Germany) using 8 pairs of Ag/AgCl electrodes. Inside the scanner, the feet of the participants were fixed to fMRI compatible custom made platforms (Right Mfg. Co., Ltd, Tokyo, Japan) with detachable Velcro stripes, to allow them to exert isometric force, and to reduce head motions inside the MRI scanner caused by the leg movement tasks (**Figure 2B**).

EEG Experiment

The EEG program for experiment instruction was created in MATLAB 2013b (The MathWorks, Inc., United States). In this experiment, additional images for blinking and set (fixation crosses indicating the participant to prepare for the task) were included. This experiment was divided into 3 modules: "Flexion vs. Extension," "Right vs. Left," and "High Force vs. Low Force," and participants were asked to take a rest after each module completion. The EEG experiment was designed in this manner attempting to reduce the potential mental fatigue of the participants (Faber et al., 2012; Talukdar and Hazarika, 2017), in consideration of the number of experimental tasks (9 motor tasks with 50 repetitions each), the introduction of task irrelevant images for blink and set (fixation crosses) events, and the condition of exerting isometric forces. Four runs composed each module and each run was repeated twice. According to the current module, each run combined two tasks and a still task, that is, in the "Flexion vs. Extension" module the tasks "LLF and LLE," "HLF and HLE," "LRF and LRE," and "HRF and HRE" and still, were included (**Figure 2C**).

In preparation for the EEG experiment, the participants were seated inside a soundproof room (AMC-3515, O'HARA & Co., Ltd.) with a 24 inches monitor to show the experiment directions. The participant feet were fixed to the platform and instructed to practice ankle flexion and extension at high and low force levels to learn to restrain co-contraction of flexor and extensor muscles (**Figure 2D**).

EEG signals were acquired with a sampling rate of 256 Hz with the ActiveTwo system and the ActiView software (BIOSEMI, Amsterdam, Netherlands), using 32 Ag/AgCl active electrodes placed accordingly to the 10–20 international system layout. Two additional electrodes were placed on both earlobes and its average was used as a reference. To place the EEG and the reference electrodes, the head cap gaps were filled with highly conductive gel and the earlobes were cleaned with 70% ethanol.

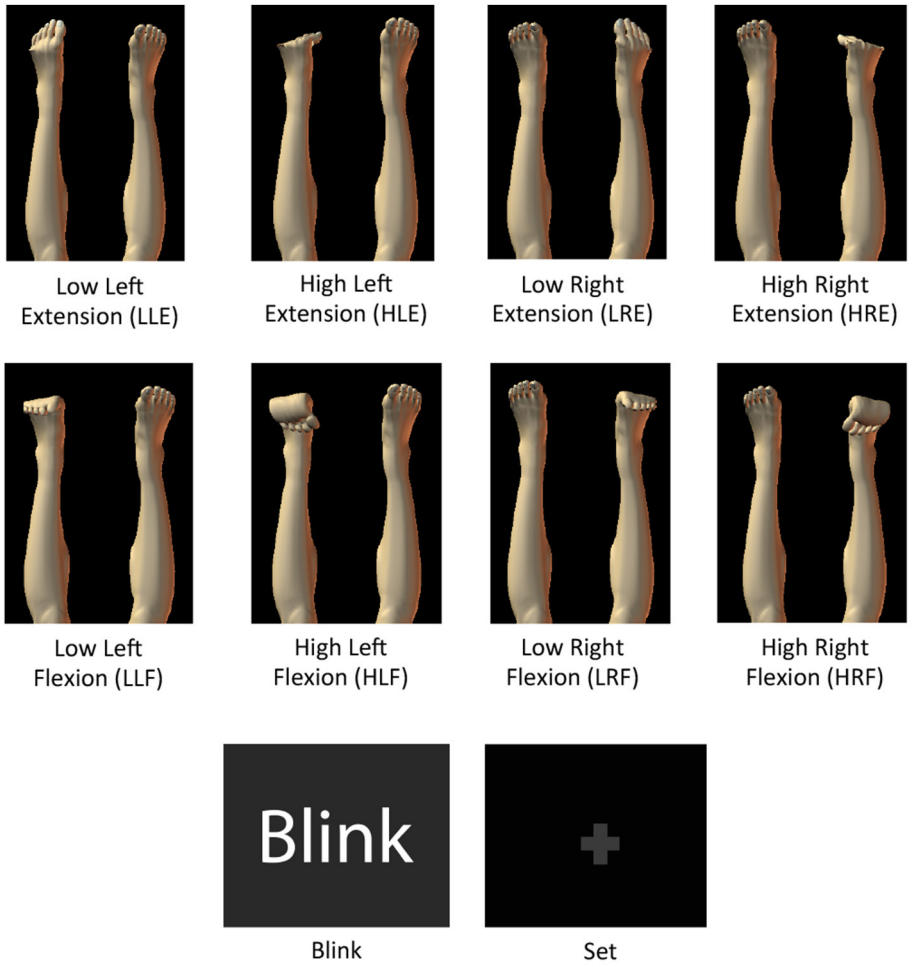

FIGURE 1 | Images with motor task instructions used during the fMRI and the EEG experiments. Blink and fixation crosses were only used for the EEG experiment.

EEG electrodes positions were recorded with a Polaris Spectra (Northern Digital Inc., Waterloo, Canada). Measurements were done in the order of nasion, right pre-auricular, left pre-auricular, and EEG electrodes according to the BIOSEMI electrodes labels.

To confirm task execution in the EEG experiment, EMG signals were recorded a sampling rate of 2,000 Hz with a Bagnoli™ Desktop EMG System (Delsys, United States) using 8 single differential electrodes on the same muscles as the fMRI experiment. EMG signal conditioning and digitalization was done with a NI-USB 6259 BNC (National Instruments, Canada).

fMRI Data Preprocessing

fMRI data was processed using SPM8 (Wellcome Department of Cognitive Neurology, UK; http://www.fil.ion.ucl.ac.uk/spm), for individual and group (second-level) analyses. In preparation for the analyses, the first five volumes of the EPI images were discarded for stabilization of the magnetization, and the last 10 volumes were discarded to avoid their use as a baseline, therefore, from the original 116 volumes, 101 volumes were used for the analyses. For the individual analyses T1-weighted axial and sagittal images were bias corrected and segmented into gray matter, white matter and cerebrospinal fluid. EPIs were corrected for differences in image acquisition time, and realigned to the mean EPI image. To register all images, the T1-weighted axial image was co-registered to the T1-weighted sagittal image and then the EPIs were co-registered to the T1-weighted axial image. It is worth mentioning that this co-registration method is not standard for fMRI analysis, and it is used only for current source estimation purpose in VBMEG. After images registration, all images were normalized to the Montreal Neurological Institute (MNI) coordinates, and smoothed with a full-width spatial Gaussian kernel of 8 mm at half maximum.

Statistical analyses were performed with a general linear model (GLM). Boxcar functions were used to model the nine periods corresponding to the nine blocks. Each execution period consisted of one block of 18 and 3 s of rest interval. These functions were then convolved with the hemodynamic response function to obtain parameters describing the blood oxygen level-dependent (BOLD) response at each stimulus presentation (task image). Finally, model parameters were estimated and statistical parametric maps were created for each participant. Using the contrasts obtained from individual analyses, a second-level

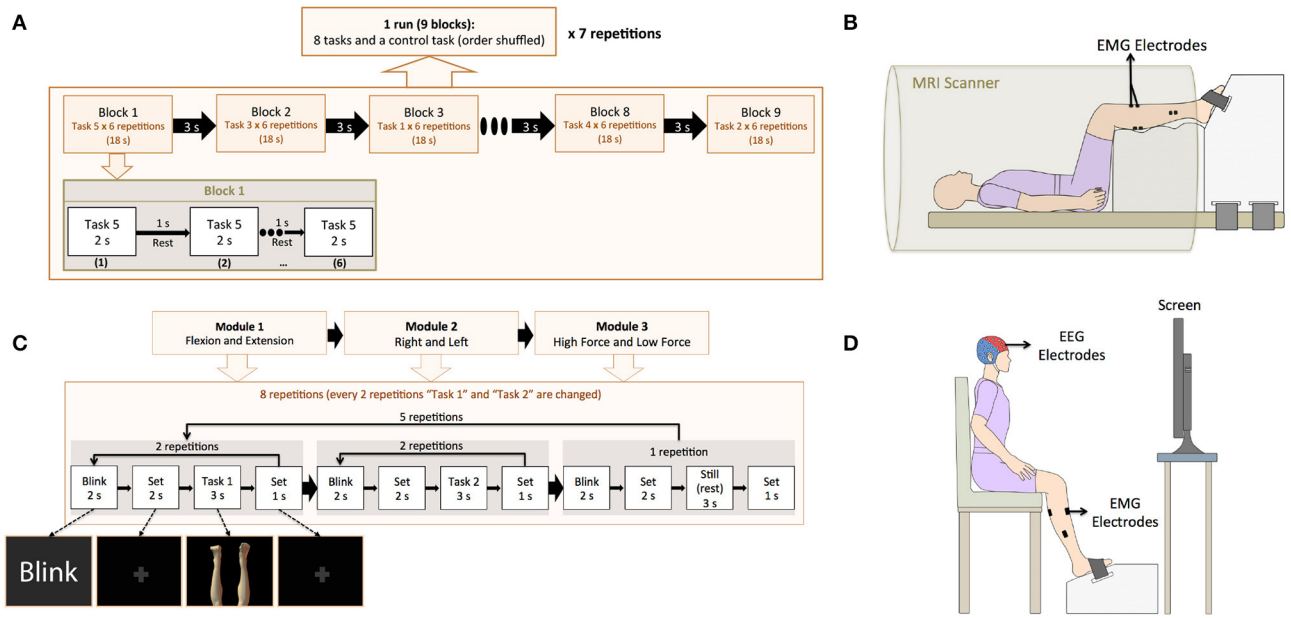

FIGURE 2 | (A) Experimental paradigm for the fMRI experiment. The fMRI experiment consisted 7 runs. In each run, 9 blocks were included (8 active tasks and a control task), and each block consisted of one experimental task and a rest interval, both repeated 6 times. **(B)** Experimental setting for the fMRI experiment. EMG electrodes were attached to the participants to confirm task execution and the feet of the participant were fixed to a custom made-platform to reduce head movements inside the scanner. **(C)** Experimental paradigm for the EEG experiment. The EEG experiment consisted of three modules: "Flexion vs. Extension," "Right vs. Left," and "High Force vs. Low Force." In each module, 2 active tasks were repeated 10 times (10 trials) and a still task was repeated 5 times (5 trials). The 2 active tasks were selected based on the module (i.e., HLE and HLF for the "Flexion vs. Extension" module). After 25 trials (10 trials for each of the 2 active tasks and 5 trials for the still task), the active tasks were changed until completing all the experimental tasks. **(D)** Experimental setting for the EEG experiment. A cap with 32 EEG electrodes and 8 EMG electrodes were attached to the participant. A custom-made platform was also used in this experiment to attach the participant's feet during the EEG experiment in order to reduce movement artifacts and allow for isometric contractions.

(group) analysis was done with a full factorial design to extract parametric maps common for all participants. Three factors were used for the design: "Factor 1: left leg and right leg," "Factor 2: flexion and extension," and "Factor 3: high force and low force." T-contrasts were obtained for each of the following conditions: (all left leg tasks) and (all right leg tasks) with $p < 0.01$ (uncorrected for multiple comparisons). Statistical parametric maps from the group analysis were masked with the anatomical atlas of Brodmann areas 4 (primary motor cortex), 6 (premotor cortex and supplementary motor area), and 3,2,1 (primary somatosensory cortex) using the WFU PickAtlas (Radiology Informatics and Imaging Laboratory, USA; http://fmri.wfubmc.edu/software/pickatlas) tool for SPM to build the area and activity priors for the purpose of cortical current sources estimation in VBMEG. The two contrasts obtained were inversely normalized into individual participant's space and merged into one activity prior and one area prior. These priors were named Group-Con.

EEG Data Preprocessing

EEG data recorded in BDF format from BIOSEMI was converted into Matlab format with EEGlab (Delorme and Makeig, 2004, https://sccn.ucsd.edu/wiki/EEGLAB), band-pass filtered from 0.5 to 40 Hz, downsampled to 200 Hz, and epoched in intervals of −0.5 s pre onset and 3 s post onset, in reference to the stimulus presentation time. This pre-processed EEG was further downsampled to 30 Hz and epoched from 0 s (onset) to 1.5 s, and these epochs of 1.5 s were used as features for the sparse logistic regression classifier, to obtain the EEG sensor signals that contributed to each of the nine experimental tasks.

Current Source Estimation with VBMEG

VBMEG is a type of distributed source method in which the MRI information provides information about the positions and orientations of dipoles, and the fMRI provides information about a region of interest and the relative amplitude of the current in each dipole (Yoshioka et al., 2008).

In conventional current estimation methods where the fMRI is also used as a prior, the fMRI information is imposed directly as the prior current variance in each dipole, and therefore the current amplitude has a low influence when the prior variance is too large or too small. In VBMEG, the prior distribution of the variance is considered a random parameter with gamma distribution, and the fMRI information is imposed on the variance distribution, rather than as the variance itself, using two hyperparameters: a variance magnification parameter (μ_0), controlling the current amplitude for a given fMRI activation, and a confidence parameter (γ_0), controlling the width of the prior distribution. This hierarchical prior provides a soft constraint on the current amplitude. A spatial

smoothness constraint with a Gaussian profile with a full width at half maximum (FWHM) of 6 mm, was incorporated in the estimation. This smoothness constraint considers that neurons within a few millimeters radius tend to fire simultaneously (Sato et al., 2004; Yoshioka et al., 2008; Toda et al., 2011; Yoshimura et al., 2012).

Because of the hierarchical prior, the estimation of the inverse filter becomes a non-linear problem that cannot be solved analytically, therefore the approximate posterior distribution is calculated by using a Variational Bayesian (VB) method, in which the current and the variance from the observed EEG data and the prior variance information given by the fMRI data are alternately estimated. The inverse filter is calculated using the estimated covariance matrix in the previous iteration (Attias, 1999; Sato, 2001). Once the inverse filter has been calculated, the current estimation becomes al linear problem.

Current sources were estimated in VBMEG following the standard procedures established in the toolbox documentation. The following steps and parameters were used to estimate cortical currents in VBMEG: firstly, a cortical surface model and a three-layer head model for each participant were extracted from the un-normalized bias-corrected T1-weighted sagittal image from the SPM analysis. The cortical surface model was created as a polygon model using FreeSurfer (Martinos Center Software, https://surfer.nmr.mgh.harvard.edu/). The cortical surface model has single-current dipoles equidistantly distributed on and perpendicular to the cortical surface, and the three-layer model has the boundary information for skull, scalp, and cerebrospinal fluid. VBMEG imports the cortical model to map the estimated current dipoles, and uses the three-layer model to create a head model for improving the accuracy in the leadfield (i.e., forward model) calculation.

Secondly, the leadfield matrix is calculated from the cortical surface model, the head model and the EEG sensor positions. Thirdly, the variance of the electrical current from EEG is estimated in the time range from −0.5 to 3 s with a baseline from −0.5 to 0 s, and the fMRI information is imposed on the prior distribution of the current variance using the hyperparameters μ_0 and γ_0. High values for both hyperparameters indicate that the brain activity was the same during both fMRI and EEG experiments. Considering the experiments were carried out in different days, and based on the previous work (Yoshimura et al., 2016), the hyperparameters values for the Group-Con area and activity priors were set as $\mu_0 = 10$ and $\gamma_0 = 1$.

To estimate the inverse filters, the whole epoch of EEG data (−0.5 to 3 s) was used for the analysis, being divided into 14 windows of 0.5 s of length with 0.25 s of overlap. This setting calculated an inverse filter for each time window corresponding to each epoch and trial. These current sources were estimated for the area and activity priors determined by Group-Con. The mean number of current dipoles estimated for each participant was of 188 ± 7.07. The time series of estimated current sources were further downsampled to 30 Hz and epoched from 0 s (onset) to 1.5 s, and these epochs of 1.5 s were used as features for the sparse logistic regression classifier, to obtain which current sources contributed most to each of the nine experimental tasks.

Multi-class Classification with Sparse Logistic Regression

Logistic regression (LR) is a well-known classifier originally developed in statistics. SLR is a Bayesian extension of LR in which a sparseness prior is imposed on LR (http://www.cns.atr.jp/~oyamashi/SLR_WEB/Readme201102.pdf). The SLR method combines the LR with the automatic relevance determination (ARD), to simultaneously perform feature selection and training of the model for classification. The ARD prunes irrelevant features by automatically setting their associated weights to zero, leading to a sparse weight vector for classification. This allows the SLR to train high-dimensional classifiers without the need of advanced feature dimension reduction, and to avoid overfitting to some extent. SLR was applied in this research using the SLR Toolbox v.1.2.1 (ATR Computational Neuroscience laboratories in Kyoto, Japan; http://www.cns.atr.jp/~oyamashi/SLR_WEB.html).

Multiclass classifications were done for the epochs of 1.5 s of estimated current sources and EEG sensor signals, using a leave-one-out (LOO) method for both current sources and pre-processed EEG data. The features for classification were obtained as described in section EEG Data Preprocessing for EEG and section Current Source Estimation with VBMEG for current sources. Mean classification accuracies from current sources, EEG and random labeled data were compared using non-parametric permutation tests (Nichols and Holmes, 2002). To evaluate the contribution of current sources and EEG sensors to each task classification, the corresponding weight values were normalized by the maximum of each trial and averaged across time points and trials. Finally, net weight values of the current sources vertices selected in each area in our ROI, and weights in each EEG sensor were averaged across participants. Location of contributing selected current sources was determined using the Anatomy toolbox v1.8 [Institute of Neuroscience and Medicine (INM-1), Germany], using the Montreal Neurological Institute (MNI) coordinates obtained from SPM.

RESULTS

Classification Results

In **Figure 3** percentage of correct classifications in the test data from current sources, EEG and random label are shown. The classification accuracy from current sources was significantly higher than chance level (Current sources: 65.64% ±4.11; $p =$ 1.19e−04), and EEG sensor signals (EEG: 22.19%; $p =$ 1.19e-04). All p-values were obtained from permutation tests and corrected for multiple comparisons using a false discovery rate of 0.05. There was no significant difference between the random label classification and the chance level.

Tables 1, **2** show the confusion matrix for the current sources classification and pre-processed EEG classification for all trials averaged across participants.

Localization of Contributing Features

Weight analyses were performed for EEG and current sources classification results. For EEG, weights were averaged and normalized across trials and participants in each EEG sensor

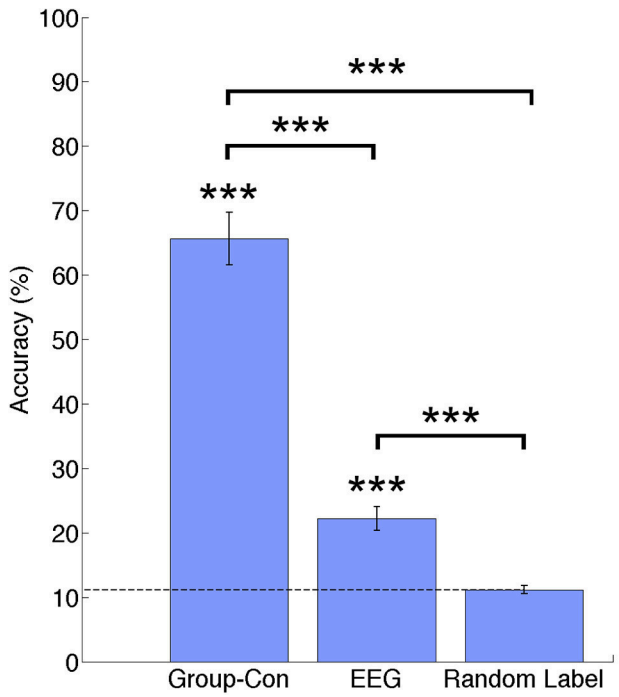

FIGURE 3 | Classification accuracies across participants for current sources estimated using priors from and fMRI group analysis (Group-Con), pre-processed EEG signals (EEG), and a random label classification for current sources. ***$p < 0.001$.

(**Figure 4**). For current sources, total weights across dipoles located in the same Brodmann area were averaged across trials and participants, and normalized per task. Current sources were obtained across Brodmann areas 1, 2, 3, 4, 6, the inferior parietal cortex (IPC) and the lateral operculum (OP3 and OP4). Finally, activation patterns were obtained for each participant showing the current sources distribution in each task (**Figure 5**).

DISCUSSION

This research presented a multi-class classification analysis of ankle motor tasks using non-invasive brain recorded signals from EEG and fMRI. As a result, we could successfully identify activation patterns for flexion and extension tasks at two different force levels in both feet. Due to the difficulty of measuring brain activity during walk related motor tasks inside the fMRI scanner, our approach focuses on the classification of ankle flexion and extension tasks that can provide an insight of control for a real time walking BCI. We obtained accuracies of 65.64% for the classification of estimated current sources, and of 22.19% for the classification of EEG sensor signals above chance level (11.11%) and no significant difference was found among classes across participants showing no disproportion of true positives.

The high classification accuracy could be attributed to the combination of VBMEG and SLR. From VBMEG, many redundant (but not identical) time series patterns of current sources are estimated and this output could give SLR many candidates for features selection from the sparse regularization point of view (Donoho, 2006). As a result, many similar time series patterns remain for classification producing high classification accuracies.

Additionally, the high-resolution fMRI prior may have also contributed to the high classification accuracy despite the use of 32 EEG channels. While a low resolution prior and a low number of electrodes affects the quality of the current sources estimated in VBMEG, and consequently the classifications results, the high spatial resolution area prior may be more important for proper current source estimation in VBMEG, than the number of EEG electrodes: a study performed by Aihara et al. (2012) showed that the detection accuracy of current sources from simulated EEG data and spatial priors at different resolutions, was largely affected by the spatial resolution of the prior than by the number of EEG sensors. Similar results were obtained with the experimental data, using 19, 31, and 64 EEG channels, and fMRI and near-infrared spectroscopy (NIRS) as priors. The fMRI prior and 64 EEG channels estimation was used as a reference. In both simulated and real data cases, the use of 19 EEG channels along with the lowest resolution prior (NIRS in the case of real data), outperformed the use of 64 EEG channels without any prior information for current source estimation.

Currently it is not possible to isolate or identify individual muscle activity from EEG recordings, however a previous study by Yoshimura et al. (2012) succeeded in reconstructing individual muscle activities (flexor carpi radialis and extensor carpi radialis brevis) from cortical current sources estimated from 32 EEG electrodes using VBMEG and a sparse regression method, in a five task experimental paradigm of wrist flexion and extension at high and low forces. These results further support the high performance of the current source estimation method with VBMEG. As for this study, we have partially succeeded in the reconstruction of ankle flexor (tibialis anterior) and extensor (soleus) muscles activities using the methods described in the paper.

As for the classification technique, we selected SLR as a classifier because it has a better classification performance in the presence of irrelevant features, when compared to more popular methods such as support vector machine (SVM) and regularized logistic regression (RLR; Yamashita et al., 2008). Additionally, in the multiclass classification each class has its own set of parameters, which allowed obtaining activation patterns of current sources that are specific to each of the experimental tasks.

Location of Features Contributive to Task Execution

The weights assigned by the classifier to EEG electrodes did not offer relevant information about the execution of the motor tasks of interest, however this result was reasonable considering the low classification accuracy of these signals. Higher weights tended to be assigned to electrodes placed over temporal and parietal lobes (P7, P8, T7, and T8; **Figure 4**). This outcome could be related to artifacts caused by eye movement or EMG artifacts during the isometric task execution.

TABLE 1 | Confusion matrix for current sources classification averaged across participants (50 test trials per class).

	Current sources classification accuracies (%)								
Target \ Selected	HLE	HLF	HRE	HRF	LLE	LLF	LRE	LRF	Control
HLE	31.63	2.63	2.25	1.25	2.25	2.63	2.00	1.63	3.75
HLF	1.00	35.50	1.25	1.88	2.50	3.25	1.38	1.00	2.25
HRE	2.38	1.38	35.38	1.38	1.38	2.00	3.25	1.00	1.88
HRF	1.00	2.25	1.63	34.63	1.00	2.38	1.88	3.13	2.13
LLE	1.50	2.75	2.00	1.38	32.75	2.75	2.13	1.88	2.88
LLF	1.88	3.38	1.25	2.38	3.25	29.75	2.13	2.00	4.00
LRE	1.25	1.75	2.13	2.63	2.63	3.13	29.75	2.38	4.38
LRF	2.00	1.50	1.00	2.25	1.13	3.38	2.13	34.25	2.38
Control	1.88	1.38	1.25	1.25	3.25	4.38	2.75	2.13	31.75
Mean accuracy per class (%)	63.26 ± 8.28	71 ± 8.90	70.76 ± 6.26	69.26 ± 6.80	65.5 ± 8.40	59.50 ± 11.99	59.50 ± 6.58	68.5 ± 6.59	63.50 ± 7.11
Mean accuracy (%)	65.64 ± 4.11								

TABLE 2 | Confusion matrix for EEG sensor signals classification averaged across participants (50 test trials per class).

	EEG sensor signals classification accuracies (%)								
Target \ Selected	HLE	HLF	HRE	HRF	LLE	LLF	LRE	LRF	Control
HLE	9.00	6.50	5.75	4.75	6.00	6.38	4.13	3.88	3.63
HLF	7.13	9.13	4.13	4.88	5.75	7.25	3.13	3.38	5.25
HRE	4.00	4.25	10.75	8.25	3.38	3.75	6.63	6.00	3.00
HRF	4.88	4.88	6.75	11.13	3.25	3.25	4.75	6.75	4.38
LLE	5.88	6.00	4.38	3.00	10.63	7.50	5.13	3.25	4.25
LLF	7.13	6.25	4.50	2.50	6.00	9.50	4.38	3.88	5.88
LRE	5.25	3.50	6.50	5.38	4.63	3.88	10.63	6.25	4.00
LRF	4.00	3.00	4.75	7.75	3.63	3.88	6.38	12.63	4.00
Control	3.13	5.25	2.25	3.50	4.38	5.38	4.38	5.25	16.50
Mean accuracy per class (%)	18 ± 3.25	18.25 ± 2.70	21.5 ± 2.76	22.25 ± 3.64	21.25 ± 3.81	19 ± 2.45	21.25 ± 3.85	25.25 ± 4.41	33 ± 8.52
Mean accuracy (%)	22.19 ± 1.85								

In the case of current sources classification, we obtained different activation patterns distributed over known brain areas involved in motor planning and execution. Vertices that were selected by the classifier as relevant for more than one task, had different signal patterns to which we attribute the higher performance classification when compared to EEG sensor signals classification. These activation patterns are shown in **Figure 5** for a representative participant. For conciseness, in **Figure 5** single task patterns were merged into (1) left leg versus right leg tasks, (2) flexion versus extension tasks, and (3) high force versus low force tasks.

The group analysis showed current sources widely distributed along our ROI of Brodmann areas 1, 2, 3 (primary somatosensory cortex), 4 (primary motor cortex), and 6 (premotor cortex and supplementary motor area), however it also showed activations in the IPC and the OP. The activations in these areas adjacent to Brodmann areas 1, 2, 3, 4, and 6 were reasonable considering the co-registration and normalization methods of fMRI and MRI data are not optimal processes, and the inverse normalization is as good as the initial normalization to the standard brain for each participant.

Current sources located in the ipsilateral side of the brain (resting leg) were observed throughout participants. While these activations were expected by the use of a single fMRI prior and co-contractions during task execution, these activations are also reasonable considering that unilateral limb movements are not exclusive of the contralateral brain and also show activations on the ipsilateral brain (Chiou et al., 2013).

Brain Areas Contributive to Task Execution

Somatosensory information from Brodmann areas 1, 2, and 3 is used in motor control: area 3 receives information relevant for proprioception and skin touch, which is processed with areas 1 and 2 (Amaral, 2013). The primary motor cortex and the primary somatosensory cortex have shown prominent activations during walking experiments (la Fougère et al., 2010), which are strongly

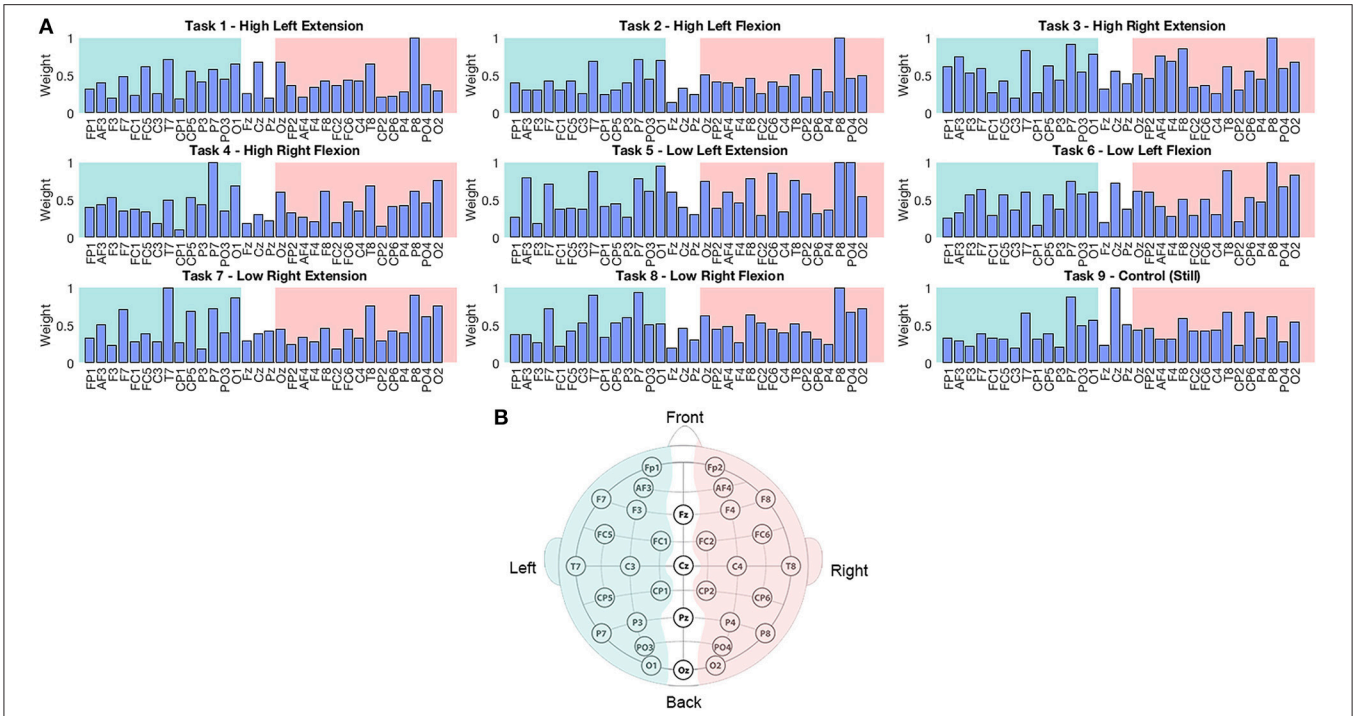

FIGURE 4 | (A) Normalized weights obtained for each task in EEG classification. Bars located on the green area correspond to the sensors located in the left hemisphere, bars in the white area correspond to the midline, and electrodes in the pink area correspond to the right hemisphere. **(B)** Location of 32 EEG electrodes over the scalp using the 10–20 extended system.

related to the goal of this study. Brodmann area 6 is involved in preparing and organizing voluntary movements (Cunnington et al., 1996; Sira and Mateer, 2014), and the highest activation in this area across participants may be related to the complexity of the task in which not only flexion and extension movements needed to be prepared for both lower limbs, but also force modulation was required. Activation in the IPC was observed in the rostral and middle areas. The rostral areas are functionally connected to motor, premotor, and somatosensory areas, thus this activation may be related to sensorimotor integration of motor task observation and task execution (Caspers et al., 2011), while middle IPC is involved visually guided attention, and it may have aroused as a result of the fixation crosses used during the EEG experiment (Caspers et al., 2013). The operculum (OP3 and OP4) is part of the secondary somatosensory cortex (SII). Studies in the role of SII in sensory-motor integration (Inoue et al., 2002) and its somatotopic map, have reported activations in SII as a result of mechanical plantar stimulation (to produce a gait-like somatosensory inflow; Labriffe et al., 2017) and somatosensory stimulation in the legs, trunk, hands and head (Disbrow et al., 2000; Eickhoff et al., 2007).

We also assessed the performance of the method in classifying tasks from each brain hemisphere (each leg separately), as a future application for patients with stroke. We created area and activity priors using the t-contrasts from only left leg tasks and only right leg tasks, and masked them with the previously described ROI. Priors in the left brain only were used for right leg tasks classification, and priors in the right brain only were used for the left leg tasks classification, resulting in 5-class classifications (4 active tasks per leg and a control task) with a chance level of 20% for each classification. Accuracies obtained from the current sources classification was significantly higher than EEG and chance level in each left leg (current sources: 70.55% $\pm$ 5.31; EEG: 31.40 $\pm$ 2.69; $p = 1.19e{-}04$ corrected for multiple comparisons) and right leg (current sources: 73.55 $\pm$ 2.82; EEG: 32.10 $\pm$ 3.07; $p = 1.19e{-}04$ corrected for multiple comparisons).

Advantage of Using Group fMRI Priors for Current Source Estimation

Various analyses using anatomical priors and fMRI priors obtained from individual analyses were also conducted in this study, obtaining current source classification accuracies similar to the group analysis (9-class mean classification accuracy in individual space: 69.25% $\pm$ 2.61). While the number of participants needs to be increased in order to draw more robust conclusions specifically for an fMRI second-level analysis, the purpose of using the group prior is to show that the methods described here are applicable using only structural MRI data, and therefore can benefit patients unable to use the MRI scanner for long sessions.

BCIs Application in Rehabilitation

Invasive BCI recordings in non-human primates have successfully been used for decoding kinematic and physiological activities (EMG), during forward and backward walking on

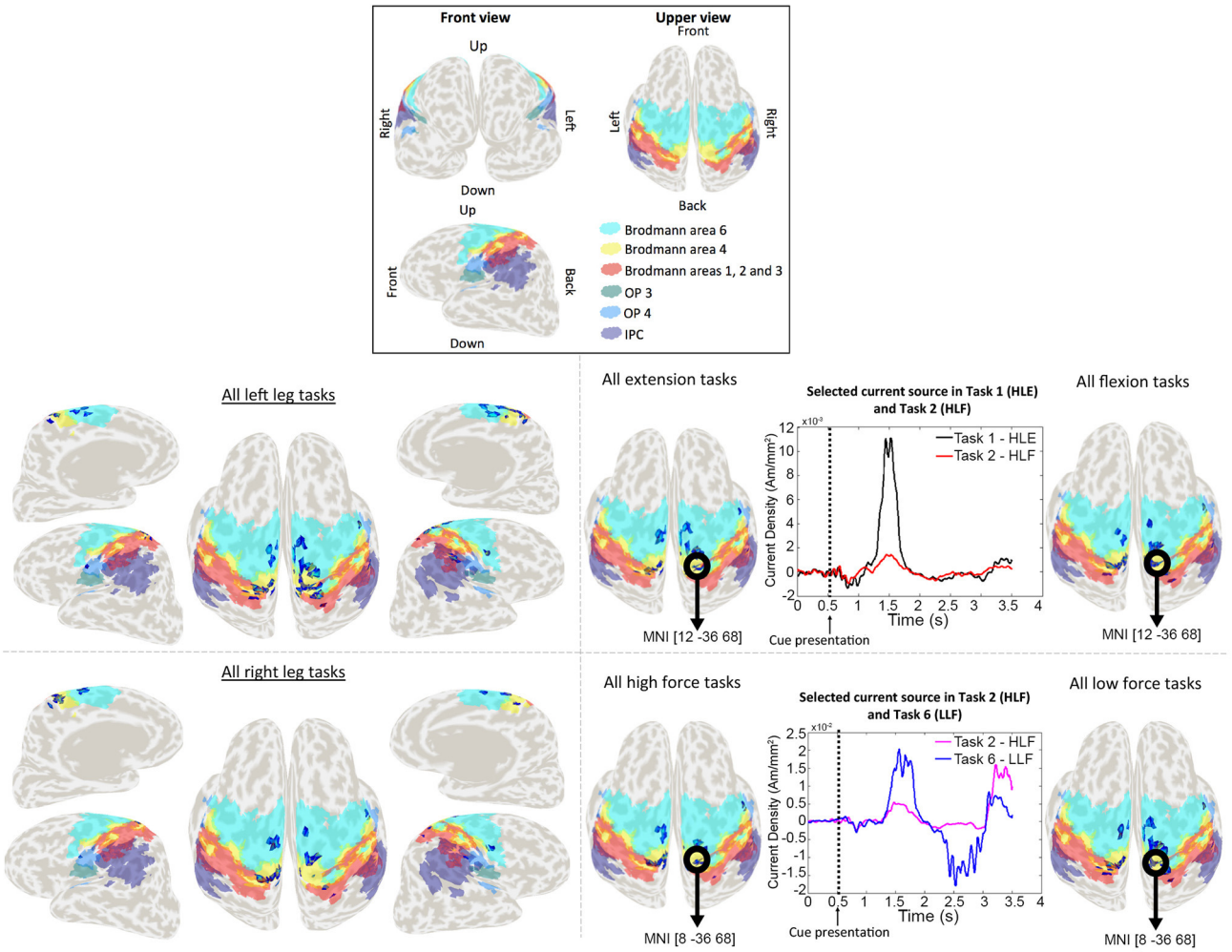

FIGURE 5 | Activation patterns for a representative participant. Colored areas show Brodmann areas 1, 2, 3, 4, 6 OP3, OP4, and the IPC. Lower left panel shows the merged activation patterns for all left and right leg tasks (all right leg tasks: HRE + HRF + LRE + LRF; all left leg tasks: HLE + HLF + LLE + LLF), and lower right panel shows the activation patterns for all extension tasks, all flexion tasks, all high force tasks and all low force tasks (all flexion tasks: HRF + HLF + LRF + LLF; all extension tasks: HRE + HLE + LRE + LLE; all high force tasks: HRF + HLF + HRE + HLE; all high force tasks: LRF + LLF + LRE + LLE). Time series represent the temporal patterns for the current source vertex in bold black circles. These signals correspond to a vertex selected by the classifier as relevant for more than one task. The vertex located in MNI [12, −36, 68], was selected by the classifier for both HLE and HLF task, and the vertex located in MNI [8, −36, 68] was selected for both HLF and LLF tasks.

a treadmill. In humans, the use of this method, along with exoskeletons or FES systems, could make it possible to create walking strategies that facilitate spinal cord plasticity to help recovering locomotion automatisms (Fitzsimmons et al., 2009). As for non-invasive techniques, the use of different strategies such as virtual reality, lower limb actuators, exoskeletons, etc., in patients with paraplegia, have already shown significant improvement in functional cortical plasticity in S1 and M1 areas (Donati et al., 2016). In this sense, the methods described here, along with high density EEG, might allow also for the prediction of kinematic variables in patients with limited mobility, aiming to design a control strategy where the patient has more control over the system than a robotic or neurostimulation solution.

In this study we have further assessed the potential of the VBMEG and SLR methods to design BCIs to control assistive and rehabilitation devices for the restoration of walking in patients with motor impairments. The highly enhanced spatial distribution of current sources over the brain cortex has the potential to identify changes in cortical plasticity in patients with stroke, to design interfaces that can identify vertices in the healthy brain relevant to the affected limb control, or to design BCIs for patients with spinal cord injury from current source estimation from motor imagery.

Challenges toward the Development of a Real-Time BCI

In order to design a reliable real time BCI, the accuracy of the system needs to be increased and a generalized classifier needs to be developed. In our experiment, blinking sessions were performed independently of task execution sessions, therefore online rejection of blinking artifacts should be implemented for the online application. One of the most challenging goals in this

project is to develop a generalized classifier able to achieve high accuracies with all participants, due to, among other factors, the non-stationary nature of brain signals, parameter tuning and training of samples, internal artifacts, etc. Finally, a limitation in this study is the small sample of participants used and therefore it is necessary to increase the sample and extend these conclusions to a larger population.

CONCLUSION

In this study we have classified ankle flexion and extension movements at different force levels in healthy participants, using non-invasive brain activity recording methods. The technique applied in this research is applicable to real-time BCIs since the filters estimation can be done offline. Also, the nature of the recordings allows for this technique to be applied to a larger population of patients with motor impairments since it does not require surgery. Finally, different combinations of area and activity priors from fMRI can be applied, and therefore specific brain areas may be used to generate control strategies in patients with stroke or spinal cord injury.

ETHICS STATEMENT

This study was carried out in accordance with the recommendations of the guidelines A14036 from Tokyo Institute of Technology and A2014-020 from the National Center of Neurology and Psychiatry, with written informed consent from all subjects. All subjects gave written informed consent in accordance with the Declaration of Helsinki. The protocol was approved by the ethics committees of the National Center of Neurology and Psychiatry and Tokyo Institute of Technology.

AUTHOR CONTRIBUTIONS

AM: designed and performed the EEG experiment, analyzed the fMRI and EEG data, reviewed literature and drafted the manuscript; RH, YO, and NY: designed and performed the fMRI experiment and analyzed data; KK, TN, and HK: performed the fMRI experiment; TH, YK, and NY: supervised the experiments and the research.

ACKNOWLEDGMENTS

This research was supported by AMED, from the Development of BMI Technologies for Clinical Application from the Strategic Research Program for Brain Sciences, and JSPS KAKENHI grants 17H05903, 15H01659, 26112004, and 15K01849.

REFERENCES

Aihara, T., Takeda, Y., Takeda, K., Wataru, Y., Sato, T., Otaka, Y., et al. (2012). Cortical current source estimation from electroencephalography in combination with near-infrared spectroscopy as a hierarchical prior. *Neuroimage* 59, 4006–4021. doi: 10.1016/j.neuroimage.2011.09.087

Amaral, D. G. (2013). "The functional organization of perception and movement," in *Principles of Neural Science*, eds E. R. Kandel, J. H. Schwartz, and T. M. Jessell (New York, NY: McGraw-Hill Companies), 356–369.

Attias, H. (1999). Inferring parameters and structure of latent variable models by variational Bayes. *Proc. Fifteenth Conf. Uncertain. Artif. Intell.* 1–5. doi: 10.1007/s13398-014-0173-7.2

Baillet, S., Mosher, J. C., and Leahy, R. M. (2001). Electromagnetic brain mapping. *IEEE Signal Process. Mag.* 18, 14–30. doi: 10.1109/79.962275

Barsotti, M., Leonardis, D., Loconsole, C., Solazzi, M., Sotgiu, E., Procopio, C., et al. (2015). "A full upper limb robotic exoskeleton for reaching and grasping rehabilitation triggered by MI-BCI," in *IEEE International Conference Rehabilitative Robotics 2015–September* (Singapore), 49–54.

Carmena, J. M., Lebedev, M. A., Crist, R. E., O'Doherty, J. E., Santucci, D. M., Dimitrov, D. F., et al. (2003). Learning to control a brain-machine interface for reaching and grasping by primates. *PLoS Biol.* 1:e42. doi: 10.1371/journal.pbio.0000042

Caspers, S., Eickhoff, S. B., Rick, T., von Kapri, A., Kuhlen, T., Huang, R., et al. (2011). Probabilistic fibre tract analysis of cytoarchitectonically defined human inferior parietal lobule areas reveals similarities to macaques. *Neuroimage* 58, 362–380. doi: 10.1016/j.neuroimage.2011.06.027

Caspers, S., Schleicher, A., Bacha-Trams, M., Palomero-Gallagher, N., Amunts, K., and Zilles, K. (2013). Organization of the human inferior parietal lobule based on receptor architectonics. *Cereb. Cortex* 23, 615–628. doi: 10.1093/cercor/bhs048

Chiou, S. Y., Wang, R. Y., Liao, K. K., Wu, Y. T., Lu, C. F., and Yang, Y. R. (2013). Co-activation of primary motor cortex ipsilateral to muscles contracting in a unilateral motor task. *Clin. Neurophysiol.* 124, 1353–1363. doi: 10.1016/j.clinph.2013.02.001

Contreras-Vidal, J. L., Bhagat, N. A., Brantley, J., Cruz-Garza, J. G., He, Y., Manley, Q., et al. (2016). Powered exoskeletons for bipedal locomotion after spinal cord injury. *J. Neural Eng.* 13, 031001–0310017. doi: 10.1088/1741-2560/13/3/031001

Cunnington, R., Bradshaw, J. L., and Iansek, R. (1996). The role of the supplementary motor area in the control of voluntary movement. *Hum. Mov. Sci.* 15, 627–647. doi: 10.1016/0167-9457(96)00018-8

Delorme, A., and Makeig, S. (2004). EEGLAB: an open source toolbox for analysis of single-trial EEG dynamics including independent component analysis. *J. Neurosci. Methods* 134, 9–21. doi: 10.1016/j.jneumeth.2003.10.009

Disbrow, E., Roberts, T., and Krubitzer, L. (2000). Somatotopic organization of cortical fields in the lateral sulcus of *Homo sapiens*: evidence for SII and PV. *J. Comp. Neurol.* 418, 1–21. doi: 10.1002/(SICI)1096-9861(20000228)418:1<1::AID-CNE1>3.0.CO;2-P

Donati, A. R. C., Shokur, S., Morya, E., Campos, D. S. F., Moioli, R. C., Gitti, C. M., et al. (2016). Long-term training with a brain-machine interface-based gait protocol induces partial neurological recovery in paraplegic patients. *Sci. Rep.* 6:30383. doi: 10.1038/srep30383

Donoho, D. L. (2006). Compressed sensing. *IEEE Trans. Inf. Theory* 52, 1289–1306. doi: 10.1109/TIT.2006.871582

Eickhoff, S. B., Grefkes, C., Zilles, K., and Fink, G. R. (2007). The somatotopic organization of cytoarchitectonic areas on the human parietal operculum. *Cereb. Cortex* 17, 1800–1811. doi: 10.1093/cercor/bhl090

Faber, L. G., Maurits, N. M., and Lorist, M. M. (2012). Mental fatigue affects visual selective attention. *PLoS ONE* 7:e48073. doi: 10.1371/journal.pone.0048073

Fitzsimmons, N. A., Lebedev, M. A., Peikon, I. D., and Nicolelis, M. A. L. (2009). Extracting kinematic parameters for monkey bipedal walking from cortical neuronal ensemble activity. *Front. Integr. Neurosci* 3:3. doi: 10.3389/neuro.07.003.2009

Gancet, J., Ilzkovitz, M., Motard, E., Nevatia, Y., Letier, P., De Weerdt, D., et al. (2012). "MINDWALKER: Going one step further with assistive lower limbs exoskeleton for SCI condition subjects," in *Proceedings of the IEEE RAS and EMBS International Conference on Biomedical Robotics and Biomechatronics* (Rome), 1794–1800.

Hochberg, L. R., Bacher, D., Jarosiewicz, B., Masse, N. Y., Simeral, J. D., Vogel, J., et al. (2012). Reach and grasp by people with tetraplegia using a neurally controlled robotic arm. *Nature* 485, 372–375. doi: 10.1038/nature11076

Inoue, K., Yamashita, T., Harada, T., and Nakamura, S. (2002). Role of human SII cortices in sensorimotor integration. *Clin. Neurophysiol*. 113, 1573–1578. doi: 10.1016/S1388-2457(02)00162-1

Jiang, N., Gizzi, L., Mrachacz-Kersting, N., Dremstrup, K., and Farina, D. (2015). A brain–computer interface for single-trial detection of gait initiation from movement related cortical potentials. *Clin. Neurophysiol*. 126, 154–159. doi: 10.1016/j.clinph.2014.05.003

Kawase, T., Yoshimura, N., Kambara, H., and Koike, Y. (2017). Controlling an electromyography-based power-assist device for the wrist using electroencephalography cortical currents. *Adv. Robot*. 31, 88–96. doi: 10.1080/01691864.2016.1215935

King, C. E., Wang, P. T., Chui, L. A., Do, A. H., and Nenadic, Z. (2013). Operation of a brain-computer interface walking simulator for individuals with spinal cord injury. *J. Neuroeng. Rehabil*. 10:77. doi: 10.1186/1743-0003-10-77

Labriffe, M., Annweiler, C., Amirova, L. E., Gauquelin-Koch, G., Ter Minassian, A., Leiber, L.-M., et al. (2017). Brain activity during mental imagery of gait versus gait-like plantar stimulation: a novel combined functional MRI paradigm to better understand cerebral gait control. *Front. Hum. Neurosci*. 11:106. doi: 10.3389/fnhum.2017.00106

la Fougère, C., Zwergal, A., Rominger, A., Förster, S., Fesl, G., Dieterich, M., et al. (2010). Real versus imagined locomotion: a [18F]-FDG PET-fMRI comparison. *Neuroimage* 50, 1589–1598. doi: 10.1016/j.neuroimage.2009.12.060

Lesser, R. P., Crone, N. E., and Webber, W. R. S. (2010). Subdural electrodes. *Clin. Neurophysiol*. 121, 1376–1392. doi: 10.1016/j.clinph.2010.04.037

Meier, J. D., Aflalo, T. N., Kastner, S., and Graziano, M. S. (2008). Complex organization of human primary motor cortex: a high-resolution fMRI study. *J. Neurophysiol*. 100, 1800–1812. doi: 10.1152/jn.90531.2008

Nichols, T. E., and Holmes, A. P. (2002). Nonparametric permutation tests for functional neuroimaging: a primer with examples. *Hum. Brain Mapp*. 15, 1–25. doi: 10.1002/hbm.1058

Pereira, J., Ofner, P., Schwarz, A., Sburlea, A. I., and Müller-Putz, G. R. (2017). EEG neural correlates of goal-directed movement intention. *Neuroimage* 149, 129–140. doi: 10.1016/j.neuroimage.2017.01.030

Sato, M. (2001). Online model selection based on the variational bayes. *Neural Comput*. 13, 1649–1681. doi: 10.1162/089976601750265045

Sato, M., Yoshioka, T., Kajihara, S., Toyama, K., Goda, N., Doya, K., et al. (2004). Hierarchical bayesian estimation for MEG inverse problem. *Neuroimage* 23, 806–826. doi: 10.1016/j.neuroimage.2004.06.037

Serruya, M. D., Hatsopoulos, N. G., Paninski, L., Fellows, M. R., and Donoghue, J. P. (2002). Instant neural control of a movement signal. *Nature* 416, 141–142. doi: 10.1038/416141a

Severens, M., Perusquia-Hernandez, M., Nienhuis, B., Farquhar, J., and Duysens, J. (2015). Using actual and imagined walking related desynchronization features in a BCI. *IEEE Trans. Neural Syst. Rehabil. Eng*. 23, 877–886. doi: 10.1109/TNSRE.2014.2371391

Shih, J. J., Krusienski, D. J., and Wolpaw, J. R. (2012). Brain-computer interfaces in medicine. *Mayo Clin. Proc*. 87, 268–279. doi: 10.1016/j.mayocp.2011.12.008

Sira, C. S., and Mateer, C. A. (2014). "Frontal lobes," in *Encyclopedia of the Neurological Sciences*, eds M. J. Aminoff and R. B. Daroff (Oxford: Elsevier Ltd.), 358–365.

Stockton, L., and Parker, D. (2002). Pressure relief behaviour and the prevention of pressure ulcers in wheelchair users in the community. *J. Tissue Viability* 12, 84–99. doi: 10.1016/S0965-206X(02)80031-6

Talukdar, U., and Hazarika, S. M. (2017). "Estimation of mental fatigue during EEG based motor imagery," in *Lecture Notes in Computer Science (Including Subseries Lecture Notes in Artificial Intelligence and Lecture Notes in Bioinformatics)*, eds A. Basu, S. Das, P. Horain, and B. Samit (Cham: Springer), 122–132.

Taylor, D. M., Tillery, S. I. H., Schwartz, A. B., Craggs, M., Wolpaw, J. R., Chapin, J. K., et al. (2002). Direct cortical control of 3D neuroprosthetic devices. *Science* 296, 1829–1832. doi: 10.1126/science.1070291

Toda, A., Imamizu, H., Kawato, M., and Sato, M. (2011). Reconstruction of two-dimensional movement trajectories from selected magnetoencephalography cortical currents by combined sparse Bayesian methods. *Neuroimage* 54, 892–905. doi: 10.1016/j.neuroimage.2010.09.057

Velliste, M., Perel, S., Spalding, M. C., Whitford, A. S., and Schwartz, A. B. (2008). Cortical control of a robotic arm for self-feeding. *Nature* 453, 1098–1101. doi: 10.1038/nature06996

Waldert, S., Preissl, H., Demandt, E., Braun, C., Birbaumer, N., Aertsen, A., et al. (2008). Hand movement direction decoded from MEG and EEG. *J. Neurosci*. 28, 1000–1008. doi: 10.1523/JNEUROSCI.5171-07.2008

Wessberg, J., Stambaugh, C. R., Kralik, J. D., Beck, P. D., Laubach, M., Chapin, J. K., et al. (2000). Real-time prediction of hand trajectory by ensembles of cortical neurons in primates. *Nature* 408, 361–365. doi: 10.1038/35042582

Wolpaw, J. R., Birbaumer, N., McFarland, D. J., Pfurtscheller, G., and Vaughan, T. M. (2002). Brain-computer interfaces for communication and control. *Clin. Neurophysiol*. 113, 767–791. doi: 10.1016/S1388-2457(02)00057-3

Xu, R., Jiang, N., Mrachacz-Kersting, N., Lin, C., Asin Prieto, G., Moreno, J. C., et al. (2014). A closed-loop brain-computer interface triggering an active ankle-foot orthosis for inducing cortical neural plasticity. *IEEE Trans. Biomed. Eng*. 61, 2092–2101. doi: 10.1109/TBME.2014.2313867

Yamashita, O., Sato, M. A., Yoshioka, T., Tong, F., and Kamitani, Y. (2008). Sparse estimation automatically selects voxels relevant for the decoding of fMRI activity patterns. *Neuroimage* 42, 1414–1429. doi: 10.1016/j.neuroimage.2008.05.050

Yang, H., Guan, C., Wang, C. C., and Ang, K. K. (2015). Detection of motor imagery of brisk walking from electroencephalogram. *J. Neurosci. Methods* 244, 33–44. doi: 10.1016/j.jneumeth.2014.05.007

Yoshimura, N., DaSalla, C. S., Hanakawa, T., Sato, M. A., and Koike, Y. (2012). Reconstruction of flexor and extensor muscle activities from electroencephalography cortical currents. *Neuroimage* 59, 1324–1337. doi: 10.1016/j.neuroimage.2011.08.029

Yoshimura, N., Nishimoto, A., Belkacem, A. N., Shin, D., Kambara, H., Hanakawa, T., et al. (2016). Decoding of covert vowel articulation using electroencephalography cortical currents. *Front. Neurosci*. 10:175. doi: 10.3389/fnins.2016.00175

Yoshioka, T., Toyama, K., Kawato, M., Yamashita, O., Nishina, S., Yamagishi, N., et al. (2008). Evaluation of hierarchical bayesian method through retinotopic brain activities reconstruction from fMRI and MEG signals. *Neuroimage* 42, 1397–1413. doi: 10.1016/j.neuroimage.2008.06.013a

Conflict of Interest Statement: The authors declare that the research was conducted in the absence of any commercial or financial relationships that could be construed as a potential conflict of interest.

The reviewer FF and handling Editor declared their shared affiliation.

frontiers in Neuroscience

ORIGINAL RESEARCH
published: 14 February 2018
doi: 10.3389/fnins.2018.00071

Gastrocnemius Myoelectric Control of a Robotic Hip Exoskeleton Can Reduce the User's Lower-Limb Muscle Activities at Push Off

Lorenzo Grazi[1*†], *Simona Crea*[1†], *Andrea Parri*[1], *Raffaele Molino Lova*[2], *Silvestro Micera*[1,3] *and Nicola Vitiello*[1,2]

[1] *The BioRobotics Institute, Scuola Superiore Sant'Anna, Pisa, Italy,* [2] *Fondazione Don Carlo Gnocchi, Firenze, Italy,* [3] *Bertarelli Foundation Chair in Translation Neuroengineering, Center for Neuroprosthetics and Institute of Bioengineering, School of Engineering, École Polytechnique Fédérale de Lausanne, Lausanne, Switzerland*

We present a novel assistive control strategy for a robotic hip exoskeleton for assisting hip flexion/extension, based on a proportional Electromyography (EMG) strategy. The novelty of the proposed controller relies on the use of the Gastrocnemius Medialis (GM) EMG signal instead of a hip flexor muscle, to control the hip flexion torque. This strategy has two main advantages: first, avoiding the placement of the EMG electrodes at the human–robot interface can reduce discomfort issues for the user and motion artifacts of the recorded signals; second, using a powerful signal for control, such as the GM, could improve the reliability of the control system. The control strategy has been tested on eight healthy subjects, walking with the robotic hip exoskeleton on the treadmill. We evaluated the controller performance and the effect of the assistance on muscle activities. The tuning of the assistance timing in the controller was subject dependent and varied across subjects. Two muscles could benefit more from the assistive strategy, namely the Rectus Femoris (directly assisted) and the Tibialis Anterior (indirectly assisted). A significant correlation was found between the timing of the delivered assistance (i.e., synchronism with the biological hip torque), and reduction of the hip flexors muscular activity during walking; instead, no significant correlations were found for peak torque and peak power. Results suggest that the timing of the assistance is the most significant parameter influencing the effectiveness of the control strategy. The findings of this work could be important for future studies aimed at developing assistive strategies for walking assistance exoskeletons.

Keywords: exoskeleton, EMG control, gait, hip orthosis, walking assistance

OPEN ACCESS

Edited by:
Yury Ivanenko,
Fondazione Santa Lucia (IRCCS), Italy

Reviewed by:
Scott A. Beardsley,
Marquette University, United States
Edwin Van Asseldonk,
University of Twente, Netherlands

****Correspondence:***
Lorenzo Grazi
lorenzo.grazi@santannapisa.it

† These authors have contributed equally to this work.

Specialty section:
This article was submitted to Neuroprosthetics, a section of the journal Frontiers in Neuroscience

Received: *31 August 2017*
Accepted: *29 January 2018*
Published: *14 February 2018*

Citation:
Grazi L, Crea S, Parri A, Molino Lova R, Micera S and Vitiello N (2018) Gastrocnemius Myoelectric Control of a Robotic Hip Exoskeleton Can Reduce the User's Lower-Limb Muscle Activities at Push Off. Front. Neurosci. 12:71. doi: 10.3389/fnins.2018.00071

INTRODUCTION

Over the last decades, several lower-limb exoskeletons have been developed for gait assistance of people with pathological gait patterns or for augmenting human performance of healthy individuals (Pons et al., 2008). Many control strategies have been proposed and tested, with different approaches depending mostly on the residual movement capabilities of the target end-users (Yan et al., 2015). The control strategies developed for people without movement capabilities

(e.g., complete spinal cord injury patients) aim to let the person stand and restore walking by means of predefined trajectory tracking of the lower-limb active joints (http://berkeleybionics.com; http://www.indego.com; http://rewalk.com; Wang et al., 2014). When people have residual lower-limb movement capabilities, the exoskeleton controller should be able to understand the user's intended movement, synchronize with the periodicity of the gait pattern and provide additional assistance in specific phases of the gait cycle. In this case, developing a control strategy that effectively interprets the information gathered from the sensors and delivers the necessary mechanical power to the user at the right time turns out fundamental for the exoskeleton to supply effective and natural assistance (Yan et al., 2015). In addition, the control strategy of a gait assistive device should be intuitive, in order to avoid burdening the user with an additional cognitive effort (Tucker et al., 2015).

A widely investigated assistive strategy for robotic exoskeletons consists of measuring the activation of the muscles involved in the movement by means of electromyographic (EMG) signals and applying an assistive torque proportional to the linear envelope (LE) of the EMGs, coherently with their agonist/antagonist action (Kiguchi and Imada, 2009; Kinnaird and Ferris, 2009; Sawicki and Ferris, 2009; Kao et al., 2010). Many examples can be found in the state of the art: HAL (http://www.cyberdyne.jp; Kawamoto et al., 2003), AFO (Kao et al., 2010), and KAFO (Sawicki and Ferris, 2009) use surface EMG signals to control the joint torques. In these cases, the main goal of the assistance is typically to restore a more efficient (physiological) gait pattern, that reduces the energy cost of walking (Ferris et al., 2008; Pons et al., 2008; Sawicki and Ferris, 2009) or muscular activation (Lenzi et al., 2013; Jackson and Collins, 2015).

Despite the intuitiveness of EMG proportional controllers, differently from AFOs or KAFOs, the development of a reliable EMG-based controller for a hip exoskeleton is challenging for two main reasons: first, the thigh cuffs that connect the device to the human might cover most of the thigh surface and the placement of electrodes under the cuffs may cause motion artifacts and discomfort to the user; second, in healthy subjects but also patients with muscle weakness of hip muscle groups (Lewis and Sahrmann, 2006), thigh muscle signals are not as powerful as ankle plantarflexors during walking, thus the detection of the onset of muscle activation might require complex signal processing techniques in real time.

To overcome these limitations, in this study we propose and validate a new myoelectric control strategy based on an ankle plantar-flexor muscle signal, i.e., the Gastrocnemius Medialis (GM) to control the flexion torque of an active pelvis orthosis (APO). We used the GM signal to control the hip flexion torque because its activation is easier to be collected compared to hip flexor muscle, i.e., the Rectus Femoris (RF) (Winter, 1990; Annaswamy et al., 1999) and it activates synergistically to the hip flexors in the late stance phase to accomplish swing initiation and forward progression (Winter, 1990; Mueller et al., 1994; Zajac et al., 2003).

The presented algorithm is a modified version of the one presented in Grazi et al. (2015). Compared to our previous work, in this study we included the possibility to slightly adjust the timing of the assistive torque based on the user's perception, in order to improve the human-robot synchrony.

Along with the description of the control strategy, we present the results of preliminary tests with eight healthy subjects, walking on the treadmill with the APO providing three levels of assistance, i.e., optimal, low, and high, customized on each subject. We assessed the performance of the GM EMG-based proportional controller during walking, by evaluating the synchrony of the delivered hip assistance with the hip flexors muscular activity and by assessing the effects of the assistance on lower-limb muscles activity.

Abbreviations: AM, Assistive mode; AOs, Adaptive oscillators; APO, Active Pelvis Orthosis; BF, Biceps Femoris; CV, Coefficient of variation; CoP, Center of pressure; CNS, Central nervous system; DOF, Degrees of freedom; EGP, Estimated gait phase; EMG, Electromyography; FBL, Final baseline; FPGA, Field programmable gate array; GM, Gastrocnemius Medialis; HS, Heel strike; LE, Linear envelope; RF, Rectus Femoris; SEA, Series elastic architecture; SOL, Soleus; ST, Semitendinosus; TA, Tibialis Anterior; TM, Transparent mode; vGRF, Vertical ground reaction force; VL, Vastus Lateralis.

MATERIALS AND METHODS

Experimental Apparatus

The experimental apparatus comprises three modules: (i) the APO (Giovacchini et al., 2015), (ii) a pair of shoes equipped with pressure-sensitive insoles (Crea et al., 2014), and (iii) a commercial EMG recording system.

APO

The APO is a lightweight lower-limb exoskeleton, conceived for assisting the hip flexion-extension movement (**Figure 1**). A horizontal C-shaped frame, surrounding the user's hips, and the back of the pelvis interfaces with the user's trunk by means of three orthotic shells (two lateral and one rear) and carries two actuation units, one for each hip flexion-extension joint, mounted on the lateral arms. The actuation unit employs a SEA architecture (Pratt and Williamson, 1995) and can provide torque up to 35 Nm. The actuated axes drive two carbon-fiber links molded with a shape sweeping from the lateral to the back side of the thigh. Thigh links are also endowed with a passive rotational Degrees of freedom (DOF) for abduction-adduction to provide a comfortable interaction and do not hinder the user's movement while walking. The control and power supply units of the APO are remotely located in order to reduce the load carried by the user.

The APO control system runs at 1 kHz on a real-time controller, a cRIO-9082 (National Instruments, TX, USA), which is endowed with a 1.33 GHz dual-core processor running a real-time operating system and a field programmable gate array (FPGA) processor Spartan-6 LX150.

Instrumented Shoes with Pressure Sensors

A pair of shoes was equipped with pressure-sensitive insoles for the measurement of the plantar pressure. Insoles consist of a

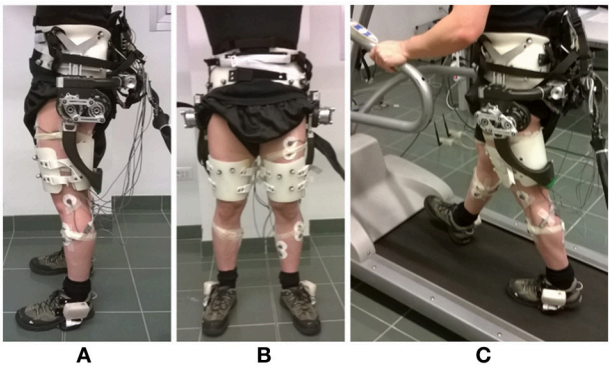

FIGURE 1 | Overview of the Active Pelvis Orthosis. **(A)** Lateral view. **(B)** Frontal view. **(C)** During treadmill walking. Instrumented shoes and EMG electrodes are also shown.

matrix of pressure sensors and an electronic board endowed with Bluetooth® modules, for communication with external devices. Pressure signals were acquired and used to online extract the position of the plantar center of pressure in the longitudinal direction (CoP) and vertical ground reaction force (vGRF) (Crea et al., 2014).

Insoles were successfully used in other online applications, such as for providing lower-limb amputees with sensory feedback related to discrete gait events (Crea et al., 2015, 2017), to control an active prosthesis during different locomotion activities (Ambrozic et al., 2014) and to control an active lower-limb exoskeleton (Yuan et al., 2015).

EMG Recording System

EMG signals were collected using pre-gelled bipolar Ag/AgCl surface electrodes (Pirrone & Co., Milan, Italy) and recorded by means of a TeleMyo 2400R EMG recording system (Noraxon Inc., AZ, USA). EMG signals were sampled at 1.5 kHz and low-pass filtered at 500 Hz by the EMG recording system. These biosignals are used both as feeding signals to the controller and to record muscles activity patterns during walking.

System Integration

The data gathered from the three modules were integrated into the control system as depicted in **Figure 2A**.

Data measured by the instrumented shoes were sent to a host PC through a Bluetooth® connection, read through a dedicated LabVIEW 2013 routine and, from the host PC, sent to the APO control board by means of a UDP connection.

The EMG recorder analog outputs were connected to the APO control board, i.e., the analog input channels of the cRIO-9082 FPGA. Data were acquired at 1 kHz and processed in real-time (**Figure 2C**).

Data were visualized on the host PC running a real-time LabVIEW 2013 Graphical User Interface (GUI). The GUI allowed also to set the parameters of the controller, and to save data for offline analysis.

APO Control Architecture

The control system is based on a two-layer hierarchical architecture (**Figure 2B**): the low-level layer, which implements the torque control loop in order to set the current to the motor drivers, and the high-level layer, which implements the assistive control strategy.

Low-level control. The low-level torque control is designed to manage the actuators in order to follow a desired torque value. The closed-loop controller is a two-pole-two-zero compensator operating on the error between the desired (τ_{des}) and actual (τ) torques. More details are reported in (Giovacchini et al., 2015).

High-level control. The high-level control relies on a two-step algorithm: the first step allows the estimation of the gait phase and the second step allows the calculation of the desired assistive torque.

Gait Phase Estimator

This block aims at estimating the current gait phase in real time by means of adaptive oscillators (AOs) (Ronsse et al., 2011, 2013). The vGRF signals from the sensorized insoles are the inputs for the AOs which, in turn, are used to estimate the current gait phase (EGP); the CoP information allows detecting the heel strike (HS) event and reset the phase given by the AOs (Yan et al., 2016). The APO control architecture using AOs and the HS event to reset the phase has been presented and validated in the work by Ruiz Garate et al. (2016). The computed gait phase ranges between 0 and 2π rad, corresponding to $[0 \div 100]$ % of the stride period (the 0% of the stride corresponding to the HS and the 100% to the subsequent HS of the same foot). The EGP is computed unilaterally for the left leg and the assumption of gait symmetry is considered.

Linear Envelope Calculator

The EMG raw signal is high-pass filtered (second-order Butterworth, cut-off frequency: 20 Hz), rectified and then low-pass filtered (second-order Butterworth, cut-off frequency: 3 Hz) to obtain a LE of the EMG signal (Kinnaird and Ferris, 2009).

Assistive Torque Generator

The computed GM LE and EGP are used to calculate the assistive torque. The assistive torque is calculated when the EGP ranges between 20 and 60%: indeed, according to Winter's data (Winter, 1990), this phase corresponds to the hip flexors and GM activity in the propulsion phase. Within the selected gait phase window, when the online LE overcomes a threshold (i.e., five times the standard deviation of the GM signal during resting, as suggested by Kinnaird and Ferris (2009) the LE is multiplied by a gain, k, to obtain the desired torque. The assistive torque could be delayed by a percentage of the gait cycle, T, based on the user's subjective perception of the assistance (1):

$$\begin{cases} \tau(t) = k \cdot LE_{GM}(t - \Delta t) \\ \Delta t = \frac{2\pi \cdot T}{|Freq_{gait}|} \end{cases} \quad (1)$$

where τ is the assistive torque, t is time, and t is the time delay corresponding to T. t is a function of the gait frequency

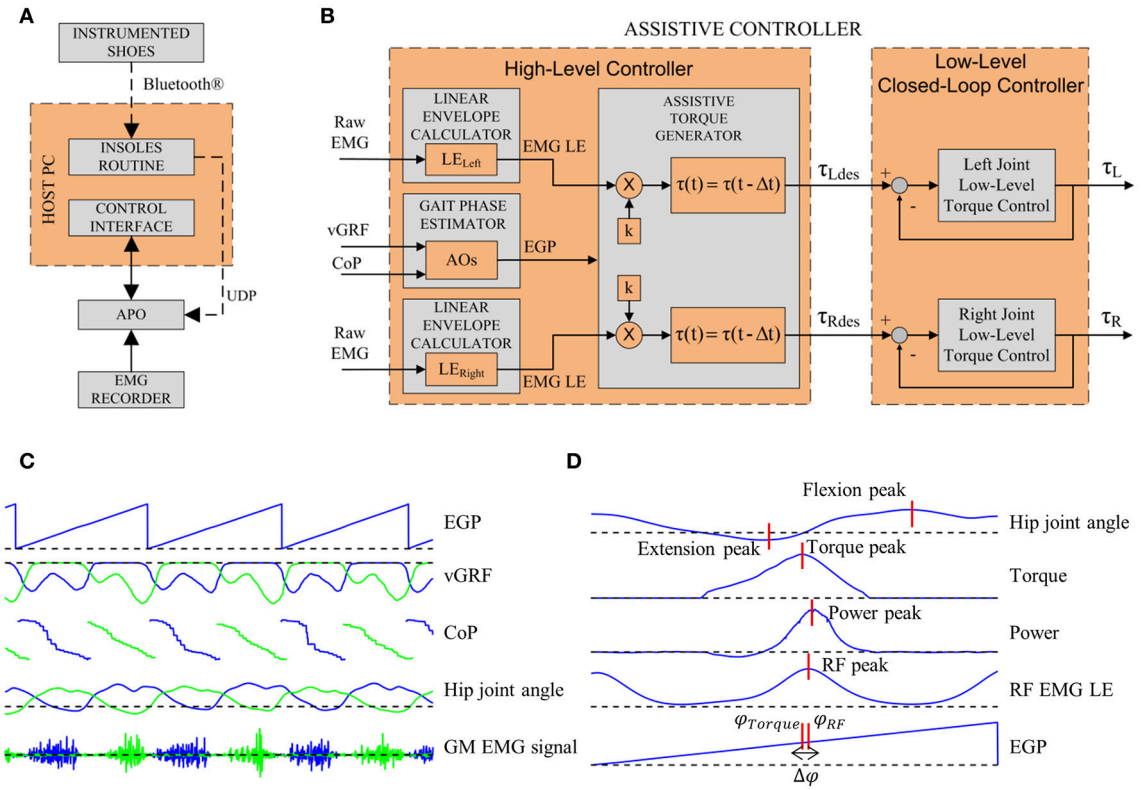

FIGURE 2 | (A) Sub-modules of the experimental apparatus. **(B)** Architecture of the assistive controller. The inputs for the high-level control layer are the left vGRF, the CoP and the raw EMG signals of left and right GM muscles. The Gait Phase Estimator block computes the EGP. The Assistive Torque Generator block computes the LE. Each LE is then multiplied by k and delayed by Δt. The outputs of the high-level control layer are the torque reference control signals for the low-level closed-loop controller. **(C)** EGP, vGRF, CoP, hip joint angle, and GM EMG signals for a few steps. Blue lines represent data from the left side, green lines represent data from the right side. **(D)** Parameters extracted.

$Freq_{gait}$–computed by the AOs—and T. T could be set up to 10%, according to the user's perception of a comfortable timing for assistance.

Experimental Procedures

Upon arrival, the participant was informed about the study and asked to sign the written informed consent. Then s/he was asked to wear short sport pants, to allow easy placement of EMG electrodes, and wear the instrumented shoes.

The EMG electrodes were placed on the subject's left limb according to SENIAM recommendations (Hermens et al., 2000). The following muscles signals were recorded: Tibialis Anterior (TA), Vastus Lateralis (VL), Soleus (SOL), RF, Biceps Femoris (BF), Semitendinosus (ST), and GM. GM was recorded on the right and left limbs since it was necessary for generating the assistive torque.

Before wearing the APO, the subject was first requested to sit for 30 s, in order to record the EMG baseline signals and calculate the threshold for LE, and then to walk on the treadmill for 3 min at self-selected speed, in order to record the initial baseline (IBL) of the EMG activity during walking.

After the IBL was measured, the subject was asked to wear the exoskeleton, with the help of the experimenter.

A familiarization session was performed to tune the parameters for the assistive controller, i.e., the gain k and the phase delay T and let the subject familiarize with the assistance, walking at self-selected speed. Manual tuning was performed in two steps: first, T was set to 0% (i.e., the delivered torque was proportional to the GM EMG activation with no delay) and k was slowly increased from 0 until the maximum value for providing comfortable assistance; second, T was slightly modified in order to further increase the perception of comfort. Some iterations of the two steps could be repeated to fine tune the combination of the two parameters.

The testing session consisted of three trials with rests in between. Within each trial 3 min walking in assistive mode (AM) and 2 min walking in transparent mode (TM) were alternated. Within each single trial, three different levels of assistance were tested: the k-value set during the familiarization session (k_{100}) was used to provide the "optimal" level of assistance (AM_{100}); k was then scaled to 50% (k_{50}) to provide the "low" level of assistance (AM_{50}), and increased of 150% (k_{150}) to provide the "high" level of assistance (AM_{150}). The order of occurrence of the three assistive levels was randomized among trials and subjects.

After completing the three testing trials, subjects were requested to perform a 3 min walking session without the exoskeleton, in order to record the final EMG baseline (FBL).

Participants

Eight healthy volunteers (5 male, age: 25 ± 1 years, height: 175.2 ± 7.2 cm, weight: 66.6 ± 4.6 kg) participated to the study.

Experimental trials were carried out at the premises of the rehabilitation center Fondazione Don Carlo Gnocchi (Florence, Italy). The experimental procedures were approved by the local Ethical Committee and carried out in accordance with the Declaration of Helsinki.

Data Analysis

EMG and exoskeleton data were saved for offline analysis. Data were segmented into strides, using the gait phase estimated online. For each trial, strides of the last minute of each condition were used to extract the following gait parameters, as depicted in **Figure 2D**:

- Maximum hip flexion angle;
- Maximum hip extension angle;
- Delivered peak hip torque, τ_{peak};
- Gait phase at the torque peak, φ_{torque};
- Power peak.

The eight LE signals were normalized by the median value of the maxima values determined in each stride of the last minute of the IBL. Normalization was done to allow inter-subject comparison. Normalized LE signals were processed to extract the following EMG parameters:

- LE peak;
- Gait phase at the RF LE peak, φ_{RF};
- Gait phase at the GM LE peak, φ_{GM};
- LE peak coefficient of variation, CV.

For each stride we calculated the parameter $\Delta\varphi$ as the difference between φ_{RF} and φ_{torque}. $\Delta\varphi$ was used to assess the synchronicity of the torque provided by the exoskeleton with the RF EMG activity. Median values and interquartile ranges of $\Delta\varphi$ were extracted for each AM in each trial. For each stride we computed $\Delta\psi$ as the difference between φ_{RF} and φ_{GM}. $\Delta\psi$ was computed for IBL and AM conditions, to quantify the phase difference among the muscles activation peak and assess the goodness of the tuning procedure for the parameter T. Moreover, across-subjects average of the coefficients of variation (CV) were computed for RF and GM peaks with the goal of assessing the variability of the control signal. CVs were calculated from IBL data.

Statistics

Friedman test was used to check for across-condition differences of gait and EMG parameters and when appropriate Wilcoxon signed-rank test was used for *post-hoc* paired comparison. The significance level was set to 0.05.

Pearson correlation was computed to check for correlations between the percentage variation of the EMG RF signal and one of the following parameters: $\Delta\varphi$, peak torque and peak power values. When significant correlation was found ($p < 0.05$), robust regression was computed and data were checked to find possible outliers by evaluating the residuals of the regression; residuals were identified by applying bisquare weighting method.

Data analysis and statistics were performed using Matlab R2017a (The Mathworks, MA, USA). All statistics were considered significant for $p < 0.05$.

RESULTS

Controller Performance

The across-subjects averaged $\Delta\varphi$ values did not show significant differences among conditions ($p = 0.19$, $\chi^2 = 3.25$, dof = 2): 8.5 ± 3.7 % for AM_{50}, 7.7 ± 3.1 % for AM_{100}, and 7.9 ± 4.2 % for AM_{150}. Positive values of $\Delta\varphi$ indicate that, within the stride, RF peaks occur later than the GM peaks. Values for each subject are reported in **Table 1**.

No significant differences were observed in the across-subjects averaged $\Delta\psi$-values among conditions ($p = 0.82$, $\chi^2 = 0.9$, dof = 3): for IBL 13.7 ± 6.6, 15.1 ± 3.0% for AM_{50}, 14.9 ± 2.1% for AM_{100}, and 15.0 ± 4.0% for AM_{150}. **Table 2** reports values for each subject.

Goodness of the tuning procedure of the parameter T was evaluated by comparing T with $\Delta\psi$ (the difference between these two parameters is $\Delta\varphi$); as the goodness of the tuning procedure decreased, $\Delta\varphi$-values increased.

Finally, the CV of the RF peak was greater than the one corresponding to the GM (0.72 compared to 0.37).

Gait Adaptation to the Assistance

Kinematics and Dynamics

Kinematic and dynamic parameters are reported only for one side. Hip angle profiles for one representative subject are shown in **Figure 3A.** The across-subject average of the maximum and minimum peak angle values increased with higher levels of assistance (**Figure 3B**), and such variations were statistically significant ($p < 0.05$, $\chi^2 = 13.63$, dof = 3 for flexion peaks; $p < 0.05$, $\chi^2 = 17.63$, dof = 3 for extension peaks).

In the k_{100} condition, the delivered torque was on average around 6.0 ± 0.8 Nm. Under k_{50}, with lower assistance, the torque peak was 3.0 ± 0.5 Nm, whereas in k_{150} condition with high assistance the torque peak was 9.0 ± 1.1 Nm. The mechanical power peak changed accordingly (17.0 ± 5.3 W for AM_{100}, 7.0 ± 2.7 W for AM_{50}, and 28.0 ± 8.3 W for AM_{150}).

EMG Analysis

EMG pattern profiles for those muscles whose activity showed differences between conditions are shown in **Figure 4A** for one representative subject; normalized EMG data are depicted in **Figure 4B** as across-subjects average values. Note that only TA peaks reported significant EMG variations across conditions ($p = 0.001$, $\chi^2 = 20.24$, dof = 5). TA, RF and GM showed increased EMG activity when subjects walked under TM compared to IBL and FBL; on the contrary, EMG activity of ST reduced. Compared to the TM condition, TA, RF, and GM peaks, in the propulsion phase, decreased in all the AM conditions. For the ST, the muscle activity increased in all AM conditions with respect to TM. In general, baselines were similar before (IBL) and

TABLE 1 | Controller parameters. Median and interquartile ranges for $\Delta\varphi$ and τ_{peak} for each subject along with T and k_{100} values.

Subject	T (%)	k_{100}	AM_{50}		AM_{100}		AM_{150}	
			$\Delta\varphi$ (%)	τ_{peak} (N·m)	$\Delta\varphi$ (%)	τ_{peak} (N·m)	$\Delta\varphi$ (%)	τ_{peak} (N·m)
1	6.5	130	10.7 (8.2–12.0)	3.00 (2.75–3.25)	8.0 (6.5–9.9)	6.40 (5.82–6.93)	7.7 (5.0–11.1)	8.44 (7.75–9.15)
2	7.5	70	6.0 (3.5–9.1)	2.44 (2.30–2.74)	5.5 (2.0–9.8)	5.77 (4.93–6.25)	5.5 (3.7–7.9)	10.22 (9.64–10.94)
3	4.5	90	10.4 (8.4–14.4)	2.58 (2.41–2.74)	10.2 (7.7–11.7)	4.69 (4.26–5.04)	15.7 (13.8–17.9)	6.86 (6.43–7.70)
4	6.0	80	13.9 (11.6–16.0)	2.53 (2.32–2.74)	10.8 (8.7–12.6)	6.28 (5.56–6.77)	11.2 (6.7–14.3)	9.84 (9.05–11.64)
5	6.5	140	9.7 (7.4–10.9)	3.55 (3.18–3.86)	9.0 (8.0–10.3)	7.55 (6.58–8.81)	9.0 (7.5–10.7)	10.39 (9.49–11.08)
6	1.5	110	10.0 (8.9–10.7)	4.08 (3.32–4.76)	10.8 (8.7–12.7)	6.75 (6.13–8.05)	8.0 (7.2–9.3)	11.84 (10.33–13.07)
7	9.0	50	2.4 (1.9–2.9)	3.35 (3.04–3.80)	2.5 (1.9–3.1)	5.74 (5.13–6.31)	3.0 (1.9–3.8)	9.39 (8.99–10.08)
8	6.5	65	4.8 (3.1–10.1)	2.35 (2.17–2.53)	4.6 (3.5–5.5)	5.08 (4.49–5.64)	3.3 (1.8–6.1)	7.46 (6.70–8.06)

TABLE 2 | $\Delta\psi$ median values and interquartile ranges for each subject for the initial baseline and all assistive conditions.

Subject	IBL	AM_{50}	AM_{100}	AM_{150}
	$\Delta\psi$ (%)	$\Delta\psi$ (%)	$\Delta\psi$ (%)	$\Delta\psi$ (%)
1	14.8 (14–16.3)	15.7 (13.4–17.6)	15.3 (13.5–16.5)	14.5 (12.2–16.9)
2	12.6 (11.8–13.5)	14.1 (12.7–15.8)	13.7 (10.3–16.1)	12.4 (11.4–15.2)
3	11.8 (10.8–12.8)	16.1 (13.8–20.9)	15.2 (6.7–17.6)	22.2 (19.8–24.5)
4	23.3 (20.8–25.4)	21.2 (19.4–23.1)	18.8 (16.7–21.5)	19.0 (14.8–21.9)
5	17 (16.2–19)	16.7 (15.4–17.5)	16.9 (15.7–18.5)	17.2 (15.6–18.7)
6	13.1 (7.4–18)	12.7 (11.8–13.3)	13.6 (11.9–15.4)	11.0 (9.8–12.1)
7	14.4 (13–16.8)	12.6 (12.0–13.3)	13.4 (12.6–14.4)	13.1 (12.3–14.1)
8	16.3 (14.4–19.5)	11.6 (9.9–14.0)	12.2 (11.1–13.3)	10.9 (10.0–14.4)

after (FBL) the experimental session, except for ST, which showed increased FBL EMG activity.

Figure 5 shows Pearson correlation analysis for RF EMG variations and $\Delta\varphi$. In the assistive conditions, correlation coefficients were found to increase with the assistance: $r = 0.52$ in AM_{50}, $r = 0.64$ in AM_{100}, $r = 0.73$ in AM_{150}; moreover, also their significance increased with the assistance: no significance was found in AM_{50} ($p = 0.18$) and AM_{100} ($p = 0.08$), whereas significance was reached in AM_{150} ($p < 0.05$). For AM_{150}, robust regression was performed and one outlier was found (corresponding to subject #6); once removed we obtained $r = 0.84$ ($p < 0.02$). No significant correlations were found for torque peaks ($p = 0.09$ in AM_{50}, $p = 0.22$ in AM_{100}, $p = 0.97$ in AM_{150}) and power peaks ($p = 0.8$ in AM_{50}, $p = 0.25$ in AM_{100}, $p = 0.19$ in AM_{150}).

DISCUSSION

Several studies showed that human Central nervous system (CNS) implements different strategies to adapt to external forces or disturbances, in order to ensure efficient locomotion (Kiguchi and Imada, 2009; Kinnaird and Ferris, 2009; Kao et al., 2010; Lewis and Ferris, 2011; Ronsse et al., 2011; Lenzi et al., 2013). In order to develop intuitive and effective control strategies for gait assistance and avoid muscle co-contractions, the assistive torque must be provided to the joint with perfect synchrony with the torque exerted by the biological limb, namely a coordination between the human and the exoskeleton must be established (Cenciarini and Dollar, 2011). To do so, state-of-the-art EMG controllers typically use the myoelectric signal measured from the muscles directly involved in the assisted action and provide an assistive torque proportional to the muscle activation (Kinnaird and Ferris, 2009; Sawicki and Ferris, 2009; Kao et al., 2010).

In the state of the art, many studies investigated the optimal assistance timing for ankle exoskeletons (Kinnaird and Ferris, 2009; Malcolm et al., 2013, 2015; Mooney et al., 2014; Collins et al., 2015; Jackson and Collins, 2015; Galle et al., 2017), whereas only few more recent studies have explored this issue for hip exoskeletons (Ding et al., 2016; Lee et al., 2017; Young et al., 2017b). Ding and colleagues investigated the effect of timing of hip extension assistance on biological joint power and metabolic cost of walking by means of a soft exosuit (Ding et al., 2016). The soft exosuit was used to deliver different hip assistive profiles, with the main goal of studying how the selection of the onset and the duration of the assistive torque can affect the metabolic cost of walking and found clear correlation between the two parameters. Similarly, Young and colleagues investigated the optimal timing to deliver the hip assistance through a hip exoskeleton and found that the subjective perception of the delivery timing did not correlate with the higher reduction in the metabolic cost (Young et al., 2017b); this result suggests that relying on this information would maybe improve the subjective perceived comfort of the user but not necessarily bring to optimal results in terms of metabolic consumption. Lee and colleagues explored the effects of different assistance timings on metabolic cost and gait parameters (e.g., step length and

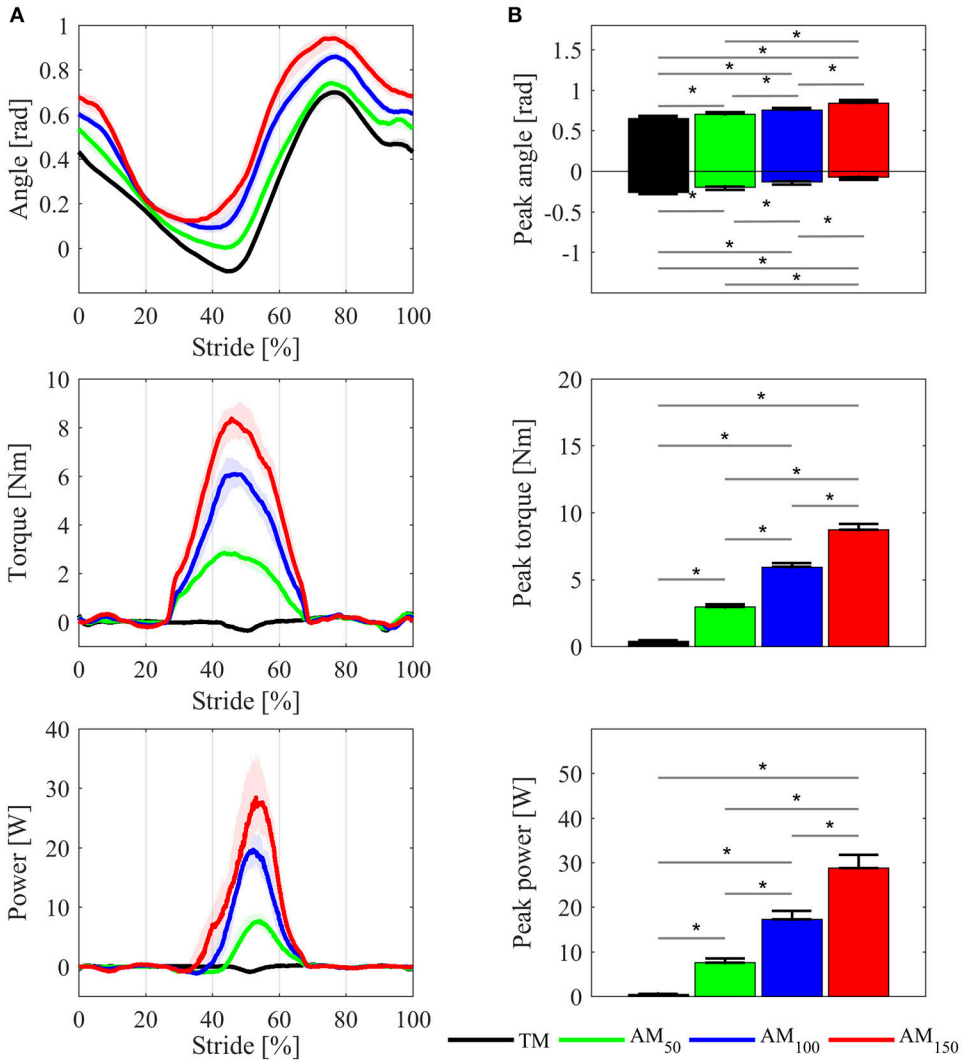

FIGURE 3 | Comparisons of the APO kinematic and dynamic variables between TM, AM_{50}, AM_{100}, and AM_{150} conditions. **(A)** Hip joint angles, delivered torque and mechanical power profiles for one representative subject; variables are plotted as median values and interquartile range contours of left hip joint. **(B)** Maximum and minimum hip flexion angle, torque peak, and power peak, averaged over all subjects: mean values ± SE. Asterisks denote $p < 0.05$.

cadence) by means of an exoskeleton conceptually similar to the APO (Lee et al., 2017). In this study, researchers explored the effect of different timing offsets between the peaks of hip joint velocity and assistance power: results showed that smaller timing offsets led to higher reductions in the metabolic cost.

The novelty of the myoelectric controller proposed in this work is that it uses a calf myoelectric signal to provide a hip flexion torque during walking. During the propulsion phase, the GM together with the Achilles tendon, generates the ankle plantar-flexion torque to propel the gait, while the RF is responsible for generating the hip flexion torque (Townsend et al., 1978; Winter, 1990); in this phase, the two muscles typically show temporal synergic actions, i.e., they have almost synchronous activations (Zajac et al., 2003). Results of this study are in line with previous works. Indeed, we observed that the assistance was more effective when the assistance peak was synchronous with the RF EMG peak.

The analysis of EMG peaks revealed that two muscles can benefit more from the assistance when compared to the TM. While the reduction of the RF signal could be a direct effect of the provided hip flexion torque, the significant reduction of the TA activation can be explained by the induced increase of the foot clearance (due to the increased hip flexion angle). In addition, the resulting increased flexion and extension hip angles in all AM conditions were in line with previous studies with hip-assistive exoskeletons (Ronsse et al., 2011; Lenzi et al., 2013; Young et al., 2017b). However, while TA normalized EMGs showed reduced activation also with respect to the baselines, RF normalized EMGs resulted higher, which could be explained by the fact that the

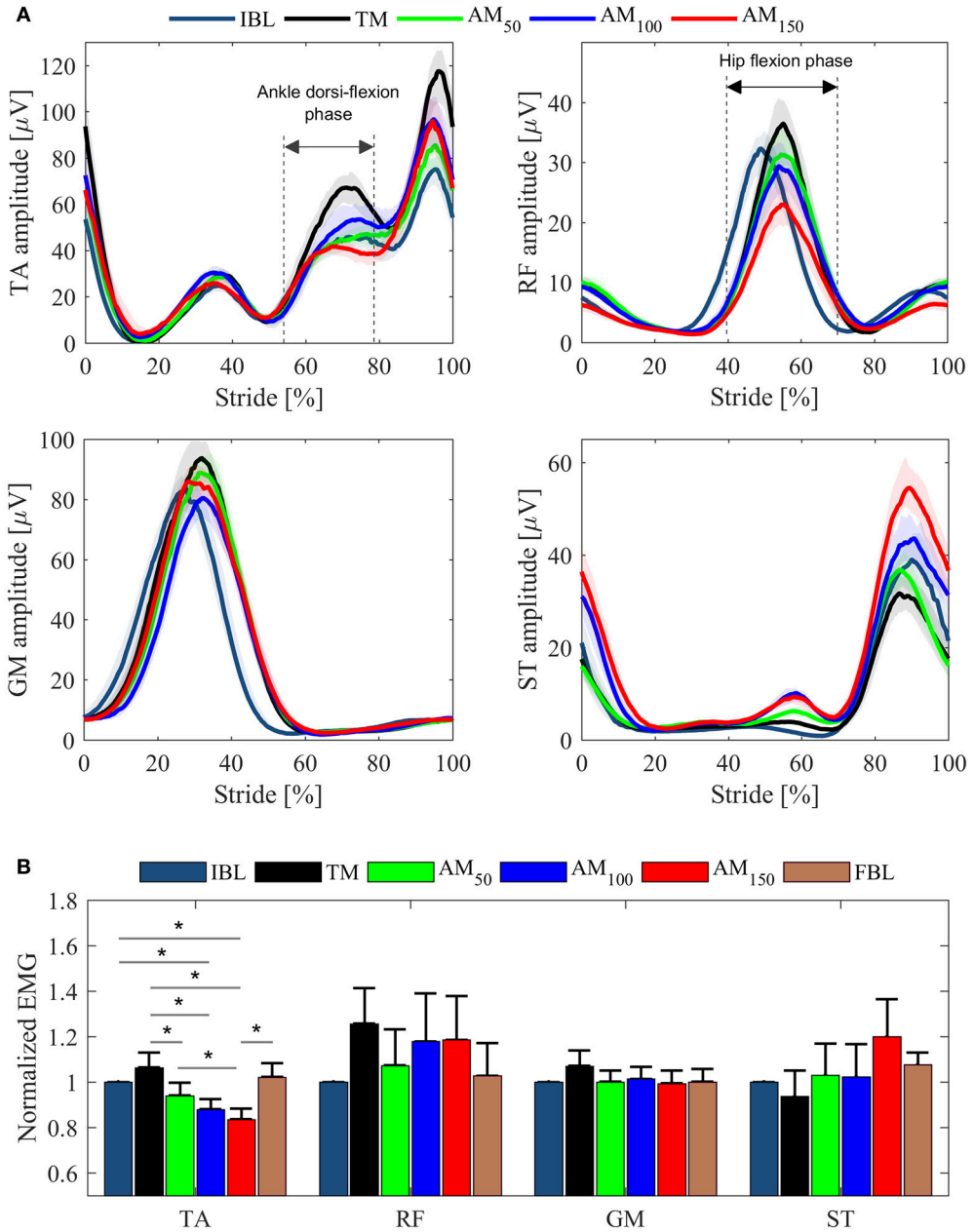

FIGURE 4 | EMG data from left leg muscles (TA, RF, GM, ST) for the last minute of each tested condition. **(A)** EMG LE activation profiles for one representative subject. Profiles are shown as median values and interquartile range contours. **(B)** EMG peaks averaged over all subjects. Mean values ± SE are shown. Data are normalized for the IBL activation peak.

synchronism between assistance and hip flexors EMG activity was not enough to reduce muscles activations even below the baseline.

Furthermore, correlation analysis was performed to observe whether the timing parameter $\Delta\varphi$ could affect the variation of the RF EMGs. Correlation was found between $\Delta\varphi$ and RF EMG peak suggesting that lower $\Delta\varphi$ could lead to higher EMG reductions. These results could support the use of the proposed control strategy and suggest, for future studies, its use to further investigate how different assistance timing could affect muscles activity. However, due to the small sample size of this study, it is difficult to draw definitive conclusions on the effect of assistance timing, although evidences from other studies support these results.

As in Young et al. (2017b), in our study we relied on the subjective perception during the tuning procedure of the assistance and adjusted the torque delivery timing. Similarly, our results show that, in some cases, the subjective perception

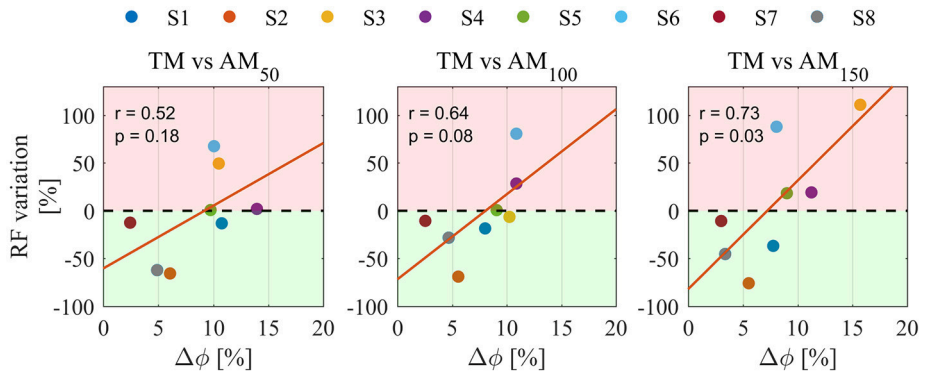

FIGURE 5 | Pearson correlation analysis between $\Delta\varphi$ and the percentage variation of RF EMGs for all assistance levels. Pearson correlation coefficient r and the level of significance p, are reported for each condition. Percentage variations are calculated for all AM conditions compared to TM. Colors are different participants. Red regions represent EMG activity increase, green regions represent EMG activity reduction. Orange lines indicate linear fit.

lead to worse synchrony between the assistance and the user's movement. Subjects may not have been able to recognize whether the assistance was synchronous enough, but could have based their judgments on the perceived comfort and stability of the gait, as pointed out in similar study (Young et al., 2017b). Furthermore, due to the poor reliability of the subjective perception, in future studies T could be rather tuned based on the computation of $\Delta\psi$ during baseline or familiarization sessions; indeed, since $\Delta\psi$ did not change across conditions, this parameter could ensure a reliable tuning procedure. In this way we could try to minimize $\Delta\varphi$ values and increase the synchrony between exoskeleton torque and hip flexors EMG activity.

Similar to other walking assistance exoskeletons (van Asseldonk et al., 2008; Ronsse et al., 2011; Winfree et al., 2011; Lenzi et al., 2012; Knaepen et al., 2014; Sylos-Labini et al., 2014) the APO "transparent mode" performance can be affected by inertia and friction, which worsen the capability of the controller to achieve null output impedance. Due to these reasons, muscular activity can increase when the exoskeletons are controlled in TM, which might be related to the resistive action of the exoskeleton on the user's movement (van Asseldonk et al., 2008; Ronsse et al., 2011; Winfree et al., 2011; Lenzi et al., 2012; Knaepen et al., 2014; Sylos-Labini et al., 2014). Similar to previous studies, our results showed that when the APO was controlled in TM, all subjects increased their RF muscular activation compared to IBL, which suggests the need to carefully consider inertia and friction compensation strategies to improve the performance in TM.

Finally, using the GM instead of the RF signal to assist the hip flexion resulted in three additional advantages. First, since the GM activation was higher than the RF activation (Winter, 1990), the signal for the control was easier to be processed online. Second, the GM signal did not suffer from motion artifacts, which, on the contrary, would have affected the RF muscle signal, due to the mechanical interaction and relative movements between the thigh cuffs and the electrodes (Young et al., 2017a). Furthermore, as reported by Winter's data (Winter, 1990), also in our data we observed that the inter-subject variability of the GM was considerably lower than the RF, thus a more reliable controller was developed.

LIMITATIONS OF THE STUDY AND FUTURE PERSPECTIVES

The goal of most robotic lower-limb exoskeletons is to reduce the metabolic cost of walking of the user (Ferris et al., 2008). Understanding how to reduce the metabolic energy expenditure of human locomotion through exoskeletons is still a complex challenge, and a huge amount of research has been done to answer this debated question (Ronsse et al., 2011; Malcolm et al., 2013, 2015; Mooney et al., 2014; Collins et al., 2015; Ding et al., 2016; Young et al., 2017b). Changes in muscles activation timing and amplitude during the utilization of lower-limb exoskeletons can be revealed by the analysis of the EMG (Ferris et al., 2008). Therefore, EMG may better reflect the changes in the metabolic energy demand with respect to, for example, the analysis of joint dynamics alone (Ferris et al., 2008). However, EMG only is still not sufficient to prove any metabolic cost reduction, thus dedicated experimental trials must be performed in future activities. Moreover, the controller presented in this study did not work with sufficient performance with all the tested subjects. The controller parameters (namely T and k) were tuned according to the user subjective perception and this might not be a reliable strategy to determine the most effective assistance profile (Young et al., 2017b); indeed, in particular the set values of T were much smaller than the baseline $\Delta\psi$ values, clearly suggesting that improvements of the tuning phase are necessary. Moreover, due to inter-subject variability, the implicit use of Winter's gait profiles as initial reference for identifying the range of the assistance timing could have introduced an additional limitation in the tuning procedure. Future developments of the control algorithm should consider automated calibration procedures to set the timing parameter. Future studies will be carried out to verify that the proposed GM-based controller improves the performance of a proportional EMG controller based on thigh muscles.

CONCLUSION

In this work, a novel assistive control strategy for an APO was presented. The GM EMG signal is recorded to provide EMG-proportional assistive torque at the hip joints.

When the assistive torque profile was synchronous with the hip flexors muscular activity, the assistance resulted in reduced activation of the assisted muscles, i.e., the RF (directly assisted) and the TA (indirectly assisted), suggesting that the proposed strategy can induce the re-modulation of muscles activations and reduce the effort.

Future works will be aimed at improving the robustness of the proposed controller by means of an automatic procedure for parameters tuning in order to reduce the source of error and maximize the synchrony of torque delivery with the hip flexors activation. Future tests will also evaluate the effects of the assistance on the metabolic consumption.

ETHICS STATEMENT

This study was carried out in accordance with the recommendations of Fondazione Don Gnocchi Ethical Committee with written informed consent from all subjects. All subjects gave written informed consent in accordance with the Declaration of Helsinki. The protocol was approved by the Fondazione Don Gnocchi Ethical Committee.

AUTHOR CONTRIBUTIONS

LG: Carried out the experimental activities and data analysis, participated in the design of the study, and drafted the manuscript; SC: Significantly contributed to the data analysis and drafted the manuscript; AP: Carried out the experimental activities and drafted the manuscript; RM: Participated in the design and supervised the study; SM and NV: Conceived the study, participated in the design, and coordination of the study; LG and SC: Equally contributed to this work. All authors approved the submitted version of the manuscript.

FUNDING

This work was supported in part by the EU within the CYBERLEGs (FP7-ICT-2011-2.1 Grant Agreement #287894) and within the CYBERLEGs Plus Plus (H2020-ICT-2016-1 Grant Agreement #731931) projects.

REFERENCES

Ambrozic, L., Gorsic, M., Geeroms, J., Flynn, L., Molino Lova, R., Kamnik, R., et al. (2014). CYBERLEGs: a user-oriented robotic transfemoral prosthesis with whole-body awareness control. *IEEE Robot. Autom. Mag.* 21, 82–93. doi: 10.1109/MRA.2014.2360278

Annaswamy, T. M., Giddings, C. J., Della Croce, U., and Kerrigan, D. C. (1999). Rectus Femoris: its role in normal gait. *Arch. Phys. Med. Rehabil.* 80, 930–934. doi: 10.1016/S0003-9993(99)90085-0

Cenciarini, M., and Dollar, A. M. (2011). Biomechanical considerations in the design of lower limb exoskeletons. *IEEE Int. Conf. Rehabil. Robot.* 2011:5975366. doi: 10.1109/ICORR.2011.5975366

Collins, S. H., Wiggin, M. B., and Sawicki, G. S. (2015). Reducing the energy cost of human walking using an unpowered exoskeleton. *Nature* 522, 212–215. doi: 10.1038/nature14288

Crea, S., Donati, M., De Rossi, S. M. M., Oddo, C. M., and Vitiello, N. (2014). A wireless flexible sensorized insole for gait analysis. *Sensors* 14, 1073–1093. doi: 10.3390/s140101073

Crea, S., Cipriani, C., Donati, M., Carrozza, M. C., and Vitiello, N. (2015). Providing time-discrete gait information by wearable feedback apparatus for lower-limb amputees: usability and functional validation. *IEEE Trans. Neural Syst. Rehabil. Eng.* 23, 250–257. doi: 10.1109/TNSRE.2014.2365548

Crea, S., Edin, B. B., Knaepen, K., Meeusen, R., and Vitiello, N. (2017). Time-discrete vibrotactile feedback contributes to improved gait symmetry in patients with lower-limb amputations: a case series. *Phys. Ther.* 97, 198–207. doi: 10.2522/ptj.20150441

Ding, Y., Panizzolo, F. A., Siviy, C. J., Malcolm, P., and Galiana, I., Holt, K. G. et al. (2016). Effect of timing of hip extension assistance during loaded walking with a soft exosuit. *J. Neuroeng. Rehabil.* 13:87. doi: 10.1186/s12984-016-0196-8

Ferris, D. P., Sawicki, G. S., and Daley, M. A. (2008). A physiologist's perspective on robotic exoskeletons for human locomotion. *Int. J. HR* 4, 507–528. doi: 10.1142/S0219843607001138

Galle, S., Malcolm, P., Collins, S. H., and De Clercq, D. (2017). Reducing the metabolic cost of walking with an ankle exoskeleton: interaction between actuation timing and power. *J. Neuroeng. Rehabil.* 14:35. doi: 10.1186/s12984-017-0235-0

Giovacchini, F., Vannetti, F., Fantozzi, M., Cempini, M., Cortese, M., Parri, A., et al. (2015). A light-weight active orthosis for hip movement assistance. *Robot. Auton. Syst.* 73, 123–134. doi: 10.1016/j.robot.2014.08.015

Grazi, L., Crea, S., Parri, A., Yan, T., and Cortese, M., Giovacchini, et al. (2015). "Gastrocnemius myoelectric control of a robotic hip exoskeleton," in *2015 37th Annual International Conference of the IEEE Engineering in Medicine and Biology Society* (Milan), 3881–3884. doi: 10.1109/EMBC.2015.7319241

Hermens, H. J., Freriks, B., Disselhorst-Klug, C., and Rau, G. (2000). Development of recommendations for SEMG sensors and sensor placement procedures. *J. Electromyogr. Kinesiol.* 10, 361–374. doi: 10.1016/S1050-6411(00)00027-4

Jackson, R. W., and Collins, S. H. (2015). An experimental comparison of the relative benefits of work and torque assistance in ankle exoskeletons. *J. Appl. Physiol.* 119, 541–557. doi: 10.1152/japplphysiol.01133.2014

Kao, P. C., Lewis, C. L., and Ferris, D. P. (2010). Invariant ankle moment patterns when walking with and without a robotic ankle exoskeleton. *J. Biomech.* 43, 203–209. doi: 10.1016/j.jbiomech.2009.09.030

Kawamoto, H., Lee, S. L. S., Kanbe, S., and Sankai, Y. (2003). "Power assist method for HAL-3 using EMG-based feedback controller," in *IEEE International Conference on Systems, Man and Cybernetics, 2003)*, Vol. 2 (Washington, DC), 1648–1653.

Kiguchi, K., and Imada, Y. (2009). "EMG-based control for lower-limb power-assist exoskeletons," in *IEEE Workshop on Robotic Intelligence in Informationally Structured Space, 2009. RIISS '09* (Nashville, TN: IEEE), 31–37. doi: 10.1109/RIISS.2009.4937901

Kinnaird, C. R., and Ferris, D. P. (2009). Medial gastrocnemius myoelectric control of a robotic ankle exoskeleton. *IEEE Trans. Neural Syst. Rehabil. Eng.* 17, 31–37. doi: 10.1109/TNSRE.2008.2008285

Knaepen, K., Beyl, P., Duerinck, S., Hagman, F., Lefeber, D., and Meeusen, R. (2014). Human-robot interaction: kinematics and muscle activity inside a powered compliant knee exoskeleton. *IEEE Trans. Neural Syst. Rehabil. Eng.* 22, 1128–1137. doi: 10.1109/TNSRE.2014.2324153

Lee, J., Seo, K., Lim, B., Jang, J., Kim, K., and Choi, H. (2017). "Effects of assistance timing on metabolic cost, assistance power, and gait parameters for a hip-type exoskeleton," in *2017 International Conference on Rehabilitation Robotics (ICORR)* (London, UK), 498–504.

Lenzi, T., Carrozza, M. C., and Agrawal, S. K. (2013). Powered hip exoskeletons can reduce the user's hip and ankle muscle activations during walking. *IEEE Trans. Neural. Syst. Rehabil. Eng.* 21, 938–948. doi: 10.1109/TNSRE.2013.2248749

Lenzi, T., De Rossi, S. M. M., Vitiello, N., and Carrozza, M. C. (2012). Intention-based EMG control for powered exoskeletons. *IEEE Trans. Biomed. Eng.* 59, 2180–2190. doi: 10.1109/TBME.2012.2198821

Lewis, C. L., and Ferris, D. P. (2011). Invariant hip moment pattern while walking with a hip robotic exoskeleton. *J. Biomech.* 44, 789–793. doi: 10.1016/j.jbiomech.2011.01.030

Lewis, C. L., and Sahrmann, S. A. (2006). Acetabular labral tears. *Phys.Ther.* 86, 110–121. doi: 10.1093/ptj/86.1.110

Malcolm, P., Derave, W., Galle, S., and De Clercq, D. (2013). A simple exoskeleton that assists plantarflexion can reduce the metabolic cost of human walking. *PLoS ONE* 8:e56137. doi: 10.1371/journal.pone.0056137

Malcolm, P., Quesada, R. E., Caputo, J. M., and Collins, S. H. (2015). The influence of push-off timing in a robotic ankle-foot prosthesis on the energetics and mechanics of walking. *J. Neuroeng. Rehabil.* 12:21. doi: 10.1186/s12984-015-0014-8

Mooney, L. M., Rouse, E. J., Herr, H. M., Patterson, M., Roberts, W., Lau, W., et al. (2014). Autonomous exoskeleton reduces metabolic cost of human walking during load carriage. *J. Neuroeng. Rehabil.* 11:80. doi: 10.1186/1743-0003-11-80

Mueller, M. J., Sinacore, D. R., Hoogstrate, S., and Daly, L. (1994). Hip and ankle walking strategies: effect on peak plantar pressures and implications for neuropathic ulceration. *Arch. Phys. Med. Rehabil.* 75, 1196–2000. doi: 10.1016/0003-9993(94)90004-3

Pons, J. L., Ceres, R., and Calderon, L. (2008). "Introduction to wearable robotics," in *Wearable Robots: Biomechatronic Exoskeletons,* ed J. L. Pons (Chichester, UK: John Wiley & Sons, Ltd).

Pratt, G. A., and Williamson, M. M. (1995). "Series elastic actuators," in *Proceedings 1995 IEEE/RSJ International Conference on Intelligent Robots and Systems*, (Pittsburgh, PA) 399–406.

Ronsse, R., Lenzi, T., Vitiello, N., Koopman, B., van Asseldonk, E., De Rossi, S. M. M., et al. (2011). Oscillator-based assistance of cyclical movements: model-based and model-free approaches. *Med. Biol. Eng. Comput.* 49, 1173–1185. doi: 10.1007/s11517-011-0816-1

Ronsse, R., De Rossi, S. M. M., Vitiello, N., Lenzi, T., Carrozza, M. C., and Ijspeert, A. J. (2013). Real-time estimate of velocity and acceleration of quasi-periodic signals using adaptive oscillators. *IEEE Trans. Robot.* 29, 783–791. doi: 10.1109/TRO.2013.2240173

Ruiz Garate, V., Parri, A., Yan, T., Munih, M., and Molino Lova, R., et. al. (2016). Walking assistance using artificial primitives: a novel bioinspired framework using motor primitives for locomotion assistance through a wearable cooperative exoskeleton. *IEEE Robot. Autom. Mag.* 23, 83–95. doi: 10.1109/MRA.2015.2510778

Sawicki, G. S., and Ferris, D. P. (2009). A pneumatically powered knee-ankle-foot orthosis (KAFO) with myoelectric activation and inhibition. *J. Neuroeng. Rehabil.* 6:23. doi: 10.1186/1743-0003-6-23

Sylos-Labini, F., La Scaleia, V., d'Avella, A., Pisotta, I., Tamburella, F., Scivoletto, G., et al. (2014). EMG patterns during assisted walking in the exoskeleton. *Front. Hum. Neurosci.* 8:423. doi: 10.3389/fnhum.2014.00423

Townsend, M. A., Lainhart, S. P., Shiavi, R., and Caylor, J. (1978). Variability and biomechanics of synergy patterns of some lower.limb muscles during ascending and descending stairs and level walking. *Med. Biol. Eng. Comput.* 16, 681–688. doi: 10.1007/BF02442448

Tucker, M. R., Olivier, J., Pagel, A., Bleuler, H., Bouri, M., Lambercy, O., et al. (2015). Control strategies for active lower extremity prosthetics and orthotics: a review. *J. Neuroengineering Rehabil.* 12:1. doi: 10.1186/1743-0003-12-1

van Asseldonk, E. H., Veneman, J. F., Ekkelenkamp, R., Buurke, J. H., van der Helm, F. C., and van der Kooij, H. (2008). The effects on kinematics and muscle activity of walking in a robotic gait trainer during zero-force control. *IEEE Trans. Neural. Syst. Rehabil. Eng.* 16, 360–370. doi: 10.1109/TNSRE.2008.925074

Wang, S., Wang, L., Meijneke, C., Asseldonk, E. V., Hoellinger, T., Cheron, G., et al. (2014). Design and evaluation of the mindwalker exoskeleton. *IEEE Trans. Neural. Syst. Rehabil. Eng.* 23, 277–286. doi: 10.1109/TNSRE.2014.2365697

Winfree, K. N., Stegall, P., and Agrawal, S. K. (2011). Design of a minimally constraining, passively supported gait training exoskeleton: ALEX II. *IEEE Int. Conf. Rehabil. Robot.* 386–391. doi: 10.1109/ICORR.2011.5975499

Winter, D. A. (1990). *The Biomechanics and Motor Control of Human Gait. Waterloo Biomechanics, 2nd Edn.* Kitchener, ON: Waterloo Biomechanics Publishing.

Yan, T., Cempini, M., Oddo, C. M., and Vitiello, N. (2015). Review of assistive strategies in powered lower-limb orthoses and exoskeletons. *Robot. Auton. Syst.* 64, 120–136. doi: 10.1016/j.robot.2014.09.032

Yan, T., Parri, A., Ruiz Garate, V., Cempini, M., Ronsse, R., and Vitiello, N. (2016). An oscillator-based smooth real-time estimate of gait phase for wearable robotics. *Auton. Robots* 41, 759–774. doi: 10.1007/s10514-016-9566-0

Young, A. J., Foss, J., Gannon, H., and Ferris, D. P. (2017b). Influence of power delivery timing on the energetics and biomechanics of humans wearing a hip exoskeleton. *Front. Bioeng. Biotechnol.* 5:4. doi: 10.3389/fbioe.2017.00004

Young, A. J., Gannon, H., and Ferris, D. P. (2017a). A biomechanical comparison of proportional electromyography control to biological torque control using a powered hip exoskeleton. *Front. Bioeng. Biotechnol.* 5:37. doi: 10.3389/fbioe.2017.00037

Yuan, K., Parri, A., Yan, T., Wang, L., Munih,M., Wang,Q., et al. (2015). "A realtime locomotion mode recognition method for an active pelvis orthosis," in *International Conference on Intelligent Robots and Systems (IROS), 2015 IEEE/RSJ* (Hamburg: IEEE), 6196–6201. doi: 10.1109/IROS.2015.7354261

Zajac, F. E., Neptune, R. R., and Kautz, S. A. (2003). Biomechanics and muscle coordination of human walking: Part II: lessons from dynamical simulations and clinical implications. *Gait Posture* 17, 1–17. doi: 10.1016/S0966-6362(02)00069-3

Conflict of Interest Statement: SC, AP, SM, and NV have commercial interests in IUVO S.r.l., a spinoff company of Scuola Superiore Sant'Anna. Currently, part of the IP protecting the APO technology described in the paper has been licensed to IUVO S.r.l. for commercial exploitation. The authors confirm that this did not affect the analysis of the results. All other authors declare that the research was conducted in the absence of any commercial or financial relationships that could be construed as a potential conflict of interest.

frontiers in Neuroscience

OPINION
published: 15 February 2018
doi: 10.3389/fnins.2018.00078

Domestic Use of the Exoskeleton for Gait Training in Patients with Spinal Cord Injuries: Ethical Dilemmas in Clinical Practice

Luciano Bissolotti[1]*, *Federico Nicoli*[2,3] and *Mario Picozzi*[2]

[1] Rehabilitation Service, Casa di Cura Domus Salutis, Fondazione Teresa Camplani, Brescia, Italy, [2] Biotechnology and Life Sciences Department, Center for Clinical Ethics, Insubria University, Varese, Italy, [3] Clinical Ethics Service, Domus Salutis Clinic, Teresa Camplani Foundation, Brescia, Italy

Keywords: exoskeleton spinal cord injury, ethics, Medical, financial, principlism, gait

INTRODUCTION

In this paper, as in our previous works[1] we evaluate some ethical questions about the domestic use of the robotic exoskeleton (ReWalk Robotics, Marlborough, MA, USA) (Esquenazi et al., 2012; Asselin et al., 2016) for gait assistance in people affected by a Spinal Cord Injury (SCI) (National spinal cord injury statistical center, 2010; Scivoletto et al., 2011). This device is presently FDA and EC market approved and it is now available in two different versions, one for hospital training and one for home-based use. The latter can be provided to the patient when a sufficient level of competence has been reached after special training. This work focuses on this second version of the ReWalk, since it was designed exclusively for domestic use.

Ethical concerns may arise because financial coverage of the home ReWalk version is still under debate for most patients; it depends mainly on personal resources in so far as home delivery is not supported by common and shared International Provisional rules.

In addition, in SCI patients the long term global consequences for health are marked by an increased risk of cardiovascular and metabolic diseases, while the paretic limbs may have a high risk of osteoporosis, skin lesions and deep venous thrombosis. Bowel constipation and pelvic floor impairment are other negative effects of SCI.

Patents with SCI, their relatives, and their health care providers frequently classify the recovery of the ability to walk as a high priority, even where great effort has been made to alleviate the aforementioned consequences (American Spinal Cord Injury Association, 1982; Nene et al., 1996).

To counteract these negative effects, Gait Retraining Programs have been operating for many years in order to exploit body-weight-supported gait on a treadmill (Sale et al., 2012), dynamic orthoses based upon passive mechanical hip-knee-ankle-foot orthoses (H-KAFO) which enable patients with SCI to ambulate over ground (Massucci et al., 1998) and/or similar synergic actions of Functional Electrical Stimulation (FES) with synchronized activation according to the different phases of the gait cycle (Nene and Patrick, 1990). Unfortunately, this type of treatment only results in obtaining a very slow gait speed with a high fatigue component.

[1]This case was initially presented at the 26th International Conference on Robotics in Alpe-Adria-Danube Region, L. Bissolotti, P. Zuccher, A. Zenorini, S. Chiari, P. Gaffurini, A. Pasini, F. Nicoli, Exoskeleton for Gait Training in Spinal Cord Injured people: clinical analysis and ethical Dilemmas, 2017 June 21-23 Tourin; and at the 31th European Conference on Philosophy of Medicine and Health Care (ESPMH), Exoskeleton for gait training in spinal cord injuried people: Should I respond to the budget or to the person?, Belgrade, Serbia 16-19 agosto 2017. A full version of this paper was accepted as chapter of the book "Advance in Service and Industrial Robotics" (eds. C.,Ferraresi, G. Quaglia) Springer, L., Bissolotti, P., Zuccher, A., Zenorini, S.,Chiari, P., Gaffurini, A Pasini, F. Nicoli. Exoskeleton for Gait Training in Spinal Cord Injuried People: Clinical Analysis and Ethical Dilemmas, 2018, pp. 759–765.

OPEN ACCESS

Edited by:
Mikhail Lebedev,
Duke University, United States

Reviewed by:
Andrea Lavazza,
Centro Universitario Internazionale, Italy
Marco Iosa,
Fondazione Santa Lucia (IRCCS), Italy

***Correspondence:**
Luciano Bissolotti
luciano.bissolotti@ancelle.it

Specialty section:
This article was submitted to Neuroprosthetics, a section of the journal Frontiers in Neuroscience

Received: *03 November 2017*
Accepted: *31 January 2018*
Published: *15 February 2018*

Citation:
Bissolotti L, Nicoli F and Picozzi M (2018) Domestic Use of the Exoskeleton for Gait Training in Patients with Spinal Cord Injuries: Ethical Dilemmas in Clinical Practice. Front. Neurosci. 12:78. doi: 10.3389/fnins.2018.00078

Given these limitations, over the past 6 years the branch of Bioengineering applied to SCI rehabilitation has progressively introduced a few powered exoskeletons to induce robotic gait in AIS A SCI patients (Chen et al., 2013). A recent systematic review of the literature supports the effectiveness of different types of exoskeletons used in a rehabilitative setting in improving some physical conditions such as spasticity and blood pressure or certain aptitudes such as balance and autonomy in transfer (Esquenazi et al., 2012).

SCIENTIFIC EVIDENCE

According to data published in the literature, training with ReWalk can be provided only once specific inclusions criteria are satisfied: patients must be 18–65 years old, with a spinal cord injury between C6 and T12, and a score on the Modified Ashworth Scale equal to or less than 3, or absence of any joint constraints as determined by clinicians (Asselin et al., 2016).

As described in a recent meta-analysis conducted by Miller et al. (2016), it is interesting to note that effectiveness and safety of exoskeletons in SCI patients appear to be well consolidated in the International scenario. In this meta-analysis including 111 patients from 14 studies (8 of them analyzed the use of ReWalk), 76% of the patients were able to walk independently with the exoskeleton at the end of the treatment period and gait speed-averaged 0.28 m/s (range: 0.031–0.71 m/s). This review also showed a reduction of spasticity in 38% of the cases and an improvement of bowel management in 61%, while the metabolic demand averaged 3.3METs at a Borg mean value of 10 in a scale from 6 to 20 points. In this review negative side effects were represented by falls (4.4%) and bone fractures (3.4%). Even though this type of technology has not proved to be effective in enhancing autonomous gait recovery in SCI patients, it can be considered both as an assistive device to realize independent assisted walking and a rehabilitation tool for its ability to provide effective benefits to specific functions (i.e., bowel movements) and structures (i.e., trunk control) of the human body. Powered exoskeletons can be considered as motorized orthoses and prescribed as devices for domestic use with the purpose of allowing standing, walking, climbing stairs, and performing activities of daily living in a standing position.

Other Authors provided the evidence of improvement in some aspects of Quality of Life (General Health and the Physical Role of the SF12) and a good overall level of satisfaction with the use of ReWalk (Platz et al., 2016).

After a selection of participants, a step-by-step procedure introduced the patients to the following phases of the program (Asselin et al., 2016). The seven different steps are represented by: Fitting (the exoskeleton is adjusted according to the patient's measures); Donning (the specific strategy used to get into the ReWalk is explained); Standing (patients receive instructions about the way to control the activation of the exoskeleton while using crutches to stand up); Standing balance (while standing, shifting the body weight and moving the trunk to induce the walking phase); Walking with crutches and progressive goals in mobility (turning by 90 and 180°, arresting gait, walking through doors, using an elevator and walking close to other people); Sitting and Doffing.

All the procedures take place while a trained instructor is assisting the patient in all the different phases of the training program. The level of intervention is progressively reduced as the patient accomplishes all of the required functional tasks.

SHOULD I RESPOND TO THE BUDGET OR TO THE PERSON?

Financial coverage for domestic use of the ReWalk is still not supported by common and shared national and international provisions. Concerns of an ethical nature may arise since the domestic use of the device depends mainly on personal resources.

Thus in hospital settings the use of the exoskeleton for therapeutic purposes seems to be ethically justified because one single device can be available to many different patients for a limited period of time, and specifically to individualized therapeutic targets (Platz et al., 2016; Raab et al., 2016). This instrument appears to be a proportionate treatment for those patients affected by SCI. But the excessive costs (around $70,000.00) seem to influence the purchase for home use: "currently the technology for enhancement of the disabled is somewhat costly, limiting access to those few who can either afford to purchase access to the technology or those lucky enough to have health insurance plans that will pay for the costs associated with using this technology" (Greenbaum, 2015).

Good medical reasoning balances risks and benefits, and the use of the exoskeleton entails many of benefits. But the ethics issue, and not only the clinical issue, concerns what type of information the physician should offer the patient (Deledda et al., 2013). It also concerns resolving an ethical doubt: is it more correct to inform the patient, who will certainly improve in any case, but not as he would if he had the tool at home, of these facts? Or would it be more ethically correct to choose not to inform the patient a priori about this possible improvement in performance using the device at home unless he is the one who specifically asks (and presumably has the financial resources to pay for it)?

Another ethically relevant question regards the content of the information that is offered to the patient by the physician—even when patients can receive information from other sources—about both the possibility of using this instrument in a hospital, and at the same time, regarding the difficulty of achieving more effective improvements where there is no continued use of the instrument at home. In particular, the initial proposal to use the exoskeleton at home should not come from the patient, even if he/she already knows this device.

Where real economic difficulties exist: should the physician recommend this device a priori also as a "tool for domestic use"? Or, should he/she present it only as an additional (but costly) possibility?

This question may be analyzed using the four-principle approach, or Principlism. It attempts to examine ethical aspects of a biomedical question. They derive from "considered judgment" (Beauchamp and Childress, 2009) in the common morality and daily activities of healthcare professionals. These principles, as presented by Beauchamp and Childress (Engelhardt, 1996), can be used to resolve bioethical controversies.

They are: Respect for autonomy (respecting the decision-making capacities of autonomous persons; enabling individuals to make rational informed choices); Non maleficence (avoiding the causation of harm; the harm should not be disproportionate to the benefits of treatment); Beneficence (it considers the balancing of the benefits of treatment against the risks and costs; the healthcare professional should act in a manner which benefits the patient); Justice (distributing benefits, risks and costs fairly; the notion that patients in similar positions should be treated in a similar manner).

THE DOMESTIC USE OF THE EXOSKELETON INVOLVES ALL FOUR OF THESE PRINCIPLES

The patient's autonomy of choice should be always maintained, even in the case of refusal of treatment for economic reasons, and even if the patient should not be left alone in the decision-making process. The doctor - patient/family relationship should be considered the most convenient setting to make a free and conscious decision about specific treatments (Nelson, 2012). In particular, regarding the domestic use of the exoskeleton, the patient often needs both the doctor's and a family member's word. The physician is always called upon to take care of his/her patients, according to the criterion of the proportionality of the treatments (Nicoli and Picozzi, 2017), by helping the patient to understand the benefits and risks of treatment in order to ensure autonomous decision-making. Even the family members have a specific role in the domestic use of the exoskeleton, because the patient needs another person to put on and to use the device. An essential requisite is to clearly and precisely show the different outcomes of the use of the exoskeleton while respecting the patient's choice (Kaldjian et al., 2005; Geppert and Shelton, 2012).

In an essential good doctor-patient relationship, special attention is asked to be paid by the doctor to the possible emotional and psychosocial difficulties (following the principle of non-maleficence) that the patient might have to face knowing that his/her therapy would be more effective if continued at home, but that he does not have the possibility of buying the exoskeleton: "There may be concerns that the availability of exoskeletons will create a dependency on the technology, and a limited availability will lead to withdrawal-like symptoms, whereby disabled individuals who may have relied on the technology, may exhibit psychosocial withdrawal-like symptoms when they lose access, either because of scarcity of the product or because they can no longer afford access to it" (Platz et al., 2016).

The third principle, that of beneficence, responds to the most important aim of medicine: to provide benefits to others. In particular, as expressed in the Hippocratic oath: "to help, or at least to do no harm" (Ama Council on Ethical Judicial Affairs, 2012).

Over the past decades this principle has often been presented in contrast with the patient's right to choose autonomously about the treatments medicine has to offer: "the principle of respect for autonomy has grounded several rights for patients, including the right to receive information, to consent to and refuse procedures, and to have confidentiality and privacy maintained. Other ethicists ground such obligations on the health care professionals' primary obligation to beneficence, which means to act for the patient's medical benefit"[2].

This argument finds its origins in the concept of *Paternalism*, an attitude according to which the physician is compared to a father and the patients to his children.

The distinction between soft and hard paternalism could better balance the principles of autonomy and beneficence. Hard paternalism seems not to consider the patient's opinion about his/her own choices, and the physician is thought of as the only well-informed individual able to perform care-planning for the patient's good. Soft paternalism seems resolve the conflict between the principle of beneficence and the principle of autonomy: it reflects "the intended beneficiary's own conception of his/her best interest, even if the intended beneficiary fails to fully understand or recognize those interests or to fully pursue them because of inadequate willfulness, commitment, or self-control"[3]. This conception of soft paternalism seems to be able to respect the autonomy of the patient, because it is oriented toward offering support so that the patient can choose the best solution for him/herself.

This is important in order to legitimize both the choice of the doctor who proposes the exoskeleton, and, the patient's option of refusing it.

The principle of justice is the last step involved in solving the ethical dilemma about the use of this device in a patient with economic difficulties. In its contemporary form, this principle is sometimes expressed as follows: "Individuals should be treated in the same manner, unless they differ in ways that are relevant to the situation in which they are involved" (Velasquez et al., 1990).

Indeed, Beauchamp and Childress underscore certain difficulties concerning the principle of justice regarding *allocating*, *rationing* and *setting priorities*.

The third aspect, the setting of priorities, is dedicated to costs, especially for insurance, new technology, deteriorating health conditions and longer life expectancy: "the question in setting priorities is how to determine what ought to be done when resources are inadequate to provide all of the health benefits that it is technically possible to provide"[4]. Unfortunately inconsistent results regarding the effectiveness

[2]Beauchamp, T. L., Childress, J. F. Principles of Biomedical Ethics. cit., 207.
[3]Beauchamp, T. L., Childress, J. F. Principles of Biomedical Ethics. cit., 210–211.
[4]Beauchamp, T. L., Childress, J. F. Principles of Biomedical Ethics, cit., 267–275.

of the use of the Exoskeleton are reported in the literature. Therefore, studies with patients who are chosen very selectively are needed to demonstrate the efficiency and effectiveness of this device in order to offer it to a larger number of patients (Datteri, 2013; Iosa et al., 2016; Raab et al., 2016).

At home, the use of the exoskeleton might be evaluated as a good choice if the economic burdens do not weigh solely on the patient: the excessive cost of the device should not eliminate a priori this possibility for the single patient.

Offering the opportunity for domestic use means building preferential paths with associative realities or foundations (e.g. patients' associations) aimed at offering specific services to a vaster number of patients, so as to increase the therapeutic efficacy and to shorten the waiting list.

CONCLUSION

In SCI patients, according to the available data, the use of exoskeletons is clinically and ethically justified. So far, the high cost of the device represents the main limiting factor for the adoption in home environments and places the issue of inequality on the access of technologically advanced assisted devices. This should not eliminate a priori this possibility for the single patient, since the health-care market is at present offering an array of solutions to various health-related problems which are based on patients' more or less limited economic possibilities.

To offer an opportunity for the domestic use of the instrument means to build preferential paths with patients' associations or foundations in order to offer specific services for a larger number of patients, so as to increase therapeutic efficacy and decrease inequality in the access to health care services and devices.

AUTHOR CONTRIBUTIONS

LB developed the theoretical formalism for rehabilitation background and exoskeletons and performed the literature research. FN developed the theoretical formalism for ethics background and rehabilitation implications and performed the literature research for this area of interest. All three authors, LB, FN, and MP contributed to the final version of the manuscript. MP supervised the project.

FUNDING

No specific fundings have been provided for the Conception, writing and editing of the manuscript. This paper represents the opinion of all three Authors and in accordance with ethical obligation as researchers, we are reporting that we don't have a financial and/or business interests in exoskeleton market and we are not consultants who receive funding from company that may be affected by the opinions reported in this lecture.

REFERENCES

Ama Council on Ethical and Judicial Affairs (2012). *Code of Medical Ethics*. Chicago, IL: American Medical Association.

American Spinal Cord Injury Association (1982). *Standards for Neurological Classification of Spinal Injured Patients*. Chicago, IL: ASIA.

Asselin, P. K., Avedissian, M., Knezevic, S., Kornfeld, S., and Spungen, A. M. (2016). Training persons with spinal cord injury to ambulate using a powered exoskeleton. *J. Vis. Exp*. 112:e54071. doi: 10.3791/54071

Beauchamp, T. L., and Childress, J. F. (2009). *Principles of Biomedical Ethics*. New York, NY: Oxford University Press.

Chen, G., Chan, C. K., Guo, Z., and Yu, H. (2013). A review of lower extremity assistive robotic exoskeletons in rehabilitation therapy. *Crit. Rev. Biomed. Eng.* 41, 343–363. doi: 10.1615/CritRevBiomedEng.2014010453

Datteri, E. (2013). Predicting the long-term effects of human-robot interaction: a reflection on responsibility in medical robotics. *Sci. Eng. Ethics.* 19, 139–160. doi: 10.1007/s11948-011-9301-3

Deledda, G., Moretti, F., Rimondini, M., and Zimmermann, C. (2013). How patients want their doctor to communicate. A literature review on primary care patients' perspectives, *Patient Educ. Couns.* 90, 297–306. doi: 10.1016/j.pec.2012.05.005

Engelhardt, H. T. Jr. (1996). *The Foundations of Bioethics*. New York, NY: Oxford University Press.

Esquenazi, A., Talaty, M., Packel, A., and Saulino, M. (2012). The ReWalk powered exoskeleton to restore ambulatory function to individuals with thoracic-level motor-complete spinal cord injury. *Am. J. Phys. Med. Rehabil.* 91, 911–921. doi: 10.1097/PHM.0b013e318269d9a3

Geppert, C. M. A., and Shelton, W. N. (2012). A comparison of general medical and clinical ethics consultation: what can we learn from each other? *Mayo Clin. Proc.* 4, 381–389. doi: 10.1016/j.mayocp.2011.10.010

Greenbaum, D. (2015). Ethical, legal and social concerns relating to exoskeletons. *Sigcas Comp. Soc.* 45, 234–239. doi: 10.1145/2874239.2874272

Iosa, M., Morone, G., Cherubini, A. and Paolucci, S. (2016). The three laws of neurorobotics: a review on what neurorehabilitation robots should do for patients and clinicians, *J. Med. Biol. Eng.* 36, 1–11. doi: 10.1007/s40846-016-0115-2

Kaldjian, L. C., Weir, R. F., and Duffy, T. P. (2005). A clinician's approach to clinical ethical reasoning. *J. Gen. Intern. Med.* 20, 306–311. doi: 10.1111/j.1525-1497.2005.40204.x

Massucci, M., Brunetti, G., Piperno, R., Betti, L., and Franceschini, M. (1998). Walking with the Advanced reciprocating GaitOrthosis (ARGO) in thoracic paraplegic patients: energy expenditure and cardiorespiratory performance. *Spinal Cord* 36, 223–227. doi: 10.1038/sj.sc.3100564

Miller, L. E., Zimmermann, A. K., and Herbert, W. G. (2016). Clinical effectiveness and safety of powered exoskeleton-assisted walking in patients with spinal cord injury: systematic review with meta-analysis. *Med. Dev.* 9, 455–466. doi: 10.2147/MDER.S103102

National spinal cord injury statistical center, I. (2010). Spinal Cord Injury Facts and Figures at a Glance. *J. Spinal Cord Med.* 33, 439–440

Nelson, C. (2012). The familiar foundation and the fuller sense: ethics consultation and narrative. *Perm. J.* 16, 60–63. doi: 10.7812/TPP/11-150

Nene, A. V., and Patrick, J. H. (1990). Energy cost of paraplegic locomotion using the ParaWalker—electrical stimulation 'hybrid' orthosis'. *Arch. Phys. Med. Rehabil.* 71, 116–120.

Nene, A. V., Hermens, H. J., and Zilvold, G. (1996). Paraplegic locomotion: a review. *Spinal Cord* 34, 507–524. doi: 10.1038/sc.1996.94

Nicoli, F., and Picozzi, M. (2017). Killing or allowing someone to die: a difference defined exclusively by the criteria of "terminal"? Making decisions regarding a patient's death. *Med. Hist.* 1, 41–48.

Platz, T., Gillner, A., Borgwaldt, N., Kroll, S., and Roschka, S. (2016). Device-Training for individuals with thoracic and lumbar spinal cord injury

using a powered exoskeleton for technically assisted mobility: achievements and user satisfaction. *BioMed. Res. Int.* 2016:8459018. doi: 10.1155/2016/8459018

Raab, K., Krakow, K., Tripp, F. and Jung, M. (2016). Effects of training with the ReWalk exoskeleton on quality of life in incomplete spinal cord injury: a single case study. *Spinal Cord Ser. Cases*. 7:15025. doi: 10.1038/scsandc.2015.25

Sale, P., Franceschini, M., Waldner, A., and Hesse, S. (2012). Use of the robot assisted gait therapy in rehabilitation of patients with stroke and spinal cord injury. *Eur. J. Phys. Rehabil. Med*. 48, 111–121.

Scivoletto, G., Farchi, S., Laurenza, L., and Molinari, M. (2011). Traumatic and non-traumatic spinal cord lesions: an Italian comparison of neurological and functional outcomes. *Spinal Cord. Med*. 49, 391–396. doi: 10.1038/sc.2010.85

Velasquez, M., Andre, C., Shanks, T. S. J., and Meyer, J. M. (1990). Justice and fairness. Issues in Ethics. *Spring* 3:2.

Conflict of Interest Statement: The authors declare that the research was conducted in the absence of any commercial or financial relationships that could be construed as a potential conflict of interest.

frontiers in Neuroscience

ORIGINAL RESEARCH
published: 02 March 2018
doi: 10.3389/fnins.2018.00069

Bi-articular Knee-Ankle-Foot Exoskeleton Produces Higher Metabolic Cost Reduction than Weight-Matched Mono-articular Exoskeleton

Philippe Malcolm[1]*, *Samuel Galle*[2], *Wim Derave*[2] and *Dirk De Clercq*[2]

[1] Department of Biomechanics, Center for Research in Human Movement Variability, University of Nebraska Omaha, Omaha, NE, United States, [2] Department of Movement and Sports Sciences, Ghent University, Ghent, Belgium

OPEN ACCESS

Edited by:
Mikhail Lebedev,
Duke University, United States

Reviewed by:
Wiktor Sieklicki,
Gdańsk University of Technology, Poland
Giuseppe Carbone,
University of Cassino, Italy
Manish Sreenivasa,
Universität Heidelberg, Germany
Jan Veneman,
Tecnalia, Spain

***Correspondence:**
Philippe Malcolm
pmalcolm@unomaha.edu

Specialty section:
This article was submitted to Neuroprosthetics, a section of the journal Frontiers in Neuroscience

Received: *07 September 2017*
Accepted: *29 January 2018*
Published: *02 March 2018*

Citation:
Malcolm P, Galle S, Derave W and De Clercq D (2018) Bi-articular Knee-Ankle-Foot Exoskeleton Produces Higher Metabolic Cost Reduction than Weight-Matched Mono-articular Exoskeleton. Front. Neurosci. 12:69. doi: 10.3389/fnins.2018.00069

The bi-articular m. gastrocnemius and the mono-articular m. soleus have different and complementary functions during walking. Several groups are starting to use these biological functions as inspiration to design prostheses with bi-articular actuation components to replace the function of the m. gastrocnemius. Simulation studies indicate that a bi-articular configuration and spring that mimic the m. gastrocnemius could be beneficial for orthoses or exoskeletons. Our aim was to test the effect of a bi-articular and spring configuration that mimics the m. gastrocnemius and compare this to a no-spring and mono-articular configuration. We tested nine participants during walking with knee-ankle-foot exoskeletons with dorsally mounted pneumatic muscle actuators. In the *bi-articular plus spring condition* the pneumatic muscles were attached to the thigh segment with an elastic cord. In the *bi-articular no-spring condition* the pneumatic muscles were also attached to the thigh segment but with a non-elastic cord. In the *mono-articular* condition the pneumatic muscles were attached to the shank segment. We found the highest reduction in metabolic cost of 13% compared to walking with the exoskeleton *powered-off* in the *bi-articular plus spring condition*. Possible explanations for this could be that the exoskeleton delivered the highest total positive work in this condition at the ankle and the knee and provided more assistance during the isometric phase of the biological plantarflexors. As expected we found that the *bi-articular conditions* reduced m. gastrocnemius EMG more than the *mono-articular condition* but this difference was not significant. We did not find that the *mono-articular condition* reduces the m. soleus EMG more than the *bi-articular conditions*. Knowledge of specific effects of different exoskeleton configurations on metabolic cost and muscle activation could be useful for providing customized assistance for specific gait impairments.

Keywords: bi-articular, mono-articular, exoskeleton, walking, gastrocnemius, soleus, metabolic cost, pneumatic muscles

INTRODUCTION

In most mainstream human-like robots (e.g., ASIMO, Sakagami et al., 2002), each degree of freedom of every joint is controlled by a separate actuator (Collins et al., 2005). Humans have not only muscles that actuate one joint but also muscles that cross two joints. These so-called bi-articular muscles, such as the m. gastrocnemius and biceps femoris, at first seem to be an unnecessarily complicated evolutionary adaptation for actions that could in principle be accomplished by mono-articular muscles. However, multiple sources of evidence point toward the benefits of biological bi-articular muscles (van Ingen Schenau, 1990). Bi-articular muscles facilitate the coupling of joint movements and allow to control distal joints via tendons connected to proximally located muscles, thereby reducing distal mass (Cleland, 1867). They also transport work from proximal mono-articular muscles to distal joints (Elftman, 1939; Van Ingen Schenau et al., 1987) while requiring lower shortening velocities from these muscles (Cleland, 1867; Bobbert and van Ingen Schenau, 1988). In walking, the bi-articular m. gastrocnemius has functions that differ from but are complementary to the functions of the mono-articular m. soleus (Neptune et al., 2001; Gottschall and Kram, 2005; Sasaki and Neptune, 2006; McGowan et al., 2008).

Several authors have proposed to use biological bi-articular muscles as inspiration in the design of robotic prostheses and exoskeletons (Ferris et al., 2007; Junius et al., 2017). Different groups are developing ankle prostheses with bi-articular components (Endo et al., 2009; Grimmer and Seyfarth, 2009; Eslamy et al., 2015; Flynn et al., 2015; Willson et al., 2015; Eilenberg, 2017) intended to mimic the function of the biological m. gastrocnemius. This gastrocnemius muscle has its origin on the medial and lateral epicondyles of the femur, inserts onto the calcaneus and performs primarily plantarflexion and secondary knee flexion. A simulation study (Eslamy et al., 2015) indicated that the addition of a gastrocnemius-mimicking bi-articular component could reduce the motor energy requirements of robotic prostheses. With respect to assistive devices that work in parallel with the body, different groups are designing exoskeletons and exosuits with multi-articular couplings (Dean, 2009; Bartenbach et al., 2015), often with non-biologically inspired configurations such as coupling plantarflexion with hip flexion (van den Bogert, 2003; van Dijk et al., 2011; Asbeck et al., 2013).

In contrast to studies in the field of prostheses, to our knowledge, no group has experimentally evaluated a configuration that mimics the biological m. gastrocnemius in exoskeletons. Exoskeletons are defined as anthropomorphic wearable devices that fit closely to the body and work in concert with the operators movements (Herr, 2009) and can be used for applications such as gait rehabilitation or assistance in clinical populations and augmentation in healthy populations. Exoskeletons with separate knee and ankle actuation have been designed (Sawicki and Ferris, 2009; Chen et al., 2016). However, a coupling similar to the m. gastrocnemius has only been evaluated in simulation.

A musculoskeletal simulation study by Arch et al. indicated that (mono-articular) ankle-foot orthoses do not sufficiently replicate the function of the m. gastrocnemius (Arch et al., 2016). Another simulation study by Baskar and Nadaradjane indicated that a bi-articular spring could potentially reduce the metabolic rate (Baskar and Nadaradjane, 2016). In their simulation they found that this bi-articular spring reduced the metabolic rate of the m. gastrocnemius, m. soleus and m. iliopsoas. It is uncertain to what extent the aforementioned simulation predictions would translate into experimental results. Previous simulation studies of exoskeletons (Farris et al., 2014; Van Dijk, 2015; Sawicki and Khan, 2016) often do not provide exact predictions of experimental results (van Dijk et al., 2011; Farris and Sawicki, 2012; Collins et al., 2015), which is likely due to the difficulty of predicting how a wearer will interact with an assistive exoskeleton (Gordon et al., 2006).

Our aim was to experimentally test the physiological and biomechanical effects of bi-articular configurations that mimic the biological m. gastrocnemius in healthy participants. To understand the specific effects of a bi-articular actuation path (based on the presence of bi-articular muscles in humans) and a bi-articular spring (based on the study by Baskar and Nadaradjane, 2016), we compared multiple configurations with bi-articular and mono-articular configurations either with or without a spring. We hypothesized that a mono-articular soleus-mimicking configuration would lead to a higher reduction in m. soleus EMG. We also hypothesized that bi-articular gastrocnemius-mimicking configurations would lead to higher reductions in m. gastrocnemius EMG. Finally, we hypothesized that bi-articular gastrocnemius-mimicking conditions would lead to higher reductions in metabolic rate compared to mono-articular conditions because they would provide additional assistance at the knee.

MATERIALS AND METHODS

Participants

We tested nine healthy participants (7♂, 2♀, 71 ± 2 kg, 177 ± 1 cm, 23 ± 1 year, values are mean ± standard error) during walking at 1.25 ms^{-1} on a treadmill (**Figure 1**). Since we did not have a prior estimate for the effect size for different exoskeleton configurations the number of participants was chosen based on other exoskeleton studies that demonstrate significant within-participant effects of different actuation types with 7–10 participants (Sawicki and Ferris, 2008; Malcolm et al., 2013; Collins et al., 2015; Mooney and Herr, 2016; Galle et al., 2017; Quinlivan et al., 2017). The walking speed of 1.25 ms^{-1} was selected to reflect the preferred walking speed of healthy adults (Rose et al., 1994) and to be similar to the speed that is used in most exoskeleton studies with healthy participants (Sawicki and Ferris, 2008; Malcolm et al., 2013; Collins et al., 2015; Galle et al., 2017). All participants of the study provided written informed consent prior to participation. The ethics committee of the Ghent University Hospital approved the protocol (Belgian registration number B670220097074).

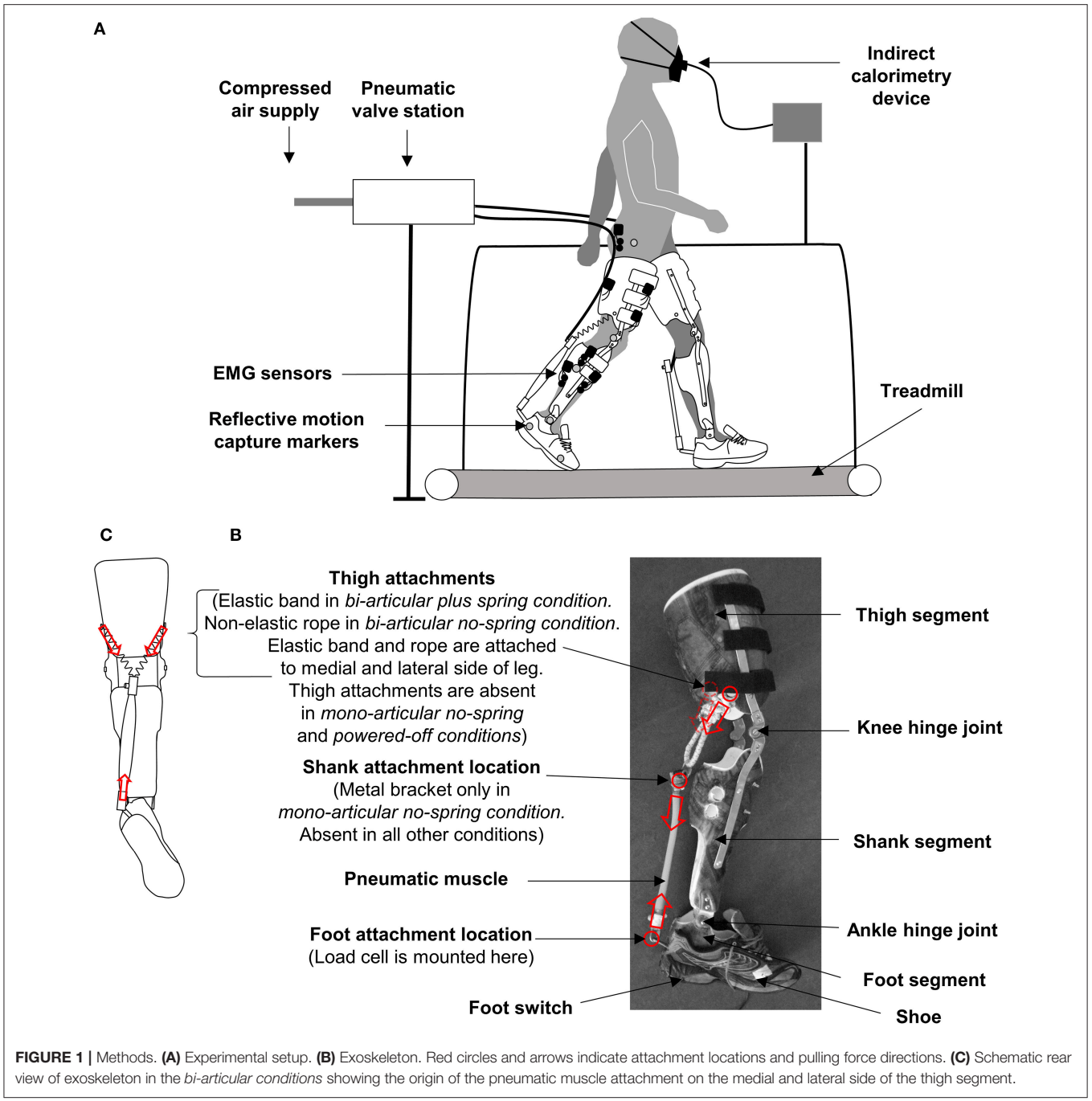

FIGURE 1 | Methods. **(A)** Experimental setup. **(B)** Exoskeleton. Red circles and arrows indicate attachment locations and pulling force directions. **(C)** Schematic rear view of exoskeleton in the *bi-articular conditions* showing the origin of the pneumatic muscle attachment on the medial and lateral side of the thigh segment.

Exoskeleton

The participants wore bilateral hinged knee-ankle-foot exoskeletons powered by pneumatic artificial muscles (**Figure 1**, **Movie 1**). The exoskeleton consisted of three shells that fit around the foot, lower leg, and thigh. The shells were molded with thermoplastic on a person with average morphology. The shells were connected with orthopedic steel bars and hinge joints. The steel bars were situated both on the medial and lateral side of the leg.

The height of the hinge joint for the knee joint was adjusted to match the participants' anthropometry. The exoskeleton was attached to the wearer by means of Velcro straps and tape around the thigh and lower leg segment. The lower leg segment of the exoskeleton weighed 0.65 kg per side, and the thigh segment of the exoskeleton weighed 1.25 kg per side. The design of our new bi-articular exoskeleton was based on our previous ankle exoskeleton (Malcolm et al., 2013) with the addition of a thigh segment. The final design of the anchor points was based on a

series of pilot tests and design modifications. The exoskeleton was tethered to a stationary power source and control unit. This type of tethered setup is similar to other knee-ankle-foot exoskeletons intended for biomechanics studies (Sawicki and Ferris, 2009) but it does not allow overground locomotion in contrast to certain other knee-ankle-foot exoskeletons (Chen et al., 2016).

Actuation Control

We actuated the exoskeletons with pneumatic artificial muscles of 3 cm in diameter. A computer program (LabView, National Instruments, Austin, TX, USA) was used to trigger the onset and end of the pneumatic muscle contraction at different percentages of the stride cycle based on signals from heel switches (Mec, Ballerup, Denmark). The pneumatic muscles were made to contract and lengthen by opening and closing of pneumatic valves (Festo, Esslingen, Germany). A constant supply pressure of 3.5 bar was used. The exact behavior of the pneumatic muscles was dependent on the inflation and deflation of the pneumatic muscles, the force-pressure-length relationship and the kinematics and the kinetics of the participant. This actuation control system was similar to the system used in Malcolm et al. (2013).

Conditions

We tested five conditions (**Figure 2**, **Movie 1**):

In the *bi-articular plus spring condition*, we attached the proximal end of the pneumatic muscles to the medial and lateral sides of the thigh segment via an elastic cord and a second non-elastic cord in parallel with the elastic cord that served to limit the maximum elongation. When pilot testing the *bi-articular plus spring condition*, we determined based on subjective perception that this second non-elastic rope was necessary to achieve an assistive effect during push-off because pneumatic muscles can only contract up to about 30% of their resting length. We intended this configuration to assist both during the eccentric and the concentric phase of the m. gastrocnemius contraction.

In the *bi-articular no-spring condition*, we attached the proximal end of the pneumatic muscles to the medial and lateral side of the thigh segment only via a non-elastic elastic cord. We intended this configuration to assist mostly with the concentric phase of the m. gastrocnemius contraction.

In the *mono-articular no-spring condition*, we attached the proximal end of the pneumatic muscles to the shank. This attachment configuration was roughly similar to that used in our previous study (Malcolm et al., 2013) except that the participants wore the non-functional thigh segment of the exoskeleton to prevent the exoskeleton mass difference from confounding the effects of differences in the actuation configuration. We did not have a mono-articular plus spring condition because we were not able to fit a pneumatic muscle that would contract over a sufficient distance and a spring within the length of the shank segment of the exoskeleton.

In the *powered-off condition*, the participants wore the entire exoskeleton without actuators.

In the *no-exoskeleton condition*, the participants walked with normal shoes without the exoskeleton.

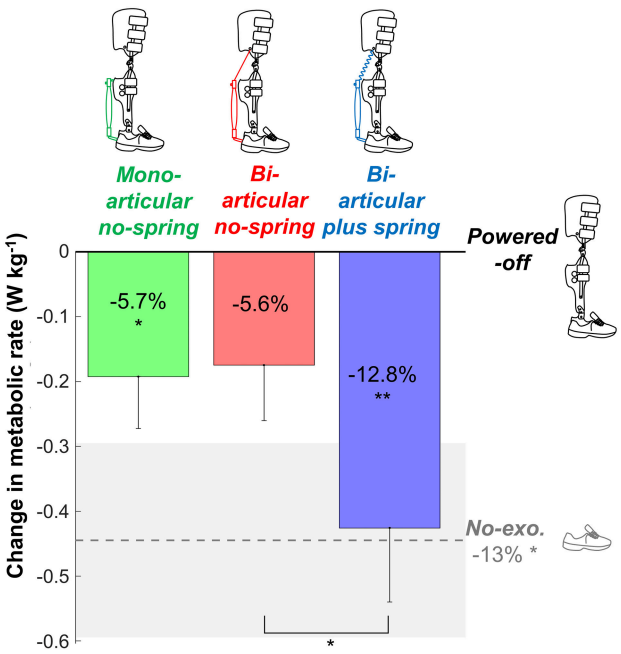

FIGURE 2 | Metabolic rate. Vertical bars show the change in metabolic rate compared to walking while wearing the exoskeleton *powered-off*. Differently colored bars represent the different exoskeleton configurations (shown in pictograms). The dashed gray line represents the difference in metabolic rate between the *no-exoskeleton* and *powered-off* conditions. Error bars indicate standard error. Shaded area indicates standard error for the *no-exoskeleton* condition. Percentages indicate percent reduction. Symbols in the vertical bars indicate significant differences compared to *powered-off*. Symbols below brackets indicate significant differences between other exoskeleton configurations. $^{**}p \leq 0.01$, $^{*}p \leq 0.05$.

In all *active conditions* (i.e., the *bi-articular plus spring*, *bi-articular no-spring*, and *mono-articular no-spring condition*) we positioned the pneumatic muscles such that they had a moment arm of ~11 cm vs. the ankle joint. In the *bi-articular conditions*, the proximal attachment was positioned on the thigh such that in the standing position, the moment arm vs. the knee joint was about half of the moment arm vs. the ankle in order to mimic the biological moment arm ratio of the m. gastrocnemius (Hof, 2001). In all three *active conditions*, we mounted the pneumatic muscles such that they appeared to be maximally elongated with the knee fully extended and ankle in 15° dorsiflexion. In the *bi-articular plus spring condition*, the elastic cord was tensioned such that it starts providing force with the knee fully extended and the ankle in 5° plantarflexion. Both adjustments were performed using tensioning screws on the pneumatic muscles while the participant stood on a 15 or 5° slope. Both angles were selected during pilot test in order to achieve that in the *bi-articular plus spring condition* the pneumatic muscles would be maximally elongated and start to apply force at initial forefoot contact (i.e. the beginning of the eccentric phase of the plantarflexors) and the *bi-articular no-spring* and *mono-articular condition* would reach maximum elongation at the beginning of the concentric phase of the plantarflexors.

Protocol

Before the metabolic and biomechanical testing protocol, the participants were allowed 18 min (Galle et al., 2013) of habituation to the different exoskeleton configurations with different timings. We used a perception-based optimization method (Caputo, 2015) to determine the optimal onset timing control input in each *active condition*. In one trial, we gradually shifted the onset timing from 23 to 53% of the stride until the participant verbally indicated that the actuation onset timing went past their perceived optimum. In another trial, we followed the same procedure in the opposite direction. We then used the mean values from the ascending and descending trials as control inputs for further metabolic and biomechanical testing. For the actuation ending, we always used a fixed control input of 60% of the stride. In the metabolic and biomechanical testing protocols, participants walked 4 min in each condition and rested while we changed the configurations. We randomized the order of the conditions.

Measurements

We recorded respiratory O_2 consumption and CO_2 production via indirect calorimetry (Oxycon Pro, Jaeger GMBH, Höchberg, Germany). We recorded the force from the pneumatic muscles at a rate of 1,000 fps with a load cell (210 Series, Richmond Industries Ltd., Rearing, United Kingdom) mounted on the distal end of the pneumatic artificial muscles such that the load cell registered the total force from the pneumatic muscle (and the series elastic cord and/or non-elastic cord in the *bi-articular conditions*). The load cell data from one participant are missing due to a device malfunction. We recorded the muscle activation on the right leg of the m. tibialis anterior, soleus, gastrocnemius medialis, gastrocnemius lateralis, vastus lateralis, rectus femoris, biceps femoris, and gluteus maximus at a rate of 1,000 fps using surface EMG sensors (Noraxon, Scottsdale, AZ, USA). We measured the kinematics of the right leg using sagittal video recording at a rate of 200 fps (Basler AG, Ahrensburg, Germany) and reflective markers on the forefoot, ankle, knee and trochanter. We recorded heel contact times using the foot switches of the exoskeleton. We processed indirect calorimetry measurements for the last 2 min of each 4-min condition. We collected load cell, EMG, kinematic, and temporal data only during the *exoskeleton conditions* (i.e., the *active conditions* and the *powered-off condition*) over a 10-second period during the last minute of each condition.

Data Processing

We calculated the metabolic rate using the Brockway equation (Brockway, 1987) and a measurement of the resting metabolic rate while standing to obtain the net metabolic rate for the walking conditions. We rectified the EMG data, applied a band pass filter (50–450 Hz) and then calculated a moving root mean square with a window of 100 ms. We normalized the EMG data to the average peak value per stride in the *powered-off* condition. We filtered the marker data with a 12-Hz Butterworth lowpass filter. Based on visual inspection, we excluded the EMG data from 24 trials (out of 288 in total) due to the presence of artifacts. We calculated the sagittal plane joint angles and angular velocities of the ankle, knee, and hip joints. For each joint angle, we subtracted the joint angle in the standing position. We estimated the total exoskeleton ankle moment by multiplying the load cell force by the moment arm vs. the ankle. In the *bi-articular condition*, we estimated the exoskeleton knee moment by multiplying the load cell force by the moment arm vs. the knee. We calculated the total exoskeleton power vs. the ankle and the knee by multiplying the exoskeleton moments by the joint angular velocities, and we calculated the positive exoskeleton work rates by integrating the positive portions of the exoskeleton power over time and dividing by the stride time. We calculated the step length by multiplying the step times obtained from foot switches by the speed of the treadmill. All time-series data were normalized vs. the stride time based on heel contact detection by the foot switches. We calculated the minima and maxima from all normalized stride time data, and we calculated the onset timing from the exoskeleton ankle moment data.

Statistics

For each time series and metric, we calculated the mean and standard error. For each metric, we tested whether there were any effects of exoskeleton condition using repeated measures ANOVA. We used Mauchly's test to verify sphericity and used the Greenhouse-Geiser correction if the sphericity assumption was violated. If the repeated measures ANOVA indicated a significant effect, we evaluated pairwise differences using paired *t*-tests using the least significant difference method. For the actuation onset timing metric, we tested whether there was a significant difference between the value in the *mono-articular no-spring condition* and the value of 42.5%, which was the average optimal timing of earlier publications with a similar mono-articular actuator configuration (Malcolm et al., 2013; Galle et al., 2017) using a one-sample *t*-test. We also tested whether the exoskeleton work rate had a significant linear effect on the reduction of the metabolic cost using mixed-model ANOVA. For the repeated measures ANOVA we reported the degrees of freedom of the condition, the degrees of freedom of the error, the *f*-value, the *p*-value, and the partial eta squared. For the *t*-tests we reported the degrees of freedom, the *t*-value, the *p*-value, and the Cohen's *d*. For the mixed-model ANOVA we reported the degrees of freedom, the *t*-value, the *p*-value, and the R^2 between the estimated metabolic cost (obtained using the equation obtained from the mixed-model ANOVA) and the actual metabolic cost. All statistical tests were conducted in MATLAB (MathWorks, Natick, MA, USA).

RESULTS

Exoskeleton Mechanics

Participants selected actuation onsets of 36.1 ± 1.6, 38.4 ± 1.3, and 40.9 ± 0.9% in the *bi-articular plus spring condition*, *bi-articular no-spring condition,* and *mono-articular no-spring condition*, respectively (**Figure 3**). Exoskeleton configuration had a significant effect on the onset timing obtained from the perception optimization ($df_{\text{cond.}} = 2$, $df_{\text{err.}} = 14$, $F = 4.080$, $p = 0.040$, $\eta^2 = 0.368$). The selected actuation onset was

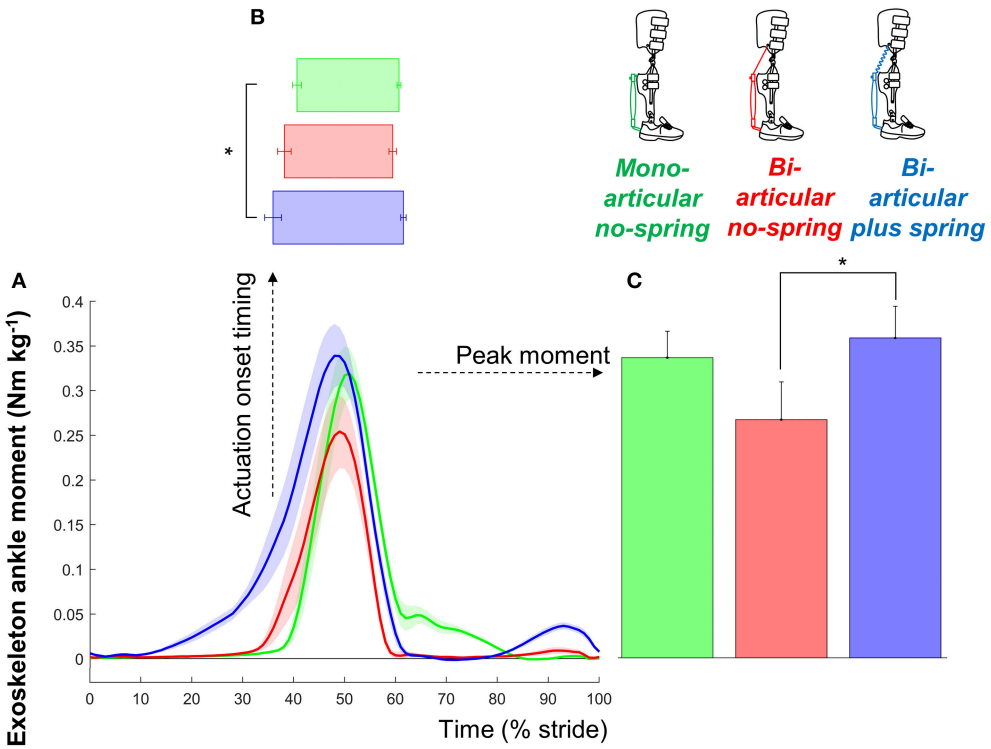

FIGURE 3 | Exoskeleton moment. **(A)** Exoskeleton ankle moment vs. stride time. Colored lines indicate the population average of different conditions (shown in pictograms). Shaded areas indicate standard error. **(B)** Actuation onset timing. **(C)** Peak moment. Differently colored bars represent the different exoskeleton configurations. Error bars indicate standard error. Symbols next to brackets indicate significant differences between exoskeleton configurations. $^*p \leq 0.05$.

significantly earlier in the *bi-articular plus spring condition* than in the *mono-articular no-spring condition* ($df = 7$, $T = 2.927$, $p = 0.022$, $d = 1.034$). The selected actuation onset in the *mono-articular no-spring condition* was not significantly different from the average value from previous publications in which similar mono-articular soleus-mimicking configurations were used (Malcolm et al., 2013; Galle et al., 2017) ($df = 7$, $T = 1.739$, $p = 0.126$, $d = 0.61$, one-sample t-test vs. 42.5%).

The peak exoskeleton ankle moments were 0.35 ± 0.04, 0.26 ± 0.04, and 0.33 ± 0.03 Nm kg^{-1} in the *bi-articular plus spring condition*, *bi-articular no-spring condition*, and *mono-articular no-spring condition*, respectively. Exoskeleton configuration had a significant effect on the peak exoskeleton moment ($df_{cond.} = 2$, $df_{err.} = 14$, $F = 5.503$, $p = 0.017$, $\eta^2 = 0.440$). The peak exoskeleton ankle moment in the *bi-articular plus spring condition* was higher than that in the *bi-articular no-spring condition* ($df = 7$, $T = 2.934$, $p = 0.022$, $d = 1.037$). The elastic cord in the *bi-articular plus* spring condition resulted in an average angular stiffness of 2.662 Nm$^{\circ -1}$ around the ankle during the phase before the pneumatic muscle contraction.

The peak exoskeleton positive ankle work rates were 0.065 ± 0.006, 0.044 ± 0.006, 0.103 ± 0.011 W kg^{-1} per side in the *bi-articular plus spring condition*, *bi-articular no-spring condition*, and *mono-articular no-spring condition*, respectively. The peak exoskeleton positive knee work rates were 0.110 ± 0.011 and 0.070 ± 0.013 W kg^{-1} per side in the *bi-articular plus spring condition* and *bi-articular no-spring condition*, respectively.

Metabolic Rate

Net metabolic rates were 2.79 ± 0.12 W kg^{-1} in the *bi-articular plus spring condition*, 3.04 ± 0.15 W kg^{-1} in the *bi-articular no-spring condition*, 3.02 ± 0.12 W kg^{-1} in the *mono-articular no-spring condition*, 3.21 ± 0.13 W kg^{-1} in the *powered-off condition*, and 2.77 ± 0.12 W kg^{-1} in the *no-exoskeleton condition* (**Figure 2**). Exoskeleton configuration had a significant effect ($df_{cond.} = 4$, $df_{err.} = 32$, $F = 4.832$, $p = 0.004$, $\eta^2 = 0.377$) on the net metabolic rate. The metabolic rate in the *bi-articular plus spring condition* was 12.8 ± 3.1% lower than that in the *powered-off condition* ($df = 8$, $T = 3.734$, $p = 0.006$, $d = 1.245$), and lower than that in the *bi-articular no-spring condition* ($df = 8$, $T = 2.920$, $p = 0.019$, $d = 0.973$). The metabolic rate in the *bi-articular no-spring* condition was on average 5.6 ± 2.7% lower than in the *powered-off* condition but this difference was not significant ($df = 8$, $T = 2.042$, $p = 0.075$, $d = 0.681$). The metabolic rate in the *mono-articular no-spring condition* was 5.7 ± 2.5% lower than in the *powered-off condition* ($df = 8$, $T = 2.400$, $p = 0.043$, $d = 0.800$). The metabolic rate was 13 ± 4% lower in the *no-exoskeleton condition* than in the *powered-off condition* ($df = 8$, $T = 2.971$,

$p = 0.018$, $d = 0.990$). None of the *exoskeleton conditions* reduced the metabolic rate below that of the *no-exoskeleton condition*.

There were significant relationships between the metabolic rate and positive ankle work ($df = 30$, $T = 0.212$, $p = 0.042$, $R^2 = 0.126$, mixed-model ANOVA), positive knee work ($df = 30$, $T = 3.392$, $p = 0.002$, $R^2 = 0.260$), and positive total joint work ($df = 30$, $T = 4.175$, $p < 0.001$, $R^2 = 0.33$) (**Figure 4**).

EMG

Exoskeleton configuration had significant effects on the peak EMG-values of the m. soleus ($df_{cond.} = 3$, $df_{err.} = 18$, $F = 8.882$, $p < 0.001$, $\eta^2 = 0.597$) and biceps femoris ($df_{cond.} = 3$, $df_{err.} = 15$, $F = 3.895$, $p = 0.031$, $\eta^2 = 0.438$) (**Figure 5**).

The peak m. soleus EMG-values in the *bi-articular plus spring condition* ($df = 7$, $T = 4.314$, $p = 0.004$, $d = 1.525$) and *mono-articular no-spring condition* ($df = 6$, $T = 4.031$, $p = 0.007$, $d = 1.524$) were lower than in the *powered-off condition*.

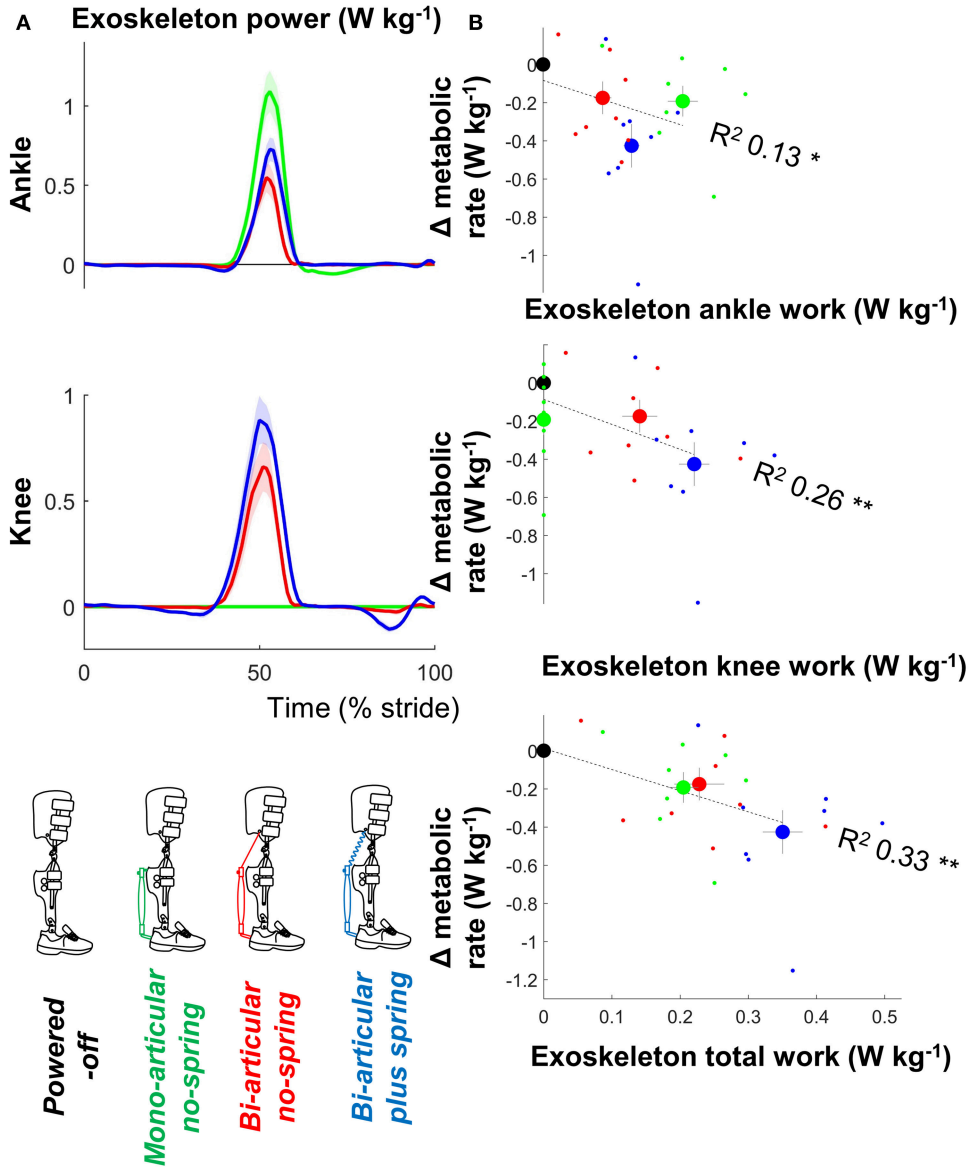

FIGURE 4 | Metabolic rate vs. exoskeleton power and work. **(A)** Exoskeleton ankle and knee power. Since pneumatic muscles can only apply a pulling force, positive ankle power indicates ankle angular velocity in the flexion direction and positive knee power indicates knee angular velocity in the flexion direction. Colored lines indicate the population average of different conditions. Shaded areas indicate standard error. **(B)** Change in metabolic rate vs. positive exoskeleton work. Large dots indicate population average for each condition. Small dots indicate individual trials. Dashed lines indicate results from regression equation from mixed-model ANOVA. R^2 values are calculated based on Pearson's correlation of estimated results from mixed-model ANOVA vs. actual metabolic results from all participants and conditions. $^{**}p \leq 0.01$, $^{*}p \leq 0.05$.

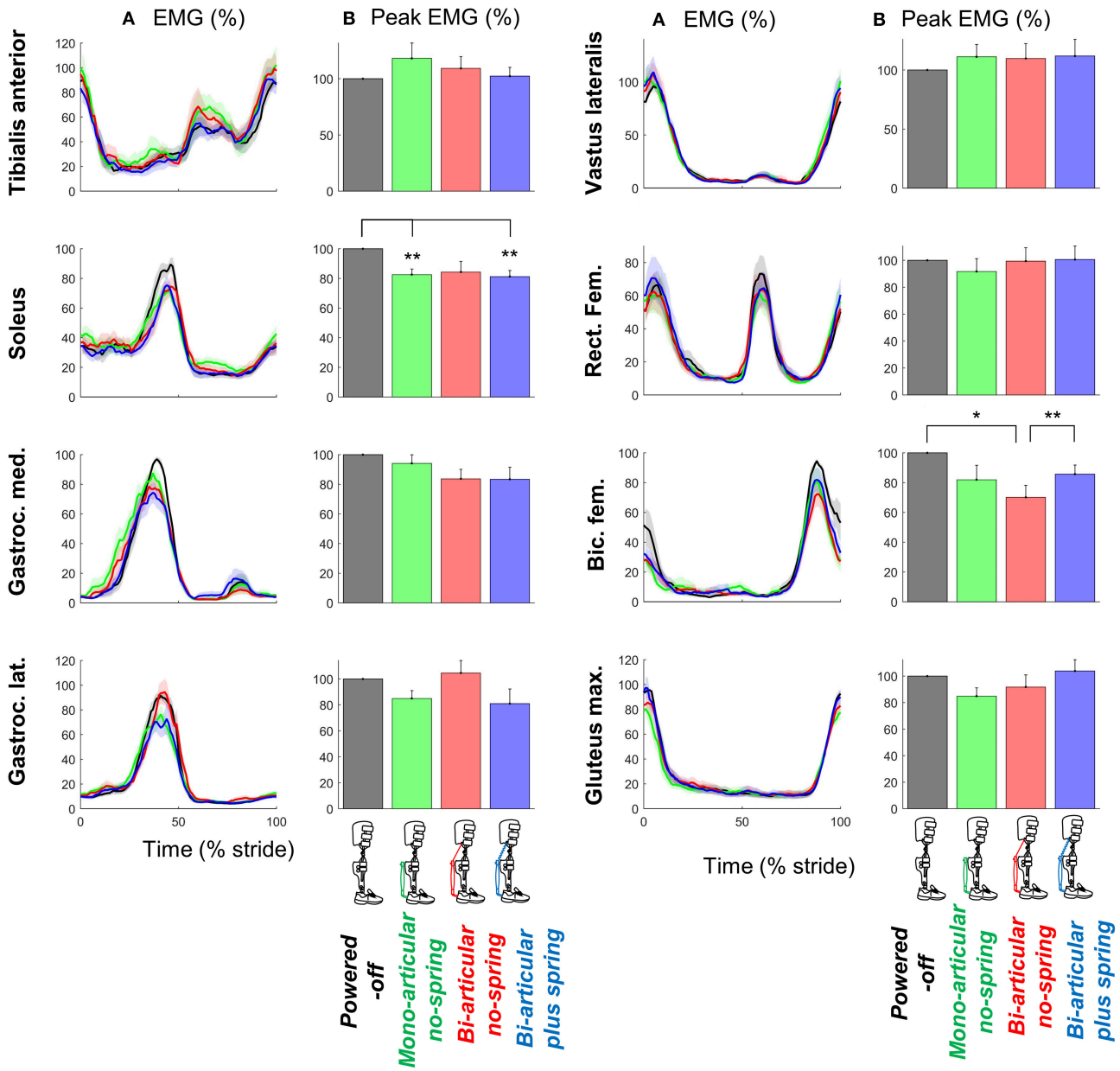

FIGURE 5 | EMG. **(A)** EMG vs. stride time. Different plots are from different muscles. Colored lines indicate the population average of different conditions (shown in pictograms). Shaded areas indicate standard error. **(B)** Peak EMG values for each muscle and condition. Differently colored bars represent the different exoskeleton configurations. Error bars indicate standard error. Symbols next to brackets indicate significant differences between exoskeleton configurations. $^{*}p \leq 0.05$. $^{**}p \leq 0.01$.

The peak m. biceps femoris in the *bi-articular no-spring condition* was also lower than that in *the powered-off condition* ($df = 5$, $T = 3.033$, $p = 0.029$, $d = 1.238$) and that in the *bi-articular plus spring condition* ($df = 5$, $T = 5.178$, $p = 0.004$, $d = 2.114$).

Kinematics

Exoskeleton configuration had significant effects on maximum plantarflexion ($df_{\text{cond.}} = 3$, $df_{\text{err.}} = 24$, $F = 44.481$, $p < 0.001$, $\eta^2 = 0.848$), maximum dorsiflexion ($df_{\text{cond.}} = 3$, $df_{\text{err.}} = 24$, $F = 12.089$, $p < 0.001$, $\eta^2 = 0.602$), and maximum knee extension ($df_{\text{cond.}} = 3$, $df_{\text{err.}} = 24$, $F = 3.709$, $p = 0.025$, $\eta^2 = 0.317$) (**Figure 6**).

Maximum plantarflexion in the *mono-articular no-spring condition* was higher than those in all other *exoskeleton conditions* ($df = 8$, all $T \geq 7.594$, all $p < 0.001$, all $d \geq 2.531$). Maximum plantarflexion in the *bi-articular plus spring condition* was higher than that in the *powered-off condition* ($df = 8$, $T = 2.949$,

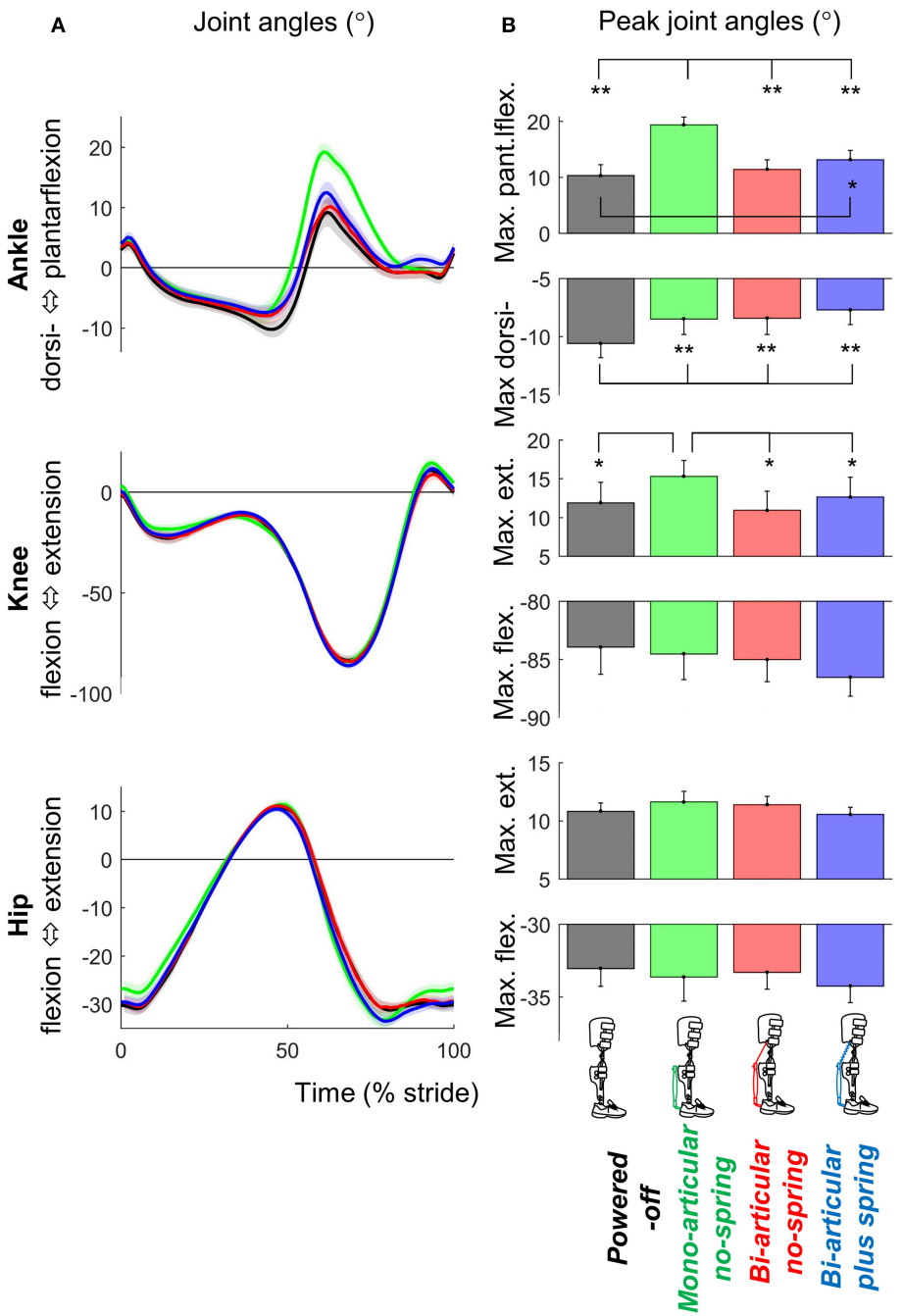

FIGURE 6 | Kinematics. **(A)** Joint angle vs. stride time. Different plots are from different joints. Colored lines indicate the population average of different conditions (shown in pictograms). Shaded areas indicate standard error. **(B)** Peak extension and flexion angles. Differently colored bars represent the different exoskeleton configurations. Error bars indicate standard error. Symbols next to brackets indicate significant differences between exoskeleton configurations. *$p \leq 0.05$. **$p \leq 0.01$.

$p = 0.019$, $d = 0.983$). In all *active exoskeleton conditions,* the maximum dorsiflexion angle before push-off was lower than that in the *powered-off condition* ($df = 8$, all $T \geq 3.720$, all $p < 0.006$, all $d \geq 1.240$).

Maximum knee extension (just before push-off) in the *mono-articular no-spring condition* was higher than those in all the other exoskeleton conditions ($df = 8$, all $T \geq 2.583$, all $p < 0.033$, all $d \geq 0.861$). We found no significant effects of exoskeleton configuration on hip joint angle or step length.

Overall, in the *bi-articular conditions* the coupling between the knee and ankle angle was more similar to the *powered-off* condition than in the *mono-articular condition* (**Figure 7**).

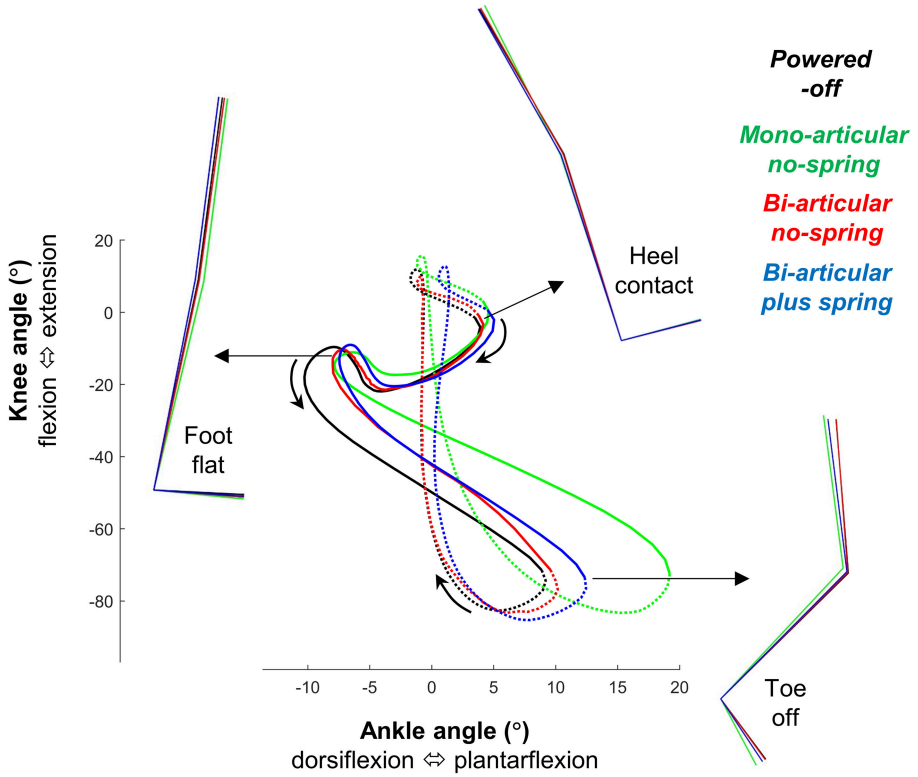

FIGURE 7 | Bi-articular coupling. Plot shows knee angle plotted on the vertical axis vs. ankle angle on the horizontal axis as in Robertson et al. (2004). Full lines indicate stance phase. Dotted lines indicate swing phase. Colored lines indicate the population average of different conditions. Stick figures indicate lower limb kinematics position at different points on the gait cycle. This figure shows that in the *bi-articular conditions* the coupling between the knee and ankle angle is more similar to the *powered-off condition*.

DISCUSSION

Our aim was to evaluate an exoskeleton with a bi-articular actuation configuration that mimicked the eccentric and concentric behavior of the m. gastrocnemius and to compare this condition with one that mimicked only the concentric behavior of the m. gastrocnemius and one that mimicked the concentric behavior of the m. soleus. We found that the *bi-articular plus spring condition* provided the highest reduction in metabolic cost (13% compared to p*owered-off*, **Figure 2**). The *bi-articular no-spring condition* and the *mono-articular no-spring condition* both provided reductions of ∼6% compared to *powered-off*. In contrast to our hypothesis we did not find the highest reduction in m. soleus EMG in the *mono-articular condition*. On average m. gastrocnemius EMG appeared to be lower in the *biarticular conditions* than in the *mono-articular condition* but this was not significant.

Peak exoskeleton ankle moment and exoskeleton ankle work rate values in the *active* conditions were respectively around 17 and 23% of the biological moment and work rate values reported in Winter (1983). In the *bi-articular* conditions there was an exoskeleton knee flexion moment and positive exoskeleton knee flexion work during the phase when the biological knee moment is in the extension direction and the biological knee work is negative (Winter, 1983) so the knee action of the exoskeleton was different than the action of the net of all the biological knee muscles. However, it is known that non-biological exoskeleton behavior can sometimes be more effective than biological behavior (Mooney and Herr, 2016; Uchida et al., 2016).

The reduction in the m. soleus EMG in the *mono-articular no-spring condition* is consistent with results from other studies showing that mono-articular ankle exoskeletons can reduce the m. soleus EMG (Sawicki and Ferris, 2008; Galle et al., 2013, 2017). The fact that the reduction in the m. soleus EMG is not the highest in the *mono-articular no-spring condition* despite the fact that in this condition the assistance is in parallel with the m. soleus may have been due to the higher maximum plantarflexion in the *mono-articular no-spring condition* (**Figure 6**). It appears that the participants utilized the exoskeleton assistance in that condition to increase plantarflexion instead of maximizing reductions in the m. soleus EMG while keeping kinematics invariant. Similar kinematic changes have also been observed in other studies with ankle exoskeletons and exosuits (Koller et al., 2015; Mooney and Herr, 2016; Quinlivan et al., 2017). The absence of a similarly large increase in plantarflexion in the *bi-articular conditions* may have been because the attachment points of the pneumatic muscle came closer to each other when the knee started to flex during push-off. Overall it appears that

the *bi-articular conditions* allowed for more natural knee and ankle kinematics than the *mono-articular condition* (**Figure 7**). For future exoskeleton designs it appears that this type of bi-articular configuration could be useful if the objective is to assist while maintaining kinematics that are as close as possible to natural biological kinematics.

Though we did not find increases in knee flexion in the *bi-articular conditions*, we did find reductions in the biceps femoris EMG at the end of swing. Because the biceps femoris is in part a knee flexor muscle it could be that the higher reduction in biceps femoris EMG is because the *bi-articular conditions* effectively assisted the knee flexion function. Although it seems logical that we did not find these reductions in the m. biceps femoris EMG in the *mono-articular condition*, we know from other studies that the m. biceps femoris EMG can actually also be reduced with a mono-articular exoskeleton, for example by providing higher assistive moments (Galle et al., 2017).

The additional assistance with knee flexion may have contributed to our finding of the highest reduction in metabolic rate in the *bi-articular plus spring condition*. We found that the sum of the positive ankle and knee work from the exoskeleton had the strongest correlation with the metabolic rate reduction (**Figure 4**). It appears that this work sum was the highest in the *bi-articular plus spring condition* due in part to the additional work delivered at the knee. Another explanation is that the *bi-articular plus spring condition* provided the highest negative work assistance at the ankle thanks to the early actuation time selected by the participants and the elastic element (**Figure 3**). Following the same hypothesis that was suggested in a study with an elastic ankle exoskeleton (Collins et al., 2015) the additional assistance during the isometric contraction phase of the biological plantarflexors could explain the higher metabolic reduction in the *bi-articular plus spring condition*.

The participants preferred earlier actuation onset timing in the *bi-articular plus spring condition* than in the *mono-articular no-spring condition*. It has been suggested that due to attributes such as low weight and elastic behavior, pneumatic muscles are useful for applications involving human interaction, such as exoskeletons (Daerden and Lefeber, 2002). However, it is also known that the contraction forces of pneumatic muscles are highest when they are elongated, and that pneumatic muscles can cause the ankle to plantarflex earlier than normal (Gordon et al., 2006). Furthermore, a simulation study of walking with an elastic ankle-foot orthosis showed that a soleus-mimicking mono-articular orthosis could cause unnatural premature knee extension during midstance (Arch et al., 2016). This inelastic pneumatic muscle behavior at maximum elongation combined with the potential to cause unnatural knee extension when actuation would be too early may explain why the participants preferred a later actuation onset timing in the *mono-articular no-spring condition*.

A limitation of our study is that the timing for each condition was selected based on perception tests. The perceived optimal timing in the *mono-articular no-spring condition* was not significantly different from the optimal timing found in previous studies (Malcolm et al., 2013; Galle et al., 2017), which suggests that the participants were relatively good at identifying their optimal timing. However, we do not have direct evidence that the participants correctly selected the optimal timing in the *bi-articular conditions*. Another limitation is that the actuator configuration was not the only difference between the conditions; there were also differences in other parameters such as timing, peak moment, work, etc. It is impossible to vary one parameter in isolation and keep every other actuation parameter constant because changes in exoskeleton parameters usually also change the kinematics (Galle et al., 2015; Koller et al., 2015; Mooney and Herr, 2016; Quinlivan et al., 2017). This challenge seems to be common in the field, and as far as we know, there are only a very small number of experimental studies that describe within-subject comparisons of exoskeleton conditions (Ding et al., 2017). In an ideal case, either a constant rate of work should be delivered in all the conditions or all the parameters of the entire actuation profile should be optimized for each condition. Delivering a constant rate of work in all conditions would allow to answer the question which is the best configuration to deliver a certain rate of work. In the current experiment it could be that the *bi-articular plus spring* provided the highest metabolic cost reduction simply because this allowed to provide more mechanical work assistance to the ankle plus the knee. However, recent studies learn that exoskeleton mechanical work only is not necessarily related to reduction in metabolic cost (Jackson and Collins, 2015; Zhang et al., 2017). Optimizing the entire actuation profile in order to identify the best profile for each configuration would require using human-in-the-loop optimization (Zhang et al., 2017). However, this approach was not feasible at the time of the data collection in our study. Another limitation in the interpretation of the results is that we only calculated the total power from the pneumatic muscle (and the series elastic cord and/or non-elastic cord in the *bi-articular conditions*). Calculating the power from each component separately would allow to discuss how each component contributes to the power delivered by the exoskeleton (Eslamy et al., 2015; Yandell et al., 2017). An alternative approach to conduct our study could have been to use two single joint actuators: one at the ankle and one at the knee. By using two separate actuators it would be possible to separate the assistive effects at the ankle and the knee. The two actuators could be programmed to behave as if there is a biarticular connection from the foot to the thigh or even different combinations of ankle and knee actuation could be tested. The fact that the actuation profiles were not fully optimized probably contributed to the fact that none of the exoskeleton conditions reduced the metabolic cost below the level of walking without an exoskeleton.

Another reason why we did not find reductions in metabolic cost below that of walking without an exoskeleton may have been the additional mass of the thigh segments of the exoskeleton. While our exoskeleton weighed relatively less than other knee-ankle-foot exoskeletons such as the ones from Chen et al. (2016) (3.5 kg for one side) and Sawicki and Ferris (2009) (2.9 kg for one side) it still weighed a considerable total of 1.9 kg per side. Based on a literature regression equation (Browning et al., 2007), we estimated that the weight of the thigh segments would have caused a penalty in metabolic cost of 6.7%. The metal bars on both the medial and lateral side of the legs might have

encumbered walking and caused participants to take wider steps. Some designs from other exoskeletons that use struts only on the lateral side of the leg might solve this problem (Suzuki et al., 2007; Esquenazi et al., 2012). Our exoskeleton design used a simple hinge joint for the knee, whereas the knee actually has a moving axis of rotation (Witte et al., 2017). The use of design principles from soft exosuits for the knee (Wehner et al., 2013; Park et al., 2014) could potentially both help reduce the weight of our device and resolve problems with joint axis alignment.

For clinical application of our exoskeleton the design and actuation profiles would need to be optimized. For example, the optimal timing could be different for every single patient as was found in stroke patients in Awad et al. (2017). It is unknown if the biarticular configuration and spring would have benefits in different populations such as patients since the current study was only conducted in a small sample of nine healthy volunteers and at a higher walking speed than patients typically use.

In conclusion, we found that a bi-articular exoskeleton configuration that mimics the m. gastrocnemius can reduce the metabolic cost of walking and reduce biceps femoris EMG. The following factors could have contributed to the higher reduction in metabolic rate in the *bi-articular plus spring condition*: closer to normal ankle and knee kinematics, additional assistance with knee flexion and higher total mechanical work assistance. However, we do not know to what extent each of these factors contributed to the metabolic cost result. Future exoskeleton designs could leverage each of these factors, possibly with different exoskeleton designs than ours, for example with separate ankle and knee actuation or with more lightweight and soft structures. Knowledge about specific effects of exoskeleton configuration on metabolic costs and muscle activation could be applied to providing customized assistance for different gait impairments or injuries and could also lead to novel experiments aimed at investigating the separate roles of the m. gastrocnemius and soleus.

AUTHOR CONTRIBUTIONS

PM, SG, WD, and DD designed the study. PM and SG performed data collection. PM performed the data analysis and drafted the manuscript. All authors edited and revised the analyses and the manuscript and gave final approval for publication.

FUNDING

SG was supported by Special Research Fund of Ghent University (BOF10/DOC/288). PM received partial support from the Center for Research in Human Movement Variability of the University of Nebraska Omaha and the NIH (P20GM109090).

SUPPLEMENTARY MATERIAL

The Supplementary Material for this article can be found online at: https://www.frontiersin.org/articles/10.3389/fnins.2018.00069/full#supplementary-material

Movie 1 | Participant walking in different exoskeleton configurations. Video shows the *bi-articular plus spring condition, bi-articular no-spring condition, mono-articular no-spring condition, powered-off condition,* and *no-exoskeleton condition.*

Data Sheet 1 | Study dataset containing results for metabolic cost, exoskeleton kinetics, EMG and kinematics. The data is saved in .mat-format and can be opened with MATLAB. Data is organized similar to exoskeleton datasets from Jackson and Collins (2015). Timeseries variables are stored as three-dimensional matrices where the first dimension is stridetime, the second dimension is participant number and the third dimension is condition number. Metric variables are stored as two-dimensional matrices where the first dimension is participant number and the second dimension is condition number. The conditions are numbered as follows: 1 = *bi-articular plus spring condition*, 2 = *bi-articular no-spring condition*, 3 = *mono-articular no-spring condition*, 4 = *powered-off condition*, 5 = *no-exoskeleton condition*.

REFERENCES

Arch, E. S., Stanhope, S. J., and Higginson, J. S. (2016). Passive-dynamic ankle–foot orthosis replicates soleus but not gastrocnemius muscle function during stance in gait: insights for orthosis prescription. *Prosthet. Orthot. Int.* 40, 606–616. doi: 10.1177/0309364615592693

Asbeck, A. T., Dyer, R. J., Larusson, A. F., and Walsh, C. J. (2013). "Biologically-inspired soft exosuit," in *IEEE International Conference on Rehabilitation Robotics* (Seattle, WA).

Awad, L. N., Bae, J., O'Donnell, K., De Rossi, S. M. M., Hendron, K., Sloot, L. H., et al. (2017). A soft robotic exosuit improves walking in patients after stroke. *Sci. Transl. Med.* 9:eaai9084. doi: 10.1126/scitranslmed.aai9084

Bartenbach, V., Schmidt, K., Naef, M., Wyss, D., and Riener, R. (2015). "Concept of a soft exosuit for the support of leg function in rehabilitation," in *IEEE International Conference on Rehabilitation Robotics* (Singapore), 125–130.

Baskar, H., and Nadaradjane, S. M. R. (2016). Minimization of metabolic cost of muscles based on human exoskeleton modeling: a simulation. *Int. J. Biomed. Eng. Sci.* 3, 1–9. doi: 10.5121/ijbes.2016.3401

Bobbert, M. F., and van Ingen Schenau, G. J. (1988). Coordination in vertical jumping. *J. Biomech.* 21, 249–262. doi: 10.1016/0021-9290(88)90175-3

Brockway, J. M. (1987). Derivation of forulae used to calculate energy expenditure in man. *Hum. Nutr. Clin. Nutr.* 41C, 463–471.

Browning, R. C., Modica, J. R., Kram, R., and Goswami, A. (2007). The effects of adding mass to the legs on the energetics and biomechanics of walking. *Med. Sci. Sports Exerc.* 39, 515–525. doi: 10.1249/mss.0b013e31802b3562

Caputo, J. M. (2015). "Chapter 5: user-optimal prosthesis design," in *Informing Ankle-Foot Prosthesis Design and Prescription through Systematic Experimentation with a Tethered Robotic Prosthesis.* Available online at: http://biomechatronics.cit.cmu.edu/publications/Caputo_2015_Dissertation.pdf#page=118

Chen, G., Qi, P., Guo, Z., and Yu, H. (2016). Mechanical design and evaluation of a compact portable knee-ankle-foot robot for gait rehabilitation. *Mech. Mach. Theory* 103, 51–64. doi: 10.1016/j.mechmachtheory.2016.04.012

Cleland, J. (1867). On the actions of muscles passing over more than one joint. *J. Anat. Physiol.* 1, 85–93.

Collins, S. H., Wiggin, M. B., and Sawicki, G. S. (2015). Reducing the energy cost of human walking using an unpowered exoskeleton. *Nature* 522, 212–215. doi: 10.1038/nature14288

Collins, S., Ruina, A., Tedrake, R., and Wisse, M. (2005). Efficient bipedal robots based on passive-dynamic walkers. *Science* 307, 1082–1085. doi: 10.1126/science.1107799

Daerden, F., and Lefeber, D. (2002). Pneumatic artificial muscles: actuators for robotics and automation. *Eur. J. Mech. Environ. Eng.* 47, 11–21. Available online

at: http://eecs.vanderbilt.edu/courses/eece258/Lab4/Pneumatic%20Artificial%20Muscles.pdf

Dean, J. C. (2009). "Development of a passive exoskeleton for swing phase gait assistance," in *Dynamic Walking Conference* (Vancouver, BC).

Ding, Y., Galiana, I., Asbeck, A. T., De Rossi, S. M. M., Bae, J., Santos, T. R. T., et al. (2017). Biomechanical and physiological evaluation of multi-joint assistance with soft exosuits. *IEEE Trans. Neural Syst. Rehabil. Eng.* 25, 119–130. doi: 10.1109/TNSRE.2016.2523250

Eilenberg, M. F. (2017). *Development and Evaluation of Biarticular Transtibial Prostheses for Level-Ground Amputee Walking*. Ph.D. thesis, MIT. Available online at: https://dspace.mit.edu/bitstream/handle/1721.1/108945/986242615-MIT.pdf?sequence=1

Elftman, H. (1939). The function of muscles in locomotion. *Am. J. Physiol.* 125, 357–366. doi: 10.1152/ajplegacy.1939.125.2.357

Endo, K., Swart, E., and Herr, H. (2009). "An artificial gastrocnemius for a transtibial prosthesis," in *Proceedings of the 31st Annual International Conference of the IEEE Engineering in Medicine and Biology Society: Engineering the Future of Biomedicine, EMBC* (Minneapolis, MN), 5034–5037.

Eslamy, M., Grimmer, M., and Seyfarth, A. (2015). "Adding passive biarticular spring to active mono-articular foot prosthesis: effects on power and energy requirement," in *IEEE-RAS International Conference on Humanoid Robots* (Madrid), 677–684.

Esquenazi, A., Talaty, M., Packel, A., and Saulino, M. (2012). The Rewalk powered exoskeleton to restore ambulatory function to individuals with thoracic-level motor-complete spinal cord injury. *Am. J. Phys. Med. Rehabil.* 91, 911–921. doi: 10.1097/PHM.0b013e318269d9a3

Farris, D. J., and Sawicki, G. S. (2012). Linking the mechanics and energetics of hopping with elastic ankle exoskeletons. *J. Appl. Physiol.* 113, 1862–1872. doi: 10.1152/japplphysiol.00802.2012

Farris, D. J., Hicks, J. L., Delp, S. L., and Sawicki, G. S. (2014). Musculoskeletal modelling deconstructs the paradoxical effects of elastic ankle exoskeletons on plantar-flexor mechanics and energetics during hopping. *J. Exp. Biol.* 217, 4018–4028. doi: 10.1242/jeb.107656

Ferris, D. P., Sawicki, G. S., and Daley, M. A. (2007). A physiologist's perspective on robotic exoskeletons for human locomotion. *Int. J. Hum. Rob.* 4, 507–528. doi: 10.1142/S0219843607001138

Flynn, L., Geeroms, J., Jimenez-Fabian, R., Vanderborght, B., Vitiello, N., and Lefeber, D. (2015). Ankle-knee prosthesis with active ankle and energy transfer: development of the CYBERLEGs alpha-prosthesis. *Rob. Auton. Syst.* 73, 4–15. doi: 10.1016/j.robot.2014.12.013

Galle, S., Malcolm, P., Collins, S. H., and De Clercq, D. (2017). Reducing the metabolic cost of walking with an ankle exoskeleton: interaction between actuation timing and power. *J. Neuroeng. Rehabil.* 14:35. doi: 10.1186/s12984-017-0235-0

Galle, S., Malcolm, P., Derave, W., and De Clercq, D. (2013). Adaptation to walking with an exoskeleton that assists ankle extension. *Gait Posture* 38, 495–499. doi: 10.1016/j.gaitpost.2013.01.029

Galle, S., Malcolm, P., Derave, W., and De Clercq, D. (2015). Uphill walking with a simple exoskeleton: plantarflexion assistance leads to proximal adaptations. *Gait Posture* 41, 246–251. doi: 10.1016/j.gaitpost.2014.10.015

Gordon, K. E., Sawicki, G. S., and Ferris, D. P. (2006). Mechanical performance of artificial pneumatic muscles to power an ankle-foot orthosis. *J. Biomech.* 39, 1832–1841. doi: 10.1016/j.jbiomech.2005.05.018

Gottschall, J. S., and Kram, R. (2005). Energy cost and muscular activity required for leg swing during walking. *J. Appl. Physiol.* 99, 23–30. doi: 10.1152/japplphysiol.01190.2004

Grimmer, M., and Seyfarth, A. (2009). "Biarticular structures to strengthen the push-off in lower leg prosthesis," in *Dynamic Walking Conference* (Vancouver, BC). Available online at: http://citeseerx.ist.psu.edu/viewdoc/download?doi=10.1.1.514.5565&rep=rep1&type=pdf

Herr, H. (2009). Exoskeletons and orthoses: classification, design challenges and future directions. *J. Neuroeng. Rehabil.* 6:21. doi: 10.1186/1743-0003-6-21

Hof, A. L. (2001). The force resulting from the action of mono- and biarticular muscles in a limb. *J. Biomech.* 34, 1085–1089. doi: 10.1016/S0021-9290(01)00056-2

Jackson, R. W., and Collins, S. H. (2015). An experimental comparison of the relative benefits of work and torque assistance in ankle exoskeletons. *J. Appl. Physiol.* 119, 541–557. doi: 10.1152/japplphysiol.01133.2014

Junius, K., Moltedo, M., Cherelle, P., Rodriguez-Guerrero, C., Vanderborght, B., and Lefeber, D. (2017). Biarticular elements as a contributor to energy efficiency: biomechanical review and application in bio-inspired robotics. *Bioinspir. Biomim.* doi: 10.1088/1748-3190/aa806e. [Epub ahead of print].

Koller, J. R., Jacobs, D. A., Ferris, D. P., and Remy, C. D. (2015). Learning to walk with an adaptive gain proportional myoelectric controller for a robotic ankle exoskeleton. *J. Neuroeng. Rehabil.* 12:97. doi: 10.1186/s12984-015-0086-5

Malcolm, P., Derave, W., Galle, S., and De Clercq, D. (2013). A simple exoskeleton that assists plantarflexion can reduce the metabolic cost of human walking. *PLoS ONE* 8:e56137. doi: 10.1371/journal.pone.0056137

McGowan, C. P., Neptune, R. R., and Kram, R. (2008). Independent effects of weight and mass on plantar flexor activity during walking: implications for their contributions to body support and forward propulsion. *J. Appl. Physiol.* 105, 486–494. doi: 10.1152/japplphysiol.90448.2008

Mooney, L. M., and Herr, H. M. (2016). Biomechanical walking mechanisms underlying the metabolic reduction caused by an autonomous exoskeleton. *J. Neuroeng. Rehabil.* 13:4. doi: 10.1186/s12984-016-0111-3

Neptune, R. R., Kautz, S. A., and Zajac, F. E. (2001). Contributions of the individual ankle plantar flexors to support, forward progression and swing initiation during walking. *J. Biomech.* 34, 1387–1398. doi: 10.1016/S0021-9290(01)00105-1

Park, Y. L., Santos, J., Galloway, K. G., Goldfield, E. C., and Wood, R. J. (2014). "A soft wearable robotic device for active knee motions using flat pneumatic artificial muscles," in *Proceedings - IEEE International Conference on Robotics and Automation* (Hong Kong), 4805–4810.

Quinlivan, B. T., Lee, S., Malcolm, P., Rossi, D. M., Grimmer, M., Siviy, C., et al. (2017). Assistance magnitude versus metabolic cost reductions for a tethered multiarticular soft exosuit. *Sci. Robot.* 2:eaah4416. doi: 10.1126/scirobotics.aah4416

Robertson, D. G. E., Caldwell, G. E., Hamill, J., Kamen, J., and Whittlesey, S. N. (2004). *Research Methods in Biomechanics*. Champaign, IL: Human Kinetics Publishers.

Rose, J., Ralston, H. J., and Gamble, J. G. (1994). "Energetics of walking," *in Human Walking. 2nd Edn.*, eds J. Rose and J. G. Gamble (Baltimore, MD: Williams & Wilkins) 45–72.

Sakagami, Y., Watanabe, R., Aoyama, C., Matsunaga, S., Higaki, N., and Fujimura, K. (2002). "The intelligent ASIMO: system overview and integration," in *IEEE/RSJ International Conference on Intelligent Robots and System* (Lausanne), 2478–2483.

Sasaki, K., and Neptune, R. R. (2006). Differences in muscle function during walking and running at the same speed. *J. Biomech.* 39, 2005–2013. doi: 10.1016/j.jbiomech.2005.06.019

Sawicki, G. S., and Ferris, D. P. (2008). Mechanics and energetics of level walking with powered ankle exoskeletons. *J. Exp. Biol.* 211, 1402–1413. doi: 10.1242/jeb.009241

Sawicki, G. S., and Ferris, D. P. (2009). A pneumatically powered knee-ankle-foot orthosis (KAFO) with myoelectric activation and inhibition. *J. Neuroeng. Rehabil.* 6:23. doi: 10.1186/1743-0003-6-23

Sawicki, G. S., and Khan, N. S. (2016). "A simple model to estimate plantarflexor muscle-tendon mechanics and energetics during walking with elastic ankle exoskeletons," in *IEEE Transactions on Biomedical Engineering*, 914–923. Available online at: http://ieeexplore.ieee.org/abstract/document/7299271/

Suzuki, K., Mito, G., Kawamoto, H., Hasegawa, Y., and Sankai, Y. (2007). Intention-based walking support for paraplegia patients with Robot Suit HAL. *Adv. Robot.* 21, 1441–1469. doi: 10.1163/156855307781746061

Uchida, T. K., Seth, A., Pouya, S., Dembia, C. L., Hicks, J. L., and Delp, S. L. (2016). Simulating ideal assistive devices to reduce the metabolic cost of running. *PLoS ONE* 11:e0163417. doi: 10.1371/journal.pone.0163417

van den Bogert, A. J. (2003). Exotendons for assistance of human locomotion. *Biomed. Eng. Online* 2:17. doi: 10.1186/1475-925X-2-17

Van Dijk, W. (2015). *Human–Exoskeleton Interaction*. Ph.D. thesis, Delft. Available online at: https://repository.tudelft.nl/islandora/object/uuid:8cf37c65-a48c-476e-8dcc-eb97c06c26d9/datastream/OBJ/download

van Dijk, W., van der Kooij, H., and Hekman, E. (2011). "A Passive Exoskeleton with Artificial Tendons," in *Proceedings of the IEEE International Conference on Rehabilitation Robotics* (Zurich), 1–6.

van Ingen Schenau, G. J. (1990). On the action of bi-articular muscles, a review. *Netherlands J. Zool.* 40, 521–540. doi: 10.1163/156854290X00073

Van Ingen Schenau, G. J., Bobbert, M. F., and Rozendal, R. H. (1987). The unique action of bi-articular muscles in complex movements. *J. Anat*. 155, 1–5.

Wehner, M., Quinlivan, B., Aubin, P. M., Martinez-Villalpando, E., Baumann, M., Stirling, L., et al. (2013). "A lightweight soft exosuit for gait assistance," in *Proceedings - IEEE International Conference on Robotics and Automation* (Karlsruhe: IEEE), 3362–3369.

Willson, A. M., Routson, R. L., Steele, K. M., Morgenroth, D. C., Czerniecki, J. M., and Aubin, P. M. (2015). "Toward a biarticular prosthesis: model development and sensistivity analysis of spring parameters," in *Young Investigator Symposium*. Available online at: http://faculty.washington.edu/paubin/wordpress/wp-content/uploads/2015/09/YIS2015BiarticularAbstract.pdf

Winter, D. A. (1983). Energy generation and absorption at the ankle and knee during fast, natural, and slow cadences. *Clin. Orthop. Relat. Res*. 175, 147–154. doi: 10.1097/00003086-198305000-00021

Witte, K. A., Fatschel, A. M., and Collins, S. H. (2017). "Design of a lightweight, tethered, torque-controlled knee exoskeleton," in *Proceedings of the IEEE International Conference on Rehabilitation Robotics* (London). doi: 10.1109/ICORR.2017.8009484

Yandell, M. B., Quinlivan, B. T., Popov, D., Walsh, C., and Zelik, K. E. (2017). Physical interface dynamics alter how robotic exosuits augment human movement: implications for optimizing wearable assistive devices. *J. Neuroeng. Rehabil*. 14:40. doi: 10.1186/s12984-017-0247-9

Zhang, J., Fiers, P., Witte, K. A., Jackson, R. W., Poggensee, K. L., Atkeson, C. G., et al. (2017). Human-in-the-loop optimization of exoskeleton assistance during walking. *Science* 356, 1280–1284. doi: 10.1126/science.aal5054

Conflict of Interest Statement: The authors declare that the research was conducted in the absence of any commercial or financial relationships that could be construed as a potential conflict of interest.

frontiers in Neuroscience

ORIGINAL RESEARCH
published: 02 March 2018
doi: 10.3389/fnins.2018.00099

Reshaping of Gait Coordination by Robotic Intervention in Myelopathy Patients After Surgery

Sandra Puentes[1,2], Hideki Kadone[2], Shigeki Kubota[3], Tetsuya Abe[3], Yukiyo Shimizu[4], Aiki Marushima[5], Yoshiyuki Sankai[6], Masashi Yamazaki[3] and Kenji Suzuki[6]*

[1] Faculty of Engineering, Information and Systems, University of Tsukuba, Ibaraki, Japan, [2] Center for Innovative Medicine and Engineering, University of Tsukuba Hospital, Ibaraki, Japan, [3] Department of Orthopaedic Surgery, Faculty of Medicine, University of Tsukuba Hospital, Ibaraki, Japan, [4] Department of Rehabilitation Medicine, Faculty of Medicine, University of Tsukuba Hospital, Ibaraki, Japan, [5] Department of Neurosurgery, Faculty of Medicine, University of Tsukuba Hospital, Ibaraki, Japan, [6] Center for Cybernics Research, University of Tsukuba, Ibaraki, Japan

The Ossification of the Posterior Longitudinal Ligament (OPLL) is an idiopathic degenerative spinal disease which may cause motor deficit. For patients presenting myelopathy or severe stenosis, surgical decompression is the treatment of choice; however, despite adequate decompression residual motor impairment is found in some cases. After surgery, there is no therapeutic approach available for this population. The Hybrid Assistive Limb® (HAL) robot suit is a unique powered exoskeleton designed to predict, support, and enhance the lower extremities performance of patients using their own bioelectric signals. This approach has been used for spinal cord injury and stroke patients where the walking performance improved. However, there is no available data about gait kinematics evaluation after HAL therapy. Here we analyze the effect of HAL therapy in OPLL patients in acute and chronic stages after decompression surgery. We found that HAL therapy improved the walking performance for both groups. Interestingly, kinematics evaluation by the analysis of the elevation angles of the thigh, shank, and foot by using a principal component analysis showed that planar covariation, plane orientation, and movement range evaluation improved for acute patients suggesting an improvement in gait coordination. Being the first study performing kinematics analysis after HAL therapy, our results suggest that HAL improved the gait coordination of acute patients by supporting the relearning process and therefore reshaping their gait pattern.

Keywords: myelopathy, motor deficit, gait coordination, kinematics, robotic therapy, gait reshaping

OPEN ACCESS

Edited by:
Yury Ivanenko, Fondazione Santa Lucia (IRCCS), Italy

Reviewed by:
Thomas Hoellinger, Université Libre de Bruxelles, Belgium
Michael James MacLellan, Louisiana State University, United States

****Correspondence:***
Sandra Puentes
sandra@ccr.tsukuba.ac.jp

Specialty section:
This article was submitted to Neuroprosthetics, a section of the journal Frontiers in Neuroscience

Received: *31 August 2017*
Accepted: *08 February 2018*
Published: *02 March 2018*

Citation:
Puentes S, Kadone H, Kubota S, Abe T, Shimizu Y, Marushima A, Sankai Y, Yamazaki M and Suzuki K (2018) Reshaping of Gait Coordination by Robotic Intervention in Myelopathy Patients After Surgery. Front. Neurosci. 12:99. doi: 10.3389/fnins.2018.00099

INTRODUCTION

The Ossification of the Posterior Longitudinal Ligament (OPLL) is an uncommon disease characterized by a pathological ectopic ligament ossification affecting usually the cervical or thoracic spine segments (Epstein, 2002; Kalb et al., 2011). This degenerative disease has high prevalence in Asian populations, with a high incidence in the Japanese community (Epstein, 2002; Kalb et al., 2011; Smith et al., 2011; Kommu et al., 2014); however, in the past years features of OPLL has been recognized also in patients from Europe and North America

(Kalb et al., 2011). The disease onset typically affect patients in their fifties, and has an incidence twice as high for males than for females (Epstein, 1992; Choi et al., 2011; Kommu et al., 2014). Surgical decompression of the spinal cord is usually necessary when the medullar compression leads to symptomatic neurological deterioration (Mehdi et al., 2016); nonetheless, despite appropriate decompression residual motor impairment is found in some patients. The degree of canal stenosis, intramedullary conditions, initial motor score and patient age have been related with the outcome where the prognosis is less optimistic for older patients with severe neurologic deficit and marked myelopathy signs (Gu et al., 2015; Kwon et al., 2015). After decompression surgery, if gait disturbances are sustained there is no available intervention to support the motor rehabilitation of such patients.

The Hybrid Assistive Limb®(HAL) robot suit is a wearable powered exoskeleton designed to assist the voluntary control of hip and knee joint motion (Kawamoto et al., 2014). It has six degrees of freedom related to the sagittal movement of the bilateral hip, knee, and ankle joints. It has four motors distributed bilaterally, located over the lateral aspects of the hip and knee joints. The motors receive information from surface electrodes which are able to collect bioelectric signals from the action potential reaching the muscles during movement preparation and initiation. Such information is processed and used by the exoskeleton to assist the patient during gait training. In previous studies where HAL was used in neurologic patients with gait disturbances, improvement in clinical scores, and walking performance, such as elongation of the stride length and increment of gait speed, was found (Kawamoto et al., 2013; Sakakima et al., 2013; Fujii et al., 2016; Kubota et al., 2016; Sczesny-Kaiser et al., 2017). A group of stroke patients treated with HAL improved their sit-to-stand movements thanks to the increment of the forward tilt angle (Kasai and Takeda, 2016). Additionally, spinal cord injury patients showed improvement in their spasticity (Ikumi et al., 2016), recovery of lower limb muscle activities (Shimizu et al., 2017), reduction of neuropathic pain (Cruciger et al., 2016) and normalization of cortical excitability and cortical plasticity (Sczesny-Kaiser et al., 2017). However, there is no available data about gait kinematics evaluation after HAL therapy.

For gait kinematic analysis, joint angle measurements were used in the past; however, the pattern of the angles of flexion-extension at the hip and ankle joints tends to differ from each subject and vary largely depending on the gait speed (Borghese et al., 1996). On the other hand, the evaluation of the lower limbs with respect to the vertical when divided in three segments has shown a stereotyped pattern across different subjects without regard to gait pattern, speed, or anatomic discrepancies (Borghese et al., 1996). Described by Borghese et al. (1996) the so-called law of intersegmental coordination is a kinematic law that describes the coordination patterns given by the correlation of the elevation angles of the lower limb divided in three segments (thigh, shank, and foot) with respect to the vertical. From this point of view, the degrees of freedom of the lower limb are reduced to 3, and when the angles are plotted against each other, they covary presenting regular loops on a plane. Intersegmental coordination analysis has been used in conditions affecting gait pattern and coordination as stroke (Chow and Stokic, 2015) and cerebellar ataxia (Martino et al., 2014); and also for assessment after therapeutic interventions as botulin toxin injections for spasticity control (Bleyenheuft et al., 2009), ankle foot orthoses in stroke patients (Bleyenheuft et al., 2013), and combined therapy for Parkinson patients (Grasso et al., 1999). However, there is no report of planar covariation analysis in patients with gait impairment receiving robotic assisted therapy.

In this study, HAL therapy was applied to OPLL patients in an acute or chronic stage after decompression surgery. Clinical scores, walking performance, and kinematics analysis was performed before the first and after the last HAL therapy session. To our knowledge, this is the first study applying kinematic analysis in OPLL patients after HAL therapy.

MATERIALS AND METHODS

Patients

Twelve patients with a diagnosis of OPLL associated to severe motor symptoms and followed by decompression surgery joined the present study. The patients were distributed in acute (3 women, 2 men, age ± 59.6 years; starting at ± 24.4 days after surgery), and chronic groups (7 men, age ± 70.1 years; starting at ± 1151.4 days after surgery) accordingly to the time interval elapsed between decompression surgery and HAL therapy (**Table 1**). All the patients included in this study were

TABLE 1 | Subjects characteristics.

Participant ID	Group	Sex	Age	Surgery-HAL interval (days)
A1	Acute	F	78	15
A2	Acute	M	64	26
A3	Acute	M	52	18
A4	Acute	F	63	32
A5	Acute	F	41	31
C1	Chronic	M	70	288
C2	Chronic	M	75	287
C3	Chronic	M	68	3,655
C4	Chronic	M	78	372
C5	Chronic	M	76	2,188
C6	Chronic	M	58	540
C7	Chronic	M	66	730
H1	Healthy	F	56	–
H2	Healthy	F	42	–
H3	Healthy	F	59	–
H4	Healthy	F	67	–
H5	Healthy	F	60	–
H6	Healthy	M	50	–
H7	Healthy	M	45	–
H8	Healthy	M	77	–

Surgery-HAL interval refers to the days elapsed from surgery to the beginning of HAL therapy.

able to voluntarily control their lower limbs. For acute patients, weight support was provided if necessary, so that the patient could produce gait by him/herself; all chronic patients were able to walk independently with or without cane support. Kinematics data from eight healthy volunteers (5 women, 3 men, age ± 57 years) who did not receive HAL treatment was also used for comparisons. This study was approved by the University of Tsukuba Hospital Ethics Committee (Approval number: H26-22) and implemented according to the ethical principles of the Declaration of Helsinki and the University Guidelines for Clinical Trials. All patients received a personalized explanation of the research contents, participation and data usage before signing an informed consent.

HAL Setup

For this study, double leg version of robot suit HAL was used. Surface electrodes were placed to detect neuromuscular activity of Iliopsoas (hip flexor), Gluteus Maximus (hip extensor), Biceps Femoris (knee flexor), and Quadriceps (vastus lateralis, knee extensor); these signals were used by the robot to support a patients' gait. Four motors were placed bilaterally beside the patient's hip and knee (two per leg). A hip motor was actuated to produce torque in proportion to a weighted difference of filtered activation of flexor and extensor muscles of the hip. In the same manner, a knee motor was actuated using filtered activation of the knee's flexor and extensor muscles. The weights multiplied on the activation of each of the antagonistic pair of the muscles, and the overall gain, were adjusted manually for each patient's comfort through the HAL therapy sessions.

Evaluation

Before starting the first HAL therapy session and after the last one, a functional evaluation was performed by using the modified Ranking Scale (mRS), Barthel Index (BI), Functional Independence Measure (FIM, motor score only), and the American Spinal Injury Association impairment scale (ASIA, motor score only) scores in order to evaluate the degree of dependence on daily life activities. Following, the patients were evaluated without fitting the robot by using the 10 m walk test where time and number of steps were counted while the patient walked 10 m in a straight line at a comfortable pace; the speed and stride length were calculated from this data.

HAL Therapy

The designed intervention consisted of 10 sessions of HAL therapy performed within the hospitalization period for acute patients. Chronic patients attended to the therapy in the hospital as outpatients. Sessions were carried out twice per week, 1 h per session divided in fitting, therapy, and releasing. Each session started by fitting HAL to the patient. A walking device (All-in-One Walking Trainer, Ropox A/S, Naestved, Denmark) with a harness was used to prevent falls, and to support body weight in some patients who needed it to walk. A HAL therapy session included 20 min of walking activity at a comfortable pace on a 25 m oval course with rest intervals. At the end of the session, the patient was released from the harness and robot. Vital signs including blood pressure, heart rate, and oxygen saturation were monitored at the beginning, end and within therapy intervals to ensure that patients were stable.

Data Collection and Analysis

Before the initial and after the final session of HAL therapy, a motion capture system (VICON MX, 16 T20s cameras, 100 Hz) was used with Plug-in gait lower limbs marker-set to record segmental kinematics. Following the method described by Borghese et al. (1996), the lower limbs of the participants were analyzed regarding the elevation angles (EA) composed by the orientation of the limb segments in the sagittal plane with respect to the vertical. The evaluated segments (**Figure 2A**) were thigh (trochanter to lateral epicondyle of the femur), shank (lateral epicondyle of the femur to lateral malleolus), and foot (posterior calcaneal tuberosity to second metatarsal). For each leg of each participant, planar covariation of the EA was calculated by using a principal component (PC) analysis, after normalization by subtracting the mean value. In normal conditions, the first (PC1) and second (PC2) components covariates over a plane describing the shape of the gait loop; we assessed the proportional width of the covariance loop by the percentage of variance (PV) of the PC2 (PV2) (Martino et al., 2014). The third component (PC3) is orthogonal to the plane, showing the data component that deviates from the covariance plane. The PV represented by the PC3 (PV3) becomes an index of planarity of the loop, where 0% corresponds to an ideal plane, evaluating the proportional deviation from the covariance plane. Standard deviation of PC2 and PC3 scores (PC2-SD and PC3-SD) were computed to assess respectively the actual width of the covariance loop and the amount deviation from the covariance plane. To compare the plane orientation before and after HAL therapy, the unit vector U3 which is normal to the covariance plane was obtained as the third eigenvector of the covariance matrix. U3 is composed of the direction cosines of the normal vector (NV) against the coordinates of the thigh, shank, and foot. NV difference between planes before and after HAL therapy was calculated for acute and chronic groups. Following, to evaluate deviation of U3 from that of the healthy group, cosine deviation was calculated by the inner product of each patient's U3 against the averaged direction cosines (U3) of healthy volunteers group. Arccosine was calculated on the result of the inner product to obtain the angular deviation of U3 vector from averaged healthy patients.

In order to evaluate changes in the movement of EA range during gait, peak comparisons for each EA were made for acute and chronic groups. Gait cycles were extracted from the original data according to the movement of the toe and heel markers. Time variable was discarded to normalize the data from 0 to 100% to represent progression of gait for each cycle, and then averaged cycle profile was obtained for each elevation angle for each subject. Comparisons from the highest and lowest peaks and their difference were calculated for each EA. Data was plotted for acute and chronic groups and data from healthy volunteers was plotted along as reference.

Following, the distance from each data point to the covariance plane was calculated and comparisons were made before and after HAL therapy for each group. To graphically present the pattern of deviation from the covariance plane through gait cycle, a Kernel

method (Kim and Scott, 2012) was used to create a heat-map. The heat-map was then plotted on the covariance plane within the three-dimensional space of thigh, shank, and foot.

Kinematic data comparisons were done by using a paired Wilcoxon signed rank test to compare between before and after HAL therapy for each of acute and chronic groups, and by using an unpaired Wilcoxon signed rank test to compare between the healthy and each of Acute-pre, Acute-post, Chronic-pre, and Chronic-post groups. Due to the sample size, a *post-hoc* power test was applied to all significant data (1,000 times replication). Significance was considered when a $p < 0.05$ accompanied by a power test >80% was found. Marginal significance was considered with $p < 0.05$ and power test >50% (Hoenig and Heisey, 2001). All statistical analysis was carried out by using custom made scripts on MATLAB [version 8.4.0.150421(R2014B)] and RStudio (version 1.0.136).

RESULTS

In the present study, we found that HAL therapy improved the walking performance; the walking speed and stride length were increased, and the time and number of steps to cover 10 m were decreased, in all acute and chronic patients (**Figure 1A**). Positive effects were also found in the motor function scores; the BI and FIM scores were increased after HAL therapy for all acute patients (**Figure 1B**). mRS score was reduced in four, and stayed the same in one, of the acute patients. On the other hand, there was no change in the mRS, BI, or FIM functional evaluation scales of the chronic patients. ASIA scores did not show relevant changes for either group (**Figure 1B**). The improvements suggested possibility of beneficial effect of HAL for OPLL patients as previous studies (Aach et al., 2014; Fujii et al., 2016; Kasai and Takeda, 2016; Kubota et al., 2016). The effect of HAL therapy could be a reinforcement of the motor learning process during training, helping patients to reshape their motor function. Necessity for further investigation was considered.

In order to understand better the effect of HAL therapy, kinematics analysis was performed on the intersegmental correlation described by the covariation of thigh, shank, and foot EA (**Figure 2A**). At a glance, the shape of the loops described by patients were distorted in contrast with healthy volunteers evidencing impaired intersegmental coordination (**Figures 2B–C**). Comparison of PC2 standard deviation (PC2-SD) before and after HAL therapy was significantly different for acute group only (**Figure 3A**, PC2-SD mean; acute-pre: 9.30 ± 3.46, acute-post: 12.43 ± 1.41, chronic-pre: 11.54 ± 2.55, chronic-post: 12.57 ± 2.62. PC2-SD *P*-values; acute pre-post: <0.01, power test: 64.4%, chronic pre-post: < 0.01, power test: 15.7%. Supplementary Tables 1, 2). The significant change of PC2-SD before and after HAL therapy for acute group seems to be beneficial regarding the results comparison contrasted to healthy volunteers; where PC2-SD increased for acute and chronic groups after HAL therapy, becoming closer to healthy participants (**Figure 3A**, PC2-SD mean; healthy: 13.40 ± 1.16. PC2-SD *P*-values; pre-acute vs. healthy: <0.01, power test: 91%; post-acute vs. healthy: 0.039, power test: 39.8%; pre-chronic vs. healthy: 0.017, power test: 67.4%; post-chronic vs. healthy: 0.355. Supplementary Tables 1, 2). Comparison of PV2 before and after HAL therapy did not differ in acute or chronic group (**Figure 3B**, PV2 mean acute-pre: 0.17 ± 0.04, acute-post: 0.15 ± 0.02, chronic-pre: 0.18 ± 0.04, chronic-post: 0.18 ± 0.05. PV2 *P*-values; acute pre-post: 0.275, chronic pre-post: 0.808. Supplementary Tables 1, 2). Additionally, PV2 difference was found before but not after HAL therapy between acute patients and healthy volunteers (**Figure 3B**, PV2 mean; healthy: 0.14±0.03. PV2 *P*-values; pre-acute vs. healthy: 0.053, power test: 55.5%; post-acute vs. healthy: 0.139; pre-chronic vs. healthy: <0.01, power test: 75.2%; post-chronic vs. healthy: <0.01, power test: 76.3%. Supplementary Tables 1, 2). These results suggest that HAL therapy improved the actual width of the gait loop on the covariance plane for both acute and chronic groups, while improvement of proportional width of the loop was observed only for acute group (**Figures 3A,B**).

Deviation from covariation plane evaluated by PC3-SD comparison did not show significant difference between before and after HAL therapy for either of acute and chronic groups (**Figure 3C**, PC3-SD mean; acute-pre: 3.65 ± 1.13, acute-post: 4.30 ± 0.64, chronic-pre: 2.99 ± 0.96, chronic-post: 3.09 ± 1.01. PC3-SD *P*-values; acute pre-post: 0.083, chronic pre-post: 0.104. Supplementary Tables 1, 2). Comparison against healthy group showed a significant difference only for acute group after HAL. (**Figure 3C**, PC3-SD mean; healthy: 3.57 ± 0.51. PC3-SD *P*-values; pre-acute vs. healthy: 0.391, post-acute vs. healthy: <0.01, power test: 82.5%; pre-chronic vs. healthy: 0.011, power test: 48.2%; post-chronic vs. healthy: 0.042, power test: 30.2%. Supplementary Tables 1, 2). However, proportional deviation from covariation plane evaluated by PV3 demonstrated a trend close to significance showing a better plane fitting after HAL therapy for acute but not for chronic group; quantitative comparison between PV3 before and after HAL therapy were close to significance for acute group only (**Figure 3D**, PV3 mean acute-pre: 0.03 ± 0.01, acute-post: 0.02 ± 0.007, chronic-pre: 0.013 ± 0.009, chronic-post: 0.012 ± 0.009. PV3 *P*-values; acute pre-post: 0.027, power test: 47.2%, chronic pre-post: 0.295. Supplementary Tables 1, 2). Comparisons against healthy volunteers showed significant difference of PV3 for acute patients before and after HAL therapy but not for chronic patients (**Figure 3D**, PV3 mean; healthy: 0.009 ± 0.002. PV3 *P*-values; pre-acute vs. healthy: <0.01, power test: 96.5%; post-acute vs. healthy: <0.01, power test: 94.6%; pre-chronic vs. healthy: 0.473; post-chronic vs. healthy: 0.447. Supplementary Tables 1, 2). Tendency of PV3 recovery was observed for acute group suggesting a positive change in planarity of coordination after HAL therapy (**Figure 3D**), although it did not reach a level comparable to healthy volunteers. On the other hand, comparisons between chronic and healthy groups did not show significant difference.

Plane orientation evaluated by the NV difference between acute and chronic groups was also significantly different (acute angle mean: 6.82 ± 4.93 deg, chronic angle mean: 2.58 ± 2.18 deg. Acute-chronic *P*-value 0.026, power test 63.1%) suggesting that plane orientation changes after HAL therapy were larger for acute group than the changes found for chronic group. The angular

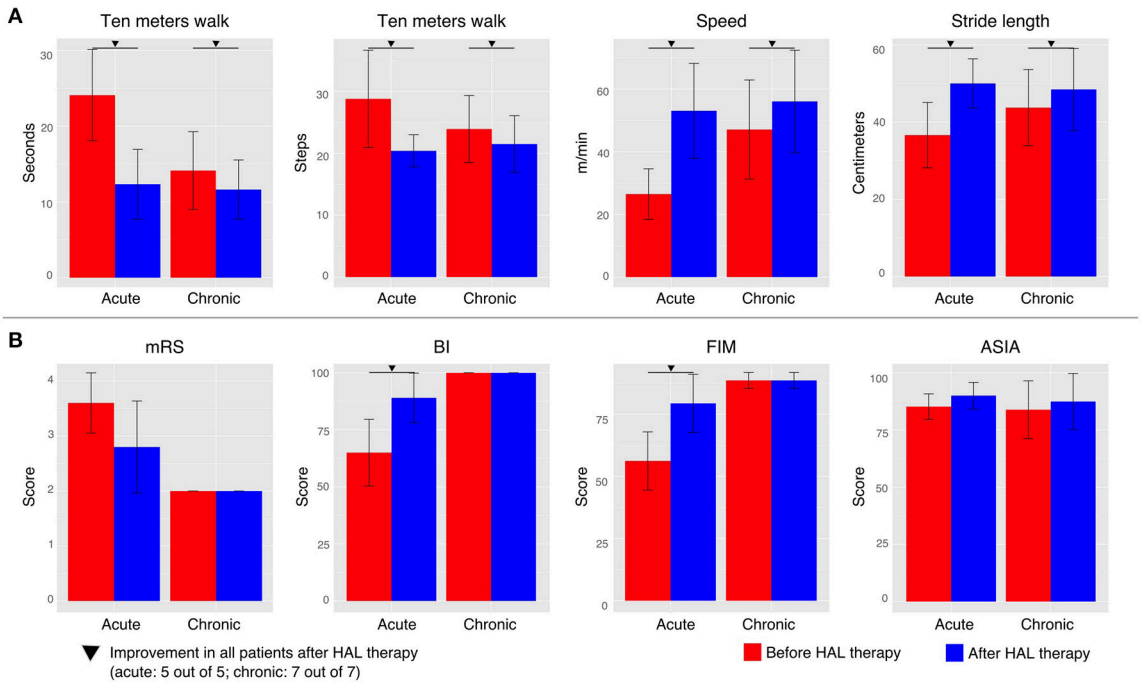

FIGURE 1 | Walking performance and clinical evaluation. **(A)** The walking performance was assessed without fitting the robot during the 10 m walk test. **(B)** Clinical evaluation was performed by using the modified Ranking Scale (mRS), Barthel Index (BI), Functional Independence Measure (FIM, motor score), and the American Spinal Injury Association impairment scale (ASIA) in order to evaluate the degree of dependency of each patient. Patients were tested before the first HAL therapy and after the last one. Inverted triangle marks indicate improvement in all patients before and after HAL therapy (5 out to 5 for acute group and 7 out of 7 for chronic group).

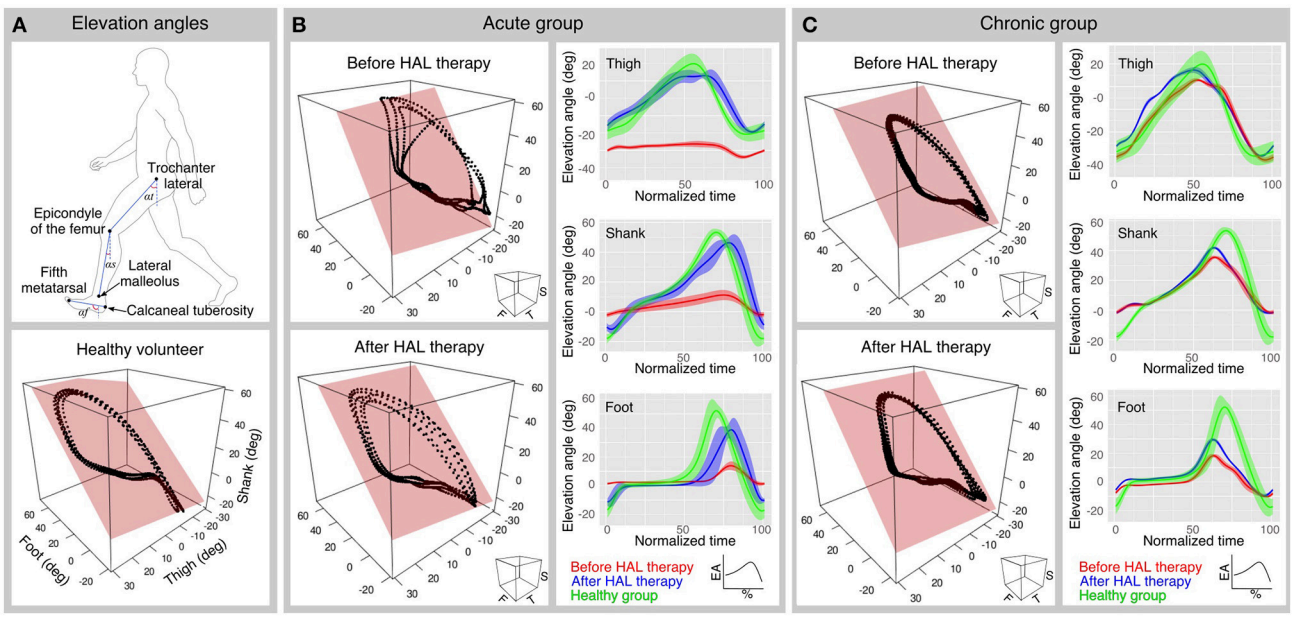

FIGURE 2 | Planar covariation and peaks analysis. **(A)** Upper panel shows the segments used to calculate the elevation angles. Lower panel shows a planar covariation analysis plot from a healthy volunteer. **(B,C)** Planar covariation analysis sample data for one acute **(B)** and one chronic **(C)** patient before and after HAL therapy (left column). Each dotted trajectory corresponds to different strides of a single subject. Elevation angle profiles also were plotted before and after HAL therapy for each segment (right column); The normalized time corresponds to the percentage of the walking cycle; solid lines represent the average and the width of the highlighted area is given by the standard deviation.

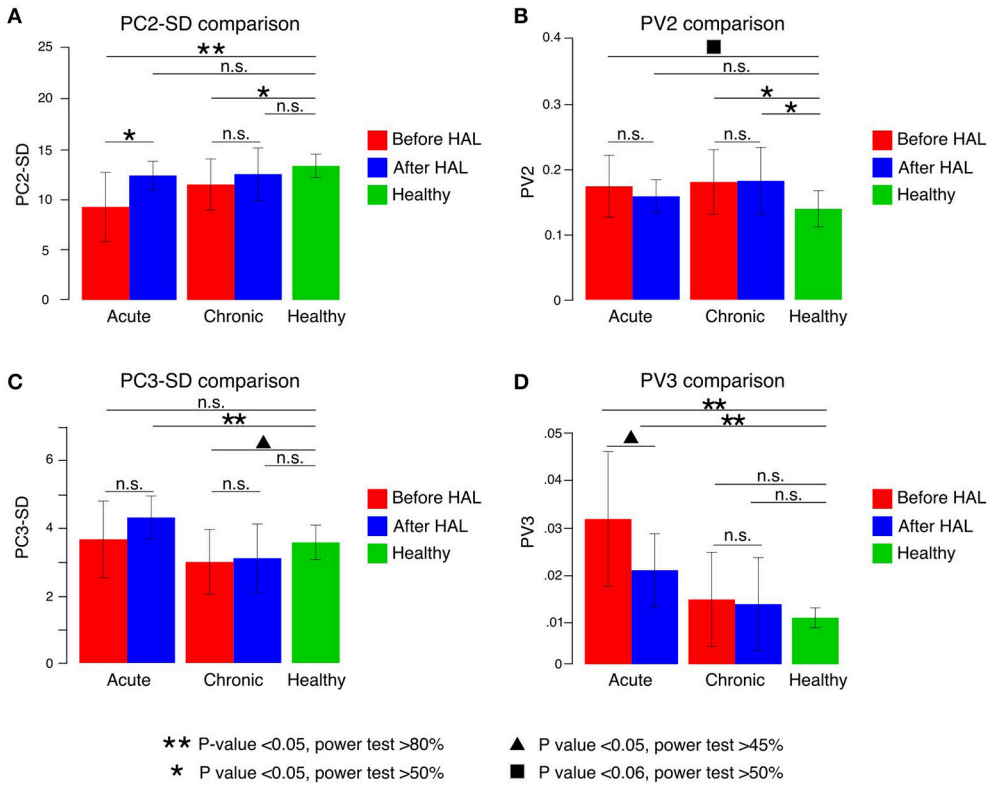

FIGURE 3 | Principal components (PC) and percentage of variance (PV) comparisons. **(A)** PC2 SD increased significantly in acute patients after HAL therapy. Significant difference when compared to healthy volunteers was found in both groups before HAL therapy but not after HAL therapy. **(B)** PV2 comparisons before and after HAL therapy did not show significant changes in either group. When compared to healthy volunteers, acute patients showed a difference close to significance before HAL therapy only. Chronic group PV2 was significantly different from healthy before and after HAL therapy. **(C)** PC3-SD comparisons only showed significant difference from healthy group for acute patients after HAL therapy and chronic patients before HAL therapy. **(D)** PV3 comparisons showed a notable reduction after HAL therapy for acute group. Despite being closer to healthy group, it was still significantly different. Double asterisk marks refer to $P < 0.05$ and power test >80%; single asterisk notes $P < 0.05$ and power test >50%; triangle mark refers to $P < 0.05$ with power test >40%; square mark notes $P < 0.06$ and power test >50% and n.s. refers to non-significant changes.

deviation of U3 vector from averaged healthy volunteers changed mainly for acute group only (U3 mean. Acute-pre: 7.720 ± 0.56 deg, acute-post: 8.168 ± 0.19 deg. *P*-value acute pre-post <0.01, power test 54.9%. Chronic-pre: 8.085 ± 0.23 deg, chronic-post: 8.1366 ± 0.278 deg. *P*-value chronic pre-post: 0.049, power test: 6.4%).

Peak comparisons before and after HAL therapy (max peak, min peak, and max-min difference) were used to evaluate the limb movement range during gait. For acute group, foot EA comparisons were significantly different for the max peak and max-min difference (max foot mean; pre: 34.01 ± 16.88 deg, post: 55.27 ± 7.44 deg, pre-post *P*-value <0.01, power test: 81.5%. min foot mean; pre: −15.48 ± 8.84 deg, post: 24.88 ± 4.58 deg, pre-post *P*-value <0.01, power test: 72%; max-min difference foot mean; pre: 49.49 ± 23.8 deg, post: 80.16 ± 9.50 deg, pre-post *P*-value<0.01, power test: 85.4%) suggesting improvement of the foot excursion. Other peaks did not show significance (*P*-values for max thigh: 0.275; max shank: 0.037, power test: 42.3%; min thigh: 0.492; min shank 0.019, power test 38.1%; max-min diff thigh: 0.083; max-min diff shank: <0.01, power test: 52.4%). On the other hand, chronic group patients did not show significant changes among peaks (*P*-values for max thigh: 0.761; max shank: 0.104; max foot: <0.01, power test: 23.7%; min thigh: 0.135; min shank: 0.583; min foot: 0.808; max-min diff thigh: <0.01, power test: 49.2%; max-min diff shank: <0.01, power test: 12.8%; max-min diff foot: <0.01, power test: 19.4%) (Supplementary Tables 3, 4). This finding may suggest that acute patients foot coordination improved giving the patients a longer stride and better foot clearance. Although shank EA peaks did not show significance for chronic patients, its difference increased after HAL therapy (shank EA difference: pre: 54.313 deg, post: 57.518 deg) (**Figures 2B,C**, right column); this increment may be related to an enlargement of movement range, and may be the reason of the larger stride length and improved limb excursion after HAL therapy in chronic patients.

Heat maps were used to assess the pattern of deviation from the covariance plane through the gait cycle. The pattern found in healthy volunteers showed hot spots in the areas related to heel strike and toe off (**Figure 4A**). However, patients from the acute group tended to have shifted hot spots which tended to recover the healthy pattern after HAL therapy (**Figure 4B**). Chronic patients had hot spots sprayed around the gait loop;

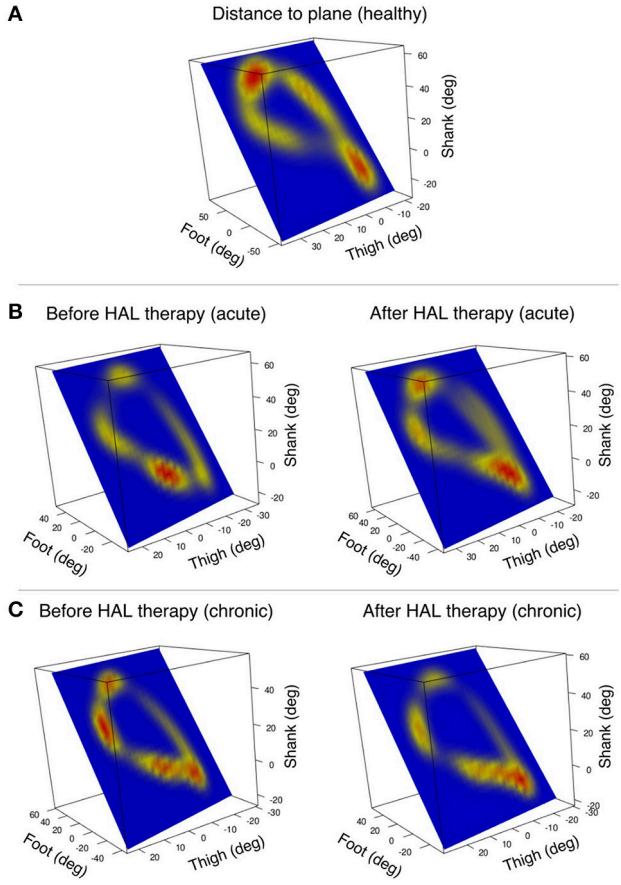

FIGURE 4 | Pattern of deviation from the covariance plane through gait cycle is visualized by heat-maps. The heat-maps are plotted on the covariance plane within the tridimensional space of thigh, shank, and foot. **(A)** An example of a healthy volunteer shows deviation from the plane mainly in the zones corresponding to heel strike and toe off. **(B)** Acute patient's deviation from the plane was shifted before HAL therapy, but the pattern was recovered after HAL therapy (one patient single leg example). **(C)** Chronic patients had several hot spots marking deviation from the plane that changed briefly after HAL therapy (one patient single leg example).

after HAL therapy, there was a tendency to reduce these hot spots (**Figure 4C**). The resemblance of acute pattern after HAL therapy to healthy volunteers suggests an improvement in limb motion and excursion. This data redistribution support our theory about coordination improvement after HAL therapy for acute OPLL patients.

DISCUSSION

It has been well-established that covariation of the EA corresponding to the lower limbs (thigh, shank, and foot) is consistent across subjects during bipedal walking in normal conditions (Borghese et al., 1996; Bianchi et al., 1998a; Ivanenko et al., 2008), and it is preserved during different gait perturbations (Bianchi et al., 1998b; Grasso et al., 1998; Ivanenko et al., 2002; Noble and Prentice, 2008). Also, there are previous studies of planar covariation in different medical conditions as stroke (Bleyenheuft et al., 2009; Chow and Stokic, 2015), lower limb amputations (Leurs et al., 2012), and cerebellar ataxia (Martino et al., 2014) where the intersegmental coordination is maintained independently of the medical condition affecting the gait pattern. However, planar covariation is preserved only in amputees when using a prosthesis independently of the adaptation time (Leurs et al., 2012). Patients with impairment of the central motor pathways often show alterations in planar covariation of the EA suggesting that it has a central origin (Ivanenko et al., 2008; Bleyenheuft et al., 2009; Martino et al., 2014; Chow and Stokic, 2015).

It is said that the central nervous system may use the intersegmental coordination as a strategy to simplify the gait control by reducing the effective degrees of freedom of muscle activation (Lacquaniti et al., 2002). Additionally, studies in toddlers have shown that the planar covariation patterns evidenced in adults starts to appear when mature gait patterns are achieved, suggesting that a coordinated behavior is controlled centrally instead of pure biomechanical constraints (Cheron et al., 2001). This observation reinforces the statement that planar covariation alterations have a central component and does not depend on a simple biomechanical effect. Therefore, the alteration of the gait coordination may suggest the central nervous system recurring to alternative strategies to provide functional motor output.

Our kinematic analysis showed that the actual width of covariation loop was broadened for both acute and chronic patients after HAL therapy (**Figure 3A**). The widths became closer to healthy controls, suggesting improvement. The proportional width and planarity were improved for acute but not for chronic patients (**Figures 3B,D**). These improvements of planar covariation suggest a beneficial effect of HAL at the level of the central nervous system, including the spinal cord and the brain especially for acute patients, the changes leading them to functional recovery of gait. In acute patients, where myelopathy started recently and poor posture due to motor disturbances may have not been established yet, the conditions to get a marked improvement were better than for chronic patients. Thus, acute patients got improvement in their walking performance and coordination after HAL therapy probably secondary to spinal remodeling and reinforcement of central pattern generators. Also, the improvement of movement range evaluation related to foot peaks suggested that HAL treatment improved central coordination rather than segment-wise adaptation. For chronic patients, where myelopathy had become a chronic condition and the patient might have developed non-ergonomic postures to achieve a functional gait, the effect of HAL therapy was evident for walking performance but subtle for coordination related to planar covariation. We believe that chronic patients had earned already a certain degree of coordination that allowed them to perform basic daily life activities before HAL therapy. Still, the walking performance was improved for them after HAL therapy. Therefore, we may infer that HAL therapy helped them to adapt their strategies of coordinated limb motion control to improve the speed and stride length.

Previous studies have shown the beneficial effects of exercising as a non-invasive treatment to provide rhythmic stimulation to the spinal cord (Sandrow-Feinberg and Houlé, 2015; Gad et al., 2017). Stimulation of spinal pathways in a rhythmic fashion may provide a beneficial effect in gait recovery by enhancing the afferent input to the spinal cord and activating the central pattern generators. This activity also increase the central nervous system plasticity, neurogenesis, and remodeling (Dunlop, 2008; Houle and Côté, 2013); however, in patients with motor disabilities regular exercise generally is not an option. Rehabilitation programs are expensive, demanding and generally cannot be offered for long periods. Additionally, post-surgical patients do not have immediate access to an exercise source during the hospitalization term. The robot suit HAL treatment offers a unique opportunity because of its ability of supplying a constant feedback from the patient's own bioelectrical signals, providing support in accordance with the patient's voluntary gait during training. We believe that the HAL's feedback exerts a direct effect on the reshaping process of muscular recruitment, accelerating the gait restructuration to generate an improved walking pattern. We also think that an intense workout program as designed for HAL therapy may induce plasticity in the spinal cord and cortex leading to neurogenesis and reorganization of the available pathways to improve motor performance. Acute patients after a recent lesion may achieve faster improvement after HAL therapy by the degree of plasticity and rewiring process in the central nervous system. On the other hand for chronic patients, there was no marked effect in coordination. However, the walking performance of these patients were improved after HAL therapy suggesting that, although plasticity and remodeling process at the spinal cord level may be slower than acute patients, a lower level of neuroplasticity is still able to induce detectable changes during voluntary gait of chronic patients.

Additionally, the coincident improvement of the clinical evaluation of functional scores (**Figure 1B**) and the recovery of the planar covariation for acute patients (**Figure 3**) may suggest an association between the changes in the walking performance and gait coordination. We consider that gait coordination analysis can be applied as an objective functional evaluation of a patient's progress during rehabilitation program.

Apart from HAL, there are other robotic assisted therapies available for gait rehabilitation. The end effector-type robotic device known as "Gait Trainer" (Werner et al., 2002; Tong et al., 2006; Peurala et al., 2009) and the exoskeleton type known as Lokomat (Mayr et al., 2007) has been used for stroke patients. The subjects showed improvement in gait performance after the intervention when evaluating gait parameters and clinical scores. The Lokomat has been used also for spinal cord injury, where beneficial effects were found in clinical scores and gait parameters (Labruyere and Van Hedel, 2014; Nam et al., 2017). Some studies have used robotic assisted therapy combined with additional treatments, also finding a beneficial effect in the patients' clinical scores (Schwartz et al., 2009; Bae et al., 2014). In contrast to these robots, HAL provides motion assistance during gait based on detected bioelectric signals of the peripheral neuro-muscular activity relevant to the lower limb joint motions, helping the user to perform intended voluntary motion in real time. This feedback is considered to compensate for the disordered loop of active motion planning, execution and sensation. We hypothesize that this function of HAL contributes to reshaping of gait and neural systems behind locomotion, as described by the gait coordination changes shown in this study. To our knowledge, this is the first report regarding analysis on gait coordination of patients before and after robotic assisted rehabilitation.

This study has limitations regarding the size of the population. Also, it was not possible to compare our results to OPLL patients that did not receive HAL therapy to discard the possibility of recovery independent of the intervention. Although data cannot be extrapolated to all the population, this study give the first insight regarding robotic rehabilitation and changes of gait coordination analyzed by planar covariation. Further studies with larger populations should be done to continue exploring the effect of HAL therapy on gait coordination.

AUTHOR CONTRIBUTIONS

SP and HK collected, analyzed, and interpreted the data; wrote and drafted the manuscript. SK recruited the patients and administered HAL therapy. TA operated all the patients from acute group. YuS supported HAL therapy. AM provided important comments for the clinical part of the study and helped developing of HAL therapy. YoS originally developed the robot suit HAL and conceived the idea of HAL therapy. MY operated all patients from chronic group, and developed HAL therapy for OPLL patients. KS designed the analysis and provided essential insight for the paper. All authors made critical revisions of the manuscript and approved the final version.

FUNDING

This study was supported by the Industrial Disease Clinical Research Grant of the Ministry of Health, Labour and Welfare, Japan (14060101-01).

ACKNOWLEDGMENTS

Authors thank Ms. Mayuko Sakamaki and Ms. Yumiko Ito of Center for Innovative Medicine and Engineering (CIME) of the University of Tsukuba Hospital for their excellent assistance during HAL intervention. We also thank Dr. Eng. Luis Carlos Manrique Ruiz for his support with the statistical analysis.

SUPPLEMENTARY MATERIAL

The Supplementary Material for this article can be found online at: https://www.frontiersin.org/articles/10.3389/fnins.2018.00099/full#supplementary-material

REFERENCES

Aach, M., Cruciger, O., Sczesny-Kaiser, M., Höffken, O., Meindl, R. Ch., Tegenthoff, M., et al. (2014). Voluntary driven exoskeleton as a new tool for rehabilitation in chronic spinal cord injury: a pilot study. *Spine J*. 14, 2847–2853. doi: 10.1016/j.spinee.2014.03.042

Bae, Y. H., Ko, Y. J., Chang, W. H., Lee, J. H., Lee, K. B., Park, Y. J., et al. (2014). Effects of robot-assisted gait training combined with functional electrical stimulation on recovery of locomotor mobility in chronic stroke patients: a randomized controlled trial. *J. Phys. Ther. Sci*. 26, 1949–1953. doi: 10.1589/jpts.26.1949

Bianchi, L., Angelini, D., and Lacquaniti, F. (1998a). Individual characteristics of human mechanics. *Pflugers Arch*. 436, 343–356. doi: 10.1007/s004240050642

Bianchi, L., Angelini, D., Orani, G. P., and Lacquaniti, F. (1998b). Kinematic coordination in human gait: relation to mechanical energy cost. *J. Neurophysiol*. 79, 2155–2170. doi: 10.1152/jn.1998.79.4.2155

Bleyenheuft, C., Cockx, S., Caty, G., Stoquart, G., Lejeune, T., and Detrembleur, C. (2009). The effect of botulinum toxin injections on gait control in spastic stroke patients presenting with a stiff-knee gait. *Gait Posture* 30, 168–172. doi: 10.1016/j.gaitpost.2009.04.003

Bleyenheuft, C., Deltombe, T., and Detrembleur, C. (2013). Influence of ankle-foot orthoses on kinematic segmental covariation among stroke patients. *Ann. Phys. Rehabil. Med.* 56, 3–13. doi: 10.1016/j.rehab.2012.11.001

Borghese, N. A., Bianchi, L., and Lacquaniti, F. (1996). Kinematic determinants of human locomotion. *J. Physiol*. 494(Pt 3), 863–879. doi: 10.1113/jphysiol.1996.sp021539

Cheron, G., Bouillot, E., Dan, B., Bengoetxea, A., Draye, J. P., and Lacquaniti, F. (2001). Development of a kinematic coordination pattern in toddler locomotion: planar covariation. *Exp. Brain Res*. 137, 455–466. doi: 10.1007/s002210000663

Choi, B. W., Song, K. J., and Chang, H. (2011). Ossification of the posterior longitudinal ligament: a review of literature. *Asian Spine J*. 5, 267–276. doi: 10.4184/asj.2011.5.4.267

Chow, J. W., and Stokic, D. S. (2015). Intersegmental coordination of gait after hemorrhagic stroke. *Exp. Brain Res*. 233, 125–135. doi: 10.1007/s00221-014-4099-2

Cruciger, O., Schildhauer, T. A., Meindl, R. C., Tegenthoff, M., Schwenkreis, P., Citak, M., et al. (2016). Impact of locomotion training with a neurologic controlled hybrid assistive limb (HAL) exoskeleton on neuropathic pain and health related quality of life (HRQoL) in chronic SCI: a case study. *Disabil. Rehabil. Assist. Technol*. 11, 529–534. doi: 10.3109/17483107.2014.981875

Dunlop, S. A. (2008). Activity-dependent plasticity: implications for recovery after spinal cord injury. *Trends Neurosci*. 8, 410–418. doi: 10.1016/j.tins.2008.05.004

Epstein, N. (1992). Diagnosis and surgical management of ossification of the posterior longitudinal ligament. *Spine J*. 2, 436–449. doi: 10.1016/S1529-9430(02)00394-7

Epstein, N. (2002). Ossification of the cervical posterior longitudinal ligament: a review. *Neurosurg. Focus* 13, 1–10. doi: 10.3171/foc.2002.13.2.16

Fujii, K., Abe, T., Kubota, S., Marushima, A., Kawamoto, H., Ueno, T., et al. (2016). The voluntary driven exoskeleton hybrid assistive limb (HAL) for postoperative training of thoracic ossification of the posterior longitudinal ligament: a case report. *J. Spinal Cord Med*. 40, 361–367. doi: 10.1080/10790268.2016.1142056

Gad, P., Gerasimenko, Y., Zdunowski, S., Turner, A., Sayenko, D., Lu., D. C., et al. (2017). Weight bearing over-ground stepping in an exoskeleton with non-invasive spinal cord neuromodulation after motor complete paraplegia. *Front. Neurosci*. 11:333. doi: 10.3389/fnins.2017.00333

Grasso, R., Bianchi, L., and Lacquaniti, F. (1998). Motor patterns for human gait: backward versus forward locomotion. *J. Neurophysiol*. 80, 1868–1885. doi: 10.1152/jn.1998.80.4.1868

Grasso, R., Peppe, A., Stratta, F., Angelini, D., Zago, M., Stanzione, P., et al. (1999). Basal ganglia and gait control: apomorphine administration and internal pallidum stimulation in Parkinson's disease. *Exp. Brain Res*. 126, 139–148. doi: 10.1007/s002210050724

Gu, Y., Shi, J., Cao, P., Yuan, W., Wu, H., Yang, L., et al. (2015). Clinical and imaging predictors of surgical outcome in multilevel cervical ossification of posterior longitudinal ligament: an analysis of 184 patients. *PLoS ONE* 10:e0136042. doi: 10.1371/journal.pone.0136042

Hoenig, J. M., and Heisey, D. M. (2001). The abuse of power: the pervasive fallacy of power calculations for data analysis. *Am. Stat*. 55, 19–24. doi: 10.1198/000313001300339897

Houle, J. D., and Côté, M. P. (2013). Axon regeneration and exercise-dependent plasticity after spinal cord injury. *Ann. N Y. Acad. Sci*. 1279, 154–163. doi: 10.1111/nyas.12052

Ikumi, A., Kubota, S., Shimizu, Y., Kadone, H., Marushima, A., Ueno, T., et al. (2016). Decrease of spasticity after hybrid assistive limb® training for a patient with C4 quadriplegia due to chronic SCI. *J. Spinal Cord Med*. 40, 5. doi: 10.1080/10790268.2016.1225913

Ivanenko, Y. P., d'Avella, A., Poppele, R. E., and Lacquaniti, F. (2008). On the origin of planar covariation of elevation angles during human locomotion. *J. Neurophysiol*. 99, 1890–1898. doi: 10.1152/jn.01308.2007

Ivanenko, Y. P., Grasso, R., Macellari, V., and Lacquaniti, F. (2002). Control of foot trajectory in human locomotion: role of ground contact forces in simulated reduced gravity. *J. Neurophysiol*. 87, 3070–3089. doi: 10.1152/jn.2002.87.6.3070

Kalb, S., Martirosyan, N. L., Perez-Orribo, L., Kalani, M. Y., and Theodore, N. (2011). Analysis of demographics, risk factors, clinical presentation, and surgical treatment modalities for the ossified posterior longitudinal ligament. *Neurosurg. Focus* 30, 3. doi: 10.3171/2010.12.FOCUS10265

Kasai, R., and Takeda, S. (2016). The effect of a hybrid assistive limb® on sit-to-stand and standing patterns of stroke patients. *J. Phys. Ther. Sci*. 28, 1786–1790. doi: 10.1589/jpts.2016.1786

Kawamoto, H., Kadone, H., Sakurai, T., Ariyasu, R., Ueno, Y., Eguchi, K., et al. (2014). Development of an assist controller with robot suit HAL for hemiplegic patients using motion data on the unaffected side. *Conf. Proc. IEEE Eng. Med. Biol. Soc*. 2014, 3077–3080. doi: 10.1109/EMBC.2014.6944273

Kawamoto, H., Kamibayashi, K., Nakata, Y., Yamawaki, K., Ariyasu, R., Sankai, Y., et al. (2013). Pilot study of locomotion improvement using hybrid assistive limb in chronic stroke patients. *BMC Neurol*. 13:141. doi: 10.1186/1471-2377-13-141

Kim, J. S., and Scott, C. D. (2012). Robust Kernel density estimation. *JMLR* 13, 2529–2565. doi: 10.1109/ICASSP.2008.4518376

Kommu, R., Sahu, B. P., and Purohit, A. (2014). Surgical outcome in patients with cervical ossified posterior longitudinal ligament: a single institutional experience. *Asian J. Neurosurg*. 9, 196–202. doi: 10.4103/1793-5482.146602

Kubota, S., Abe, T., Fujii, K., Marushima, A., Ueno, T., Haginoya, A., et al. (2016). Improvement of walking ability using hybrid assistive limb training in a patient with severe thoracic myelopathy caused by ossification of the posterior longitudinal ligament - a case report. *J. Spine* S7:003. doi: 10.4172/2165-7939.S7-003

Kwon, S. Y., Shin, J. J., Lee, J. H., and Cho, W. H. (2015). Prognostic factors for surgical outcome in spinal cord injury associated with ossification of the posterior longitudinal ligament (OPLL). *J. Orthop. Surg. Res*. 10, 94. doi: 10.1186/s13018-015-0235-3

Labruyere, R., and Van Hedel, H. J. (2014). Strength training versus robot-assisted gait training after incomplete spinal cord injury: a randomized pilot study in patients depending on walking assistance. *J. Neuroeng. Rehabil*. 9, 11–14. doi: 10.1186/1743-0003-11-4

Lacquaniti, F., Ivanenko, Y. P., and Zago, M. (2002). Kinematic control of walking. *Arch. Ital. Biol*. 140, 263–272. doi: 10.4449/aib.v140i4.485

Leurs, F., Bengoetxea, A., Cebolla, A. M., De Saedeleer, C., Dan, B., and Cheron, G. (2012). Planar covariation of elevation angles in prosthetic gait. *Gait Posture* 35, 647–652. doi: 10.1016/j.gaitpost.2011.12.017

Martino, G., Ivanenko, Y. P., Serrao, M., Ranavolo, A., d'Avella, A., Draicchio, F., et al. (2014). Locomotor patterns in cerebellar ataxia. *J. Neurophysiol*. 112, 2810–2821. doi: 10.1152/jn.00275.2014

Mayr, A., Kofler, M., Quirbach, E., Matzak, H., Fröhlich, K., and Saltuari, L. (2007). Prospective, blinded, randomized crossover study of gait rehabilitation in stroke patients using the Lokomat gait orthosis. *Neurorehabil. Neural Repair* 21, 307–314. doi: 10.1177/1545968307300697

Mehdi, S. K., Alentado, V. J., Lee, B. S., Mroz, T. E., Benzel, E. C., and Steinmetz, M. P. (2016). Comparison of clinical outcomes in decompression and fusion versus decompression only in patients with ossification of the posterior longitudinal ligament: a meta-analysis. *Neurosurg. Focus* 40, 6. doi: 10.3171/2016.3.FOCUS1630

Nam, K. Y., Kim, H. J., Kwon, B. S., Park, J. W., Lee, H. J., and Yoo, A. (2017). Robot-assisted gait training (Lokomat) improves walking function and activity

in people with spinal cord injury: a systematic review. *J. Neuroeng. Rehabil.* 14, 24. doi: 10.1186/s12984-017-0232-3

Noble, J. W., and Prentice, S. D. (2008). Intersegmental coordination while walking up inclined surfaces: age and ramp angle effects. *Exp. Brain Res.* 189, 249–255. doi: 10.1007/s00221-008-1464-z

Peurala, S. H., Airaksinen, O., Huuskonen, P., Jäkälä, P., Juhakoski, M., Sandell, K., et al. (2009). Effects of intensive therapy using gait trainer or floor walking exercises early after stroke. *J. Rehabil. Med.* 41, 166–173. doi: 10.2340/16501977-0304

Sakakima, H., Ijiri, K., Matsuda, F., Tominaga, H., Biwa, T., Yone, K., et al. (2013). A newly developed robot suit hybrid assistive limb facilitated walking rehabilitation after spinal surgery for thoracic ossification of the posterior longitudinal ligament: a case report. *Case Rep. Orthop*. 2013:621405. doi: 10.1155/2013/621405

Sandrow-Feinberg, H. R., and Houlé, J. D. (2015). Exercise after spinal cord injury as an agent for neuroprotection, regeneration and rehabilitation. *Brain Res.* 1619, 12–21. doi: 10.1016/j.brainres.2015.03.052

Schwartz, I., Sajin, A., Fisher, I., Neeb, M., Shochina, M., Katz-Leurer, M., et al. (2009). The effectiveness of locomotor therapy using robotic-assisted gait training in subacute stroke patients: a randomized controlled trial. *PMR* 1, 516–523. doi: 10.1016/j.pmrj.2009.03.009

Sczesny-Kaiser, M., Kowalewski, R., Schildhauer, T. A., Aach, M., Jansen, O., Grasmücke, D., et al. (2017). Treadmill training with HAL exoskeleton -a novel approach for symptomatic therapy in patients with limb-girdle muscular dystrophy - Preliminary study. *Front Neurosci.* 11:449. doi: 10.3389/fnins.2017.00449

Shimizu, Y., Kadone, H., Kubota, S., Suzuki, K., Abe, T., Ueno, T., et al. (2017). Voluntary ambulation by upper limb-triggered HAL® in patients with complete quadri/paraplegia due to chronic spinal cord injury. *Front. Neurosci.* 11:649. doi: 10.3389/fnins.2017.00649

Smith, Z. A., Buchanan, C. C., Raphael, D., and Khoo, L. T. (2011). Ossification of the posterior longitudinal ligament: pathogenesis, management, and current surgical approaches. a review. *Neurosurg. Focus* 30, 3. doi: 10.3171/2010.12.FOCUS10283

Tong, R. K., Ng, M. F., and Li, L. S. (2006). Effectiveness of gait training using an electromechanical gait trainer, with and without functional electric stimulation, in subacute stroke: a randomized con- trolled trial. *Arch. Phys. Med. Rehabil.* 87, 1298–1304. doi: 10.1016/j.apmr.2006.06.016

Werner, C., Von Frankenberg, S., Treig, T., Konrad, M., and Hesse, S. (2002). Treadmill training with partial body weight support and an electromechanical gait trainer for restoration of gait in subacute stroke patients. *Stroke* 33, 2895–2901. doi: 10.1161/01.STR.0000035734.61539.F6

Conflict of Interest Statement: YoS is the C.E.O., shareholder, and director of CYBERDYNE Inc. which produces the robot suit HAL. CYBERDYNE was not involved in study design, data collection, analysis, writing, or submission of this article.

The other authors declare that the research was conducted in the absence of any commercial or financial relationships that could be construed as a potential conflict of interest.

frontiers in Neuroscience

CASE REPORT
published: 22 March 2018
doi: 10.3389/fnins.2018.00134

Impact of Powered Knee-Ankle Prosthesis on Low Back Muscle Mechanics in Transfemoral Amputees: A Case Series

*Chandrasekaran Jayaraman[1,2], Shenan Hoppe-Ludwig[1], Susan Deems-Dluhy[1], Matt McGuire[1], Chaithanya Mummidisetty[1], Rachel Siegal[1], Aileen Naef[1,3], Brian E. Lawson[4], Michael Goldfarb[4], Keith E. Gordon[2] and Arun Jayaraman[1,2]**

[1] Max Nader Lab for Rehabilitation Technologies & Outcomes Research, Center for Bionic Medicine, Shirley Ryan Ability Lab, Chicago, IL, United States, [2] Department of Physical Therapy and Human Movement Sciences, Northwestern University, Chicago, IL, United States, [3] School of Life Sciences, Swiss Federal Institute of Technology in Lausanne, Lausanne, Switzerland, [4] Department of Mechanical Engineering, Vanderbilt University, Nashville, TN, United States

Regular use of prostheses is critical for individuals with lower limb amputations to achieve everyday mobility, maintain physical and physiological health, and achieve a better quality of life. Use of prostheses is influenced by numerous factors, with prosthetic design playing a critical role in facilitating mobility for an amputee. Thus, prostheses design can either promote biomechanically efficient or inefficient gait behavior. In addition to increased energy expenditure, inefficient gait behavior can expose prosthetic user to an increased risk of secondary musculoskeletal injuries and may eventually lead to rejection of the prosthesis. Consequently, researchers have utilized the technological advancements in various fields to improve prosthetic devices and customize them for user specific needs. One evolving technology is powered prosthetic components. Presently, an active area in lower limb prosthetic research is the design of novel controllers and components in order to enable the users of such powered devices to be able to reproduce gait biomechanics that are similar in behavior to a healthy limb. In this case series, we studied the impact of using a powered knee-ankle prostheses (PKA) on two transfemoral amputees who currently use advanced microprocessor controlled knee prostheses (MPK). We utilized outcomes pertaining to kinematics, kinetics, metabolics, and functional activities of daily living to compare the efficacy between the MPK and PKA devices. Our results suggests that the PKA allows the participants to walk with gait kinematics similar to normal gait patterns observed in a healthy limb. Additionally, it was observed that use of the PKA reduced the level of asymmetry in terms of mechanical loading and muscle activation, specifically in the low back spinae regions and lower extremity muscles. Further, the PKA allowed the participants to achieve a greater range of cadence than their predicate MPK, thus allowing them to safely ambulate in variable environments and dynamically control speed changes. Based on the results of this case series, it appears that there is considerable potential for powered prosthetic components to provide safe and efficient gait for individuals with above the knee amputation.

Keywords: powered knee-ankle prosthesis, amputees, gait, variability, musculoskeletal injuries, microprocessor knee, low back pain

OPEN ACCESS

Edited by:
Mikhail Lebedev,
Duke University, United States

Reviewed by:
Raoul Huys,
Centre National de la Recherche Scientifique (CNRS), France
Robert Gregg,
University of Texas at Dallas, United States

***Correspondence:**
Arun Jayaraman
ajayaraman@sralab.org

Specialty section:
This article was submitted to Neuroprosthetics, a section of the journal Frontiers in Neuroscience

Received: *01 September 2017*
Accepted: *20 February 2018*
Published: *22 March 2018*

Citation:
Jayaraman C, Hoppe-Ludwig S, Deems-Dluhy S, McGuire M, Mummidisetty C, Siegal R, Naef A, Lawson BE, Goldfarb M, Gordon KE and Jayaraman A (2018) Impact of Powered Knee-Ankle Prosthesis on Low Back Muscle Mechanics in Transfemoral Amputees: A Case Series. Front. Neurosci. 12:134. doi: 10.3389/fnins.2018.00134

INTRODUCTION & BACKGROUND

Prostheses are defined as devices that help to restore a missing function that has occurred as the result of limb loss. While many factors affect an amputee's ability to return to their pre-amputation functional level, the design of the prosthetic device itself can impact function by contributing to normalization of gait and body symmetry. In the United States, prescription of a specific type of device for a user depends on the type of amputation and their clinically designated mobility level [i.e., K levels or Medicare Functional Classifications Level (MFCL); CMS, 2001].

Consequently, various types of prosthetic device designs have evolved over decades, with the goal of facilitating normative (reproducing healthy limb behavior) biomechanical gait behavior in amputees. Broadly, there are three main categories of prosthetic knee and ankle components available for transfemoral (above knee) amputees when considering energetic control, namely, (i) mechanical passive devices (non-powered) (Michael, 1999), (ii) microprocessor-controlled passive devices (Grimes et al., 1977; Peeraer et al., 1989, 1990; Aeyels et al., 1992; Popović et al., 1995; Taylor et al., 1996; Otto Bock Orthopedic Industry, 1998; Zlatnik et al., 2002; Ossur, 2017), and (iii) powered devices (Tomovic and McGhee, 1966; Flowers, 1974; Au et al., 2008, 2009; Sup et al., 2009; Hitt et al., 2010). The powered devices for the transfemoral population can be further divided into powered knees, powered ankles, and powered knee-ankle devices (Cappozzo and Gazzani, 1982; Au et al., 2008, 2009; Holgate et al., 2008; Bergelin et al., 2010; Eilenberg et al., 2010; Hitt et al., 2010; Suzuki et al., 2011; Bergelin and Voglewede, 2012; Caputo and Collins, 2014; Cherelle et al., 2014).

Walking using traditional non-powered prostheses is very energy inefficient (incurring ∼60% more energy usage) when compared to able-bodied individuals resulting in reduced everyday mobility or even immobility (Hafner et al., 2002). Additionally, transfemoral amputees commonly exhibit compensatory biomechanics resulting in body motions that are atypical to normal human locomotion. These compensatory mechanisms arise due to chronic imbalance or prosthetic derived muscle/movement activations that alter the normal biomechanics and motion. Over time, these factors increase the risk of secondary musculoskeletal injuries such as severe chronic pain in the low back and the contralateral (non-amputated) side resulting in inactivity or surgical interventions (Cappozzo and Gazzani, 1982; Michaud et al., 2000; Klein Horsman et al., 2007; Goujon-Pillet et al., 2008; Molina Rueda et al., 2013; Devan et al., 2014; Hendershot and Wolf, 2014; Shojaei et al., 2016). Therefore, any enhancement to the mechanical or control systems design of prostheses which can reproduce a biomechanical behavior similar to a healthy limb is very beneficial.

In the pursuit of normalizing some of the abnormal gait mechanics that are commonly seen in transfemoral amputees, a coordinated powered knee and ankle prosthesis (Generation 3) was developed at Vanderbilt University to provide power generation similar to an anatomical joint. While there are commercially available, independent prosthetic knees and feet that provide power to a single joint, there are no available versions that have integrated power and communication between both the knee and ankle components. Thus, implementation of the PKA in transfemoral participants has the potential to improve lower limb prosthesis performance.

Congruent with this tenet, literature indicates that the Vanderbilt Generation 3 powered knee-ankle prosthesis (PKA) may provide significant biomechanical benefits to users, compared to conventional passive devices (Goldfarb et al., 2013; Lawson et al., 2013, 2014, 2015; Shultz et al., 2016). Furthermore, most lower-limb amputation studies have historically focused on comparing the performance of a traditional mechanically passive prostheses to microprocessor-controlled knee prostheses (MPK) with variable damping. These studies suggest that in comparison to mechanical passive devices, consistent use of MPK prostheses reduced energy consumption, improved smoothness of gait, and decreased the work done by the affected side hip muscles during walking (Taylor et al., 1996; Schmalz et al., 2002; Johansson et al., 2005).

However, presently it is not clear if implementing a PKA in unilateral transfemoral amputees that currently use a microprocessor controlled knee (MPK) could offer improved biomechanical benefits. Such biomechanical benefits, if any, could pave the way for them to reproduce a normalized gait similar to the healthy limb in comparison to their predicate MPK device. Additionally improving body biomechanics in transfemoral amputees could potentially minimize the risk of exposure of the low back region and contralateral side, to abnormal loading-based secondary musculoskeletal injuries in transfemoral amputees (a serious health-concern in transfemoral amputees; Devan et al., 2017). Consequently, this case series investigated the potential benefits the PKA could offer to transfemoral amputees who are currently using a MPK as their predicate device. To achieve this, a clinical comparison of the performance between the PKA and the participants predicate MPK devices was conducted in two transfemoral amputees.

Through this case series we hope to provide two novel insights. It is the first to report a performance comparison between the PKA and MPK prosthetic device in unilateral transfemoral amputee literature. Secondly, this case series compared the low back (L3 lumbar erector spinae region) muscle activation in unilateral transfemoral amputees ambulating with the PKA and their MPK. Low back muscle activation and injury has been very scarcely studied in transfemoral prosthetic literature (Yoder et al., 2015; Shojaei et al., 2016). The novel information from this case series will provide novel insights that can aid in improving our understanding on potential benefits the PKA could offer over the MPK devices. In terms of low back muscle loading pattern (i.e., reduce activation asymmetry in the contralateral vs. ipsilateral side).

METHODS

Ethics

All study procedures were approved by the Institutional Review Board at Northwestern University. Both participants provided voluntary signed informed consent before beginning the study.

The cases discussed here are part of a larger clinical trial that can be found at https://clinicaltrials.gov/ct2/show/NCT03204513.

Case Description

The basic demographic information and prosthetic device specifications of the two study participants are provided in Table S1 (Supplementary Material).

Even though both study participants utilize a MPK prosthesis, they have clinical differences based on age, residual limb length, clinically perceived activity level, and everyday community mobility. CS01 is a 25 y/o male with a knee disarticulation amputation, who currently has a clinically identified functional level of MFCL K4, indicating that he "has the ability [or potential] for prosthetic ambulation that exceeds basic ambulation skills, exhibiting high impact, stress or energy levels which is typical of an active adult or athlete" (CMS, 2001). CS01 is a student athlete, who plays basketball 3–5 times a week. CS02 is a 58 y/o male with a medium length transfemoral amputation whose current MFCL level is K3, indicating that he "has the ability [or potential] for ambulation with variable cadence. Typical of the community ambulators who have the ability to traverse most environmental barriers and may have vocational, therapeutic or exercise activity that demands prosthetic utilization beyond simple locomotion" (CMS, 2001). CS02 is employed as a computer engineer. His personal life includes maintenance of a large piece of land and care of multiple large breed dogs. He has already had a total knee replacement of the intact limb. The differences in the lengths of the residual limbs can play an important factor in the control of a prosthesis. The shorter the residual limb, the less control a participant would have due to loss of muscle, nerve and bony lever arm. Significantly, CS01's level of amputation, a knee disarticulation, provides almost fully intact hip adductors and the vast majority of the major muscle group's bulk remaining. This is not the case in CS02's mid length amputation, transecting all of the major muscle groups of the thigh, reducing his capacity to generate force. In general, a shorter residuum means additional work of the smaller remaining muscles with less biomechanical advantage. Over time, these imbalances can cause compensations in other areas of the body. Additionally, a longer residual limb may require differences in the prosthetic knee height compared to the anatomical knee axis, which may contribute to inequalities in gait kinematics.

On participants' similarities at the time of the study, both had been using their current MPK devices for over 2 years. Both subjects demonstrated reduced hip extension compared to normative range of motion, though they were both able to achieve functional hip range of motion through compensatory motions of the lumbar spine. When a hip flexion contracture is present, the step length of the sound limb is restricted as well. This impacts a participant's overall gait, including the quality of steps, speed and distance covered. In order to accommodate the hip flexion contracture, motion usually occurs within the spine.

Photographs of both participants with their predicate prosthetic device and the PKA have been provided in the Supplementary Material (Figures S1, S2).

Study Design

Participants were randomized to start either with their predicate MPK-1 (Genium in case of participant CS01), and MPK-2 (Rheo-3 in case of participant CS02), or the PKA. Following the consent process, an experienced prosthetist evaluated the participants' prosthetic sockets for appropriate component fitting with the study device (PKA) or predicate device (MPK-1 for CS01 and MPK-2 for CS02). Any adjustments to the sockets or the device settings were made during the fitting sessions.

Prosthetic Device Fitting

The knee and ankle parameters for the PKA were individually configured for each participant during the fitting sessions. In brief, the impedance parameters at the ankle and knee joints during three states (sitting, standing, and stepping), and the push-off trigger angle and push-off strength thresholds were manually tuned starting with reference parameters used from the data of healthy individuals (Sup et al., 2008). The ankle motor power to enable ankle push-off strength was also individually adjusted to suit the participants comfort level for the three cadence levels (slow, default, and fast speeds).

Additionally, qualitative feedback from the participant and external observation by the clinicians were used to fine tune the parameters so that any undesirable aspects of gait arising from compensations, such as vaulting, hip hiking, and circumduction were minimized. The goal of the tuning process was to adjust the PKA device to maximize participant's ability to ambulate with a biomechanical behavior similar to a healthy limb. The overall process of tuning the PKA device for a participant is similar to the process followed by prosthetist in aligning and adjusting any passive or powered prosthetic device. The procedure for this customized parameter tuning for the PKA has been discussed in extensive detail in literature (Lawson et al., 2013, 2014, 2015; Shultz et al., 2016). The finalized parameters for the two participants are provided in the Supplementary Material (Table S2, Figures S3, S4).

Prosthetic Device Training

Once proper prosthetic fit was clinically confirmed, participants underwent up to 12 training sessions of intense functional training with the device. Subject's body mechanics were evaluated and training was provided to maximize control of the prostheses and minimize compensations. The training included performing a battery of activities indoors and outdoors, and emulating walking environments encountered in daily living conditions (e.g., level and uneven indoor and outdoor surfaces including obstacle avoidance, crossing streets, and varied pavement). Participants were also specifically acclimated to treadmill walking. Safe and independent performance of the benchmark activities over three of the training sessions was used as a threshold to indicate the successful completion of training with the device (Supplementary Material, Table S3). These training procedures were performed with the participant's predicate devices (MPK-1 for CS01 and MPK-2 for CS02), as well as the PKA. Training for both the devices was carried out to maximize device usage in the training environment and minimize any confounding effects arising due to the training protocol adopted.

Once the fitting, training, and testing phases for the first study device were completed, a washout period of at least 2 months was given before the participant was scheduled to cross-over to the second device. This was done to minimize the carry-over effect of one device influencing the performance outcomes of the second device. The order of the post-training assessment tests for both devices were held similar for each participant.

Data Collection Procedures

Three different strands of tests were conducted to compare the performance between MPKs and the PKA. Ankle and knee kinematics were analyzed to investigate if using a PKA enabled participants to emulate an ankle and knee behavior similar in biomechanics to the behavior of a healthy limb. Muscle activation was recorded from the lower limb muscles on the contralateral side (non-amputated side) and the low back lumbar L3 region(bilateral). The muscle activation during ambulation was compared to study the muscle loading trends between the prosthetic devices. A modified Graded Treadmill Test (GTT) was performed to investigate the energy efficiency and the ranges of variable cadence the participants achieved with these devices. Finally, to assess the prosthetic devices on a functional task, an outdoor cross-walk test was performed to represent a common activity of daily living. Participants performed all the tests with both the devices.

Biomechanics

A 10 camera motion capture system (Qualysis, Gothenburg Sweden) was used to record the kinematics, ground reaction forces (GRF), and muscle activation (EMG) during walking. In total, 38 reflective markers were placed on the lower limbs, pelvis, and trunk based on the six degrees of freedom cluster marker configuration (Acasio et al., 2017) The motion capture data was sampled at 100 Hz. GRF were collected using six AMTI force plates (AMTI, Watertown, MA) sampled at 1,000 Hz. Muscle activation using wireless EMG sensors (Delsys Inc.) were collected from bilateral erector spinae muscles at the lumbar L3 level (RES-L3 and LES-L3) and on lower extremity muscles [medial gastrocnemius (MGC), rectus femoris (RF)] on the limb contralateral to the prosthesis. The EMG's were sampled at 2,000 Hz. All data was collected during walking at the participants self-selected speed along a seven-foot walkway embedded with force plates.

Modified Graded Treadmill Test (VO2 and Variable Cadence)

This test was used to determine each participant's cardio-vascular response to walking at different speeds on a motorized treadmill. Participants were secured to an overhead safety harness during this test as they walked for up to 2 min at progressively increasing speeds on the treadmill. Speeds were varied between 0.2 m/s up to 2.0 m/s at increments of 0.2 m/s. Before increasing the speed to the next stage, participants were given the choice to stop or continue with the test. The test was stopped if the participant opted to do so, or if the clinician decided to stop the test based on achieving age-based target maximum heart rate threshold. The maximum heart rate threshold was calculated as 80% of their maximum heart rate (220-Age). Participants' cardiovascular and metabolic responses (Duffield et al., 2004) were monitored frequently and recorded during the entire test using a COSMED K4B2 device (Duffield et al., 2004). Additionally, inertial measurement units (IMUs–Actigraph GT9X Link, Actigraph, LLC. Pensacola, FL, USA.; Rothney et al., 2008; John and Freedson, 2012), were mounted bilaterally on the dorsum of the shoes to capture acceleration signatures during walking. This was post-processed to extract cadence (step counts/min) and stride times.

Outdoor Overground Walking (EMG)—MC10

Participants performed a cross walk blinking signal test. This test measured the time taken to cross a designated two-lane street with curb cuts at the transition to the sidewalk. The walkway distance was ∼20 m. The muscle activation of the MGC was also recorded from the contralateral limb using the BioStampRC, a novel high resolution skin conformable flexible Bluetooth based sensor (Yuhao et al., 2018). The EMG module sampled at 1,000 Hz while the acceleration modules sampled at 31.25 Hz. Both EMG and acceleration were recorded simultaneously during the task. Participants performed three trials.

DATA ANALYSIS

Standard data analysis procedures were employed to post-process the data and extract the outcome metrics of interest. Custom developed MATLAB scripts were used for all data analysis. All the outcome metrics were computed and compared between the devices (i.e., PKA and the respective predicate MPK devices for CS01 and CS02) to study various aspects within the context to performance, safety (potential to minimize injury) and function.

Healthy Controls

To compare the prosthetic device performance for knee and ankle kinematics, the healthy benchmark data from literature was used (Winter, 1991). This approach is a commonly adopted procedure in prosthetic literature in order to compare biomechanical behavior (Goldfarb et al., 2013; Lawson et al., 2013, 2014, 2015; Shultz et al., 2016).

Biomechanics

All motion capture data was post-processed using Visual3D (C-Motion, Germantown, MD) and custom MATLAB (version R2016, Mathworks, Natick, MA) scripts. Any missing marker data was gap-filled and low-pass filtered (Butterworth, cut-off frequency 6 Hz). GRF's were low-pass filtered (Butterworth, cut-off frequency 20 Hz). The gait cycle was identified based on the heel strike events from motion data. Each gait cycle was then normalized from 0 to 100%. In total, six strides were analyzed. All data was averaged over three walking trials (i.e., six steady state strides).

Joint Kinematics

An inverse kinematics pipeline was executed in Visual 3D to compute the ankle and knee joint kinematics from the motion

capture data. The knee and the ankle joint kinematics from each of the devices were then benchmarked with the knee and ankle joint kinematics from the healthy controls data obtained from literature (Winter, 1991). Pearson correlation coefficients were then computed between the joint kinematics obtained from each of the prosthetic devices and that of the healthy controls from literature (Winter, 1991). The strength of this correlation (positive correlation value between 0 and 1) indicated the degree of closeness of a particular device to reproduce kinematic behavior similar to a healthy limb. A correlation value of zero indicates that the knee/ankle kinematics trajectory behavior while using that prosthetic device did not linearly correlate (temporally) with the joint kinematic behavior of a healthy limb as obtained from literature (Winter, 1991).

Vertical Ground Reaction Force (VGRF)

The vertical ground reaction force (VGRF) from the contralateral and ipsilateral sides was extracted from the force plate recordings. The VGRF was then averaged over the gait cycles to obtain the mean VGRF, and then normalized using the participant's weight (participant+device) in kilograms (i.e., N/kg). The ratio of, the *peak weight- normalized VGRF following the heel strike* (F_{Z1} N/kg), *over the peak weight-normalized VGRF at ankle push-off* (F_{Z2} N/kg) *during stance phase was computed* (refer schematic in Figure S5). A value of unity for this ratio indicates that the peak VGRF during these two instances of stance phase were of equal magnitude. A deviation of this ratio from unity marks the degree of asymmetry between the peak VGRF during stance phase of gait. The PKA provides push off power at the ankle during the terminal stance phase of the gait unlike the MPK. In order to study the benefit of the ankle push off in normalizing the VGRF peaks, this ratio measure was chosen. This ratio from both the prosthetic devices (MPKs and PKA) was then benchmarked with the ratio of VGRF obtained for the healthy controls data from literature (Winter, 1991).

EMG Data Analysis

The EMG data was band pass filtered (Butterworth, band pass frequency 30–500 Hz). From each of the three walking trials, two steady state gait cycles were extracted bilaterally. The cycle wise gait data was extracted based on the heel strike events. Each gait cycle was then normalized from 0 to 100%. The area under the curve (AUC) was then computed for each muscle group from each of the gait cycle. This value was then averaged over the gait cycles and averaged over the trials for each side. This was computed for the right and left erector spinae at lumbar L3 level (RES-L3 and LES-L3), MGC and RF of the contralateral limb. In order to study the symmetry of lumbar muscle activation between the contralateral and ipsilateral sides during the overall gait cycle, the ratio of the AUC between both these sides was computed. A ratio closer to unity indicates overall symmetric EMG activation (i.e., in terms of gross magnitude of AUC) bilaterally on the erector spinae muscles at the L3 level.

Clinical Recordings

The first minute in each speed during the GTT was used to attain the steady state locomotion and hence was not used for data analysis. All outcome metrics for the GTT were computed for the second minute of each speed during the GTT.

COSMED

Manufacturer provided proprietary software was used to extract the VO2 and energy expenditure from the COSMED K4B2 during the modified GTT. The VO2 and energy expenditure were computed for the second minute of each speed during the GTT. The energy expenditure was used to study the energy efficiency of the PKA vs. the predicate MPK devices. The metabolic outcomes were weight normalized (participant weight + device weight). The gross oxygen cost (mL/kg/m) [i.e., from every second minute (steady state) over the entire trial] was also computed to use as an overall index to compare the gait efficiency while ambulating with different prosthetic devices.

IMU's

The vertical acceleration (A_y) from the IMUs placed on the dorsum of each foot was used to compute the cadence (step count/min) and stride time during the modified GTT. The data from the second minute of each time series was extracted based on the IMU time stamp. Then a continuous wavelet transform was used on the A_y component to compute the stride times and step counts (Zijlstra and Hof, 2003). At each speed range, the mean, standard deviation (*SD*), and the coefficient of variation [CV% = (SD/mean) *100] were computed for the stride time data. Custom developed MATLAB scripts were used for all IMU data post-processing.

RESULTS

The results are presented in three sections (i) biomechanics, (ii) clinical outcomes from GTT, and (iii) functional outcomes from outdoor testing. Both participants completed the protocol within the described timeline and there were no adverse events.

PKA Parameter Tuning

The participant-wise final parameters set for the PKA devices are provided in Table S2 in the Supplementary Material. Participant CS01 preferred a lower strength for the ankle push off power from the PKA device in comparison to CS02 (Table S2, Figures S3, S4 from Supplementary Material). The ankle reference trajectories (Figures S3, S4) were adjusted for each participant in order to allow them to clear the foot during swing phase while walking at various speeds. During the swing phase of the gait, the controller of the PKA is designed such that the knee and the ankle followed the reference trajectories.

Biomechanics

The mean values of the temporal spatial variables, including walking speed, stride time, and stance time (% of gait cycle) when walking with the MPKs and PKA are provided in the **Table 1**. The mean speed, mean stride time, and mean stance time (% gait cycle) were similar between both the devices for the participants.

Joint Kinematics

Figures 1A1,B1 shows a representative plot comparing the ankle joint kinematics for the two participants (CS01 and CS02) while

TABLE 1 | Temporal spatial parameters.

Gait parameter	CS01		CS02	
	MPK-1 (Genium)	PKA	MPK-2 (Rheo-3)	PKA
Walking speed (m/s)	1.3 (0.08)	1.3 (0.11)	1.2 (0.11)	1.3 (0.07)
Intact leg stride time (s)	1.1 (0.02)	1.1 (0.03)	1.2 (0.05)	1.2 (0.05)
Prosthetic leg stride time (s)	1.1 (0.02)	1.1 (0.05)	1.2 (.03)	1.2 (0.05)
Intact leg stance time (% gait cycle)	65 (1.1)	65 (4.0)	70 (4.0)	71 (2.0)
Prosthetic leg stance time (% gait cycle)	62 (1.1)	64 (2.0)	61 (2.0)	60 (2.0)
Intact leg stance phase: Ratio of VGRF (F_{Z1}/F_{Z2})	1.18 (0.1)	1.07 (0.03)	1.13 (0.11)	1.01 (0.03)
Prosthetic leg stance phase: Ratio of VGRF (F_{Z1}/F_{Z2})	1.17 (0.2)	1.00 (0.03)	1.12 (0.02)	1.00(.02)

using their predicate MPK devices and the PKA. The ankle joint kinematics while using PKA (Pearson's correlation coefficient: rho $\geq$ 0.6) were closer in kinematics to a healthy limb gait behavior than the MPK devices (correlation coefficient: rho $\leq$ 0.3). A similar observation was noted for knee kinematics when using the PKA (Pearson's correlation coefficient: PKA: rho $_{PKA}$ $\geq$ 0.95; MPKs: 0.92 $\leq$rho $_{MPKs}$ $\leq$ 0.95).This observation is consistent with the literature (Sup et al., 2009; Lawson et al., 2013, 2015). This showed that both the participants reproduced ankle and knee kinematics closer to that observed in healthy limb while ambulating using the PKA. Similarity in kinematics to a healthy limb have been shown to lead to symmetric joint loading profile during gait (Sup et al., 2009; Lawson et al., 2013, 2015). To further understand the implication, here we study two aspects, (i) the symmetry in ratio of peak VGRF (i.e., F_{Z1}/F_{Z2}) and, (ii) the overall low back muscle activation (erector spinae at lumbar L3 EMG AUC) while walking with the predicate MPKs and the PKA.

Ratio of Peak VGRF (F_{Z1}/F_{Z2})

The ratio of the peak *VGRF* from the contralateral and the ipsilateral sides are furnished in **Table 1**. The ratio of peak VGRF between the contralateral and the ipsilateral side while using the different devices are compared with the healthy control in **Figures 1A2,B2**. Both participants had at least a 12% difference between the magnitude of the ratio of the peak VGRF (VGRF $_{FZ1}$ > VGRF $F_{Z2,}$ varied between 12 and 18%, **Table 1**). In comparison to the MPK, this ratio was lower (<7% difference) while using the PKA in both participants (**Table 1**, **Figures 1A2,B2**). The peak VGRF magnitudes encountered while walking with both the MPKs and PKA fell well within the standard norm (i.e., 100–120% of body weight). However, based on the *ratio of the VGRF*, both participants reproduced behavior more similar to healthy controls when using the PKA.

EMG Activation (AUC)

In comparison to the MPKs, the erector spinae muscle activation (LES-L3 and RES-L3) was relatively more symmetrical (magnitude of AUC) between the contralateral and ipsilateral sides while using the PKA (**Figures 1A3,B3**). However, in both participants using the MPK, the activation of the RES-L3 was approximately five times higher than that of the LES-L3 (**Figures 1A3,B3**), implying a degree of asymmetry in muscle activation while using the MPK. In contrast, while using the PKA, this asymmetry was far less pronounced. Complimenting this observation, it was observed that the muscle activation (AUC) of the RF on the contralateral side decreased considerably while using the PKA in both participants. The MGC activation on the contralateral lateral side increased for CS02 while using the PKA (**Figure 1B4**). However, for participant CS01, the MGC showed only a slight increase in activation in contralateral side when using the PKA (**Figure 1A4**).

Clinical Outcomes (GTT)

The summary of the GTT results are shown in **Figure 2**.

Speed Ranges

Participant CS01 was able to reach a maximum speed of 1.8 m/s while using the MPK-1 and reached a maximum speed of 1.6 m/s while using the PKA. Participant CS01 transitioned from walking into running when the speed was switched from 1.6 to 1.8 m/s while using MPK-1. In contrast, participant CS02 was able to reach a higher walking speed of 1.4 m/s while using the PKA compared to a maximum speed of 1.2 m/s with the MPK-2.

Energy Expenditure (EE)

The overall energy expenditure (EE) trends during the GTT task showed a marginal benefit using the PKA in comparison to the MPK for participant CS01. For participant CS02 energy benefits were observed at certain speed ranges while using the MPK-2 (**Figure 2B2**). These comparisons are based on the minute-by-minute outcomes and for matched gait speed. Moreover, despite being approximately twice as heavy as the predicate MPKs' weight, the PKA did not require additional energy expenditure during the GTT task (**Figures 2A2,B2**). In addition to looking at the minute-to-minute EE, a gross measure of the overall oxygen cost (i.e., gait efficiency; Darter et al., 2013) was also calculated. Based on the oxygen cost the gross gait efficiency during the entire GTT test was as follows, CS01 [(MPK-1 $_{GTT}$ = 0.16 mL/kg/m); PKA $_{GTT}$ = 0.14 mL/Kg/m)], CS02 [(MPK-2 $_{GTT}$ = 0.22 mL/kg/m); PKA $_{GTT}$ = 0.22 mL/Kg/m)]. Based on the gait efficiency, using the PKA was more energy efficient for CS01 and incurred the same energy cost as the MPK-2 for CS02.

Variable Cadence

The stride times computed from the foot IMUs were used to compare the ranges of variable cadence achievable between

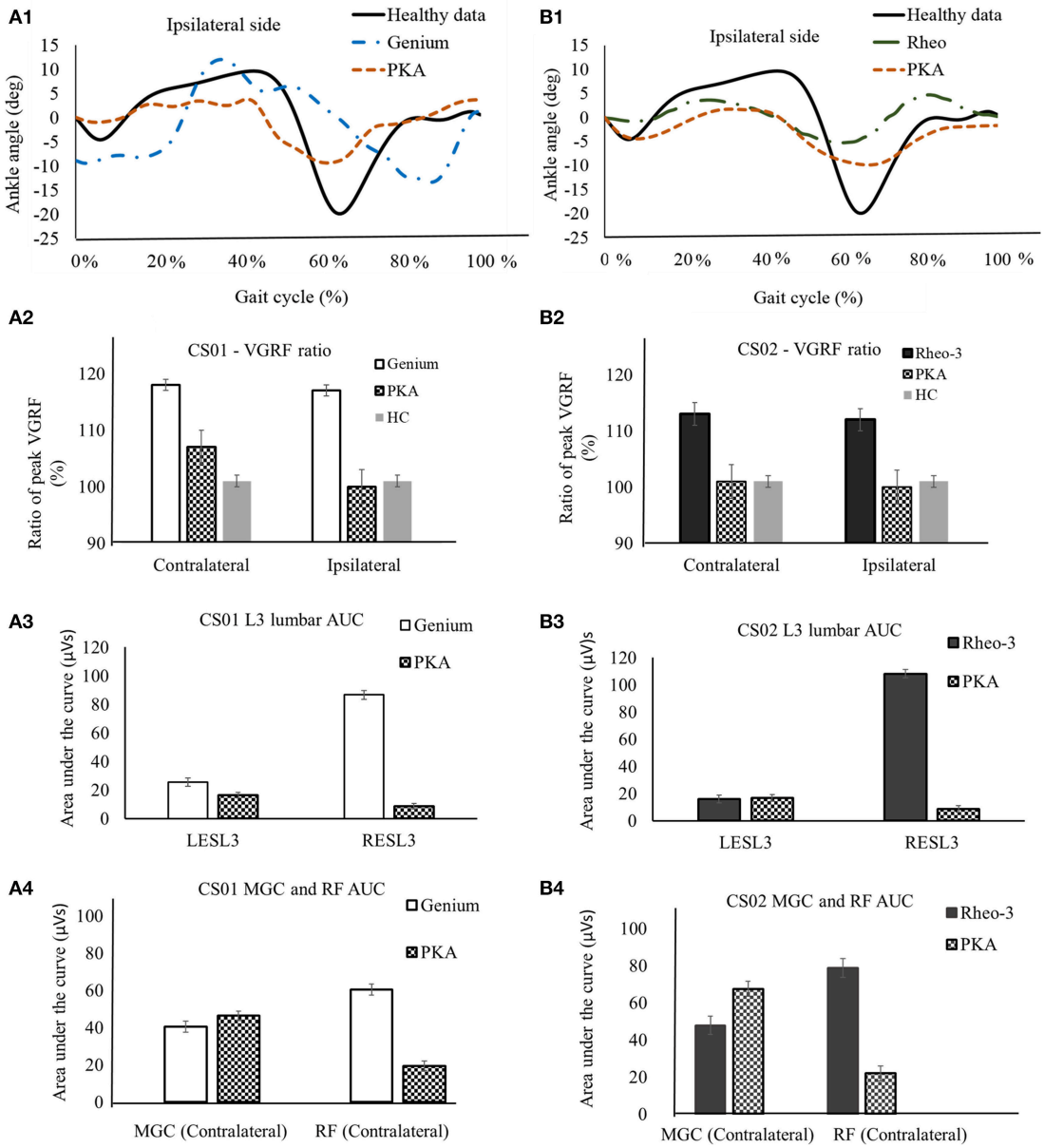

FIGURE 1 | A representative data showing comparison of biomechanics outcome metrics between MPK and PKA. Panels **(A1–A4)** are for participant CS01. **(A1)** compares the ankle joint kinematics between PKA, MPK1- (Genium), and healthy data (Winter, 1991) for the ipsilateral side for CS01. **(A2)** Shows comparison of the ratio of peak VGRF (Fz1/Fz2) during the stance phase between MPK-1 (Genium), PKA, and healthy data (Winter, 1991). It was observed that using the PKA led to a VGRF behavior closer to healthy limb on both the contralateral and the ipsilateral sides. **(A3)** EMG activation profile between MPK-1(Genium) and PKA at right and left side L3 erector spinae muscles in low back. The EMG activation profile was indexed as area under the curve (AUC) of the EMG signal. It can be observed that using PKA reduces the asymmetry in EMG activation between the LES-L3 and the RES-L3 muscles. **(A4)** EMG activation (AUC) for lower extremity muscles MGC and RF on contralateral side. It was observed that using the PKA lead to higher activation in the MGC and reduced activation in the RF on the contralateral side. Panels **(B1–B4)** are for participant CS02. **(B1)** compares the ankle joint kinematics between PKA, MPK2- Rheo-3, and healthy data (Winter, 1991) for the ipsilateral side for CS02. **(B2)** Comparison of the ratio of peak VGRFs during the stance phase between MPK-2 (Rheo-3), PKA, and healthy data (Winter, 1991). It was observed that using the PKA led to a VGRF behavior close to healthy limb on both, the contralateral and the ipsilateral sides. **(B3)** EMG activation profile between MPK-2 (Rheo-3) and PKA at right and left side L3 erector spinae muscles in low back. The EMG activation profile was indexed as area under the curve (AUC) of the EMG signal. It can be observed that using PKA reduces the asymmetry in EMG activation between the LESL3 and the RESL3 muscles. **(B4)** EMG activation (AUC) for lower extremity muscles MGC and the RF on contralateral side. It was observed that using the PKA lead to higher activation in the MGC and reduced activation in the RF on the contralateral side.

the PKA and MPK during the modified GTT. It was observed that at all speed levels during the GTT, participants were able to walk with variable cadence while using both prostheses (i.e., their respective predicate MPK-1, or MPK-2 and the PKA; **Figures 2A1,B1**). However, at speed ranges >0.6 m/s, the variability in stride times indexed as the

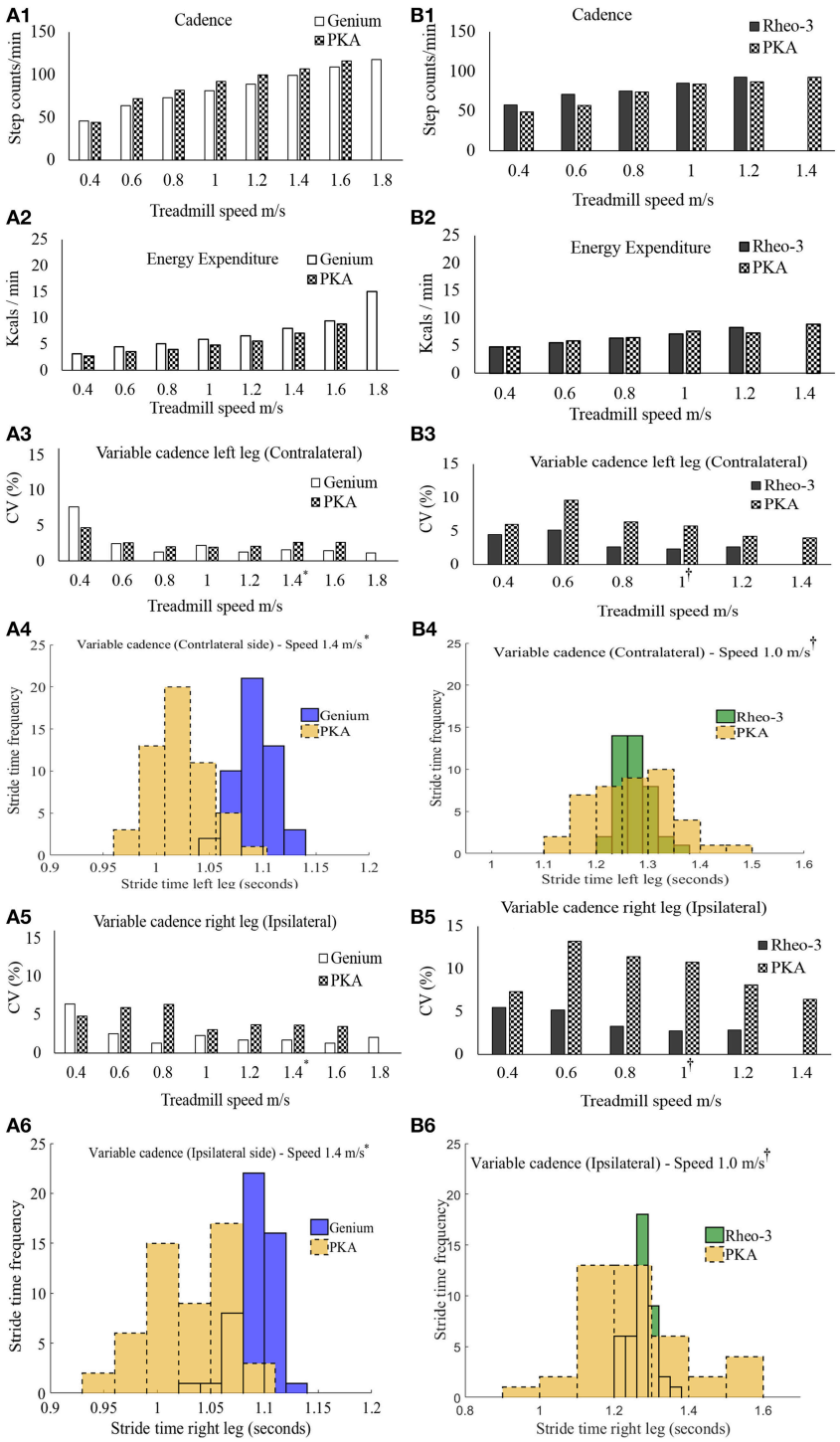

FIGURE 2 | Summary of outcome metrics from the modified graded treadmill test (GTT). Panels **(A1–A6)** are GTT outcome metrics for participant CS01 and panels **(B1–B6)** are GTT outcome metrics for participant CS02. **(A1,B1)** compares the cadence during the GTT between the MPK-1(Genium) vs. PKA and MPK-2(Rheo-3) vs. PKA respectively. **(A2,B2)** compares the EE during GTT between the MPK-1 (Genium) vs. PKA and MPK-2 (Rheo-3) vs. PKA respectively. **(A3,B3)** Compares the coefficient of variation (CV%) for the stride time between the MPK-1(Genium) vs. PKA (in panel **A3**) and MPK-2(Rheo-3) vs. PKA (in panel **B3**) respectively for the contralateral limb. **(A4,B4)** shows the stepwise stride time for the contralateral side during a representative 1 min treadmill walk for MPK-1(Genium) vs. PKA [(in panel **A4**): at treadmill speed of 1.4 m/s (*preferred treadmill speed of the participant CS01)] and MPK-2(Rheo-3) vs. PKA [(in panel **B4**): at treadmill speed of 1 m/s (†preferred treadmill speed of the participant CS02)]. **(A5,B5)** Compares the coefficient of variation (CV%) for the stride time between the MPK-1(Genium) vs. PKA (in panel **A5**) and MPK-2(Rheo-3) vs. PKA (in panel **B5**) respectively for the ipsilateral limb. **(A6,B6)** shows the stepwise stride time for the contralateral side during a representative 1 min treadmill walk for MPK-1(Genium) vs. PKA [(in panel **A6**): at treadmill speed of 1.4 m/s] and MPK-2(Rheo-3) vs. PKA [(in panel **B6**): at treadmill speed of 1 m/s].

coefficient of variation (CV%) was relatively higher for the PKA for both users bilaterally. This suggests that the PKA offered greater ranges of variable cadence to both the contralateral (**Figures 2A3,B3,A4,B4**) and the ipsilateral side limbs (**Figures 2A5,B5,A6,B6**). Perhaps the ability of the PKA device to offer, (i) greater range of variable cadence and, (ii) ankle push off, facilitated marginally better performance in terms of EE/endurance. Indeed, literature shows that cadence and energy expenditure are positively correlated in lower limb amputee population (Rowe et al., 2014).

Outdoor

The participants were able to cross the street to demonstrate community mobility and speed modulation (walking speeds: $CS01_{Genium} = 1.9$ m/s, $CS01_{PKA} = 1.6$ m/s, $CS02_{Rheo-3} = 1.6$ m/s, $CS02_{PKA} = 1.3$ m/s). This showed that both the MPKs and PKA can be used to complete this day-to-day functional task. It was observed that for CS01, the MGC activation followed a similar trend between the outdoor and the indoor tests (level ground walking during the indoor motion capture test; **Figure 3A**). However, for CS02, the trend for activation of MGC showed opposing trends (i.e., the MPK-2 $_{AUC}$ > PKA $_{AUC}$; **Figure 3B**) between the outdoor walking and indoor walking (level ground walking during the indoor motion capture test). We speculate that this change in trend for CS02 could have been due to environmental factors such as the uneven terrain and the subject's decreased ability to control frontal plane forces in this environment.

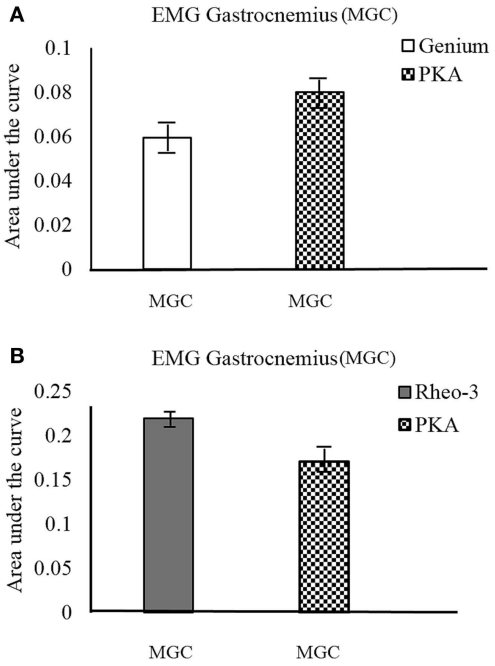

FIGURE 3 | MGC muscle EMG activation profile during outdoor cross walk testing. The EMG activation was indexed as area under the curve (AUC) of the EMG signal. **(A)** compares the MGC muscle activation on the contralateral side between the MPK-1(Genium) and the PKA device. **(B)** compares the MGC muscle activation on the contralateral side between the MPK-2(Rheo-3) and the PKA device for CS02.

DISCUSSION

In this two-participant case series we investigated the efficacy of the PKA that incorporates both a powered knee and powered ankle (PKA) system. The main aim was to investigate if the PKA could offer potential benefits to users in terms of gait performance, metabolic performance (EE), and back muscle activation which has implications for minimization of risk of low back pain.

Benchmarking Outcome Variables With Literature

The mean temporal spatial gait parameters (**Table 1**), cadence ranges and the mean oxygen cost from the two participants in this case series compared well with mean values reported in literature for transfemoral amputees (Jarvis et al., 2017). The observations on knee and ankle kinematics were also consistent with literature (Sup et al., 2009; Lawson et al., 2013, 2015). Benchmarking our outcome metrics with previous literature provides support for the validity of the data collected and the overall findings.

Performance

Energy Expenditure and Endurance

CS01, a young adult, achieved a faster gait speed with his predicate device (MPK-1, Genium) on the treadmill in comparison to the PKA. The participant transitioned from walking to running with the MPK at a speed of 1.8 m/s. There are three potential reasons thatCS01 was unable to reach higher speed while using the PKA: (i) the long length of CS01's residual limb, (ii) a lower ankle push-off setting chosen by CS01, which limited him from taking full advantage of the PKA's potential benefit (Supplementary Material, Figure S3) in comparison to CS02, and (iii) there was no "run mode controller" on the Gen-3 PKA used for this study and considering the safety of the participant, we terminated the test before the participant could break into running.

CS02, an older adult, was able to walk at a higher speed with the PKA than the MPK-2 (Rheo-3) during the modified GTT test. CS02 chose to have an ankle pulse setting far higher (Supplementary Material, Figure S4) than that of CS01. Based on this, for an older adult the ankle push off offered by the PKA could be beneficial in terms of facilitating higher walking speed/endurance. Higher walking speed/endurance is generally related to higher quality of living in older adults (Studenski et al., 2011; Busch Tde et al., 2015). However, this tenet may not be generalizable (Hafner et al., 2016). Increased speed/endurance may have occurred due to integration of power at the ankle and knee and been facilitated by the variable cadence feature offered by the PKA.

CS02 had nearly similar gross oxygen cost, (i.e., gait efficiency) during walking on the treadmill with both the MPK-2 and the PKA. However, for the same oxygen cost, CS02 was able to achieve a higher speed and walked longer with the PKA. Participant CS01 had a detectable improvement in gait efficiency while using the PKA (expended less oxygen cost). The gait efficiency while walking with the MPK-1 was 0.02 mL/kg/m higher than that of the PKA for CS01. The minimal

detectable change (MDC) threshold for a true change in walking performance (gait efficiency) is 0.01 mL/kg/m (Darter et al., 2013). This showed that the participant CS01 benefitted energetically while using the PKA, while CS02 benefitted in terms of endurance while using the PKA.

Quality of Gait Biomechanics and Safety

Kinematics

The ankle joint kinematics while using the PKA reproduced a trajectory that is more similar in behavior [Pearson's correlation (rho $\geq$ 0.6)] to that of a healthy limb in comparison to the MPK devices. The PKA device achieves this by virtue of two of its main design features. First, the PKA controller is designed to make the knee and the ankle joints follow an enforced reference trajectory that is similar to a healthy limb trajectory during gait (Supplementary Material, Figures S3, S4) and (ii) the ankle motor in the PKA provides ankle push off power to suit the level of cadence. The PKA also has a powered knee, which provides stabilization throughout the stance phase and provides power to propel the leg during swing phase. Both the predicate devices are energetically passive (i.e., the foot spring stores and releases energy during gait cycle), unlike the PKA, which provides additional power through motors. Both the predicate MPKs and the PKA device reproduced a knee trajectory (kinematics) that was similar to a healthy limb. Previous literature has shown similar results for knee and ankle kinematics. However, they compared the PKA device with a mechanical passive prosthetic device (Goldfarb et al., 2013; Lawson et al., 2013, 2014, 2015; Shultz et al., 2016). This is the first work to report such kinematic comparison between the PKA and MPK devices.

Erector Spinae EMG

Both participants showed considerable asymmetry (i.e., magnitude of AUC) between the muscle activation level in LES-L3 and RES-L3 level while using their respective MPK devices. In contrast to the muscle activation trends observed with the MPKs, use of the PKA reduced the degree of asymmetry in muscle activation between the RES-L3 and LES-L3 (**Figures 1A3,B3**) during walking in both participants. There are three potential reasons that could have led to the reduction in muscle activation asymmetry while using the PKA. First, by virtue of the PKAs design, the energy provided by the active motors at the knee and ankle which propelled the ipsilateral side during the terminal stance and swing phases could have reduced the load on the erector spinae back muscles. Second, from the trends of the VGRF it can be seen that the PKA led to similar magnitude peak VGRF (i.e., F_{Z1}/F_{Z2}) as opposed to the MPKs. Third, it was observed that the activation level (AUC) of the contralateral RF muscle was considerably higher when ambulating with the MPK devices in comparison to the PKA for both the participants (**Figures 1A4,B4**). A similar muscle activation trend was seen for the contralateral MGC muscle activation in participant CS02. However, this MGC trend was subtle for CS01. These factors could have cumulatively facilitated the reduction of asymmetry in the lumbar L3 muscle activation pattern between the contralateral and the ipsilateral side while using the PKA. In contrast to the PKA, while using the MPK (passive energy) there is no power assist during the gait cycle.

This novel finding could hold implications for minimizing the chance of occurrence of low back injury and pain in transfemoral users over long term device use. This observation is significant because low back muscle activation and injury has been very scarcely studied in transfemoral prosthetic literature (Yoder et al., 2015; Shojaei et al., 2016). Asymmetry in lumbar erector spinae activation during gait is a typical muscle activation pattern in individuals with chronic low back pain (Cappozzo and Gazzani, 1982; Michaud et al., 2000; Lamoth et al., 2006a; Goujon-Pillet et al., 2008; Morgenroth et al., 2010; Hendershot and Nussbaum, 2013; Hendershot et al., 2013; Molina Rueda et al., 2013; Devan et al., 2014; Hendershot and Wolf, 2014; Shojaei et al., 2016). Indeed, such asymmetry has been linked to loss of mobility, debilitating quality of life and surgical interventions (Madeleine et al., 2008; Shojaei et al., 2016). It is highly possible that the muscle activation asymmetry, (**Figures 1A3,B3**) observed in the erector spinae at the L3 region while using the MPKs for locomotion could predispose these users to a higher risk of low back pain and injury in the future.

Based on this case series, we maintain that using the PKA led to more symmetric back muscle activation patterns for both our participants in comparison to their predicate MPKs.

This study is the first to systematically study lumbar muscle activation during different prosthesis use. Also, ours is the first study to report the lumbar muscle activation while using a PKA. From a clinical standpoint, the results observed have significant implications for consequences pertaining to return to work activities and the burden of long term costs. Further studies in this direction are warranted.

Variable Cadence

Both users were able to achieve wider ranges of cadence while using the PKA (**Figures 2A3,A5,B3,B5**) on both the contralateral and the ipsilateral side. With a wide range of cadence, the PKA could offer improved potential in different walking environments over the predicate MPKs. Furthermore, it was observed that for most speed ranges higher than 0.4 m/s, the variability in stride time (CV%) was relatively higher while using the PKA than while using a MPK for both the contralateral and ipsilateral sides (**Figures 2A3,A5,B3,B5**). Indeed, in general, it is well-known that change in variability of movement and musculoskeletal injuries are related (Lamoth et al., 2006b; Madeleine et al., 2008; Lomond and Côté, 2010; Stergiou and Decker, 2011; Srinivasan and Mathiassen, 2012; Steele et al., 2014; Jayaraman et al., 2016). As far as this case study goes, it is too soon to comment if the higher variability that manifests while using the PKA is good or bad. However, unlike the MPK devices, the PKA device offers the clinician more control to fine-tune the leg parameters. To modulate gait variability. In general, changes in the variability of the movement that happen over time have been shown to be related to musculoskeletal injuries occurring due to repetitive movements. Only a structured longitudinal study focused on these outcomes can determine if such a feature is beneficial.

CONCLUDING REMARKS

This case series provide early stage results from a larger on-going clinical trial and thus are not broadly generalizable.

However, the initial results from this ongoing trial of the PKA are promising for walking performance. Both users in this study were trained through just 12 sessions on the PKA and could perform as well as or in some cases better than MPK devices which the users have utilized full time for at least 2 years. In comparison to the MPKs, using the PKA led to more normalized knee and ankle kinematics, more normalized VGRF, and symmetric lumbar muscle activation at the erector spinae region. Additionally, CS01 showed better gait efficiency while using the PKA and CS02 demonstrated better endurance by achieving a higher walking speed. Based on these observations, we maintain that pursuing further research and development of such PKA devices for different terrains could potentially lead to the improvement of transfemoral prosthetic users mobility. The symmetric loading bear implications for minimizing the risk of secondary musculoskeletal injury occurring due to repetitive use. These findings hold potential implications for improving long-term device use and overall quality of life in transfemoral amputees.

AUTHOR CONTRIBUTIONS

CJ, SD-D, SH-L and AJ: carried out the experimental activities, data analysis, participated in the design of the study, and drafted the manuscript; CM, MM, AN, and RS: carried out the experimental activities, data analysis, and drafting of the manuscript; BL, KG, and MG: assisted in the design of the study and in data collection. All authors approved the submitted version of the manuscript.

FUNDING

This work has been funded by a grant from the Department of Defense, Award W81XWH-15-2-0041, and by Max Nader Lab for Rehabilitation Technologies & Outcomes Research.

ACKNOWLEDGMENTS

We would like to thank the Center for Bionic Medicine for support of this clinical trial and the clinical staff of the Shirley Ryan Ability Lab for assistance in recruitment of appropriate subjects.

SUPPLEMENTARY MATERIAL

The Supplementary Material for this article can be found online at: https://www.frontiersin.org/articles/10.3389/fnins.2018.00134/full#supplementary-material

REFERENCES

Acasio, J., Wu, M., Fey, N. P., and Gordon, K. E. (2017). Stability-maneuverability trade-offs during lateral steps. *Gait Posture* 52, 171–177. doi: 10.1016/j.gaitpost.2016.11.034

Aeyels, B., Peeraer, L., Vander Sloten, J., and Van der Perre, G. (1992). Development of an above-knee prosthesis equipped with a microcomputer-controlled knee joint: first test results. *J. Biomed. Eng.* 14, 199–202. doi: 10.1016/0141-5425(92)90052-M

Au, S., Berniker, M., and Herr, H. (2008). Powered ankle-foot prosthesis to assist level-ground and stair-descent gaits. *Neural Netw.* 21, 654–666. doi: 10.1016/j.neunet.2008.03.006

Au, S. K., Weber, J., and Herr, H. (2009). Powered ankle-foot prosthesis improves walking metabolic economy. *Robot. IEEE Trans.* 25, 51–66. doi: 10.1109/TRO.2008.2008747

Bergelin, B. J., Mattos, J. O., Wells, J. G. Jr., and Voglewede, P. A. (2010). Concept through preliminary bench testing of a powered lower limb prosthetic device. *J. Mech. Robot.* 2, 41005–41013. doi: 10.1115/1.4002205

Bergelin, B. J., and Voglewede, P. A. (2012). Design of an active ankle-foot prosthesis utilizing a four-bar mechanism. *ASME J. Mech. Des.* 134:061004. doi: 10.1115/1.4006436

Busch Tde, A., Duarte, Y. A., Pires Nunes, D., Lebrão, M. L., Satya Naslavsky, M., Dos Santos Rodrigues, A., et al. (2015). Factors associated with lower gait speed among the elderly living in a developing country: a cross-sectional population-based study. *BMC Geriatr.* 15:35. doi: 10.1186/s12877-015-0031-2

Cappozzo, A., and Gazzani, F. (1982). "Spinal loading during abnormal walking," in *Biomechanics: Principles and Applications,* eds V. C. D. Huiskes and R. De Wijn (The hague; Boston, MA; London: Martinus Nijhoff), 141–148.

Caputo, J. M., and Collins, S. H. (2014). A universal ankle-foot prosthesis emulator for human locomotion experiments. *J. Biomech. Eng.* 136:035002. doi: 10.1115/1.4026225

Cherelle, P., Grosu, V., Matthys, A., Vanderborght, B., and Lefeber, D. (2014). Design and validation of the Ankle Mimicking Prosthetic (AMP-) foot 2.0. *IEEE Trans. Neural Syst. Rehabil. Eng.* 22, 138–148. doi: 10.1109/TNSRE.2013.2282416

CMS (2001). *HCFA Common Procedure Coding System HCPCS 2001* [Online]. Washington, DC: US Government Printing Office. Available online: https://www.cgsmedicare.com/jc/mr/pdf/mr_checklist_llp.pdf

Darter, B. J., Rodriguez, K. M., and Wilken, J. M. (2013). Test–retest reliability and minimum detectable change using the K4b(2): oxygen consumption, gait efficiency, and heart rate for healthy adults during submaximal walking. *Res. Q. Exerc. Sport* 84, 223–231. doi: 10.1080/02701367.2013.784720

Devan, H., Hendrick, P., Hale, L., Carman, A., Dillon, M. P., and Ribeiro, D. C. (2017). Exploring factors influencing low back pain in people with nondysvascular lower limb amputation: a national survey. *PM R* 9, 949–959. doi: 10.1016/j.pmrj.2017.02.004

Devan, H., Hendrick, P., Ribeiro, D. C., Hale, L. A., and Carman, A. (2014). Asymmetrical movements of the lumbopelvic region: is this a potential mechanism for low back pain in people with lower limb amputation? *Med. Hypotheses* 82, 77–85. doi: 10.1016/j.mehy.2013.11.012

Duffield, R., Dawson, B., Pinnington, H. C., and Wong, P. (2004). Accuracy and reliability of a Cosmed K4b2 portable gas analysis system. *J. Sci. Med. Sport* 7, 11–22. doi: 10.1016/S1440-2440(04)80039-2

Eilenberg, M. F., Geyer, H., and Herr, H. (2010). Control of a powered ankle-foot prosthesis based on a neuromuscular model. *IEEE Trans. Neural Syst. Rehabil. Eng.* 18, 164–173. doi: 10.1109/TNSRE.2009.2039620

Flowers, W. C. (1974). Use of an amputee-computer interactive facility in above-knee prosthesis research. *Proc. ACM Annu. Conf.* 1, 355–339. doi: 10.1145/800182.810421

Goldfarb, M., Lawson, B. E., and Shultz, A. H. (2013). Realizing the promise of robotic leg prostheses. *Sci. Transl. Med.* 5:210ps215. doi: 10.1126/scitranslmed.3007312

Goujon-Pillet, H., Sapin, E., Fodé, P., and Lavaste, F. (2008). Three-dimensional motions of trunk and pelvis during transfemoral amputee gait. *Arch. Phys. Med. Rehabil.* 89, 87–94. doi: 10.1016/j.apmr.2007.08.136

Grimes, D., Flowers, Wc, and Donath, M. (1977). Feasibility of an active control scheme for above-knee prostheses. *J. Biomech. Eng.* 99, 215–221. doi: 10.1115/1.3426293

Hafner, B. J., Morgan, S. J., Askew, R. L., and Salem, R. (2016). Psychometric evaluation of self-report outcome measures for prosthetic applications. *J. Rehabil. Res. Dev.* 53, 797–812. doi: 10.1682/JRRD.2015.12.0228

Hafner, B. J., Sanders, J. E., Czerniecki, J., and Fergason, J. (2002). Energy storage and return prostheses: does patient perception correlate with biomechanical analysis? *Clin. Biomech.* 17, 325–344. doi: 10.1016/S0268-0033(02)00020-7

Hendershot, B. D., Bazrgari, B., and Nussbaum, M. A. (2013). Persons with unilateral lower-limb amputation have altered and asymmetric trunk mechanical and neuromuscular behaviors estimated using multidirectional trunk perturbations. *J. Biomech.* 46, 1907–1912. doi: 10.1016/j.jbiomech.2013.04.018

Hendershot, B. D., and Nussbaum, M. A. (2013). Persons with lower-limb amputation have impaired trunk postural control while maintaining seated balance. *Gait Posture* 38, 438–442. doi: 10.1016/j.gaitpost.2013.01.008

Hendershot, B. D., and Wolf, E. J. (2014). Three-dimensional joint reaction forces and moments at the low back during over-ground walking in persons with unilateral lower-extremity amputation. *Clin. Biomech.* 29, 235–242. doi: 10.1016/j.clinbiomech.2013.12.005

Hitt, J. K., Sugar, T. G., Holgate, M., and Bellman, R. (2010). An active foot-ankle prosthesis with biomechanical energy regeneration. *J. Med. Dev.* 4:011003. doi: 10.1115/1.4001139

Holgate, M., Bohler, A., and Sugar, T. (2008). "Control algorithms for ankle robots: a reflection on the state-of-the-art and presentation of two novel algorithms," in *Proceedings of IEEE/RASEMBS Conference Biomedical Robotics Biomechatronics* (Scottsdale, AZ), 97–102. doi: 10.1109/BIOROB.2008.4762859

Jarvis, H. L., Bennett, A. N., Twiste, M., Phillip, R. D., Etherington, J., and Baker, R. (2017). Temporal spatial and metabolic measures of walking in highly functional individuals with lower limb amputations. *Arch. Phys. Med. Rehabil.* 98, 1389–1399. doi: 10.1016/j.apmr.2016.09.134

Jayaraman, C., Moon, Y., and Sosnoff, J. J. (2016). Shoulder pain and time dependent structure in wheelchair propulsion variability. *Med. Eng. Phys.* 38, 648–655. doi: 10.1016/j.medengphy.2016.04.005

Johansson, J. L., Sherrill, D. M., Riley, P. O., Bonato, P., and Herr, H. (2005). A clinical comparison of variable-damping and mechanically passive prosthetic knee devices. *Am. J. Phys. Med. Rehabil.* 84, 563–575. doi: 10.1097/01.phm.0000174665.74933.0b

John, D., and Freedson, P. (2012). ActiGraph and Actical physical activity monitors: a peek under the hood. *Med. Sci. Sports Exerc.* 44, S86–S89. doi: 10.1249/MSS.0b013e3182399f5e

Klein Horsman, M. D., Koopman, H. F., van der Helm, F. C., Prosé, L. P., and Veeger, H. E. (2007). Morphological muscle and joint parameters for musculoskeletal modelling of the lower extremity. *Clin. Biomech.* 22, 239–247. doi: 10.1016/j.clinbiomech.2006.10.003

Lamoth, C. J., Daffertshofer, A., Meijer, O. G., and Beek, P. J. (2006a). How do persons with chronic low back pain speed up and slow down? Trunk-pelvis coordination and lumbar erector spinae activity during gait. *Gait Posture* 23, 230–239. doi: 10.1016/j.gaitpost.2005.02.006

Lamoth, C. J., Meijer, O. G., Daffertshofer, A., Wuisman, P. I., and Beek, P. J. (2006b). Effects of chronic low back pain on trunk coordination and back muscle activity during walking: changes in motor control. *Eur. Spine J.* 15, 23–40. doi: 10.1007/s00586-004-0825-y

Lawson, B. E., Mitchell, J., Truex, D., Schultz, A., Ledoux, E., and Goldfarb, M. (2014). "A robotic leg prosthesis - design, control, and implementation," in *IEEE Robotics and Automation Magazine,* 70–81. doi: 10.1109/MRA.2014.2360303

Lawson, B. E., Ruhe, B., Shultz, A., and Goldfarb, M. (2015). A powered prosthetic intervention for bilateral transfemoral amputees. *IEEE Trans. Biomed. Eng.* 62, 1042–1050. doi: 10.1109/TBME.2014.2334616

Lawson, B. E., Varol, H. A., Huff, A., Erdemir, E., and Goldfarb, M. (2013). Control of stair ascent and descent with a powered transfemoral prosthesis. *IEEE Trans. Neural Syst. Rehabil. Eng.* 21, 466–473. doi: 10.1109/TNSRE.2012.2225640

Lomond, K. V., and Côté, J. N. (2010). Movement timing and reach to reach variability during a repetitive reaching task in persons with chronic neck/shoulder pain and healthy subjects. *Exp. Brain Res.* 206, 271–282. doi: 10.1007/s00221-010-2405-1

Madeleine, P., Voigt, M., and Mathiassen, S. E. (2008). The size of cycle-to-cycle variability in biomechanical exposure among butchers performing a standardised cutting task. *Ergonomics* 51, 1078–1095. doi: 10.1080/00140130801958659

Michael, J. W. (1999). Modern prosthetic knee mechanisms. *Clin. Orthop. Relat. Res.* 361, 339–347. doi: 10.1097/00003086-199904000-00006

Michaud, S. B., Gard, S. A., and Childress, D. S. (2000). A preliminary investigation of pelvic obliquity patterns during gait in persons with transtibial and transfemoral amputation. *J. Rehabil. Res. Dev.* 37, 1–10.

Morgenroth, D. C., Orendurff, M. S., Shakir, A., Segal, A., Shofer, J., and Czerniecki, J. M. (2010). The relationship between lumbar spine kinematics during gait and low-back pain in transfemoral amputees. *Am. J. Phys. Med. Rehabil.* 89, 635–643. doi: 10.1097/PHM.0b013e3181e71d90

Molina Rueda, F., Alguacil Diego, I. M., Molero Sánchez, A., Carratalá Tejada, M., Rivas Montero, F. M., and Miangolarra Page, J. C. (2013). Knee and hip internal moments and upper-body kinematics in the frontal plane in unilateral transtibial amputees. *Gait Posture* 37, 436–439. doi: 10.1016/j.gaitpost.2012.08.019

Otto Bock Orthopedic Industry, I. (1998). *Manual for the 3c100 Otto Bock C-Leg 1st Edn*. Duderstadt: Otto Bock Orthopedic Industry.

Ossur (2017). *Ossur - The Power Knee* [Online]. Available online at: https://www.ossur.com/prosthetic-solutions/products/dynamic-solutions/power-knee

Peeraer, L., Aeyels, B., and Van der Perre, G. (1990). Development of EMG-based mode and intent recognition algorithms for a computer-controlled above-knee prosthesis. *J. Biomed. Eng.* 12, 178–182. doi: 10.1016/0141-5425(90)90037-N

Peeraer, L., Tilley, K., and Van Der Perre, G. (1989). A computer-controlled knee prosthesis: a preliminary report. *J. Med. Eng. Technol.* 13, 134–135. doi: 10.3109/03091908909030213

Popović D., Oguztöreli, M. N., and Stein, R. B. (1995). Optimal control for an above-knee prosthesis with two degrees of freedom. *J. Biomech.* 28, 89–98. doi: 10.1016/0021-9290(95)80010-7

Rothney, M. P., Schaefer, E. V., Neumann, M. M., Choi, L., and Chen, K. Y. (2008). Validity of physical activity intensity predictions by ActiGraph, Actical, and RT3 accelerometers. *Obesity* 16, 1946–1952. doi: 10.1038/oby.2008.279

Rowe, D. A., McMinn, D., Peacock, L., Buis, A. W., Sutherland, R., Henderson, E., et al. (2014). Cadence, energy expenditure, and gait symmetry during music-prompted and self-regulated walking in adults with unilateral transtibial amputation. *J. Phys. Act. Health* 11, 320–329. doi: 10.1123/jpah.2012-0056

Schmalz, T., Blumentritt, S., and Jarasch, R. (2002). Energy expenditure and biomechanical characteristics of lower limb amputee gait: the influence of prosthetic alignment and different prosthetic components. *Gait Posture* 16, 255–263. doi: 10.1016/S0966-6362(02)00008-5

Shojaei, I., Hendershot, B. D., Wolf, E. J., and Bazrgari, B. (2016). Persons with unilateral transfemoral amputation experience larger spinal loads during level-ground walking compared to able-bodied individuals. *Clin. Biomech.* 32, 157–163. doi: 10.1016/j.clinbiomech.2015.11.018

Shultz, A. H., Lawson, B. E., and Goldfarb, M. (2016). Variable cadence walking and ground adaptive standing with a powered ankle prosthesis. *IEEE Trans. Neural Syst. Rehabil. Eng.* 24, 495–505. doi: 10.1109/TNSRE.2015.2428196

Srinivasan, D., and Mathiassen, S. E. (2012). Motor variability in occupational health and performance. *Clin. Biomech.* 27, 979–993. doi: 10.1016/j.clinbiomech.2012.08.007

Steele, J., Bruce-Low, S., Smith, D., Jessop, D., and Osborne, N. (2014). Lumbar kinematic variability during gait in chronic low back pain and associations with pain, disability and isolated lumbar extension strength. *Clin. Biomech.* 29, 1131–1138. doi: 10.1016/j.clinbiomech.2014.09.013

Stergiou, N., and Decker, L. M. (2011). Human movement variability, nonlinear dynamics, and pathology: is there a connection? *Hum. Mov. Sci.* 30, 869–888. doi: 10.1016/j.humov.2011.06.002

Studenski, S., Perera, S., Patel, K., Rosano, C., Faulkner, K., Inzitari, M., et al. (2011). Gait speed and survival in older adults. *JAMA* 305, 50–58. doi: 10.1001/jama.2010.1923

Sup, F., Bohara, A., and Goldfarb, M. (2008). Design and control of a powered transfemoral prosthesis. *Int. J. Rob. Res.* 27, 263–273. doi: 10.1177/0278364907084588

Sup, F., Varol, H. A., Mitchell, J., Withrow, T. J., and Goldfarb, M. (2009). Preliminary evaluations of a self-contained anthropomorphic transfemoral prosthesis. *IEEE ASME Trans. Mechatron.* 14, 667–676. doi: 10.1109/TMECH.2009.2032688

Suzuki, R., Sawada, T., Kobayashi, N., and Hofer, E. P. (2011). "Control method for powered ankle prosthesis via internal model control design," in *Proceedings of IEEE International Conference on Mechatronics Automation* (Beijing), 237–242. doi: 10.1109/ICMA.2011.5985663

Taylor, M. B., Clark, E., Offord, E. A., and Baxter, C. (1996). A comparison of energy expenditure by a high level trans-femoral amputee using the Intelligent Prosthesis and conventionally damped prosthetic limbs. *Prosthet. Orthot. Int.* 20, 116–121.

Tomovic, R., and McGhee, R. B. (1966). A finite state approach to the synthesis of bioengineering control systems. *IEEE Trans. Hum. Factors Electron.* 7, 65–69. doi: 10.1109/THFE.1966.232325

Winter, D. A. (1991). *Biomechanics and Motor Control of Human Gait: Normal, Elderly and Pathological*. Waterloo, ON: Waterloo Biomechanics Press.

Yoder, A. J., Petrella, A. J., and Silverman, A. K. (2015). Trunk-pelvis motion, joint loads, and muscle forces during walking with a transtibial amputation. *Gait Posture* 41, 757–762. doi: 10.1016/j.gaitpost.2015.01.016

Yuhao, L., Limei, T. R., M. S., Matthew, C., Yinji, M., Siyi, M., and Rogers, A. (2018). Intraoperative monitoring of neuromuscular function with soft, skin-mounted wireless devices nature digital medicine (In press).

Zijlstra, W., and Hof, A. L. (2003). Assessment of spatio-temporal gait parameters from trunk accelerations during human walking. *Gait Posture* 18, 1–10. doi: 10.1016/S0966-6362(02)00190-X

Zlatnik, D., Steiner, B., and Schweitzer, G. (2002). Finite-State Control of a Trans-Femoral (Tf) Prosthesis. *IEEE Trans. Control Syst. Technol.* 10, 408–420. doi: 10.1109/87.998030

Conflict of Interest Statement: MG and BL reports patents US 20130310949, US 9289317 B2, US 20130268090 A1, US 20150209159 A1, US 20120221119 A1 broadly relevant to this work.

The other authors declare that the research was conducted in the absence of any commercial or financial relationships that could be construed as a potential conflict of interest.

frontiers in Neuroscience

ORIGINAL RESEARCH
published: 10 April 2018
doi: 10.3389/fnins.2018.00159

A Control Scheme That Uses Dynamic Postural Synergies to Coordinate a Hybrid Walking Neuroprosthesis: Theory and Experiments

Naji A. Alibeji[1], *Vahidreza Molazadeh*[2], *Brad E. Dicianno*[2] *and Nitin Sharma*[2,3]*

[1] Department of Biomedical Engineering, Case Western Reserve University, Cleveland, OH, United States, [2] Department of Mechanical Engineering and Materials Science, University of Pittsburgh, Pittsburgh, PA, United States, [3] Department of Bioengineering, University of Pittsburgh, Pittsburgh, PA, United States

OPEN ACCESS

Edited by:
Irina N. Beloozerova, Barrow Neurological Institute (BNI), United States

Reviewed by:
Shinya Aoi, Kyoto University, Japan
Boris Prilutsky, Georgia Institute of Technology, United States

***Correspondence:**
Nitin Sharma
nis62@pitt.edu

Specialty section:
This article was submitted to Neuroprosthetics, a section of the journal Frontiers in Neuroscience

Received: *01 September 2017*
Accepted: *27 February 2018*
Published: *10 April 2018*

Citation:
Alibeji NA, Molazadeh V, Dicianno BE and Sharma N (2018) A Control Scheme That Uses Dynamic Postural Synergies to Coordinate a Hybrid Walking Neuroprosthesis: Theory and Experiments. Front. Neurosci. 12:159. doi: 10.3389/fnins.2018.00159

A hybrid walking neuroprosthesis that combines functional electrical stimulation (FES) with a powered lower limb exoskeleton can be used to restore walking in persons with paraplegia. It provides therapeutic benefits of FES and torque reliability of the powered exoskeleton. Moreover, by harnessing metabolic power of muscles via FES, the hybrid combination has a potential to lower power consumption and reduce actuator size in the powered exoskeleton. Its control design, however, must overcome the challenges of actuator redundancy due to the combined use of FES and electric motor. Further, dynamic disturbances such as electromechanical delay (EMD) and muscle fatigue must be considered during the control design process. This ensures stability and control performance despite disparate dynamics of FES and electric motor. In this paper, a general framework to coordinate FES of multiple gait-governing muscles with electric motors is presented. A muscle synergy-inspired control framework is used to derive the controller and is motivated mainly to address the actuator redundancy issue. Dynamic postural synergies between FES of the muscles and the electric motors were artificially generated through optimizations and result in key dynamic postures when activated. These synergies were used in the feedforward path of the control system. A dynamic surface control technique, modified with a delay compensation term, is used as the feedback controller to address model uncertainty, the cascaded muscle activation dynamics, and EMD. To address muscle fatigue, the stimulation levels in the feedforward path were gradually increased based on a model-based fatigue estimate. A Lyapunov-based stability approach was used to derive the controller and guarantee its stability. The synergy-based controller was demonstrated experimentally on an able-bodied subject and person with an incomplete spinal cord injury.

Keywords: hybrid neuroprosthesis, synergy, nonlinear control, neuromuscular stimulation, Lyapunov

1. INTRODUCTION

Paraplegia in persons with spinal cord injury (SCI) impairs walking function and lowers their quality of life. Functional electrical stimulation (FES) and powered exoskeletons are two potential technologies that aim to reanimate lower-limb function in these persons. FES is an artificial application of electrical potential across a muscle group to produce a desired limb function and is prescribed as an intervention to rehabilitate or restore gait function in individuals with mobility-impairements (Peckham and Gray, 1996). FES was used for the first time in the 1960s by Kantrowitz (1960) and Liberson et al. (1961) to produce gait patterns and to correct drop foot, respectively. Since then FES systems that use either percutaneous or surface electrodes have been used to produce gait (Bajd et al., 1983; Marsolais and Kobetic, 1987; Kralj and Bajd, 1989; Granat et al., 1993; Kobetic et al., 1997; Hardin et al., 2007). Despite this progress, the issue of rapid onset of FES-induced muscle fatigue remains unresolved. To reduce the effects of muscle fatigue, FES has been used in conjunction with a passive orthosis (Solomonow et al., 1988; Goldfarb et al., 2003; Farris et al., 2009; Kobetic et al., 2009). The addition of an orthosis mitigates fatigue effects by lowering stimulation duty cycle of FES because it can be used to support the user's weight during standing. However, the gait is still powered by FES during the swing movement and is affected by FES-induced muscle fatigue.

Powered exoskeletons by their virtue of generating high, rapid, and reliable torque are actively being used to provide gait therapy or restoration (Farris et al., 2011; Neuhaus et al., 2011; Strausser and Kazerooni, 2011). Compared to sole FES-based walking systems, however, they may have higher power consumption to operate high torque motors. Bulky high torque motors and larger batteries increase weight and reduce wearability. A hybrid device that combines an FES system with a powered exoskeleton (del Ama et al., 2012, 2014; Ha et al., 2012; Kirsch et al., 2013, 2014a) can overcome these limitations by reducing power consumption and actuator size in the powered exoskeleton. Moreover, the use of FES provides therapeutic benefits to a user.

In Quintero et al. (2012), FES was combined with a powered exoskeleton to control knee extension by using an adaptive gain-based controller and a PD controller. In del Ama et al. (2014) a cooperative knee joint controller was used in a hybrid knee-ankle-foot exoskeleton. The approach was tested on able-bodied subjects. A PID controller and an iterative learning controller were used to stimulate the quadriceps muscle and the knee flexors, respectively while a variable stiffness controller computed the knee electric motor stiffness based on the measured interaction torque between the user and the exoskeleton. In Ha et al. (2015), another cooperative control approach was used to coordinate hip motors with the stimulation of the hamstrings and knee motors with the stimulation of quadriceps muscle. The approach was tested on three subjects with SCI. The motors were controlled using a high-bandwidth position feedback and the FES control was modified by the difference between the estimated muscle torque and the reference torque profile.

In our previous research, a dynamic optimization method was used to optimize a hybrid walking system (FES + passive orthosis) (Sharma et al., 2014). However, the method computes FES control inputs offline. Motivated to develop an optimization method for a real-time implementation, in Kirsch et al. (2014b), a linear model predictive control (MPC) method was proposed to dynamically allocate control in a hybrid knee joint control system composed of FES and an electric motor. However, a linearized musculoskeletal model was used for the linear MPC method, which may lose control performance outside the region of linearization. Therefore a nonlinear model predictive controller (NMPC) for an FES only case was developed in Kirsch and Sharma (2017) to elicit knee extension in able-bodied participants.

Aforementioned research papers in hybrid neuroprosthesis control focused primarily on coordinating FES and the motors at a single joint, even though some of these papers provided pioneering evidence of its benefits. Motivated to provide a general framework that coordinates stimulation of multiple muscles and exoskeleton actuators at multiple joints, a muscle synergy-inspired controllers were presented in Alibeji et al. (2015b, 2017). In Alibeji et al. (2015b), simulations of the synergy inspired controller for single stepping motion were shown. This controller was further improved to incorporate effects of fatigue and electromechanical delay (EMD) in Alibeji et al. (2017). The experimental evidence of the synergy-inspired controller was provided using standing-cyclical experiments.

Motivated to extend the synergy-based controller, in this paper, dynamic postural synergies were used in a control scheme to generate walking with a hybrid exoskeleton. The dynamic postural synergies are artificial synergies designed to drive the system to key dynamic postures when activated. Then sequential activation of these dynamic postural synergies drive the system to produce gait motions. An adaptive update law was used to modify the synergy activation profiles to compensate for parametric changes in the model. A PID-based feedback component was used to make the controller robust to uncertainity and disturbances. The controller uses dynamic surface control (DSC) (Alibeji et al., 2017) to avoid the use of acceleration signals in the control design. This DSC framework was also modified to include a delay compensation term to account for the EMD. To counter muscle fatigue effects, the control input terms were scaled by the fatigue estimate's inverse. In addition, a scaling factor gain is added to the feedforward component in case there is mismatch in model and subjects strength during experiments. Model-based estimators were designed to estimate the fatigue and activation state variables. The individual components of this controller have been validated experimentally and through simulations in Sharma et al. and Alibeji et al. and have been shown to provide improved performance compared with traditional PID controllers (Sharma et al., 2011; Alibeji et al., 2015a,b, 2017). Finally, experiments were performed on an able-bodied subject and a person with an incomplete spinal cord injury to show the feasibility of coordinating multiple muscles and electric motors with the synergy-inspired controller.

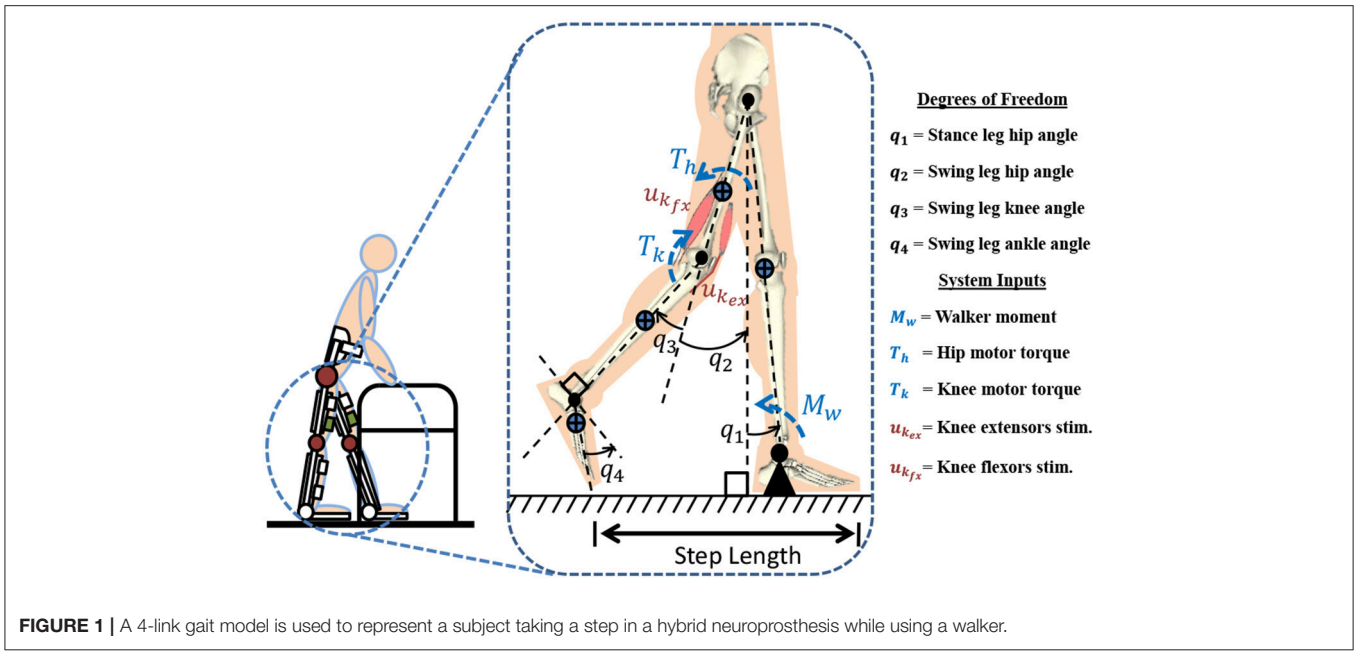

FIGURE 1 | A 4-link gait model is used to represent a subject taking a step in a hybrid neuroprosthesis while using a walker.

2. METHODS

2.1. Walking Hybrid Neuroprosthesis Model

Figure 1 represents the 4-link model which is used for modeling a hybrid neuroprosthesis and a walker. The 4-link model considers a hybrid neuroprosthesis that uses electric motors and FES via surface electrodes, which non-selectively apply an external voltage potential to a muscle group to generate a contraction. The stance leg is modeled as one rigid segment simulating the locking of the knee joint and the ankle is fixed to the ground because only half of the gait cycle is considered. The swing leg has a thigh, shank, and foot segment but only the hip and knee joints have active actuation. The knee joint uses 3 actuators: motor and FES for flexion and extension of antagonistic muscle pairs. The model only uses electric motors at the hip joints because it can be difficult to stimulate the hip flexors and extensors, as these muscle are not easily accessible using surface electrodes. The trunk dynamics were neglected in the model because the use of a walker allows the user to stabilize their truck. However, the model assumes the trunk is fixed at the vertical orientation. The walker is modeled as a moment acting on the stance leg to help propel the body forward and also to keep it upright. The lower limb model is given as:

$$M\left(q\right)\ddot{q} + C(q,\dot{q})\dot{q} + G(q) + f(q,\dot{q}) + \Gamma_d(t) + \Gamma_{ext}(t) = \Gamma, \quad (1)$$

where $q,\ \dot{q},\ \ddot{q} \in \mathbb{R}^4$ are the angular positions, velocities, and accelerations of the leg segments, respectively. In (1), $M(q) \in \mathbb{R}^{4\times4}$ is the combined inertia of the hybrid neuroprosthesis and human limbs, $C(q,\dot{q}) \in \mathbb{R}^{4\times4}$ is the centripetal/Coriolis matrix, $G(q) \in \mathbb{R}^4$ is the gravity vector, $f(q,\dot{q}) \in \mathbb{R}^4$ is the viscoelastic vector term that models the passive muscle dynamics, $\Gamma_{ext} \in \mathbb{R}^4$ is the torque generated at each joint due to contact with the ground and walker moment (M_W), and $\Gamma_d \in \mathbb{R}^4$ is any unmodeled effects or disturbances in the system. The active torques at the joints are generated by including the musculoskeletal dynamics due to FES (Popović et al., 1999), an electric motor attached at each joint, and the moment generated by the walker force. The torque term is defined as

$$\Gamma = b(q,\dot{q})\phi(t)\mu(t), \quad (2)$$

where $\mu(t) \in \mathbb{R}^4$ is the intermediate normalized activation vector containing activation states for the actuators, and is defined as

$$\mu \triangleq \left[\begin{array}{cccc} \mu_{k_{fx}} & \mu_{k_{ex}} & \mu_{h_m} & \mu_{k_m} \end{array}\right]^{\mathrm{T}},$$

where, $\mu_{k_{fx}} \in \mathbb{R}$ is knee flexor muscle activation, $\mu_{k_{ex}} \in \mathbb{R}$ is knee extensor muscle activation, $\mu_{k_m} \in \mathbb{R}$ is normalized current for the knee motor and $\mu_{h_m} \in \mathbb{R}$ is normalized current for the hip motor. In (2), $\phi(t) \in \mathbb{R}^{4\times4}$ is the fatigue matrix that contains the fatigue factor corresponding to each stimulated muscle and is defined as

$$\phi \triangleq diag\left(\left[\begin{array}{cccc} \phi_{k_{fx}} & \phi_{k_{ex}} & 1 & 1 \end{array}\right]\right),$$

and $b(q,\dot{q}) \in \mathbb{R}^{4\times4}$ is the control gain matrix defined as

$$b = \left[\begin{array}{cccc} 0 & 0 & \psi_{k_{fx}} & 0 \\ 0 & 0 & -\psi_{k_{ex}} & 0 \\ 0 & \kappa_h & 0 & 0 \\ 0 & 0 & \kappa_k & 0 \end{array}\right]^T, \quad (3)$$

In (3), $\psi_{i_{fx}},\ \psi_{i_{ex}}$ are the torque-length and torque-velocity relationships of the flexor and extensor muscles and the

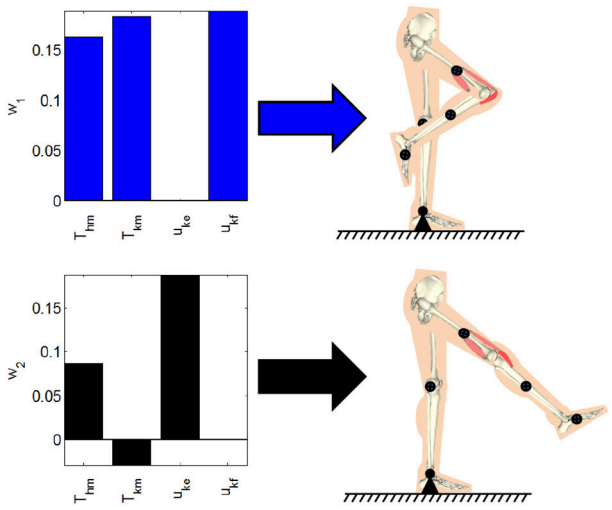

FIGURE 2 | The dynamic postural synergies computed through the optimizations and the dynamic postures they result in when activated.

conversion constants (current to torque) of the electric-motor drives is κ_i.

The activation state is governed by the following first order differential equation

$$\dot{\mu}_{i_j} = -\omega_{i_j}\mu_{i_j} + \omega_{i_j}u_{i_j}(t - \tau_{i_j}), \tag{4}$$

where subscripts $i = h,\ k$ stand for the hip and knee joints of the swing leg and $(j = fx,\ ex,\ m)$ for the type of actuator. In (4), $\omega_{i_j} \in \mathbb{R}^+$ is the actuator decay constant, u_{i_j} is the normalized input, and τ_{i_j} is the input delay.

The fatigue dynamics of the muscles, $\phi_{i_j} \in \mathbb{R}$ is generated from the first order differential equation (Riener et al., 1996)

$$\dot{\phi}_{i_j} = \frac{1}{T_{f_{i_j}}}(\phi_{\min_{i_j}} - \phi_{i_j})\mu_{i_j} + \frac{1}{T_{r_{i_j}}}(1 - \phi_{i_j})(1 - \mu_{i_j}), \tag{5}$$

where $\phi_{\min} \in (0, 1)$ is the unknown minimum fatigue constant of a muscle, and $T_f,\ T_r \in \mathbb{R}^+$ are unknown time constants for fatigue and recovery in the muscle, respectively. Because $\mu \in [u_{min}, u_{max}]$ for muscles, it can be shown that $\phi \in [\phi_{\min}, 1]$, where $\phi = 1$ when the muscle is fully rested, and $\phi = \phi_{\min}$ when the muscle is fully fatigued. The fatigue state for the motors in the fatigue matrix are set to one because the motors do not fatigue.

The stimulation applied to the muscle is bounded by two stimulation levels v_{min} and v_{max} to avoid under/over stimulating the muscles. This allows the normalization of the input function $u(t) \in \mathbb{R}^4$, which is modeled by a piecewise linear recruitment curve (Schauer et al., 2005), as

$$u(t) = sat[v(t)] = \begin{cases} 0 & v < v_{min} \\ \frac{v(t) - v_{min}}{v_{max} - v_{min}} & v_{min} \le v \le v_{max} \\ 1 & v > v_{max} \end{cases} \tag{6}$$

where $v_{\min}, v_{\max} \in \mathbb{R}^4$ are the minimum/maximum input magnitudes for each actuator (stimulation or motor) and $v(t) \in \mathbb{R}^4$ is the input to the system. Based on (4) and (6), a linear differential inequality can be developed to show that $\mu \in [u_{\min}, u_{\max}]$. The $u_{\min}, u_{\max}$ values are $[0, 1]$ for muscles because they are unidirectional and $[-1, 1]$ for electric motors because they are bidirectional actuators.

2.2. Dynamic Postural Synergies

The purpose of muscle synergies in human motor control is to reduce the complexity of the system by reducing the input space and redundant DOF. In this paper, an alternative form of synergies called dynamic postural synergies are introduced. Unlike other methods which identify synergies by using statistical analysis tools on collected EMG data or simulation results, this form of synergies is computed independently to create a reduced input space for a system that can be used to more efficiently control a system. The dynamic postural synergies generated in this paper are artificial synergies that are designed to drive the system to key dynamic postures, which are defined as the joint positions at any moment during a movement pattern. Then motions such as walking can be segmented into a finite number of dynamic postures and a dynamic postural synergy can be computed for each dynamic posture. These artificial synergies can then be activated sequentially to drive the system from one dynamic posture to the next to create the original motion.

In Bajd et al. (1983) rudimentary gait was recreated in subjects with SCI by stimulating the peroneal nerve and then the quadriceps to produce two key dynamic postures; the withdrawal reflex and knee extension. The withdrawal reflex is a spinal reflex that protects the body from damaging stimuli and can be triggered by activating the pain receptors at the bottom of the foot or stimulating the peroneal nerve. The reflex consists of the flexing of the hip, knee, and ankle joints to immediately lift the leg off of the ground or the source of the pain. In this work, the artificial synergies, defined as $W \in \mathbb{R}^{4\times2}$, that produce these dynamic postures were computed using dynamic optimizations. Then, another set of dynamic optimizations were used to find the optimal activation of these artificial synergies, defined as $c_d \in \mathbb{R}^2$, to reproduce gait trajectories, q_d. Below, the dynamics, excluding the fatigue factor ϕ, are written in terms of the kinematic trajectories (q_d) and the activation state generated from the dynamic postural synergies and their optimal activation (i.e., $\mu_d = Wc_d$) as

$$\begin{aligned} M(q_d)\ddot{q}_d + C(q_d, \dot{q}_d)\dot{q}_d + G(q_d) + f(q_d, \dot{q}_d) \\ \equiv b(q_d, \dot{q}_d)\mu_d(t) - \Gamma^*_{ext}, \end{aligned} \tag{7}$$

where Γ^*_{ext} is the ground reaction forces and walker moment, M_W, resulting from the optimal trajectories (q_d).

2.2.1. Computing the Synergies

The dynamic postural synergies are computed using optimizations that use the 4-link walking model in (1). The 4-link walking model was modified to reflect the hybrid neuroprosthesis testbed, therefore, only the hip motors, knee

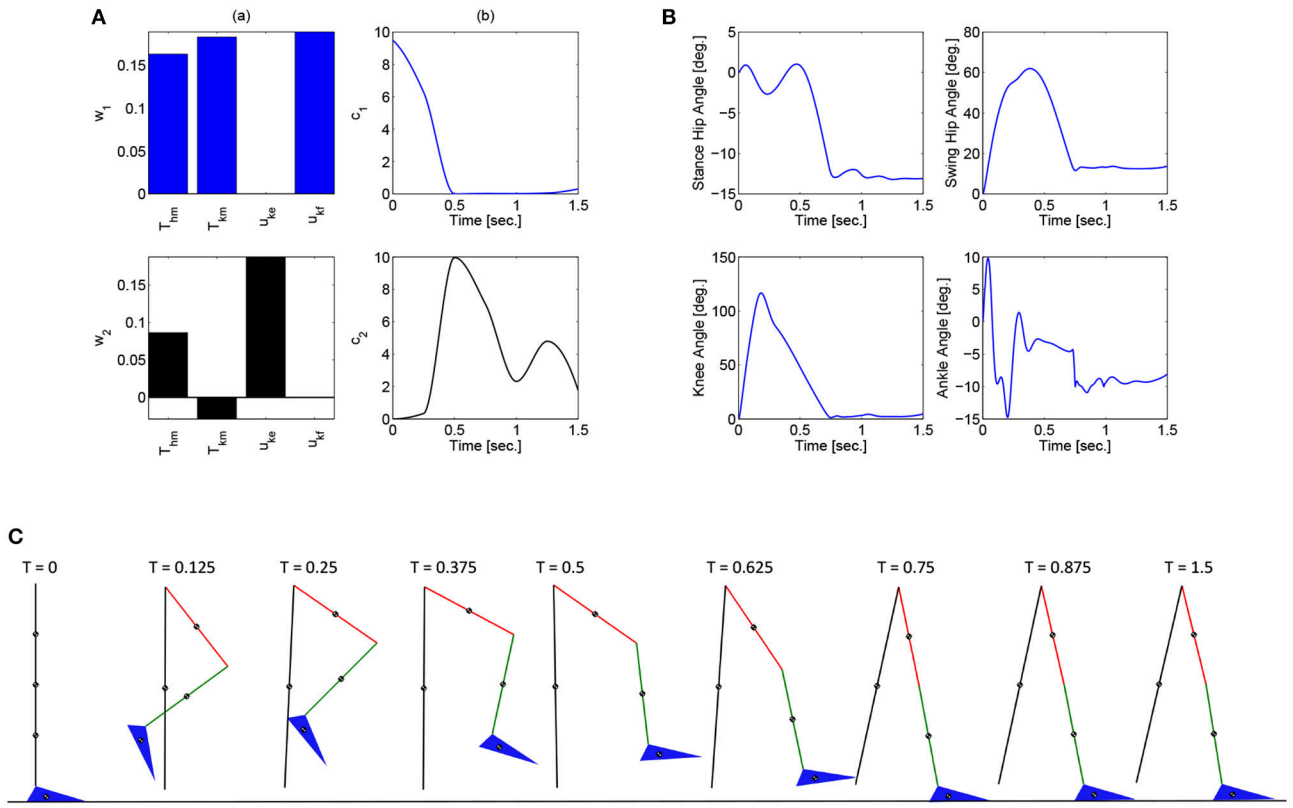

FIGURE 3 | (A) The dynamic postural synergies (a) and their activation to produce a half step (b), **(B)** the joint trajectories they produce, **(C)** the gait sequence for the half step.

motors, and the antagonistic muscle pairs of the knee joint are used. The parameters used for this model were taken from Popović et al. (1999) for an able bodied person. Optimizations were conducted to compute the synergies that distribute the effort to the 4 inputs that minimize the error between the desired dynamic posture and the resulting motion. The joint angles for the desired dynamic postures were taken from the optimal trajectories in Alibeji et al. (2015b). For these optimizations, the convex cost function's objective was to minimize the dynamic posture's position error and minimize the activation states of the system and is defined as

$$\min_{W} \ \Pi = \int_{t_0}^{t_f} \left(E_1(t)^T Q_1 E_1(t) + \mu(t)^T R_1 \mu(t) \right) dt \qquad (8)$$

$$\text{subject to: } M\left(q\right)\ddot{q} + C(q,\dot{q})\dot{q} + G(q) + f(q,\dot{q}) = b(q,\dot{q})\mu - \Gamma_{ext},$$

$$\mu \in [\mu_l, \mu_u]$$

where dynamic posture's position error is defined as $E_1 = q_{dp} - q$ and q_{dp} is the joint positions for the desired dynamic posture. In (8), $Q_1 \in \mathbb{R}^{4\times4}$ is a weight on the position tracking error, the matrix $R_1 \in \mathbb{R}^{4\times4}$ is a positive-definite matrix of weights on the activation vector, and the lower and upper bound on the activations are defined as μ_l and $\mu_u \in \mathbb{R}^4$. Based on the selection of the input weight matrix R_1, the distribution of the effort from the motors or stimulation can be emphasized. These optimizations were performed by using Matlab's fmincon function (MathWorks, Inc., USA). The dynamic postural synergies computed through the optimization and the postures they produce; withdrawal reflex and knee extension, can be seen in **Figure 2**. The first dynamic postural synergy activates the hip motor to produce a moment at the hip in the flexion direction, and activates the knee motor and knee flexor to produce a moment at the knee in the flexion direction, to produce the withdrawal reflex. The second dynamic postural synergy activates the hip motor to produce a smaller moment at that hip to maintain the hip joint's position, and activates the knee motor and knee extensor to produce a moment at the knee to fully extend the knee joint.

2.2.2. Computing the Synergies' Activation

Unlike the synergies extracted through statistical methods, such as principal component analysis in Alibeji et al. (2015b), these dynamic postural synergies were determined using separate optimizations prior to these dynamic optimizations. Using these already computed dynamic postural synergies, these dynamic optimizations now compute the optimal synergies' activations in order to complete a step.

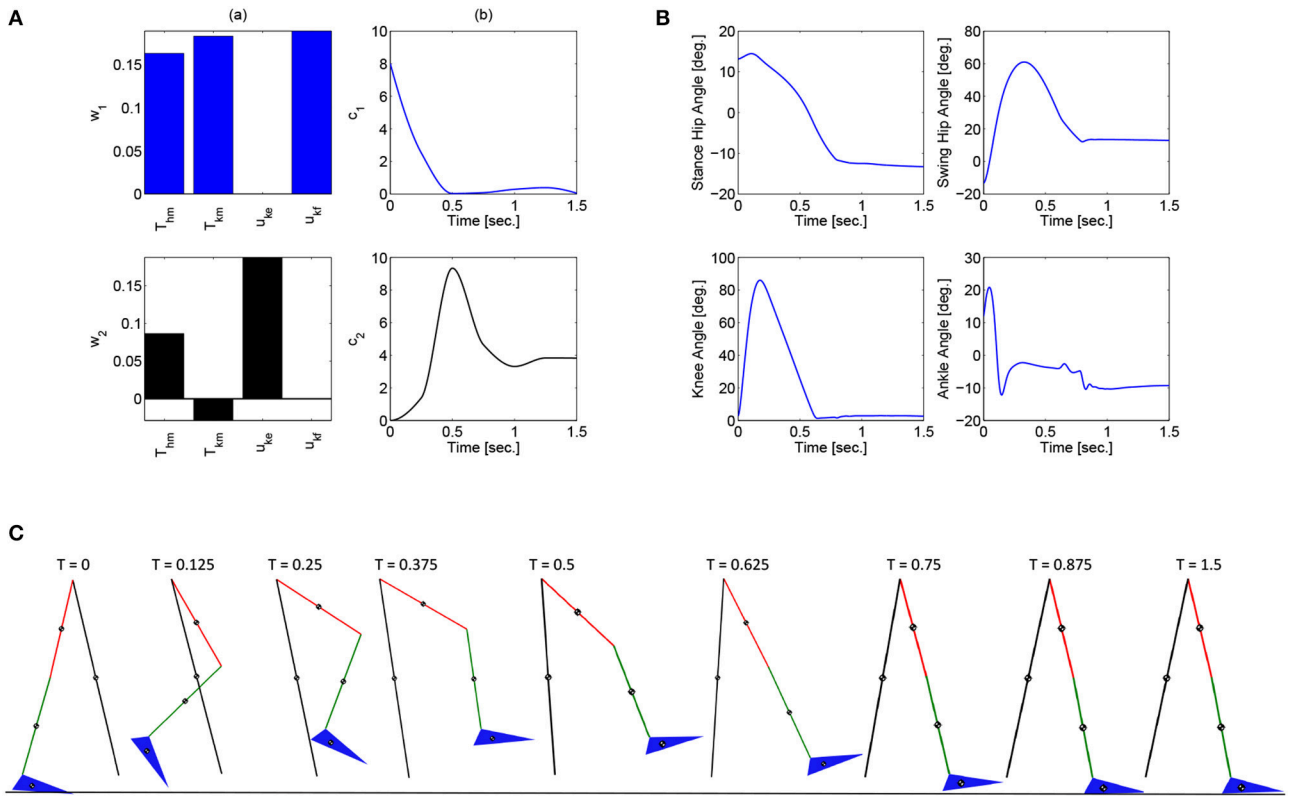

FIGURE 4 | (A) The dynamic postural synergies (a) and their activation to produce a full step (b), **(B)** the joint trajectories they produce, **(C)** the gait sequence for the full step.

In order to consistently and easily maintain the initial condition during experimentation, the subject will start the gait process while standing upright. Therefore, two sets of dynamic optimizations are computed; one for a half step (0.2 meters) and the second for a full step (0.4 meters).

These dynamic optimizations also include the double support phase (DSP) part of the gait sequence, i.e, when the body is supported by both legs. During the DSP the load transfers from the stance leg to the swing leg and the legs switch roles, i.e., the stance leg from the previous step becomes the swing leg for the next step and vice versa. To include the DSP, the swing leg has to the reach the desired position, where the swing leg makes contact with the ground, in the allotted time, $t_{step} = 1$ s., and maintain that position, i.e., maintain contact with the ground, for a predetermined duration, $t_{DSP} = 0.5$ s. For these optimizations, the convex cost function's objective was to minimize the synergy activation for the full duration and the final position error from $t = t_{step}$ to $t = t_{DSP}$. The cost function is defined as

$$\begin{aligned} \min_{c,M_w} \ \Pi = & \int_{t_0}^{t_f} c(t)^T R_2 c(t) dt + \int_{t_{step}}^{t_f} E_2(t)^T Q_2 E_2(t) dt \\ & + \Pi_{extra} \\ \text{subject to: } & c \in [c_l, c_u] \end{aligned} \tag{9}$$

where final position error is defined as $E = q_f - q$, q_f is the final joint positions for a complete step, $R_2 \in \mathbb{R}^{2\times 2}$ is the positive-definite weight matrix for the synergy activation, $Q_2 \in \mathbb{R}^{4\times 4}$ is the positive-definite weight matrix for the the joint angle errors, and the lower and upper bound on the synergy activations are defined as c_l and $c_u \in \mathbb{R}^2$. In the cost function t_0 is the time in which the step begins and t_f is the final time for the step and is defined as $t_f = t_{step} + t_{DSP}$. The last variable in the cost function, Π_{extra} is an additional cost that is activated when certain undesirable events occur in the solution, e.g., the foot drags on the ground or the swing leg overshoots.

These optimizations were performed in Matlab using a genetic algorithm particle swarm optimization (GAPSO) method to minimize the cost function. The dynamic postural synergies, their activations computed through the optimizations, the joint trajectories they produce, and the gait sequence for the half step and full step can be seen in **Figures 3**, **4**, respectively. From the gait sequences, it can be observed that the optimizations computed the synergy activations to complete the step, whether half or full, and maintained contact with the ground throughout the DSP while interacting with the ground reaction model. In addition, it can be seen that the dynamic postural synergies are activated in sequence as intended, i.e., for the first 0.5 s. primarily the first synergy is activated and then for the remainder of time primarily the second synergy is activated. Even though the model completes the step by around 1 s. the second synergy is still

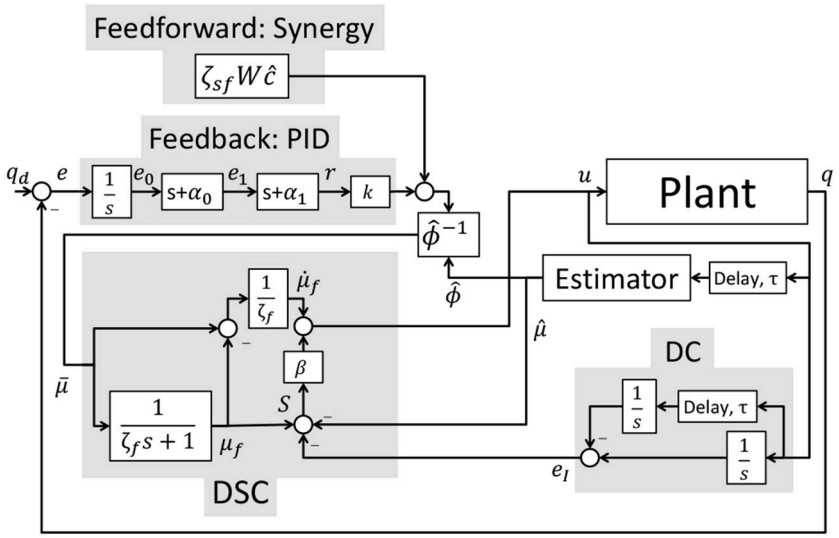

FIGURE 5 | The control schematic for the implementation of the overall controller.

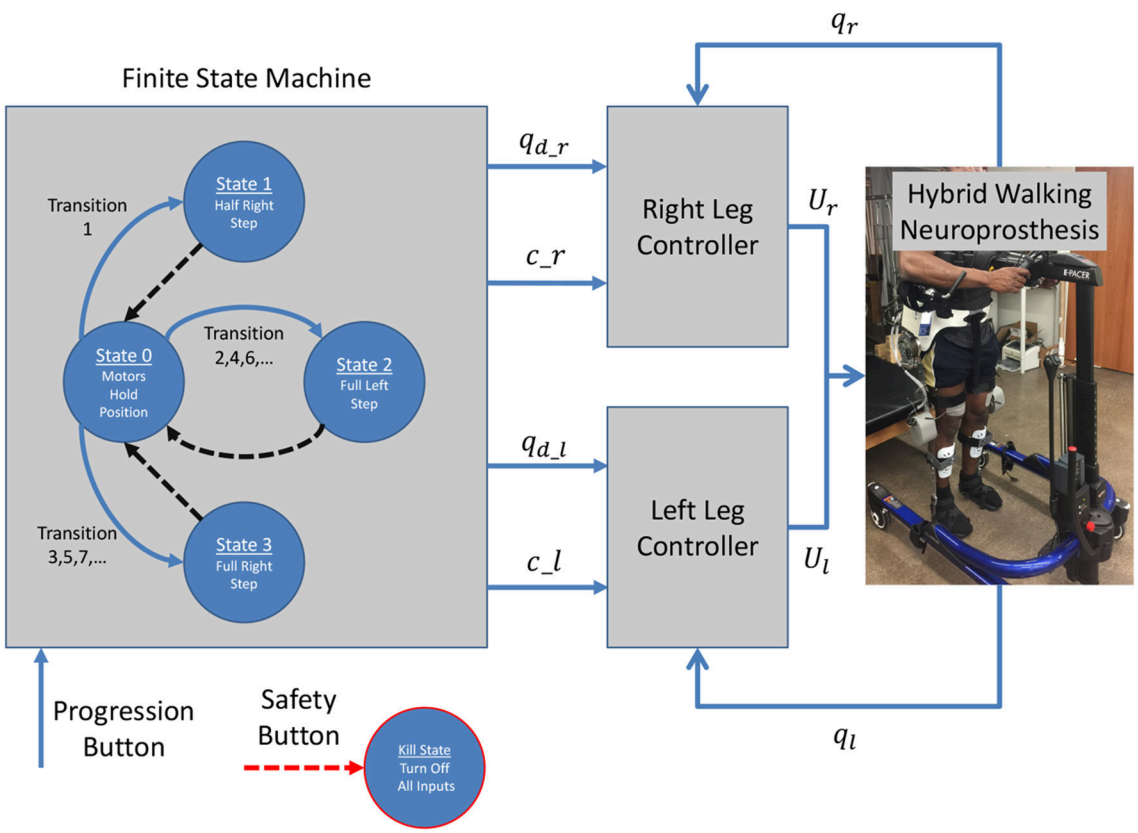

FIGURE 6 | The Finite State Machine determines the desired trajectories and synergy activations based on what state is activated; either half right step, full left step, or full right step. Then two controllers are used, one for each leg, which work in tandem to produce gait.

activated for the remainder of the time; this is to keep the knee from buckling since both legs are supporting the body during this phase.

Note that for the full step results, as the swing leg leaves the ground, the stance leg is tilted posteriorly which is not typical for normal gait. This is because this system does not currently

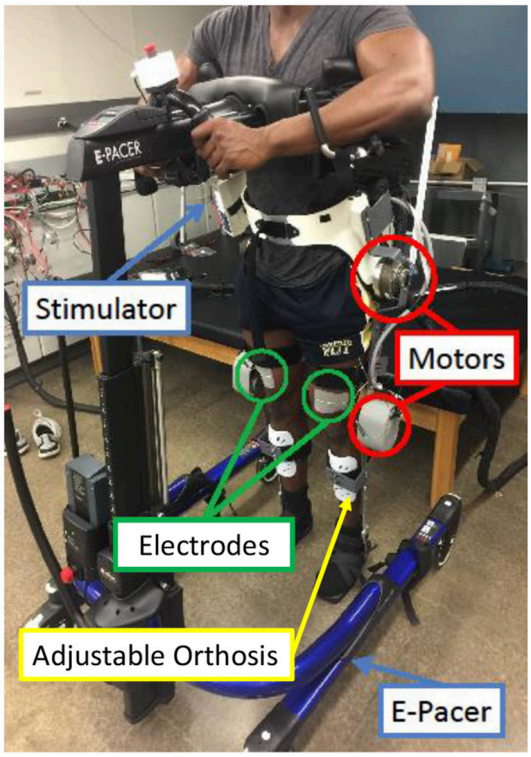

FIGURE 7 | The walking hybrid neuroprosthesis and the gait support device used in the experimental demonstration of the synergy-based control system. This system uses an electric motor at the hip and knee joints of each leg and FES of the hamstrings and quadriceps muscle group of each leg.

include actuation at the ankle joints to produce push off. During normal gait the first part of the gait sequence is push off, as a result of the plantar-flexion of the ankle, to propel the body forward. The differences between gait with and without push off can be seen when comparing these results to the walking simulation results in Alibeji et al. (2015b) where ankle actuation is present. If the push off phase is to be included in this system, it would have its own dynamic postural synergy.

2.3. Control Development and Stability Analysis

2.3.1. Control Objective

The control objective is to track a continuously differentiable desired trajectory $q_d \in \mathbb{R}^4$. The tracking error, $e \in \mathbb{R}^4$, is defined as

$$e \triangleq q_d - q. \tag{10}$$

To facilitate the control design and stability analysis, the auxiliary error signals $e_1(t),\ r(t) \in \mathbb{R}^4$ are defined as

$$e_1 \triangleq \dot{e}_0 + \alpha_0 e_0, \tag{11}$$

$$r \triangleq \dot{e}_1 + \alpha_1 e_1, \tag{12}$$

where $\alpha_0,\ \alpha_1 \in \mathbb{R}^+$ are control gains and $e_0(t) \in \mathbb{R}^4$ is an auxiliary signal defined as Downey et al. (2015)

$$e_0 \triangleq \int_{t_0}^{t} e(s)ds, \tag{13}$$

in order to incorporate integral control. To simplify the derivations, the following notations are used: (1) the time dependence of a function is dropped [e.g., $e(t) \rightarrow e$] and (2) a signal delayed by τ is notated as a subscript [e.g., $u(t-\tau) \rightarrow u_\tau$]. In addition, to facilitate the control development and stability analysis, the following assumptions were made.

Assumption 1: Only motion in the sagittal plane is considered.

Assumption 2: The unmodeled effects or disturbances, τ_d, are bounded as $|\tau_d| \leq \epsilon_1$ where $\epsilon_1 \in \mathbb{R}^+$ is a constant.

Assumption 3: The dynamic postural synergies, W, are bounded constants and their activation, c_d, are bounded vectors.

Assumption 4: The desired trajectory, $q_d \in \mathbb{R}^n$, and its derivatives, $\dot{q}_d,\ \ddot{q}_d \in \mathbb{R}^n$, are bounded.

2.3.2. Closed-Loop Error System

The open-loop error is derived by multiplying the time derivative of (12) with $M(q)$ and substituting the dynamics in (1) and (2) to obtain

$$M\dot{r} = M\ddot{q}_d + C\dot{q} + G + f + d - b\phi\mu + M\alpha_0\ddot{e}_0 + M\alpha_1\dot{e}_1. \tag{14}$$

where d is the lumped disturbances and is defined as $d = \Gamma_d + \Gamma_{ext}$. This expression can be written in the form

$$M\dot{r} = -Cr + \tilde{N} + N_d + d - b\phi\mu - e_1 - b_d\phi e_I, \tag{15}$$

where $b_d = b(q_d, \dot{q}_d)$, $e_I \in \mathbb{R}^4$, is defined as $e_{I_{i_j}} \triangleq \int_{t-\tau_{i_j}}^{t} u_{i_j}(\theta)d\theta$ for each actuator and $\tilde{N} \in \mathbb{R}^4$, is defined as $\tilde{N} \triangleq N - N_d$. The auxiliary signals $N(q, \dot{q}, e, \dot{e}, e_I, t)$ and $N_d(t)$ are defined as

$$\begin{aligned} N \triangleq\ & M\ddot{q}_d + C\left(\dot{q}_d + (\alpha_0 + \alpha_1)\, e_1 - \alpha_0^2 e_0\right) + G + f \\ & + M\alpha_0\left(r - (\alpha_1 + \alpha_0)\, e_1 + \alpha_0^2 e_0\right) \\ & + M\alpha_1\left(r - \alpha_1 e_1\right) + e_1 + b_d\phi e_I, \end{aligned}$$

$$N_d \triangleq M(q_d)\ddot{q}_d + C(q_d, \dot{q}_d)\dot{q}_d + G(q_d) + f(q_d, \dot{q}_d).$$

The term $\tilde{N}$ in (15) can be upper bounded by using the Mean Value Theorem as

$$\left\|\tilde{N}\right\| \leq \rho_1(\|z\|)\,\|z\|, \tag{16}$$

where $\rho_1(\|z\|) \in \mathbb{R}$ is a positive monotonic bounded function and $z \in \mathbb{R}^{16}$ is defined as

$$z = [\ e_0^T\ \ e_1^T\ \ r^T\ \ e_I^T\ ]^T.$$

Note that the auxiliary signal N_d is equal to the left hand side of the desired muscle dynamics in (7). Therefore, (15) can be rewritten as

$$M\dot{r} = -Cr + \tilde{N} + D + b_d\mu_d - b\phi\mu - e_1 - b_d\phi e_I, \tag{17}$$

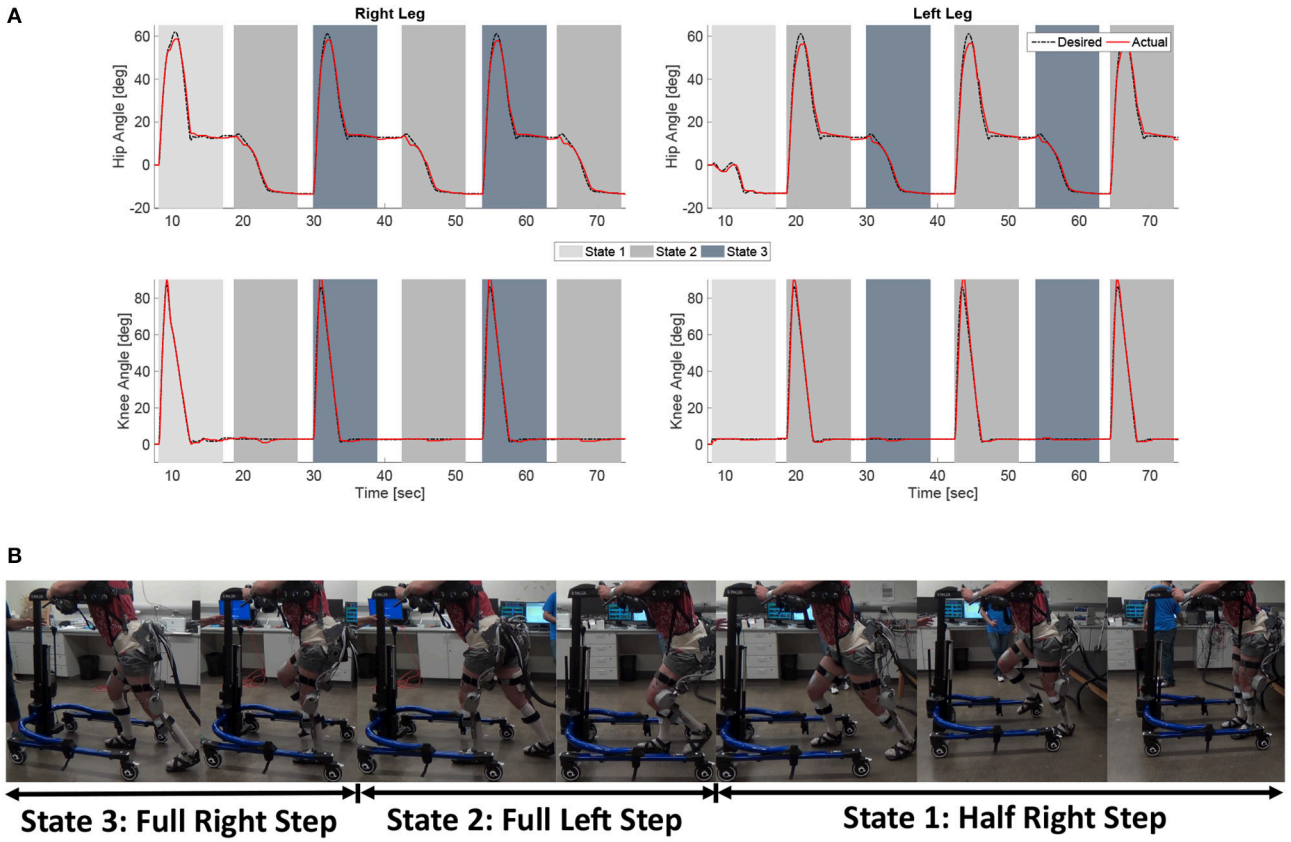

FIGURE 8 | (A) The desired and actual joint angles of the right and left hip and knee joints resulting from using the developed synergy-based DSC/DC control system in conjunction with the FSM on a subject with an incomplete SCI. The shaded regions indicate which state of the FSM is active at that time. **(B)** A sequence of photos illustrating the gait produce during the experiments. The depicted individual provided written and informed consent for the publication of this image.

where $D = d - \Gamma^*_{ext}$. After adding and subtracting the terms $b_d\hat{\phi}\bar{\mu}$, $b_d\phi\bar{\mu}$, $b_d\phi\hat{\mu}$, $b_d\phi\mu$, and $b_d\phi\mu_f$ where $\hat{\mu} \in \mathbb{R}^4$ and $\hat{\phi} \in \mathbb{R}^{4\times4}$ are estimates of the activation state and the fatigue state, $\bar{\mu} \in \mathbb{R}^4$ is the desired activation to be later defined, and $\mu_f \in \mathbb{R}^4$ is a filtered desired activation, and rearranging the terms, (17) becomes

$$M\dot{r} = -Cr + b_d\phi S + b_d\phi y + \tilde{N} + D + b_d\mu_d + \tilde{b}\phi\mu + b_d\phi\tilde{\mu} + b_d\tilde{\phi}\bar{\mu} - b_d\hat{\phi}\bar{\mu} - e_1, \quad (18)$$

where $\tilde{b} \in \mathbb{R}^{4\times4}$ is defined as $\tilde{b} \triangleq b_d - b$, $\tilde{\phi} \in \mathbb{R}^{4\times4}$ is defined as $\tilde{\phi} \triangleq \hat{\phi} - \phi$, and $\tilde{\mu} \in \mathbb{R}^4$ is defined as $\tilde{\mu} \triangleq \hat{\mu} - \mu$.

The estimates of the activation and fatigue states in (4) and (5) are generated through the following dynamics

$$\dot{\hat{\mu}}_{i_j} = -\hat{w}_{i_j}\hat{\mu}_{i_j} + \hat{w}_{i_j}u_{i_j}(t - \tau_{i_j}), \quad (19)$$

$$\dot{\hat{\phi}}_{k_j} = \frac{1}{\hat{T}_{f_{k_j}}}(\hat{\phi}_{\min_{k_j}} - \hat{\phi}_{k_j})\hat{\mu}_{k_j} + \frac{1}{\hat{T}_{r_{k_j}}}(1 - \hat{\phi}_{k_j})(1 - \hat{\mu}_{k_j}), \quad (20)$$

where $\hat{w}_{i_j}$, $\hat{T}_{f_{k_j}}$, $\hat{T}_{r_{k_j}}$, and $\hat{\phi}_{\min_{k_j}}$ are bounded estimates of the real parameters that can be determined through system identification experiments (Kirsch, 2016; Alibeji et al., 2017). Note that these estimators are governed by first-order differential equations, thus the estimates are bounded as $\hat{\mu} \in [u_{\min}, u_{\max}]$ and $\hat{\phi} \in [\hat{\phi}_{\min}, 1]$.

In (18), the surface error, $S \in \mathbb{R}^4$, is defined as

$$S \triangleq \mu_f - \hat{\mu} - e_I. \quad (21)$$

The delay compensation term, e_I, is added to the surface error, S, to deal with the input delay in the actuator dynamics. The boundary layer error, $y \in \mathbb{R}^4$, for μ is defined as

$$y \triangleq \bar{\mu} - \mu_f. \quad (22)$$

The filtered desired activation μ_f is obtained by passing $\bar{\mu}$ through a low-pass filter such as

$$\zeta_f\dot{\mu}_f + \mu_f = \bar{\mu}; \quad \mu_f(0) = \bar{\mu}(0), \quad (23)$$

where $\zeta_f \in \mathbb{R}^+$ is the low-pass filter time constant.

To felicitate the control design the desired activation, $\bar{\mu}$, is defined as

$$\bar{\mu} = \hat{\phi}^{-1}\left[\zeta_{sf}W\hat{c} + kr\right], \quad (24)$$

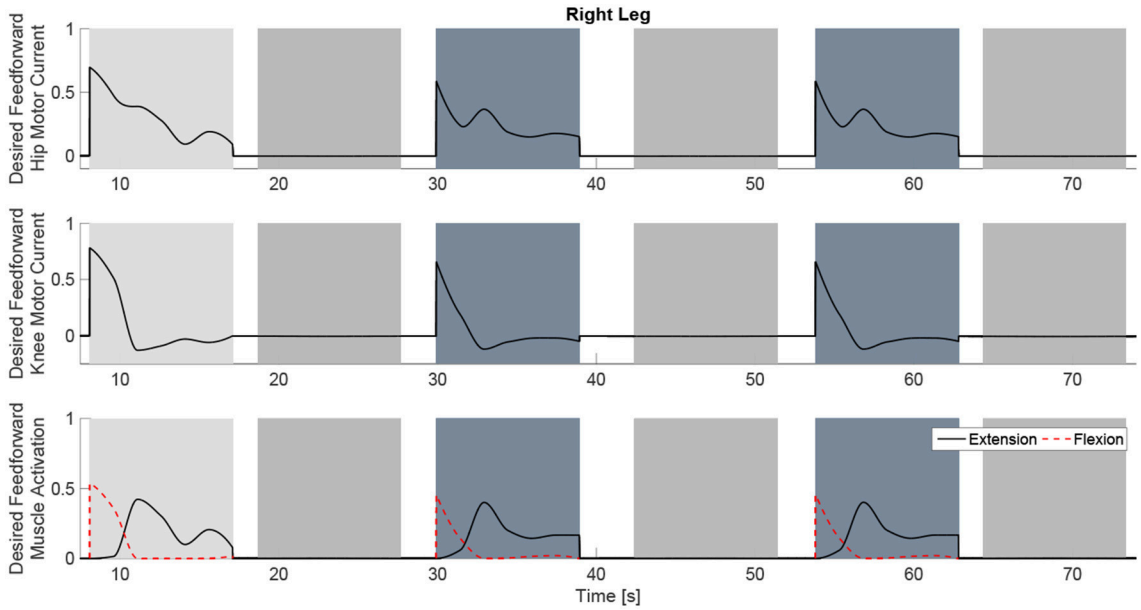

FIGURE 9 | The desired feedforward component of $\bar{\mu}$ for all of the system inputs. This component is generated from the dynamic postural synergies and their activation after adaptation and with the scaling up from the fatigue estimate and the scaling factor control gain.

where $\hat{c} \in \mathbb{R}^2$ is the estimate of c_d, $\zeta_{sf} \in \mathbb{R}^{4\times4}$ is a control gain matrix and $k \in \mathbb{R}^{4\times4}$ is the feedback gain matrix that is chosen to only influence the electric motors.

In $\bar{\mu}$, the feedforward component, $\zeta_{sf} W\hat{c}$, and the feedback component, kr, are scaled by the inverse of the fatigue estimate. This feature is included in the controller so that as a muscle fatigues, the stimulation input to that muscle increases gradually to counteract the effects of the fatigue. The estimate of the synergy activation updates according to the following update law with the projection algorithm (Dixon et al., 2003).

$$\dot{\hat{c}} = \text{proj}\left(\dot{c}_d + FW^T\zeta_{sf}^T b_d^T r\right), \tag{25}$$

where $F \in \mathbb{R}^{2\times2}$ is a symmetric positive definite gain matrix. After using (24), (18) becomes

$$\begin{aligned} M\dot{r} = &- Cr + b_d\phi S + b_d\phi y + \tilde{N} + D + b_d\zeta_{sf} W\tilde{c} \\ &+ b_d(I - \zeta_{sf})Wc_d + \tilde{b}\phi\mu + b_d\phi\tilde{\mu} \\ &+ b_d\tilde{\phi}\hat{\phi}^{-1}\zeta_{sf} W\hat{c} + b_d\tilde{\phi}\hat{\phi}^{-1}kr - b_d kr - e_1, \end{aligned} \tag{26}$$

where I is the identity matrix and $\tilde{c} \in \mathbb{R}^2$ is defined as

$$\tilde{c} = c_d - \hat{c}.$$

Using the Mean Value Theorem, Assumption 4, and the property of projection algorithm the following terms can be bounded as

$$\begin{aligned} &\left\|\tilde{b}\phi\mu\right\| \le \rho_2(\|z\|)\|z\|, \quad \left\|b_d\right\| \le \zeta, \quad \|D\| \le \epsilon_1 \\ &\left\|b_d(I - \zeta_{sf})Wc_d\right\| \le \epsilon_2, \quad \left\|b_d\tilde{\phi}\hat{\phi}^{-1}\zeta_{sf} W\hat{c}\right\| \le \epsilon_3 \end{aligned} \tag{27}$$

where $\rho_2(\|z\|) \in \mathbb{R}$ is a positive monotonically increasing bounded function and $\epsilon_1, \epsilon_2, \epsilon_3, \zeta \in \mathbb{R}^+$ are constants.

The surface error dynamics are derived by taking the time derivative of (21) and using (19), resulting in

$$\dot{S} = \dot{\mu}_f + \hat{w}\hat{\mu} - \hat{w}u_\tau - (u - u_\tau). \tag{28}$$

Based on the subsequent stability analysis, the normalized input u is designed as

$$u = \beta S + \dot{\mu}_f, \tag{29}$$

where $\beta \in \mathbb{R}^+$ is a control gain.

Therefore, the closed-loop surface error dynamics can be written as

$$\dot{S} = -\beta S + \hat{w}\hat{\mu} + (1 - \hat{w})u_\tau. \tag{30}$$

The boundary layer error dynamics are found by taking the time derivative of (22) and using (23), which results in

$$\dot{y} = \eta - \frac{y}{\zeta_f}, \tag{31}$$

where $\eta(e, r, S, y, t)$ is a continuous nonlinear function defined as $\eta = \frac{d}{dt}[\bar{\mu}]$. Based on the definition of u in (29), the control law v is designed as

$$v = \left[\beta S + \frac{\hat{\phi}^{-1}\left[\zeta_{sf} W\hat{c} + kr\right] - \mu_f}{\zeta_f} - u_{min}\right]\frac{\Delta v}{\Delta u} + v_{\min}, \tag{32}$$

where $\Delta v = v_{\max} - v_{\min}$ and $\Delta u = u_{\max} - u_{\min}$. The desired feedback activation, kr, defined in (24) can be expressed

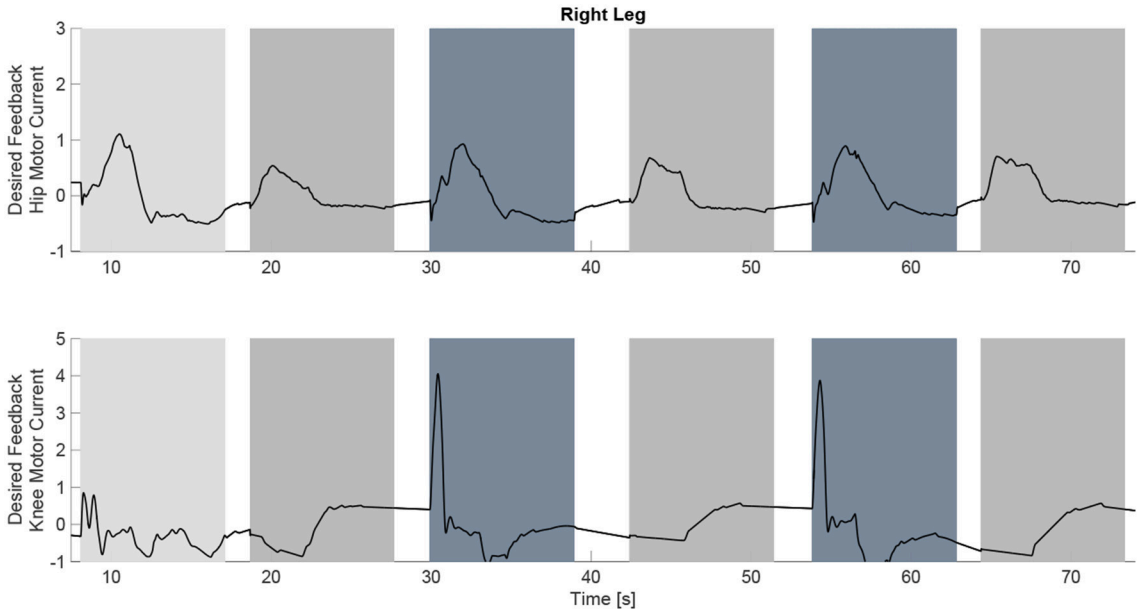

FIGURE 10 | The desired feedback component of $\bar{\mu}$ which is only applied to the four motors at the hip and knee joints of each leg. It can be observed that they majority of the effort is occurring during the swing phase of each leg.

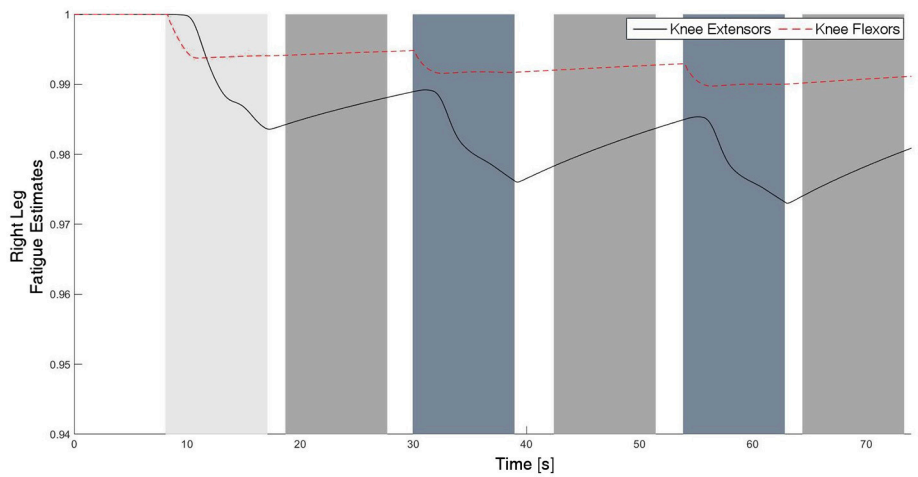

FIGURE 11 | The fatigue estimates for the knee flexors and extensors of the right leg. The fatigue estimate ranges from 1 to ϕ_{min}, which corresponds to no fatigue to fully fatigued, respectively. It can be observed that the fatigue occurs during the swing phase, and the muscles recover during the stance phase since there is no stimulation.

in standard PID form as $K_P e + K_D \dot{e} + K_I \int_0^t e(\theta) d\theta$ where $K_P,\ K_D,\ K_I \in \mathbb{R}^+$ are the proportional, derivative, and integral control gains and are defined as $K_P = k(\alpha_0 + \alpha_1)$, $K_D = k$, and $K_I = k\alpha_0\alpha_1$. The control schematic for the implementation of the overall controller is represented in **Figure 5**.

2.4. Finite State Machine

The hybrid neuroprosthesis used for experimental demonstration uses 4 electric motors; one on each hip joint and knee joint, and 4 stimulation channels; the quadriceps and hamstrings of each leg. The hybrid neuroprosthesis is controlled using two of the adaptive synergy-based PID-DSC controller with delay compensation working in tandem to produce gait, one for each leg. The Finite State Machine, shown in **Figure 6**, is used to determine which trajectories and synergy activations of the gait sequence are used; i.e., either half right step (State 1), full left step (State 2), or full right step (State 3). In between the active states; State 1–3, the standby state (State 0) is activated by default, in which the motors at the joints hold their positions and the synergy activations are set to zero. When a leg is activated

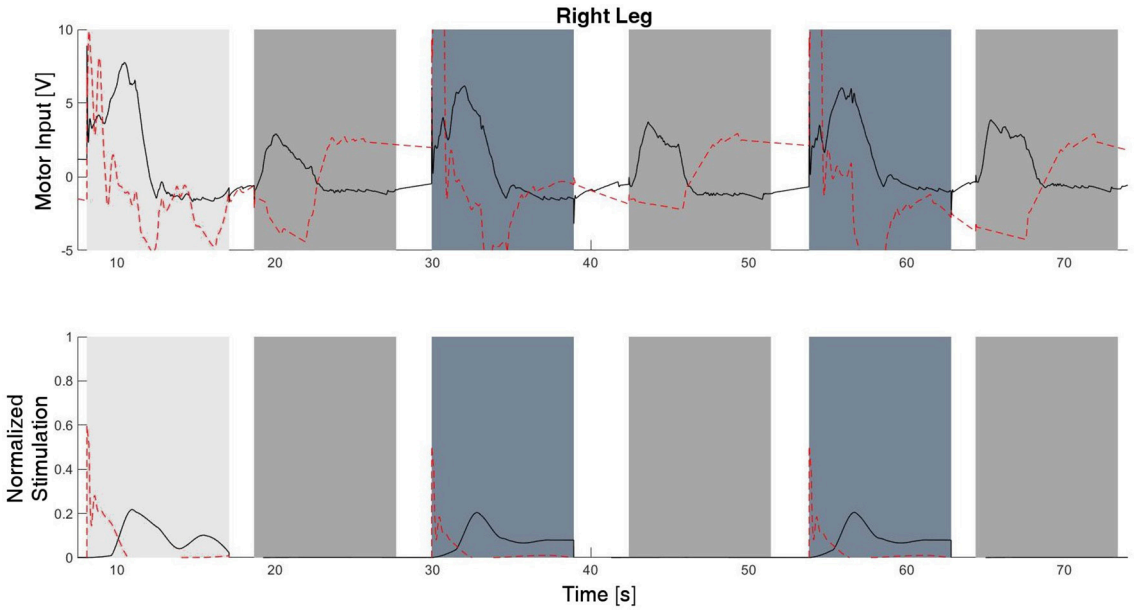

FIGURE 12 | The inputs to all of the system inputs, including feedback and feedforward, for this experimental trial. Note that there is no stimulation occurring during the stance phase of each leg.

in a state, it becomes the swing leg and its counterpart becomes the stance leg. When a leg becomes the stance leg the controller only uses feedback to track the stance hip trajectory and hold the position of the knee joint. The progression of the FSM is determined by the progression button, in which the first time it is pressed State 1 is activated, then each time it is pressed after that the even transitions activate State 2 and the odd transitions activate State 3. In addition to the progression button, there is a safety button which turns off all inputs when pressed.

2.5. Experimental Demonstration

The hybrid neuroprosthesis testbed, shown in **Figure 7**, can be broken down into four primary components: an adjustable orthosis, electric motors, a stimulation unit, and an assistive support device. The orthosis is designed to be adjustable to comfortably fit a wide variety of body types while maintaining the alignment of the joints between the orthosis and subject. Custom motor mount brackets were fabricated to attach the electric motors at the joints of the orthosis. The electric motors (Harmonic Drive LLC, MA, USA) at the hip joints can generate a maximum torque of 50 Nm. The knee electric motor were EC90 brushless motors (Maxon Motor, Switzerland) combined with a Harmonic Gear CSD-25-100-2UH (Harmonic Drive LLC, MA, USA). The knee motor can generate a maximum torque of 56 Nm. A RehaStim 8-channel stimulator (Hasomed Inc., DE) was used to generate the current modulated biphasic pulse trains used to elicit muscle contractions. A set of transcutaneous electrodes was placed on the quadriceps and hamstring muscle groups. The current modulated pulse train with a frequency of 35 Hz and a 400 μs pulse width is typically used for all experiments. An assistive support device, called an E-Pacter (Rifton, USA), is used for the experiments to help the subjects maintain their balance and propel themselves forward. An xPC target (SpeedGoat, CH) was used to interface with the different sensors and motor drivers and implement the controller in real-time at 1 kHz. The control algorithms were coded in Simulink (MathWorks Inc, USA) and used Simulink's (MathWorks Inc, USA) real-time toolbox software running on a Windows machine (Intel Xeon 3.10 GHz processor). The hybrid neuroprosthesis is controlled using a button to control the progression of gait and an emergency stop button to stop all the inputs.

The overall control system was experimentally demonstrated on an able-bodied subject (male; 27 years old, height: 1.80 m, weight: 90 kg) and a person with an incomplete SCI (male; 41 years old, height 1.70 m, weight 70 kg, injury: T10 AIS A). For these experiments it is assumed that the behavior of the right and left leg are similar, therefore, both States 2 and 3 use the same synergies and activations computed in the previous sections. The optimizations to compute the synergies, their activations, and the trajectories they produce were performed using the subject's height and weight, but the model used the muscle parameters reported in Popović et al. (1999) for an able-bodied subject and person with SCI, respectively. If this system is to be implemented on a subject with a condition in which a injury/disorder in which one of his or her leg's response is much different than his or her other leg such as in hemiplegia due to a stroke, it would probably be more beneficial to use multiple subject-specific models, one for each leg.

Prior to any experimentation, an approval from the Institutional Review Board at the University of Pittsburgh was obtained. The consent procedure for human participants was written and informed. During the experiments, the subject was instructed to relax and refrain from voluntarily interfering with the hybrid exoskeleton. The estimates of the EMD, activation time constants, and fatigue/recovery rates were estimated in system identification experiments in a leg extension machine and

TABLE 1 | The root mean squared of the input voltage to the motors.

Subject	Joint	Synergy-based Controller		RISE	
		RMSE [deg.]	RMS V [V]	RMSE [deg.]	RMSV [V]
Incomplete SCI	Right Hip	1.35	2.25	1.68	2.49
	Right Knee	1.68	3.10	3.52	3.36
Able Bodied	Right Hip	1.56	3.22	2.70	3.39
	Right Knee	0.92	2.50	3.03	3.70

Note that the Synergy-based controller uses less motor input which means less power consumption and results in better tracking performance.

assumed to be the same for both legs. During the experiments, the subjects used a gait assistive device called the E-Pacer (Rifton, USA) to help support and propel themselves forward. The progression and safety buttons were operated by a separate user and were used to control the FSM. The experiments were run for 6 steps, including the half right step. In order to compare the difference in power consumption between a powered exoskeleton, just motors, and a hybrid neuroprosthesis, motors and FES, the testbed was tested with two different control systems. For the first control system for the hybrid neuroprosthesis configuration, the adaptive synergy-based PID-DSC controller was used to govern the input to the FES and motors. For the second control system for the powered exoskeleton configuration, a Robust Integral of the Sign of the Error (RISE) (Xian et al., 2004) controller was used to govern the input to the motors. This controller was used for this case because it contains a unique integral signum term which can accommodate for sufficiently smooth bounded disturbances like the friction in the harmonic drive motors used in this testbed.

3. RESULTS

The experimental results from the subject with the incomplete SCI can be seen in **Figures 8–12**. The tracking performance for the both right and left hip and knee joints can be seen in **Figure 8A**. **Figure 8B** shows a sequence of frames from the video footage illustrating the gait produced using the control system[1]. The root mean squared errors (RMSE) and root mean squared voltages (RMSV) for the hip and knee joints for the right leg are presented in **Table 1**. From the results it can be seen that not only did the synergy-based controller result in better tracking performance, but it did so while consuming less energy compared to the RISE controller. In addition, the hybrid neuroprosthesis testbed, when using the synergy-based controller, also includes theraputic health benefits due to the use of FES. The desired feedforward component, $\hat{\phi}^{-1}\zeta_{sf}W\hat{c}$, and desired feedback component, kr, in $\bar{\mu}$ can be seen in **Figures 9**, **10**. The contribution of the inverse of the fatigue estimate scaling factor is not apparent in the experimental results as there is little change in the desired feedfoward activations, as seen in **Figure 9**. This is due to the small changes in the estimate of the fatigue, as seen in **Figure 11**. This is due to the fatigue parameters identified for the subject with an incomplete SCI. Since his injury level is incomplete, his muscles had not atrophied and resistant to fatigue. However, for the subjects with advanced muscle atrophy as a result of their complete SCI, muscle fatigue would occur more rapidly, hence this is still a practical feature in the controller. The actual input signals for all 8 inputs of the system can be seen in **Figure 12**. It can be observed, that when a leg takes the role of the stance leg, the synergy activation is zero which results in zero stimulation and zero desired feedforward motor activation. Hence, only feedback control of the motors is used to lock the knee joint of the stance leg. From the inputs, we can see that the timing of the stimulation is sensible as for each step the flexors is activated first to produce the withdrawal reflex and then the extensors to fully extend the knee.

[1]The video footage of testing of the dynamic postural synergy-based controller on a subject with an incomplete SCI can be seen in the Supplementary Files.

4. DISCUSSION

As researchers, we often analyze biological systems to devise innovative solutions to real world applications. To overcome the challenge of actuator redundancy, we studied how scientists believed the human body solves its high degree of freedom and actuator redundancy problem to achieve fluid and coordinated movements such as gait. It is hypothesized that the human central nervous system (CNS) activates multiple muscle fibers in groups or patterns called muscle synergies, or motor primitives, to efficiently perform complex movements such as reaching, hand manipulations, or posture control (Sherrington, 1910; d'Avella and Tresch, 2001; Ting, 2007; Vinjamuri, 2008; Vinjamuri et al., 2010). The benifit of synergies is their function of transforming a higher dimensional and complex systems into lower dimensional and simpler systems that are easier to control (Tresch and Jarc, 2009). In Neptune et al. (2009), muscle synergies for human locomotion were extracted and successfully applied to complex human walking models to reproduce realistic gait motions. For a more thorough literature review on synergies, readers are referred to these references (Vinjamuri, 2008; Tresch and Jarc, 2009).

In this research, a synergy-based control system is used to distribute the control effort to the multiple actuators of a walking hybrid neuroprosthesis. This approach is inspired from the human motor control concept of muscle synergies. In most studies, muscle synergies are proposed as a basis employed during human motor control and found by decomposing recorded EMG signals (collected from multiple muscles) to extract muscle synergies. Unlike these studies, in this paper dynamic postural synergies are designed, using dynamic optimizations, to be used as a basis for the control system for the walking hybrid neuroprosthesis. This synergy design approach, using optimizations to distribute the control effort among the available actuators, offers multiple advantages and convenience such as allowing for the incorporation of external inputs, i.e., electric motors and FES. Another benefit for this method of designing dynamic postural synergies is the ease of adding

additional restrictions on the synergies, i.e., no co-activation or no negative stimulation. Based on the synergy principle, fewer control signals are used to control multiple actuators in a hybrid neuroprosthesis, therefore the use of synergies will not only solve the actuator redundancy problem similarly to how the body is hypothesized to do so, but it will do it in a more computationally efficient way. However, there are still other remaining challenges that could hamper the effectiveness of a closed-loop synergy-based control system if not addressed. These remaining challenges are EMD, actuator dynamics, and muscle fatigue. Therefore, Lyapunov-based control design approaches were used to derive this class of synergy-based controllers that are robust to EMD and compensate for activation dynamics and muscle fatigue. While the developed control system was capable of reproducing gait, the finite state machine can still be scaled-up to achieve motions other than gait such as sitting/standing and ascending/descending.

5. CONCLUSION

In this paper, the adaptive synergy-based DSC controller is developed and experimentally tested on an able-bodied subject and person with an incomplete SCI using a walking hybrid neuroprosthesis. This control system used dynamic postural synergies designed to reproduce the key dynamic posture; the withdrawal reflex and knee extension, which have been shown to be able to reproduce gait. Dynamic optimizations were then used to compute the optimal synergies' activation to produce a half step and full step. A finite state machine was developed to switch between the trajectories and synergy activations depending on three states; half right step, full right step, and full left step. The control system then used two of the synergy-based DSC controller, one for each leg, working in tandem to reproduce gait. The overall control system was able to recreate gait using the hybrid neuroprosthesis and the gait assistive device.

AUTHOR CONTRIBUTIONS

NA designed the controller, developed dynamic postural synergies, performed experiments, and wrote the paper. VM performed optimizations, BD recruited subjects for the study and supervised and provided advise on conducting experiments with subjects with SCI, and NS designed and conceptualized the control design, study, experiments, and edited the manuscript.

ACKNOWLEDGMENTS

This work was funded in part by the NSF award numbers: 1462876 and 1511139. Any opinions, findings, and conclusions or recommendations expressed in this material are those of the author(s) and do not necessarily reflect the views of the National Science Foundation. Research reported in this article was also supported in part by Eunice Kennedy Shriver National Institute of Child Health and Human Development of the National Institutes of Health under award number: R03HD086529. The content is solely the responsibility of the authors and does not necessarily represent the official views of the National Institutes of Health. NA is with the Department of Biomedical Engineering at Case Western Reserve University, Cleveland, OH, USA. VM and NS, Ph.D. are with the Department of Mechanical Engineering and Materials Science, University of Pittsburgh, Pittsburgh, PA, USA 15261. BD, MD, is with the Department of Physical Medicine and Rehabilitation Science, University of Pittsburgh, Pittsburgh, PA.

SUPPLEMENTARY MATERIAL

The Supplementary Material for this article can be found online at: https://www.frontiersin.org/articles/10.3389/fnins.2018.00159/full#supplementary-material

REFERENCES

Alibeji, N., Kirsch, N., Farrokhi, S., and Sharma, N. (2015a). Further results on predictor-based control of neuromuscular electrical stimulation. *IEEE Trans. Neural Syst. Rehabil. Eng.* 3, 1095–1105. doi: 10.1109/TNSRE.2015.2418735

Alibeji, N. A., Kirsch, N. A., and Sharma, N. (2015b). A muscle synergy-inspired adaptive control scheme for a hybrid walking neuroprosthesis. *Front. Bioeng. Biotechnol.* 3:203. doi: 10.3389/fbioe.2015.00203

Alibeji, N., Kirsch, N., and Sharma, N. (2017). An adaptive low-dimensional control to compensate for actuator redundancy and fes-induced muscle fatigue in a hybrid neuroprosthesis. *Control Eng. Pract.* 59, 204–219. doi: 10.1016/j.conengprac.2016.07.015

Bajd, T., Kralj, A., Turk, R., Benko, H., and Sega, J. (1983). The use of a four-channel electrical stimulator as an ambulatory aid for paraplegic patients. *Phys. Ther.* 63, 1116–1120. doi: 10.1093/ptj/63.7.1116

d'Avella, A., and Tresch, M. C. (2001). "Modularity in the motor system: decomposition of muscle patterns as combinations of time-varying synergies," in *Advances in Neural Information Processing Systems*, Vol. 14, eds T. G. Dietterich, S. Becker, and Z. Ghahramani (Vancouver, BC: MIT Press), 141–148.

del Ama, A. J., Gil-Agudo, A., Pons, J., and Moreno, J. C. (2014). Hybrid FES-robot cooperative control of ambulatory gait rehabilitation exoskeleton. *J. NeuroEng. Rehabil.* 11:27. doi: 10.1186/1743-0003-11-27

del Ama, A. J., Koutsou, A. D., Moreno, J. C., de-los Reyes, A., Gil-Agudo, A., and Pons, J. L. (2012). Review of hybrid exoskeletons to restore gait following spinal cord injury. *J. Rehabil. Res. Dev.* 49, 497–514. doi: 10.1682/JRRD.2011.03.0043

Dixon, W. E., Behal, A., Dawson, D. M., and Nagarkatti, S. (2003). *Nonlinear Control of Engineering Systems: A Lyapunov-Based Approach*. New York, NY: Birkhäuser Boston.

Downey, R. J., Cheng, T. H., Bellman, M. J., and Dixon, W. E. (2015). "Switched tracking control of a human limb during asynchronous neuromuscular electrical stimulation," in *Proceedings of American Control Conference* (Chicago, IL), 4504–4508.

Farris, R. J., Quintero, H. A., and Goldfarb, M. (2011). Preliminary evaluation of a powered lower limb orthosis to aid walking in paraplegic individuals. *IEEE Trans. Neural Syst. Rehabil. Eng.* 19, 652–659. doi: 10.1109/TNSRE.2011.2163083

Farris, R., Quintero, H., Withrow, T., and Goldfarb, M. (2009). "Design and simulation of a joint-coupled orthosis for regulating FES-aided gait," in *IEEE International Conference on Robotics and Automation* (Kobe), 1916–1922.

Goldfarb, M., Korkowski, K., Harrold, B., and Durfee, W. (2003). Preliminary evaluation of a controlled-brake orthosis for FES-aided gait. *IEEE Trans. Neural Syst. Rehabil. Eng.* 11, 241–248. doi: 10.1109/TNSRE.2003.816873

Granat, M. H., Ferguson, A. C., Andrews, B. J., and Delargy, M. (1993). The role of functional electrical stimulation in the rehabilitation of patients with

incomplete spinal cord injury-observed benefits during gait studies. *Spinal Cord* 31, 207–215. doi: 10.1038/sc.1993.39

Ha, K. H., Murray, S., and Goldfarb, M. (2015). An approach for the cooperative control of FES with a powered exoskeleton during level walking for persons with paraplegia. *IEEE Trans. Neural Syst. Rehabil. Eng.* 24, 455–466. doi: 10.1109/TNSRE.2015.2421052

Ha, K. H., Quintero, H. A., Farris, R. J., and Goldfarb, M. (2012). "Enhancing stance phase propulsion during level walking by combining FES with a powered exoskeleton for persons with paraplegia," in *Annual International Conference of the IEEE Engineering in Medicine and Biology Society* (San Diego, CA), 344–347.

Hardin, E., Kobetic, R., Murray, L., Corado-Ahmed, M., Pinault, G., Sakai, J., et al. (2007). Walking after incomplete spinal cord injury using an implanted FES system: a case report. *J. Rehabil. Res. Dev.* 44, 333–346. doi: 10.1682/JRRD.2007.03.0333

Kantrowitz, A. (1960). *Electronic Physiologic Aids. Report of the Maimonides Hospital*, Brooklyn, NY. 4–5.

Kirsch, N. (2016). *Control Methods for Compensation and Inhibition of Muscle Fatigue in Neuroprosthetic Devices*. Doctoral Dissertation, University of Pittsburgh.

Kirsch, N. A., Alibeji, N., Fisher, L., Gregory, C., and Sharma, N. (2014a). "A semi-active hybrid neuroprosthesis for restoring lower limb function in paraplegics," in *IEEE Annual International Conference of the IEEE Engineering in Medicine and Biology Society* (Chicago, IL).

Kirsch, N., Alibeji, N., and Sharma, N. (2014b). "Model predictive control-based dynamic control allocation in a hybrid neuroprosthesis," in *Proceedings of ASME Dynamic Systems and Control Conference* (San Antonio, TX).

Kirsch, N., Alibeji, N. A., and Sharma, N. (2013). "Optimized control of different actuation strategies for FES and orthosis aided gait," in *Proceedings of ASME Dynamic Systems and Control Conference* (Palo Alto, CA).

Kirsch, N., Alibeji, N., and Sharma, N. (2017). Nonlinear model predictive control of functional electrical stimulation. *Control Eng. Pract.* 58, 319–331. doi: 10.1016/j.conengprac.2016.03.005

Kobetic, R., To, C. S., Schnellenberger, J. R., Audu, M. L., Bulea, T. C., Gaudio, R., et al. (2009). Development of hybrid orthosis for standing, walking, and stair climbing after spinal cord injury. *J. Rehabil. Res. Dev.* 46, 447–462. doi: 10.1682/JRRD.2008.07.0087

Kobetic, R., Triolo, R., and Marsolais, E. (1997). Muscle selection and walking performance of multichannel FES systems for ambulation in paraplegia. *IEEE Trans. Rehabil. Eng.* 5, 23–29. doi: 10.1109/86.559346

Kralj, A., and Bajd, T. (1989). *Functional Electrical Stimulation: Standing and Walking after Spinal Cord Injury*. Boca Raton, FL: CRC.

Liberson, W., Holmquest, H., Scot, D., and Dow, M. (1961). Functional electrotherapy: stimulation of the peroneal nerve synchronized with the swing phase of the gait of hemiplegic patients. *Arch. Phys. Med.* 42, 101–105.

Marsolais, E. B., and Kobetic, R. (1987). Functional electrical stimulation for walking in paraplegia. *J. Bone Joint Surg.* 69, 728–733. doi: 10.2106/00004623-198769050-00014

Neptune, R. R., Clark, D. J., and Kautz, S. A. (2009). Modular control of human walking: a simulation study. *J. Biomech.* 42, 1282–1287. doi: 10.1016/j.jbiomech.2009.03.009

Neuhaus, P. D., Noorden, J. H., Craig, T. J., Torres, T., Kirschbaum, J., and Pratt, J. E. (2011). "Design and evaluation of mina: a robotic orthosis for paraplegics," in *IEEE International Conference on Rehabilitation Robotics* (Zurich), 1–8.

Peckham, P. H., and Gray, D. B. (1996). Functional neuromuscular stimulation. *J. Rehabil. Res. Dev.* 33, 9–11. doi: 10.1109/86.750554

Popović, D., Stein, R., Oğuztöreli, M., Lebiedowska, M., and Jonić, S. (1999). Optimal control of walking with functional electrical stimulation: a computer simulation study. *IEEE Trans. Rehabil. Eng.* 7, 69–79.

Quintero, H. A., Farris, R. J., Ha, K., and Goldfarb, M. (2012). Preliminary assessment of the efficacy of supplementing knee extension capability in a lower limb exoskeleton with FES. *IEEE Eng. Med. Biol. Soc.* 2012, 3360–3363. doi: 10.1109/EMBC.2012.6346685

Riener, R., Quintern, J., and Schmidt, G. (1996). Biomechanical model of the human knee evaluated by neuromuscular stimulation. *J. Biomech.* 29, 1157–1167. doi: 10.1016/0021-9290(96)00012-7

Schauer, T., Negard, N. O., Previdi, F., Hunt, K. J., Fraser, M. H., Ferchland, E., et al. (2005). Online identification and nonlinear control of the electrically stimulated quadriceps muscle. *Control Eng. Pract.* 13, 1207–1219. doi: 10.1016/j.conengprac.2004.10.006

Sharma, N., Bhasin, S., Wang, Q., and Dixon, W. E. (2011). Predictor-based control for an uncertain euler-lagrange system with input delay. *Automatica* 47, 2332–2342. doi: 10.1016/j.automatica.2011.03.016

Sharma, N., Mushahwar, V., and Stein, R. (2014). Dynamic optimization of fes and orthosis-based walking using simple models. *IEEE Trans. Neural Syst. Rehabil. Eng.* 22, 114–126. doi: 10.1109/TNSRE.2013.2280520

Sherrington, C. S. (1910). Flexion-reflex of the limb, crossed extension-reflex, and reflex stepping and standing. *J. Physiol.* 40, 28–121. doi: 10.1113/jphysiol.1910.sp001362

Solomonow, M., Baratta, R., Shoji, H., Ichie, M., Hwang, S., Rightor, N., et al. (1988). "FES powered locomotion of paraplegics fitted with the LSU reciprocating gait orthoses (RGO)," in *Proceedings of the Annual International Conference of the IEEE Engineering in Medicine and Biology Society* (New Orleans, LA), Vol. 4, 1672.

Strausser, K., and Kazerooni, H. (2011). "The development and testing of a human machine interface for a mobile medical exoskeleton," in *Proceedings of the IEEE/RSJ International Conference on Intelligent Robots and Systems* (San Francisco, CA), 4911–4916.

Ting, L. H. (2007). Dimensional reduction in sensorimotor systems: a framework for understanding muscle coordination of posture. *Prog. Brain. Res.* 165, 299–321. doi: 10.1016/S0079-6123(06)65019-X

Tresch, M. C., and Jarc, A. (2009). The case for and against muscle synergies. *Curr. Opin. Neurobiol.* 19, 601–607. doi: 10.1016/j.conb.2009.09.002

Vinjamuri, R., Sun, M., Chang, C.-C., Lee, H.-N., Sclabassi, R. J., and Mao, Z.-H. (2010). *Dimensionality Reduction in Control and Coordination of the Human Hand,* PhD thesis. University of Pittsburgh.

Vinjamuri, R. K. (2008). *Dimensionality Reduction in Control and Coordination of the Human Hand*, PhD thesis, Swanson School of Engineering, University of Pittsburgh.

Xian, B., Dawson, D. M., de Queiroz, M. S., and Chen, J. (2004). A continuous asymptotic tracking control strategy for uncertain nonlinear systems. *IEEE Trans. Autom. Control* 49, 1206–1211. doi: 10.1109/TAC.2004.831148

Conflict of Interest Statement: The authors declare that the research was conducted in the absence of any commercial or financial relationships that could be construed as a potential conflict of interest.

frontiers in Neuroscience

ORIGINAL RESEARCH
published: 25 April 2018
doi: 10.3389/fnins.2018.00276

Lateral Symmetry of Synergies in Lower Limb Muscles of Acute Post-stroke Patients After Robotic Intervention

Chun Kwang Tan[1], Hideki Kadone[2], Hiroki Watanabe[3], Aiki Marushima[3], Masashi Yamazaki[4], Yoshiyuki Sankai[5,6] and Kenji Suzuki[1,5,6]*

[1] Artificial Intelligence Laboratory, University of Tsukuba, Tsukuba, Japan, [2] Center for Innovative Medicine and Engineering, University of Tsukuba Hospital, Tsukuba, Japan, [3] Department of Neurosurgery, Faculty of Medicine, University of Tsukuba, Tsukuba, Japan, [4] Department of Orthopaedic Surgery, Faculty of Medicine, University of Tsukuba, Tsukuba, Japan, [5] Center for Cybernics Research, University of Tsukuba, Tsukuba, Japan, [6] Faculty of Engineering, University of Tsukuba, Tsukuba, Japan

Gait disturbance is commonly associated with stroke, which is a serious neurological disease. With current technology, various exoskeletons have been developed to provide therapy, leading to many studies evaluating the use of such exoskeletons as an intervention tool. Although these studies report improvements in patients who had undergone robotic intervention, they are usually reported with clinical assessment, which are unable to characterize how muscle activations change in patients after robotic intervention. We believe that muscle activations can provide an objective view on gait performance of patients. To quantify improvement of lateral symmetry before and after robotic intervention, muscle synergy analysis with Non-Negative Matrix Factorization was used to evaluate patients' EMG data. Eight stroke patients in their acute phase were evaluated before and after a course of robotic intervention with the Hybrid Assistive Limb (HAL), lasting over 3 weeks. We found a significant increase in similarity between lateral synergies of patients after robotic intervention. This is associated with significant improvements in gait measures like walking speed, step cadence, stance duration percentage of gait cycle. Clinical assessments [Functional Independence Measure-Locomotion (FIM-Locomotion), FIM-Motor (General), and Fugl-Meyer Assessment-Lower Extremity (FMA-LE)] showed significant improvements as well. Our study shows that muscle synergy analysis can be a good tool to quantify the change in neuromuscular coordination of lateral symmetry during walking in stroke patients.

Keywords: muscle synergies, gait symmetry, stroke rehabilitation, robotic intervention, hybrid assistive limb

OPEN ACCESS

Edited by:
Yury Ivanenko, Fondazione Santa Lucia (IRCCS), Italy

Reviewed by:
Tetsuro Funato, University of Electro-Communications, Japan
Germana Cappellini, Università degli Studi di Roma Tor Vergata, Italy

****Correspondence:***
Chun Kwang Tan
chunkwang@ai.iit.tsukuba.ac.jp

Specialty section:
This article was submitted to Neuroprosthetics, a section of the journal Frontiers in Neuroscience

Received: *31 December 2017*
Accepted: *09 April 2018*
Published: *25 April 2018*

Citation:
Tan CK, Kadone H, Watanabe H, Marushima A, Yamazaki M, Sankai Y and Suzuki K (2018) Lateral Symmetry of Synergies in Lower Limb Muscles of Acute Post-stroke Patients After Robotic Intervention. Front. Neurosci. 12:276. doi: 10.3389/fnins.2018.00276

1. INTRODUCTION

Stroke is a serious neurological disease commonly associated with gait disturbance (Verma et al., 2012; Esquenazi et al., 2017). This points to a need for asssitive devices that can help in patients' therapy process and personal mobility. In reviews done by Díaz et al. (2011) and Esquenazi et al. (2017), there appears to be an increasing trend in the use of exoskeletons for therapy. This has led

to the development of several commercially available exoskeletons for therapy. Some examples of these exoskeletons are the Hybrid Assistive Limb (HAL) (Hayashi et al., 2005), ReWalk (Zeilig et al., 2012), Lokomat (Jezernik et al., 2003), and Lopes (Veneman et al., 2007).

Although improvements to stroke patients' gait can be clinically verified after robotic intervention, the effects of such interventions from the viewpoint of muscle activations are not well studied. Typically, studies involving the use of exoskeletons focus on clinical metrics describing the performance of patients before and after a course of therapy (Aach et al., 2014; Watanabe et al., 2014). Louie and Eng (2016) did a review on various studies that looked into the effects of exoskeletons on therapy and listed methods and results from them. It was also noted that all of the studies listed in their review used mainly only clinical measures to evaluate improvement in patients. Díaz et al. (2011) also concluded that there is a need to develop standardized protocols to obtain reliable assessment data, as clinical measures are currently not sufficient and require many clinical trials in order to be widely accepted and implemented. Although clinical measures are a good indication of the general wellbeing of patients, they are unable to reflect changes in the way muscles are coordinated in a task. We believe having knowledge in how muscle synergies change after therapy would help determine accurately if the patient has regained their mobility.

One measure where clinical measures do not quantify well is gait symmetry. However, such a measure is turning out to be an important measure to evaluate post stroke patients. Verma et al. (2012) did an extensive review on characterization of such asymmetries and found that asymmetries arise on the unaffected side due to compensation and adaptation. They also found that such asymmetries lead to inefficient energy expenditure, falls, abnormal joint loading, joint pain, deformity and pain. Since gait asymmetry is such a serious issue, having tools like muscle synergy analysis (MSA) would allow us to assess patient gait performance accurately, and thus, customize treatments. Further support for measuring gait asymmetries come from Patterson et al. (2010), who analyzed patient gait data up to a mean of 82 months, post stroke. They found that spatial and temporal gait symmetry parameters (stance time, swing time, step length symmetry), actually show a worsening of gait in those patients, whereas parameters like velocity, neurological deficit and lower extremity motor impairment did not reveal any significant worsening of gait. They conclude that gait asymmetry should be given more attention both in clinical situation and research.

Previous studies have proposed that co-activation of muscles, also known as muscle synergies or motor modules, are sufficient to describe various postural or locomotion tasks in humans (Ivanenko et al., 2007; Torres-Oviedo and Ting, 2007). These synergies can be considered strategies that the human body employs to facilitate control of limbs in various tasks. Such a method, known as muscle synergy analysis (MSA), has recently seen interest in the stroke therapy. Studies by Clark et al. (2010), Barroso et al. (2017), and Gizzi et al. (2011) used MSA to assess gait performance of stroke patients. One related work by Routson et al. (2013) employed MSA to quantify walking performance of stroke patients before and after therapy. These studies highlight the importance of having such measures, in addition to clinical measures, in order to predict stroke patient performance and to customize therapies.

In our study, we investigate muscle activation changes with MSA in stroke patients who underwent a course of robotic therapy using the HAL Lower Limb exoskeleton (Hayashi et al., 2005). Muscle synergies are extracted with Non-Negative Matrix Factorization (NNMF) (Gelsy Torres-Oviedo and Ting, 2006) and compared to evaluate changes in muscle activation of stroke patients before and after robotic therapy. This study aims to quantify gait symmetry of post stroke patients with lateral symmetry of muscle synergies on both sides of the body, when they are walking.

2. METHODS

This study was carried out in accordance with the recommendations of the University Guidelines for Clinical Trials, Institutional Review Board of University of Tsukuba Hospital, with written informed consent from all subjects. All subjects gave written informed consent in accordance with the Declaration of Helsinki. The protocol was approved by the Institutional Review Board of University of Tsukuba Hospital. The University Guidelines for Clinical Trials conforms to the ethical principles of the Declaration of Helsinki.

2.1. Participants

Eight post stroke patients in their acute phase after onset participated in the study (**Table 1**). Among the eight participants, there were four females and four males, aged between 43 and 80 (average: 59.3 $\pm$ 12.2) yrs. Four of them had hemiparesis on the left side, and the other four on the right side. Medical diagnosis included Atherothrombotic Cerebral Infarction (ACI), Subcortical Hemorrhage (SH), Brain Stem Infarction (BSI), Lacunar Infarct (LI) and Atherothrombotic Brain Stem Infarction (ABSI). Clinical evaluation of their Functional Ambulation Category (FAC) before starting the robotic intervention ranged from 1 (ambulation under substantial

TABLE 1 | Participants characteristics.

ID	Age (years)	Gender	Diagnosis	Affected side	FAC before HAL	Onset-HAL duration (days)
S1	67	F	ACI	L	1	10
S2	52	F	SH	R	2	17
S3	71	F	BSI	L	1	11
S4	55	M	LI	L	2	10
S5	55	F	ABSI	L	3	16
S6	43	M	LI	R	2	11
S7	51	F	ACI	R	2	18
S8	80	M	ACI	R	2	16

Diagnosis was Atherothrombotic Cerebral Infarction (ACI), Subcortical Hemorrhage (SH), Brain Stem Infarction (BSI), Lacunar Infarct (LI) or Atherothrombotic Brain Stem Infarction (ABSI).

physical assistance) to 3 (independent ambulation under observation). These patients were included in the study 10–18 (average: 13.6 ± 3.4) days after onset.

2.2. Robotic Intervention

Since all participants were hemiparetic, single leg version of Robot Suit HAL was used. The robot was composed of three rigid structures corresponding to lumbar, thigh and shank, and shoe, of the paretic side, weighing 9 kg in total. These parts were serially connected by joints allowing relative sagittal motion, realizing joint motion of hip, knee and ankle in the sagittal plane. Electric motors were embedded at the hip and knee joints, and controlled according to the bioelectric signals detected by surface electrodes attached on the skin surface of the relevant muscles. In equation, the hip and knee motors were controlled in real time to provide assistive joint torque as $T_{hip} = G_{hip,\,flex} * A_{hip,\,flex} - G_{hip,\,ext} * A_{hip,\,ext}$ and $T_{knee} = G_{knee,\,flex} * A_{knee,\,flex} - G_{knee,ext} * A_{knee,\,ext}$, where $A_{hip,\,flex}$, $A_{hip,\,ext}$, $A_{knee,\,flex}$ and $A_{knee,\,ext}$ are respectively filtered activation of Illiopsoas (hip flexor), Gluteus maximus (hip extensor), Hamstrings (knee flexor) and Vastus Lateralis (knee extensor) muscles. $G_{hip,\,flex}$, $G_{hip,\,ext}$, $G_{knee,\,flex}$, and $G_{knee,\,ext}$ are gain parameters adjusted according to wearer's comfort through the sessions.

Robotic intervention was started within the participants' acute period (**Table 1**). Intervention sessions were performed three times per week for 3 weeks, and therefore nine times in total, for each patient. An intervention session lasted approximately 60 min, including clinical examination, attaching the robot, 20 min of walking training using the robot including rest when necessary, and detaching the robot. During walking training, the patient walked repetitively in a 25 m course composed of two straight lines and two semicircles, on a flat surface. For safety reasons, a walking device (All-in-One Walking Trainer, Ropox A/S, Naestved, Denmark) with a harness was used to prevent falls, and heart rate and oxygen saturation were monitored time to time.

2.3. Data Measurement

Gait of the patients was measured during straight walking at a self-selected speed without wearing HAL, 1–3 days before the first HAL session (pre HAL) and after the last HAL session (post HAL). Lower limb muscle activity and foot motion were recorded using a measurement system. All-In-One Walking Trainer (Ropox A/S, Denmark), with a harness, was used during the walking test to prevent falls. The harness was adjusted so that it did not provide any weight support. The patients walked for 6 m several times (Lam et al., 2010), until three consecutive steady steps were obtained. Data that did not fit the criteria of three consecutive steady steps were discarded. Also, the initiation and termination of walking during each 6 meters walking trial were discarded as well.

2.3.1. Electromyography

Skin preparation included wiping down the muscle bellies with alcohol swabs. Twelve wireless, surface EMG electrodes were placed bilaterally over the muscle bellies of: Vastus Medialis (VM), Hamstrings (HAM), Tibialis Anterior (TA), Gastrocnemius (GAS), Adductor Longus (ADD), Gluteus Maximus (Gmax), using a TrignoTM Lab Wireless electromyography (EMG) system (Delsys Inc., Boston, MA, USA). EMG data was sampled at 2,000 Hz.

2.3.2. Motion Capture System

Motion tracking of subjects was achieved with a motion capture system (VICON MX System with 16 T20S Cameras, Vicon, Oxford, UK), in synchronization with EMG and sampled at 100 Hz. Sixteen autoreflective markers were placed bilaterally on the anterior superior iliac spine, posterior superior iliac spine, lower lateral 1/3 surface of the thigh, flexion-extension axis of the knee, lower lateral 1/3 surface of shank, lateral malleolus for the ankle, posterior peak of the calcaneus for the heel and the lateral second metatarsal bone of the toe. These marker positions were used for gait phase detection during locomotion.

2.4. Data Analysis

2.4.1. Preprocessing

From the synchronized tracks of EMG and motion data, three consecutive steady steps starting from a heel strike and ending with a succeeding heel strike were extracted in the middle of 6 m walking for each leg (Right and Left), pre and post HAL, for each of the participants. EMG data was first band-passed with a 4th order, zero-lag Butterworth band-pass filter at 30–400 Hz. The bandpassed EMG was then filtered with a Hampel filter, with the parameters, time window, $\text{win} = 200$ and a threshold of $\sigma = 4$ (standard deviations), to remove artifacts. Finally, EMG data was fully rectified and low-passed with a 4th order, zero-lag Butterworth low-pass filter at 6 Hz to obtain the EMG envelope. The EMG envelope is then time-normalized and resampled to 100 times points.

2.4.2. Extraction of EMG Based on Kinematic Data

We segmented the EMG data into windows based on the phases of walking (Stance, Swing, Cycle). Stance is defined as the period starting from a heel strike and ending with toe off. Swing is defined as the period between starting from the toe off to heel strike. The Cycle is defined as starting from a heel strike and ending at the next heel strike.

Segmented data is further divided into sides (Affected and Unaffected). Each muscle vector in each segment was divided by its own standard deviation in that particular segment (e.g., Cycle muscle vectors are divided with the standard deviation of muscle vectors in the Cycle segment). This is based on the "UnitPer" definition (standard deviation per trial) of Banks et al. (2017), who evaluated the effect of different EMG normalization methods with NNMF MSA. This provides a consistent effect size for varying muscle synergies and timing coefficients.

Data segments from 3 consecutive walking cycles were separated and concatenated, based on their phase in the gait cycle and side of the patient, thus obtaining 6 matrices in total (Affected_Stance, Affected_Swing, Affected_Cycle, Unaffected_Stance, Unaffected_Swing, Unaffected_Cycle). Oliveira et al. (2014) noted that for intra-subject comparisons, muscle synergies extracted from concatenated signals yielded higher reconstruction quality, as compared to muscle synergies

from averaged signals. This processing method was adopted as we would like extracted synergies to be representative of the subject's muscle activations. Also, we think averaging the EMG signals would mask step-to-step variability of muscle activations in hemeparetic patients.

2.4.3. Muscle Synergy Extraction With NNMF

NNMF was then used to extract muscle synergies from the concatenated EMG data. This was performed with Matlab's NNMF function, using the multiplicative update algorithm. Parameters for the tolerance for the residual (TolFun) was given as $1e-6$ and the tolerance for the relative change in elements (TolX) was given as $1e-4$. The algorithm was repeated 50 times and results with the lowest root mean square residual were taken to be the best. Synergies were allowed to vary per condition.

The choice of number of synergies were determined with the criteria of when the variance-accounted-for (VAF_{total}) between the reconstructed and original EMG envelope was above 90% and subsequent increase of the number of synergies did not give more than a 5% increase in VAF. We also imposed a local criteria where the reconstruction VAF (VAF_{muscle}) for each muscle vector was above 75% (Torres-Oviedo and Ting, 2007). The VAF is defined as 100 ∗ (uncentered Pearson correlation coefficient), which requires the total sum of squares to be taken with respect to zero (Gelsy Torres-Oviedo and Ting, 2006). This is given as:

$$VAF = 100 \cdot \left(\frac{(\sum_{j=1}^{m} \sum_{i=1}^{n} X_{nm} \cdot Y_{nm})^2}{(\sum_{j=1}^{m} \sum_{i=1}^{n} X_{nm}^2) \cdot (\sum_{j=1}^{m} \sum_{i=1}^{n} Y_{nm}^2)} \right) \quad (1)$$

where n is the number of datapoints for each channel, and m is the number of channels. X_{nm} and Y_{nm} are the matrices containing the reconstructed and original signal respectively. VAF calculation code is adapted from the "rsqr_uncentered" function in the file "PosturalData_NMFvsPCA_GUI_July2013" given in Neuromechanics Lab (2016).

The mean muscle VAF was calculated for each extracted muscle synergy vector ($\frac{1}{n} \sum_{i=1}^{n} \mathrm{VAF}_{muscle}^{i}$, where i = number of synergies and n = number of muscle channels), and were used as a basis in the sorting of muscle synergy vectors. Synergy vectors were sorted according to the mean muscle VAF in descending order (i.e., a synergy with highest mean reconstruction muscle VAF, as compared to other synergies, were placed as the first synergy).

2.4.4. Synergy Analysis

Lateral synergy symmetry was determined by comparing the sorted synergies (described in section 2.4.3) from the affected side and unaffected side with the general Pearson correlation coefficient (r). Muscle synergy matrices were compared with the corresponding synergy matrix for the other side of the body (e.g., $\mathrm{Synergy}_{affected}$ with $\mathrm{Synergy}_{unaffected}$ and so on). Such comparisons were performed for muscle synergies extracted from the concatenated EMG data (section 2.4.2) during different phases of gait. Note that only muscle synergies that belong to the same gait phase were compared (e.g., muscle synergies from the full cycle phase, on the affected side of the body, were compared only with the muscle synergies from the full cycle phase, on the unaffected side of the body). The motivation for this comparison is to provide a single value measure for similarity.

Synergy vector comparison with the scalar dot product (Cheung et al., 2012) was also performed to evaluate the changes in contents of the muscle synergy vectors. Muscle synergy matching was also performed to discover the presence of similar muscle synergy vectors on both sides of the body. Muscle synergies with the highest scalar dot product score are selected, matched and removed from the pool of muscle synergies. This process continues until no more muscle synergies are left to match.

2.4.5. Software

Data extraction was done using scripts on MATLAB 8.4 (Mathworks, Natick, MA, USA). NNMF and the rest of the processing were performed with scripts on MATLAB 9.3 (Mathworks, Natick, MA, USA).

2.5. Clinical Assessments

Physical therapists also evaluated the patients before and after the course of therapy. The below measures were used to evaluate patient motor functions:

1. Functional Independence Measure-Locomotion (FIM-Locomotion)
2. Functional Independence Measure-Motor (General) [FIM-Motor (General)]
3. Fugl-Meyer Assessment, Lower Extremity (FMA-LE)

For the kinematics, we measured the walking speed, step cadence, absolute lateral difference of step length and the percentage of stance in relation to gait cycle. The absolute lateral difference of step length was derived from the step length variable. The absolute difference in step length between both sides of the body was calculated to account for the differences in compensatory walking strategies employed by the patients. Step length does not take into consideration the compensatory gait patterns hemiparetic patients exhibit. For example, some patients start their swing phase with their affected leg and bring their unaffected leg to their center for stabilization (Verma et al., 2012). This causes the affected step length to be longer than the unaffected side. Similarly, patients who drag their affected leg during walking would have a longer step length on their unaffected side.

2.6. Statistical Analysis

Normality of the data were tested with the Shapiro-Wilk test, with the significance level set to 5%. Statistical comparison performed with the T-test (for normally distributed data) and the Mann-Whitney U-test (for non-normal distribution). For each paired dataset, both pairs would have to fulfill the criteria of the Shapiro-Wilk test before the T-test was applied. Otherwise, the U-Test was used instead. Significance was considered in comparisons with $p < 0.05$.

3. RESULTS

3.1. Clinical Assessments

Significant improvement in the kinematic measurements of the patients was observed (**Figure 1**). Statistically significant increase was observed in walking speed [Pre : 14.36 ± 12, Post : 31.47 ± 12.11 m/min, ($p < 0.05$)] and step cadence [Pre : 22.95 ± 9.04, Post : 35.32 ± 8.45 steps/min, ($p < 0.05$)], together with a decrease in the percentage of stance duration, in relation to the whole gait cycle [Pre Affected : 72.17 ± 6.12, Post Affected : 64.04 ± 4.51 %, ($p < 0.05$)] [Pre Unaffected : 80.89 ± 7.63, Post Unaffected : 70.76 ± 4.96 %, ($p < 0.05$)]. There was no significant improvement in absolute lateral difference of step length. [Pre : 0.0783 ± 0.0473, Post : 0.0575 ± 0.0153 m, ($p > 0.05$)]. Only the range of movement for the affected hip show significant improvement [Pre Affected Hip : 30.33 ± 10.15, Post Affected Hip : 39.63 ± 6.98 degrees ($p < 0.05$)].

The FIM-Locomotion score, FIM-Motor (General) score, FMA-LE scores improved after robotic intervention (**Table 2**). Only 1 patient (S7) did not show an improvement in FIM-Locomotion scores, however, the other measures (FIM-Motor(General) and FMA-LE) indicated improvement.

3.2. Number of Muscle Synergies in Patients

The figure below (**Figure 2**) details the mean overall reconstruction VAF and mean reconstruction VAF for each muscle vector (**Figure 3**) according to the number of muscle synergies for all subjects. Error bars denote the standard deviation.

The table below (**Table 3**) details the change in the number of muscle synergies per subject in different conditions. The number of synergies selected for each subject is based on both the overall reconstruction VAF ($VAF_{total} > 90\%$) and local reconstruction VAF ($VAF_{muscle} > 75\%$) (Torres-Oviedo and Ting, 2007) for each subject. We found that 3 subjects required an increase of the number of muscle synergies by 1, No change for 3 subjects, and 1 subject required a decrease in the number of muscle synergies for their affected side. The exception to this case is S3, reduced the number of muscle synergies by 1 after therapy. We also found changes in the unaffected side of patients, with S2, S3, and S4

TABLE 2 | Clinical Measures Pre-Post robotic intervention.

	FIM-Locomotion (Pre)	FIM-Locomotion (Post)	FIM-Motor (General) (Pre)	FIM-Motor (General) (Post)	FMA-LE (Pre)	FMA-LE (Post)
S1	1	**3**	46	**73**	13	**18**
S2	1	**5**	40	**82**	19	**26**
S3	1	**2**	40	**55**	18	**28**
S4	2	**7**	52	**77**	26	**29**
S5	2	**7**	78	**90**	20	**27**
S6	1	**6**	66	**83**	21	**25**
S7	1	1	53	**62**	14	**22**
S8	1	**5**	50	**65**	17	**20**

Numbers in bold denote improvement in scores.

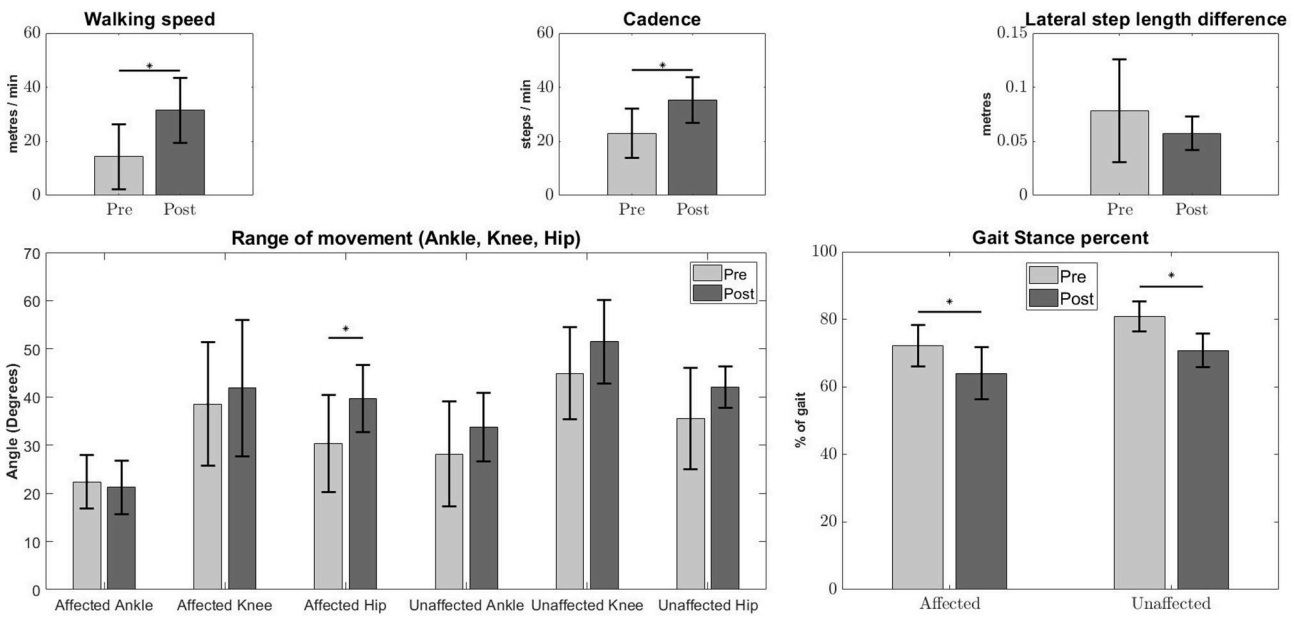

FIGURE 1 | Kinematic measures Pre-Post conditions. Error bars denote the standard deviation. Improvements were observed in walking speed **(Top Left)**, step cadence **(Top Middle)**, stance duration percentage of affected and unaffected side **(Bottom Right)**, and Pre-Post affected hip angles **(Bottom Left)**. The Lateral step length difference **(Top Right)** and other joint angles **(Bottom Left)** do not show any significant differences. The asterisks indicate statistical significance.

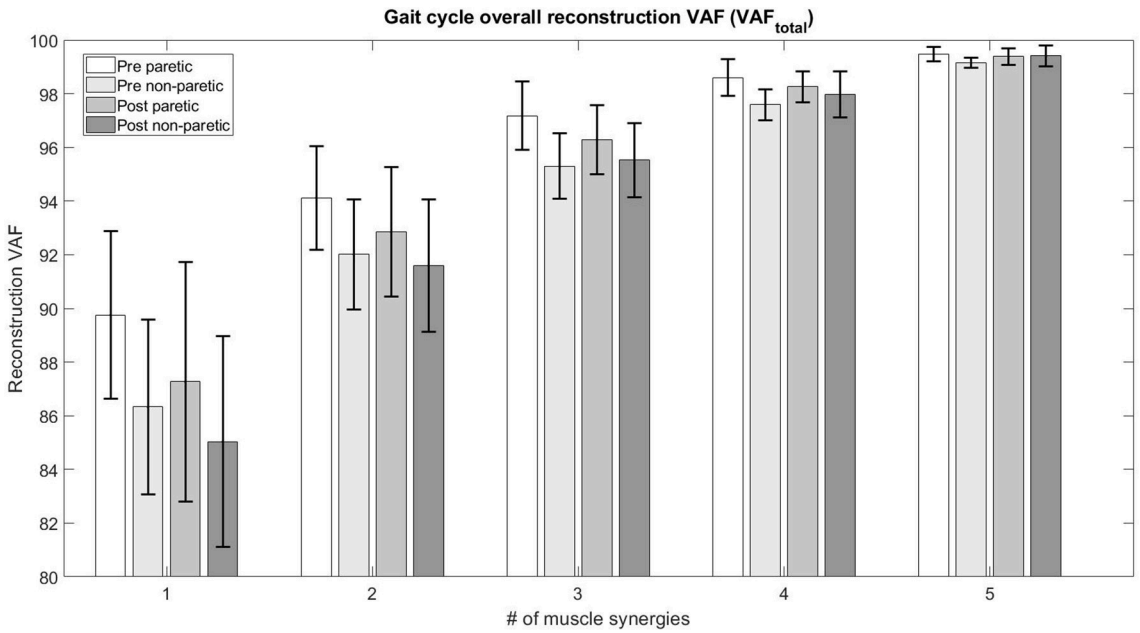

FIGURE 2 | Total variability accounted for (VAF_{total}) based on the number of muscle synergies.

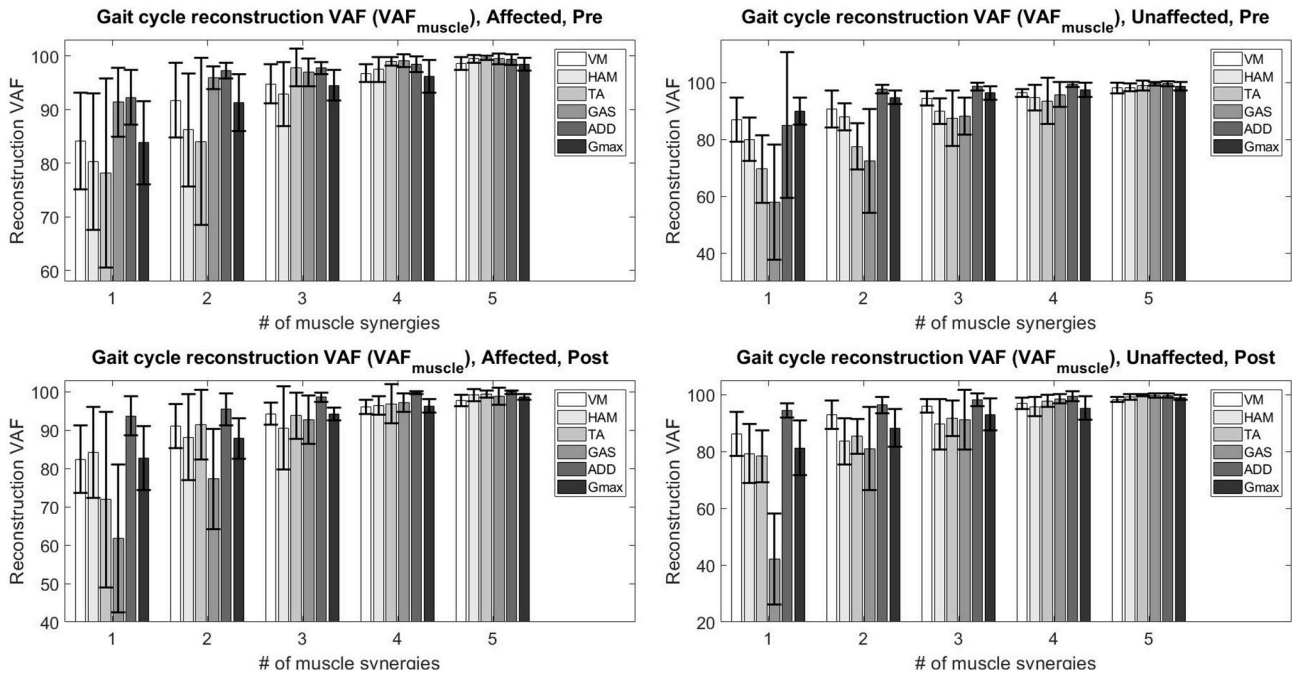

FIGURE 3 | Total variability accounted for (VAF_{muscle}) based on the number of muscle synergies and condition.

showing a decrease in muscle synergies. The exception to this case were S5 and S6, who had an increase in the number of muscle synergies in the unaffected side.

To determine the number of synergies for comparison between sides per subject, we selected the maximum number of synergy for both the affected and unaffected side in the comparison condition (e.g., In **Table 3**, the number of synergy for S2 is determined to be 3 for Side Similarity in the pre-intervention condition, and 2 for the post-intervention condition. However, for the same subject, the number of synergies for Pre-Post Similarity comparisons would be 3 for the unaffected side).

3.3. Muscle Synergies, EMG Waveforms and Kinematics

S2 was picked as the representative subject for reporting as this subject displays the greatest improvement in FIM (General) scores and reasonably good improvement in both FIM locomotion and FMA lower limb scores. **Figures 4, 5** shows the muscle synergy vectors, timing coefficients, original EMG envelopes and reconstructed EMGs, for the affected side of S2, during the pre-intervention and post-intervention conditions respectively. Raw EMG waveforms and joint angles for S2 in the pre-intervention and post-intervention conditions (**Figures 6**, **7**, respectively) were presented.

Overall reconstruction VAF for S2 is high (>90%) for both conditions, although certain abnormal looking EMG envelopes can be seen. To explain them, the raw EMG waveforms, and their corresponding joint angles, for both pre and post intervention conditions, are examined (**Figures 6, 7**). Due to ethical reasons, we are unable to provide the raw EMG values, hence the vertical axes of EMG plots remain unlabeled. In the Pre-intervention condition (**Figure 6**, Affected side), subject's VM and GAS muscles are active for most of the gait cycle (**Stance percent**: 80.56 ± 7.24). This can be observed in the slow rate of increase in the knee angles. ADD muscles are also highly active in the pre-intervention condition, so as to provide stability for the hip joint, where hip angles hover around values between 10 and 20° for most of the stance phase. In the post-intervention condition (**Figure 7**, Affected Side), the subject has an overly active TA post rehabilitation, contributing to abnormal dorsal flexion of the ankle throughout the gait cycle. We observed the VM muscles are active longer than usual in the stance phase. The timing of the GAS muscles were later, as compared to the unaffected side. The HAM muscles appear to be weaker than the unaffected side, where short activations were noted. The knee angle trajectory shows a slight parabolic curve on the Affected knee, as opposed to a relatively straight trajectory on the Unaffected knee.

TABLE 3 | Number of muscle synergies required pre and post robotic intervention for affected and unaffected sides.

	Affected Pre	Post	Change	Unaffected Pre	Post	Change
S1	1	**2**	+1	2	2	0
S2	2	2	0	3	**2**	−1
S3	3	**2**	−1	4	**2**	−2
S4	2	**3**	+1	3	**2**	−1
S5	3	**4**	+1	2	**4**	+2
S6	3	3	0	3	**4**	+1
S7	1	1	0	2	2	0
S8	1	**3**	+2	3	3	0

Bold numbers indicate the change in the number of muscle synergies.

3.4. Synergy Changes After Robotic Intervention

Muscle synergy similarity was quantified with the Pearson correlation coefficient (r) to provide an overall view of the lateral symmetry of the muscle synergies.

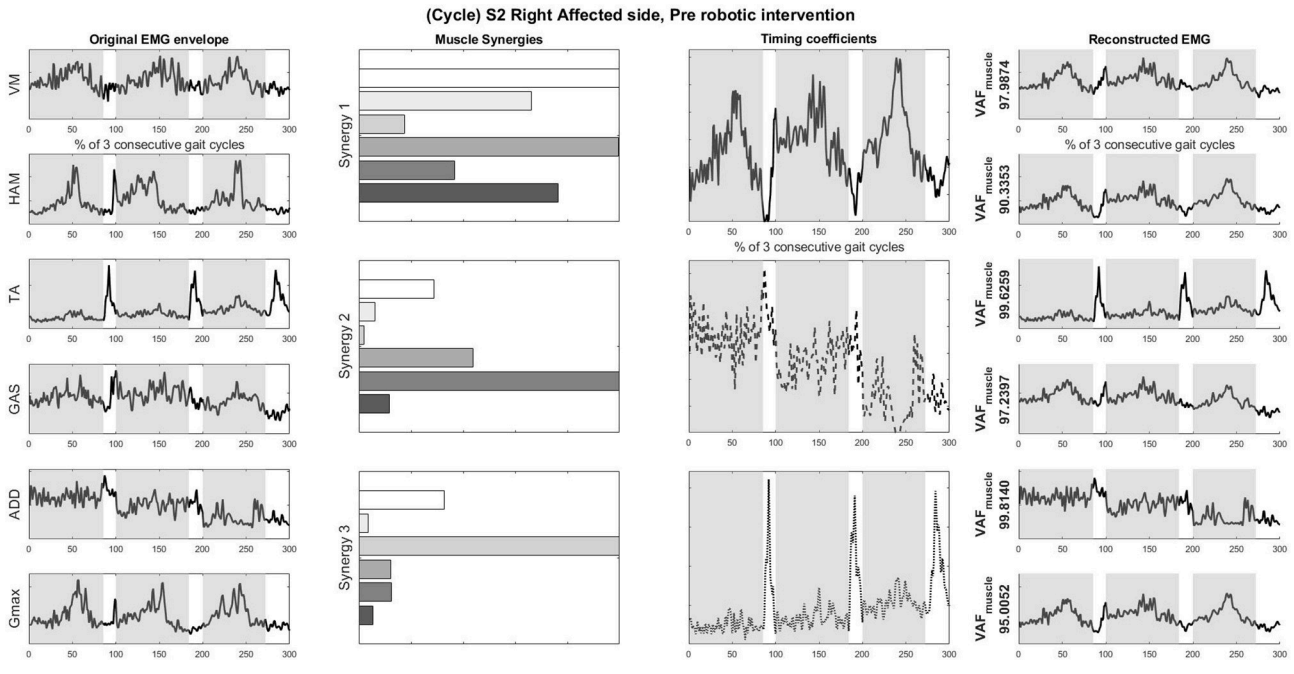

FIGURE 4 | Original EMG envelope, muscle synergies, timing coefficients and Reconstructed EMGs for affected side, pre HAL intervention, computed by NNMF with 3 synergies. Each bar of the synergy set is matched with the order of muscles in the "Original EMG" (Left) column, namely (from top bar to bottom bar) VM, HAM, TA, GAS, ADD, Gmax. Similarly, each plot in the "Individual Reconstructed EMG" column is matched with the order of the muscles in the "Original EMG" (Left) column. Each line pattern represents the reconstructed EMG from each motor module. Shaded areas denote stance phases.

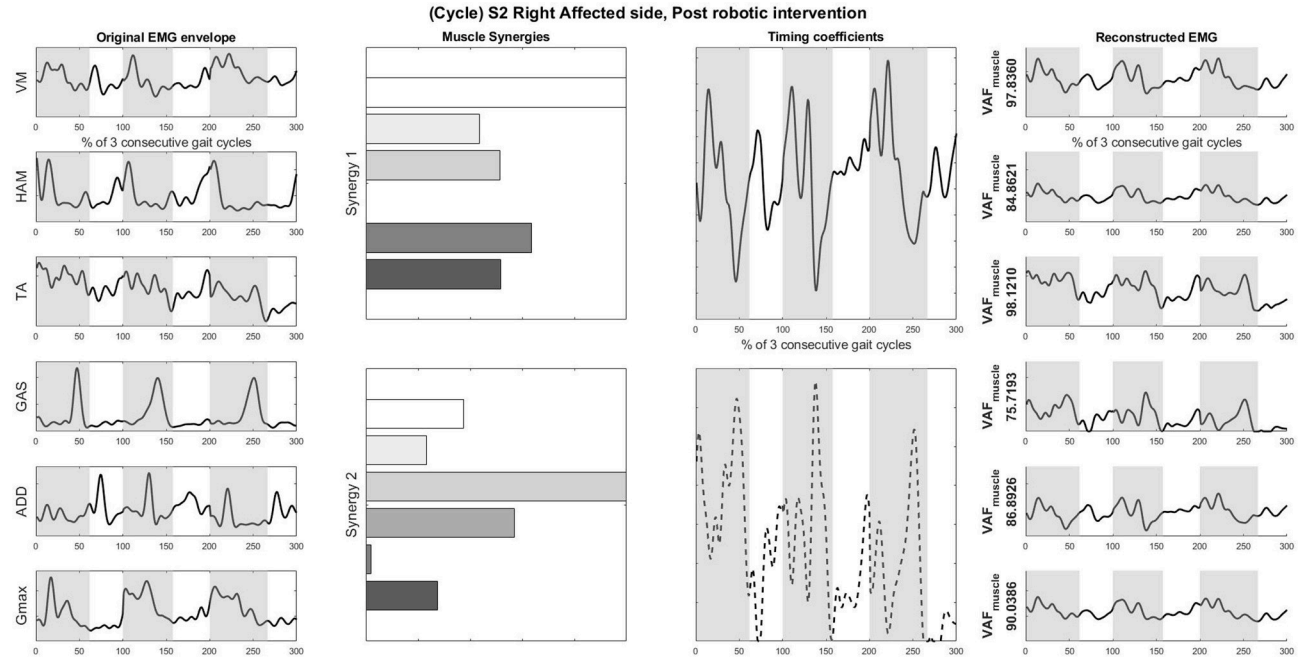

FIGURE 5 | Original EMG envelope, muscle synergies, timing coefficients and Reconstructed EMGs for affected side, post HAL intervention, computed by NNMF with 2 synergies. Each bar of the synergy set is matched with the order of muscles in the "Original EMG" (Left) column, namely (from top bar to bottom bar) VM, HAM, TA, GAS, ADD, Gmax. Similarly, each plot in the "Individual Reconstructed EMG" column is matched with the order of the muscles in the "Original EMG" (Left) column. Each line pattern represents the reconstructed EMG from each motor module. Shaded areas denote stance phases.

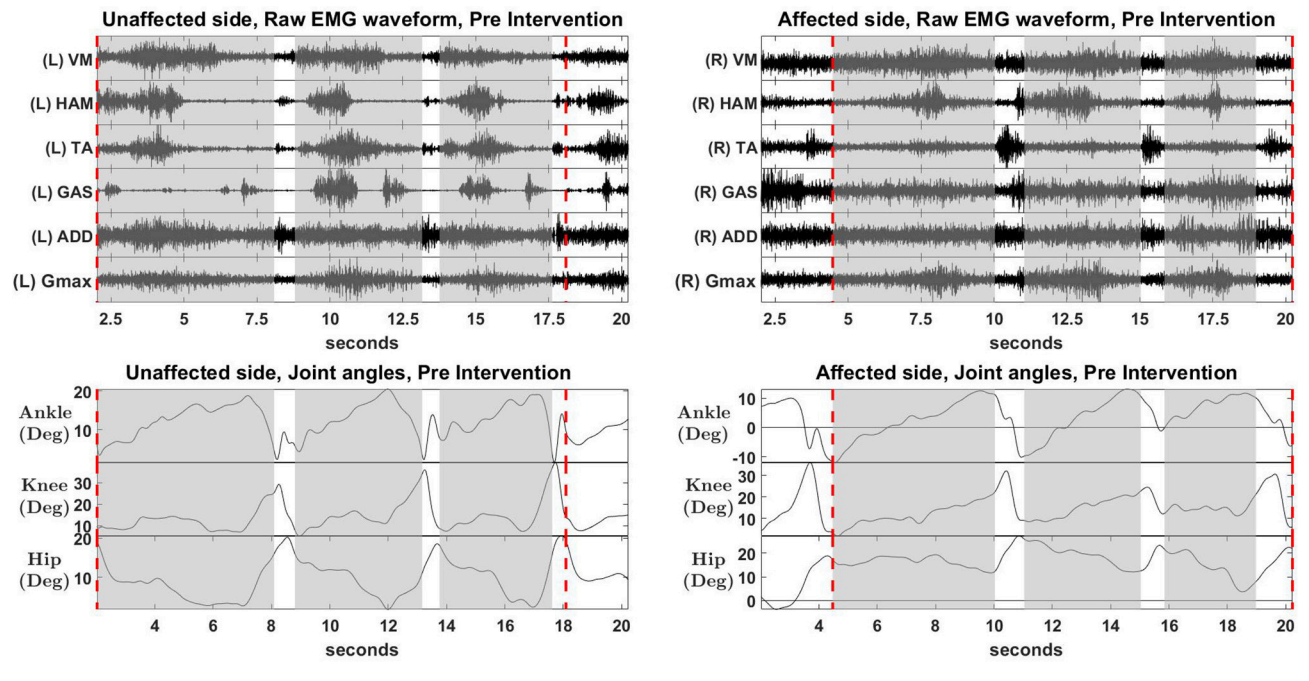

FIGURE 6 | Raw EMG waveform and joint angles, pre intervention. Positive values in angles indicate flexion, while negative values indicate extension.

A significant increase in the bilateral symmetry in the swing phase was observed (Pre : -0.0987 ± 0.349, Post : 0.272 ± 0.291, $p < 0.05$) (**Figure 8**, Second column, Bottom). However, no significance were found for other phases of gait, although a upward trend can be observed. **Stance** (Pre : 0.251 ± 0.352, Post : 0.39 ± 0.514, $p > 0.05$), **Cycle** (Pre : 0.129 ± 0.368, Post : 0.344 ± 0.323, $p > 0.05$).

Pre-Post similarities between the affected and unaffected side for all phases were also not significant, although the variability in r for the affected side is much higher than the unaffected side,

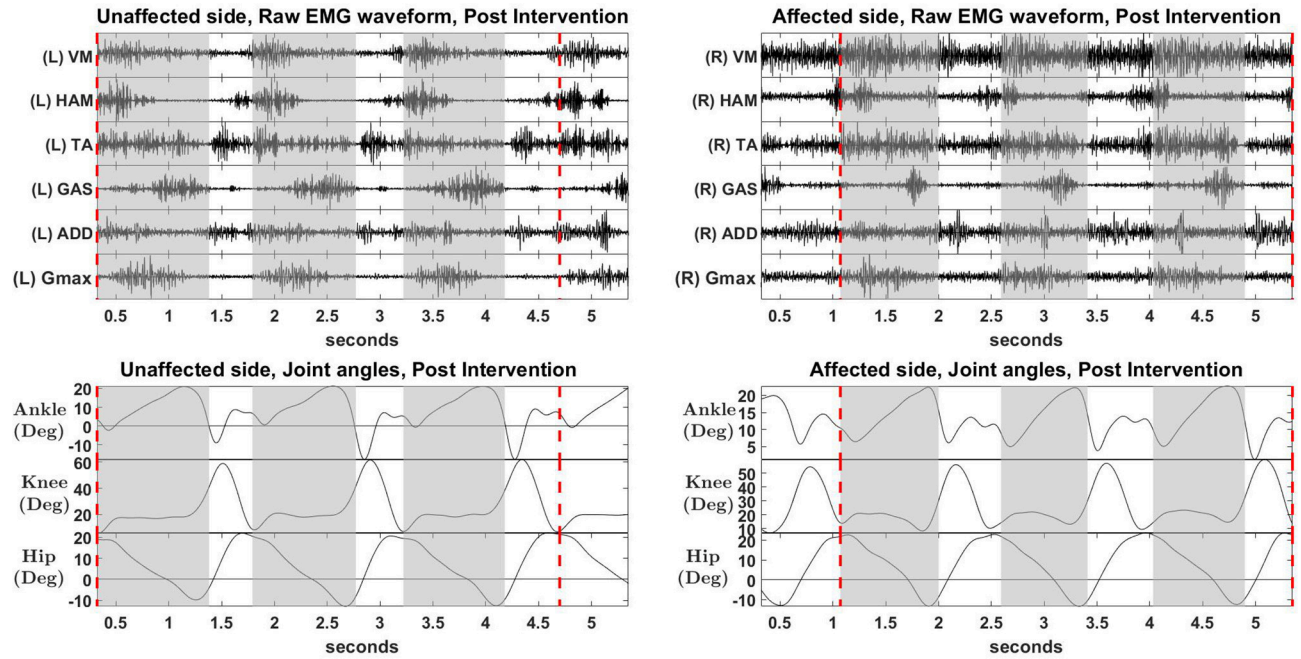

FIGURE 7 | Raw EMG waveform and joint angles, post intervention. Positive values in angles indicate joint flexion, while negative values indicate extension.

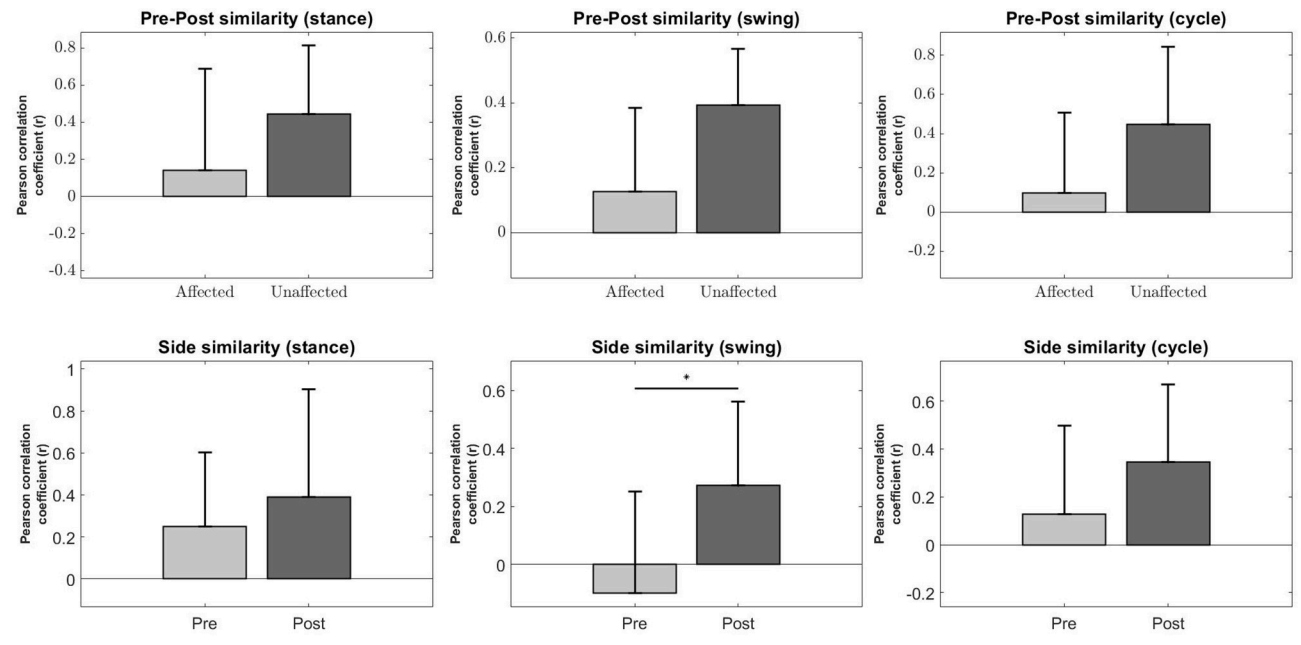

FIGURE 8 | Synergy comparison between conditions. Error bars denote standard deviation. Pre-Post comparison of r between affected and unaffected side during Stance, Swing and Full gait cycle **(Top Row)**. Side comparison of r before and after robotic intervention during Stance, Swing and Fully gait cycle **(Bottom Row)**. The asterisks indicate statistical significance.

possibly indicating a greater change in muscle synergies after robotic intervention. **Stance** (Pre : 0.142 ± 0.548, Post : 0.443 ± 0.371, $p > 0.05$), **Swing** (Pre : 0.128 ± 0.257, Post : 0.393 ± 0.174, $p > 0.05$), **Cycle** (Pre : 0.0988 ± 0.41, Post : 0.446 ± 0.397, $p > 0.05$) (**Figure 8**, Top Row).

We also evaluated muscle synergy vectors on an individual basis as well. **Figures 10, 11** show our results for Subject 2. **Figure 9** labels the muscles shown in **Figures 10, 11**.

Pre-intervention (**Figure 10**), it can be observed that muscle synergies on the affected side are different from muscle synergies on the unaffected side, when sorted by task contribution levels.

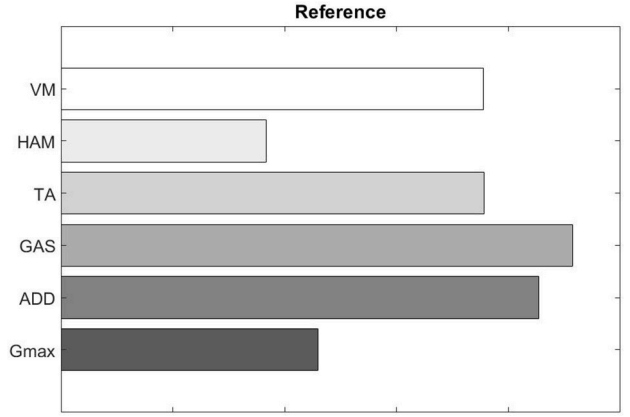

FIGURE 9 | Reference plot displaying the arrangement of muscles in **Figures 10**, **11**.

For example, the first synergy on the affected side has that largest similarity to the second synergy on the unaffected side. This differences in task contribution levels of similar muscle synergies could lead to the observed asymmetric gait (**Figure 6**).

In the post-intervention condition (**Figure 11**), similar muscle synergies, denoted by a high scalar dot product value, now has similar task contribution levels, and this probably lead to a more symmetric gait (**Figure 7**).

4. DISCUSSIONS AND CONCLUSIONS

Our current study attempts to provide a method to measure lateral symmetry by evaluating the number of synergies for each side of the body and contents of the muscle synergy vectors. We think this is a better representation of how the patient is moving, since these synergies quantify muscle activations. By comparing these muscle synergies, we can assess gait symmetries of patients. Although the usual method for previous studies to assess the performance of stroke patients is to compare them with healthy subjects (Bowden et al., 2010; Gizzi et al., 2011; Routson et al., 2013; Hayes et al., 2014; Barroso et al., 2016; Pérez-Nombela et al., 2017), we show that lateral symmetry can still be used as a relative measure by comparing the sides of the patients. Future considerations would be to analyze healthy subjects to test the accuracy of this method.

The increase in lateral symmetry is also associated with the improvement in clinical assessment and gait characteristics. This shows that robotic intervention is helpful for stroke patients

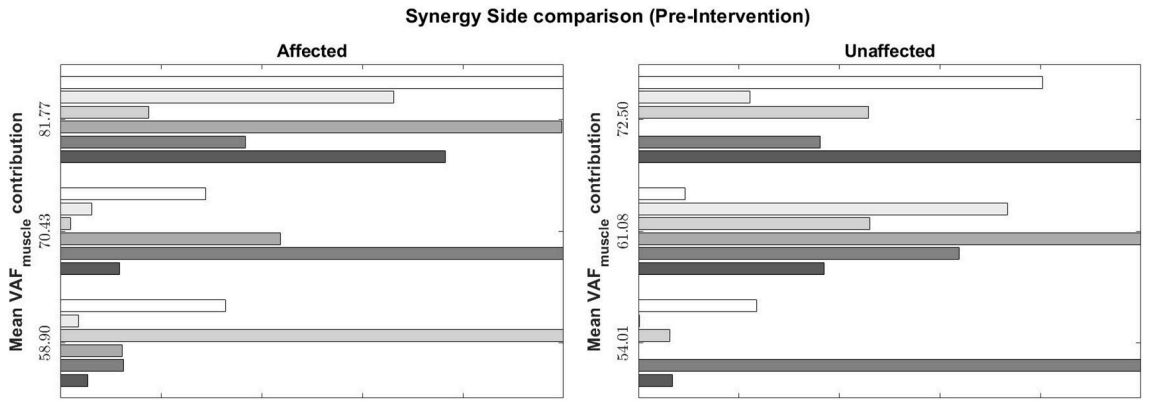

Scalar product similarity matrix

	Unaffected Syn 1	Unaffected Syn 2	Unaffected Syn 3
Affected Syn 1	0.75778	0.80267	0.36241
Affected Syn 2	0.45306	0.69599	0.91875
Affected Syn 3	0.54415	0.45627	0.24392

FIGURE 10 | Muscle synergy vectors of Subject 2, Pre intervention, Full Gait cycle. VAF to original states the contribution of each synergy to the original EMG. A higher value indicates a higher contribution. The scalar product similarity matrix shows results of comparing each synergy vector on the Affected side with all synergy vectors on the Unaffected side. Muscle synergies with the highest score are selected, matched and removed from the pool of muscle synergies. This process continues until no more muscle synergies are left to match. The synergies are matched in the sequence given by the color codes: 1st, Light gray; 2nd, Dark gray; 3rd, Black. The 1st synergy on the affected side is matched with the 2nd synergy on the unaffected side. Similarly, the 3rd synergy on the affected side is matched with the 1st synergy on the unaffected.

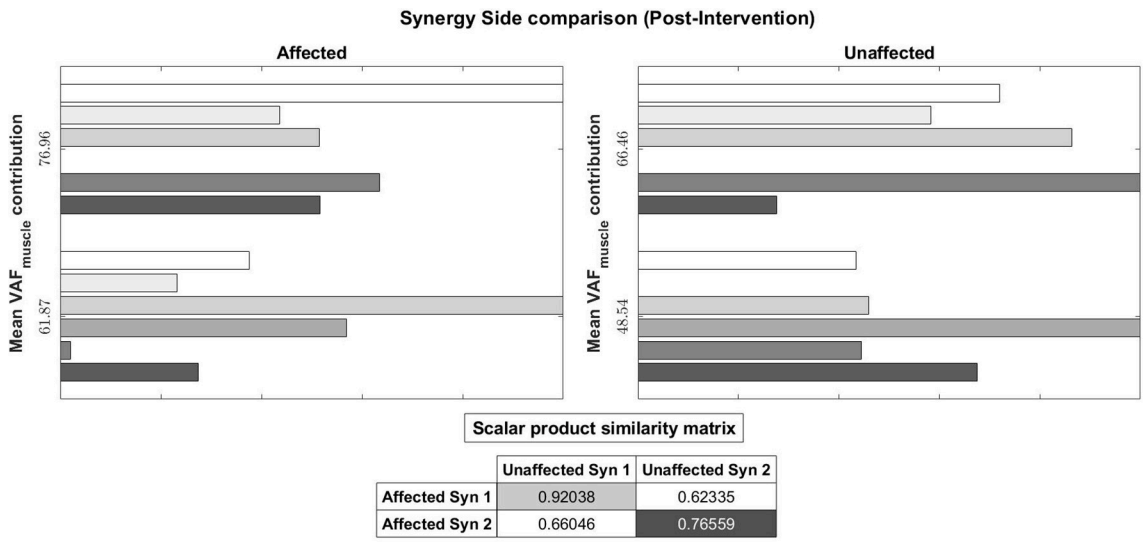

FIGURE 11 | Muscle synergy vectors of Subject 2, Post intervention, Full Gait cycle. With the same muscle synergy matching method, The order of muscle synergies for Subject 2 on the affected side was matched with the order of muscle synergies on the unaffected side (1st synergy on the affected side is matched with the 1st synergy on the unaffected and so on).

(**Figure 1** and **Table 2**). Among the kinematic measures, only absolute lateral difference of step length did not show significant improvement (**Figure 1**, Top Right). This is because we think the step length variable, which is the basis for absolute step length difference, is too vague as a measure. As was described in section 2.5, this variable does not consider the side favored by the patient during walking.

In our study, we utilized a sorting method to arrange muscle synergies according to their contributions for a particular task. One reason for the sorting is because the NNMF algorithm randomly orders the factorized synergies. Another reason is to account for the lack of age-matched controls. Although cluster analysis (Martino et al., 2015; Cappellini et al., 2016) is also an important method to match muscle synergies and indicate the presence of similar muscle synergies on both side of the body, muscle synergies should also be evaluated in context of the task. Nazifi et al. (2017) and Torres-Oviedo and Ting (2010) show that task-specific muscle synergies are dynamically recruited for different tasks, in addition to common muscle synergies found in all subjects. Chvatal and Ting (2013) noted that muscle synergies may be recruited by different neural circuits for a common motor task. These studies suggest that the task might influence the recruitment of muscle synergies, hence analysis should be done in context of the task. We do not expect our subjects to possess similar muscle synergies, due to differences in descending neural commands from the motor cortex caused by stroke. Hence, sorting muscle synergies would help standardize comparison to the task level, allowing muscle synergies with similar contribution levels on both sides of the body to be compared.

Our results show that stroke patients have reduced number of muscle synergies on their affected side as compared to their unaffected side pre intervention (**Table 3**, Affected Pre and Unaffected Pre). This agrees with the previous studies on MSA of stroke patients (Clark et al., 2010; Cheung et al., 2012). However, we have also observed patients who have decreased number of synergies on their unaffected side pre intervention [**Table 3**, S3 (Affected Side), and S2, S3, S4 (Unaffected Side)]. Although this appears to be contradictory, a study by Hashiguchi et al. (2016) found that subacute stroke patients exhibit both fractionation and merging of muscle synergies. They conclude that the number of muscle synergies do not consistently change with the recovery phase. They also found that the merging of synergies is associated with decrease in muscle strength and range of movement in the ankle joint, while fractionation is only related to improvement in the Barthel index.

We also noticed that the unaffected side tends to match the number of synergies on the affected side, with S2, S3, and S4 showing a decrease in the number of synergies, and S5 and S6 showing an increase in the number of synergies. This seems to agree with our results of patients having increased lateral symmetry in muscle synergies while walking. We think that the decrease in the number of synergies on the unaffected side could be due to the central nervous system trying to match the number of synergies on both sides of the body (Decrease in unaffected side of S2, S3, S4). Similarly, when the affected side sees an increase in the number of synergies, the unaffected side would probably require an increase in the number of synergies as well, in order to cater for the increased variety of movement (Increase in unaffected side of S5 and S6). A possible explanation for this phenomena is put forth by Graziadio et al. (2012), who studied bilateral reorganization of the corticospinal system of stroke patients with hemiparesis. They found that the corticospinal system appears to prioritize

symmetrical recovery, even if it is achieved at the expense of the non-lesioned side.

We think that once the affected side regains sufficient motor function, there is no need for the unaffected side to compensate for the affected side, hence leading to a change in the number and contents of synergies, thus, achieving gait symmetry. This could be beneficial for the patients, as gait asymmetries would lead to further complications in future if left untreated (Verma et al., 2012). We hypothesize that this might be the central nervous system's way of regaining symmetry. Indeed, results by Clark et al. (2010) suggest that the organization of muscle synergies are similar in the legs of both healthy and post-stroke patients, with the only difference being the ability to activate muscle synergies independently, where reduction in this ability leads to merged synergies. This is also seen in the study of Cheung et al. (2012). However, associating the number of degrees of freedom to number of muscle synergies seem to contradict our results, where we observed a reduction in the number of synergies post robotic intervention, and those of Hashiguchi et al. (2016), which indicate fractionation can also occur in postacute stroke patients. As Cheung et al. (2012) pointed out, the motor system is a complex mix of descending and ascending neural pathways that interact with each other, and that changes also occur in subcortical areas. More work in understanding muscle synergies in the context of both the cortical and subcortical neural circuits have to be done before any concrete conclusions can be drawn.

Our hypothesis of HAL was that, by its function of actually performing intended motion in real time based on the detected peripheral neuromuscular activity, it can assist neurorehabilitation of the original neuro-muscular motor function of the affected limb. This is in contrast to conventional physical therapy, in which the unaffected side was trained to perform compensatory motions, with orthoses and/or walking aids prescribed to help regain functional independence in daily life (Verma et al., 2012). It was also noted by Verma et al. (2012) that the adult human brain is capable of reorganization after stroke and can be manipulated with movement stimuli involving lower limbs. Shimizu et al. (2017) showed that recovery of neuromuscular activity is possible even in patients with chronic complete spinal cord injury with quadri/paraplegia. They used HAL to allow patients to trigger voluntary ambulation with residual muscle activations in their arms. This supports our hypothesis of HAL's effect on neurorehabilitation after stroke observed in this study.

It is also widely discussed that the synergy modules of muscular activation extracted by NNMF represents the way the central nervous system organizes the coordinated control of multiple muscles by descending commands to the peripheral (Ting et al., 2015). The improvement of lateral synergy after robotic intervention using HAL shown in this study suggests possible contribution of HAL in the improvement of neuronal organization of gait by the central nervous system, in the acute phase post-stroke patients.

4.1. Limitations of Study

Limitation of the study includes the lack of control patients who did not receive HAL treatment. However, we do note that Louie and Eng (2016) have performed an extensive review of various clinical trials utilizing robotic intervention for post-stroke treatment, with findings that robotic intervention is safe and beneficial for stroke patients. Hence, this study is focused on developing methods to quantify the effects of robotic intervention. Nevertheless, comparison to control group and investigation of synergy organization during sessions remain for future consideration.

We acknowledge that the variety of impaired gait in stroke patients cannot be fully captured with 8 subjects. However, our study would like to show that muscle synergies are able to quantify gait asymmetries in stroke patients and hope that this method would inspire others to use and refine our methods. That said, increasing the number of subjects remains a consideration for future studies.

AUTHOR CONTRIBUTIONS

CT and HK collected, analyzed and interpreted the data; wrote and drafted the manuscript. HW and AM planned and administered HAL treatment. AM diagnosed the patients and prescribed HAL treatment. MY provided important comments for the clinical part of the study and helped developing HAL treatment. YS originally developed the robot suit HAL and conceived the idea of HAL treatment. KS designed the analysis and provided essential insight for the paper. All authors made critical revisions of the manuscript and approved the final version.

FUNDING

This study was supported by the Industrial Disease Clinical Research Grant of the Ministry of Health, Labour and Welfare, Japan (14060101-01) and Empowerment Informatics Program of University of Tsukuba.

ACKNOWLEDGEMENT

Authors thank Ms. Mayuko Sakamaki and Ms. Yumiko Ito of Center for Innovative Medicine and Engineering (CIME) of University of Tsukuba Hospital, for their excellent assistance during HAL treatments.

REFERENCES

Aach, M., Cruciger, O., Sczesny-Kaiser, M., Höffken, O., Meindl, R. C., Tegenthoff, M., et al. (2014). Voluntary driven exoskeleton as a new tool for rehabilitation in chronic spinal cord injury: a pilot study. *Spine J.* 14, 2847–2853. doi: 10.1016/j.spinee.2014.03.042

Banks, C. L., Pai, M. M., McGuirk, T. E., Fregly, B. J., and Patten, C. (2017). Methodological choices in muscle synergy analysis impact differentiation of physiological characteristics following stroke. *Front. Comput. Neurosci.* 11:78. doi: 10.3389/fncom.2017.00078

Barroso, F. O., Torricelli, D., Bravo-Esteban, E., Taylor, J., Gómez-Soriano, J., Santos, C., et al. (2016). Muscle synergies in cycling after incomplete spinal

cord injury: correlation with clinical measures of motor function and spasticity. *Front. Hum. Neurosci.* 9:706. doi: 10.3389/fnhum.2015.00706

Barroso, F. O., Torricelli, D., Molina-Rueda, F., Alguacil-Diego, I. M., de-la Cuerda, R. C., Santos, C., et al. (2017). Combining muscle synergies and biomechanical analysis to assess gait in stroke patients. *J. Biomech.* 63(Suppl. C):98–103. doi: 10.1016/j.jbiomech.2017.08.006

Bowden, M. G., Clark, D. J., and Kautz, S. A. (2010). Evaluation of abnormal synergy patterns poststroke: relationship of the fugl-meyer assessment to hemiparetic locomotion. *Neurorehabil. Neural Repair* 24, 328–337. doi: 10.1177/1545968309343215

Cappellini, G., Ivanenko, Y. P., Martino, G., MacLellan, M. J., Sacco, A., Morelli, D., et al. (2016). Immature spinal locomotor output in children with cerebral palsy. *Front. Physiol.* 7:478. doi: 10.3389/fphys.2016.00478

Cheung, V. C. K., Turolla, A., Agostini, M., Silvoni, S., Bennis, C., Kasi, P., et al. (2012). Muscle synergy patterns as physiological markers of motor cortical damage. *Proc. Natl. Acad. Sci. U.S.A.* 109, 14652–14656. doi: 10.1073/pnas.1212056109

Chvatal, S., and Ting, L. (2013). Common muscle synergies for balance and walking. *Front. Comput. Neurosci.* 7:48. doi: 10.3389/fncom.2013.00048

Clark, D. J., Ting, L. H., Zajac, F. E., Neptune, R. R., and Kautz, S. A. (2010). Merging of healthy motor modules predicts reduced locomotor performance and muscle coordination complexity post-stroke. *J. Neurophysiol.* 103, 844–857. doi: 10.1152/jn.00825.2009

Díaz, I., Gil, J. J., and Sánchez, E. (2011). Lower-limb robotic rehabilitation: literature review and challenges. *J. Robot.* 2011:759764. doi: 10.1155/2011/759764

Esquenazi, A., Talaty, M., and Jayaraman, A. (2017). Powered exoskeletons for walking assistance in persons with central nervous system injuries: a narrative review. *PM & R* 9, 46–62. doi: 10.1016/j.pmrj.2016.07.534

Gelsy Torres-Oviedo, J. M. M., and Ting, L. H. (2006). Muscle synergy organization is robust across a variety of postural perturbations. *J. Neurophysiol.* 96, 1530–1546. doi: 10.1152/jn.00810.2005

Gizzi, L., Feldbæ k Nielsen, J., Felici, F., Ivanenko, Y. P., and Farina, D. (2011). Impulses of activation but not motor modules are preserved in the locomotion of subacute stroke patients. *J. Neurophysiol.* 106, 202–210. doi: 10.1152/jn.00727.2010

Graziadio, S., Tomasevic, L., Assenza, G., Tecchio, F., and Eyre, J. (2012). The myth of the "unaffected" side after unilateral stroke: is reorganisation of the non-infarcted corticospinal system to re-establish balance the price for recovery? *Exp. Neurol.* 238, 168–175. doi: 10.1016/j.expneurol.2012.08.031

Hashiguchi, Y., Ohata, K., Kitatani, R., Yamakami, N., Sakuma, K., Osako, S., et al. (2016). Merging and fractionation of muscle synergy indicate the recovery process in patients with hemiplegia: the first study of patients after subacute stroke. *Neural Plast.* 2016:7. doi: 10.1155/2016/5282957

Hayashi, T., Kawamoto, H., and Sankai, Y. (2005). "Control method of robot suit hal working as operator's muscle using biological and dynamical information," in *2005 IEEE/RSJ International Conference on Intelligent Robots and Systems* (Edmonton), 3063–3068.

Hayes, H. B., Chvatal, S. A., French, M. A., Ting, L. H., and Trumbower, R. D. (2014). Neuromuscular constraints on muscle coordination during overground walking in persons with chronic incomplete spinal cord injury. *Clin. Neurophysiol.* 125, 2024–2035. doi: 10.1016/j.clinph.2014.02.001

Ivanenko, Y. P., Cappellini, G., Dominici, N., Poppele, R. E., and Lacquaniti, F. (2007). Modular control of limb movements during human locomotion. *J. Neurosci.* 27, 11149–11161. doi: 10.1523/JNEUROSCI.2644-07.2007

Jezernik, S., Colombo, G., Keller, T., Frueh, H., and Morari, M. (2003). Robotic orthosis lokomat: a rehabilitation and research tool. *Neuromodulation* 6, 108–115. doi: 10.1046/j.1525-1403.2003.03017.x

Lam, H. S. P., Lau, F. W. K., Chan, G. K. L., and Sykes, K. (2010). The validity and reliability of a 6-metre timed walk for the functional assessment of patients with stroke. *Physiother. Theory Pract.* 26, 251–255. doi: 10.3109/09593980903015235

Louie, D. R., and Eng, J. J. (2016). Powered robotic exoskeletons in post-stroke rehabilitation of gait: a scoping review. *J. NeuroEng. Rehabil.* 13:53. doi: 10.1186/s12984-016-0162-5

Martino, G., Ivanenko, Y. P., d'Avella, A., Serrao, M., Ranavolo, A., Draicchio, F., et al. (2015). Neuromuscular adjustments of gait associated with unstable conditions. *J. Neurophysiol.* 114, 2867–2882. doi: 10.1152/jn.00029.2015

Nazifi, M. M., Yoon, H. U., Beschorner, K., and Hur, P. (2017). Shared and task-specific muscle synergies during normal walking and slipping. *Front. Hum. Neurosci.* 11:40. doi: 10.3389/fnhum.2017.00040

Neuromechanics Lab, E. U. (2016). *Software Sharing: Non-Negative Matrix Factorization Tutorial and Matlab Code, Tutorials 2&3: Postural Control and Walking Examples.* Available online at: http://neuromechanicslab.emory.edu/resources/software.html

Oliveira, A. S., Gizzi, L., Farina, D., and Kersting, U. G. (2014). Motor modules of human locomotion: influence of emg averaging, concatenation, and number of step cycles. *Front. Hum. Neurosci.* 8:335. doi: 10.3389/fnhum.2014.00335

Patterson, K. K., Gage, W. H., Brooks, D., Black, S. E., and McIlroy, W. E. (2010). Changes in gait symmetry and velocity after stroke: a cross-sectional study from weeks to years after stroke. *Neurorehabil. Neural Repair* 24, 783–790. doi: 10.1177/1545968310372091

Pérez-Nombela, S., Barroso, F., Torricelli, D., de los Reyes-Guzmán A, del Ama, A. J., Gómez-Soriano, J., et al. (2017). Modular control of gait after incomplete spinal cord injury: differences between sides. *Spinal Cord* 55, 79–86. doi: 10.1038/sc.2016.99

Routson, R. L., Clark, D. J., Bowden, M. G., Kautz, S. A., and Neptune, R. R. (2013). The influence of locomotor rehabilitation on module quality and post-stroke hemiparetic walking performance. *Gait Posture* 38, 511–517. doi: 10.1016/j.gaitpost.2013.01.020

Shimizu, Y., Kadone, H., Kubota, S., Suzuki, K., Abe, T., Ueno, T., et al. (2017). Voluntary ambulation by upper limb-triggered hal® in patients with complete quadri/paraplegia due to chronic spinal cord injury. *Front. Neurosci.* 11:649. doi: 10.3389/fnins.2017.00649

Ting, L. H., Chiel, H. J., Trumbower, R. D., Allen, J. L., McKay, J. L., Hackney, M. E., et al. (2015). Neuromechanical principles underlying movement modularity and their implications for rehabilitation. *Neuron* 86, 38–54. doi: 10.1016/j.neuron.2015.02.042

Torres-Oviedo, G., and Ting, L. H. (2007). Muscle synergies characterizing human postural responses. *J. Neurophysiol.* 98, 2144–2156. doi: 10.1152/jn.01360.2006

Torres-Oviedo, G., and Ting, L. H. (2010). Subject-specific muscle synergies in human balance control are consistent across different biomechanical contexts. *J. Neurophysiol.* 103, 3084–3098. doi: 10.1152/jn.00960.2009

Veneman, J. F., Kruidhof, R., Hekman, E. E. G., Ekkelenkamp, R., Asseldonk, E. H. F. V., and van der Kooij, H. (2007). Design and evaluation of the lopes exoskeleton robot for interactive gait rehabilitation. *IEEE Trans. Neural Syst. Rehabil. Eng.* 15, 379–386. doi: 10.1109/TNSRE.2007.903919

Verma, R., Arya, K. N., Sharma, P., and Garg, R. (2012). Understanding gait control in post-stroke: implications for management. *J. Bodywork Movement Ther.* 16, 14–21. doi: 10.1016/j.jbmt.2010.12.005

Watanabe, H., Tanaka, N., Inuta, T., Saitou, H., and Yanagi, H. (2014). Locomotion improvement using a hybrid assistive limb in recovery phase stroke patients: a randomized controlled pilot study. *Arch. Phys. Med. Rehabil.* 95, 2006–2012. doi: 10.1016/j.apmr.2014.07.002

Zeilig, G., Weingarden, H., Zwecker, M., Dudkiewicz, I., Bloch, A., and Esquenazi, A. (2012). Safety and tolerance of the rewalk™ exoskeleton suit for ambulation by people with complete spinal cord injury: a pilot study. *J. Spinal Cord Med.* 35, 96–101. doi: 10.1179/2045772312Y.0000000003

Conflict of Interest Statement: YS is the C.E.O., shareholder, and director of CYBERDYNE Inc. which produces the robot suit HAL. CYBERDYNE was not involved in study design, data collection, analysis, writing or submission of this article.

The other authors declare that the research was conducted in the absence of any commercial or financial relationships that could be construed as a potential conflict of interest.

frontiers in Neuroscience

CORRECTION
published: 21 February 2020
doi: 10.3389/fnins.2020.00113

Corrigendum: Lateral Symmetry of Synergies in Lower Limb Muscles of Acute Post-stroke Patients After Robotic Intervention

Chun Kwang Tan[1]*, *Hideki Kadone*[2], *Hiroki Watanabe*[3], *Aiki Marushima*[3], *Masashi Yamazaki*[4], *Yoshiyuki Sankai*[5,6] and *Kenji Suzuki*[1,5,6]

[1] Artificial Intelligence Laboratory, University of Tsukuba, Tsukuba, Japan, [2] Center for Innovative Medicine and Engineering, University of Tsukuba Hospital, Tsukuba, Japan, [3] Department of Neurosurgery, Faculty of Medicine, University of Tsukuba, Tsukuba, Japan, [4] Department of Orthopaedic Surgery, Faculty of Medicine, University of Tsukuba, Tsukuba, Japan, [5] Center for Cybernics Research, University of Tsukuba, Tsukuba, Japan, [6] Faculty of Engineering, University of Tsukuba, Tsukuba, Japan

Keywords: muscle synergies, gait symmetry, stroke rehabilitation, robotic intervention, hybrid assistive limb

OPEN ACCESS

Edited and reviewed by:
Yury Ivanenko,
Santa Lucia Foundation (IRCCS), Italy

***Correspondence:**
Chun Kwang Tan
chunkwang@ai.iit.tsukuba.ac.jp

Specialty section:
This article was submitted to Neuroprosthetics, a section of the journal Frontiers in Neuroscience

Received: *20 January 2020*
Accepted: *29 January 2020*
Published: *21 February 2020*

Citation:
Tan CK, Kadone H, Watanabe H, Marushima A, Yamazaki M, Sankai Y and Suzuki K (2020) Corrigendum: Lateral Symmetry of Synergies in Lower Limb Muscles of Acute Post-stroke Patients After Robotic Intervention. Front. Neurosci. 14:113. doi: 10.3389/fnins.2020.00113

A Corrigendum on

Lateral Symmetry of Synergies in Lower Limb Muscles of Acute Post-stroke Patients After Robotic Intervention

by Tan, C. K., Kadone, H., Watanabe, H., Marushima, A., Yamazaki, M., Sankai, Y., et al. (2018). Front. Neurosci. 12:276. doi: 10.3389/fnins.2018.00276

In the original article, there was a mistake in **Table 1** as published. **The gender of S7 is wrongly listed as "M," where it should be "F."** The corrected **Table 1** appears below.

Additionally, there was a mistake in **Table 2** as published. **The FMA-LE (Pre) of S6 is wrongly listed as "23," where it should be "21."** The corrected **Table 2** appears below.

The authors apologize for this error and state that this does not change the scientific conclusions of the article in any way. The original article has been updated.

TABLE 1 | Participants characteristics.

ID	Age (years)	Gender	Diagnosis	Affected side	FAC before HAL	Onset-HAL duration (days)
S1	67	F	ACI	L	1	10
S2	52	F	SH	R	2	17
S3	71	F	BSI	L	1	11
S4	55	M	LI	L	2	10
S5	55	F	ABSI	L	3	16
S6	43	M	LI	R	2	11
S7	51	F	ACI	R	2	18
S8	80	M	ACI	R	2	16

Diagnosis was Atherothrombotic Cerebral Infarction (ACI), Subcortical Hemorrhage (SH), Brain Stem Infarction (BSI), Lacunar Infarct (LI) or Atherothrombotic Brain Stem Infarction (ABSI).

TABLE 2 | Clinical Measures Pre-Post robotic intervention.

	FIM-Locomotion (Pre)	FIM-Locomotion (Post)	FIM-Motor (General) (Pre)	FIM-Motor (General) (Post)	FMA-LE (Pre)	FMA-LE (Post)
S1	1	**3**	46	**73**	13	**18**
S2	1	**5**	40	**82**	19	**26**
S3	1	**2**	40	**55**	18	**28**
S4	2	**7**	52	**77**	26	**29**
S5	2	**7**	78	**90**	20	**27**
S6	1	**6**	66	**83**	21	**25**
S7	1	1	53	**62**	14	**22**
S8	1	**5**	50	**65**	17	**20**

Numbers in bold denote improvement in scores.

frontiers in Neuroscience

ORIGINAL RESEARCH
published: 01 June 2018
doi: 10.3389/fnins.2018.00374

Supplemental Stimulation Improves Swing Phase Kinematics During Exoskeleton Assisted Gait of SCI Subjects With Severe Muscle Spasticity

Andrew Ekelem and Michael Goldfarb*

Department of Mechanical Engineering, Center for Rehabilitation Engineering and Assistive Technology, Vanderbilt University, Nashville, TN, United States

Spasticity is a common comorbidity associated with spinal cord injury (SCI). Robotic exoskeletons have recently emerged to facilitate legged mobility in people with motor complete SCI. Involuntary muscle activity attributed to spasticity, however, can prevent such individuals from using an exoskeleton. Specifically, although most exoskeleton technologies can accommodate low to moderate spasticity, the presence of moderate to severe spasticity can significantly impair gait kinematics when using an exoskeleton. In an effort to potentially enable individuals with moderate to severe spasticity to use exoskeletons more effectively, this study investigates the use of common peroneal stimulation in conjunction with exoskeleton gait assistance. The electrical stimulation is timed with the exoskeleton swing phase, and is intended to acutely suppress extensor spasticity through recruitment of the flexion withdrawal reflex (i.e., while the stimulation is activated) to enable improved exoskeletal walking. In order to examine the potential efficacy of this approach, two SCI subjects with severe extensor spasticity (i.e., modified Ashworth ratings of three to four) walked in an exoskeleton with and without supplemental stimulation while knee and hip motion was measured during swing phase. Stimulation was alternated on and off every ten steps to eliminate transient therapeutic effects, enabling the acute effects of stimulation to be isolated. These experiments indicated that common peroneal stimulation on average increased peak hip flexion during the swing phase of walking by 21.1° (236%) and peak knee flexion by 14.4° (56%). Additionally, use of the stimulation decreased the swing phase RMS motor current by 228 mA (15%) at the hip motors and 734 mA (38%) at the knee motors, indicating improved kinematics were achieved with reduced effort from the exoskeleton. Walking with the exoskeleton did not have a significant effect on modified Ashworth scores, indicating the common peroneal stimulation has only acute effects on suppressing extensor tone and aiding flexion. This preliminary data indicates that such supplemental stimulation may be used to improve the quality of movement provided by exoskeletons for persons with severe extensor spasticity in the lower limb.

Keywords: spinal cord injury, spasticity, exoskeleton, functional electrical stimulation, locomotion, rehabilitation

OPEN ACCESS

Edited by:
Yury Ivanenko,
Fondazione Santa Lucia (IRCCS), Italy

Reviewed by:
Ranu Jung,
Florida International University, United States
Elena Yu. Shapkova,
State Research Institute for Phthysiopulmonology, St. Petersburg, Russia

****Correspondence:***
Andrew Ekelem
ekelem90@gmail.com

Specialty section:
This article was submitted to Neuroprosthetics, a section of the journal Frontiers in Neuroscience

Received: *01 September 2017*
Accepted: *14 May 2018*
Published: *01 June 2018*

Citation:
Ekelem A and Goldfarb M (2018) Supplemental Stimulation Improves Swing Phase Kinematics During Exoskeleton Assisted Gait of SCI Subjects With Severe Muscle Spasticity. Front. Neurosci. 12:374. doi: 10.3389/fnins.2018.00374

INTRODUCTION

Spasticity is a common comorbidity resulting from spinal cord injury (SCI), where ∼68–75% of individuals with SCI experience spasticity and 20–40% have problematic spasticity that restricts activities of daily living (Adams and Hicks, 2005). Spasticity is commonly defined as involuntary muscle activity initiated by uninhibited reflex circuits, and can be categorized as intrinsic tonic, intrinsic phasic, or extrinsic nocuous (Decq, 2003; Adams and Hicks, 2005). Tonic and phasic spasticity are thought to be caused by the hyperactive stretch reflex circuits after central neurologic impairment of the corticospinal inhibitory pathways. Symptoms of spasticity include a counter torque proportional to the angular velocity about the joint and an increase in muscle tone. Spasticity is ordinarily evaluated through the Modified Ashworth Scale (MAS) which involves a trained assessor rapidly advancing a joint through its range of motion and evaluating the stiffness of the joint on a scale from zero to four, see **Table 1** (Bohannon and Smith, 1987; Biering-Sørensen et al., 2006). Significant tonic and/or phasic spasticity can be problematic for attempts to restore mobility to a paretic or paralyzed limb.

Spasticity may be managed to achieve a balance between useful and detrimental effects by progressing from physical rehabilitation, pharmacological intervention, injection, intrathecal baclofen, and surgery (Adams and Hicks, 2005). Useful effects of spasticity induced muscle activity include: reduced muscle atrophy and improved blood circulation, which can reduce predispositions to other comorbidities that commonly result from frequent wheelchair use (Demirel et al., 1998; Adams and Hicks, 2005). Therefore, spasticity is typically managed to a level that best balances comfort and quality of life (QOL).

Recently, lower limb exoskeletons have begun to emerge onto the commercial marketplace. Such devices can facilitate legged mobility for individuals with SCI. These devices have the potential to improve the QOL of people with lower limb paralysis by enabling them to walk, generally via actuated knee and hip joints (Contreras-Vidal et al., 2016). Exoskeletons have been shown to enable safe over-ground weighted walking and gait training for the mobility impaired, particularly for individuals with SCI (Contreras-Vidal et al., 2016). The presence of severe spasticity, however, can severely impair the ability of an exoskeleton to provide a viable walking movement (Esquenazi et al., 2012; Aach et al., 2013; Kolakowsky-Hayner, 2013). Severe extensor spasticity, in particular, can preclude hip and knee flexion during the swing phase of walking, thereby largely nullifying the ability of the exoskeleton to provide effective legged mobility.

TABLE 1 | Modified ashworth scale description (Bohannon and Smith, 1987).

Modified ashworth scale	Description
0	No increase in muscle tone
1	Slight increase in muscle tone, manifested by a catch and release or by minimal resistance at the end range of motion when the affected parties moved in flexion or extension
1+	Slight increase in muscle tone, manifested by a catch, followed by minimal resistance throughout the remainder (less than half) of the range of motion
2	More marked increase in muscle tone through most of the range of motion, but the affect part is easily moved
3	Considerable increase in muscle tone, passive movement is difficult
4	Affected part is rigid in flexion or extension

Functional electrical stimulation (FES) applies artificial electrical impulses to initiate action potentials in muscle and nerves for a functional response. FES has proven effective in enabling ambulation in the SCI population, and promoting neural recovery for incomplete the SCI population (Graupe and Bazo, 2015; Young, 2015). Depending primarily on FES alone for gait can be metabolically taxing, is prone to rapid fatigue, and may lack limb control and stability. For these reasons effort has gone into combining FES with orthotic devices, generally called hybrid FES systems, which can provide several advantages relative to using FES alone (Andrews et al., 1988; Isakov et al., 1992; Goldfarb et al., 2003; Bulea et al., 2013; del-Ama et al., 2014; Chang et al., 2017; Anaya et al., 2018), and one prior study investigated a hybrid FES system that couples FES with a robotic exoskeleton (Ha et al., 2016). That study specifically coupled a lower limb exoskeleton with FES of the quadriceps and hamstrings muscle groups of each leg, and demonstrated reduced exoskeleton motor torque and power when used in a hybrid FES manner.

The intent of this research is to investigate the potential of supplementing a lower limb exoskeleton with FES for the purpose of enabling individuals with severe extensor spasticity to effectively walk in a lower limb exoskeleton when those individuals would otherwise have difficulty to do so. Preliminary studies indicate that exoskeleton walking may have beneficial effects with respect to mitigating spasticity (Esquenazi et al., 2012; Aach et al., 2013; Contreras-Vidal et al., 2016), and as such, making this technology available for individuals with moderate to severe spasticity may have particular value for this sub-population. In order to do so, the authors propose here to supplement an exoskeleton with stimulation of the common peroneal nerve with the intent of exciting the flexion withdrawal reflex. Common peroneal nerve stimulation has been shown to assist neurologically impaired individuals during the swing phase of gait by initiating a concerted flexion of the hip, knee, and ankle (Zehr et al., 1997; Bajd et al., 1999; Embrey et al., 2010; O'Dell et al., 2014; Street and Singleton, 2017). Stimulation of the common peroneal nerve activates the flexor withdrawal reflex, which comprises afferent neurons activating motor units responsible for flexion, as well as inhibitory interneurons that inhibit ipsilateral extensors while activating contralateral extensors (Sherrington, 1910). As such, the hypothesis behind peroneal stimulation is twofold: first, the reflex is hypothesized to temporarily inhibit the extensor tone resulting from severe extensor spasticity, and second, the reflex is expected to recruit the lower limb flexors, and therefore supplement the exoskeleton motors during swing. In order to evaluate this hypothesis, a lower limb exoskeleton system was

configured to incorporate supplemental FES of the common peroneal nerve, and experiments were conducted on two SCI subjects with severe extensor spasticity to evaluate the effect of supplemental peroneal stimulation on exoskeleton-generated swing phase movement.

METHODS

Clinical Status

Two subjects were recruited for these experiments. The subjects met the inclusions criteria of having thoracic-level motor-complete SCI (i.e., ASIA A or B) to exclude voluntary motor control of the lower limbs; had right and left leg extensor spasticity rated on the MAS of three or greater in one or more joints; and were responsive to stimulation of the flexor withdrawal reflex. Subject characteristics relevant to the experiments are given in **Table 2**, and respective MAS scores given in **Table 3**. This study was conducted with the informed consent of each subject and with the approval of the Vanderbilt University Internal Review Board.

Indego Exoskeleton

The walking controller was implemented on a lower-limb exoskeleton prototype, shown in **Figure 1**. The prototype utilizes a commercially-available lower-limb exoskeleton (Indego Exoskeleton, Parker Hannifin Corp) as a hardware platform, but replaced the commercial version of the software with experimental control software written by the authors—in this case, the walking controller with supplemental stimulation of the common peroneal nerve on each leg. The experimental control software was implemented in MATLAB Simulink/Stateflow (Mathworks Inc) through a controller area network (CAN) serial cable which was plugged into a CAN port in the exoskeleton. The Indego exoskeleton hardware platform incorporates four motors for powered movement of bilateral hip and knee joints in the sagittal plane, in addition to built-in ankle-foot-orthoses (AFOs) at both ankle joints to provide ankle stability and transfer the weight of the exoskeleton to the ground. Onboard electronic sensors include encoders at each joint that provide the respective joint angles and angular velocities, and a six-axis inertial measurement unit (IMU) in each thigh link, which provide the left and right thigh angles with respect to the vertical. The total mass of the exoskeleton including the battery is ∼12 kg (26 lbs). Further details regarding the Indego exoskeleton functions can be found in (Quintero et al., 2011; Hartigan et al., 2015).

A custom stimulator was developed on an embedded system, which was controlled in the same MATLAB Simulink/Stateflow environment used to control the exoskeleton, and connected via the same CAN cable. As such, the sensor information and control associated with the exoskeleton and stimulator were fully synchronized. The custom stimulator employed a charge-balanced bipolar stimulation waveform with 200 μs pulse widths at a frequency of 50 hz. The device controls the peak current output with a maximum amplitude of 80 mA. Square sticky-gel 3.8 x 3.8 cm (1.5 x 1.5 in) electrodes were placed over the common peroneal nerve on each leg, see **Figure 2**. One electrode was positioned over the fibula head, near the underlying common peroneal nerve, and the second electrode was over the tibialis anterior, ∼4 cm below the tibial tuberosity. Surface electrodes produce a diffuse electric fields so precision (<1 cm) is not necessary. This electrode arrangement avoided significant eversion of the ankle while enabling the flexor withdrawal to be sufficiently activated. A total of two stimulator channels were

TABLE 2 | Subject characteristics.

Subject ID	S1	S2
ASIA	T11 B	T4 B
Level	T11	T4-5
DOI	Mar 2010	Dec 2013
Body Mass (kg)	66	88
Height (m)	1.83	1.73

TABLE 3 | Modified ashworth scale ratings for each subject.

Muscle Group	S1 R/L	S2 R/L
Hip flexors	1+/1	0/1
Hip extensors	2/1	0/0
Knee flexors	2/2	2/2
Knee extensors	3/3	3/3
Hip adductors	3/3	3/3
Hip abductors	0/0	0/0
Ankle dorsiflexors	0/0	0/0
Ankle plantarflexors	3/3	4/3

FIGURE 1 | Indego exoskeleton. Photograph courtesy of Parker-Hannifin.

FIGURE 2 | Typical electrode placement for stimulation of the common peroneal nerve.

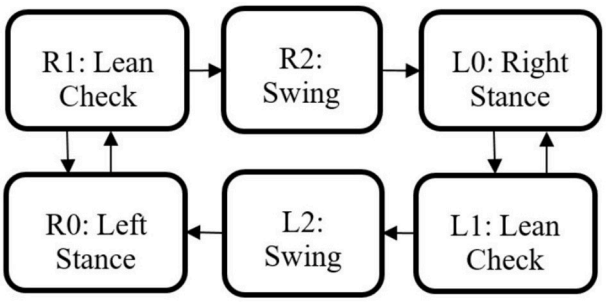

FIGURE 3 | Walking state machine with corresponding transition conditions in **Table 4**.

TABLE 4 | State machine transition conditions.

Transition	Condition
R0 to R1 or L0 to L1	Rear thigh angle exceeds lean threshold
R1 to R0 or L1 to L0	Rear thigh angle less than lean threshold
R1 to R2 or L1 to L2	State timer exceeds 200 ms
R2 to L0 or L2 to R0	State timer exceeds 1.1 s

used, one for each leg. The stimulation amplitude was set prior to donning the exoskeleton to a level that elicited strong ankle dorsiflexion, but not so high as to raise the heel off the ground while in a seated position. The stimulation amplitude for the subjects, respectively, were set to 28 and 44 mA on the right, and 28 and 54 mA on the left.

Hybrid Controller

The state machine for the Indego walking controller is shown in **Figure 3** with state transition conditions described in **Table 4**. To account for the latency of the stimulation to produce movement, the stimulation was activated during the lean check state, which identifies the user's intent to take a step by maintaining a forward lean (i.e., forward movement of the estimated center of pressure), as measured by inertial sensors in the exoskeleton, for 200 ms. Once swing is initiated, the stimulation remains on for 40% of the swing phase, during which the majority of flexion occurs. **Figure 4** shows the desired joint trajectories commanded by the exoskeleton controller as the state machine cycles through a right and left step, along with the corresponding timing of the stimulation pulse. When the stimulation is off, the stimulation amplitude is maintained at zero.

Experimental Procedure

Participants were fit with the exoskeleton and given practice sessions (<4 h per day) walking with FES on and off, until they could comfortably walk, and advance the balance aid (i.e., the walker), see **Figure 5**, for 1 h taking breaks as needed. The practice sessions were scheduled approximately a week apart and did not have an appreciable effect on the subjects' spasticity during any term of the study. After sufficient training sessions, each subject had a data session where they donned the FES system, Indego, and XSens MVN Awinda system (Xsens Technologies B.V., Netherlands) motion capture system and walked for ∼1 h, taking rest breaks as needed. The Xsens wireless sensor based motion tracking system was used to capture the kinematic data of the lower limbs during each session. This system includes seven sensors, one sensor for each limb segment (two feet, two shanks, two thighs, and one hip). The sensors were orientated as recommended by Xsens except the thigh sensors were placed medial rather than lateral as to not interfere with the exoskeleton. The Xsens system was calibrated in stance before each 6 min walk session. Data was saved every 6 min as to not overload the computer and risk a loss of data. Neither the environment nor exoskeleton created substantial interference with the Xsens measurement, as validated via Xsens calibration procedures. The trajectories measured by Xsens motion tracker were then processed in MATLAB to identify the peak flexion angle of each joint for each step. For these experiments, the stimulation was programmed to alternate on and off every 10 steps to assess the relative value of stimulation on exoskeleton motion. Gait data was recorded during the data

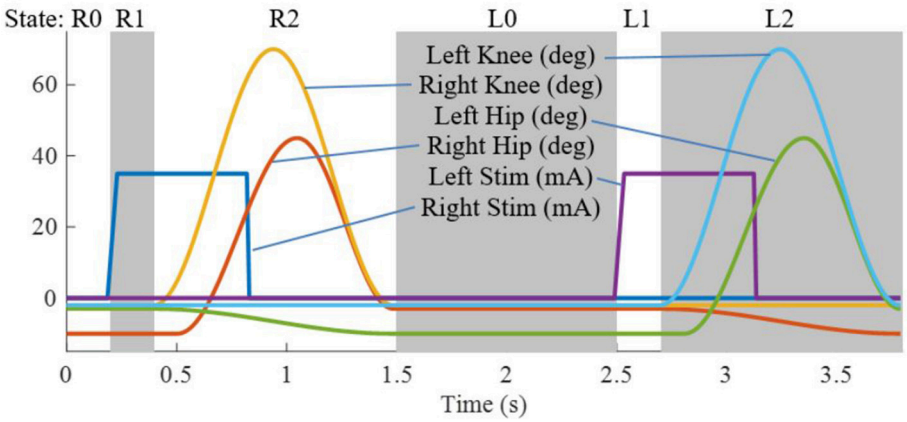

FIGURE 4 | Trajectories for the four exoskeleton joints and the stimulation amplitude for the right and left legs as the state machine progresses through two steps.

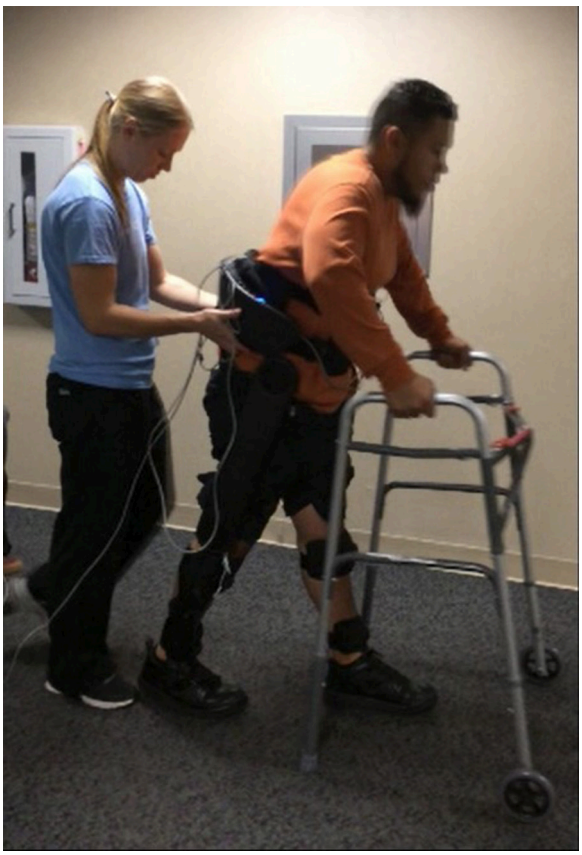

FIGURE 5 | Subject walking with the exoskeleton and stimulator, using a walker for balance. The physical therapist monitors the gait as a precaution in accordance with the Vanderbilt IRB. The subject has consented to the use of this photograph.

session, totaling 232 steps for S1, and 329 steps for S2. MAS were evaluated prior to donning the equipment and after doffing the equipment.

RESULTS

Common peroneal stimulation increased the step length for both subjects, which was reflected in the kinematic data. The hip and knee angles of a representative walking session is plotted in **Figure 6**. The colored dots/hashes indicate the peaks found with a MATLAB algorithm, and does not include half steps, which are the steps in and out of neutral stance (when both hip equilibrium positions are equivalent). The gray bands indicate periods where FES is off. As seen in the data, the subject was able to achieve significantly greater hip and knee flexion with FES, which is indicative of larger steps and greater toe clearance.

The peak flexion angle during swing was parsed for each swing joint per step and grouped by FES on or off and by subject. The median peak flexion of all steps (right and left) for the hip and knee joints of each subject are plotted in **Figure 7**, with error bars denoting plus and minus half the interquartile range. Stimulation assistance increased the median hip peak flexion angles by 21.1° (236%) and the median peak knee angle by 14.4° (56%). Significance in differences in the peak flexion angles were assessed using the Wilcoxon tests for the intra-participant peaks, which indicated that the differences in peak knee and hip joint flexion between the FES-on and FES-off cases were significant with greater than a 99% confidence level. Wilcoxon was chosen due to the non-normality of the data as indicated by the Lilliefors test.

Motor current data from the exoskeleton was logged and analyzed to evaluate the effects of FES assistance on motor torques. Specifically, RMS motor current provides a direct indication of how much effort is being exerted by the exoskeleton to move the paretic limbs. The RMS motor current for the swing leg was parsed for each step (right and left) and grouped into FES-on and FES-off for each subject. The median swing motor current plus and minus half of the interquartile range is shown in **Figure 8** for each subject with FES on and off. Across subjects FES decreased the swing RMS current by 228 mA (15.0%) at the hip motors and 734 mA (37.8%) at the knee motors. Additionally, the intra-participant median swing RMS currents with FES-on and

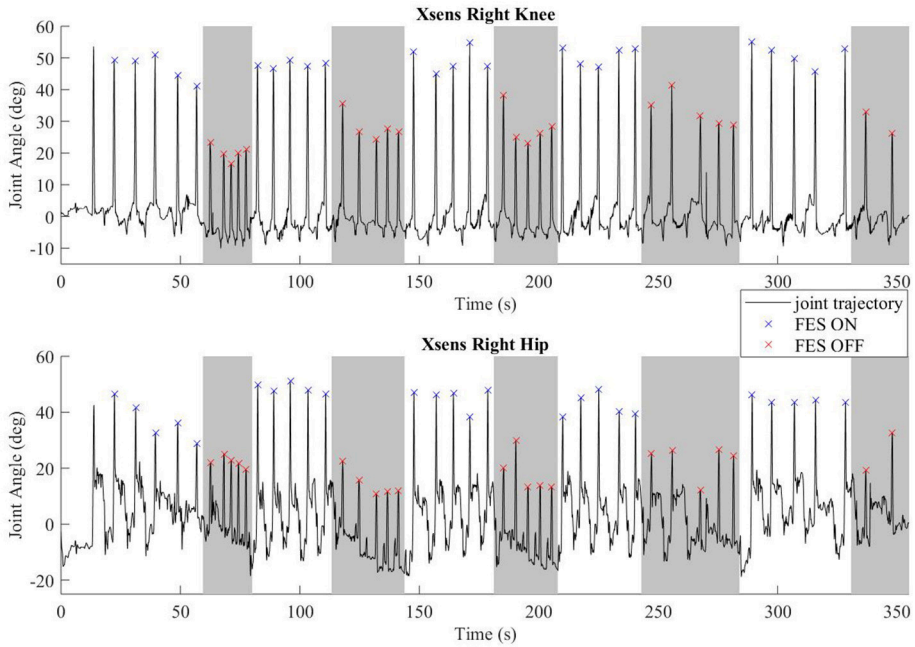

FIGURE 6 | Representative joint angles from walking trial with subject S2. The gray bars indicate periods with FES off and the white bars indicate steps taken with FES on. Flexion peaks are identified by hash marks; blue for steps with FES assistance, red for steps without FES assistance.

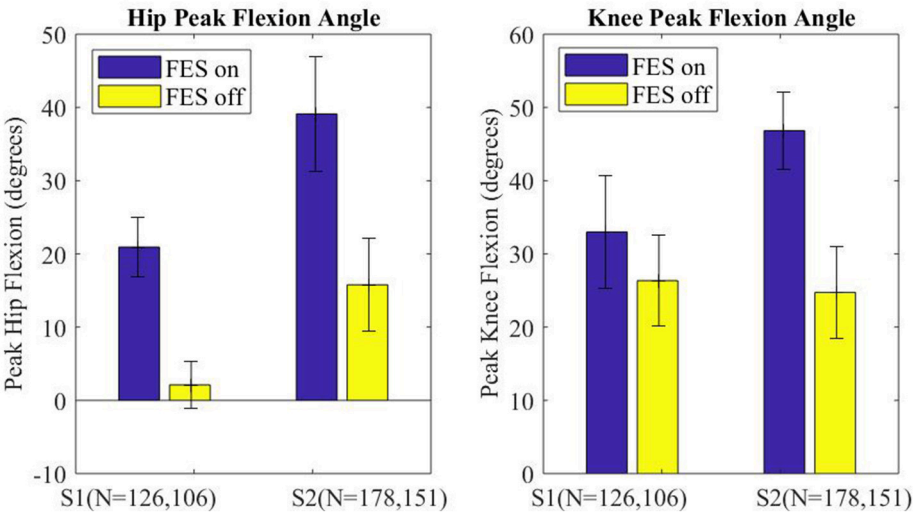

FIGURE 7 | Median peak joint angle across all steps for each subject plotted for FES assistance on and FES assistance off. Error bars mark plus and minus half of the interquartile range. Wilcoxon analysis determines FES on and off had significantly different medians for each joint of each subject, $p < 0.01$.

FES-off were significantly different with a 99% confidence level for both subjects, per Wilcoxon tests of the data.

DISCUSSION

Stimulation of the flexion withdrawal reflex improved the flexion kinematics significantly during exoskeleton assisted gait for participants with severe extensor spasticity. Qualitatively, both subjects had difficulty achieving toe clearance while walking with the exoskeleton without stimulation (i.e., toes consistently dragged on the ground). Adding stimulation greatly improved the gait kinematics and enabled these participants to take significantly larger strides.

Stimulation values were set while sitting and remained constant throughout the session that lasted over 1 h.

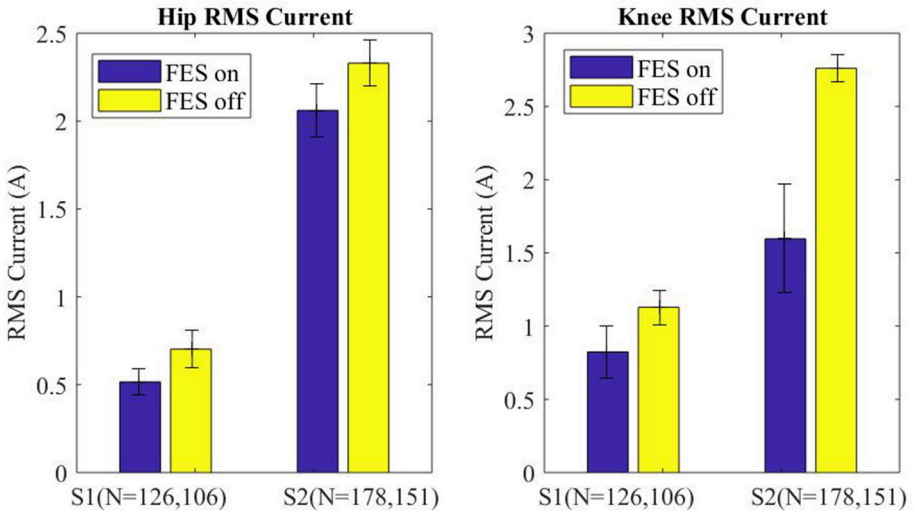

FIGURE 8 | Median of the RMS current of the swing leg for all steps plotted for FES assistance on and FES assistance off. Error bars mark plus and minus half of the interquartile range. Wilcoxon analysis determines FES on and off are significantly different for each joint of each subject, $p < 0.01$.

Accommodation during the span of the trial was not assessed. It is possible that switching the FES off every ten steps effects accommodation. Continued research that specifically explores accommodation and varying FES amplitude should be performed. The stimulation amplitude was intentionally set below a level that would saturate the withdrawal reflex. Based on the experiments performed here, a relatively low-level of reflex stimulation appears to be sufficient to suppress extensor spasticity. A stronger reflex may have increased the observed effect, but may also increase habituation. FES duration during each step was established at a level that coincided with the exoskeleton flexion, accounting for the reflex delay ∼100 ms; duration was not systematically evaluated. Continued studies that explore the physiological response (e.g., electromyography) of spasticity and peroneal stimulation is encouraged.

Additionally FES has been shown to provide therapeutic value for persons with SCI by activating the dormant neuromuscular tissue of the paralyzed limbs. The improved blood flow furthermore may reduce the likelihood of some comorbidities associated with SCI. For these reasons the addition of flexor withdrawal stimulation may be beneficial to all SCI individuals, including individuals with minimal spasticity.

Although some prior studies indicate a possible reduction in spasticity resulting from the use of exoskeletons, in this research, the MAS scores did not change significantly from before to after the walking session. The inherent limitations of the MAS test due to the coarse scoring and human dependent evaluation may attribute to unperceivable change in spasticity. Another consideration is severe spasticity may be more resistant to fatigue than mild spasticity. Furthermore, the focus of the study was acute spasticity (intra-step); a study that examines long term changes in spasticity should account for variables such as intervention duration, rest frequency and duration, and possibly include multiple MAS evaluators or other test for spasticity.

The significant reduction in the motor RMS current per step in conjunction with improved peak flexion is clear indication that extensor tone (spasticity) impedes the exoskeleton assisted flexion, and that flexor stimulation concerted with the exoskeleton flexion can restore a typical range of motion. The significance of the RMS current reductions is that the improved kinematics coincided with a reduction in exoskeleton effort, therefore, the improved flexion can be attributed exclusively to the FES of the common peroneal nerve. Electrical stimulation increased the electrical efficiency and improved performance by adding synergy between man and machine, muscles and motors.

Discrepancies between the exoskeleton kinematic data and the Xsens measured joint angles were perceivable suggesting that the human-robot interface (straps, soft tissue) allows for considerable deformation, especially when spasticity impedes exoskeleton motion. The Xsens provided successful means for motion capture of the user within the exoskeleton. Optical options for motion capture were not feasible due to the coverage of the exoskeleton, as well as the necessity of a very large motion capture arena for over-ground gait. Precaution was taken to securely fasten the Xsens sensors with elastic Velcro straps; trials where a Xsens sensor slipped substantially were not included.

A greater number of subjects should be evaluated to make generalized claims regarding the use of supplemental FES for subjects with severe extensor spasticity. Furthermore, the rehabilitation community would benefit from studies that explore the broader impact of exoskeletal walking in the SCI population.

CONCLUSION

In two motor-complete-thoracic-level SCI subjects with severe lower limb extensor spasticity, supplemental stimulation of the common peroneal nerve during swing was shown to significantly

enhance walking movements generated by the exoskeleton, and to significantly reduce the current demand on the exoskeleton motors. Results of more subjects would strengthen the conclusion of this work. The authors hope that employing supplemental FES as described here will make exoskeletal walking a viable option for individuals with SCI and severe extensor spasticity.

ETHICS STATEMENT

This study was carried out in accordance with the recommendations of the Vanderbilt Internal Review Board with written informed consent from all subjects. All subjects gave written informed consent in accordance with the Declaration of Helsinki. The protocol was approved by the Vanderbilt Internal Review Board.

AUTHOR CONTRIBUTIONS

AE conceived and conducted the study, performed data analysis and wrote and edited the manuscript. MG coordinated the study and wrote and edited the manuscript.

FUNDING

Funding for this research was provided in part by USAMRMC award no. W81XWH-15-2-0068.

ACKNOWLEDGMENTS

The authors would like to thank Christina Durrough, DPT, and the SCI subjects for making this study possible.

REFERENCES

Aach, M., Meindl, R., Hayashi, T., Lange, I., Geßmann, J., Sander, A., et al. (2013). "Exoskeletal neuro-rehabilitation in chronic paraplegic patients – initial results," in *Converging Clinical and Engineering Research on Neurorehabilitation*, eds J. L. Pons, D. Torricelli, and M. Pajaro (Berlin; Heidelberg: Springer Berlin Heidelberg), 233–36.

Adams, M. M., and Hicks, A. L. (2005). Spasticity after spinal cord injury. *Spinal Cord* 43, 577–586. doi: 10.1038/sj.sc.3101757

Anaya, F., Thangavel, P., and Yu, H. (2018). Hybrid FES–robotic gait rehabilitation technologies: a review on mechanical design, actuation, and control strategies. *Int. J. Intell. Robot. Appl.* 2, 1–28. doi: 10.1007/s41315-017-0042-6

Andrews, B. J., Baxendale, R. H., Barnett, R., Phillips, G. F., Yamazaki, T., Paul, J. P., et al. (1988). Hybrid FES orthosis incorporating closed loop control and sensory feedback. *J. Biomed. Eng.* 10, 189–195. doi: 10.1016/0141-5425(88)90099-4

Bajd, T., Kralj, A., Stefancic, M., and Lavrac, N. (1999). Use of functional electrical stimulation in the lower extremities of incomplete spinal cord injured patients. *Artif. Organs* 23, 403–409. doi: 10.1046/j.1525-1594.1999.06360.x

Biering-Sørensen, F., Nielsen, J. B., and Klinge, K. (2006). Spasticity-assessment: a review. *Spinal Cord* 44, 708–722. doi: 10.1038/sj.sc.3101928

Bohannon, R. W., and Smith, M. B. (1987). Interrater reliability of a modified ashworth scale of muscle spasticity. *Phys. Ther.* 67, 206–207. doi: 10.1093/ptj/67.2.206

Bulea, T. C., Kobetic, R., Audu, M. L., Schnellenberger, J. R., and Triolo, R. J. (2013). Finite State Control of a Variable Impedance Hybrid Neuroprosthesis for Locomotion After Paralysis. *IEEE Trans. Neural Syst. Rehab. Eng.* 21, 141–151. doi: 10.1109/TNSRE.2012.2227124

Chang, S. R., Kobetic, R., and Triolo, R. J. (2017). Effect of exoskeletal joint constraint and passive resistance on metabolic energy expenditure: implications for walking in paraplegia. *PLoS ONE* 12:e0183125. doi: 10.1371/journal.pone.0183125

Contreras-Vidal, J. L., A Bhagat, N., Brantley, J., Cruz-Garza, J. G., He, Y., Manley, Q., et al. (2016). Powered exoskeletons for bipedal locomotion after spinal cord injury. *J. Neural Eng.* 13:031001. doi: 10.1088/1741-2560/13/3/031001

Decq, P. (2003). Pathophysiology of spasticity. *Neuro-Chirurgie* 49 (2–3 Pt 2), 163–184.

del-Ama, A. J., Gil-Agudo, A., Pons, J. L., and Moreno, J. C. (2014). Hybrid FES-robot cooperative control of ambulatory gait rehabilitation exoskeleton. *J. Neuro Eng. Rehab.* 11:27. doi: 10.1186/1743-0003-11-27

Demirel, G., Yilmaz, H., Paker, N., and Onel, S. (1998). Osteoporosis after spinal cord injury. *Spinal Cord* 36, 822–826. doi: 10.1038/sj.sc.3100704

Embrey, D. G., Holtz, S. L., Alon, G., Brandsma, B. A., and McCoy, S. W. (2010). Functional electrical stimulation to dorsiflexors and plantar flexors during gait to improve walking in adults with chronic Hemiplegia. *Arch. Phys. Med. Rehab.* 91, 687–696. doi: 10.1016/j.apmr.2009.12.024

Esquenazi, A., Talaty, M., Packel, A., and Saulino, M. (2012). The rewalk powered exoskeleton to restore ambulatory function to individuals with thoracic-level motor-complete spinal cord injury. *Am. J. Phys. Med. Rehab.* 91, 911–921. doi: 10.1097/PHM.0b013e318269d9a3

Goldfarb, M., Korkowski, K., Harrold, B., and Durfee, W. (2003). Preliminary evaluation of a controlled-brake orthosis for FES-Aided Gait. *IEEE Trans. Neural Syst. Rehab. Eng.* 11, 241–248. doi: 10.1109/TNSRE.2003.816873

Graupe, D., and Bazo, H. A. C. (2015). Thoracic level complete Paraplegiaâ¿'walking performance, training and medical benefits with the PARASTEP FES system. *Int. J. Phys. Med. Rehab.* 3:298. doi: 10.4172/2329-9096.1000298

Ha, K. H., Murray, S. A., and Goldfarb, M. (2016). An approach for the cooperative control of FES with a powered exoskeleton during level walking for persons with paraplegia. *IEEE Trans. Neural Syst. Rehab. Eng.* 24, 455–466. doi: 10.1109/TNSRE.2015.2421052

Hartigan, C., Kandilakis, C., Dalley, S., Clausen, M., Wilson, E., Morrison, S., et al. (2015). Mobility outcomes following five training sessions with a powered exoskeleton. *Topics Spinal Cord Injury Rehab.* 21, 93–99. doi: 10.1310/sci2102-93

Isakov, E., Douglas, R., and, Berns, P. (1992). Ambulation using the reciprocating gait orthosis and functional electrical stimulation. *Spinal Cord* 30, 239–245. doi: 10.1038/sc.1992.62

Kolakowsky-Hayner, S. A. (2013). Safety and feasibility of using the eksotm bionic exoskeleton to aid ambulation after spinal cord injury. *J. Spine*. S4:003. doi: 10.4172/2165-7939.S4-003

O'Dell, M. W., Dunning, K., Kluding, P., Wu, S. S., Feld, J., Ginosian, J., et al. (2014). Response and prediction of improvement in gait speed from functional electrical stimulation in persons with poststroke drop foot. *PM&R* 6, 587–601. doi: 10.1016/j.pmrj.2014.01.001

Quintero, H. A., Farris, R. J., Hartigan, C., Clesson, I., and Goldfarb, M. (2011). A powered lower limb orthosis for providing legged mobility in paraplegic individuals. *Topics Spinal Cord Injury Rehab.* 17, 25–33. doi: 10.1310/sci1701-25

Sherrington, C. S. (1910). Flexion-reflex of the limb, crossed extension-reflex, and reflex stepping and standing. *J. Physiol.* 40 (1–2), 28–121. doi: 10.1113/jphysiol.1910.sp001362

Street, T., and Singleton, C. (2017). A clinically meaningful training effect in walking speed using functional electrical stimulation for motor-incomplete spinal cord injury. *J. Spinal Cord Med.* 41, 361–366. doi: 10.1080/10790268.2017.1392106

Young, W. (2015). Electrical stimulation and motor recovery. *Cell Trans.* 24, 429–446. doi: 10.3727/096368915X686904

Zehr, E. P., Komiyama, T., and Stein, R. B. (1997). Cutaneous reflexes during human gait: electromyographic and kinematic responses to electrical stimulation. *J. Neurophysiol.* 77, 3311–3325. doi: 10.1152/jn.1997.77.6.3311

Conflict of Interest Statement: MG is an inventor on intellectual property that has been licensed by Vanderbilt University to the Parker Hannifin Corporation for use in the Indego exoskeleton.

The other author declares that the research was conducted in the absence of any commercial or financial relationships that could be construed as a potential conflict of interest.

frontiers in Neuroscience

ORIGINAL RESEARCH
published: 13 July 2018
doi: 10.3389/fnins.2018.00471

A Prototype of a Neural, Powered, Transtibial Prosthesis for the Cat: Benchtop Characterization

Hangue Park[1,2†], Muhammad S. Islam[3], Martha A. Grover[4], Alexander N. Klishko[2], Boris I. Prilutsky[2] and Stephen P. DeWeerth[1,5]*

[1] School of Electrical and Computer Engineering, Georgia Institute of Technology, Atlanta, GA, United States, [2] Biomechanics and Motor Control Laboratory, School of Biological Sciences, Georgia Institute of Technology, Atlanta, GA, United States, [3] Wallace H. Coulter Department of Biomedical Engineering, Georgia Institute of Technology, Atlanta, GA, United States, [4] School of Chemical & Biomolecular Engineering, Georgia Institute of Technology, Atlanta, GA, United States, [5] P.C. Rossin College of Engineering and Applied Science, Lehigh University, Bethlehem, PA, United States

OPEN ACCESS

Edited by:
Daniel P. Ferris, University of Florida, United States

Reviewed by:
Elliott J. Rouse, University of Michigan, United States
Corey Pew, University of Texas at Austin, United States

***Correspondence:**
Boris I. Prilutsky
boris.prilutsky@ap.gatech.edu

†Present address:
Hangue Park, Department of Electrical and Computer Engineering, Texas A&M University, College Station, TX, United States

Specialty section:
This article was submitted to Neuroprosthetics, a section of the journal Frontiers in Neuroscience

Received: *30 December 2017*
Accepted: *21 June 2018*
Published: *13 July 2018*

Citation:
Park H, Islam MS, Grover MA, Klishko AN, Prilutsky BI and DeWeerth SP (2018) A Prototype of a Neural, Powered, Transtibial Prosthesis for the Cat: Benchtop Characterization. Front. Neurosci. 12:471. doi: 10.3389/fnins.2018.00471

We developed a prototype of a neural, powered, transtibial prosthesis for the use in a feline model of prosthetic gait. The prosthesis was designed for attachment to a percutaneous porous titanium implant integrated with bone, skin, and residual nerves and muscles. In the benchtop testing, the prosthesis was fixed in a testing rig and subjected to rhythmic vertical displacements and interactions with the ground at a cadence corresponding to cat walking. Several prosthesis functions were evaluated. They included sensing ground contact, control of transitions between the finite states of prosthesis loading, and a closed-loop modulation of the linear actuator gain in each loading cycle. The prosthetic design parameters (prosthesis length = 55 mm, mass = 63 g, peak extension moment = 1 Nm) corresponded closely to those of the cat foot-ankle with distal shank and the peak ankle extension moment during level walking. The linear actuator operated the prosthetic ankle joint using inputs emulating myoelectric activity of residual muscles. The linear actuator gain was modulated in each cycle to minimize the difference between the peak of ground reaction forces (GRF) recorded by a ground force sensor and a target force value. The benchtop test results demonstrated a close agreement between the GRF peaks and patterns produced by the prosthesis and by cats during level walking.

Keywords: bone-anchored transtibial prosthesis, sensing and powered prosthesis, closed-loop control, cat, ground reaction force

INTRODUCTION

Individuals with lower limb loss wearing a unilateral passive prosthesis frequently show asymmetric walking, which can lead to undesirable compensations and subsequent degenerative musculoskeletal conditions (Burke et al., 1978; Jaegers et al., 1995; Struyf et al., 2009). Among the variety of underlying reasons causing locomotor asymmetry, the inappropriate motor output and the lack of somatosensory feedback from the prosthetic limb are probably most important (Hof et al., 2007; Kannape and Herr, 2014). To correct these motor and sensory deficits, it is necessary to establish a bidirectional communication interface between the nervous system and the prosthesis.

Recent studies have shown the feasibility of replicating tactile sensory feedback from the amputated, phantom limb by electrical stimulation to residual cutaneous nerves (Dhillon et al., 2004; Ortiz-Catalan et al., 2014; Tan et al., 2014; Davis et al., 2016; Graczyk et al., 2016). Myoelectric signals with built-in pattern recognition algorithms enable fine motor control in arm prostheses, even without any sensory feedback (Li et al., 2010; Tkach et al., 2014). Likewise, it might be possible to improve locomotor outcome measures (e.g., walking symmetry) by controlling a powered prosthesis or orthosis using myoelectric signals from residual or intact muscles (Sawicki and Ferris, 2009; Herr and Grabowski, 2012; Takahashi et al., 2015; Kannape and Herr, 2016).

Recent developments of bone-anchored lower limb prostheses have improved the load transmission to the skeletal system, range of motion, comfort, and osseoperception (Hagberg and Branemark, 2009; Juhnke et al., 2015; Leijendekkers et al., 2016). In addition, bone-anchored limb prostheses may potentially allow for a secure and stable neural interface between the residual nerves and muscles and the prosthesis (Pitkin et al., 2012; Al-Ajam et al., 2013; Ortiz-Catalan et al., 2014).

We have used rodent and feline animal models to test integration of skin-and-bone integrated pylons (SBIP) with the residual tissue (Pitkin et al., 2009; Farrell et al., 2014b,c; Jarrell et al., 2018). These studies have demonstrated the potential of the SBIP implant to provide secure, infection-free fixation of the prosthesis to the residual limb. This type of implant can also be used as a gateway for transmission of nerve and myoelectric signals between the residual limb and prosthesis (Pitkin et al., 2012). For example, pressure applied to the prosthesis during the stance phase of walking can be transmitted to the nervous system via electrical stimulation of residual cutaneous nerves (Park et al., 2015, 2016), whereas myoelectric activity recorded in residual muscles can be used to drive prosthetic actuators.

Although bone-anchored powered transtibial prostheses integrated with sensory and motor nerve fibers or muscles via a percutaneous pylon have the great potential for improving quality of prosthetic locomotion as discussed above, there have been no rigorous studies on animal models that tested the feasibility and performance of such prostheses. Prior to implementing this technology in people with limb loss, preclinical animal studies should address the following important questions: (i) Do these prostheses improve symmetry of locomotion and to what extent? (ii) How does continual electrical stimulation of peripheral nerves affect the nerve structural integrity and function? (iii) Does stimulation of sensory nerves engage proper reflex responses and how they change over time? (iv) Do residual muscles and their myoelectric activity controlling prosthetic actuators degrade over time to a degree that cannot be compensated by the control system? (v) Does the porous titanium implant serving as a prosthesis-body gateway allow for skin ingrowth and reduction of the infection rate, etc.

The use of animal models for testing sensing, powered prostheses during locomotion may be challenging. The first challenge is securing a limb prosthesis on the animal. Rodents, cats, and dogs are notorious for removing externally attached assistive devices (Mich, 2014); therefore, the use of bone-anchored implants for prosthesis attachment appears a viable option (Fitzpatrick et al., 2011; Farrell et al., 2014b; Jarrell et al., 2018). Another challenge is strict limitations on prosthesis small size and mass and a relatively high power output. For the cat of 3 to 4 kg, for example, the half of tibia length is approximately 55 mm (Klishko et al., 2014); mass of the foot with half of the shank is ∼80 g (Hoy and Zernicke, 1985); the average peak of the ankle moment during level walking is 0.73–0.75 Nm (Gregor et al., 2006; Prilutsky et al., 2011); and the average peak of ankle positive power in the same conditions is 0.86 W (Prilutsky et al., 2011). Thus, each component of the prosthesis [prosthetic foot, sensors, actuator, battery, neural stimulator and amplifier, microprocessor unit (MCU), and electronics] should be carefully selected to satisfy these requirements. ABS plastic, carbon fiber, or fiberglass are lightweight materials with high ultimate strength and can be used for prosthetic foot fabrication (Delussu et al., 2013; Farrell et al., 2014b; Corbett et al., 2018). Options for appropriate prosthetic actuators and batteries are more limited as they need to satisfy the conflicting requirements for lightweight and high power output. Soft pneumatic actuators, satisfying the above requirements, have been recently developed and used in limb prosthetic and orthotic applications in people and animals (Ferris et al., 2005; Roche et al., 2014; Florez et al., 2017). However, these actuators require large off-board air pressure regulators and therefore are better suited for rehabilitation and research of assisted locomotion on a treadmill. Linear electromechanical actuators has demonstrated sufficient power production in relatively light wearable, powered prosthetic ankles during human walking (Blaya and Herr, 2004; Garcia et al., 2011; Realmuto et al., 2011). Considering the above limitations on size, weight, and moment production for the cat prosthetic ankle, a miniature linear actuator (PQ12-63-06-P, Actuonix, BC, Canada) appears to be a good choice. With its small weight of 15 g, stroke length of 20 mm, and maximum force of 45 N, it should produce an extension ankle moment of ∼1 Nm with the moment arm of ∼0.025 m corresponding to that of the cat Achilles tendon (Prilutsky et al., 1996). A further challenge is the selection of an appropriate feedback control law for the prosthesis. Although a wide variety of feedback control laws are employed by terrestrial animals including humans during locomotion (Edwards and Prilutsky, 2017), proportional-derivative control laws are often used in orthotic-prosthetic ankle emulators controlled by powerful off-board electric motors or pressure regulators to reproduce either the desired joint moment or joint position (Sawicki and Ferris, 2009; Caputo and Collins, 2014). In wearable powered prostheses, finite-state controllers are often used that do not require exact tracking of a desired joint moment or angular trajectory (Au et al., 2007; Shultz et al., 2016) and thus permit the use of lighter and less powerful actuators.

The goal of this work was to develop and benchtop characterize a prototype of a bone-anchored, powered, and sensing transtibial prosthesis for a feline animal model of prosthetic gait. The developed prototype included an ABS plastic foot with force sensor, stimulator of a sensory nerve, EMG amplifier, linear actuator, battery, and microprocessor. The prototype satisfied the design criteria for prosthesis weight and

moment production. In benchtop testing, the performance of a finite-state control scheme for the prosthesis was evaluated by subjecting the prosthesis to rhythmic loading that simulated the stance and swing phases of locomotion. A force sensor on the ground detected two motion states – the stance and swing, and the linear actuator generated an extension and flexion moment, respectively. An empirical relationship between muscle activity and ankle moment developed using our previous data were simplified by a step function with a variable gain. The gain of the extension moment was adjusted in each cycle automatically via a wireless interface and off-board PC to reduce the error between the desired peak of the ground reaction force (GRF) and the measured peak. The prosthetic prototype was able to reproduce the desirable GRF peaks within several cycles.

MATERIALS AND METHODS

Prosthesis Design

Prosthesis Components

The prosthesis comprised (1) MCU, (2) EMG amplifier, (3) current stimulator, (4) force-position sensor, (5) linear actuator, (6) battery and coil, (7) power management, and (8) prosthetic foot. (1) The MCU model CC2510F32 (Texas Instruments, TX, United States) included 8051 microcontroller and wireless transceiver with low-power consumption. (2) EMG amplifier INA128 with gain of 1000 (V/V) (Texas Instruments, TX, United States) included an embedded Sallen-Key active band-pass filter to suppress both motion artifact and ambient noise. (3) Current stimulator had discrete n-type field effect transistors (nFETs) and p-type field effect transistors (pFETs) designed to generate biphasic current pulses, while a programmable resistor AD5162 (Analog Devices, MA, United States) adjusted the current level of the pulses using current steering. The stimulator was tested in walking cats – electrical stimulation was applied to the distal tibial nerve during the stance phase of walking and reduced or reversed effects of paw pad anesthesia on the duty factor and step length symmetry (Park et al., 2015, 2016). (4) ThinPot linear force-position sensor (Spectra Symbol, UT, United States) was fixed on the bottom of the J-shaped foot, between the J-shaped plastic foot and the rubber layer. The sensor can record normal force with the 1-bit resolution at a threshold of 0.7 N. This is sufficient to detect paw contact during walking in cats (Park et al., 2015, 2016). (5) A miniature linear actuator PQ12-63-06-P (Actuonix, BC, Canada) with a brushed DC motor and transmission gear with a 63:1 ratio can produce a 20-mm stroke, which corresponds approximately to muscle-tendon unit length changes of a cat ankle extensor (soleus, SO) during locomotion (Gregor et al., 2006). This single linear actuator with an H-bridge motor driver (DRV8837, Texas Instruments, TX, United States) could extend and flex the prosthetic joint and thus reproduce actions of the ankle extensors (e.g., SO) and flexors (e.g., tibialis anterior, TA). (6) A Li-polymer rechargeable battery GM053040 (550 mAh, 5 mm × 30 mm × 40 mm) was selected as the power source. Its maximum discharge current (550 mA) corresponds to the maximum stall current of the linear actuator PQ12-63-06-P. We estimated the battery would last before recharging for 1.5 h based on current requirements of the linear actuator to generate force of 20 N (∼200 mA), current requirements for other electronic components (<20 mA), the DC–DC conversion ratio (∼2:1) and efficiency (∼85%), and walking duty cycle (<75%). The inductive coil was provided for wireless recharging. (7) Power management generated 3V outputs for the MCU and foot force-position sensor, 5 V outputs for the EMG amplifier and current stimulator, and a 6 V output for the linear actuator. (8) J-shaped foot was 3D printed from the ABS plastic capable of withstanding forces of 60–90 N that exceed peak ground reaction forces (GRF) during cat walking by two to three times (Corbett et al., 2018). The diagram in **Figure 1** illustrates the signal and power flow between the prosthetic components. The signal flow from the ThinPot linear force-position sensor on the foot (4) to the current stimulator (3) represents the sensory pathway (green arrows), whereas the signal flow from the EMG amplifier (2) to the linear actuator (5) – the motor pathway (blue arrows).

The prosthesis was wirelessly connected with external devices, i.e., a force sensing resistor FSR406 (Interlink Electronics, CA, United States) mounted on the floor and a computer monitoring GRF and adjusting a motor gain of the linear actuator in real time. An external MCU with a wireless transceiver and microcontroller provided communications between the external devices (**Figure 2**) and the prosthesis.

Prosthesis Assembly

A rectangular aluminum bar (6061-T6511, Metalsdepot, KY, United States) 55 mm in length served as a structural frame for the prosthesis (**Figure 3**). The bar was connected to the J-shaped plastic foot via a pivot. The aluminum bar was also connected to the percutaneous pylon that would be implanted into the medullary cavity of the cat tibia and interfaced with residual cutaneous nerves and SO and TA muscles via implanted electrodes.

The linear actuator (see above) was attached to a posterior side of the aluminum bar at a 25-mm distance from the ankle pivot (this distance approximately corresponds to the moment arm of the cat Achilles tendon with respect to the ankle (Goslow et al., 1973; Prilutsky et al., 1996). Two separate printed circuit boards (PCBs) were placed to the right of the linear actuator and the flat part of the J-shaped foot. The MCU, wireless interface, EMG amplifier, and power management integrated with the PCB were placed to the right of the linear actuator. The motor driver, sensor interface, and stimulator integrated with the PCB were fixed on the flat part of J-shaped foot. Finally, a Li-polymer rechargeable battery was mounted to the left of the linear actuator.

The prosthesis components were selected to satisfy the design criteria for prosthesis weight and moment production. As a result, the prosthesis mass was 63 g with the maximum available moment (stall moment) of 1 Nm. The stall moment was calculated from the maximum push/pull force of the linear actuator (40 N) and the actuator moment arm with respect to the pivot (note that we measured the maximum force of the linear actuator and the obtained value of 40 N was slightly lower that

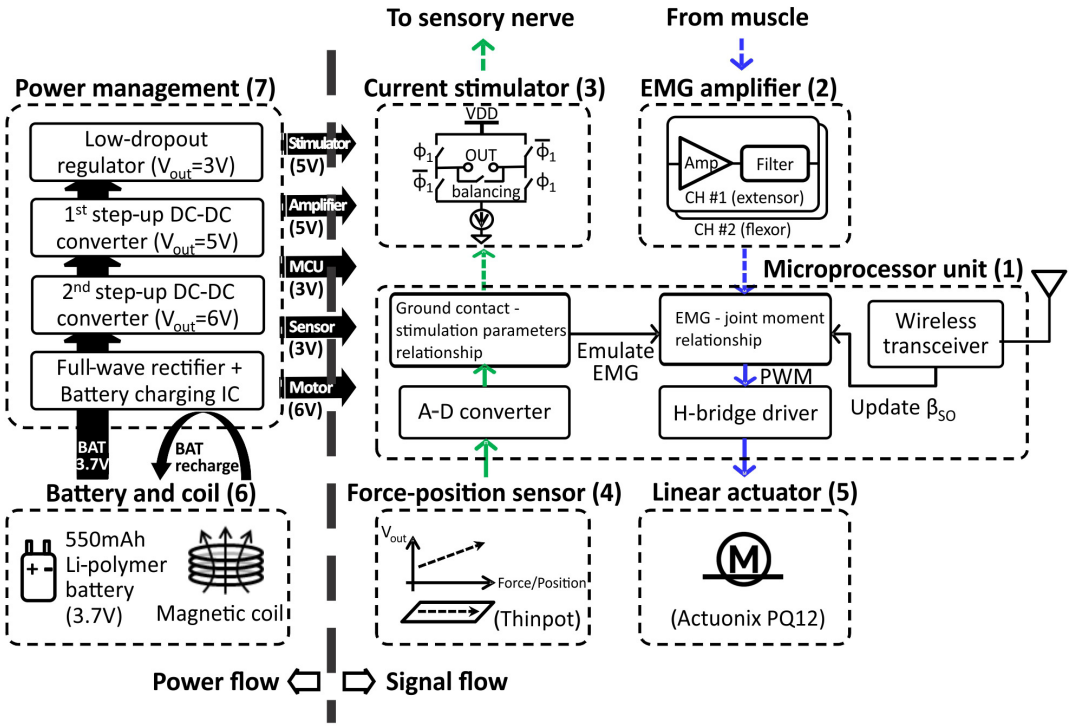

FIGURE 1 | Block diagram illustrating power flow (on left) and signal flow (on right) between prosthetic components. The sensory pathway of signal flow on right is indicated by the green arrows; the motor pathway is indicated by blue arrows. The pathways represented by dashed arrows are not implemented in the prosthetic prototype, but will be implemented when the prosthesis is worn by the cat. See text for details.

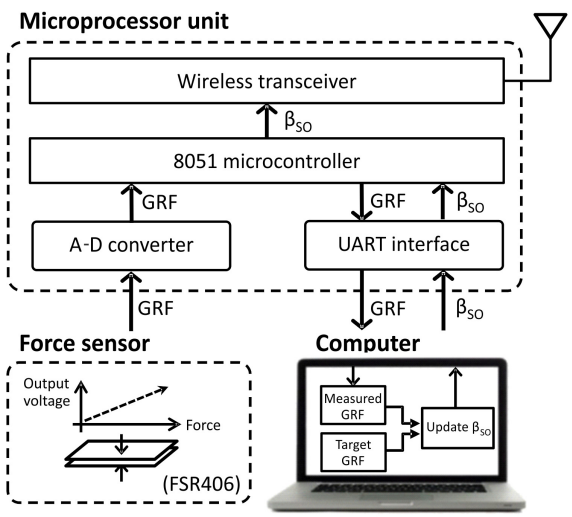

FIGURE 2 | Block diagram of external devices (computer, ground force sensor, and microprocessor unit) that update the extension gain β_{SO}, based on the ground reaction force (GRF) peak, and transmit it wirelessly to the prosthesis. See text for details.

45 N reported by manufacturer). The value of 1 Nm is close to the maximum ankle moment during level walking in the cat (McFadyen et al., 1999; Gregor et al., 2006; Prilutsky et al., 2011).

Prosthesis Control

Finite-State Controller

A simple finite-state machine controller was implemented to control the linear actuator (**Figure 4A**). Transitions between the two states – stance and swing – depended on the presence of contact with the ground and EMG activity of a residual ankle extensor and flexor muscles. Transition from the stance to swing state was triggered by (i) foot unloading (interruption of contact with the ground), (ii) terminating EMG activity of the ankle extensor, and (iii) initiating EMG activity of the ankle flexor (**Figure 4A**). These three conditions triggered a pushing stroke of the linear actuator leading to a flexor moment at the ankle. Transition from the swing to stance state was initiated by (i) onset of ground contact with the foot, (ii) onset of EMG activity of the ankle extensor, and (iii) offset of EMG activity of the ankle flexor. These conditions triggered a pulling stroke of the linear actuator producing an extension ankle moment.

Ankle Moment–EMG Relationship

To modulate the output of the linear actuator during the stance and swing states of walking, we established a relationship between EMG activities recorded from ankle extensor and flexor muscles and the resultant ankle moment (motor pathway, **Figure 1**).

The relationship between EMG activity of an ankle extensor SO and ankle flexor TA and ankle moment during level walking in the cat was obtained from previously recorded EMGs and ankle moment (Prilutsky et al., 2011;

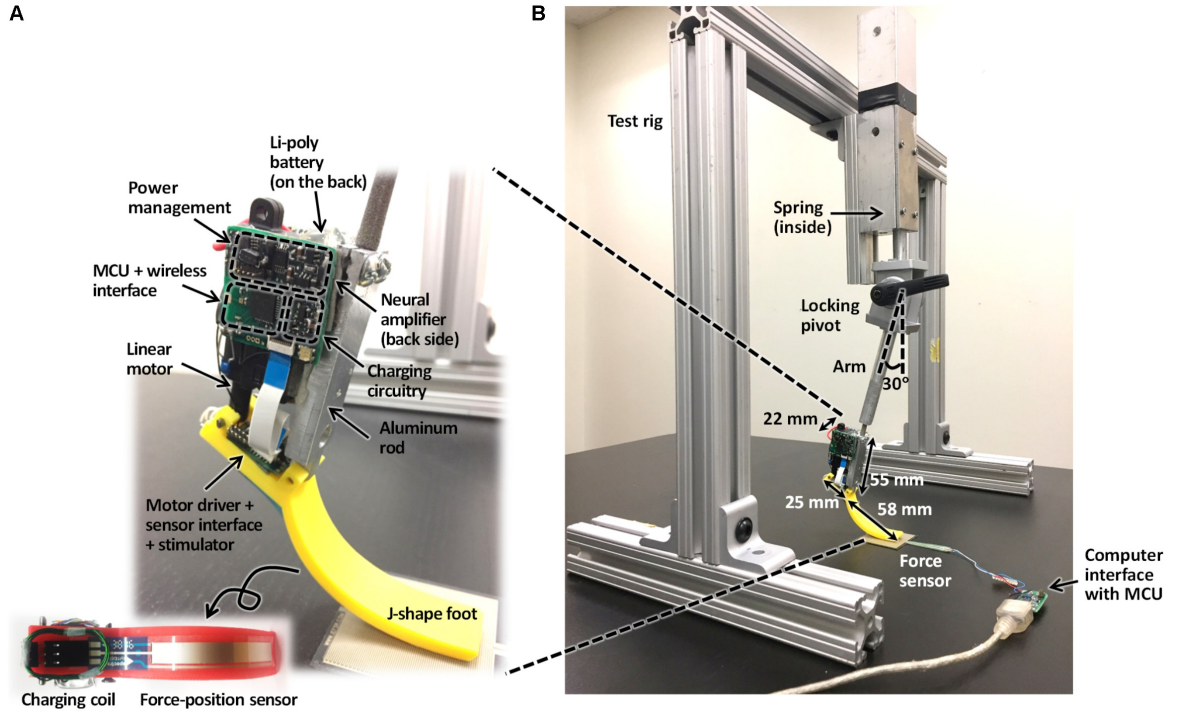

FIGURE 3 | Prosthesis prototype **(A)** and test rig with the attached prosthesis **(B)**.

Markin et al., 2012) using a multivariate linear regression analysis in software STATISTICA 7 (StatSoft, United States). The equation had the following form (Prilutsky et al., 2005):

$$M_{ANK}(t) = \beta_0 + \beta_{SO} EMG_{SO}(t - \Delta t) + \beta_{TA} EMG_{TA}(t - \Delta t), \quad (1)$$

where M_{ANK} is the ankle joint moment in Nm; EMG_{SO} and EMG_{TA} are normalized EMG activities of SO and TA muscles, changing from 0 to 1; t is time and $\Delta t \approx 60$ ms is the electromechanical delay between the appearance of EMG activity and the onset of the resultant joint moment (Gregor et al., 2006); $\beta_o \approx 0$ (see Results), β_{SO} and β_{TA} are empirical constants (measured in Nm). Approximately two-thirds of total 22 walking cycles ($n = 15$) from three cats were randomly selected and used to derive regression equation (1). The remaining cycles ($n = 7$) were used to compare the predicted ankle moment M_{ANK} with the experimental one. The detailed description of how the joint moments and EMG activities were obtained and processed can be found in the original publications (Prilutsky et al., 2005, 2011; Markin et al., 2012).

Ground Contact Pressure and Tactile Perception

In our preliminary studies (Park et al., 2015, 2016), we have established the relationship between output of the force-position sensor under the cat hindpaw and electrical stimulation of the distal tibial nerve (sensory pathway, **Figure 1**) that apparently perceived by the cat as contact with the ground during walking. When the output of the force sensor exceeded a threshold (indicating the stance phase), the current stimulator delivered stimulation (trains of 200-μs biphasic rectangular pulses, 100 Hz, 1.2 T) to the distal tibial nerve. This sensory nerve stimulation reduced or reversed effects of local anesthesia of the ipsilateral hind- and forepaws on the step length symmetry and duty factor (Park et al., 2015, 2016).

Implementation of Control During Benchtop Testing

For benchtop testing of the developed prosthesis outside the animal in this study, both the sensory and motor pathways were simplified. The simplified sensory pathway transmitted information about the timing of ground contact, measured by the force-position sensor on the foot, to the linear actuator instead of the current stimulator (**Figure 1**). The timing of ground contact was described as a unit step function $S(t)$:

$$S(t) = H(F(t) - F_{TH}), \quad (2)$$

where $F(t)$ is the recorded force-position sensor output, F_{TH} is the force detection threshold, and $H(x)$ is a Heaviside step function, i.e., $H(x) = 1$ if $x > 0$ and $H(x) = 0$ if $x \leq 0$. Function $S(t)$ defined the stance and swing phases (finite states of the system; **Figure 4A**), and this phase information was used to emulate a simplified motor pathway, i.e., the relationship between the ankle moment and EMG of SO and TA muscles. Specifically, EMG activity of SO and TA muscles was emulated by unit step functions representing the timing of muscle activity derived from the ground contact information. SO EMG was computed as

$$EMG_{SO}(t) = S(t - \Delta t_{SO}) - S(t - (\Delta t_{SO} + T_{SO})), \quad (3)$$

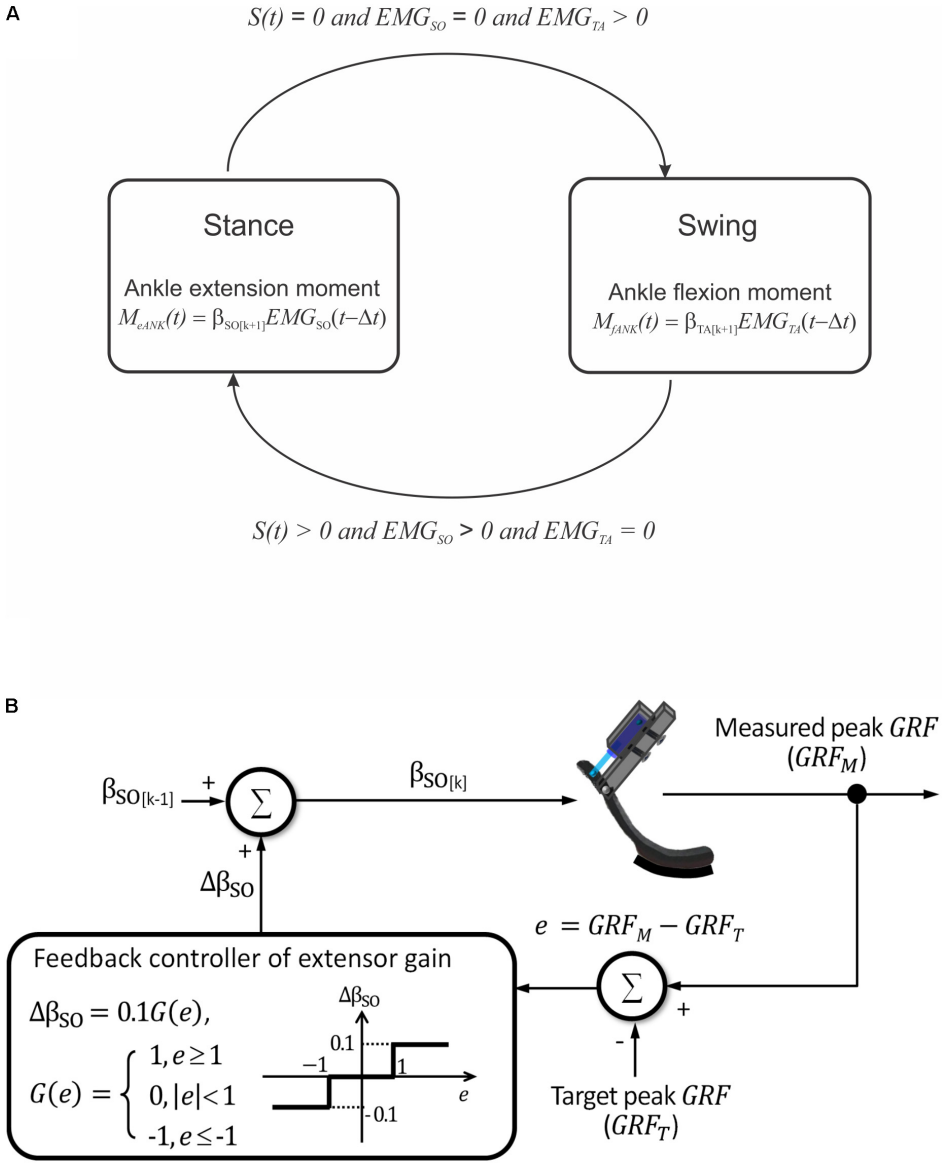

FIGURE 4 | Schematics illustrating prosthesis control. **(A)** Two finite states of prosthesis loading and conditions for transitions between them. *S(t)* is a step function indicating presence [*S(t)* > 0] or absence [*S(t)* = 0] of ground contact. EMG_{SO} and EMG_{TA} are step functions indicating presence or absence of EMG activity in ankle extensor soleus (SO) and ankle flexor tibialis anterior (TA), respectively. **(B)** Closed-loop modulation of extension gain b_{SO}. The gain is changed by 10% in each cycle *k* depending on the value of error *e* between the measured and target peaks of ground reaction force (GRF).

where Δt_{SO} is the phase delay between the previous stance phase offset and subsequent SO EMG onset, T_{SO} is the duration of EMG_{SO} activity, *S(t)* is the step function representing contact information (see Eq. 2). In the tests described here, the following parameters of Eq. 3 were used (Prilutsky et al., 2005, 2011; Markin et al., 2012): Δt_{SO} = 100 ms and T_{SO} = 500 ms.

TA EMG activity was computed as

$$EMG_{TA}(t) = S(t - \Delta t_{TA}) - S(t - (\Delta t_{TA} + T_{TA})) \quad (4)$$

where Δt_{TA} is the phase delay between the previous stance phase onset and subsequent TA EMG onset, T_{TA} is the duration of EMG_{TA} activity; Δt_{TA} = 400 ms and T_{TA} = 200 ms (Prilutsky et al., 2005, 2011; Markin et al., 2012).

The emulated EMG signals (Eqs 3 and 4) were used to control the linear actuator with a dual polarity. The ankle joint moment was calculated using Eq. 1 and emulated EMG activity of SO and TA obtained from Eqs 3 and 4 (**Figure 4A**). Because SO and TA during walking have reciprocal activity and β_0 is close to zero (see Eq. 1 and Results), calculations of the ankle extension and flexion moments were simplified as $M_{e\,ANK}(t) = \beta_{SO}\, EMG_{SO}(t - \Delta t)$, and $M_{f\,ANK}(t) = \beta_{TA}\, EMG_{TA}(t - \Delta t)$, respectively (see **Figure 4A**). In these equations, β_{SO} and β_{TA} are extension and flexion motor gains.

Closed-Loop Updates of Extension Motor Gain

The maximum of extension gain β_{SO} was set at 1 Nm. The updated value of the gain in a next cycle could be increased or decreased by 10% depending on the difference $e = GRF_M - GRF_T$ between the measured GRF peak (GRF_M) and a target GRF peak (GRF_T), respectively, in the current cycle (**Figure 4B**):

$$\beta_{SO[K]} = \beta_{SO[K-1]} + 0.1\,G(e) \quad (5)$$

where k is the cycle number and $G(e) = 1$ *if* $e \geq 1$, $G(e) = 0$ *if* $|e| < 1$, $G(e) = -1$ *if* $e \leq -1$. Thus, if the GRF_M exceeded or was less than the target value by 1 N or more, the current extension gain would be decreased or increased by 10%, respectively; otherwise, the gain would not change (**Figure 4B**).

Benchtop Characterization of Prosthesis

During the benchtop characterization, we imposed rhythmic loading on the prosthesis to simulate the stance and swing phases of walking and to test the finite-state machine controller (**Figure 4A**) with a closed-loop modulation of the extension gain in real time (**Figure 4B**).

Design of a Test Rig

To perform benchtop characterization, we designed a test rig made of aluminum bars with L-shaped connectors, a zinc-plated compression spring, locking pivot, and prosthesis support arm (**Figure 3B**). The force produced by the compressed spring, along with the weight of the prosthesis and its support arm, caused loading of the prosthesis during contact with the ground that was comparable to GRF exerted by the hindpaw during normal level walking in the cat. The support arm was set at a vertical angle of 30° so that the J-shaped prosthetic foot could be in contact with the ground starting at both full flexion (at foot contact) until full extension (foot off) of the ankle joint.

Test Procedure

Each test cycle started from onset of the swing state of the controller – the prosthesis foot was positioned just above the ground, prosthetic ankle was fully extended, and the linear actuator started producing a flexion ankle moment. This prosthesis position corresponded to full relaxation of the compression spring. The researcher raised the prosthesis by the hand to a height of ∼40 mm, at which the spring was fully compressed, and then the prosthesis was released. The fully compressed spring accelerated the prosthesis toward the ground vertically. Given spring deformation of ∼40 mm and stiffness of 0.36 N/mm, the spring applied ∼14 N to the prosthesis when it was released by the hand.

When the prosthesis touched the ground, the foot force-position sensor detected the ground contact and the conditions for the swing to stance state transition were satisfied: $S(t) > 0$ (Eq. 2), $EMG_{SO} > 0$ (Eq. 3), and $EMG_{TA} = 0$ (Eq. 4). At that instant, the linear motor initiated a pull stroke and generated extension ankle moment (M_{eANK}, see **Figure 4A**). When the prosthetic joint reached the maximum extension at the end of stance phase, the prosthesis was lifted by the experimenter's hand and raised against the compression spring as described above. As soon as ground contact was lost, the conditions for the stance to swing state transition were satisfied: $S(t) = 0$ (Eq. 2), $EMG_{SO} = 0$ (Eq. 3), and $EMG_{TA} > 0$ (Eq. 4). At that instant, a flexion ankle moment was generated (M_{fANK}, see **Figure 4A**), and the prosthesis joint angle returned to the fully flexed position. Cadence of prosthesis loading in these tests corresponded to a typical cadence of walking cats (Gregor et al., 2006).

We also tested the ability of the feedback controller to modulate the extension gain β_{SO} and thus the magnitude of the exerted ankle moment (M_{eANK}, **Figures 4A,B**) in real-time. The produced peak GRF (GRF_M) was measured by the force sensor FSR406, mounted on the ground under the prosthesis foot (**Figure 3B**). The target value of GRF_T was set and compared with the GRF_M value in a custom designed LabView (National Instruments, TX, United States) application on the off-board computer. Based on the operating principle of the DC motor, we assumed that the extension gain β_{SO} (and thus extension moment M_{eANK}) was proportional to the duty cycle of pulse-width modulation (PWM) of control signal (Weber, 1965). The maximum value of extension gain ($\beta_{SO} = 1$ Nm) corresponded to the extension ankle moment $M_{eANK} = 1$ Nm and PWM = 100%. With this maximum gain, the linear actuator produced the maximum force of 40 N and could generate the maximum ground reaction peak of ∼13–15 N (see Results). The extension gain β_{SO} (corresponding to PWM) was updated in each test cycle based on Eq. 5 (**Figure 4B**). The closed-loop control system was tested at three target values of GRF_T: 14, 6, and 12 N. These three target forces were pre-programmed in the microprocessor to occur at the onset of testing, at the end of cycle 2 and at the end of cycle 8, respectively. During testing, the flexion gain β_{TA} was set at the maximum value of −1 Nm and not changed (**Figure 4A**).

RESULTS

Ankle Moment-EMG Relationship

Rectified and low-pass filtered EMG activities of SO and TA, as well as the corresponding ankle joint moments, recorded in Prilutsky et al. (2011), Markin et al. (2012) during 22 cycles of level walking in three cats (**Figures 5A–C**), were used to obtain the regression Eq. 1. The empirical constants in Eq. 1 were $\beta_0 = 0.023528$ Nm, $\beta_{S0} = 0.969663$ Nm, and $\beta_{TA} = 0.052416$ Nm. The coefficient of multiple correlation for Eq. 1 was $r = 0.874$ ($p < 0.05$). The ankle moment as a function of the normalized cycle time computed from SO and TA EMGs using Eq. 1 was generally within one standard deviation from the mean experimental moment (**Figure 5D**). As explained in Materials and Methods, SO and TA EMG activity was simplified for the purpose of the benchtop testing of the prosthesis by step functions EMG_{SO} and EMG_{TA} (Eqs 3 and 4). These step functions are shown in **Figures 5A,B** by red dashed rectangles.

Finite State Controller With Closed-Loop Update of Extension Gain

During rhythmic loading of the prosthesis, the finite state controller correctly identified the stance and swing states based

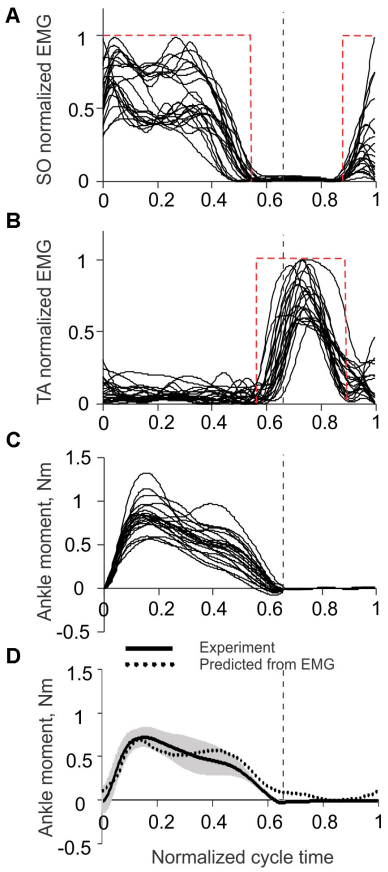

FIGURE 5 | Ankle joint moment and EMG activity of soleus (SO) and tibialis anterior (TA) muscles during level walking in the cat. The vertical dashed lines separate the stance and swing phases. Experimental EMG and ankle moment data are taken from 22 cycles of level walking of three cats (mass 3.55 ± 0.65 kg; mean ± SD) (Prilutsky et al., 2011; Markin et al., 2012). **(A)** Normalized SO EMG during level walking in the cat. The red dashed rectangle corresponds to emulated SO EMG signal (see text for details). **(B)** Normalized TA EMG during level walking in the cat. The red dashed rectangle corresponds to emulated TA EMG signal (see text for details). **(C)** Ankle joint moment during level walking in the cat; positive values correspond to extension (plantar flexion). **(D)** Ankle moment obtained experimentally (solid line with gray shade, mean ± SD) and predicted from SO and TA EMGs using Eq. 1 (dotted line). Positive values correspond to extension (plantar flexion).

on the signal from the force-position sensor on the bottom of the foot. The linear actuator produced pulling strokes (extension ankle moments) in the stance state and pushing strokes (flexion moments) in the swing state. In the example in **Figure 6A**, the prosthesis produced GRF in 14 cycles of rhythmic loading; the corresponding changes in the PWM duty cycle are shown in **Figure 6B**. In the first two cycles, the target GRF force was 14 N, which corresponded to the maximum capacity of the linear actuator (PWM duty cycle was 100%). Since the GRF peaks produced in these cycles were within ±1 N of the target value, the extension gain β_{SO}, and PWM were not changed (**Figure 6B**, Eq. 5). At the end of stance phase of cycle 2, when the target force was reduced from 14 to 6 N, the force error *e* (Eq. 5) was detected in stance of cycle 3 and the extension gain β_{SO}, and PWM were reduced by the control system by 10% in cycles 4 through 6 until the peak GRF error during stance became smaller than 1 N in cycle 7 (**Figure 6**). The peaks of GRF in cycles 7 and 8 were maintained near the target force of 6 N within ±1 N, and no changes in PWM occurred. After the target force changed at the end of cycle 8 from 6 to 12 N, the controller detected the force difference *e* in stance of cycle 9 and increased PWM by 10% in cycle 10. Since the measured GRF peaks in cycles 10 and 11 were lower than the target value, PWD was increased again by 10% in cycles 11 and 12. Since the GRF peaks in cycles 13 and 14 were within ±1 N from the target value of 12 N, no changes in PWD occurred in these cycles (**Figure 6**).

The peak GRF values during the transition period from the target change to achieving the target by the system (cycles 3 through 7 and 8 through 12; **Figure 6A**) could be considered the system step response to the error *e* input (**Figure 6B**). In the current control system design, the response time corresponded to the duration of one cycle. The prosthesis closely reproduced the target GRF peaks in steady state cycles 1–3, 7–9, and 12–14 (**Figure 6A**). The absolute error of peak GRF across all three target values was 0.31 ± 0.23 N (mean ± SD), and the relative error (absolute error normalized to the target value) was 3.49 ± 3.06%.

Ground Reaction Forces Produced by the Prosthesis

The time profiles of GRF measured under the prosthetic foot in 14 consecutive cycles had a double-peak pattern (**Figure 6A**). The mean GRF peak in cycles 1 through 3, where the PWM duty cycle was set to 100% to produce maximal GRF peaks, was 13.8 ± 0.5 N. This value was within one standard deviation of the GRF mean peak (14.9 ± 1.6 N) obtained in walking cats (**Figure 7**).

The comparison of the prosthetic GRF profiles averaged across cycles 1 through 3 with the experimental GRF recorded previously during level walking in cats (Prilutsky et al., 2011) – the same 22 cycles from which ankle moments and EMG patterns in **Figure 5** were obtained, demonstrated close qualitative and quantitative agreements (**Figure 7**). Specifically, both patterns had two peaks – one in the early stance phase (leg contact) and the other one in the late stance phase.

DISCUSSION

We developed a powered, sensing transtibial prosthesis for the use in the feline animal model of prosthetic gait. This animal model is needed for testing feasibility and performance of bone-anchored limb prostheses integrated with residual sensory nerves and muscles during locomotion (see Introduction). The size, mass, and maximum extension moment of the prosthesis closely matched the corresponding parameters of the cat foot-ankle with the distal shank and the peak ankle extension moment produced during level walking in the cat (Gregor et al., 2006, 2018; Prilutsky et al., 2011). The prosthetic powered ankle joint was designed for control of the linear actuator by the recorded EMG activity of the residual ankle extensor and

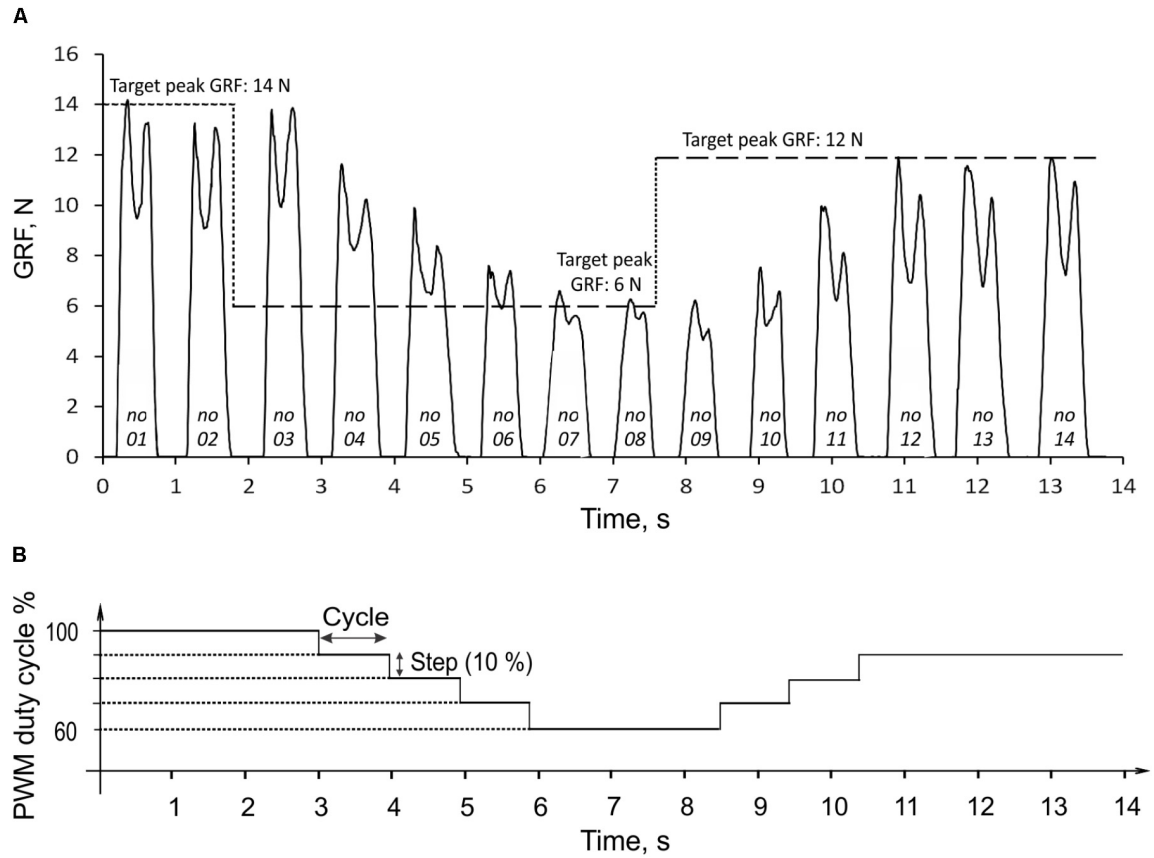

FIGURE 6 | Ground reaction force (GRF) during 14 cycles of prosthesis loading **(A)** and the corresponding changes in PWM duty cycle of the actuator **(B)**. The three target values of GRF peak (14, 6, and 12 N) are indicated by the horizontal dashed lines in **(A)**. The numbers at bottom of force traces indicate the cycle number. For details, see text.

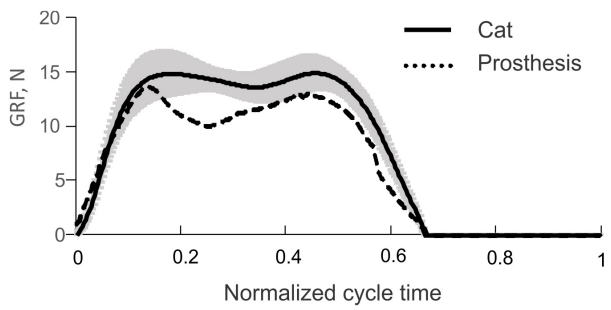

FIGURE 7 | Vertical ground reaction force (GRF) recorded during level walking in the cat (solid line and shade, mean ± SD; computed using data from Prilutsky et al., 2011) and mean GRF recorded during the first three cycles of prosthesis testing (dashed line), see **Figure 6A**.

flexor muscles. The ability of the prosthesis to detect timing of ground contact will allow for delivering tactile sensory feedback by phase dependent stimulation of sensory nerves. The foot force-position sensor detecting touch with the ground in this study was used in the past to trigger electrical stimulation of the distal tibial nerve during the stance phase of walking and to provide tactile feedback to the nervous system of walking cats with the anesthetized hindpaw (Park et al., 2015, 2016).

In the present benchtop testing of the prosthesis, only selected prosthesis functions were characterized. They included detecting timing of ground contact onset and offset, control of transitions between the stance and swing states by the finite-state machine controller, and a real-time automatic modulation of the extension gain based on the measured GRF peak in each loading cycle (**Figure 4**). The results of testing demonstrated that the prosthesis was able to produce the extension and flexion ankle moments in the appropriate loading states. The prosthesis was also able to generate appropriate GRF peaks by modulating the extension gain in a closed-loop real time control. In addition, the prosthesis was capable of generating realistic GRF forces similar to those observed during normal level walking in the cat. Although the maximum GRF peaks were slightly lower than the desired value of 15 N (a typical GRF peak during level walking in the cat) and much lower than peak forces during 27°-upslope walking (17-22 N; Gregor et al., 2006; Prilutsky et al., 2011), we expect that proximal joints may be able to compensate for this difference during cat walking with the powered prosthesis. This expectation is based on a recent study

demonstrating that cats walking with a passive bone-anchored transtibial prosthesis with no active ankle extension are able to generated ∼70 and ∼50% of the normal GRF peak observed in intact level and 27°-upslope walking, respectively (Jarrell et al., 2018).

The double-peak GRF profiles generated by the prosthesis (**Figure 6**) were not expected because the control system was designed to reproduce just a target GRF peak. It appears that the observed GRF profile is a result of interactions between the constant moment produced by the linear actuator and passive dynamics of the prosthesis and its support system. The two GRF peaks had different magnitudes, and the second peak was lower than the first (**Figure 6**).

The magnitude of the second peak of vertical GRF depends on the magnitude of ankle extension moment in the late-stance phase of prosthetic walking in humans. For example, reduction in passive foot stiffness leads to a parallel decrease in the second GRF peak and ankle extension moment peak (Fey et al., 2011). The use of powered ankle prostheses decreases or eliminates the differences in second GRF peak and ankle extension moment magnitude between the intact and prosthetic limbs in humans (Rabago et al., 2016; Shultz et al., 2016). Since our powered prosthesis with its control system is designed to maintain a target GRF peak, we do not expect a close match of the generated GRF profile with that of the intact animal. This expected mismatch should not necessarily lead to asymmetric walking unless there is a substantial mismatch in the GRF impulse.

The linear actuator PQ12-63-06-P was selected for the cat transtibial prosthesis because it satisfied strict limitations on the size and mass of the cat foot-ankle and distal shank. To maximize the force output of the actuator to ensure it could produce its maximum moment of 1 Nm, we increased its duty cycle from its optimum value of 20%, recommended by the manufacturer as the most efficient, to 100%. We verified consistency of the actuator operation with the duty cycle of 100% over multiple cycles in our benchtop prosthesis testing. We found that this linear actuator at the duty cycle of 100% could generate consistent levels of GRF for over 100 cycles. This number of cycles is sufficient for a single recording session in the cat.

It may be necessary to increase the moment arm of the linear actuator with respect to ankle joint or replace this actuator with a larger one if testing in the animal would demonstrate its inability to generate sufficient ankle moment and power. However, a larger size of the actuator and battery would increase demands on the knee and hip flexor muscles during the swing phase of walking and could lead to abnormal asymmetric locomotor pattern.

In our benchtop testing of the prosthesis prototype, the force sensing resistor FSR406 mounted on the floor (**Figure 3B**) measured vertical GRF peaks, and the linear force-position sensor (ThinPot) attached to the bottom of the foot (**Figure 3A**) detected ground contact timing used to emulate extensor and flexor EMG bursts and determined onset-offset times of the linear actuator (**Figure 4A**). In the actual implementation of the prosthesis in the animal, we plan to mount the force-sensing resistor FSR406 or a similar one on the bottom of the prosthetic foot to serve both functions, i.e., detecting ground contact and measuring GRF peaks. In that case, wireless communication between the prosthesis and external computer will be used to monitor, modify, and record characteristics of the control system (target GRF peaks, actuator gains, stimulation parameters, EMG, etc.).

One potential limitation of the force-sensing resistor FSR406 for monitoring the peak GRF is that it can only measure the normal component of the 3D GRF vector (vertical component in this study, **Figures 6A**, **7**), although the other two GRF components are also important for accurate description of foot interaction with the ground (Aubin et al., 2008). During level cat walking, the normal peak GRF force exceeds the anterior-posterior and medial-lateral peaks by ∼5 and >10 times, respectively (Farrell et al., 2014a). Thus, the peak of the normal GRG component might still be used to monitor and modify the prosthesis output during level walking in the cat. However, during 27°-upslope cat walking the normal and tangential (in progression direction) peaks are comparable (Gregor et al., 2006, 2018; Prilutsky et al., 2011). Therefore, for this walking condition some modifications in the GRF target or control algorithm may be necessary.

In the animal testing, the GRF peak measured by the force sensor FSR406 on the foot in each walking cycle will be compared with a preset target value, and gains β_{SO} and β_{TA} will be changed in real time if necessary. Information about ground contact onset and offset determined by the same sensor will be used to control timing of electrical stimulation of the sensory nerves. We could use the timing of ground contact to control the linear actuator as demonstrated in this study. However, we plan to use recorded EMG signals from residual SO and TA to estimate the ankle moment (Eq. 1) and use either the estimated moment peak or moment profile for control of the linear actuator. Gains β_{SO} and β_{TA} could be modified based on the measured GRF peaks (**Figure 4B**) or/and predicted ankle moment peak. This type of control seems more intuitive for the user (Ortiz-Catalan et al., 2014; Kannape and Herr, 2016) since it includes a highly adaptive living system in the control of the prosthesis output.

In our planned animal studies, we will evaluate the contribution of sensory nerve stimulation to SO and TA EMG activity magnitude, to symmetry of walking and to other locomotor characteristics by comparing walking with and without phase dependent stimulation of sensory nerves. Changes in quality of EMG signals and in activation thresholds of sensory nerves [recorded action potentials in the sciatic nerve in response to stimulation of the distal tibial, sural or superficial peroneal nerves while the animal is sedated (Ollivier-Lanvin et al., 2011; Park et al., 2016)] will be determined over several months. During testing the prosthesis in the animal model, we plan to add another sensory feedback signal – contact force from the dorsal surface of the prosthetic foot. Another force sensor FSR406 will detect contact of the dorsal surface of the prosthetic foot with an external object and trigger electrical stimulation of the superficial peroneal nerve if the contact occurs in the swing phase of locomotion. The superficial peroneal nerve is a cutaneous

nerve innervating skin on the dorsum of the foot (Crouch, 1969). Electrical stimulation of this nerve during swing elicits stumbling corrective response in the cat (Forssberg, 1979; Wand et al., 1980; Quevedo et al., 2005), which helps the animal avoid tripping by enhancing stepping over the obstacle.

In the end of the study, the animals will be euthanized and the residual limb with the porous titanium implant, residual muscles, and nerves with implanted electrodes will be harvested for histological analysis (Farrell et al., 2014b,c). This analysis will reveal the extent of skin and bone ingrowth into the percutaneous implant and integrity of implanted muscles and nerves. The results of our planned animal studies will inform future designs of transtibial prostheses integrated with the residual limb in people.

CONCLUSION

In conclusion, the designed prototype of a feline bone-anchored, sensing, powered transtibial prosthesis demonstrated the ability to reproduce values and patterns of the GRF observed during normal walking in the cat. The prosthesis dimensions, mass, and extension moment produced were similar to the corresponding characteristics of the cat. The prosthesis was designed for use with a porous titanium pylon implanted in tibia (Pitkin et al., 2012; Farrell et al., 2014b; Jarrell et al., 2018) that could serve as a gateway for transmission of feedback (from the prosthesis to the peripheral sensory nerves) and feedforward (from implanted muscle electrodes to the prosthetic actuator) signals between the prosthesis and the residual limb.

AUTHOR CONTRIBUTIONS

BP and SD did conception and design of research; HP, MI, BP, and SD did prosthesis design; HP, MG, AK, and PB did design of control algorithm; HP and MI did experimental recordings; HP analyzed data; HP, AK, and PB prepared figures. HP, MG, AK, BP, and SD interpreted results of experiments; HP and BP drafted manuscript; HP, MI, MG, AK, BP, and SD edited and revised manuscript and approved final version of manuscript.

FUNDING

The study was supported by U.S. Department of Defense Grant W81XWH-16-1-0791.

REFERENCES

Al-Ajam, Y., Lancashire, H., Pendegrass, C., Kang, N., Dowling, R. P., Taylor, S. J., et al. (2013). The use of a bone-anchored device as a hard-wired conduit for transmitting EMG signals from implanted muscle electrodes. *IEEE Trans. Biomed. Eng.* 60, 1654–1659. doi: 10.1109/TBME.2013.2241060

Au, S. K., Herr, H., Weber, J., and Martinez-Villalpando, E. C. (2007). Powered ankle-foot prosthesis for the improvement of amputee ambulation. *Conf. Proc. IEEE Eng. Med. Biol. Soc.* 2007, 3020–3026.

Aubin, P. M., Cowley, M. S., and Ledoux, W. R. (2008). Gait simulation via a 6-DOF parallel robot with iterative learning control. *IEEE Trans. Biomed. Eng.* 55, 1237–1240. doi: 10.1109/TBME.2007.908072

Blaya, J. A., and Herr, H. (2004). Adaptive control of a variable-impedance ankle-foot orthosis to assist drop-foot gait. *IEEE Trans. Neural Syst. Rehabil. Eng.* 12, 24–31. doi: 10.1109/TNSRE.2003.823266

Burke, M. J., Roman, V., and Wright, V. (1978). Bone and joint changes in lower limb amputees. *Ann. Rheum. Dis.* 37, 252–254. doi: 10.1136/ard.37.3.252

Caputo, J. M., and Collins, S. H. (2014). A universal ankle-foot prosthesis emulator for human locomotion experiments. *J. Biomech. Eng.* 136:035002. doi: 10.1115/1.4026225

Corbett, C. E., Allen, E. V., Prilutsky, B. I., and Childers, W. L. (2018). "CatWalk: a passive prosthetic foot for felines with a transtibial amputation," in *Proceedings of the Annual Meeting of the American Academy of Orthotists and Prosthetists*, (Washington, DC: American Academy of Orthotists and Prosthetists).

Crouch, J. E. (1969). *Text-Atlas of Cat Anatomy*. Philadelphia, PA: Lea & Febiger.

Davis, T. S., Wark, H. A., Hutchinson, D. T., Warren, D. J., O'neill, K., Scheinblum, T., et al. (2016). Restoring motor control and sensory feedback in people with upper extremity amputations using arrays of 96 microelectrodes implanted in the median and ulnar nerves. *J. Neural Eng.* 13:036001. doi: 10.1088/1741-2560/13/3/036001

Delussu, A. S., Brunelli, S., Paradisi, F., Iosa, M., Pellegrini, R., Zenardi, D., et al. (2013). Assessment of the effects of carbon fiber and bionic foot during overground and treadmill walking in transtibial amputees. *Gait Posture* 38, 876–882. doi: 10.1016/j.gaitpost.2013.04.009

Dhillon, G. S., Lawrence, S. M., Hutchinson, D. T., and Horch, K. W. (2004). Residual function in peripheral nerve stumps of amputees: implications for neural control of artificial limbs. *J. Hand Surg. Am.* 29, 605–615; discussion 616–608. doi: 10.1016/j.jhsa.2004.02.006

Edwards, D. H., and Prilutsky, B. I. (2017). "Sensory feedback in the control of posture and locomotion," in *Neurobiology of Motor Control: Fundamental Concepts and New Directions*, eds S. L. Hooper and A. Büschges (New York, NY: Wiley), 263–304.

Farrell, B. J., Bulgakova, M. A., Beloozerova, I. N., Sirota, M. G., and Prilutsky, B. I. (2014a). Body stability and muscle and motor cortex activity during walking with wide stance. *J. Neurophysiol.* 112, 504–524. doi: 10.1152/jn.00064.2014

Farrell, B. J., Prilutsky, B. I., Kistenberg, R. S., Dalton, J. F. T., and Pitkin, M. (2014b). An animal model to evaluate skin-implant-bone integration and gait with a prosthesis directly attached to the residual limb. *Clin. Biomech.* 29, 336–349. doi: 10.1016/j.clinbiomech.2013.12.014

Farrell, B. J., Prilutsky, B. I., Ritter, J. M., Kelley, S., Popat, K., and Pitkin, M. (2014c). Effects of pore size, implantation time, and nano-surface properties on rat skin ingrowth into percutaneous porous titanium implants. *J. Biomed. Mater. Res. A* 102, 1305–1315. doi: 10.1002/jbm.a.34807

Ferris, D. P., Sawicki, G. S., and Domingo, A. (2005). Powered lower limb orthoses for gait rehabilitation. *Top. Spinal Cord Inj. Rehabil.* 11, 34–49. doi: 10.1310/6GL4-UM7X-519H-9JYD

Fey, N. P., Klute, G. K., and Neptune, R. R. (2011). The influence of energy storage and return foot stiffness on walking mechanics and muscle activity in below-knee amputees. *Clin. Biomech.* 26, 1025–1032. doi: 10.1016/j.clinbiomech.2011.06.007

Fitzpatrick, N., Smith, T. J., Pendegrass, C. J., Yeadon, R., Ring, M., Goodship, A. E., et al. (2011). Intraosseous transcutaneous amputation prosthesis (ITAP) for limb salvage in 4 dogs. *Vet. Surg.* 40, 909–925. doi: 10.1111/j.1532-950X.2011.00891.x

Florez, J. M., Shah, M., Moraud, E. M., Wurth, S., Baud, L., Von Zitzewitz, J., et al. (2017). Rehabilitative soft exoskeleton for rodents. *IEEE Trans. Neural Syst. Rehabil. Eng.* 25, 107–118. doi: 10.1109/TNSRE.2016.2535352

Forssberg, H. (1979). Stumbling corrective reaction: a phase-dependent compensatory reaction during locomotion. *J. Neurophysiol.* 42, 936–953. doi: 10.1152/jn.1979.42.4.936

Garcia, E., Arevalo, J. C., Munoz, G., and Gonzalez-De-Santos, P. (2011). On the biomimetic design of agile-robot legs. *Sensors* 11, 11305–11334. doi: 10.3390/s111211305

Goslow, G. E. Jr., Reinking, R. M., and Stuart, D. G. (1973). The cat step cycle: hind limb joint angles and muscle lengths during unrestrained locomotion. *J. Morphol.* 141, 1–41. doi: 10.1002/jmor.1051410102

Graczyk, E. L., Schiefer, M. A., Saal, H. P., Delhaye, B. P., Bensmaia, S. J., and Tyler, D. J. (2016). The neural basis of perceived intensity in natural and artificial touch. *Sci. Transl. Med.* 8:362ra142. doi: 10.1126/scitranslmed.aaf5187

Gregor, R. J., Maas, H., Bulgakova, M. A., Oliver, A., English, A. W., and Prilutsky, B. I. (2018). Time course of functional recovery during the first 3 mo after surgical transection and repair of nerves to the feline soleus and lateral gastrocnemius muscles. *J. Neurophysiol.* 119, 1166–1185. doi: 10.1152/jn.00661.2017

Gregor, R. J., Smith, D. W., and Prilutsky, B. I. (2006). Mechanics of slope walking in the cat: quantification of muscle load, length change, and ankle extensor EMG patterns. *J. Neurophysiol.* 95, 1397–1409. doi: 10.1152/jn.01300.2004

Hagberg, K., and Branemark, R. (2009). One hundred patients treated with osseointegrated transfemoral amputation prostheses–rehabilitation perspective. *J. Rehabil. Res. Dev.* 46, 331–344. doi: 10.1682/JRRD.2008.06.0080

Herr, H. M., and Grabowski, A. M. (2012). Bionic ankle-foot prosthesis normalizes walking gait for persons with leg amputation. *Proc. Biol. Sci.* 279, 457–464. doi: 10.1098/rspb.2011.1194

Hof, A. L., Van Bockel, R. M., Schoppen, T., and Postema, K. (2007). Control of lateral balance in walking. Experimental findings in normal subjects and above-knee amputees. *Gait Posture* 25, 250–258. doi: 10.1016/j.gaitpost.2006.04.013

Hoy, M. G., and Zernicke, R. F. (1985). Modulation of limb dynamics in the swing phase of locomotion. *J. Biomech.* 18, 49–60. doi: 10.1016/0021-9290(85)90044-2

Jaegers, S. M., Arendzen, J. H., and De Jongh, H. J. (1995). Prosthetic gait of unilateral transfemoral amputees: a kinematic study. *Arch. Phys. Med. Rehabil.* 76, 736–743. doi: 10.1016/S0003-9993(95)80528-1

Jarrell, J., Farrell, B. J., Kistenberg, R. S., Dalton, J. F. T., Pitkin, M., and Prilutsky, B. I. (2018). Kinetics of individual limbs during level and slope walking with a unilateral transtibial bone-anchored prosthesis in the cat. *J. Biomech.* doi: 10.1016/j.jbiomech.2018.05.021 [Epub ahead of print].

Juhnke, D. L., Beck, J. P., Jeyapalina, S., and Aschoff, H. H. (2015). Fifteen years of experience with Integral-Leg-Prosthesis: cohort study of artificial limb attachment system. *J. Rehabil. Res. Dev.* 52, 407–420. doi: 10.1682/JRRD.2014.11.0280

Kannape, O. A., and Herr, H. M. (2014). Volitional control of ankle plantar flexion in a powered transtibial prosthesis during stair-ambulation. *Conf. Proc. IEEE Eng. Med. Biol. Soc.* 2014, 1662–1665. doi: 10.1109/EMBC.2014.6943925

Kannape, O. A., and Herr, H. M. (2016). Split-belt adaptation and gait symmetry in transtibial amputees walking with a hybrid EMG controlled ankle-foot prosthesis. *Conf. Proc. IEEE Eng. Med. Biol. Soc.* 2016, 5469–5472. doi: 10.1109/EMBC.2016.7591964

Klishko, A. N., Farrell, B. J., Beloozerova, I. N., Latash, M. L., and Prilutsky, B. I. (2014). Stabilization of cat paw trajectory during locomotion. *J. Neurophysiol.* 112, 1376–1391. doi: 10.1152/jn.00663.2013

Leijendekkers, R. A., Staal, J. B., Van Hinte, G., Frolke, J. P., Van De Meent, H., Atsma, F., et al. (2016). Long-term outcomes following lower extremity press-fit bone-anchored prosthesis surgery: a 5-year longitudinal study protocol. *BMC Musculoskelet. Disord.* 17:484. doi: 10.1186/s12891-016-1341-z

Li, G., Schultz, A. E., and Kuiken, T. A. (2010). Quantifying pattern recognition-based myoelectric control of multifunctional transradial prostheses. *IEEE Trans. Neural Syst. Rehabil. Eng.* 18, 185–192. doi: 10.1109/TNSRE.2009.2039619

Markin, S. N., Lemay, M. A., Prilutsky, B. I., and Rybak, I. A. (2012). Motoneuronal and muscle synergies involved in cat hindlimb control during fictive and real locomotion: a comparison study. *J. Neurophysiol.* 107, 2057–2071. doi: 10.1152/jn.00865.2011

McFadyen, B. J., Lavoie, S., and Drew, T. (1999). Kinetic and energetic patterns for hindlimb obstacle avoidance during cat locomotion. *Exp. Brain Res.* 125, 502–510. doi: 10.1007/s002210050708

Mich, P. M. (2014). The emerging role of veterinary orthotics and prosthetics (V-OP) in small animal rehabilitation and pain management. *Top. Companion Anim. Med.* 29, 10–19. doi: 10.1053/j.tcam.2014.04.002

Ollivier-Lanvin, K., Krupka, A. J., Auyong, N., Miller, K., Prilutsky, B. I., and Lemay, M. A. (2011). Electrical stimulation of the sural cutaneous afferent nerve controls the amplitude and onset of the swing phase of locomotion in the spinal cat. *J. Neurophysiol.* 105, 2297–2308. doi: 10.1152/jn.00385.2010

Ortiz-Catalan, M., Hakansson, B., and Branemark, R. (2014). An osseointegrated human-machine gateway for long-term sensory feedback and motor control of artificial limbs. *Sci. Transl. Med.* 6:257re256. doi: 10.1126/scitranslmed.3008933

Park, H., Mehta, R., Deweerth, S. P., and Prilutsky, B. I. (2015). "Modulation of afferent feedback from paw pad afferents affects interlimb coordination and adaptation to split-belt treadmill locomotion in the cat," in *Society for Neuroscience Meeting*, Chicago, IL.

Park, H., Oh, K., Prilutsky, B. I., and Deweerth, S. P. (2016). "A real-time closed-loop control system for modulating gait characteristics via electrical stimulation of peripheral nerves," in *Proceedings of the 2016 IEEE Biomedical Circuits and Systems Conference (BioCAS)*, (Shanghai: IEEE), 95–98. doi: 10.1109/BioCAS.2016.7833733

Pitkin, M., Cassidy, C., Muppavarapu, R., and Edell, D. (2012). Recording of electric signal passing through a pylon in direct skeletal attachment of leg prostheses with neuromuscular control. *IEEE Trans. Biomed. Eng.* 59, 1349–1353. doi: 10.1109/TBME.2012.2187784

Pitkin, M., Raykhtsaum, G., Pilling, J., Shukeylo, Y., Moxson, V., Duz, V., et al. (2009). Mathematical modeling and mechanical and histopathological testing of porous prosthetic pylon for direct skeletal attachment. *J. Rehabil. Res. Dev.* 46, 315–330. doi: 10.1682/JRRD.2008.09.0123

Prilutsky, B. I., Herzog, W., and Leonard, T. (1996). Transfer of mechanical energy between ankle and knee joints by gastrocnemius and plantaris muscles during cat locomotion. *J. Biomech.* 29, 391–403. doi: 10.1016/0021-9290(95)00054-2

Prilutsky, B. I., Maas, H., Bulgakova, M., Hodson-Tole, E. F., and Gregor, R. J. (2011). Short-term motor compensations to denervation of feline soleus and lateral gastrocnemius result in preservation of ankle mechanical output during locomotion. *Cells Tissues Organs* 193, 310–324. doi: 10.1159/000323678

Prilutsky, B. I., Sirota, M. G., Gregor, R. J., and Beloozerova, I. N. (2005). Quantification of motor cortex activity and full-body biomechanics during unconstrained locomotion. *J. Neurophysiol.* 94, 2959–2969. doi: 10.1152/jn.00704.2004

Quevedo, J., Stecina, K., Gosgnach, S., and Mccrea, D. A. (2005). Stumbling corrective reaction during fictive locomotion in the cat. *J. Neurophysiol.* 94, 2045–2052. doi: 10.1152/jn.00175.2005

Rabago, C. A., Aldridge Whitehead, J., and Wilken, J. M. (2016). Evaluation of a powered ankle-foot prosthesis during slope ascent gait. *PLoS One* 11:e0166815. doi: 10.1371/journal.pone.0166815

Realmuto, J., Klute, G., and Devasia, S. (2011). Nonlinear passive cam-based springs for powered ankle prostheses. *J. Med. Dev.* 9:011007. doi: 10.1115/1.4028653

Roche, E. T., Wohlfarth, R., Overvelde, J. T., Vasilyev, N. V., Pigula, F. A., Mooney, D. J., et al. (2014). A bioinspired soft actuated material. *Adv. Mater.* 26, 1200–1206. doi: 10.1002/adma.201304018

Sawicki, G. S., and Ferris, D. P. (2009). A pneumatically powered knee-ankle-foot orthosis (KAFO) with myoelectric activation and inhibition. *J. Neuroeng. Rehabil.* 6:23. doi: 10.1186/1743-0003-6-23

Shultz, A. H., Lawson, B. E., and Goldfarb, M. (2016). Variable cadence walking and ground adaptive standing with a powered ankle prosthesis. *IEEE Trans. Neural Syst. Rehabil. Eng.* 24, 495–505. doi: 10.1109/TNSRE.2015.2428196

Struyf, P. A., Van Heugten, C. M., Hitters, M. W., and Smeets, R. J. (2009). The prevalence of osteoarthritis of the intact hip and knee among traumatic leg amputees. *Arch. Phys. Med. Rehabil.* 90, 440–446. doi: 10.1016/j.apmr.2008.08.220

Takahashi, K. Z., Lewek, M. D., and Sawicki, G. S. (2015). A neuromechanics-based powered ankle exoskeleton to assist walking post-stroke: a feasibility study. *J. Neuroeng. Rehabil.* 12:23. doi: 10.1186/s12984-015-0015-7

Tan, D. W., Schiefer, M. A., Keith, M. W., Anderson, J. R., Tyler, J., and Tyler, D. J. (2014). A neural interface provides long-term stable natural touch perception. *Sci. Transl. Med.* 6:257ra138. doi: 10.1126/scitranslmed.3008669

Tkach, D. C., Young, A. J., Smith, L. H., Rouse, E. J., and Hargrove, L. J. (2014). Real-time and offline performance of pattern recognition myoelectric control using a generic electrode grid with targeted muscle reinnervation patients. *IEEE Trans. Neural Syst. Rehabil. Eng.* 22, 727–734. doi: 10.1109/TNSRE.2014.2302799

Wand, P., Prochazka, A., and Sontag, K. H. (1980). Neuromuscular responses to gait perturbations in freely moving cats. *Exp. Brain Res.* 38, 109–114. doi: 10.1007/BF00237937

Weber, H. F. (1965). Pulse-width modulation DC motor control. *IEEE Trans. Ind. Electron. Control Instrum.* 1, 24–28. doi: 10.1109/TIECI.1965.229545

Conflict of Interest Statement: The authors declare that the research was conducted in the absence of any commercial or financial relationships that could be construed as a potential conflict of interest.

frontiers in Human Neuroscience

REVIEW
published: 06 August 2018
doi: 10.3389/fnhum.2018.00312

EEG-Based BCI Control Schemes for Lower-Limb Assistive-Robots

*Madiha Tariq, Pavel M. Trivailo and Milan Simic**

School of Engineering, RMIT University Melbourne, Melbourne, VIC, Australia

Over recent years, brain-computer interface (BCI) has emerged as an alternative communication system between the human brain and an output device. Deciphered intents, after detecting electrical signals from the human scalp, are translated into control commands used to operate external devices, computer displays and virtual objects in the real-time. BCI provides an augmentative communication by creating a muscle-free channel between the brain and the output devices, primarily for subjects having neuromotor disorders, or trauma to nervous system, notably spinal cord injuries (SCI), and subjects with unaffected sensorimotor functions but disarticulated or amputated residual limbs. This review identifies the potentials of electroencephalography (EEG) based BCI applications for locomotion and mobility rehabilitation. Patients could benefit from its advancements such as wearable lower-limb (LL) exoskeletons, orthosis, prosthesis, wheelchairs, and assistive-robot devices. The EEG communication signals employed by the aforementioned applications that also provide feasibility for future development in the field are sensorimotor rhythms (SMR), event-related potentials (ERP) and visual evoked potentials (VEP). The review is an effort to progress the development of user's mental task related to LL for BCI reliability and confidence measures. As a novel contribution, the reviewed BCI control paradigms for wearable LL and assistive-robots are presented by a general control framework fitting in hierarchical layers. It reflects informatic interactions, between the user, the BCI operator, the shared controller, the robotic device and the environment. Each sub layer of the BCI operator is discussed in detail, highlighting the feature extraction, classification and execution methods employed by the various systems. All applications' key features and their interaction with the environment are reviewed for the EEG-based activity mode recognition, and presented in form of a table. It is suggested to structure EEG-BCI controlled LL assistive devices within the presented framework, for future generation of intent-based multifunctional controllers. Despite the development of controllers, for BCI-based wearable or assistive devices that can seamlessly integrate user intent, practical challenges associated with such systems exist and have been discerned, which can be constructive for future developments in the field.

Keywords: brain-computer interface (BCI), electroencephalography (EEG), spinal cord injury (SCI), exoskeletons, orthosis, assistive-robot devices

OPEN ACCESS

Edited by:
Mikhail Lebedev,
Duke University, United States

Reviewed by:
Vera Talis,
Institute for Information Transmission Problems (RAS), Russia
Yuri Levik,
Institute for Information Transmission Problems (RAS), Russia

***Correspondence:**
Milan Simic
milan.simic@rmit.edu.au

Received: *03 May 2018*
Accepted: *16 July 2018*
Published: *06 August 2018*

Citation:
Tariq M, Trivailo PM and Simic M (2018) EEG-Based BCI Control Schemes for Lower-Limb Assistive-Robots. Front. Hum. Neurosci. 12:312. doi: 10.3389/fnhum.2018.00312

INTRODUCTION

The field of assistive technologies, for mobility rehabilitation, is ameliorating by the introduction of electrophysiological signals to control these devices. The system runs independent of physical, or muscular interventions, using brain signals that reflect user's intent to control devices/limbs (Millán et al., 2010; Lebedev and Nicolelis, 2017), called brain-computer interface (BCI). Commonly used non-invasive modality to record brain signals is electroencephalography (EEG). EEG signals are deciphered to control commands in order to restore communication between the brain and the output device when the natural communication channel i.e., neuronal activity is disrupted. Recent reviews on EEG-BCI for communication and rehabilitation of lower-limbs (LL) could be found in (Cervera et al., 2018; Deng et al., 2018; He et al., 2018a; Lazarou et al., 2018; Semprini et al., 2018; Slutzky, 2018).

About five decades ago, EEG-BCIs used computer cursor movements to communicate user intents for patient-assistance in various applications (Vidal, 1973; Wolpaw et al., 2002; Lebedev and Nicolelis, 2017). The applications are now widespread, as machine learning has become one essential component of BCI, functional in different fields of neurorobotics and neuroprosthesis. For lower extremity, applications include human locomotion assistance, gait rehabilitation, and enhancement of physical abilities of able-bodied humans (Deng et al., 2018). Devices for locomotion, or mobility assistance, vary from wearable to (non-wearable) assistive-robot devices. Wearable devices such as exoskeletons, orthosis, prosthesis, and assistive-robot devices including wheelchairs, guiding humanoids, telepresence and mobile robots for navigation are the focus of our investigation.

Control schemes, offered by these systems, rely on the inputs derived from electrophysiological signals, electromechanical sensors from the device, and the deployment of finite state controller that attempts to implicate user's motion intention, to generate correct walking trajectories with wearable robots (Duvinage et al., 2012; Jimenez-Fabian and Verlinden, 2012; Herr et al., 2013; Contreras-Vidal et al., 2016). Input signals are typically extracted from the residual limb/muscles i.e., amputated or disarticulated lower-limbs (LL), via electromyography (EMG), from users with no cortical lesion or intact cognitive functions. Such solutions consequently preclude patient groups whose injuries necessitate direct cortical input to the BCI controller, for instance users with neuromotor disorders such as spinal cord injury (SCI) and stroke, or inactive efferent nerves/synergistic muscle groups. In this case direct cortical inputs from EEG could be the central-pattern-generators (CPG) that generate basic motor patterns at the supraspinal or cortical level (premotor and motor cortex); or the LL kinesthetic motor imagery (KMI) signals (Malouin and Richards, 2010). The realization of BCI controllers solely driven by EEG signals, for controlling LL wearable/assistive devices, is therefore possible (Lee et al., 2017). Several investigations reinstate that CPG with less supraspinal control is involved in the control of bipedal locomotion (Dimitrijevic et al., 1998; Beloozerova et al., 2003; Tucker et al., 2015). This provides the basis for the development of controllers, directly driven from cortical activity in correlation to the user intent for volitional movements (Nicolas-Alonso and Gomez-Gil, 2012; Angeli et al., 2014; Tucker et al., 2015; Lebedev and Nicolelis, 2017) instead of EMG signals. Consequently, controllers with EEG-based activity mode recognition for portable assistive devices, have become an alternative to get seamless results (Presacco et al., 2011b). However, when employing EEG signals as input to the BCI controller, there necessitates a validation about the notion that EEG signals from the cortex can be useful for the locomotion control.

Though cortical sites encode movement intents, the kinetic and kinematic changes necessary to execute the intended movement, are essential factors to be considered. Studies indicate that the selective recruitment of embedded "muscle synergies" provide an efficient means of intent-driven, selective movement, i.e., these synergies, stored as CPGs, specify spatial organization of muscle activation and characterize different biomechanical subtasks (Chvatal et al., 2011; Chvatal and Ting, 2013). According to Maguire et al. (2018), during human walking, Chvatal and Ting (2012) identified different muscle synergies for the control of muscle activity and coordination. According to Petersen et al. (2012), the swing-phase was more influenced by the central cortical control, i.e., dorsiflexion in early stance at heel strike, and during pre-swing and swing phases for energy transfer from trunk to leg. They also emphasized the importance of cortical activity during steady unperturbed gait for the support of CPG activity. Descending cortical signals communicate with spinal networks to ensure that accurate changes in limb movement have appropriately integrated into the gait pattern (Armstrong, 1988). The subpopulations of motor-cortical neurons activate sequentially amid the step cycle particularly during the initiation of pre-swing and swing (Drew et al., 2008). The importance of cortical activation upon motor imagery (MI) of locomotor tasks has been reported in Malouin et al. (2003) and Pfurtscheller et al. (2006b). Similarly, the confirmation of electrocortical activity coupled to gait cycle, during treadmill walking or LL control, for applications as EEG-BCI exoskeletons and orthotic devices, has been discerned by (He et al., 2018b, Gwin et al. (2010, 2011), Wieser et al. (2010), Presacco et al. (2011a), Presacco et al. (2011b), Chéron et al. (2012), Bulea et al. (2013), Bulea et al. (2015), Jain et al. (2013), Petrofsky and Khowailed (2014), Kumar et al. (2015), and Liu et al. (2015). This provides the rationale for BCI controllers that incorporate cortical signals for high-level commands, based on user intent to walk/bipedal locomotion or kinesthetic motor imagery of LL.

While BCIs may not require any voluntary muscle control, they are certainly dependent on brain response functions therefore the choice of BCI depends on the user's sensorimotor lesion and adaptability. Non-invasive types of BCI depend on EEG signals used for communication, which elicit under specific experimental protocols. Deployed electrophysiological signals that we investigate, include oscillatory/sensorimotor rhythms (SMR), elicited upon walking intent, MI or motor execution (ME) of a task, and evoked potentials as event-related potentials (ERP/P300) and visual evoked potentials (VEP). Such BCI functions as a bridge to bring sensory input into the brain, bypassing damages sight, listening or sensing abilities. **Figure 1**

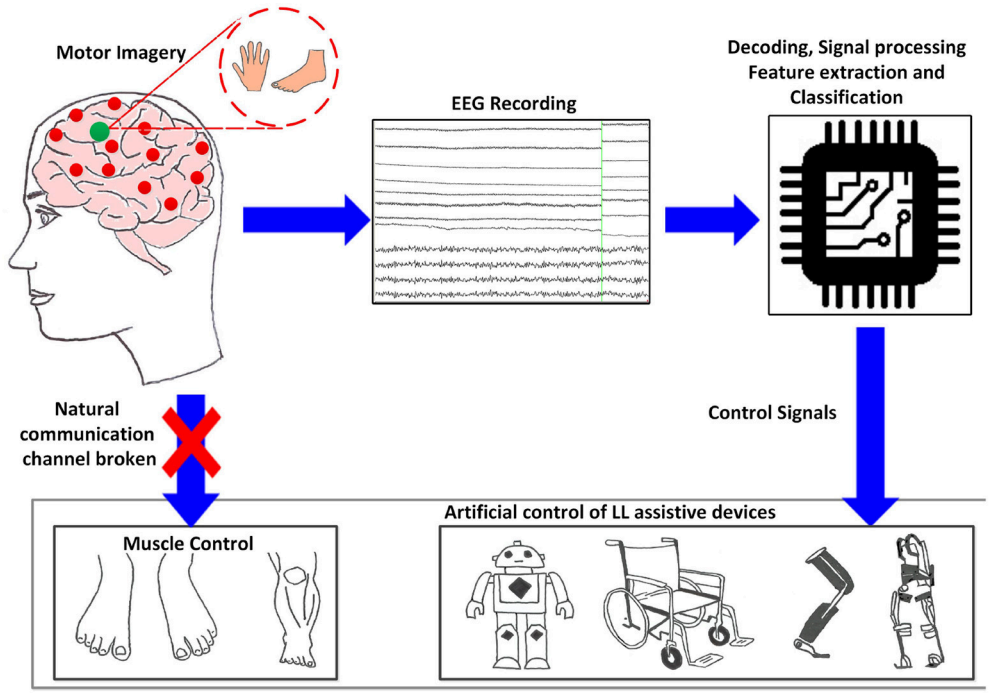

FIGURE 1 | Generic concept/function diagram of BCI controlled assistive LL devices based on motor imagery.

shows a schematic description of a BCI system based on MI, adapted from He et al. (2015). The user performs MI of limb(s), which is encoded in EEG reading; features representing the task are deciphered, processed and translated to commands in order to control assistive-robot device.

Reviewed control schemes deployed by wearable LL and assistive-robots are presented in a novel way, i.e., in form of a general control framework fitting in hierarchical layers. It shows the informatic interactions, between the user, the BCI operator, the shared controller, and the robot device with environment. The BCI operator is discussed in detail in the light of the feature extraction, classification and execution methods employed by all reviewed systems. Key features of present state-of-the-art EEG-based BCI applications and its interaction with the environment are presented and summarized in the form of a table. Proposed BCI control framework can cater similar systems based on fundamentally different classes. We expect a progress in the incorporation of the novel framework for the improvement of user-machine adaptation algorithms in a BCI.

The reviewed control schemes indicated that the MI/ME of LL tasks, as aspects of SMR-based BCI have not been extensively used compared to upper limbs (Tariq et al., 2017a,b, 2018). This is due to the small representation area of LL, in contrast to upper limbs, located inside the interhemispheric fissure of the sensorimotor cortex (Penfield and Boldrey, 1937). The review is an effort to progress the development of user's mental task related to LL for BCI reliability and confidence measures.

Challenges presently faced by EEG-BCI controlled wearable and assistive technology, for seamless control in real-time, to regain natural gait cycle followed by a minimal probability of non-volitional commands, and possible future developments in these applications, are discussed in the last section.

GENERAL CONTROL FRAMEWORK FOR BCI WEARABLE LOWER-LIMB AND ASSISTIVE-ROBOT DEVICES

In order to structure the control architecture adopted by various BCI wearable LL and assistive robot-devices, a general framework is presented in **Figure 2**. This framework was extended from Tucker et al. (2015) applicable to a range of EEG-BCI controlled devices for LL assistance, including portable exoskeletons, orthosis, prosthesis, and assistive-robots (wheelchairs, humanoids, and navigation/telepresence robots).

Figure 2 reflects the generalized control framework, where electrophysiological and transduced signal interactions, along the feedforward and feedback loops, are shown for motion intent recognition, during activity mode. Integral parts of the framework include a user of the assistive robot-device, the assistive-robot device itself, a BCI operator structure with sub-level controls, shared control, communication protocol and the interaction with environment. The BCI operator structure constitutes of three sub-layers which are the feature extraction, translation and execution layer, respectively. As a precaution to ensure human-robot interaction safety, safety layers are used

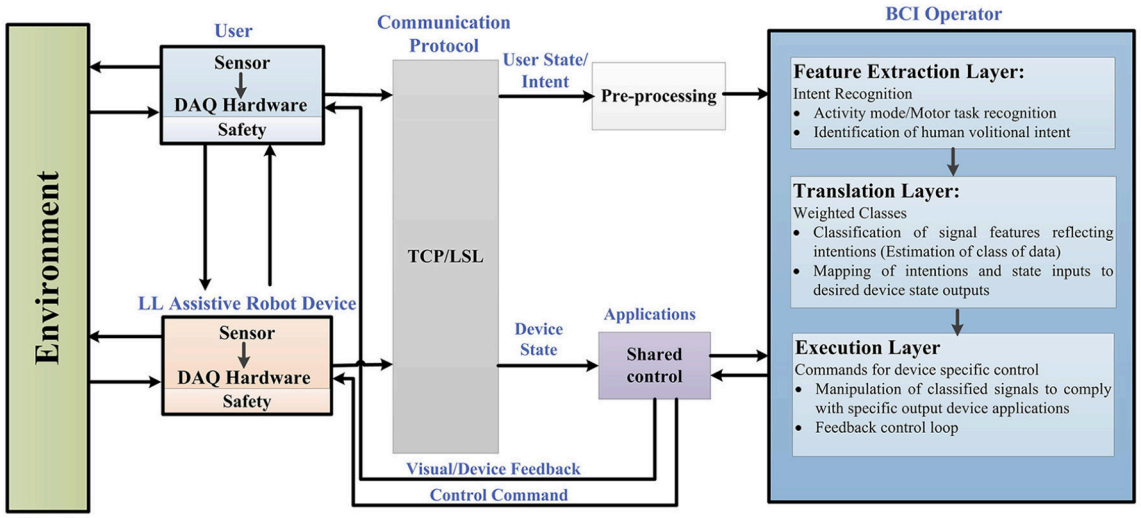

FIGURE 2 | Generalized framework in BCI controlled wearable LL and assistive devices for rehabilitation.

with the user and the robotic device parts of the framework. The control framework is in a generalized form applicable to all brain-controlled assistive robots.

BCI control is driven from the recognition of user's motion intentions; therefore we begin from the point of origin where motion intentions arise (cortical levels). The first step involves how to perceive and interpret the user's physiological state (i.e., MI/ME or ERP) acquired via EEG. Following this, the status of physical interaction between the user and the environment (and vice versa), and the robotic device and the environment (and vice versa) are checked. The assistive-robot's state is determined via electromechanical sensors. The user and assistive-robot status inputs to the BCI operator and shared controller, respectively.

Raw signals from the user and assistive LL device pass through the communication protocol which directs them to the connected client i.e., BCI operator via pre-processing and shared control module. Real-time signal acquisition and operating software could be used to assign event markers to the recorded data e.g., OpenViBE, BioSig, BCI++, BCI2000 etc. (Schalk et al., 2004; Mellinger and Schalk, 2007; Renard et al., 2010). The streaming connection can be made using TCP (when the time synchronization requirements do not need accuracy <100 ms) or LSL which incorporates built-in network and synchronization capabilities (with accuracy of 1 ms) recommended for applications based on ERPs.

Under the control framework components, BCI operator is the core part comprising of three sub layers, described in detail in section BCI Operator.

At feature extraction layer (intent recognition), user's intent of activities related to LL movements are perceived, discerned and interpreted. Signal features associated to user's kinesthetic intent/execution of motor task (in case of SMR) are encoded in form of feature vector (Lotte, 2014). The activity-mode recognition for ERP, against displayed oddball menu for specific location, uses frequency, or time domain features. It is the user's direct volitional control that lets voluntarily manipulate the state of the device (e.g., joint position, speed, velocity and torque).

Translation layer (weighted class) takes account of the translation of extracted signal features to manipulate the robotic device, via machine understandable commands, which carry the user's intent. This is done by supervised, or unsupervised learning (classification algorithm) which essentially estimates the weighted class, represented by the feature vector, and identifies the cognitive patterns for mapping to the desired state (unique command).

The desired state of user intent is carried to the execution layer (commands for device-specific control) where an error approximation is done with reference to current state. The state of the device is also sent to the execution layer via shared controller, as a feedforward control, in order to comply with the execution layer. The execution layer sends control commands to the actuator(s) of the device and visual feedback to the user via shared control unit in order to minimize the possible error. The feedback control plays a vital role in achieving the required output (usually accounts for the kinematic or kinetic properties of the robot-device).

This closes the overall control loop and the robotic device actuates to perform the required task(s). As the wearable assistive-robot is physically placed in close contact with the user, and that the powered device is likely to generate output force, safety mechanisms are kept into consideration with the user and hardware in the control framework. Inter-networking between subsystems of the generalized control architecture relies on the exchange of information sent at signal-level as well as physical-level.

USER ADAPTABILITY AND EEG SIGNAL ACQUISITION

The type of BCI is directed based on the user's lesion level and extent of adaptability to adhere with the specific BCI protocol.

User Adaptability

In order for the portable LL wearable-BCI controllers to be compliant with residual neuromusculoskeletal structures, the sensorimotor control loop of human locomotion is taken into account, since the volitional and reflex-dependent modulation of these locomotion patterns emerges at the cortical levels (Armstrong, 1988; Kautz and Patten, 2005; Bakker et al., 2007; Zelenin et al., 2011; Pons et al., 2013; Angeli et al., 2014; Marlinski and Beloozerova, 2014; Capogrosso et al., 2016). This may essentially preclude the direct control of LL via neural activity alone, while keeping a balance and orientation during dynamic tasks. However, the sole employment of cortical activity is still useful for providing high-level commands to the controller of the device to execute volitional movements (Carlson and Millan, 2013; Contreras-Vidal and Grossman, 2013; Kilicarslan et al., 2013), for patients whose injuries necessitate a direct input from cortex to the robotic device controller. Therefore, the critical aspect for a functional portable LL device is the lesion measure and the physiological constraints based on which the user can adapt to the BCI protocol. The physiological constraints in such cases can be compensated through assistance, like shared control.

EEG Signal Acquisition

The neuronal activity can be divided into spikes and field potentials. Spikes show action potentials of neurons individually and are detected via invasive microelectrodes. Field potentials on the other hand can be measured by EEG and they reflect the combined synaptic, axonal and neuronal activity of the neuron groups (Yang et al., 2014; He, 2016).

The communication components in EEG activity useful for BCI include, the oscillatory activity comprising of delta, theta, alpha/mu, beta and gamma rhythms; the ERP (P300), the VEP, and slow cortical potentials (SCP). Oscillatory rhythms fluctuate according to the states of brain activity; some rhythms are distinguished depending on these states (Semmlow and Griffel, 2014). The *Mu* and *beta* rhythms are also termed SMR. The SMR elicit event-related desynchronization (ERD) or event-related synchronization (ERS) which are directly related to proportional power decrease upon ME/MI of limb(s) movement or power increase in the signal upon rest, respectively; they are non-phase locked signals (Kalcher and Pfurtscheller, 1995). Evoked potentials on the other hand are phase-locked. A BCI system employs evoked potentials when requiring less or no training from the user i.e., a system based on stimulus-evoked EEG signals that provides task-relevant information (Baykara et al., 2016), useful for locked-in or multiple sclerosis patients. This involves the presentation of an odd-ball paradigm in case of P300 or multiple visual stimuli flashing, e.g., letters, digits on screen in case of VEP. The P300 is derived from user response that evokes approximately 300 ms after stimulus triggering and corresponds to positive voltage peak (Lazarou et al., 2018). VEP measures the time for the visual stimulus to travel from the eye to occipital cortex.

Users can generally be grouped based on their physical and mental state, for instance locked-in patients with intact eye muscles, can communicate via ERP signals, whereas patients with motor complete but sensory incomplete SCI can utilize SMR signals based on MI. **Figure 3** shows the electrophysiological signals that are extensively employed by BCI system for communication; however EEG signals employed by the wearable LL and assistive devices are highlighted for this study.

Deployed Oscillatory Rhythms

For assistive devices, the two commonly used SMR acquired from the motor cortex are *mu* (8–11 Hz) and *beta* (12–30 Hz) rhythms, which elicit upon ME/MI tasks. The ME task is based on the physical motion of the user's limbs that activate the motor cortex; this includes the development of muscular tension, contraction or flexion. The MI is a covert cognitive process based on the kinesthetic imagination of the user's own limb movement with no muscular activity also termed "kinesthetic motor imagery" (KMI) (Mokienko et al., 2013). Motor tasks can generally be upper or lower limb related (Malouin et al., 2008). The upper limb motor tasks activate hand area (Vasilyev et al., 2017) and LL motor tasks activate foot representation area of the cortex respectively (Wolpaw and Wolpaw, 2012). The advantage with MI signals is that they are free of proprioceptive feedback unlike ME tasks.

It was suggested by Wolpaw and Mcfarland (2004), that the use of *mu* and *beta* rhythms could give similar results as those presented by invasive methods for motor substitution. A non-invasive BCI could clinically support medical device applications (as discussed in section Lower-Limb Assistive-Robot Applications in Different Environments). The BCIs for control of medical device applications are reported in Allison et al. (2007); Daly and Wolpaw (2008), and Frolov et al. (2017). It was observed that BCI employed by assistive-robot devices for control purposes was focused on upper limb MI (Belda-Lois et al.,

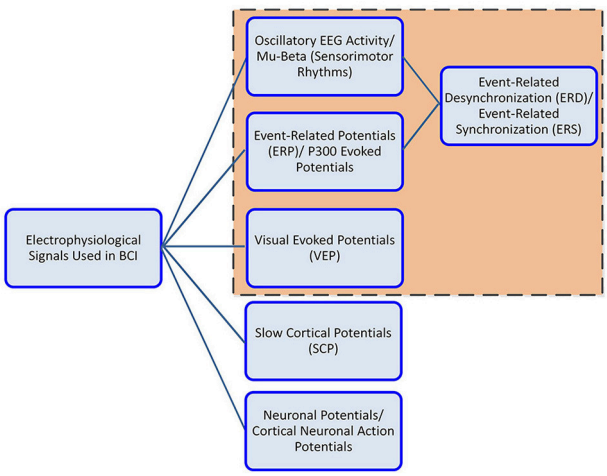

FIGURE 3 | Electrophysiological signals used in BCI controlled wearable LL and assistive-robot devices.

2011) such as hand and fingers, for applications including BCI hand orthotics and exoskeleton (Schwartz et al., 2006; Soekadar et al., 2015). This is because the foot representation area is near the mantelkante, which is situated deep within interhemispheric fissure of the human sensorimotor cortex (Penfield and Boldrey, 1937). However, it never withheld progress into this direction. Research on LL, precisely the foot MI/ME for controlling assistive robots, is in progress (Pfurtscheller et al., 2006a; Hashimoto and Ushiba, 2013; Tariq et al., 2017b, 2018). It was proved that the induction of *beta* ERS in addition to *mu-beta* ERD, improved the discrimination between left and right foot imagery and stepping tasks, as accurate as hand MI (Pfurtscheller et al., 2005, 2006a; Pfurtscheller and Solis-Escalante, 2009; Hashimoto and Ushiba, 2013; Liu et al., 2018) which provides a basis for research in BCI controlled foot neuroprosthesis. To our knowledge no literature on explicit employment of knee or hip KMI tasks in any BCI experimental protocol is available except for (Tariq et al., 2017a).

Besides the KMI of LL, cortical signals arising from the sensorimotor control loop of human locomotion intent is taken into account, for the portable LL wearable-BCI controllers to be compliant with the residual neuromusculoskeletal structures (La Fougere et al., 2010) suggested that brain areas underlying walking MI overlie the supplementary motor area and pre-frontal cortex. The idea of walking from thought based on foot imagery has also been presented in Pfurtscheller et al. (2006b). A novel way of therapy that earlier provided limited grade of motor-function recovery for chronic gait function impaired subjects due to foot-drop was described (Do et al., 2011, 2012). They integrated EEG-based BCI with non-invasive functional electrical stimulation (FES) system. It resulted in enabling the brain-control of foot dorsiflexion directly in healthy individuals. Takahashi et al. (2009, 2012) validated the feasibility of short-term training by employing ERD and FES based on dorsiflexion of paralyzed ankle experiments. Beta corticomuscular coherence (CMC) gave a measure of communication amid sensorimotor cortex and muscles. García-Cossio et al. (2015) demonstrated the possibility to decode walking intentions from cortical patterns. Raethjen et al. (2008) found coherence in EEG at stepping frequency and electromyography (EMG) anterior tibial muscles pattern for rhythmic foot movements.

Work on analyzing EEG signals for detection of unexpected obstacles during walking was presented recently (Salazar-Varas et al., 2015). Observation of electrocortical activity related to walking gait-cycle and balancing experiments has been reported in Presacco et al. (2011b). Electrocortical activity resulting from gait-like movements and balancing with treadmill, Erigo R tilt table, and customized stationary bicycle with rigid reclined backboard (as pedaling device) have been discussed in Wieser et al. (2010), Gwin et al. (2011), Presacco et al. (2011a), Jain et al. (2013), Petrofsky and Khowailed (2014), Bulea et al. (2015), Kumar et al. (2015), and Liu et al. (2015).

Deployed Event-Related and Evoked Potentials

ERPs have successfully been deployed in ambulatory and motor conditions without affecting the recorded EEG data. P300 showed to improve the performance of an EEG-based BCI system during ambulatory conditions or foot dorsiflexion/plantar-flexion condition (Lotte et al., 2009; Castermans et al., 2011b; Duvinage et al., 2012). They used similar experimental protocol i.e., oddball paradigm while subjects were physically walking or moving feet in dorsiflexion or plantar-flexion direction. In addition to this, the somatosensory evoked potentials (SEP) were deployed in assistive technologies. These potentials commonly elicit by bipolar transcutaneous electrical stimulation applied on the skin over the trajectory of peripheral nerves of the upper limb (the median nerve) or LL (the posterior tibial nerve), and then recorded from the scalp (Sczesny-Kaiser et al., 2015). In addition to the wearable devices, assistive technologies as EEG-BCI controlled wheelchairs and humanoid robots have successfully deployed the P300 (Rebsamen et al., 2007, 2010; Pires et al., 2008; Iturrate et al., 2009b; Palankar et al., 2009; Lopes et al., 2011; Kaufmann et al., 2014) and VEP signals (Bell et al., 2008). However, the only drawback, with employment of ERP and VEP signals in a BCI for the control of assistive devices precisely wearables, is the presence of visual stimulus set-up within the device that makes it less convenient for portable applications.

COMMUNICATION PROTOCOL

Like a basic communication system, the BCI for control of assistive devices has an input, an output, translation components for converting input to output, and a protocol responsible for the real-time operation onset, offset and timing.

Acquired EEG signals are transferred to the BCI operator via a communication protocol. Similarly sensor output from the robot device is directed to the shared control unit via communication protocol, **Figure 2**. Communication protocol could be a transmission control/internet protocol (TCP/IP), a suite of communication protocols used to interconnect network devices on the internet or a private network. For instance, in EEG-BCI controlled humanoids, the data (visual feedback images from the humanoid monocular camera and motion commands from the BCI system) were transmitted using wireless TCP/IP communication between the humanoid and other systems (Chae et al., 2011a,b, 2012).

An alternate approach is the lab streaming layer (LSL), which allows synchronization of the streaming data across devices. Information can be streamed over the network from "Presentation to the LSL" (Iturrate et al., 2009b; Renard et al., 2010; Kothe and Makeig, 2013; Gramann et al., 2014). Recent assistive applications (Galán et al., 2008; Millán et al., 2009) such as wheelchairs, and mobile robots, use controller area network (CAN) bus which is a robust vehicle bus standard. It is designed to allow microcontrollers and devices to communicate in applications without a host computer and follows a message-based protocol. It is a low cost, fault tolerant communication system, with the data transfer rates in the range of 40 Kbit/s to 1 Mbit/s.

BCI OPERATOR

After passing through the communication protocol, acquired EEG signals are directed to connected

client, i.e., the BCI operator, but are pre-processed first.

Preprocessing

The acquired raw EEG signals are pre-processed, as they are susceptible to noise and artifacts. It could be hardware/environmental noise, experimental error or physiological artifact. As hardware and environmental noise are not brain-related, it is best to remove them before converting raw EEG to signal features.

Removal of Noise

Hardware noise in the EEG signal usually occurs due to instrument degradation, electrode wear, mains interference (AC power lines), electromagnetic wave sources as computers, mobile phones, notebooks, wireless routers or other electronic equipment. High noise frequencies in the signal can be removed by notch filters (50 or 60 Hz for power lines). To block electromagnetic waves, electromagnetic shields could be used.

Removal of Artifacts

EEG artifacts arise due to physiological activities such as skin impedance fluctuations, electrooculography activity, eye blinks, electrocardiographic activity, facial/body muscle EMG activity and respiration. As the frequency ranges, for the aforementioned physiological signals are typically known, the bandpass filter can be an effective preprocessing tool. Most EEG-based BCI systems for assistive technologies have shown the successful implementation of simple low-pass, high-pass, or bandpass filters to remove physiological artifacts. Other methods for artifact removal include temporal filtering, spatial filtering, independent component analysis (ICA) (Viola et al., 2009), principal component analysis (PCA), linear regression, blind source separation (BSS) (Ferdousy et al., 2010), wavelet transform, autoregressive moving average, nonlinear adaptive filtering, source dipole analysis (Fatourechi et al., 2007) or thresholding of meaningful parameters (e.g., channel variance) based on a prior statistical analysis (Nolan et al., 2010).

Feature Extraction Layer

After preprocessing of data, different brain activities are classified based on their selected features.

Band Power Features

The band power features, usually used, are the time-frequency components of ERD/ERS. After bandpass filtering, resulting signal is squared to obtain its power $p\,[t] = x^2\,[t]$, where x is the filtered single band EEG signal amplitudes and p is the resulting band-power values. To smooth-out (average) the signal, a w-sized smoothing window operation is used. This is followed by a logarithm of the processed signal sample, using Equation 1:

$$\overline{p}\,[n] = \ln\left(\frac{1}{w}\sum_{k=0}^{w} p\,[n-k]\right) \tag{1}$$

where $\overline{p}\,[n]$ are the smoothed band-power values, and w is the smoothing window size. In their work (Presacco et al., 2011b; Contreras-Vidal and Grossman, 2013), the feature extraction method employed by EEG-BCI lower exoskeleton, for neural decoding of walking pattern, included power spectral density (PSD) analysis of the kinematic data and adaptive Thompson's multitaper for each channel of EEG recorded, during rest and walking tasks. Decoding method employed a time-embedded linear Wiener filter, independently designed and cross-validated for each extracted gait pattern. Parameters of the model were calculated with Gaussian distribution method. This ensured the feasibility of successfully decoding human gait patterns with EEG-BCI LL exoskeleton. Similarly, the results tested a on paraplegic subject for BCI controlled lower exoskeleton (Kilicarslan et al., 2013) reflect the method of decoding closed loop implementation structure of user intent with evaluation accuracy of 98%. Data was filtered in *delta* band (0.1–2 Hz) using 2nd order Butterworth filter. The filtered data was standardized and separate channels were used, to create feature matrix to extract *delta* band features.

In 2012 (Noda et al., 2012) proposed an exoskeleton robot that could assist user stand-up movements. For online decoding they used 9th order Butterworth filter for 7–30 Hz band. After down-sampling, Laplace filter and common average subtraction were applied for voltage bias removal. The covariance matrix of the processed data was used as input variable for the two-class classifier; the results were productive. Other EEG-BCI lower exoskeletons (Gancet et al., 2011, 2012) considered employing steady-state VEP (SSVEP) for motion intention recognition. Proprioceptive artifacts removal (during walk) is aimed to be removed using ICA. Other recent work on LL exoskeleton controlled via SSVEP includes (Kwak et al., 2015). In the SEP-controlled LL exoskeleton (Sczesny-Kaiser et al., 2015), SEP signals were sampled at 5 kHz and bandpass filtered between 2 and 1,000 Hz. In total 800 evoked potentials were recorded in epochs from 30 before to 150 ms after the stimulus, and then averaged. Paired-pulse suppression was expressed as a ratio of the amplitudes of second and first peaks, which was the primary outcome parameter. For correlation analysis, they calculated the difference of mean amplitude ratios.

For a BCI controlled robotic gait orthosis (Do et al., 2011, 2013) an EEG prediction model was generated to exclude EEG channels with excessive artifacts. The EEG epochs corresponding to idling and walking states were then transformed into frequency domain, their PSD were integrated over 2 Hz bins, followed by dimensionality reduction using class-wise principal component analysis (CPCA). The results established feasibility of the application.

BCI and shared control wheelchairs, based on MI signals to ensure interference free navigation protocol, was presented in Millán et al. (2009) and Carlson and Millan (2013). They estimated PSD in the 4–48 Hz band with a 2 Hz resolution. ERD was observed in the *mu* band power 8–13 Hz. These changes were detected by estimating the PSD features every 16 times/s using Welch method with five overlapped (25%) Hanning windows of 500 ms. In order to select subject-specific features, that maximize the separability between different tasks (based on training data cross validation) the canonical variate analysis (CVA) was used. In a similar work presented by Galán et al. (2008) for BCI controlled wheelchair, feature selection

was done by picking stable frequency components. The stability of frequency components was assessed using CVA one per frequency component on the training set.

Time-Domain Parameters

The time-domain parameters compute time-varying power of the first k derivatives of the signal; $p_i(t) = \frac{d^i x(t)}{dt^i}$ where $i = 0, 1, \ldots, k$ and x is the initial EEG signal. Resulting derivatives are smoothed using exponential moving average and logarithm, used in feature vector generation, as given in Equation 2:

$$\overline{p_i}[n] = \ln\left(u\, p_i[n] - (1-u)\, p_i[n-1]\right) \tag{2}$$

where $\overline{p}$ is the smoothed signal derivatives, u is the moving average parameter, $u \in [0; 1]$.

EEG-BCI for control of LL orthosis (Taylor et al., 2001; Duvinage et al., 2012) combined a human gait model based on a CPG and a classic but virtual P300 to decipher user's intent for four different speeds. P300 was used to control the CPG model and the orthosis device by sending high-level commands. The frequency band for P300 were high-pass filtered (temporal) at 1 Hz cut off frequency using 4th order Butterworth filter. This was followed by designing of an xDAWN-based spatial filter, by linearly combining EEG channels. When EEG signals were projected into this subspace, P300 detection was enhanced. The resulting signal was epoched using time window that started after stimulus, averaged and sent to the classifier. In another related work (Lotte et al., 2009), the epoching of P300 signal was done by selection of related time window, followed by bandpass filtering in 1–12 Hz range using 4th order Butterworth filter. Post this; winsorizing for each channel was done by replacing values within 5% most extreme values by most extreme values from remaining 95% samples from that window. A subset of the features was selected using the sequential forward floating (SFFS) feature selection algorithm that ensured the maximization of performance of the BCI system.

The EEG-BCI for foot orthosis reported in Xu et al. (2014), employed bandpass filtering (0–3 Hz). The system was based on the detection of movement-related cortical potentials (MRCP). The data between 0.5 and before 1.5 s, after the movements, were extracted as the "signal intervals" while others were extracted as the "noise intervals." The measure analysis of variance, ANOVA, was used for statistical analysis.

The P300-BCI wheelchair incorporated bandpass filtering between 0.5 and 30 Hz and characterized the P300 signal in the time domain. For each EEG channel, 1-s sample recordings were extracted after each stimulus onset and filtered using the moving average technique. The resulting data segments for each channel selected were concatenated, creating a single-feature vector (Iturrate et al., 2009a,b).

Common Spatial Patterns

The common spatial pattern (CSP) features are sourced from a preprocessing technique (filter) used to separate a multivariate signal into subcomponents that have maximum differences in variance (Müller-Gerking et al., 1999). The difference allows simple signal classification. Generally, the filter can be described as a spatial coefficient matrix W, as shown in Equation 3:

$$S = W^T E \tag{3}$$

where S is the filtered signal matrix, E is the original EEG signal vector. Columns of W denote spatial filters, while W^{T} are the spatial patterns of EEG signal. In their work (Choi and Cichocki, 2008) used SMR to control wheelchair. For pre-processing they employed the second order BSS algorithm using a modified and improved real-time AMUSE algorithm that enabled a rapid and reliable estimation of independent components with automatic ranking (sorting) according to their increasing frequency contents and/or decreased linear predictability. The AMUSE algorithm worked as 2 consecutive PCAs; one applied to the input data and the second applied to the time-delayed covariance matrix of the output from the previous stage. For feature extraction, CSP filter was used that distinguish each data group optimally from the multichannel EEG signals.

SMR-based humanoid robots used the KMI of left hand, right hand, and foot as control signals (Chae et al., 2011b, 2012). Sampled EEG signals were spatially filtered with large Laplacian filter. During the overall BCI protocols, Laplacian waveforms were subjected to an autoregressive spectral analysis. For amplitude features extraction, every 250 ms observation segment was analyzed by the autoregressive algorithm, and the square root of power in 1 Hz wide frequency bands within 4–36 Hz was calculated.

Translation Layer

After passing through the feature extraction layer, the feature vector is directed to the translation layer to identify user intent brain signals, and manipulate the robotic device via machine understandable commands for interfacing. Different classification techniques for distinct features are used. Classification algorithms, calibrated via supervised or unsupervised learning, during training phase, are able to detect brain-signal patterns during the testing stage. This essentially estimates the weighted class, represented by the feature vector for mapping to the desired state (unique command). A recent review on most commonly used classification algorithms for EEG-BCIs has been reported by (Lotte et al., 2018). Some of the commonly used classification methods in EEG-BCI controllers for LL assistance are LDA, SVM, GMM, and ANN (Delorme et al., 2010, 2011).

Linear Discriminant Analysis

One of the most extensive and successfully deployed classification algorithms, in EEG-BCI for assistive technologies is the linear discriminant analysis (LDA). The method employs discriminant hyper-plane(s) in order to separate data representing two or more classes. Since it has low computational requirements, it is most suitable for online BCI systems. A feature a can be projected onto a direction defined by a unit vector $\hat{\omega}$, resulting in a scalar projection b, given by Equation 4:

$$b = \vec{a} \cdot \hat{\omega}^2 \tag{4}$$

The aim of LDA classification is to find a direction $\hat{\omega}$, such that, when projecting the data onto $\hat{\omega}$ it maximizes the distance between the means and minimizes the variance of the two classes (dimensionality reduction). It assumes a normal data distribution along with an equal covariance matrix for both classes (Lotte et al., 2007). LDA minimizes the expression given by Equation 5:

$$\frac{\left(m_\phi - m_\Psi\right)^2}{s_\phi^2 + s_\Psi^2} \tag{5}$$

where m_ϕ and m_Ψ are the means and s_ϕ and s_Ψ are the standard deviations of the two respective classes, after projecting the features onto $\hat{\omega}$. EEG-BCI lower exoskeletons used LDA for the reduction of data dimensionality (Kilicarslan et al., 2013). EEG-BCI lower orthosis employed a 12-fold LDA using voting rule for decision making in selection of speed (Lotte et al., 2009; Duvinage et al., 2012). Dimensionality reduction, using CPCA and approximate information discriminant analysis (AIDA), were used in the robotic gait orthosis system (Do et al., 2011, 2013). The BCI-driven orthosis (Xu et al., 2014) used the manifold based non-linear dimensionality reduction method, called locality preserving projection (LPP), along with LDA, to detect MRCPs. EEG-BCI wheelchairs successfully deployed LDA (Galán et al., 2008; Iturrate et al., 2009a,b). LDA was successfully used for translation of EEG signal into movement commands in humanoids (Chae et al., 2011a,b, 2012).

Support Vector Machine

The goal of SVM classifier is to maximize the distance between the separating hyper plane and the nearest training point(s) also termed support vectors. The separating hyper plane in the 2D feature space is given by the Equation 6:

$$y = \omega^T x + b \tag{6}$$

where ω, $x \in R^2$ and $b \in R^1$. The hyper plane (also called the decision border) divides the feature space into two parts. Classified results depend on which side of the hyper plane the example is located. In SVM, the distances between a hyper plane and the nearest examples are called margins.

Though SVM is a linear classifier, it can be made with non-linear decision boundaries using non-linear kernel functions, such as Gaussian or radial basis functions (known as RBF). The non-linear SVM offers a more flexible decision boundary, resulting in an increase in classification accuracy. The kernel functions, however, could be computationally more demanding. EEG-BCI wheelchairs have successfully used linear SVM for dynamic feature classification (Bell et al., 2008; Choi and Cichocki, 2008; Ferreira et al., 2008; Rebsamen et al., 2010; Belluomo et al., 2011). It was also successfully implemented in EEG-BCI humanoid (Bell et al., 2008) and mobile robots (Ferreira et al., 2008; Belluomo et al., 2011).

Gaussian Mixture Model

The GMM is an unsupervised classifier. This implies that the training samples of a classifier are not labeled to show their class. More precisely, what makes GMM unsupervised is that during the training of the classifier, estimation is done for the underlying probability density functions of the observations (Scherrer, 2007). Several EEG-BCI applications utilized the GMM as a feature classifier, such as lower exoskeletons, wheelchairs and mobile robots (Galán et al., 2008; Millán et al., 2009; Carlson and Millan, 2013; Kilicarslan et al., 2013).

Artificial Neural Network

The ANNs are non-linear classifiers inspired by human's nervous system ability to adaptively react to changes in surroundings. They are commonly used in pattern recognition problems, due to their post-training capability to recognize sets of training-data-related patterns. ANNs comprise of assemblies of artificial neurons that allow the drawing of non-linear decision boundaries. They can be used in different algorithms including multilayer perception, Gaussian classifier, learning vector quantization, RBF neural networks, etc. (Anthony and Bartlett, 2009). In their proposed model for lower exoskeleton (Gancet et al., 2011, 2012), they aim at adopting processing method as dynamic recurrent neural network (DRNN).

Execution Layer

Once classified, the desired state of user intent is carried to the execution layer for an error approximation. The approximation in reference to the present state of the device is used to drive the actuator for reducing any error. The execution layer of control is highly device-specific. It could rely on feedforward or feedback loops (Tucker et al., 2015).

Feedforward control needs some model to predict the system's future state, based on the past and present set of inputs and the device state. Aforementioned control inputs can be effective for reducing the undesired interaction forces, that could occur due to the added mass, inertia and friction of the device (Murray and Goldfarb, 2012). On the contrary feedback controllers do not require a model of the system, but require an estimate of the current state. The controller compares current state with the desired state of the device and modulates the power input to the device accordingly (Millán et al., 2009; Duvinage et al., 2012; Noda et al., 2012; Contreras-Vidal and Grossman, 2013; Do et al., 2013; Kilicarslan et al., 2013; Xu et al., 2014; Contreras-Vidal et al., 2016).

SHARED CONTROL

Shared control is used to couple the user's intelligence, i.e., cognitive signals with precise capabilities of the robotic device given the context of surroundings, resulting in reduced workload for the user to continuously deliver commands to drive the robotic device. Inputs to the shared control module are sensory readings of the robotic device and output of the BCI operator (classified signal). The classified signal is combined with the robot's precise parameter e.g., velocity to generate smoother driving output. Several assistive technologies for motor impairment have successfully employed shared controllers for navigational assistance to maneuver the assistive devices in different directions, independently and safely (Galán et al., 2008;

Millán et al., 2009; Tonin et al., 2010, 2011; Carlson and Millan, 2013).

This refers to the idea of switching between operators, i.e., if the user needs no navigational assistance he will be granted full control over the robotic device; otherwise, sole mental commands will be used and modified by the system. One key aspect of shared control is the two-way communication between the human and the robot. The shared control is beneficial primarily for navigational directions. In the case of robots with only three possible steering mental commands such as forward, left, and right, there is a need of assistance by the device for fine maneuvering. Secondly, the cognitive commands might not always be perfect, i.e., could be vague. In the case of errors, an extra navigational safety is required by the system to interpret the meaning of the command. In this way the system would be able to perceive any new environment.

LOWER-LIMB ASSISTIVE-ROBOT APPLICATIONS IN DIFFERENT ENVIRONMENTS

The last integral part, of the control framework, is the robotic device, as observed in **Figure 2**. In this section, the current state-of-the-art EEG-based activity mode recognition in a BCI for control of LL assistive devices is summarized in **Table 1**.

BCI Exoskeletons

In order to control a LL robotic exoskeleton (NeuroRex), Contreras-Vidal and Grossman (2013) and Kilicarslan et al. (2013) decoded neural data for human walking from Presacco et al. (2011b). They evaluated the degree of cognitive-motor-body adaptations while using portable robot. Their results proved that NeuroRex can be regarded as an augmented system of locomotor therapy (LT) by reviewing its initial validation in a paraplegic patient having SCI. They also performed comprehensive clinic assessments for user safety protection.

The MINDWALKER (Gancet et al., 2011, 2012) is another project where researchers proposed a novel idea of presenting the SCI patients with intact brain capabilities. The facility of crutch-less assistive LL exoskeleton is based on brain neural-computer interface (BNCI) control for balanced walking patterns. It also evaluated the potential effects of Virtual Reality (VR) based technology that could support patient/user training for reaching a high confidence level for controlling the exoskeleton virtually before the real transition. Other brain controlled exoskeletons are reported in Noda et al. (2012), Kwak et al. (2015), Sczesny-Kaiser et al. (2015), and Lee et al. (2017).

BCI Orthosis

EEG-based activity mode recognition for orthotic devices has been investigated by Duvinage et al. (2012). They proved the concept of considering user's intent by combining CPG-based human gait model and classic P300-BCI for five different states; three speed variations, a stop state and a non-control state. Using unnatural P300 command by augmented reality eyewear (from Vuzix, Rchester, USA) decision was sent to the Virtual Reality Peripheral Network (VRPN) server to be exploited while wearing LL orthosis. This was based on the pilot study carried by Lotte et al. (2009), where a solution to the constraints, such as deterioration of signals (during ambulation), was avoided by using slow P300 for control during sitting, walking and standing. Authors of Castermans et al. (2011a) used an experimental protocol to limit movement artifacts present in EEG signals compared to real walk on treadmill. They suggested that rhythmic EEG activity could be exploited for driving a user intent-based foot-ankle orthosis built on PCPG algorithm. Similar investigation was conducted by Raethjen et al. (2008).

In their work, Do et al. (2013) proposed a novel approach of BCI controlled lower extremity orthotics to restore LL ambulation for partially and complete SCI subjects suffering from cardiovascular disease, osteoporosis, metabolic derangements and pressure ulcers. They developed an EEG prediction model to operate the BCI online and tested the commercial robotic gait orthosis system (RoGO) for two states, idling and walking KMI. Similarly, testing for intuitive and self-paced control of ambulation was also done with an avatar in a virtual reality environment (VRE) (Wang et al., 2012; King et al., 2013). Other similar investigations are reported in Wang et al. (2010) and Do et al. (2011).

The BCI driven motorized ankle-foot orthoses, known as (BCI-MAFO), intended for stroke rehabilitation was presented in Xu et al. (2014). Their system was able to detect imaginary dorsiflexion movements (for walking gait) within a short latency, by analyzing MRCPs. Upon each detection, the MAFO was triggered to elicit passive dorsiflexion, hence, providing the user a binary control of robotic orthosis. The MEP was elicited by transcranial magnetic stimulation (TMS); the results reflected an effective way to induce cortical plasticity for motor function rehabilitation.

BCI Wheelchairs, Humanoids, and Mobile Robots

Assistive technologies such as wheelchairs controlled via EEG-BCI have extensively been researched. In their work, Carlson and Millan (2013) proposed the idea of combining a commercial wheelchair and BCI with a shared control protocol. The paradigm was based on KMI of left/right hand, both feet, or in idle state; each against three distinct tasks as move left/right or forward by avoiding obstacles. Modifications in the commercial mid-wheel drive model (by Invacare Corporation) were directly controlled by a laptop. An interface module, based on remote joystick, was used between the laptop and wheelchair's CANBUS-based control network. Wheel-encoders were added for motion feedback alongside sonar sensors and webcams for environment feedback to the controller using cheap sensors compared to other systems. Previous solution required continuous commands from the user, in order to drive the wheelchair, that ended up in high user workload (Millán et al., 2009). Other similar systems were proposed by Vanacker et al. (2007) and Galán et al. (2008).

Research on the challenges faced during fully control automated wheelchairs with BCI was done by Rebsamen et al. (2007, 2010). Their results proved that if synchronous evoked

TABLE 1 | Key features of EEG-based activity mode recognition exoskeletons, orthosis, wheelchairs and assistive robots for rehabilitation.

Devices	Brain activity	Pre-processing and feature extraction	Classifier	Classifi-cation accuracy (%)	Key findings	Type of support and applications	References
NeuroRex	Oscillatory rhythms	Bandpass filter, PSD analysis	GMM, LDA	-, >90 (GMM), -	For standing-up, self-balancing, walking and backing, turning, ascending and descending stairs applications. An augmented form of Locomotor Therapy (LT)	Lower body exoskeleton based on user intent control for walking independently for subjects with paraparesis, complete paraplegia, stroke and SCI	Noda et al., 2012; Contreras-Vidal and Grossman, 2013; Kilicarslan et al., 2013
MIND-WALK-ER	SSVEP*	ICA	DRNN Chéron et al., 2011, KNN	-, -, 92.6% (online)	Exploitation of motor cortex EEG signals for generating online legs kinematics angles corresponding to walking pattern and pace as imagined by user deploying VR	Crutch-less assistive LL exoskeleton for walk empowering (dynamic balance) for SCI patients with intact brain capabilities	Gancet et al., 2011, 2012; Kwak et al., 2015
HAL® Exo-skeleton	SEP	Bandpass filter	-		Significant improvement in paired-pulse SEP in SCI patients compared to the controls at baseline following training. The robotic-assisted BWSTT in SCI patients is capable of inducing cortical plasticity following highly repetitive, active locomotive use of paretic legs.	HAL® exoskeleton-assisted bodyweight supported treadmill training (BWSTT) for improving walking function in SCI patients	Sczesny-Kaiser et al., 2015
Five-State Foot Lifter	P300*	Temporal high-pass filter, xDAWN-based spatial filter Rivet et al., 2009, epoch averaging, SFFS	LDA (using voting rule for decision making)	83 ± 15.5% (walking) 75% (walking)	Proof of the concept of combining a human gait model based on CPG widely used in robotics and P300 based BCI to consider user's intent. This CPG allowed to automatically generate a periodic gait pattern/behavior of the patient and his desired speed. No required training by the user to manage the P300 paradigm provided by augmented reality eyewear for external stimulus presentation.	A five-state foot lifter orthosis for sitting, standing and walking at four speeds & a non-control state for stroke patients unable to lift their feet or foot drop problems Pilot study for ambulatory BCI	Lotte et al., 2009; Duvinage et al., 2012

(Continued)

TABLE 1 | Continued

Devices	Brain activity	Pre-processing and feature extraction	Classifier	Classifi-cation accuracy (%)	Key findings	Type of support and applications	References
BCI-RoGO	Oscillatory rhythms**	FFT, PSD, CPCA	AIDA, linear Bayesian classifier	>85%, -, -	Development of EEG prediction model based on idling and KMI states. Preliminary evidence from results reflect the feasibility of restoring brain-controlled walking after SCI.	BCI Robotic gait orthosis for SCI, tetraplegia, and paraplegia patients to improve neurological outcomes beyond those of standard therapy to improve ambulation	Wang et al., 2010; Do et al., 2011, 2013
BCI-MAFO	MRCP***	Bandpass filter, large Laplacian filter, ANOVA	LPP and LDA	73 ± 10.3%.	Efficient induction of cortical neuroplasticity in healthy subjects with a short intervention procedure to use self-paced BCI for binary control of the robotic orthosis.	BCI-driven motorized ankle-foot orthosis (MAFO). An ambulatory rehabilitation-tool for stroke patients	Xu et al., 2014
BCI Wheel-chair	Oscillatory rhythms	Spatial filter (CAR), Laplacian filter, PSD (Welch method), CVA, Bandpass filter, FFT	Gaussian model, LDA	≥90%, -, ≥80%, 80%	Reduced cognitive workload due to BCI protocol coupled with shared control, compared to previous systems. Spontaneous control given to user to move left, right or forward and avoid obstacles automatically by perceiving surrounding environment, no waiting for external cues compared to synchronous P300 protocol. Based on combination of cheaper sensors for providing controller with environmental feedback.	Brain-actuated wheelchair for users with severe mobility impairment. Suitable for experienced/inexperienced users to continuously and safely operate with even complex navigation independently	Vanacker et al., 2007; Galán et al., 2008; Millán et al., 2009; Carlson and Millan, 2013
P300 BCI Wheel-chair	P300, ERP	Bandpass filter, moving average filter	SVM, Gaussian model, LDA	≈100%, ≈100%, ≥94%, ≥94%, 100%, 100%, ≥95%, ≥85.8%	Successfully targeted people suffering from a very low information transfer rate using the P300 paradigm, using virtual guiding paths and predictable trajectories. Incorporation of *mu/beta* (a faster BCI) to stop wheelchair. Provision of destination selection from predefined localities in the menu.	BCI wheelchair for locked-in or ALS patients. Intelligent and safe BCI wheelchair where known surroundings as, toilet, kitchen, bedroom and living room in house is highlighted by standard oddball paradigm.	Rebsamen et al., 2007, 2010; Pires et al., 2008; Iturrate et al., 2009a,b; Palankar et al., 2009; Lopes et al., 2011; Kaufmann et al., 2014

(Continued)

TABLE 1 | Continued

Devices	Brain activity	Pre-processing and feature extraction	Classifier	Classifi-cation accuracy (%)	Key findings	Type of support and applications	References
BMI wheel-chair	Oscillatory rhythms*	2nd order BSS with AMUSE algorithm, CSP filter, Bandpass filter	SVM	-	Effective feedback training method resulting in multi DOFs/freely controlling wheelchair parallel to controlling with a joystick	BCI wheelchair based on MI protocol for motor impaired patients.	Choi and Cichocki, 2008
BCI mobile robot/humanoid	Oscillatory rhythms	Bandpass filter, Laplacian filter, PSD (Welch method)	Statistical Gaussian model	74%, ≥75.6%, 81%, ≥75.6%, -, -	Allow subjects to complete complex tasks in same time and with same number of commands as required by manual control	BCI based telepresence robot for left/right steering via imagination of left/ right hand or feet movement of physically impaired people. Control navigation of humanoid robot via MI.	Millan et al., 2004; Tonin et al., 2010, 2011; Chae et al., 2011a,b, 2012
BCI mobile robot/humanoid	SMR, ERP, P300*	Spatial filter, temporal filter, Bandpass filter	SVM	95%, -, 95%, ≥93%, 80.5%	Development of an interactive BCI system to control twin coordinated mobile robot movements via two EEG signals (imagery left-right arm). The concentration and relaxation states of visual cortex, was used to allow operator to successfully control a robot without using hands. Successful control of BCI humanoid for sophisticated interaction with the environment, involving not only navigation but also manipulation and transport of objects.	BCI controlled mobile and telepresence robots for navigation in required direction for motor disability assistance. BCI controlled humanoid for navigation assistance as well as transportation of objects.	Bell et al., 2008; Ferreira et al., 2008; Belluomo et al., 2011; Escolano et al., 2012; De Venuto et al., 2017

They used combined EEG and EMG modalities in their system.

**They used combined EEG, FES, and EMG modalities in their BCI orthosis.*

***They used combined EEG and TMS modalities for brain signal acquisition and for classification purposes, they used additional features from EMG in their BCI orthosis.*

P300 signals are used for mobile commands, and oscillatory rhythms are used for stop command, the system is efficient and safe enough to drive the real-time wheelchair in possible directions. They used Yamaha JW-I power wheelchair with two optical rotary encoders attached to glide-wheels for odometry, a bar code scanner for global positioning and a proximity sensor mounted in front of the wheelchair for collision avoidance. User could reach the destination, by selecting amongst a list of pre-defined locations. This was primarily for patients with lost voluntary muscle control, but intact cognitive behavior who could use a BCI, such as LL amputees.

Other P300-BCI wheelchairs' research include work done by Iturrate et al. (2009a,b) where the system relied on synchronous stimulus-driven protocol. The work done by Palankar et al. (2009) focused on, completely and partially locked-in patients, and provided them with an effective model of a 9-DOF wheelchair-mounted robotic arm (WMRA) system. Pires et al. (2008) and Lopes et al. (2011) contributed in visual P300 based BCI for steering wheelchair assisted by shared-control. Kaufmann et al. (2014) validated the feasibility of a BCI based on tactually-evoked ERP for wheelchair control. Other wheelchairs controlled via EEG-based BCI include (Choi and Cichocki, 2008; Tsui et al., 2011; Huang et al., 2012; De Venuto et al., 2017).

In their report (Tonin et al., 2010, 2011) presented a BMI-controlled telepresence robot for people with motor impairment that could allow them completion of complex tasks, in similar time as that consumed by healthy subjects. They were able to steer Robotino^{TM} (by FESTO), via asynchronous KMI of left/right hand and feet. The system incorporated shared control for obstacle avoidance, safety measures and for interpreting user intentions to reach goal autonomously. A similar project was earlier presented by Millan et al. (2004) for mobile robot control in indoor environment via EEG. In order to recognize environment situations, a multilayer perception was implemented. Sensory readings were mapped to 6 classes of environmental states: forward movement, turn left, follow left wall, right turn, follow right wall and stop. These environmental states were generated against mental tasks as relax, KMI of left/right hand, cube rotation imagery, subtraction and word association. Research for control of two coordinated mobile robots, via SMR and ERP, that could be useful for motor impaired people, is done by Belluomo et al. (2011). Similarly mobile robot (Pioneer 2-DX) control based on *mu* ERD/ERS was done by Ferreira et al. (2008).

As per our knowledge, reflected from the literature, there is no viable active prosthetic ankle-foot, or prosthetic LL device, controlled via EEG-BCI for amputees.

PRACTICAL CHALLENGES

In order to design a controller for an assistive-robot device there is a need of a seamless integration between the BCI operator, and the execution of required tasks from the output device with minimal cognitive disruption. However, there are challenges associated to the real-time implementation of the system, when dealt with motor impaired population. Some open problems and challenges associated to wearable systems have recently been summarized in (Deng et al., 2018; Lazarou et al., 2018; Semprini et al., 2018). The following sections discuss in detail practical challenges associated to EEG-BCI wearable and assistive technologies.

Wearable Lower-Limb Device Challenges

A critical need for reliable EEG-BCI is required that could interpret user intent and make context-based decisions from the user's present internal state. This would allow a direct and voluntary operation of the wearable LL devices beyond the user's affected physical, cognitive or sensory capabilities. With wearable LL devices it is observed that they did not embed shared controllers. The system should involve the development of reliable discrete classifiers, combined with continuous (model-based) neural interfaces, to predict the subject's intent without needing continuous supervisory control, but an *"assist-as-needed"* control from the BCI. Wearable LL technologies should embed features such as, self-calibration, self-analysis (with backward-forward failure attribution analysis) and error-correction. This is followed by adopting appropriate behavioral testing methods for performance evaluations of the system.

Clinical evaluation of wearables needs standardized safety and tolerability assessment of important factors such as cardiometabolic, musculoskeletal, skin, and biomechanical risks, followed by the assessment of cognitive-behavioral discrepancies that define the user profile. Cardiorespiratory safety is of principal importance as individuals with stroke and SCI may have autonomic instability that can alter the pressure of blood-flow. Their heart rates may not respond correctly to increased cardiorespiratory demands, depending on the lesion intensity. The cardiorespiratory demands of supported BCI-exoskeleton/orthosis usage must primarily be assessed and carefully monitored also for reasons as: (1) the mean peak heart fitness levels after SCI vary considerably depending on the lesion characteristics, but are generally much lower than normal; and (2) the skeletal muscle after SCI (or any central-nervous system injury) shifts in a shortfall severity from slow to a fast jerk molecular composition. Patients with abnormal gait biomechanics and fitness levels must show adequate cardiorespiratory tolerance based on subject perceived exertion scales, and objective monitoring of metabolic profiles. This metabolic surveillance, along with careful clinical measures, to assess muscle injury, is inevitable for validating the cardiorespiratory, metabolic, and muscle safety during exoskeleton/orthosis use.

During rehabilitation, the wearable robotics may impose unusual joint kinetics and kinematics that could potentially injure bone or skin, particularly in stroke or SCI patients that usually have osteoporosis, unusual spasticity patterns, or contractures. For safe utilization a standard screening for assessment of bone health using dual X-ray absorptiometry and identification of abnormal torque or impulses ahead of time, could retain from injury. There should be a careful consideration between engineers, clinicians, and subjects with neurological disability to rightly apply this new technology.

Substantial research and understanding of the cortical representations, for the perception of bipedal locomotion, is vital for evaluating changes in cortical dynamics when wearing closed-loop BCI portable devices, and gauging on how these changes are correlated with gait adaptation. As the BCI wearable devices are designed to be stable, they have to finish one complete cycle of gait before stopping, resulting in a slow time-response compared to the model's output. This is why in some systems the subject has to keep standing, as long as he can, after stopping the robot for continuously recording the model's output state.

With P300-wearable LL devices, the decision time is relatively slow for real-time applications such as walking. The solution could involve implementation of more complex pipelines that include artifact removal techniques specific to gait-artifacts, followed by a better management of stimulus presentation duration. The P300 pipeline does not allow working asynchronously, which is an important aspect for the patient's comfort (can be tiring). Following this, the poor experimental paradigm that usually includes a screen on a treadmill is not applicable for street walking; accordingly, an augmented reality eyewear seems to be indispensable.

Assistive-Robot Challenges

Clinical evaluations revealed that subjects with poor BCI performance require an extra need for assistance while maneuvering assistive-robots during complex path plans such as narrow corridors, despite the arduous BCI training.

The use of adaptive assistance with BCI wheelchairs increases the task performance of the user; however, the fixed activation levels of the system do not integrate the user's performance. This is due to the varying fatigue and hormone levels of the user, due to which the shared controller may not offer constant level of assistance. Consequently, similar system behavior is always activated when the activation threshold is reached, even though an experienced user might still be able to recover from the disorientation on its own. System performance could be increased, if a user model is built at runtime, and the level of experience to determine the thresholds is estimated when the system behavior is activated.

Various customized filtering approaches have been deployed by researchers during different states of wheelchair use, for instance, the regular on and off switching of filter in between sessions of start and stop. Given in Kwak et al. (2015), when the filter was switched on or off, the subject was required to use another mental mode (or at least adapt its existing one) as the driving system was different when the filtering was applied. This resulted in a confusion mode which is a common problem in shared control systems. When the subject's acquired strategies are built up using one driving system (i.e., without filtering) and applied to the other situation (i.e., with filtering), it ends up in a weak performance, leading to a situation where the environmental filter is actually working against the user's intention. With present BCI-wheelchairs that incorporate shared controllers, if the activation levels of the system do not integrate the user's performance, it could lead to degradation or loss of function.

Reportedly P300-wheelchairs were too slow to stop in real-time, after the selection of a sub-goal from menu, the user has to focus on a validation option, due to which the wheelchair stops and waits for the next command (followed by validation) from the user. Consequently this ends up in more stationary positions than actually moving to specific destinations.

CONCLUSIONS

In this paper, we have presented a comprehensive review of the state-of-the-art EEG-BCI controlled wearable and assistive technologies for users having neuromotor disorder, SCI, stroke, disarticulation or amputation of residual LL. All reviewed applications are presented in the form of a generalized BCI control framework. The control framework is inclusive of the user, the BCI operator, the shared controller, and the robot device with the environment. Each element of the control framework was discussed in detail. The BCI operator is based on sub-layers, each of which is highlighting the feature extraction, classification and execution methods respectively, employed by each application. The reviewed applications comprised of oscillatory rhythms, event-related and evoked potentials as input signals. The EEG-BCI based portable and assistive device applications included exoskeletons, orthosis, wheelchairs, mobile/navigation robots and humanoids. Key features from each application were discussed and presented in the **Table 1**.

Based on the review we concluded that LL tasks, such as knee, or hip joint movements, have never been explicitly employed as MI or ME tasks in any BCI experimental protocol. Only foot or upper limb kinesthetic tasks are deployed. Additionally, it is observed that the EEG-based activity mode recognition, used to control wearable LL devices, only comprise of exoskeletons and orthosis. No viable prosthetic ankle-foot, or prosthetic LL device, employing EEG signals, for activity mode recognition, is currently available.

In most applications based on P300, strong output signals were observed that resulted in accurate command functions. It was followed by a slow performance pace and a loss in the user concentration due to stimulus presentation. On the contrary, applications employing SMR, where no stimulus protocol is involved, reflected a faster performance speed, followed by a weaker output signal during asynchronous mode.

Performance of EEG-based BCI, deployed by assistive technologies, is constrained due to the design of non-invasive modalities, compared to invasive ones and due to the limited size of features employed. In the case of complex movements more sets of parameters are required to execute a seamless output. This is still one of the challenging problems that require expertise to develop efficient and robust algorithms to apprehend user's motion intention.

In the most of the reviewed applications, there is a lack of quantitative performance indicators for the algorithms' evaluations. There is no explicit signal classification, percentage given. Error measurements between expected and real system trajectories are missing. There is no indication about the

measurements of the user-energy consumption, the walking endurance and the system costs. Finally, an important issue of carrying tests under realistic conditions, with patients having LL pathologies, needs special attention, provided the observations make the comparison of the dynamic behavior of each application difficult.

AUTHOR CONTRIBUTIONS

MT devised, drafted, structured, analyzed, and coordinated reading and writing of this review. She contributed text throughout, generated the figures and developed the structure of the generalized control framework and provided final approval of the manuscript. PT contributed to analysis, critical revision, provided feedback and final approval on the manuscript. MS contributed to the **Figure 1**, analyzed, critically revised, provided feedback and final approval on the manuscript. All authors read and approved the final version of the manuscript. All authors agree to be accountable for all aspects of the work in ensuring that questions related to the accuracy or integrity of any part of the work are appropriately investigated and resolved.

ACKNOWLEDGMENTS

Authors acknowledge the financial support received for this research provided by RMIT University Ph.D. International Scholarship (RPIS).

REFERENCES

Allison, B. Z., Wolpaw, E. W., and Wolpaw, J. R. (2007). Brain–computer interface systems: progress and prospects. *Expert Rev. Med. Devices* 4, 463–474. doi: 10.1586/17434440.4.4.463

Angeli, C. A., Edgerton, V. R., Gerasimenko, Y. P., and Harkema, S. J. (2014). Altering spinal cord excitability enables voluntary movements after chronic complete paralysis in humans. *Brain* 137, 1394–1409. doi: 10.1093/brain/awu038

Anthony, M., and Bartlett, P. L. (2009). *Neural Network Learning*: *Theoretical Foundations*. London: Cambridge University Press.

Armstrong, D. M. (1988). The supraspinal control of mammalian locomotion. *J. Physiol.* 405, 1–37. doi: 10.1113/jphysiol.1988.sp017319

Bakker, M., Verstappen, C., Bloem, B., and Toni, I. (2007). Recent advances in functional neuroimaging of gait. *J. Neural Transm.* 114, 1323–1331. doi: 10.1007/s00702-007-0783-8

Baykara, E., Ruf, C. A., Fioravanti, C., Käthner, I., Simon, N., Kleih, S. C., et al. (2016). Effects of training and motivation on auditory P300 brain-computer interface performance. *Clin. Neurophysiol.* 127, 379–387. doi: 10.1016/j.clinph.2015.04.054

Belda-Lois, J.-M., Mena-Del Horno, S., Bermejo-Bosch, I., Moreno, J. C., Pons, J. L., Farina, D., et al. (2011). Rehabilitation of gait after stroke: a review towards a top-down approach. *J. Neuroeng. Rehabil.* 8, 66. doi: 10.1186/1743-0003-8-66

Bell, C. J., Shenoy, P., Chalodhorn, R., and Rao, R. P. (2008). Control of a humanoid robot by a noninvasive brain–computer interface in humans. *J. Neural Eng.* 5, 214. doi: 10.1088/1741-2560/5/2/012

Belluomo, P., Bucolo, M., Fortuna, L., and Frasca, M. (2011). "Robot control through brain computer interface for patterns generation," in *AIP Conference Proceedings* (Halkidiki), 1031–1034.

Beloozerova, I. N., Sirota, M. G., and Swadlow, H. A. (2003). Activity of different classes of neurons of the motor cortex during locomotion. *J. Neurosci.* 23, 1087–1097. doi: 10.1523/JNEUROSCI.23-03-01087.2003

Bulea, T. C., Kilicarslan, A., Ozdemir, R., Paloski, W. H., and Contreras-Vidal, J. L. (2013). Simultaneous scalp electroencephalography (EEG), electromyography (EMG), and whole-body segmental inertial recording for multi-modal neural decoding. *J. Vis. Exp.* 77:e50602. doi: 10.3791/50602

Bulea, T. C., Kim, J., Damiano, D. L., Stanley, C. J., and Park, H.-S. (2015). Prefrontal, Posterior parietal and sensorimotor network activity underlying speed control during walking. *Front. Hum. Neurosci.* 9:247. doi: 10.3389/fnhum.2015.00247

Capogrosso, M., Milekovic, T., Borton, D., Wagner, F., Moraud, E. M., Mignardot, J.-B., et al. (2016). A brain–spine interface alleviating gait deficits after spinal cord injury in primates. *Nature* 539, 284–288. doi: 10.1038/nature20118

Carlson, T., and Millan, J. D. R. (2013). Brain-controlled wheelchairs: a robotic architecture. *IEEE Rob. Autom. Mag.* 20, 65–73. doi: 10.1109/MRA.2012.2229936

Castermans, T., Duvinage, M., Hoellinger, T., Petieau, M., Dutoit, T., and Cheron, G. (2011a). "An analysis of EEG signals during voluntary rhythmic foot movements," in *2011 5th International IEEE/EMBS Conference on the Neural Engineering (NER)* (Cancún), 584–588.

Castermans, T., Duvinage, M., Petieau, M., Hoellinger, T., De Saedeleer, C., Seetharaman, K., et al. (2011b). "Optimizing the performances of a P300-based brain–computer interface in ambulatory conditions," in *IEEE Journal on Emerging and Selected Topics in Circuits and Systems,* Vol. 1 (New York, NY), 566–577.

Cervera, M. A., Soekadar, S. R., Ushiba, J., Millán, J. D. R., Liu, M., Birbraumer, N., et al. (2018). Brain-computer interfaces for post-stroke motor rehabilitation: a meta-analysis. *Ann. Clin. Transl. Neurol.* 5, 651–663. doi: 10.1002/acn3.544

Chae, Y., Jeong, J., and Jo, S. (2011a). "Noninvasive brain-computer interface-based control of humanoid navigation," in *2011 IEEE/RSJ International Conference on the Intelligent Robots and Systems (IROS)* (San Francisco, CA), 685–691.

Chae, Y., Jeong, J., and Jo, S. (2012). Toward brain-actuated humanoid robots: asynchronous direct control using an EEG-based BCI. *IEEE Trans. Rob.* 28, 1131–1144. doi: 10.1109/TRO.2012.2201310

Chae, Y., Jo, S., and Jeong, J. (2011b). "Brain-actuated humanoid robot navigation control using asynchronous brain-computer interface," in *2011 5th International IEEE/EMBS Conference on the Neural Engineering (NER)* (Cancún), 519–524.

Chéron, G., Duvinage, M., Castermans, T., Leurs, F., Cebolla, A., Bengoetxea, A., et al. (2011). "Toward an integrative dynamic recurrent neural network for sensorimotor coordination dynamics," in *Recurrent Neural Networks for Temporal Data Processing,* Vol. 5, ed H. Cardot (Rijeka: InTech), 67–80.

Chéron, G., Duvinage, M., De Saedeleer, C., Castermans, T., Bengoetxea, A., Petieau, M., et al. (2012). From spinal central pattern generators to cortical network: integrated BCI for walking rehabilitation. *Neural Plast.* 2012:375148. doi: 10.1155/2012/375148

Choi, K., and Cichocki, A. (2008). Control of a wheelchair by motor imagery in real time. *Intell. Data Eng. Autom. Learn.* 2008, 330–337. doi: 10.1007/978-3-540-88906-9_42

Chvatal, S. A., and Ting, L. H. (2012). Voluntary and reactive recruitment of locomotor muscle synergies during perturbed walking. *J. Neurosci.* 32, 12237–12250. doi: 10.1523/JNEUROSCI.6344-11.2012

Chvatal, S. A., and Ting, L. H. (2013). Common muscle synergies for balance and walking. *Front. Comput. Neurosci.* 7:48. doi: 10.3389/fncom.2013.00048

Chvatal, S. A., Torres-Oviedo, G., Safavynia, S. A., and Ting, L. H. (2011). Common muscle synergies for control of center of mass and force in nonstepping and stepping postural behaviors. *J. Neurophysiol.* 106, 999–1015. doi: 10.1152/jn.00549.2010

Contreras-Vidal, J. L., Bhagat, N. A., Brantley, J., Cruz-Garza, J. G., He, Y., Manley, Q., et al. (2016). Powered exoskeletons for bipedal locomotion after spinal cord injury. *J. Neural Eng.* 13:031001. doi: 10.1088/1741-2560/13/3/031001

Contreras-Vidal, J. L., and Grossman, R. G. (2013). "NeuroRex: A clinical neural interface roadmap for EEG-based brain machine interfaces to a lower body

robotic exoskeleton," in *2013 35th Annual International Conference of the IEEE Engineering in Medicine and Biology Society (EMBC)* (Osaka), 1579–1582.

Daly, J. J., and Wolpaw, J. R. (2008). Brain–computer interfaces in neurological rehabilitation. *Lancet Neurol.* 7, 1032–1043. doi: 10.1016/S1474-4422(08)70223-0

Delorme, A., Kothe, C., Vankov, A., Bigdely-Shamlo, N., Oostenveld, R., Zander, T. O., et al. (2010). *MATLAB-Based Tools for BCI Research*. London: Springer, Brain-computer interfaces.

Delorme, A., Mullen, T., Kothe, C., Acar, Z. A., Bigdely-Shamlo, N., Vankov, A., et al. (2011). EEGLAB, SIFT, NFT, BCILAB, and ERICA: new tools for advanced EEG processing. *Comput. Intell. Neurosci.* 2011:10. doi: 10.1155/2011/130714

Deng, W., Papavasileiou, I., Qiao, Z., Zhang, W., Lam, K.-Y., and Han, S. (2018). Advances in automation technologies for lower-extremity neurorehabilitation: a review and future challenges. *IEEE Rev. Biomed. Eng.* 11, 289–305. doi: 10.1109/RBME.2018.2830805

De Venuto, D., Annese, V. F., and Mezzina, G. (2017). "An embedded system remotely driving mechanical devices by P300 brain activity," in *Proceedings of the Conference on Design, Automation & Test in Europe, European Design and Automation Association* (Lausanne), 1014–1019.

Dimitrijevic, M. R., Gerasimenko, Y., and Pinter, M. M. (1998). Evidence for a spinal central pattern generator in humans. *Ann. N. Y. Acad. Sci.* 860, 360–376. doi: 10.1111/j.1749-6632.1998.tb09062.x

Do, A. H., Wang, P. T., King, C. E., Abiri, A., and Nenadic, Z. (2011). Brain-computer interface controlled functional electrical stimulation system for ankle movement. *J. Neuroeng. Rehabil.* 8:49. doi: 10.1186/1743-0003-8-49

Do, A. H., Wang, P. T., King, C. E., Chun, S. N., and Nenadic, Z. (2013). Brain-computer interface controlled robotic gait orthosis. *J. Neuroeng. Rehabil.* 10:111. doi: 10.1186/1743-0003-10-111

Do, A. H., Wang, P. T., King, C. E., Schombs, A., Cramer, S. C., and Nenadic, Z. (2012). "Brain-computer interface controlled functional electrical stimulation device for foot drop due to stroke," in *2012 Annual International Conference of the IEEE Engineering in Medicine and Biology Society (EMBC)* (San Diego, CA), 6414–6417.

Drew, T., Kalaska, J., and Krouchev, N. (2008). Muscle synergies during locomotion in the cat: a model for motor cortex control. *J. Physiol.* 586, 1239–1245. doi: 10.1113/jphysiol.2007.146605

Duvinage, M., Castermans, T., Jiménez-Fabián, R., Hoellinger, T., De Saedeleer, C., Petieau, M., et al. (2012). "A five-state P300-based foot lifter orthosis: Proof of concept," in *Biosignals and Biorobotics Conference (BRC)*, *2012 ISSNIP* (Manaus: IEEE), 1–6.

Escolano, C., Antelis, J. M., and Minguez, J. (2012). A telepresence mobile robot controlled with a noninvasive brain–computer interface. *IEEE Trans. Syst. Man Cybern. B Cybern.* 42, 793–804. doi: 10.1109/TSMCB.2011.2177968

Fatourechi, M., Bashashati, A., Ward, R. K., and Birch, G. E. (2007). EMG and EOG artifacts in brain computer interface systems: a survey. *Clin. Neurophysiol.* 118, 480–494. doi: 10.1016/j.clinph.2006.10.019

Ferdousy, R., Choudhory, A. I., Islam, M. S., Rab, M. A., and Chowdhory, M. E. H. (2010). "Electrooculographic and electromyographic artifacts removal from EEG," in *2010 2nd International Conference on the Chemical, Biological and Environmental Engineering (ICBEE)* (Cairo), 163–167.

Ferreira, A., Celeste, W. C., Cheein, F. A., Bastos-Filho, T. F., Sarcinelli-Filho, M., and Carelli, R. (2008). Human-machine interfaces based on EMG and EEG applied to robotic systems. *J. Neuroeng. Rehabil.* 5:10. doi: 10.1186/1743-0003-5-10

Frolov, A. A., Mokienko, O., Lyukmanov, R., Biryukova, E., Kotov, S., Turbina, L., et al. (2017). Post-stroke rehabilitation training with a motor-imagery-based brain-computer interface (BCI)-controlled hand exoskeleton: a randomized controlled multicenter trial. *Front. Neurosci.* 11:400. doi: 10.3389/fnins.2017.00400

Galán, F., Nuttin, M., Lew, E., Ferrez, P. W., Vanacker, G., Philips, J., et al. (2008). A brain-actuated wheelchair: asynchronous and non-invasive brain–computer interfaces for continuous control of robots. *Clin. Neurophysiol.* 119, 2159–2169. doi: 10.1016/j.clinph.2008.06.001

Gancet, J., Ilzkovitz, M., Cheron, G., Ivanenko, Y., Van Der Kooij, H., Van Der Helm, F., et al. (2011). "MINDWALKER: a brain controlled lower limbs exoskeleton for rehabilitation. Potential applications to space," in *11th Symposium on Advanced Space Technologies in Robotics and Automation* (Noordwijk), 12–14.

Gancet, J., Ilzkovitz, M., Motard, E., Nevatia, Y., Letier, P., De Weerdt, D., et al. (2012). "MINDWALKER: going one step further with assistive lower limbs exoskeleton for SCI condition subjects," in *2012 4th IEEE RAS & EMBS International Conference on the Biomedical Robotics and Biomechatronics (BioRob)* (Rome), 1794–1800.

García-Cossio, E., Severens, M., Nienhuis, B., Duysens, J., Desain, P., Keijsers, N., et al. (2015). Decoding sensorimotor rhythms during robotic-assisted treadmill walking for brain computer interface (BCI) applications. *PLoS ONE* 10:e0137910. doi: 10.1371/journal.pone.0137910

Gramann, K., Ferris, D. P., Gwin, J., and Makeig, S. (2014). Imaging natural cognition in action. *Int. J. Psychophysiol.* 91, 22–29. doi: 10.1016/j.ijpsycho.2013.09.003

Gwin, J. T., Gramann, K., Makeig, S., and Ferris, D. P. (2010). Removal of movement artifact from high-density EEG recorded during walking and running. *J. Neurophysiol.* 103, 3526–3534. doi: 10.1152/jn.00105.2010

Gwin, J. T., Gramann, K., Makeig, S., and Ferris, D. P. (2011). Electrocortical activity is coupled to gait cycle phase during treadmill walking. *Neuroimage* 54, 1289–1296. doi: 10.1016/j.neuroimage.2010.08.066

Hashimoto, Y., and Ushiba, J. (2013). EEG-based classification of imaginary left and right foot movements using beta rebound. *Clin. Neurophysiol.* 124, 2153–2160. doi: 10.1016/j.clinph.2013.05.006

He, B. (2016). *Neural Engineering*. New York, NY: Springer, U. S.

He, B., Baxter, B., Edelman, B. J., Cline, C. C., and Wenjing, W. Y. (2015). Noninvasive brain-computer interfaces based on sensorimotor rhythms. *Proc. IEEE* 103, 907–925. doi: 10.1109/JPROC.2015.2407272

He, Y., Eguren, D., Azorín, J. M., Grossman, R. G., Luu, T. P., and Contreras-Vidal, J. L. (2018a). Brain-machine interfaces for controlling lower-limb powered robotic systems. *J. Neural Eng.* 15:021004. doi: 10.1088/1741-2552/aaa8c0

He, Y., Luu, T. P., Nathan, K., Nakagome, S., and Contreras-Vidal, J. L. (2018b). A mobile brain-body imaging dataset recorded during treadmill walking with a brain-computer interface. *Sci. Data* 5:180074. doi: 10.1038/sdata.2018.74

Herr, H. M., Weber, J. A., Au, S. K., Deffenbaugh, B. W., Magnusson, L. H., Hofmann, A. G., et al. (2013). *Powered Ankle-Foot Prothesis*. Google Patents No. 60/934,223. Cambridge, MA: Massachusetts Institute of Technology.

Huang, D., Qian, K., Fei, D.-Y., Jia, W., Chen, X., and Bai, O. (2012). Electroencephalography (EEG)-based brain–computer interface (BCI): a 2-D virtual wheelchair control based on event-related desynchronization/synchronization and state control. *IEEE Trans. Neural Syst. Rehabil. Eng.* 20, 379–388. doi: 10.1109/TNSRE.2012.2190299

Iturrate, I., Antelis, J., and Minguez, J. (2009a). "Synchronous EEG brain-actuated wheelchair with automated navigation," in *IEEE International Conference on the Robotics and Automation ICRA'09* (Kobe), 2318–2325.

Iturrate, I., Antelis, J. M., Kubler, A., and Minguez, J. (2009b). A noninvasive brain-actuated wheelchair based on a P300 neurophysiological protocol and automated navigation. *IEEE Trans. Rob.* 25, 614–627. doi: 10.1109/TRO.2009.2020347

Jain, S., Gourab, K., Schindler-Ivens, S., and Schmit, B. D. (2013). EEG during pedaling: evidence for cortical control of locomotor tasks. *Clin. Neurophysiol.* 124, 379–390. doi: 10.1016/j.clinph.2012.08.021

Jimenez-Fabian, R., and Verlinden, O. (2012). Review of control algorithms for robotic ankle systems in lower-limb orthoses, prostheses, and exoskeletons. *Med. Eng. Phys.* 34, 397–408. doi: 10.1016/j.medengphy.2011.11.018

Kalcher, J., and Pfurtscheller, G. (1995). Discrimination between phase-locked and non-phase-locked event-related EEG activity. *Electroencephalogr. Clin. Neurophysiol.* 94, 381–384. doi: 10.1016/0013-4694(95)00040-6

Kaufmann, T., Herweg, A., and Kübler, A. (2014). Toward brain-computer interface based wheelchair control utilizing tactually-evoked event-related potentials. *J. Neuroeng. Rehabil.* 11:7. doi: 10.1186/1743-0003-11-7

Kautz, S. A., and Patten, C. (2005). Interlimb influences on paretic leg function in poststroke hemiparesis. *J. Neurophysiol.* 93, 2460–2473. doi: 10.1152/jn.00963.2004

Kilicarslan, A., Prasad, S., Grossman, R. G., and Contreras-Vidal, J. L. (2013). "High accuracy decoding of user intentions using EEG to control a

lower-body exoskeleton," in *2013 35th Annual International Conference of the IEEE Engineering in Medicine and Biology Society (EMBC)* (Osaka), 5606–5609.

King, C. E., Wang, P. T., Chui, L. A., Do, A. H., and Nenadic, Z. (2013). Operation of a brain-computer interface walking simulator for individuals with spinal cord injury. *J. Neuroeng. Rehabil.* 10:77. doi: 10.1186/1743-0003-10-77

Kothe, C. A., and Makeig, S. (2013). BCILAB: a platform for brain–computer interface development. *J. Neural Eng.* 10:056014. doi: 10.1088/1741-2560/10/5/056014

Kumar, D., Aggarwal, G., Sehgal, R., Das, A., Lahiri, U., and Dutta, A. (2015). "Engagement-sensitive interactive neuromuscular electrical therapy system for post-stroke balance rehabilitation-a concept study," in *2015 7th International IEEE/EMBS Conference on the Neural Engineering (NER)* (Montpellier), 190–193.

Kwak, N.-S., Müller, K.-R., and Lee, S.-W. (2015). A lower limb exoskeleton control system based on steady state visual evoked potentials. *J. Neural Eng.* 12:056009. doi: 10.1088/1741-2560/12/5/056009

La Fougere, C., Zwergal, A., Rominger, A., Förster, S., Fesl, G., Dieterich, M., et al. (2010). Real versus imagined locomotion: a [18 F]-FDG PET-fMRI comparison. *Neuroimage* 50, 1589–1598. doi: 10.1016/j.neuroimage.2009.12.060

Lazarou, I., Nikolopoulos, S., Petrantonakis, P. C., Kompatsiaris, I., and Tsolaki, M. (2018). EEG-based brain-computer interfaces for communication and rehabilitation of people with motor impairment: a novel approach of the 21st century. *Front. Hum. Neurosci.* 12:14. doi: 10.3389/fnhum.2018.00014

Lebedev, M. A., and Nicolelis, M. A. (2017). Brain-machine interfaces: from basic science to neuroprostheses and neurorehabilitation. *Physiol. Rev.* 97, 767–837. doi: 10.1152/physrev.00027.2016

Lee, K., Liu, D., Perroud, L., Chavarriaga, R., and Millán, J. D. R. (2017). *Endogenous Control of Powered Lower-Limb Exoskeleton*. Basel: Springer: Wearable Robotics: Challenges and Trends.

Liu, Y.-H., Lin, L.-F., Chou, C.-W., Chang, Y., Hsiao, Y.-T., and Hsu, W.-C. (2018). Analysis of electroencephalography event-related desynchronisation and synchronisation induced by lower-limb stepping motor imagery. *J. Med. Biol. Eng.* 4, 1–16. doi: 10.1007/s40846-018-0379-9

Liu, Y.-H., Zhang, B., Liu, Q., Hsu, W.-C., Hsiao, Y.-T., Su, J.-Y., et al. (2015). "A robotic gait training system integrating split-belt treadmill, footprint sensing and synchronous EEG recording for neuro-motor recovery," in *2015 37th Annual International Conference of the IEEE Engineering in Medicine and Biology Society (EMBC)* (Milan), 3573–3577.

Lopes, A. C., Pires, G., Vaz, L., and Nunes, U. (2011). "Wheelchair navigation assisted by human-machine shared-control and a P300-based brain computer interface," in *2011 IEEE/RSJ International Conference on the IEEE Intelligent Robots and Systems (IROS)* (San Francisco, CA), 2438–2444.

Lotte, F. (2014). *A Tutorial on EEG Signal-Processing Techniques for Mental-State Recognition in Brain–Computer Interfaces*. London: Springer, Guide to Brain-Computer Music Interfacing.

Lotte, F., Bougrain, L., Cichocki, A., Clerc, M., Congedo, M., Rakotomamonjy, A., et al. (2018). A review of classification algorithms for EEG-based brain-computer interfaces: a 10 year update. *J. Neural Eng.* 15:031005. doi: 10.1088/1741-2552/aab2f2

Lotte, F., Congedo, M., Lécuyer, A., Lamarche, F., and Arnaldi, B. (2007). A review of classification algorithms for EEG-based brain–computer interfaces. *J. Neural Eng.* 4:R1. doi: 10.1088/1741-2560/4/2/R01

Lotte, F., Fujisawa, J., Touyama, H., Ito, R., Hirose, M., and Lécuyer, A. (2009). "Towards ambulatory brain-computer interfaces: A pilot study with P300 signals," in *Proceedings of the International Conference on Advances in Computer Enterntainment Technology,* (Athens: ACM), 336–339.

Maguire, C. C., Sieben, J. M., and De Bie, R. A. (2018). Movement goals encoded within the cortex and muscle synergies to reduce redundancy pre and post-stroke. The relevance for gait rehabilitation and the prescription of walking-aids. A literature review and scholarly discussion. *Physiother. Theory Pract.* 5, 1–14. doi: 10.1080/09593985.2018.1434579

Malouin, F., and Richards, C. L. (2010). Mental practice for relearning locomotor skills. *Phys. Ther.* 90, 240–251. doi: 10.2522/ptj.20090029

Malouin, F., Richards, C. L., Durand, A., and Doyon, J. (2008). Clinical assessment of motor imagery after stroke. *Neurorehabil. Neural Repair.* 22, 330–340. doi: 10.1177/1545968307313499

Malouin, F., Richards, C. L., Jackson, P. L., Dumas, F., and Doyon, J. (2003). Brain activations during motor imagery of locomotor-related tasks: a PET study. *Hum. Brain Mapp.* 19, 47–62. doi: 10.1002/hbm.10103

Marlinski, V., and Beloozerova, I. N. (2014). Burst firing of neurons in the thalamic reticular nucleus during locomotion. *J. Neurophysiol.* 112, 181–192. doi: 10.1152/jn.00366.2013

Mellinger, J., and Schalk, G. (2007). *BCI2000: A General-Purpose Software Platform for BCI Research*. Cambridge, MA: Towards Brain-Computer Interfacing.

Millán, J. D. R., Galán, F., Vanhooydonck, D., Lew, E., Philips, J., and Nuttin, M. (2009). "Asynchronous non-invasive brain-actuated control of an intelligent wheelchair," in *Annual International Conference of the IEEE Engineering in Medicine and Biology Society (EMBC)* (Minneapolis, MN), 3361–3364.

Millán, J. D. R., Rupp, R., Müller-Putz, G. R., Murray-Smith, R., Giugliemma, C., Tangermann, M., et al. (2010). Combining brain–computer interfaces and assistive technologies: state-of-the-art and challenges. *Front. Neurosci.* 4:161. doi: 10.3389/fnins.2010.00161

Millan, J. R., Renkens, F., Mourino, J., and Gerstner, W. (2004). Noninvasive brain-actuated control of a mobile robot by human EEG. *IEEE Trans. Biomed. Eng.* 51, 1026–1033. doi: 10.1109/TBME.2004.827086

Mokienko, O., Chervyakov, A., Kulikova, S., Bobrov, P., Chernikova, L., Frolov, A., et al. (2013). Increased motor cortex excitability during motor imagery in brain-computer interface trained subjects. *Front. Comput. Neurosci.* 7:168. doi: 10.3389/fncom.2013.00168

Müller-Gerking, J., Pfurtscheller, G., and Flyvbjerg, H. (1999). Designing optimal spatial filters for single-trial EEG classification in a movement task. *Clin. Neurophysiol.* 110, 787–798. doi: 10.1016/S1388-2457(98)00038-8

Murray, S., and Goldfarb, M. (2012). "Towards the use of a lower limb exoskeleton for locomotion assistance in individuals with neuromuscular locomotor deficits," in *2012 Annual International Conference of the IEEE Engineering in Medicine and Biology Society (EMBC)*, (San Diego, CA: IEEE), 1912–1915.

Nicolas-Alonso, L. F., and Gomez-Gil, J. (2012). Brain computer interfaces, a review. *Sensors* 12, 1211–1279. doi: 10.3390/s120201211

Noda, T., Sugimoto, N., Furukawa, J., Sato, M.-A., Hyon, S.-H., and Morimoto, J. (2012). "Brain-controlled exoskeleton robot for BMI rehabilitation," in *2012 12th IEEE-RAS International Conference on Humanoid Robots (Humanoids)* (Osaka: IEEE), 21–27.

Nolan, H., Whelan, R., and Reilly, R. (2010). FASTER: fully automated statistical thresholding for EEG artifact rejection. *J. Neurosci. Methods* 192, 152–162. doi: 10.1016/j.jneumeth.2010.07.015

Palankar, M., De Laurentis, K. J., Alqasemi, R., Veras, E., Dubey, R., Arbel, Y., et al. (2009). "Control of a 9-DoF wheelchair-mounted robotic arm system using a P300 brain computer interface: Initial experiments," in *2008 IEEE International Conference on Robotics and Biomimetics, ROBIO* (Bangkok: IEEE), 348–353. doi: 10.1109/ROBIO.2009.4913028

Penfield, W., and Boldrey, E. (1937). Somatic motor and sensory representation in the cerebral cortex of man as studied by electrical stimulation. *Brain* 60, 389–443. doi: 10.1093/brain/60.4.389

Petersen, T. H., Willerslev-Olsen, M., Conway, B. A., and Nielsen, J. B. (2012). The motor cortex drives the muscles during walking in human subjects. *J. Physiol.* 590, 2443–2452. doi: 10.1113/jphysiol.2012.227397

Petrofsky, J. S., and Khowailed, I. A. (2014). Postural sway and motor control in trans-tibial amputees as assessed by electroencephalography during eight balance training tasks. *Med. Sci. Monit.* 20: 2695–2704. doi: 10.12659/MSM.891361

Pfurtscheller, G., Brunner, C., Schlögl, A., and Da Silva, F. L. (2006a). Mu rhythm (de) synchronization and EEG single-trial classification of different motor imagery tasks. *Neuroimage* 31, 153–159. doi: 10.1016/j.neuroimage.2005.12.003

Pfurtscheller, G., Leeb, R., Keinrath, C., Friedman, D., Neuper, C., Guger, C., et al. (2006b). Walking from thought. *Brain Res.* 1071, 145–152. doi: 10.1016/j.brainres.2005.11.083

Pfurtscheller, G., Neuper, C., Brunner, C., and Da Silva, F. L. (2005). Beta rebound after different types of motor imagery in man. *Neurosci. Lett.* 378, 156–159. doi: 10.1016/j.neulet.2004.12.034

Pfurtscheller, G., and Solis-Escalante, T. (2009). Could the beta rebound in the EEG be suitable to realize a "brain switch"? *Clin. Neurophysiol.* 120, 24–29. doi: 10.1016/j.clinph.2008.09.027

Pires, G., Castelo-Branco, M., and Nunes, U. (2008). "Visual P300-based BCI to steer a wheelchair: a Bayesian approach," in *2008 30th Annual International Conference of the IEEE Engineering in Medicine and Biology Society EMBS* (Vancouver, BC: IEEE), 658–661.

Pons, J., Moreno, J., Torricelli, D., and Taylor, J. (2013). "Principles of human locomotion: a review," in *2013 35th Annual International Conference of the IEEE Engineering in Medicine and Biology Society (EMBC)* (Osaka: IEEE), 6941–6944.

Presacco, A., Forrester, L., and Contreras-Vidal, J. L. (2011a). "Towards a non-invasive brain-machine interface system to restore gait function in humans," in *2011 Annual International Conference of the IEEE Engineering in Medicine and Biology Society, EMBC* (Boston, MA: IEEE), 4588–4591.

Presacco, A., Goodman, R., Forrester, L., and Contreras-Vidal, J. L. (2011b). Neural decoding of treadmill walking from noninvasive electroencephalographic signals. *J. Neurophysiol.* 106, 1875–1887. doi: 10.1152/jn.00104.2011

Raethjen, J., Govindan, R., Binder, S., Zeuner, K. E., Deuschl, G., and Stolze, H. (2008). Cortical representation of rhythmic foot movements. *Brain Res.* 1236, 79–84. doi: 10.1016/j.brainres.2008.07.046

Rebsamen, B., Burdet, E., Guan, C., Zhang, H., Teo, C. L., Zeng, Q., et al. (2007). Controlling a wheelchair indoors using thought. *IEEE Intell. Syst.* 22, 18–24. doi: 10.1109/MIS.2007.26

Rebsamen, B., Guan, C., Zhang, H., Wang, C., Teo, C., Ang, M. H., et al. (2010). A brain controlled wheelchair to navigate in familiar environments. *IEEE Trans. Neural Syst. Rehabil. Eng.* 18, 590–598. doi: 10.1109/TNSRE.2010.2049862

Renard, Y., Lotte, F., Gibert, G., Congedo, M., Maby, E., Delannoy, V., et al. (2010). Openvibe: an open-source software platform to design, test, and use brain–computer interfaces in real and virtual environments. *Presence* 19, 35–53. doi: 10.1162/pres.19.1.35

Rivet, B., Souloumiac, A., Attina, V., and Gibert, G. (2009). xDAWN algorithm to enhance evoked potentials: application to brain–computer interface. *IEEE Trans. Biomed. Eng.* 56, 2035–2043. doi: 10.1109/TBME.2009.2012869

Salazar-Varas, R., Costa, Á., Iáñez, E., Úbeda, A., Hortal, E., and Azorín, J. (2015). Analyzing EEG signals to detect unexpected obstacles during walking. *J. Neuroeng. Rehabil.* 12, 101. doi: 10.1186/s12984-015-0095-4

Schalk, G., Mcfarland, D. J., Hinterberger, T., Birbaumer, N., and Wolpaw, J. R. (2004). BCI2000: a general-purpose brain-computer interface (BCI) system. *IEEE Trans. Biomed. Eng.* 51, 1034–1043. doi: 10.1109/TBME.2004.827072

Scherrer, B. (2007). *Gaussian Mixture Model Classifiers*. Lecture Notes, February.

Schwartz, A. B., Cui, X. T., Weber, D. J., and Moran, D. W. (2006). Brain-controlled interfaces: movement restoration with neural prosthetics. *Neuron* 52, 205–220. doi: 10.1016/j.neuron.2006.09.019

Sczesny-Kaiser, M., Höffken, O., Aach, M., Cruciger, O., Grasmücke, D., Meindl, R., et al. (2015). HAL® exoskeleton training improves walking parameters and normalizes cortical excitability in primary somatosensory cortex in spinal cord injury patients. *J. Neuroeng. Rehabil.* 12, 68. doi: 10.1186/s12984-015-0058-9

Semprini, M., Laffranchi, M., Sanguineti, V., Avanzino, L., De Icco, R., De Michieli, L., et al. (2018). Technological approaches for neurorehabilitation: from robotic devices to brain stimulation and beyond. *Fronti. Neurol.* 9:212. doi: 10.3389/fneur.2018.00212

Semmlow, J. L., and Griffel, B. (2014). *Biosignal and Medical Image Processing*. Cambridge, MA: CRC press.

Slutzky, M. W. (2018). Brain-machine interfaces: powerful tools for clinical treatment and neuroscientific investigations. *Neuroscientist*. doi: 10.1177/1073858418775355. [Epub ahead of print].

Soekadar, S. R., Witkowski, M., Vitiello, N., and Birbaumer, N. (2015). An EEG/EOG-based hybrid brain-neural computer interaction (BNCI) system to control an exoskeleton for the paralyzed hand. *Biomed. Tech. (Berl)* 60, 199–205. doi: 10.1515/bmt-2014-0126

Takahashi, M., Gouko, M., and Ito, K. (2009). "Fundamental research about electroencephalogram (EEG)-functional electrical stimulation (FES) rehabilitation system," in 2009 *IEEE International Conference on, IEEE Rehabilitation Robotics, (2009) ICORR* (Kyoto), 316–321.

Takahashi, M., Takeda, K., Otaka, Y., Osu, R., Hanakawa, T., Gouko, M., et al. (2012). Event related desynchronization-modulated functional electrical stimulation system for stroke rehabilitation: a feasibility study. *J. Neuroeng. Rehabil.* 9, 56. doi: 10.1186/1743-0003-9-56

Tariq, M., Trivailo, P. M., and Simic, M. (2017a). "Detection of knee motor imagery by Mu ERD/ERS quantification for BCI based neurorehabilitation applications," in *2017 11th Asian Control Conference (ASCC)*, (Gold Coast, QLD), 2215–2219.

Tariq, M., Trivailo, P. M., and Simic, M. (2018). Event-related changes detection in sensorimotor rhythm. *Int. Rob. Autom. J.* 4, 119–120. doi: 10.15406/iratj.2018.04.00105

Tariq, M., Uhlenberg, L., Trivailo, P., Munir, K. S., and Simic, M. (2017b). "Mu-beta rhythm ERD/ERS quantification for foot motor execution and imagery tasks in BCI applications," in *2017 8th IEEE International Conference on Cognitive Infocommunications (CogInfoCom)* (Debrecen), 000091–000096.

Taylor II, R. M., Hudson, T. C., Seeger, A., Weber, H., Juliano, J., and Helser, A. T. (2001). "VRPN: a device-independent, network-transparent VR peripheral system," in *Proceedings of the ACM Symposium on Virtual Reality Software and Technology*, (Baniff, AB: ACM), 55–61.

Tonin, L., Carlson, T., Leeb, R., and Millán, J. D. R. (2011). "Brain-controlled telepresence robot by motor-disabled people," in *2011 Annual International Conference of the IEEE Engineering in Medicine and Biology Society, EMBC* (Boston, MA: IEEE), 4227–4230.

Tonin, L., Leeb, R., Tavella, M., Perdikis, S., and Millán, J. D. R. (2010). "The role of shared-control in BCI-based telepresence," in *2010 IEEE International Conference on Systems Man and Cybernetics*, (Istanbul: IEEE), 1462–1466.

Tsui, C. S. L., Gan, J. Q., and Hu, H. (2011). A self-paced motor imagery based brain-computer interface for robotic wheelchair control. *Clin. EEG Neurosci.* 42, 225–229. doi: 10.1177/155005941104200407

Tucker, M. R., Olivier, J., Pagel, A., Bleuler, H., Bouri, M., Lambercy, O., et al. (2015). Control strategies for active lower extremity prosthetics and orthotics: a review. *J. Neuroeng. Rehabil.* 12, 1. doi: 10.1186/1743-0003-12-1

Vanacker, G., Del R Millán, J., Lew, E., Ferrez, P. W., Moles, F. G., Philips, J., et al. (2007). Context-based filtering for assisted brain-actuated wheelchair driving. *Comput. Intell. Neurosci.* 2007, 3–3. doi: 10.1155/2007/25130

Vasilyev, A., Liburkina, S., Yakovlev, L., Perepelkina, O., and Kaplan, A. (2017). Assessing motor imagery in brain-computer interface training: psychological and neurophysiological correlates. *Neuropsychologia* 97, 56–65. doi: 10.1016/j.neuropsychologia.2017.02.005

Vidal, J. J. (1973). Toward direct brain-computer communication. *Annu. Rev. Biophys. Bioeng.* 2, 157–180. doi: 10.1146/annurev.bb.02.060173.001105

Viola, F. C., Thorne, J., Edmonds, B., Schneider, T., Eichele, T., and Debener, S. (2009). Semi-automatic identification of independent components representing EEG artifact. *Clin. Neurophysiol.* 120, 868–877. doi: 10.1016/j.clinph.2009.01.015

Wang, P. T., King, C., Chui, L. A., Nenadic, Z., and Do, A. (2010). "BCI controlled walking simulator for a BCI driven FES device," in *Proceedings of RESNA Annual Conference*, (Arlington: VA: RESNA).

Wang, P. T., King, C. E., Chui, L. A., Do, A. H., and Nenadic, Z. (2012). Self-paced brain–computer interface control of ambulation in a virtual reality environment. *J. Neural Eng.* 9:056016. doi: 10.1088/1741-2560/9/5/056016

Wieser, M., Haefeli, J., Bütler, L., Jäncke, L., Riener, R., and Koeneke, S. (2010). Temporal and spatial patterns of cortical activation during assisted lower limb movement. *Exp. Brain Res.* 203, 181–191. doi: 10.1007/s00221-010-2223-5

Wolpaw, J., and Wolpaw, E. W. (2012). Brain-*Computer Interfaces*: *Principles* and *Practice*, New York, NY: Oxford University Press.

Wolpaw, J. R., Birbaumer, N., McFarland, D. J., Pfurtscheller, G., and Vaughan, T. M. (2002). Brain-computer interfaces for communication and control. *Clin. Neurophysiol.* 113, 767–791. doi: 10.1016/S1388-2457(02)00057-3

Wolpaw, J. R., and Mcfarland, D. J. (2004). Control of a two-dimensional movement signal by a noninvasive brain-computer interface in humans. *Proc. Natl. Acad. Sci. U.S.A.* 101, 17849–17854. doi: 10.1073/pnas.0403504101

Xu, R., Jiang, N., Mrachacz-Kersting, N., Lin, C., Prieto, G. A., Moreno, J. C., et al. (2014). A closed-loop brain–computer interface triggering an active ankle–foot orthosis for inducing cortical neural plasticity.

IEEE Trans. Biomed. Eng. 61, 2092–2101. doi: 10.1109/TBME.2014.2313867

Yang, Z., Wang, Y., and Ouyang, G. (2014). Adaptive neuro-fuzzy inference system for classification of background EEG signals from ESES patients and controls. *ScientificWorldJournal* 2014:140863. doi: 10.1155/2014/140863

Zelenin, P. V., Deliagina, T. G., Orlovsky, G. N., Karayannidou, A., Dasgupta, N. M., Sirota, M. G., et al. (2011). Contribution of different limb controllers to modulation of motor cortex neurons during locomotion. *J. Neurosci.* 31, 4636–4649. doi: 10.1523/JNEUROSCI.6511-10.2011

Conflict of Interest Statement: The authors declare that the research was conducted in the absence of any commercial or financial relationships that could be construed as a potential conflict of interest.

frontiers in Neuroscience

ORIGINAL RESEARCH
published: 11 September 2018
doi: 10.3389/fnins.2018.00639

Balance in Blind Subjects: Cane and Fingertip Touch Induce Similar Extent and Promptness of Stance Stabilization

*Stefania Sozzi[1], Francesco Decortes[2], Monica Schmid[2], Oscar Crisafulli[3] and Marco Schieppati[4]**

[1] Centro Studi Attività Motorie, Istituti Clinici Scientifici Maugeri, Pavia, Italy, [2] Centro di Riabilitazione Visiva, Istituti Clinici Scientifici Maugeri, Pavia, Italy, [3] Department of Neurosciences, Rehabilitation, Ophthalmology, Genetics and Maternal Child Health, University of Genoa, Genoa, Italy, [4] Department of Exercise and Sport Science, LUNEX International University of Health, Exercise and Sports, Differdange, Luxembourg

Subjects with low vision often use a cane when standing and walking autonomously in everyday life. One aim of this study was to assess differences in the body stabilizing effect produced by the contact of the cane with the ground or by the fingertip touch of a firm surface. Another aim was to estimate the promptness of balance stabilization (or destabilization) on adding (or withdrawing) the haptic input from cane or fingertip. Twelve blind subjects and two subjects with severe visual impairment participated in two experimental protocols while maintaining the tandem Romberg posture on a force platform. In one protocol, subjects lowered the cane to a second platform on the ground and lifted it in sequence at their own pace. In the other protocol, they touched an instrumented pad with the index finger and withdrew the finger from the pad in sequence. In both protocols, subjects were asked to exert a force not granting mechanical stabilization. Under steady-state condition, the finger touch or the contact of the cane with the ground significantly reduced (to ∼78% and ∼86%, respectively) the amplitude of medio-lateral oscillation of the centre of foot pressure (CoP). Oscillation then increased when haptic information was removed. The delay to the change in body oscillation after the haptic shift was longer for addition than withdrawal of the haptic information (∼1.4 s and ∼0.7 s, respectively; $p < 0.001$), but was not different between the two haptic conditions (finger and cane). Similar stabilizing effects of input from cane on the ground and from fingertip touch, and similar latencies to integrate haptic cue from both sources, suggest that the process of integration of the input for balance control is initiated by the haptic stimulus at the interface cane-hand. Use of a tool is as helpful as the fingertip input, and does not produce different stabilization. Further, the latencies to haptic cue integration (from fingertip or cane) are similar to those previously found in a group of sighted subjects, suggesting that integration delays for automatic balance stabilization are not modified by visual impairment. Haptic input from a tool is easily exploited by the neural circuits subserving automatic balance stabilization in blind people, and its use should be enforced by sensory-enhancing devices and appropriate training.

Keywords: haptics, cane, finger touch, blindness, stance control

OPEN ACCESS

Edited by:
Mikhail Lebedev,
Duke University, United States

Reviewed by:
Thorsten Stein,
Karlsruher Institut für Technologie (KIT), Germany
Suresh Munuswamy,
Public Health Foundation of India, India

***Correspondence:**
Marco Schieppati
marco.schieppati@lunex-university.net

Specialty section:
This article was submitted to Neuroprosthetics, a section of the journal Frontiers in Neuroscience

Received: *10 May 2018*
Accepted: *28 August 2018*
Published: *11 September 2018*

Citation:
Sozzi S, Decortes F, Schmid M, Crisafulli O and Schieppati M (2018) Balance in Blind Subjects: Cane and Fingertip Touch Induce Similar Extent and Promptness of Stance Stabilization. Front. Neurosci. 12:639. doi: 10.3389/fnins.2018.00639

INTRODUCTION

Subjects with visual impairment often use a cane to move autonomously in everyday life (Jeka, 1997). The cane helps to partially overcome the mobility restriction associated with low vision, by assisting subjects in detecting obstacles along their path thereby decreasing the risk of falling (White et al., 2015), by conferring them a sense of stability (Bateni and Maki, 2005; Virgili and Rubin, 2010) and by providing a haptic cue to help estimate heading direction and orientation of the body in the gravitational field (Lederman and Klatzky, 2009; Lacquaniti et al., 2015).

Pioneering studies by Holden et al. (1994), Jeka and Lackner (1994), and Jeka et al. (1996) in sighted subjects showed that the simple contact by a finger with a solid frame is as effective as the sight of the surrounding environment in reducing postural sway when compared to no contact, eyes closed condition. Remarkably, the force levels exerted by the finger or by the cane were below those necessary to provide significant mechanical stabilization. Several studies followed, and all arrived at the conclusion that a light fingertip touch improves the control of standing by providing additional somatosensory information (Clapp and Wing, 1999; Baldan et al., 2014; Honeine and Schieppati, 2014; Schieppati et al., 2014; Bernard-Demanze et al., 2015; Honeine et al., 2015). Contact of a cane with the ground has been shown to be similarly effective in reducing postural sway in both sighted subjects and in small cohorts of non-sighted subjects as well (Jeka et al., 1996; Albertsen et al., 2010).

Sway stabilization must be rapid, in order to promptly adapt balance control to the haptic supplementation. The time that elapses from the instant of the haptic cue to postural stabilization is a critical period, during which the nervous system integrates the additional sensory input and prepares to shift to the new 'postural set.' This time period would be especially important in visually impaired subjects during their daily life activities. The latency of the postural resetting in response to the new haptic input from fingertip touch was estimated in sighted subjects standing with eyes closed (Rabin et al., 2006; Sozzi et al., 2011, 2012) and found to be in the order of 1 s. This was considered the time necessary for the integration and reweighting of the new information by the circuits responsible for balance control (Honeine et al., 2015). Conversely, the time period elapsing from the withdrawal of the finger touch to the increase in body sway was significantly shorter than that observed on addition of the haptic input. The latencies to the changes in CoP oscillation after the contact of a cane to the ground (or its removal) were estimated in a group of young sighted subjects (Sozzi et al., 2017). These latencies were similar to those occurring on fingertip touch, suggesting a substantial equivalence of the haptic information derived from "direct" fingertip contact and "indirect" cane contact with the floor. The latencies to fingertip light touch had been also estimated in a small population of blind subjects (Schieppati et al., 2014). They proved to be broadly similar to those of sighted people, except in a few congenital blind subjects that appeared to react early to the haptic finger cue.

Aim of the present investigation was: (a) to assess in a new population of blind subjects the effect on body sway of the haptic sensory input produced by the contact of a cane with the ground in stabilizing the standing body, and (b) to compare these effects to those produced by the light finger touch in the same cohort. Moreover, in the assumption that a prompt reaction to the haptic input would be a priority, we wanted (c) to estimate and compare in this same cohort the time necessary to achieve stabilization or destabilization, on adding or withdrawing the haptic input from either cane or finger touch.

In the background of this study stays the issue of the capacity of the blind subjects to exploit haptic inputs from a cane as an effective aid to reach balance stabilization and maintain equilibrium. Do subjects with severe visual impairment have an edge by using the cane compared to using a finger? Or does appropriate cane use require a higher level of conscious control than the finger touching task (Honeine et al., 2017) or larger anticipatory postural adjustments (Chabran et al., 2001) that might attenuate the incoming input (Starr and Cohen, 1985) and interfere with the promptness of stabilization?

Further, the two haptic inputs would depend on the activation of separate receptors and travel through separate central pathways; the distance of the supports from the body is different, and cane input from a distant point may have different effects on postural steadiness than the finger has, since light touch may be integrated as the horizontal distance between body center of mass and the haptic surface (Assländer et al., 2018); the preparation of the reaching movement to catch either of the two stable structures, and its control, would require a distinct set of postural adjustments as well (Aruin and Latash, 1996; Castellote et al., 2004; Krishnan et al., 2012) potentially leading to context-dependent modulation of tactile input (Juravle et al., 2013); different arm orientations and task features might produce changes in arm proprioception and cutaneous feedback (Rabin et al., 1999; Chapman and Beauchamp, 2006); and the difference in the features of the cutaneous stimuli may produce different cortical activation (Kojima et al., 2018). As a consequence, the integration and weighting of the two haptic inputs (direct with the finger, indirect with the cane) might produce a different degree of stabilization or need a different time interval before the stabilizing effects on balance are fully expressed. Further, the information from the cane contact with the ground would be processed by the blind subjects in a different way than that from the finger touch, because the cane also conveys some information about the free open space around them and about their orientation in that space, or because cross-modal brain plasticity might have differently affected the tactile and haptic sensory channel (Kupers et al., 2006; Fiehler and Rösler, 2010; see for a review, Parreira et al., 2017).

MATERIALS AND METHODS

Subjects

Twelve blind subjects (according to the ICD-10 classification, with visual acuity < 1/20) and two subjects with severe visual impairment (visual acuity < 2/10) participated in this study (**Table 1**). Their mean (±SD) age, weight and height were 47.1 years ± 14.8, 81.4 kg ± 21.9 and 171.1 cm ± 9.2. The

TABLE 1 | Characteristics of the participants.

Subject/sex	Diagnosis	Visual acuity	Age at diagnosis/cane user for # years
1/F	Age-related macular degeneration	0, ability to tell light from dark	Late/7
2/M	Aniridia and nystagmus	1/20	Early/1
3/M	Retinopathy of prematurity	0, ability to tell light from dark	Early/8
4/M	Cortical blindness (multifocal leukoencephalopathy in AIDS)	0	Late/2
5/F	Stargardt macular degeneration	1/50	Late/4
6/M	Retinitis pigmentosa	2/10	Late/2
7/F	Leber congenital amaurosis	0	Early/11
8/M	Congenital glaucoma	0	Late/30
9/M	Angioblastoma with ocular nerves damage	0, ability to tell light from dark	Late/30
10/F	Meningioma of olfactory groove	0, ability to tell light from dark	Late/12
11/F	Tapetoretinal degeneration	RE: 1/50, LE: 1/20	Early/0
12/M	Age-related macular degeneration and glaucoma	1/20	Late/0
13/M	Bilateral retinal detachment and glaucoma	0, ability to tell light from dark	Late/10
14/M	Stargardt macular degeneration	RE 1/10, LE: counting finger at 30 cm distance	Late/0

Early, <5 years; late, >5 years; RE, right eye; LE, left eye.

blindness was of varied etiology. Three of the subjects had severe visual impairment from infancy (early, age <5 years), eleven had vision problems starting later in life (late, age >5 years) and became gradually blind still later. All of them had received an orienteering and training course except three, which were receiving the course at the time of their recruitment in the study.

All subjects were naïve to the experimental task and had not participated previously in balance control investigations. All of them, before participating in the experiments, signed the informed consent form approved by the ethics committee of the Istituti Clinici Scientifici Maugeri (# 757 CEC) in accordance with the Declaration of Helsinki.

The experiments took place in a normally lit room. Subjects participated in two different experimental protocols, performed in two sessions taking place in different days, maintaining the tandem Romberg posture with eyes closed (EC) on a force platform, with the great toe of the rear foot just behind the heel of the front foot (**Figure 1**). Seven subjects chose the right foot as the rear foot. This posture was utilized in order to magnify the medio-lateral (M-L) sway variations connected to the changes in haptic information (Sozzi et al., 2011, 2012, 2013; Honeine et al., 2015). For the entire duration of the experiments, an operator stood near the subjects in order to help them if they lost balance. This never happened and no subject even lifted a foot during the trial. The overall duration of each session (periods of rest included) lasted about 2 h.

Centre of Foot Pressure (CoP) Oscillation

Platforms force (Kistler 9286BA) signals were acquired at 140 Hz (SMART-D system, BTS, Italy). The output of the platform was the instantaneous position of the centre of foot pressure (CoP) along the sagittal (antero-posterior, A-P) and the frontal plane (M-L). To quantify the amplitude of the CoP oscillations, the CoP M-L and A-P position traces were high-pass filtered with a second order Butterworth filter (cut-off frequency 0.1 Hz) and rectified with a software developed in Labview (National Instruments, United States) before averaging. No low pass filtering was applied.

Finger Touch

Subjects slowly flexed the right hand to lightly touch a pad with the tip of the index finger, or to withdraw the finger from the pad, after a verbal go-signal given by the operator. Subjects were asked not to move in a reaction-time mode on hearing the verbal signal, but to self-pace the finger movement when ready. The touch-pad was horizontally oriented and positioned in front of the subject's right hemi-body at about the height of the flexed forearm (**Figure 1A**). In order to facilitate the light touch of the pad, the height of the touch pad was adjusted for each subject. The touch-pad was instrumented with a strain gauge. The signal recorded from the strain gauge was stored in a PC and then utilized to detect the time at which the touch occurred or the finger was removed from the pad, and to calculate the force applied on the pad. A few practice trials were run to obtain touch forces on the pad smaller than 1 N (Jeka and Lackner, 1994). These touching and withdrawing tasks were repeated in sequence. The time intervals between each movement varied pseudo-randomly between 15 s and 25 s.

Cane Touch

Subjects held with their dominant hand (right hand for 13 subjects) a straight plastic cane of 1 m length and 100 g weight (**Figure 1B**). Except for this, the protocol mirrored the 'finger-touch' protocol described above. The force applied by the cane on the ground and the time instant of the contact of the cane with the ground (or of cane lifting) were identified from the force signal

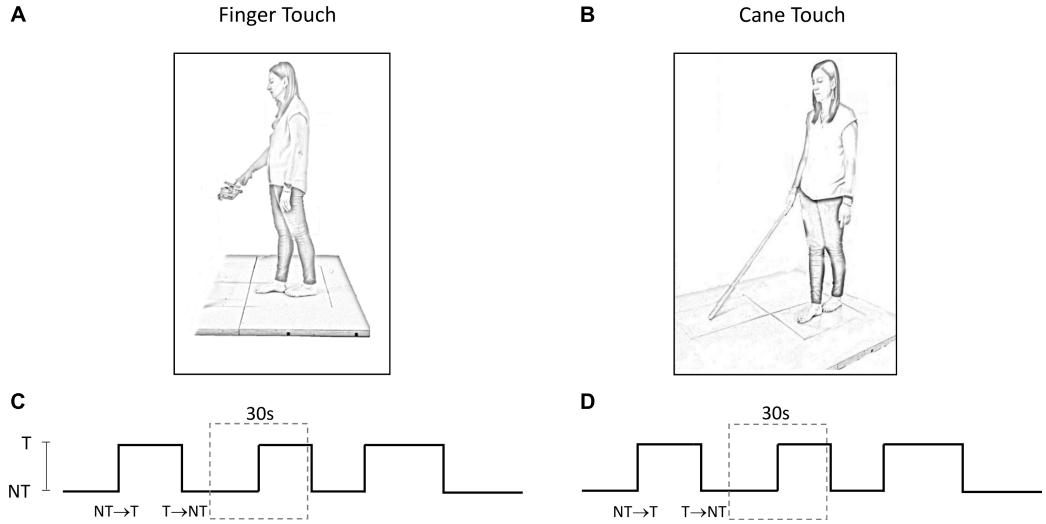

FIGURE 1 | (A,B) Subject stood with feet in tandem position on a force platform and performed a series of trials under 'Finger touch' **(A)** and 'Cane touch' condition **(B)**. **(C,D)** The duration of the time intervals that contained the haptic changes varied randomly from 15 s to 25 s (three such periods are shown). For the analysis, each acquisition epoch was then divided in periods of 30 s duration (dotted rectangles) centered on the change in haptic condition.

recorded by a second force platform. This platform was placed in front of the subject and laterally spaced from the platform on which the subject stood (there were 55 cm from the center of the first platform to the center of the second platform). Again, subjects were asked not to move the cane in a reaction-time mode on hearing the verbal signal, but to self-pace the movement necessary for lowering or lifting the cane from the ground when they felt so.

Data Acquisition and Treatment

The methods below have been used in similar published studies (Sozzi et al., 2012, 2017; Schieppati et al., 2014). Briefly, for each protocol, each subject provided a series of 60 trials per direction of haptic shift (Touch → NoTouch, T-NT; NoTouch → Touch, NT-T). The two protocols (finger–cane) were spaced by a week or more. The order of conditions was randomized across the subjects. The 60 trials were acquired by performing a series of 10 successive acquisition epochs of 240 s each (for both the 'finger touch' condition and the 'cane touch' condition). Between these acquisition epochs rest periods were allowed, during which subjects were free to sit or move around. Each epoch contained six haptic changes in which the finger touched the pad, or the cane was lowered onto the ground (NT-T), and six changes in which the finger was withdrawn from the pad or the cane was lifted from the ground (T-NT). Each acquisition epoch was divided in periods of 30 s duration centered on the change in haptic condition at t = 15 s (**Figures 1C,D**). The exact time instant of the haptic shift was identified on the signal recorded by the strain-gauge of the pad on which the finger was leant or by the force signal recorded by the platform on which the cane was lowered. The abrupt rise in the force signals marked the contact of the finger or of the cane with the stable surface, a brusque return to zero marked the instant of finger or cane detachment. Then, equal-condition trials were aligned at the instant of the haptic shift and averaged. The big trial numbers (n = 60 per haptic shift direction: NT-T and T-NT, cane and finger) were necessary in order to get consistent mean values for body oscillation, and to estimate reliably the time following the shift in haptic information, at which body sway modifications occurred. Repetition rate, and rest periods, would not have affected the stabilizing effects of the haptic cue, since stabilization had been observed during both continuous and intermittent light finger touch (Johannsen et al., 2014).

Levels of Body Oscillation With and Without Haptic Cue

For every trial recorded in each subject, the mean A-P and M-L oscillations of the CoP were computed under all haptic (NT and T, cane and finger) conditions at steady state. These mean oscillation values were calculated on the first and last 10 s periods of each trial period. In this way, the steady state periods did not contain the 5-s intervals just before and just after the sensory shift, and were considered to be stationary and unaffected by the sensory shift (Sozzi et al., 2011, 2012; Honeine et al., 2015).

Mean Latency of the Changes in Body Sway Oscillations Following the Sensory Shifts

For each subject and condition of haptic shift (addition or withdrawal, both for finger and cane touch), we assessed the latency following the sensory shift at which the CoP oscillation started to diminish, or to increase, depending on the haptic-shift direction (NT-T or T-NT). The latency was estimated on the averaged CoP traces (n = 60), centered on the sensory shift. These latencies were assessed only for the frontal plane, because under tandem stance the presence or absence of haptic information produced a much larger gap in the oscillation level in the M-L

than in the A-P direction. This allowed a secure application of the statistical procedure used to detect the time at which the oscillations began to change.

In order to estimate the time instant at which the change in haptic condition began to affect the CoP oscillation, each successive value of the averaged trace following the instant of the sensory shift was compared to the mean value of the trace computed during the 15 s before the haptic shift by one-sample Student's *t*-test with *n* = number of repetitions. The time-interval after the shift, at which the *t*-value of the successive comparisons bypassed the critical value corresponding to a 0.05 probability (one-tailed *t*-test) and remained above that value for at least 100 ms, was taken as the time at which the presence or absence of the haptic information began to affect the postural control mode (Sozzi et al., 2012; Schieppati et al., 2014).

Time to Reach Steady State Condition

After the initial change in CoP oscillation, the averaged CoP value gradually reached a new steady state pertaining to the new sensory condition. The trace representing the time-course of the CoP oscillation was fitted for each subject and condition with an exponential model ($y = A + B\ e^{-t/\tau}$) by the Excel® Solver Utility (Sozzi et al., 2011, 2012; Schieppati et al., 2014). The parameter τ of the exponential model was the time constant of the recovery, A was the value at steady state, and A+B the intercept with the ordinate. A, B, and τ were computed by using the minimum sum squared algorithm by the iterative conjugate gradient method of the Solver utility. The curve of the mean CoP oscillation was fitted from t = latency of changes after the haptic shift until the end of the 30 s time window.

Statistical Analyses

The mean levels of CoP oscillation calculated at steady state were compared by a 3-way repeated-measure ANOVA with direction of oscillation (M-L and A-P), cane or finger touch condition and the presence or absence of haptic information (NT or T) as independent factors. Two 2-way repeated-measure ANOVAs with cane or finger touch condition and direction of haptic shift (NT-T or T-NT) were used to compare the mean latencies of the change in M-L CoP oscillation level after the sensory shift and to compare the mean time constant (τ) to reach the steady state condition. All *post hoc* comparisons was made with the Tukey's HSD test. Where the differences were significant, the Cohen's *d* effect sizes were also reported in order to highlight the strength of the difference (with $d = 0.2$, 0.5, and 0.8 considered as small, medium and large effect size, respectively). The mean forces exerted by the cane or by the finger were compared between 'Finger touch' or 'Cane touch' condition by the paired Student's *t*-test, and the Cohen's *d* effect size was calculated. The software package used was Statistica (StatSoft, United States).

RESULTS

Figure 2 shows the averaged traces of the signals recorded in one representative subject standing on the force platform during the T-NT (left panels) and NT-T (right panels) haptic shifts for the finger touch (**Figures 2A–D**) and cane touch (**Figures 2E–H**) protocols. During the touch periods, the force exerted by the subject by means of the finger or by the cane was always less than 1N (**Figures 2A,B,E,F**). When subjects lifted the finger from the touch pad (**Figure 2A**) or lifted the cane from the ground (**Figure 2E**), the values of the oscillations (**Figures 2C,G**, respectively) increased after a short delay from the instant of the sensory shift. Conversely, after the NT-T shift [finger on the touch pad (**Figure 2B**) or cane lowered onto the ground (**Figure 2F**)], the values of the M-L CoP oscillations (**Figures 2D,H**) diminished in amplitude. All subjects referred that when they touched the touch pad or lowered the cane on the ground they felt more stable than in the absence of the haptic reference.

Body Sway Under Steady State Condition

Figure 3 shows the mean values of the CoP M-L and A-P oscillations calculated at steady state, with (T) or without (NT) the haptic information. The oscillations (finger and cane condition collapsed) were larger along the M-L (left panel) than the A-P (right panel) direction [$F(1,13) = 12.41$, $p < 0.05$; Cohen's $d = 3.92$] during both NT and T conditions. Oscillations were larger in both M-L and A-P directions during the NT (black bars) than during the T period (white bars) [NT vs. T; $F(1,13) = 27.57$, $p < 0.001$; $d = 5.8$]. There was no difference in the CoP oscillations (M-L and A-P collapsed) between cane touch and finger touch conditions [Cane vs. Finger; $F(1,13) = 0.41$, $p = 0.53$]. There were significant interactions between NT or T condition and cane or finger touch condition [$F(1,13) = 15.41$, $p < 0.05$; $d = 4.33$] and between direction of oscillation (M-L or A-P) and cane or finger touch condition [$F(1,13) = 5.39$, $p < 0.05$; $d = 2.56$]. There were no interactions between direction of oscillation and NT or T condition [$F(1,13) = 1.18$, $p = 0.29$] and between direction of oscillation, cane or finger touch condition and NT or T condition [$F(1,13) = 1.6$, $p = 0.23$]. The *post hoc* test showed that the oscillations were always larger under NT than T condition ($p < 0.001$, $d > 0.6$ for all four comparisons), and were slightly smaller in the M-L direction when holding the cane without touching the ground than during the finger no-touch condition ($p < 0.001$, $d = 1.1$).

Figure 4A shows the mean values of the force exerted by the cane or by the finger during the touch periods and the mean values of M-L oscillations of the CoP (**Figure 4B**) at steady state, with (T) or without (NT) the haptic information. All subjects collapsed, there was a difference between the force exerted by the cane and the finger (paired *t*-test, $p < 0.05$; $d = 2.13$), because nine subjects did not succeed in maintaining a force contact of the cane with the ground below 1N (mean force was 2.3 N ± 1.05, dark gray bar in **Figure 4A**), even if the force exerted by their finger was always smaller than 1N. In the other five subjects (light gray bar), the cane exerted less force, and there was no difference between the force applied by the cane to the ground (0.58 N ± 0.09) and that applied by the finger to the touch-pad (0.45 N ± 0.16) (paired *t*-test, $p = 0.17$). Of note (**Figure 4B**), there was no difference in the mean levels of CoP oscillation while

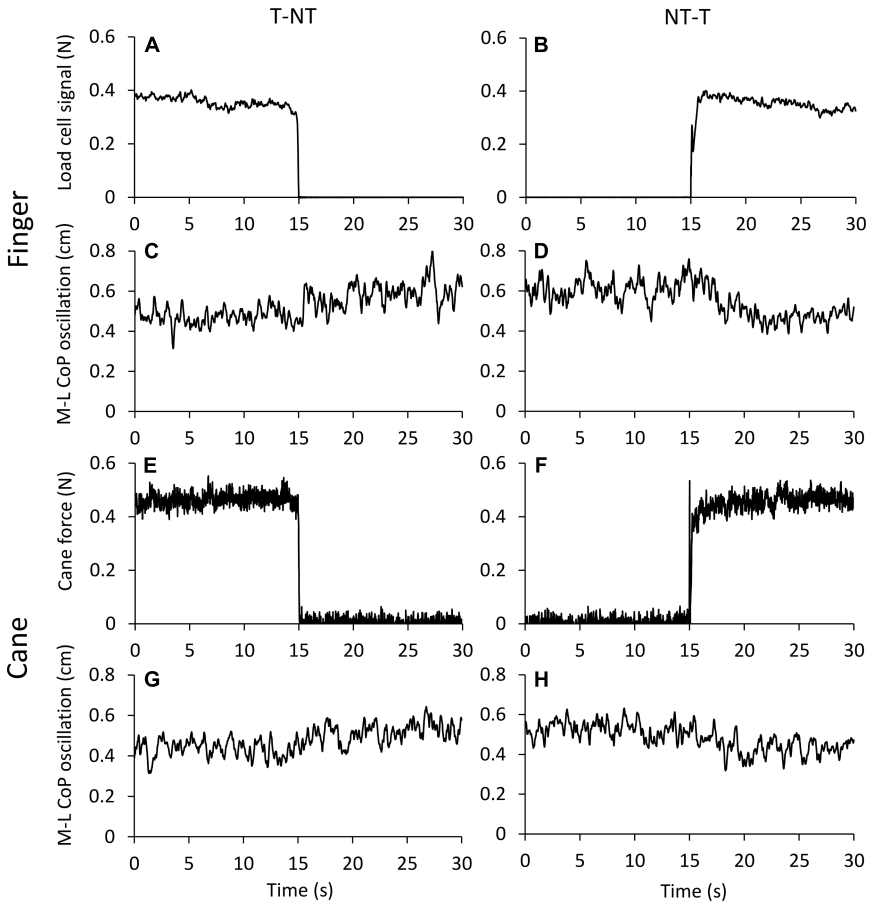

FIGURE 2 | (A–D) Average traces (n = 60) recorded from one subject under the 'finger touch' protocol. **(E–H)** Average traces recorded from the same subject as in **(A–D)**, but under the 'cane touch' protocol. The forces exerted with the finger **(A,B)** and the cane **(E,F)** were less than 1N. After withdrawal of the haptic information from finger **(C)** or cane **(G)** the values of M-L CoP oscillation increased at a short delay from the instant (t = 15 s) of the shift in haptic condition. When the haptic information entered, both by finger **(D)** and by cane **(H)** contact, the values of M-L CoP oscillation diminished in amplitude.

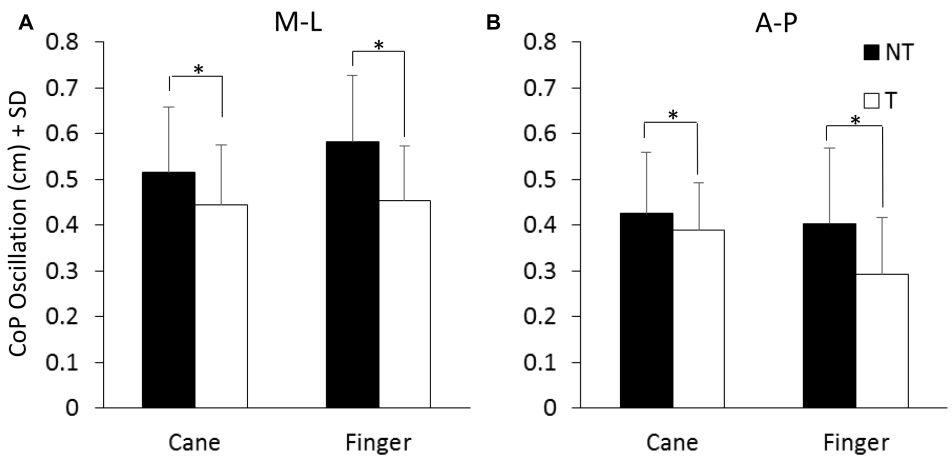

FIGURE 3 | Mean levels of M-L and A-P **(A,B)** CoP oscillation calculated at steady state under NT (black bars) and T (white bars) condition. The oscillation was greater along the frontal (M-L) than the sagittal (A-P) plane and greater under NT than T condition. *Indicates a significant difference ($p < 0.05$).

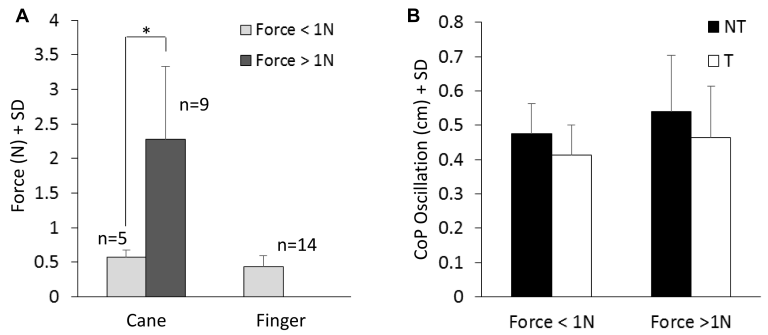

FIGURE 4 | (A) Mean value of force exerted by cane or finger during the touch period. The dark column refers to the subjects that exerted more than 1N force. **(B)** Shows the mean M-L CoP oscillations in the two sub-group of subjects **(A)** standing with the cane during NT (black bars) and T (white bars) periods. The oscillations during T (cane) are not related to the level of force exerted onto the ground.

standing with a cane between the two groups of subjects applying a lower or a higher force level (white bars in **Figure 4B**, *t*-test, $p = 0.51$).

Latencies of Changes in M-L CoP Oscillation Following the Sensory Shift

The latencies of the changes in body sway on touching the ground with the cane or the solid surface with the finger (or vice versa, lifting the cane off ground or removing the finger from the touch-pad) were estimated for each subject on the mean M-L CoP oscillation trace.

As shown in **Figures 5A,B**, at a short delay following the shift in haptic condition (t = 15 s), the oscillations decreased when the haptic information from cane or finger was available (NT-T condition) or increased when the haptic information was removed (T-NT condition). Latencies of these changes were estimated by comparing each mean oscillation value after the haptic shift with the mean oscillation value calculated for the 15-s period before the shift (**Figures 5C,D**).

Figure 5E shows that, across subjects, for the NT-T haptic shift, mean latencies ranged from 0.96 s to 2.1 s for the cane-touch condition and from 0.99 s to 1.8 s for the finger-touch condition. For the T-NT shift, latencies ranged from 0.4 s to 1 s for the cane and from 0.5 s to 1.2 s for the finger condition. In the **Figure 5**, the mean latencies across subjects for the two sensory shifts (NT-T and T-NT) and for the two touch conditions are also reported. There was no difference in the mean latencies between the cane-touch and the finger-touch condition [$F(1,13) = 1.59$, $p = 0.23$]. There was a difference between NT-T and T-NT condition, since latencies were longer for addition than withdrawal of haptic information [$F(1,13) = 61.29$, $p < 0.001$; $d = 6.25$] and there was no interaction between cane or finger touch condition and haptic shift direction [$F(1,13) = 0.79$, $p = 0.39$].

Some subjects were equally slow in responding to both cane and finger input, and some fast on both cane and finger input. On the other hand, all subjects were equally fast on withdrawing the haptic input, from either source. However, there was a large variance in the latencies. Within each haptic shift (NT-T or T-NT), the relationships between the cane and finger latencies were not significant (linear regression for T-NT: $y = 0.04x + 0.78$, $R^2 = 0.003$, $p = 0.85$; for NT-T: $y = 0.21x + 1.09$, $R^2 = 0.08$, $p = 0.3$). The difference between the values of the intercepts with the ordinate of the two linear regressions was similar to the difference between the mean latencies of the NT-T and T-NT conditions. All data points collapsed, there was a good relationship between finger and cane data ($y = 0.52x + 0.57$, $R^2 = 0.44$, $p < 0.001$, regression line not drawn in the **Figure 5**).

Across all subjects, we found no significant relationship between latencies (in any condition) and age at first diagnosis of visual impairment ($p > 0.16$ for the slope of the regression lines drawn for all four conditions). Neither was there any significant regression between latencies and the number of years that subjects had been using the cane at the time of this study ($p > 0.45$ for the slope of the regression lines drawn for all four conditions), in spite of the ample year range (9.9 years $\pm$ 9.7).

Time Course of the Changes in M-L CoP Oscillation

The time necessary to gradually reach a new steady state (time constant, τ) after the earliest detectable changes in body sway connected with the sensory shift was also estimated for each subject, based on the time course of the mean M-L CoP oscillation trace. In the case of the NT-T, after the latency period from the instant of the shift, the M-L CoP oscillation decreased until it reached a new steady state (for both cane or finger touch), vice versa after the T-NT shift. The mean time constant calculated for the two haptic shifts under both cane and finger touch condition are reported in **Figure 6**. There was a large τ variability across subjects under all conditions. There was no difference between the time constants of cane and finger touch condition [$F(1,13) = 0.08$, $p = 0.78$], no difference between directions of haptic shift [NT-T vs. T-NT: $F(1,13) = 1.84$, $p = 0.19$] and no interaction between cane or finger touch condition and haptic shift direction [$F(1,13) = 0.12$, $p = 0.74$].

DISCUSSION

In standing blind subjects, we investigated the stabilizing effect produced by the contact of the cane with the ground and

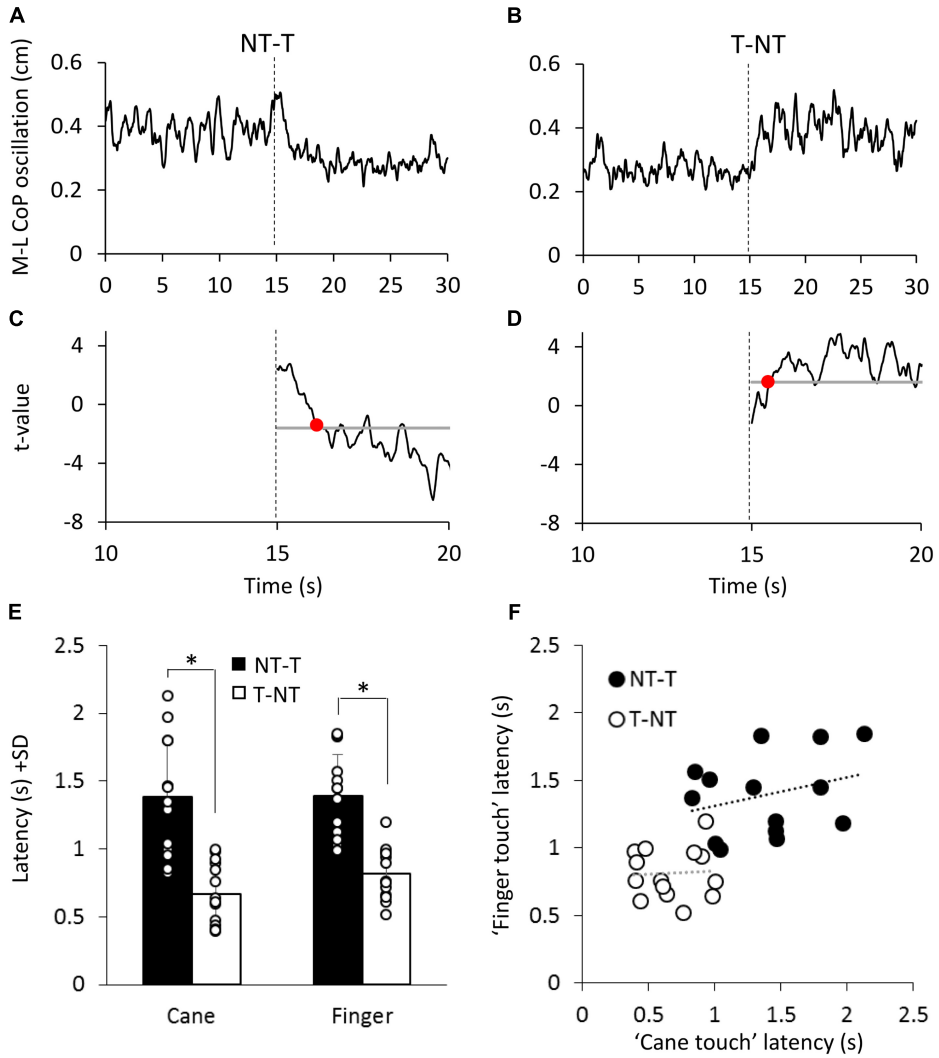

FIGURE 5 | (A,B) Mean M-L CoP oscillation of one subject during NT-T and T-NT haptic shift (dotted line at 15 s) under the 'cane touch' condition. **(C,D)** The traces show the *t*-values calculated by comparing all the successive mean values of oscillation with the mean value of all pre-shift period. The horizontal line indicates the critical t value corresponding to $\alpha = 0.05$ probability. The time at which the *t*-value bypassed the critical value and remained above or below it for at least 100 ms (red dot in **C,D**) was set as the latency at which the haptic shift began to significantly affect the M-L CoP oscillation. **(E)** Mean time intervals from the haptic shift to the change in CoP oscillation. These latencies were longer for the addition (NT-T, black bars) than for the withdrawal (T-NT, white bars) of the haptic information. There was no difference in latency between cane touch and finger touch condition. **(F)** For each subject, the latency calculated for the 'finger touch' condition is plotted against the latency of the 'cane touch' condition both for the NT-T (black circles) and for T-NT shift (open circles). Across subjects, there was no significant relationship between the latencies of cane and touch within condition. *Indicates a significant difference ($p < 0.05$).

those produced by a fingertip touch of a firm surface. We also estimated the promptness of balance stabilization (or destabilization) on adding (or withdrawing) the haptic inputs. We found that both the contact of the finger with the cue surface and the contact of the cane with the ground reduced the amplitude of oscillation of the CoP to a similar extent. The delay to the change in body oscillation on reaching the haptic surface was significantly longer for addition than withdrawal of the haptic information, but was not different between the two haptic conditions. The findings show that using a cane provides an aid to enhance body steadiness, as effective as a finger touch, and that both haptic cues are processed by the nervous system within an equal time interval.

Haptic information derived from fingertip or cane contact with a surface, even with a level of contact force not granting mechanical stabilization (Jeka et al., 1996; Lackner et al., 2001; Kouzaki and Masani, 2008; Sozzi et al., 2012, 2017), is sufficient for consistently reducing body sway. The haptic cues arising from cutaneous, kinesthetic, and proprioceptive sense (Lederman and Klatzky, 2009) provide useful information in terms of specifying body position in space much as vision (Peterka, 2002; Honeine et al., 2015). Haptic information can substitute for the absence of vestibular (Bernard-Demanze et al., 2015), visual (Jeka et al.,

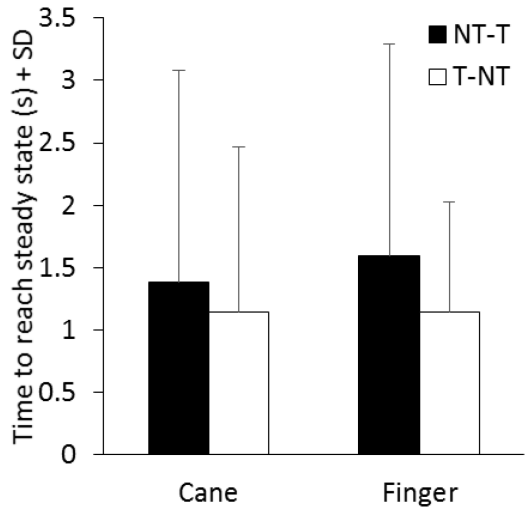

FIGURE 6 | Mean time constants of the recovery of the oscillations to a new steady state pertaining to the new sensory condition. There is no significant difference in the time constant between conditions (cane or finger touch) and between directions of haptic shift (NT-T or T-NT).

1996; Sozzi et al., 2012; Honeine et al., 2015) or somatosensory information (Kotecha et al., 2012) in the control of balance and gait. Haptic cues improves postural control in the elderly (Baccini et al., 2007; Albertsen et al., 2012), and can even help Parkinsonian patients during stance and walking (Rabin et al., 2013, 2015). Bolton et al. (2011) revealed a facilitation of the late cortical response to electrical stimulation of a nerve from the hand during haptic balance tasks. They suggested that task-specific regulation of the cortical representation of fingertip afferent input occurs when it is relevant to providing stable cues for balance control. These findings imply the relevance of the haptic input and the complexity of the changes in the cortical excitability induced by the haptic stabilization during stance. The latency from the haptic cue to the onset of balance stabilization more than accounts for the delays connected with supraspinal, possibly cortical processing (Tokuno et al., 2009; Onishi et al., 2010; see for a discussion, Sozzi et al., 2017).

In blind subjects, haptic information normally originates from touching a solid surface with the hand or fingers, or from using a tool, normally a cane. This can serve for mechanical support of the body (Maeda et al., 1998; Bateni and Maki, 2005; Virgili and Rubin, 2010), for exploration of the shape of the walking path or ground texture (Nunokawa and Ino, 2010; Ranavolo et al., 2011), or for referencing the body to the ground and to the vertical in the absence of vision (Jeka et al., 1996; Albertsen et al., 2012; Lacquaniti et al., 2015). Here, we were interested in comparing the extent and the promptness of the balance stabilization by finger touch to a cue-surface close to the body and by cane contact to the ground in visually impaired subjects, in search of a difference connected to the different features of the haptic tasks.

Cane and Finger Touch Stabilization

In this population of adult blind subjects, standing in tandem Romberg position eyes closed, we found that the effects on body sway exerted by the haptic information either from the cane or from the fingertip was undistinguishable. This were true also for the two subjects with visual acuity < 2/10. In passing, all these subjects used their preferred hand for reaching with the cane or finger much as sighted subjects do (Stone and Gonzalez, 2014), indicating that blindness did not affect the way deliberate movements in search of stabilizing sensory cues are controlled.

Not only the extent of stabilization under steady-state sensory condition was similar, but the latency of the changes in body sway on both adding or withdrawing the haptic information from either source (cane, finger) was similar as well. Further, the time course for the body sway to reach the level corresponding to the given postural condition (with or without the haptic input) was also similar, suggesting no changes in the integration and re-weighting processes of haptic cues from cane and finger.

What matters in the postural stabilization seems to be the presence (or absence) of the haptic information itself rather than the source of the haptic input or the way it is achieved. A contact far from the body, like that from the cane tip, with the arm somewhat flexed and abducted, assists balance as much as the touch with the tip of the index finger, with the hand placed very close to the body. Further, the possible prevalence of the coarser proprioceptive input in the case of the cane than the finger (Buchthal, 1982; Schieppati and Ducati, 1984; Phillips and Johnson, 1985) did not seem to count. Broadly similar stabilizing effects between different passive tactile cues had been described by Rogers et al. (2001).

We also noted that some subjects exerted more than 1 N force with the cane on the force platform, but that the level of their stabilized sway was indistinguishable from that observed when the same subjects exerted less than 1 N with the finger or from that of the subjects that exerted less than 1 N with the cane. Different forces would produce a different afferent input, but either the differences are negligible, or it is the mere haptic information from the environment that matters. As to the level of force exerted, others have shown in sighted subjects that standing while lightly or forcefully touching a wall does not produce significant difference in body sway between the two touching conditions (Watanabe et al., 2010; Ustinova and Langenderfer, 2013; Baldan et al., 2014). Similar results were obtained by Jeka et al. (1996): they asked the subjects (sighted and blind subjects) to maintain the tandem Romberg stance without the cane or while holding the cane in a perpendicular or slanted orientation and to apply two different level of force (<2 N or as much force as they desired). They found that the postural sway attenuation was greatest with a slanted cane, irrespective of the level of force applied.

Time Course of Haptic Stabilization

The latency and time-course to stabilization (or destabilization on withdrawing the haptic input) were also similar between cane and finger touch. This would imply that lowering (or raising) of the cane by a complex coordinate movement entailing a postural

adjustment (although minor, given the light weight of the cane) does not produce a longer latency than the simple lowering (or raising) of the index finger. Since the instruction was to exert a very low force level during the task, we were expecting a stronger control during cane than finger lowering to the haptic surface, possibly accompanied a greater cognitive effort that would have delayed the integration process (Honeine et al., 2017). Again, what matters seems to be the contact itself, producing the sensory haptic volley.

Of course, a sizeable difference in latency was observed, as expected, between addition and subtraction of the sensory input. The origin of this difference has been discussed at length in previous papers (Sozzi et al., 2011, 2012; Schieppati et al., 2014; Honeine et al., 2017). We found here that there was no significant interaction between cane and finger or addition and withdrawal of the haptic stimulus. The control of the tool and the calibration of its contact force, which would have been expected to require a greater attention cost than the finger's (Williams et al., 1998; Saradjian et al., 2013; Johannsen et al., 2014), was apparently not critical to the processing of the haptic information. Since attention can effectively modulate tactile change detection (Spence and Gallace, 2007; Van Hulle et al., 2013), we would also argue that under this challenging stance condition the same level of attention was likely devoted to both finger touch and cane haptic input. The brain is obviously capable of detecting meaningful haptic transients, regardless of the sensory channel through which these are conveyed (proprioceptive, tactile) and of the concurrent motor action. The peripheral receptors are designed for this. And the brain anticipates the transition (Chapman, 1994), contributing to enhanced performance during both cane and finger touch, by preparing the postural centers to assign the appropriate functional value to the relevant haptic input (Schieppati and Nardone, 1995). This process may be the same as that observed in the visual stabilization of posture in sighted subjects (Sozzi et al., 2011, 2012) pointing again to the similar processing of stabilizing cues from different modalities.

Comparison to Sighted Subjects' Haptic Stabilization

In this population of blind subjects, the extent of the stabilization in response to cane or finger touch was similar to that of a population of sighted subjects studied previously (Sozzi et al., 2012, 2017). The latency, at which the body sway began to diminish in response to the haptic input (or to increase after its withdrawal) and the time-course for the body sway to reach the steady-state level (with or without the haptic input) were also similar to that described in sighted subjects.

It appears that blindness did not confer any advantage to the processing of the haptic input, from either cane or finger, toward a better or more prompt stabilization of balance. These considerations do not necessarily run counter to the hypothesis that blind subjects recruit visual-related cortices to process information from other perceptual sensory modalities through cross-modal plasticity (Lewis et al., 2010; Voss et al., 2016), or that adapted sensory-motor functions take place in multimodal integration regions (Easton et al., 1998; Ortiz-Terán et al., 2016). It is not clear whether new circuits are being recruited more promptly during the haptic-induced postural stabilization in low-vision subjects. What is known already is that body sway in blind and low-vision subjects is not lesser than in sighted subjects eyes closed (Schmid et al., 2007; Russo et al., 2017), indicating no superior capacity of exploiting the cutaneous input from the foot sole (Roll et al., 2002) or finger (Bolton et al., 2011) or the proprioceptive inflow from the postural muscles (Schieppati and Nardone, 1999; Marchand-Pauvert et al., 2005). The level of sway reached on obtaining the haptic cues (from either cane or finger touch) is also similar to that of sighted subjects. Under different experimental conditions, testing whether visual and haptic map learning yield functionally equivalent spatial images in working memory, Giudice et al. (2011) have shown no reliable differences between sighted and blind subjects for orientation and turning time measures, and suggested that the equivalent behavior was mediated by an amodal spatial image. Kim et al. (2014) found equivalence of sighted and low-vision subjects in the perception of tactile stimuli in terms of haptic perception and user interface needs, and suggested that the everyday use of residual visual capacities was less likely to have enhanced their haptic capabilities via brain plasticity. One of the reasons for not finding the expected edge in low-vision subjects might be connected to their inability to exploit the enhanced tactile acuity, which is normally enabled by vision in sighted subjects (Kennett et al., 2001; Serino and Haggard, 2010; Konen and Haggard, 2014; Colino et al., 2017). Even in sighted subjects, when vision is not available, proprioceptive information from the support can substitute for vision (Krishnan and Aruin, 2011). All in all, it seems that the basic mechanisms whereby stance support modulates the 'postural set' (Ivanenko and Gurfinkel, 2018) and reduces body postural oscillations are common to both blind and sighted subjects.

Limitations in the Assessment of the Latency to Sway Changes

As far as the rapidity with which the haptic input is integrated in the control of standing balance, the picture is not unequivocal. In a previous communication, we found that the latency to body sway change on touching a firm surface with the finger was somewhat shorter in a very small cohort of early blind subjects than in late blinds (Schieppati et al., 2014). That finding was suggested to be a sign of learning to re-weight the haptic cues in order to obtain a rapid integration of the stabilizing input, possibly connected with the brain plasticity in the early years of these subjects (Dormal et al., 2012). Those short latencies did not recur in the presently studied population. The latencies of the subjects whose vision became severely impaired early in life (3/14) is within the range of the entire population of low-vision subjects. Therefore, we would be reluctant in shedding any firm divide between congenital or early blind subjects and late blind subjects or subject with severely impaired vision, based on the extent of the stabilization (see also Soares et al., 2011) or on the latency of their postural adaptation to haptic input.

We would point out again (Schieppati et al., 2014) that our method of estimating latencies is based on statistical assumptions

and is affected by the number of trials averaged, the individual mean level and variability of the center of pressure oscillation during the trials and the criteria set for the assessment. There must have been a change at the CNS level prior to the value determined by a significant *t*-test, but this statistical procedure cannot detect the 'true' time at which a change in the balancing pattern occurs. These uncertainties, though, would have affected to the same extent the measures taken in both the cane and finger condition or, for that matter, in both blind and sighted subjects. Moreover, under conditions where repeated trials are being performed, the learning ratio of different subjects of different cohorts might affect the outcome (Postma et al., 2007). Fortin et al. (2008), studying navigational proficiency in blind persons, found no differences in their superior skills and hippocampal volume, regardless of their blindness being congenital or acquired. Thus, whether or not brain plasticity in the early blindness confers an advantage in the capacity to use egocentric haptic information (Postma et al., 2007; Ruggiero et al., 2012) and to exploit it for balance stabilization would require further investigations in larger cohorts of subjects. In this context, we note that further understanding of neuroplasticity would be welcome because of its casual role in the embodiment of neural prostheses (Lebedev and Nicolelis, 2006).

Perspectives

Recent studies demonstrated that a vibratory noise applied to the fingertip while standing with eyes closed and touching a solid surface improved postural stability more than merely touching the surface (Magalhães and Kohn, 2011a,b). Whether adding a concurrent sensory stimulation through a different modality channel can also diminish the latency to integrate the haptic input into the balance control process in low-vision subjects is an open question worth investigating (see Lebedev and Ossadtchi, 2018, for a general discussion about instructing the brain to improve learning of haptic feedback).

Various devices have been developed to aid blind or visually impaired subjects in avoiding obstacles during walking (Tzovaras et al., 2004; Penrod et al., 2005; Nunokawa et al., 2014; Buchs et al., 2017; see for a review Pawluk et al., 2015). For instance, ultrasonic or infrared sensors were mounted on the cane in order to estimate the distance between the user and an obstacle, or to judge hardness of an object. Instrumentation of the cane, taking into account the time necessary to integrate haptic information, could help blind subjects to feel more stable and more confident during the activities of everyday life including gait, since dynamic stability is reduced in low-vision subjects (Hallemans et al., 2010). The latency to stabilization in response to haptic input should also be considered when designing devices to help visually impaired subjects orienting themselves while stepping along a path unbeknownst to them but with guide lines detectable by an instrumented cane (as for instance in Hirahara et al., 2006).

CONCLUSION

The haptic input can and does stabilize balance under challenging conditions, such as the tandem Romberg posture. The haptic effect is broadly similar regardless of the source of the information, finger or cane. The haptic input is given priority by the brain, independently of task differences while aiming at the haptic target. Drawing from findings by Rabin and Gordon (2004, 2006) obtained in a different perspective, one would argue that the spatially meaningful tactile cues and the proprioceptive feedback from the entire upper limb are integrated based on the specific task priority of the current task.

There does not appear to be differences between these blind subjects and the sighted subjects studied in a previous recent investigation (Sozzi et al., 2017). The similarities between cane and finger effects on balance stabilization and the similar behavior of low-vision and sighted subjects are expression of a normal processing of haptic input in low vision, and constitute a rationale for inclusion in their rehabilitation (Meyniel et al., 2017) of orienteering and training course with emphasis on the use of the cane (Kimura et al., 2012). The similarities of cane and finger input and the effectiveness of cane contact would also warrant use of the cane and instrumentation of it in order to enhance the sensory feedback when necessary, as when postural orientation is modified (Bisdorff et al., 1996) or when aging degrades haptic sense (Kalisch et al., 2008; Giudice et al., 2017).

AUTHOR CONTRIBUTIONS

SS contributed with data collection, data analysis and drafted parts of the manuscript. FD and MoS recruited and diagnosed the patients. OC contributed with data collection and data analysis. MaS contributed with project creation, data analysis, and wrote and edited the manuscript.

FUNDING

This study was supported in part by a Ricerca Finalizzata grant (RF-2011-02352379) from the Italian Ministry of Health.

REFERENCES

Albertsen, I. M., Temprado, J. J., and Berton, E. (2010). Effect of haptic supplementation on postural stabilization: a comparison of fixed and mobile support conditions. *Hum. Mov. Sci.* 29, 999–1010. doi: 10.1016/j.humov.2010.07.013

Albertsen, I. M., Temprado, J. J., and Berton, E. (2012). Effect of haptic supplementation provided by a fixed or mobile stick on postural stabilization in elderly people. *Gerontology* 58, 419–429. doi: 10.1159/000337495

Aruin, A. S., and Latash, M. L. (1996). Anticipatory postural adjustments during self-initiated perturbations of different magnitude triggered by a standard motor action. *Electroencephalogr. Clin. Neurophysiol.* 101, 497–503. doi: 10.1016/S0013-4694(96)95219-4

Assländer, L., Smith, C. P., and Reynolds, R. F. (2018). Sensory integration of a light touch reference in human standing balance. *PLoS One* 13:e0197316. doi: 10.1371/journal.pone.0197316

Baccini, M., Rinaldi, L. A., Federighi, G., Vannucchi, L., Paci, M., and Masotti, G. (2007). Effectiveness of fingertip light contact in reducing

postural sway in older people. *Age Ageing* 36, 30–35. doi: 10.1093/ageing/afl072

Baldan, A. M., Alouche, S. R., Araujo, I. M., and Freitas, S. M. (2014). Effect of light touch on postural sway in individuals with balance problems: a systematic review. *Gait Posture* 40, 1–10. doi: 10.1016/j.gaitpost.2013.12.028

Bateni, H., and Maki, B. E. (2005). Assistive devices for balance and mobility: benefits, demands, and adverse consequences. *Arch. Phys. Med. Rehabil.* 86, 134–145. doi: 10.1016/j.apmr.2004.04.023

Bernard-Demanze, L., Temprado, J. J., Elzière, M., Albertsen, I. M., Retornaz, F., Lavieille, J. P., et al. (2015). Effects of haptic supplementation on postural stability in unilateral vestibular loss patients. *Neurosci. Lett.* 592, 70–75. doi: 10.1016/j.neulet.2015.03.008

Bisdorff, A. R., Wolsley, C. J., Anastasopoulos, D., Bronstein, A. M., and Gresty, M. A. (1996). The perception of body verticality (subjective postural vertical) in peripheral and central vestibular disorders. *Brain* 119, 1523–1534. doi: 10.1093/brain/119.5.1523

Bolton, D. A., McIlroy, W. E., and Staines, W. R. (2011). The impact of light fingertip touch on haptic cortical processing during a standing balance task. *Exp. Brain Res.* 212, 279–291. doi: 10.1007/s00221-011-2728-6

Buchs, G., Simon, N., Maidenbaum, S., and Amedi, A. (2017). Waist-up protection for blind individuals using the EyeCane as a primary and secondary mobility aid. *Restor. Neurol. Neurosci.* 35, 225–235. doi: 10.3233/RNN-160686

Buchthal, F. (1982). Human nerve potentials evoked by tactile stimuli. II. Stimulus parameters and recruitment of components. *Acta. Physiol. Scand. Suppl.* 502, 19–32.

Castellote, J. M., Valls-Solé, J., and Sanegre, M. T. (2004). Ballistic reactions under different motor sets. *Exp. Brain Res.* 158, 35–42. doi: 10.1007/s00221-004-1866-5

Chabran, E., Maton, B., Ribreau, C., and Fourment, A. (2001). Electromyographic and biomechanical characteristics of segmental postural adjustments associated with voluntary wrist movements, influence of an elbow support. *Exp. Brain Res.* 141, 133–145. doi: 10.1007/s002210100823

Chapman, C. E. (1994). Active versus passive touch: factors influencing the transmission of somatosensory signals to primary somatosensory cortex. *Can. J. Physiol. Pharmacol.* 72, 558–570. doi: 10.1139/y94-080

Chapman, C. E., and Beauchamp, E. (2006). Differential controls over tactile detection in humans by motor commands and peripheral reafference. *J. Neurophysiol.* 96, 1664–1675. doi: 10.1152/jn.00214.2006

Clapp, S., and Wing, A. M. (1999). Light touch contribution to balance in normal bipedal stance. *Exp. Brain Res.* 125, 521–524. doi: 10.1007/s002210050711

Colino, F. L., Lee, J. H., and Binsted, G. (2017). Availability of vision and tactile gating: vision enhances tactile sensitivity. *Exp. Brain Res.* 235, 341–348. doi: 10.1007/s00221-016-4785-3

Dormal, G., Lepore, F., and Collignon, O. (2012). Plasticity of the dorsal "spatial" stream in visually deprived individuals. *Neural Plast.* 2012:687659. doi: 10.1155/2012/687659

Easton, R. D., Greene, A. J., DiZio, P., and Lackner, J. R. (1998). Auditory cues for orientation and postural control in sighted and congenitally blind people. *Exp. Brain Res.* 118, 541–550. doi: 10.1007/s002210050310

Fiehler, K., and Rösler, F. (2010). Plasticity of multisensory dorsal stream functions: evidence from congenitally blind and sighted adults. *Restor. Neurol. Neurosci.* 28, 193–205.

Fortin, M., Voss, P., Lord, C., Lassonde, M., Pruessner, J., Saint-Amour, D., et al. (2008). Wayfinding in the blind: larger hippocampal volume and supranormal spatial navigation. *Brain* 131, 2995–3005. doi: 10.1093/brain/awn250

Giudice, N. A., Bennett, C. R., Klatzky, R. L., and Loomis, J. M. (2017). Spatial updating of haptic arrays across the life span. *Exp. Aging Res.* 43, 274–290. doi: 10.1080/0361073X.2017.1298958

Giudice, N. A., Betty, M. R., and Loomis, J. M. (2011). Functional equivalence of spatial images from touch and vision: evidence from spatial updating in blind and sighted individuals. *J. Exp. Psychol. Learn Mem. Cogn.* 37, 621–634. doi: 10.1037/a0022331

Hallemans, A., Ortibus, E., Meire, F., and Aerts, P. (2010). Low vision affects dynamic stability of gait. *Gait Posture* 32, 547–551. doi: 10.1016/j.gaitpost.2010.07.018

Hirahara, Y., Sakurai, Y., Shiidu, Y., Yanashima, K., and Magatani, K. (2006). Development of the navigation system for the visually impaired by using white cane. *Conf. Proc. IEEE Eng. Med. Biol. Soc.* 1, 4893–4896.

Holden, M., Ventura, J., and Lackner, J. R. (1994). Stabilization of posture by precision contact of the index finger. *J. Vestib. Res.* 4, 285–301.

Honeine, J. L., Crisafulli, O., and Schieppati, M. (2017). Body sway adaptation to addition but not withdrawal of stabilizing visual information is delayed by a concurrent cognitive task. *J. Neurophysiol.* 117, 777–785. doi: 10.1152/jn.00725.2016

Honeine, J. L., Crisafulli, O., Sozzi, S., and Schieppati, M. (2015). Processing time of addition or withdrawal of single or combined balance-stabilizing haptic and visual information. *J. Neurophysiol.* 114, 3097–3110. doi: 10.1152/jn.00618.2015

Honeine, J. L., and Schieppati, M. (2014). Time-interval for integration of stabilizing haptic and visual information in subjects balancing under static and dynamic conditions. *Front. Syst. Neurosci.* 8:190. doi: 10.3389/fnsys.2014.00190

Ivanenko, Y., and Gurfinkel, V. S. (2018). Human postural control. *Front. Neurosci.* 12:171. doi: 10.3389/fnins.2018.00171

Jeka, J. J. (1997). Light touch contact as a balance aid. *Phys. Ther.* 77, 476–487. doi: 10.1093/ptj/77.5.476

Jeka, J. J., Easton, R. D., Bentzen, B. L., and Lackner, J. R. (1996). Haptic cues for orientation and postural control in sighted and blind individuals. *Percept. Psychophys.* 58, 409–423. doi: 10.3758/BF03206817

Jeka, J. J., and Lackner, J. R. (1994). Fingertip contact influences human postural control. *Exp. Brain Res.* 100, 495–502. doi: 10.1007/BF02738408

Johannsen, L., Lou, S. Z., and Chen, H. Y. (2014). Effects and after-effects of voluntary intermittent light finger touch on body sway. *Gait Posture* 40, 575–580. doi: 10.1016/j.gaitpost.2014.06.017

Juravle, G., McGlone, F., and Spence, C. (2013). Context-dependent changes in tactile perception during movement execution. *Front. Psychol.* 4:913. doi: 10.3389/fpsyg.2013.00913

Kalisch, T., Tegenthoff, M., and Dinse, H. R. (2008). Improvement of sensorimotor functions in old age by passive sensory stimulation. *Clin. Interv. Aging.* 3, 673–690. doi: 10.2147/CIA.S3174

Kennett, S., Taylor-Clarke, M., and Haggard, P. (2001). Non-informative vision improves the spatial resolution of touch in humans. *Curr. Biol.* 11, 1188–1191. doi: 10.1016/S0960-9822(01)00327-X

Kim, H. N., Smith-Jackson, T., and Terpenny, J. (2014). Haptic perception of users with low vision and their needs in haptic-incorporated user interfaces. *Disabil. Rehabil. Assist. Technol.* 9, 195–208. doi: 10.3109/17483107.2013.769121

Kimura, T., Kouzaki, M., Masani, K., and Moritani, T. (2012). Unperceivable noise to active light touch effects on fast postural sway. *Neurosci. Lett.* 506, 100–103. doi: 10.1016/j.neulet.2011.10.058

Kojima, S., Onishi, H., Miyaguchi, S., Kotan, S., Sasaki, R., Nakagawa, M., et al. (2018). Modulation of corticospinal excitability depends on the pattern of mechanical tactile stimulation. *Neural Plast.* 2018:5383514. doi: 10.1155/2018/5383514

Konen, C. S., and Haggard, P. (2014). Multisensory parietal cortex contributes to visual enhancement of touch in humans: a single-pulse TMS study. *Cereb. Cortex* 24, 501–507. doi: 10.1093/cercor/bhs331

Kotecha, A., Webster, A. R., Wright, G., Michaelides, M., and Rubin, G. S. (2012). Standing balance stability and the effects of light touch in adults with profound loss of vision – An exploratory study. *Invest. Ophthalmol. Vis. Sci.* 57, 5053–5759. doi: 10.1167/iovs.16-19606

Kouzaki, M., and Masani, K. (2008). Reduced postural sway during quiet standing by light touch is due to finger tactile feedback but not mechanical support. *Exp. Brain Res.* 188, 153–158. doi: 10.1007/s00221-008-1426-5

Krishnan, V., and Aruin, A. S. (2011). Postural control in response to a perturbation: role of vision and additional support. *Exp. Brain Res.* 212, 385–397. doi: 10.1007/s00221-011-2738-4

Krishnan, V., Kanekar, N., and Aruin, A. S. (2012). Feedforward postural control in individuals with multiple sclerosis during load release. *Gait Posture* 36, 225–230. doi: 10.1016/j.gaitpost.2012.02.022

Kupers, R., Fumal, A., de Noordhout, A. M., Gjedde, A., Schoenen, J., and Ptito, M. (2006). Transcranial magnetic stimulation of the visual cortex induces somatotopically organized qualia in blind subjects. *Proc. Natl. Acad. Sci. U.S.A.* 103, 13256–13260. doi: 10.1073/pnas.0602925103

Lackner, J. R., Rabin, E., and DiZio, P. (2001). Stabilization of posture by precision touch of the index finger with rigid and flexible filaments. *Exp. Brain Res.* 139, 454–464. doi: 10.1007/s002210100775

Lacquaniti, F., Bosco, G., Gravano, S., Indovina, I., La Scaleia, B., Maffei, V., et al. (2015). Gravity in the brain as a reference for space and time perception. *Multisens. Res.* 28, 397–426. doi: 10.1163/22134808-00002471

Lebedev, M. A., and Nicolelis, M. A. (2006). Brain–machine interfaces: past, present and future. *Trends Neurosci.* 29, 536–546. doi: 10.1016/j.tins.2006.07.004

Lebedev, M. A., and Ossadtchi, A. (2018). Commentary: injecting instructions into premotor cortex. *Front. Cell. Neurosci.* 12:65. doi: 10.3389/fncel.2018.00065

Lederman, S. J., and Klatzky, R. L. (2009). Haptic perception: a tutorial. *Atten. Percept. Psychophys.* 71, 1439–1459. doi: 10.3758/APP.71.7.1439

Lewis, L. B., Saenz, M., and Fine, I. (2010). Mechanisms of cross-modal plasticity in early-blind subjects. *J. Neurophysiol.* 104, 2995–3008. doi: 10.1152/jn.00983.2009

Maeda, A., Nakamura, K., Otomo, A., Higuchi, S., and Motohashi, Y. (1998). Body support effect on standing balance in the visually impaired elderly. *Arch. Phys. Med. Rehabil.* 79, 994–997. doi: 10.1016/S0003-9993(98)90100-9

Magalhães, F. H., and Kohn, A. F. (2011a). Vibration-enhanced posture stabilization achieved by tactile supplementation: may blind individuals get extra benefits? *Med. Hypotheses.* 77, 301–304. doi: 10.1016/j.mehy.2011.04.040

Magalhães, F. H., and Kohn, A. F. (2011b). Vibratory noise to the fingertip enhances balance improvement associated with light touch. *Exp. Brain Res.* 209, 139–151. doi: 10.1007/s00221-010-2529-3

Marchand-Pauvert, V., Nicolas, G., Marque, P., Iglesias, C., and Pierrot-Deseilligny, E. (2005). Increase in group II excitation from ankle muscles to thigh motoneurones during human standing. *J. Physiol.* 566, 257–271. doi: 10.1113/jphysiol.2005.087817

Meyniel, C., Bodaghi, B., and Robert, P. Y. (2017). Revisiting vision rehabilitation. *Front. Syst. Neurosci.* 11:82. doi: 10.3389/fnsys.2017.00082

Nunokawa, K., and Ino, S. (2010). An experimental study on target recognition using white canes. *Conf. Proc. IEEE Eng. Med. Biol. Soc.* 2010, 6583–6586. doi: 10.1109/IEMBS.2010.5627121

Nunokawa, K., Seki, Y., Ino, S., and Doi, K. (2014). Judging hardness of an object from the sounds of tapping created by a white cane. *Conf. Proc. IEEE Eng. Med. Biol. Soc.* 2014, 5876–5879. doi: 10.1109/EMBC.2014.6944965

Onishi, H., Oyama, M., Soma, T., Kubo, M., Kirimoto, H., Murakami, H., et al. (2010). Neuromagnetic activation of primary and secondary somatosensory cortex following tactile-on and tactile-off stimulation. *Clin. Neurophysiol.* 121, 588–593. doi: 10.1016/j.clinph.2009.12.022

Ortiz-Terán, L., Ortiz, T., Perez, D. L., Aragón, J. I., Diez, I., Pascual-Leone, A., et al. (2016). Brain plasticity in blind subjects centralizes beyond the modal cortices. *Front. Syst. Neurosci.* 10:61. doi: 10.3389/fnsys.2016.00061

Parreira, R. B., Grecco, L. A. C., and Oliveira, C. S. (2017). Postural control in blind individuals: a systematic review. *Gait Posture* 57, 161–167. doi: 10.1016/j.gaitpost.2017.06.008

Pawluk, D. T., Adams, R. J., and Kitada, R. (2015). Designing haptic assistive technology for individuals who are blind or visually impaired. *IEEE Trans. Haptics* 8, 258–278. doi: 10.1109/TOH.2015.2471300

Penrod, W., Corbett, M. D., and Blash, B. (2005). A master trainer class for professionals in teaching the ultracane electronic travel device. *J. Vis. Impairment Blind.* 99, 711–714.

Peterka, R. J. (2002). Sensorimotor integration in human postural control. *J. Neurophysiol.* 88, 1097–1118. doi: 10.1152/jn.2002.88.3.1097

Phillips, J. R., and Johnson, K. O. (1985). Neural mechanisms of scanned and stationary touch. *J. Acoust. Soc. Am.* 77, 220–224. doi: 10.1121/1.392262

Postma, A., Zuidhoek, S., Noordzij, M. L., and Kappers, A. M. (2007). Differences between early-blind, late-blind, and blindfolded-sighted people in haptic spatial-configuration learning and resulting memory traces. *Perception* 36, 1253–1265. doi: 10.1068/p5441

Rabin, E., Bortolami, S. B., DiZio, P., and Lackner, J. R. (1999). Haptic stabilization of posture: changes in arm proprioception and cutaneous feedback for different arm orientations. *J. Neurophysiol.* 82, 3541–3549. doi: 10.1152/jn.1999.82.6.3541

Rabin, E., Chen, J., Muratori, L., DiFrancisco-Donoghue, J., and Werner, W. G. (2013). Haptic feedback from manual contact improves balance control in people with Parkinson's disease. *Gait Posture* 38, 373–379. doi: 10.1016/j.gaitpost.2012.12.008

Rabin, E., Demin, A., Pirrotta, S., Chen, J., Patel, H., Bhambri, A., et al. (2015). Parkinsonian gait ameliorated with a moving handrail, not with a banister. *Arch. Phys. Med. Rehabil.* 96, 735–741. doi: 10.1016/j.apmr.2014.07.427

Rabin, E., DiZio, P., and Lackner, J. R. (2006). Time course of haptic stabilization of posture. *Exp. Brain Res.* 170, 122–126. doi: 10.1007/s00221-006-0348-3

Rabin, E., and Gordon, A. (2006). Prior experience and current goals affect muscle-spindle and tactile integration. *Exp. Brain Res.* 169, 407–16. doi: 10.1007/s00221-005-0154-3

Rabin, E., and Gordon, A. M. (2004). Influence of fingertip contact on illusory arm movements. *J. Appl. Physiol.* 96, 1555–1560. doi: 10.1152/japplphysiol.01085.2003

Ranavolo, A., Conte, C., Iavicoli, S., Serrao, M., Silvetti, A., Sandrini, G., et al. (2011). Walking strategies of visually impaired people on trapezoidal- and sinusoidal-section tactile ground surface indicators. *Ergonomics* 54, 246–256. doi: 10.1080/00140139.2010.548533

Rogers, M. W., Wardman, D. L., Lord, S. R., and Fitzpatrick, R. C. (2001). Passive tactile sensory input improves stability during standing. *Exp. Brain Res.* 136, 514–522. doi: 10.1007/s002210000615

Roll, R., Kavounoudias, A., and Roll, J. P. (2002). Cutaneous afferents from human plantar sole contribute to body posture awareness. *Neuroreport* 13, 1957–1961. doi: 10.1097/00001756-200210280-00025

Ruggiero, G., Ruotolo, F., and Iachini, T. (2012). Egocentric/allocentric and coordinate/categorical haptic encoding in blind people. *Cogn. Process.* 13(Suppl 1), S313–S317. doi: 10.1007/s10339-012-0504-6

Russo, M. M., Lemos, T., Imbiriba, L. A., Ribeiro, N. L., and Vargas, C. D. (2017). Beyond deficit or compensation: new insights on postural control after long-term total visual loss. *Exp. Brain Res.* 235, 437–446. doi: 10.1007/s00221-016-4799-x

Saradjian, A. H., Tremblay, L., Perrier, J., Blouin, J., and Mouchnino, L. (2013). Cortical facilitation of proprioceptive inputs related to gravitational balance constraints during step preparation. *J. Neurophysiol.* 110, 397–407. doi: 10.1152/jn.00905.2012

Schieppati, M., and Ducati, A. (1984). Short-latency cortical potentials evoked by tactile air-jet stimulation of body and face in man. *Electroencephalogr. Clin. Neurophysiol.* 58, 418–425. doi: 10.1016/0013-4694(84)90138-X

Schieppati, M., and Nardone, A. (1995). Time course of 'set'-related changes in muscle responses to stance perturbation in humans. *J. Physiol.* 487, 787–796. doi: 10.1113/jphysiol.1995.sp020918

Schieppati, M., and Nardone, A. (1999). Group II spindle afferent fibers in humans: their possible role in the reflex control of stance. *Prog. Brain Res.* 123, 461–472. doi: 10.1016/S0079-6123(08)62882-4

Schieppati, M., Schmid, M., and Sozzi, S. (2014). Rapid processing of haptic cues for postural control in blind subjects. *Clin. Neurophysiol.* 125, 1427–1439. doi: 10.1016/j.clinph.2013.11.011

Schmid, M., Nardone, A., De Nunzio, A. M., Schmid, M., and Schieppati, M. (2007). Equilibrium during static and dynamic tasks in blind subjects: no evidence of cross-modal plasticity. *Brain* 130, 2097–2107. doi: 10.1093/brain/awm157

Serino, A., and Haggard, P. (2010). Touch and the body. *Neurosci. Biobehav. Rev.* 34, 224–236. doi: 10.1016/j.neubiorev.2009.04.004

Soares, A. V., Oliveira, C. S., Knabben, R. J., Domenech, S. C., and Borges Junior, N. G. (2011). Postural control in blind subjects. *Einstein (Sao Paulo).* 9, 470–476. doi: 10.1590/S1679-45082011AO2046

Sozzi, S., Crisafulli, O., and Schieppati, M. (2017). Haptic cues for balance: use of a cane provides immediate body stabilization. *Front. Neurosci.* 11:705. doi: 10.3389/fnins.2017.00705

Sozzi, S., Do, M. C., Monti, A., and Schieppati, M. (2012). Sensorimotor integration during stance: processing time of active or passive addition or withdrawal of visual or haptic information. *Neuroscience* 212, 59–76. doi: 10.1016/j.neuroscience.2012.03.044

Sozzi, S., Honeine, J. L., Do, M. C., and Schieppati, M. (2013). Leg muscle activity during tandem stance and the control of body balance in the frontal plane. *Clin. Neurophysiol.* 124, 1175–1186. doi: 10.1016/j.clinph.2012.12.001

Sozzi, S., Monti, A., De Nunzio, A. M., Do, M. C., and Schieppati, M. (2011). Sensori-motor integration during stance: time adaptation of control mechanisms on adding or removing vision. *Hum. Mov. Sci.* 30, 172–189. doi: 10.1016/j.humov.2010.06.002

Spence, C., and Gallace, A. (2007). Recent developments in the study of tactile attention. *Can. J. Exp. Psychol.* 61, 196–207. doi: 10.1037/cjep2007021

Starr, A., and Cohen, L. G. (1985). 'Gating' of somatosensory evoked potentials begins before the onset of voluntary movement in man. *Brain Res.* 348, 183–186. doi: 10.1016/0006-8993(85)90377-4

Stone, K. D., and Gonzalez, C. L. (2014). Grasping without sight: insights from the congenitally blind. *PLoS One* 9:e110175. doi: 10.1371/journal.pone.0110175

Tokuno, C. D., Taube, W., and Cresswell, A. G. (2009). An enhanced level of motor cortical excitability during the control of human standing. *Acta Physiol. (Oxf.)* 195, 385–395. doi: 10.1111/j.1748-1716.2008.01898.x

Tzovaras, D., Nikolakis, G., Fergadis, G., Malasiotis, S., and Stavrakis, M. (2004). Design and implementation of haptic virtual environments for the training of the visually impaired. *IEEE Trans. Neural. Syst. Rehabil. Eng.* 12, 266–278. doi: 10.1109/TNSRE.2004.828756

Ustinova, K. I., and Langenderfer, J. E. (2013). Postural stabilization by gripping a stick with different force levels. *Gait Posture* 38, 97–103. doi: 10.1016/j.gaitpost.2012.10.020

Van Hulle, L., Van Damme, S., Spence, C., Crombez, G., and Gallace, A. (2013). Spatial attention modulates tactile change detection. *Exp. Brain Res.* 224, 295–302. doi: 10.1007/s00221-012-3311-5

Virgili, G., and Rubin, G. (2010). Orientation and mobility training for adults with low vision. *Cochrane Database Syst. Rev.* CD003925. doi: 10.1002/14651858.CD003925

Voss, P., Alary, F., Lazzouni, L., Chapman, C. E., Goldstein, R., Bourgoin, P., et al. (2016). Crossmodal processing of haptic inputs in sighted and blind individuals. *Front. Syst. Neurosci.* 10:62. doi: 10.3389/fnsys.2016.00062

Watanabe, S., Kobara, K., and Ishida, H. (2010). Influence of fingertip contact with a wall on postural sway and electromyographic activity of the soleus muscle. *Electromyogr. Clin. Neurophysiol.* 50, 229–233.

White, U. E., Black, A. A., Wood, J. M., and Delbaere, K. (2015). Fear of falling in vision impairment. *Optom. Vis. Sci.* 92, 730–735. doi: 10.1097/OPX.0000000000000596

Williams, S. R., Shenasa, J., and Chapman, C. E. (1998). Time course and magnitude of movement-related gating of tactile detection in humans, I. Importance of stimulus location. *J. Neurophysiol.* 79, 947–963. doi: 10.1152/jn.1998.79.2.947

Conflict of Interest Statement: The authors declare that the research was conducted in the absence of any commercial or financial relationships that could be construed as a potential conflict of interest.

frontiers in Neuroscience

ORIGINAL RESEARCH
published: 09 October 2018
doi: 10.3389/fnins.2018.00719

Reshaping of Bilateral Gait Coordination in Hemiparetic Stroke Patients After Early Robotic Intervention

Sandra Puentes[1,2], Hideki Kadone[2], Hiroki Watanabe[3], Tomoyuki Ueno[4], Masashi Yamazaki[5], Yoshiyuki Sankai[3], Aiki Marushima[6] and Kenji Suzuki[3]*

[1] Faculty of Engineering, Information and Systems, University of Tsukuba, Tsukuba, Japan, [2] Center for Innovative Medicine and Engineering, University of Tsukuba Hospital, Tsukuba, Japan, [3] Center for Cybernics Research, University of Tsukuba, Tsukuba, Japan, [4] Department of Rehabilitation Medicine, University of Tsukuba Hospital, Tsukuba, Japan, [5] Department of Orthopaedic Surgery, University of Tsukuba Hospital, Tsukuba, Japan, [6] Department of Neurosurgery, University of Tsukuba Hospital, Tsukuba, Japan

Hemiparetic gait is a common condition after stroke which alters importantly the quality of life of stroke survivors. In recent years, several robotic interventions have been developed to support and enhance rehabilitation strategies for such population. The Hybrid Assistive Limb® (HAL) robot suit is a unique device able to collect in real time bioelectric signals from the patient to support and enhance voluntary gait. HAL has been used before in early stages of stroke showing gait improvement after the intervention. However, evaluation of the coordination of gait has not been done yet. Coordination is a key factor for an adequate gait performance; consequently, its changes may be closely related to gait recovery. In this study, we used planar covariation to evaluate coordination changes in hemiparetic stroke patients after early HAL intervention. Before starting, impaired intersegmental coordination for the paretic and non-paretic side was evident. HAL intervention was able to induce recovery of the covariation loop shape and deviation from the covariation plane improving intersegmental coordination. Also, there was a tendency of recovery for movement range evidenced by comparison of peak elevation angles of each limb segment of the patients before and after HAL intervention, and also when compared to healthy volunteers. Our results suggest that early HAL intervention contributed to the improvement of gait coordination in hemiparetic stroke patients by reinforcing central pattern generators and therefore reshaping their gait pattern.

Trial registration: UMIN000022410 2016/05/23.

Keywords: stroke, hemiparesis, robot suit HAL, gait coordination, early intervention

OPEN ACCESS

Edited by:
Yury Ivanenko,
Fondazione Santa Lucia (IRCCS), Italy

Reviewed by:
Tetsuro Funato,
The University of Electro-Communications, Japan
Fan Gao,
University of Kentucky, United States

****Correspondence:***
Sandra Puentes
sandra@ccr.tsukuba.ac.jp

Specialty section:
This article was submitted to Neuroprosthetics, a section of the journal Frontiers in Neuroscience

Received: *27 June 2018*
Accepted: *19 September 2018*
Published: *09 October 2018*

Citation:
Puentes S, Kadone H, Watanabe H, Ueno T, Yamazaki M, Sankai Y, Marushima A and Suzuki K (2018) Reshaping of Bilateral Gait Coordination in Hemiparetic Stroke Patients After Early Robotic Intervention. Front. Neurosci. 12:719. doi: 10.3389/fnins.2018.00719

Abbreviations: 6MWD, 6-Minute Walk Distance; EA, elevation angles; FAC, Functional Ambulation Classification; FIM, Functional Independence Measure; FMA, Fugl-Meyer Assessment; HAL, Hybrid Assistive Limb; max peaks, maximum peaks; min peaks, minimum peaks; max-min difference, maximum peak to minimum peak difference; np-pre, non-paretic side before HAL intervention; np-post, non-paretic side after HAL intervention; par-post, paretic side after HAL intervention; par-pre, paretic side before HAL intervention; PC2SD, PCA second component standard deviation; PC3SD, PCA third component standard deviation; PCA, Principal Component Analysis; PV2, PCA second component percentage of variance; PV3, PCA third component percentage of variance.

INTRODUCTION

Stroke is known as a leading cause of motor impairment, whose burden in terms of disability continue increasing worldwide (Feigin et al., 2017; Benjamin et al., 2018). Exercise is the most common intervention to improve walking performance (Eng and Tang, 2007) and previous studies have shown proof that early interventions designed to be intense and repetitive depending on the patient tolerance are able to improve functional outcome when compared to conventional rehabilitation (Salter et al., 2006; Eng and Tang, 2007; Peurala et al., 2007). Additionally, it has been found that patients admitted within the first 30 days of stroke onset to rehabilitation programs experience greater functional improvement accompanied by reduction in length of hospital stay (Salter et al., 2006). In recent years, the development of new technologies to improve the outcome of exercise training in patients with gait disturbances has opened the path to the development of variated exoskeleton models (Chen et al., 2013; Esquenazi et al., 2017).

The Hybrid Assistive Limb® (HAL) robot suit, is a wearable exoskeleton able to provide bilateral or unilateral leg support. The single-leg version is used to assist patients presenting hemiparesis. This HAL version has three degrees of freedom related to the sagittal movement of hip, knee, and ankle joints of the braced side. Using surface electrodes, HAL is able to collect bioelectric signals from the action potentials reaching flexor and extensor muscles of the hip and knee during movement preparation and initiation. This information is processed by an on-board processor to control two motors located over the lateral aspects of the supported hip and knee joints, respectively, in order to assist the voluntary control of the patient joints motion during gait training in real time (Kawamoto et al., 2013). Previous studies have established the feasibility and safety of HAL intervention in early stages of stroke (Ueba et al., 2013; Ogata et al., 2015). These studies did not report major secondary effects. However, patients with intracerebral hemorrhage and low functional scores tended to present orthostatic hypotension. Regarding performance and HAL intervention, one study examining intracerebral hemorrhage patients found better outcome for patients with right intracerebral hemorrhage exclusively when compared to patients who received standard rehabilitation (Ogata et al., 2015); however, the authors reported that HAL intervention group displayed larger hematoma volumes and a trend of increased severity at the initial evaluation when compared to control group (Ogata et al., 2015). Other study including ischemic and hemorrhagic stroke patients reported gait improvement, better torso posture and ability to stand with HAL assist for patients treated with the exoskeleton (Ueba et al., 2013).

There are previous studies using other robotic interventions implemented within the first 30 days after stroke onset. Patients with severe impairment of the motor function using the end-effector-type robotic device denominated as Gait Trainer showed improvement of the motor outcome which was sustained after 2 years (Peurala et al., 2007; Morone et al., 2012). The exoskeleton Lokomat was able to induce motor recovery and improvement of cardiopulmonary fitness which is an issue for bedridden patients (Chang et al., 2012). Finally, a study implementing the gait assistance robot GAR found motor and functional recovery but it was not significantly different from regular rehabilitation; however, the extensor muscle torque improved bilaterally, being significant only for the non-paretic side (Ochi et al., 2015).

These studies focused their analysis on the comparison of functional scales and gait parameters, but there are no additional measurements to evaluate coordination changes after robotic intervention. It is known that coordination impairment is an underlying cause of gait deficit after stroke (Bleyenheuft et al., 2009; Chow and Stokic, 2015); hemiparesis alters the stabilization of head and thorax which contribute to the deviation of walking trajectories and poor balance during gait generation (Lamontagne et al., 2005). Also, muscle weakness from the hemiparetic side affect the initiation of movement and proper flexion and extension of the ipsilateral hip, knee, and ankle (Quervain et al., 1996). Likewise, post-stroke patients have more difficulties regulating their walking speed, step frequency, and step length which are important elements to execute stable gait when walking in complex environments (Hak et al., 2013). However, despite unilateral brain damage, abnormal patterns of movement are also found in the non-paretic side during gait generation (Quervain et al., 1996) accompanied by increment of the bilateral kinematic variability. These changes have been associated to asymmetry and lack of coordination of the left-right stepping phase (Meijer et al., 2011). Additionally, these conditions impair the ability to avoid obstacles bilaterally, becoming more prominent under time pressure (Otter et al., 2005). Bilateral coordination is an important component of gait pattern; therefore, evaluation of its changes may help to elucidate the impact of robotic interventions.

Kinematic analysis of gait has been attempted before by measuring changes in joint angles; however, the pattern of the flexion-extension angles of hip and knee joints tends to generate a large variation in inter-patients and inter-trial results (Boudarham et al., 2013) and becomes dependent on the gait speed (Borghese et al., 1996). Since the gait pattern is drastically altered after stroke due to hemiparesis and march instability, perturbing patients' balance and speed (Quervain et al., 1996; Goldie et al., 2001); it is ideal to collect data using a method able to obtain reproducible results despite these gait characteristics. Analysis of the EA of the lower limbs has shown a stereotyped pattern in healthy volunteers despite gait pattern, speed variation, or anatomic discrepancies (Borghese et al., 1996; Ivanenko et al., 2008). The EA are calculated by the relationship of lower limb thigh, shank, and foot segments to the vertical. When plotted against each other, these angles covary describing regular loops over a plane (Borghese et al., 1996; Ivanenko et al., 2008). The correlation of the coordination patterns among the EA of the lower limb segments during locomotion is known as the law of intersegmental coordination (Borghese et al., 1996; Barliya et al., 2009). It has been suggested that this planar law represents the coordinated kinematic synergies of the body in charge of the maintenance of dynamic equilibrium during gait progression and anticipatory locomotor adjustments to environmental changes (Maclellan and McFadyen, 2010). This analysis has been previously used for gait analysis of stroke patients (Bleyenheuft et al., 2009; Chow and Stokic, 2015) and we

previously reported a planar covariation analysis of myelopathy patients after HAL intervention (Puentes et al., 2018); however; to our knowledge, this is the first study examining planar covariation after an early robotic intervention as a measure of gait coordination in stroke patients.

MATERIALS AND METHODS

Participants

Eleven patients hospitalized with a diagnosis of acute stroke were selected for this study (8 women and 3 men). As inclusion criteria, patients within 40 to 80 years old, displaying hemorrhagic or ischemic stroke causing hemiparesis; with a stroke onset within 7 to 14 days were selected. Only first-time episode patients with a FAC higher than 4 before the stroke onset, able to give consent for the study and physically suitable for HAL fitting were included. All patients were able to control their lower extremities voluntarily, but minimal weight support was provided if necessary. One patient was excluded due to anxiety over using an exoskeleton and interference with a previous spinal surgery (included patients n = 10, age 60.7 ± 11 years; **Table 1**). As control, kinematics data from nine healthy age-matched volunteers (5 women and 4 men, age 58.2 ± 11 years; **Table 1**) was used. This study was approved by the Ethics Committee of the University of Tsukuba Hospital (approval number: H27-257) and implemented according to the ethical principles stipulated in the Declaration of Helsinki and the University Guidelines for Clinical Trials. All patients received a personalized explanation of the study, participation and data usage before signing an informed consent.

HAL Intervention

The intervention consisted in 9 HAL sessions performed within the hospitalization period three times per week. Each session started with HAL fitting and both patient and robot were secured to the All-In-One® walking trainer (Ropox A/S, Naestved, Denmark). This support system provides individual harnesses for the patient and the robot in order to ensure safety during the sessions and support the robot weight (14 kg). Once the patient was ready, the HAL treatment started consisting of 20 min of walking activity in a 25 m oval course at a comfortable pace. The condition of each patient was assessed by monitoring their blood pressure, heart rate, and oxygen saturation at the beginning, end, and within treatment intervals to ensure that patients were stable. At the end of the treatment, the patients were released from the robot and harness. In total, HAL intervention takes about 1 h from HAL fitting to release.

HAL Configuration

The single leg version of the robot suit HAL was used to support the hemiparetic side of stroke patients only. The neuromuscular activity of the Iliopsoas (hip flexor), Gluteus Maximus (hip extensor), Biceps Femoris (knee flexor), and the Quadriceps (vastus lateralis and knee extensor) of the affected side was detected through surface electrodes and processed by HAL to assist the patients' gait. The robot locates two motors beside the patient's hip and knee; when actuated by muscle signals, these motors are able to produce torque in proportion to the weighted difference of filtered activation of the ipsilateral flexor and extensor muscles corresponding to the hip and knee, respectively. The weights multiplied on the activation of the antagonistic muscles and the overall gain were adjusted individually depending on patient's

TABLE 1 | Characteristics of the participants.

ID	Included participants	Gender	Age	Diagnostic	Lesion	Paretic side	Interval (days)
S1	Stroke	F	67	Atherothrombotic cerebral infarction	Posterior limb of the internal capsule	Left	10
S2	Stroke	F	52	Intracerebral hemorrhage (subcortical)	Parietal lobe	Right	17
S3	Stroke	F	71	Brain stem infarction	Pons: paramedial left side	Left	11
S4	Stroke	M	55	Lacunar infarct	Right basal ganglia to corona radiata	Left	10
S5	Stroke	F	55	Atherothrombotic cerebral infarction	Anterior cerebral artery territory	Left	16
S6	Stroke	M	43	Lacunar infarct	Lateral thalamus	Right	11
S7	Stroke	F	51	Atherothrombotic cerebral infarction	Left basal ganglia to corona radiata	Right	18
S8	Stroke	M	80	Atherothrombotic cerebral infarction	Putamen	Right	16
S9	Stroke	F	61	Cerebral hemorrhage	Thalamus, third ventricle	Left	12
S10	Stroke	F	72	Hypertensive intracerebral hemorrhage	Thalamus	Right	14
H1	Healthy	F	56	–	–	–	–
H2	Healthy	F	42	–	–	–	–
H3	Healthy	F	59	–	–	–	–
H4	Healthy	F	67	–	–	–	–
H5	Healthy	F	60	–	–	–	–
H6	Healthy	M	50	–	–	–	–
H7	Healthy	M	45	–	–	–	–
H8	Healthy	M	77	–	–	–	–
H9	Healthy	M	68	–	–	–	–

Interval refers to the days elapsed from stroke onset to the beginning of HAL intervention. One patient excluded from the study is not listed.

electromyography signals, gait performance, and verbally reported subjective perception through HAL intervention sessions.

Evaluation

Before starting the first HAL session and after the last one, the degree of dependence on daily life activities of stroke patients was evaluated by using the FAC, FMA, and the FIM (total and locomotion only). Following, the patients were evaluated by using the 6MWD. Recordings were used to calculate the stride length, cadence, and speed (**Figure 1**). All evaluations were performed without using HAL.

Data Collection and Analysis

Segmental kinematics were recorded by using a motion capture system (VICON MX, 16 T20s cameras, 100 Hz) with Plug-in Gait lower limbs marker-set before the first and after the last HAL intervention for 10 stroke patients, and during a single session for 9 healthy volunteers. For data collection, patients were asked to walk 10 m over a straight line; the initial and final steps were discarded to collect the steps with best performance. Six to 24 cycles were used for analysis. For the last three patients, segmental kinematics were recorded on days 1, 4, and 7 before and during HAL intervention. Since the number of patients was not enough for statistical comparison, only data from one patient was used as an example of planar covariation changes before, during, and after HAL intervention. The EA of the lower limbs were analyzed regarding the orientation of the limb segments in the sagittal plane with respect to the vertical as described before (Borghese et al., 1996). The evaluated segments (**Figure 2A**) were denominated as thigh (from the trochanter to the lateral epicondyle of the femur), shank (from the lateral epicondyle of the femur to the lateral malleolus), and foot (from the posterior calcaneal tuberosity to the second metatarsal). Following, planar covariation of the EA for each lower limb was calculated by using a principal component (PC) analysis after data normalization by subtracting the mean value.

Previous studies have described in healthy volunteers that the first (PC1) and second (PC2) components covariates over a plane describing the shape of the gait loop; nevertheless, the third component (PC3) is orthogonal to the plane, representing the data component that deviates from the covariance plane (Borghese et al., 1996). We calculated the standard deviation of PC2 and PC3 (PC2-SD and PC3-SD) to evaluate the actual width of the covariance loop and the deviation from the covariance plane, respectively. Additionally, we evaluated the proportional width of the covariance loop determined by the percentage of variance (PV) of the PC2 (PV2) and the proportional deviation from the plane determined by the PV of PC3 (PV3) as described before (Martino et al., 2014). The PV3 becomes an index of planarity of the loop, where 0% corresponds to an ideal plane fitting, thus evaluating the proportional deviation from the covariance plane.

In order to visualize the deviation pattern from the covariance plane through gait cycle, the distance from each point to the covariance plane was measured and a Kernel method (Kim and Scott, 2012) was used to create a heat map. This plot was performed over the covariance plane within the three-dimensional space of thigh, shank, and foot EA.

To evaluate the changes in the movement range of the EAs during gait performance, peak comparisons for each EA were performed. Gait cycles were extracted from the original data according to the movement of the toe and heel markers. To normalize the data, the time variable was discarded and the gait progression was accounted from 0 to 100% for each subject. The averaged cycle profile was obtained for each EA of each limb and comparisons were made from the max peaks, min peaks, and max-min difference. The obtained data was plotted for each patient' individual limbs and split in EA before and after HAL intervention. Data from all healthy volunteers was averaged and plotted along as reference. Peak comparisons also were performed as described above for joint angles. Cycles were extracted from the original kinematic data for hip, knee, and ankle joints.

Statistical analysis was done by using a Wilcoxon signed rank test (paired for side comparisons and before-after HAL intervention; unpaired for patients' comparisons against volunteers) analyzing the evolution of patients before and after HAL intervention or either condition against healthy volunteers. Due to sample size, a power test was applied after each analysis (10,000 times replication). Significance was considered when a P-value <0.05 was accompanied by an observed power (OP) $>50\%$ (Hoenig and Heisey, 2001). All statistical analysis was carried out by using custom made scripts on MATLAB [version 8.4.0.150421 (R2014B)] and RStudio (version 1.0.136).

RESULTS

Walking performance analysis showed an improvement in cadence (mean; pre: 52.54 $\pm$ 25.5 steps/min, post: 70.48 $\pm$ 16.6 steps/min, P-value: 0.04, OP: 25%) and a significant improvement in 6MWD (mean; pre: 97.93 $\pm$ 66.1 m, post: 217 $\pm$ 77.9 m, P-value: <0.01, OP: 74.5%), stride length (mean; pre: 0.29 $\pm$ 0.1 m, post: 0.42 $\pm$ 0.08 m, P-value: 0.015, OP: 59.4%) and walking speed (**Figure 1A**; mean; pre: 16.45 $\pm$ 10.1 m/min, post: 31.4 $\pm$ 13.2 m/min, P-value: <0.01, OP: 51.2%). Functional scores also showed a tendency of recovery for FMA (mean; pre: 20.6 $\pm$ 5.4, post: 25.5 $\pm$ 4.2, P-value: <0.01, OP: 35.4%), and significant improvement for FAC (mean; pre: 1.90 $\pm$ 0.7, post: 3.7 $\pm$ 0.6, P-value: <0.01, OP: 98%), FIM (mean; pre: 88.7 $\pm$ 13.4, post: 109.3 $\pm$ 10.7, P-value: <0.01, OP: 77.6%), and FIM locomotion (mean; pre: 55.5 $\pm$ 12.6, post: 75.2 $\pm$ 11.1, P-value: <0.01, OP: 73.4%) after HAL intervention (**Figure 1B**).

Kinematics analysis was used to understand changes in coordination given by alteration in the planar covariation of thigh, shank, and foot limb segments (**Figure 2A**, elevation angles). Healthy volunteers displayed a tear drop shaped pattern as previously described (**Figure 2A**, volunteer). In contrast, the loops corresponding to the patients' analysis were distorted in both paretic and non-paretic limbs (**Figure 2B**). Additionally, the distribution size of the data over the plane was importantly reduced for patients before HAL intervention evidencing impaired intersegmental coordination (**Figure 2B**,

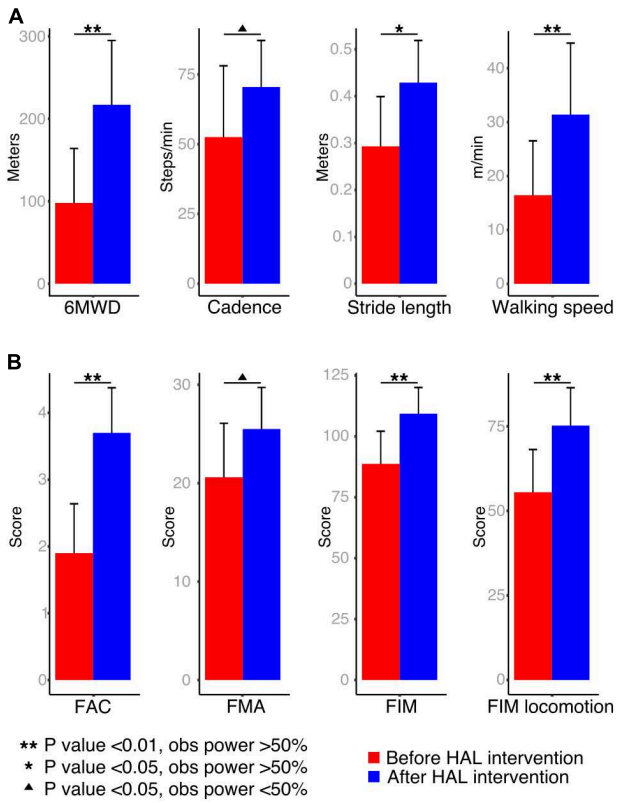

FIGURE 1 | Walking performance and clinical scores: **(A)** patients were assessed during a 6-min walking distance test and cadence, stride length and walking speed were calculated from recordings. **(B)** To evaluate the degree of functionality of patients, the Functional Ambulation Classification (FAC), Fugl-Meyer Assessment (FMA), Functional Independence Measure (FIM) total, and locomotion scores were performed.

before HAL intervention). An example from one patient (S7, **Table 1**) showed progressive loop recovery at the days of the first, fourth, and seventh HAL interventions where enlargement of the loop width is evident and the paretic side tendency to recover the tear drop shape of the loop was noticeable (**Figure 2B**, day 18, 25, and 35 after stroke). After complete HAL intervention, recovery of the loop width for both sides (paretic and non-paretic) was found, with recovery of tear drop like pattern more accentuated for the paretic side (**Figure 2B**, after HAL intervention).

Comparisons of PC2 standard deviation (PC2-SD) were significantly different from paretic and non-paretic limbs before and after HAL intervention when compared to healthy group. However, there was a tendency to recover for both sides after HAL intervention [**Figure 2C**, PC2-SD comparison and **Supplementary Tables S1**, **S2**. PC2-SD *P*-values; Par-pre Vs healthy volunteers (healthy): <0.01, OP: 96.1%; par-post Vs healthy: <0.01, OP: 96.3%; np-pre Vs healthy: <0.01, OP: 99.5%; np-post Vs healthy: <0.01, OP: 89.4%]. The PV as well showed a tendency of recovery for paretic and non-paretic limbs of patients after HAL intervention (**Figure 2C**, PV2 comparison; PV2 *P*-values; par-pre Vs par-post: 0.013, OP: 26.4%). These results suggest that HAL intervention induced a recovery trend by improving the actual and proportional width of the gait loop on the covariance plane.

Deviation from the covariance plane evaluated by PC3-SD comparisons showed improvement mainly for the np-post (**Figure 2C**, PC3-SD comparison and **Supplementary Tables S1**, **S2**. *P*-values; np-post Vs par-post: 0.019, OP: 57.1%; par-pre Vs healthy: 0.04, OP: 53.8%; par-post Vs healthy: <0.01, OP: 81.7%). Proportional deviation from covariation plane evaluated by PV3 demonstrated a tendency of recovery from patients after HAL intervention for non-paretic side as well (**Figure 2C**, PV3 comparison and PV3 *P*-values; par-pre Vs healthy: 0.03, OP: 53%). For paretic side, tendency of recovery was found when comparing between paretic and non-paretic limbs before and after HAL intervention (PV3 Par-pre Vs par-post *P*-value: 0.02, OP: 26.6%) and only paretic limbs before the intervention were significantly different from healthy volunteers. After HAL intervention, the PV3 reached values similar to healthy volunteers without exhibiting a statistical difference (**Figure 2C**; PV3 comparison *P*-values; np-pre Vs healthy: <0.01, OP: 92.2%; np-post Vs healthy: <0.01, OP: 74.6%). This tendency of recovery of PV3 suggests positive changes in planarity of coordination after HAL intervention. Other comparisons did not show significant differences.

Heat maps were used to graphically assess the deviation pattern from the covariance plane. The pattern found in healthy volunteers corresponded to a loop with two main hot spots in the areas related to heel strike and toe off (**Figure 2D**). Patients showed distorted patterns which differed importantly from the healthy pattern, encompassing a smaller surface, and evidencing one small hot spot (**Figure 2D**, before HAL). However, after HAL therapy, the loop shape was recovered for both sides (paretic and non-paretic), and the loop shape was closer to the volunteer conditions (**Figure 2D**, after HAL). The resemblance of heat maps after HAL intervention to healthy suggests an improvement in limb motion and plane stability.

Peak comparisons before and after HAL intervention were used to evaluate the range of movement of each EA. Patients before HAL intervention showed lower peaks with an increased variability when compared to plots after HAL intervention; where the SD was smaller and the pattern resembled the healthy group data (**Figure 3A**). Statistical comparisons of max peaks, min peaks, and max-min difference were also performed (**Figure 3B** and **Supplementary Tables S3**, **S4**). Max peaks for non-paretic side did not show any significance related to thigh EA. Shank and foot showed significant difference from healthy volunteers before and after HAL intervention, but a tendency of recovery was noticed (shank *P*-value; np-pre Vs np-post: 0.04, OP: 44%; np-pre Vs healthy: <0.01, OP: 99.1%; np-post Vs healthy: <0.01, OP: 76.6%. Foot *P*-value; np-pre Vs np-post: 0.019, OP: 42.4%; np-pre Vs healthy: < 0.01, OP: 98.1%; np-post Vs healthy: 0.04, power test: 56.4%). On the paretic side, significant differences between thigh, shank, and foot before HAL intervention and healthy group were found; (thigh *P*-value; par-pre Vs healthy: <0.01, OP: 73.2%. Shank *P*-value: par-pre Vs healthy: <0.01, OP: 99.9%; par-post Vs healthy: <0.01, OP: 81.5%. Foot *P*-value; par-pre Vs healthy: <0.01, power test 99.9%; par-post Vs healthy: <0.01, power test: 99%). Peak comparisons before and after HAL

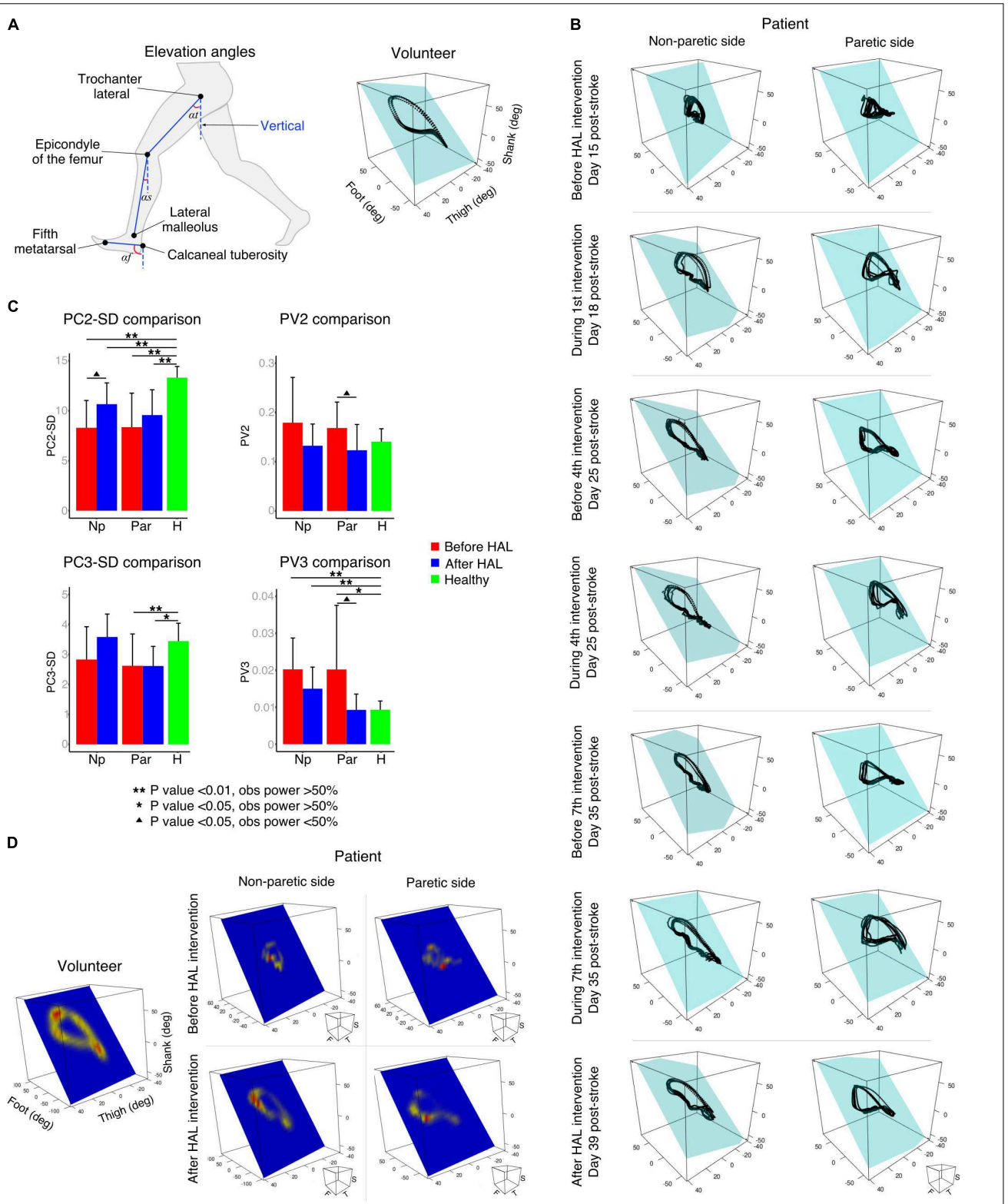

FIGURE 2 | Planar covariation of elevation angles. **(A)** Left: thigh, shank, and foot limb segments used to calculate the elevation angles. Right: planar covariation sample from one healthy volunteer leg. **(B)** Planar covariation sample from one patient paretic and non-paretic leg before, during and after HAL intervention. Each dotted line corresponds to different strides of the same limb **(C)** PCA comparisons using second (PC2) and third (PC3) components. Comparisons of the actual data were done with the standard deviation (SD). The proportional variance of both components was also analyzed (PV2 and PV3). **(D)** Heat maps were used to plot the deviation from the plane for each participant. Sample from one volunteer leg and one patient paretic and non-paretic leg before and after HAL are shown.

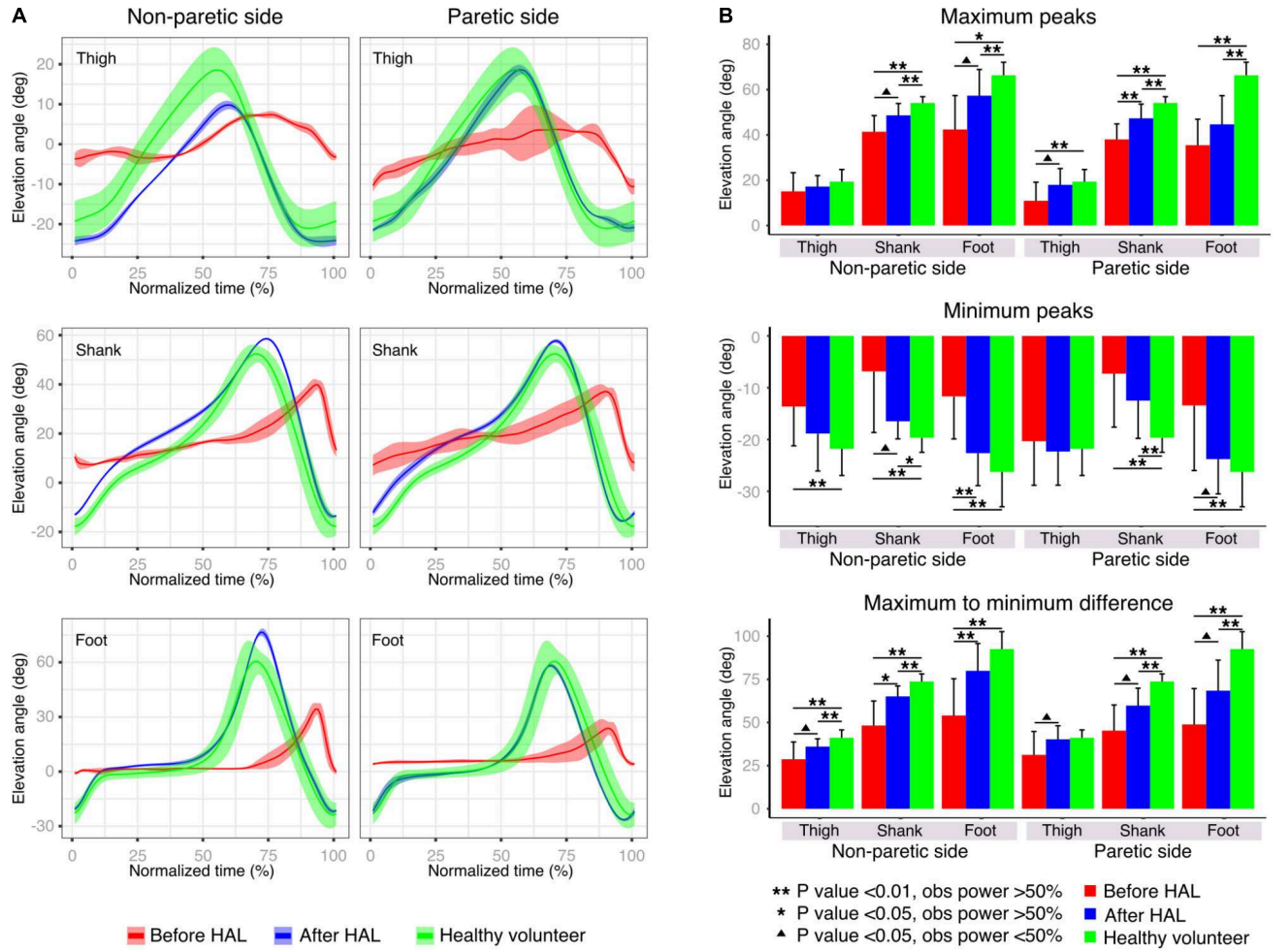

FIGURE 3 | Peak analysis. **(A)** Elevation angle profiles were plotted before and after HAL therapy for each limb segment of one example patient's paretic and non-paretic leg. The solid line represents the profile mean and width of highlighted area represents the standard deviation. Healthy volunteer plot (green line) is given by the averaged results of all healthy volunteer participants. **(B)** Maximum peaks, minimum peaks, and maximum to minimum peaks differences were compared for paretic and non-paretic side before and after HAL. As control, results from healthy volunteers were also included.

intervention showed significant difference only for shank (*P*-value: par-pre Vs par-post: <0.01, OP: 60.7%) but tendency of recovery was evident for all EA. Min peaks showed a tendency of recovery more marked for the non-paretic side, where thigh EA peaks showed a significant difference before HAL intervention and healthy but not after HAL intervention and healthy (thigh *P*-value; np-pre Vs healthy: <0.01, OP: 75.9%; np-post Vs healthy: 0.22). Shank min peaks showed statistical difference before and after HAL intervention against healthy, but tendency of recovery also was found (shank *P*-value; np-pre Vs np-post: <0.01, OP: 41.5%; np-pre Vs healthy: <0.01, OP: 84.4%; np-post Vs healthy: <0.02, OP: 59.63%). Foot min peaks showed a significant difference before and after HAL intervention, and also, significant difference was found before HAL intervention and healthy only (foot *P*-value; np-pre Vs np-post: <0.01, OP: 66.04%; np-pre Vs healthy: <0.01, power test 98.2%; np-post Vs healthy: 0.22). On the paretic limb, there were no relevant changes for thigh min peaks. On the other hand, shank and foot min peaks showed a tendency of recovery being more marked for foot peaks where significant difference was found only before HAL intervention and healthy volunteers (shank *P*-value; par-pre Vs healthy: <0.01, OP: 88.6%; par-post Vs healthy: <0.01, OP: 76.0%. Foot *P*-value; par-pre Vs healthy: <0.01, power test 75.4%; par-post Vs healthy: 0.43). Finally, the max-min difference showed a tendency of recovery mainly marked for non-paretic foot where a significant difference was found before and after HAL intervention and between before HAL intervention and healthy group only (thigh *P*-value; np-pre Vs healthy: <0.01, OP: 89.2%; np-post Vs healthy: <0.01, OP: 69.2%. Shank *P*-value; np-pre Vs np-post: 0.019, OP: 68.3%; np-pre Vs healthy: <0.01, OP: 99.4%; np-post Vs healthy: <0.01, OP: 92.4%. Foot *P*-value; np-pre Vs np-post: <0.01, OP: 58.4%; np-pre Vs healthy: <0.01, power test 99.5%; np-post Vs healthy: 0.051). The paretic side also showed a tendency of improvement before and after HAL intervention. Results from shank and foot evidenced significance when comparing peaks

before and after HAL to healthy volunteers. However, peaks obtained after HAL intervention tended to increase to the level of the healthy group (shank *P*-value; par-pre Vs par-post: <0.01, OP: 43.7%; par-pre Vs healthy: <0.01, OP: 99.7%; par-post Vs healthy: <0.01, OP: 94.2%. Foot *P*-value; par-pre Vs par-post: <0.01, OP: 35.4%; par-pre Vs healthy: <0.01, OP: 99.9%; par-post Vs healthy: <0.01, OP: 92.8%). Peak analysis results showed important changes related principally to the foot EA for non-paretic side and thigh EA for paretic side. Despite the maintained significance between patients after HAL intervention and healthy volunteers, and overall tendency of recovery was also found for shank EA. These changes may represent an improvement in toe clearance and limb excursion induced by HAL intervention.

In addition to EA analysis, peaks comparison was also performed for hip, knee, and ankle joint angles (**Supplementary Figure S1**). Before HAL, patients showed relatively flat plots. However, after HAL intervention, resemblance to healthy volunteers improved (**Supplementary Figure S1A**). Max peaks comparison showed a tendency of recovery for knee angle of the non-paretic side (**Supplementary Figure S1B** and **Supplementary Tables S5**, **S6**. Knee *P*-value: np-pre Vs healthy: <0.01, OP: 97.9%; np-post Vs healthy: 0.017, OP: 65.8%) although pre-post comparisons did not show significance. Min peaks comparisons did not find significance related to improvement. Max to min peaks comparison of non-paretic side showed marginal significance before and after HAL intervention for knee joint (*P*-value np-pre Vs np-post: 0.03, OP: 33.3%) and significant difference when comparing patients before and after HAL intervention against healthy volunteers (*P*-value np-pre Vs healthy: <0.01, OP: 99.8%; np-post Vs healthy: <0.01, OP: 93.4%). However, a tendency of recovery was noted. Comparisons for the paretic side evidenced significance related to improvement for hip joint angle, where comparisons before and after HAL intervention showed a marginal improvement (*P*-value: < 0.01, OP: 42.1). Additionally, comparisons before HAL intervention and healthy were statistically different, but when comparing healthy volunteers to patients after HAL intervention, significance was not found (*P*-value par-pre Vs healthy: <0.01, OP: 85.3; par-post Vs healthy: 0.29). This data reinforces the findings related to thigh and shank EA improvement after HAL intervention. Lack of significance related to other joint peaks may be related to the high variability found on joint angles analysis between subjects and between trials in healthy volunteers (Borghese et al., 1996). Due to gait deterioration in stroke patients, gait cycle variability inter-trial and inter-subject is expected to be larger. Given their stereotyped characteristics (Borghese et al., 1996; Ivanenko et al., 2008), EA analysis allows collection of less variable data which is desirable in populations with gait disturbances as stroke patients.

DISCUSSION

Gait generation is a complex dynamic process with spinal circuits able to generate basic locomotion patterns, altered by descending pathways carrying information from the brain. The system also has feedback from muscle receptors, skin afferents, and senses which help to gather information to adapt the locomotion pattern to the environment (Belda-Lois et al., 2011). However, the disruption of the descending pathways after the ischemia onset induce muscle co-activation of the paretic limb (Beyaert et al., 2015) instead of selective control of individual joint movements adapting to the new conditions in order to stabilize gait (Verma et al., 2012). In hemiparesis, the underlying mechanisms of asymmetry are poor single limb support and lack of forward movement control (Verma et al., 2012) summed to the disproportion between hemilateral motor commands leading to bilateral coordination deficit (Meijer et al., 2011). This asymmetry leads to compensation strategies leaning on the capabilities of the non-paretic limb. The achieved walking pattern is characterized by a higher proportion of the gait cycle spent in the unaffected single limb support and bipedal support in comparison to the supporting time provided by the hemiparetic leg (Olney and Richards, 1996), drifting away from regaining a coordinated gait pattern.

It has been acknowledged that planar covariation of limb segments may be a way used by the central nervous system to reduce the effective degrees of freedom thus simplifying the control of posture and locomotion (Lacquaniti et al., 1990, 2002; Ivanenko et al., 2008). During gait, the rotation of EA belonging to thigh, shank, and foot limb segments covary tracing a tridimensional trajectory of temporal changes lying close to a plane in healthy subjects (Borghese et al., 1996; Ivanenko et al., 2008). The planar law of intersegmental coordination is discussed to be representing the strategy of modularized control of the lower limbs by the central nervous system in terms of limb orientation and length (Ivanenko et al., 2007, 2008). Since healthy subjects' trajectories correspondence to plane has minimal variation, plane fitting related data may not be so relevant; however, distorted gait patterns have an effect over this aspect. Previous studies using planar covariation analysis in different pathologies affecting locomotion as Parkinson (Grasso et al., 1999), stroke (Bleyenheuft et al., 2009; MacLellan et al., 2013; Chow and Stokic, 2015), myelopathy (Puentes et al., 2018), and cerebellar ataxia (Martino et al., 2014) have demonstrated the preservation of intersegmental coordination to some extent despite the underlying condition; however, impaired intersegmental coordination was found in all cases. Interestingly, an additional research documenting changes in planar covariation of amputees found preservation of the gait loop and adequate intersegmental coordination on novice and experienced prostheses users (Leurs et al., 2012). The integrity of the central nervous system and the preserved intersegmental coordination in such patients suggest that the relationship between segments may have a central control and that it is not dependent on biomechanical constrains (Ivanenko et al., 2008; Leurs et al., 2012). The improvement of planar covariation, may suggest changes related to neural plasticity leading to coordination and gait recovery (Poppele and Bosco, 2003; Ivanenko et al., 2008).

In the present study, the initial evaluation before HAL intervention confirmed the conservation of the law of intersegmental coordination. However, the hemiparetic gait induced distortion and size reduction of the gait loop showing impaired intersegmental coordination for both paretic and non-paretic limbs (**Figure 2B**). Early HAL intervention was able to induce recovery of the covariation loop shape and distance to plane distribution (**Figures 2B,D**). PCA comparisons also showed a tendency of recovery for the actual width of the loop and plane stability more accentuated for the non-paretic limb (PC2-SD, **Figure 2C**). On the other hand, the proportion of variance of loop width and proportional plane stability recovery was more prominent for the paretic side (PV3, **Figure 2C**). The tendency of recovery shown by the planar covariation analysis suggests a beneficial effect of HAL intervention on improvement of gait coordination.

Previous studies have shown lack of recovery of spatiotemporal coordination in gait of stroke patients after conventional rehabilitation despite improvement of balance ability and walking velocity (Patterson et al., 2008, 2014). Foot drag during swing phase, foot slap, unstable support, and weak propulsion during stance phase are the reasons which lead the non-paretic limb to adopt compensatory movements to compromise gait. The compensatory movements deviate the non-paretic limb from its original movement pattern, even to deteriorate lateral asymmetry of gait (Olney and Richards, 1996). We hypothesize that HAL intervention was able to modify gait coordination by providing functional control to the paretic limb at the earliest possible occasion post stroke. HAL allowed to perform voluntary control of the paretic leg by its function to provide joint motion assistance in accordance with the patients' bioelectrical activity. This feature enabled patients to perform larger foot excursion during swing phase, smoother landing, better support stability, and empowered propulsion during stance phase. This characteristic may have saved the non-paretic limb from the demand to take compensatory movements through recovery, probably contributing to bilateral improvement of gait coordination. By using the patient's own bioelectric signals, the gait output can be perceived natural and coherent, generating sensory feedback of the performed motion over to the central nervous system. A recent report by our group (Tan et al., 2018) analyzed the muscle synergies of some of the patients included in our research before and after HAL intervention. It was found that before HAL intervention, stroke patients had a reduced number of muscle synergies of the paretic leg when comparing to the contralateral limb. HAL intervention improved in some cases the synergies of the paretic side but in some cases also a reduction of synergies in the non-paretic side was found. This synergies reduction of the non-paretic side may be a strategy to balance bilateral muscle control to improve gait coordination. In contrast to conventional rehabilitation strategies, where the goal is to adapt compensatory movements to enhance performance in daily life activities (Verma et al., 2012), HAL provided support allowing a more natural recovery process thus improving coordination.

Peak analysis of the EA showed a trend of recovery more accentuated for thigh peaks in the paretic limb; on the other hand, shank and foot peak recovery seemed to be more favored for the non-paretic limb (**Figure 3B**). We think HAL intervention improved the range of movement of lower limbs during gait through improvement of hip flexion which is known to be affected in hemiparetic gait (Olney and Richards, 1996). Also, we think that HAL support to the hemiparetic side allowed a better performance of the non-paretic leg, balancing the gait and allowing a normal time for swing and stance phases of both limbs reducing the early foot contact of the non-paretic limb evidenced in stroke patients (Olney and Richards, 1996). Joint angle analysis showed tendency of improvement of knee angle in the non-paretic side and also hip angle of the paretic side (**Supplementary Figure S1B**), detecting less significant comparisons than the EA analysis. We consider that the main difference in the results is related to the high variability of joint angles regarding gait pattern and velocity in contrast to the stereotyped pattern found on EA (Borghese et al., 1996).

It is known that exercising is an effective non-invasive treatment able to induce neuroplasticity in the central nervous system and increase resistance to the brain damage (Cotman and Berchtold, 2002; Sandrow-Feinberg and Houlé, 2015). Offering rehabilitation in the early stages of stroke increases the functional recovery and reduces hospitalization time, favoring the patient to continue rehabilitation in the outpatient clinic. However, delayed admission to rehabilitation program is common for stroke patients leading to poor outcomes and long-term disability (Salter et al., 2006). We believe that HAL intervention may have a higher impact in an early stage avoiding the establishment of compensatory strategies which affect importantly gait coordination in this population. Additionally, studies analyzing adaptability changes in the post-stroke brain have found evident contralesional activation in the early stages which returns to normal in the subacute and chronic stages of the disease (Beyaert et al., 2015). This activation is supposed to correspond to automatic and intentional cognitive processes for support, balance, and progression that help patients to find strategies to generate gait despite hemiparesis (Beyaert et al., 2015). We hypothesize that patients receiving early HAL intervention may use this mechanism to find better strategies to improve motor output reducing abnormal postures and allowing a better gait recovery process.

This study has limitations with respect to the size of the population included for analysis. Also, we have not included a control group of stroke patients undergoing conventional rehabilitation to compare with patients after HAL intervention. Additionally, changes in the non-paretic side and its improvement after HAL intervention lead us to the question whether hemiparetic patients may respond differently to HAL if the double leg version is used to support also the non-paretic side. Further studies shall enlarge the population size, adding

a control group of patients receiving standard rehabilitation only and comparing the output in stroke patients after an early intervention by using the single leg and double leg HAL exoskeleton.

AUTHOR CONTRIBUTIONS

SP and HK collected, analyzed, and interpreted the data, and wrote and drafted the manuscript. HW administered HAL therapy and collected the data for clinical scores. TU and MY contributed in the development of HAL intervention program. YS originally developed the robot suit HAL and conceived the idea of HAL intervention. AM diagnosed the patients and prescribed HAL intervention, also provided important comments for the clinical part of the study, and contributed in the design of HAL intervention protocol. KS designed the analysis and provided essential insight for the paper. All authors made critical revisions of the manuscript and approved the final version. All authors read and approved the final manuscript.

FUNDING

This study was supported by the Industrial Disease Clinical Research Grant of the Ministry of Health, Labour and Welfare, Japan (14060101-01).

ACKNOWLEDGMENTS

We thank Ms. Mayuko Sakamaki and Ms. Yumiko Ito of Center for Innovative Medicine and Engineering (CIME) of the University of Tsukuba Hospital for their excellent technical assistance during HAL intervention. We also thank Dr. Eng. Luis Carlos Manrique Ruiz for his advice on statistical analysis.

SUPPLEMENTARY MATERIAL

The Supplementary Material for this article can be found online at: https://www.frontiersin.org/articles/10.3389/fnins.2018.00719/full#supplementary-material

REFERENCES

Barliya, A., Omlor, L., Giese, M. A., and Flash, T. (2009). An analytical formulation of the law of intersegmental coordination during human locomotion. *Exp. Brain Res.* 193, 371–385. doi: 10.1007/s00221-008-1633-0

Belda-Lois, J. M., del Horno, S. M., Bermejo-Bosch, I., Moreno, J. C., Pons, J. L., Farina, D., et al. (2011). Rehabilitation of gait after stroke: a review towards a top-down approach. *J. Neuroeng. Rehabil.* 8:66. doi: 10.1186/1743-0003-8-66

Benjamin, E. J., Virani, S. S., Callaway, C. W., Chamberlain, A. M., Chang, A. R., Cheng, S., et al. (2018). Heart disease and stroke statistics-2018 update: a report from the american heart association. *Circulation* 137, e67–e492. doi: 10.1161/CIR.0000000000000558

Beyaert, C., Vasa, R., and Frykberg, G. E. (2015). Gait post-stroke: pathophysiology and rehabilitation strategies. *Neurophysiol. Clin.* 45, 335–355. doi: 10.1016/j.neucli.2015.09.005

Bleyenheuft, C., Cockx, S., Caty, G., Stoquart, G., Lejeune, T., and Detrembleur, C. (2009). The effect of botulinum toxin injections on gait control in spastic stroke patients presenting with a stiff-knee gait. *Gait Posture* 30, 168–172. doi: 10.1016/j.gaitpost.2009.04.003

Borghese, N. A., Bianchi, L., and Lacquaniti, F. (1996). Kinematic determinants of human locomotion. *J. Physiol.* 494(Pt 3), 863–879. doi: 10.1113/jphysiol.1996.sp021539

Boudarham, J., Roche, N., Pradon, D., Bonnyaud, C., Bensmail, D., and Zory, R. (2013). Variations in kinematics during clinical gait analysis in stroke patients. *PLoS One* 8:e66421. doi: 10.1371/journal.pone.0066421

Chang, W. H., Kim, M. S., Huh, J. P., Lee, P. K., and Kim, Y. H. (2012). Effects of robot-assisted gait training on cardiopulmonary fitness in subacute stroke patients: a randomized controlled study. *Neurorehabil. Neural Repair* 26, 318–324. doi: 10.1177/1545968311408916

Chen, G., Chan, C. K., Guo, Z., and Yu, H. (2013). A review of lower extremity assistive robotic exoskeletons in rehabilitation therapy. *Crit. Rev. Biomed. Eng.* 41, 343–363. doi: 10.1615/CritRevBiomedEng.2014010453

Chow, J. W., and Stokic, D. S. (2015). Intersegmental coordination of gait after hemorrhagic stroke. *Exp. Brain Res.* 233, 125–135. doi: 10.1007/s00221-014-4099-2

Cotman, C., and Berchtold, N. (2002). Exercise: a behavioral intervention to enhance brain health and plasticity. *Trends Neurosci.* 25, 295–301. doi: 10.1016/S0166-2236(02)02143-4

Eng, J. J., and Tang, P. F. (2007). Gait training strategies to optimize walking ability in people with stroke: a synthesis of the evidence. *Expert Rev. Neurother.* 7, 1417–1436. doi: 10.1586/14737175.7.10.1417

Esquenazi, A., Talaty, M., and Jayaraman, A. (2017). Powered exoskeletons for walking assistance in persons with central nervous system injuries: a narrative review. *PM R* 9, 46–62. doi: 10.1016/j.pmrj.2016.07.534

Feigin, V. L., Norrving, B., and Mensah, G. A. (2017). Global burden of stroke. *Circ. Res.* 120, 439–448. doi: 10.1161/CIRCRESAHA.116.308413

Goldie, P. A., Matyas, T. A., and Evans, O. M. (2001). Gait after stroke: initial deficit and changes in temporal patterns for each gait phase. *Arch. Phys. Med. Rehabil.* 82, 1057–1065. doi: 10.1053/apmr.2001.25085

Grasso, R., Peppe, A., Stratta, F., Angelini, A., Zago, M., Stanzione, P., et al. (1999). Basal ganglia and gait control: apomorphine administration and internal pallidum stimulation in Parkinson's disease. *Exp. Brain Res.* 126, 139–148. doi: 10.1007/s002210050724

Hak, L., Houdijk, H., Wurff, P., van der Prins, M. R., Mert, A., Beek, P. J., et al. (2013). Stepping strategies used by post-stroke individuals to maintain margins of stability during walking. *Clin. Biomech.* 28, 1041–1048. doi: 10.1016/j.clinbiomech.2013.10.010

Hoenig, J. M., and Heisey, D. M. (2001). The abuse of power: the pervasive fallacy of power calculations for data analysis. *Am. Stat.* 55, 19–24. doi: 10.1198/000313001300339897

Ivanenko, Y. P., Cappellini, G., Dominici, N., Poppele, R. E., and Lacquaniti, F. (2007). Modular control of limb movements during human locomotion. *J. Neurosci.* 27, 11149–11161. doi: 10.1523/JNEUROSCI.2644-07.2007

Ivanenko, Y. P., d' Avella, A., Poppele, R. E., and Lacquaniti, F. (2008). On the origin of planar covariation of elevation angles during human locomotion. *J. Neurophysiol.* 99, 1890–1898. doi: 10.1152/jn.01308.2007

Kawamoto, H., Kamibayashi, K., Nakata, Y., Yamawaki, K., Ariyasu, R., Sankai, Y., et al. (2013). Pilot study of locomotion improvement using hybrid assistive limb in chronic stroke patients. *BMC Neurol.* 13:141. doi: 10.1186/1471-2377-13-141

Kim, J. S., and Scott, C. D. (2012). Robust Kernel density estimation. *JMLR* 13, 2529–2565.

Lacquaniti, F., Ivanenko, Y. P., and Zago, M. (2002). Kinematic control of walking. *Arch. Ital. Biol.* 140, 263–272.

Lacquaniti, F., Taillanter, L. M., Lopiano, L., and Maioli, C. (1990). The control of limb geometry in cat posture. *J. Physiol.* 426, 177–192. doi: 10.1113/jphysiol.1990.sp018132

Lamontagne, A., Serres, S. J., De Fung, J., and Paquet, N. (2005). Stroke affects the coordination and stabilization of head, thorax and pelvis during voluntary horizontal head motions performed in walking. *Clin. Neurophysiol.* 116, 101–111. doi: 10.1016/j.clinph.2004.07.027

Leurs, F., Bengoetxea, A., Cebolla, A. M., De Saedeeler, C., Dan, B., and Cheron, G. (2012). Planar covariation of elevation angles in prosthetic gait. *Gait Posture* 35, 647–652. doi: 10.1016/j.gaitpost.2011.12.017

Maclellan, M. J., and McFadyen, B. J. (2010). Segmental control for adaptive locomotor adjustments during obstacle clearance in healthy young adults. *Exp. Brain Res.* 202, 307–318. doi: 10.1007/s00221-009-2133-6

MacLellan, M. J., Richards, C. L., Fung, J., and McFayden, B. J. (2013). Use of segmental coordination analysis of nonparetic and paretic limbs during obstacle clearance in community-dwelling persons after stroke. *PM R* 5, 381–391. doi: 10.1016/j.pmrj.2013.02.003

Martino, G., Ivanenko, Y. P., Serrao, M., Ranavolo, A., d' Avella, A., Draicchio, F., et al. (2014). Locomotor patterns in cerebellar ataxia. *J. Neurophysiol.* 112, 2810–2821. doi: 10.1152/jn.00275.2014

Meijer, R., Plotnik, M., Zwaaftink, E. G., Lummel, R. C., van Ainsworth, E., Martina, J. D., et al. (2011). Markedly impaired bilateral coordination of gait in post-stroke patients: is this deficit distinct from asymmetry? A cohort study. *J. Neuroeng. Rehabil.* 8:23. doi: 10.1186/1743-0003-8-23

Morone, G., Iosa, M., Bragoni, M., Angelis, D., De Venturiero, V., Coiro, P., et al. (2012). Who may have durable benefit from robotic gait training?: a 2-year follow-up randomized controlled trial in patients with subacute stroke. *Stroke* 43, 1140–1142. doi: 10.1161/STROKEAHA.111.638148

Ochi, M., Wada, F., Saeki, S., and Hachisuka, K. (2015). Gait training in subacute non-ambulatory stroke patients using a full weight-bearing gait-assistance robot: a prospective, randomized, open, blinded-endpoint trial. *J. Neurol. Sci.* 353, 130–136. doi: 10.1016/j.jns.2015.04.033

Ogata, T., Abe, H., Samura, K., Hamada, O., Nonaka, M., Iwaasa, M., et al. (2015). Hybrid assistive limb (HAL) rehabilitation in patients with acute hemorrhagic stroke. *Neurol. Med. Chir.* 55, 901–906. doi: 10.2176/nmc.oa.2015-0209

Olney, S. J., and Richards, C. (1996). Hemiparetic gait following stroke. Part I: characteristics. *Gait Posture* 4, 136–148. doi: 10.1016/0966-6362(96)01063-6

Otter, A. R., Den Geurts, A. C., Haart, M., de Mulder, T., and Duysens, J. (2005). Step characteristics during obstacle avoidance in hemiplegic stroke. *Exp. Brain Res.* 161, 180–192. doi: 10.1007/s00221-004-2057-0

Patterson, K., Mansfield, A., Biasin, L., Brunton, K., Inness, E., and McIlroy, W. (2014). Longitudinal changes in poststroke spatiotemporal gait asymmetry over inpatient rehabilitation. *Neurorehabil. Neural Repair* 29, 153–162. doi: 10.1177/1545968314533614

Patterson, K. K., Parafianowicz, I., Danells, C. J., Closson, V., Verrier, M. C., Staines, W. R., et al. (2008). Gait asymmetry in community-ambulating stroke survivors. *Arch. Phys. Med. Rehabil.* 89, 304–310. doi: 10.1016/j.apmr.2007.08.142

Peurala, S. H., Airaksinen, O., Jäkälä, P., Tarkka, I. M., and Sivenius, J. (2007). Effects of intensive gait-oriented physiotherapy during early acute phase of stroke. *J. Rehabil. Res. Dev.* 44, 637–648. doi: 10.1682/JRRD.2006.05.0039

Poppele, R., and Bosco, G. (2003). Sophisticated spinal contributions to motor control. *Trend Neurosci.* 26, 269–276. doi: 10.1016/S0166-2236(03)00073-0

Puentes, S., Kadone, H., Kubota, S., Abe, T., Shimizu, Y., Marushima, A., et al. (2018). Reshaping of gait coordination by robotic intervention in myelopathy patients after surgery. *Front. Neurosci.* 12:99. doi: 10.3389/fnins.2018.00099

Quervain, I. A., De Simon, S. R., Leurgans, S., Pease, W. S., and McAllister, D. (1996). Gait pattern in the early recovery period after stroke. *J. Bone Joint Surg. Am.* 78, 1506–1514. doi: 10.2106/00004623-199610000-00008

Salter, K., Jutai, J., Hartley, M., Foley, N., Bhogal, S., Bayona, N., et al. (2006). Impact of early vs delayed admission to rehabilitation on functional outcomes in persons with stroke. *J. Rehabil. Med.* 38, 113–117. doi: 10.1080/16501970500314350

Sandrow-Feinberg, H. R., and Houlé, J. D. (2015). Exercise after spinal cord injury as an agent for neuroprotection, regeneration and rehabilitation. *Brain Res.* 1619, 12–21. doi: 10.1016/j.brainres.2015.03.052

Tan, C. K., Kadone, H., Watanabe, H., Marushima, A., Yamazaki, M., Sankai, Y., et al. (2018). Lateral symmetry of synergies in lower limb muscles of acute post-stroke patients after robotic intervention. *Front. Neurosci.* 12:276. doi: 10.3389/fnins.2018.00276

Ueba, T., Hamada, O., Ogata, T., Inoue, T., Shiota, E., and Sankai, Y. (2013). Feasibility and safety of acute phase rehabilitation after stroke using the hybrid assistive limb robot suit. *Neurol. Med. Chir.* 53, 287–290. doi: 10.2176/nmc.53.287

Verma, R., Arya, K. N., Sharma, P., and Garg, R. K. (2012). Understanding gait control in post-stroke: implications for management. *J. Bodyw. Mov. Ther.* 16, 14–21. doi: 10.1016/j.jbmt.2010.12.005

Conflict of Interest Statement: YS is the CEO, shareholder, and director of CYBERDYNE Inc. which manufacture the robot suit HAL. CYBERDYNE was not involved in the study design, data collection, analysis, writing or submission of this article.

The remaining authors declare that the research was conducted in the absence of any commercial or financial relationships that could be construed as potential conflict of interest.

frontiers in Neuroscience

ORIGINAL RESEARCH
published: 29 March 2019
doi: 10.3389/fnins.2019.00259

A Randomized and Controlled Crossover Study Investigating the Improvement of Walking and Posture Functions in Chronic Stroke Patients Using HAL Exoskeleton – The HALESTRO Study (HAL-Exoskeleton STROke Study)

Matthias Sczesny-Kaiser[1], Rebecca Trost[1], Mirko Aach[2], Thomas A. Schildhauer[3], Peter Schwenkreis[1] and Martin Tegenthoff[1]*

[1] Department of Neurology, BG University Hospital Bergmannsheil Bochum, Bochum, Germany, [2] Department of Spinal Cord Injury, BG University Hospital Bergmannsheil Bochum, Bochum, Germany, [3] Department of General and Trauma Surgery, BG University Hospital Bergmannsheil Bochum, Bochum, Germany

OPEN ACCESS

Edited by:
Irina N. Beloozerova, Georgia Institute of Technology, United States

Reviewed by:
Yongtian He, University of Houston, United States
Antonio Oliviero, Fundación del Hospital Nacional de Parapléjicos, Spain

***Correspondence:**
Matthias Sczesny-Kaiser
matthias.sczesny-kaiser@rub.de

Specialty section:
This article was submitted to Neuroprosthetics, a section of the journal Frontiers in Neuroscience

Received: *09 November 2018*
Accepted: *05 March 2019*
Published: *29 March 2019*

Citation:
Sczesny-Kaiser M, Trost R, Aach M, Schildhauer TA, Schwenkreis P and Tegenthoff M (2019) A Randomized and Controlled Crossover Study Investigating the Improvement of Walking and Posture Functions in Chronic Stroke Patients Using HAL Exoskeleton – The HALESTRO Study (HAL-Exoskeleton STROke Study). Front. Neurosci. 13:259. doi: 10.3389/fnins.2019.00259

Background: The exoskeleton HAL (hybrid assistive limb) has proven to improve walking functions in spinal cord injury and chronic stroke patients when using it for body-weight supported treadmill training (BWSTT). Compared with other robotic devices, it offers the possibility to initiate movements actively. Previous studies on stroke patients did not compare HAL-BWSTT with conventional physiotherapy (CPT). Therefore, we performed a crossover clinical trial comparing CPT and HAL-BWSTT in chronic stroke patients with hemiparesis, the HALESTRO study. Our hypothesis was that HAL-training would have greater effects on walking and posture functions compared to a mixed-approach CPT.

Methods: A total of 18 chronic stroke patients participated in this study. Treatment consisted of 30 CPT sessions and of 30 sessions of BWSTT with a double leg type HAL exoskeleton successively in a randomized, crossover study design. Primary outcome parameters were walking time and speed in 10-meter walk test (10MWT), time in timed-up-and-go test (TUG) and distance in 6-min walk test (6MWT). Secondary outcome parameters were the functional ambulatory categories (FAC) and the Berg-Balance Scale (BBS). Data were assessed at baseline, at crossover and at the end of the study, all without using and wearing HAL.

Results: Our study demonstrate neither a significant difference in walking parameters nor in functional and balance parameters. When HAL-BWSTT was applied to naïve patients, it led to an improvement in walking parameters and in balance abilities. Pooling all data, we could show a significant effect in 10MWT, 6MWT, FAC and BBS, both therapies sequentially applied over 12 weeks. Thereby, FAC improve from dependent to independent category (3 to 4). One patient dropped out of the study due to intensive fatigue after each training session.

Conclusion: HAL-BWSTT and mixed-approach CPT were effective therapies in chronic stroke patients. However, compared with CPT, HAL training with 30 sessions over 6 weeks was not more effective. The combination of both therapies led to an improvement of walking and balance functions. Robotic rehabilitation of walking disorders alone still lacks the proof of superiority in chronic stroke. Robotic treatment therapies and classical CPT rehabilitation concepts should be applied in an individualized therapy program.

Keywords: stroke rehabilitation, exoskeleton, hybrid assistive limb, physiotherapeutic approach, locomotor training

INTRODUCTION

Stroke is a growing medical and socioeconomical problem these days (Feigin et al., 2015). Epidemiologic studies estimated an yearly incidence of 800,000 in the United States to 1.0 million in the European Union (EU) (Truelsen et al., 2006; Mozaffarian et al., 2016). Incidence and prevalence increased over the last 20 years, while mortality decreased remarkably due to improving emergency medicine (Reeves et al., 2008; Koton et al., 2014). Stroke incidence is supposed to raise to 1.5 million per year in 2025 in the EU (Truelsen et al., 2006). Total costs of stroke care were expected to increase up to $184.1 billion in the United States for the year 2030 (Ovbiagele et al., 2013). In the next years, stroke therapy will become an even greater burden for national socioeconomic systems. While acute stroke therapies mainly focus on reducing infarcted brain tissue, reducing expected acute functional deficits and stroke survival, rehabilitation therapies in chronic stroke patients usually focus on restoration and reducing existing and persisting functional deficits. Both treatment approaches are necessary to lower resulting costs for the public healthcare system. Therefore, studies in both stroke settings (acute/chronic) are needed to limit persisting disabilities and analyze the best possible rehabilitation options.

Today, it is generally accepted that outpatient physiotherapy and other therapies would not lead to a significant functional recovery in chronic stroke.

The functional recovery curve reaches saturation after 6 months with only few fluctuations (Duncan et al., 1994; Jørgensen et al., 1995; Kwakkel et al., 2004; Langhorne et al., 2011). However, only few studies have addressed whether modern rehabilitation tools could induce significant functional recovery even in chronic stages. First positive evidence was given by innovative robotic devices for arm and walking training (Kwakkel et al., 2004; Huang and Krakauer, 2009; Reinkensmeyer et al., 2009; Lo et al., 2010). The results indicated that functional recovery might be possible even in chronic stages of stroke. The implementation of recent scientific knowledge on neurorehabilitation and neuronal plasticity like task-specificity, context-specificity and/or high-intensity and repetitive practice is a great advantage of new rehabilitation approaches. Several different robotic devices for locomotor support have been developed over the last 10 years. Most of them serve primarily as a medical and nursing device for walking support, but can be used as a training tool as well. For example, the ReWalk exoskeleton (ReWalk Robotics Ltd., Yokneam, Isreal) and the Indego bionic exoskeleton (Parker Hannifin Corporation, Cleveland, OH, United States) allow people with paraparesis due to spinal cord injury (SCI) to stand up, walk with a defined pattern and climb stairs. Induced locomotion is passive, not neurological self-induced and not based on any biological signal. Both robots use pre-programmed walking patterns that were executed irrespective of patient's remaining walking abilities. ReWalk and Indego have the intention to be applied predominantly as a walking aid for outdoor use. For walking rehabilitation, different robotic devices and gait trainers have been developed (e.g., Locomat, Gait Trainer GT a. s. o.). Even though, scientists showed therapeutic effects on walking parameters and disability, so far, in larger studies, they failed to show superiority when compared with conventional physiotherapies (Mehrholz and Pohl, 2012; Chang and Kim, 2013; Swinnen et al., 2014). Neither Locomat nor Gait Trainer GT uses neurobiological signal for locomotion control.

In contrast, the exoskeleton hybrid assistive limb (HAL) is controlled voluntarily by the patient's own muscle signals detected by surface electrodes. This self-initiated movement is capable to induce a somatosensory feedback-loop that enhances neural plasticity and locomotor learning (Sczesny-Kaiser et al., 2015). Pilot studies on patients with SCI, and chronic stroke showed safety and beneficial effects on walking functions (Kawamoto et al., 2013; Aach et al., 2014; Cruciger et al., 2014; Nilsson et al., 2014; Yoshimoto et al., 2015; Grasmücke et al., 2017; Jansen et al., 2017). In SCI, our study group demonstrated that HAL-assisted and body-weight supported treadmill training with supervision of a specialized physiotherapist led to a significant improvement of walking parameters and ambulatory capacity as indicated by the Walking Index for SCI II. These effects were observed in acute and chronic SCI patients, even up to 19 years after ictus (Aach et al., 2014; Grasmücke et al., 2017). Treadmill- and HAL-associated parameters like walking distance, speed and time as well as independent parameters like 10-meter walk test and 6-min walk test increased significantly up to 50% (Grasmücke et al., 2017). Moreover, these improvements could be detected in chronic tetraplegic and paraplegic patients. Older age (>50 years) and spastic motor behavior were non-significant negative predictors for walking endurance improvements. In stroke patients, similar results for HAL-assisted and body-weight supported treadmill training were demonstrated by several study groups in Japan

and Sweden (Wada et al., 2010; Kawamoto et al., 2013, 2014; Nilsson et al., 2014; Yoshimoto et al., 2015) The therapeutic target was hemiparesis in all studies, and predominantly, patients with hemispheric insult were enrolled. In addition to technical requirements, safety and feasibility (Kawamoto et al., 2014; Nilsson et al., 2014), effects on treadmill-bound and treadmill-independent parameters were investigated (Kawamoto et al., 2013; Yoshimoto et al., 2015, 2016; Mizukami et al., 2017). Again, study results showed significant improvements, and even promising results indicating significant improvements in the functional ambulatory category (FAC) (Kawamoto et al., 2013). In spite of these encouraging positive results of HAL-training, most of these studies were performed in an uncontrolled design, e.g., using a conventional and mixed physiotherapy setup as control group. Thus, these results encourage to perform controlled studies using HAL-assisted treadmill training in chronic stroke patients. To become an established part of neurorehabilitation programs, HAL has to be compared with conventional physiotherapy (CPT) which is the cornerstone, today. Here, Bobath's concept and proprioceptive neuromuscular facilitation (PNF) were used regularly (Dickstein et al., 1986; Lincoln et al., 1999; Luke et al., 2004; Wang et al., 2005).

We hypothesized that, in chronic stroke patients, HAL-assisted body-weight supported treadmill training would be more effective in recovery of walking parameters than CPT (provided according to current standards of practice). We further hypothesized that exoskeletal HAL training would improve outcome parameters reflecting functional independence more than conventional therapy.

MATERIALS AND METHODS

Study Design and Patients

This study was performed in a monocentric, controlled, randomized, two-period crossover design to test the efficacy of HAL-assisted body-weight supported treadmill training compared to CPT on walking parameters in chronic stroke patients. The study was done in accordance with the Declaration of Helsinki. It was approved by the local Ethics Committee of the Medical Faculty of Ruhr University Bochum (reg. no. 4894-14). All patients provided written informed consent before participating. The study has been registered in German Clinical Trials Register (DRKS-ID: DRKS00006821). **Figure 1** shows our study design. Patients were randomly assigned to Group 1 or to Group 2 using a computer-generated list. Masking to treatment allocation for therapist and patients was not feasible. 18 ambulatory, chronic stroke patients with incomplete hemiparesis were enrolled. The inclusion criteria were (1) incomplete paresis of the leg after single incident of ischemic or hemorrhagic stroke, at least 6 months prior and (2) age between 18 and 75 years. Exclusion criteria were (1) severely impaired communication due to native language or aphasia, (2) impaired cardiorespiratory capacity, (3) severe multimodal neglect, (4) history of severe infection or history of infection with multiresistant bacteria, (5) complete paralysis of the leg, (6) history of more than 1 stroke, (7) decubital ulcer of the lower extremities and the sacral region, (8) severe osteoporosis and fractures, (9) history of deep vein thrombosis and pulmonary embolism, (10) contracture of the leg, (11) body weight > 100 kg, (12) epilepsy, (13) electric medical devices like cardiac pacemaker, (14) metal implants like ventriculoperitoneal shunt. To characterize patients' impairments in activities of daily living at baseline and cognition, the Barthel index, the FAC and the Montreal Cognitive Assessment (MoCA) were assessed (Holden et al., 1986; Nasreddine et al., 2005; Hachinski et al., 2006; Sivakumar et al., 2014). All demographic and clinical characteristics of the patients are shown in **Tables 1**, **2**. Except patient no. 7 (pontine infarction), all patients had hemispheric lesions supplied by the middle cerebral artery.

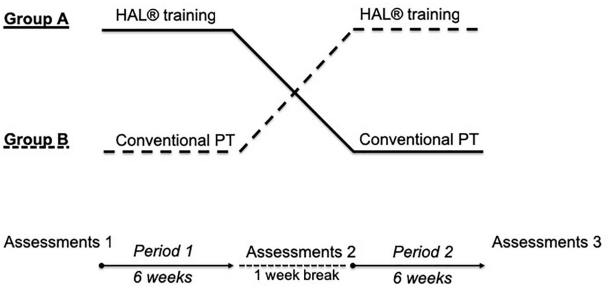

FIGURE 1 | Study design. Two-period, controlled crossover design. Each period included 30 therapy sessions. 1-week break was held between both periods. Before, at crossover and at the end of the study, assessments were done. HAL = hybrid assistive limb, Group 1 = HAL-CPT; Group 2 = CPT-HAL.

HAL Therapy

In both Groups, all patients underwent a 6-week HAL-assisted, supervised, body-weight supported treadmill training (BWSTT). Each patient was scheduled for a 30 min training session 5 times a week, resulting in 30 sessions. The therapy was supervised by one to two stroke-specialized and HAL-qualified physiotherapists. HAL is an exoskeleton with a patient size-adjustable frame and robotic actuators that attaches to the patient's lower limbs. The joint movements are supported by electric motors. The exoskeleton percutaneously detects minimal bioelectric signals initiated by the patient's voluntary muscle activities (hip and knee flexors and extensors) via electromyography (EMG) electrodes and/or the floor reaction force signals caused by patient's intended weight shifts. Through a cable connection between the exoskeleton and the patient, this system allows a voluntary robotic-supported range of motion (cybernic voluntary control mode = CVC mode) to occur at each motor and joint separately. The electric motor support at the hip and knee joints is gradually adjustable according to the patient's own remnant flexor and extensor muscle function. This leads to independent individual hip and knee joint motion support synchronous with the patients' voluntary drive, so it enables individualized and adjustable muscle group locomotion training to be established for bilateral hip and knee flexors and extensors. The CVC mode has been used for the paretic leg. For the non-paretic leg, the CIC mode (cybernic impedance control) was chosen. It compensates for

TABLE 1 | Demographic and clinical characteristics of the patients.

#	Sex	Age	Group	Time since stroke, months	Etiology	Side of paralysis	Assistive device	FAC	Barthel index	MoCA
1	m	52	1	108	ischemia	L	walking cane	4	100	22
2	m	65	1	81	ischemia	L	walking cane	4	100	21
3	m	61	1	69	hemorrhage	R	walking cane	5	100	21
4	f	61	1	95	ischemia	R	wheelchair	2	70	22
5	m	73	1	81	ischemia	L	walking cane	3	90	16
6	f	70	2	355	ischemia	R	none	4	100	17
7	m	62	2	10	ischemia	L	walking cane	4	100	18
8	f	57	1	30	hemorrhage	R	wheeled walker	4	100	28
9	m	72	2	32	ischemia	L	walking cane	4	100	25
10	m	71	1	45	ischemia	L	wheelchair	2	85	21
11	m	60	2	115	ischemia	L	wheelchair	4	80	23
12	m	69	2	204	ischemia	R	FES*	5	100	23
13	m	71	1	24	hemorrhage	R	walking cane	5	100	26
14	m	57	2	26	hemorrhage	R	none	5	100	23
15	m	58	2	120	ischemia	L	none	5	95	28
16	f	74	2	27	ischemia	L	none	4	85	21
17	f	58	1	29	ischemia	L	none	4	80	26
18	m	75	2	30	ischemia	R	wheelchair	0	45	20

*f = female, m = male, L = left, R = right, FAC = functional ambulation categories. Patient #17 was a drop-out because of massive fatigue after each training session. Group 1 = HAL-CPT, Group 2 = CPT-HAL; *FES = functional electrical stimulation for drop foot (ActiGate®).*

TABLE 2 | Demographic and clinical characteristics of the groups.

	Group 1	Group 2	*p*-value
n	9	9	
Age (mean)	63	66	0.371
Sex (m/f)	6/3	7/2	NA
Time since stroke, months (mean)	62	102	0.331
Side of paralysis (L/R)	5/4	5/4	NA
Type of stroke (ischemic/hemorrhage)	6/3	8/1	NA
FAC (mean)	3.6	3.9	0.730
Barthel index (mean)	92	89	0.760
MoCA (mean)	22.6	22.0	0.740

f = female, m = male, L = left, R = right, FAC = functional ambulation categories, MoCA = Montreal Cognitive Assessment. Group 1 = HAL-CPT; Group 2 = CPT-HAL; NA = not assessable.

the weight of the device and the friction, without having any therapeutic effect. With the treadmill system (Woodway USA, Inc., Waukesha, WI, United States), the walking speed could be adjusted from 0 km/h to approximately 4.5 km/h. During treatment, the velocity of the treadmill was set individually between comfortable and maximum speed tolerated by the patient. Initially, the harness system supported approximately 25 to 50% of each patient's body weight. This was individually reduced in subsequent training sessions depending on patient's feedback and therapeutic progress. HAL robot suit and training setting are presented in **Figure 2**.

Conventional Physiotherapy

All patients received CPT 5 times a week for 6 weeks resulting in 30 sessions. Patient #10 missed two sessions because of logistic trouble resulting in 28 session. All other patients underwent 30 HAL-sessions. The therapy was performed by one stroke-specialized physiotherapist. Each session lasted about 30–45 min individually based on patient's daily condition. CPT was performed as mixed intervention consisting of different approaches and concepts, e.g., Bobath's neurophysiological concept, PNF and motor (re-)learning programs referenced to Carr and Shepherd (1987). Main therapeutic aims were gait stability, physiological walking pattern, utilization of assistive devices, controlled activation of distinct muscle groups, and regulation of spasticity.

Primary Outcomes: Walking Performance

The 10-meter walking test (10MWT) was measured at each training session. It detects the time to walk a 10 m distance (Bohannon, 1997; Perera et al., 2006). The timed-up-and-go test (TUG) describes the time and assistance required for standing up from a chair, to walk 3 meters, turn around, walk back and

FIGURE 2 | HAL exoskeleton and training setting. Left part of the figure shows HAL exoskeleton with its electronic actuators for hip and knee joints ("power units"), its battery pack and controller at the top and its EMG-electrodes and cables for detection of bioelectrical signals. Right part of the figure demonstrates the training setting with the treadmill, the body-weight support and the exoskeleton. Official picture of Cyberdyne Inc., the person was not subject of the published study and has been engaged and paid for commercials. Copyright Cyberdyne, Inc., published with kindly permission.

sit down (Podsiadlo and Richardson, 1991). The 6-min walking test (6MWT) evaluates the distance covered over a time of 6 min (Harada et al., 1999). The TUG test and 6MWT were assessed at baseline, at crossover and at the end of the study. All tests were performed without HAL exoskeleton.

Secondary Outcomes: Functional and Balance Performance

The FAC is a functional walking test to evaluate ambulation ability. Patients were rated on 5 categories (0 = patient cannot walk, 5 = patient can walk independently anywhere) (Holden et al., 1986; Mehrholz et al., 2007). We used FAC for classification of our patients group as well as a secondary outcome parameter. Previous studies using HAL in subacute stroke patients reported a significant improvement in FAC score (Nilsson et al., 2014; Watanabe et al., 2014). The Berg-Balance Scale (BBS) is an assessment tool to evaluate balance skills and to predict falls. It contains of 14 items with a 5-point (range from 0 to 4) scale. Maximum score is 56 points. Static and dynamic activities of varying difficulty have to be performed. A score of <45 points indicates individuals with a higher risk of falls (Berg et al., 1992; Flansbjer et al., 2012). Both measurements have been tested at baseline, at crossover and at the end of the study.

Statistics

At first, to rule out carry-over effects and test our study for validity a pre-test was performed by calculating the sum of the measured values in the periods for each patient and compared across the two groups by an unpaired t-test (Wellek and Blettner, 2012). When p was greater than 0.05, we proved that no carryover effects existed and that our "wash-out" phase was sufficiently long enough (1 week). As a second step, we calculated the within-subject difference in our outcome parameters between both study periods. To prove a statistical difference between the treatment effects HAL and CPT, two-sided Student's unpaired t-test was carried out. Significance was assumed at the 5% alpha level ($p > 0.05$). If no statistical effect for one therapy was present, repeated measurement analysis of variance (rmANOVA) was performed to assess significant differences between both Groups (1 = HAL-CPT vs. 2 = CPT-HAL). We defined "time" as within-subject factor and "Group" as between-subject factor. Where it was appropriate, *post hoc* t-test were subsequently applied. For these tests, the significance level was adjusted by dividing it by the Number of comparisons (0.05/3 = 0.017; Bonferroni correction). Additionally, for pure analysis of HAL-BWSTT effects on walking parameters, BBS and FAC within therapy-naïve patients, Student's two-sided, paired t-test has been performed with data of the first therapy period. This analysis was not the primary aim of the HALESTRO study, but it has been important to evaluate the therapeutic effect of HAL itself and, therefore, to enable a comparison of our data with previous work from other HAL-groups.

RESULTS

Demographic and Clinical Characteristics of Both Groups

We did not find statistical differences for "age" and "time since stroke" between both groups (age: mean Group 1 = 63 years, mean Group 2 = 66 years, $p = 0.371$; time since stroke: mean Group 1 = 62 months, mean Group 2 = 102 months, $p = 0.331$). Looking at clinical characteristics like independence in activities of daily living (Barthel index), ambulation ability (FAC) and cognitive impairment (MoCA), statistical analysis revealed no significant differences between Group 1 and 2 (Barthel index: mean Group 1: 92, mean Group 2: 89, $p = 0.760$; FAC: mean Group 1 = 3.6, mean Group 2 = 3.9, $p = 0.730$; MoCA: mean Group 1: 22.6, mean Group 2: 22.0, $p = 0.740$). For results see **Table 2**.

Crossover Analysis

The first step of our analysis was to look for carryover effects between both study periods. Statistical analysis revealed no carryover effects for all primary outcome parameters (walking abilities: 10MWT: $p = 0.805$, 6MWT: $p = 0.529$ and TUG: $p = 0.692$) as well as for the secondary outcome parameters FAC and BBS (FAC: $p = 0.244$, BBS: $p = 0.949$). As the next step, we looked for significant differences between the therapeutic effects of "HAL-BWSTT" and "CPT." None of primary and secondary outcome parameters showed a significant difference between both treatments (10MWT: $p = 0.071$, 6MWT: $p = 0.840$, TUG: $p = 0.835$, FAC: $p = 0.088$, BBS: $p = 0.737$). **Table 3** shows mean values for walking parameters, standard deviation and mean period effects. **Figures 3**, **4** demonstrate results of our primary and secondary outcome parameters. Additionally, whisker-box plots and scatter plots are available in the **Supplementary Materials**.

Analysis of Variance and *post hoc* t-Tests

We performed rmANOVA to show differences between both groups. For 10MWT, rmANOVA revealed a significant effect

TABLE 3 | Data sheet with mean values for walking parameters, standard deviation and mean period effects.

10MWT [s] and *speed (m/s)*						
	Pre		**Crossover**		**Post**	
	mean	***SD***	***mean***	***SD***	***mean***	***SD***
Group 1 (HAL®-CPT)	25.29	13.66	21.72	11.46	19.34	8.99
Group 2 (CPT-HAL®)	27.15	35.25	13.68	4.57	23.28	30.23
Group 1 (HAL®-CPT)	0.49	0.21	0.56	0.23	0.60	0.22
Group 2 (CPT-HAL®)	0.64	0.29	0.80	0.26	0.73	0.3
Training effect 10MWT [s], mean of intraindividual differences						
Group 1 (HAL®-CPT)	–2.69				±2.21	
Group 2 (CPT-HAL®)	–3.77				±7.42	
6MWT [m]						
	Pre		**Crossover**		**Post**	
	mean	***SD***	***mean***	***SD***	***mean***	***SD***
Group 1 (HAL®-CPT)	169.33	81.87	190.38	87.98	203.25	86.53
Group 2 (CPT-HAL®)	242.50	132.15	243.06	102.62	236.78	115.03
Training effect 6MWT [m], mean of intraindividual differences						
Group 1 (HAL®-CPT)		+12.88			±22.61	
Group 2 (CPT-HAL®)		+15.83			±34.66	
TUG [s]						
	Pre		**Crossover**		**Post**	
	mean	***SD***	***mean***	***SD***	***mean***	***SD***
Group 1 (HAL®-CPT)	34.54	23.79	29.32	17.27	27.22	20.26
Group 2 (CPT-HAL®)	37.20	55.56	23.83	5.42	25.65	33.86
Training effect TUG [s], mean of intraindividual differences						
Group 1 (HAL®-CPT)		+2.10			±10.61	
Group 2 (CPT-HAL®)		–1.46			±46.18	

Ten MWT = 10-meter walk test, 6 MWT = 6-min walk test, TUG = timed-up-and-go, SD = standard deviation.

for the within-subject factor "time" ($F_{2,30}$ = 14.459, $p < 0.000$). No significant interactions could be demonstrated for the interaction between "time" and between-subject factor "Group" ($F_{2,30}$ = 1.346, p = 0.276) and for the between-subject factor "Group" ($F_{1,15}$ = 0.028, p = 0.870). *Post hoc t*-test showed significant effects between baseline and crossover (p = 0.002), and between baseline and the end of the study (p = 0.001). For 6MWT, rmANOVA showed a significant interaction between the factors "time" and "Group" ($F_{2,30}$ = 4.338, p = 0.022). All other rmANOVA analysis were without significant effects (within-subject factor "time": $F_{2,30}$ = 2.035, p = 0.148; between-subject factor "Group": $F_{1,15}$ = 0.819, p = 0.380). *Post hoc t*-test revealed significant effect for Group 1 (HAL-CPT) between baseline and end of the study (p = 0.013). Looking at the third primary outcome parameter TUG, statistical analysis demonstrated a significant effect for the within-subject factor "time" ($F_{2,30}$ = 3.832, p = 0.033), but not for the interaction between "time" and "Group" ($F_{2,30}$ = 0.248, p = 0.782). Again, between-subject factor "Group" revealed no significant effect ($F_{1,15}$ = 0.020, p = 0.888). *Post hoc t*-tests revealed no significant differences (pre-cross: p = 0.06, cross-post: p = 0.993, pre-post: p = 0.039). For our secondary outcome parameter, significant effects were seen for the BBS. RmANOVA showed significance for the factor "time" ($F_{1,2}$ = 12.294, $p < 0.000$). Again, interaction between "time" and "Group" and the between-subject factor "Group" itself revealed no significant effects ($F_{2,30}$ = 1.801, p = 0.183; $F_{1,15}$ = 0.015, p = 0.904). *Post hoc t*-tests showed significant effects between baseline and crossover assessments as well as between baseline and the end of the study (p = 0.003; p = 0.001). FAC data analysis showed significant effect for within-subject factor "time" ($F_{2,30}$ = 9.900, $p < 0.000$) but not for interaction between "time" and "Group" ($F_{2,30}$ = 2.363, p = 0.111) and the between-subject factor "Group" itself

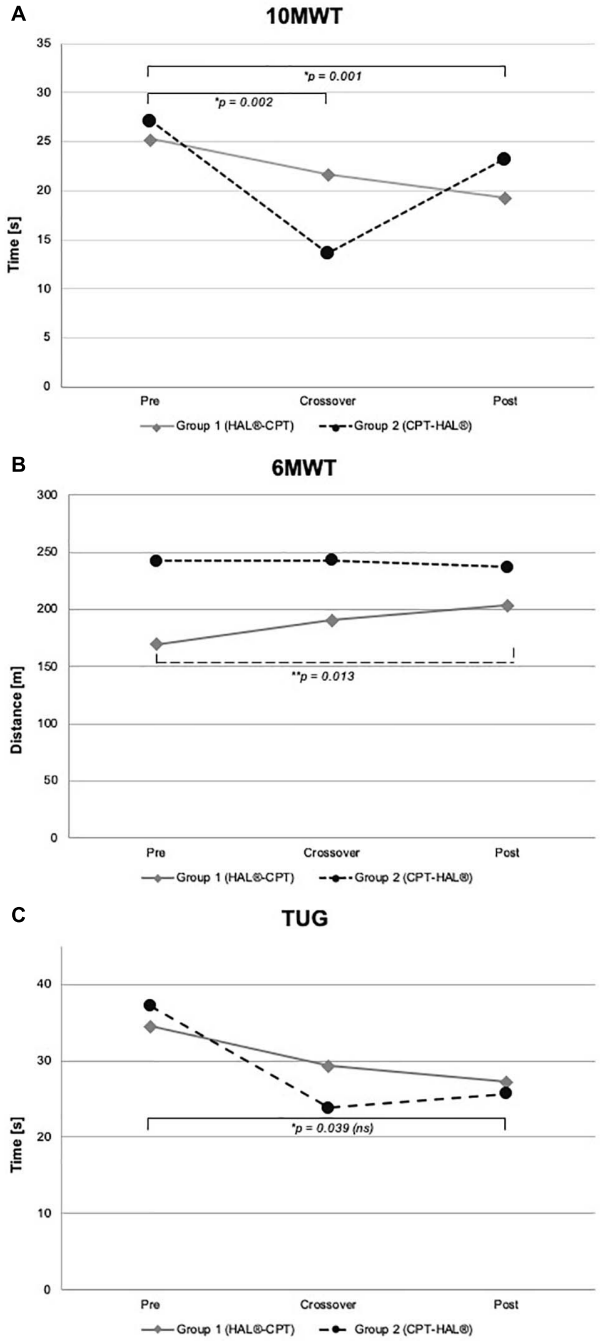

FIGURE 3 | Walking performance parameter. Walking abilities at baseline, crossover and at the end of the study. Figure shows mean values for Group 1 (HAL-CPT) and Group 2 (CPT-HAL). Ten MWT = 10-meter walking test **(A)**, 6 MWT = 6-min walking test **(B)**, TUG = timed-up-and-go test **(C)**. * indicated *post hoc t*-tests after significant effect for factor "time," ** indicated *post hoc t*-test after significant interaction between "time" and "Group" (see "Results" section for details). *p*-threshold < 0.017 (Bonferroni correction).

($F_{1,15}$ = 0.814, p = 0.381). *Post hoc t*-test showed significant effects between baseline measurements and the end of the study (p = 0.001).

Analysis of First Period Effects in Group 1 (HAL-BWSTT Effects on Naïve Chronic Stroke Patients)

Student's paired *t*-test showed significant effects of HAL-therapy on therapy-naïve patients for the following parameters: 10MWT (p = 0.003), 10MWT-speed (p = 0.001), TUG (p = 0.047) and BBS (p = 0.014). Mean values and standard deviations are presented in **Table 3**. No significant effect could be seen for 6MWT and FAC ($p > 0.05$).

Analysis of First Period Effects in Group 2 (CPT Effects on Naïve Chronic Stroke Patients)

Student's paired *t*-test showed no significant effects of mixed CPT on therapy-naïve patients for following parameters: 10 MWT (p = 0.099), TUG (p = 0.203), 6MWT (p = 0.197) and BBS (p = 0.081). A tendency can be observed for FAC (p = 0.051). Mean values and standard deviations are presented in **Table 3**.

DISCUSSION

The main finding of our study is that HAL-assisted BWSTT in chronic stroke patients did not improve walking functions and balance abilities significantly more than CPT in a mixed concept, each provided for 5 times a week for 6 weeks. Whereas, the sequential combination of both therapies, notwithstanding the order, achieved a significant improvement of walking functions, FAC and balance abilities. Although our study might stand partly in contradiction to other studies using HAL exoskeleton in stroke patients, it is the first HAL-study provided in a controlled, randomized and crossover design in chronic stroke. Besides, our study showed again that HAL-training itself can improve walking and balance functions in chronic stroke patients, like it has been reported by other study groups before (Kawamoto et al., 2013; Yoshimoto et al., 2016). The applied treatments have to be analyzed in detail to answer the question why robotic-assisted locomotor training with HAL failed to be more effective compared to CPT in chronic stroke patients.

HAL-Treatment

We observed that our HAL-BWSTT protocol led to similar results as Kawamoto et al. (2013) and Yoshimoto et al. (2015) reported in their studies on chronic stroke patients. In our study, when HAL-BWSTT was applied to "naïve" patients (i.e., Group 1, first study period), it led to an improvement in walking parameters (10MWT, TUG) and in balance abilities (BBS), but not in functional ambulation. Comparing the mean values mentioned in the other studies with our data, our results are in line with previously published studies. Walking parameter in our study and in Kawamoto's study improved by approximately 20%. Interestingly, in Yoshimoto's study, the effect was greater, approximately 50%. Moreover, Yoshimoto and coworkers proved that HAL-training was more effective than CPT; their study was performed in a parallel group design. Although HAL-training was an effective therapy in our

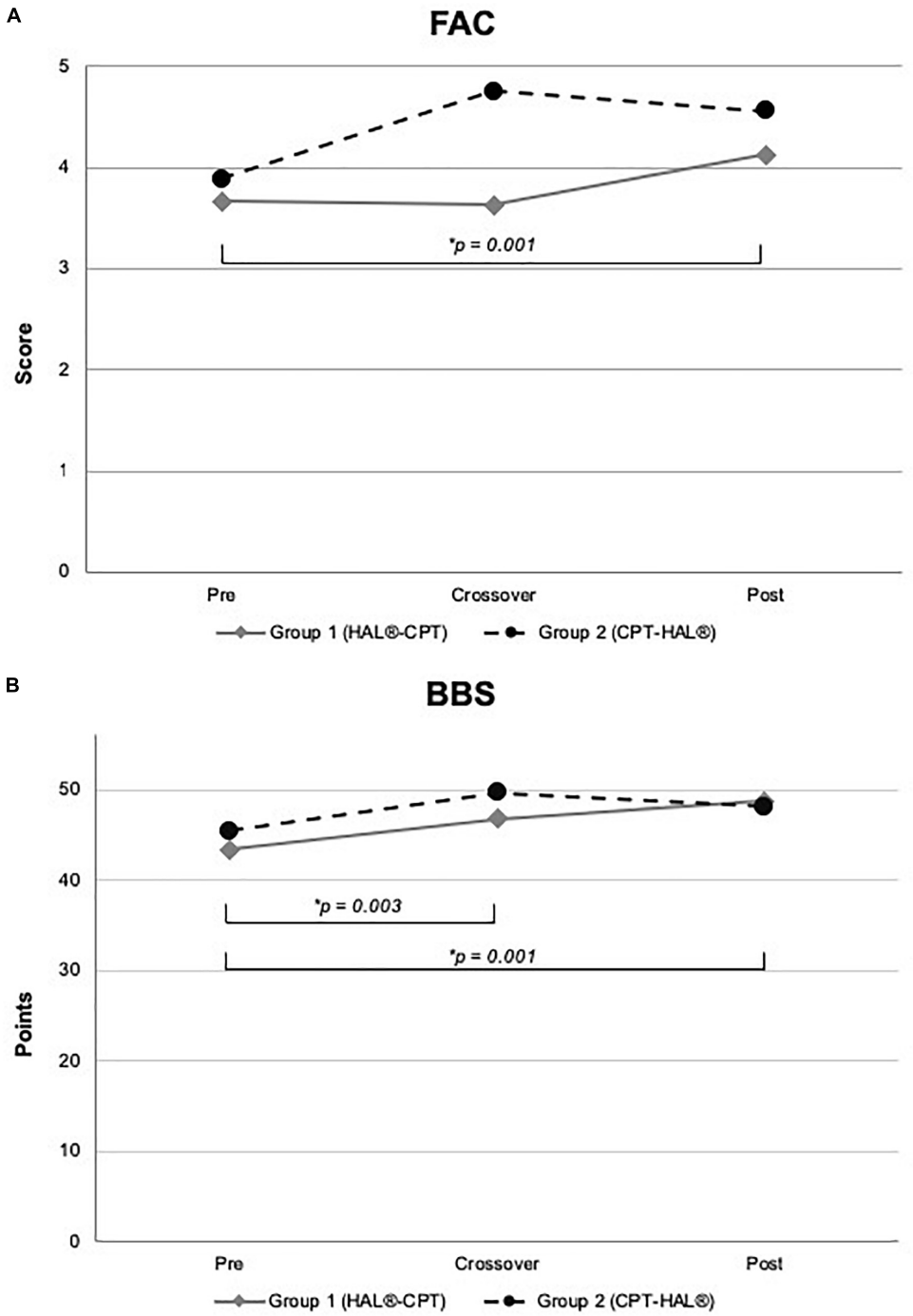

FIGURE 4 | Functional outcome and Berg-Balance Scale. Figure shows mean values for Group 1 (HAL-CPT) and Group 2 (CPT-HAL). FAC = Functional ambulation categories **(A)**, BBS = Berg-Balance-Scale **(B)**. * indicated *post hoc t*-tests after significant effect for factor "time." *p*-threshold < 0.017 (Bonferroni correction).

patients as well, there were several differences in the design of robotic training as well as in the CPT period. In our opinion, both issues might have contributed to different results at the end of our controlled, crossover study. First, Kawamoto et al. (2013) and Yoshimoto et al. (2015) did not apply (body-weight supported) treadmill training to their patients. Patients wore a harness connected to a mobile suspension system called the All-In-One Walking Trainer (Ropox A/S, Denmark) and walked freely on a floor with therapeutic assistance. Second, in both studies, the total number of HAL sessions and the frequency were considerably lower [Kawamoto et al. (2013): 16 sessions, 2/week, Yoshimoto et al. (2015): 8 sessions, 1/week, HALESTRO:

30 sessions, 5/week]. Third, and this might be the substantial difference to the HAL training in our study, Yoshimoto et al. (2015) have used a higher walking speed in order to compensate lower amount of training sessions. In contrast, we increased the number of sessions while using a lower walking speed. Both approaches are generally accepted concepts of modern stroke rehabilitation (Langhorne et al., 2011). Looking at our treadmill data (not published), Group 1 reached a median speed of 0.78 km/h (SD: ±0.22) to 1.34 km/h (SD: ±0.37) after 6 weeks of HAL training; after 6 weeks of CPT, Group 2 accomplished a median speed of 1.11 km/h (SD: ±0.28) to 1.48 km/h (SD: ±0.36) after 6 weeks of HAL-training. Yoshimoto et al. (2015) did not mention the individual walking speed on the treadmill. Less relevant, Yoshimoto et al. (2015) used the single leg version of the HAL robot suit (Kawamoto et al., 2009). Recently, it has been discussed how far single leg type is more suitable for patients with medium to low functional impairment and the double leg type is recommended for patients with severe functional impairment (indicated by FAC $\leq$ 1) (Nishimura et al., 2018). Studies investigating the efficiency of both types have not been performed yet. General recommendations do not exist. Therefore, we decided to apply the combination of CVC and CIC mode as mentioned above. Patients did not report discomfort or any disturbances. Summarizing, the HALESTRO study proved the efficiency of HAL robot suit for locomotor und posture functions using a high frequency BWSTT protocol with a comfortable treadmill speed. Like in classical walking training with a physiotherapist, HAL locomotor training offers the possibility of variations that are capable to modify the training outcome, like Yoshimoto's study has shown. It remains unclear which training type is superior and which HAL type (single vs. double leg version) is recommended for which patient. Low-frequency and high-speed HAL training seems to be more effective.

CPT in HALESTRO Study

Our study demonstrates no significant difference in walking, functional, and balance metrics between HAL-BWSTT and CPT. Because HAL-BWSTT has proven a significant effect after 6 weeks in naïve chronic stroke patients, one has to consider what was the characteristic of CPT in HALESTRO study. For the study design, it was very important for us to create a physiotherapeutic setting that is "real" and not artificially assembled only for the HALESTRO study. For this purpose, our physiotherapist was encouraged to perform an ambulatory care therapy that not only aimed on walking and gait but included the whole patient as a complex interrelated biological system. This might have been one reason why HAL-BWSTT effects were equalized. Again, we have to compare our results with Yoshimoto's stroke study (Yoshimoto et al., 2016), especially because they could prove that HAL-therapy was significantly more effective than CPT. But, there were differences to our CPT design, leading to different results. At first, and the most important and most powerful difference was that we applied a so called "mixed" physiotherapy concept. In Pollock's comprehensive meta-analysis, a number of CPT-approaches failed to prove superiority in rehabilitation of walking impairment after stroke (Pollock et al., 2007). Interestingly, it was insufficient to conclude that any therapy approach is more effective in promoting recovery of disability than any other. For physiotherapeutic intervention, using a "mix" of components from different approaches was more effective compared to a treatment control (Pollock et al., 2007). Indeed, it remained unclear which concept the therapists in Yoshimoto et al. (2015) have used. Instead of performing CPT one to 2 times a week for 40 min, absolutely no change of mean values of 10MWT, TUG and BBS were observed. Again, this is in contrast to our data; we clearly observed effects of CPT on all parameters. Since, there are basic differences in CPT approaches, our study failed to prove superiority of one therapeutic regime. CPT in our study was more effective than in Yoshimoto's work. In fact, CPT is a strong instrument in walking rehabilitation as previous neurorehabilitation studies have demonstrated. Compared with the Locomat (Husemann et al., 2007; Mayr et al., 2007), with the Gait Trainer (Peurala et al., 2005), and with solely additional use of a treadmill (Duncan et al., 2011; Mehrholz et al., 2017a), hands-on physiotherapy based on "mixed" approach has proven its superiority and high efficiency on functional independence, walking speed and motor function (Pollock et al., 2007; Langhorne et al., 2009, 2011).

Global Study Effects

Indeed, the HALESTRO study could not verify a significant superiority of robotic-assisted treadmill therapy with HAL or for hands-on physiotherapy for locomotor rehabilitation in chronic stroke patients. But our data have shown a clearly significant effect on the walking parameters 10MWT, 6MWT, FAC and BBS (see **Figures 3**, **4**) when both therapies were sequentially applied over 12 weeks. For BBS and 10MWT, we have seen significant effects after the first study period (baseline – crossover). These significant effects were seen after pooling data of all subjects irrespective of therapeutic group and intervention/interventional sequence. An interesting detail is the improvement in FAC (see **Table 4** and **Figure 4**). Although the functional recovery curve after stroke reaches saturation after 6 months with only few fluctuations, in our small study group of 18 resp. 17 patients, we could see a functionally important improvement depicted by FAC. The mean FAC exceeded the category level 3 and reached category level 4. Category 3 represents the ambulator-dependent level, category 4 the ambulator-independent level. So, patients could not only improve their results in the 10MWT or 6MWT, but also their daily relevant independency. As well as for FAC, patients benefit from enhanced balance functions and posture. Many patients reported a close relationship between both improvements; more stability led to more confidence, which led to more independency. However, these effects were not specific to one of both interventions, but for the combination of both therapies. This is a conclusion that not only we could state for our study, but also were made in greater and larger stroke rehabilitation studies. Recently, Mehrholz et al. (2017b) published an update of their Cochrane review examining the effects of electromechanical and robot-assisted gait training devices for improving walking after stroke very detailly. Finally, 36 trials with 1.472 participants were

TABLE 4 | Data sheet with mean values for functional ambulatory categories and Berg-Balance-Scale.

FAC						
	Pre		**Crossover**		**Post**	
	mean	***SD***	***Mean***	***SD***	***mean***	***SD***
Group 1 (HAL®-CPT)	3.67	1.12	3.63	1.19	4.13	1.13
Group 2 (CPT-HAL®)	3.89	1.54	4.75	0.46	4.56	1.01
Training effect FAC, mean of intraindividual differences						
Group 1 (HAL®-CPT)		0.5			± 0.53	
Group 2 (CPT-HAL®)		0.11			± 0.33	
BBS [points]						
	Pre		**Crossover**		**Post**	
	mean	***SD***	***mean***	***SD***	***mean***	***SD***
Group 1 (HAL®-CPT)	43.33	9.18	46.75	9.79	48.75	6.65
Group 2 (CPT-HAL®)	45.44	13.14	49.63	8.23	48.11	10.34
Training effect BBS [points], mean of intraindividual differences						
Group 1 (HAL®-CPT)		2.00			± 5.29	
Group 2 (CPT-HAL®)		1.33			± 2.40	

FAC = functional ambulatory categories, BBS = Berg-Balance-Scale, SD = standard deviation.

included. Outcome parameters were independency in walking, walking velocity and capacity also. Like in our study, the authors found in this meta-analysis that the combination of electromechanical-assisted training with physiotherapy after stroke is more likely to achieve independent walking than people who received gait trainings without those devices. Interestingly, the subgroup analysis of Mehrholz' meta-analysis reported a result regarding HAL-therapy in stroke patients which can be confirmed by us: acute and subacute stroke patients as well as patients who are not ambulatory are more likely to achieve independent walking when they receive electromechanical-assisted gait training than without. Watanabe and coworkers have shown significant improvements in independent walking after 12 session of HAL therapy compared to conventional gait therapy (outcome parameter FAC). Their study has been performed in a parallel group design on 24 subacute stroke patients. Even though it was no primary aim of the HALESTRO study and a subgroup analysis would not be reliable due to small number of subjects, we also observed that the lower the FAC score and the lower the walking speed in 10MWT, the more improvement our patients could gain. It might be a ceiling effect. But Mehrholz et al. (2017b) results encourage to propose that there is a systematic effect behind this observation. In fact, our study does not allow any conclusions about this issue; further studies aiming on this topic should be carried out.

Limitations

Certain limitations of our study should be noted. One point is its crossover design. For a better comparability of different therapeutic effects within one patient (each patient serves as her/his own control) and to avoid problems of comparability of study and control group, we decided to perform our study in a crossover design. To rule out a carryover effect, we specified a so called "washout phase" of 1 week. The duration of 1 week was assessed by other rehabilitation study previously performed in the field of stroke rehabilitation. Statistical analysis showed that no carryover effect was present. However, is it really possible to "washout" motor movements and coordinative motoric that one has learned within 1 week? Can these complex locomotor pattern really be forgotten within 1 week? Studies focusing extinction motor learning are ongoing. First evidence for distinct brain areas like the primary motor cortex could be delivered as areas of memory retrieval and extinction whereas the sensory cortices are supposed to be essential for long-term memory (Guo et al., 2017). A specific time period allowing for safe extinction or "washout" has not been identified so far. Statistically, we could deny any carryover effect for sure, but one must assume that certain new acquired locomotor sequences endured the "washout phase." Therefore, these reflections underline the concept of synergistic effects of "conservative" physiotherapy and "innovative" robotic therapy. Moreover, it underlines the meaningfulness of combined therapy in crossover studies and not in parallel group design. Another limitation is the statistical power was low due to the small number of patients. One may note that the recruitment was very difficult. Furthermore, we missed to investigate the after effects. Notably, Watanabe and coworkers assessed follow-up examinations for subacute stroke patients and found promising results for HAL-intervention (Watanabe et al., 2017). Similar outlasting results have been reported by our group for SCI patients (Grasmücke et al., 2017; Jansen et al., 2017).

CONCLUSION

In conclusion, our results indicate that BWSTT with HAL® exoskeleton applied with moderate walking speed 5 times a week for 6 weeks (30 sessions) is not more effective in chronic stroke patients with moderate to severe impairment than mixed approach CPT. But both therapies combined sequentially, notwithstanding the order, is likely to achieve independent walking even in chronic stroke patients. The duration of these improvements remains unclear and further studies are needed.

DATA AVAILABILITY

All datasets generated for this study are included in the manuscript and/or the **Supplementary Files**.

AUTHOR CONTRIBUTIONS

MS-K, RT, PS, and MT acquired and analyzed the data, participated in its design, and drafted the manuscript. MA and TS participated in the design and data collection and helped to draft the manuscript.

FUNDING

This study was partially funded by a grant from New Energy and Industrial Technology Development Organization, Japan (NEDO).

ACKNOWLEDGMENTS

We would like to thank Professor Dr. Yoshiyuki Sankai, CEO of Cyberdyne Inc., that produces the HAL exoskeleton. He provided exclusively technical and advisory support. We would speak out special thanks to our physiotherapist Caro who performed mixed approach CPT section and a lot of HAL trainings. You are the best! Last but not least, we want to thank all patients who took part in our study! We are very grateful for all engagement you put in this study! It was outstanding! We thank Dr. Emre Yilmaz for proofreading. We also thank PD Dr. Johannes Dietrich for his statistical and graphical support.

SUPPLEMENTARY MATERIAL

The Supplementary Material for this article can be found online at: https://www.frontiersin.org/articles/10.3389/fnins.2019.00259/full#supplementary-material

REFERENCES

Aach, M., Cruciger, O., Sczesny-Kaiser, M., Höffken, O., Meindl, R. C., Tegenthoff, M., et al. (2014). Voluntary driven exoskeleton as a new tool for rehabilitation in chronic spinal cord injury: a pilot study. *Spine J.* 14, 2847–2853. doi: 10.1016/j.spinee.2014.03.042

Berg, K. O., Maki, B. E., Williams, J. I., Holliday, P. J., and Wood-Dauphinee, S. L. (1992). Clinical and laboratory measures of postural balance in an elderly population. *Arch. Phys. Med. Rehabil.* 73, 1073–1080.

Bohannon, R. W. (1997). Comfortable and maximum walking speed of adults aged 20-79 years: reference values and determinants. *Age Ageing* 26, 15–19. doi: 10.1093/ageing/26.1.15

Carr, J., and Shepherd, R. B. (1987). *A Motor Relearning Programme for Stroke*, 2nd Edn. Oxford: Butterworth-Heinemann Ltd.

Chang, W. H., and Kim, Y.-H. (2013). Robot-assisted therapy in stroke rehabilitation. *J. Stroke* 15, 174–181. doi: 10.5853/jos.2013.15.3.174

Cruciger, O., Tegenthoff, M., Schwenkreis, P., Schildhauer, T. A., and Aach, M. (2014). Locomotion training using voluntary driven exoskeleton (HAL) in acute incomplete SCI. *Neurology* 83:474. doi: 10.1212/WNL.0000000000000645

Dickstein, R., Hocherman, S., Pillar, T., and Shaham, R. (1986). Stroke rehabilitation. Three exercise therapy approaches. *Phys. Ther.* 66, 1233–1238. doi: 10.1093/ptj/66.8.1233

Duncan, P. W., Goldstein, L. B., Horner, R. D., Landsman, P. B., Samsa, G. P., and Matchar, D. B. (1994). Similar motor recovery of upper and lower extremities after stroke. *Stroke* 25, 1181–1188. doi: 10.1161/01.STR.25.6.1181

Duncan, P. W., Sullivan, K. J., Behrman, A. L., Azen, S. P., Wu, S. S., Nadeau, S. E., et al. (2011). Body-weight-supported treadmill rehabilitation after stroke. *N. Engl. J. Med.* 364, 2026–2036. doi: 10.1056/NEJMoa1010790

Feigin, V. L., Krishnamurthi, R. V., Parmar, P., Norrving, B., Mensah, G. A., Bennett, D. A., et al. (2015). Update on the global burden of ischemic and hemorrhagic stroke in 1990-2013: the GBD 2013 study. *Neuroepidemiology* 45, 161–176. doi: 10.1159/000441085

Flansbjer, U.-B., Blom, J., and Brogårdh, C. (2012). The reproducibility of berg balance scale and the single-leg stance in chronic stroke and the relationship between the two tests. *PM R* 4, 165–170. doi: 10.1016/j.pmrj.2011.11.004

Grasmücke, D., Zieriacks, A., Jansen, O., Fisahn, C., Sczesny-Kaiser, M., Wessling, M., et al. (2017). Against the odds: what to expect in rehabilitation of chronic spinal cord injury with a neurologically controlled hybrid assistive limb® exoskeleton. A subgroup analysis of 55 patients according to age and lesion level. *Neurosurg. Focus* 42:E15. doi: 10.3171/2017.2.FOCUS171

Guo, R., Ge, R., Zhao, S., Liu, Y., Zhao, X., Huang, L., et al. (2017). Associative memory extinction is accompanied by decayed plasticity at motor cortical neurons and persistent plasticity at sensory cortical neurons. *Front. Cell. Neurosci.* 11:168. doi: 10.3389/fncel.2017.00168

Hachinski, V., Iadecola, C., Petersen, R. C., Breteler, M. M., Nyenhuis, D. L., Black, S. E., et al. (2006). National institute of neurological disorders and stroke-canadian stroke network vascular cognitive impairment harmonization standards. *Stroke* 37, 2220–2241. doi: 10.1161/01.STR.0000237236.88823.47

Harada, N. D., Chiu, V., and Stewart, A. L. (1999). Mobility-related function in older adults: assessment with a 6-minute walk test. *Arch. Phys. Med. Rehabil.* 80, 837–841. doi: 10.1016/S0003-9993(99)90236-8

Holden, M. K., Gill, K. M., and Magliozzi, M. R. (1986). Gait assessment for neurologically impaired patients. Standards for outcome assessment. *Phys. Ther.* 66, 1530–1539. doi: 10.1093/ptj/66.10.1530

Huang, V. S., and Krakauer, J. W. (2009). Robotic neurorehabilitation: a computational motor learning perspective. *J. NeuroEng. Rehabil.* 6, 5–13. doi: 10.1186/1743-0003-6-5

Husemann, B., Müller, F., Krewer, C., Heller, S., and Koenig, E. (2007). Effects of locomotion training with assistance of a robot-driven gait orthosis in hemiparetic patients after stroke: a randomized controlled pilot study. *Stroke* 38, 349–354. doi: 10.1161/01.STR.0000254607.48765.cb

Jansen, O., Schildhauer, T. A., Meindl, R. C., Tegenthoff, M., Schwenkreis, P., Sczesny-Kaiser, M., et al. (2017). Functional outcome of neurologic-controlled HAL-exoskeletal neurorehabilitation in chronic spinal cord injury: a pilot with

one year treatment and variable treatment frequency. *Global Spine J.* 7, 735–743. doi: 10.1177/2192568217713754

Jørgensen, H. S., Nakayama, H., Raaschou, H. O., and Olsen, T. S. (1995). Recovery of walking function in stroke patients: the copenhagen stroke study. *Arch. Phys. Med. Rehabil.* 76, 27–32. doi: 10.1016/S0003-9993(95)80038-7

Kawamoto, H., Hayashi, T., Sakurai, T., Eguchi, K., and Sankai, Y. (2009). Development of single leg version of HAL for hemiplegia. *Conf. Proc. IEEE Eng. Med. Biol. Soc.* 2009, 5038–5043. doi: 10.1109/IEMBS.2009.5333698

Kawamoto, H., Kamibayashi, K., Nakata, Y., Yamawaki, K., Ariyasu, R., Sankai, Y., et al. (2013). Pilot study of locomotion improvement using hybrid assistive limb in chronic stroke patients. *BMC Neurol.* 13:141. doi: 10.1186/1471-2377-13-141

Kawamoto, H., Kandone, H., Sakurai, T., Ariyasu, R., Ueno, Y., Eguchi, K., et al. (2014). Development of an assist controller with robot suit HAL for hemiplegic patients using motion data on the unaffected side. *Conf. Proc. IEEE Eng. Med. Biol. Soc.* 2014, 3077–3080. doi: 10.1109/EMBC.2014.6944273

Koton, S., Schneider, A. L. C., Rosamond, W. D., Shahar, E., Sang, Y., Gottesman, R. F., et al. (2014). Stroke incidence and mortality trends in US communities, 1987 to 2011. *JAMA* 312, 259–268. doi: 10.1001/jama.2014.7692

Kwakkel, G., Kollen, B., and Lindeman, E. (2004). Understanding the pattern of functional recovery after stroke: facts and theories. *Restor. Neurol. Neurosci.* 22, 281–299.

Langhorne, P., Bernhardt, J., and Kwakkel, G. (2011). Stroke rehabilitation. *Lancet* 377, 1693–1702. doi: 10.1016/S0140-6736(11)60325-5

Langhorne, P., Coupar, F., and Pollock, A. (2009). Motor recovery after stroke: a systematic review. *Lancet Neurol.* 8, 741–754. doi: 10.1016/S1474-4422(09)70150-4

Lincoln, N. B., Parry, R. H., and Vass, C. D. (1999). Randomized, controlled trial to evaluate increased intensity of physiotherapy treatment of arm function after stroke. *Stroke* 30, 573–579. doi: 10.1161/01.STR.30.3.573

Lo, A. C., Guarino, P. D., Richards, L. G., Haselkorn, J. K., Wittenberg, G. F., Federman, D. G., et al. (2010). Robot-assisted therapy for long-term upper-limb impairment after stroke. *N. Engl. J. Med.* 362, 1772–1783. doi: 10.1056/NEJMoa0911341

Luke, C., Dodd, K. J., and Brock, K. (2004). Outcomes of the Bobath concept on upper limb recovery following stroke. *Clin. Rehabil.* 18, 888–898. doi: 10.1191/0269215504cr793oa

Mayr, A., Kofler, M., Quirbach, E., Matzak, H., Fröhlich, K., and Saltuari, L. (2007). Prospective, blinded, randomized crossover study of gait rehabilitation in stroke patients using the Lokomat gait orthosis. *Neurorehabil. Neural Repair* 21, 307–314. doi: 10.1177/1545968307300697

Mehrholz, J., and Pohl, M. (2012). Electromechanical-assisted gait training after stroke: a systematic review comparing end-effector and exoskeleton devices. *J. Rehabil. Med.* 44, 193–199. doi: 10.2340/16501977-0943

Mehrholz, J., Thomas, S., and Elsner, B. (2017a). Treadmill training and body weight support for walking after stroke. *Cochrane Database Syst. Rev.* 34:CD002840. doi: 10.1002/14651858.CD002840.pub4

Mehrholz, J., Thomas, S., Werner, C., Kugler, J., Pohl, M., and Elsner, B. (2017b). Electromechanical-assisted training for walking after stroke: a major update of the evidence. *Stroke* doi: 10.1161/STROKEAHA.117.018018 [Epub ahead of print].

Mehrholz, J., Wagner, K., Rutte, K., Meissner, D., and Pohl, M. (2007). Predictive validity and responsiveness of the functional ambulation category in hemiparetic patients after stroke. *Arch. Phys. Med. Rehabil.* 88, 1314–1319. doi: 10.1016/j.apmr.2007.06.764

Mizukami, M., Yoshikawa, K., Kawamoto, H., Sano, A., Koseki, K., Asakwa, Y., et al. (2017). Gait training of subacute stroke patients using a hybrid assistive limb: a pilot study. *Disabil. Rehabil. Assist. Technol.* 12, 197–204. doi: 10.3109/17483107.2015.1129455

Mozaffarian, D., Benjamin, E. J., Go, A. S., Arnett, D. K., Blaha, M. J., Cushman, M., et al. (2016). Heart disease and stroke statistics-2016 update: a report from the american heart association. *Circulation* 133, e38–e360. doi: 10.1161/CIR.0000000000000350

Nasreddine, Z. S., Phillips, N. A., Bédirian, V., Charbonneau, S., Whitehead, V., Collin, I., et al. (2005). The montreal cognitive assessment, MoCA: a brief screening tool for mild cognitive impairment. *J. Am. Geriatr. Soc.* 53, 695–699. doi: 10.1111/j.1532-5415.2005.53221.x

Nilsson, A., Vreede, K. S., Häglund, V., Kawamoto, H., Sankai, Y., and Borg, J. (2014). Gait training early after stroke with a new exoskeleton–the hybrid assistive limb: a study of safety and feasibility. *J. NeuroEng. Rehabil.* 11:92. doi: 10.1186/1743-0003-11-92

Nishimura, M., Kobayashi, S., Kinjo, Y., Hokama, Y., Sugawara, K., Tsuchida, Y., et al. (2018). Factors leading to improved gait function in patients with subacute or chronic central nervous system impairments who receive functional training with the robot suit hybrid assistive limb. *Neurol. Med. Chir.* 58, 39–48. doi: 10.2176/nmc.oa.2017-0082

Ovbiagele, B., Goldstein, L. B., Higashida, R. T., Howard, V. J., Johnston, S. C., Khavjou, O. A., et al. (2013). Forecasting the future of stroke in the United States: a policy statement from the American heart association and American stroke association. *Stroke* 44, 2361–2375. doi: 10.1161/STR.0b013e31829734f2

Perera, S., Mody, S. H., Woodman, R. C., and Studenski, S. A. (2006). Meaningful change and responsiveness in common physical performance measures in older adults. *J. Am. Geriatr. Soc.* 54, 743–749. doi: 10.1111/j.1532-5415.2006.00701.x

Peurala, S. H., Tarkka, I. M., Pitkänen, K., and Sivenius, J. (2005). The effectiveness of body weight-supported gait training and floor walking in patients with chronic stroke. *Arch. Phys. Med. Rehabil.* 86, 1557–1564. doi: 10.1016/j.apmr.2005.02.005

Podsiadlo, D., and Richardson, S. (1991). The timed "Up & Go": a test of basic functional mobility for frail elderly persons. *J. Am. Geriatr. Soc.* 39, 142–148. doi: 10.1111/j.1532-5415.1991.tb01616.x

Pollock, A., Baer, G., Langhorne, P., and Pomeroy, V. (2007). Physiotherapy treatment approaches for the recovery of postural control and lower limb function following stroke: a systematic review. *Clin. Rehabil.* 21, 395–410. doi: 10.1177/0269215507073438

Reeves, M. J., Bushnell, C. D., Howard, G., Gargano, J. W., Duncan, P. W., Lynch, G., et al. (2008). Sex differences in stroke: epidemiology, clinical presentation, medical care, and outcomes. *Lancet Neurol.* 7, 915–926. doi: 10.1016/S1474-4422(08)70193-5

Reinkensmeyer, D. J., Maier, M. A., Guigon, E., Chan, V., Akoner, O., Wolbrecht, E. T., et al. (2009). Do robotic and non-robotic arm movement training drive motor recovery after stroke by a common neural mechanism? Experimental evidence and a computational model. *Conf. Proc. IEEE Eng. Med. Biol. Soc.* 2009, 2439–2441. doi: 10.1109/IEMBS.2009.5335353

Sczesny-Kaiser, M., Höffken, O., Aach, M., Cruciger, O., Grasmücke, D., Meindl, R., et al. (2015). HAL exoskeleton training improves walking parameters and normalizes cortical excitability in primary somatosensory cortex in spinal cord injury patients. *J. NeuroEng. Rehabil.* 12:68. doi: 10.1186/s12984-015-0058-9

Sivakumar, L., Kate, M., Jeerakathil, T., Camicioli, R., Buck, B., and Butcher, K. (2014). Serial montreal cognitive assessments demonstrate reversible cognitive impairment in patients with acute transient ischemic attack and minor stroke. *Stroke* 45, 1709–1715. doi: 10.1161/STROKEAHA.114.004726

Swinnen, E., Beckwée, D., Meeusen, R., Baeyens, J.-P., and Kerckhofs, E. (2014). Does robot-assisted gait rehabilitation improve balance in stroke patients? A systematic review. *Top Stroke Rehabil.* 21, 87–100. doi: 10.1310/tsr2102-87

Truelsen, T., Piechowski-Jozwiak, B., Bonita, R., Mathers, C., Bogousslavsky, J., and Boysen, G. (2006). Stroke incidence and prevalence in Europe: a review of available data. *Eur. J. Neurol.* 13, 581–598. doi: 10.1111/j.1468-1331.2006.01138.x

Wada, Y., Kondo, I., Sonoda, S., Miyasaka, H., Teranishi, T., Nagai, S., et al. (2010). Preliminary trial to increase gait velocity with high speed treadmill training for patients with hemiplegia. *Am. J. Phys. Med. Rehabil.* 89, 683–687. doi: 10.1097/PHM.0b013e3181e29d27

Wang, R.-Y., Chen, H.-I., Chen, C.-Y., and Yang, Y.-R. (2005). Efficacy of Bobath versus orthopaedic approach on impairment and function at different motor

recovery stages after stroke: a randomized controlled study. *Clin. Rehabil.* 19, 155–164. doi: 10.1191/0269215505cr850oa

Watanabe, H., Goto, R., Tanaka, N., Matsumura, A., and Yanagi, H. (2017). Effects of gait training using the Hybrid Assistive Limb in recovery-phase stroke patients: a 2-month follow-up, randomized, controlled study. *NeuroRehabilitation* 40, 363–367. doi: 10.3233/NRE-161424

Watanabe, H., Tanaka, N., Inuta, T., Saitou, H., and Yanagi, H. (2014). Locomotion improvement using a hybrid assistive limb in recovery phase stroke patients: a randomized controlled pilot study. *Arch. Phys. Med. Rehabil.* 95, 2006–2012. doi: 10.1016/j.apmr.2014.07.002

Wellek, S., and Blettner, M. (2012). On the proper use of the crossover design in clinical trials. *Dtsch. Arztebl. Int.* 109, 276–281. doi: 10.3238/arztebl.2012.0276

Yoshimoto, T., Shimizu, I., and Hiroi, Y. (2016). Sustained effects of once-a-week gait training with hybrid assistive limb for rehabilitation in chronic stroke: case study. *J. Phys. Ther. Sci.* 28, 2684–2687. doi: 10.1589/jpts.28.2684

Yoshimoto, T., Shimizu, I., Hiroi, Y., Kawaki, M., Sato, D., and Nagasawa, M. (2015). Feasibility and efficacy of high-speed gait training with a voluntary driven exoskeleton robot for gait and balance dysfunction in patients with chronic stroke: nonrandomized pilot study with concurrent control. *Int. J. Rehabil. Res.* 38, 338–343. doi: 10.1097/MRR.0000000000000132

Conflict of Interest Statement: TS was a consultant for Cyberdyne, Inc. at the time the study was conducted.

The remaining authors declare that the research was conducted in the absence of any commercial or financial relationships that could be construed as a potential conflict of interest.

frontiers in Neuroscience

ORIGINAL RESEARCH
published: 30 July 2019
doi: 10.3389/fnins.2019.00732

Kinematic and Functional Gait Changes After the Utilization of a Foot Drop Stimulator in Pediatrics

*Kiran K. Karunakaran[1,2,3,4], Rakesh Pilkar[1,3], Naphtaly Ehrenberg[1,4], Katherine S. Bentley[3,4], JenFu Cheng[3,4] and Karen J. Nolan[1,3,4]**

[1] Center for Mobility and Rehabilitation Engineering Research, Kessler Foundation, West Orange, NJ, United States, [2] Department of Biomedical Engineering, New Jersey Institute for Technology, Newark, NJ, United States, [3] Department of Physical Medicine and Rehabilitation, Rutgers – New Jersey Medical School, Newark, NJ, United States, [4] Children's Specialized Hospital, Mountainside, NJ, United States

Foot drop is one of the most common secondary conditions associated with hemiplegia post stroke and cerebral palsy (CP) in children, and is characterized by the inability to lift the foot (dorsiflexion) about the ankle. This investigation focuses on children and adolescents diagnosed with brain injury and aims to evaluate the orthotic and therapeutic effects due to continuous use of a foot drop stimulator (FDS). Seven children (10 ± 3.89 years) with foot drop and hemiplegia secondary to brain injury (stroke or CP) were evaluated at baseline and after 3 months of FDS usage during community ambulation. Primary outcome measures included using mechanistic (joint kinematics, toe displacement, temporal-spatial asymmetry), and functional gait parameters (speed, step length, time) to evaluate the orthotic and therapeutic effects. There was a significant correlation between spatial asymmetry and speed without FDS at 3 months ($r = 0.76$, $p < 0.05$, df = 5) and no correlation between temporal asymmetry and speed for all conditions. The results show orthotic effects including significant increase in toe displacement ($p < 0.025$ $N = 7$) during the swing phase of gait while using the FDS. A positive correlation exists between toe displacement and speed (with FDS at 3 months: $r = 0.62$, $p > 0.05$, without FDS at 3 months: $r = 0.44$, $p > 0.05$). The results indicate an orthotic effect of increased dorsiflexion and toe displacement during swing with the use of the FDS in children with hemiplegia. Further, the study suggests that there could be a potential long-term effect of increased dorsiflexion during swing with continuous use of FDS.

Keywords: functional electrical stimulation, foot drop, hemiplegia, stroke, cerebral palsy, gait, pediatric rehabilitation

OPEN ACCESS

Edited by:
Yoshio Sakurai, Doshisha University, Japan

Reviewed by:
Brooke M. Odle, Case Western Reserve University, United States
Monireh Ahmadi Bani, University of Social Welfare and Rehabilitation Sciences, Iran

***Correspondence:**
Karen J. Nolan
knolan@kesslerfoundation.org

Specialty section:
This article was submitted to Neuroprosthetics, a section of the journal Frontiers in Neuroscience

Received: *13 July 2018*
Accepted: *01 July 2019*
Published: *30 July 2019*

Citation:
Karunakaran KK, Pilkar R, Ehrenberg N, Bentley KS, Cheng J and Nolan KJ (2019) Kinematic and Functional Gait Changes After the Utilization of a Foot Drop Stimulator in Pediatrics. Front. Neurosci. 13:732. doi: 10.3389/fnins.2019.00732

INTRODUCTION

Children with hemiplegia due to stroke or cerebral palsy (CP) have unilateral motor deficits due to paralysis or weakness. Currently, 500,000 children under the age of 18 with CP (Prevalence of Cerebral Palsy, 2018) and 1 in 1,600 neonate, and 13 per 100,000 older children are affected by stroke each year in the United States (Bernson-Leung and Rivkin, 2009). Foot drop is one of the common secondary conditions associated with hemiplegia and is characterized by the inability to

lift the foot (dorsiflexion) about the ankle due to paralysis or weakness of the peroneal and anterior tibialis muscles (Stewart, 2008). Foot drop, can affect the ability of the toes to clear the floor during the swing, and can also impair stability during the stance. Reduced toe clearance impedes the ability to walk efficiently and may cause reduced functional mobility. One of the most common deficits for individuals with hemiplegia is decreased dorsiflexion during swing leading to deficits in walking (Winters et al., 1987). Consequently, compensatory mechanisms like steppage gait (Dubin, 2014), hip hiking (Kerrigan et al., 2000; Dubin, 2014), toe walking(Dubin, 2014), etc. are used to successfully ambulate. These pathological deviations from the healthy walking result in slower walking speed (Sheffler and Chae, 2015), shorter step length (Sheffler and Chae, 2015), increased risk of falls due to kinematic changes (Winters et al., 1987) and decreased inter-limb temporal and spatial symmetry (Patterson et al., 2010; Nadeau, 2014).

Currently, custom molded ankle foot orthosis (AFO), a passive compensation device, is predominantly used to clinically treat foot drop. AFOs provide support and stability to the foot and ankle during stance phase, and provide clearance to the foot during the swing phase as the foot is always maintained at a predetermined angle (Lehmann et al., 1983; Gök et al., 2003). Though AFOs provide the necessary orthotic effect for foot drop, they can restrict the passive and active ankle range of motion (ROM) (Gök et al., 2003). This restricted ROM may lead to reduced muscle activity (Geboers et al., 2002).

Recent research is focusing on restoring function through the use of functional electrical stimulation (FES) (Cauraugh et al., 2010; Khamis et al., 2018). An FES device or foot drop stimulator (FDS) electrically stimulates the peroneal nerve to activate the peroneal and tibialis anterior muscles to dorsiflex the foot during swing phase (Selzer et al., 2006). Research suggests that FES can not only provide sufficient dorsiflexion to clear the foot during the swing but may also provide the user with rehabilitative benefits, as it would not restrict the user's passive and active ROM (Comeaux et al., 1997; Van Der Linden et al., 2008; Laufer et al., 2009). Previous research on adults with foot drop has shown significant orthotic and therapeutic improvements in walking speed (Burridge et al., 1997; Voigt and Sinkjaer, 2000), temporal and spatial gait symmetry (Comeaux et al., 1997; Lin et al., 2006; Balasubramanian et al., 2007; Patterson et al., 2008), spasticity, and energy consumption with the use of FES (Yan et al., 2006). In addition, using neurophysiological measures, Stein et al. have shown that the therapeutic effects in functional outcome measures are in response to the neuroplastic changes resulting from the use of FES (Everaert et al., 2010). Extensive evidence supporting the efficacy of FES in treating foot drop is available for adults but similar evidence is not currently available in children. Previous research on children with foot drop have shown changes in functional outcome measures such as increased walking speed (Cauraugh et al., 2010; Prosser et al., 2012; Prenton et al., 2018), increased stride length (Pool et al., 2014), reduced use of compensatory mechanisms (Pool et al., 2014), and decreased mean energy expenditures (El-Shamy and Abdelaal, 2016) with the use of FES, but they have not investigated the kinematic and inter-limb asymmetry changes, and its association with functional outcomes due to immediate (orthotic) and continuous (therapeutic) use of FES. Though walking speed reflects overall gait performance, it does not depict underlying impairments in joint mechanisms and inter-limb coordination during gait, and their recovery. Winter et al. observed that ankle joint angle changes in young adults, howsoever small, could significantly improve toe clearance (Winter, 1992). Research in percutaneous stimulation and FES in children and adolescents have shown increased dorsiflexion with no significant changes in speed, but have shown changes in musculature(Orlin et al., 2005). Therefore, understanding the joint kinematic changes could provide insight into the mechanistic effects of FDS even when evidence is lacking in functional outcomes. Studying mechanistic changes could provide quantitative information about sub-clinical kinematic outcomes (Hausdorff et al., 2001).

Temporal and spatial symmetry have previously been studied to understand pathological walking patterns (Patterson et al., 2010). Studies have reported that temporal asymmetry is a significant predictor of hemiparetic walking performance such as walking speed and falls in adults (Roth et al., 1997; Patterson et al., 2010). In healthy individuals, the variability in temporal and spatial parameters is minimal (Patterson et al., 2010). In contrast, individuals with hemiplegia present with higher asymmetry between their limbs, leading to the ambulatory deficits (Patterson et al., 2010). Understanding the asymmetry characteristics during gait will help improve the design of rehabilitation interventions for individuals with deficits in functional ambulation (Wall and Turnbull, 1986). Quantifying the change in asymmetry would help us further understand the effect of using FDS on functional/clinical outcomes such as falls, etc. (Hausdorff et al., 2001).

The objective of this exploratory investigation is to evaluate the orthotic and therapeutic effects of using FDS for children and adolescents by evaluating mechanistic and functional outcomes. Orthotic effect is defined as the improvement while using the device (FDS is active on the affected limb) and the therapeutic effect is defined as any lasting effect once the device is removed (FDS is inactive or removed). The secondary objective will explore the adaptive effect, which is defined as the changes in orthotic effect over time. The primary hypotheses were that the use of a FDS will result in increased toe clearance (displacement) and temporal-spatial symmetry. The secondary hypotheses were that toe displacement and temporal-spatial symmetry will correlate with gait speed. This investigation will provide preliminary evidence for utilization of FDS in pediatric rehabilitation.

METHODOLOGY

Participants

Eleven participants with foot drop and hemiplegia secondary to brain injury (age: between 5 and 17 years) were recruited. Only data from seven participants (four male and three female) were available for analysis because kinematic data were not available, participants did not complete both time points or participants were discharged due to FDS non-compliance. The demographics

of the seven participants are shown in **Table 1**. Additional inclusion criteria stated that participants: (1) were > 6 months post diagnosis of brain injury; (2) had no history of injury or pathology in the unaffected leg within the past 90 days; (3) were able to walk independently for 10 m without any assistive device; (4) had no history of Botulinum toxin injection to the lower limbs within 3 months of enrollment and no Botulinum toxin injection during the course of study; (5) had no severe cognitive or communication impairment; and (6) were not involved in any other interventions or were not using any devices/medications that might interfere with the study. Individuals with additional orthopedic, neuromuscular, or neurological pathologies that would interfere with their ability to walk were not included in this study. The protocol was approved by the Kessler Foundation Institutional Review Board (IRB), and consent was obtained before study participation from each participant's parent/guardian (in addition assent was obtained for participants > 13 years). All participants used an AFO for community ambulation prior to their participation in the study, and they were encouraged to use the FDS without an AFO during the course of the study.

FIGURE 1 | Subject wearing the FDS.

Foot Drop Stimulator

Functional electrical stimulation was provided through a commercially available FDS device (WalkAide®, Innovative Neurotronics, Austin, TX, United States). The WalkAide device uses surface electrodes in a single cuff located at the proximal end of the tibia about the peroneal nerve to stimulate during the swing phase of the gait cycle with customized frequency (17–33 Hz), pulse width (25–300 μs), and intensity of the generated electrical pulse to produce the desired dorsiflexion during gait. The FDS timing is controlled by a tilt sensor and accelerometer that will determine when to stimulate the peroneal nerve by monitoring the wearer's leg position during gait. The small device [87.9 g, 8.2 cm (H) × 6.1 cm (W) × 2.1 cm (T)] is attached to a molded cuff located just below the knee, secured with a latch, and properly aligned using anatomical landmarks and visual indicators (**Figure 1**).

Procedures

All participants completed up to eight study visits including screening, fitting, and device adjustment visits. These were followed by three data collection sessions (baseline, 1 month and 3 months). At their first visit, participants were screened and consented by a member of the study staff. Each participant was then fitted with a FDS by a licensed clinician at their second visit. During the device adjustment visits, a clinician provided training including review of device usage (donning and doffing), electrode placement, stimulation intensity adjustments, and a review of safety precautions. Following the adjustment visits, baseline data collection was conducted, and at the completion of the baseline session, all participants were given the device to use for community ambulation. All participants were instructed to use the device for everyday community ambulation for the entire duration of the study. Follow-up data collection was conducted at 1-month, and 3-month time points to assess the effect of continuous use of the device during community ambulation. This study was part of a larger investigation, and data from the baseline and 3-month visits were used for data analysis as 1-month data was not available for some participants. During each data collection session, retroreflective markers were placed on anatomical landmarks of the participants based on a modified

TABLE 1 | Subject demographics.

Subject	Condition	Affected side	Gender	Age at consent (years)	Height at baseline (m)	Weight at baseline (Kg)	Height at 3 months (m)	Weight at 3 Months (Kg)	Years since injury
1	CP	Right	F	16	1.45	45.00	1.47	47.70	16
2	CP	Right	F	9	1.51	40.28	1.55	41.4	9
3	Stroke	Right	F	6	1.22	26.10	1.24	26.55	5
4	CP	Left	M	7	1.30	30.60	1.33	34.20	7
5	Stroke	Left	M	15	1.83	71.21	1.83	70.65	15
6	Stroke	Right	M	8	1.35	23.85	1.35	23.85	8
7	CP	Right	M	10	1.57	52.65	1.60	56.70	10
Mean ± (SD)				10.14 ± 3.89	1.46 ± 0.20	41.38 ± 16.77	1.48 ± 0.199	43.01 ± 16.79	

Helen-Hayes marker configuration (Davis et al., 1991). Gait kinematics in the sagittal, frontal, and transverse planes were collected using a 12-camera motion capture system (Motion Analysis Corporation, Santa Rosa, CA, United States) at 60 Hz. At every data collection session, all seven participants performed in two conditions: (1) with FDS; and (2) without FDS, for a total of up to 24 walks (12 walking trials per condition). The order was randomized between with and without FDS condition for all subjects. During each trial, all participants were instructed to walk approximately 10 m on an unobstructed walkway at a self-selected speed. All participants wore shoes and did not wear any other assistive device during the data collection sessions. Participants were monitored during each trial and permitted to rest or take breaks at any time during testing to minimize the effects of fatigue.

Data Processing and Analysis

All marker positions and joint angle data were collected, processed, and exported using Motion Analysis's Cortex software (Motion Analysis Corporation, Santa Rosa, CA, United States) and analyzed using MATLAB (The Mathworks Inc., Natick, MA, United States). The Cartesian and joint kinematics data was exported from Cortex and filtered using a fourth order low pass filter. MATLAB was used to analyze the gait trajectories for each session with and without the FDS. The exported data was further divided into gait cycles, with a gait cycle being defined as the period from ground contact of one foot to the subsequent ground contact of the same foot. A minimum of 10 and a maximum of 25 gait cycles per condition, and per session were available for each subject and used for data analysis. The outcome measures and the analyses are shown in **Table 2**.

RESULTS

Sagittal Kinematics

Figure 2 shows the average sagittal plane kinematics of the ankle joint for the unaffected and affected legs with and without FDS for both sessions. At 3 months compared to baseline with FDS (adaptation effect), there is an increased mean dorsiflexion during swing on the affected side as well as increased plantar flexion during the beginning of stance phase (**Figure 2A**) but at 3 months compared to baseline without FDS (therapeutic effect), there is only a small increase in mean dorsiflexion during swing (**Figure 2B**) on the affected side. Also, at 3 months, increased mean dorsiflexion was observed during swing with FDS compared to without FDS (**Figures 2A,B**), and at baseline a small increase in mean dorsiflexion with FDS compared to without FDS (orthotic effect). No difference was observed between baseline and 3 months on the unaffected side with and without FDS (**Figures 2C,D**). However, the mean dorsiflexion angle during swing of the affected ankle was close to the unaffected ankle with use of FDS at 3 months (**Figures 2A,C**), and the ankle angle profile with FDS at 3 months is similar to that of the healthy control (**Figure 2A**).

Figure 3 shows the average sagittal plane kinematics of the knee for the unaffected and affected legs with FDS for both sessions. The results show that at 3 months compared to baseline with FDS, there is a small increase in mean flexion at the beginning of swing on the affected side (**Figure 3A**) but was within standard deviation (SD). At 3 months compared to baseline without FDS, there is a small increase in mean flexion at the beginning of swing (**Figure 3B**) on the affected side but was within SD. No difference was observed at baseline or at 3 months in knee flexion/extension between with and without FDS on the affected (**Figures 3A,B**) and unaffected sides (**Figures 3C,D**). Increased flexion was observed in the knee angles of both legs in the healthy control participant compared to the mean knee angles of participants with disability.

Figure 4 shows the average sagittal plane kinematics of the hip for the unaffected and affected legs with FDS for both sessions. No difference was observed between baseline and 3 months or between with and without FDS at baseline or at 3 months on the affected (**Figures 4A,B**) and unaffected legs (**Figures 4C,D**).

Toe Displacement

On comparing toe displacement of the affected leg while walking with and without FDS both at baseline and at 3 months, following results were obtained:

There was no significant effect of duration of use (i.e., from baseline to 3 months [$F(1,6) = 5.08$, $p > 0.05$, $N = 7$], Cohen's d effect size = 0.9) but there was a significant effect of FDS (i.e., with vs. without device [[$F(1,6) = 18.79$, $p < 0.005$, $N = 7$], Cohen's d effect size = 0.76) and there was no significant interaction effect ([$F(1,6) = 3.58$, $p > 0.05$, $N = 7$], Cohen's d effect size = 0.37) using repeated measures ANOVA. At 3 months compared to baseline with FDS, participants showed no significant difference in toe displacement in the affected leg, but participants 1, 4, 5, 6, and 7 increased their mean toe displacement (**Figure 5A**). Also, at 3 months compared to baseline without FDS (therapeutic effect), participants showed no significant difference [$t(-6) = 1.44$, $p > 0.05$, Cohen's d effect size = 0.54] in the affected leg, but participants 2, 3, 4, and 7 increased their mean toe displacement while subject 6 decreased their mean toe displacement (**Figure 5A**). At baseline, participants 1, 2, 4, 5, and 6 increased their mean toe displacement in the affected leg when walking with FDS compared to without FDS (orthotic effect), though no significant difference was observed between the two groups after Bonferroni correction [$t(6) = 2.79$, $p > 0.025$, $N = 7$, Cohen's $d = 1.05$]. At 3 months, there was a significant difference due to the FDS compared to without FDS (orthotic effect) after Bonferroni correction [$t(6) = 3.54$, $p < 0.025$, $N = 7$, Cohen's $d = 1.0$] on the affected leg, where participants 1, 2, 4, 5, 6, and 7 showed increased toe displacement with FDS.

Walking Speed

There was no significant main effect of device (i.e., with vs. without device [F(1,6) = 3.71, $p > 0.05$, N = 7], Cohen's d effect size = 0.78) or duration of use (i.e., baseline to 3 months[(F(1,6) = 5.74, $p > 0.05$, N = 7]), Cohen's d effect size = 0.9) or interaction effect ([F(1,6) = 3.58, $p > 0.05$, N = 7], Cohen's d effect size = 0.58) using repeated measures ANOVA. The results show that at 3 months compared to baseline with FDS, participants 2, 4, 5, 6, and 7 increased their mean speed (**Figure 5B**). Additionally, at 3 months compared to

TABLE 2 | Outcome measures.

Outcome measure	Description	Statistical analysis
Sagittal plane kinematics	The knee and ankle angles were computed for each gait cycle and averaged for each subject	
Toe displacement	The toe displacement was calculated as the maximum of the normalized difference in Cartesian y position of the toe (*ytoe*) and the heel (*yheel*) as shown in the equation below (y position data was normalization with respect to the foot position on the floor during stance). The average toe displacement was calculated for each subject $Max(normalized\ (ytoe - yheel))$ (1)	Shapiro-Wilk test ($p > 0.05$) of normality showed that data was normal. Repeated measures analysis of variance (ANOVA) was used to determine the effect of FDS and the effect of duration of use (Baseline to 3 months). Further, a *post hoc* test (pairwise comparison) with Bonferroni correction was performed to determine the difference between the conditions
Walking speed	The average walking speed was computed as the linear distance with respect to time to complete a gait cycle	Shapiro–Wilk test ($p > 0.05$) of normality showed that data was normal. Repeated measures analysis of variance (ANOVA) was used to determine the effect of FDS and the effect of duration of use (Baseline to 3 months) on walking speed
Step length	The average step length for each gait cycle was computed as the forward linear displacement between foot contact of the ipsilateral leg to foot contact of the contralateral leg during each gait cycle	Shapiro–Wilk test ($p > 0.05$) of normality showed that data was normal. Repeated measures analysis of variance (ANOVA) was used to determine the effect of FDS and the effect of duration of use (Baseline to 3 months) on step length
Temporal measures	Total time was computed as the time between foot contact of one leg to the subsequent foot contact of the same leg. The average total time was computed for each gait cycle. Further, average swing time for each subject during each condition was computed as the time between the foot off the floor of one leg to foot contact of the same leg during the gait cycle	Shapiro–Wilk test ($p > 0.05$) of normality showed that data was normal. Repeated measures analysis of variance (ANOVA) was used to determine the effect of FDS on total time. Further, a *post hoc* test (pairwise comparison) with Bonferroni correction was performed to determine the difference between the conditions A Friedman non-parametric test was used to determine the effect of FDS and the effect of duration of use (Baseline to 3 months) on swing time, as the data did not pass the test for normality ($p < 0.05$) using Shapiro–Wilk test
Temporal-spatial symmetry	The swing and stance time of each foot during each gait cycle was computed, and the following ratios were used to compute the temporal asymmetry: $\text{Temporal swing stance symmetry} = (\text{swing time})/(\text{stance time})$ (2) Equation 2 was computed for both affected and unaffected limbs $\text{Overall temporal asymmetry} = \text{abs}\left(1 - \left(\frac{\text{affected swing stance symmetry}}{\text{unaffected swing stance symmetry}}\right)\right)$ (3) The step length of each foot was computed for each gait cycle, and the spatial asymmetry ratio was calculated as follows: $\text{Spatial asymmetry} = \text{abs}\left(1 - \left(\frac{\text{unaffected step length}}{\text{affected step length}}\right)\right)$ (4)	Shapiro–Wilk test ($p > 0.05$) of normality showed that data was normal. Repeated measures analysis of variance (ANOVA) was used to determine the effect of FDS and the effect of duration of use (Baseline to 3 months) on temporal asymmetry. Further, a *post hoc* test (pairwise comparison) with Bonferroni correction was performed to determine the difference between the conditions A Friedman non-parametric test was used to determine the effect of FDS and the effect of duration of use (Baseline to 3 months) on spatial asymmetry, as the data did not pass the test for normality ($p < 0.05$) using Shapiro–Wilk test of normality

baseline without FDS, participants 2, 3, 4, 5, and 7 increased their speed, and participants 1 and 6 decreased their mean speed (**Figure 5B**). At baseline, participants 1, 2, 3, 5, 6, and 7 (**Figure 5B**) showed a decrease in speed with FDS compared to without FDS. At 3 months, Participants 1, 4, and 6 (**Figure 5B**) increased their mean speed with FDS compared to without FDS, but participants 3 and 7 decreased their speed with FDS compared to without FDS.

Step Length

There was no significant effect of device or duration of use with the repeated measures ANOVA. The results show that at 3 months compared to baseline with use of FDS, participants 2 and 5 increased their mean step length by over 20 mm (**Table 3**). Also, at 3 months compared to baseline without the use of FDS, participants 2, 3, 4, and 5 increased their step length by over 20 mm, but participants 1 and 6 decreased their mean step length by over 20 mm (**Table 3**). At baseline, subject 2 showed an over 20 mm increase in their mean step length (**Table 3**) when walking without FDS compared to with FDS. At 3 months, participants 3 and 7 showed an over 20 mm increase in their mean step length (**Table 3**), but subject 6 showed a decrease in mean step length when walking without FDS compared to with FDS.

Total Time

There was a significant effect of device and duration of use but there was no interaction effect using the repeated measures

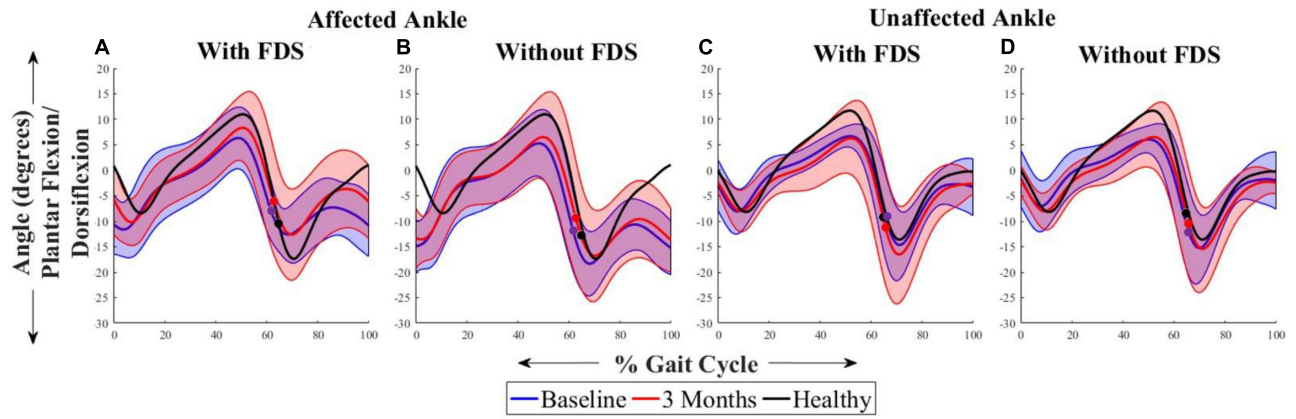

FIGURE 2 | Mean ± Standard deviation (SD) ankle plantarflexion/dorsiflexion of the **(A)** affected ankle with FDS, **(B)** affected ankle without FDS **(C)** unaffected ankle with FDS and **(D)** unaffected ankle without FDS, at baseline and 3 months of all participants. The black line represents the mean ankle plantarflexion/dorsiflexion of one representative healthy child. The dots represent the start of swing phase.

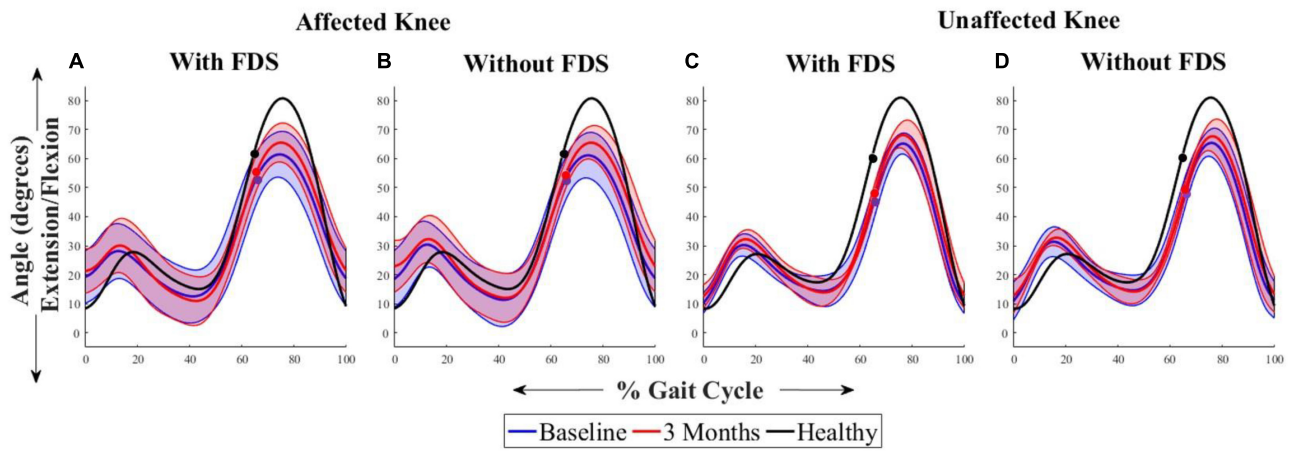

FIGURE 3 | Mean ± Standard deviation (SD) knee plantarflexion/dorsiflexion of the **(A)** affected knee with FDS, **(B)** affected knee without FDS **(C)** unaffected knee with FDS and **(D)** unaffected knee without FDS, at baseline and 3 months of all participants. The black line represents the mean knee plantarflexion/dorsiflexion of one representative healthy child. The dots represent the start of swing phase.

ANOVA. The results show that the mean total time at 3 months compared to baseline with the use of FDS ($p > 0.025$, N = 7) did not show a significant effect after Bonferroni correction, but participants 2, 4, and 7 showed a decrease in mean total time (**Table 3**) of over 0.05 s. The mean total time at 3 months compared to baseline without the use of FDS ($p < 0.025$, N = 7) showed a significant effect after Bonferroni correction, where participants 2, 4, and 7 showed a decrease in mean total time (**Table 3**) of over 0.05 s. At baseline, there was no significant effect after Bonferroni correction ($p > 0.025$, N = 7) in mean total time between with and without FDS, but participants 1, 2, 5, 6, and 7 showed a decrease in mean total time of over 0.05 s while walking without the FDS compared with FDS (**Table 3**). At 3 months, there was no significant effect ($p < 0.025$, N = 7) in mean total time while walking without the FDS compared with FDS (**Table 3**). No participants showed a change in mean total time greater than 0.05 s.

Swing Time

There was no significant effect of device but there was a significant effect of duration of use but there was no significant interaction effect using the repeated measures ANOVA. No significant change in swing time was observed between baseline and 3 months with the use of FDS (**Table 3**). The results show that at 3 months compared to baseline with the use of FDS, participants 1, 2, 3, 5, 6, and 7 showed a decrease in mean swing time (**Table 3**). Also, at 3 months compared to baseline without the use of FDS, participants 1, 2, 3, 5, 6, and 7 showed a decrease in mean swing time (**Table 3**).

At baseline, the mean swing time increased for participants 1, 2, 5, 6 and decreased for subject 7 with use of FDS compared to without use of FDS (**Table 3**). At 3 months, the mean swing time increased for participant 3 with use of FDS compared to without use of FDS (**Table 3**).

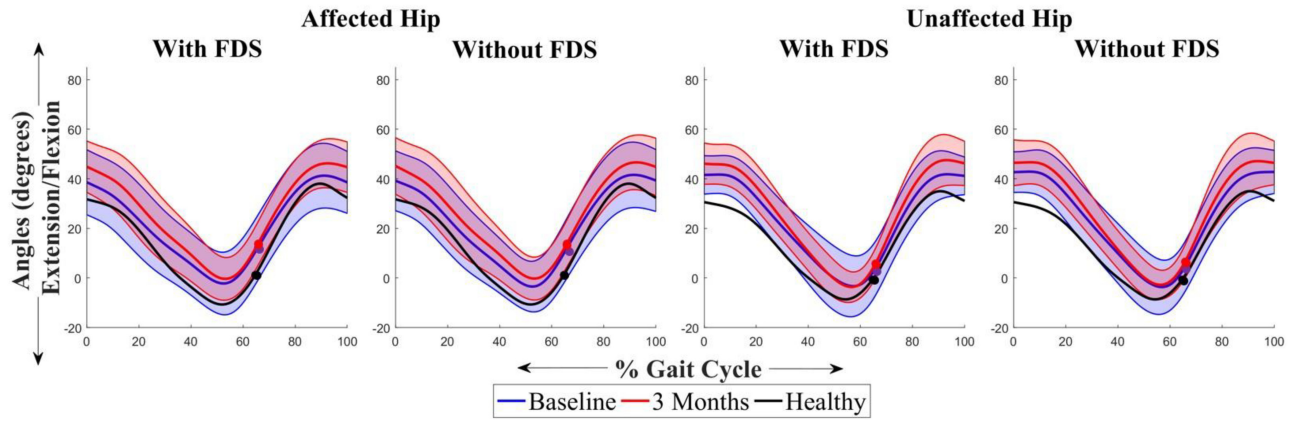

FIGURE 4 | Mean ± Standard deviation (SD) hip plantarflexion/dorsiflexion of the **(A)** affected hip with FDS, **(B)** affected hip without FDS **(C)** unaffected hip with FDS and **(D)** unaffected hip without FDS, at baseline and 3 months of all participants. The black line represents the mean hip plantarflexion/dorsiflexion of one representative healthy child. The dots represent the start of swing phase.

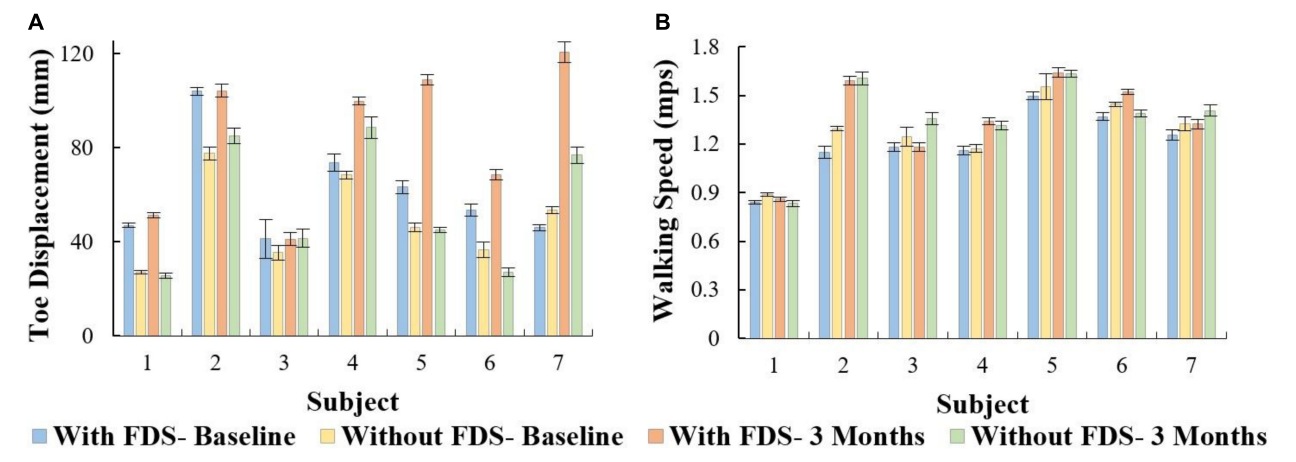

FIGURE 5 | (A) Mean ± Standard error of toe displacement of the affected side with and without FDS. **(B)** Mean ± Standard error of walking speed for the affected side with and without FDS.

Correlation Between Toe Displacement and Speed

All conditions showed no significant Pearson's r correlation between toe displacement and speed (With FDS- Baseline: $r = 0.07$, $p > 0.05$, df = 5 Without FDS- Baseline: $r = 0.20$, $p > 0.05$, df = 5 With FDS- 3 Months: $r = 0.62$, $p > 0.05$, df = 5 Without FDS- 3 Months: $r = 0.44$, $p > 0.05$, df = 5). However, high positive correlation was observed between toe displacement and speed at 3 months with FDS compared to without FDS (**Figure 6**).

Temporal and Spatial Symmetry

There was no significant effect of device (i.e., with and without device [$F(1,6) = 5.724$, $p > 0.005$, $N = 7$], Cohen's d effect size = 0.48) or duration of use (i.e., baseline to 3 months[($F(1,6) = 1.871$, $p > 0.05$, $N = 7$]), Cohen's d effect size = 0.24)and there was no significant ([$F(1,6) = 3.426$, $p > 0.05$, $N = 7$], Cohen's d effect size = 0.4) interaction effect using the repeated measures ANOVA on temporal symmetry (**Figure 7a**). Overall, temporal asymmetry was higher with FDS at baseline compared to without FDS in participants 1, 2, 5, and 7. At 3 months, subject 4 showed higher asymmetry with FDS compared to without FDS, while subject 6 showed higher asymmetry without FDS compared to with FDS. Participants 2, 3 and 7 showed decreased asymmetry from baseline to 3 months without FDS. Participants 4 and 6 showed increased asymmetry from baseline to 3 months without FDS.

There was no significant effect of device or duration of use using the Friedman Non-parametric test ($p > 0.05$) on spatial symmetry (**Figure 7b**). Spatial asymmetry was higher with FDS at baseline compared to without FDS for participants 2 and 7. Subject 1 showed decreased asymmetry with FDS at 3 months compared to without FDS, while participants 3, 4, and 5 showed increased asymmetry at 3 months with FDS compared to without FDS. Participants

TABLE 3 | The table shows the Mean ± Standard error of total time, step length, and swing time of the affected side.

Subject	With FDS- baseline	Without FDS- baseline	With FDS- 3 Months	Without FDS- 3 Months
Step Length (mm)				
1	488.12 ± 6.14	502.38 ± 5.46	479.92 ± 7.65	470.58 ± 7.33
2	600.14 ± 9.02	623.33 ± 7.19	686.43 ± 14.62	699.90 ± 16.10
3	411.21 ± 11.06	424.52 ± 14.76	427.61 ± 12.24	483.91 ± 18.89
4	553.90 ± 22.10	552.55 ± 7.23	563.95 ± 10.88	572.33 ± 9.16
5	758.83 ± 10.56	762.15 ± 30.92	786.26 ± 15.23	802.34 ± 7.27
6	616.17 ± 6.92	617.94 ± 6.69	621.08 ± 8.06	549.16 ± 9.74
7	676.62 ± 7.15	680.69 ± 10.14	627.80 ± 16.66	675.48 ± 0.019
Total time (seconds)				
1	1.15 ± 0.009	1.12 ± 0.009	1.14 ± 0.013	1.12 ± 0.010
2	1.10 ± 0.022	1.03 ± 0.009	0.94 ± 0.009	0.93 ± 0.020
3	0.89 ± 0.011	0.88 ± 0.024	0.89 ± 0.016	0.85 ± 0.019
4	1.02 ± 0.012	1.01 ± 0.017	0.91 ± 0.014	0.93 ± 0.006
5	1.11 ± 0.008	1.08 ± 0.01	1.07 ± 0.009	1.06 ± 0.01
6	0.94 ± 0.013	0.90 ± 0.007	0.85 ± 0.007	0.87 ± 0.009
7	1.19 ± 0.019	1.13 ± 0.03	1.09 ± 0.017	1.07 ± 0.011
Swing Time (s)				
1	0.44 ± 0.005	0.40 ± 0.004	0.39 ± 0.006	0.38 ± 0.006
2	0.40 ± 0.006	0.38 ± 0.004	0.36 ± 0.003	0.35 ± 0.007
3	0.35 ± 0.006	0.35 ± 0.007	0.33 ± 0.007	0.31 ± 0.01
4	0.33 ± 0.007	0.34 ± 0.008	0.35 ± 0.008	0.34 ± 0.008
5	0.48 ± 0.005	0.45 ± 0.015	0.45 ± 0.004	0.44 ± 0.004
6	0.39 ± 0.005	0.37 ± 0.003	0.34 ± 0.003	0.36 ± 0.005
7	0.38 ± 0.007	0.42 ± 0.013	0.36 ± 0.01	0.36 ± 0.004

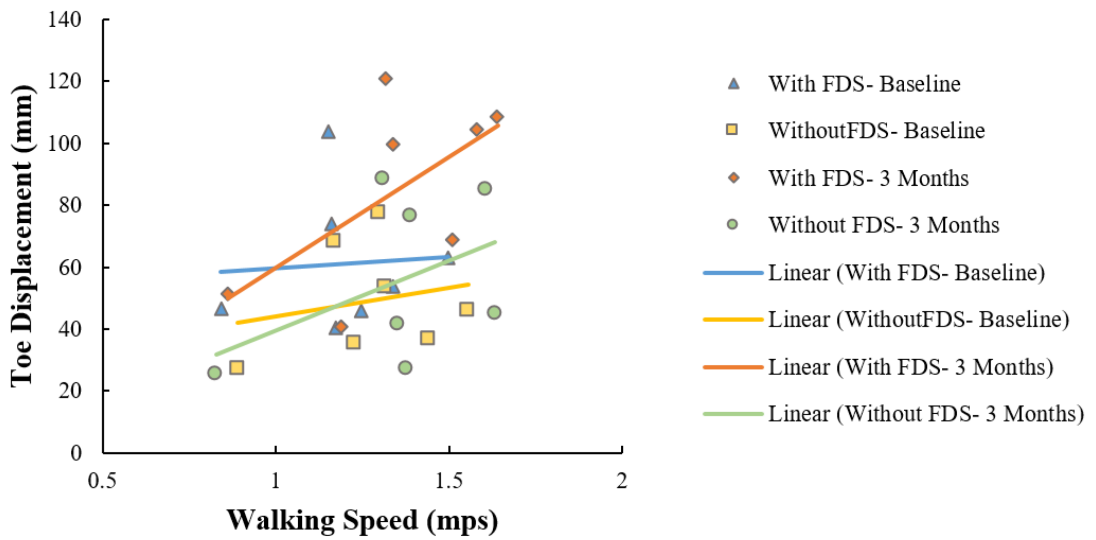

FIGURE 6 | Correlation between toe displacement and speed of the affected side with and without FDS at baseline and 3 months.

3, 4, and 5 showed decreased asymmetry from baseline to 3 months without FDS.

No significant Pearson's r correlation was observed between temporal asymmetry and speed in all conditions (With FDS- Baseline [r = 0.01, p > 0.05, df = 5], with FDS- 3 Months [r = 0.49, p > 0.05, df = 5] without FDS- Baseline. [r = 0.481, p > 0.05, df = 5] and without FDS- 3 Months[r = 0.261, p > 0.05, df = 5]) (**Figure 7c**).

Significant Pearson's r correlation was observed between spatial asymmetry and speed at without FDS- 3 months [r = 0.76, p < 0.05, df = 5] (**Figure 7d**). No significant correlation was

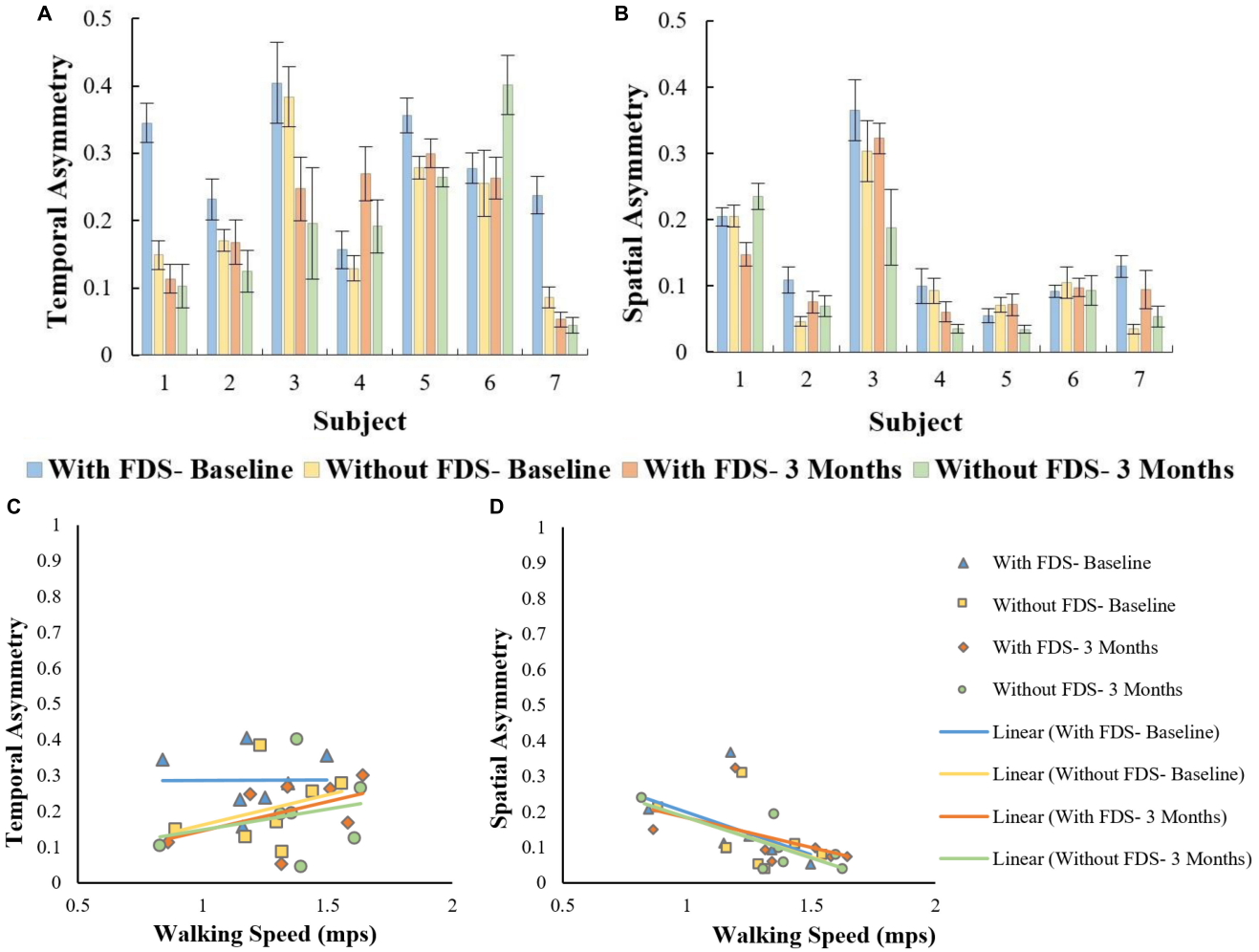

FIGURE 7 | (A) Overall asymmetry of the affected side with and without FDS at baseline and 3 months. **(B)** Spatial asymmetry of the affected side with and without FDS at baseline and 3 months. **(C)** Correlation between temporal asymmetry and speed of the affected side with and without FDS at baseline and 3 months. **(D)** Correlation between spatial asymmetry and speed of the affected side with and without FDS at baseline and 3 months.

observed between spatial asymmetry and speed in the other conditions (With FDS- Baseline [$r = 0.46$, $p > 0.05$], Without FDS- Baseline [$r = 0.481$, $p > 0.05$, df = 5] With FDS- 3 Months [$r = 0.49$, $p > 0.05$, df = 5]).

DISCUSSION

Children and adolescents with foot drop have difficulty clearing their foot off the floor during swing, hence producing inefficient gait with altered gait kinematics and interlimb symmetry. This, in turn, results in reduced speed and step length, and increased gait cycle duration when walking. Current research is focused on reducing these deficits with the use of FDS, and on understanding both the orthotic and therapeutic effects of FDS. In this study, the efficacy of FDS usage for 3-month was investigated by evaluating the changes in mechanistic outcomes such as kinematics, inter-limb asymmetry, and functional outcomes such as speed, step length, and gait cycle duration. This study evaluates mechanistic parameters, using outcomes such as symmetry and toe displacement, which have not been considered in other research investigating FDS in children. Following the use of FDS, increased dorsiflexion of the ankle was observed, aiding in foot clearance. While no significant increase in speed or step length was found, a correlation between toe displacement and speed, and between spatial asymmetry and speed was observed.

The results showed that participants increased their toe displacement with FDS compared to without FDS, demonstrating that the FDS device is assisting in clearing the foot, as shown in **Figure 5A**. This is further supported by the mean dorsiflexion angle during swing (**Figure 2**), where the mean ankle angle with FDS is greater than the angle without FDS by over 3 degrees, as Winter et al. showed that a small change in dorsiflexion angle could have a considerable effect on toe displacement (Winter, 1992). These results are also in accordance with the results observed by other researchers (Van Der Linden et al., 2008; Prosser et al., 2012; Damiano et al., 2013), who found that using FDS produced increased dorsiflexion during swing

phase in children. Further, a similar orthotic effect of increased dorsiflexion was also observed with percutaneous electrical stimulation (Pierce et al., 2004a,b; Postans and Granat, 2005). Additionally, an adaptive effect was observed from baseline to 3 months, where both mean dorsiflexion and toe displacement increased with the use of FDS. This could be due to the participants adapting to the FDS with time. This effect may partially explain the decrease in temporal and spatial symmetry, and walking speed with FDS compared to without FDS in some of the participants at baseline.

Though some of the participants showed an increase in walking speed at the 3-month visit when walking with the FDS compared to without FDS, they did not exhibit any statistically significant change in walking speed between conditions as shown in **Figure 5B**. This result is in concordance with Prosser et al., where they showed an increase in dorsiflexion angle but no statistically significant change in walking speed after a 3-month intervention with FES in "free- and fast-speed" trials (Prosser et al., 2012). Similar results were also observed by Orlin et al. with percutaneous stimulation, where they achieved improvements in kinematics but no significant change in walking speed (Orlin et al., 2005). Bertoti et al. reported a step length increase in a child with CP after 7 months of gait training with percutaneous stimulation, but no change in walking speed (Bertoti et al., 1997). One possible explanation for the lack of significant changes in walking speed could be that most of the participants in the study were already ambulating with a healthy walking speed at the time of enrollment, which limited further significant improvement. Unlike results from research in adults with hemiplegia post-stroke, where adult participants presented with slower walking speeds and have shown significant increases in speed after the use of FDS (Burridge et al., 1997). Based on our study, we can infer that walking speed in itself might not be an indicator of the deficit or of the recovery in certain populations with walking impairments. Hence, other mechanistic outcomes need to be used to better understand the deficit and recovery that may take place.

A positive correlation (r = 0.62) between toe displacement and speed was observed with the use of FDS and a moderate correlation (r = 0.44) without FDS at 3 months. This could indicate that an increase in toe displacement may be a contributing factor to the observed increase in walking speed. These results were not statistically significant which could be due to the small sample size, however, the trend could be clinically important. After continuous use of the FDS, some participants increased mean ankle dorsiflexion even while walking without the FDS from baseline to 3 months during the swing phase (**Figure 2B**), and 4 out of 7 participants increased toe displacement (**Figure 5**). These effects, however, were not statistically significant and also were not observed in all participants. These clinical improvements while walking without FDS in some participants may indicate that continuous use of the FDS may have resulted in a therapeutic effect but a larger sample is required to further conclusively prove the effect of duration of use.

Spatial asymmetry and speed showed a negative correlation in all conditions, suggesting that an increase in speed is associated with a decrease in spatial asymmetry. The negative correlation was higher at 3 months compared to baseline indicating that a decrease in asymmetry could have contributed to the increase in speed. Though there was no change in step length on the affected side, the symmetry between the two legs improved, indicating that the step length of both legs became more equivalent. Studies on hemiparetic gait have reported that temporal asymmetry is more of a predictor of walking speed than spatial asymmetry (Lin et al., 2006; Balasubramanian et al., 2007; Patterson et al., 2008, 2010; Nadeau, 2014); however, in this study, temporal asymmetry showed a lower correlation with speed compared to spatial asymmetry.

Prior to the start of the study, all the participants were exclusively relying on an AFO for community ambulation to prevent foot drop. In growing children and adolescents, AFOs needs to be fabricated multiple times, thus increasing the incurred expense over time. On the contrary, a FDS device that can be affordably adjusted to accommodate for user growth rather than being periodically replaced might be a more cost-effective solution for foot drop. In addition, the results of this study indicate the potential of FDS to providing not only an orthotic effect to the wearer but also a therapeutic effect as well, without the ROM restriction of an AFO.

A potential limitation of the current study is that participant activity in the community was not monitored. It is possible that increased activity in the community while wearing the FDS device could provide additional therapeutic advantage over time since increased steps would positively correlate with increased stimulation dosing. Researchers did not want to adjust participant behavior so no instructions were provided to increase community ambulation, instructions for community utilization were to wear the FDS device as much as possible while at home and in the community. Additionally, FDS device compliance and usage was not standardized throughout the investigation. Therefore, the individual clinical benefits from wearing the device may be related to device adoption or use. The combination between community ambulation and device usage is important to consider when evaluating the clinical benefits of FDS. In this pilot investigation, evaluating the effect of FDS in pediatric population, we were able to begin to identify relevant outcomes to consider in pediatrics when deciding if a FDS is appropriate for clinical use. Another limitation of this research is the limited sample size. The data indicated some promising results for orthotic and therapeutic effects that should continue to be explored in a larger sample.

CONCLUSION

This study indicates that there is an orthotic effect of increased dorsiflexion and toe displacement during swing with the use of the FDS in children with hemiplegia. Further, the study suggests that there could be a potential long-term effect of increased dorsiflexion during swing with continuous use of FDS. The current results are promising, but future studies with a larger sample in a controlled environment would be required to further understand the efficacy of the FDS in children and adolescents and to confirm any training effect conclusively.

ETHICS STATEMENT

This study was carried out in accordance with the recommendations of Kessler Foundation IRB with written informed consent from all subjects. All subjects gave written informed consent in accordance with the Declaration of Helsinki. The protocol was approved by the Kessler Foundation IRB.

AUTHOR CONTRIBUTIONS

KN designed the study with assistance from KB and JC. KK, NE, and KN collected the data. KK, RP, and NE analyzed the data. KK drafted the manuscript. RP, NE, KB, JC, and KN revised, reviewed, and finalized the manuscript.

FUNDING

This research was supported by Kessler Foundation (West Orange, NJ, United States) and Children's Specialized Hospital (Mountainside, NJ, United States).

ACKNOWLEDGMENTS

We would like to thank Hanger Clinic – Prosthetics and Orthotics (West Orange, NJ, United States) for their assistance in this investigation. We would also like to acknowledge Arvind Ramanujam, Ghaith Androwis, Kathleen Chervin, and Gregory Ames for their assistance in data collection.

REFERENCES

Balasubramanian, C. K., Bowden, M. G., Neptune, R. R., and Kautz, S. A. (2007). Relationship between step length asymmetry and walking performance in subjects with chronic hemiparesis. *Arch. Phys. Med. Rehabil.* 88, 43–49. doi: 10.1016/j.apmr.2006.10.004

Bernson-Leung, M. E., and Rivkin, M. J. (2009). [Stroke in neonates and children]. *Rev. Neurol.* 165, 889–900.

Bertoti, D. B., Stanger, M., Betz, R. R., Akers, J., Maynahon, M., and Mulcahey, M. J. (1997). Percutaneous intramuscular functional electrical stimulation as an intervention choice for children with cerebral palsy. *Pediatr. Phys. Ther.* 9, 123–127.

Burridge, J. H., Taylor, P. N., Hagan, S. A., Wood, D. E., and Swain, I. D. (1997). The effects of common peroneal stimulation on the effort and speed of walking: a randomized controlled trial with chronic hemiplegic patients. *Clin. Rehabil.* 11, 201–210. doi: 10.1177/026921559701100303

Cauraugh, J. H., Naik, S. K., Hsu, W. H., Coombes, S. A., and Holt, K. G. (2010). Children with cerebral palsy: a systematic review and meta-analysis on gait and electrical stimulation. *Clin. Rehabil.* 24, 963–978. doi: 10.1177/0269215510371431

Comeaux, P., Patterson, N., Rubin, M., and Meiner, R. (1997). Effect of neuromuscular electrical stimulation during gait in children with cerebral palsy. *Pediatr. Phys. Ther.* 9, 103–109.

Damiano, D. L., Prosser, L. A., Curatalo, L. A., and Alter, K. E. (2013). Muscle plasticity and ankle control after repetitive use of a functional electrical stimulation device for foot drop in cerebral palsy. *Neurorehabil. Neural Repair.* 27, 200–207. doi: 10.1177/1545968312461716

Davis, R. B., Õunpuu, S., Tyburski, D., and Gage, J. R. (1991). A gait analysis data collection and reduction technique. *Hum. Mov. Sci.* 10, 575–587. doi: 10.1016/0167-9457(91)90046-z

Dubin, A. (2014). Gait. The role of the ankle and foot in walking. *Med. Clin. North Am.* 98, 205–211. doi: 10.1016/j.mcna.2013.10.002

El-Shamy, S. M., and Abdelaal, A. A. M. (2016). walkaide efficacy on gait and energy expenditure in children with hemiplegic cerebral palsy. *Am. J. Phys. Med. Rehabil.* 95, 629–638. doi: 10.1097/PHM.0000000000000514

Everaert, D. G., Thompson, A. K., Chong, S. L., and Stein, R. B. (2010). Does functional electrical stimulation for foot drop strengthen corticospinal connections? *Neurorehabil. Neural Repair* 24, 168–177. doi: 10.1177/1545968309349939

Geboers, J. F., Drost, M. R., Spaans, F., Kuipers, H., and Seelen, H. A. (2002). Immediate and long-term effects of ankle-foot orthosis on muscle activity during walking: a randomized study of patients with unilateral foot drop. *Arch. Phys. Med. Rehabil.* 83, 240–245. doi: 10.1053/apmr.2002.27462

Gök, H., Küçükdeveci, A., Altinkaynak, H., Yavuzer, G., and Ergin, S. (2003). Effects of ankle-foot orthoses on hemiparetic gait. *Clin. Rehabil.* 17, 137–139. doi: 10.1191/0269215503cr605oa

Hausdorff, J. M., Rios, D. A., and Edelberg, H. K. (2001). Gait variability and fall risk in community-living older adults: a 1-year prospective study. *Arch. Phys. Med. Rehabil* 82, 1050–1056. doi: 10.1053/apmr.2001.24893

Kerrigan, D. C., Frates, E. P., Rogan, S., and Riley, P. O. (2000). Hip hiking and circumduction: quantitative definitions. *Am. J. Phys. Med. Rehabil.* 79, 247–252. doi: 10.1097/00002060-200005000-00006

Khamis, S., Herman, T., Krimus, S., and Danino, B. (2018). Is functional electrical stimulation an alternative for orthotics in patients with cerebral palsy? A literature review. *Eur. J. Paediatr. Neurol.* 22, 7–16. doi: 10.1016/j.ejpn.2017.10.004

Laufer, Y., Ring, H., Sprecher, E., and Hausdorff, J. M. (2009). Gait in individuals with chronic hemiparesis: one-year follow-up of the effects of a neuroprosthesis that ameliorates foot drop. *J. Neurol. Phys. Ther.* 33, 104–110. doi: 10.1097/NPT.0b013e3181a33624

Lehmann, J. F., Esselman, P. C., Ko, M. J., Smith, J. C., DeLateur, B. J., and Dralle, A. J. (1983). Plastic ankle-foot orthoses: evaluation of function. *Arch. Phys. Med. Rehabil.* 64, 402–407.

Lin, P. Y., Yang, Y. R., Cheng, S. J., and Wang, R. Y. (2006). The relation between ankle impairments and gait velocity and symmetry in people with stroke. *Arch. Phys. Med. Rehabil.* 87, 562–568. doi: 10.1016/j.apmr.2005.12.042

Nadeau, S. (2014). Understanding spatial and temporal gait asymmetries in Individuals Post Stroke. *Int. J. Phys. Med. Rehabil.* 2:201. doi: 10.1016/j.physbeh.2013.11.004

Orlin, M. N., Pierce, S. R., Stackhouse, C. L., Smith, B. T., Johnston, T., Shewokis, P. A., et al. (2005). Immediate effect of percutaneous intramuscular stimulation during gait in children with cerebral palsy: a feasibility study. *Dev. Med. Child Neurol.* 47, 684–690. doi: 10.1111/j.1469-8749.2005.tb01054.x

Patterson, K. K., Gage, W. H., Brooks, D., Black, S. E., and McIlroy, W. E. (2010). Evaluation of gait symmetry after stroke: a comparison of current methods and recommendations for standardization. *Gait Posture* 31, 241–246. doi: 10.1016/j.gaitpost.2009.10.014

Patterson, K. K., Parafianowicz, I., Danells, C. J., Closson, V., Verrier, M. C., Staines, W. R., et al. (2008). Gait asymmetry in community-ambulating stroke survivors. *Arch. Phys. Med. Rehabil.* 89, 304–310. doi: 10.1016/j.apmr.2007.08.142

Pierce, S. R., Laughton, C. A., Smith, B. T., Orlin, M. N., Johnston, T. E., and McCarthy, J. J. (2004a). Direct effect of percutaneous electric stimulation during gait in children with hemiplegic cerebral palsy: a report of 2 cases. *Arch. Phys. Med. Rehabil.* 85, 339–343. doi: 10.1016/s0003-9993(03)00473-8

Pierce, S. R., Orlin, M. N., Lauer, R. T., Johnston, T. E., Smith, B. T., and McCarthy, J. J. (2004b). Comparison of percutaneous and surface functional electrical stimulation during gait in a child with hemiplegic cerebral palsy. *Am. J. Phys. Med. Rehabil.* 83, 798–805. doi: 10.1097/01.phm.0000137318.92035.8c

Pool, D., Blackmore, A. M., Bear, N., and Valentine, J. (2014). Effects of short-term daily community walk aide use on children with unilateral spastic cerebral palsy. *Pediatr. Phys. Ther.* 26, 308–317. doi: 10.1097/pep.0000000000000057

Postans, N., and Granat, M. (2005). Effect of functional electrical stimulation, applied during walking, on gait in spastic cerebral palsy. *Dev. Med. Child* 47, 46–52. doi: 10.1111/j.1469-8749.2005.tb01039.x

Prenton, S., Hollands, K. L., Kenney, L. P. J., and Onmanee, P. (2018). Functional electrical stimulation and ankle foot orthoses provide equivalent therapeutic effects on foot drop: a meta-analysis providing direction for future research. *J. Rehabil. Med.* 50, 129–139. doi: 10.2340/16501977-2289

Prevalence of Cerebral Palsy (2018). *Prevalence of Cerebral Palsy*. Available at: http://www.cerebralpalsy.org/about-cerebral-palsy/prevalence-and-incidence (accessed December 3, 2018).

Prosser, L. A., Curatalo, L. A., Alter, K. E., and Damiano, D. L. (2012). Acceptability and potential effectiveness of a foot drop stimulator in children and adolescents with cerebral palsy. *Dev. Med. Child Neurol.* 54, 1044–1049. doi: 10.1111/j.1469-8749.2012.04401.x

Roth, E. J., Merbitz, C., Mroczck, K., Dugan, S. A., and Suh, W. W. (1997). Hemiplegic gait: relationships between walking speed and other temporal parameters. *Am. J. Phys. Med. Rehabil.* 76, 128–133. doi: 10.1097/00002060-199703000-00008

Selzer, M., Clarke, S., Cohen, L., Dumcan, P., and Gage, F. (2006). *Textbook of Neural Repair and Rehabilitation," Medical Neurorehabilitation*. Cambridge: Cambridge University Press.

Sheffler, L. R., and Chae, J. (2015). Hemiparetic Gait. *Phys. Med. Rehabil. Clin. North Am.* 26, 611–623. doi: 10.1016/j.pmr.2015.06.006

Stewart, J. D. (2008). Foot drop: where, why and what to do? *Pract. Neurol.* 8:3. doi: 10.1136/jnnp.2008.149393

Van Der Linden, M. L., Hazlewood, M. E., Hillman, S. J., and Robb, J. E. (2008). Functional electrical stimulation to the dorsiflexors and quadriceps in children with cerebral palsy. *Pediatr. Phys. Ther.* 20, 23–29. doi: 10.1097/PEP.0b013e31815f39c9

Voigt, M., and Sinkjaer, T. (2000). Kinematic and kinetic analysis of the walking pattern in hemiplegic patients with foot-drop using a peroneal nerve stimulator. *Clin. Biomech.* 15, 340–351. doi: 10.1016/s0268-0033(99)00082-0

Wall, J. C., and Turnbull, G. I. (1986). Gait asymmetries in residual hemiplegia. *Arch. Phys. Med. Rehabil.* 67, 550–553.

Winter, D. A. (1992). Foot trajectory in human gait: a precise and multifactorial motor control task. *Phys. Ther.* 72, 45–53; discussion54–56.

Winters, T. F., Gage, J. R., and Hicks, R. (1987). Gait patterns in spastic hemiplegia in children and young adults. *J. Bone Joint Surg. Am.* 69, 437–441. doi: 10.2106/00004623-198769030-00016

Yan, T., Hui-Chan, C. W., and Li, L. S. (2006). [Effects of functional electrical stimulation on the improvement of motor function of patients with acute stroke: a randomized controlled trial]. *Zhonghua Yi Xue Za Zhi* 86, 2627–2631.

Conflict of Interest Statement: The authors declare that the research was conducted in the absence of any commercial or financial relationships that could be construed as a potential conflict of interest.

frontiers in Neuroscience

ORIGINAL RESEARCH
published: 25 May 2020
doi: 10.3389/fnins.2020.00416

Exoskeleton Walk Training in Paralyzed Individuals Benefits From Transcutaneous Lumbar Cord Tonic Electrical Stimulation

Elena Y. Shapkova[1,2], Elena V. Pismennaya[3], Dmitriy V. Emelyannikov[1] and Yury Ivanenko[4]*

[1] The Spinal Center of Saint-Petersburg State Research Institute of Phthisiopulmonology, Saint Petersburg, Russia, [2] Institute of Translational Biomedicine, Saint Petersburg State University, Saint Petersburg, Russia, [3] Institute of Mechanics, Lomonosov Moscow State University, Moscow, Russia, [4] IRCCS Santa Lucia Foundation, Rome, Italy

In recent years, advanced technologies featuring wearable powered exoskeletons and neuromodulation of lumbosacral spinal networks have been developed to facilitate stepping and promote motor recovery in humans with paralysis. Here we studied a combined effect of spinal cord electrical stimulation (SCES) and exoskeleton walk training (EWT) during an intensive 2-week rehabilitative protocol in spinal cord injury individuals (n = 19, American Spinal Injury Association Impairment Scale (AIS) A-11, B-5, C-3). The purpose of this study was to evaluate the compatibility of methods and to explore the main effects of combined SCES and EWT. All participants had a chronic state of paralysis (1–11 years after trauma). In addition, in the control group (n = 16, AIS A-7, B-5, C-4), we performed EWT without SCES. For EWT, we used a powered exoskeleton (ExoAtlet), while stability was assisted by crutches, with automatic arrest of stepping if excessive torques were detected. SCES was applied to the level of the mid-lumbar cord over the Th12 vertebra at 1 or 3 pulses/s (4 individuals with severe spasticity were also stimulated in an anti-spastic mode 67 pulses/s). The vertical component of the ground reaction force was recorded using the F-Scan system at the onset and after training with SCES. EWT with SCES significantly increased the foot loading forces, could decrease their asymmetry and 8 out of 19 subjects improved their Hauser Ambulation Index. The anti-spastic mode of stimulation also allowed individuals with severe spasticity to walk with the aid of the exoskeleton. Participants reported facilitation when walking with SCES, paresthesia in leg muscles and new non-differential sensation of passive motion in leg joints. Neurological examination showed an increase of tactile (7) and/or pain (7) sensation and an increase of the AIS motor scale in 9 individuals, including both incomplete and complete paralysis. Improvements in the neurological scores were, however, limited in the control group (EWT without SCES). The results suggest that SCES may facilitate training and walking in the exoskeleton by activating the locomotor networks and augmenting compensative sensitivity.

Keywords: spinal cord injury, exoskeleton, spinal cord electrical stimulation, spasticity, locomotion, neurorehabilitation

OPEN ACCESS

Edited by:
Jose Luis Contreras-Vidal, University of Houston, United States

Reviewed by:
Filipe Oliveira Barroso, Consejo Superior de Investigaciones Científicas (CSIC), Spain
Leonardo Gizzi, University of Stuttgart, Germany
Antonio J. del-Ama, Rey Juan Carlos University, Spain

****Correspondence:***
Elena Y. Shapkova
eyshapkova@gmail.com

Specialty section:
This article was submitted to Neuroprosthetics, a section of the journal Frontiers in Neuroscience

Received: *09 September 2019*
Accepted: *06 April 2020*
Published: *25 May 2020*

Citation:
Shapkova EY, Pismennaya EV, Emelyannikov DV and Ivanenko Y (2020) Exoskeleton Walk Training in Paralyzed Individuals Benefits From Transcutaneous Lumbar Cord Tonic Electrical Stimulation. Front. Neurosci. 14:416. doi: 10.3389/fnins.2020.00416

INTRODUCTION

In the last decade, interest has grown around the use of exoskeleton-induced walk for the rehabilitation of paralyzed patients. Exoskeletons (Exo) have been shown to enable over-ground weighted walking and gait training for the mobility impaired persons, particularly for individuals with spinal cord injury (SCI) (del-Ama et al., 2012; Sylos-Labini et al., 2014; Onose et al., 2016). Single case reports of supplemental functional stimulation of leg muscles (Ekelem and Goldfarb, 2018) and spinal cord neuromodulation (Gad et al., 2017) during Exo-assisted gait have shown improved kinematics and muscle activity patterns in motor complete SCI individuals. Nevertheless, the efficacy of Exo training for individuals with SCI is still under discussion (Contreras-Vidal et al., 2016; Fisahn et al., 2016; Scivoletto et al., 2019).

Earlier works suggested a beneficial effect of spinal cord electrical stimulation on activating spinal locomotor circuits (Dimitrijevic and Larsson, 1981; Shapkov et al., 1996) and controlling spinal spasticity (Richardson and McLone, 1978; Siegfried et al., 1978; Vodovnik et al., 1984). The effectiveness of different stimulation parameters has also been explored (Iwahara et al., 1992; Dimitrijevic et al., 1998; Shapkova, 2004). In our clinic, for more than 25 years we have been developing a method of transcutaneous spinal cord electrical stimulation (SCES) to activate the neuronal locomotor networks in paralyzed individuals (Shapkov et al., 1996; Shapkova and Schomburg, 2001; Shapkova, 2004). In particular, we demonstrated that application of tonic (either epidural or transcutaneous) electrical stimulation at the mid-lumbar enlargement (about L3-L5 spinal segments, Th12 vertebrae) could evoke well-coordinated, alternating, step-like movements in individuals with complete and incomplete paralysis (Shapkova, 2004). Because the frequency of "stepping" was generally independent of the SCES frequency and rhythmic movements could continue for many cycles after the end of stimulation, the induced activity was considered to be centrally generated by activating the spinal pattern generation circuitry. Using such approaches, many researchers have put significant effort into assessing and modulating the functional state of the spinal locomotor circuits in humans (Mayr et al., 2016; Ivanenko et al., 2017; Gill et al., 2018; Hofstoetter et al., 2018; Taccola et al., 2018; Wagner et al., 2018; Megía García et al., 2020). Similar concepts have been developed using animal models (Musienko et al., 2012; Lavrov et al., 2015; Wenger et al., 2016). Epidural stimulation is typically more localized and requires less current of stimulation, while transcutaneous stimulation is non-invasive, although both techniques seem to largely activate the posterior root fibers (even if it is difficult to fully rule out that the stimulation is also acting on the neural circuitry in the cord) (see Hofstoetter et al., 2018 for a review). Since common neural structures are activated by epidural and transcutaneous lumbar spinal cord stimulation with a similar effect (Hofstoetter et al., 2018), the use of non-invasive SCES has become widely spread over for both basic and clinical research (Shapkova, 2004; Gerasimenko et al., 2015; Hofstoetter et al., 2015; Mayr et al., 2016; Solopova et al., 2017; Barroso et al., 2019).

In the context of looking for adaptive therapies for entraining the spinal locomotor circuitry, it may be of interest to explore the effect of combined interventions since the efficiency of SCES at rest might be limited without a concurrent locomotor function training, which may entrain activity-dependent plasticity of spinal neuronal networks. A combination of two highly intensive methods, such as powered exoskeleton walk training (EWT) and spinal cord electrical stimulation, stimulating afferent and efferent inputs within a functional task, may lead to effective neural plasticity that provides a basis for recovery. Therefore, the purpose of this study was to evaluate the compatibility of methods and to explore the main effects of combined SCES and EWT. To this end, thirty five participants with complete and incomplete SCI were enrolled in this exploratory study and were grouped according to the stimulation (frequency of SCES) method.

MATERIALS AND METHODS

Participants

Thirty five adults with traumatic chronic SCI participated in this study (10♀, 25♂, post-trauma period from 1 to 11 years). **Figure 1A** illustrates a general scheme of participants' groups and **Table 1** shows the characteristic of participants. The criteria for inclusion were: SCI with paralysis estimated as class A, B, or C of American Spinal Injury Association Impairment Scale (AIS); decompression and stabilization of spine in anamnesis, confirmed by MRI and/or CT data; post-trauma period more than 12 mo; age within 18–55 years; ability to stand for 30 min without pathological orthostatic reactions; high motivation to motor recovery; written informed consent to participate in the study. The exclusion criteria were: low extremities' bone fractures within post-trauma period; the thrombosis in the vessels of lower extremities (ultrasound or Doppler data); decubitus or maceration of the skin; other neurological diseases. All subjects gave written informed consent. This study was reviewed and approved by the Ethics Committee of the Saint-Petersburg State Research Institute of Phthisiopulmonology and carried out in accordance with the Declaration of Helsinki.

Nineteen volunteers [4♀, 15♂, 31.2 ± 8.6 years (mean ± SD)] performed EWT with SCES (Groups 1–3). Fifteen participants had a lesion at thoracic level, two participants at thoracic-lumbar level, two participants at low-cervical level with partly/mostly saved functions of the arms. According to ASIA standards, neurological state of participants was estimated as class A (11), B (5), and C (3) (**Table 1**). The functional mobility of participants varied from 0 to 7 (3.7 ± 1.7, Rivermead Mobility Index), activities of daily living – from 8 to 90 (on average 57.8 ± 20, Barthel Index). For ambulation, all subjects used a wheelchair: ambulation was estimated as 8 and 9 by the Hauser Index (restricted to wheelchair) in 13 individuals, and as 7 (walking limited to several steps with bilateral support, less than 8 m, using a wheelchair for most activities) in 6 persons.

Sixteen participants (6♀, 10♂, 33.3 ± 9.3 years, AIS A-7, B-5, and C-4 individuals) performed EWT without SCES (Group 4, 12 training sessions), with similar inclusion/exclusion criteria and limitation for the level of spasticity MAS $\leq$ 3 (Modified Ashworth

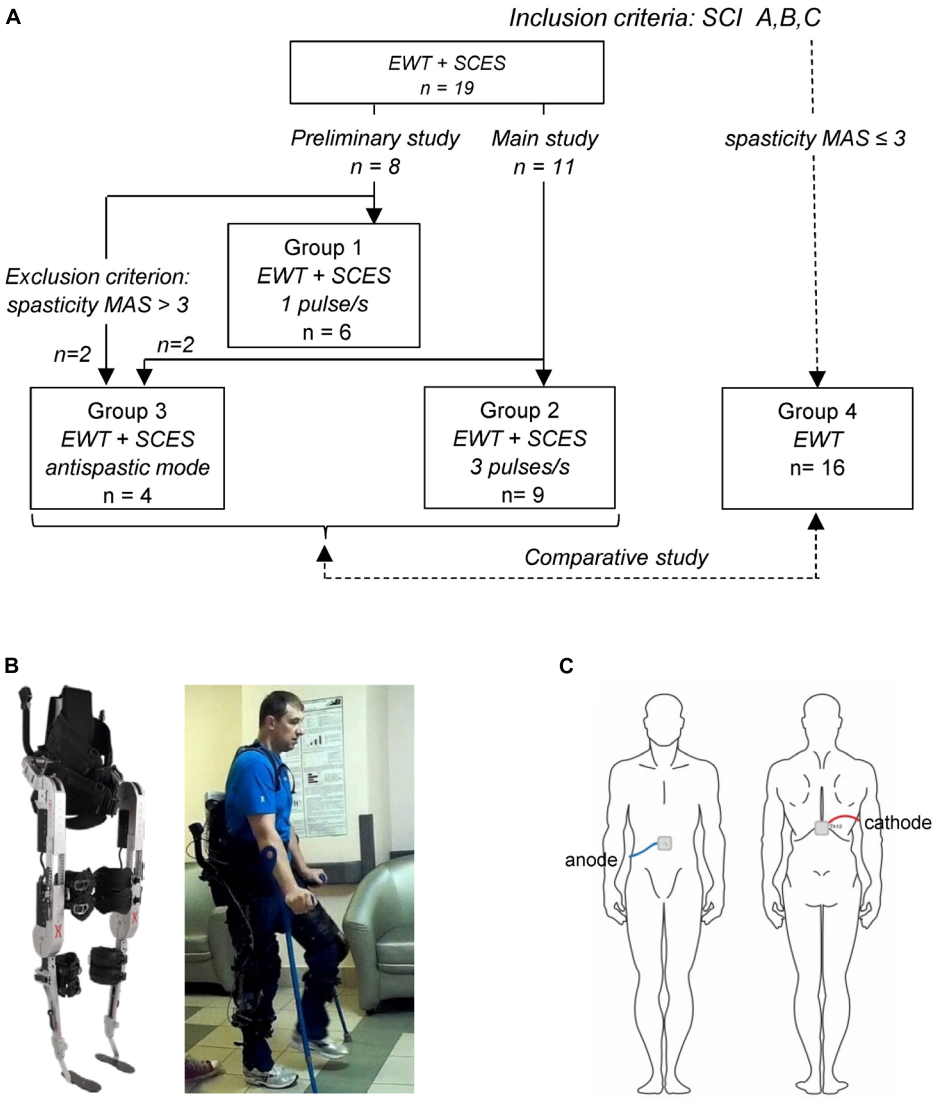

FIGURE 1 | Experimental setup. **(A)** General scheme of participant groups and corresponding inclusion criteria. **(B)** Wearable powered exoskeleton (left) and an example of walking in the exoskeleton in the SCI participant (P12, AIS B, 11 years post-injury, see **Table 1**) without the assistance of the physiotherapist at the end of 2-week training (written informed consent was obtained from the individual for the publication of this image). The exoskeleton is attached to the wearer at five main locations: footplate, shank, thigh, pelvis, and torso. In each leg, hip flexion/extension and knee flexion/extension) are powered by actuators, providing appropriate kinematics of joint angle motion, 8 different walking modes and 3 speeds (corresponding to the cycle duration of T = 3, 4, or 5 s), and an automatic arrest of stepping if excessive torques are detected. **(C)** Schematic illustration of electrode placements.

Scale). Most participants had a lesion at thoracic level (n = 12), three at thoracic-lumbar level, and one at low-cervical high-thoracic level with mostly unimpaired functions of the arms. The functional mobility of participants varied from 2 to 4 (3.1 ± 0.6, Rivermead Mobility Index), activities of daily living – from 40 to 90 (on average 63.4 ± 13.8, Barthel Index), and the Hauser Ambulation Index was estimated as 7 (7) and 8 (9) (**Table 1**).

Walking in the Exoskeleton

Wearable exoskeleton ExoAtlet Global is designed to empower lower limb disable people to walk on level ground (European patent WO 2017/069652 A1, Berezij et al., 2017)[1]. The exoskeleton weighs 23 kg including battery and it bears its own weight by transferring the weight via its footplates to the ground. It is attached to the wearer at five main locations: footplate, shank, thigh, pelvis, and torso (**Figure 1**). Its shank, thigh and foot segment lengths and pelvic widths can be accommodated to different subject height/statures (weight up to 100 kg and height 1.55–1.95 m). Footplates are made of carbon fiber to host human feet (**Figure 1B**) so that one degree of freedom (ankle dorsi/plantar flexion) is passively sprung with

[1]https://www.exoatlet.com/en

TABLE 1 | General information about the participants of the study.

Patient	Gender	Age, years	Level of spine damage	Level of spinal cord damage	Duration of paralysis, yrs	Rivermead Mobility Index	Barthel Index	AIS	AIS motor before/ after training	AIS sensory LT before/ after training	AIS sensory PP before/ after training	Muscle tone, for spasticity: MAS before and after training	# of training sessions	# of training sessions with SCES	Total training duration, min	Averaged session duration, min	Walk duration, min	Max non-stop walk, min	Previous experience	Hauser Ambulation Index (0–9) before/ after training
Group 1 (1 pulse/s SCES)																				
P1	Ì	37	Th9	D9	1.5	4	65	A	0/0	60/60	60/60	Spastic R2/2, L2/2	15	9	872	58	380	8.7	SCES	**8/7**
P2	F	33	Th4-5	D4	4.8	3	30	A	0/0	**44/48**	**46/48**	Normal R0/0, L0/0	13	7	625	48	262	5.3	–	8/8
P3	Ì	21	Th5-7	D4	2	0	25	A	1/1	**40/43**	43/43	Spastic R2/3, L2/3	13	7	785	60	265	9.5	–	8/8
P4	Ì	37	Th12-L1	D10-12	2.5	4	75	C	19/19	**87/90**	**87/90**	Low	12	8	743	62	394	15.2	SCES	**7/6**
P5	Ì	38	Th10-12	D10	6	4	60	A	0/0	64/64	64/64	Low	12	8	616	51	315	21.5	–	8/8
P6	F	55	Ñ6-7	C8	10	3	60	B	0/0	74/74	42/42	Low	8	7	294	37	166	3.5	–	**9/8**
mean ± SD													13	8	656 ± 202	53 ± 10	297 ± 85	10.6 ± 6.7		
Group 2 (3 pulses/s SCES)																				
P7	Ì	38	Th10	D9	2.5	3	65	A	**0/1**	62/62	64/64	Spastic R1/0, L1/0	10	9	432	43	302	37.6	EXO, SCES	**7/6**
P8	F	34	Th5	D4	6	3	60	A	**0/1**	44/44	44/44	Normal R0/0, L0/0	10	8	428	43	278	37.2	EXO, SCES	8/8
P9	Ì	20	Th5-6	D4	11	3	65	À	6/6	78/78	66/66	Low with distal clonus	10	9	395	40	271	21.5	SCES	8/8
P10	Ì	21	Th5	D5	4	4	55	A	**0/1**	44/44	**44/45**	Spastic R3/3, L3/2	9	9	348	39	205	25.4	EXO, SCES	8/8
P11	Ì	32	Th5-6	D4	4.5	2	60	À	0/0	44/44	44/44	Low with distal clonus	10	8	415	42	274	23.8	SCES	8/8
P12	Ì	37	Th12, L1-2	L2	11	3	75	B	**6/9**	107/107	103/103	Low	7	7	460	66	380	185.0	EXO	8/8
P13	F	27	Th10	D11	3	7	75	B	**0/3**	**89/91**	**91/93**	Low with distal clonus	10	9	404	40	286	40.8	EXO	**7/6**
P14	Ì	20	Th5-6	D7	2	7	90	B	0/0	58/58	58/58	Spastic R3/3, L2/2	7	6	223	33	137	18.4	EXO	**7/6**
P15	Ì	24	Th12	L2	1.5	7	65	C	**12/13**	**98/100**	**100/102**	Spastic R1/1, L1 + /1 +	9	7	226	25	157	21.9	EXO	**7/6**
mean ± SD (*excluding P12)													9	8	370 ± 88	41 ± 11	255 ± 76	28.3 ± 8.2*		
Group 3 (67 + 3 pulses/s SCES)																				
P16	Ì	27	Th5-8	D6	9	3	50	A	0/0	**60/63**	**60/63**	Spastic R4/3, L4/3	11	8	766	70	278	8.15	–	8/8
P17	Ì	28	Th5-7	D5	1.5	3	40	Â	**0/3**	68/68	**56/58**	Spastic R4/3, L4/4	10	9	408	41	279	31.7	EXO, SCES	8/8
P18	Ì	31	Th7	D7	1	3	8	À	**0/2**	52/52	52/52	Spastic R4/3, L4/3	11	10	507	46	388	40.4	EXO, SCES	8/8
P19	Ì	32	C5-7, Th1	D3	4	4	75	C	**12/14**	**110/112**	75/75	Spastic R4/3, L4/3	9	8	308	34	204	14.2	SCES	**7/6**
mean ± SD													10	9	497 ± 197	48 ± 15	287 ± 76	23.6 ± 15.0		

(Continued)

TABLE 1 | Continued

Patient	Gender	Age, years	Level of spine damage	Level of spinal cord damage	Duration of paralysis, yrs	Rivermead Mobility Index	Barthel Index	AIS	AIS motor before/ after training	AIS sensory LT before/ after training	AIS sensory PP before/ after training	Muscle tone, for spasticity: MAS before and after training	# of training sessions	# of training sessions with SCES	Total training duration, min	Averaged session duration, min	Walk duration, min	Max non-stop walk, min	Previous experience	Hauser Ambulation Index (0–9) before/ after training
Group 4 (control, without SCES)																				
P20	M	36	Th7	D11	3	3	55	A	0/0	73/73	73/73	LOW with distal clonus	12	0	526	44	422	39	–	8/8
P21	M	28	Th12	L1	2	3	55	B	2/2	78/78	78/78	Spastic R1/1,L1/1	12	0	479	40	384	40	–	7/7
P22	M	44	Th12	L3	6	3	55	C	**17/18**	**88/90**	**90/92**	Spastic R2/2,L3/2	12	0	469	39	390	39	–	7/7
P23	M	33	Th12-L1	L2	11	4	85	C	16/16	94/94	92/92	Low	12	0	502	42	419	41	–	7/7
P24	F	20	Th5-6, Th9-10	D4	2	4	65	A	52/52	44/44	69/69	Normal R0/0,L0/0	12	0	581	48	381	24	–	8/8
P25	M	38	C7-Th1	D3	10	4	90	B	2/2	68/68	35/35	Spastic R3/3,L3/3	12	0	377	31	290	32	–	**7/6**
P26	M	38	Th12	D7	10	4	75	A	12/12	88/88	88/88	Low	12	0	462	39	400	42	–	**7/6**
P27	F	39	Th12	D12	10	3	45	A	0/0	74/74	72/72	Low	12	0	304	25	221	27	–	8/8
P28	M	44	Th12	L1	5	3	65	C	78/78	78/78	**63/67**	Spastic R1+/1+, L1+/1+	12	0	347	29	166	17	–	8/8
P29	F	27	Th3	D1	7	2	40	A	0/0	42/42	40/40	Spastic R3/3,L3/3	12	0	450	37	306	26	–	8/8
P30	F	18	Th12-L1	L1	5	3	65	B	6/6	78/78	78/78	Low	12	0	359	30	280	41	–	7/7
P31	F	21	Th11-L1	D10	4	3	75	B	0/0	72/72	64/64	Low	12	0	387	32	272	17	–	7/7
P32	F	27	Th7	D7	7	3	60	B	0/0	82/82	52/52	Spastic R3/3,L3/3	12	0	237	20	114	12	–	8/8
P33	M	49	Th7-9	D10	2	2	55	C	15/15	**72/82**	64/64	Spastic R3/3,L3/3	12	0	222	19	138	16	–	8/8
P34	M	41	Th6-7	D7	2	3	75	A	1/1	64/64	57/57	Spastic R1/1,L1/1	12	0	411	34	340	33	–	8/8
P35	M	30	Th8-9	D8	3	3	55	A	0/0	**58/60**	58/58	spastic R2/2,L0/2	12	0	437	36	285	14	–	8/8
mean ± SD													12	0	409 ± 100	34 ± 8	300 ± 100	28.8 ± 11.0		

*AIS, American Spinal Injury Association Impairment Scale (LT, light touch; PP, pin-prick), MAS, Modified Ashworth Scale before/after training for both right (R) and left (L) sides. Previous experience of SCES refers to ∼2–3 weeks of SCES (∼1 h per day) in the supine position, ∼1 year prior to the study, to activate the spinal locomotor networks. Previous experience of EXO refers to advanced EXO-walkers (practice for ∼6–12 months) with no experience in SCES. Previous experience of "EXO, SCES" refers to experience in both SCES and EWT ∼1 year prior to this study. We marked in bold changes in neurological indicators (AIS) and in the Hauser Ambulation Index after training. *Patient (P12) was excluded from calculating the max non-stop walk (marked by the asterisk) because of his outstanding personal results (outlier).*

certain stiffness (150 Nm/rad). The control of the exoskeleton is initiated/performed via a PC tablet or a "smart crutch" for experienced users. The control system of the ExoAtlet is unique and allows different functions and control modes: it collects data from body angles, allows to set the height and length of the step, sitting, performing sit-to-stand, standing still, stepping in place, level walking with different cycle durations, walking on angled surface, stepping over obstacles, and comfortable walking up and down stairs (Berezij et al., 2017; Pais-Vieira et al., 2020). Comparative characteristics of the exoskeleton ExoAtlet can be found in a review (Onose et al., 2016). In each lower limb, hip flexion/extension and knee flexion/extension are powered by actuators, providing appropriate kinematics of joint angle motion. The walking trajectories during the swing phase (reference joint angles) were defined based on ensemble-averaged walking patterns of 8 neurologically intact individuals during normal overground walking at the natural self-selected speed, recorded by means of a 16-cameras Vicon system at 120 Hz (Oxford, United Kingdom) (Berezij et al., 2017). The swing phase durations were similar across conditions, however, other parameters could vary in order to allow the SCI participants to incrementally increase their performance with training by selecting shorter cycle durations and/or longer stride lengths. Hip and knee flexion angles were decreased (scaled) during swing (relative to the reference trajectories recorded in neurologically intact individuals) to ensure more stable walking of paralyzed individuals, so that the selected program for stepping determined the kinematics of the Exo-gait with three different stride lengths (about 0.6, 0.75, and 0.9 m) and three different cycle durations (3, 4, and 5 s). Sensors built into each motor provide an automatic arrest of stepping if excessive torques (exceeding by 40% the reference hip or knee joint torques during walking in the exoskeleton in neurologically intact individuals) are detected (Berezij et al., 2017). The reference hip/knee joint torques were defined based on ensemble-averaged joint torques of neurologically intact individuals walking in the exoskeleton, recorded by means of torque sensors of the exoskeleton (Berezij et al., 2017). The exoskeleton was designed to walk with crutches (since it cannot provide full balance), which can bear a significant portion of body weight since SCI individuals use their upper limbs and body to assist foot loading and stepping. The design also included two rear handholds for one or two assistants for physical help and/or safety (typically used in the initial sessions but not for advanced pilots, see **Supplementary Videos**). An example of walking in the exoskeleton in the SCI subject before and after EWT with SCES is illustrated in **Figure 1B** and **Supplementary Videos**.

Electrical Stimulation of the Spinal Cord

The stimulation method is thoroughly described in our previous studies (Shapkova and Schomburg, 2001; Shapkova, 2004). SCES was applied to the level of the mid-lumbar cord using the Viking Select stimulator (United States), the pair of conductive self-adhesive electrodes (3 cm× 4 cm) being placed on the skin over the Th12 vertebra (cathode) and centrally on the abdomen (anode) (**Figure 1C**). Once electrodes were mounted, the participant was placed in the supine position to determine the intensity of SCES. The magnitude of SCES (0.5 ms monophasic square-wave pulses) was about 1.3–1.4 of motor threshold in leg muscles. To determine the motor threshold, the electromyographic (EMG) activity was recorded bilaterally in 4 muscles (RF, rectus femoris; BF, biceps femoris; GL, gastrocnemius lateralis; TA, tibialis anterior), and the stimulation intensity was adjusted using 3 mA increments until a response was observed in at least 4 muscles (in some SCI individuals, not all muscles could be activated, see section "Results"). EMG activity was recorded at 2 kHz using bipolar surface electrodes (Nicolet Viasys Viking Select EMG System, United States). If leg muscle responses were low/absent or required too high amplitude currents (>70 mA), we considered the visible response of the abdominal muscles (multisegmental muscle responses were absent in two participants). In the anti-spastic mode, the magnitude of SCES was below the motor threshold. All SCES-procedures were painless. Some participants had previous experience of SCES and/or EWT (**Table 1**). We grouped participants according to the frequency of SCES (**Table 1**) and below we summarize the experimental procedure.

For our tasks, we set the frequency of SCES to 1 (Group 1), 3 (Group 2), and 67 (Group 3) pulses/s. In addition, in the control group (Group 4), we performed EWT without SCES. A general scheme of participant groups is illustrated in **Figure 1A**. First (in the preliminary study), in Group 1 of participants (**Figure 1A** and **Table 1**), with SCES at 1 pulse/s, we evaluated the compatibility of EWT and SCES in the context of potential disturbing influences and benefits, taking in account its strong influence on excitability of motor neurons and potential disturbing effects on body balance. Indeed, electrical stimulation *per se* may evokes perceptual or mechanical disturbing effects (for instance, it stimulates erector spinae and abdominal muscles), as well as even low frequency stimulation at 1 Hz may facilitate motor responses (Shapkova, 2004; Solopova et al., 2014). The rationale for using SCES at 3 pulses/s (Group 2, main study, **Figure 1A**) was to activate the spinal pattern generator networks (Shapkova and Schomburg, 2001; Shapkova, 2004). This frequency has been shown also to be effective in evoking stepping in the decerebrate cat (Iwahara et al., 1992). However, in the first session, two participants from the preliminary study and two participants from the main study were unable to use the exoskeleton because of severe spasticity (MAS 4) since the exoskeleton arrested after a few steps. These participants were excluded from Group 1 and 2, and formed Group 3 (**Figure 1A**). In this group, to perform EWT, we applied an anti-spastic SCES at 67 pulses/s beginning from the second or third session. After 2–3 sessions with 67 pulses/s, we used an alternating (changing every 10 min) stimulation at 67 pulses/s (to suppress spasticity, Pinter et al., 2000; Hofstoetter et al., 2014) and 3 pulses/s (to activate spinal locomotor networks, Shapkova, 2004). Using this stimulation method, they were able to complete the whole training program (9–11 training sessions with a comparable session duration as in Group 1 and 2, **Table 1**) and were included in the analysis as Group 3.

Exoskeleton Walk Training With SCES

The study included short (∼2 weeks) intensive rehabilitative period of exoskeleton walk training with transcutaneous

electrical stimulation of the spinal cord. All subjects received daily 40 min SCES in the stationary (supine) position prior to the EWT session. All participants were clinically stable at the time of examination and capable of walking in the exoskeleton with crutches and with the assistance of physiotherapist. The novices begun the course with learning to wear the exoskeleton, to stand up and sit down, to stand with crutches, to step in place and to walk straight. In the initial sessions, they required assistance by two or three physiotherapists. The number of sessions needed for novices to achieve independent stable walking with the exoskeleton was about 3–6 (**Table 1**). When a participant demonstrated stable walk with one assistant for safety (from the 3–6 session for novices, and from the first or second session for experienced exoskeleton walkers), electrical stimulation of the spinal cord was applied during EWT. On average, the total number of sessions over the 2 weeks of training was 7–15 depending on the subject, and the total duration of walking in the exoskeleton was ∼250–300 min. Participants in each group received about 8 sessions (range 6–10) of combined EWT and SCES (**Table 1**). The total session duration (wearing the exoskeleton), the duration of walking and the maximal non-stop walk duration per each subject are described in **Table 1**.

Neurological Examination and Biomechanical Measurements

Spinal cord injury participants were admitted to the hospital for the purposes of this study and were submitted to neurological evaluation, routine radiological and neurophysiological tests. Radiological tests included available neuroimaging techniques of the spine and the spinal cord (CT, MRI). Neurological examination was performed before and after the training course using the American Spinal Injury Association Impairment Scale (AIS), spasticity – by the Modified Ashworth Scale (MAS), and ambulation was estimated using the Hauser Ambulation Index (HAI). Spinal motoneurons excitability was assessed by evaluating H-reflex responses (in the lateral gastrocnemius muscle of both legs), and the multisegmental muscle responses (in the rectus femoris, biceps femoris, lateral gastrocnemius, and tibialis anterior) to the electrical stimulus (0.5 ms) applied between vertebras Th11-12 (Emeliannikov et al., 2016). The GL H-reflex was evoked by stimulation of n. tibialis in popliteal fossa (0.5 ms). H-reflex and multisegmental muscle responses were recorded consecutively, without changing EMG electrodes position, on diagnostic complex Viking Select (Nicolet, United States). For the H-reflex, the peak-to-peak amplitude of the M-wave (over the 5–20 ms period after the stimulus) and the H-reflex (25–60 ms after the stimulus) was calculated from each sweep (Solopova et al., 2003; Emeliannikov et al., 2016). Using 5 mA increments, the stimulation intensity was incrementally adjusted from 5 mA to ∼100 mA and the H_{max}/M_{max} ratio was also computed.

The vertical component of the ground reaction force was recorded in 13 participants by means of in-shoe sensors using the F-Scan System (Tekscan, United States) in two circumstances: the first time when the participants were able to perform stable exoskeleton-induced walking with one assistant for safety and second time after 6–7 sessions of training in the presence of SCES. The individual sensor elements of the F-Scan System were elastic and arranged in a matrix insole. The local vertical force sensed by each element was recorded at 100 Hz. The insole was interposed between the participant's foot and the sole of the shoes. Before each trial, the mean level of each sensor was measured while the foot was unloaded (lifted) for 3–5 s and this value was used as a zero level. A measure for asymmetry index (ASI) (Kim and Eng, 2003; Aruin and Kanekar, 2013) was used to assess the GRF right-left symmetry (absolute value) between the participant's left (L) and right (R) limbs:

$$ASI = abs(L\text{-}R)/[0.5 \times (L + R)] \times 100\% \quad (1)$$

An ASI = 0 represents perfect symmetry. The max vertical feet loading (normalized to the body weight and averaged across strides, left and right side being pooled together) was also calculated.

Effects of EWT (with and without SCES) were assessed based on the results of neurological examination at the beginning and at the end of course (performed by an independent neurologist, not involved in the study). Due to unique individual variability, idiosyncrasies and the relationship between clinical factors and the extent to which rehabilitation potential is realized, some additional method details for individual subjects are provided in the Results. The descriptive statistics included means and standard deviation of the mean (SD). Repeated measures analysis of variance (RM ANOVA) was used (after determination that the data were normally distributed, Kolmogorov-Smirnov test) to assess the effect of EWT with SCES on changes in the foot loading force when walking in the exoskeleton with crutches. Given the heterogeneity of the sample and the treatments given, we mostly showed averaged data and we indicated individual neurological scores for all participants and groups. The characteristics of participants, neurological evaluation and durations of training are described in **Table 1**.

RESULTS

Learning to Walk in the Exoskeleton

While experienced exoskeleton walkers received SCES starting with the first or second session, novices required several sessions of training with the exoskeleton before we could apply SCES. After positioning the SCI participants in the upright posture, first, they were asked to learn to perform stepping in place movements and maintain balance while alternatingly loading the crutches with their upper limbs. After learning stepping in place movements, they were asked to walk forward along a 30-m walkway and could incrementally increase their performance with training. Specifically, we started EWT with the cycle duration 4–5 s and the shortest stride length (∼0.6 m). If the participant succeeded with stepping, we asked whether it would be comfortable for him/her to walk faster (i.e., to decrease the stride duration to 4 and 3 s and increase the stride length to ∼0.75 or 0.9 m) and, accordingly, we incrementally increased the walking speed throughout the course of 2-weeked EWT. Typical total duration of the experimental session was ∼1 h (**Table 1**). All

subjects showed strong motivation since the first trial and throughout testing.

While the kinematics of Exo-gait was determined by the appropriate control of the exoskeleton actuators (Berezij et al., 2017), its functioning also depended on the interaction between the exoskeleton program and activity of a pilot, who could "follow" or "resist" stepping performance. The exoskeleton contained multiple force sensors and the control program provided an automatic arrest of walking if excessive torques were detected. In this case, the control of the exoskeleton changed to the posture maintenance mode (fixed joint angles) preventing the subject from falling. Thus, there was a period of "learning" for the subject to produce a minimal influence on the robot and SCI participants first performed standard training of walking in the exoskeleton (without SCES) to achieve stable gait. In fact, the duration of non-stop walk was shorter in the first sessions with respect to the final sessions (see below). All SCI participants were able to walk in the exoskeleton with crutches and/or assistance of two or three physiotherapists in the initial sessions. When they accomplished relatively stable walking with one assistant for safety (after a few training sessions), SCES was applied during EWT in all remaining sessions. The participants of Group 3 accomplished walking in the exoskeleton only using an anti-spastic SCES at 67 pulses/s (or an alternating, changing every 10 min, stimulation at 67 pulses/s to suppress spasticity and 3 pulses/s to activate spinal locomotor networks).

Foot Loading in SCI Individuals During Walking in the Exoskeleton

Spinal cord injury participants achieved the control of balance holding the crutches, as well as being assisted by the physiotherapists in the initial sessions (see **Supplementary Videos**). During Exo-walking, the body weight is distributed between the feet and crutch support. The beginners rely more on crutches, whereas with experience the participants increase loading on the feet. An example of foot pressure recordings is illustrated in **Figures 2A,B** for subject P5 (AIS A). Note a significant increase in foot loading following EWT with SCES (**Figures 2A,B**). Local loadings of the plantar side of the foot were variable for different subjects. The coefficient of variation in the max foot loading across strides was similar before [7.5 ± 2.6% (mean ± SD across subjects)] and after (6.9 ± 2.5%) the training course though the GRF right-left asymmetry index (ASI) decreased from 25 ± 16% (range 3–60%) to 15 ± 9% (range 3–33%). However, overall, there was a significant increment of the max feet loading after 2 weeks of exoskeleton walk training with SCES across all subjects (RM ANOVA, $F = 16.2$, $p = 0.001$, $n = 13$, **Figure 2C**), likely related to a lesser support of the body weight by crutches and increments in the walking speed/cadence after training.

The time course of the net vertical ground reaction force varied across participants, from a simple bell-shaped trajectory (with the timing of the maximum force around midstance, **Figure 2B**) to a two-peaked profile with the two maxima at the beginning and the end of stance. The latter profile has an apparent similarity with the shape of the vertical GRF force curve

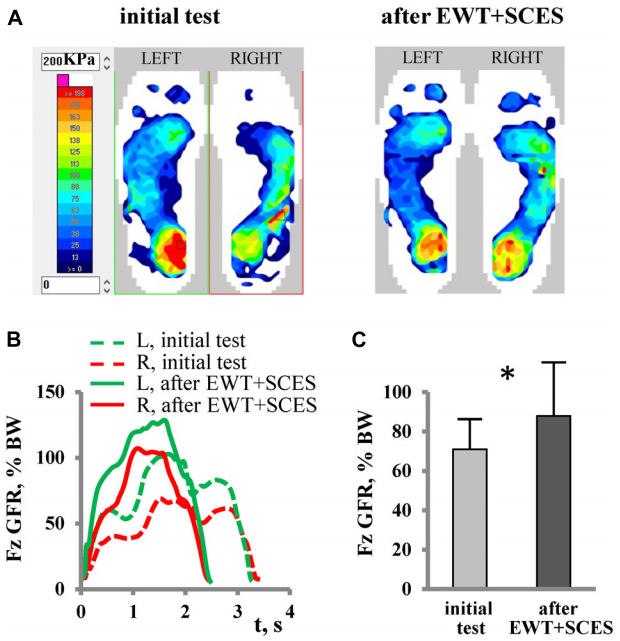

FIGURE 2 | Foot loading characteristics. **(A)** An example of plantar pressure recordings at the end of the stance phase (during maximum foot loading of the right leg and of the left leg) in subject P5 (AIS A, fracture at Th10-12, 6 years post-trauma) during the initial test (2nd session, left panel) and after EWT with SCES (8th session, right panel). **(B)** Vertical component of GRF (Fz) expressed in% of body weight (BW) during the stance phase (averaged across 12 strides) in the same subject. **(C)** Max vertical foot loading force across all recorded subjects (mean + SD, $n = 13$, left and right foot data were pooled together) during the initial test and after a short course of EWT with SCES (asterisk denotes significant difference, RM ANOVA, $F = 16.2$, $p < 0.001$, $n = 13$). Note more symmetrical loading of both feet **(A)** and a significant increase in the foot loading **(C)** following EWT with SCES.

during normal over-ground walking or at moderate levels of body weight support in neurologically intact individuals (Ivanenko et al., 2002), but it cannot be interpreted in the same way because of the extra support by crutches and/or a more "passive" nature of foot loading forces in SCI individuals (e.g., a lack of the power in the ankle joint extensors at the end of stance). For instance, the distribution of foot pressure at the end of the stance phase in most paraplegic subjects showed typical loading on both forefoot and heel areas (**Figure 2A**), while the anterior-posterior center-of-pressure excursion is substantial in neurologically intact individuals during stance and results in merely forefoot loading at push-off (Ivanenko et al., 2002).

Facilitation of Exoskeleton-Induced Walking and the Effect of Training

The most evident effect of SCES on stepping was observed in Group 3 (MAS∼4). In participants with severe spasticity, it was typically difficult to start the training session since the exoskeleton automatically stopped after a few steps due to an excessive resistance (**Figure 3**, upper panel). In two participants, muscle spasms occurred during the sit-to-stand transition before the Exo-walk started. To prevent this, the participants first

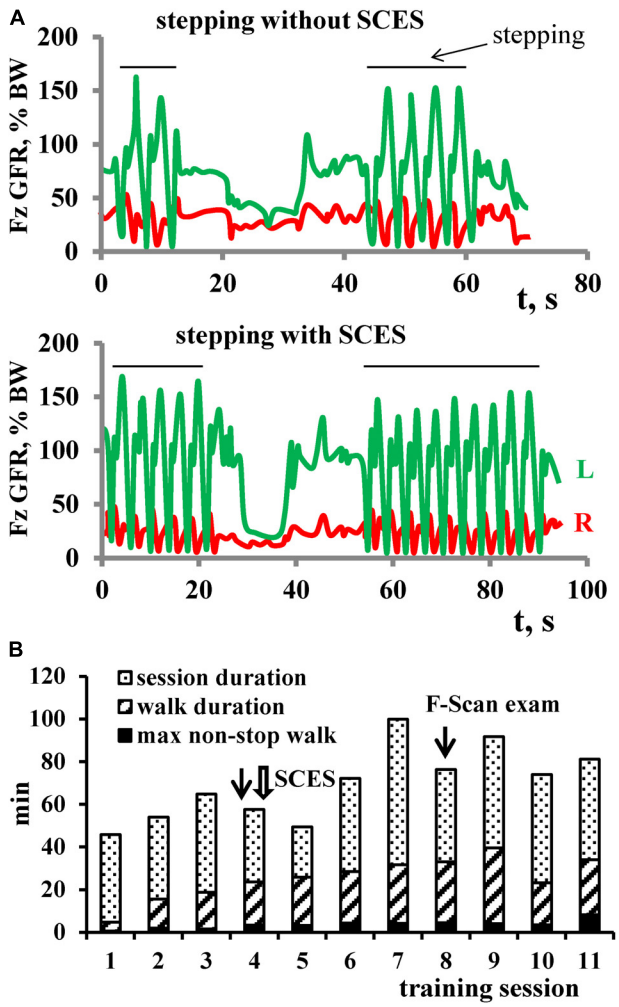

FIGURE 3 | Facilitation of stepping with SCES (in the anti-spastic mode) in subject P16 with severe spasticity (AIS B, MAS 4). **(A)** Examples of vertical GRF in the 4th session of EWT (1st session with SCES) without (upper panel) and with (lower panel) SCES. Each panel shows 2 attempts of stepping in the exoskeleton (indicated by horizontal lines), corresponding to the initial and final series of alternating foot loading, respectively. Note more steps performed with SCES. **(B)** Diagram of EWT across 11 sessions: session duration (column as a whole), total duration of walking (oblique stripes) and maximal non-stop walk duration (black). Session (#4), in which SCES started, is marked by a wide arrow. Sessions, in which F-Scan recordings were performed, are marked by thin arrows.

donned the exoskeleton in the supine position and then we placed them directly to the upright position avoiding a sit-to-stand maneuver. The application of SCES in the anti-spastic mode (67 pulses/s) immediately increased the number of Exo-steps (**Figure 3A**, lower panel). With training, the duration of the non-stop step sequences gradually increased (**Figure 3B**). In the first session with SCES, subject P16 increased the maximum non-stop duration from 22 to 50 strides and performed 122 strides at the end of the training course. Subject P19 increased the max non-stop duration from 34 to 121 strides beginning from the 3rd session and performed 284 strides (14 min) already in the 4th session. Subjects P17 and P18 performed up to 32 and 40 min of non-stop walking at the end of EWT.

Overall, the average duration of walking in Group 3 did not differ significantly from Group 1 and 2 (**Table 1**). The max non-stop duration in the Groups 3 and 2 was comparable (23.6 ± 15 min vs. 28.3 ± 8.2 min) and exceeded that of the Group 1 value (10.6 ± 6.7 min). Thus, application of SCES in the anti-spastic mode allowed individuals with severe spasticity to walk in the exoskeleton, and the amount of training within the course was comparable to other groups. Furthermore, it is also worth noting that, in all participants of the Group 3, the level of spasticity decreased after EWT with SCES (**Table 1**).

The positive effect of training was observed in both motor incomplete and complete paraplegic subjects. **Figure 4A** illustrates a diagram of training (lower left panel) and an example of changes in the foot pressure characteristics during EWT with SCES (right panels) in subject P4 with incomplete paraplegia. After 6 sessions of training, there was a twofold increase in the amplitude of GRF. Also, after EWT with SCES, P4 subject increased an ability to walk over-ground using a walker for support and balance (without exoskeleton) from 3 to 40 strides. The subject noted the emergence of paresthesia in leg muscles and new "feeling of support" with an increase of sensation (by + 3 AIS score for both light touch and pin-prick, **Table 1**).

All participants of the Group 1 and 2 also reported facilitation of exoskeleton walking when SCES was applied. The participants of the Group 1 (SCES at 1 pulse/s) attributed this facilitation to improvements in the sensitivity of the body below the lesion. Group 2 participants (SCES at 3 pulses/s) noted an ability to walk for a greater distance and/or with less fatigue. The latter could be illustrated in subject P12 (**Figure 4B**). P12 is actively engaged in sports, as an actual member of the National Russian Paralympic Team in curling. In the second training session with SCES, this participant improved his achievement of non-stop walking in the exoskeleton from 120 min (previous achievement) to 185 min and set the new record. After 6 sessions of training, the pressure under the feet increased and spread to the front part of the foot, and the amplitude of GRF increased from ∼75% BW up to ∼100–105% BW (**Figure 4B**). Also, at the end of EWT, his AIS motor scale increased by 3 points (from 6 to 9, **Table 1**).

Excitability of Spinal Motor Neurons

Excitability of the spinal motor neurons was assessed by the presence/amplitude of H-reflex responses and by the evoked multisegmental muscle responses to supramaximal electrical stimulus at the level of Th11-12 vertebrae. **Figure 5** illustrates an example of such responses before and after EWT with SCES. Excitability of the spinal motor neurons below lesion was observed in most SCI participants. In some subjects we failed to observe muscle responses: M- and H-responses in the lateral gastrocnemius muscle were not detected bilaterally in 2 subjects and the H-response was not found in 5 subjects (bilaterally in 4 subjects and unilaterally in 1 subject). After the training period, we detected the M-response in one of those subjects and the H-response in another one. The magnitude of the H-reflex varied within 0.1–3.2 mV across all subjects, and the H_{max}/M_{max} ratio – within 0.07-1.0. In 6 participants with an initially low H_{max}/M_{max}

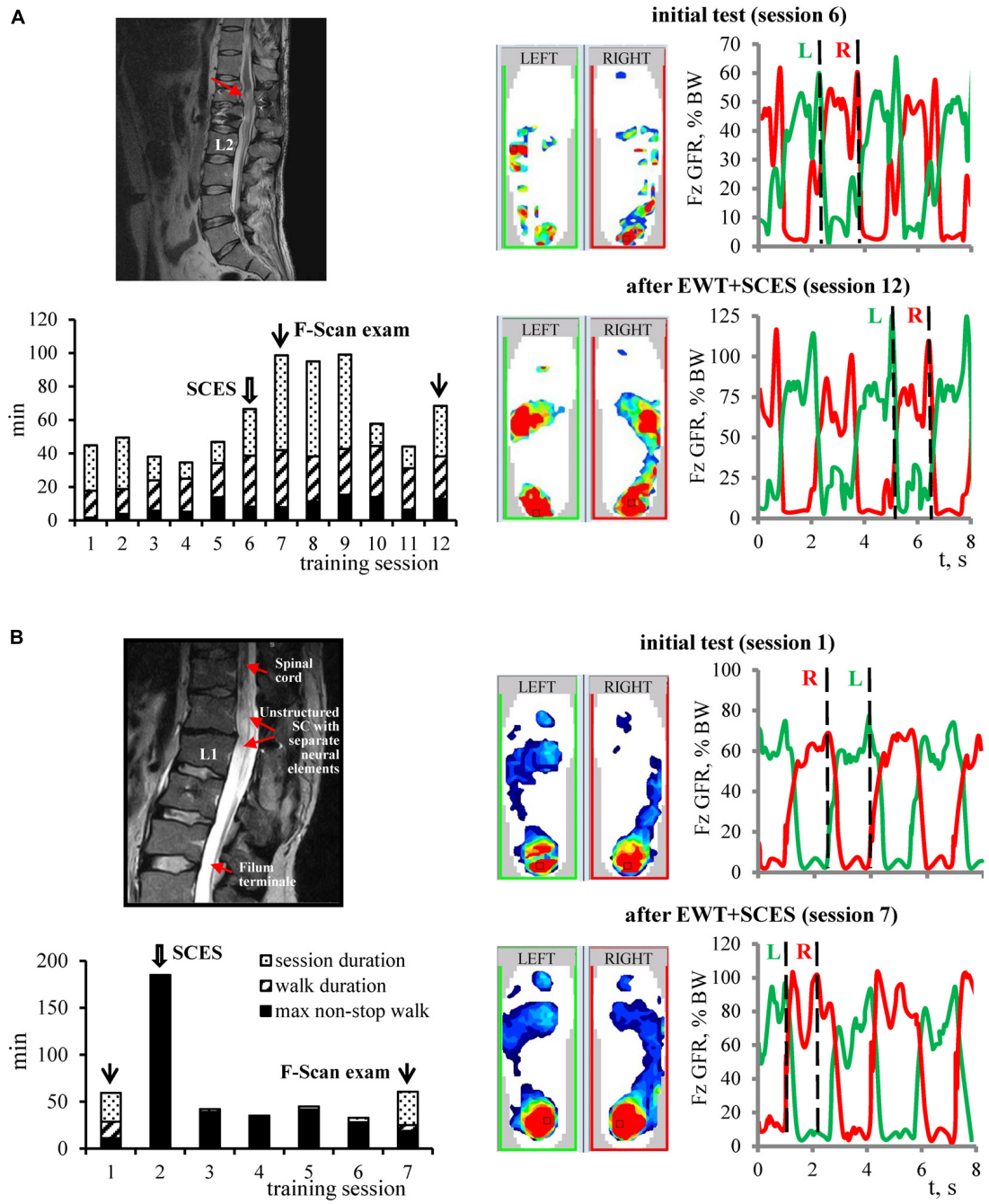

FIGURE 4 | Examples of changes in the foot pressure characteristics during EWT with SCES in subjects with motor incomplete **(A)** and complete **(B)** paraplegia. For each example: MRI image, diagram of EWT (same format as in **Figure 3B**), plantar pressure recordings and vertical foot loading forces (right) during the initial test and after EWT with SCES are shown. Vertical dashed lines on the right panels correspond to the time when plantar pressure distribution patterns are illustrated on the middle panels (corresponding to the maximum foot loading at the end of the stance phase). **(A)** Subject P4 (AIS C, 2.5 years post-trauma). MRI: structural changes of the spinal cord with post-traumatic gliosis. After 6 sessions of training, there was a twofold increase of the plantar pressure and the amplitude of GRF. Also, P4 subject increased an ability to walk over-ground using a walker for balance (without exoskeleton) from 3 to 40 strides. The subject noted the emergence of paresthesia in leg muscles and new "feeling of support" with an increase of sensation (by + 3 AIS score for both light touch and pin-prick). **(B)** Subject P12 (AIS B, motor – 3, sensory 103/103, 11 years post-trauma), advanced EXO-walker. MRI: non-structured spinal cord at the level for lumbar enlargement (Th12-L1) with separated neural elements. Complicated L1 vertebral fracture with SC compression. Surgery: SC decompression and instrumental fixation. P12 is actively engaged in sports, as an actual member of the National Russian Paralympic Team in curling. In the first training session with SCES, the subject improved his achievement of non-stop walking in the exoskeleton from 120 min (previous achievement) to 185 min and set the new record. After 6 sessions of training, the pressure under the feet increased and spread to the front part of the foot, and the amplitude of GRF increased from ∼75% BW up to ∼100–105% BW. Wide arrows – sessions in which SCES started, and thin arrows – sessions in which F-Scan recordings were performed.

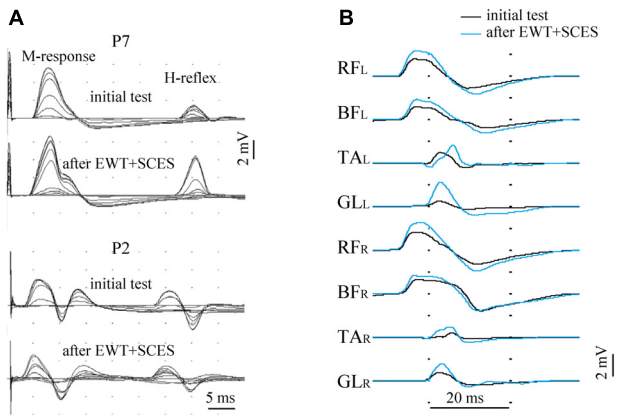

FIGURE 5 | Excitability of lumbar motor neurons before and after the course of EWT with SCES assessed by the presence/amplitude of the H-reflex [**(A)**, superposition of 12 records with gradually increased stimulus magnitude in two subjects] and by the evoked multisegmental muscle responses to supramaximal electrical stimulus at the level of Th11-12 vertebrae **(B)** in subject P7 (AIS A, 2.5 years post-injury). The H-reflex was evaluated in the lateral gastrocnemius muscle and was illustrated for two participants **(A)**: with an initially low H_{max}/M_{max} ratio (subject P7, upper panels) and with an initially high H_{max}/M_{max} ratio (subject P2). After the 2 weeks of training, the H-reflex significantly increased in P7 and decreased in P2 (a kind of "normalization" toward an optimal 0.4–0.6 value for the H_{max}/M_{max} ratio). RF, rectus femoris; BF, biceps femoris; TA, tibialis anterior; GL, gastrocnemius lateralis (R, right; L, left).

ratio, we observed an increase of this ratio by more than 30% (**Figure 5A**) and a decrease in 3 subjects with an initially high ratio. Thus, there was a kind of "normalization" of this parameter toward an optimal 0.4–0.6 value after the 2 weeks of training.

Multisegmental muscle responses to the electrical stimulus applied between vertebras Th11-12 allowed to assess the excitability of multiple motor pools (we recorded EMG responses in 8 leg muscles) and they varied across muscles and subjects (0.1–8.5 mV). Multisegmental muscle responses were recorded in 17 subjects and were absent in two participants. They could be evoked in all (14/19) muscles or in the part (3/19) of them, and the number of muscles with evoked responses was the same before and after training. Not all changes in the excitability of different motor pools of the lumbosacral enlargement could be clearly interpreted because of technical reasons (due to some differences in the skin impedance and/or electrode placement). Nevertheless, both methods of the neurophysiological examination showed the excitability of at least a part of motor neurons of motor pools in most SCI subjects.

Changes in the Neurological State

During the course of EWT with SCES, 15 out of 19 participants reported occurrence and subsequent strengthening of paresthesia in leg muscles, new non-differential feeling of passive motion in leg joints and a "sense of support." In one subject (P4), paresthesia reached the level of pain, interfering with night's sleep and requiring medication using non-steroidal anti-inflammatory drug injections. Nevertheless, at the request of the subject, EWT with SCES was continued and 2 days later the subject reported an overhauled feeling of "whole legs" instead of mosaic sensations in some parts of the thigh and foot.

Table 1 shows overall changes in the neurological state (AIS, MAS) and locomotor ability (HAI) in all SCI participants after EWT with SCES, and **Figure 6** illustrates the proportion of participants with neurological improvements in motor and sensory AIS depending on completeness of spinal cord damage (ASIA-class), time after injury, and frequency of SCES. Neurologic examination at the end of the training course showed an increase in pain sensitivity in 8 subjects, tactile sensitivity in 7 subjects and the leg muscle strength in 9 subjects (**Table 1**). After training we obtained some motor or sensory improvements in all AIS-C subjects (3/3) and in more than a half of AIS-A (7/11) and B (3/5) subjects (**Figure 6A**). There was no clear dependence of the rate of neurological progress on the time after injury (**Figure 6B**), though the progress in motor and sensory AIS seemed to be more often observed in the participants during the period of 2–5 years after injury.

In Group 1 (stimulation at 1 pulse/s), there were no improvements in the motor scale (**Figure 6C**, left panel), while in Group 2 (3 pulses/s) and Group 3 ("67 + 3" pulses/s), the proportion of individuals with improvements in the AIS motor scale was comparable (6/9 and 3/4, respectively). After the training course, 8 out of 19 subjects improved the Hauser Ambulation Index (**Table 1**). Two participants (AIS C), who were initially unable to walk, started to walk using walkers and stopped using a wheelchair when ambulating indoors.

In Group 4 (EWT without SCES), we also observed increments in foot loading with training (68 ± 10% BW before and 89 ± 11% BW after training). However, a substantially smaller proportion of individuals showed improvements in the AIS motor and sensory scales (especially in SCI-A and SCI-B participants) after the course of training with respect to the groups with SCES (**Figure 6A**, see also **Table 1**).

DISCUSSION

In this study, we evaluated the compatibility of EWT and tonic electrical stimulation of the lumbar enlargement and explored the main effects of 2-weeked combined SCES and EWT. We explored diverse stimulation parameters and tested 35 individuals with post-traumatic impairment of the spinal cord (**Table 1**). The results demonstrated that SCES and EWT are well compatible, and SCES may facilitate training and walking in the exoskeleton in SCI individuals by activating the locomotor networks and augmenting compensative sensitivity. Facilitation of stepping with SCES was noticed by all participants, but the nature of such effects requires further investigations.

Benefits of Combined EWT and SCES

There might be several benefits of EWT with a non-invasive SCES in regard to locomotor training on a treadmill with a body weight support. Stepping in the exoskeleton provides a unique opportunity to experience over-ground weight bearing stepping. Moreover, it allows to use the upper body and arm muscles to assist leg movements and to challenge balance control

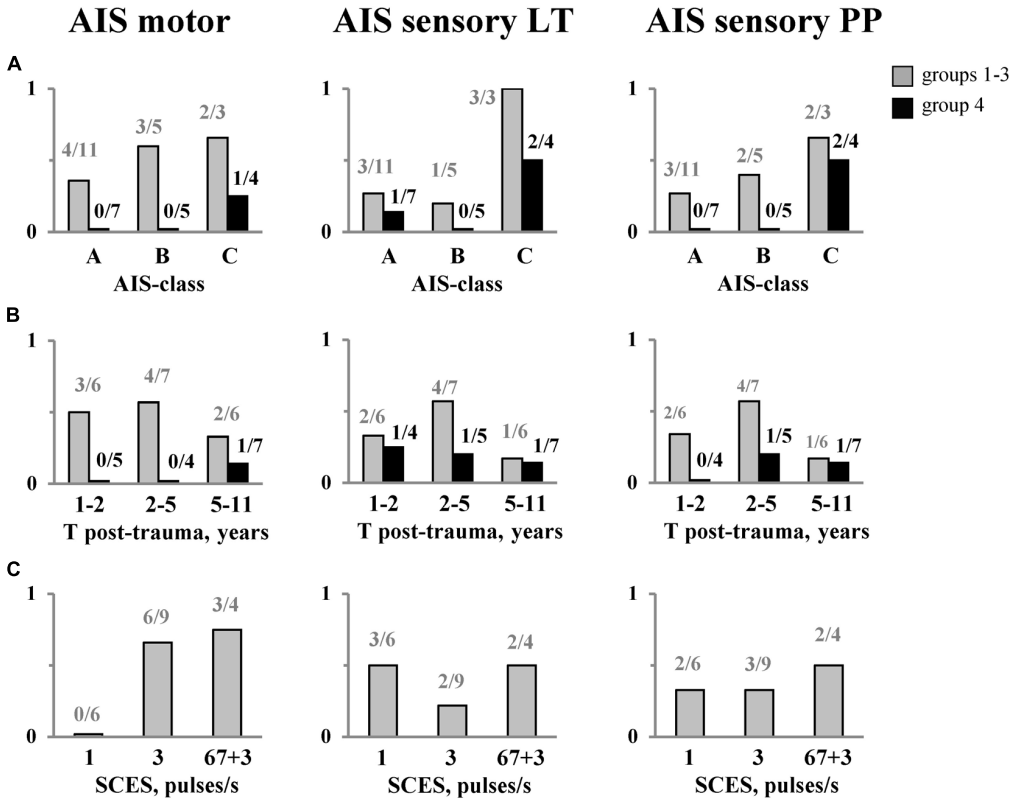

FIGURE 6 | The proportion of subjects with neurological improvements in motor and sensory (LT &PP) AIS after EWT with SCES depending on: completeness of spinal cord damage **(A)**, time after injury **(B)**, and frequency of SCES **(C)**. The number of subjects is also indicated. The data for the group 4 (EWT without SCES) are shown separately and marked in black. LT, light touch; PP, pin-prick. Note a significantly smaller proportion of subjects in group 4 showing improvements in the neurological indicators [especially in SCI **(A,B)**] with respect to the groups with SCES [**(A)**, see also **Table 1**].

by coordinating the movements between the arms, trunk and lower limbs, thus promoting connections between lumbosacral and cervical enlargements (Sylos-Labini et al., 2014; Gad et al., 2017). Reflex-related activity of lower limb muscles innervated from the spinal segments below the lesion during assisted walking in the exoskeleton (Sylos-Labini et al., 2014; Gad et al., 2017) might also be beneficial for potential gait rehabilitation since there is a relationship between facilitation of segmental reflexes and the ability to recover gait (Dietz et al., 2009; Thompson and Wolpaw, 2014). SCES aims at activating the spinal locomotor networks below the lesion, changing them to a physiologically active state and reinforcing synaptic connections of the spinal pattern generation circuitry and supraspinal-spinal connectivity (Shapkova, 2004; Gill et al., 2018; Hofstoetter et al., 2018; Wagner et al., 2018). Thus, in addition to gait assistive aspects of exoskeleton robotic devices in severely paralyzed individuals, the proposed approach of EWT with SCES may also be beneficial for gait rehabilitation.

After the training course of 2 weeks, the SCI individuals, initially able to ambulate with walkers, increased the walking distance but did not stop to use a wheelchair. The ability to walk 20–30 using a walker for balance did not change significantly their life. However, two participants, who were initially unable to walk, started to walk using walkers and stopped to use a wheelchair indoors. In our understanding, it was a drastic change in their lifestyle and future quality of life.

After 2 weeks of intensive training, we obtained some motor or sensory improvements in all AIS-C subjects (3/3) and in more than a half of AIS-A and B subjects (10/16). We did not find a dependence of the rate of neurological progress on the time after injury (within 1–11 years, **Figure 6B**). A traditional view and prognosis of chronic SCI is based on extensive atrophy in the spinal circuitries distal to the lesion (Dietz and Müller, 2004) and on limited plasticity and functional recovery after more than a year after a spinal complete lesion. Our findings may challenge a traditional prognosis for chronic SCI. Finally, improvements in the neurological scores were substantially limited in the Group 4 (especially in SCI A and B patients) with respect to the groups with SCES (**Table 1** and **Figure 6**). Nevertheless, since multiple factors might play a role, further investigations are needed to develop personalized neuromodulatory interventions to meet the specific needs of individuals with spinal cord injury (James et al., 2018).

Frequency-Dependent Effects of SCES

The interventions tested included EWT with non-invasive spinal cord stimulation at 1 pulse/s (Group 1, **Table 1**), 3 pulses/s (Group 2) and high-frequency anti-spastic stimulation (Group

3). The most evident is an anti-spastic effect of SCES at 67 pulses/s. The usage of the spinal cord electrical stimulation to relieve spasticity dates back to the end of seventies (Richardson and McLone, 1978; Siegfried et al., 1978; Vodovnik et al., 1984) and is associated mostly with epidural stimulation (Hunter and Ashby, 1994; Midha and Schmitt, 1998; Pinter et al., 2000). It has been shown that epidural stimulation with the electrodes placed over the lumbar posterior roots in the frequency range of 50 Hz–100 Hz can significantly suppress severe lower limb spasticity (Pinter et al., 2000). The effect was accounted for by changes in the excitability of neural circuits in the lumbar spinal cord through continuous posterior root activation. Technologies with the implantation of anti-spastic stimulants have demonstrated moderate efficacy as compared to their high cost and did not find a widespread application. Nowadays, after obtaining evidence of a comparable effect of epidural and percutaneous electrical stimulation (Hofstoetter et al., 2018), an interest in the anti-spastic electrical stimulation has been revived (Hofstoetter et al., 2014). Despite some technical differences between our method and the one described by Hofstoetter et al. (2014) in the location of the electrodes and stimulation frequency (67 vs. 50 pulses/s), both methods are based on the same principle and produce similar anti-spastic effect. The application of SCES in the anti-spastic mode had an immediate effect on the number of non-stop steps and facilitated stepping in the exoskeleton (**Figure 3**), with some improvements in the motor and sensory AIS after 2 weeks of training (**Figure 6C**).

Spinal cord electrical stimulation at 1 pulse/s is routinely used in our clinic to increase excitability of motor neurons in flaccid paralysis. In this study, the frequency of 1 pulse/s (Group 1, **Table 1**) was chosen to test a possible disturbing effect of SCES on the exoskeleton-induced walking. Despite the magnitude of stimulation exceeded the motor threshold and the sensitivity to stimulus increased with the number of sessions, no subject reported any disturbances associated with SCES. The subjects noticed "the returning feeling of the lower body or the whole leg instead of the part of it" and a new feeling of ground support. Subjective impressions of participants were supported by the results of the neurological examination: in Group 1, improvements in sensitivity were found more often as compared to Group 2 (**Figure 6C**, middle panel). Based on these observations, we suggest that such stimulation gives a greater impact on sensitivity rather than results in improvements in the motor scale (**Figure 6C**).

For EWT with SCES at 3 pulses/s, we assumed to activate the spinal locomotor networks and/or potentiate their activity (Shapkova and Schomburg, 2001; Shapkova, 2004). It is also worth noting that this frequency was found to be most effective in inducing locomotion in the decerebrate cat (Iwahara et al., 1992). The experienced exoskeleton-walkers reported that with 3 pulses/s SCES they were able to walk longer without fatigue. For instance, potentiation of the locomotor ability was clearly demonstrated by the subject P12. This advanced exoskeleton-walker significantly improved his best achievement for the non-stop walk duration in the exoskeleton in the 2nd training session of EWT with SCES (**Figure 4B**). At the end of the training course, we also found significant changes in the F-Scan recordings (**Figure 4B**) and an increase of the muscle strength (by 3 points in the AIS motor score, **Table 1**). Taking into account the high physical conditions of P12 (active member of the National Paralympic Team) and 3-year experience with EWT, we explain such effects by the efficacy of SCES in activating spinal neural structures and/or increasing their excitability. Overall, in the subjects receiving 3 pulses/s SCES, an increase in the muscle strength was observed more often than in the Group 1 (**Figure 6C**).

Limitations of the Study

The results of the study are encouraging but need to be confirmed in a larger SCI population, also because the effects may be heterogeneous due to multiple clinical or methodological factors. For instance, we used SCES during both stationary (supine) condition and during EWT so that its duration was overall twice longer as compared to the EWT duration. We performed SCES in the stationary condition to activate the locomotor networks and thus to reinforce the potential effect of combined training but we do not know its relative effect. Also, there might be subject-specific or condition-specific optimal parameters of SCES. Various techniques have been developed to stimulate the central pattern generators (CPGs) for stepping, which may include both diffuse and quite specific tuning effects, although tonic and rhythmic spinal activity control are not separate phenomena but are closely integrated to properly sustain CPG functioning (Hofstoetter et al., 2017; Ivanenko et al., 2017). For instance, differential spinal cord segment stimulation (epidural or transcutaneous) is a promising tool to restore the functioning of the CPG circuitry in both animals (Capogrosso et al., 2016; Wenger et al., 2016) and humans (Solopova et al., 2017; Angeli et al., 2018; Gill et al., 2018; Wagner et al., 2018), and such stimulation techniques might take into account differential activation of spinal segments to selectively drive neuroprostheses depending on walking conditions (Dewolf et al., 2019) and individual affordability and efficacy of such approaches (James et al., 2018).

Nevertheless, the activation of CPG circuits largely depends on the presence of a sustained tonic excitatory drive, as it can be elicited by electrical spinal cord stimulation, or by specific pharmacological neuromodulation (Hofstoetter et al., 2017). In our study using tonic SCES, the subjective reports, increments in the max non-stop walk duration (**Figure 3**), the differential effect of the SCES frequency (**Figure 6C** left panel) and limited improvements in the neurological scores in the control group of subjects for EWT without stimulation (**Figure 6**), point to a facilitatory effect of stimulation. The findings also corroborate a general notion about a facilitatory outcome of SCES on the functioning of the locomotor pattern generation circuitry (Shapkova, 2004; Gill et al., 2018; Hofstoetter et al., 2018; Wagner et al., 2018), as well as the results of a recent case study that spinal cord stimulation enhances the level of effort that the subject can generate while stepping in the exoskeleton along with changes in autonomic functions including cardiovascular and thermoregulation (Gad et al., 2017). Also, no clinical changes were observed in the previous study on exoskeleton walk training in motor complete paraplegic individuals in the absence of concurrent SCES (Sylos-Labini et al., 2014), consistent with a limited effectiveness of robot-assisted gait training in severely

paralyzed persons (Swinnen et al., 2010; Roy et al., 2012; Sale et al., 2012). Thus, EWT with SCES represents a considerable potential for gait rehabilitation after chronic spinal cord injury. The neurological improvement obtained after the short intensive course of combined SCES and EWT in chronic SCI individuals also suggests that a similar or greater improvement may be expected in acute paraplegic persons.

While improvements of stepping in the exoskeleton (**Figures 2–4**) and neurological improvements in the motor and sensory scales were observed (**Figure 6**), the course of 2 weeks is apparently too short and we have to find an optimal course duration and/or the number of courses to provide clinically significant and stable results for both acute and chronically paralyzed persons. Also, given that neurological improvements were observed in participants who previously received EWT or SCES interventions (**Table 1**), one could probably expect a cumulative effect of a series of courses.

CONCLUSION

This study showed that percutaneous electrical stimulation of the lumbar enlargement and exoskeleton-induced walking are well compatible and provide walking assistance for SCI individuals. The exoskeleton assists both posture and leg movements, and SCES may facilitate training and walking in the exoskeleton in individuals with chronic SCI. The results also suggest that facilitation may be frequency dependent (3 pulses/s to activate the locomotor networks, 1 pulse/s to augment compensative sensitivity) though further investigations with a larger sample of participants are necessary to understand the benefits of training with different modes of stimulation and the underlying mechanisms. SCES in the anti-spastic mode can decrease spasticity and thus makes the exo-walk training possible for individuals with severe spasticity. The 2-week intensive synergistic effect of EWT with SCES enriched the locomotor ability and evoked neurological improvements in chronic SCI individuals, including complete paralysis, being beneficial for gait rehabilitation after SCI.

DATA AVAILABILITY STATEMENT

The datasets generated for this study are available on request to the corresponding author.

ETHICS STATEMENT

The studies involving human participants were reviewed and approved by the Local Ethical Committee of the Saint-Petersburg State Research Institute of Phthisiopulmonology. The patients/participants provided their written informed consent to participate in this study.

AUTHOR CONTRIBUTIONS

ES organized and conducted the study, analyzed the clinical data, and wrote the draft of the manuscript. EP conceived and initiated the study and performed the biomechanical measurements and data analysis. DE conducted the study, performed the neurophysiological examination, and prepared illustrations. YI discussed the clinical and biomechanical data at all stages of the study, initiated the manuscript writing, and edited the manuscript.

FUNDING

The work was supported in part by the manufacturer of the "ExoAtlet" exoskeleton by covering travel expenses and accommodation for the participants, the Saint Petersburg State University (project #51134206) and by the Italian Ministry of Health (Ricerca corrente, IRCCS Fondazione Santa Lucia).

ACKNOWLEDGMENTS

We are grateful to our colleagues Ekaterina Styrina, Ekaterina Grigorjeva, Yulia Larionova, and to volunteers of the public association "Energy of Life" for the help with EWT. Our special thanks to Dr. Kira Petrushanskaya for the help with biomechanical data processing. Many thanks to our SCI participants for their enthusiasm and active collaboration, which made the study possible.

SUPPLEMENTARY MATERIAL

The Supplementary Material for this article can be found online at: https://www.frontiersin.org/articles/10.3389/fnins.2020.00416/full#supplementary-material

VIDEO S1 | Video fragments of stepping in the exoskeleton of subject P4 – initial test.

VIDEO S2 | Video fragments of stepping in the exoskeleton of subject P4 – after EWT with SCES. Written informed consent was obtained from the individual for the publication of these videos and recognizable image.

REFERENCES

Angeli, C. A., Boakye, M., Morton, R. A., Vogt, J., Benton, K., Chen, Y., et al. (2018). Recovery of over-ground walking after chronic motor complete spinal cord injury. *N. Engl. J. Med.* 379, 1244–1250. doi: 10.1056/NEJMoa1803588

Aruin, A. S., and Kanekar, N. (2013). Effect of a textured insole on balance and gait symmetry. *Exp. Brain Res.* 231, 201–208. doi: 10.1007/s00221-013-3685-z

Barroso, F. O., Pascual-Valdunciel, A., Torricelli, D., Moreno, J. C., Ama-Espinosa, A. D., Laczko, J., et al. (2019). Noninvasive modalities used in spinal cord injury rehabilitation. *Spinal Cord Inj. Ther.* Avaliable online at:

https://www.intechopen.com/books/spinal-cord-injury-therapy/noninvasive-modalities-used-in-spinal-cord-injury-rehabilitation

Berezij, E., Pismennaya, E., Kuzmichev, A., and Lavrovskiy, E. (2017). *Exoskeleton ExoAtlet*. Patent WO 2017/069652. Avaliable online at: https://patentscope.wipo.int/search/en/detail.jsf?docId=WO2017069652&tab=PCTBIBLIO

Capogrosso, M., Milekovic, T., Borton, D., Wagner, F., Moraud, E. M., Mignardot, J.-B., et al. (2016). A brain-spine interface alleviating gait deficits after spinal cord injury in primates. *Nature* 539, 284–288. doi: 10.1038/nature20118

Contreras-Vidal, J. L., Bhagat, A. N., Brantley, J., Cruz-Garza, J. G., He, Y., Manley, Q., et al. (2016). Powered exoskeletons for bipedal locomotion after spinal cord injury. *J. Neural Eng.* 13:031001. doi: 10.1088/1741-2560/13/3/031001

del-Ama, A. J., Koutsou, A. D., Moreno, J. C., de-los-Reyes, A., Gil-Agudo, A., and Pons, J. L. (2012). Review of hybrid exoskeletons to restore gait following spinal cord injury. *J. Rehabil. Res. Dev.* 49, 497–514.

Dewolf, A. H., Ivanenko, Y. P., Zelik, K. E., Lacquaniti, F., and Willems, P. A. (2019). Differential activation of lumbar and sacral motor pools during walking at different speeds and slopes. *J. Neurophysiol.* 122, 872–887. doi: 10.1152/jn.00167.2019

Dietz, V., Grillner, S., Trepp, A., Hubli, M., and Bolliger, M. (2009). Changes in spinal reflex and locomotor activity after a complete spinal cord injury: a common mechanism? *Brain* 132, 2196–2205.

Dietz, V., and Müller, R. (2004). Degradation of neuronal function following a spinal cord injury: mechanisms and countermeasures. *Brain* 127, 2221–2231. doi: 10.1093/brain/awh255

Dimitrijevic, M. R., Gerasimenko, Y., and Pinter, M. M. (1998). Evidence for a spinal central pattern generator in humans. *Ann. N. Y. Acad. Sci.* 860, 360–376.

Dimitrijevic, M. R., and Larsson, L. E. (1981). Neural control of gait: clinical neurophysiological aspects. *Appl. Neurophysiol.* 44, 152–159.

Ekelem, A., and Goldfarb, M. (2018). Supplemental stimulation improves swing phase kinematics during exoskeleton assisted gait of SCI subjects with severe muscle spasticity. *Front. Neurosci.* 12:374. doi: 10.3389/fnins.2018.00374

Emeliannikov, D. V., Shapkova, E. Y., Moshonkina, T. R., and Gerasimenko, Y. P. (2016). Evaluation of motor neuron excitability in lumbosacral spinal cord: transcutaneous spinal cord stimulation as compared to H-reflex. *Fiziol. Cheloveka* 42, 32–36.

Fisahn, C., Aach, M., Jansen, O., Moisi, M., Mayadev, A., Pagarigan, K. T., et al. (2016). The effectiveness and safety of exoskeletons as assistive and rehabilitation devices in the treatment of neurologic gait disorders in patients with spinal cord injury: a systematic review. *Glob. Spine J.* 6, 822–841. doi: 10.1055/s-0036-1593805

Gad, P., Gerasimenko, Y., Zdunowski, S., Turner, A., Sayenko, D., Lu, D. C., et al. (2017). Weight bearing over-ground stepping in an exoskeleton with non-invasive spinal cord neuromodulation after motor complete paraplegia. *Front. Neurosci.* 11:333. doi: 10.3389/fnins.2017.00333

Gerasimenko, Y., Gorodnichev, R., Moshonkina, T., Sayenko, D., Gad, P., and Reggie Edgerton, V. (2015). Transcutaneous electrical spinal-cord stimulation in humans. *Ann. Phys. Rehabil. Med.* 58, 225–231. doi: 10.1016/j.rehab.2015.05.003

Gill, M. L., Grahn, P. J., Calvert, J. S., Linde, M. B., Lavrov, I. A., Strommen, J. A., et al. (2018). Neuromodulation of lumbosacral spinal networks enables independent stepping after complete paraplegia. *Nat. Med.* 24, 1677–1682. doi: 10.1038/s41591-018-0175-7

Hofstoetter, U. S., Freundl, B., Binder, H., and Minassian, K. (2018). Common neural structures activated by epidural and transcutaneous lumbar spinal cord stimulation: elicitation of posterior root-muscle reflexes. *PLoS One* 13:e0192013. doi: 10.1371/journal.pone.0192013

Hofstoetter, U. S., Knikou, M., Guertin, P. A., and Minassian, K. (2017). Probing the human spinal locomotor circuits by phasic step-induced feedback and by tonic electrical and pharmacological neuromodulation. *Curr. Pharm. Des.* 23, 1805–1820. doi: 10.2174/1381612822666161214144655

Hofstoetter, U. S., Krenn, M., Danner, S. M., Hofer, C., Kern, H., McKay, W. B., et al. (2015). Augmentation of voluntary locomotor activity by transcutaneous spinal cord stimulation in motor-incomplete spinal cord-injured individuals. *Artif. Organs* 39, E176–E186. doi: 10.1111/aor.12615

Hofstoetter, U. S., McKay, W. B., Tansey, K. E., Mayr, W., Kern, H., and Minassian, K. (2014). Modification of spasticity by transcutaneous spinal cord stimulation in individuals with incomplete spinal cord injury. *J. Spinal Cord Med.* 37, 202–211. doi: 10.1179/2045772313Y.0000000149

Hunter, J. P., and Ashby, P. (1994). Segmental effects of epidural spinal cord stimulation in humans. *J. Physiol.* 474, 407–419.

Ivanenko, Y. P., Grasso, R., Macellari, V., and Lacquaniti, F. (2002). Control of foot trajectory in human locomotion: role of ground contact forces in simulated reduced gravity. *J. Neurophysiol.* 87, 3070–3089.

Ivanenko, Y. P., Gurfinkel, V. S., Selionov, V. A., Solopova, I. A., Sylos-Labini, F., Guertin, P. A., et al. (2017). Tonic and rhythmic spinal activity underlying locomotion. *Curr. Pharm. Des.* 23, 1753–1763. doi: 10.2174/1381612823666170125152246

Iwahara, T., Atsuta, Y., Garcia-Rill, E., and Skinner, R. D. (1992). Spinal cord stimulation-induced locomotion in the adult cat. *Brain Res. Bull.* 28, 99–105.

James, N. D., McMahon, S. B., Field-Fote, E. C., and Bradbury, E. J. (2018). Neuromodulation in the restoration of function after spinal cord injury. *Lancet Neurol.* 17, 905–917. doi: 10.1016/S1474-4422(18)30287-4

Kim, C. M., and Eng, J. J. (2003). Symmetry in vertical ground reaction force is accompanied by symmetry in temporal but not distance variables of gait in persons with stroke. *Gait Posture* 18, 23–28.

Lavrov, I., Musienko, P. E., Selionov, V. A., Zdunowski, S., Roy, R. R., Edgerton, V. R., et al. (2015). Activation of spinal locomotor circuits in the decerebrated cat by spinal epidural and/or intraspinal electrical stimulation. *Brain Res.* 1600, 84–92. doi: 10.1016/j.brainres.2014.11.003

Mayr, W., Krenn, M., and Dimitrijevic, M. R. (2016). Epidural and transcutaneous spinal electrical stimulation for restoration of movement after incomplete and complete spinal cord injury. *Curr. Opin. Neurol.* 29, 721–726. doi: 10.1097/WCO.0000000000000382

Megía García, A., Serrano-Mu??oz, D., Taylor, J., Avenda??o-Coy, J., and Gómez-Soriano, J. (2020). Transcutaneous spinal cord stimulation and motor rehabilitation in spinal cord injury: a systematic review. *Neurorehabil. Neural Repair* 34, 3–12. doi: 10.1177/1545968319893298

Midha, M., and Schmitt, J. K. (1998). Epidural spinal cord stimulation for the control of spasticity in spinal cord injury patients lacks long-term efficacy and is not cost-effective. *Spinal Cord* 36, 190–192.

Musienko, P. E., Zelenin, P. V., Lyalka, V. F., Gerasimenko, Y. P., Orlovsky, G. N., and Deliagina, T. G. (2012). Spinal and supraspinal control of the direction of stepping during locomotion. *J. Neurosci.* 32, 17442–17453. doi: 10.1523/JNEUROSCI.3757-12.2012

Onose, G., Cârdei, V., Crăciunoiu, ??T., Avramescu, V., Opri??, I., Lebedev, M. A., et al. (2016). Mechatronic wearable exoskeletons for bionic bipedal standing and walking: a new synthetic approach. *Front. Neurosci.* 10:343. doi: 10.3389/fnins.2016.00343

Pais-Vieira, C., Khazraei, M., Perrotta, A., Neves-Amado, J., Morya, E., Moioli, R., et al. (2020). Method for positioning and rehabilitation training with the ExoAtlet §powered exoskeleton. *MethodsX* 7:100849. doi: 10.1016/j.mex.2020.100849

Pinter, M. M., Gerstenbrand, F., and Dimitrijevic, M. R. (2000). Epidural electrical stimulation of posterior structures of the human lumbosacral cord: 3. Control Of spasticity. *Spinal Cord* 38, 524–531.

Richardson, R. R., and McLone, D. G. (1978). Percutaneous epidural neurostimulation for paraplegic spasticity. *Surg. Neurol.* 9, 153–155.

Roy, R. R., Harkema, S. J., and Edgerton, V. R. (2012). Basic concepts of activity-based interventions for improved recovery of motor function after spinal cord injury. *Arch. Phys. Med. Rehabil.* 93, 1487–1497.

Sale, P., Franceschini, M., Waldner, A., and Hesse, S. (2012). Use of the robot assisted gait therapy in rehabilitation of patients with stroke and spinal cord injury. *Eur. J. Phys. Rehabil. Med.* 48, 111–121.

Scivoletto, G., Galli, G., Torre, M., Molinari, M., and Pazzaglia, M. (2019). The overlooked outcome measure for spinal cord injury: use of assistive devices. *Front. Neurol.* 10:272. doi: 10.3389/fneur.2019.00272

Shapkov, Y. T., Shapkova, E. Y., and Mushkin, A. Y. (1996). Electrostimulation of the spinal cord as a method of inducing locomotor activity in children (clinical aspects and technical problems). *Med. Tekh* 4, 3–5.

Shapkova, E. Y. (2004). "Spinal locomotor capability revealed by electrical stimulation of the lumbar enlargement in paraplegic patients," in *Progress in Motor Control*, eds M. Latash and M. Levin (Champaign, IL: Human Kinetics), 253–289.

Shapkova, E. Y., and Schomburg, E. D. (2001). Two types of motor modulation underlying human stepping evoked by spinal cord electrical stimulation (SCES). *Acta Physiol. Pharmacol. Bulg.* 26, 155–157.

Siegfried, J., Krainick, J. U., Haas, H., Adorjani, C., Meyer, M., and Thoden, U. (1978). Electrical spinal cord stimulation for spastic movement disorders. *Appl. Neurophysiol.* 41, 134–141.

Solopova, I. A., Kazennikov, O. V., Deniskina, N. B., Levik, Y. S., and Ivanenko, Y. P. (2003). Postural instability enhances motor responses to transcranial magnetic stimulation in humans. *Neurosci. Lett.* 337, 25–28.

Solopova, I. A., Selionov, V. A., Kazennikov, O. V., and Ivanenko, Y. P. (2014). Effects of transcranial magnetic stimulation during voluntary and non-voluntary stepping movements in humans. *Neurosci. Lett.* 579, 64–69.

Solopova, I. A., Sukhotina, I. A., Zhvansky, D. S., Ikoeva, G. A., Vissarionov, S. V., Baindurashvili, A. G., et al. (2017). Effects of spinal cord stimulation on motor functions in children with cerebral palsy. *Neurosci. Lett.* 639, 192–198. doi: 10.1016/j.neulet.2017.01.003

Swinnen, E., Duerinck, S., Baeyens, J.-P., Meeusen, R., and Kerckhofs, E. (2010). Effectiveness of robot-assisted gait training in persons with spinal cord injury: a systematic review. *J. Rehabil. Med.* 42, 520–526.

Sylos-Labini, F., La Scaleia, V., d'Avella, A., Pisotta, I., Tamburella, F., Scivoletto, G., et al. (2014). EMG patterns during assisted walking in the exoskeleton. *Front. Hum. Neurosci.* 8:423. doi: 10.3389/fnhum.2014.00423

Taccola, G., Sayenko, D., Gad, P., Gerasimenko, Y., and Edgerton, V. R. (2018). And yet it moves: recovery of volitional control after spinal cord injury. *Prog. Neurobiol.* 160, 64–81. doi: 10.1016/j.pneurobio.2017.10.004

Thompson, A. K., and Wolpaw, J. R. (2014). Operant conditioning of spinal reflexes: from basic science to clinical therapy. *Front. Integr. Neurosci.* 8:25. doi: 10.3389/fnint.2014.00025

Vodovnik, L., Bowman, B. R., and Hufford, P. (1984). Effects of electrical stimulation on spinal spasticity. *Scand. J. Rehabil. Med.* 16, 29–34.

Wagner, F. B., Mignardot, J.-B., Le Goff-Mignardot, C. G., Demesmaeker, R., Komi, S., Capogrosso, M., et al. (2018). Targeted neurotechnology restores walking in humans with spinal cord injury. *Nature* 563, 65–71. doi: 10.1038/s41586-018-0649-2

Wenger, N., Moraud, E. M., Gandar, J., Musienko, P., Capogrosso, M., Baud, L., et al. (2016). Spatiotemporal neuromodulation therapies engaging muscle synergies improve motor control after spinal cord injury. *Nat. Med.* 22, 138–145. doi: 10.1038/nm.4025

Conflict of Interest: The powered exoskeleton for this study was granted by its manufacturer "ExoAtlet". EP is the major constructor of the "ExoAtlet" exoskeleton.

The remaining authors declare that the research was conducted in the absence of any commercial or financial relationships that could be construed as a potential conflict of interest.

frontiers in Neuroscience

BRIEF RESEARCH REPORT
published: 15 March 2021
doi: 10.3389/fnins.2021.613844

Improving the Selectivity of an Osseointegrated Neural Interface: Proof of Concept For Housing Sieve Electrode Arrays in the Medullary Canal of Long Bones

Augusto X. T. Millevolte[1,2†], Aaron M. Dingle[1†], Jared P. Ness[2], Joseph Novello[2], Weifeng Zeng[1], Yan Lu[3], Rashea L. Minor[3], Brett Nemke[3], Mark D. Markel[3], Aaron J. Suminski[2,3,4], Justin C. Williams[2,4] and Samuel O. Poore[1,2]*

[1] Division of Plastic Surgery, Department of Surgery, University of Wisconsin – Madison, Madison, WI, United States, [2] Department of Biomedical Engineering, College of Engineering, University of Wisconsin – Madison, Madison, WI, United States, [3] Department of Medical Sciences, University of Wisconsin – Madison, Madison, WI, United States, [4] Department of Neurological Surgery, University of Wisconsin – Madison, Madison, WI, United States

OPEN ACCESS

Edited by:
Mikhail Lebedev,
Duke University, United States

Reviewed by:
Melanie Gay Urbanchek,
University of Michigan, United States
Vidhi Desai,
Abbott (United States), United States

***Correspondence:**
Samuel O. Poore
poore@surgery.wisc.edu

[†] These authors have contributed equally to this work

Specialty section:
This article was submitted to Neuroprosthetics, a section of the journal Frontiers in Neuroscience

Received: 04 October 2020
Accepted: 16 February 2021
Published: 15 March 2021

Citation:
Millevolte AXT, Dingle AM, Ness JP, Novello J, Zeng W, Lu Y, Minor RL, Nemke B, Markel MD, Suminski AJ, Williams JC and Poore SO (2021) Improving the Selectivity of an Osseointegrated Neural Interface: Proof of Concept For Housing Sieve Electrode Arrays in the Medullary Canal of Long Bones. Front. Neurosci. 15:613844. doi: 10.3389/fnins.2021.613844

Sieve electrodes stand poised to deliver the selectivity required for driving advanced prosthetics but are considered inherently invasive and lack the stability required for a chronic solution. This proof of concept experiment investigates the potential for the housing and engagement of a sieve electrode within the medullary canal as part of an osseointegrated neural interface (ONI) for greater selectivity toward improving prosthetic control. *The working hypotheses* are that (A) the addition of a sieve interface to a cuff electrode housed within the medullary canal of the femur as part of an ONI would be capable of measuring efferent and afferent compound nerve action potentials (CNAPs) through a greater number of channels; (B) that signaling improves over time; and (C) that stimulation at this interface generates measurable cortical somatosensory evoked potentials through a greater number of channels. The modified ONI was tested in a rabbit (n = 1) amputation model over 12 weeks, comparing the sieve component to the cuff, and subsequently compared to historical data. Efferent CNAPs were successfully recorded from the sieve demonstrating physiological improvements in CNAPs between weeks 3 and 5, and somatosensory cortical responses recorded at 12 weeks postoperatively. This demonstrates that sieve electrodes can be housed and function within the medullary canal, demonstrated by improved nerve engagement and distinct cortical sensory feedback. This data presents the conceptual framework for housing more sophisticated sieve electrodes in bone as part of an ONI for improving selectivity with percutaneous connectivity toward improved prosthetic control.

Keywords: regenerative neural interface, neural interface, osseointegrated neural interface, amputation, amputation neuroma, neural prosthetic, prosthetic control, somatosensory evoked potential (SSEP)

INTRODUCTION

With an estimated 500 new cases every day within the United States, there is an increasing pool of amputees, living long and otherwise healthy lives (Ziegler-Graham et al., 2008; Mioton and Dumanian, 2018). A significant challenge in developing advanced motorized and sensate prosthetic devices is establishing neural interfaces that are highly selective, stable and capable of enhanced longevity (Navarro et al., 2005; Ortiz-Catalan et al., 2014; Ghafoor et al., 2017; Valerio et al., 2020). Electrode selectivity – i.e., the ability of a peripheral neural interface (PNI) to selectively stimulate or record from individual nerves – is a critical parameter inherently linked to the degrees of freedom a PNI is capable of controlling, as well as the differentiation between motor and sensory signals (Grill et al., 2009; Micera and Navarro, 2009; Horch et al., 2011; Tan et al., 2014, 2015; Cheesborough et al., 2015; Ghafoor et al., 2017). Sieve electrodes represent a type of PNI with the greatest potential for selectivity resulting from their well-spaced specificity within the nerve. These devices involve invasive nerve transection (Navarro et al., 2005; MacEwan et al., 2016; Desai et al., 2017; Ghafoor et al., 2017), and rely on robust neural regeneration through electrode transit zones, assimilating the PNI into the nerve. In the amputation setting, it may be possible to simply interface the sieve array with the residual nerve end, taking advantage of the regenerative process that would otherwise lead to neuroma formation.

Amputation neuroma is a non-tumorigenic bulbous mass that develops at the terminal end of the residual nerve, representing the innate capacity for the transected nerve to regenerate. Neuromas are a significant cause of neuropathic pain and can preclude use of a traditional socket prosthetic (Davis, 1993; Gallagher and Maclachlan, 2001). Symptomatic neuroma can be addressed utilizing a multitude of techniques including transposition into muscle and targeted muscle reinnervation (Woo et al., 2016; Mioton and Dumanian, 2018). Another proven treatment to handle neuropathic pain resulting from amputation neuromas transposes the affected nerve via a corticotomy into the intramedullary canal of long bones (Boldrey, 1943; Goldstein and Sturim, 1985; Israel et al., 2018).

Based on this clinical operation, Dingle et al. (2020a) have developed an osseointegrated neural interface (ONI) in a rabbit model that consists of an intramedullary array capable of both efferent and afferent signal transmission and demonstrates physiological and histological signs of regeneration over 3 months. Cuff electrodes are renowned as the least invasive, and least selective interfaces on the PNI spectrum, with sieve electrodes at the opposing end of the spectrum, being the most invasive and offering the most selectivity (Navarro et al., 2005). A confounding factor in this justification is that sieve electrodes are typically tested in neurorrhaphy models in rodents, a model that is well known for its robust neural regeneration and return of function of intact distal target organs (Vela et al., 2020), but is not reflective of the amputation paradigm, in which regeneration is typically haphazard in the absence of a distal target, leading to neuroma formation. Dingle et al. (2020a) demonstrated that the robust three-dimensional axonal sprouting associated with neuroma formation can be passively redirected through transit zones of a dummy sieve electrode housed within the medullary canal. Given this evidence, we believe that the invasive procedure of transecting a nerve in order to insert a sieve electrode is a moot point in the amputation setting, as neurotmesis is unavoidable and the true distal targets are lost. Alternatively, we propose that the neural regeneration giving rise to problematic neuromas can be utilized to innervate sieve electrodes and ultimately restore function though a neuroprosthetic.

In this research report we explore the idea and concept of housing a sieve interface within the medullary canal of long bones as part of an ONI as a method for improving selectivity within this model. This sieve is designed to abut the terminal end of residual nerve and capitalize on the axonal regeneration that would otherwise lead to neuroma formation. *The working hypotheses* are that (A) the addition of a sieve interface to a cuff electrode housed within the medullary canal of the femur as part of an ONI would be capable of measuring bi-directional (efferent and afferent) compound nerve action potentials (CNAPs) through a greater number of channels; (B) that signaling improves over time; and C) that stimulation at this interface generates measurable cortical somatosensory evoked potentials (SSEPs) through a greater number of channels. The cuff electrode allows for comparison to historic data utilizing our amputation model and cuff based ONI (Dingle et al., 2020a). The mechanical stability of the bone may help mitigate damage to the interface resulting from micro-motion while simultaneously providing an electrically insulated environment less prone to myoelectric noise. In addition to the favorable neural interface environment, the intramedullary canal enables the osseointegrated percutaneous integration of a prosthetic, which can simplify the percutaneous routing of leads (Ortiz-Catalan et al., 2014).

METHODS

Experimental Design

This experiment was designed to examine the concept that the medullary canal represents an ideal environment for the stable housing and engagement of a sieve electrode, as part of an ONI. In order to achieve proof of concept we performed a short-term experiment in a single animal wherein modifications were made to the intramedullary array of our previously published ONI (Dingle et al., 2020a) to include radial electrodes with substantial transit zones for the nerve regeneration (MacEwan et al., 2016). The modifications made to the array served as a less-expensive and more rapidly produced model to measure osseointegrated neural function for confirming proof of concept. Successful proof of concept was predetermined as the ability to record efferent and stimulate afferent signals through the sieve interface comparable to those generated through the original cuff component. This modified ONI was implanted in one New Zealand White rabbit (n = 1, Female, 2.7 kg), monitored with repeated electrophysiology measurements (18–34 randomized trials per stimulation) at four time points over a 12-week period to determine nerve engagement with the sieve

electrodes and confirmed by complementary engagement of the cuff electrode. Engagement of the cuff was qualitatively compared to historic data (Dingle et al., 2020a). Histological assessment of regeneration was attempted, however, tissue was substantially damaged during retrieval from within the bone. This study was not intended to demonstrate the preferential function of any specific sieve interface design; rather, the intention was to demonstrate proof of concept for stably housing a sieve interface within the medullary canal in an amputation model, supporting rigorous studies of more advanced electrodes toward clinical applicability. All animal procedures were approved by the University of Wisconsin Institutional Animal Care and Use Committee (IACUC, #V005256), the United States Army Medical Research and Material Command (USAMRMC, #DARPA-8728), and the Animal Care and Use Review Office (ACURO, #DARPA-8728).

Device Fabrication

ONI Device

The ONI device (**Figure 1**) consists of two arrays constructed from silicon cuff tubes with embedded electrodes, each connected to a printed circuit board (PCB, Tucker-Davis Technologies (TDT), Florida, United States) secured to an osseointegrated, percutaneous screw (M4 × 50 mm cup point grub screw, ACCUGROUP, Huddersfield, United Kingdom) (Dingle et al., 2020a). In addition to basic cuff electrodes, three platinum iridium wires (Pt/Ir) with 1mm of insulation removed were placed through the distal end of the intramedullary cuff extending radially into the lumen to create a sieve electrode interface, with three 1 mm^2 transit zones for sub-chronic electrophysiological interrogation of axonal engagement (**Figures 1B–E**). The sieve electrodes were based on previously published designs to maximize transit zones (MacEwan et al., 2016), and only added to the distal intramedullary array that interfaces with the terminal end of the amputated nerve within the bone (**Figure 1F**). The proximal array, connected via insulated Pt/Ir wire, is interfaced outside of the bone and required to perform stimulation and recording of CNAPs under anesthesia. Arrays consisted of silicone tubing (A-M Systems silicone tubing, 1.98 mm inner diameter, 0.6 mm wall thickness) and Pt/Ir wires (A-M Systems 125 μm Pt/Ir PFA coated wire). For the proximal array, tubing was 7.5 mm in length, electrode wires placed at 2 and 4.75 mm apart from the center. For the intramedullary array, tubing was 10 mm in length, cuff electrodes placed at 2.5 and 5 mm with sieve electrodes placed 1mm from the distal end (**Figures 1B,C**). All electrode wires were secured with quick setting silicone (Kwik-Sil, World Precision Instruments, Sarasota, Florida, United States). The proximal array was connected to the PCB via 7cm of Pt/Ir wire, while the intramedullary array was connected to a separate PCB via 4cm of Pt/Ir wire. Both PCBs and Pt/IR wires were affixed to the percutaneous screw with UV curable dental acrylic (Flow-It Accelerated Light Cure, PENTORN, Orange, CA, United States).

Micro-Electrocorticography Array

A custom 16-channel Micro-electrocorticography array (μECoG) array was fabricated using a previously described photolithography lift-off process (Thongpang et al., 2011). The array measured 4 mm × 4 mm with 16 circular platinum electrodes in a 4 × 4 grid spaced 500 μm apart on parylene. Each electrode measured 200 μ m in diameter.

Surgical Procedures

Surgical Creation of the ONI

The surgical creation of an ONI consists of a transfemoral amputation and subsequent implantation of the ONI device in New Zealand White rabbits as previously described (Dingle et al., 2020a). Prior to surgery animals were given one dose of Combi-Pen 48 antibiotic (500,000 IU/kg SQ. Bimdeda, Oakbrook Terrace, IL, United States). Rabbits were induced with ketamine (10–15 mg/kg IM), midazolam (0.5–2.0 mg/kg IM), and inhaled isoflurane (0–5% in 100% oxygen). After general anesthesia was reached the anesthetic plane was maintained through isoflurane (0–5% inhaled with O_2) Vitals including O_2 and CO_2 saturation, temperature, blood pressure, and heart rate were monitored through the duration of surgery (Cardel Veterinary Monitor 9,500 HD, Midmark, Dayton, OH, United States). A corticotomy is drilled 2 cm above the midpoint of the femur before a mid-femoral amputation is performed. The transected sciatic nerve was threaded through the corticotomy and inserted into the intramedullary array so that the terminal nerve end abuts the sieve (**Figure 1D**). The intramedullary array is secured to the nerve with an epineurial stitch and both are pressed back into the medullary canal, followed by the intramedullary screw and secured with veterinary bone cement (BioMedtrix, Boonton, New Jersey, United States). The proximal cuff was then wrapped around sciatic nerve outside the bone, roughly 3 cm proximal to the intramedullary array, secured with an epineurial stitch and the amputation site closed.

Craniotomy

At the experimental endpoint of 12 weeks, a craniotomy was performed under anesthesia over the somatosensory cortex contralateral to the amputation to place a custom μECoG array to record SSEPs in an acute procedure. The craniotomy was initiated near Bregma, creating a window 5 mm by 8 mm, measured by the coronal and sagittal suture, respectively. After the craniotomy and electrode placement were completed the animal was taken off of general anesthesia. Subsequent continuous IV infusion of dexmedetomidine (0.06–0.12 mg/kg/hr) and ketamine (15–25 mg/kg/hr) enabled cortical recordings.

Electrophysiology Procedures

Compound Nerve Action Potentials

In this experiment, we aim to address the working hypotheses that (A) the addition of a sieve interface to a cuff electrode housed within the medullary canal of the femur as part of an ONI would be capable of measuring bi-directional (efferent and afferent) CNAPs through a greater number of channels, and (B) that signaling improves over time. Electrophysiology was performed at weeks 3, 5, 8, and 12 post-implantation under general anesthesia. Printed circuit boards (PCBs) percutaneously connected to implanted electrodes were connected to a TDT system via a zero insertion force (ZIF) clip headstage. Prior to each recording session impedance of each electrode was

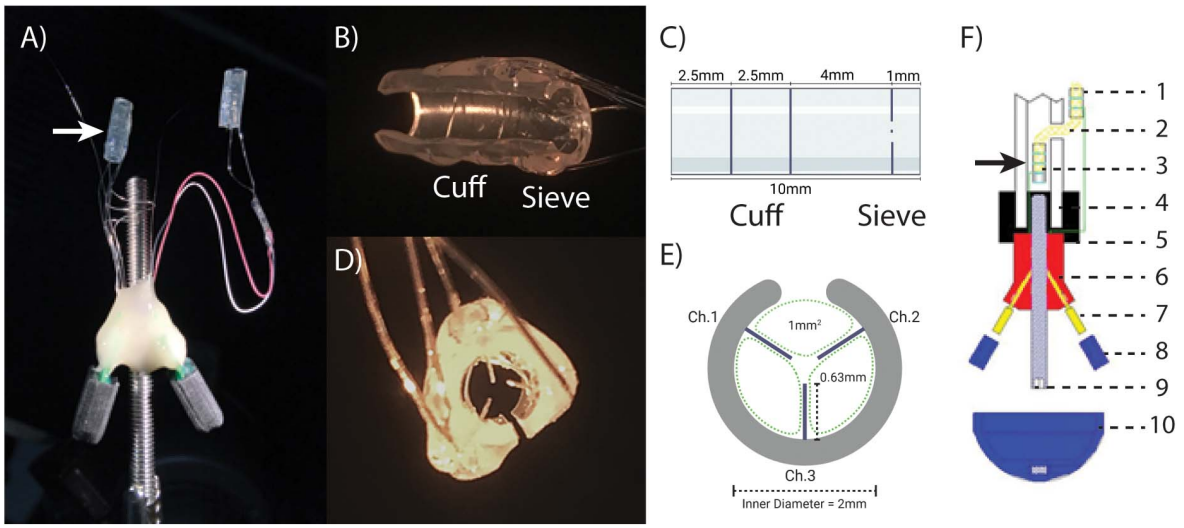

FIGURE 1 | The osseointegrated neural interface (ONI): **(A)** Photograph of the implanted ONI, with a modified intramedullary array (white arrow), containing an additional sieve interface. **(B,C)** A photograph and schematic, (respectively), of the modified intramedullary array, showing the placement of cuff and sieve electrodes. **(D,E)** A photograph and schematic, (respectively), of the sieve electrodes highlighting transit zones (green dotted lines, 1 mm^2) around the electrodes and channel designation, representative of the implanted electrode. The cut along the silicon tubing visible in **(B,D,E)** is to enable implantation around the nerve. **(F)** A schematic diagram of an implanted ONI highlighting the placement of the modified intramedullary array (black arrow) as well as the proximal array (1), nerve entering bone via the corticotomy (2), intramedullary array consisting of a cuff and sieve (3), bone (4), bone cement (5), epoxy resin (6), PCB (7), PCB cap (8), intramedullary screw (9), cap to protect PCBs (10). Green lines indicate Pt/Ir wire used to create electrode contacts (1 and 2), and connect to independent PCBs (7).

measured at 1,120 Hz using the PZ5 Neurodigitizer (Tucker Davis Technologies). Evoked potentials were recorded using a TDT PZ5 Neurodigitizer with a sampling rate of 25 kHz. CNAPs were generated through monophasic constant current pulses with a phase duration of 30 μs across a range of amplitudes (100 μV–8 mA), this range of amplitudes was used to find the stimulation threshold and confirm a graded response. The resulting CNAPs were low pass filtered (4th order Butterworth corner frequency = 5 kHz) and averaged to identify peak response from each of the stimulation-evoked CNAPs (n = 18–35 randomized trials per stimulation amplitude) and averaged across trials. Peak amplitude measurements were taken at 3 and 5 weeks and compared at 5 mA herein. Direction of stimulation was controlled through stimulation of the proximal or intramedullary array. Stimulation via the proximal array and recorded through the intramedullary array prompted efferent CNAPS. Conversely, afferent CNAPs were prompted through stimulation of intramedullary array and measured by the proximal array. Stimulations and recordings with the intramedullary array were performed sequentially though the cuff and each of the three sieve electrodes.

Somatosensory Evoked Potentials

In this experiment, we aim to address the working hypothesis (C) that stimulation at this interface generates measurable cortical SSEPs through a greater number of channels. The capacity to elicit somatosensory potentials from a sieve interface via an ONI was tested in an acute experiment at 12 weeks post-surgery. Stimulation was delivered to the terminal end of the nerve via the intramedullary array, stimulating through the cuff and each of the sieve electrodes separately. Responses evoked by stimulation were recorded via μECoG placed over somatosensory cortex contralateral to the amputation. Charge balanced single biphasic pulses (amplitude 100 μA–8 mA, phase 30 μs) were applied to confirm graded responses using an A-M Systems Isolated Pulse Stimulator Model 2100, controlled by a TDT Rz2 BioAmp Processor which was connected to a PCB on the μECoG via ZIF clip. Cortical responses evoked by stimulation from 30 randomized trials (n = 30) were amplified (×2), bandpass filtered (corner frequencies: 2.2 Hz–2.7 kHz) and digitized at 6 kHz using a PZ5 Neurodigitizer (TDT) (Dingle et al., 2020a).

Statistics

A total of seven data points were extracted around the time of peak response from each CNAP post filtering and averaged across time and trials in order to quantify the neural response. A two-way ANOVA with Tukey-Kramer *post hoc* test was performed on CNAP peak to peak response as evoked by stimulation amplitude for each of the recording electrodes (cuff, sieve electrode 1–3). All electrophysiological data analysis was performed in Matlab (Mathworks).

RESULTS

This work demonstrates proof of concept that a sieve interface can be housed and function within the medullary canal as part of an ONI. The previously published cuff based ONI (Dingle et al., 2020a) was successfully modified to contain an additional sieve interface (**Figure 1**). This modification consisted of three radial electrodes to form a sieve electrode based on previously

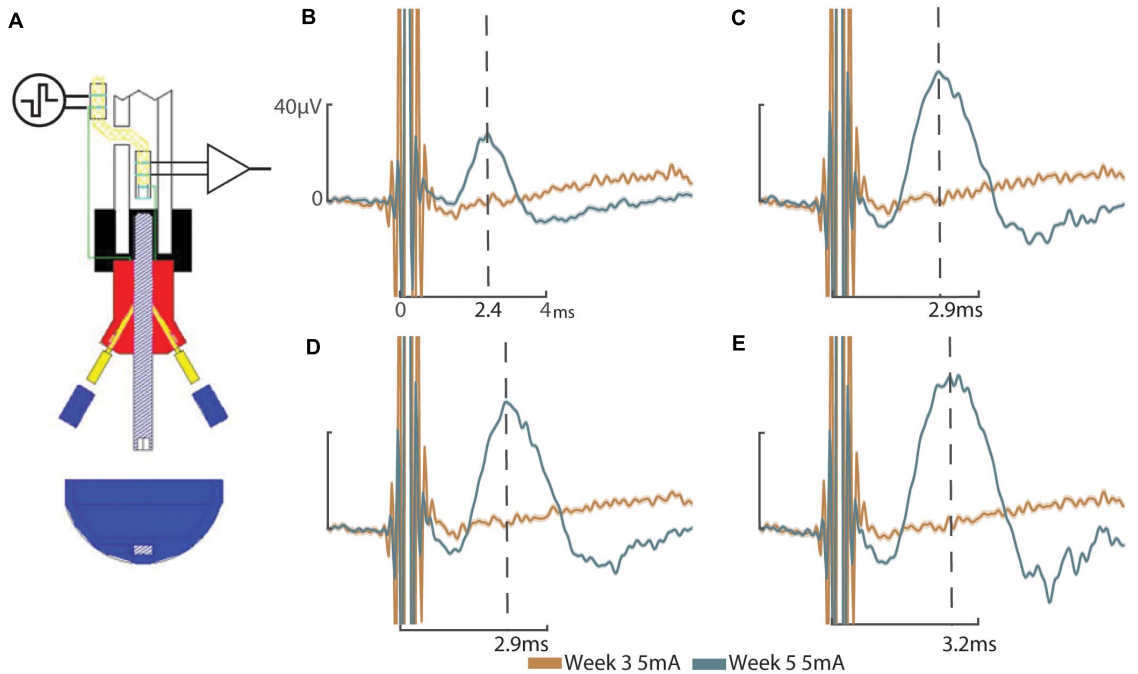

FIGURE 2 | Compound nerve action potentials: **(A)** Schematic representation of efferent stimulation through the ONI demonstrating application of electrical stimuli to the nerve via the proximal cuff and measured evoked potentials using the intramedullary cuff. Efferent CNAPs evoked from stimulation of the proximal cuff where recorded through the cuff and each of the sieve electrodes. **(B)** CNAPs recorded through the cuff at week 3 (peak amplitude = 0.82 ± 2.5 μV) and week 5 (peak amplitude = 27.72 ± 0.88 μV). **(C)** CNAPs recorded through Sieve Ch. 1 at 3 weeks (peak amplitude = 0.78 ± 3.61 μV) and 5 weeks (peak amplitude = 53.78 ± 0.64 μV. **(D)** CNAPs recorded through Sieve Ch. 2 at 3 weeks (peak amplitude = 2.91 ± 1.04 μV) and 5 weeks (peak amplitude = 52.60 ± 0.59 μV). **(E)** CNAPs recorded through Sieve Ch. 3 at 3 weeks (peak amplitude = 3.20 ± 1.12 μV) and 5 weeks (62.40 ± 1.30 μV). Peak amplitude at 3 weeks was determined manually, based on the timing of peak amplitude at 5 weeks, indicated by the dotted lines with times annotated on the *x*-axis **(B–E)**. Stimulation at 5 mA shown. Uniform scale bars **(B–E)** depict 0–40 microvolts (μV, *y*-axis) and 0–4 ms (ms, *x*-axis) as annotated in **(B)**. Standard deviation is shown underlying they average response **(B–E)**.

published designs to combine both sieve and cuff interfaces (Kim et al., 2020) and maximize transit zones (MacEwan et al., 2016). The modifications did not impact surgical implantation and the animal recovered well and remained unremarkable throughout the 12-week experimental period.

Electrophysiology

Compound Nerve Action Potentials

These results address the working hypotheses that (A) the addition of a sieve interface to a cuff electrode housed within the medullary canal of the femur as part of an ONI would be capable of measuring bi-directional (efferent and afferent) CNAPs through a greater number of channels, and (B) that signaling improves over time. At week three neither the cuff (impedance = 3.8 kΩ, peak amplitude = 0.82 ± 2.5 μV) nor the sieve electrodes (impedances = 13.6, 13.9, and 9.5 kΩ, peak amplitudes = 0.78 ± 3.61 μV, 2.91 ± 1.04 μV, and 3.20 ± 1.12 μV for channels 1–3, respectively) were able to successfully engage the nerve. Given another 2 weeks (week 5) engagement was achieved across all channels demonstrating improved electrophysiological function of the nerve in bone. At week 5, efferent responses are not equal across all channels, demonstrating a two-fold increase in peak amplitude response from the sieve electrodes (impedances = 13.0, 15.1, and 9.2 kΩ, peak amplitudes = 53.78 ± 0.64 μV, 52.60 ± 0.59 μV, and 62.40 ± 1.30 μV for channels 1–3, respectively, average peak amplitude = 56.26 μV) compared to the cuff (impedance = 2.4 kΩ, peak amplitude = 27.72 ± 0.88 μV) (**Figure 2**). Statistical analysis revealed a significant main effect of stimulation amplitude ($F_{3,245}$ = 902.51, P = 4.49e^{-132}) and electrode ($F_{3,245}$ = 178.98, P = 1.88e^{-61}) on the magnitude of evoked CNAPs, demonstrating consistently higher amplitudes through all three sieve electrodes compared to the cuff, and one sieve electrode (Ch. 3) above all others (**Figure 3**). A confounding factor in this experiment was that the proximal array was lost due to visibly broken wires found at the percutaneous site at the week 8 recording session. The broken wires were confirmed as an open circuit with impedance testing (≥536 kΩ) and the irreparable nature was confirmed via x-ray. While this array is not considered an essential component of a true ONI, it is required for conducting stimulation and recording under anesthesia. Afferent CNAPs were not successfully recorded.

Somatosensory Evoked Potentials

These results address the working hypothesis (C), that stimulation at this interface generates measurable cortical SSEPs through a greater number of channels. The intramedullary array remained functional throughout the sub-chronic 12-week

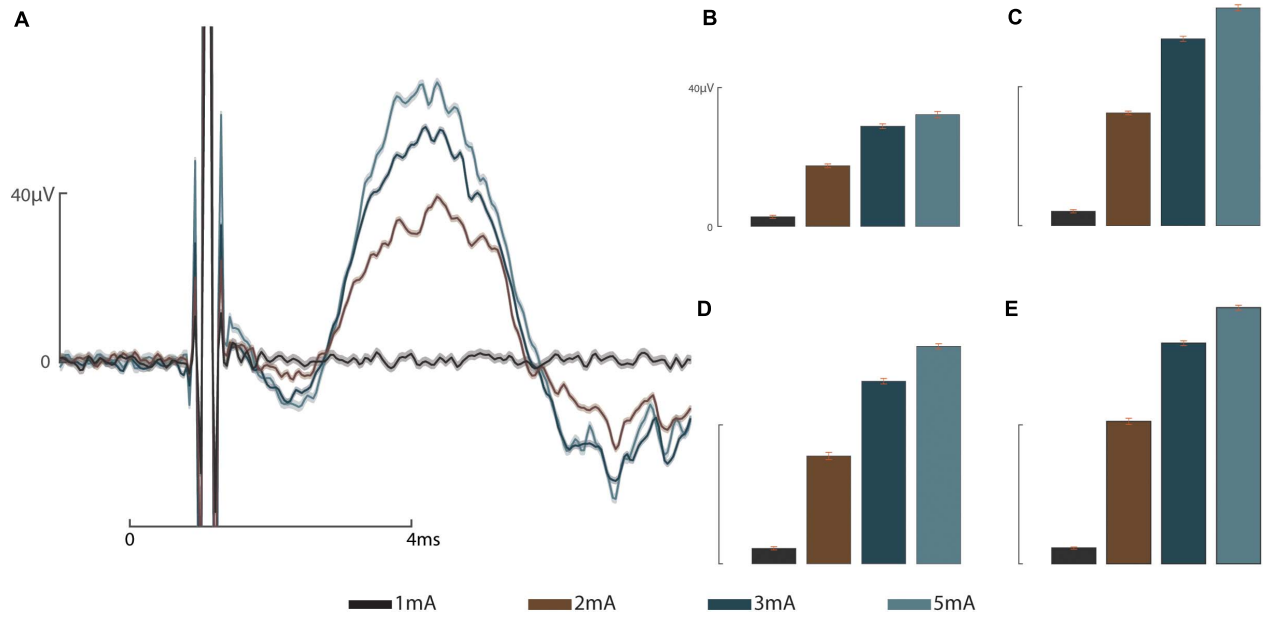

FIGURE 3 | Graded response to stimulus: **(A)** Representative graded response to stimulation at 1, 2, 3, and 5 mA from sieve Ch. 3. **(B)** Graded response to stimulation recorded by the intramedullary cuff electrode. **(C)** Graded response to stimulation recorded through sieve Ch. 1. **(D)** Graded response to stimulation recorded through sieve Ch. 2. **(E)** Graded response to stimulation recorded through sieve Ch. 3. Scale bars depict 0–40 microvolts (μV, *y*-axis) as annotated in **(A,B)**, and 0–4 ms (ms, *x*-axis, **A**).

period, as demonstrated by the ability to elicit SSEPs through the cuff electrode and each of the sieve electrodes (**Figure 3**). Nerve engagement through the three sieve electrodes varies from channel to channel, though statistically relevant spatiality between electrodes cannot be concluded. The strongest responses were recorded by μECoG electrodes 4, 7, and 8 (**Figure 3**). The three sieve electrodes demonstrate similar waveforms, all of which are greater than responses achieved through the cuff. Spatiality can be determined in the sense that stimulation elicits a response in some cortical regions (e.g., Ch. 4) and not others (e.g., Ch. 16).

DISCUSSION

Out of the myriad of potential peripheral nerve interfaces (PNIs), those with greater selectivity are considered to be the most invasive, which results in the shortest longevity and stability (Navarro et al., 2005; Ghafoor et al., 2017). Sieve electrodes enable close contact with individual nerve bundles or even individual fibers within the perineurium, resulting in greater selectivity than can be achieved with extraneural PNIs (MacEwan et al., 2016; Urbanchek et al., 2016). This increased selectively can ultimately translate to improved prosthetic control (Tyler and Durand, 2002; Ghafoor et al., 2017; Straka et al., 2018). The downside of such intimate contact is the potential for damage resulting from micro-motion (Branner et al., 2004; Desai et al., 2017; Wurth et al., 2017). Additionally, the classification of sieve electrodes as most invasive is based on the neurorrhaphy model in which they are tested (Navarro et al., 2005) and are not necessarily reflective of the amputation setting. We have previously developed a trans-femoral amputation model in rabbits based on the clinical transposition of nerve into bone to treat symptomatic neuroma that serves as the basis for creating an ONI for prosthetic control (Israel et al., 2018; Dingle et al., 2020b).

In this proof of concept study, we explore the concept of securely housing sieve electrodes in the medullary canal as part of an ONI as a potential method for increasing selectivity. By abutting sieve electrodes to the terminal end of the amputated nerve we demonstrate neural engagement improves over time comparable to a cuff electrode in the same animal (**Figure 2**) and historic data (Dingle et al., 2020a). Sieve electrodes demonstrated greater neural engagement (two-fold) than cuff electrodes (**Figure 2**). Furthermore, statistical analysis reveals that each of the sieve electrodes records a significantly higher magnitude than cuff electrodes (**Figure 3**), demonstrating resistance of the epineurium (Yoshida et al., 2000; Branner et al., 2004; Ghafoor et al., 2017). Histological examination of regeneration through transit zones was attempted, but failed due to tissue damage when retrieving the interface from the osseointegrated hardware within the bone. Neural regeneration through transit zones has been demonstrated previously in this model in the absence of osseointegration and associated electrode hardware. The loss of the proximal array after the fifth week precluded electrophysiological time points matching our previous studies, including the recording of afferent CNAPS from 8 weeks post-operatively (Dingle et al., 2020a).

Despite the complication of losing the proximal array after 5 weeks, the intramedullary array remained operational and viability was confirmed by the recording of afferent

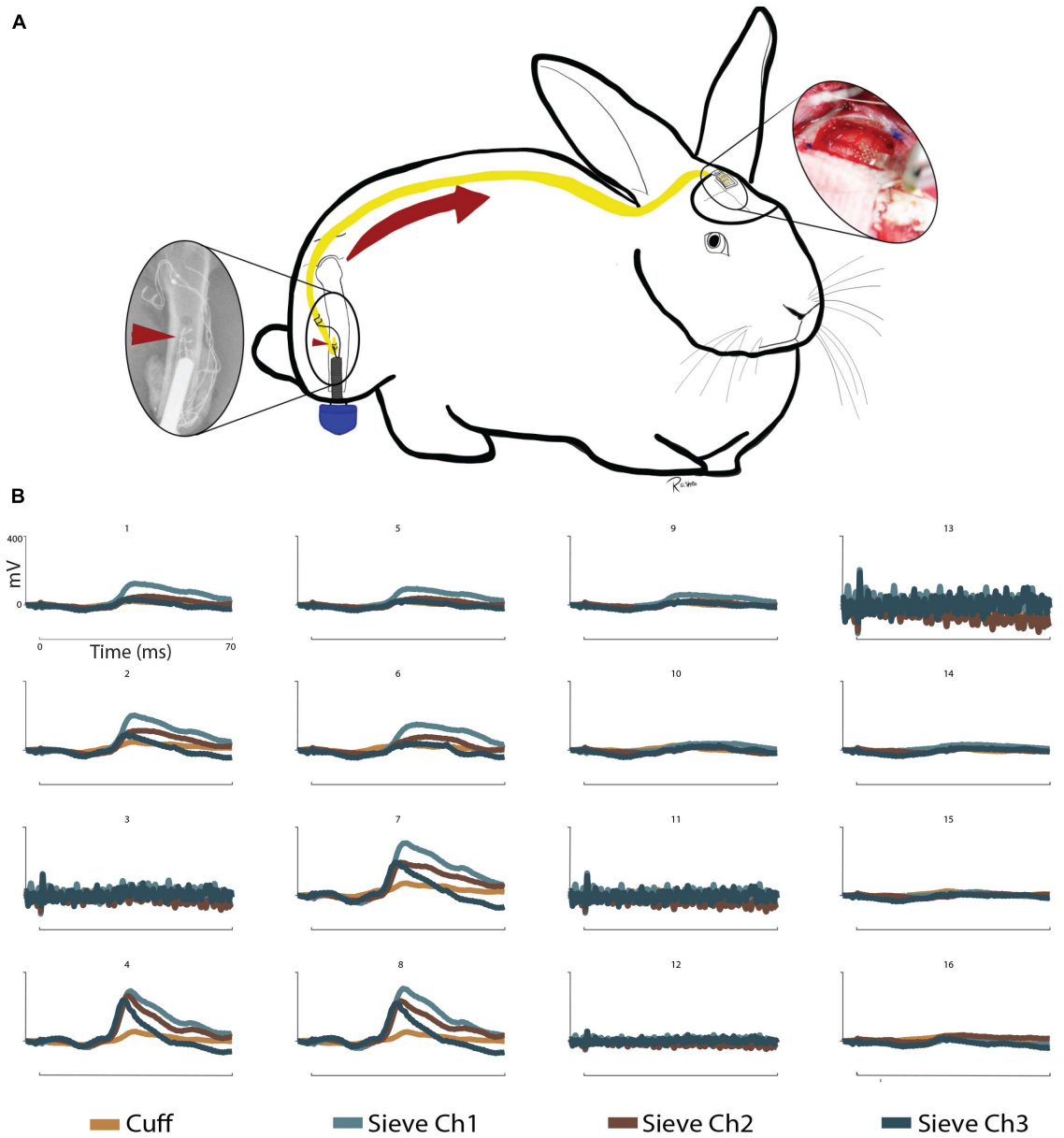

FIGURE 4 | Somatosensory evoked potentials: **(A)** Schematic representation of sensory information written to the CNS via a sieve interface as part of an ONI. Left to right: The intramedullary array (red arrowheads) stimulates the sciatic nerve within the medullary canal of the femur. Afferent action potentials travel from the PNS to the CNS (red arrow) and are recorded over the contralateral somatosensory cortex via μECoG. **(B)** SSEPs recorded via 16 channel micro-electrocorticography in a terminal operation at week 12. Stimulation was provided through the cuff and sieve electrodes. Stimulation results in cortical spatiality as demonstrated by clear signals in channels 4, 7, and 8 from the sieve electrodes and weaker responses from the cuff. Reduced cortical responses can be seen in channels 1, 2, 5, 6, and 9 and no clear signals in channels 10, 14–16. Channels 3, 11, 12, and 13 of the μECoG were not functional at the time of recording. Stimulation at 5 mA shown. Uniform scale bars (channels 1–16) depict 0–400 mV (mV, *y*-axis) and 0–70 ms (ms, *x*-axis) as annotated in B1.

cortical responses to stimulation 12-weeks post implantation (**Figure 4**). Cuff and sieve electrodes demonstrated nerve engagement with signals propagating to cortical brain regions. The strongest responses were recorded by μECoG electrodes 4, 7, and 8, (**Figure 4**). Sieve Ch. 3 had the strongest efferent CNAPs in week 5 (**Figures 2**, **3**) but the weakest afferent SSEPs through to the cortical regions in week 12 (**Figure 4**). In cortical regions of stimulation, the similarity in the waveforms indicates sieve electrodes are activating similar cortical regions signifying selectivity between these electrodes is poor. This is expected given the rudimentary construction of the array. Spatiality of the cortical response can be observed in the sense that responses to cuff and sieve electrodes differ enough to indicate each electrode simulates different areas of cortex with substantial overlap (**Figure 4**). As with CNAPs, SSEPs evoked through stimulation of the sieve demonstrated

greater peak amplitudes than those achieved with the cuff, supporting the requirement for lower stimulation thresholds with more intimate neural contact (Tyler and Durand, 2002; Ghafoor et al., 2017).

This study was *not* intended to demonstrate the preferential function of any specific sieve interface; rather, the intention was to demonstrate proof of concept for stably housing a sieve interface within the medullary canal and engaging with transposed nerves in an amputation model based on a clinical procedure for treating neuroma (Israel et al., 2018). The ONI model for peripheral nerve interfacing and prosthetic attachment is amenable to the application of more sophisticated sieve electrodes capable of greater selectivity for improved prosthetic control. Our simplified design demonstrates the capacity for bi-directional (efferent CNAPs and afferent SSEPs) stimulation and recording aided by percutaneous connectivity of an osseointegrated prosthetic abutment. Our results support the ability for osseointegrated prosthetics to handle percutaneous neural interface connections, confirming the stability of routing wires (Ortiz-Catalan et al., 2014).

CONCLUSION

This proof of concept experiment successfully demonstrates the working hypotheses that (A) sieve interface can be housed within the medullary canal of long bones in conjunction with a cuff electrode as part of an ONI capable of recording efferent CNAPs from a greater number of channels, (B) that the signal improves over time; and (C) that afferent stimulation through the sieve can generate SSEPs, demonstrating the ability to elicit SSEPs through a greater number of channels, contributing to the literature concerning osseointegrated neural interfacing. The ONI allows the application of a sieve electrode on the terminal end of amputated nerves, secured within the bone with direct connectivity afforded by percutaneous osseointegration. This proof of concept supports future work for the application of more sophisticated sieve electrodes within the medullary canal as part of an ONI for improved prosthetic control.

DATA AVAILABILITY STATEMENT

The raw data supporting the conclusions of this article will be made available by the authors, without undue reservation.

ETHICS STATEMENT

All animal procedures were approved by the University of Wisconsin Institutional Animal Care and Use Committee (IACUC, #V005256), the United States Army Medical Research and Material Command (USAMRMC, #DARPA-8728), and the Animal Care and Use Review Office (ACURO, #DARPA-8728).

AUTHOR CONTRIBUTIONS

SP, AD, JW, AS, and MM: conceptualization. AD, JPN, JN, and AM: data curation. AD, JPN, JN, AS, and AM: data analysis. SP and JW: funding acquisition. AD, JPN, JN, BN, YL, AM, and RM: investigation. SP, YL, BN, AD, JN, JPN, AS, JW, MM, RM, and AM: methodology. AD and BN: project administration. SP, JW, MM, and BN: resources. AS, JPN, and JN: software. SP, JW, MM, BN, and AD: supervision. AD and AS: validation. AD, JPN, JN, and AS: visualization. AD and AM: writing – original draft preparation. AD, JPN, AM, and RM: writing – figures. AM, AD, JPN, JN, WZ, YL, RM, BN, MM, AS, JW, and SP: writing – review and editing. All authors contributed to the article and approved the submitted version.

FUNDING

This work was sponsored by the Defense Advanced Research Projects Agency (DARPA), Biological Technologies Office (BTO), and Hand Proprioception and Touch Interfaces (HAPTIX) program through the DARPA Contracts Management Office Grant/Contract No. HR0011-17-2-0050.

REFERENCES

Boldrey, E. (1943). Amputation neuroma in nerves implanted in bone. *Ann. Surg.* 118, 1052–1057. doi: 10.1097/00000658-194312000-00011

Branner, A., Stein, R. B., Fernandez, E., Aoyagi, Y., and Normann, R. A. (2004). Long-term stimulation and recording with a penetrating microelectrode array in cat sciatic nerve. *IEEE Trans. Biomed. Eng.* 51, 146–157. doi: 10.1109/tbme.2003.820321

Cheesborough, J. E., Smith, L. H., Kuiken, T. A., and Dumanian, G. A. (2015). Targeted muscle reinnervation and advanced prosthetic arms. *Semin. Plast. Surg.* 29, 062–072. doi: 10.1055/s-0035-1544166

Davis, R. W. (1993). Phantom sensation, phantom pain, and stump pain. *Arch. Phys. Med. Rehabil.* 74, 79–91.

Desai, V. H., Spearman, B. S., Shafor, C. S., Natt, S., Teem, B., and Graham, J. B. (2017). "Design, fabrication, and characterization of a scalable tissue-engineered-electronic-nerve-interface (TEENI) device," in *Proceedings of the 2017 8th International IEEE/EMBS Conference on Neural Engineering (NER)*, (Shanghai, China: IEEE), 203–206.

Dingle, A. M., Ness, J. P., Novello, J., Israel, J. S., Sanchez, R., and Millevolte, A. X. T. (2020a). Methodology for creating a chronic osseointegrated neural interface for prosthetic control in rabbits. *J. Neurosci. Methods* 331:108504. doi: 10.1016/j.jneumeth.2019.108504

Dingle, A. M., Ness, J. P., Novello, J., Millevolte, A. X. T., Zeng, W., and Sanchez, R. (2020b). Experimental basis for creating an osseointegrated neural interface for prosthetic control: a pilot study in rabbits. *Mil. Med.* 185 (Supplement_1), 462–469. doi: 10.1093/milmed/usz246

Gallagher, P., and Maclachlan, M. (2001). Adjustment to an artificial limb: a qualitative perspective. *J. Health Psychol.* 6, 85–100. doi: 10.1177/135910530100600107

Ghafoor, U., Kim, S., and Hong, K.-S. (2017). Selectivity and longevity of peripheral-nerve and machine interfaces: a review. *Front. Neurorobot.* 11:59.

Goldstein, S. A., and Sturim, H. S. (1985). Intraosseous nerve transposition for treatment of painful neuromas. *J. Hand Surg.* 10, 270–274. doi: 10.1016/s0363-5023(85)80120-9

Grill, W. M., Norman, S. E., and Bellamkonda, R. V. (2009). Implanted neural interfaces: biochallenges and engineered solutions. *Annu. Rev. Biomed. Eng.* 11, 1–24. doi: 10.1146/annurev-bioeng-061008-124927

Horch, K., Meek, S., Taylor, T. G., and Hutchinson, D. T. (2011). Object discrimination with an artificial hand using electrical stimulation of peripheral tactile and proprioceptive pathways with intrafascicular electrodes. *IEEE Trans. Neural Syst. Rehabil. Eng.* 19, 483–489. doi: 10.1109/tnsre.2011.2162635

Israel, J. S., Dingle, A. M., Sanchez, R. J., Kapur, S. K., Brodnick, S., and Richner, T. J. (2018). Neuroma implantation into long bones: clinical foundation for a novel osseointegrated peripheral nerve interface. *Plast. Reconstr. Surg. Global Open* 6:e1788. doi: 10.1097/gox.0000000000001788

Kim, H., Dingle, A. M., Ness, J. P., Baek, D.-H., Bong, J., and Lee, I.-K. (2020). Cuff and sieve electrode (CASE): the combination of neural electrodes for bi-directional peripheral nerve interfacing. *J. Neurosci. Methods* 336:108602. doi: 10.1016/j.jneumeth.2020.108602

MacEwan, M. R., Zellmer, E. R., Wheeler, J. J., Burton, H., and Moran, D. W. (2016). Regenerated sciatic nerve axons stimulated through a chronically implanted macro-sieve electrode. *Front. Neurosci.* 10:557.

Micera, S., and Navarro, X. (2009). Chapter 2 bidirectional interfaces with the peripheral nervous system. *Int. Rev. Neurobiol.* 86, 23–38. doi: 10.1016/s0074-7742(09)86002-9

Mioton, L. M., and Dumanian, G. A. (2018). Targeted muscle reinnervation and prosthetic rehabilitation after limb loss. *J. Surg. Oncol.* 118, 807–814. doi: 10.1002/jso.25256

Navarro, X., Krueger, T. B., Lago, N., Micera, S., Stieglitz, T., and Dario, P. (2005). A critical review of interfaces with the peripheral nervous system for the control of neuroprostheses and hybrid bionic systems. *J. Peripher. Nerv. Syst.* 10, 229–258. doi: 10.1111/j.1085-9489.2005.10303.x

Ortiz-Catalan, M., Hakansson, B., and Branemark, R. (2014). An osseointegrated human-machine gateway for long-term sensory feedback and motor control of artificial limbs. *Sci. Transl. Med.* 6:257re6.

Straka, M., Shafer, B., Vasudevan, S., Welle, C., and Rieth, L. (2018). Characterizing longitudinal changes in the impedance spectra of in-vivo peripheral nerve electrodes. *Micromachines* 9:587. doi: 10.3390/mi9110587

Tan, D. W., Schiefer, M. A., Keith, M. W., Anderson, J. R., and Tyler, D. J. (2015). Stability and selectivity of a chronic, multi-contact cuff electrode for sensory stimulation in human amputees. *J. Neural Eng.* 12:026002. doi: 10.1088/1741-2560/12/2/026002

Tan, D. W., Schiefer, M. A., Keith, M. W., Anderson, J. R., Tyler, J., and Tyler, D. J. (2014). A neural interface provides long-term stable natural touch perception. *Sci. Transl. Med.* 6:257ra138. doi: 10.1126/scitranslmed.3008669

Thongpang, S., Richner, T. J., Brodnick, S. K., Schendel, A., Kim, J., and Adam Wilson, J. (2011). A micro-electrocorticography platform and deployment strategies for chronic BCI applications. *Clin. EEG Neurosci.* 42, 259–265. doi: 10.1177/155005941104200412

Tyler, D. J., and Durand, D. M. (2002). Functionally selective peripheral nerve stimulation with a flat interface nerve electrode. *IEEE Trans. Neural Syst. Rehabil. Eng.* 10, 294–303. doi: 10.1109/tnsre.2002.806840

Urbanchek, M. G., Kung, T. A., Frost, C. M., Martin, D. C., Larkin, L. M., and Wollstein, A. (2016). Development of a regenerative peripheral nerve interface for control of a neuroprosthetic limb. *BioMed. Res.* 2016:5726730.

Valerio, I., Schulz, S. A., West, J., Westenberg, R. F., and Eberlin, K. R. (2020). Targeted muscle reinnervation combined with a vascularized pedicled regenerative peripheral nerve interface. *Plast. Reconstr. Surg. Global Open* 8:e2689. doi: 10.1097/gox.0000000000002689

Vela, F. J., Martínez-Chacón, G., Ballestín, A., Campos, J. L., Sánchez-Margallo, F. M., and Abellán, E. (2020). Animal models used to study direct peripheral nerve repair: a systematic review. *Neural Regen. Res.* 15, 491–502. doi: 10.4103/1673-5374.266068

Woo, S. L., Kung, J. A., Brown, D. L., Leonard, J. A., Kelly, B. M., and Cederna, P. S. (2016). Regenerative peripheral nerve interfaces for the treatment of postamputation neuroma pain: a pilot study. *Plast. Reconstr. Surg. Global Open* 4:e1038.

Wurth, S., Capogrosso, M., Raspopovic, S., Gandar, J., Federici, G., Kinany, N., et al. (2017). Long-term usability and bio-integration of polyimide-based intra-neural stimulating electrodes. *Biomaterials* 122, 114–129.

Yoshida, K., Jovanoviæ, K., and Stein, R. B. (2000). Intrafascicular electrodes for stimulation and recording from mudpuppy spinal roots. *J. Neurosci. Methods* 96, 47–55.

Ziegler-Graham, K., MacKenzie, E. J., Ephraim, P. L., Travison, T. G., and Brookmeyer, R. (2008). Estimating the prevalence of limb loss in the United States: 2005 to 2050. *Arch. Phys. Med. Rehabil.* 89, 422–429.

Conflict of Interest: JW has ownership interests in NeuroOne Medical Inc., and Neuronexus Technologies, companies which produce and market micro-electrode technologies, including peripheral neural interfaces. JW and SP own intellectual property related to the material discussed in this manuscript which has been assigned to the Wisconsin Alumni Research Foundation.

The remaining authors declare that the research was conducted in the absence of any commercial or financial relationships that could be construed as a potential conflict of interest.

frontiers in Neuroscience

ORIGINAL RESEARCH
published: 21 May 2021
doi: 10.3389/fnins.2021.607905

Surface Electromyography and Electroencephalogram-Based Gait Phase Recognition and Correlations Between Cortical and Locomotor Muscle in the Seven Gait Phases

Pengna Wei, Jinhua Zhang, Baozeng Wang and Jun Hong*

The Key Laboratory of Education Ministry for Modern Design and Rotor-Bearing System, School of Mechanical Engineering, Xi'an Jiaotong University, Xi'an, China

The classification of gait phases based on surface electromyography (sEMG) and electroencephalogram (EEG) can be used to the control systems of lower limb exoskeletons for the rehabilitation of patients with lower limb disorders. In this study, the slope sign change (SSC) and mean power frequency (MPF) features of EEG and sEMG were used to recognize the seven gait phases [loading response (LR), mid-stance (MST), terminal stance (TST), pre-swing (PSW), initial swing (ISW), mid-swing (MSW), and terminal swing (TSW)]. Previous researchers have found that the cortex is involved in the regulation of treadmill walking. However, corticomuscular interaction analysis in a high level of gait phase granularity remains lacking in the time–frequency domain, and the feasibility of gait phase recognition based on EEG combined with sEMG is unknown. Therefore, the time–frequency cross mutual information (TFCMI) method was applied to research the theoretical basis of gait control in seven gait phases using beta-band EEG and sEMG data. We firstly found that the feature set comprising SSC of EEG as well as SSC and MPF of sEMG was robust for the recognition of seven gait phases under three different walking speeds. Secondly, the distribution of TFCMI values in eight topographies (eight muscles) was different at PSW and TSW phases. Thirdly, the differences of corticomuscular interaction between LR and MST and between TST and PSW of eight muscles were not significant. These insights enrich previous findings of the authors who have carried out gait phase recognition and provide a theoretical basis for gait recognition based on EEG and sEMG.

Keywords: electroencephalogram, surface electromyography, gait phases, pattern recognition, time–frequency cross mutual information

OPEN ACCESS

Edited by:
Kyuhwa Lee,
Wyss Center for Bio and Neuroengineering, Switzerland

Reviewed by:
Yongtian He,
University of Houston, United States
Giovanna Catavitello,
Catholic University of Louvain, Belgium

****Correspondence:***
Jinhua Zhang
jjshua@mail.xjtu.edu.cn

Specialty section:
This article was submitted to Neuroprosthetics, a section of the journal Frontiers in Neuroscience

Received: *18 September 2020*
Accepted: *06 April 2021*
Published: *21 May 2021*

Citation:
Wei PN, Zhang JH, Wang BZ and Hong J (2021) Surface Electromyography and Electroencephalogram-Based Gait Phase Recognition and Correlations Between Cortical and Locomotor Muscle in the Seven Gait Phases. Front. Neurosci. 15:607905. doi: 10.3389/fnins.2021.607905

INTRODUCTION

Human locomotor disorder seriously affects the quality of life. Nontraumatic gait disorder is caused by brain damage and is a feature of many neurological disorders such as stroke, cerebral palsy, and Parkinson's disease (Louie and Eng, 2016; Ziegler et al., 2018). Surface electromyography (sEMG)-based rehabilitative devices or robots have been developed for neurological injury rehabilitation of

lower limb functions (Veneman et al., 2007; Banala et al., 2008). The classification results of gait phases from sEMG can be used to control the gait of lower limb exoskeletons for the rehabilitation of patients with lower limb disorders (Joshi et al., 2013). The human gait cycle is divided into stance and swing phases (Taborri et al., 2016). In this study, the stance phase is then subdivided into loading response (LR), mid-stance (MST), terminal stance (TST), and pre-swing (PSW). Similarly, the swing phase is divided into the initial swing (ISW), mid-swing (MSW), and terminal swing (TSW). More information about gait partitioning methods is available elsewhere in the literature (Taborri et al., 2016).

However, sEMG signals change due to muscle fatigue and sweat. Patients will suffer from muscle fatigue after training. Therefore, gait phase recognition methods only using sEMG signals are limited, meaning they cannot identify all seven gait phases. For instance, Li et al. (2016) utilized sEMG signals to recognize five gait phases, while Wei et al. applied sEMG and kinematic data from both legs to recognize five gait phases (Wei et al., 2018). However, electroencephalogram (EEG) signals will counteract these shortcomings (susceptible to fatigue and sweating) of sEMG. The cortex is activated during walking and EEG signals will enrich the gait information for gait prediction. EEG and sEMG signals, generated before movement, can be used to predict gait (Gao et al., 2018; Ziegler et al., 2018). Nevertheless, the theoretical basis of gait phase recognition based on EEG combined with sEMG has not been researched.

Human bipedal walking is an automatic activity. It includes top-down pathways (from the brain toward the spinal cord and periphery) to generate a motor action, while it also includes feedback from the periphery to the brain to correct the motion. Several research groups have observed significant cortical activation (for example, in the premotor, supplementary motor, and primary sensorimotor regions) during walking (la Fougère et al., 2010; Bradford et al., 2016; Artoni et al., 2017). In 2019, Jensen and colleagues found that the motor cortex contributes to both ankle plantar flexor muscle activity and forward propulsion during gait (Jensen et al., 2019). The authors of recent studies have found that the gait phase is associated with cortical activity modulations (Wagner et al., 2012, 2014; Bradford et al., 2016). However, corticomuscular connectivity remains unclear during walking.

Various researchers have used either coherence or correlation analysis methods to measure corticomuscular coherence (Artoni et al., 2017; Jensen et al., 2019), such as Jensen et al. who performed frequency domain analysis of the correlation between EEG–EMG and EMG–EMG. However, coherence and correlation analysis are suitable for linear signals, while both EEG and sEMG signals are nonlinear (Popivanov and Dushanova, 1999). The nonlinear characteristics include point-wise correlation dimension, Kolmogorov entropy, and largest Lyapunov exponents as functions of time. The time–frequency cross mutual information (TFCMI) method can be utilized to calculate mutual information between two time–frequency domain signals (Lu et al., 2011; Anmin Gong et al., 2018). The TFCMI method integrates the time and frequency components of the signal, then the nonlinear correlation calculation method is used to estimate the similarity of multichannel physiological signals. We used TFCMI to estimate the interaction between EEG and sEMG channels during walking.

In this study, we firstly used sEMG, EEG signals, and 3D motion trajectory data (Taborri et al., 2016) for lower limbs to predict all seven gait phases. The robustness of sEMG and EEG-based neural interface was analyzed because people cannot always walk at a fixed speed (Marchal-Crespo and Reinkensmeyer, 2009; Tefertiller et al., 2011).

Therefore, we predict the gait phases at three speeds. Secondly, we calculated TFCMI values between beta-band EEG and sEMG channels in the seven gait phases to research the theoretical basis of gait phase recognition based on EEG and sEMG (Oliveira et al., 2018; Li et al., 2019).

MATERIALS AND METHODS

Participants and Ethical Approval

Nine healthy participants (seven males and two females, aged 23–26; body weight: 62 ± 10 kg; height: 171 ± 6 cm) were recruited from Xi'an Jiaotong University. All study procedures performed were approved by the Institutional Review Board of Xi'an Jiaotong University and carried out according to the Helsinki Declaration of 1975.

Experimental Device

The custom-designed equipment used in this experiment included a treadmill, an electrode cap, an amplifier with a built-in three-axis acceleration sensor, eight sEMG electrodes, 10 motion capture cameras, and 16 Vicon reflector balls, as shown in **Figure 1A**. We utilized a 32-channel LiveAmp Cap with multitrodes to record EEG and sEMG signals during treadmill walking. This LiveAmp Cap was a customized, wireless, lightweight, wearable device, meaning it caused minimum disturbance to the participants' movement while EEG and sEMG were recorded. A gaze screen with a cross symbol was used to focus the participants, as shown in **Figures 1B,C** shows the lower limb model in a motion capture system. All participants walked on the treadmill using their typical walking style. Participants choose a comfortable treadmill speed of 2.0 km/h during the experiment. The speeds of 1.4 and 2.6 km/h were also selected to simulate slow and fast walking speeds in everyday life.

Data Collection

All participants walked on a treadmill at three speeds (1.4, 2.0, and 2.6 km/h), respectively, in fifteen 30-s time blocks. There was a break between any two trials. Participants were asked to walk as usual, as well as to relax and minimize eye blinks, head rotation, and swallowing during the study. Participants were also asked to fix their gaze to the cross symbol, as shown in **Figure 1B**. The experiments were conducted in a quiet room.

EEG and sEMG signals and lower limb trajectory data were simultaneously recorded. Twenty-four-channel EEG signals (Fp1, Fp2, F3, F4, C3, C4, P3, P4, O1, O2, F7, F8, T7, T8, P7, P8, Fz, Cz, Pz, Oz, M1, M2, FPz, and VEOG) and eight muscles [biceps femoris (BF), vastus medialis (VM), tibialis anterior (TA), and gastrocnemius medialis (GM), bilaterally]

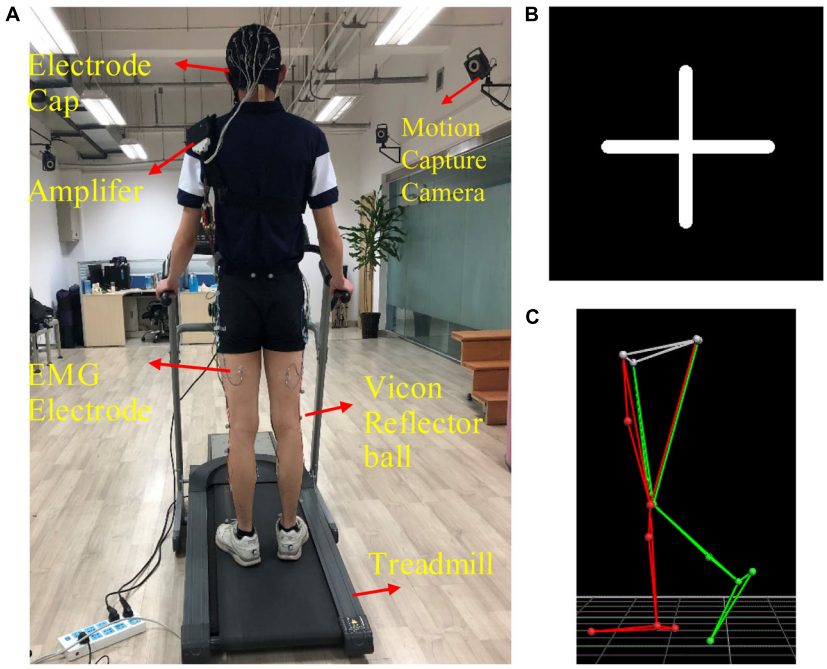

FIGURE 1 | (A) The experimental device, **(B)** the cross symbol, and **(C)** the lower limb model in the motion capture system. The 16 positions of the Vicon reflector balls are the anterior superior iliac, posterior superior iliac, thigh, knee, tibia, ankle, heel, and toe, bilaterally.

of the lower limb sEMG signals were collected by the 32Ch LiveAmp Cap at a sampling rate of 500 Hz. Twenty-four unipolar channels were collected in the cap, and electrodes for eight bipolar sEMG were recorded at the BF, VM, TA, and GM. These muscles were selected as they are related to the entire gait cycle (Perry and Davids, 1992; Petersen et al., 2012). Locations for sEMG electrodes were selected based on the SENIAM guidelines[1] (Artoni et al., 2017), while EEG electrodes were placed following the international 10–20 electrode system. The impedance of EEG and sEMG electrodes was kept under 20 kΩ throughout the experiment (Gwin et al., 2011).

Signals were amplified using a wireless LiveAmp amplifier (Brain Products Inc., Gilching, Germany). The track of 16 positions of the lower limbs was acquired by 16 reflective markers, using a 10-camera motion capture system Nexus 2.6 (VICON T40S, United Kingdom) at a sampling rate of 100 Hz. Reflective markers' positions are presented in **Figure 1C**. The motion capture system was synchronized with the wireless LiveAmp amplifier *via* the LiveAmp sensor and trigger extension. 3D marker data were resampled and aligned to EEG and sEMG data using a MATLAB (MathWorks Natick, MA, United States) script, based on the EEGLAB toolbox (Delorme and Makeig, 2004) before further preprocessing.

Data Processing

EEG and sEMG Data Processing

Raw EEG data were preprocessed using Brain Vision Analyzer 2.1 (Brain Products Inc., Gilching, Germany) and a MATLAB (MathWorks, Natick, MA, United States) script based on the EEGLAB toolbox, thus minimizing motion and other artifacts (Kline et al., 2015). The raw signal processing flow can be seen in **Supplementary Figure 1**. The default reference position of the electrode cap is FCz. However, FCz was too close to other EEG electrodes. Therefore, raw data were re-referenced to the mastoid, and the mean of the left and the right mastoid signal was calculated as a new reference. The EEG, EOG, and three-axis acceleration channels were selected. EEG signals were then high-pass filtered using a zero-phase 0.5 Hz cutoff, second-order Butterworth filter, and low-pass filtered using a zero-phase 50 Hz.

The EEG and sEMG data were resampled to 1,000 Hz and independent component analysis (ICA) (Sun et al., 2005) was used to decompose EEG signals into many independent components (ICs). The ICs which most correlated to lateral and vertical eye movement were marked and removed. sEMG signals were passed through an elliptic bandpass filter of 30–450 Hz bandwidth, while an FIR least-square bandstop notch filter of 50 Hz was used to remove low and high frequencies and residual line noise from raw sEMG signals. Wavelet denoising technology was used to remove noise in sEMG signals. The basic functions of the wavelet we adopted were "wden" and "db4." EEG and sEMG channels with obvious artifacts were removed following a visual inspection.

Gait Cycle Segmentation and Gait Phase Segmentation

3D marker data from the five positions were used to divide the gait cycle during treadmill walking. The z-direction corresponds to the vertical direction, the y-direction is the anteroposterior.

[1]www.seniam.org

The *z*-direction trajectory of the right heel with a more obvious periodicity of the gait cycle was applied to divide EEG and sEMG signals into single gait cycles (see **Supplementary Figure 2**). The seven gait phases are demarcated according to 3D marker data from the five positions (Perry and Davids, 1992; Ryu and Kim, 2014). The MSW is the period until the right foot is horizontal [vertical position of the right heel (Heel_RZ) equal to that of the right toe (Toe_RZ)] after ISW. TSW is the period until the distance between the left and right feet is the farthest at the first time[that is the first largest difference between the anteroposterior displacement of the right heel (Heel_RY) and that of the left heel (Heel_LY)] after the MSW. LR is the period until the right leg is being apart from land [vertical position of the right heel (Heel_RZ) equal to that of the left heel (Heel _LZ)] after TSW. MST is the period until the heel of the right leg is at the highest position after LR. TST is the period until the right foot is horizontal again after MST. PSW is the period until the distance between the left and right feet is the smallest after TST. ISW is the period until the end of the gait cycle. The gait phase segmentation result can be seen in **Figure 2**.

Feature Extraction

Feature extraction is a technique used to draw representation information from preprocessed input data. To analyze sEMG and EEG signals, feature extraction methods tend to include the time domain (TD), frequency domain (FD), and time–frequency (TFD) domain (Asghari Oskoei and Hu, 2007; Phinyomark et al., 2017; Martín-Clemente et al., 2018). In this study, slope sign change (SSC) and mean power frequency (MPF) were utilized to classify the seven gait phases. SSC is a time domain feature that also reflects signal frequency information. MPF is a mean frequency that is expressed as the sum of sEMG and EEG power frequency, divided by the total sum of the spectrum intensity. These extract features were combined and inputted to the library for support vector machine (LIBSVM) for classification. Three feature sets were combined. They were the SSC and MPF features of sEMG ([7 × 100, 8 × 2]), the SSC and MPF features of sEMG and the SSC feature of EEG ([7 × 100, (8 + 21) × 3]), the SSC and MPF features of sEMG, and the MPF feature of EEG ([7 × 100, (8 + 21) × 3]). In brackets are the feature set dimensions, 7 is the seven gait phases, 100 is the number of the feature values, 8 is the number of the sEMG channels, 21 is the number of the EEG channels, and 2 and 3 are the number of features (such as SSC of sEMG, SSC of EEG, etc.). Finally, two-thirds of the combined feature sets as training dataset were inputted to the support vector machine (SVM) to train the classifier. Then, one-thirds of the combined feature sets as testing dataset were inputted to the trained classifier to classify the seven gait phases. SVM parameters were optimized using the particle swarm optimization (PSO) method.

Time–Frequency Analysis Using TFCMI

TFCMI values were calculated to estimate the time–frequency correlation between EEG and sEMG channels. EEG and sEMG signals were normalized due to their large power

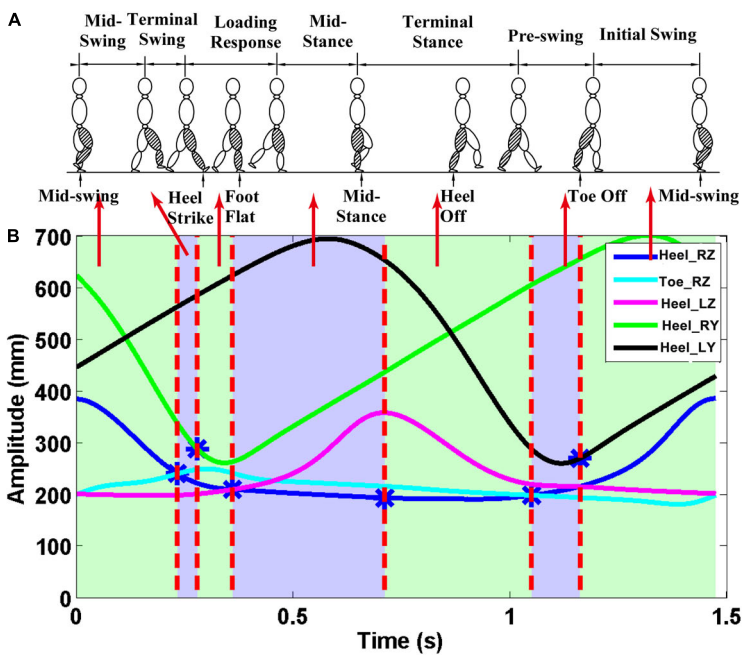

FIGURE 2 | Gait phase division results. The *z*-direction corresponds to the vertical direction, and the *y*-direction is the anteroposterior. **(A)** Seven gait phases of the gait cycle; **(B)** trajectory data. The first vertical red line—the first intersection of Heel_RZ and Toe_RZ. The second vertical red line—the point with the largest difference between Heel_RY and Heel_LY. The third vertical red line—the first intersection of the Heel_RZ and Heel_LZ. The fourth vertical red line—the maximum point of the Heel_LZ. The fifth vertical red line—the second intersection of the Heel_RZ and the Toe_RZ. Finally, the sixth vertical red line—the point with the smallest difference between the Heel_RY and the Heel_LY.

difference before TFCMI was calculated. The calculation process can be seen below.

Morlet wavelet transformation, which contains both time and frequency domain information, was utilized to transform the EEG signal into the time–frequency domain (Vialatte et al., 2007). Time–frequency power maps of each channel for beta (16–25 Hz) data were created. Therefore, the two maps were 10 × 2,000 and 16 × 2,000, respectively. Ten and 16 represent the frequency from 16 to 25 Hz and 30 to 45 Hz, while 2,000 represents the sample points. The mean of beta-band powers was calculated, respectively, before two 1 × 2,000 power curves were created in each channel.

Cross mutual information (CMI) between any two channels was calculated using the mean power signals. CMI maps were created by computing the entropy and mutual information, which can be expressed as:

$$\boldsymbol{H}\left(\boldsymbol{F}_i\right) = -\sum_{b=1}^{40} \boldsymbol{p}\left(\boldsymbol{F}_{i,b}\right) \log_2 \boldsymbol{p}\left(\boldsymbol{F}_{i,b}\right)$$

$$\begin{aligned} \boldsymbol{TFMI}\left(\boldsymbol{F}_i, \boldsymbol{F}_j\right) &= \boldsymbol{H}\left(\boldsymbol{F}_i\right) + \boldsymbol{H}\left(\boldsymbol{F}_j\right) - \boldsymbol{H}\left(\boldsymbol{F}_i, \boldsymbol{F}_j\right) \\ &= \sum_{b=1}^{40} \boldsymbol{p}\left(\boldsymbol{F}_{i,b}, \boldsymbol{F}_{j,b}\right) \log_2 \frac{\boldsymbol{p}\left(\boldsymbol{F}_{i,b}, \boldsymbol{F}_{j,b}\right)}{\boldsymbol{p}\left(\boldsymbol{F}_{i,b}\right)\boldsymbol{p}\left(\boldsymbol{F}_{j,b}\right)} \end{aligned}$$

where $\boldsymbol{H}\left(\boldsymbol{F}_i\right)$ denotes entropy, $\boldsymbol{F}_i$ is the mean power signals at the ith channel, $\boldsymbol{p}\left(\boldsymbol{F}_{i,b}\right)$ is the probability density function (PDF) of $\boldsymbol{F}_i$, $\boldsymbol{p}\left(\boldsymbol{F}_{i,b}, \boldsymbol{F}_{j,b}\right)$ is the joint probability density function (JPDF) of $\boldsymbol{F}_i$, while $\boldsymbol{F}_j$ $b = 1, 2, \cdots, 40$ is the bin number of the histogram used to construct the approximated PDF. Some 40 bins were selected based on both previous research and our data (Fraser and Swinney, 1986; Tamburri et al., 2002).

Finally, TFCMI values between any two channels were obtained to create a 31 × 31 (23 EEG and 8 sEMG channels) TFCMI map (**Supplementary Figure 3A**). Each entry of the 31× 31 matrices is the value of mutual information from TF power between a pair of channels. TFCMI values from the ith to the jth as well as the jth to the ith are the same. Therefore, the TFCMI map is symmetrical. Since TFCMI values were normalized, the diagonal TFCMI value (self-relevance) is equal to one. TFCMI values from the 13 EEG (lower limb movement-related electrodes: F3, F4, C3, C4, P3, P4, F7, F8, P7, P8, Fz, Cz, and Pz) and eight sEMG channels were extracted from the 31 × 31 matrices. We then calculated the mean of TFCMI values between 13 EEG and 8 sEMG channels in all trials, which were illustrated as a 13-channel topographic map. The map of mean coupling strength from the Oz channel to all EEG channels as well as the Fpz channel to all EEG channels can be seen in **Supplementary Figure 3B**.

RESULTS

Gait Phase Recognition Results

It should be noted that the sEMG data of two participants are unavailable due to surface electrode malfunction. Therefore, this analysis is based on seven participants. Gait phase recognition

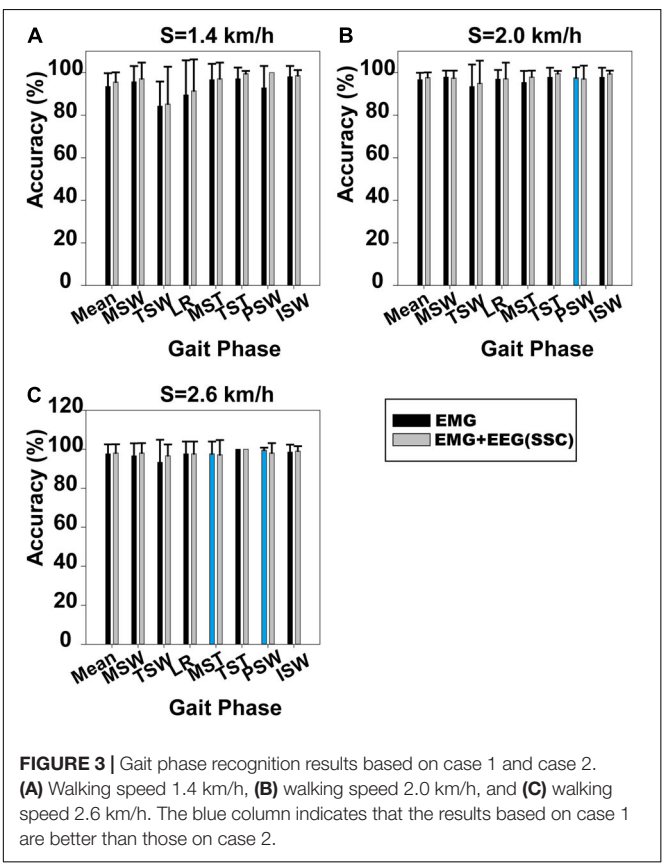

FIGURE 3 | Gait phase recognition results based on case 1 and case 2. **(A)** Walking speed 1.4 km/h, **(B)** walking speed 2.0 km/h, and **(C)** walking speed 2.6 km/h. The blue column indicates that the results based on case 1 are better than those on case 2.

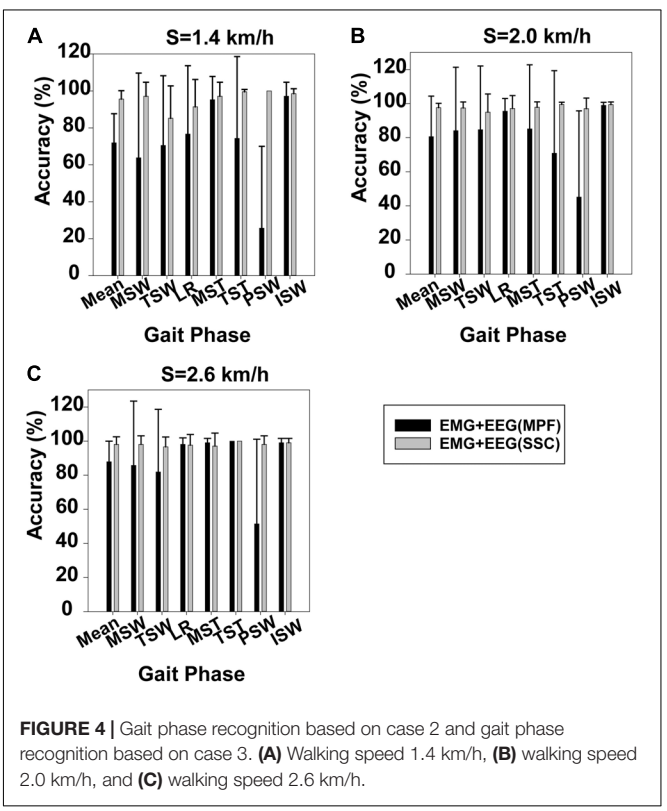

FIGURE 4 | Gait phase recognition based on case 2 and gait phase recognition based on case 3. **(A)** Walking speed 1.4 km/h, **(B)** walking speed 2.0 km/h, and **(C)** walking speed 2.6 km/h.

was based on the SSC and MPF features of the sEMG and EEG signals. For easy understanding, we define the SSC and MPF features of sEMG as case 1, define the SSC and MPF features of sEMG and the SSC feature of EEG as case 2, and define the SSC and MPF features of sEMG and the MPF feature of EEG as case 3. Firstly, we compared gait phase recognition based on case 1 and case 2. Secondly, gait phase recognition using case 2 was compared with recognition using case 3.

Difference Between sEMG and EEG Signal Features

Gait phase identification based on case 1 and case 2 is shown in **Figure 3**. Gait phase identification in the seven gait phases and the three speeds (1.4, 2.0, and 2.6 km/h) can be seen in **Figures 3A–C**, respectively. **Figure 3A** demonstrates that the mean accuracy of recognition of the seven gait phases using case 1 and case 2 was 93.47 and 95.58%. Also, the standard deviation (SD) decreased from 0.062 to 0.045. The mean accuracy has increased when the SSC of EEG was applied. The same can be observed in **Figures 3B,C**. In **Figure 3B**, the mean accuracy of identifying the seven gait phases increased from 96.69 to 97.63%, while the SD decreased from 0.032 to 0.025. In **Figure 3C**, the mean accuracy of identifying the seven gait phases increased from 97.62 to 98.10%, while the SD decreased from 0.048 to 0.044.

The Mann–Whitney *U*-test was used to analyze whether the difference in gait phase recognition between case 1 and case 2 was significant. We found that the difference between case 1 and case 2 was significant at 1.4 km/h (p = 0.034), but not at 2.0 km/h (p = 0.244) and 2.6 km/h (p = 0.746). The results for each participant based on case 1 and case 2 can be seen in **Supplementary Figures 4–6**.

Difference Between the EEG Features of the SSC and MPF

Figure 4 displays gait phase recognition based on case 2 and gait phase recognition based on case 3. Gait phase recognition in the seven phases at three speeds (1.4, 2.0, and 2.6 km/h) can be seen in **Figures 4A–C**, respectively. These figures demonstrate that the mean accuracy of recognition of the seven gait phases decreased

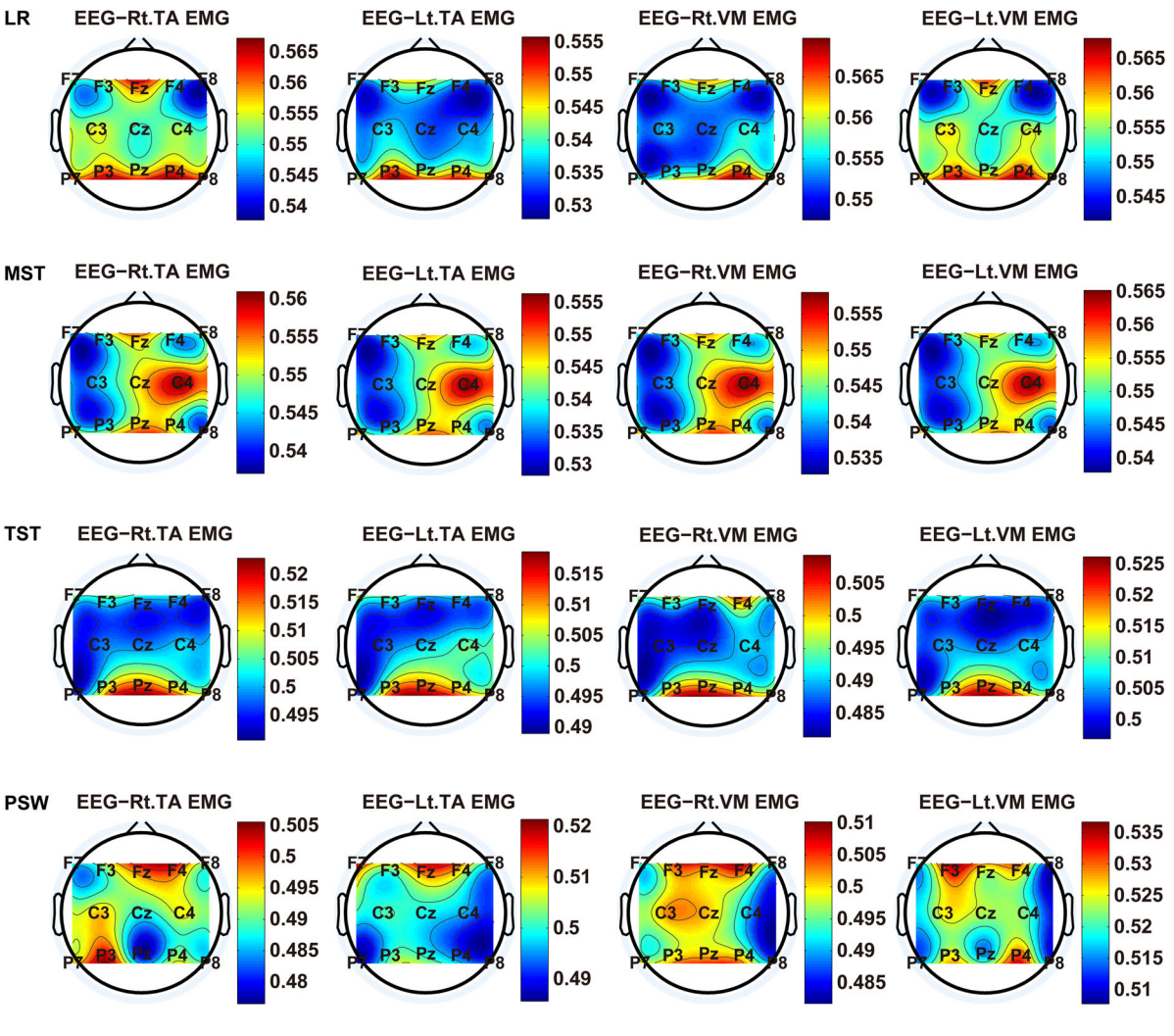

FIGURE 5 | The TFCMI topography between EEG (beta band) and sEMG (TA and VM) of the stance phase (LR, MST, TST, and PSW).

from 95.58 to 71.90%, 97.63 to 80.63%, and 98.10 to 87.89%, respectively, while the SD increased from 0.045 to 0.158, 0.025 to 0.23, and 0.044 to 0.121, respectively, when the SSC of EEG was replaced by the MPF of EEG. Some gait phase recognition results based on case 3 were below 60%, for example, PSW in **Figures 4A–C**. Using the Mann–Whitney *U*-test, we found that the gait phase recognition difference between the two sets was significant at 1.4 km/h ($p = 0.003$) but not significant at 2.0 km/h ($p = 0.092$) and 2.6 km/h ($p = 0.123$).

Time–Frequency Analysis of EEG and sEMG Signals in Seven Gait Phases Using TFCMI

We carried out a time–frequency analysis of the EEG and sEMG signals using TFCMI at a comfortable speed (2.0 km/h). TFCMI topography between EEG data (beta band) and sEMG can be seen in **Figures 5–8**. The results in **Figures 5**, **6** are based on the sEMG channels of the right (Rt.) and left (Lt.) TA as well as the right and left VM. Results in **Figures 7**, **8** are based on the sEMG channels of BF and GM of both legs. In **Figures 5–8**, we can observe that the distribution of TFCMI values of eight topographies was different in PSW ($p < 0.05$) and TSW ($p < 0.05$).

TFCMI values of the frontal, central, and parietal lobes were calculated and can be seen in **Figure 9**. One-way ANOVA was utilized to explore whether the difference between TFCMI values for the seven gait phases of eight muscles was significant. The results showed that the difference between TFCMI values for the seven gait phases of each muscle was significant ($p < 0.05$). Multiple comparisons were used to explore which two phases of the eight muscles differed significantly. The gait phases with no significant difference can be seen in **Table 1** due to the fact that there were too many phases with significant differences.

DISCUSSION

Gait phase recognition based on case 2 was better than recognition based on case 1 and case 3, as can be seen in **Figures 3**, **4**. The use of near-infrared spectroscopy (NIRS) (Miyai et al., 2001) and functional magnetic resonance imaging (fMRI) (Cunnington et al., 2005) has shown that the cortex is involved in steady-state walking. This suggests that the addition of SSC features of EEG will enrich gait information contained in sEMG features and improve the accuracy of gait phase recognition. However, the difference in gait phase recognition between case 1 and case 2 and between case 2 and case 3

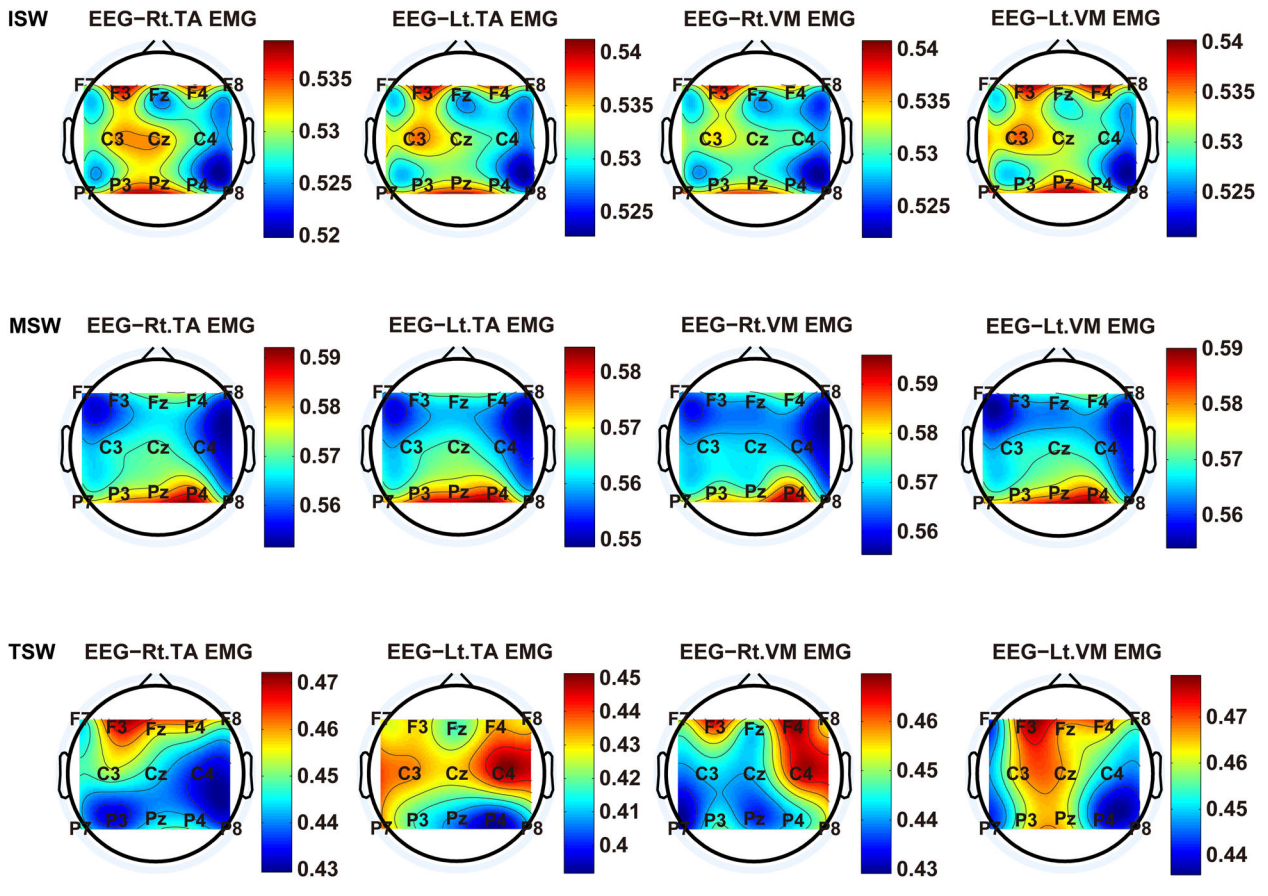

FIGURE 6 | The TFCMI topography between EEG (beta band) and sEMG (TA and VM) of the swing phase (ISW, MSW, and TSW).

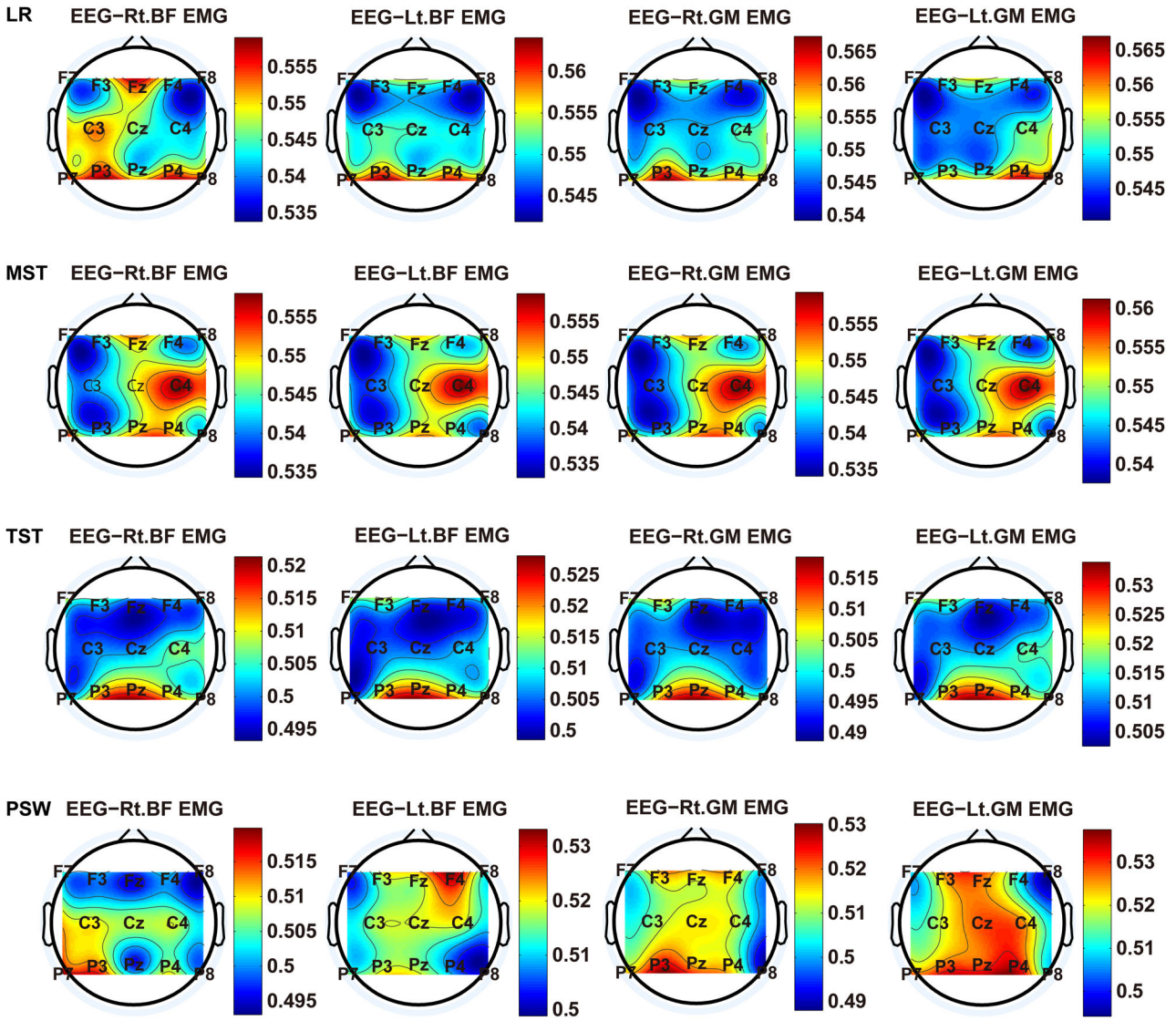

FIGURE 7 | TFCMI topography between EEG (beta band) and sEMG (BF and GM) of the stance phase (LR, MST, TST, and PSW).

was significant (p = 0.034, p = 0.003) only at the lowest speed (1.4 km/h), although the accuracy of gait phase recognition increased using case 2 at speeds of 2.0 and 2.6 km/h. This may be because relatively faster walking speeds reduced sensorimotor beta-band power (Nordin et al., 2019a), and this indicates that sensorimotor cortices process more sensory feedback than slow walking (Pfurtscheller and Lopes Da Silva, 1999; Nordin et al., 2019b). Previous research showed that bilateral coordination decreased in slow than in fast walking (Plotnik et al., 2013). This suggests that people need to pay more attention to slow walking than fast walking (Plotnik et al., 2013). Furthermore, we speculated that the contribution of the EEG features to gait phase recognition was reduced at faster rather than slower speeds. Overall, the mean accuracy of gait recognition using case 2 was significantly higher (95.58%) than those using other cases (case 1: 93.47%, case 3: 71.90%) at 1.4 km/h. Therefore, the gait phase recognition based on case 2 is suitable for a relatively low speed of walking.

We also investigated the difference in the results of gait phase recognition among the three walking speeds based on case 1 and case 2, respectively. The Mann–Whitney U-test showed that the difference of the results of gait phase recognition among the three walking speeds based on case 1 and case 3 was significant (p = 0.015 and p = 0.045). However, the difference in the results of gait phase recognition among the three walking speeds based on case 2 was not significant (p = 0.224). Case 2 was more robust than case 1 although the difference in gait phase recognition between the two feature sets was not significant at a faster speed (2.0 and 2.6 km/h).

Gait phase recognition for seven participants using case 2 can be seen in **Supplementary Figures 4–6**. Gait phase recognition based on case 1 was better than that based on case

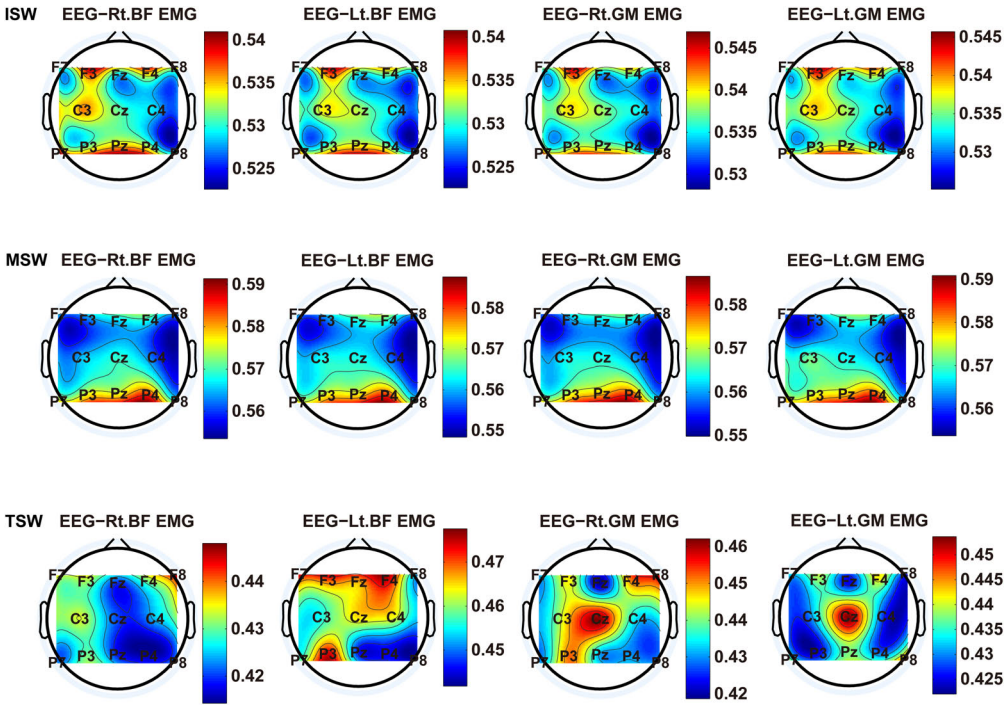

FIGURE 8 | TFCMI topography between EEG (beta band) and sEMG (BF and GM) of the stance phase (ISW, MSW, and TSW).

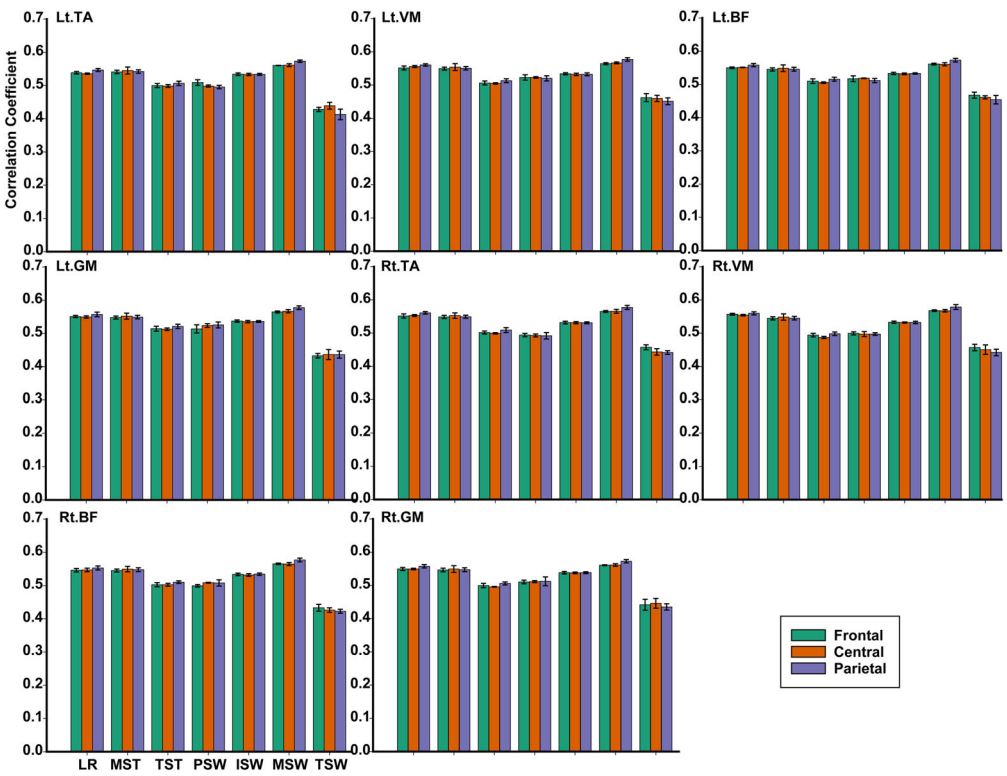

FIGURE 9 | The TFCMI values of the frontal, central, and parietal lobes in seven gait phases for eight muscles.

TABLE 1 | Multiple comparison results of the seven gait phases for the beta band.

Muscle	Gait phases	*p*-value
Lt. TA	LR and MST	0.688
	TST and PSW	0.802
Lt. VM	LR and MST	0.075
Lt. BF	TST and PSW	0.126
Lt. GM	LR and MST	0.214
	TST and PSW	0.172
Rt. VM	TST and PSW	0.135
Rt. BF	LR and MST	0.475
	TST and PSW	0.763
Rt. GM	LR and MST	0.095

2 in certain gait phases. For instance, gait phase recognition based on case 1 was better than that of case 2 in LR for subject 1 at 2.0 km/h. This suggests a small difference in the individual's level of cortex participation during walking. Case 3 performed poorly, although case 2 achieved accurate gait recognition (**Figure 4**). This demonstrates that gait phase information weakened when combining sEMG features with MPF of EEG. MPF is a kind of frequency domain feature. Lee et al. (2019) reported that time domain features achieved the highest accuracy than the frequency domain and common spatial patterns in multiclass MI. Therefore, we speculated that the MPF of EEG is not suitable for fusing with sEMG features to identify the gait phase.

Cortical activation is time-locked to the gait cycle, as has been demonstrated by several researchers (Gwin et al., 2011; Kline et al., 2016; Artoni et al., 2017). However, leg muscles drive leg movement directly, while corticomuscular interaction analysis in a high level of gait phase granularity was not investigated in the time–frequency domain. The latter is critical for the rehabilitation of gait disorders, especially non-traumatic gait disorders. By computing TFCMI values between EEG and sEMG using beta-band EEG data and sEMG data (**Figures 5–8**), we found that the distribution of TFCMI values of eight topographies (eight muscles) was different at PSW ($p < 0.05$) and TSW phases ($p < 0.05$), which indicates that the cerebral cortex area is more actively involved in the regulation of eight muscles during PSW and TSW. Additionally, similar cortex areas were activated in the eight muscles at other gait phases. Previous authors have suggested that corticomuscular connectivity was stronger in the muscles of swing legs than those of stance legs (Artoni et al., 2017). These findings do not contradict ours. The PSW and TSW gait phases are the beginning and end of swing phases, respectively, therefore, our study also showed the corticomuscular connectivity was more active in the swing phases than in the stance phases. The different cerebral cortex areas are involved in the regulation of eight muscles during PSW and TSW. However, the recognition accuracies of PSW (97.05%) and TSW (94.97%) based on case 2 were lower than other phases at the speed of 2.0 km/h. One explanation is that the different distribution of TFCMI values of eight topographies (eight muscles) reduces the separability of sEMG and EEG features. For example, in **Supplementary Figure 7**, there is no clear line of the SSC of sEMG and EEG at PSW and TSW.

For each muscle, corticomuscular interaction analysis for the seven gait phases has not been previously investigated in the time–frequency domain using the TFCMI method. However, are the differences in TFCMI values significant in the seven gait phases? We calculated TFCMI values for the frontal, central, and parietal lobes, and the results can be seen in **Figure 9** (beta-band EEG signals). We found that TFCMI value differences between LR and MST and between TST and PSW of each muscle were not significant (**Table 1**). Therefore, the differences in corticomuscular interaction between LR and MST and between TST and PSW were not significant. This can be proven by gait recognition results based on case 3. The *post-hoc* tests of the gait phase recognition results based on case 3 showed that the differences of recognition results between LR and MST ($p = 0.594$) and between TST and PSW ($p = 0.191$) were not significant. The TFCMI results also can be used to explain the bad performance of the recognition results of TST and PSW based on case 3 at the speed of 2.0 km/h.

Based on this study, a high level of gait phase granularity recognition during treadmill walking by EEG and sEMG signals of the participant is available. This can be applied to the control system of a gait rehabilitation device for people with gait disorders. The gait phase recognition based on case 2 is suitable for patients with a relatively low speed, and based on case 1, case 2, and case 3, it is suitable for patients with a relatively high speed. Also, case 2 was more robust than case 1 and case 3. The cerebral cortex area is more actively involved in the regulation of eight muscles during PSW and TSW. Therefore, targeted rehabilitation training for PSW and TSW will improve the function of the gait-related cortex. Furthermore, there is no clear line of the SSC of sEMG and EEG at PSW and TSW; thus, case 2 is not suitable for gait phase recognition at the speed of 2.0 km/h. The differences of corticomuscular interaction between LR and MST and between TST and PSW were not significant. The performance of the recognition results of TST and PSW based on case 3 at the speed of 2.0 km/h was poor. Therefore, other strategies should be used to classify TST and PSW at the speed of 2.0 km/h. Our results can guide rehabilitation physicians as they develop a rehabilitation plan for each phase of a patient's gait.

DATA AVAILABILITY STATEMENT

The raw data supporting the conclusions of this article will be made available by the authors, without undue reservation.

ETHICS STATEMENT

The studies involving human participants were reviewed and approved by the Institutional Review Boards of Xi'an Jiaotong

University. The patients/participants provided their written informed consent to participate in this study.

AUTHOR CONTRIBUTIONS

PW designed the study, conducted, supervised the experimental process, analyzed the experimental data, and wrote this manuscript. JZ guided the experimental process. BW co-designed the study. JH supervised the data analysis. All authors revised and approved the manuscript.

FUNDING

This work was supported by the Equipment Advance Research Foundation of China (grant no. 61400030701) and the Fundamental Research Funds for the Central Universities (grant no. sxzy022019050).

ACKNOWLEDGMENTS

We thank the participants who enrolled in these experiments.

SUPPLEMENTARY MATERIAL

The Supplementary Material for this article can be found online at: https://www.frontiersin.org/articles/10.3389/fnins.2021.607905/full#supplementary-material

REFERENCES

Artoni, F., Fanciullacci, C., Bertolucci, F., Panarese, A., Makeig, S., Micera, S., et al. (2017). Unidirectional brain to muscle connectivity reveals motor cortex control of leg muscles during stereotyped walking. *Neuroimage* 159, 403–416. doi: 10.1016/j.neuroimage.2017.07.013

Asghari Oskoei, M., and Hu, H. (2007). Myoelectric control systems-a survey. *Biomed. Signal Process. Control* 2, 275–294. doi: 10.1016/j.bspc.2007.07.009

Banala, S. K., Kim, S. H., Agrawal, S. K., and Scholz, J. P. (2008). "Robot assisted gait training with active leg exoskeleton (ALEX)", in *Proceedings of the 2nd Bienn. IEEE/RAS-EMBS International Conference of Biomedical Robotic and Biomechatronics*, Scottsdale, AZ. 653–658. doi: 10.1109/BIOROB.2008.4762885

Bradford, J. C., Lukos, J. R., and Ferris, D. P. (2016). Electrocortical activity distinguishes between uphill and level walking in humans. *J. Neurophysiol.* 115, 958–966. doi: 10.1152/jn.00089.2015

Cunnington, R., Windischberger, C., and Moser, E. (2005). Premovement activity of the pre-supplementary motor area and the readiness for action: studies of time-resolved event-related functional MRI. *Hum. Mov. Sci.* 24, 644–656. doi: 10.1016/j.humov.2005.10.001

Delorme, A., and Makeig, S. (2004). EEGLAB: an open source toolbox for analysis of single-trial EEG dynamics including independent component analysis. *J. Neurosci. Methods* 134, 9–21. doi: 10.1016/j.jneumeth.2003.10.009

Fraser, A. M., and Swinney, H. L. (1986). Independent coordinates for strange attractors from mutual information. *Phys. Rev. A* 33, 1134–1140.

Gao, Y., Ren, L., Li, R., and Zhang, Y. (2018). Electroencephalogram-electromyography coupling analysis in stroke based on symbolic transfer entropy. *Front. Neurol.* 8:716. doi: 10.3389/fneur.2017.00716

Gong, A., Liu, J., Chen, S., and Fu, Y. (2018). Time–frequency cross mutual information analysis of the brain functional networks underlying multiclass motor imagery. *J. Mot. Behav.* 50, 254–267. doi: 10.1080/00222895.2017.1327417

Gwin, J. T., Gramann, K., Makeig, S., and Ferris, D. P. (2011). Electrocortical activity is coupled to gait cycle phase during treadmill walking. *Neuroimage* 54, 1289–1296. doi: 10.1016/j.neuroimage.2010.08.066

Jensen, P., Frisk, R., Spedden, M. E., Geertsen, S. S., Bouyer, L. J., Halliday, D. M., et al. (2019). Using corticomuscular and intermuscular coherence to assess cortical contribution to ankle plantar flexor activity during gait. *J. Mot. Behav.* 51, 668–680. doi: 10.1080/00222895.2018.1563762

Joshi, C. D., Lahiri, U., and Thakor, N. V. (2013). "Classification of gait phases from lower limb EMG: Application to exoskeleton orthosis," in *Proceedings of the 2013 IEEE Point-of-Care Healthcare Technologies*, Bangalore, 228–231. doi: 10.1109/PHT.2013.6461326

Kline, J. E., Huang, H. J., Snyder, K. L., and Ferris, D. P. (2015). Isolating gait-related movement artifacts in electroencephalography during human walking. *J. Neural Eng.* 12:46022. doi: 10.1088/1741-2560/12/4/046022

Kline, J. E., Huang, H. J., Snyder, K. L., and Ferris, D. P. (2016). Cortical spectral activity and connectivity during active and viewed arm and leg movement. *Front. Neurosci.* 10:91. doi: 10.3389/fnins.2016.00091

la Fougère, C., Zwergal, A., Rominger, A., Förster, S., Fesl, G., Dieterich, M., et al. (2010). Real versus imagined locomotion: a [18F]-FDG PET-fMRI comparison. *Neuroimage* 50, 1589–1598. doi: 10.1016/j.neuroimage.2009.12.060

Lee, S. B., Kim, H. J., Kim, H., Jeong, J. H., Lee, S. W., and Kim, D. J. (2019). Comparative analysis of features extracted from EEG spatial, spectral and temporal domains for binary and multiclass motor imagery classification. *Inf. Sci.* 502, 190–200. doi: 10.1016/j.ins.2019.06.008

Li, J., Dimitrakopoulos, G. N., Thangavel, P., Chen, G., Sun, Y., Guo, Z., et al. (2019). What are spectral and spatial distributions of EEG-EMG correlations in overground walking? An exploratory study. *IEEE Access* 7, 43935–143946. doi: 10.1109/access.2019.2945602

Li, Y., Gao, F., Chen, H., and Xu, M. (2016). "Gait recognition based on EMG with different individuals and sample sizes," in *Proceedings of the Chinese Control Conference CCC*, (New York, NY: IEEE), 4068–4072. doi: 10.1109/ChiCC.2016.7553988

Louie, D. R., and Eng, J. J. (2016). Powered robotic exoskeletons in post-stroke rehabilitation of gait: a scoping review. *J. Neuroeng. Rehabil.* 13:53. doi: 10.1186/s12984-016-0162-5

Lu, C. F., Teng, S., Hung, C. I., Tseng, P. J., Lin, L. T., Lee, P. L., et al. (2011). Reorganization of functional connectivity during the motor task using EEG time-frequency cross mutual information analysis. *Clin. Neurophysiol.* 122, 1569–1579. doi: 10.1016/j.clinph.2011.01.050

Marchal-Crespo, L., and Reinkensmeyer, D. J. (2009). Review of control strategies for robotic movement training after neurologic injury. *J. Neuroeng. Rehabil.* 6:20. doi: 10.1186/1743-0003-6-20

Martín-Clemente, R., Olias, J., Thiyam, D. B., Cichocki, A., and Cruces, S. (2018). Information theoretic approaches for motor-imagery BCI systems: review and experimental comparison. *Entropy* 20:7. doi: 10.3390/e20010007

Miyai, I., Tanabe, H. C., Sase, I., Eda, H., Oda, I., Konishi, I., et al. (2001). Cortical mapping of gait in humans: a near-infrared spectroscopic topography study. *Neuroimage* 14, 1186–1192. doi: 10.1006/nimg.2001.0905

Nordin, A. D., Hairston, W. D., and Ferris, D. P. (2019a). Faster gait speeds reduce alpha and beta EEG spectral power from human sensorimotor cortex. *IEEE Trans. Biomed. Eng.* 67, 842–853. doi: 10.1109/tbme.2019.2921766

Nordin, A. D., Hairston, W. D., and Ferris, D. P. (2019b). Human electrocortical dynamics while stepping over obstacles. *Sci. Rep.* 9:4693. doi: 10.1038/s41598-019-41131-2

Oliveira, A. S., Arguissain, F. G., and Andersen, O. K. (2018). Cognitive processing for step precision increases beta and gamma band modulation during overground walking. *Brain Topogr.* 31, 661–671. doi: 10.1007/s10548-018-0633-z

Perry, J. K. S. T., and Davids, J. R. (1992). Gait analysis: normal and pathological function. *J. Pediatr. Orthop* 12:815.

Petersen, T. H., Willerslev-Olsen, M., Conway, B. A., and Nielsen, J. B. (2012). The motor cortex drives the muscles during walking in human subjects. *J. Physiol.* 590, 2443–2452. doi: 10.1113/jphysiol.2012.227397

Pfurtscheller, G., and Lopes Da Silva, F. H. (1999). Event-related EEG/MEG synchronization and desynchronization: basic principles. *Clin. Neurophysiol.* 110, 1842–1857. doi: 10.1016/S1388-2457(99)00141-8

Phinyomark, A., Khushaba, R. N., Ibáñez-Marcelo, E., Patania, A., Scheme, E., and Petri, G. (2017). Navigating features: a topologically informed chart of electromyographic features space. *J. R. Soc. Interface* 14:20170734. doi: 10.1098/rsif.2017.0734

Plotnik, M., Bartsch, R. P., Zeev, A., Giladi, N., and Hausdorff, J. M. (2013). Effects of walking speed on asymmetry and bilateral coordination of gait. *Gait Posture* 38, 864–869. doi: 10.1016/j.gaitpost.2013.04.011

Popivanov, D., and Dushanova, J. (1999). Non-linear EEG dynamic changes and their probable relation to voluntary movement organization. *Neuroreport* 10, 1397–1401. doi: 10.1097/00001756-199905140-00003

Ryu, J. H., and Kim, D. H. (2014). "Multiple gait phase recognition using boosted classifiers based on sEMG signal and classification matrix," in *Proceedingsof the 8th International Conference. Ubiquitous Information Management and Communication ICUIMC 2014*, New York, NY. doi: 10.1145/2557977.2557993

Sun, L., Liu, Y., and Beadle, P. J. (2005). "Independent component analysis of EEG signals," in *Proceedings of 2005 IEEE International Workshop. VLSI Design Video Technology. IWVDVT 2005*, Suzhou, 219–222. doi: 10.1109/iwvdvt.2005.1504590

Taborri, J., Palermo, E., Rossi, S., and Cappa, P. (2016). Gait partitioning methods: a systematic review. *Sensors (Switzerland)* 16:66. doi: 10.3390/s16010066

Tamburri, L. M., Hix, C. D., and Sole, M. L. (2002). Revising a book chapter written by a previous author. *Nurse Author Ed.* 12, 7–9.

Tefertiller, C., Pharo, B., Evans, N., and Winchester, P. (2011). Efficacy of rehabilitation robotics for walking training in neurological disorders: a review. *J. Rehabil. Res. Dev.* 48, 387–416. doi: 10.1682/JRRD.2010.04.0055

Veneman, J. F., Kruidhof, R., Hekman, E. E. G., Ekkelenkamp, R., Van Asseldonk, E. H. F., and Van Der Kooij, H. (2007). Design and evaluation of the LOPES exoskeleton robot for interactive gait rehabilitation. *IEEE Trans. Neural Syst. Rehabil. Eng.* 15, 379–386. doi: 10.1109/TNSRE.2007.903919

Vialatte, F. B., Martin, C., Dubois, R., Haddad, J., Quenet, B., Gervais, R., et al. (2007). A machine learning approach to the analysis of time-frequency maps, and its application to neural dynamics. *Neural Netw.* 20, 194–209. doi: 10.1016/j.neunet.2006.09.013

Wagner, J., Solis-Escalante, T., Grieshofer, P., Neuper, C., Müller-Putz, G., and Scherer, R. (2012). Level of participation in robotic-assisted treadmill walking modulates midline sensorimotor EEG rhythms in able-bodied subjects. *Neuroimage* 63, 1203–1211. doi: 10.1016/j.neuroimage.2012.08.019

Wagner, J., Solis-Escalante, T., Scherer, R., Neuper, C., and Müller-Putz, G. (2014). It's how you get there: walking down a virtual alley activates premotor and parietal areas. *Front. Hum. Neurosci.* 8:93. doi: 10.3389/fnhum.2014.00093

Wei, P. N., Xie, R., Tang, R., Li, C., Kim, J., and Wu, M. (2018). sEMG based gait phase recognition for children with Spastic cerebral palsy. *Ann. Biomed. Eng.* 47, 223–230. doi: 10.1007/s10439-018-02126-8

Ziegler, J., Gattringer, H., and Mueller, A. (2018). "Classification of gait phases based on bilateral EMG data using support vector machines," in *in Proceedings of the 2018 7th IEEE International Conference on Biomedical Robotics and Biomechatronics (Biorob)*, Enschede. 978–983. doi: 10.1109/BIOROB.2018.8487750

Conflict of Interest: The authors declare that the research was conducted in the absence of any commercial or financial relationships that could be construed as a potential conflict of interest.

frontiers in Neuroscience

ORIGINAL RESEARCH
published: 12 August 2021
doi: 10.3389/fnins.2021.700672

Bilateral Intracranial Beta Activity During Forced and Spontaneous Movements in a 6-OHDA Hemi-PD Rat Model

Soheil Mottaghi[1,2,3], Sandra Kohl[1,2], Dirk Biemann[1,2], Samuel Liebana[4,5], Ruth Eneida Montaño Crespo[1,2], Oliver Buchholz[1,2], Mareike Wilson[1,2], Carolin Klaus[1,2], Michelle Uchenik[6], Christian Münkel[1,2], Robert Schmidt[7] and Ulrich G. Hofmann[1,2,3]*

[1] Neuroelectronic Systems, Department of Neurosurgery, Medical Center, University of Freiburg, Freiburg, Germany, [2] Faculty of Medicine, University of Freiburg, Freiburg, Germany, [3] Technical Faculty, University of Freiburg, Freiburg, Germany, [4] Department of Engineering, University of Cambridge, Cambridge, United Kingdom, [5] Department of Physiology, Anatomy, and Genetics, University of Oxford, Oxford, United Kingdom, [6] Biomedical Department, Faculty of Engineering, University of Minnesota, Minneapolis, MN, United States, [7] Department of Psychology, The University of Sheffield, Sheffield, United Kingdom

OPEN ACCESS

Edited by:
Kyuhwa Lee, Wyss Center for Bio and Neuroengineering, Switzerland

Reviewed by:
Lohitash Karumbaiah, University of Georgia, United States
Nandakumar Narayanan, The University of Iowa, United States

***Correspondence:**
Soheil Mottaghi
soheilmottaghi@gmail.com

Specialty section:
This article was submitted to Neuroprosthetics, a section of the journal Frontiers in Neuroscience

Received: *26 April 2021*
Accepted: *20 July 2021*
Published: *12 August 2021*

Citation:
Mottaghi S, Kohl S, Biemann D, Liebana S, Montaño Crespo RE, Buchholz O, Wilson M, Klaus C, Uchenik M, Münkel C, Schmidt R and Hofmann UG (2021) Bilateral Intracranial Beta Activity During Forced and Spontaneous Movements in a 6-OHDA Hemi-PD Rat Model. Front. Neurosci. 15:700672. doi: 10.3389/fnins.2021.700672

Cortico-basal ganglia beta oscillations (13–30 Hz) are assumed to be involved in motor impairments in Parkinson's Disease (PD), especially in bradykinesia and rigidity. Various studies have utilized the unilateral 6-hydroxydopamine (6-OHDA) rat PD model to further investigate PD and test novel treatments. However, a detailed behavioral and electrophysiological characterization of the model, including analyses of popular PD treatments such as DBS, has not been documented in the literature. We hence challenged the 6-OHDA rat hemi-PD model with a series of experiments (i.e., cylinder test, open field test, and rotarod test) aimed at assessing the motor impairments, analyzing the effects of Deep Brain Stimulation (DBS), and identifying under which conditions excessive beta oscillations occur. We found that 6-OHDA hemi-PD rats presented an impaired performance in all experiments compared to the sham group, and DBS could improve their overall performance. Across all the experiments and behaviors, the power in the high beta band was observed to be an important biomarker for PD as it showed differences between healthy and lesioned hemispheres and between 6-OHDA-lesioned and sham rats. This all shows that the 6-OHDA hemi-PD model accurately represents many of the motor and electrophysiological symptoms of PD and makes it a useful tool for the pre-clinical testing of new treatments when low β (13–21 Hz) and high β (21–30 Hz) frequency bands are considered separately.

Keywords: 6-hydroxydopamine, Hemi Parkinson's, deep brain stimulation, animal model, neuroprosthetic, local field potential, beta oscillation, biomarker

INTRODUCTION

Parkinson's disease (PD) is a neurodegenerative disorder which affects an estimated 10 million patients worldwide (Dorsey et al., 2018). The disease is characterized by both motor and non-motor symptoms, including decreased and inhibited movements, resting tremor, rigidity, sleep issues, cognitive dysfunction, and depression (DeMaagd and Philip, 2015). It has been shown that

neural loss in the nigral dopaminergic inputs to the striatum is one of the main causes of the condition. This leads to a major alteration in the neural activity in the cortico-basal ganglia loop, which adversely affects the ability to make voluntary movements (Brown et al., 2001; Levy et al., 2002; Kühn et al., 2005). In the presence of normal dopaminergic drive, the activity of cortico-basal ganglia loop neurons is largely desynchronized. However, upon the loss of dopaminergic neurons, in idiopathic PD and experimental models of the disease, neurons of the subthalamic nucleus (STN), (internal and external) globus pallidus (GP) and substantia nigra pars reticulata (SNr), lose their independence and show increases in burst firing, and synchronization of activity (Filion et al., 1991; Nini et al., 1995).

The synchronized neural oscillations in the aforementioned areas mostly have frequencies within the beta band (13–30 Hz), a frequency band which has been shown to correlate with bradykinesia and rigidity in PD patients (Kühn et al., 2008). Research to-date suggests that common treatments for bradykinesia, such as levodopa medication or high-frequency deep brain stimulation (DBS), work by suppressing the synchronized beta band oscillations in the cortico-thalamo-basal ganglia circuit (Levy et al., 2002; Kühn et al., 2005; Dorval et al., 2010; Delaville et al., 2015). This suppression is predominantly observed in the STN (Plenz and Kital, 1999; Gatev et al., 2006; Stein and Bar-Gad, 2013) and the motor cortex (Yamawaki et al., 2008) of PD patients. It is, however, important to note that this suppression of neural activity in the cortico-thalamo-basal ganglia circuit only leads to motor improvements in patients who already present deteriorated capabilities, and will instead impair the performance of PD patients whose motor capabilities are within normal limits (Chen et al., 2011).

Adaptive deep brain stimulation (aDBS) is emerging as a promising enhanced treatment for PD which overcomes several limitations of conventional DBS (Little and Brown, 2020). Since physiological biomarkers derived from cortico-basal ganglia loop beta band oscillations are currently the front-runners as control signals for aDBS (Little et al., 2013, 2014; Castaño-Candamil et al., 2017), the development of future control algorithms for this treatment (Hoang et al., 2017; Neumann et al., 2019) will surely benefit from a framework for the systematic testing of these biomarkers using accessible and established animal models of PD.

In this study we present an investigation on the suitability of the unilateral 6-hydroxydopamine (6-OHDA) hemi-PD rat model (Ungerstedt, 1968) as a framework for PD pre-clinical research. The unilateral 6-OHDA rat model simulates certain symptoms of PD by unilaterally injecting the highly specific neurotoxin 6-hydroxydopamine (6-OHDA) into either the medial forebrain bundle (MFB) or the substantia nigra, causing substantial ipsilateral dopamine loss (Ungerstedt, 1968; Henderson et al., 2003). This creates what is known as a hemi-parkinsonian (hemi-PD) rat, where one hemisphere of the rat brain is significantly damaged, and the contralateral side to the lesion serves as an in-animal control allowing for electrophysiological comparisons within the rat (Lundblad et al., 2005). Throughout this paper, lesioned animals are interchangeably referred to as 6-OHDA, hemi-PD, or PD animals. We use the last two names to highlight the model's capability to simulate several symptoms of PD, though we would like to make clear that the disease model does not capture all the aspects of PD, as will be demonstrated later.

Our work aims to quantify the motor impairments displayed by the unilateral 6-OHDA model. In addition it characterizes the conditions under which an excess in the spectral power of the beta frequency band is exhibited in the neural oscillations of the primary motor cortex (M1) and the subthalamic nucleus (STN) of animals lesioned according to this. To achieve this, a series of tests assessing the different movement capabilities of the animals were performed, including the cylinder, open field, and rotarod tests. Furthermore, the characterization of the lesion's influence on animal's motor capabilities, the effect of standard DBS on the improvement of motor impairments and the alterations of beta oscillations were investigated through the above tests as well. Finally, all throughout our study we assessed the suitability of beta power in the STN as a biomarker to control stimulation in aDBS.

MATERIALS AND METHODS

All animal procedures were conducted in conformity with relevant institutional rules in compliance with the guidelines of the German Council on Animal Protection. Protocols were approved by the Animal Care Committee of the University of Freiburg under the supervision of the Regierungspräsidium Freiburg (approval G15/031) in accordance with the guidelines of the European Union Directive 2010/63/UE.

Surgical Procedure

Two groups of adult female Sprague-Dawley rats (290–310 g), consisting of 13 6-OHDA lesioned hemi-parkinsonian rats (PD-group) and 12 non-lesioned rats (sham-group), were used for this study. All animals were acquired from Charles River Laboratories (Germany) and were housed under temperature-controlled conditions in a 12-h light-dark cycle, with access to water and food *ad libitum*. Rats were allowed to acclimate to these conditions for a minimum of 2 weeks prior to any experimental procedures in order to reduce unnecessary stress.

Prior to surgery, all rats underwent at least 7 days of handling to familiarize them with the experimenter. During each surgery, the rats were anesthetized with oxygen (0.15 l/min) and isoflurane (Abbvie, United States). Anesthesia was induced with 4% isoflurane and gradually lowered to 1.5% after placing the animal into the stereotaxic frame (David Kopf, United States). Breathing, reflexes, and depth of anesthesia were monitored throughout the duration of the surgery.

All PD-group animals underwent two consecutive stereotaxic surgeries, with a 2-week recovery time between each surgery. In the first, the 6-OHDA was injected, and in the second, custom-made microelectrodes for stimulation and recording were implanted. During each surgery, holes were drilled at the injection or implantation site, and the dura was resected using a fine needle. The injection canula or electrode was subsequently lowered manually at a rate of approximately 200 μm/s. Four minutes were allowed to pass after each injection, with the needle still inserted, to allow the 6-OHDA to adequately diffuse into the

target. After electrode implantation, the skull aperture around the implanted electrode was filled with bone wax. Once in place, electrodes were fixed to a nearby stainless-steel screw anchor (0–80 × 1/8; Plastics One) using a 2-compound dental cement (Palapress; Heraeus Holding GmbH; Germany).

Sham animals (n = 12) were subjected to a unilateral MFB injection of saline, following the same procedure as that of the lesion for the 6-OHDA-group (see section "6-OHDA Lesion and Apomorphine Test"). The sham rats were subsequently subjected to an electrode implantation surgery, which followed the same procedure as the implantation surgery of the PD group (see section "Electrode Implantation" for more details). This protocol ensures that the impairment observed in the hemi-PD rats is solely due to the 6-OHDA treatment and not due to the surgical procedures that the rats were subjected to.

6-OHDA Lesion and Apomorphine Test

Animals assigned to the PD group were unilaterally lesioned with a 6-OHDA solution (3.6 mg 6-OHDA, 20 mg ascorbic acid, and 10 ml 0.9% NaCl) injected into the right medial forebrain bundle (**Figure 1**). **Table 1** contains the lesion coordinates, 6-OHDA volume and the injection rate. The Apomorphine rotation test was performed after a recovery period of 2 weeks to test dopamine depletion intensity. Animals were deemed sufficiently lesioned if at least 3 contralateral (to the lesion) rotations on average were observed per minute for 30 min after the subcutaneous injection of a 0.1ml/100 gr. Apomorphine solution (1 mg Apomorphine, 2 mg ascorbic acid acquired from Sigma-Aldrich Chemie GmbH, Germany and 20 ml NaCl).

Electrode Implantation

All rats received a bilateral implantation of Platinum-Iridium (70% Pt, 30% Ir) bipolar recording electrodes with 10 and 75 μm tip diameter and separation, respectively (Science Products GmbH, Germany) into the primary motor cortex (M1) and STN, to achieve a total of eight recording sites for each rat brain (**Figure 2**). The coordinates of the implants are available in **Table 2**. Additionally, rats in the PD group received custom-made bipolar stimulation electrodes, made of intertwined 50 μm Platinum-Iridium (70% Pt, 30% Ir) microwires (Science Products GmbH, Germany). The stimulation electrodes were implanted into the STN ipsilateral to the lesion and adjacent to the recording electrodes (**Figure 2**).

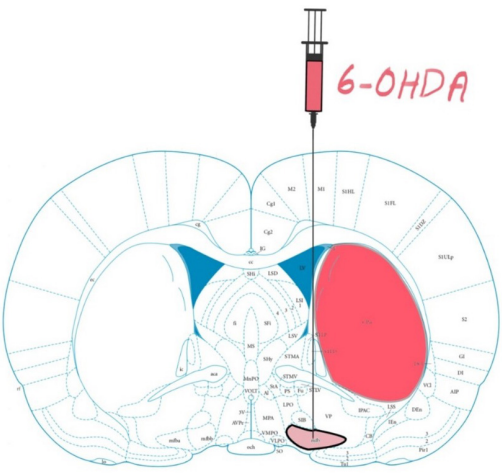

FIGURE 1 | Rat brain atlas; 6-hydroxydopamine (6-OHDA) Parkinson's Disease (PD) models are made by administering 6-OHDA into nigrostriatal pathway, in this case the medial forebrain bundle (mfb). From 6-14 days post lesioning, the dopaminergic cells in the striatum (Caudate Putamen CPu) degenerate. Figure adapted from Mottaghi (2020).

TABLE 1 | Lesion coordinates in MFB, quantity of 6-OHDA per coordinate and injection rate.

	AP (mm)	ML (mm)	DV (mm)	Quantity	Injec. Rate
MFB	−4.4	−1.2	−7.8	2.5 μl	1 μl/min
	−4.0	−0.8	−7.2	3.0 μl	1 μl/min

Animal Experiments

In all experiments, video recordings of animal behavior and electrophysiological recordings of brain signals were collected. Electrophysiological data in the form of local field potentials (LFP, 0.3–300 Hz filtered using a 20th-order Butterworth filter) was recorded from the bilaterally implanted recording electrodes in the STN and M1. Data was collected using a 32-channel wireless head stage (Multi-channel System GmbH, Germany) and an AlphaLab SnR system (AlphaOmega, Israel). Prior to all behavioral tests, an adequate stimulation strength for each animal of the PD group was individually determined by titrating the current amplitude such that explorative behavior was observed, but stimulation-related side effects were not. In this way, we compensated for possible variations in electrode placement and shape. Stimulation was applied at a frequency of 130 Hz using a biphasic rectangular pulse and a pulse width of 65 μs in each of the following behavioral tests. Depending on the behavioral paradigm being tested, DBS stimulation was turned on/off at different points throughout the experiment for a fixed period of time to compare the behavior of the animals during on/off periods.

Cylinder Test

The cylinder test measures spontaneous forelimb use, body movement and exploratory activities (Cenci and Lundblad, 2005). Animals were not introduced to the cylinder prior to the experiment in order to test their motivation and capability to explore a novel environment.

Each rat was placed in a transparent cylinder (acrylic glass, 19 cm diam., 35 cm ht.) for a total of 2 min (see **Figures 3A,B**). A Logitech C920 HD video camera (Logitech, Switzerland) was used to record the animals from a ventral viewpoint (30fps). Rats belonging to the PD group (n = 13) were split into two groups, those receiving DBS during the experiment (PD-DBS ON, n = 7) and those which did not (PD-DBS OFF, n = 6). Sham rats (n = 12) never received DBS. The experimental schedule is shown in **Figure 3C**.

The observed behavior of all rats was classified into three distinct patterns: rearing, stepping and inactive behavior. During

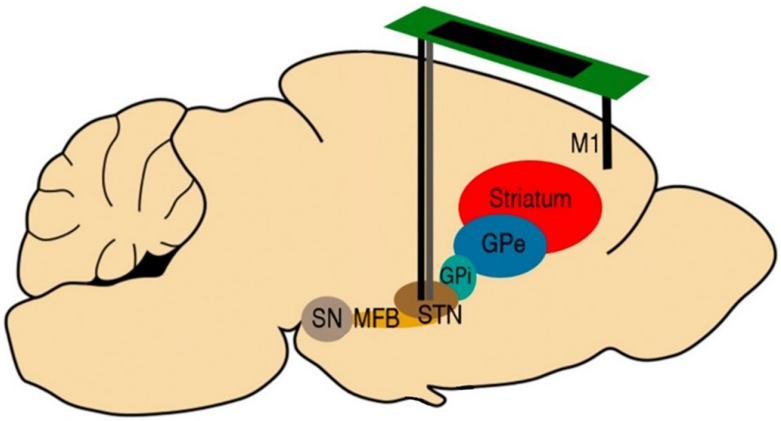

FIGURE 2 | Schematic description of the electrode implantation sites. All rats received bilateral implantations of Platinum-Iridium bipolar recording electrodes (10 mm diameter, black) to both the STN and M1. Rats in the PD group were also implanted with bipolar stimulation electrodes (50 mm diameter, gray) in the STN ipsilateral to the lesion, adjacent to the recording electrodes. Figure adapted from Mottaghi (2020).

rearing, rats stand on their hind limbs while their forelimbs touch the cylinder wall to maintain balance (**Figure 3A**). Stepping was defined as episodes where the orientation of the animal's body shifted > 45 degrees while its forepaws alternated between touching the ground and being held in the air (**Figure 3B**). Any behavior that could not be defined as either rearing or stepping was classified as inactive.

To quantitatively assess the amount of time spent in each of the three behavioral categories, the distinct positions of the rat's forelimbs were identified and converted into a four-digit binary code, updated every 0.25s. The first two digits represent the left and right forelimb, respectively, and indicate whether the paws touch the cylinder wall (1) or not (0). Similarly, the last two digits show whether the forelimb paws touch the ground (e.g., 1100 = both front paws on wall, 0011 = both front paws on floor, 0000 = rearing with no support, 0110 = right paw on wall and left paw on floor). The body rotation was also measured (in θ/s) using Tracker video analysis software (©2016, Douglas Brown[1]) combined with a virtual protractor overlay on the video, with the protractor vertex centered on the center of the urinary meatus of the rat. The endpoint of one protractor leg was aligned with the upper chest of the animal while the remaining leg served as a reference for rotation. After collection, the binary forelimb states and rotation measurements were subsequently analyzed in MATLAB (MathWorks, United States).

Open Field Test

To measure the animal's locomotor performance and explorative behavior in a novel environment, an open field test (Seibenhener and Wooten, 2015) was performed. The rats were placed in a featureless square chamber (74 × 74 × 30 cm) and left free to explore for 10 min while their location was tracked using BioObserve Viewer II software (BioObserve GmbH, Germany, 25 fps). The experimental layout, together with the superimposed trajectories of the tested animals, are depicted in **Figure 3D**. The experiment was divided into three episodes. During the first 3 min (episode 1), no rat ($n = 25$) received DBS stimulation. Next, PD-group animals were divided into two subgroups; one received DBS for 4 min (PD-DBS ON, $n = 7$) while the other did not (PD-DBS OFF, $n = 6$). In the last episode, DBS was turned off for all the PD rats ($n = 13$) and stayed off for the remaining 3 min. Sham rats ($n = 12$) were left free to explore with no DBS for the entirety of the experiment. The environment was cleaned after each trial to prevent any lingering olfactory signals from interfering with behavior. As in the cylinder test, electrophysiological and video tracking data was collected and subsequently analyzed offline.

[1]https://physlets.org/tracker

TABLE 2 | Electrode implantation coordinates in M1 and STN.

	AP (mm)	ML (mm)	DV (mm)
M1	+2.5	±3.0	−1.6
STN	−3.8	±2.4	8.0

Rotarod

The rotarod test, first described by Dunham and Miya (1957), is widely used to assess the effect of brain injuries or experimental drugs on motor function in rodents (Cartmell et al., 1991; Bohlen et al., 2009). No experienced observer or nominal scoring procedure is required, as the test yields a discretely measurable variable (time or speed) which can be used to quantify motor behavior in an objective manner. To perform this test, the rat is placed on a rotating rod that mimics a treadmill. The rod is suspended high enough over the ground so that the rat is naturally motivated to avoid falling, but low enough to avoid any injuries should a fall occur. The rotational speed of the rod is then gradually increased until, when the rat eventually loses its grip or balance, it falls onto a switch plate beneath the rod. Both the speed of the rod and the time that the animals remained on the rotarod are measured and recorded (**Figure 4A**).

The experimental schedule spans over 2 days: on the first day, all rats ($n = 25$) were trained on a rotarod (Rat Rota-Rod 47700; UGO Basile S.R.L. Gemonio, Italy) in three sessions with

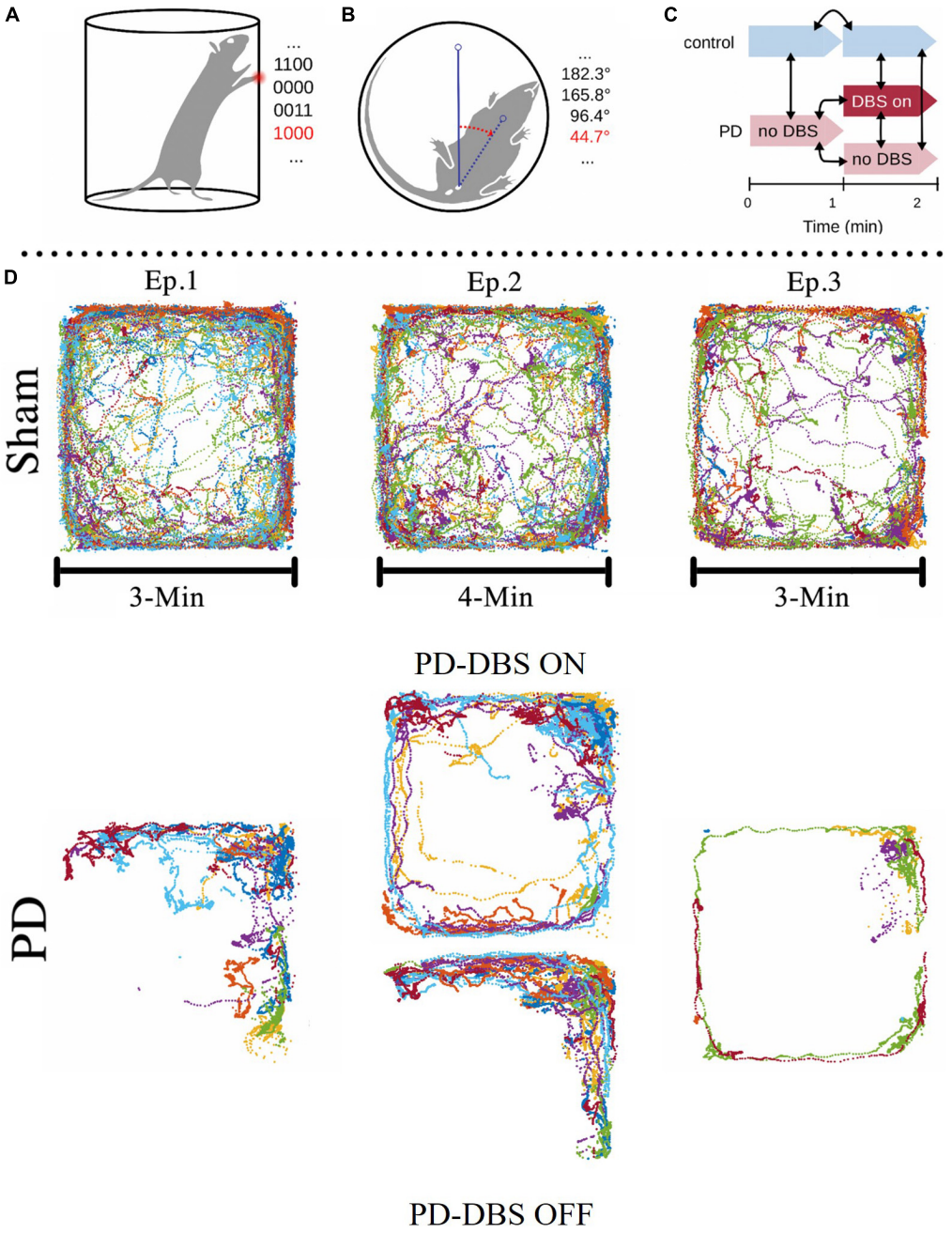

FIGURE 3 | Depictions of the cylinder test and open field test experimental setups. **(A,B)** The body angle of the animal and the position of its forepaws were measured and the latter was recorded using a binary code. The first two digits of the 4-bit code represent whether the forepaws were touching the cylinder walls and the last two represent whether they were touching the cylinder floor (e.g., 1100 = both front paws on wall, 0000 = rearing with no support, 0011 = both front paws on floor, 1000 = left paw on wall and right paw not in contact). **(C)** The animals were monitored for 2 min. A subgroup of PD animals received DBS treatment at the onset of the second minute, while the rest of the PD group remained untreated. **(D)** Open field area, a 74 cm × 74 cm square box, with the exploratory activities of different PD and Sham rats during 10 min superimposed. Note how sham rats explore most of the area available to them (with a tendency to avoid the center which is a natural reaction for rats), whereas unstimulated PD rats remain on the corners and explore much less than sham rats. Notice the significant difference in the trajectories between stimulated PD rats (episode 2, top) and non-stimulated PD rats [episode 1, 2 (bottom) and 3]. This shows that DBS considerably increases the rats' ability or motivation to explore and corrects major motor impairments. Figure adapted from Mottaghi (2020).

20 min between each session. The sessions consisted of 8 trials with different velocity settings of the rod (12, 16, 19, 21, 24, 26, 28, and 38 rpm) and a maximal duration of 60s. Each trial was followed by a resting period of 1 min (**Figure 4B**). On the second day, the rotarod was set to accelerate from 2 to 60 rpm with 1 rpm steps over the course of 7 min. 52 s. All rats performed the test

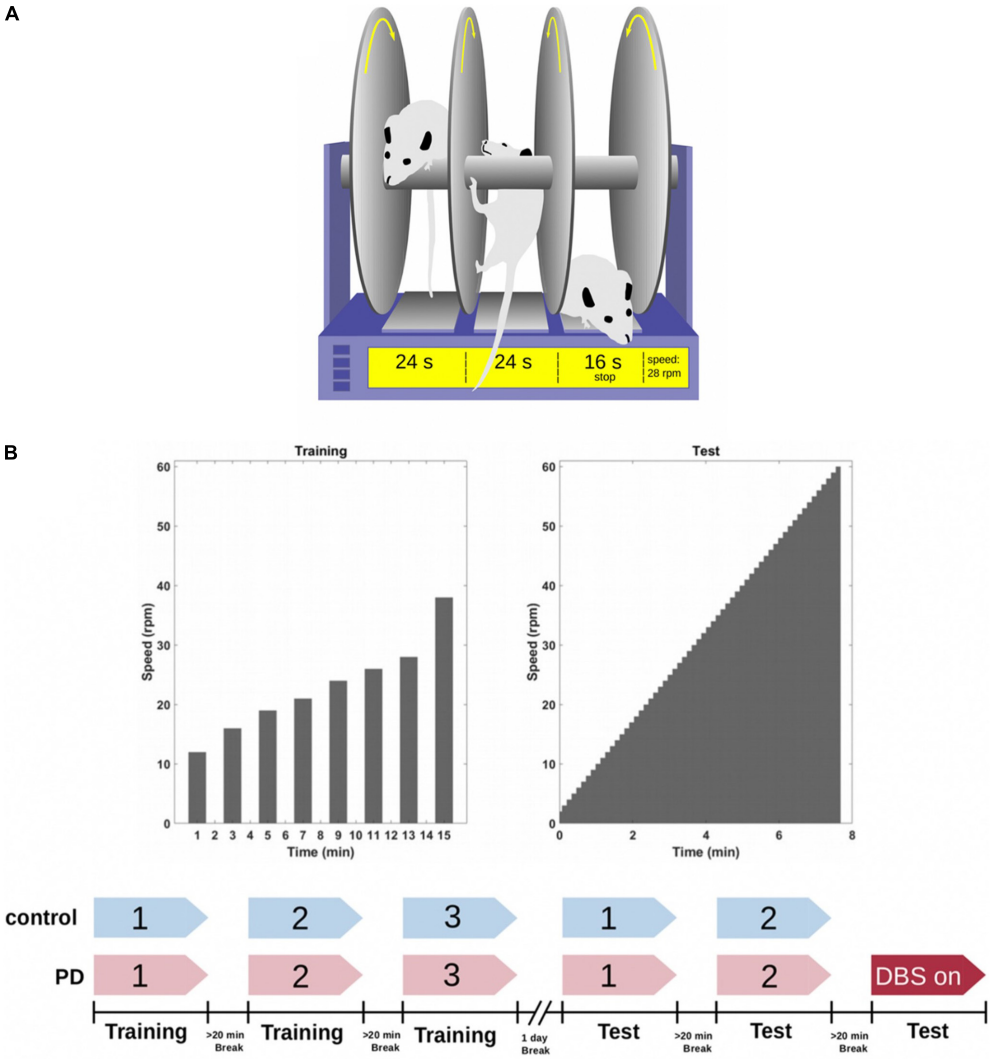

FIGURE 4 | (A) The rotarod is a device consisting of a rotating rod on which rats have to walk without falling for as long as they can. A timer records how long the rats walk on the rod before they fall and trip a switch which stops the timer. **(B)** All the animals (n = 25) were trained on the rotarod 1 day prior to the test day. They trained for three sessions (with a maximum duration of 60 s) with a 20 min break between each session. On the next day, both the sham and PD group performed two sessions of testing without DBS. A subgroup of the PD rats (n = 7) performed a third round while receiving DBS treatment. The other subgroup performed the third round without DBS (n = 6). Figure adapted from Mottaghi (2020).

in two sessions with a break of at least 20 min in between the sessions. The PD rats were then split into two groups where PD-DBS ON rats (n = 7) performed an additional third session while constantly receiving DBS and PD-DBS OFF (n = 6) did the same but without DBS (**Figure 4B**).

Electrophysiological Analysis

All of our data analysis was performed in MATLAB 2017a (Mathworks, United States) and Python (Python Software Foundation, CWI). LFP signals were resampled at 1.1 kHz. Power spectral density (PSD) was calculated using Thomson's multitaper PSD estimate (5 Slepian tapers). In this paper, the right hemisphere of PD-group animals corresponds to the lesioned side, while the left hemisphere is the intact (unlesioned) side. Sham rats only had recording electrodes and hence both of their hemispheres were intact.

The Euclidean Distances (ED) between the averaged PSD's of different brain regions were used to quantitatively compare electrophysiological behavior across the brain. In our experiments these were used to quantify the difference in beta band power (13–30 Hz) between sham rats and PD rats as follows:

$$ED_{PSD_{sham}} - PSD_{PD} = \sqrt{\sum_{f=13Hz}^{30Hz} PSD(f)_{sham^2} - \sum_{f=13Hz}^{30Hz} PSD(f)_{PD^2}} \quad (1)$$

The behavioral results and normalized band power were statistically analyzed using a non-parametric Wilcoxon rank-sum test, unless mentioned otherwise. Kendall's rank correlation

coefficient was used to assess the linear correlation between band power and speed.

Euthanasia and Histology

After having finalized all experimental testing, chronically implanted rats were euthanized with an overdose of isoflurane and were perfused transcardially with a 4% formaldehyde solution (PFA in phosphate buffer). Their brains were removed, post-fixed in PFA for 7 days and stored in 30% sucrose, after which they were cut into coronal sections (40 μm) along the probe's implantation trajectory with a cryostat (CryoStar NX70, Thermo Fisher Scientific, United States). Sections were collected on glass slides and stored at 4°C until further processing. Tyrosine Hydroxylase TH staining (Primary AB: T-1299 Sigma 0.2 ml −20°C) was then used as a marker to identify the presence (or lack of) dopaminergic neurons and thus assess the success of the lesion. The sections were also used to verify the correct positioning of the recording and stimulating electrodes.

RESULTS

Using a series of different experimental paradigms, we provided an in-depth characterization of the motor impairments caused by the unilateral 6-OHDA lesion of the hemi-PD rat model and investigated the conditions under which excessive beta power can be observed in the STN and M1 of animals lesioned according to this model. For each experimental paradigm we analyzed the behavior and compared the impairments of the PD group with the motor abilities of the sham group. Furthermore, we investigated the differences in neural activity arising from the different behaviors. To this end, the recorded LFP signal (0.3–300 Hz) was filtered into θ (6–12 Hz), low (13–21 Hz), and high (21–30 Hz) β bands (see **Figure 5**).

DBS Restores Exploratory Movement Patterns in the 6-OHDA Hemi-PD Rat

The cylinder and open field (OF) tests investigated exploratory movement patterns in both the PD and sham animal groups, since the animals were free to move and explore in both environments. The cylinder environment favored rearing and other stationary activities while the OF challenged their locomotion capabilities.

In the cylinder test, the time that each animal spent in each of the 3 behavioral categories (i.e., rearing, stepping, and inactive) was measured and analyzed individually for each category. To establish a baseline behavioral pattern, the performance of the sham rats during the first minute of the experiment was compared to their performance during the second minute; thus focusing on any behavioral changes resulting uniquely from the time spent in the cylinder. A significant decrease in the sham rats' rearing time and a significant increase in the duration and frequency of their inactive episodes was observed from this comparison ($p_{rear} < 0.05$, $p_{inactive} < 0.01$). However, the difference in the time spent stepping was insignificant (see **Figure 6A**). This shows that there is a natural tendency for the rats to explore less the longer they spend in the cylinder environment. These results are useful to gauge the scale of the natural decrease in exploratory behavior over time, allowing a more accurate estimation of the effects caused by the 6-OHDA lesion.

A similar comparison between the PD and sham groups over the first minute shows that PD rats spent significantly less time stepping and rearing, and instead spent more time in the inactive state ($p_{stepping} < 0.05$, $p_{rear} < 0.001$, $p_{inactive} < 0.001$) (**Figure 6B**). The first minute differences in the time spent stepping between PD and sham rats are slightly more pronounced than comparable first to second minute sham rats' efforts ("Stepping," **Figure 6B** vs. **Figure 6A**). The differences in time spent rearing and in the inactive state are however much more pronounced between PD and sham rats than among sham rats only ("Rearing" and "Inactive," **Figure 6B** vs. **Figure 6A**).

To evaluate the effect of DBS on the behavior of PD rats, the PD-group was divided into two subgroups: one PD subgroup (n = 7, PD-DBS ON) was exposed to STN-DBS at the onset of the second minute of the experiment, while the other subgroup remained untreated (n = 6, PD-DBS OFF). The results indicate that PD-DBS ON rats exhibited a similar behavioral pattern to the sham group during the second minute, whereas PD-DBS OFF rats exhibited significantly less stepping ($p_{Sham-PD-DBSOFF} < 0.001$ and $p_{PD-DBSON\ -PD-DBSOFF} < 0.01$, respectively) and rearing ($p_{Sham-PD-DBSOFF} < 0.01$ and $p_{PD-DBSON\ -PD-DBSOFF} < 0.01$, respectively), and instead spent significantly longer periods of time in the inactive state ($p_{Sham-PD-DBSOFF} < 0.001$ and $p_{PD-DBSON\ -\ PD-DBSOFF} < 0.01$, respectively) compared to the sham and PD-DBS ON groups (see **Figure 6C**).

The data from the OF test showed similar results to that of the cylinder test. This data was analyzed for all groups by dividing the tracking data into three episodes: (1) the first 3 min of the experiment without electrical stimulation; (2) minutes 4 to 8, where only the PD-DBS ON subgroup (n = 7) received DBS, and the rest of the groups continued untreated; (3) the last 3 min, where once again no DBS was applied to any of the groups. Subsequently, we compared the behavioral patterns exhibited in each of the episodes across groups.

Figure 3D illustrates tracking data for sham and PD group animals in each episode. Similar to the cylinder test, it can be seen that the sham rats' exploration drive declined as time progressed. **Figure 3D** also shows that sham rats explored significantly more than PD-group rats, where PD animals tend to move less and like to stick to the walls of the arena. Although DBS increased the extent of exploratory behavior of PD rats in episode 2, when it was removed during episode 3, PD animals returned to their mostly inactive behavior.

In order to quantify and statistically compare these behavioral differences, four parameters were considered: average velocity (see **Figure 7A**), average time showing large movements (LM) (speed > 4 cm/s, t > 2 s) (see **Figure 7B**), total distance traveled (see **Figure 7C**) and average time spent immobile (speed < 0.5 cm/s, t > 2 s) (see **Figure 7D**). Sham rats showed a decrease in average velocity, average time spent in LM and distance traveled if we compare the results from the first and third

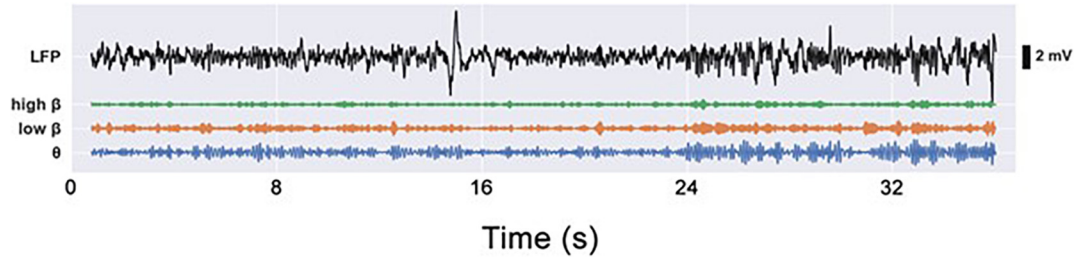

FIGURE 5 | Electrophysiological LFP signals (0.3–300 Hz), as well as video footage, were captured during each experiment simultaneously and were analyzed offline. LFP signals were filtered into G (6–12 Hz), low p (13–21 Hz), and high p (21–30 Hz) frequency bands.

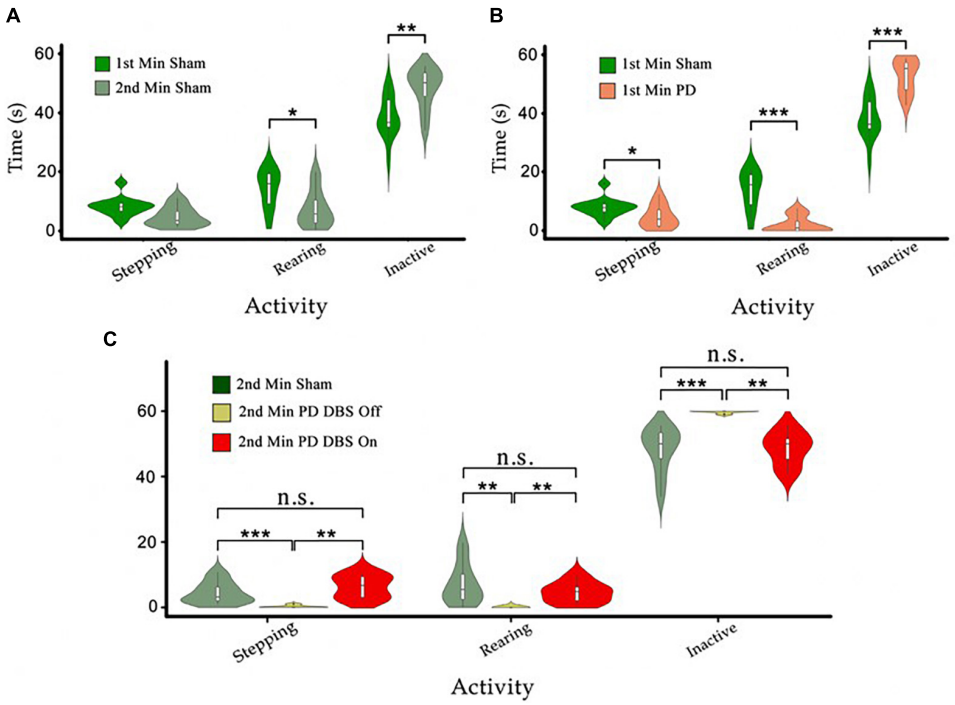

FIGURE 6 | (A) The time sham animals spend in stepping, rearing, and inactivity during the first minute of the tests was compared to the second minute. We observe decreases in stepping and rearing behavior and an increase in the time spent in the inactive state. **(B)** Comparison in the same behaviors as in **(A)** between PD and sham rats during the first minute. **(C)** The behavioral patterns of PD-DBS ON, PD-DBS OFF, and sham animals during the second minute of the cylinder test. We see a similar pattern for PD-DBS ON and sham rats and a drastically impaired pattern in PD-DBS OFF rats, which spend nearly all of their time in the inactive state. Level of significance (*$p < 0.05$, **$p < 0.01$, ***$p < 0.001$, and n.s. stands for not significant). Figure adapted from Mottaghi (2020).

episodes. On the other hand, the average time sham rats spent immobile increased throughout this timespan. This corroborates habituation observed in the cylinder test.

During the first and third episodes (where DBS was not applied to any animal), significant differences in all four parameters were seen between the sham and PD groups (p_{speed}, p_{LM}, $p_{tr.dist.}$, and $p_{immob.} < 0.001$). In the second episode, no significant difference was observed between any of the measured parameters for sham rats and the PD-DBS-ON subgroup, however the PD-DBS-OFF subgroup exhibited significantly less exploratory behavior in comparison.

The behavioral results from both the cylinder and OF tests hence show that we can reestablish severely impaired movement capabilities to close-to-healthy levels through the use of STN-DBS on subjects of the hemi-PD rat model.

Distinct Movement-Dependent PSD Profiles in 6-OHDA Hemi-PD Rats

Having characterized the behavioral differences between the sham, PD, and DBS groups, we next examined how these differences were reflected on a neural level. To relate the animals' behavior with the measured neural activity, the digitized behavioral patterns of the animals' forelimbs in the cylinder test were synchronized with the time-frequency power analysis of the electrophysiological recordings in order to identify possible movement-dependent patterns. A digitized value > 0100 (4 in

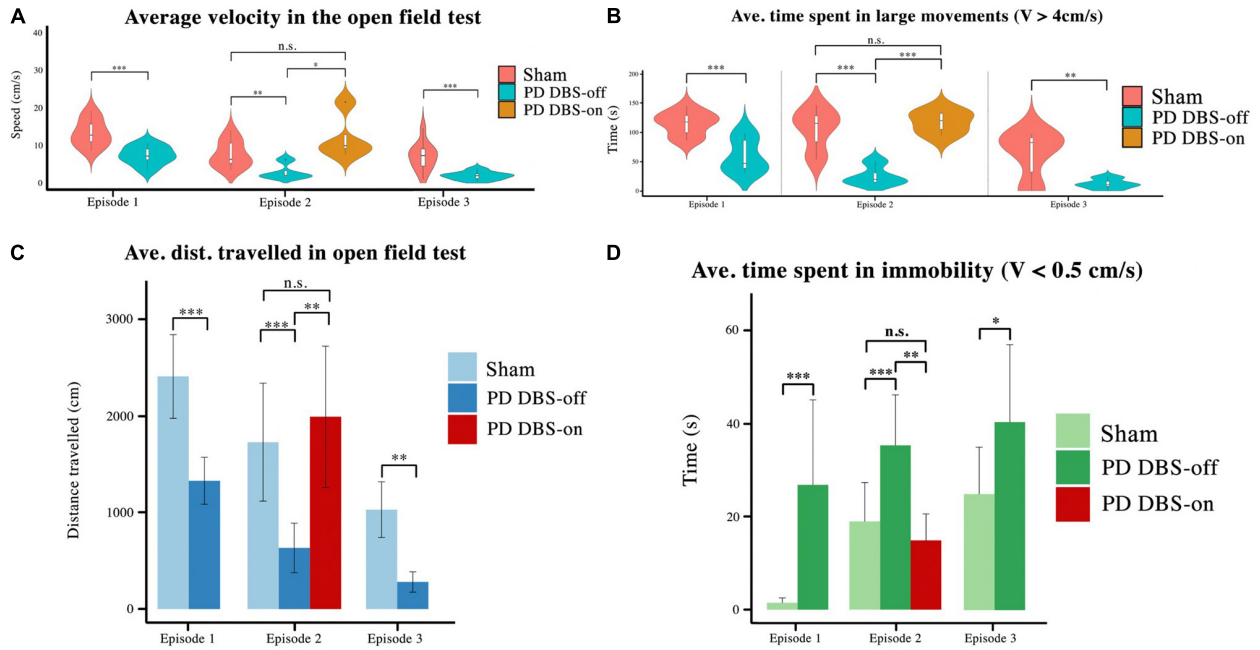

FIGURE 7 | Four behavioral features of the OF test were analyzed using the animals' tracking data. **(A)** The average velocity, **(B)** time spent in large movements, **(C)** distance traveled, **(D)** and the time spent in immobility were selected as variables to compare across groups. It is shown here that unstimulated animals exhibit lower velocity, distance traveled, and time spent in large movements than stimulated or healthy animals, and instead spend more time in immobility. However, the subgroup that received DBS exhibits significant exploratory improvements and a significant reduction in their immobility spells. Level of significance: (*$p < 0.05$, **$p < 0.01$, ***$p < 0.001$, and n.s. stands for not significant). Figure adapted from Mottaghi (2020).

its decimal representation) encodes for a rearing position as here at least one of the animal's forelimb paws is touching the wall (1100 = both front paws on wall, 0000 = rearing with no support, 0011 = both front paws on floor, and 1000 = left paw on wall and right paw not in contact).

Figure 8 shows spectrograms from an electrophysiological recording from both the M1 of the unlesioned and lesioned sides of one exemplary PD rat, synchronized with a plot showing the rat's progression through different forelimb positions. The lesioned hemisphere in this PD rat shows a strong increase in beta power (13–30 Hz) compared to its unlesioned (intact) hemisphere in moments when the rat was entering the rearing position (see arrowheads below spectrograms, **Figure 8**). A similar analysis applied across all rats (see **Figure 9**) confirms the findings of Degos et al. (2009) who also observed an excess in beta band power in the lesioned hemisphere of rats from the unilateral 6-OHDA model. The correspondence of the peak in beta power with rearing episodes shows that the model is affecting neural activity during movement planning and initiation, which could explain the tendency of PD rats to remain in the inactive state (see **Figure 6B** and **Figure 7D**).

For both sham and PD rats, we also calculated the average band power within the frequency bands of interest [i.e., theta (6–12 Hz), low beta (13–21 Hz), and high beta (21–30 Hz)] for signals corresponding to the three behavioral patterns of the cylinder test (see **Figure 9**). The results show distinct low and high beta band power differences between intact and lesioned hemispheres during rearing, significant differences only in low beta band power during stepping and no significant differences at any of the three frequency bands during inactive episodes. As a control, we also looked at the differences in the band power between the two intact hemispheres of sham rats, finding no significant differences. This hence confirms that the differences in band power for PD rats were due to the lesion.

These results show us that the differences in the spectra of electrophysiological recordings from the left and right M1 of PD and sham rats change depending on the behavior of the rats. In particular during active episodes (**Figures 9A–D**), the spectra of intact and lesioned hemispheres differ more than in no-movement episodes (**Figure 9F**). Motor symptoms of PD are apparently related to an alteration of LFP spectra. In addition, the differences in spectra between lesioned and intact hemispheres were preferentially visible in the beta band (both low and high), hinting at the beta band's importance as a potential indicator for the presence of PD symptoms.

Excessive Beta Power Is More Prominent in M1 Than in the STN

The prominence of excessive beta power in the lesioned hemisphere of PD rats was compared between recordings from M1 and the STN of PD and sham rats performing the cylinder test. To this end, we computed the PSD of M1 and STN recordings for all animals during rearing and stepping

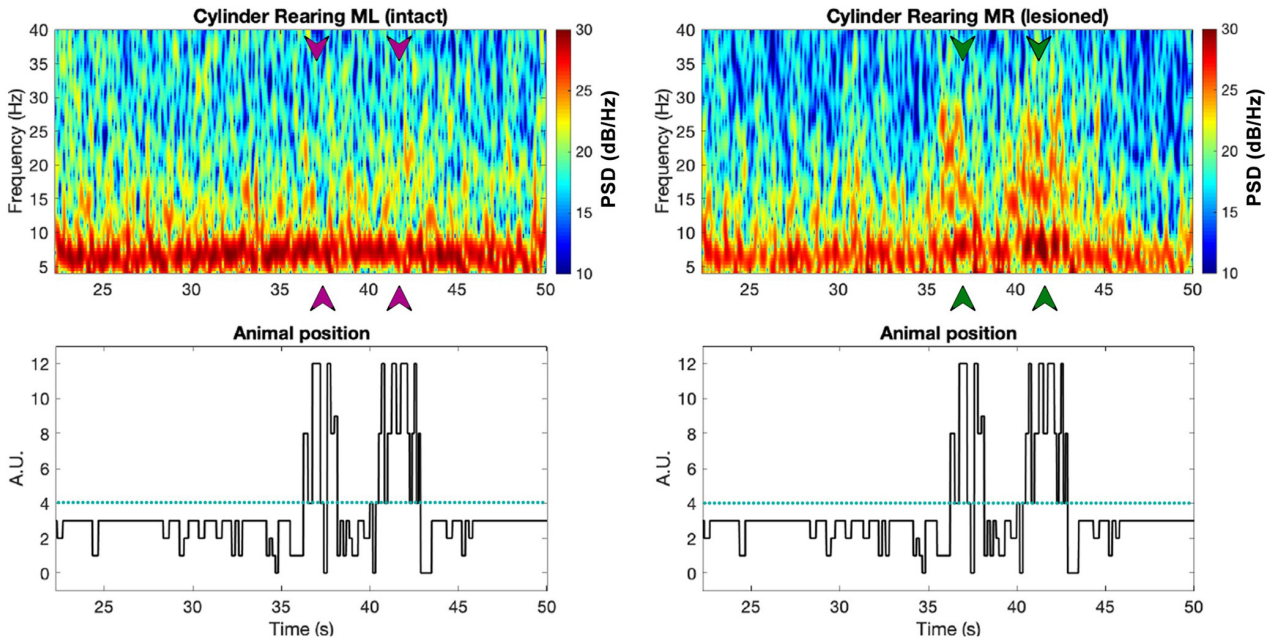

FIGURE 8 | The top two plots show spectrogram examples from the intact (left) vs. lesioned (right) hemispheres captured from bilateral M1 of a PD rat (R21), with the digitized behavioral pattern shown below each spectrogram. Note that the arrows in the spectrograms point at the times in which the animal was rearing, as can be seen from the forelimb position plot below (green and purple correspond to the lesioned and intact hemispheres, respectively). Figure adapted from Mottaghi (2020).

episodes – where the difference in beta power between intact and lesioned hemispheres had been found to be significant.

Figure 10 illustrates the PSD analysis of recordings from the STN and M1 of the lesioned hemisphere of PD rats during DBS-OFF and ON episodes, as well as from the corresponding intact regions of the sham group. In order to quantify the difference between the PSD's from different regions, the Euclidean Distances (ED) between the averaged PSD's were calculated as in Eq. 1.

The PSD plots show how, in both rearing and stepping episodes, the excess in beta power of the DBS-OFF recordings from the lesioned regions is less prominent in STN (**Figures 10A,C** left) than in M1 (**Figures 10A,C** right). In addition, we observe that the application of DBS suppresses this excessive beta power in both regions during these episodes. The results of the ED analysis show in rearing episodes (compared to no stimulation) DBS substantially lowers the ED's in the low beta band for both the STN and M1 (**Figure 10B**). A similar analysis for stepping episodes shows a significant reduction in the ED's for the low beta band only in M1 (not in the STN, **Figure 10D**).

As the LFPs from M1 had more clear and marked differences between the electrophysiological signals coming from lesioned and healthy hemispheres, this indicates they may be better suited for biomarker applications. Furthermore, differences in the M1 signals were also observed in a wider range of behaviors (i.e., both rearing and stepping) compared to the STN signals. In addition, in line with the results from the previous section, differences in the beta band power between the lesioned and healthy hemispheres were more pronounced as the animals' activities become more complex and intensive. Finally, the therapeutic effects of DBS also returned the beta band power of PD rats close to the levels of healthy rats.

The Low Beta Band Is Related to Locomotion

Next, in the context of bradykinesia in PD, we investigated the correlation between movement speed and spectral power in sham and PD rats. This was done selecting time periods involving locomotion from the OF test. For each locomotion speed in the range 1–16 cm/s (1cm/s resolution), we analyzed LFP signals recorded from M1. Due to low sample points, higher speeds were excluded from the analysis. In order to assess the effect of movement speed on the power in the different frequency bands, the average band power calculated over 5-s windows was determined at each speed. Violin plots on the right side of each subplot in **Figure 11** represent the distribution of the power in each band. Additionally, the raster plots placed along the top of **Figure 11**'s subplots indicate statistical significance for the difference in power between the sham and PD group (blue and red, respectively) at each speed.

Comparing the normalized power within theta, low, and high beta bands at each observed speed between healthy (blue) and PD (red) animals revealed little differences at individual speeds, but significant differences overall. Compared to sham group rats, PD rats demonstrate lower theta and higher low beta power.

The results of this experiment tell us that the speed of free movement is hardly reflected by the band power in both sham or hemi-parkinsonian rats. However, overall utilization of spectral power differs between healthy and lesioned animals (violin plots),

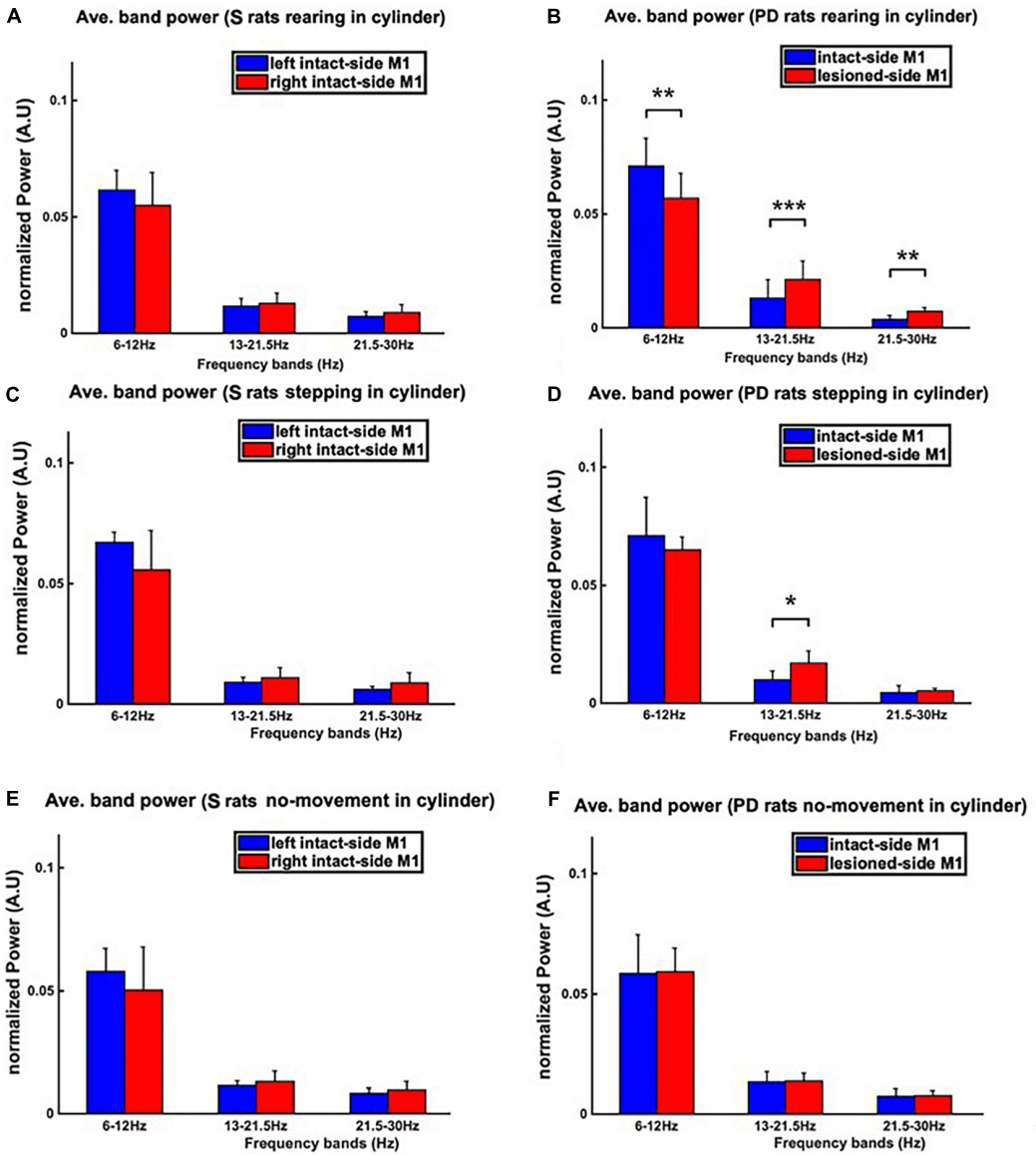

FIGURE 9 | The power spectral density (PSD) during the three behavioral patterns of the cylinder test (i.e., rearing, stepping, and no-movement) was analyzed. The PSD was averaged over theta, low beta, and high beta bands measured from both hemispheres, resulting in three bins, one for each band. The averaged-PSD comparison of the right vs. left M1 of sham rats is shown in the left column **(A,C,E)**, whilst the same comparison for PD rats is shown in the right column **(B,D,F)**. **(B)** During rearing in PD rats, both the low and high beta power from the lesioned hemisphere (right hemisphere) is significantly higher than in the intact hemisphere. **(D)** During stepping episodes, however, only the power in the low beta band is significantly higher in the lesioned than in the intact hemisphere. **(F)** No significant differences between hemispheres can be observed for any band during inactive episodes in PD rats. **(A,C,E)** Similarly, no significant differences are found by comparing the power in PD animals to that of sham group animals for inactive episodes. Level of significance: (*$p < 0.05$, **$p < 0.01$, and ***$p < 0.001$). Figure adapted from Mottaghi (2020).

but only in the low beta band the PD animals' power appears more pronounced than in the healthy animals (correlation lines). In other bands the verdict is not that clear and hardly any of the differences in speed-power-pairs shows a significant difference. As a useful indicator should exhibit some kind of specific feature, this casts doubt on the beta band power to be suitable for revealing acute impediments in the movement of PD animals upon which to trigger a stimulator.

DBS Restores Locomotion and Balance During Forced Movements

Both the cylinder and OF tests assessed exploratory behavior, allowing the animal to start and stop movements freely. It was shown in **Figures 6**, **7** that PD animals tend to explore less than sham group animals. This motivated us to challenge their locomotion capability further by employing the rotarod test, in which the rats were forced to initiate movement and continue to

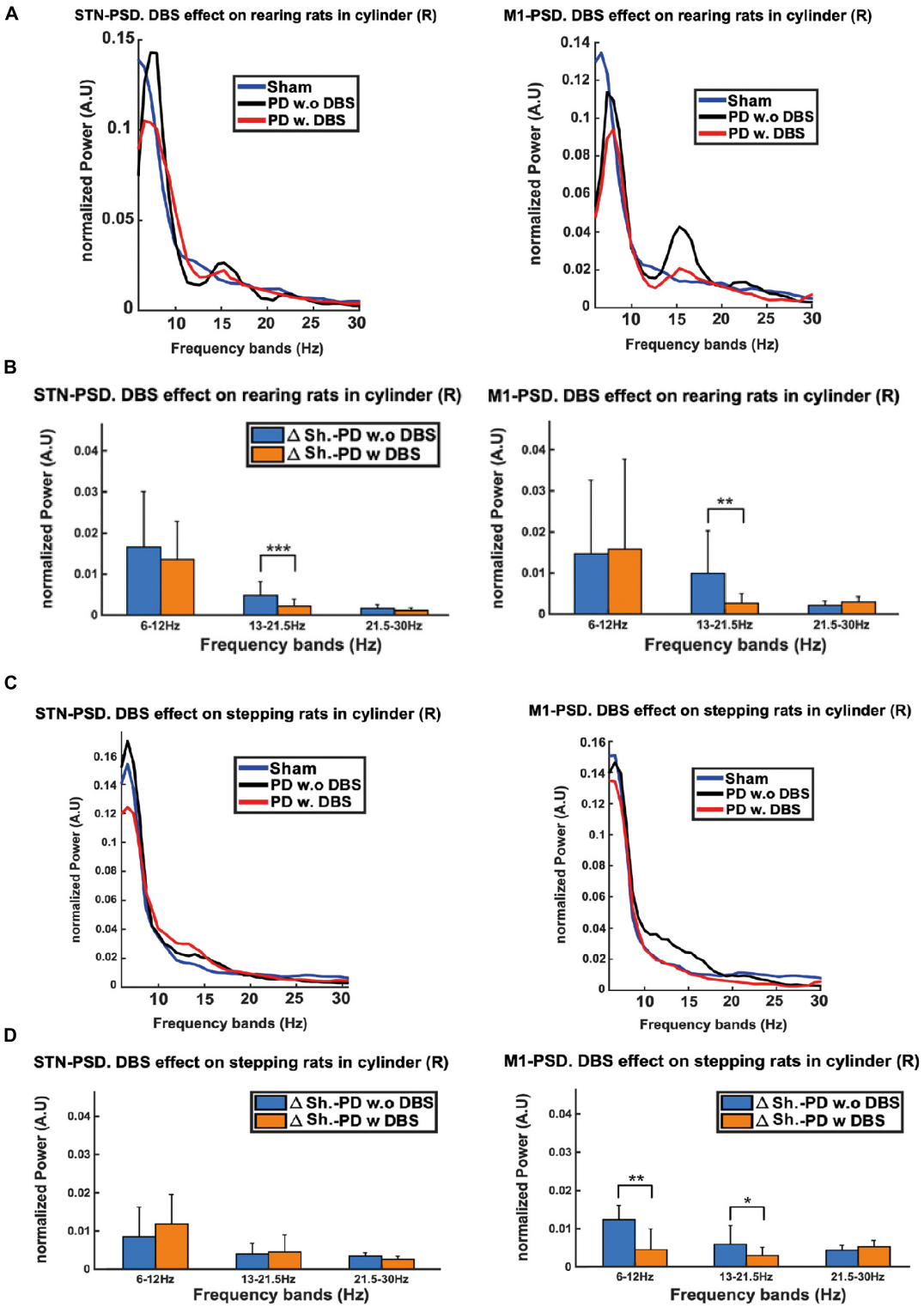

FIGURE 10 | The excessive beta power of PD rats during stepping and rearing was compared between STN and M1 regions. **(A)** Although excessive beta can be seen in both regions, the M1 exhibits a more pronounced excess during rearing as compared to the STN. **(C)** The beta power excess during stepping only becomes apparent for M1 and not for the STN. We also observe that the administration of DBS lowers the beta excess power in both rearing and stepping episodes. **(B,D)** Euclidean Distance (ED) was used to quantify the differences between the PSDs of PD DBS-ON vs. sham and PD DBS-OFF vs. sham rats. The low beta band shows significant decreases in the ED's upon stimulation, which can be observed in both the STN and M1 during rearing, but only in M1 during stepping. Level of significance: (*$p < 0.05$, **$p < 0.01$, and ***$p < 0.001$). Figure adapted from Mottaghi (2020).

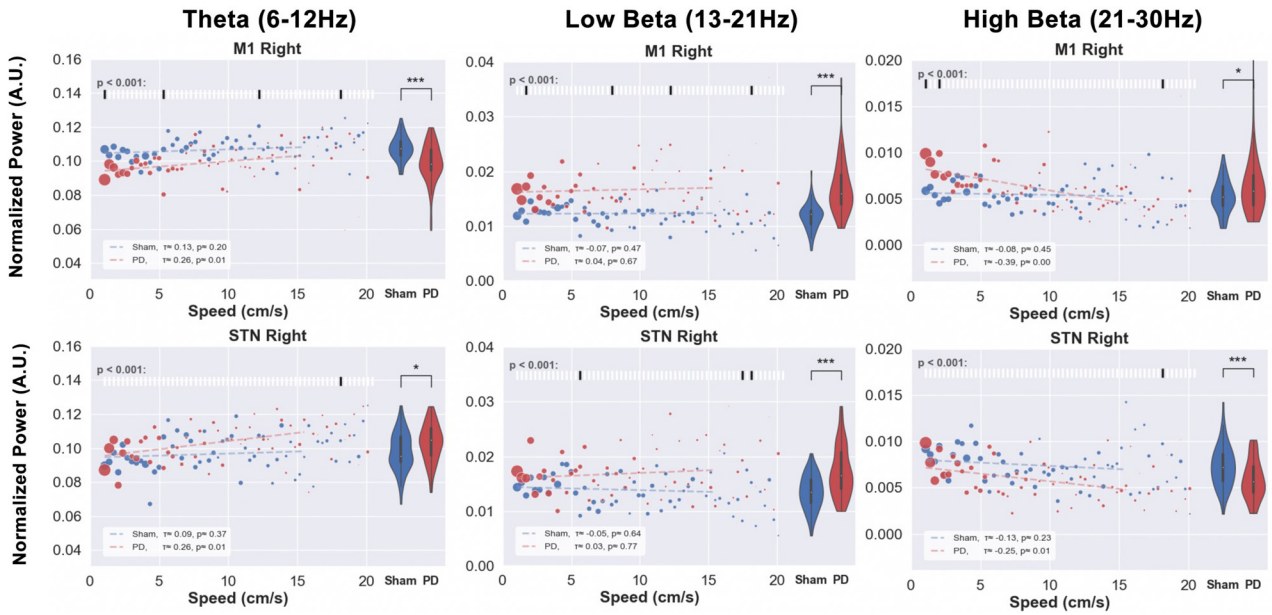

FIGURE 11 | Speed-power relationship was analyzed in order to investigate the correlation between behavioral impairments and electrophysiological indicators. The locomotion speed of each animal was computed using the tracking data. Electrophysiological signals from M1 and STN of the same timestamps were filtered in theta, low, and high beta bands. The scatter plots above illustrate the median value of the band power at each specific speed (red for PD and blue for sham). The size of each point represents the relative amount of data (number of animals exhibiting that speed) per point. The violin plots on the right side of each figure represent the distribution of power over all the speed bins. Kendall's rank correlation coefficient (x) was computed to assess the correlation between speed and power band values, as shown in the white box in the bottom-left corner of each subfigure. Significance tests between PD and sham band power values at each speed were performed and are shown in the raster plot along the top of each subfigure. Note: Except for the low beta band, PD animals' LFP power does not exceed healthy animals' power with the exemption of high beta power at low speeds in the M1. Level of significance: (*$p < 0.05$ and ***$p < 0.001$). Figure adapted from Mottaghi (2020).

walk to avoid falling. We measured the maximum speed and time that each rat was able to stay on the rotarod and compared results across groups (see **Figure 12**).

As no significant difference was found between the first and the second round of trials in the sham group, we compared the results of any of the two sham rounds to the other trials. Overall, we found that PD rats stayed a significantly shorter (on average 100 s vs. 200 s for sham) on the rotarod compared to the sham group when no DBS was applied. However, remarkably, the administration of DBS greatly increases the time spent on the rotarod for PD rats ($n = 7$) as compared to PD rats without DBS ($n = 6$). Moreover, no significant differences were evident between the sham and PD-DBS group.

These results demonstrate that the movement capabilities of lesioned animals were also impaired for forced movements involving balance, and that DBS is capable of restoring performance back to healthy levels.

Impairment of Movement Initiation in Hemi-Parkinsonian Rats Is Accompanied by Alterations in Frequency Band Power

Finally, we examined how power in different frequency bands related to the performance of the animals in the rotarod test (**Figure 13**). In the examined theta and beta bands, significant differences were exhibited between the speed-power pairs of PD and sham group animals (see raster plots). The signal power was significantly lower for the PD rats in the theta band and higher in the two beta bands for all speeds as compared to sham rats. Interestingly, significant differences between the power at each speed in the low beta bands were present only during the early phase of the experiment, and disappeared when the speed reached 4 cm/s. The theta and high beta bands instead show strong differences at higher speeds. Therefore, the speed determined whether there was a difference in the speed-power pairs between the groups, which we did not see in the analysis of the OF test (**Figure 12**). Moreover, contrasting with the results from the OF test, the analysis of recordings from the STN showed patterns similar to those from M1.

DISCUSSION

Closed-loop or adaptive DBS (aDBS) is hoped to ameliorate PD patient's symptoms by turning on the stimulation only when needed to reduce PD's motor symptoms. Clearly, a reliable indicator is needed to trigger the stimulating device and excessive beta-band activity was proposed for that purpose (Little et al., 2013).

Enhanced beta oscillatory activity throughout the cortico-thalamo-basal ganglia loop has been repeatedly reported in PD patients and pre-clinical animal models of the disease

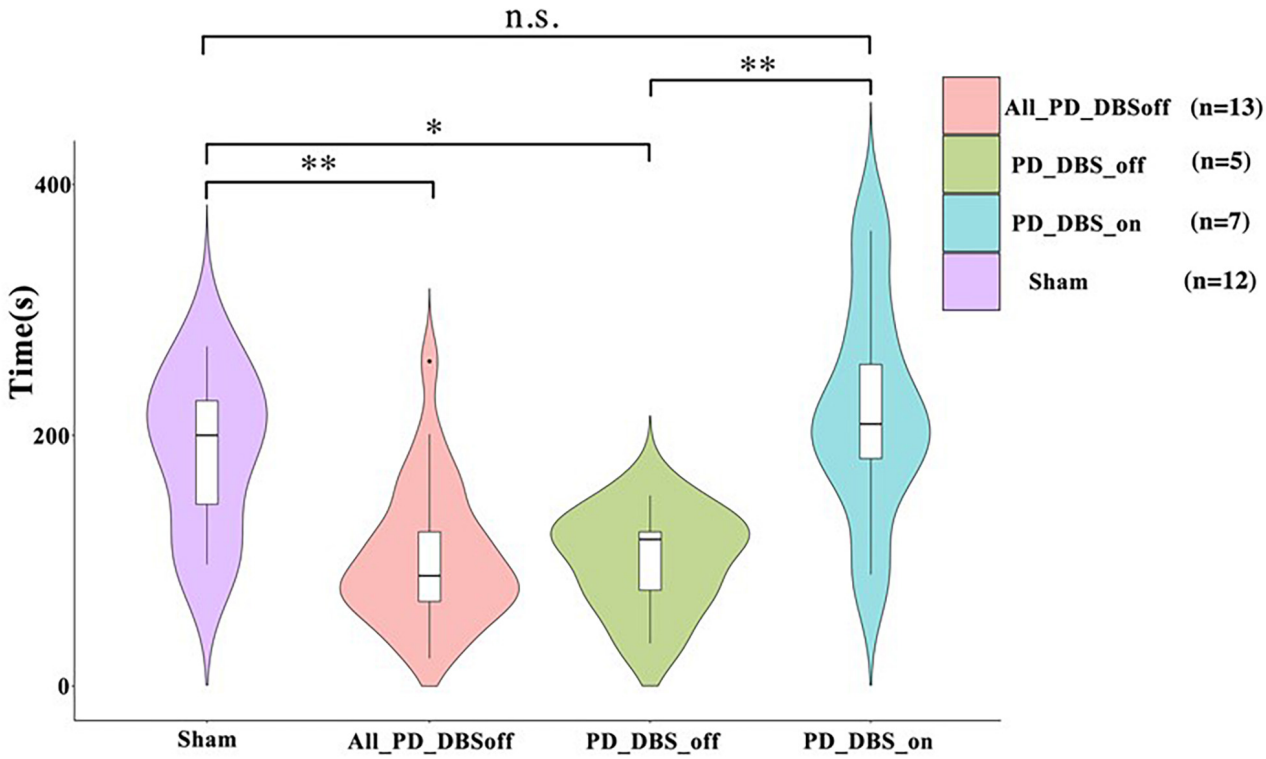

FIGURE 12 | The rotarod test challenges the motor and balance capabilities of animals by forcing them to move at the speed of the elevated rotating rod they are placed on. All the animals underwent two test sessions while no DBS treatment was applied. A subgroup of PD animals performed a third test session while receiving DBS (n = 7), whereas the rest of the PD group performed the third round while DBS was off (n = 6). The maximum time and speed each animal could remain on the rotarod was recorded and compared across groups. The performance of the PD and sham group during the first two rounds were compared (sham vs. All PDDBSoff). The PD group remained a significantly shorter period of time on the rotarod compared to the sham group. As for the third round, the performance difference between the PDDBSon and sham animals was not significant. However, the performance of the PDDBSoff subgroup was significantly worse compared to the sham and PDDBSon. Level of significance: (*$p < 0.05$, **$p < 0.01$, and n.s. stands for not significant). Figure adapted from Mottaghi (2020).

(Levy et al., 2002; Brown, 2006; Kühn et al., 2008; Dorval et al., 2010; Delaville et al., 2015). Studies show that it is mainly related to bradykinesia and akinesia symptoms and is thought to be an antikinetic feature of the disease. Dopamine replacement therapies (Heimer et al., 2002; Levy et al., 2002; Williams, 2002; Priori et al., 2004; Sharott et al., 2005) and DBS treatments (Wingeier et al., 2006) have been observed to lower its severity.

In an earlier study of a preclinical PD model, Degos et al. observed such an excessive increase of beta band oscillations in the motor cortex of awake PD rats, unfortunately after the bradykinetic/akinetic symptoms of their model became apparent (Degos et al., 2009).

In the present study we provide a deep behavioral and electrophysiological characterization of the 6-OHDA rat model of PD using three different behavioral paradigms. In each we evaluated motor symptoms, potential electrophysiological indicators, and the efficacy of DBS at recovering motor impairments. Whereas most research with PD models focuses on the basal ganglia's effect (Dorval and Grill, 2014; Anderson et al., 2015; Hoang et al., 2017) we included LFP recordings from the motor cortex into our data set. Hence our results provide new insights both on the 6-OHDA model as on the quest for a reliable biomarker for aDBS. This is of particular interest as the beta power already has been contested in literature (Swan et al., 2019).

Motor impairments observed in the model (less exploration, slower locomotion speeds, longer immobility) can be linked to bradykinesia and akinesia, while no resting tremor was observed in any of the PD animals in our study which agrees with previous reports on the model (Asakawa et al., 2016). We noticed that excessive beta power was not measured during inactive episodes, corroborating results published by Degos et al. (2009). Similarly (Degos et al., 2009; Asakawa et al., 2016) our hemi-PD animals expressed less exploratory behavior as compared to healthy animals in the cylinder, OF and rotarod tests. We found that DBS treatment improved the performance of hemi-PD animals across all the tested experimental settings, suggesting an analogous mode of operation of DBS in rats to that of humans.

Among the behavior evaluated in unrestrained movement experiments, rearing showed the most prominent increase in the beta band power in lesioned hemispheres. In contrast, we observed when the animal was forced to move on the rotarod, at all speeds, the excessive beta power was detected more easily than during self-guided movements. We speculate that staying atop the rotating rod required better synchronized and more

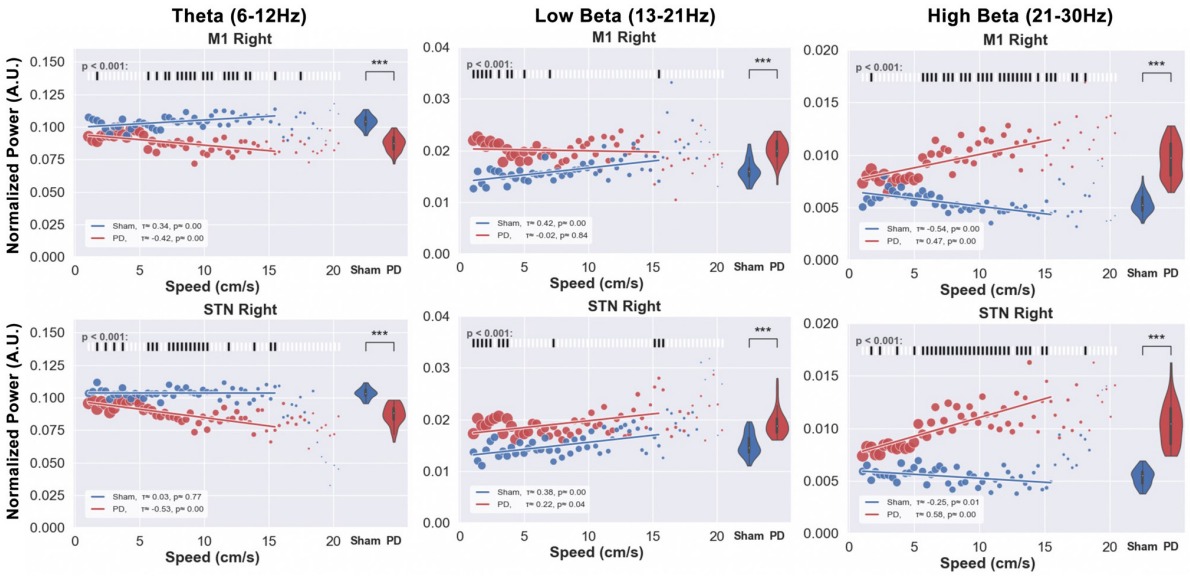

FIGURE 13 | The relation between speed and band power in forced movements on the rotarod was investigated for PD and sham rats. The speeds of the rotarod as well as the electrophysiological signals (M1 and STN) of the same time stamps were plotted for theta, low, and high beta bands. Each data point represents the median of the band power measured at each speed. The size of each point represents the relative amount of data per point. The distribution of the power, over all the speeds is represented by the violin plots on the right side of each subfigure, and the results from the significance test of the difference between the PD and sham band power, at each speed are illustrated in the raster plots above the figures. The theta power, measured from both the right STN and M1 regions over all the speeds (1Ű16 cm/s) are significantly lower in PD rats compared to the sham group, while both low and high beta power showed higher values for PD compared to sham rats. Unlike the results from the OF test, the results from the STN are in line with the results from M1. Additionally, the low beta band shows stronger significant differences between PD and sham speed-power pairs only at lower speeds (<4 cm/s) while theta and high beta bands exhibit significant differences at higher speeds (>4 cm/s). Level of significance: (***$p < 0.001$). Figure adapted from Mottaghi (2020).

widespread brain networks to be activated thus contributing to a stronger signal in the beta band.

Interestingly, when analyzing the low and the high beta bands separately, we observed in the lesioned hemisphere a cross-over in significance levels at around 4 cm/s forced speed. Below that critical speed, the low beta power was higher in lesioned than in healthy animals, whereas above 4 cm/s high beta is presented stronger by PD animals. This is in line with the literature which assumes high beta band power to be an important indicator for cortico-subthalamic interactions, strongly affected by PD (Lalo et al., 2008; Hirschmann et al., 2013; Cao et al., 2019). With an increase in forced speed high beta energy increases both in the M1 and the STN as compared to the high beta contribution in healthy animals. This divergence is not observed in self-motivated movements.

Low beta power on the contrary is attributed to slower walking behavior and freezing in humans (Singh et al., 2013). A more prominent low beta contribution can be seen in PD animals during the slow phases of the forced motion experiments. Self-motivated movement doesn't show such a clear distinction. The low-frequency effects of the 6-OHDA model were studied in Alberico et al. (2017), where it was shown that increased delta field potential power correlates with dyskinesias in 6-OHDA-lesioned mice. This low-frequency effect agrees well with our hypothesis that the interference with lower frequencies in both human PD and the 6-OHDA model leads to the disruption of slow movements or movements made when stationary. Although Alberico et al. (2017) were measuring activity in the striatum to demonstrate the correlation, the projections between the STN, M1 and striatum could explain why we have similar findings.

This difference shows that, depending on the speed and the involvement of additional brain circuits, a generalized beta band power tends to ignore important and subtle differences in its subbands. Across all the experiments and behaviors, the power in the high beta band was observed to be an important indicator in PD animals as it showed differences between healthy and lesioned hemispheres and between PD and sham rats.

Previous studies used behavioral tests in 6-OHDA hemi-PD rodent models and quantitatively evaluated the severity of PD symptoms, to investigate the effects of novel therapeutic interventions and to gain insights into PD pathophysiology (Iancu et al., 2005). However, like other neurotoxic models, a limitation is the acute neurodegenerative property of the 6-OHDA model, as it lacks the progressive, age-dependent effects of PD. Nor does it cover the occurrence of Lewy bodies found in humans (Potashkin et al., 2010). We also observed that the 6-OHDA model does not simulate resting tremor, an important symptom of PD in humans. Thus no salient features were detected in signals recorded during periods of inactivity, which would be crucial as aDBS trigger.

The main findings of our experiments were that the 6-OHDA PD model emulates the motor and balance impairments of PD in both free and forced motion and that STN-DBS is well suited to restore animals' impaired capabilities back to healthy levels.

We also discovered that excessive beta power is prominent in PD rats in all experimental settings i.e., in free and forced motion at all speeds – except when animals remain immobile. An analysis between speed and spectral power further revealed significant correlations only in forced movement which were positive in the beta band and negative in the theta band. We also noticed that excessive beta power was more prominent in high beta and M1 than in the STN.

When generously projecting our results from an animal model of PD toward treatments of human patients with adaptive DBS, we advocate to take contextual information of the surroundings into account. Self-paced walking may produce different LFP signals than walking on a treadmill. In addition, control algorithm might strongly benefit from more than one recording location in the brain, as our results showed differences in recordings from STN (the usual implant locationin humans) and the motor cortex.

All in all, we want to express our hope that the use of a better validated animal model might prove beneficial for the treatment of PD patients.

DATA AVAILABILITY STATEMENT

The raw data supporting the conclusions of this article will be made available by the authors, without undue reservation.

ETHICS STATEMENT

All animal procedures were conducted in conformity with relevant institutional rules in compliance with the guidelines of the German Council on Animal Protection. Protocols were approved by the Animal Care Committee of the University of Freiburg under the supervision of the Regierungspräsidium Freiburg (approval G15/031) in accordance with the guidelines of the European Union Directive 2010/63/UE.

AUTHOR CONTRIBUTIONS

SM designed the experiments and performed the surgeries. SM, SK, DB, SL, RM, MW, and CK contributed to the experimental performance. SM and DB analyzed the results. CM performed the histology. RS and UH supervised the experimental and analysis work. All authors contributed to manuscript revision, read and approved the submitted version.

FUNDING

This study was supported by BMBF-project FMT (13GW0230A).

REFERENCES

Alberico, S. L., Kim, Y. C., Lence, T., and Narayanan, N. S. (2017). Axial levodopa-induced dyskinesias and neuronal activity in the dorsal striatum. *Neuroscience* 343, 240–249. doi: 10.1016/j.neuroscience.2016.11.046

Anderson, C. J., Sheppard, D. T., Huynh, R., Anderson, D. N., Polar, C. A., and Dorval, A. D. (2015). Subthalamic deep brain stimulation reduces pathological information transmission to the thalamus in a rat model of parkinsonism. *Front. Neural Circuits* 9:31. doi: 10.3389/fncir.2015.00031

Asakawa, T., Fang, H., Sugiyama, K., Nozaki, T., Hong, Z., Yang, Y., et al. (2016). Animal behavioral assessments in current research of Parkinson's disease. *Neurosci. Biobehav. Rev.* 65, 63–94. doi: 10.1016/j.neubiorev.2016.03.016

Bohlen, M., Cameron, A., Metten, P., Crabbe, J. C., and Wahlsten, D. (2009). Calibration of rotational acceleration for the rotarod test of rodent motor coordination. *J. Neurosci. Methods* 178, 10–14. doi: 10.1016/j.jneumeth.2008.11.001

Brown, P. (2006). Bad oscillations in Parkinson's disease. *J. Neural Transmis. Supplement.* 70, 27–30. doi: 10.1007/978-3-211-45295-0_6

Brown, P., Oliviero, A., Mazzone, P., Insola, A., Tonali, P., and Di Lazzaro, V. (2001). Dopamine dependency of oscillations between subthalamic nucleus and pallidum in Parkinson's disease. *J. Neurosci.* 21, 1033–1038. doi: 10.1523/jneurosci.21-03-01033.2001

Cao, C., Huang, P., Wang, T., Zhan, S., Liu, W., Pan, Y., et al. (2019). Cortico-subthalamic coherence in a patient with dystonia induced by chorea-acanthocytosis: a case report. *Front. Hum. Neurosci.* 13:163. doi: 10.3389/fnhum.2019.00163

Cartmell, S. M., Gelgor, L., and Mitchell, D. (1991). A revised rotarod procedure for measuring the effect of antinociceptive drugs on motor function in the rat. *J. Pharmacol. Methods* 26, 149–159. doi: 10.1016/0160-5402(91)90063-B

Castaño-Candamil, S., Mottaghi, S., Coenen, V. A., Hofmann, U. G., and Tangermann, M. (2017). "Closed-Loop deep brain stimulation system for an animal model of parkinson's disease: a pilot study," in *Proceedings of the 7th Graz Brain-Computer Interface Conference 2017* (Graz), doi: 10.3217/978-3-85125-533-1-12

Cenci, M., and Lundblad, M. (2005). "Chapter B7 – Utility of 6-hydroxydopamine lesioned rats in the preclinical screening of novel treatments for parkinson disease," in *Animal Models of Movement Disorders*, 1st Edn (Cambridge, MA: Academic Press), 193–208. doi: 10.1016/B978-012088382-0/50016-5

Chen, J., Liu, J. L., Chen, X., Qian, H., Xian, W. B., Zhou, H. Y., et al. (2011). *Zhonghua yi Xue za Zhi*, Vol. 91, 291–295.

Degos, B., Deniau, J.-M., Chavez, M., and Maurice, N. (2009). Chronic but not acute dopaminergic transmission interruption promotes a progressive increase in cortical beta frequency synchronization: relationships to vigilance state and akinesia. *Cereb. Cortex* 19, 1616–1630. doi: 10.1093/cercor/bhn199

Delaville, C., McCoy, A. J., Gerber, C. M., Cruz, A. V., and Walters, J. R. (2015). Subthalamic nucleus activity in the awake hemiparkinsonian rat: relationships with motor and cognitive networks. *J. Neurosci.* 35, 6918–6930. doi: 10.1523/JNEUROSCI.0587-15.2015

DeMaagd, G., and Philip, A. (2015). Parkinson's disease and its management part 1: disease entity, risk factors, pathophysiology, clinical presentation, and diagnosis. *P T* 40, 504–532.

Dorsey, E. R., Sherer, T., Okun, M. S., and Bloemd, B. R. (2018). The emerging evidence of the Parkinson pandemic. *J. Parkinson's Dis.* 8, S3–S8. doi: 10.3233/JPD-181474

Dorval, A. D., and Grill, W. M. (2014). Deep brain stimulation of the subthalamic nucleus reestablishes neuronal information transmission in the 6-OHDA rat model of parkinsonism. *J. Neurophysiol.* 111, 1949–1959. doi: 10.1152/jn.00713.2013

Dorval, A. D., Kuncel, A. M., Birdno, M. J., Turner, D. A., and Grill, W. M. (2010). Deep brain stimulation alleviates parkinsonian bradykinesia by regularizing pallidal activity. *J. Neurophysiol.* 104, 911–921. doi: 10.1152/jn.00103.2010

Dunham, N. W., and Miya, T. S. (1957). A note on a simple apparatus for detecting neurological deficit in rats and mice. *J. Am. Pharm. Associat. Am. Pharm. Associat.* 46, 208–209. doi: 10.1002/jps.3030460322

Filion, M., Tremblay, L., and Bédard, P. J. (1991). Effects of dopamine agonists on the spontaneous activity of globus pallidus neurons in monkeys with MPTP-induced parkinsonism. *Brain Res.* 547, 152–161.

Gatev, P., Darbin, O., and Wichmann, T. (2006). Oscillations in the basal ganglia under normal conditions and in movement disorders. *Movem. Dis.* 21, 1566–1577. doi: 10.1002/mds.21033

Heimer, G., Bar-Gad, I., Goldberg, J. A., and Bergman, H. (2002). Dopamine replacement therapy reverses abnormal synchronization of pallidal neurons in the 1-methyl-4-phenyll-1,2,3,6-tetrahydropyridine primate model of parkinsonism. *J. Neurosci.* 22, 7850–7855. doi: 10.1523/jneurosci.22-18-07850.2002

Henderson, J. M., Watson, S., Halliday, G. M., Heinemann, T., and Gerlach, M. (2003). Relationships between various behavioural abnormalities and nigrostriatal dopamine depletion in the unilateral 6-OHDA-lesioned rat. *Behav. Brain Res.* 139, 105–113. doi: 10.1016/S0166-4328(02)00087-6

Hirschmann, J., Özkurt, T. E., Butz, M., Homburger, M., Elben, S., Hartmann, C. J., et al. (2013). Differential modulation of STN-cortical and cortico-muscular coherence by movement and levodopa in Parkinson's disease. *NeuroImage* 68, 203–213. doi: 10.1016/j.neuroimage.2012.11.036

Hoang, K. B., Cassar, I. R., Grill, W. M., and Turner, D. A. (2017). Biomarkers and stimulation algorithms for adaptive brain stimulation. *Front. Neurosci.* 11:564. doi: 10.3389/fnins.2017.00564

Iancu, R., Mohapel, P., Brundin, P., and Paul, G. (2005). Behavioral characterization of a unilateral 6-OHDA-lesion model of Parkinson's disease in mice. *Behav. Brain Res.* 162, 1–10. doi: 10.1016/j.bbr.2005.02.023

Kühn, A. A., Kempf, F., Brucke, C., Gaynor Doyle, L., Martinez-Torres, I., Pogosyan, A., et al. (2008). High-frequency stimulation of the subthalamic nucleus suppresses oscillatory beta activity in patients with Parkinson's disease in parallel with improvement in motor performance. *J. Neurosci.* 28, 6165–6173. doi: 10.1523/JNEUROSCI.0282-08.2008

Kühn, A. A., Trottenberg, T., Kivi, A., Kupsch, A., Schneider, G. H., and Brown, P. (2005). The relationship between local field potential and neuronal discharge in the subthalamic nucleus of patients with Parkinson's disease. *Exp. Neurol.* 194, 212–220. doi: 10.1016/j.expneurol.2005.02.010

Lalo, E., Thobois, S., Sharott, A., Polo, G., Mertens, P., Pogosyan, A., et al. (2008). Patterns of bidirectional communication between cortex and basal ganglia during movement in patients with Parkinson disease. *J. Neurosci.* 28, 3008–3016. doi: 10.1523/JNEUROSCI.5295-07.2008

Levy, R., Ashby, P., Hutchison, W. D., Lang, A. E., Lozano, A. M., and Dostrovsky, J. O. (2002). Dependence of subthalamic nucleus oscillations on movement and dopamine in Parkinson's disease. *Brain* 125, 1196–1209. doi: 10.1093/brain/awf128

Little, S., and Brown, P. (2020). Debugging adaptive deep brain stimulation for Parkinson's disease. *Move. Disord. Off. J. Mov. Disorder Soc.* 35, 555–561. doi: 10.1002/mds.27996

Little, S., Pogosyan, A., Neal, S., Zavala, B., Zrinzo, L., Hariz, M., et al. (2013). Adaptive deep brain stimulation in advanced Parkinson disease. *Ann. Neurol.* 74, 449–457. doi: 10.1002/ana.23951

Little, S., Pogosyan, A., Neal, S., Zrinzo, L., Hariz, M., Foltynie, T., et al. (2014). Controlling Parkinson's disease with adaptive deep brain stimulation. *J. Vis. Exp.* 89:51403. doi: 10.3791/51403

Lundblad, M., Usiello, A., Carta, M., Håkansson, K., Fisone, G., and Cenci, M. A. (2005). Pharmacological validation of a mouse model of L-DOPA-induced dyskinesia. *Exp. Neurol.* 194, 66–75. doi: 10.1016/j.expneurol.2005.02.002

Mottaghi, S. (2020). Sampling the parameter space of cDBS in a Hemi-PD Rat Model (urn:nbn:de:bsz:25-freidok-1943136) [PhD thesis, Abert-Ludwigs-Universitaet Freiburg]. *FreiDok Plus*. doi: 10.6094/UNIFR/194313

Neumann, W. J., Turner, R. S., Blankertz, B., Mitchell, T., Kühn, A. A., and Richardson, R. M. (2019). Toward electrophysiology-based intelligent adaptive deep brain stimulation for movement disorders. *Neurotherapeutics* 16, 105–118. doi: 10.1007/s13311-018-00705-0

Nini, A., Feingold, A., Slovin, H., and Bergman, H. (1995). Neurons in the globus pallidus do not show correlated activity in the normal monkey, but phase-locked oscillations appear in the MPTP model of parkinsonism. *J. Neurophysiol.* 74, 1800–1805. doi: 10.1152/jn.1995.74.4.1800

Plenz, D., and Kital, S. T. (1999). A basal ganglia pacemaker formed by the subthalamic nucleus and external globus pallidus. *Nature* 400, 677–682. doi: 10.1038/23281

Potashkin, J. A., Blume, S. R., and Runkle, N. K. (2010). Limitations of animal models of Parkinson's disease. *Parkinsons Dis.* 2011:658083. doi: 10.4061/2011/658083

Priori, A., Foffani, G., Pesenti, A., Tamma, F., Bianchi, A. M., Pellegrini, M., et al. (2004). Rhythm-specific pharmacological modulation of subthalamic activity in Parkinson's disease. *Exp. Neurol.* 189, 369–379. doi: 10.1016/j.expneurol.2004.06.001

Seibenhener, M. L., and Wooten, M. C. (2015). Use of the open field maze to measure locomotor and anxiety-like behavior in mice. *J. Visual. Exp.* 96:e52434.

Sharott, A., Magill, P. J., Harnack, D., Kupsch, A., Meissner, W., and Brown, P. (2005). Dopamine depletion increases the power and coherence of β-oscillations in the cerebral cortex and subthalamic nucleus of the awake rat. *Eur. J. Neurosci.* 21, 1413–1422. doi: 10.1111/j.1460-9568.2005.03973.x

Singh, A., Plate, A., Kammermeier, S., Mehrkens, J. H., Ilmberger, J., and Bötzel, K. (2013). Freezing of gait-related oscillatory activity in the human subthalamic nucleus. *Basal Ganglia* 3, 25–32. doi: 10.1016/j.baga.2012.10.002

Stein, E., and Bar-Gad, I. (2013). Beta oscillations in the cortico-basal ganglia loop during parkinsonism. *Exp. Neurol.* 245, 52–59. doi: 10.1016/j.expneurol.2012.07.023

Swan, C. B., Schulte, D. J., Brocker, D. T., and Grill, W. M. (2019). Disorders of the nervous system beta frequency oscillations in the subthalamic nucleus are not sufficient for the development of symptoms of parkinsonian bradykinesia/akinesia in rats. *eNeuro* 6:ENEURO.0089-19.2019. doi: 10.1523/ENEURO.0089-19.2019

Ungerstedt, U. (1968). 6-hydroxy-dopamine induced degeneration of central monoamine neurons. *Eur. J. Pharmacol.* 5, 107–110. doi: 10.1016/0014-2999(68)90164-7

Williams, D. (2002). Dopamine-dependent changes in the functional connectivity between basal ganglia and cerebral cortex in humans. *Brain* 125, 1558–1569. doi: 10.1093/brain/awf156

Wingeier, B., Tcheng, T., Koop, M. M., Hill, B. C., Heit, G., and Bronte-Stewart, H. M. (2006). Intra-operative STN DBS attenuates the prominent beta rhythm in the STN in Parkinson's disease. *Exp. Neurol.* 197, 244–251. doi: 10.1016/j.expneurol.2005.09.016

Yamawaki, N., Stanford, I. M., Hall, S. D., and Woodhall, G. L. (2008). Pharmacologically induced and stimulus evoked rhythmic neuronal oscillatory activity in the primary motor cortex in vitro. *Neuroscience* 151, 386–395. doi: 10.1016/j.neuroscience.2007.10.021

Conflict of Interest: The authors declare that the research was conducted in the absence of any commercial or financial relationships that could be construed as a potential conflict of interest.

Advantages of publishing in Frontiers

OPEN ACCESS
Articles are free to read for greatest visibility and readership

FAST PUBLICATION
Around 90 days from submission to decision

HIGH QUALITY PEER-REVIEW
Rigorous, collaborative, and constructive peer-review

TRANSPARENT PEER-REVIEW
Editors and reviewers acknowledged by name on published articles

Frontiers
Avenue du Tribunal-Fédéral 34
1005 Lausanne | Switzerland

Visit us: www.frontiersin.org
Contact us: frontiersin.org/about/contact

REPRODUCIBILITY OF RESEARCH
Support open data and methods to enhance research reproducibility

DIGITAL PUBLISHING
Articles designed for optimal readership across devices

FOLLOW US
@frontiersin

IMPACT METRICS
Advanced article metrics track visibility across digital media

EXTENSIVE PROMOTION
Marketing and promotion of impactful research

LOOP RESEARCH NETWORK
Our network increases your article's readership